



**FuelSolutions™ W74 Canister Transportation
Safety Analysis Report**

*Revision 10
September 2006*

*Document No. WSNF-123
Docket No. 71-9276*

Prepared by:

EnergySolutions Spent Fuel Division, Inc.
Campbell, California

©2006 EnergySolutions Spent Fuel Division, Inc.
All Rights Reserved

Approved for Release:

Revision: 10

Digitally signed by Steven E. Sisley
Reason: Approved for release
Date: 2006.10.02 15:46:42 -07'00'

TABLE OF CONTENTS

<u>Section</u>	<u>Title</u>	<u>Page</u>
1.	GENERAL INFORMATION	1-1
1.1	Introduction	1.1-1
1.2	Package Description	1.2-1
1.2.1	Packaging	1.2-1
1.2.1.1	FuelSolutions™ W74 Canister	1.2-2
1.2.1.2	Other FuelSolutions™ Canister Features	1.2-6
1.2.1.3	Non-Packaging Support Equipment	1.2-8
1.2.2	Operational Features	1.2-8
1.2.2.1	Horizontal Canister Transfer	1.2-9
1.2.2.2	Vertical Canister Transfer	1.2-9
1.2.2.3	Canister Loading, Closure, and Opening	1.2-9
1.2.3	Contents of Packaging	1.2-9
1.2.3.1	Spent Fuel to be Transported.....	1.2-9
1.2.3.2	Radionuclide Inventory	1.2-12
1.2.3.3	Maximum Payload Weight.....	1.2-12
1.2.3.4	Maximum Decay Heat.....	1.2-12
1.2.3.5	Maximum Pressure Buildup.....	1.2-12
1.2.4	Compliance with 10CFR71	1.2-12
1.3	Appendices	1.3-1
1.3.1	General Arrangement Drawings	1.3-1
1.3.2	Product Literature	1.3-3
1.3.2.1	Borated Stainless Steel Literature	1.3-3
1.3.2.2	Electroless Nickel Plating Literature.....	1.3-5
1.3.3	Glossary of Terms	1.3-7
2.	STRUCTURAL EVALUATION	2-1
2.1	Structural Design.....	2.1-1
2.1.1	Discussion	2.1-1
2.1.1.1	Shell Assembly	2.1-1

TABLE OF CONTENTS (continued)

<u>Section</u>	<u>Title</u>	<u>Page</u>
	2.1.1.2 Basket Assembly	2.1-1
	2.1.1.3 Damaged Fuel Can	2.1-3
2.1.2	Design Criteria	2.1-4
	2.1.2.1 Basic Design Criteria.....	2.1-4
	2.1.2.2 Load Combinations	2.1-5
	2.1.2.3 Miscellaneous Structural Failure Modes.....	2.1-6
2.2	Weights and Center of Gravity.....	2.2-1
2.3	Mechanical Properties of Materials	2.3-1
2.4	General Standards for All Packages.....	2.4-1
	2.4.1 Minimum Package Size.....	2.4-1
	2.4.2 Tamper Indicating Device.....	2.4-1
	2.4.3 Positive Closure	2.4-1
	2.4.4 Chemical and Galvanic Reactions	2.4-1
2.5	Lifting and Tiedown Standards	2.5-1
2.6	Normal Conditions of Transport	2.6-1
	2.6.1 Heat 2.6-1	
	2.6.1.1 Summary of Pressures and Temperatures	2.6-1
	2.6.1.2 Differential Thermal Expansion	2.6-2
	2.6.1.3 Stress Calculations	2.6-6
	2.6.1.4 Fatigue Evaluation.....	2.6-13
	2.6.1.5 Comparison with Allowable Stresses.....	2.6-20
	2.6.2 Cold 2.6-29	
	2.6.3 Reduced External Pressure.....	2.6-29
	2.6.4 Increased External Pressure	2.6-29
	2.6.5 Vibration2.6-30	
	2.6.5.1 General and LTP Spacer Plates	2.6-30
	2.6.5.2 Engagement Spacer Plate	2.6-32
	2.6.5.3 Support Tubes and Support Sleeves.....	2.6-33
	2.6.5.4 Guide Tubes.....	2.6-35

TABLE OF CONTENTS (continued)

<u>Section</u>	<u>Title</u>	<u>Page</u>
	2.6.5.5 Vibration Summary	2.6-38
2.6.6	Water Spray.....	2.6-47
2.6.7	Free Drop	2.6-47
	2.6.7.1 General and LTP Spacer Plates	2.6-47
	2.6.7.2 Engagement Spacer Plate	2.6-53
	2.6.7.3 Support Tubes.....	2.6-54
	2.6.7.4 Guide Tubes.....	2.6-55
	2.6.7.5 Canister Shell Assembly.....	2.6-61
	2.6.7.6 Free Drop Summary	2.6-61
2.6.8	Corner Drop	2.6-71
2.6.9	Compression.....	2.6-71
2.6.10	Penetration	2.6-71
2.7	Hypothetical Accident Conditions	2.7-1
	2.7.1 Free Drop	2.7-1
	2.7.1.1 End Drop	2.7-2
	2.7.1.2 Side Drop.....	2.7-23
	2.7.1.3 Corner Drop.....	2.7-37
	2.7.1.4 Oblique Drop.....	2.7-45
2.7.2	Crush 2.7-91	
2.7.3	Puncture 2.7-91	
2.7.4	Thermal 2.7-91	
2.7.5	Immersion - Fissile Material	2.7-91
2.7.6	Immersion - All Packages	2.7-92
2.7.7	Summary of Damage.....	2.7-92
2.8	Special Requirements for Irradiated Nuclear Fuel Shipments	2.8-1
2.9	Internal Pressure Test.....	2.9-1
2.10	Special Form	2.10-1
2.11	Fuel Rods.....	2.11-1
2.12	Appendices	2.12-1

TABLE OF CONTENTS (continued)

<u>Section</u>	<u>Title</u>	<u>Page</u>
2.12.1	General and LTP Spacer Plate Tributary Weights.....	2.12-1
2.12.2	Free Drop Equivalent Static Design Loads.....	2.12-9
2.12.2.1	W74 Canister Frequency Analysis.....	2.12-9
2.12.2.2	Equivalent Static Accelerations.....	2.12-13
2.12.3	General and LTP Spacer Plate Stress Evaluation Points.....	2.12-15
2.12.4	Finite Element Model Descriptions.....	2.12-17
2.12.4.1	General and LTP Spacer Plate Models.....	2.12-17
2.12.4.2	Engagements Spacer Plate Finite Element Models.....	2.12-22
2.12.4.3	Guide Tube Half-Symmetry Periodic Model.....	2.12-28
2.12.4.4	Canister Top Shield Plug Model.....	2.12-29
2.12.4.5	Canister Shell Axisymmetric Finite Element Model.....	2.12-30
2.12.4.6	Canister Shell Half-Symmetry Finite Element Model.....	2.12-32
2.12.5	Canister Shell Stress Evaluation Points.....	2.12-51
3.	THERMAL EVALUATION.....	3-1
3.1	Discussion.....	3.1-3
3.1.1	Design Features.....	3.1-3
3.1.1.1	W74 Canister.....	3.1-4
3.1.1.2	Transportation Cask.....	3.1-5
3.1.2	Design Basis Thermal Load Conditions.....	3.1-6
3.1.3	Design Basis Axial Heat Generation Profile.....	3.1-7
3.1.3.1	Development of the Design Basis Axial Heat Generation Profile.....	3.1-8
3.1.3.2	Application of Axial Heat Profiles for Canister Analysis.....	3.1-9
3.1.3.3	Compliance with Transportation Cask Thermal Requirements .	3.1-10
3.1.4	Temperature Summary.....	3.1-10
3.1.5	Transportation Cask Internal Pressure Summary.....	3.1-11
3.2	Summary of Thermal Properties of Materials.....	3.2-19
3.2.1	W74 Canister.....	3.2-19
3.2.2	Big Rock Point Fuel.....	3.2-20

TABLE OF CONTENTS (continued)

<u>Section</u>	<u>Title</u>	<u>Page</u>
3.3	Technical Specification of Components	3.3-1
3.3.1	W74 Canister.....	3.3-1
3.3.2	Fuel Cladding Allowable Temperatures	3.3-2
3.4	Thermal Evaluation for Normal Conditions of Transport.....	3.4-7
3.4.1	Thermal Models	3.4-7
3.4.1.1	Analytical Thermal Models.....	3.4-7
3.4.1.2	Test Thermal Model	3.4-13
3.4.2	Maximum Temperatures	3.4-13
3.4.3	Minimum Temperatures.....	3.4-15
3.4.4	Maximum Internal Pressures	3.4-15
3.4.4.1	Fuel Rod Fill Gas.....	3.4-16
3.4.4.2	Fuel Rod Fission Gas Generation.....	3.4-17
3.4.4.3	Transportation Cask MNOP	3.4-18
3.4.5	Maximum Thermal Stresses.....	3.4-19
3.4.6	Evaluation of Package Performance for Normal Conditions of Transport	3.4-19
3.5	Thermal Evaluation for Hypothetical Accident Conditions.....	3.5-45
3.5.1	Thermal Model.....	3.5-45
3.5.1.1	Analytical Thermal Model	3.5-45
3.5.1.2	Test Thermal Model	3.5-46
3.5.2	Package Conditions and Environment	3.5-46
3.5.3	Package Temperatures	3.5-47
3.5.4	Maximum Internal Pressures	3.5-48
3.5.5	Maximum Thermal Stresses.....	3.5-48
3.5.6	Evaluation of Package Performance for Hypothetical Accident Conditions	3.5-48
3.6	Appendices	3.6-55
3.6.1	Canister Internal Convection	3.6-55
3.6.2	Other Modes of Heat Transfer	3.6-58
3.6.3	Impact Of Fission Gas Release On Thermal Performance	3.6-60

TABLE OF CONTENTS (continued)

<u>Section</u>	<u>Title</u>	<u>Page</u>
3.6.4	Big Rock Point Mixed-Oxide (MOX) Fuel	3.6-63
3.6.4.1	Heat Generation of BRP MOX Fuel	3.6-63
3.6.4.2	Axial Heat Generation Profile of BRP MOX Fuel.....	3.6-63
3.6.4.3	Effective Thermal Conductivity of BRP MOX Fuel.....	3.6-64
3.6.4.4	Allowable Cladding Temperature for BRP MOX Fuel.....	3.6-64
3.6.4.5	Canister Internal Pressure for BRP MOX Fuel	3.6-65
3.6.4.6	Thermal Summary for BRP MOX Fuel	3.6-65
3.6.5	Big Rock Point Damaged Fuel.....	3.6-65
3.6.5.1	Heat Generation of BRP Damaged Fuel	3.6-66
3.6.5.2	Axial Heat Generation Profile of BRP Damaged Fuel.....	3.6-66
3.6.5.3	Effective Thermal Conductivity of BRP Damaged Fuel.....	3.6-66
3.6.5.4	Allowable Cladding Temperature for BRP Damaged Fuel.....	3.6-68
3.6.5.5	Estimated Cladding Temperature for BRP Damaged Fuel	3.6-68
3.6.5.6	Estimated Cladding Temperature for BRP Fuel Rubble	3.6-69
3.6.5.7	Canister Internal Pressure for BRP Damaged Fuel	3.6-70
3.6.5.8	Thermal Summary for BRP Damaged Fuel Assemblies	3.6-70
3.6.6	Big Rock Point Partial Fuel Assemblies	3.6-71
3.6.6.1	Maximum Canister Thermal Rating for BRP Partial Fuel Assemblies.....	3.6-71
3.6.6.2	Effective Thermal Conductivity of BRP Partial Fuel Assemblies.....	3.6-71
3.6.6.3	Thermal Summary for BRP Partial Fuel Assemblies.....	3.6-71
3.6.7	Computer Code Descriptions	3.6-72
3.6.7.1	Thermal Desktop® Computer Code.....	3.6-72
3.6.7.2	SINDA/FLUINT® Computer Code	3.6-72
3.6.7.3	RadCAD® Computer Code.....	3.6-73
4.	CONTAINMENT	4-1
4.1	Description of Containment System	4.1-3
4.1.1	Containment Boundary	4.1-3

TABLE OF CONTENTS (continued)

<u>Section</u>	<u>Title</u>	<u>Page</u>
4.1.2	Codes and Standards	4.1-3
4.1.3	Special Requirements for Damaged Spent Nuclear Fuel.....	4.1-3
4.2	Containment Under Normal Conditions of Transport.....	4.2-1
4.2.1	Pressurization of Containment Vessel	4.2-1
4.2.2	Containment Criteria.....	4.2-1
4.2.3	Compliance with Containment Criteria	4.2-1
4.3	Containment Under Hypothetical Accident Conditions.....	4.3-1
4.3.1	Pressurization of Containment Vessel	4.3-1
4.3.2	Containment Criteria.....	4.3-1
4.3.3	Compliance with Containment Criteria	4.3-1
5.	SHIELDING EVALUATION	5-1
5.1	Discussion and Results.....	5.1-1
5.1.1	FuelSolutions™ TS125 Transportation Cask Shielding Design Features ...	5.1-1
5.1.2	FuelSolutions™ W74 Canister Shielding Design Features	5.1-1
5.1.3	Shielding Results.....	5.1-2
5.2	Source Specification.....	5.2-1
5.2.1	FuelSolutions™ Generic Decay Library.....	5.2-1
5.2.2	Gamma Source Terms.....	5.2-2
5.2.2.1	Active Fuel Primary Gamma Sources	5.2-2
5.2.2.2	End Fitting and Plena Region Gamma Sources	5.2-3
5.2.2.3	Secondary Gamma Sources	5.2-4
5.2.2.4	Axial Distribution of Gamma Sources	5.2-4
5.2.3	Neutron Source Terms	5.2-5
5.2.3.1	Neutron Source Strengths.....	5.2-5
5.2.3.2	Neutron Energy Spectrum	5.2-5
5.2.3.3	Axial Neutron Distribution.....	5.2-6
5.3	Model Specification	5.3-1
5.3.1	Description of Radial and Axial Shielding Configuration.....	5.3-1
5.3.1.1	Overview	5.3-1

TABLE OF CONTENTS (continued)

<u>Section</u>	<u>Title</u>	<u>Page</u>
5.3.1.2	Treatment of Voids, Streaming Paths, and Other Geometry Irregularities	5.3-1
5.3.1.3	Differences Between Normal and Accident Models	5.3-2
5.3.1.4	Dose Point Locations.....	5.3-2
5.3.1.5	TS125 Cask Body Geometry	5.3-3
5.3.1.6	W74 Canister Geometry	5.3-3
5.3.2	Shield Regional Densities	5.3-5
5.3.2.1	FuelSolutions™ W125 Transportation Cask Shield Regional Densities	5.3-5
5.3.2.2	FuelSolutions™ W74 Canister Shield Regional Densities	5.3-5
5.4	Shielding Evaluation	5.4-1
5.4.1	Methodology	5.4-1
5.4.2	Results	5.4-2
5.5	Supplemental Data	5.5-1
5.5.1	BRP Mixed-Oxide (MOX) Fuel Assembly Qualification	5.5-1
5.5.2	BRP Partial Fuel Assembly Qualification	5.5-3
5.5.3	BRP Damaged Fuel Assembly Qualification.....	5.5-3
6.	CRITICALITY EVALUATION	6-1
6.1	Discussion and Results.....	6.1-1
6.2	Package Fuel Loading	6.2-1
6.3	Model Specification	6.3-1
6.3.1	Description of Calculational Model.....	6.3-1
6.3.1.1	Hypothetical Accident Conditions	6.3-5
6.3.1.2	Normal Conditions of Transport	6.3-8
6.3.1.3	Criticality Models for MOX, Partial, and Damaged BRP Fuel....	6.3-9
6.3.2	Package Regional Densities	6.3-11
6.4	Criticality Evaluation	6.4-1
6.4.1	Calculational Method.....	6.4-1
6.4.2	Fuel Loading Optimization	6.4-1

TABLE OF CONTENTS (continued)

<u>Section</u>	<u>Title</u>	<u>Page</u>
	6.4.2.1 Package Array	6.4-1
	6.4.2.2 Single Package.....	6.4-7
	6.4.3 Criticality Results.....	6.4-8
6.5	Criticality Benchmark Experiments	6.5-1
6.6	Supplemental Analyses	6.6-1
6.6.1	Big Rock Point Mixed-Oxide Fuel Assembly Criticality Evaluation.....	6.6-1
	6.6.1.1 MOX Fuel Criticality Analyses.....	6.6-1
	6.6.1.2 MOX Fuel Criticality Benchmarks	6.6-7
6.6.2	Big Rock Point Partial Fuel Assembly Criticality Evaluation.....	6.6-11
	6.6.2.1 Partial Assemblies with Missing Corner Rods.....	6.6-11
	6.6.2.2 Partial Assemblies with Missing Array-Interior or Array-Edge Rods.....	6.6-13
6.6.3	Big Rock Point Damaged Fuel Assembly Criticality Evaluation	6.6-16
	6.6.3.1 W74 Canister Model for the Damaged Assembly Analyses	6.6-17
	6.6.3.2 Damaged Fuel Can Contents Model Description.....	6.6-18
	6.6.3.3 Damaged Assembly Criticality Analysis Results.....	6.6-20
	6.6.3.4 Damaged Fuel Can Preferential Flooding Analysis	6.6-24
	6.6.3.5 Damaged BRP MOX Assembly Analyses	6.6-25
	6.6.3.6 Other Allowable Damaged Fuel Can Contents	6.6-27
6.6.4	The W74 Canister Inside the TS125 Transportation Cask	6.6-28
7.	OPERATING PROCEDURES	7-1
7.1	Procedures for Loading the Cask in the Spent Fuel Pool.....	7.1-1
	7.1.1 Preparation of an Empty Canister for Fuel Loading.....	7.1-1
	7.1.2 Installing an Empty Canister into the Transportation Cask.....	7.1-1
	7.1.3 Load Fuel into the Canister.....	7.1-1
	7.1.4 Drain and Backfill Canister with Helium	7.1-2
7.2	Procedures for Unloading Package	7.2-1
7.3	Preparation of Empty Package for Transport.....	7.3-1
7.4	Appendix	7.4-1

TABLE OF CONTENTS (continued)

<u>Section</u>	<u>Title</u>	<u>Page</u>
8.	ACCEPTANCE TESTS AND MAINTENANCE PROGRAM.....	8-1

LIST OF TABLES

<u>Tables</u>	<u>Title</u>	<u>Page</u>
Table 1.0-1	- FuelSolutions™ Transportation SAR Regulatory Compliance Cross-Reference Matrix (13 pages).....	1-8
Table 1.2-1	- Principal Characteristics of the FuelSolutions™ W74 Canister	1.2-14
Table 1.2-2	- Matrix of FuelSolutions™ W74 Canister Configurations.....	1.2-15
Table 1.2-3	- FuelSolutions™ W74 Canister Design Criteria Summary (3 pages).....	1.2-16
Table 1.2-4	- FuelSolutions™ W74 Canister SNF Assembly Acceptance Criteria for Transport (6 pages).....	1.2-19
Table 1.2-5	- FuelSolutions™ W74 Canister SNF Fuel Assembly Classes Acceptable for Transport.....	1.2-25
Table 1.2-6	- FuelSolutions™ W74 Canister UO ₂ SNF Fuel Assemblies Acceptable for Transport ⁽¹⁾	1.2-26
Table 1.2-7	- FuelSolutions™ W74 Canister MOX SNF Assemblies Acceptable for Transport ⁽¹⁾	1.2-27
Table 2.1-1	- FuelSolutions™ W74 Canister Minimum Design Margins for NCT Loading Conditions.....	2.1-9
Table 2.1-2	- FuelSolutions™ W74 Canister Minimum Design Margins for HAC Loading Conditions.....	2.1-10
Table 2.1-3	- Summary of FuelSolutions™ W74 Canister Component Functions and Design Codes	2.1-11
Table 2.1-4	- Canister Shell Allowable Stress Criteria	2.1-12
Table 2.1-5	- Canister Basket Allowable Stress Criteria	2.1-12
Table 2.1-6	- Summary of NCT Load Combinations	2.1-13
Table 2.1-7	- Summary of HAC Load Combinations	2.1-13
Table 2.2-1	- W74 Canister Weights and Centers of Gravity	2.2-1
Table 2.3-1	- FuelSolutions™ W74M Canister Materials Summary.....	2.3-3
Table 2.3-2	- FuelSolutions™ W74T Canister Material Summary	2.3-4
Table 2.3-3	- Type 316 Stainless Steel Material Properties.....	2.3-5
Table 2.3-4	- Type 316 Stainless Steel Plastic Material Properties	2.3-5
Table 2.3-5	- Type 304 Stainless Steel Material Properties.....	2.3-6
Table 2.3-6	- Type XM-19 Stainless Steel Material Properties	2.3-7
Table 2.3-7	- ASTM A36 Carbon Steel Material Properties	2.3-8
Table 2.3-8	- A514, Grades F or P Carbon Steel Material Properties	2.3-9
Table 2.3-9	- SA-517, Grade F or P Carbon Steel Material Properties	2.3-10
Table 2.3-10	- Neutron Absorber Material Properties	2.3-11
Table 2.3-11	- A516, Grades 55 and 60 Carbon Steel Material Properties	2.3-12
Table 2.6-1	- Summary of W74 Canister Temperatures	2.6-21
Table 2.6-2	- W74 General Spacer Plate Stress Intensities (20 Highest Values) - NCT Cold Environment Thermal Loading.....	2.6-22
Table 2.6-3	- W74 LTP Spacer Plate Stress Intensities (20 Highest Values) - NCT Cold Environment Thermal Loading.....	2.6-23
Table 2.6-4	- Summary of W74 NCT Thermal Stress Design Margins.....	2.6-24
Table 2.6-5	- Summary of W74 Canister NCT Vibration Design Margins	2.6-40
Table 2.6-6	- W74 Guide Tube Longitudinal Seam Weld Stresses due to NCT Vibration Loading (Horizontal Panel)	2.6-41
Table 2.6-7	- W74 Guide Tube Longitudinal Seam Weld Stresses due to NCT Vibration Loading (Vertical Panel).....	2.6-42

LIST OF TABLES (continued)

<u>Table</u>	<u>Title</u>	<u>Page</u>
Table 2.6-8	- Summary of W74 Canister NCT Free Drop Design Margins	2.6-62
Table 2.6-9	- W74 General Spacer Plate Allowable Buckling Stresses for NCT Conditions	2.6-63
Table 2.6-10	- W74 LTP Spacer Plate Allowable Buckling Stresses for NCT Conditions	2.6-64
Table 2.6-11	- W74 Spacer Plate NCT Side Drop Ligament Stresses and Buckling Interaction Ratios	2.6-65
Table 2.7-1	- Summary of W74 Canister Basket Assembly HAC End Drop Design Margins.....	2.7-20
Table 2.7-2	- W74 Canister Shell HAC End Drop Stress Analysis Results	2.7-21
Table 2.7-3	- W74 Spacer Plate 60g Side Drop Elastic Stress Analysis Results.....	2.7-33
Table 2.7-4	- Summary of W74 Canister Basket Assembly HAC Side Drop Design Margins.....	2.7-34
Table 2.7-5	- Summary of W74 Canister HAC Corner Drop Design Margins.....	2.7-44
Table 2.7-6	- W74 Canister General and LTP Spacer Plate Maximum Stress Intensities for 36g Transverse Loading.....	2.7-73
Table 2.7-7	- W74 Canister General and LTP Spacer Plate Maximum Stresses for HAC Oblique Drop Secondary Impact	2.7-73
Table 2.7-8	- W74 General Spacer Plate Allowable Buckling Stresses.....	2.7-74
Table 2.7-9	- W74 LTP Spacer Plate Allowable Buckling Stresses.....	2.7-75
Table 2.7-10	- W74 General Spacer Plate Buckling Interaction Ratios for HAC Slapdown Impact Loading without Thermal	2.7-76
Table 2.7-11	- W74 General Spacer Plate Buckling Interaction Ratios for Combined HAC Slapdown Impact and NCT Thermal Loading.....	2.7-77
Table 2.7-12	- W74 LTP Spacer Plate Buckling Interaction Ratios for HAC Slapdown Impact Loading without Thermal	2.7-78
Table 2.7-13	- W74 LTP Spacer Plate Buckling Interaction Ratios for Combined HAC Slapdown Impact and NCT Thermal Loading	2.7-79
Table 2.7-14	- Guide Tube Neutron Absorber Sheet Retainer Weld Shear Stresses – HAC Oblique Drop Slapdown Impact	2.7-80
Table 2.7-15	- W74 Canister Shell Assembly HAC Oblique Drop Slapdown Impact Stress Analysis Results.....	2.7-81
Table 2.7-16	- Summary of W74 Canister HAC Oblique Drop Design Margins.....	2.7-82
Table 2.12-1	- W74M Spacer Plate Tributary Weights – Uniform Fuel Loading	2.12-4
Table 2.12-2	- W74T Spacer Plate Tributary Weights – Uniform Fuel Loading	2.12-5
Table 2.12-3	- BRP Fuel Grid Spacer Positions and Tributary Weights	2.12-6
Table 2.12-4	- W74M Spacer Plate Tributary Weights – Concentrated Fuel Loading.....	2.12-7
Table 2.12-5	- W74T Spacer Plate Tributary Weights – Concentrated Fuel Loading.....	2.12-8
Table 2.12-6	- W74 Canister Equivalent Static Free Drop G-Loads	2.12-14
Table 3.1-1	- Transportation Design Basis Thermal Conditions	3.1-13
Table 3.1-2	- W74 Canister Design-Basis Axial Heat Profile	3.1-14
Table 3.1-3	- W74 Canister Maximum Thermal Ratings for Transportation	3.1-15
Table 3.1-4	- W74 Canister Thermal Ratings vs. SNF Burnup	3.1-15
Table 3.1-5	- Transportation Cask Internal Pressures with Loaded W74 Canister.....	3.1-16
Table 3.2-1	- W74 Canister Homogenous Material Properties (2 pages)	3.2-22
Table 3.2-2	- W74 Canister Surface Emissivities	3.2-24
Table 3.2-3	- W74 Canister Material Properties, Fluids	3.2-25
Table 3.3-1	- W74 Canister Component Allowable Temperatures.....	3.3-5
Table 3.4-1	- FuelSolutions™ W74 Canister Maximum System Temperatures for NCT	3.4-20
Table 3.4-2	- Transportation Package NCT Internal Pressures.....	3.4-21

LIST OF TABLES (continued)

<u>Table</u>	<u>Title</u>	<u>Page</u>
Table 3.4-3	- W74 Canister SNF Gas	3.4-22
Table 3.4-4	- W74 Canister Free Volume and MNOP ⁽¹⁾	3.4-23
Table 3.5-1	- W74/TS125 System Temperature For HAC Fire	3.5-50
Table 3.5-2	- W74 Canister and Transportation Cask Internal Pressures for HAC Fire Event	3.5-51
Table 3.6-1	- FuelSolutions™ W74 Canister Maximum System Temperatures With and Without Fission Gas Release	3.6-74
Table 3.6-2	- W74 Damaged Fuel Effective Conductivity	3.6-75
Table 5.1-1	- Summary of W125/W74 Maximum Dose Rates	5.1-3
Table 5.1-2	- W74 Canister Shielding Design Features	5.1-4
Table 5.2-1	- BWR Source Term Calculation Input Parameters	5.2-8
Table 5.2-2	- W74 UO ₂ Fuel Gamma Sources	5.2-9
Table 5.2-3	- W74 Assembly Hardware Gamma Source Strengths	5.2-10
Table 5.2-4	- BWR Fuel Axial Gamma Profiles	5.2-11
Table 5.2-5	- W74 Normalized Neutron Source Spectrum	5.2-12
Table 5.2-6	- W74 Axial Neutron Source Profiles	5.2-13
Table 5.3-1	- Roadmap to W74 Shielding Models	5.3-7
Table 5.3-2	- W74 Canister Component Dimensions	5.3-8
Table 5.3-3	- Canister Interior Source Zone Dimensions (in.)	5.3-9
Table 5.3-4	- Raw Material Atom Densities	5.3-10
Table 5.3-5	- W74 Active Fuel Region Densities	5.3-11
Table 5.3-6	- W74 Plenum Region Densities	5.3-12
Table 5.3-7	- W74 Bottom End Densities	5.3-13
Table 5.3-8	- W74 Top End Densities	5.3-14
Table 5.3-9	- W74 “Center” Region Densities ⁽¹⁾	5.3-15
Table 5.4-1	- W74 Normal Condition Results (3 pages)	5.4-4
Table 5.4-2	- W74 Accident Condition Results	5.4-7
Table 5.5-1	- ORIGEN 2.1 Data for BRP MOX Fuel Assemblies	5.5-5
Table 5.5-2	- BRP MOX Fuel Gamma Source Strengths	5.5-6
Table 5.5-3	- BRP MOX Fuel Gamma Source Strength Comparison	5.5-7
Table 5.5-4	- BRP MOX Assembly Total Neutron Source Strengths	5.5-8
Table 5.5-5	- W74 MOX Fuel Normal Condition Results (3 pages)	5.5-9
Table 5.5-6	- W74 MOX Fuel Accident Condition Results	5.5-12
Table 6.1-1	- W74 Canister Fuel Specification for Big Rock Point	6.1-3
Table 6.2-1	- Specific Fuel Assembly Parameters	6.2-3
Table 6.3-1	- Worst-Case Material and Fabrication Tolerances for the FuelSolutions™ W74 Canister	6.3-13
Table 6.3-2	- W74 Basket Model Differences Between Intact, Partial, MOX, and Damaged BRP Assembly Criticality Analyses	6.3-14
Table 6.3-3	- UO ₂ Number Densities as a Function of Enrichment	6.3-15
Table 6.3-4	- Water Number Densities as a Function of Density	6.3-16
Table 6.3-5	- Zircaloy-4 Number Densities	6.3-17
Table 6.3-6	- 304 Stainless Steel Number Densities	6.3-17
Table 6.3-7	- Borated Stainless Steel Number Densities (1.0 w/o natural boron)	6.3-18
Table 6.3-8	- Borated Stainless Steel Number Densities (1.25 w/o natural boron)	6.3-18
Table 6.3-9	- 316 Stainless Steel Number Densities	6.3-19

LIST OF TABLES (continued)

<u>Table</u>	<u>Title</u>	<u>Page</u>
Table 6.3-10	- 517 P Carbon Steel Number Densities	6.3-19
Table 6.3-11	- XM-19 Stainless Steel Number Densities	6.3-20
Table 6.3-12	- Depleted Uranium Number Densities	6.3-20
Table 6.3-13	- Solid Neutron Shield Number Densities	6.3-21
Table 6.4-1	- MCNP Results for the Canister Design Case Studies	6.4-10
Table 6.4-2	- Material and Fabrication Tolerance Results for the FuelSolutions™ W74 Canister	6.4-11
Table 6.4-3	- Optimum Interspersed Moderator Case Results for the FuelSolutions™ W74 Canister	6.4-12
Table 6.4-4	- Optimum Interior Moderator Case Results for the FuelSolutions™ W74 Canister	6.4-13
Table 6.4-5	- MCNP Results for the FuelSolutions™ W74 Canister and Big Rock Point Fuel Assemblies with Variable Fuel Rod Enrichments	6.4-14
Table 6.4-6	- MCNP Results for the FuelSolutions™ W74 Canister and Big Rock Point Fuel Assemblies with Lattice Average Fuel Rod Enrichments.....	6.4-15
Table 6.4-7	- Multiple-Package Array, Hypothetical Accident Condition Results to Determine the Bounding Fuel Assembly Configuration (4.1% Enriched Fuel)	6.4-16
Table 6.4-8	- Big Rock Point Fuel Assembly USL Value Ranges	6.4-16
Table 6.4-9	- Multiple-Package Array, Normal Operating Condition Results	6.4-17
Table 6.4-10	- MCNP Results for the Single-Package Models	6.4-17
Table 6.5-1	- Benchmark Critical Experiments (2 Pages)	6.5-3
Table 6.6-1	- Uranium Isotope Atom Densities for UO ₂ Fuel Rods in BRP MOX Assemblies.....	6.6-32
Table 6.6-2	- BRP Assembly MOX Fuel Pin Isotope Densities (atom/barn-cm)	6.6-33
Table 6.6-3	- MCNP Calculated K _{eff} Values for W74 Baskets Fully Loaded with BRP MOX Fuel (Full Water Density).....	6.6-34
Table 6.6-4	- MCNP Calculated K _{eff} for MOX Fuel vs. W74 Interior Water Density (G-Pu Fuel Assemblies).....	6.6-35
Table 6.6-5	- W74 Canister MOX Fuel Specifications.....	6.6-36
Table 6.6-6	- MOX Fuel Benchmark Critical Experiments.....	6.6-38
Table 6.6-7	- Upper Sub-Critical Limit Formulas for the MOX Only, UO ₂ Only, and MOX + UO ₂ Sets of Critical Experiments	6.6-39
Table 6.6-8	- Parameter Ranges Covered by Critical Experiments and BRP MOX Fuel Assemblies.....	6.6-40
Table 6.6-9	- Calculated K _{eff} Values for BRP Assemblies with Missing Array Corner Rods.....	6.6-41
Table 6.6-10	- Calculated K _{eff} vs. Fuel Rod Pitch for 4.1% Enriched GE 9x9 BRP Assembly Fuel Rods (Single Assembly with Full Water Reflection)	6.6-41
Table 6.6-11	- Calculated K _{eff} vs. Fuel Rod Pitch for 4.1% Enriched Siemens 11x11 BRP Assembly Fuel Rods (Single Assembly with Full Water Reflection).....	6.6-42
Table 6.6-12	- Calculated K _{eff} for BRP Partial Assemblies at Maximum Allowable Enrichment (Optimum Pitch ⁽¹⁾ Fuel Rod Arrays Inside the W74 Canister).....	6.6-42
Table 6.6-13	- Physical Parameters and USL Values for the Optimum BRP Fuel Rod Arrays	6.6-43
Table 6.6-14	- Calculated K _{eff} Values for a W74 Canister w/ Eight Damaged Fuel Cans Containing a Square Array of 0.471-inch Diameter Fuel Cylinders (Guide Tubes Contain Partial 9x9 BRP Assembly Configurations).....	6.6-43

LIST OF TABLES (continued)

<u>Table</u>	<u>Title</u>	<u>Page</u>
Table 6.6-15	- Calculated K_{eff} Values for a W74 Canister w/ Eight Damaged Fuel Cans Containing a Square Array of 0.3715-inch Diameter Fuel Cylinders (Guide Tubes Contain Partial 9x9 BRP Assembly Configurations).....	6.6-44
Table 6.6-16	- Calculated K_{eff} Values for a W74 Canister w/ Eight Damaged Fuel Cans Containing a Hexagonal Array of 0.471-inch Diameter Fuel Cylinders (Guide Tubes Contain Partial 9x9 BRP Assembly Configurations).....	6.6-44
Table 6.6-17	- Calculated K_{eff} Values for a W74 Canister w/ Eight Damaged Fuel Cans Containing a Hexagonal Array of 0.3715-inch Diameter Fuel Cylinders (Guide Tubes Contain Partial 9x9 BRP Assembly Configurations).....	6.6-45
Table 6.6-18	- Calculated K_{eff} Values for a W74 Canister w/ Eight Damaged Fuel Cans Containing a Hexagonal Array of 0.9 cm Diameter Fuel Spheres (Guide Tubes Contain Partial 9x9 BRP Assembly Configurations).....	6.6-45
Table 6.6-19	- Calculated K_{eff} Values for a W74 Canister w/ Eight Damaged Fuel Cans Containing a Square Array of 0.3715-inch Diameter Fuel Cylinders (Guide Tubes Contain Intact 11x11 BRP Assembly Configurations).....	6.6-46
Table 6.6-20	- W74 Damaged Assembly 10CFR71 Criticality Margin Calculation (0.655-inch Pitch Square Array of 0.3715-inch Diameter Fuel Cylinders in All Damaged Fuel Cans).....	6.6-46
Table 6.6-21	- H-to- ²³⁵ U Ratio vs. Array Dimension for Various UO ₂ Fuel Rod Diameters and MOX Fuel Rod Material Compositions ⁽¹⁾	6.6-47
Table 6.6-22	- Final k_{eff} vs. Fuel Cylinder Diameter and H-to- ²³⁵ U Ratio ⁽¹⁾	6.6-48
Table 6.6-23	- Final k_{eff} vs. H-to- ²³⁵ U Ratio for Various Fuel Sphere Diameters.....	6.6-49
Table 6.6-24	- Final k_{eff} vs. Particle Diameter for UO ₂ Fuel Cylinders and Spheres (at optimum H-to- ²³⁵ U ratio).....	6.6-49
Table 6.6-25	- Transportation Cask Comparison Case Results for the FuelSolutions™ W74 Canister.....	6.6-50
Table 6.6-26	- MCNP Results for the TS125 Cask Single-Package Models.....	6.6-51
Table 7.1-1	- Helium Backfill Gas Quantities for the FuelSolutions™ W74 Canister.....	7.1-3

This page intentionally left blank.

LIST OF FIGURES

<u>Figures</u>	<u>Title</u>	<u>Page</u>
Figure 1.0-1	- FuelSolutions™ Spent Fuel Management System Elements.....	1-6
Figure 1.0-2	- FuelSolutions™ Transportation Package Certification Application Approach.....	1-7
Figure 1.2-1	- FuelSolutions™ Spent Fuel Management System.....	1.2-28
Figure 1.2-2	- Expanded View of FuelSolutions™ W74 Canister	1.2-29
Figure 2.1-1	- FuelSolutions™ W74 Canister Support Tube Assembly Detail.....	2.1-14
Figure 2.1-2	- FuelSolutions™ W74 Damaged Fuel Can.....	2.1-15
Figure 2.2-1	- FuelSolutions™ W74 Canister Center of Gravity Diagram	2.2-3
Figure 2.6-1	- W74 Canister Support Tube and End Spacer Plate Curvature Due to Lateral Thermal Gradients	2.6-25
Figure 2.6-2	- W74 General Spacer Plate NCT Cold Environment Thermal Gradient	2.6-26
Figure 2.6-3	- W74 LTP Spacer Plate NCT Cold Environment Thermal Gradient.....	2.6-27
Figure 2.6-4	- W74 Canister Engagement Spacer Plate NCT Cold Environment Thermal Gradient	2.6-28
Figure 2.6-5	- W74 Guide Tube NCT Vibration S.I. Contour Plot (Middle Fiber).....	2.6-43
Figure 2.6-6	- W74 Guide Tube NCT Vibration S.I. Contour Plot (Top Fiber).....	2.6-44
Figure 2.6-7	- W74 Guide Tube NCT Vibration S.I. Contour Plot (Bottom Fiber)	2.6-45
Figure 2.6-8	- W74 Spacer Plate NCT Free Drop Loading Diagram	2.6-66
Figure 2.6-9	- W74 Guide Tube S.I. Contour Plot (Middle Fiber) - 15g NCT Side Drop, Uniform Fuel Loading	2.6-67
Figure 2.6-10	- W74 Guide Tube S.I. Contour Plot (Top Fiber) - 15g NCT Side Drop, Uniform Fuel Loading	2.6-68
Figure 2.6-11	- W74 Guide Tube S.I. Contour Plot (Bottom Fiber) - 15g NCT Side Drop, Uniform Fuel Loading	2.6-69
Figure 2.7-1	- W74 Canister Guide Tube HAC End Drop Buckling Evaluation Boundary Conditions.....	2.7-22
Figure 2.7-2	- W74 Canister General and LTP Spacer Plate HAC Side Drop Impact Orientations Evaluated.....	2.7-35
Figure 2.7-3	- W74 Canister Engagement Spacer Plate HAC Side Drop Impact Orientations Evaluated	2.7-36
Figure 2.7-4	- W74 Guide Tube S.I. Contour Plot (Middle Fiber) - 62g Slapdown, Uniform SNF Loading, Elastic Analysis.....	2.7-83
Figure 2.7-5	- W74 Guide Tube S.I. Contour Plot (Top Fiber) - 62g Slapdown, Uniform SNF Loading, Elastic Analysis	2.7-84
Figure 2.7-6	- W74 Guide Tube S.I. Contour Plot (Bottom Fiber) - 62g Slapdown, Uniform SNF Loading, Elastic Analysis.....	2.7-85
Figure 2.7-7	- W74 Guide Tube S.I. Contour Plot (Middle Fiber) - 64.5g Slapdown Load, Concentrated SNF Loading, Plastic Analysis.....	2.7-86
Figure 2.7-8	- W74 Guide Tube S.I. Contour Plot (Top Fiber) - 64.5g Slapdown Load, Concentrated SNF Loading, Plastic Analysis.....	2.7-87
Figure 2.7-9	- W74 Guide Tube S.I. Contour Plot (Bottom Fiber) - 64.5g Slapdown Load, Concentrated SNF Loading, Plastic Analysis.....	2.7-88
Figure 2.7-10	- W74 Guide Tube Permanent Deformation Resulting from HAC Slapdown Impact Loading	2.7-89
Figure 2.7-11	- Canister Shell Stress Intensity Contour Plot for 87g HAC Slapdown Load.....	2.7-90
Figure 2.12-1	- W74 Canister General and LTP Spacer Plate Stress Evaluation Points	2.12-16

LIST OF FIGURES (continued)

<u>Figure</u>	<u>Title</u>	<u>Page</u>
Figure 2.12-2	- W74 Canister General and LTP Spacer Plate Plane-Stress Finite Element Model.....	2.12-34
Figure 2.12-3	- W74 Canister General and LTP Spacer Plate Loading Diagram.....	2.12-35
Figure 2.12-4	- W74 General Spacer Plate Full Multi-Span Finite Element Model.....	2.12-36
Figure 2.12-5	- W74 General Spacer Plate Buckling Shell Finite Element Model.....	2.12-37
Figure 2.12-6	- W74 Canister Engagement Spacer Plate Half-Symmetry Plane-Stress Finite Element Model.....	2.12-38
Figure 2.12-7	- W74 Canister Engagement Spacer Plate Full Plane-Stress Finite Element Model.....	2.12-39
Figure 2.12-8	- W74 Canister Engagement Spacer Plate Solid Quarter-Symmetry Modal Analysis Model.....	2.12-40
Figure 2.12-9	- W74 Canister Engagement Spacer Plate HAC End Drop Modal Analysis Mass Distribution.....	2.12-41
Figure 2.12-10	- W74 Canister Engagement Spacer Plate HAC End Drop Solid Quarter-Symmetry Model Boundary Conditions.....	2.12-42
Figure 2.12-11	- W74 Canister Engagement Spacer Plate HAC End Drop Solid Quarter-Symmetry Model Pressure Loading.....	2.12-43
Figure 2.12-12	- W74 Canister Guide Tube Finite Element Model.....	2.12-44
Figure 2.12-13	- W74 Canister Top Shield Plug Quarter Symmetry Model.....	2.12-45
Figure 2.12-14	- W74 Canister Top Shield Plug Quarter Symmetry Model Adjusted Density Regions.....	2.12-46
Figure 2.12-15	- Bounding Canister Shell Assembly Axisymmetric Finite Element Model.....	2.12-47
Figure 2.12-16	- Canister Shell Half-Symmetry Finite Element Model.....	2.12-48
Figure 2.12-17	- Canister Shell Assembly Half-Symmetry Finite Element Model, Shell Assembly Mesh.....	2.12-49
Figure 2.12-18	- Canister Shell Assembly Half-Symmetry Finite Element Model - Spacer Plate Mesh and Loading.....	2.12-50
Figure 2.12—19	- Canister Shell Axisymmetric Model Stress Evaluation Locations - Top and Bottom End Regions.....	2.12-52
Figure 2.12—20	- Canister Shell Axisymmetric Model Stress Evaluation Locations - Cavity Region.....	2.12-53
Figure 3.1-1	- Design Basis Axial Heat Profile for W74 Canister Analysis.....	3.1-17
Figure 3.1-2	- Max. Peaking Factor vs. Burnup for BWR Fuel.....	3.1-17
Figure 3.4-1	- FuelSolutions™ W74M Canister Thermal Submodel Layout.....	3.4-24
Figure 3.4-2	- Node Layout for W74 Canister Bottom End.....	3.4-25
Figure 3.4-3	- Typical Node Layout Between W74 Spacer Plates.....	3.4-26
Figure 3.4-4	- Node Layout for W74 Canister Fuel Load Configuration.....	3.4-27
Figure 3.4-5	- Typical Node Layout for W74 Spacer Plate.....	3.4-28
Figure 3.4-6	- Isometric View of Node Layout Between Typical Set of W74 Spacer Plates.....	3.4-29
Figure 3.4-7	- Node Layout for W74 Canister Mid-Length Section.....	3.4-30
Figure 3.4-8	- Node Layout for W74 Top End.....	3.4-31
Figure 3.4-9	- Assumed Flow Pattern within Horizontal Canister.....	3.4-32
Figure 3.4-10	- Sensitivity of W74 Canister and TS125 Transportation Cask Components to Heat Load.....	3.4-33
Figure 3.4-11	- W74/TS125 Axial Temperature Distribution; NCT Hot (100°F), 180° Rotation From Bottom.....	3.4-34

LIST OF FIGURES (continued)

<u>Figure</u>	<u>Title</u>	<u>Page</u>
Figure 3.4-12	- W74/TS125 Cask Axial Temperature Distribution; NCT Hot (100°F), 15° Rotation From Bottom	3.4-35
Figure 3.4-13	- W74/TS125 Cask Radial Temperature Distribution; NCT Hot (100°F), 15° Rotation From Bottom	3.4-36
Figure 3.4-14	- W74/TS125 Cask Axial Temperature Distribution; NCT Cold (-20°F), 15° Rotation From Bottom	3.4-37
Figure 3.4-15	- W74/TS125 Cask Radial Temperature Distribution; NCT Cold (-20°F), 15° Rotation From Bottom	3.4-38
Figure 3.4-16	- Hottest W74 Stainless Steel Spacer Plate Temperature Distribution, NCT Hot (100°F).....	3.4-39
Figure 3.4-17	- Hottest W74 Carbon Steel Spacer Plate Temperature Distribution, NCT Hot (100°F).....	3.4-40
Figure 3.4-18	- W74 Engagement Plate Temperature Distribution, NCT Hot (100°F).....	3.4-41
Figure 3.4-19	- Hottest W74 Stainless Steel Spacer Plate Temperature Distribution, NCT Cold (-20°F).....	3.4-42
Figure 3.4-20	- Hottest W74 Carbon Steel Spacer Plate Temperature Distribution, NCT Cold (-20°F).....	3.4-43
Figure 3.4-21	- W74 Engagement Plate Temperature Distribution, NCT Cold (-20°F).....	3.4-44
Figure 3.5-1	- HAC Fire Transient, FuelSolutions™ W74 Canister, Hot Initial Conditions	3.5-52
Figure 3.5-2	- HAC Fire Transient, FuelSolutions™ W74 Canister, Cold Initial Conditions.....	3.5-53
Figure 3.6-1	- Gas Node and Flow Pattern in a Horizontal Canister	3.6-76
Figure 3.6-2	- Circulation Pattern within NUHOMS® 24 Unit DSC	3.6-77
Figure 3.6-3	- Temperature Distribution in NUHOMS® 24 Unit Basket.....	3.6-78
Figure 3.6-4	- Double Open-Ended Cavity with Two Heated Walls	3.6-78
Figure 3.6-5	- Gas Mixture Thermal Conductivity vs. Fission Gas Mole Fraction	3.6-79
Figure 3.6-6	- Change in Buoyancy Forces Due to Addition of Fission Gases To Helium Backfill Gases	3.6-79
Figure 3.6-7	- Combined Effect on Convection Heat Transfer Due to Addition of Fission Gases.....	3.6-80
Figure 3.6-8	- Effect of Reconfigured, Damaged Fuel on W74 Canister Temperatures Within W150 Transfer Cask	3.6-81
Figure 4.1-1	- W74 Damaged Fuel Can	4.1-5
Figure 5.3-1	- Normal Condition Detector Locations.....	5.3-16
Figure 5.3-2	- Accident Condition Detector Locations.....	5.3-17
Figure 5.3-3	- W74 Side R-Z Gamma Model (normal conditions).....	5.3-18
Figure 5.3-4	- W74 Neutron R-Z Model (normal conditions)	5.3-19
Figure 5.3-5	- W74 Gamma and Neutron R-Z Model (accident conditions).....	5.3-20
Figure 5.3-6	- W74 Bottom End Gamma Model (normal and accident conditions).....	5.3-21
Figure 5.3-7	- W74 Top End Gamma Model (normal and accident conditions)	5.3-22
Figure 6.3-1	- FuelSolutions™ W74 Basket (Nominal Dimensions)	6.3-22
Figure 6.3-2	- FuelSolutions™ W74 Type A Guide Tube Assembly (Nominal Dimensions)	6.3-23
Figure 6.3-3	- FuelSolutions™ W74 Type B Guide Tube Assembly (Nominal Dimensions)	6.3-24
Figure 6.3-4	- FuelSolutions™ W74 Shell Assembly and Representative Transportation Cask.....	6.3-25
Figure 6.3-5	- FuelSolutions™ W74 Shell Assembly and TS125 Transportation Cask.....	6.3-26
Figure 6.3-6	- Horizontal Cross-Section of MCNP Model.....	6.3-27
Figure 6.3-7	- Side View of Lower Portion of FuelSolutions™ W74 HAC Model (cut-away).....	6.3-28

LIST OF FIGURES (continued)

<u>Figure</u>	<u>Title</u>	<u>Page</u>
Figure 6.3-8	- Side View of Middle Portion of the FuelSolutions™ W74 HAC Model (cut-away).....	6.3-29
Figure 6.3-9	- Side View of Upper Portion of the FuelSolutions™ W74 HAC Model (cut-away).....	6.3-30
Figure 6.3-10	- FuelSolutions™ W74 Fuel Pattern No. 1 Basket Configuration	6.3-31
Figure 6.3-11	- FuelSolutions™ W74 Pattern No. 2 Basket Configuration	6.3-32
Figure 6.3-12	- FuelSolutions™ W74 Pattern No. 3 Basket Configuration	6.3-33
Figure 6.3-13	- W74 Canister Post-Drop Guide Tube Deformation.....	6.3-34
Figure 6.3-14	- Side View of Lower Portion of FuelSolutions™ W74 NCT Model (cut-away)	6.3-35
Figure 6.3-15	- Side View of Middle Portion of FuelSolutions™ W74 NCT Model (cut-away).....	6.3-36
Figure 6.3-16	- Side View of Upper Portion of the FuelSolutions™ W74 NCT Model (cut-away).....	6.3-37
Figure 6.3-17	- FuelSolutions™ W74 Basket Model for MOX and Damaged Assembly Analyses (Nominal Dimensions)	6.3-38
Figure 6.3-18	- W74 Damaged Fuel Can Configuration	6.3-39
Figure 6.4-1	- Multiple Pin Enrichment Pattern 1 for the Big Rock Point GE 9x9 Fuel	6.4-18
Figure 6.4-2	- Multiple Pin Enrichment Pattern 2 for the Big Rock Point GE 9x9 Fuel Assembly.	6.4-19
Figure 6.4-3	- Multiple Pin Enrichment Pattern 3 for the Big Rock Point GE 9x9 Fuel Assembly	6.4-20
Figure 6.4-4	- Multiple Pin Enrichment Pattern 4 for the Big Rock Point Siemens 9x9 Fuel Assembly	6.4-21
Figure 6.4-5	- Multiple Pin Enrichment Pattern 1 for the Big Rock Point Siemens 11x11 Fuel Assembly	6.4-22
Figure 6.4-6	- Multiple Pin Enrichment Pattern 2 for the Big Rock Point Siemens 11x11 Fuel Assembly	6.4-23
Figure 6.4-7	- Multiple Pin Enrichment Pattern 3 for the Big Rock Point Siemens 11x11 Fuel Assembly	6.4-24
Figure 6.4-8	- Multiple Pin Enrichment Pattern 4 for the Big Rock Point Siemens 11x11 Fuel Assembly	6.4-25
Figure 6.6-1	- J2 (9x9) BRP MOX Assembly Array	6.6-52
Figure 6.6-2	- DA (11x11) BRP MOX Assembly Array	6.6-53
Figure 6.6-3	- G-Pu (11x11) BRP MOX Assembly Array	6.6-54
Figure 6.6-4	- UO ₂ 9x9 BRP Assembly with Two Inserted MOX Rods	6.6-55
Figure 6.6-5	- D72 Partial Assembly Array - J2 Assembly Type.....	6.6-56
Figure 6.6-6	- D73 Partial Assembly Array - J2 Assembly Type.....	6.6-57
Figure 6.6-7	- G01 Partial Assembly Array - G-Pu Assembly Type.....	6.6-58
Figure 6.6-8	- G02 Partial Assembly Array - G-Pu Assembly Type.....	6.6-59
Figure 6.6-9	- K _{eff} vs. H-to- ²³⁵ U Ratio for GE 9x9 BRP Fuel Rod Arrays (Single Assembly Sized Fuel Rod Array with Full Water Reflection)	6.6-60
Figure 6.6-10	- K _{eff} vs. H-to- ²³⁵ U Ratio for Siemens 11x11 BRP Fuel Rod Arrays (Single Assembly Sized Fuel Rod Array with Full Water Reflection)	6.6-61
Figure 6.6-11	- K _{eff} vs. H / ²³⁵ U Ratio for a Square Array of 0.471-inch Diameter Fuel Cylinders.....	6.6-62
Figure 6.6-12	- K _{eff} vs. H / ²³⁵ U Ratio for a Square Array of 0.3715-inch Diameter Fuel Cylinders.....	6.6-63

LIST OF FIGURES (continued)

<u>Figure</u>	<u>Title</u>	<u>Page</u>
Figure 6.6-13	- K_{eff} vs. H / ^{235}U Ratio for a Hexagonal Array of 0.471-inch Diameter Fuel Cylinders.....	6.6-64
Figure 6.6-14	- K_{eff} vs. H / ^{235}U Ratio for a Hexagonal Array of 0.3715-inch Diameter Fuel Cylinders.....	6.6-65
Figure 6.6-15	- K_{eff} vs. H / ^{235}U Ratio for a Hexagonal Array of 0.9 cm Diameter Fuel Spheres.....	6.6-66
Figure 6.6-16	- W74 Canister k_{eff} vs. Damaged Fuel Can Interior and Canister Interior Moderator Densities.....	6.6-67

This page intentionally left blank.

1. GENERAL INFORMATION

Overview

This Safety Analysis Report (SAR) provides the technical basis for the design, fabrication, and operation of the FuelSolutions™ W74 canister related to transportation within the FuelSolutions™ TS125 Transportation Cask and serves to demonstrate compliance with the applicable requirements of 10CFR71.¹ The FuelSolutions™ W74 canister is used for both storage and transport of spent nuclear fuel (SNF) assemblies, and is the central component of the FuelSolutions™ Spent Fuel Management System (SFMS). The corresponding safety analysis of the FuelSolutions™ TS125 Transportation Cask is documented in the companion FuelSolutions™ TS125 Transportation Cask SAR.²

The FuelSolutions™ W74 canister has a capacity of up to 64 Big Rock Point Boiling Water Reactor (BWR) SNF assemblies. There are an additional ten center cell locations in the FuelSolutions™ W74 canister that are designed to remain empty. The FuelSolutions™ W74 canister is used to safely dry store SNF on-site in an Independent Spent Fuel Storage Installation (ISFSI), in accordance with the requirements of 10CFR72,³ as described in the FuelSolutions™ W74 Canister Storage Final Safety Analysis Reports (FSARs).⁴ The FuelSolutions™ W74 canister is also used to safely transport SNF assemblies off-site, in accordance with 10CFR71, as described and analyzed in the subsequent chapters of this SAR.

The FuelSolutions™ SFMS is a fully integrated, canister-based system that provides for the storage and transport of a broad range of SNF assembly classes. The components and support equipment that comprise the FuelSolutions™ SFMS are shown in Figure 1.0-1. The transportation packaging components of the FuelSolutions™ SFMS include the FuelSolutions™ W74 canister described in this SAR, and the FuelSolutions™ TS125 Transportation Cask and impact limiters described in the FuelSolutions™ TS125 Transportation Cask SAR. Taken together, these SARs are intended to demonstrate compliance with 10CFR71 for certification of the FuelSolutions™ Transportation Package in accordance with Subpart C of 10CFR71. The modular organization of the SARs for the FuelSolutions™ transportation certification application is shown schematically in Figure 1.0-2.

A FuelSolutions™ Transportation Package, comprised of the FuelSolutions™ transportation packaging and its payload, is used for off-site transport of the SNF assemblies by rail, barge, or heavy haul truck in accordance with the requirements of 10CFR71 and 49CFR173.⁵ The

¹ Title 10, Code of Federal Regulations, Part 71 (10CFR71), *Packaging and Transportation of Radioactive Material*, U.S. Nuclear Regulatory Commission, October 2004.

² WSNF-120, *FuelSolutions™ TS125 Transportation Cask Safety Analysis Report*, Docket No. 71-9276, EnergySolutions Spent Fuel Division, Inc.

³ Title 10, Code of Federal Regulations, Part 72 (10CFR72), *Licensing Requirements for the Independent Storage of Spent Nuclear Fuel and High-Level Radioactive Waste*, U.S. Nuclear Regulatory Commission, 1995.

⁴ WSNF-223, *FuelSolutions™ W74 Canister Storage Final Safety Analysis Report*, Docket No. 72-1026, BNG Fuel Solutions Corporation.

⁵ Title 49, Code of Federal Regulations, Part 173 (49CFR173), *Shippers-General Requirements for Shipments and Packagings*, U.S. Department of Transportation, October 2004.

FuelSolutions™ SFMS support equipment that interfaces with the transportation package to facilitate handling and transport operations is described in Chapter 1 of the FuelSolutions™ TS125 Transportation Cask SAR.

The FuelSolutions™ W74 canister (including the damaged fuel cans) is classified as “important to safety” in accordance with Regulatory Guide 7.10.⁶ The safety classifications of other FuelSolutions™ Transportation System components and support equipment are discussed in Chapter 1 of the FuelSolutions™ TS125 Transportation Cask SAR. The safety analysis for off-site transport conditions is provided only for the FuelSolutions™ W74 canister in this SAR. The safety analysis for the other FuelSolutions™ canisters is provided in their respective FuelSolutions™ Canister Transportation SAR. The safety analysis for the FuelSolutions™ TS125 Transportation Cask and impact limiters is provided in the FuelSolutions™ TS125 Transportation Cask SAR.

By this SAR and its companion FuelSolutions™ TS125 Transportation Cask SAR, U. S. Nuclear Regulatory Commission (NRC) approval of the FuelSolutions™ Transportation Package design is sought by EnergySolutions Spent Fuel Division (EnergySolutions SFD) in accordance with 10CFR71, Subpart C. Upon review and acceptance by the NRC, the resulting Certificate of Compliance (C of C) would include the FuelSolutions™ W74 canister, in conjunction with the reviewed and approved FuelSolutions™ TS125 Transportation Cask and impact limiters, for the off-site transport of SNF assemblies. Fabrication and operation of the certified FuelSolutions™ Transportation Package may then be implemented by the licensee (qualified cask user/operator) in accordance with the general license provisions of 10CFR71.

In addition to meeting the specific requirements of 10CFR71, the generic design basis and the corresponding safety analysis of the FuelSolutions™ transportation packaging contained in this SAR and the FuelSolutions™ TS125 Transportation Cask SAR are intended to bound the SNF assembly characteristics, design conditions, and interfaces that exist at many domestic power reactor sites in the contiguous United States. These FuelSolutions™ transportation SARs also provide the basis for component fabrication and acceptance, and the requirements for safe operation and maintenance of the FuelSolutions™ transportation packaging components that must be met by the licensee, consistent with the design basis and safety analysis documented herein.

Quality Assurance

All quality-affecting activities associated with this license application and package certification are being controlled under an NRC-approved quality assurance (QA) program meeting the requirements of 10CFR50,⁷ Appendix B; 10CFR71, Subpart H; and 10CFR72, Subpart G, as discussed in Section 1.3.1 of the FuelSolutions™ TS125 Transportation Cask SAR. The licensee’s QA program is to be used to control activities performed by the licensee (qualified cask user/operator) in accordance with 10CFR71.

⁶ Regulatory Guide 7.10, *Establishing Quality Assurance Programs for Packaging Used in the Transport of Radioactive Material*, U.S. Nuclear Regulatory Commission, June 1974.

⁷ Title 10, U.S. Code of Federal Regulations, Part 50 (10CFR50), *Domestic Licensing of Production and Utilization Facilities*, Nuclear Regulatory Commission, 1995.

Licensing Approach

BFS has elected to use a modular approach to organization of the FuelSolutions™ transportation SARs, as illustrated in Figure 1.0-2, which separates the system elements that are common to all canisters from those that are canister-specific. In addition, the generic system descriptions, design criteria, and analysis methodologies applicable to the safety evaluations performed for all system components are included in the FuelSolutions™ TS125 Transportation Cask SAR, to the maximum extent possible. Similarly, the generic operating procedures and maintenance requirements applicable to all system components are included in the FuelSolutions™ TS125 Transportation Cask SAR. Chapters 1 through 8 of this FuelSolutions™ W74 Canister Transportation SAR contain the following information:

1. A description of the FuelSolutions™ W74 canister. Delineation of the acceptable canister contents.
2. The structural design and analysis of the FuelSolutions™ W74 canister for all loading conditions.
3. The thermal design and analysis of the FuelSolutions™ W74 canister and its contents for all design conditions.
4. Reference to the transportation containment boundary analysis contained in the FuelSolutions™ TS125 Transportation Cask SAR.
5. The package shielding design and analysis for the FuelSolutions™ W74 canister and the resulting package dose rates, including tabulation of the acceptable cooling times for the SNF assemblies qualified to be loaded into the FuelSolutions™ W74 canister.
6. The criticality safety analysis for the FuelSolutions™ W74 canister and tabulation of the maximum acceptable initial enrichment for each SNF assembly class qualified to be loaded into the canister.
7. Reference to the generic FuelSolutions™ Transportation System operating procedures contained in the FuelSolutions™ TS125 Transportation Cask SAR.
8. Reference to the acceptance criteria and maintenance requirements contained in the FuelSolutions™ W74 Canister Storage FSAR.

Chapters 1 through 8 of the FuelSolutions™ TS125 Transportation Cask SAR contain the following information:

1. Identification of all FuelSolutions™ Transportation System components and support equipment. A description of the FuelSolutions™ TS125 Transportation Cask, including the impact limiters and cask cavity spacer. A general description of the FuelSolutions™ TS125 transportation packaging contents.
2. The structural design and analysis of the FuelSolutions™ TS125 Transportation Cask (including the impact limiters) for all loading conditions, including the design basis canister interface loadings. A synopsis of the test program performed to verify the performance of the impact limiters and the methodology used to develop the design basis cask drop loadings.

3. The thermal design and analysis of the FuelSolutions™ TS125 Transportation Cask for all design conditions, including the design basis canister interface thermal conditions.
4. The design and analysis of the FuelSolutions™ TS125 Transportation Cask containment boundary.
5. Descriptions of the FuelSolutions™ Transportation Package shielding design features, excluding those that are unique to a particular canister design, if any. The shielding analysis of the FuelSolutions™ TS125 Transportation Cask, excluding that which is unique to a particular canister design.
6. A summary of the criticality analysis approach. Reference to the criticality safety analysis contained in each FuelSolutions™ Canister Transportation SAR.
7. The generic operating procedures for the FuelSolutions™ Transportation System, excluding those that are unique to a particular canister design, if any.
8. The acceptance criteria and maintenance requirements applicable to the FuelSolutions™ TS125 Transportation Cask and impact limiters.

The purpose of this approach is that once the application is reviewed and the FuelSolutions™ Transportation Package is certified by the NRC, the C of C can more easily be amended to include additional or alternate FuelSolutions™ canister designs or payloads without having to re-review the information contained in the FuelSolutions™ TS125 Transportation Cask SAR, which is applicable to all FuelSolutions™ canisters.

To facilitate this approach, canister interface parameters with the transportation cask such as canister size, weight, heat load, and dose rates are established. Values for these canister interface parameters are defined in the FuelSolutions™ TS125 Transportation Cask SAR, within which all acceptance criteria for the transportation packaging are met. Using this approach, all FuelSolutions™ canisters and their contents that remain within the acceptance values established for these interface parameters, as demonstrated in the respective FuelSolutions™ Canister Transportation SARs, and that meet all the applicable acceptance criteria for the canister itself are qualified for use with the FuelSolutions™ TS125 Transportation Cask. This is accomplished by submittal of additional or revised FuelSolutions™ Canister Transportation SARs for review and approval by the NRC, which will rely on the FuelSolutions™ TS125 Transportation Cask SAR as approved by the NRC.

Safety Analysis Report Preparation

The format and content of this SAR and the associated FuelSolutions™ TS125 Transportation Cask SAR are based on Regulatory Guide 7.9⁸ and NUREG-1617.⁹ The provisions of these guidance documents and the regulatory requirements of 10CFR71 are addressed in this SAR for the FuelSolutions™ W74 canisters and payloads, and in the companion SAR for the FuelSolutions™ TS125 Transportation Cask and impact limiters. Table 1.0-1 provides a matrix

⁸ Regulatory Guide 7.9, *Standard Format and Content of Part 71 Applications for Approval of Packaging of Radioactive Material*, Revision 2 (Draft), U.S. Nuclear Regulatory Commission, 1986.

⁹ NUREG-1617, *Standard Review Plan for Transportation Packages for Spent Nuclear Fuel*, Final Report, U.S. Nuclear Regulatory Commission, March 2000.

of the topics in NUREG-1617 and Regulatory Guide 7.9, the corresponding 10CFR71 requirements, and a reference to the applicable FuelSolutions™ transportation SAR section that addresses each topic. The formatting guidelines provided in Regulatory Guide 7.9 were closely followed when possible; however, in order to address the review criteria delineated by NUREG-1617, amended or additional subsections were added to this SAR.

In complying with the guidance provided by the draft NUREG-1617 and Regulatory Guide 7.9, efforts have been made to report the same information only once in the most relevant location in a particular SAR to avoid the potential for conflicts, contradictions and ambiguities, and to facilitate the maintenance and future updates to these SARs as required by 10CFR71.

Appropriate cross-references are provided to aid the reader in locating information provided elsewhere in the SARs, when necessary to support the discussions of a particular SAR section, rather than to repeat the same information in that section.

The FuelSolutions™ Storage System is addressed independently by a separate series of FSARs under Docket No. 72-1026, which comply with the requirements of 10CFR72. The FuelSolutions™ Storage System includes the FuelSolutions™ W150 Storage Cask and the FuelSolutions™ W100 Transfer Cask as the primary components. The FuelSolutions™ canister subsystem includes various FuelSolutions™ canisters designed to meet both the transport requirements of 10CFR71 and the storage requirements of 10CFR72, and thus are dual-certified components.

This SAR chapter provides a general description of the FuelSolutions™ Transportation Package, but principally addresses the FuelSolutions™ W74 canisters and their allowable radioactive contents, or payloads. Summary discussions of the FuelSolutions™ TS125 Transportation Cask and impact limiters are provided to identify the cask as part of the transportation packaging. Further information is provided in the FuelSolutions™ TS125 Transportation Cask SAR. General arrangement drawings of the FuelSolutions™ W74 canister are provided in Section 1.3.1.

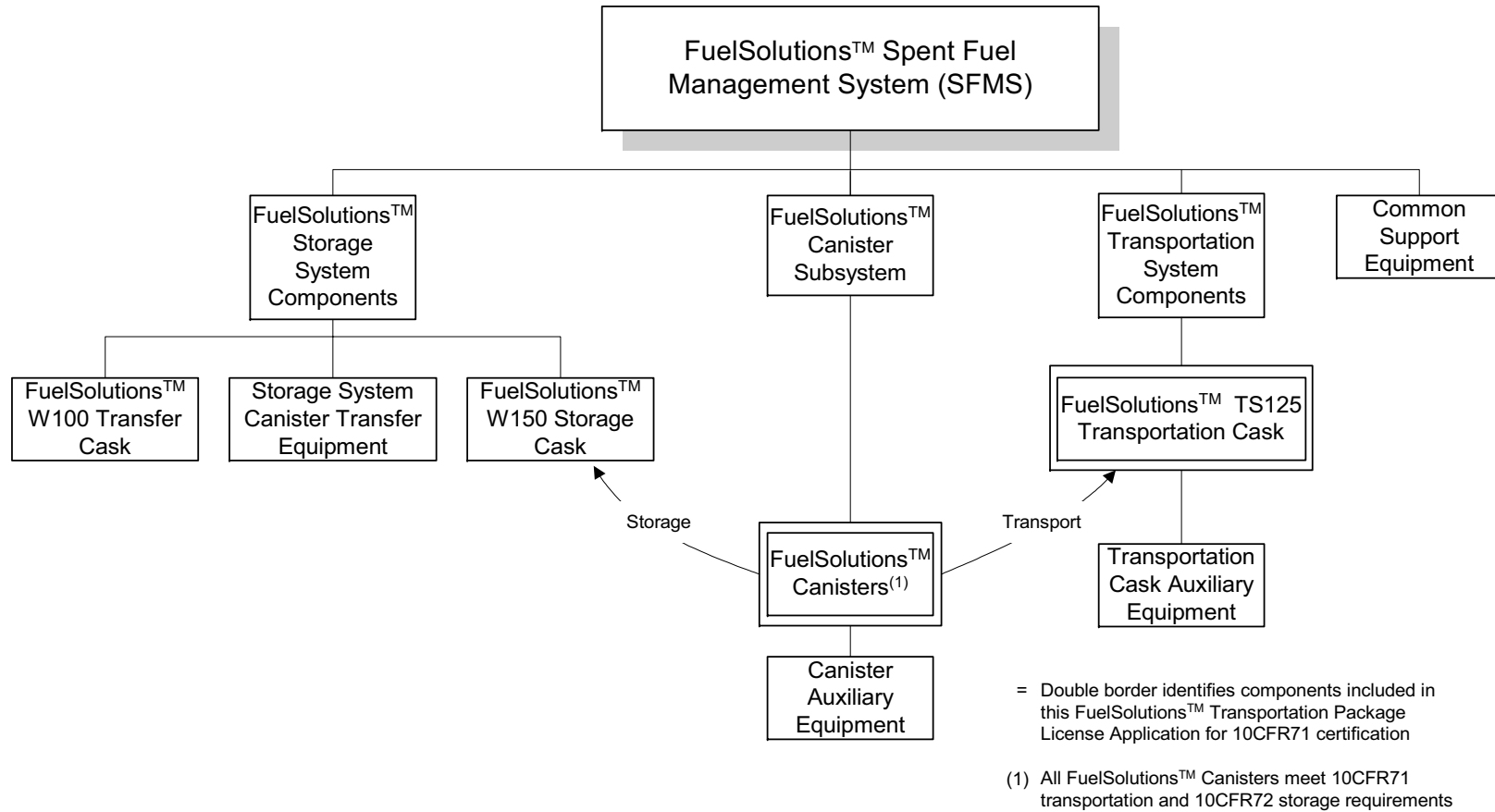


Figure 1.0-1 - FuelSolutions™ Spent Fuel Management System Elements

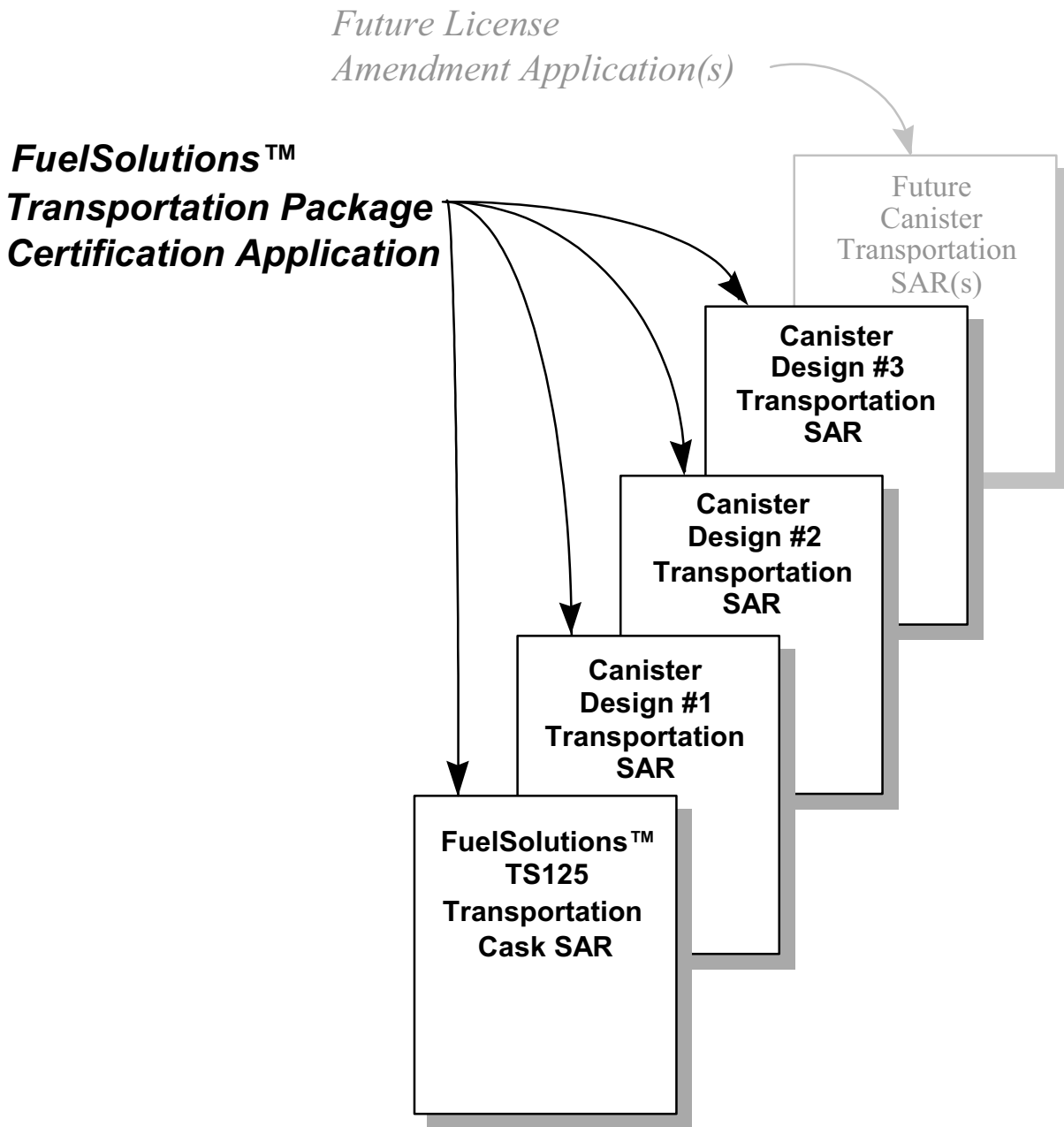


Figure 1.0-2 - FuelSolutions™ Transportation Package Certification Application Approach

Table 1.0-1 - FuelSolutions™ Transportation SAR Regulatory Compliance Cross-Reference Matrix (13 pages)

Regulatory Guide 7.9 Section and Content	NUREG-1617 Review Criteria	Applicable 10CFR71 Requirement	FuelSolutions™ Transportation Cask SAR	FuelSolutions™ Canister Transportation SAR
1. General Information				
1. General Information	1.5.1 General SAR Format	10CFR71.31	1.0	1.0
1.1 Introduction	1.5.2 Package Design Information	10CFR71.31(a)(1) 10CFR71.31(a)(2) 10CFR71.31(b) 10CFR71.31(c) 10CFR71.33(a)(1) 10CFR71.33(a)(2) 10CFR71.33(a)(3) 10CFR71.35(b) 10CFR71.59	1.1	1.1
1.2 Package Description	1.5.3 Package Description	10CFR71.33 10CFR71.35 10CFR71.43	1.2	1.2
1.2.1 Packaging	1.5.3.1 Packaging	10CFR71.31(a)(1) 10CFR71.45	1.2.1	1.2.1
1.2.2 Operational Features	1.5.3.2 Operational Features	10CFR71.87	1.2.2	1.2.2
1.2.3 Contents of Packaging	1.5.3.3 Contents	10CFR71.55	1.2.3	1.2.3
--	1.5.4 Compliance with 10 CFR Part 71	10CFR71.31(a)(2) 10CFR71.35(a) 10CFR71.41(a)	1.2.4	1.2.4
1.3 Appendix	1.5.5 Appendix	10CFR71.37 10CFR71.33(a)(5) 10CFR71.43(a) 10CFR71.43(b) 10CFR71.43(c) 10CFR71.43(d) 10CFR71.43(e) 10CFR71.31(c)	1.3	1.3
2. Structural Evaluation				
2.1 Structural Design	2.5.1 Description of Structural Design	--	2.1	2.1

Table 1.0-1 - FuelSolutions™ Transportation SAR Regulatory Compliance Cross-Reference Matrix (13 pages)

Regulatory Guide 7.9 Section and Content	NUREG-1617 Review Criteria	Applicable 10CFR71 Requirement	FuelSolutions™ Transportation Cask SAR	FuelSolutions™ Canister Transportation SAR
2.1.1 Discussion	--	10CFR71.31(a)(1) 10CFR71.33(a)(5)	2.1.1	2.1.1
2.1.2 Design Criteria	2.5.1.2 Codes and Standards	10CFR71.31(c)	2.1.2	2.1.2
2.2 Weights and Centers of Gravity	2.5.1.1 Descriptive Information including Weights and Centers of Gravity	10CFR71.33(a)(2) 10CFR71.33(a)(5) 10CFR71.33(b)(6)	2.2	2.2
2.3 Mechanical Properties of Materials	2.5.2 Material Properties	10CFR71.33(a)(5)	2.3	2.3
--	2.5.2.1 Materials and Material Specifications	10CFR71.33(a)(5)	2.1, 2.3	2.1, 2.3
2.4 General Standards for All Packages	--	10CFR71.43	2.4	2.4
2.4.1 Minimum Package Size	--	10CFR71.43(a)	2.4.1	--
2.4.2 Tamperproof Feature	--	10CFR71.43(b)	2.4.2	--
2.4.3 Positive Closure	--	10CFR71.43(c)	2.4.3	--
2.4.4 Chemical and Galvanic Reactions	2.5.2.2 Prevention of Chemical, Galvanic, or Other Reactions	10CFR71.43(d)	2.4.4	2.4.4
-- (Valves)	--	10CFR71.43(e)	2.4.5	--
-- (Cask Design)	--	10CFR71.43(f)	2.4.6	--
-- (External Temperatures)	--	10CFR71.43(g)	2.4.7	--
-- (Venting)	--	10CFR71.43(h)	2.4.8	--

Table 1.0-1 - FuelSolutions™ Transportation SAR Regulatory Compliance Cross-Reference Matrix (13 pages)

Regulatory Guide 7.9 Section and Content	NUREG-1617 Review Criteria	Applicable 10CFR71 Requirement	FuelSolutions™ Transportation Cask SAR	FuelSolutions™ Canister Transportation SAR
2.5 Lifting and Tiedown Standards for All Packages	2.5.3 Lifting and Tiedown Standards for All Packages	10CFR71.45	2.5	2.5
2.5.1 Lifting Devices	2.5.3.1 Lifting Devices	10CFR71.45(a)	2.5.1	--
2.5.2 Tiedown Devices	2.5.3.2 Tiedown Devices	10CFR71.45(b)	2.5.2	--
--	2.5.4 General Considerations for Structural Evaluation of Packaging	10CFR71.31(a)(2) 10CFR71.35(a) 10CFR71.41(a) 10CFR71.71 10CFR71.73	2.6, 2.7	2.6, 2.7
2.6 Normal Conditions of Transport	2.5.5 Normal Conditions of Transport	10CFR71.35(a) 10CFR71.41(a) 10CFR71.43(f) 10CFR71.51(a)(1) 10CFR71.55(d)(4) 10CFR71.71	2.6	2.6
2.6.1 Heat	2.5.5.1 Heat	10CFR71.71(c)(1)	2.6.1	2.6.1
2.6.2 Cold	2.5.5.2 Cold	10CFR71.71(c)(2)	2.6.2	2.6.2
2.6.3 Reduced External Pressure	2.5.5.3 Reduced External Pressure	10CFR71.71(c)(3)	2.6.3	--
2.6.4 Increased External Pressure	2.5.5.4 Increased External Pressure	10CFR71.71(c)(4)	2.6.4	--
2.6.5 Vibration	2.5.5.5 Vibration	10CFR71.71(c)(5)	2.6.5	2.6.5
2.6.6 Water Spray	2.5.5.6 Water Spray	10CFR71.71(c)(6)	2.6.6	--
2.6.7 Free Drop	2.5.5.7 Free Drop	10CFR71.71(c)(7)	2.6.7	2.6.7
2.6.8 Corner Drop	2.5.5.8 Corner Drop	10CFR71.71(c)(8)	2.6.8	2.6.8
2.6.9 Compression	2.5.5.9 Compression	10CFR71.71(c)(9)	2.6.9	--
2.6.10 Penetration	2.5.5.10 Penetration	10CFR71.71(c)(10)	2.6.10	--

Table 1.0-1 - FuelSolutions™ Transportation SAR Regulatory Compliance Cross-Reference Matrix (13 pages)

Regulatory Guide 7.9 Section and Content	NUREG-1617 Review Criteria	Applicable 10CFR71 Requirement	FuelSolutions™ Transportation Cask SAR	FuelSolutions™ Canister Transportation SAR
2.7 Hypothetical Accident Conditions	2.5.6 Hypothetical Accident Conditions	10CFR71.35(a) 10CFR71.41(a) 10CFR71.51(a)(2) 10CFR71.73	2.7	2.7
2.7.1 Free Drop	2.5.6.1 Free Drop	10CFR71.73(c)(1)	2.7.1	2.7.1
---	2.5.6.2 Crush	10CFR71.73(c)(2)	2.7.2	2.7.2
2.7.2 Puncture	2.5.6.3 Puncture	10CFR71.73(c)(3)	2.7.3	--
2.7.3 Thermal	2.5.6.4 Thermal	10CFR71.73(c)(4)	2.7.4	2.7.3
2.7.4 Immersion - Fissile Material	2.5.6.5 Immersion - Fissile Material	10CFR71.73(c)(5)	2.7.5	--
2.7.5 Immersion - All Packages	2.5.6.6 Immersion - All Material	10CFR71.73(c)(6)	2.7.6	--
2.7.6 Summary of Damage	--	--	2.7.7	2.7.7
--	2.5.7 Special Requirement for Irradiated Nuclear Fuel Shipments	10CFR71.61	2.8	--
--	2.5.8 Internal Pressure Test	10CFR71.85(b)	2.9	--
2.8 Special Form	--	10CFR71.75 10CFR71.77	2.10	2.10
2.9 Fuel Rods	--	--	2.11	2.11
2.10 Appendix	2.5.9 Appendix	10CFR71.73(c)(1)	2.12	2.12

Table 1.0-1 - FuelSolutions™ Transportation SAR Regulatory Compliance Cross-Reference Matrix (13 pages)

Regulatory Guide 7.9 Section and Content	NUREG-1617 Review Criteria	Applicable 10CFR71 Requirement	FuelSolutions™ Transportation Cask SAR	FuelSolutions™ Canister Transportation SAR
3. Thermal Evaluation				
3.1 Discussion	3.5.1 Description of the Thermal Design	10CFR71.31(a)(1) 10CFR71.31(c) 10CFR71.33(a)(5) 10CFR71.33(a)(6) 10CFR71.33(b)(1) 10CFR71.33(b)(3) 10CFR71.33(b)(5) 10CFR71.33(b)(7) 10CFR71.33(b)(8) 10CFR71.51(c)	3.1	3.1
3.2 Summary of Thermal Properties of Materials	3.5.2.1 Material Properties	10CFR71.31(a)(1) 10CFR71.33(a)(5)	3.2	3.2
3.3 Technical Specifications of Components	3.5.2.2 Technical Specifications of Component	10CFR71.31(a)(1) 10CFR71.33(a)(5)	3.3	3.3
--	3.5.3 General Considerations for Thermal Evaluations	10CFR71.31(a)(2) 10CFR71.35(a) 10CFR71.41(a)	3.4, 3.5	3.4, 3.5
--	3.5.4 Evaluation of Accessible Surface Temperatures	10CFR71.43(g)	3.4	3.4,
3.4 Thermal Evaluation for Normal Conditions of Transport	3.5.5 Thermal Evaluation under Normal Conditions of Transport	10CFR71.43(f) 10CFR71.51(a)(1) 10CFR71.71	3.4	3.4
3.4.1 Thermal Model	--	10CFR71.71	3.4.1	3.4.1
3.4.2 Maximum Temperatures	3.5.5.1 Heat and Cold	10CFR71.71(c)(1)	3.4.2	3.4.2
3.4.3 Minimum Temperatures	3.5.5.1 Heat and Cold	10CFR71.71(c)(2)	3.4.3	3.4.3

Table 1.0-1 - FuelSolutions™ Transportation SAR Regulatory Compliance Cross-Reference Matrix (13 pages)

Regulatory Guide 7.9 Section and Content	NUREG-1617 Review Criteria	Applicable 10CFR71 Requirement	FuelSolutions™ Transportation Cask SAR	FuelSolutions™ Canister Transportation SAR
3.4.4 Maximum Internal Pressures	3.5.5.2 Maximum Normal Operating Pressure (MNOP)	10CFR71.71(b)	3.4.4	3.4.4
3.4.5 Maximum Thermal Stresses	3.5.5.3 Maximum Thermal Stresses	10CFR71.71	3.4.5	3.4.5
3.4.6 Evaluation of Package Performance for Normal Conditions of Transport	--	10CFR71.71	3.4.6	3.4.6
3.5 Hypothetical Accident Thermal Evaluation	3.5.6 Thermal Evaluation under Hypothetical Accident Conditions	10CFR71.73	3.5	3.5
3.5.1 Thermal Model	--	10CFR71.73	3.5.1	3.5.1
3.5.2 Package Conditions and Environment	3.5.6.1 Initial Conditions 3.5.6.2 Fire Test	10CFR71.73(b)	3.5.2	3.5.2
3.5.3 Package Temperatures	3.5.6.3 Maximum Temperatures and Pressures	10CFR71.73(b)	3.5.3	3.5.3
3.5.4 Maximum Internal Pressures	3.5.6.3 Maximum Temperatures and Pressures	10CFR71.73(b)	3.5.4	3.5.4
3.5.5 Maximum Thermal Stresses	3.5.6.4 Maximum Thermal Stresses	10CFR71.73(c)(4)	3.5.5	3.5.5
3.5.6 Evaluation of Package Performance for Hypothetical Accident Thermal Conditions	--	10CFR71.73	3.5.6	3.5.6
3.6 Appendix	3.5.7 Appendix	--	3.6	3.6

Table 1.0-1 - FuelSolutions™ Transportation SAR Regulatory Compliance Cross-Reference Matrix (13 pages)

Regulatory Guide 7.9 Section and Content	NUREG-1617 Review Criteria	Applicable 10CFR71 Requirement	FuelSolutions™ Transportation Cask SAR	FuelSolutions™ Canister Transportation SAR
4. Containment				
4.1 Containment Boundary	4.5.1 Description of the Containment System	10CFR71.31(a)(1) 10CFR71.31(c) 10CFR71.33(a)(4) 10CFR71.33(a)(5) 10CFR71.33(b)(7) 10CFR71.43(c) 10CFR71.43(e)	4.1	--
4.1.1 Containment Vessel		10CFR71.43(c)	4.1.1	--
4.1.2 Containment Penetrations		10CFR71.43(e)	4.1.2	--
4.1.3 Seals and Welds		10CFR71.43(c) 10CFR71.43(h)	4.1.3	--
4.1.4 Closure		10CFR71.43(c)	4.1.4	--
4.2 Requirements for Normal Conditions of Transport	4.5.2 Containment under Normal Conditions of Transport	10CFR71.31(a)(2) 10CFR71.33(b)(5) 10CFR71.35(a) 10CFR71.41(a) 10CFR71.43(f) 10CFR71.43(h) 10CFR71.51(a)(1) 10CFR71.51(c)	4.2	--
4.2.1 Containment of Radioactive Material	4.5.2.3 Compliance with Containment Criteria	10CFR71.51(a)(1)	4.2.1	--
4.2.2 Pressurization of Containment Vessel	4.5.2.1 Pressurization of Containment Vessel	10CFR71.71(b)	4.2.2	--
4.2.3 Containment Criterion	4.5.2.2 Containment Criteria	10CFR71.43(f)	4.2.3	--
--	--	10CFR71.87(i)	4.2.4	--

Table 1.0-1 - FuelSolutions™ Transportation SAR Regulatory Compliance Cross-Reference Matrix (13 pages)

Regulatory Guide 7.9 Section and Content	NUREG-1617 Review Criteria	Applicable 10CFR71 Requirement	FuelSolutions™ Transportation Cask SAR	FuelSolutions™ Canister Transportation SAR
4.3 Containment Requirements for Hypothetical Accident Conditions	4.5.3 Containment under Hypothetical Accident Conditions	10CFR71.31(a)(2) 10CFR71.35(a) 10CFR71.41(a) 10CFR71.51(a)(2) 10CFR71.51(c)	4.3	4.3
4.3.1 Fission Gas Products	4.5.3.2 Containment Criteria	10CFR71.33(b)(1) 10CFR71.33(b)(2) 10CFR71.33(b)(3)	4.3.1	4.3.1
4.3.2 Containment of Radioactive Material	4.5.3.2 Containment Criteria	10CFR71.51(a)(2)	4.3.2	--
4.3.3 Containment Criterion	4.5.3.3 Compliance with Containment Criteria	10CFR71.51(a)(2)	4.3.3	--
4.4 Special Requirements	--	10CFR71.63	4.4	--
4.5 Appendix	4.5.4 Appendix	--	--	4.5
5. Shielding Evaluation				
5.1 Discussion and Results	5.5.1 Description of the Shielding Design	10CFR71.31(a)(1) 10CFR71.31(c) 10CFR71.33(a)(5)	5.1	5.1
5.2 Source Specification	5.5.2 Source Specification	10CFR71.31(a)(1) 10CFR71.33(b)(1) 10CFR71.33(b)(2) 10CFR71.33(b)(3)	--	5.2
5.2.1 Gamma Source	5.5.2.1 Gamma Source		--	5.2.2
5.2.2 Neutron Source	5.5.2.2 Neutron Source		--	5.2.3
5.3 Model Specification	5.5.3 Model Specification	10CFR71.31(a) 10CFR71.31(b)	5.3	5.3
5.3.1 Description of Radial and Axial Shielding Configuration	5.5.3.1 Configuration of Source and Shielding	--	5.3.1	5.3.1
5.3.2 Shield Regional Densities	5.5.3.2 Material Properties	--	5.3.2	5.3.2

Table 1.0-1 - FuelSolutions™ Transportation SAR Regulatory Compliance Cross-Reference Matrix (13 pages)

Regulatory Guide 7.9 Section and Content	NUREG-1617 Review Criteria	Applicable 10CFR71 Requirement	FuelSolutions™ Transportation Cask SAR	FuelSolutions™ Canister Transportation SAR
5.4 Shielding Evaluation	5.5.4 Evaluation	10CFR71.31(a)(2) 10CFR71.35(a) 10CFR71.41(a) 10CFR71.43(f) 10CFR71.47(b) 10CFR71.51(a)(1) 10CFR71.51(a)(2)	5.4	5.4
5.5 Appendix	5.5.5 Appendix	--	5.5	5.5
6. Criticality Evaluation				
6.1 Discussion and Results	6.5.1 Description of the Criticality Design	10CFR71.31(a)(1) 10CFR71.31(c) 10CFR71.33(a)(5) 10CFR71.35(b) 10CFR71.59(b)	--	6.1
6.2 Package Fuel Loading	6.5.2 Spent Nuclear Fuel Contents	10CFR71.31(a)(1) 10CFR71.33(b)(1) 10CFR71.33(b)(2) 10CFR71.33(b)(3) 10CFR71.83	--	6.2
6.3 Model Specification	6.5.3 General Considerations for Evaluations	10CFR71.31(a)(2) 10CFR71.35(a) 10CFR71.41(a)	--	6.3
6.3.1 Description of Calculational Model	6.5.3.1 Model Configuration		--	6.3.1
6.3.2 Package Regional Densities	6.5.3.2 Material Properties		--	6.3.2

Table 1.0-1 - FuelSolutions™ Transportation SAR Regulatory Compliance Cross-Reference Matrix (13 pages)

Regulatory Guide 7.9 Section and Content	NUREG-1617 Review Criteria	Applicable 10CFR71 Requirement	FuelSolutions™ Transportation Cask SAR	FuelSolutions™ Canister Transportation SAR
6.4 Criticality Calculation	6.5.4 Single Package Evaluation	10CFR71.35 10CFR71.43(f) 10CFR71.51(a)(1) 10CFR71.55(b) 10CFR71.55(d) 10CFR71.55(e)	--	6.4.2.2
	6.5.5 Evaluation of Package Arrays under Normal Conditions of Transport	10CFR71.35 10CFR71.59	--	6.4.2.1
	6.5.6 Evaluation of Package Arrays under Hypothetical Accident Conditions	10CFR71.35 10CFR71.59	--	6.4.2.1
6.4.1 Calculational or Experimental Method	6.5.3.3 Computer Codes and Cross Section Libraries	--	--	6.4.1
6.4.2 Fuel Loading or Other Contents Loading Optimization	6.5.3.4 Demonstration of Maximum Reactivity	10CFR71.55 10CFR71.63	--	6.4.2
6.4.3 Criticality Results	6.5.4 Single Package Evaluation	10CFR71.55	--	6.4.3
	6.5.5 Evaluation of Package Arrays under Normal Conditions of Transport			
	6.5.6 Evaluation of Package Arrays under Hypothetical Accident Conditions			

Table 1.0-1 - FuelSolutions™ Transportation SAR Regulatory Compliance Cross-Reference Matrix (13 pages)

Regulatory Guide 7.9 Section and Content	NUREG-1617 Review Criteria	Applicable 10CFR71 Requirement	FuelSolutions™ Transportation Cask SAR	FuelSolutions™ Canister Transportation SAR
6.5 Critical Benchmark Experiments	6.5.7 Benchmark Evaluations	10CFR71.31(a)(2) 10CFR71.35	--	6.5
6.5.1 Benchmark Experiments and Applicability	6.5.7.1 Experiments and Applicability		--	6.5.1
6.5.2 Details of Benchmark Calculations	6.5.7.2 Bias Determination		--	6.5.2
6.5.3 Results of Benchmark Calculations			--	6.5.3
--	6.5.8 Burnup Credit	--	--	--
6.6 Appendix	6.5.9 Appendix	--	--	6.6
7. Operating Procedures				
7.1 Procedures for Loading Package	7.5.1 Package Loading	10CFR71.31(c) 10CFR71.35(c) 10CFR71.43(g) 10CFR71.47(b) 10CFR71.47(c) 10CFR71.47(d) 10CFR71.87 10CFR71.89	7.1	7.1
7.2 Procedures for Unloading Package	7.5.2 Package Unloading	10CFR71.35(c)	7.2	7.2
7.3 Preparation of Empty Package for Transport	7.5.3 Preparation of Empty Package for Transport	10CFR71.87(i)	7.3	--
--	7.5.4 Other Procedures	10CFR71.35(c)	--	--
7.4 Appendix	7.5.5 Appendix	10CFR71.51(a)	7.4	--

Table 1.0-1 - FuelSolutions™ Transportation SAR Regulatory Compliance Cross-Reference Matrix (13 pages)

Regulatory Guide 7.9 Section and Content	NUREG-1617 Review Criteria	Applicable 10CFR71 Requirement	FuelSolutions™ Transportation Cask SAR	FuelSolutions™ Canister Transportation SAR
8. Acceptance Tests and Maintenance Program				
8.1 Acceptance Tests	8.2.4 Review Procedures	10CFR71.31(c) 10CFR71.37 10CFR71.85 10CFR71.87 10CFR71.93(b)	8.1	--
8.1.1 Visual Inspection	8.2.4.1 Visual Inspections and Measurements 8.2.4.2 Weld Inspections	10CFR71.85(a) 10CFR71.87(b)	8.1.1	--
8.1.2 Structural and Pressure Tests	8.2.4.3 Structural and Pressure Tests	10CFR71.41(a) 10CFR71.45(a) 10CFR71.71(c) 10CFR71.73(c) 10CFR71.85(b)	8.1.2	--
8.1.3 Leak Tests	8.2.4.4 Leakage Test	10CFR71.37(b) 10CFR71.43(f) 10CFR71.87(c)	8.1.3	--
8.1.4 Component Tests	8.2.4.5 Component Tests	10CFR71.43(d) 10CFR71.73(c)(1) 10CFR71.87(e)	8.1.4	--
8.1.5 Tests for Shielding Integrity	8.2.4.6 Shielding Tests	10CFR71.87(j)	8.1.5	--
8.1.6 Thermal Acceptance Tests	8.2.4.8 Thermal Tests	10CFR71.33(b)(7) 10CFR71.71(c) 10CFR71.73(c)	8.1.6	--
8.1.4.3 Miscellaneous	8.2.4.7 Neutron Absorber Tests	10CFR71.87(g) 10CFR71.85(c)	8.1.7	--
8.2 Maintenance Program	8.3.4 Review Procedures	10CFR71.31(c) 10CFR71.37 10CFR71.85(a) 10CFR71.87(b) 10CFR71.93(b)	8.2	--
--	--	10CFR71.85(a) 10CFR71.87(b)	8.2.1	--

Table 1.0-1 - FuelSolutions™ Transportation SAR Regulatory Compliance Cross-Reference Matrix (13 pages)

Regulatory Guide 7.9 Section and Content	NUREG-1617 Review Criteria	Applicable 10CFR71 Requirement	FuelSolutions™ Transportation Cask SAR	FuelSolutions™ Canister Transportation SAR
8.2.1 Structural and Pressure Tests	8.3.4.1 Structural and Pressure Tests	--	8.2.2	--
8.2.2 Leak Tests	8.3.4.2 Leakage Tests	10CFR71.37(b) 10CFR71.43(f) 10CFR71.87(c)	8.2.3	--
8.2.3 Subsystem Maintenance	--	10CFR71.85(a) 10CFR71.87(b)	8.2.4	--
8.2.4 Valves, Rupture Discs, and Gaskets on Containment Vessel	8.3.4.3 Component Tests	10CFR71.87(c) 10CFR71.87(e)	8.2.5	--
8.2.5 Shielding	--	--	8.2.6	--
8.2.6 Thermal	8.3.4.5 Thermal Tests	10CFR71.85(a) 10CFR71.87(b)	8.2.7	--
8.2.7 Miscellaneous	8.3.4.4 Neutron Absorber Tests	10CFR71.87(g)	8.2.8	--

1.1 Introduction

The FuelSolutions™ SFMS is a fully integrated, canister-based system that provides for the storage and transport of a broad range of SNF assembly classes. The FuelSolutions™ SFMS is designed to be suitable for most commercial reactor sites in the contiguous United States. The FuelSolutions™ SFMS is also designed to be suitable for the U.S. Department of Energy's (DOE) Centralized Interim Storage Facility (CISF) and a Mined Geologic Disposal System (MGDS). In addition, it is also suitable for use at private CISFs.

The FuelSolutions™ SFMS is comprised of four basic system components. These components can be used in a variety of ways to satisfy a particular licensee's requirements throughout the life of the plant. A synopsis for each of the four basic components of the FuelSolutions™ SFMS is as follows:

1. A *FuelSolutions™ Canister* is designed for dry storage of SNF in accordance with 10CFR72 and for transportation of SNF in accordance with 10CFR71. The canister is placed in an overpack cask for fuel loading, closure, transfer, on-site storage, and off-site transport. It provides confinement for storage, criticality control and passive heat removal for storage and transport, and biological shielding for closure and handling operations for the enclosed SNF. The canister interfaces are standardized to be compatible with each of the system cask components identified below. The various FuelSolutions™ canister designs are addressed in their respective FuelSolutions™ Canister Storage FSARs and Transportation SARs.
2. The *FuelSolutions™ TS125 Transportation Cask and Impact Limiters* are designed and licensed in accordance with 10CFR71 and are used for off-site shipment of a FuelSolutions™ canister. The transportation cask can be used to load or unload a canister with SNF in a spent fuel pool or a shielded hot cell. The transportation cask can also be used to transfer a sealed canister to and from either the storage cask via the transfer cask or to and from the transfer cask. It provides containment, structural protection, biological shielding, and passive heat removal for the enclosed canister and SNF. The FuelSolutions™ TS125 Transportation Cask and impact limiters are addressed in the FuelSolutions™ TS125 Transportation Cask SAR.
3. A *FuelSolutions™ W150 Storage Cask* provides passive vertical dry storage of a loaded canister in an on-site ISFSI or at an off-site CISF, in accordance with 10CFR72. The storage cask is capable of accommodating both vertical or horizontal canister transfer to the transfer cask. It provides biological shielding, structural protection, and passive convective heat removal for the enclosed canister and SNF. The FuelSolutions™ W150 Storage Cask is addressed in the FuelSolutions™ Storage System FSAR.¹⁰
4. A *FuelSolutions™ W100 Transfer Cask* provides canister loading, closure, and handling capability, in accordance with 10CFR50 and 10CFR72. The transfer cask has the capability to be used in the following operational modes:

¹⁰ WSNF-220, *FuelSolutions™ Storage System Final Safety Analysis Report*, NRC Docket No. 72-1026, BNG Fuel Solutions Corporation.

- Loading or unloading of a canister with SNF in a spent fuel pool, in a cask receiving area using an SNF assembly shuttle cask and shielded loading collar, or in a shielded hot cell,
- Vertical transfer of a sealed canister to or from a FuelSolutions™ W150 Storage Cask inside the plant's fuel building or a licensed cask handling facility,
- Horizontal transfer of a sealed canister to or from a FuelSolutions™ W150 Storage Cask within an ISFSI or the licensee's owner-controlled area,
- Vertical transfer of a sealed canister to or from a FuelSolutions™ TS125 Transportation Cask inside the plant's fuel building or a licensed cask handling facility, or
- Horizontal transfer of a sealed canister to or from a FuelSolutions™ TS125 Transportation Cask within an ISFSI or the licensee's owner-controlled area.

The transfer cask provides biological shielding, structural protection, and passive heat removal for the enclosed canister and SNF. The FuelSolutions™ W100 Transfer Cask is addressed in the FuelSolutions™ Storage System FSAR.

FuelSolutions™ W74 Canister Description

The FuelSolutions™ canister, Model No. W74, is designed to be used together with a FuelSolutions™ TS125 Transportation Cask and impact limiters as a FuelSolutions™ packaging for the safe transport of SNF assemblies. Key criteria and features of the FuelSolutions™ W74 canister design are as follows:

- The shell assembly pressure-retaining components are designed, analyzed, and fabricated in accordance with the applicable provisions of the American Society of Mechanical Engineers (ASME) Boiler and Pressure Vessel (B&PV) Code, Section III, Subsection NB,¹¹ as discussed in Section 2.1.2 of the FuelSolutions™ W74 Canister Storage FSAR. Double closure plates and seal welds are used on the top end of the canister. No credit is taken for the containment capability of the canister for the off-site transport of SNF.
- The internal basket assembly is designed, analyzed, and fabricated in accordance with the applicable provisions of ASME B&PV Code, Section III, Subsection NG,¹² as discussed in Section 2.1.2 of the FuelSolutions™ W74 Canister Storage FSAR. Fixed borated neutron absorbers for criticality control are integral with the basket assembly.
- Thick shield plugs are provided at the canister top and bottom ends to maintain occupational exposures as low as reasonably achievable (ALARA).
- Basket assembly and top shield plug carbon steel components are electroless nickel plated for corrosion protection.

¹¹ American Society of Mechanical Engineers (ASME) Boiler and Pressure Vessel Code, Section III, Division 1, Subsection NB, *Class 1 Components*, 1998 Edition.

¹² American Society of Mechanical Engineers (ASME) Boiler and Pressure Vessel Code, Section III, Division 1, Subsection NG, *Core Support Structures*, 1998 Edition.

These criteria and design features comply with the requirements of 10CFR71 and are consistent with those used for other SNF transportation packages previously approved by the NRC. The design of the FuelSolutions™ W74 canister is described further in Section 1.2.1.1.

FuelSolutions™ W74 Canister Operations Overview

The principal FuelSolutions™ W74 canister operations performed under the plant's 10CFR50 license, a stand-alone storage and/or cask handling facility's 10CFR72 license, or the certificate holder's 10CFR71 C of C for off-site transport are as follows:

- A FuelSolutions™ W74 canister is wet loaded with SNF in a spent fuel pool using conventional methods, while within a FuelSolutions™ W100 Transfer Cask or a FuelSolutions™ TS125 Transportation Cask.

Alternatively, a FuelSolutions™ W74 canister may be loaded with SNF while within a FuelSolutions™ W100 Transfer Cask outside the spent fuel pool, but inside the plant's fuel building or a licensed cask handling facility using a fuel assembly shuttle cask and a shielded loading collar, as described in the respective FuelSolutions™ Canister Storage FSAR.

Following SNF loading, the FuelSolutions™ W74 canister is vacuum dried and helium backfilled using conventional methods. Canister seal welding uses remote automated welding equipment.

- A sealed FuelSolutions™ W74 canister can be transferred horizontally to or from a FuelSolutions™ TS125 Transportation Cask, using a FuelSolutions™ W100 Transfer Cask within an ISFSI or CISF, or the licensee's owner-controlled area.

Alternatively, a sealed FuelSolutions™ W74 canister can be transferred vertically to or from a FuelSolutions™ TS125 Transportation Cask or W150 Storage Cask, using a FuelSolutions™ W100 Transfer Cask inside the plant's (or CISFs) cask receiving bay or a licensed cask handling facility.

- A FuelSolutions™ W74 canister, which is sealed in the cavity of a FuelSolutions™ TS125 Transportation Cask and fully configured with impact limiters and secured to the intermodal skid, is transported off-site by rail, barge, or heavy-haul trailer.

The operations of a FuelSolutions™ W74 canister for off-site transport are described further in Section 1.2.2 and the FuelSolutions™ TS125 Transportation Cask SAR.

Spent Fuel to be Transported

The FuelSolutions™ W74 canister is designed to dimensionally accommodate only Big Rock Point BWR SNF assemblies. Up to sixty-four (64) Big Rock Point SNF assemblies may be stored and transported in a FuelSolutions™ W74 canister. The SNF assemblies include intact zircaloy-clad fuel assemblies, damaged fuel assemblies, partial fuel assemblies, and MOX fuel assemblies. The SNF assembly acceptance criteria and the corresponding bases for the structural, thermal, radiological, and criticality safety evaluations are provided in this SAR and the FuelSolutions™ TS125 Transportation Cask SAR. The contents of the FuelSolutions™ W21 canister are discussed further in Section 1.2.3.

This page intentionally left blank.

1.2 Package Description

The FuelSolutions™ Transportation System consists of the components and equipment that provide for the handling, transfer, and off-site transport of SNF in sealed canisters. A schematic of the FuelSolutions™ SFMS components and equipment, including those associated with the FuelSolutions™ Transportation System, is shown in Figure 1.2-1. The FuelSolutions™ Transportation System components that are classified as important to safety are also identified in Figure 1.2-1. The quality classifications for the FuelSolutions™ Transportation System components and equipment are shown in Table 1.2-1 of the FuelSolutions™ TS125 Transportation Cask SAR.

The FuelSolutions™ Transportation Package described in this SAR is a FuelSolutions™ transportation packaging with a payload of SNF assemblies. The FuelSolutions™ transportation packaging is comprised of two primary components—a FuelSolutions™ TS125 Transportation Cask with impact limiters and a FuelSolutions™ W74 canister. The FuelSolutions™ W74 canister satisfies the dimensional, weight, thermal, radiological, and subcriticality constraints of the cask, as described in Section 1.2.3 of the FuelSolutions™ TS125 Transportation Cask SAR. The features of the FuelSolutions™ W74 canister design provided to meet the performance requirements of 10CFR71 include:

- A robust structural steel basket assembly, which provides support to maintain the spacing of the SNF assemblies.
- A conservative “flux trap” basket design that does not require either burnup credit or moderator exclusion for criticality control.
- A basket assembly that uses fixed borated neutron absorber materials for criticality control.
- Integral gamma shielding at both ends provides axial shielding capability.

The FuelSolutions™ W74 canister is designed for 100 years of service while satisfying the applicable regulatory requirements, as discussed in Section 2.1.2 of the FuelSolutions™ W74 Canister Storage FSAR.

This SAR section provides a description of the FuelSolutions™ Transportation Package, focusing mainly on the FuelSolutions™ W74 canister and its radioactive contents, or payload. The principal characteristics of the FuelSolutions™ W74 canister are summarized in Table 1.2-1, and a matrix of the FuelSolutions™ W74 canister configurations is provided in Table 1.2-2. A summary of the design criteria for the FuelSolutions™ W74 canister is provided in Table 1.2-3. General arrangement drawings of the FuelSolutions™ W74 canister are provided in Section 1.3.1. Descriptions of the FuelSolutions™ TS125 Transportation Cask, the impact limiters, and FuelSolutions™ Transportation System support equipment are provided in Section 1.2 of the FuelSolutions™ TS125 Transportation Cask SAR.

1.2.1 Packaging

The FuelSolutions™ transportation packaging consists of a FuelSolutions™ TS125 Transportation Cask and impact limiters, together with a FuelSolutions™ W74 canister. These components assure compliance with the packaging requirements of 10CFR71. The

FuelSolutions™ packaging as it pertains to the FuelSolutions™ TS125 Transportation Cask is described in Section 1.2.1 of the FuelSolutions™ TS125 Transportation Cask SAR.

A typical FuelSolutions™ canister includes a shell assembly that provides for confinement of all radioactive materials during dry storage, and an internal basket assembly that provides geometric spacing and criticality control for the SNF assemblies for both storage and transport conditions. A FuelSolutions™ W74 canister provides an additional containment boundary, structural support, an inert helium atmosphere, criticality control, and axial shielding for the SNF assemblies during transport, although no credit is taken for the additional containment capability. Figure 1.2-2 shows an expanded view of the major FuelSolutions™ W74 canister components. These components are described in the sections that follow.

1.2.1.1 FuelSolutions™ W74 Canister

The FuelSolutions™ W74 canister, shown in Figure 1.2-2, is designed for both on-site dry storage and off-site transport of SNF assemblies in accordance with the requirements of 10CFR71 and 10CFR72. All canister external dimensions and maximum weights are standardized so that support equipment, methods of handling, and the interfaces with the FuelSolutions™ TS125 Transportation Cask are consistent for the various FuelSolutions™ canisters. The principal characteristics of the FuelSolutions™ W74 canister are summarized in Table 1.2-1. General arrangement drawings for the FuelSolutions™ W74 canister are provided in Section 1.3.1.

The FuelSolutions™ W74 canister shell assembly is a high-integrity pressure vessel that provides confinement of the SNF during dry storage and maintains an inert helium atmosphere in contact with the SNF. The helium atmosphere assures corrosion protection and enhances heat removal. For conservatism, no credit is taken for the added capability of the canister shell to confine or contain the radioactive materials during transport. However, credit is taken for the capability of the canister shell to maintain the helium atmosphere for design basis conditions during transport.

The FuelSolutions™ W74 canister shell assembly also includes biological shielding at both ends to maintain exposures ALARA during canister and cask loading, handling, storage, and transport operations. Within each FuelSolutions™ W74 canister, there is a basket assembly that provides structural support and criticality control for the SNF assemblies. A conservative “flux trap” design is used that does not require either burnup credit or moderator exclusion for criticality control.

The FuelSolutions™ W74 canister basket assembly has 74 cell locations with a capacity for up to 64 undamaged Big Rock Point BWR SNF assemblies, as discussed in Section 1.2.3. The additional ten cell locations at the center of the basket are mechanically blocked to prevent fuel assemblies from being loaded into these locations. Upper and lower basket assemblies, each containing 32 SNF assemblies, stack on top of each other. The FuelSolutions™ W74 canister is shielded at both ends to facilitate and allow a full range of operational alternatives and to provide flexibility. The top shield plate contains 37 independent shield plugs to facilitate canister fuel loading with a single element transfer cask outside the plant’s spent fuel pool. Alternatively, a solid top shield plate is used for conventional canister fuel loading in the plant’s spent fuel pool.

Design Characteristics

The FuelSolutions™ canister subsystem includes two different classes of FuelSolutions™ canister assemblies. The two classes are as follows:

- The FuelSolutions™ W74M class Multi-Purpose Canister (MPC) for storage, transportation, and disposal (top shield plug with individual plugs or solid plate).
- The FuelSolutions™ W74T class Transportable Storage Canister (TSC) for storage and transportation (top shield plug with individual plugs or solid plate).

Unlike other FuelSolutions™ canister types, the FuelSolutions™ W74 canister design includes only one canister length and cavity size, as shown in Table 1.2-1. Only carbon steel shield plugs are used with the top shield plug assembly comprised of a shield plate with individual shield plugs or a solid plate. No fuel assembly spacers are used. The configurations of the two FuelSolutions™ W74 canister classes are described in Table 1.2-2.

The FuelSolutions™ W74 canister is comprised of a shell assembly and an internal basket assembly, as shown in Figure 1.2-2. The pressure-retaining components of the FuelSolutions™ W74 canister shell assembly (i.e., the confinement boundary for storage) are designed and fabricated as an ASME Section III, Class 1 pressure vessel, in accordance with the applicable requirements of Subsection NB, as discussed in Section 2.1.2 of the FuelSolutions™ W74 Canister Storage FSAR. These include the canister shell, the top and bottom closure plates, the ports, and the associated welds, as described below. The non-pressure retaining components of the canister shell assembly are designed and fabricated as an ASME Section III, Class 1 component support in accordance with the applicable requirements of Subsection NF. These include the top and bottom shield plug assemblies and the associated welds, as described below. The basket assembly is designed and fabricated as an ASME Section III core support structure, in accordance with the applicable requirements of Subsection NG, as discussed in Section 2.1.2 of the FuelSolutions™ W74 Canister Storage FSAR.

All FuelSolutions™ W74 canister shell assembly confinement boundary material and basket assembly structural materials are ASME Code-approved stainless steel or carbon steel materials. Welding of these materials is also in accordance with the applicable requirements of the ASME Code. The corresponding material and welding specifications and properties are shown on the drawings in Section 1.3.1, and described in Section 2.3 of this SAR. The associated fracture toughness requirements are described in Section 2.1.2 of this SAR.

The canister shell assembly consists of a right circular cylindrical shell with a top end inner closure plate, a top end outer closure plate, and a bottom closure plate. The canister shell assembly also includes a shell extension and a bottom end plate that are non-pressure retaining. In addition, vent, drain, instrumentation, and leak test ports are provided. Each FuelSolutions™ W74 canister shell assembly, including both the W74M class and the W74T class canisters, contains a top and bottom carbon steel shield plug that are non-pressure retaining. The bottom shield plug is encased by the canister bottom closure plate, the shell extension, and the bottom end plate. The top shield plug is an assembly comprised of a thick shield plate with 37 independent shield plugs aligned with each upper basket storage location. Alternatively, the shield plug is comprised of a solid plate.

The FuelSolutions™ W74 canister design provides criticality control under all NCT and HAC. The FuelSolutions™ W74 basket assembly uses a conservative “flux trap” design (i.e., the neutron-absorbing materials are separated by water-filled channels that thermalize the fast neutrons and reduce the reactivity of the fuel matrix) to maintain criticality control. The effective neutron multiplication factor, k_{eff} , meets the regulatory acceptance limits for storage and transportation conditions with optimum fresh water moderation and close reflection considering all biases and uncertainties. The FuelSolutions™ W74 basket is designed to accommodate enriched fresh (unburned) fuel without the need for burnup credit (i.e., credit for fissile material depletion due to in-reactor fission reactions). Neutron moderation is provided in the FuelSolutions™ W74 basket assembly by the geometric spacing of the guide tube assemblies and by borated stainless steel neutron-absorbing material incorporated into the guide tube assemblies. The geometric spacing is maintained by the spacer plates that support the guide tubes and the SNF assemblies. The borated neutron absorber panels are secured to the guide tubes by welded stainless steel retainers. The borated neutron absorber materials in the basket are non-structural members, and no structural credit is taken for borated materials.

The FuelSolutions™ W74 upper and lower canister basket assemblies consist of a series of circular spacer plates with machined openings, held in position axially by four welded support tubes that run through support sleeves placed between the spacer plates. The bottom end of the upper basket assembly is equipped with a thick stainless steel engagement plate that rests on top of the lower basket support tubes. The engagement plate provides support for the SNF assemblies in the upper basket with the canister in the vertical orientation. The basket openings are fitted with guide tube assemblies that consist of built-up layers of an inner structural tube and borated neutron absorber sheets (borated stainless). Additional product literature that describes the properties of the borated stainless material is provided in Section 1.3.2.1. The properties of borated stainless steel, including its chemical composition, physical properties, minimum boron content and means of verification, are discussed further in Section 6.3.2 of this SAR. No borated materials are formed/bent, welded, or used as structural members.

The basket spacer plates and support tubes are fabricated from high-strength carbon steel or stainless steel to provide maximum strength, optimize thermal performance, and minimize weight. The carbon steel basket components are plated with electroless nickel (EN) for corrosion protection following canister fabrication and during the brief period when the canister is filled with water for SNF loading, prior to backfilling with a non-corrosive inert gas (i.e., helium). High phosphorus EN plating with a thickness that is suitable for moderate service conditions is specified, and is to be applied in accordance with the requirements of ASTM B733.¹³ EN plating has been used extensively over the past 50 years in a broad range of industrial applications. EN plating has been studied and tested extensively over the last 25 years, and nationally recognized industry standards and specifications have been developed for its use. The use of EN plating for the FuelSolutions™ W74 canister and its service environment, including interactions with other materials, has been thoroughly evaluated by BFS and found to meet all the applicable performance requirements. The use of EN is discussed further in Section 2.4.4 of this SAR. Additional product literature that describes the properties of the EN plating used for this application is provided in Section 1.3.2.2.

¹³ ASTM B733, “Standard Specification for the Autocatalytic (Electroless) Nickel-Phosphorus Coatings on Metal,” 1997.

The FuelSolutions™ W74M basket spacer plates are fabricated from EN-plated, high-strength carbon steel and high-strength stainless steel. The FuelSolutions™ W74T basket spacer plates are fabricated from EN-plated high-strength carbon steel, except for the bottom spacer plate. The bottom spacer plate is fabricated from high-strength stainless steel to facilitate a welded attachment of the guide tube retainer clip. The support tubes for both the FuelSolutions™ W74T and the W74M basket are constructed of high-strength stainless steel. All basket support sleeves are constructed of stainless steel. The basket openings are fitted with guide tube assemblies that consist of built-up layers of an inner structural tube and borated neutron absorber sheets. The inner structural tube is constructed of austenitic stainless steel for both the FuelSolutions™ W74T and W74M class basket assemblies. The borated stainless steel neutron absorbers are attached to the inner tubes with welded stainless steel retainers. The specific material designations for the FuelSolutions™ W74T class basket assemblies are shown on the drawings in Section 1.3.1.

The FuelSolutions™ W74 canister top end closure consists of a thick shield plug assembly, an inner closure plate with an instrument port cover, a vent port cover, a drain port cover, and an outer closure plate with leak test port cover. The shield plug assembly provides biological shielding for loading of the SNF assemblies in the upper basket and for canister closure operations. The inner and outer closure plates and port covers provide redundant welded closures to assure that the canister maintains confinement function during dry storage. All canister top end closure welds are liquid dye penetrant, including the inner closure welds at the root and final weld passes, and the outer closure weld at the root, intermediate, and final weld passes. In addition, the top end inner closure welds (with the exception of the vent, drain, and leak test port covers) are helium pressure tested and leak tested. This assures that the inert helium atmosphere, the integrity of the canister basket assemblies, and the contained SNF assemblies are maintained during storage and transport. Additional discussion of the FuelSolutions™ canister closure is provided in Section 2.5.2 of the FuelSolutions™ W74 Canister Storage FSAR.

The bottom end closure welding, examination, pressure testing, and leak testing is performed during canister fabrication. All longitudinal and circumferential seam welds in the canister shell are 100% radiographically examined, full penetration butt welds. The canister bottom end plate includes a weld neck to facilitate a full penetration weld to the canister shell. The canister bottom end plate weld to the canister shell is 100% radiographically examined. In addition, the bottom end plate weld and canister shell seam welds are helium pressure tested and leak tested. The canister shell extension and bottom end plate attachment welds are non-pressure retaining welds and are liquid dye penetrant examined.

Gross Weight and Dimensions

The maximum gross shipping weight of a FuelSolutions™ Transportation Package, including the FuelSolutions™ TS125 Transportation Cask with impact limiters, the canister, and the SNF payload, is nominally 285,000 lbs. The package weight is addressed further in Section 1.2.1.5 of the FuelSolutions™ TS125 Transportation Cask SAR.

The breakdown of weights for both FuelSolutions™ W74 canister classes with the associated SNF assembly classes and configurations are provided in Section 2.2 of this SAR. The maximum loaded dry weight of a sealed FuelSolutions™ W74 canister is approximately 77,500 lbs. This is

within the design criteria used for the transportation cask discussed in Section 1.2.3 of the FuelSolutions™ TS125 Transportation Cask SAR.

The overall dimensions of each type of FuelSolutions™ W74 canister are summarized in Table 1.2-2 and shown on the drawings contained in Section 1.3.1. These canister dimensions conform to the standardized physical interface with the FuelSolutions™ TS125 Transportation Cask, as discussed in the FuelSolutions™ TS125 Transportation Cask SAR.

1.2.1.2 Other FuelSolutions™ Canister Features

Receptacles, Valves, Testing/Sampling Ports

The ports on a FuelSolutions™ W74 canister include a drain port, a vent port, and an instrument port. The drain and vent ports are used to drain the canister cavity and to backfill it with helium following canister fuel loading, to provide an inert atmosphere for dry storage and transport. The instrument port is for pressure monitoring during FuelSolutions™ W74 canister refueling, if unloading is necessary. Additional discussion of the canister design features used for canister fuel loading and unloading are provided in Section 1.2.1.3 of the FuelSolutions™ W74 Canister Storage FSAR.

The FuelSolutions™ W74 canister ports are not part of the FuelSolutions™ Transportation Package containment boundary. The location of receptacles, valves, and ports on the containment boundary of the FuelSolutions™ TS125 Transportation Cask is addressed in Section 1.2.1.6 of the FuelSolutions™ TS125 Transportation Cask SAR.

Heat Dissipation

The design basis heat load of the radioactive contents for a FuelSolutions™ W74 canister for transportation is 22,000 watts, with a maximum linear heat generation rate (LHGR) of 192 watts/inch. The design basis axial heat generation profile for the FuelSolutions™ W74 canister is discussed in Section 3.1.3 of this SAR. Heat dissipation from a FuelSolutions™ TS125 Transportation Cask is addressed in Section 1.2.3.4 of the FuelSolutions™ TS125 Transportation Cask SAR.

Coolants

No coolants are used within a FuelSolutions™ W74 canister other than helium within the canister cavity, as discussed in Chapter 3 of this SAR. Coolants for the FuelSolutions™ TS125 Transportation Cask are addressed in Section 1.2.1.6 of the FuelSolutions™ TS125 Transportation Cask SAR.

Protrusions

There are no protrusions on a FuelSolutions™ W74 canister. Protrusions on the FuelSolutions™ TS125 Transportation Cask are addressed in Section 1.2.1.6 of the FuelSolutions™ TS125 Transportation Cask SAR.

Lifting and Tiedown Devices

The device for lifting a FuelSolutions™ W74 canister to facilitate canister transfer is the top end outer closure plate, which has threaded counterbores for attaching a vertical lift fixture.

Additional discussion of the canister design features used for canister transfer are provided in Section 1.2.1.3 of the FuelSolutions™ W21 Canister Storage FSAR.

Since the FuelSolutions™ W21 canister is transported inside of a FuelSolutions™ TS125 Transportation Cask, the requirements for lifting and tiedown devices are not applicable to a FuelSolutions™ W74 canister. The design of the FuelSolutions™ TS125 Transportation Cask for lifting and tie down is addressed in Section 1.2.1.6 of the FuelSolutions™ TS125 Transportation Cask SAR.

Pressure Relief System

The FuelSolutions™ W74 canister is a seal welded pressure vessel with no penetrations that is designed to withstand the maximum internal pressure for all design basis conditions. Thus, there is no pressure relief system on a FuelSolutions™ W74 canister. Pressure relief for the FuelSolutions™ TS125 Transportation Cask is addressed in Section 1.2.1.6 of the FuelSolutions™ TS125 Transportation Cask SAR.

Shielding

A FuelSolutions™ W74 canister loaded with SNF assemblies contains both gamma and neutron radiation sources. Biological shielding for the package is provided as follows:

- For the attenuation of gamma radiation, shielding between the radioactive contents and the exterior surface of a package is provided by the FuelSolutions™ TS125 Transportation Cask and also by the FuelSolutions™ W74 canister (the internal basket assembly, cylindrical shell, shield plugs at each end, redundant top closure plates, the bottom closure plate, and the bottom end plate).
- For attenuation of neutron radiation, the center region of the transportation cask body between the impact limiters and the bottom end of the cask have a layer of hydrogenous, solid neutron shielding material.

Further discussion of the shielding characteristics of the FuelSolutions™ W74 canister is provided in Chapter 5 of this SAR. The shielding features for the FuelSolutions™ TS125 Transportation Cask are described in Section 1.2.1.6 of the FuelSolutions™ TS125 Transportation Cask SAR.

Miscellaneous Features

An SNF fuel assembly that is considered to be a damaged fuel assembly, as defined in Section 1.2.3, is placed in a Fuel Solutions™ W74 damaged fuel can to assure that the associated fissile and radioactive materials remain within the damaged fuel can. The damaged fuel can is designed and fabricated using the same material to the same criteria as the canister basket guide tubes. The damaged fuel can is sized to accommodate an SNF assembly and incorporates borated stainless steel neutron absorbers for criticality control. The damaged fuel can has a bottom plate and lid with screened holes to provide for water drainage and vacuum drying following canister fuel loading. The damaged fuel can lid is removable and has mechanical catches that secure it to the can assembly. The lid has lifting handles to allow the lid and the damaged fuel can to be handled and placed in the Fuel Solutions™ W74 canister basket. The damaged fuel cans are placed in the support tubes of the upper and lower basket assemblies, which are oversized for

this purpose. Drawings for the Fuel Solutions™ W74 damaged fuel can are provided in Section 1.3.1.

Permanent FuelSolutions™ W74 canister identification information is provided on the outside of the top closure plate and the bottom end plate. The permanent identification markings on the FuelSolutions™ W74 canister are discussed further in Section 9.1.7.2 of the FuelSolutions™ W74 Canister Storage FSAR.

1.2.1.3 Non-Packaging Support Equipment

The FuelSolutions™ support equipment used to facilitate FuelSolutions™ W74 canister loading, closure, and transfer operations is shown schematically in Figure 1.2-1 and described in Section 1.2.1.4 of the FuelSolutions™ Storage System FSAR. In addition, FuelSolutions™ support equipment is used to handle and transport the FuelSolutions™ Transportation Package, as described in Section 1.2.1.7 of the FuelSolutions™ TS125 Transportation Cask SAR.

1.2.2 Operational Features

The operations associated with the FuelSolutions™ TS125 Transportation Cask and the FuelSolutions™ W74 canisters are similar to other licensed transportation packages. The FuelSolutions™ W74 canisters are designed to be loaded in a spent fuel pool while inside a FuelSolutions™ TS125 Transportation Cask. However, a FuelSolutions™ W74 canister being loaded for on-site storage prior to off-site transport would typically be loaded while inside a FuelSolutions™ W100 Transfer Cask, as described in Section 1.2.2 of the FuelSolutions™ W74 Canister Storage FSAR. After interim storage on-site, a loaded FuelSolutions™ W74 canister can be transferred from a FuelSolutions™ W150 Storage Cask into a FuelSolutions™ TS125 Transportation Cask using a FuelSolutions™ W100 Transfer Cask. With a transfer cask, a loaded FuelSolutions™ W74 canister can be transferred into a FuelSolutions™ TS125 Transportation Cask either vertically or horizontally using FuelSolutions™ SFMS support equipment. These capabilities and equipment are discussed further in Section 1.2.2 of the FuelSolutions™ TS125 Transportation Cask SAR.

FuelSolutions™ W74 Canister

The FuelSolutions™ W74 canister incorporates several design features to facilitate off-site canister transportation operations. These features include the following:

- Top and bottom shield plugs, which allow vertical or horizontal canister transfer while maintaining occupational exposures ALARA.
- Threaded counterbores on the outer top closure plate for vertical lifting fixture attachment and installation of the horizontal transfer pintle.
- Threaded counterbores on the bottom end plate for installation of the horizontal transfer pintle.

FuelSolutions™ TS125 Transportation Cask

The FuelSolutions™ TS125 Transportation Cask design incorporates several design features that facilitate the transfer of a FuelSolutions™ canister. Key operational features of the transportation

cask and impact limiters are discussed further in Section 1.2.2 of the FuelSolutions™ TS125 Transportation Cask SAR.

1.2.2.1 Horizontal Canister Transfer

The FuelSolutions™ W74 canister is designed for horizontal transfer from or to a storage cask, and from or to a transportation cask via a transfer cask. The basic operations are discussed further in Section 1.2.2.1 of the FuelSolutions™ TS125 Transportation Cask SAR.

1.2.2.2 Vertical Canister Transfer

The FuelSolutions™ W74 canister is designed for vertical transfer from or to a transportation cask, and from or to a storage cask via a transfer cask. The basic operations for a typical vertical transfer of a canister from a storage cask to a transportation cask are discussed further in Section 1.2.2.3 of the FuelSolutions™ TS125 Transportation Cask SAR.

1.2.2.3 Canister Loading, Closure, and Opening

Basic SNF loading, closure, and opening operations for the FuelSolutions™ W74 canister are described in Sections 1.2.2.1 and 1.2.2.2 of the FuelSolutions™ Storage System FSAR. Canister-specific operations are provided in Sections 1.2.2.1 and 1.2.2.2 of the FuelSolutions™ W74 Canister Storage FSAR.

1.2.3 Contents of Packaging

1.2.3.1 Spent Fuel to be Transported

The FuelSolutions™ W74 canister is designed to accommodate up to 64 SNF assemblies (up to 32 each in the upper and lower baskets). Mechanical stops are placed over the remaining center guide tube openings of the basket to prevent fuel assemblies from being loaded at those locations. The FuelSolutions™ W74 canister accommodates Big Rock Point (BRP) BWR SNF assemblies without flow channels. The acceptance criteria that must be satisfied by the licensee to qualify SNF assemblies for transportation in the FuelSolutions™ W74 canister are delineated in Table 1.2-4. It is the responsibility of the licensee to assure that the fuel assemblies to be placed in the FuelSolutions™ W74 canister meet these criteria.

In addition to dimensional acceptance (specified in Table 1.2-5), the SNF assemblies to be stored in the FuelSolutions™ W74 canister must be zircaloy-clad fuel. Missing fuel rods may be replaced with dummy rods that displace an equal amount of water as the original rods to permit such fuel assemblies to be transported in the FuelSolutions™ W74 canister.

The FuelSolutions™ W74 canister may be loaded with fewer than 64 fuel assemblies, provided that dummy fuel assemblies are placed in the remaining empty canister guide tubes (other than the center guide tubes). The dummy fuel assemblies maintain the minimum total package weight and the center of gravity near the centerline of the canister. The dummy fuel assemblies are required to have approximately the same cross-section width, length, and total weight shown in Table 1.2-5 for the fuel assembly class to be loaded.

The structural analysis of the FuelSolutions™ W74 canister for the bounding BRP fuel assembly (maximum total weight and maximum weight per unit length) described in Chapter 2 of this

SAR, qualifies the BRP fuel assemblies (see Table 1.2-5) for storage in either FuelSolutions™ W74 canister class (see Table 1.2-1 and Table 1.2-2). In addition, the maximum total loaded weight of the FuelSolutions™ W74 canister is shown to be bounded by or equivalent to the design basis canister weight used in the structural analysis of the FuelSolutions™ TS125 Transportation Cask, as documented in Section 1.2.3 of the FuelSolutions™ TS125 Transportation Cask SAR.

Thermal qualification of the SNF assembly classes listed in Table 1.2-5 for transport in the FuelSolutions™ W74 canister is based on the maximum decay heat load and the axial peaking profile over the active fuel length of the SNF assembly, as described in Section 3.1.3 of this SAR. The licensee is required to assure that these values are not exceeded for each SNF assembly, based on the characteristics of the unburned SNF assembly (uranium content and initial enrichment), the characteristics of the SNF assembly at the time of reactor discharge (burnup and axial peaking profile), and the time since discharge (cooling time). The combinations of initial enrichment, burnup, and cooling time for each SNF assembly class accommodated by the FuelSolutions™ W74 canister are to be determined such that the thermal acceptance criteria for the FuelSolutions™ Transportation Package are satisfied, as described in Section 3.1.4 of this SAR and the FuelSolutions™ TS125 Transportation Cask SAR.

Radiological qualification of the SNF assembly classes listed in Table 1.2-5 to be transported in the FuelSolutions™ W74 canister is also dependent on the characteristics of the unburned fuel assembly, the characteristics of the fuel assembly at the time of reactor discharge, and the time since discharge (cooling time). A range of combinations of initial enrichment, burnup, and cobalt content is included in the development of radiological source terms, as documented in Section 5.2 of this SAR. The required minimum cooling time is determined such that the regulatory dose limits for the FuelSolutions™ Transportation Package are satisfied as the basis for radiological fuel qualification. The resulting minimum acceptable cooling time for the BRP UO₂ fuel assemblies accommodated by the FuelSolutions™ W74 canister is provided in Table 1.2-6.

Criticality safety qualification of the SNF assembly classes listed in Table 1.2-5 to be transported in the FuelSolutions™ W74 canister is dependent on the initial enrichment, the theoretical UO₂ density of the fuel pellet, and the geometry of the fuel assembly components. The criticality analysis for the most reactive BRP fuel assemblies (documented in Section 6.4 of this SAR) qualifies the fuel assemblies listed in Table 1.2-5 that meet the fuel assembly parameters listed in Table 6.1-1 of this SAR for transport in either FuelSolutions™ W74 canister class (see Table 1.2-1 and Table 1.2-2). The resulting maximum acceptable initial enrichments, regardless of burnup or cooling time for the fuel assembly, for the BRP UO₂ fuel assemblies are provided in Table 1.2-6.

The FuelSolutions™ W74 canister, as designed, will also accommodate BRP MOX, partial, and damaged SNF assemblies, as discussed in the paragraphs that follow.

1.2.3.1.1 Mixed-Oxide (MOX) Fuel Assemblies

The BRP MOX fuel assemblies have the same envelope dimensions and weight as the BRP UO₂ fuel assemblies shown in Table 1.2-5. Thus, the structural evaluation for the FuelSolutions™ W74 canister and basket described in Chapter 2 of this SAR is the same for BRP UO₂ and MOX fuel assemblies.

BRP MOX fuel assemblies have significantly longer minimum cooling times than those required for BRP UO₂ fuel assemblies, as indicated in Table 1.2-7. The BRP MOX fuel assemblies are shown to have thermal source terms that are bounded by the design basis BRP UO₂ fuel assembly thermal source, as discussed in Section 3.6.4 of this SAR.

Similarly, the longer cooling times required for the BRP MOX fuel assemblies, as indicated in Table 1.2-7, result in dose rates that are bounded by those of the design basis BRP UO₂ fuel assemblies, as discussed in Section 5.5.1 of this SAR.

Since there are different BRP MOX fuel assembly designs, as indicated in Table 1.2-7, the criticality qualification for BRP MOX fuel assemblies is performed explicitly for each BRP MOX fuel assembly design, as discussed in Section 6.6.1 of this SAR.

1.2.3.1.2 Partial Fuel Assemblies

Partial BRP fuel assemblies have one or more full-length fuel rods missing but are otherwise intact, and thus, are not required to be placed in a damaged fuel can. The envelope dimensions and weight of the partial BRP fuel assemblies are bounded by or are the same as that of the intact BRP fuel assemblies shown in Table 1.2-5. Thus, the structural evaluation for the FuelSolutions™ W74 canister and basket described in Chapter 2 of this SAR for intact BRP fuel assemblies is bounding for partial BRP fuel assemblies.

The thermal and radiological sources for damaged BRP fuel assemblies are likewise bounded by those for intact BRP fuel assemblies, and thus have the same minimum cooling time as intact BRP fuel assemblies. Thus, the thermal and radiological evaluations of the W74 canister for intact BRP fuel assemblies are bounding for partial BRP fuel assemblies, as discussed in Sections 3.6.5 and 5.5.2 of this SAR.

Partial BRP fuel assemblies have different initial enrichment limits than those of intact fuel assemblies due to the potential for a more reactive assembly configuration, as discussed in Section 6.6.2 of this SAR.

1.2.3.1.3 Damaged Fuel Assemblies

Damaged BRP fuel assemblies are those with fuel rod cladding damage in excess of pinhole leaks or hairline cracks. Fuel assemblies with damaged grid spacers (defined as damaged to a degree where fuel rod structural integrity cannot be assured, or where grid spacers have shifted vertically from their design position) are also considered damaged fuel assemblies. Damaged BRP fuel assemblies are to be placed in damaged fuel cans, as discussed in Section 1.2.1.2.

Damaged BRP fuel assemblies that have been placed in damaged fuel cans are to be loaded into the FuelSolutions™ W74 canister basket support tubes, which are oversized for this purpose. The combined weight of the fuel assembly and the damaged fuel can is considered in the structural analysis of the FuelSolutions™ W74 canister, as discussed in Section 2.2 of this SAR.

The thermal and radiological sources for partial BRP fuel assemblies are bounded by those for the intact BRP fuel assemblies. However, the damaged fuel can provides an additional item through which the decay heat of the fuel assembly is to be removed, as discussed in Section 3.6.6 of this SAR. The damaged fuel can provides additional radiological shielding, thus the radiological evaluations of the W74 canister for intact BRP fuel assemblies bound those for damaged BRP fuel assemblies, as discussed in Section 5.5.3 of this SAR.

Damaged fuel assemblies have different enrichment limits than those of intact fuel assemblies, due to the potential for a more reactive assembly configuration, as discussed in Section 6.6.3 of this SAR.

1.2.3.2 Radionuclide Inventory

The design basis gamma and neutron source terms for the total payload contents of a FuelSolutions™ W74 canister for transportation are $4.9E+16$ gammas/sec-canister and $3.2E+09$ neutrons/sec-canister, respectively, as discussed in Section 5.2 of this SAR. A breakdown of the gamma and neutron source terms by energy group is also provided in Section 5.2 of this SAR. The corresponding radionuclide inventory is provided in Section 4.3 of this SAR. A higher canister neutron source strength is permitted for a FuelSolutions™ W74 canister containing mixed-oxide Big Rock Point assemblies, as discussed in Section 5.5 of this SAR. All existing mixed-oxide Big Rock Point fuel is shown to be radiologically qualified as discussed in Section 5.5.1.

1.2.3.3 Maximum Payload Weight

The maximum payload weight for the SNF radioactive contents within a FuelSolutions™ W74 canister is 31,360 pounds, as discussed in Section 2.2 of this SAR. This weight occurs for the FuelSolutions™ W74 canister SNF assemblies that are the heaviest of all allowable contents. A breakdown of the specific payload weights and total canister weights are provided in Section 2.2 of this SAR.

1.2.3.4 Maximum Decay Heat

The maximum design basis decay heat load for FuelSolutions™ W74 canister is 22,000 watts, as discussed in Section 3.1.4 of this SAR. The basis for this value and a discussion of the FuelSolutions™ W74 canister thermal characteristics are provided in Section 3.1.4 of this SAR.

1.2.3.5 Maximum Pressure Buildup

The FuelSolutions™ TS125 Transportation Cask is designed for a maximum internal pressure of 75 psig, as discussed in Section 1.2.3.5 of the FuelSolutions™ TS125 Transportation Cask SAR. The maximum normal operating pressure (MNOP) of 10.7 psig and the maximum HAC pressure of 29.3 for the FuelSolutions™ W74 canister are bounded by the maximum design pressure for the transportation cask, as discussed in Section 3.1.5 of this SAR. Note that although no credit is taken for the containment capability of the canister shell assembly, the transportation cask would only be subjected to these internal pressures if the canister shell is leaking or is breached.

Since no credit is taken for the containment capability of the canister shell assembly, the external pressure requirements of 10CFR71.61 do not apply.

1.2.4 Compliance with 10CFR71

The FuelSolutions™ W74 canister described in this SAR, together with the FuelSolutions™ TS125 Transportation Cask and impact limiters described in the FuelSolutions™ TS125 Transportation Cask SAR, fully comply with the requirements of 10CFR71. These include the general standards for all packages specified in 10CFR71.43, the requirements for NCTs defined in 10CFR71.71, and the requirements for HACs defined in 10CFR71.73. The specific SAR

sections that address these 10CFR71 requirements are identified in Table 1.0-1. The structural, thermal, containment, shielding, and criticality requirements of 10CFR71 are addressed in Chapters 2 through 6 of this SAR and the FuelSolutions™ TS125 Transportation Cask SAR. The operational requirements of 10CFR71 are addressed in Chapter 7 of the FuelSolutions™ TS125 Transportation Cask SAR. Operations that are specific to the FuelSolutions™ W74 canister are addressed in Chapter 7 of this SAR. The acceptance test and maintenance program requirements for the FuelSolutions™ W21 canister are addressed in Chapter 9 of the FuelSolutions™ W74 Canister Storage FSAR.

Table 1.2-1 - Principal Characteristics of the FuelSolutions™ W74 Canister

Characteristic	W74M ⁽²⁾	W74T ⁽²⁾
Gross Weight (empty)	44,900 lbs.	42,700 lbs.
Materials of Construction for Canister Shell ⁽¹⁾	Stainless Steel	
Materials Used As Neutron Absorbers and Moderators	Borated Stainless Steel	
External Dimensions: Diameter Length	66 inches	
	192.25 inches	
Cavity Size: Diameter Length	64.75 inches	
	173.0 inches	
Internal Structures	Coated Carbon Steel Spacer Plates and Stainless Steel Support Tube Basket Assembly	
External Structures	None	
Receptacles	N/A	
Valves	Vent & Drain Fittings	
Sampling Ports	Instrument Port Available during Canister Reflooding, Outer Closure Plate Leak Test Port	
Means of Passive Heat Dissipation	Conduction, Convection, and Radiation	
Volume of Coolant	N/A	
Type of Coolant	N/A	
Outer Protrusions	None	
Inner Protrusions	Vent & Drain Port Bodies and Drain Tube	
Lifting Devices	Separate Lifting Fixture	
Impact Limiters	N/A	
Amount of Shielding: Radial Bottom End Top End	5/8-inch thick Stainless Steel	
	5.75-inch Carbon Steel / 2.75-inch Stainless Steel	
	7.25-inch Carbon Steel / 3.00-inch Stainless Steel	
Pressure Relief Systems	None	
Closures	Welded Inner and Outer Top Cover Plates	
Means of Confinement	All Welded Construction with No Penetrations or Mechanical Seals	
Model Number-Cavity Designator	W74M	W74T
Description of How Individual Casks Will Be Identified	Individually Stamped (see Section 9.1.7.2 of the FuelSolutions™ W74 Canister Storage FSAR)	

Notes:

- (1) Structural confinement materials for storage only.
- (2) All dimensions are nominal.

Table 1.2-2 - Matrix of FuelSolutions™ W74 Canister Configurations

Canister Configuration⁽²⁾	W74M⁽¹⁾	W74T⁽¹⁾
Overall Length, inch	192.25	192.25
Outside Diameter, inch	66.00	66.00
Shell Thickness, inch	0.63	0.63
Upper Basket		
Basket Length (including engagement sleeve), inch	87.25	87.25
Number of Spacer/Engagement Plates	15	14
CS Spacer Plate Thickness, inch	0.75	0.75
SS Spacer Plate Thickness, inch	2.00	NA
SS Engagement Spacer Plate Thickness, inch	2.00	2.00
Borated Neutron Absorber Panel Thickness, inch	0.075	0.075
Lower Basket		
Basket Length, inch	85.25	85.25
Number of Spacer Plates	14	13
CS Spacer Plate Thickness, inch	0.75	0.75
SS Spacer Plate Thickness, inch	2.00	NA
Borated Neutron Absorber Panel Thickness, inch	0.075	0.075
Basket Support and Guide Tubes		
Number of Support Tubes, each basket	4	4
SS Support Tube Inside Dimension (square), inch	7.40	7.40
SS Support Tube Thickness, inch	0.63	0.63
Number of Guide Tubes, each basket	28	28
SS Guide Tube Inside Dimension (square), inch	6.90	6.90
SS Guide Tube Thickness, inch	0.09	0.09
Top Closure		
Shield Plug ⁽²⁾ Thickness, inch	7.25	7.25
Shield Plug ⁽²⁾ Material	Carbon Steel	Carbon Steel
Inner Closure Plate Thickness, inch	1.00	1.00
Outer Closure Plate Thickness, inch	2.00	2.00
Bottom Closure		
End Plate Thickness, inch	1.75	1.75
Shield Plug Thickness, inch	5.75	5.75
Shield Plug Material	Carbon Steel	Carbon Steel
Closure Plate Thickness, inch	1.00	1.00
Cavity Length, inch	173.00	173.00

Notes:

- (1) All dimensions are nominal.
- (2) Top shield plug with individual plugs or solid plate.
- (3) CS - Carbon Steel, SS - Stainless Steel.

Table 1.2-3 - FuelSolutions™ W74 Canister Design Criteria Summary (3 pages)

Type	Criteria or Reference	Basis ⁽¹⁾
Design Life:	-	-
Design	100 yrs.	W74 Canister Storage FSAR Section 2.1.2
Regulatory:	-	-
Storage	20 yrs.	10CFR72.230
Transportation	5 yrs.	10CFR71.38 & C of C
Contents of Application:	-	-
The applicant shall identify any established codes and standards proposed for use in the package design, fabrication, assembly, testing, maintenance, and use:	-	10CFR71.31(c)
Containment Boundary	Provided by TS125 Transportation Cask (see WSNF-120, Chapter 4)	Reg. Guide 7.6, Section B
Shell and Closure Plates	ASME Code, Section III, Subsection NB	Reg. Guide 7.6, Section B
Basket Assembly	ASME Code, Section III, Subsection NG	Reg. Guide 7.6, Section B
Outer Closure Plate Vertical Lifting Points	NUREG-0612 & ANSI N14.6	NUREG-1567
Package Description:	-	-
Classification	See WSNF-120, Section 1.1	10CFR71.33(a)(1)
Max. Gross Weight (dry)	See Table 2.2-1	10CFR71.33(a)(2)
Max. Live Load (fuel only)	See Table 2.2-1	10CFR71.33(a)(2)
External Dimensions	See Table 1.2-1	NUREG-1617
Cavity Size	See Table 1.2-1	NUREG-1617
Model Number	W74	10CFR71.33(a)(3)
Containment System Identification	Provided by TS125 Transportation Cask	10CFR71.33(a)(4)
Specific Materials of Construction, Weights, Dimensions, and Fabrication Methods for:	-	-
Receptacles	None	10CFR71.33(a)(5)(i)

Table 1.2-3 - FuelSolutions™ W74 Canister Design Criteria Summary (3 pages)

Type	Criteria or Reference	Basis⁽¹⁾
Nonfissile Neutron Absorbers or Moderators	See Table 1.2-1	10CFR71.33(a)(5)(ii)
Internal/External Structures Supporting/Protecting Receptacles	See Table 1.2-1	10CFR71.33(a)(5)(iii)
Valves, Sampling Ports, Lifting Devices, and Tiedown Devices	N/A (for transportation)	10CFR71.33(a)(5)(iv)
Structural/Mechanical Means to Transfer/Dissipate Heat	None (Passive)	10CFR71.33(a)(5)(v)
Identification/Volumes of Any Receptacles Containing Coolant	None	10CFR71.33(a)(6)
Package Contents:	-	-
Identification and Maximum Radioactivity of Radioactive Constituents	See Section 1.2.3	10CFR71.33(b)(1)
Identification and Maximum Quantities of Fissile Constituents	See Section 5.2	10CFR71.33(b)(2)
Chemical/Physical Form	See Section 1.2.3	10CFR71.33(b)(3)
Extent of Reflection	See Section 6.3.1	10CFR71.33(b)(4)
Amount/Identity of Nonfissile Materials Used as Neutron Absorbers or Moderators	See Section 6.3.1	10CFR71.33(b)(4)
Atomic Ratio of Moderator to Fissile Constituents	See Section 6.3.1	10CFR71.33(b)(4)
Maximum Normal Operating Pressure (MNOP)	10.7 psig	10CFR71.33(b)(5)
Maximum Weight:	See Maximum Gross Weight	10CFR71.33(b)(6)
Maximum Amount of Decay Heat	22,000 watts	10CFR71.33(b)(7)
Identification/Volumes of Any Coolants	N/A	10CFR71.33(b)(8)
Package Evaluation:	-	-
Allowable Number of Packages that May Be Transported in the Same Vehicle	One Canister per TS125 Transportation Cask, Exclusive Use Shipments	10CFR71.35(b)

Table 1.2-3 - FuelSolutions™ W74 Canister Design Criteria Summary (3 pages)

Type	Criteria or Reference	Basis ⁽¹⁾
General Package Standards	See Table 1.2-3 in TS125 Transportation Cask SAR	10CFR71.43
Lifting/Tiedown Standards:	-	-
Lifting Devices	NUREG-0612 & ANSI N14.6	10CFR71.45(a)
Tiedown Devices	N/A	10CFR71.45(b)(1)
External Radiation Standards: Radiation levels	See Table 1.2-3 in TS125 Transportation Cask SAR	10CFR71.47(a)
General Requirements for Fissile Material Packages	See Table 1.2-3 in TS125 Transportation Cask SAR	10CFR71.55
Special Requirements for Irradiated Nuclear Fuel Shipments	See Table 1.2-3 in TS125 Transportation Cask SAR	10CFR71.61
Unknown Contents Properties Assumptions	(2)	10CFR71.83
Preliminary Determinations	See Table 1.2-3 in TS125 Transportation Cask SAR	10CFR71.85
Routine Determinations	See Table 1.2-3 in TS125 Transportation Cask SAR	10CFR71.87
Opening Instructions	See Table 1.2-3 in TS125 Transportation Cask SAR	10CFR71.89
Quality Assurance	See Table 1.2-3 in TS125 Transportation Cask SAR	10CFR71.101(b)
Handling, Storage, and Shipping	See Table 1.2-3 in TS125 Transportation Cask SAR	10CFR71.127
Additional Criteria:	-	-
Thermal:	-	-
Maximum Design (Allowable) Material Temperatures	See Tables 2.1-3, 2.1-4, and 2.3-3 through 2.3-9	-
Insulation	Protected by TS125 Transportation Cask	10CFR71.71(c)(1)
Retrievability (NCT and HAC):	No Encroachment on Spent Fuel	-
NCT Loads and Conditions	See Table 1.2-3 in TS125 Transportation Cask SAR	-
HAC Design Events and Conditions	See Table 1.2-3 in TS125 Transportation Cask SAR	-

Notes:

(1) See Table 1.0-1 for cross-references to applicable SAR sections.

(2) The FuelSolutions™ W74 canister is not evaluated for failed fuel in this SAR; therefore, no assumptions have been made relative to unknown properties of fissile materials.

**Table 1.2-4 - FuelSolutions™ W74 Canister SNF Assembly
Acceptance Criteria for Transport (6 pages)**

Payload Designation	<u>W74-1</u>: Intact UO₂ Fuel Assemblies
SNF Parameter	Loading/Acceptance Criteria
Payload Description	<p>≤ 64 Big Rock Point BWR intact^(1, 2) UO₂ fuel assemblies, as defined in Table 1.2-5. Any remaining empty canister basket guide tubes and/or support tubes may be loaded with fuel assemblies meeting any of the acceptable payload specifications W74-2 through W74-6, subject to the limitations of those specifications.</p> <p>If less than 64 total fuel assemblies are loaded, a dummy fuel assembly is to be placed into each empty canister basket guide tube and/or support tube. Each dummy fuel assembly is to be the approximate weight and size of the intact fuel assembly, as defined in Table 1.2-5.</p>
Cladding Material/Condition	Zircaloy cladding with no known or suspected cladding defects greater than hairline cracks or pinhole leaks.
Maximum Weight	≤ 485 pounds per fuel assembly, as defined in Table 1.2-5.
Maximum Heat Load	≤ 0.344 kW per fuel assembly.
Maximum Uranium Loading	≤ 142.1 kg, as defined in Table 1.2-6.
Maximum Initial Enrichment ⁽³⁾	≤ 4.10 w/o ²³⁵ U, as defined in Table 1.2-6 for the fuel assembly parameters defined in Table 6.1-1 of this SAR.
Maximum Burnup	≤ 32,000 MWd/MTU, as defined in Table 1.2-6.
Minimum Cooling Time	≥ 6.0 years, irrespective of fuel assembly type, enrichment, burnup; and total cobalt content, as defined in Table 1.2-6. The effects of the maximum acceptable gamma and neutron sources are incorporated into the minimum cooling time determination. ⁽⁴⁾

W74-1 Notes:

- (1) Intact fuel assemblies include those BRP fuel assemblies with 1 to 4 corner rods missing, and BRP 9x9 fuel assemblies with 1 rod missing from a non-corner location. This includes assemblies with partial length rods, or rod fragments inside stainless tubes, in any of the array corner locations. It also includes 9x9 assemblies with 11x11 assembly rods in corner locations.
- (2) Intact assemblies may have any number of fuel rods replaced with solid zircaloy or stainless steel rods, or with poison rods. They may also have any object other than fuel rods placed in the empty array or guide tube locations, including all forms of inserts or control components.
- (3) Defined as the maximum array-average enrichment, which is the peak planar average initial enrichment considering all elevations along the assembly axis.
- (4) If an SNF assembly has been further irradiated after having fuel rods replaced by dummy stainless rods, an evaluation must be performed that shows that the active fuel region non-fuel gamma source strength is bounded by that described in Section 5.2.2.1 of this SAR.

**Table 1.2-4 - FuelSolutions™ W74 Canister SNF Assembly
 Acceptance Criteria for Transport (6 pages)**

Payload Designation	W74-2: Intact MOX Fuel Assemblies
SNF Parameter	Loading/Acceptance Criteria
Payload Description	<p>≤ 64 Big Rock Point BWR intact MOX fuel assemblies, as defined in Table 1.2-6. Any remaining empty canister basket guide tubes and/or support tubes may be loaded with fuel assemblies meeting any of the acceptable payload specifications W74-1 and W74-3 through W74-6, subject to the limitations of those specifications.</p> <p>If less than 64 total fuel assemblies are loaded, a dummy fuel assembly must be placed into each empty canister basket guide tube and/or support tube. Each dummy fuel assembly must be the approximate weight and size of the intact fuel assembly, as defined in Table 1.2-5.</p>
Cladding Material/Condition	Zircaloy cladding with no known or suspected cladding defects greater than hairline cracks or pinhole leaks.
Maximum Weight	≤ 485 pounds per fuel assembly, as defined in Table 1.2-5.
Maximum Heat Load	≤ 0.344 kW per fuel assembly.
Maximum Heavy Metal Loading	The heavy metal loading varies by fuel assembly type and must not exceed the maximum values defined in Table 1.2-7.
Maximum Initial Enrichment	The fuel rod initial enrichment varies by fuel assembly type and must not exceed the maximum values defined in Table 1.2-7 for MOX fuel assembly arrays bounded by those shown in Figures 6.6-1 through 6.6-4 of this SAR.
Maximum Burnup	The burnup varies by fuel assembly type and must not exceed the maximum values defined in Table 1.2-7.
Minimum Cooling Time	The cooling time varies by fuel assembly type and must not be less than the minimum values defined in Table 1.2-7. The effects of the maximum acceptable gamma and neutron sources are incorporated into the minimum cooling time determination.

W74-2 Note:

Notes 1, 2, and 4 for W74-1 apply to W74-2.

**Table 1.2-4 - FuelSolutions™ W74 Canister SNF Assembly
 Acceptance Criteria for Transport (6 pages)**

Payload Designation	W74-3: Partial UO₂ Fuel Assemblies
SNF Parameter	Limit/Specification
Payload Description	<p>≤ 64 Big Rock Point BWR partial UO₂ fuel assemblies, as defined in Table 1.2-6. Partial fuel assemblies are defined as those assemblies having one or more full-length fuel rods missing from the intact fuel assemblies defined in Table 1.2-6 (except as permitted by W74-1 Note 1). The affected array locations may contain nothing, partial length rods, hollow zircaloy or stainless steel rods, neutron source rods, or any other non-fissile material object that displaces less water than a full-length fuel rod. Any remaining empty canister basket guide tubes and/or support tubes may be loaded with fuel assemblies meeting any of the acceptable loading specifications W74-1, W74-2, and W74-4 through W74-6, subject to the limitations of those specifications.</p> <p>If less than 64 total fuel assemblies are loaded, a dummy fuel assembly must be placed into each empty canister basket guide tube and/or support tube. Each dummy fuel assembly must be the approximate weight and size of the intact fuel assembly, as defined in Table 1.2-5.</p>
Cladding Material/Condition	Zircaloy cladding with no known or suspected cladding defects greater than hairline cracks or pinhole leaks.
Maximum Weight	≤ 485 pounds per fuel assembly, as defined in Table 1.2-5.
Maximum Heat Load	≤ 0.344 kW per fuel assembly.
Maximum Uranium Loading	≤ 142.1 kg, as defined in Table 1.2-6.
Maximum Initial Enrichment ⁽¹⁾	<p>≤ 3.55 w/o ²³⁵U (missing array interior or edge rods - 9x9)</p> <p>≤ 3.6 w/o ²³⁵U (missing array interior or edge rods - 11x11)</p>
Maximum Burnup	≤ 32,000 MWd/MTU, as defined in Table 1.2-6.
Minimum Cooling Time	≥ 6.0 years, irrespective of fuel assembly type, enrichment, burnup; and total cobalt content, as defined in Table 1.2-6. The effects of the maximum acceptable gamma and neutron sources are incorporated into the minimum cooling time determination.

W74-3 Notes:

- (1) Defined as the maximum array average initial enrichment, which is the peak planar average initial enrichment considering all elevations along the fuel assembly axis. The averaging is applied only to those fuel rods that are present in the partial array.
- (2) Notes 2 and 4 for W74-1 apply to W74-3.

**Table 1.2-4 - FuelSolutions™ W74 Canister SNF Assembly
 Acceptance Criteria for Transport (6 pages)**

Payload Designation	W74-4: Partial MOX Fuel Assemblies
SNF Parameter	Loading/Acceptance Criteria
Payload Description	<p>≤ 64 Big Rock Point BWR partial MOX fuel assemblies, as defined in Table 1.2-7. Partial fuel assemblies are defined as those assemblies having one or more full-length fuel rods missing from the intact fuel assemblies defined in Table 1.2-7 (except as permitted by W74-1 Note 1). The affected array locations may contain nothing, partial length rods, hollow zircaloy or stainless steel rods, neutron source rods, or any other non-fissile material object that displaces less water than a full-length fuel rod. Any remaining empty canister basket guide tubes and/or support tubes may be loaded with fuel assemblies meeting any of the acceptable loading specifications W74-1 through W74-3, W74-5, and W74-6, subject to the limitations of those specifications.</p> <p>If less than 64 fuel assemblies are loaded, a dummy fuel assembly must be placed into each empty canister basket guide tube and/or support tube. Each dummy fuel assembly must be the approximate weight and size of the intact fuel assembly, as defined in Table 1.2-5.</p>
Cladding Material/Condition	Zircaloy cladding with no known or suspected cladding defects greater than hairline cracks or pinhole leaks.
Maximum Weight	≤ 485 pounds per fuel assembly, as defined in Table 1.2-5.
Maximum Heat Load	≤ 0.344 kW per fuel assembly.
Maximum Heavy Metal Loading	The heavy metal loading varies by fuel assembly type and must not exceed the maximum values defined in Table 1.2-7.
Maximum Initial Enrichment	The fuel rod initial enrichment varies by fuel assembly type and must not exceed the maximum values defined in Table 1.2-7 for the partial MOX fuel assembly arrays bounded by those shown in Figures 6.6-5 through 6.6-8 of this SAR.
Maximum Burnup	The burnup varies by fuel assembly type and must not exceed the maximum values defined in Table 1.2-7.
Minimum Cooling Time	The cooling time varies by fuel assembly type and must not be less than the minimum values defined in Table 1.2-7. The effects of the maximum acceptable gamma and neutron sources are incorporated into the minimum cooling time determination.

W74-4 Note:

Note 4 for W74-1 applies to W74-4.

**Table 1.2-4 - FuelSolutions™ W74 Canister SNF Assembly
 Acceptance Criteria for Transport (6 pages)**

Payload Designation	W74-5: Damaged UO₂ Fuel Assemblies
SNF Parameter	Limit/Specification
Payload Description	<p>≤ 8 Big Rock Point BWR damaged UO₂ fuel assemblies. Damaged fuel assemblies are defined as those with fuel rod damage in excess of hairline cracks or pinhole leaks. Fuel assemblies with damaged grid spacers (defined as damaged to a degree where fuel rod structural integrity cannot be assured, or where grid spacers have shifted vertically from their design position) are also considered to be damaged fuel assemblies.</p> <p>Each fuel assembly designated as damaged must be placed within a damaged fuel can and loaded into one of the four basket support tube locations in the upper and lower basket of the canister. The remaining empty canister basket guide tubes and support tubes may be loaded with fuel assemblies meeting any of the acceptable loading specifications W74-1 through W74-4 and W74-6, subject to the limitations of those specifications, for a total of ≤ 64 Big Rock Point BWR fuel assemblies.</p> <p>If less than 64 fuel assemblies are loaded, a dummy fuel assembly must be placed into each empty canister basket guide tube and/or support tube. Each dummy fuel assembly must be the approximate weight and size of the intact fuel assembly, as defined in Table 1.2-5.</p>
Cladding Material/Condition	Zircaloy cladding with fuel rod damage in excess of hairline cracks or pinhole leaks.
Maximum Weight	≤ 685 pounds per canned fuel assembly.
Maximum Heat Load	≤ 0.344 kW per fuel assembly.
Maximum Uranium Loading	≤ 142.1 kg, as defined in Table 1.2-6.
Maximum Initial Enrichment	≤ 4.61 w/o ²³⁵ U peak fuel pellet initial enrichment.
Maximum Burnup	≤ 32,000 MWd/MTU, as defined in Table 1.2-6.
Minimum Cooling Time	≥ 6.0 years, irrespective of fuel assembly type, enrichment, burnup; and total cobalt content, as defined in Table 1.2-6. The effects of the maximum acceptable gamma and neutron sources are incorporated into the minimum cooling time determination.

W74-5 Note:

Note 4 for W74-1 applies to W74-5.

**Table 1.2-4 - FuelSolutions™ W74 Canister SNF Assembly
 Acceptance Criteria for Transport (6 pages)**

Payload Designation	W74-6: Damaged MOX Fuel Assemblies
SNF Parameter	Limit/Specification
Payload Description	<p>≤ 8 Big Rock Point BWR damaged MOX fuel assemblies. Damaged fuel assemblies are defined as those with fuel rod damage in excess of hairline cracks or pinhole leaks. Fuel assemblies with damaged grid spacers (defined as damaged to a degree where the fuel rod structural integrity cannot be assured, or where the grid spacers have shifted vertically from their design position) are also considered to be damaged fuel assemblies.</p> <p>Each fuel assembly designated as damaged must be placed within a damaged fuel can and loaded into one of the four basket support tube locations in the upper and lower basket of the canister. The remaining empty canister basket guide tubes and support tubes may be loaded with fuel assemblies meeting any of the acceptable loading specifications W74-1 through W74-5, subject to the limitations of those specifications, for a total of ≤ 64 Big Rock Point BWR fuel assemblies.</p> <p>If less than 64 fuel assemblies are loaded, a dummy fuel assembly must be placed into each empty canister basket guide tube and/or support tube. Each dummy fuel assembly must be the approximate weight and size of the intact fuel assembly, as defined in Table 1.2-5.</p>
Cladding Material/Condition	Zircaloy cladding with fuel rod damage in excess of hairline cracks or pinhole leaks.
Maximum Weight	≤ 685 pounds per canned fuel assembly.
Maximum Heat Load	≤ 0.344 kW per fuel assembly.
Maximum Heavy Metal Loading	The heavy metal loading varies by fuel assembly type and must not exceed the maximum values defined in Table 1.2-7.
Maximum Initial Enrichment	≤ 4.61 w/o ²³⁵ U peak fuel pellet initial enrichment for all MOX fuel assembly types defined in Table 1.2-7, based on the formula $E_{U-235} + 0.7 \times P_{PU}$, where E_{U-235} is the ²³⁵ U initial enrichment of the uranium in the fuel pellet, and P_{PU} is the overall w/o of plutonium in the fuel pellet.
Maximum Burnup	The burnup varies by fuel assembly type and must not exceed the maximum values defined in Table 1.2-7.
Minimum Cooling Time	The cooling time varies by fuel assembly type and must not be less than the minimum values defined in Table 1.2-7. The effects of the maximum acceptable gamma and neutron sources are incorporated into the minimum cooling time determination.

W74-6 Note:

Note 4 for W74-1 applies to W74-6.

Table 1.2-5 - FuelSolutions™ W74 Canister SNF Fuel Assembly Classes Acceptable for Transport

BWR Fuel Assembly Class	Maximum Length⁽¹⁾ (in)	Width (in)	Weight (lb)	FuelSolutions™ Canister Class⁽¹⁾
Fuel Assemblies without Flow Channels				
Big Rock Point 9x9	84.8	6.52	485	M and T ⁽²⁾
Big Rock Point 11x11	84.8	6.52	485	M and T ⁽²⁾

Notes:

- (1) Maximum fuel assembly length includes an allowance for irradiation and thermal growth.
- (2) Canister class definitions are provided in Section 1.2.1.1.

Table 1.2-6 - FuelSolutions™ W74 Canister UO₂ SNF Fuel Assemblies Acceptable for Transport⁽¹⁾

Assembly Class ^{(2),(3)}	Assembly Type	Maximum Uranium Loading (kg)	Maximum Initial Enrichment (w/o ²³⁵ U)	Maximum Burnup (MWd/MTU)	Minimum Cooling Time ⁽⁴⁾ (years)	Criticality Class ⁽⁵⁾
Big Rock Point	9x9 GE	142.1	4.1	32,000	6.0	GE 9x9
	9x9 ANF	142.1	4.1	32,000	6.0	Siemens 9x9
	11x11 ANF	142.1	4.1	32,000	6.0	Siemens 11x11
	Other ⁽⁶⁾					

Notes:

- (1) Applicable to fuel acceptance specifications W74-1, W74-3, and W74-5.
- (2) Assembly Class is defined per EIA Spent Fuel Discharge Report.¹⁴
- (3) Fuel assembly dimensions and weights for each fuel assembly class are provided in Table 1.2-5.
- (4) For any versions of these assembly types that contain more than 2.9 grams cobalt in the non-fuel hardware in the core zone, the minimum cooling time is 6 years. Assemblies with over 15 grams cobalt in the non-fuel hardware in the core zone are not qualified for transport in the W74 canister.
- (5) Criticality Class definitions are per Table 6.1-1 of this SAR, and include definitions of cladding type and other fuel assembly characteristics relevant to criticality safety.
- (6) Other fuel assemblies that meet the defined parameters are qualified for transport.

¹⁴ Energy Information Administration, *Spent Nuclear Fuel Discharges from U.S. Reactors 1993*, U.S. Department of Energy, 1995.

**Table 1.2-7 - FuelSolutions™ W74 Canister MOX SNF Assemblies
 Acceptable for Transport⁽¹⁾**

Assembly Class ⁽²⁾	Assembly Type	Maximum Heavy Metal Loading (kg)	Maximum Burnup (MWd/MTIHM)	Maximum Fuel Rod Initial Enrichment (w/o)	Minimum Cooling Time (years)
Big Rock Point	J2 (9x9) ⁽³⁾	124	22,820	²³⁵ U - 4.50 PuO ₂ - 3.65	22
	DA (11x11) ⁽³⁾	126	21,850	²³⁵ U - 2.40 PuO ₂ - 2.45	22
	G-Pu (11x11) ⁽³⁾	127	34,220	²³⁵ U - 4.60 PuO ₂ - 5.45	15
	UO ₂ (9x9) w/2 MOX rods ⁽⁴⁾	(see Table 1.2-6)			

Notes:

- (1) Applicable to fuel acceptance specifications W74-2, W74-4, and W74-6.
- (2) Assembly Class is defined per EIA Spent Fuel Discharge Report.
- (3) Cobalt content is to be ≤2.9 g in the active fuel region.
- (4) This qualification specifically applies to BRP assemblies E65 and E72.

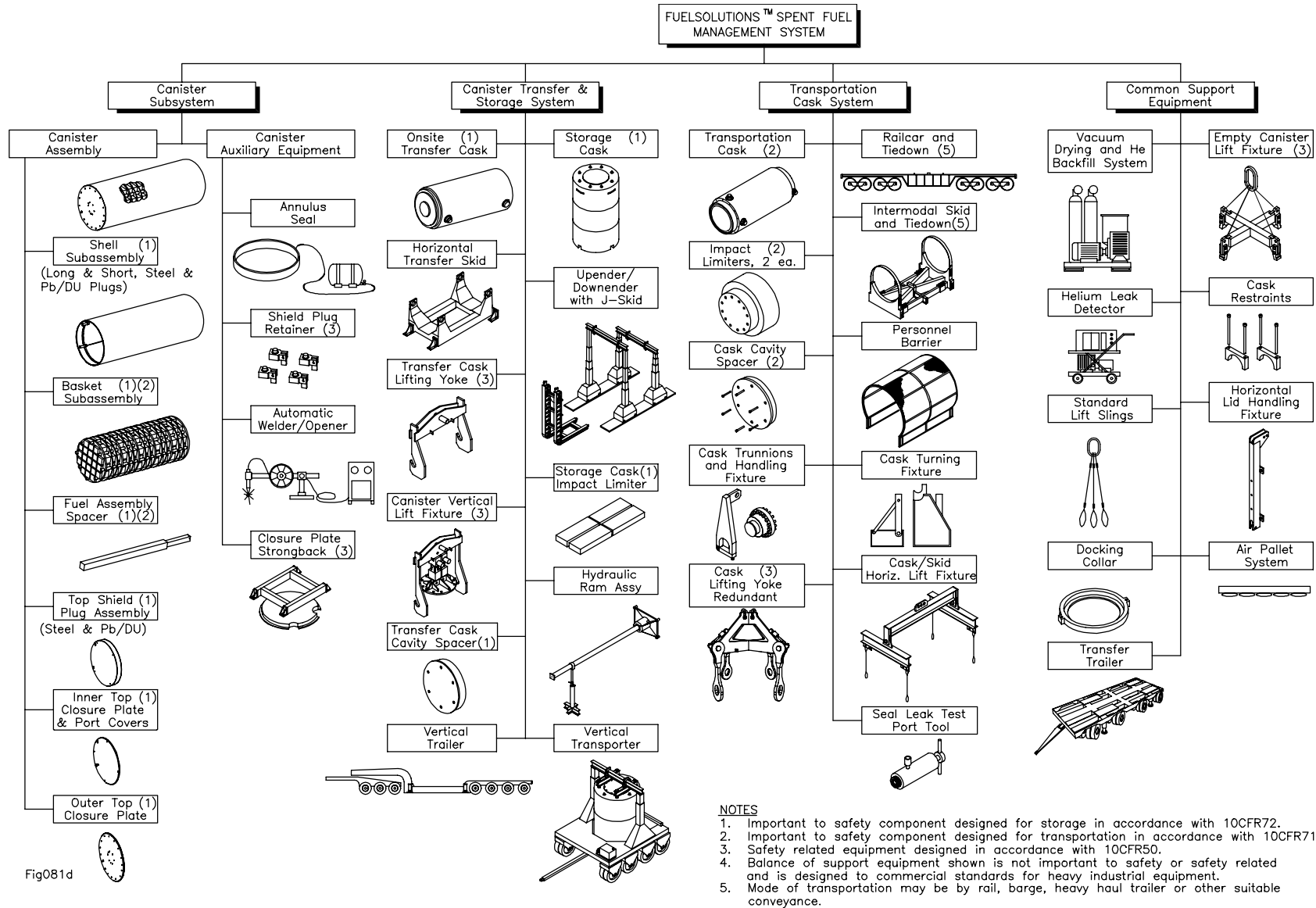


Figure 1.2-1 - FuelSolutions™ Spent Fuel Management System

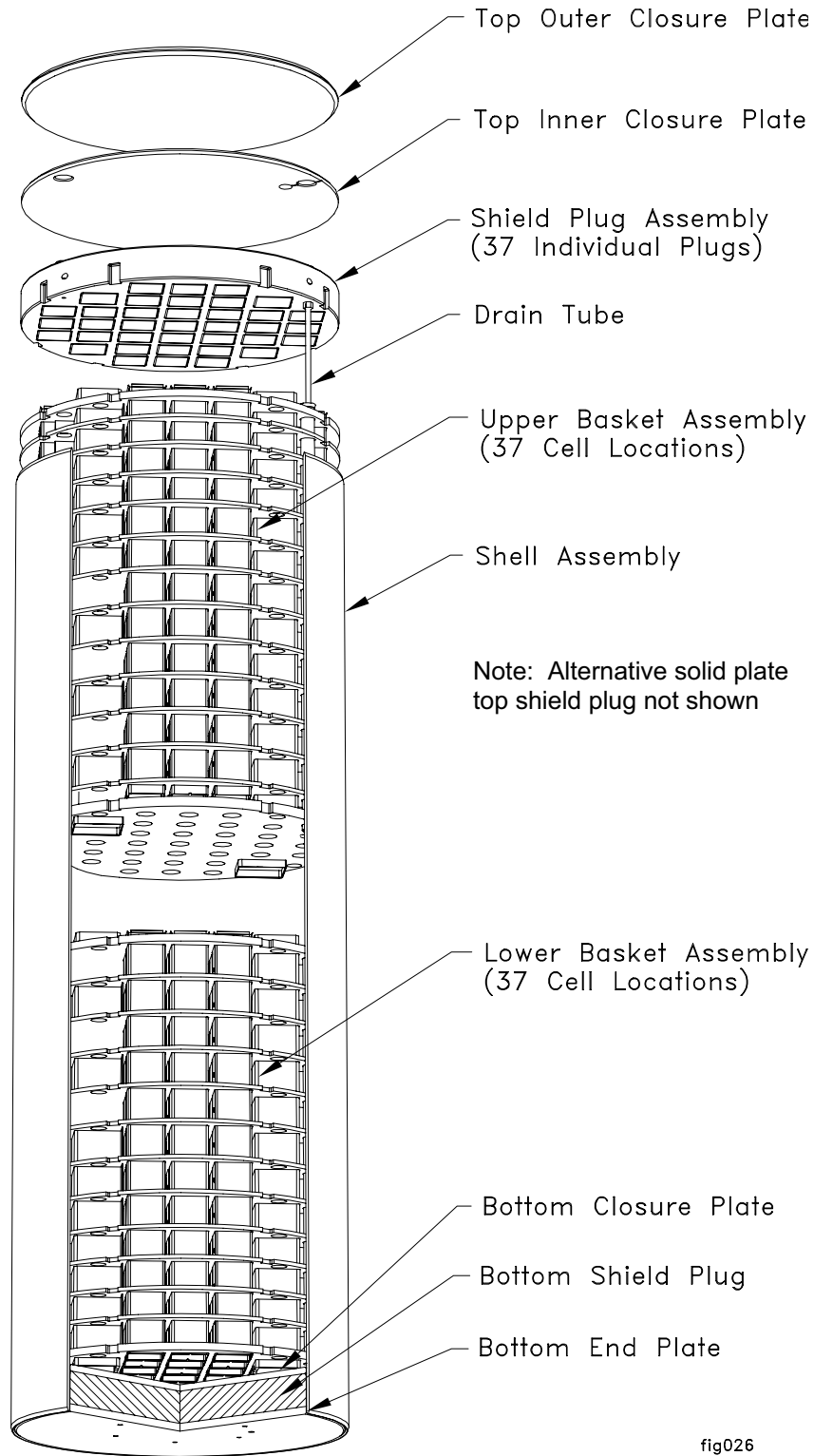


Figure 1.2-2 - Expanded View of FuelSolutions™ W74 Canister

This page intentionally left blank.

1.3 Appendices

1.3.1 General Arrangement Drawings

The following general arrangement drawings of the FuelSolutions™ W74M and W74T class canisters are provided in this section:

- W74-110, FuelSolutions™ W74 Canister Assembly
- W74-120, FuelSolutions™ W74 Canister Basket Assembly
- W74-121, FuelSolutions™ W74 Canister Spacer Plates
- W74-122, FuelSolutions™ W74 Canister Basket Guide Tube Assembly
- W74-130, FuelSolutions™ W74 Canister Shell Assembly
- W74-140, FuelSolutions™ Canister Shield Plug Assembly
- W74-150, FuelSolutions™ Canister Top Closure Plates and Port Covers
- 3319, FuelSolutions™ W74 Assembly and Detail Damaged Fuel Can
- W74-200, FuelSolutions™ TS125 Transportation Package Configuration for W74 Canisters
- W74-205, FuelSolutions™ W74 Canister Assembly Transfer Configurations

Drawings withheld on the basis of
“Security-Related Information.”

1.3.2 Product Literature

Literature describing special materials used for the FuelSolutions™ W74 canister is provided in this section.

1.3.2.1 Borated Stainless Steel Literature

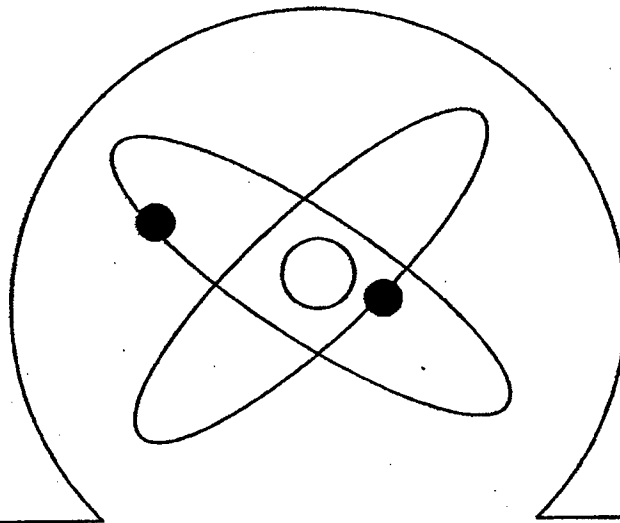
Literature describing typical borated stainless steel neutron absorbing materials used for the FuelSolutions™ W74 canister basket assembly is provided in this section (pages 1 - 18). Note that this information is considered to be typical and the accompanying nomogram does not imply that product forms are limited to the range shown.

This page intentionally left blank.

BOHLER SPECIAL PLATES -
DO THE JOB ALL OVER THE WORLD

 **BÖHLER**
BLECHE

BÖHLER NEUTRONIT A976



**SHEET AND PLATE
FOR NUCLEAR ENGINEERING**

Dr. A. KÜGLER

APPLICATIONS

In nuclear engineering borated stainless steels are predominantly used as a shielding material for radwaste disposal equipment, such as

- ⇒ components for compact storage racks (intermediate storage)
- ⇒ transportation baskets

The main demands made on sheet and plate used for these applications are:

- ⇒ largest possible thermal neutron absorption cross section which is uniform over the whole surface area
- ⇒ toughness
- ⇒ resistance to general types of corrosion
- ⇒ intergranular corrosion resistance
- ⇒ weldability

Based on persistent research and development work BÖHLER BLECHE GMBH are able to offer stainless steel grades with different boron contents which fully meet these requirements.

NEUTRON ABSORPTION

The neutron absorption properties of boron alloyed stainless steel depend on the content of B10 isotope. The boron isotope B10 has an absorption cross section for thermal neutrons of more than 3800 barns. B10 is exceeded only by Gadolinium and Samarium.

σ_{abs} of	Cd 113	20.000 barn
	Sm 149	41.000 barn
	Gd 155	61.000 barn
	Gd 157	247.000 barn

Among all elements having large absorption cross sections for thermal neutrons, up to now only boron is of importance for steelmaking. The reason is that production of shielding material is not only a physical but an economical problem and metallurgical problem as well.

Natural boron is commonly used as starting material for the production of Ferrobor. Natural boron consists of more than 19.6 at.-% B10. This level may also be expected in boron stainless steel products, because it is influenced neither by the melting process nor by forming operations.

The cross sections of the alloying elements chromium, molybdenum and nickel are considerably smaller and may be disregarded for the evaluation of neutron absorption capacity.

METALLURGICAL BACKGROUND

The solubility of boron in steel is very low, at room temperature negligible small. 100 % of the boron content in steel is precipitated in the form of borides, predominantly with the tetragonal structure Fe_2B . With increasing boron content in steel both the size of the precipitates and the number of particles increase. But even for 2 % boron the particles are of microscopical size.

The transition elements Cr, Ni, Mn and Mo form boride structures very similar to Fe. Furthermore Carbon, which is always present in steel can replace Boron on some lattice places. The boride in stainless steel can therefore be described for the annealed equilibrium condition as:



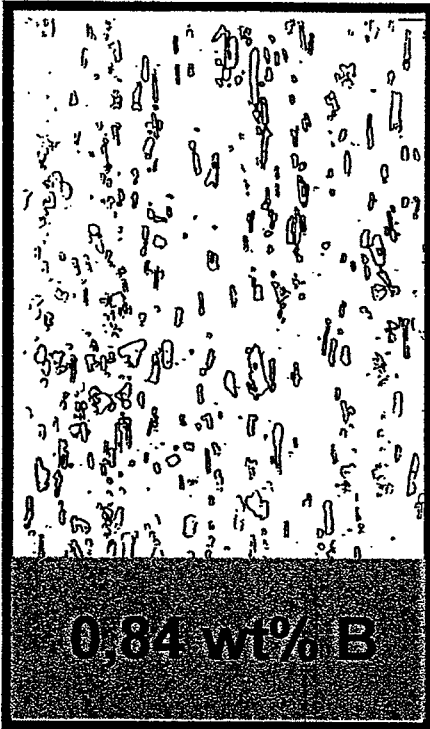
The boride is very hard, e.g. comparable with the hardness of a carbide. Furthermore, the boride is very resistant to oxidation and chemical attack e.g. the boride is completely resistant against corrosion attack under the environmental conditions of a nuclear power station.

The carbon of the stainless steel is completely bound to the precipitated boride particles. A boron alloyed stainless steel therefore reacts like a stabilized stainless steel type which is very important for the application of welded components.

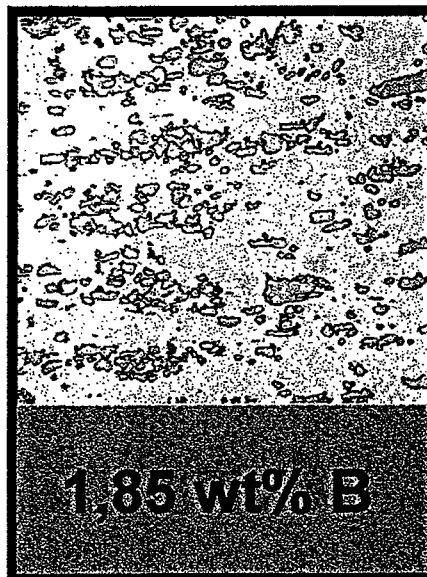
There is a practical upper limit for alloying boron into steel. This limit is about 1.9 % because of the tendency of boron to produce the low melting point eutectic together with iron and some accompanying elements. Such eutectic makes it impossible to roll the material to a sheet. During hot rolling, the melting eutectic creates surface cracks. These surface cracks may lead to a fracture of the material. The risk of such a fracture can be minimized by taking certain steps e.g. preforming. In view of this, the fabrication of a boron alloyed stainless steel sheet with more than 1.9 % boron has always an unsatisfying result.

BOHLER SPECIAL PLATES -
DO THE JOB ALL OVER THE WORLD

BÖHLER
BLECHE



**MICROSTRUCTURE
BÖHLER
NEUTRONIT A976**



magnification 500x
etched

VERIFICATION OF BORON CONTENT

Boron alloyed stainless steel has a heterogen structure. But nevertheless, the boron distribution is macroscopically uniform. Only when investigated by microscope, there is a discontinuity in distribution which has no practical effect.

The boron content is certificated both for heat analysis and product analysis. Determination is effected by the wet chemical or spectroscopic method with an error of less than 0.03 % B (95% confidential level).

BÖHLER BLECHE GMBH has the unique possibility to subject each sheet of a batch to nondestructive neutron control using portable test equipment JEN3 developed by the **Office des Rayonnements Ionisants**, Section d'Application des Radioéléments, Saclay, France.

This test equipment consists of a neutron source (Cf 252) and a scintillation counter and is used for determining the absorption of a neutron flux passing twice through the plate. This equipment allows a 100 % material identification test and provides proof of the homogeneous distribution of boron.

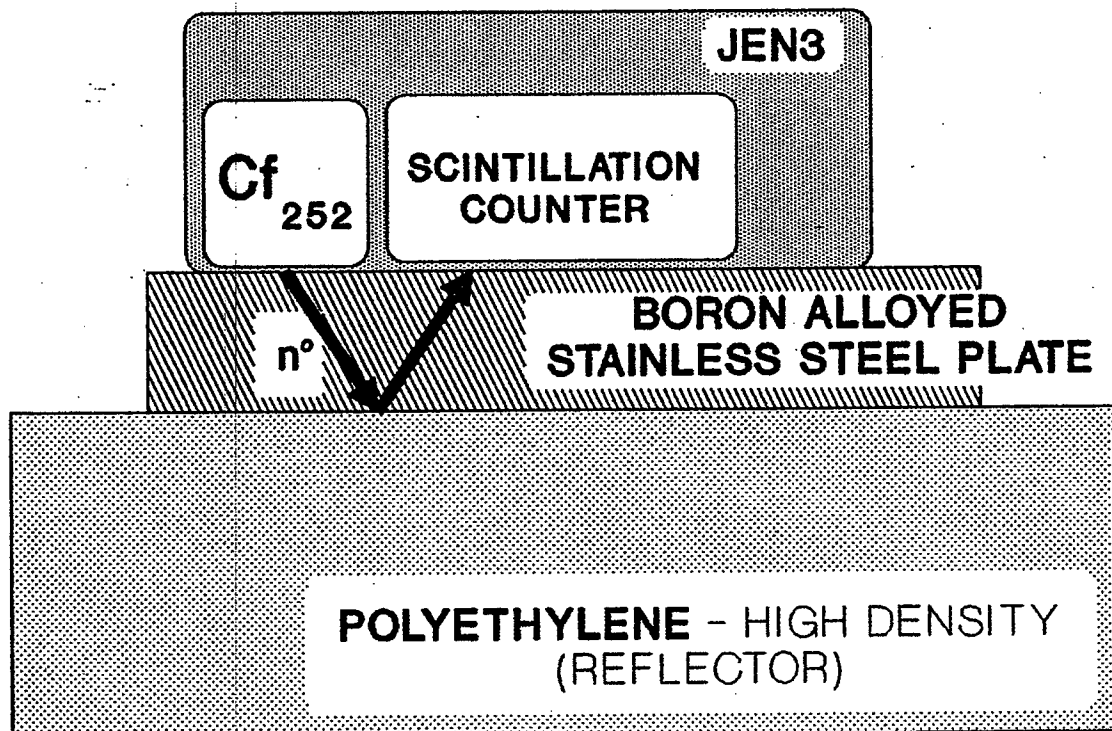
By comparative measurements using sheets made from steel with different boron contents including standard stainless grades the test equipment can be calibrated to indicate the content of B10-isotope. If only natural boron is used for steel melting, the counting rate of JEN3 indicates the content of boron. The result can be compared with the result of the standard chemical analysis.

This test is the only method to check whether enriched boron is used for alloying by comparing the result of the chemical analysis with the counting rate of JEN3.

BOHLER SPECIAL PLATES -
DO THE JOB ALL OVER THE WORLD

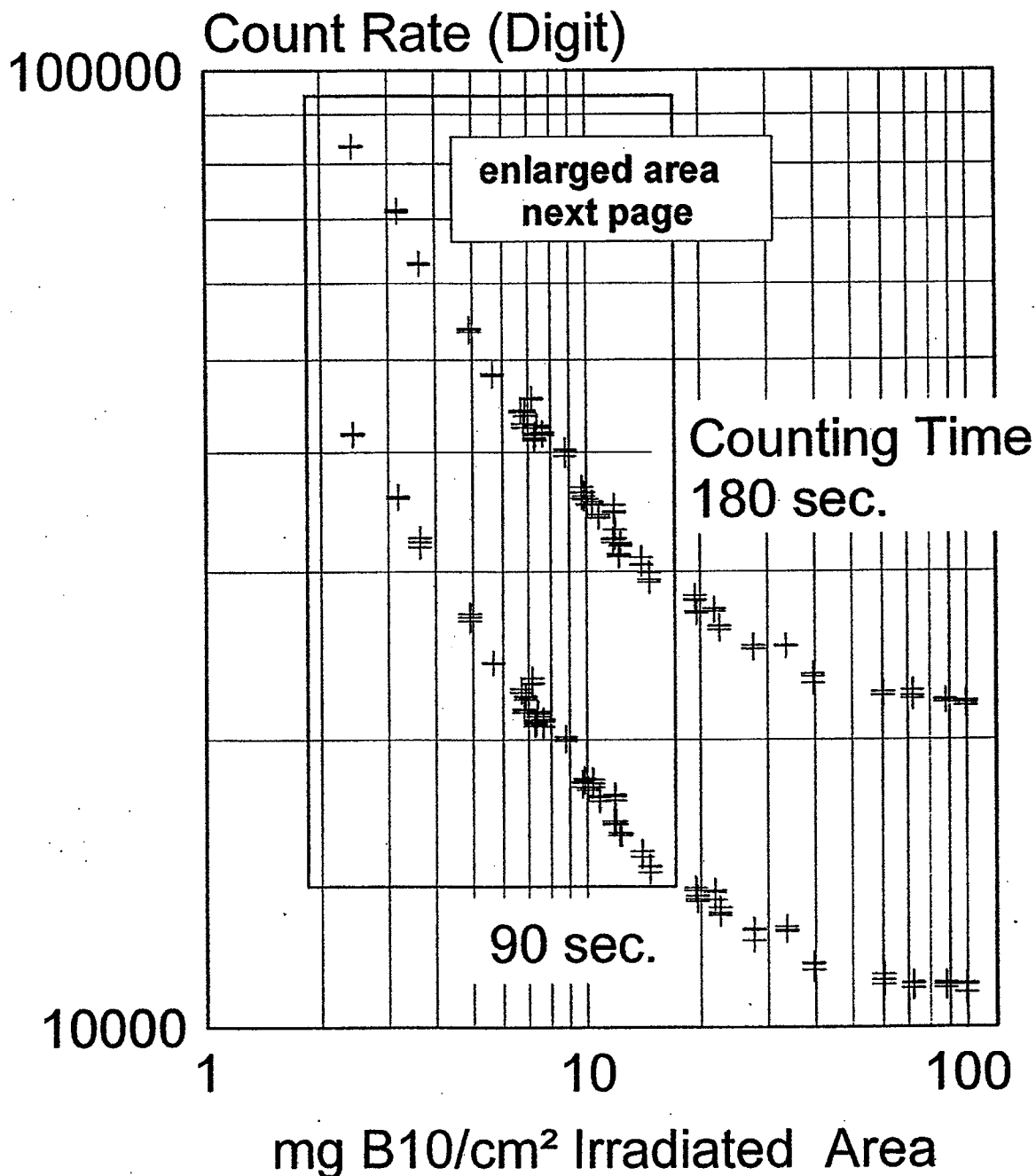
BÖHLER
BLECHE

JEN3 TRANSPORTABLE TEST EQUIPMENT



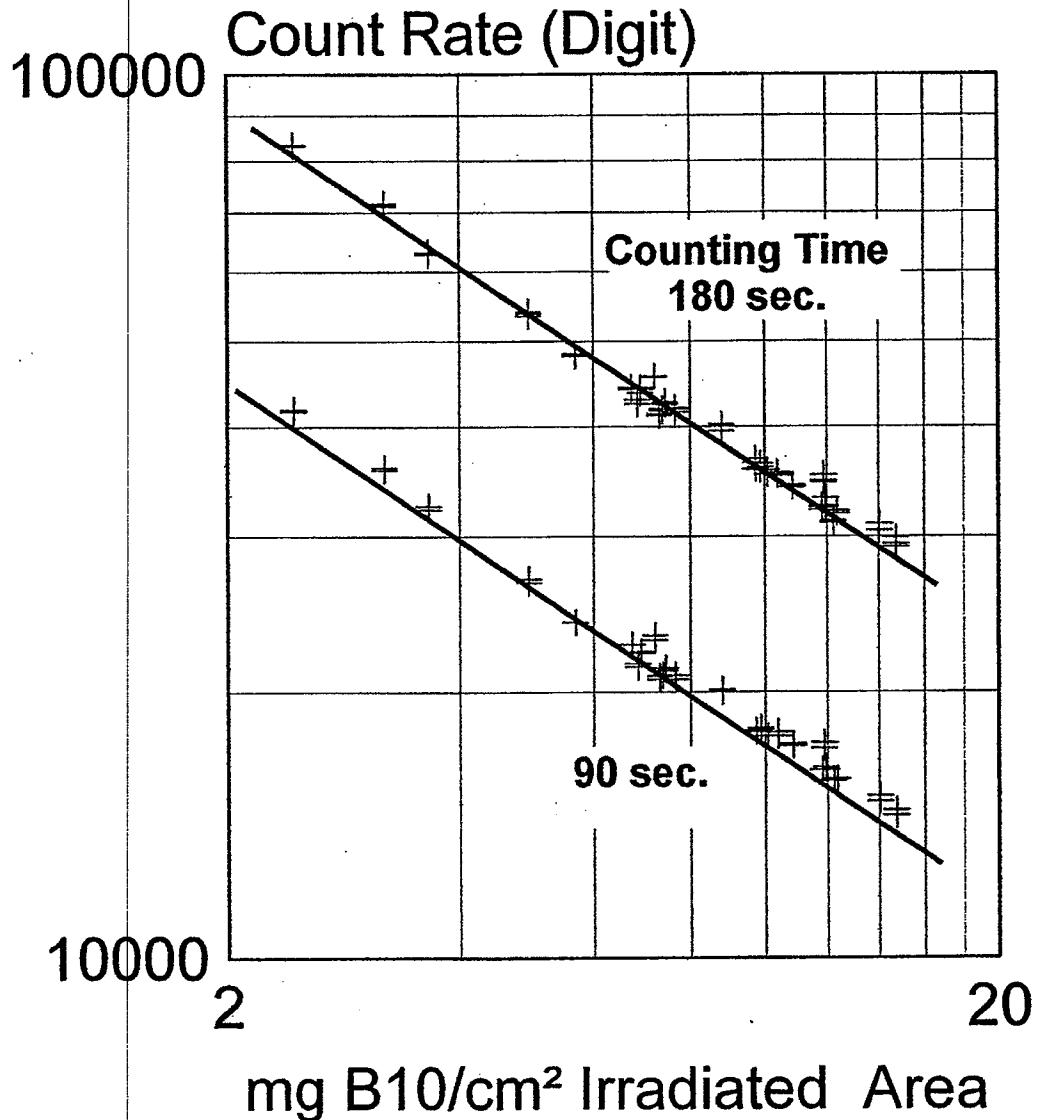
JEN3 is the only method to check in the state of delivery whether the stainless plate is boron alloyed or not.

CORRELATION BETWEEN B10-CONTENT AND JEN3-COUNT RATE



Notice : Absolute value of count rate depends on the actual
activity of the neutron source Cf 252

**CORRELATION BETWEEN
B10-CONTENT AND JEN3-COUNT RATE
In-linear between 2 - 17 mg B10/cm²**



Notice : Absolute value of count rate depends on the actual activity of the neutron source Cf 252

**BOHLER SPECIAL PLATES -
DO THE JOB ALL OVER THE WORLD**

 **BÖHLER**
BLECHE

PROPERTIES OF BORON ALLOYED STEEL

The properties of the steel are closely correlated with the heterogeneity of the structure. Because of this and a comparable hardness between borides and carbides boron alloyed stainless steel behaves similar to high alloyed tool steel types in the annealed condition.

It is evident that for mechanical properties and corrosion resistance only the total boron content is of importance and not the B10-content.

CHEMICAL COMPOSITION

The special boron alloyed **BÖHLER NEUTRONIT** steel grades are based on the AISI type 304.

AVERAGE VALUES					
BÖHLER NEUTRONIT	C	Cr	Ni	Co	B
A 976	0,04 max.	18,5	13	0,20 max.	acc. spec.

The **Nickel** content is increased to 13 % as compared with AISI type 304 to obtain a stable austenitic structure with better forming properties.

The **Boron** content is according to the customer specification. Most common are Boron values similar to ASTM A887, type B3, B4 and B6.

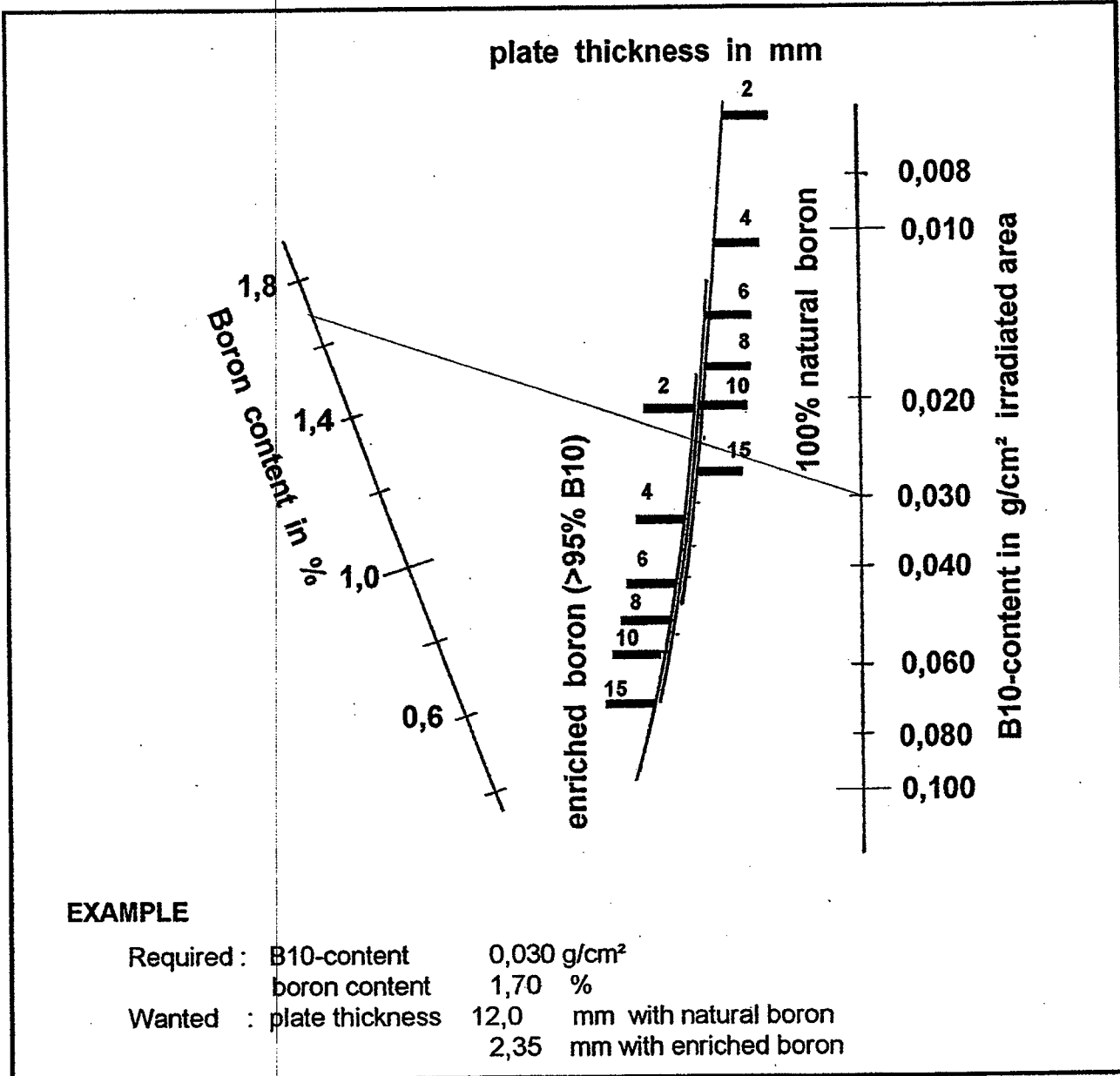
In addition to ASTM A887 a **Molybdenum** alloyed type **BÖHLER NEUTRONIT A978** can be supplied on special request too. This steel type is capable of meeting the most stringent requirements for corrosion resistance, but not necessary for standard application conditions.

On special request, the **Chromium** content can be increased to 22 % for the same reason.

Both changes in chemical analysis need a surcharge in price because of higher alloying costs.

After producing more than 2000 tons of boron alloyed stainless steel **BÖHLER BLECHE GMBH** is in the position to guarantee a uniform distribution of boron within all sheets of one heat.

NOMOGRAM for the calculation of the plate thickness of borated stainless steel Böhler NEUTRONIT A976



NUC08.PRS

MECHANICAL PROPERTIES

Tensile strength and hardness rise with increasing boron content while toughness is reduced.

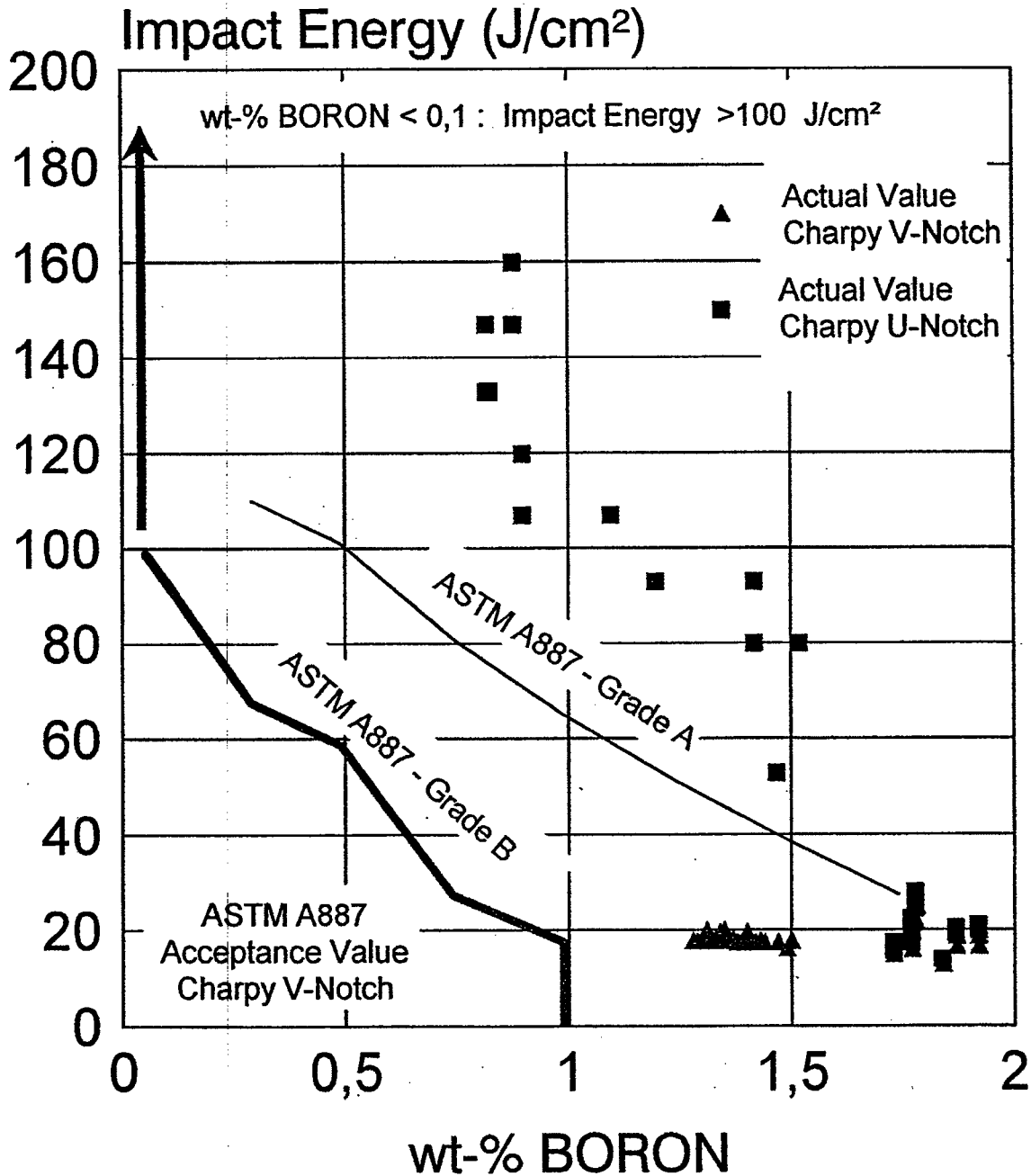
Boron content %	Yield strength MPa min.	Tensile strength MPa min.	Elongation in $L_0=5t_0$ %, min.
0,8	250	550	19
0,9 - 1,2			16
1,4 - 1,6			13
> 1,7			6

The loss of toughness is due to the bi-phase structure. Impact strength decreases with increasing proportions of hard borides in the structure, but fracture is not yet 100 % brittle, even in case of boron content of about 1,9 %. After fracture the specimen show a marked reduction of area which is due to the fine distribution of borides and to the increased nickel content of the matrix.

Toughness properties are retained both at low and elevated temperatures.

The mechanical properties of **BÖHLER NEUTRONIT A976** are conform to the requirements specified in ASTM A887, Grade B.

Toughness of BÖHLER NEUTRONIT A976



NOTE :

ASTM A887 requires standard size of thickness(=10 mm)

Usual sheet thickness 2,5 - 4,5 mm, e.g. actual tests only with subsized specimen possible.

CORROSION RESISTANCE

Corrosion resistance has proven satisfactory under the conditions encountered in practice.

Because of the chromium content of the borides, the precipitates extract chromium from the matrix. Therefore, corrosion resistance is less than it could be expected from the heat analysis but nevertheless similar to a AISI 321 type.

The chromium value in the matrix is depending on the boron content. For **BÖHLER NEUTRONIT A976** with about 1.2 % boron no corrosion attack under reactor conditions is known to us. Higher boron contents might be a problem. An analogous increase of the chromium content to about 21.5 % could solve the problem, if there is any.

Due to the fact that the carbon is dissolved with the borides, no sensitivity takes place even after welding plate material or after specific heat treatment cycles for simulation of a cast process. Intergranular corrosion is not a problem for boron alloyed stainless steel types.

An additional limitation of the carbon content to 0.03% - compared with the ASTM-requirement of max. 0.08 % - is a further step to minimize the risk of intergranular corrosion attack in the heat affected zone.

BOHLER SPECIAL PLATES -
DO THE JOB ALL OVER THE WORLD



INSPECTION AND QUALITY ASSURANCE

Unless otherwise specified in the order, material tests are conducted on the basis of DIN or ASTM, quality specifications for stainless steels. All tests and inspections are performed by our shop independent Quality Control Department. We are able to comply with all national standards and special customer requirements for production inspection, testing and final inspection.

We have been granted a **Quality Assurance Certificate** according to **ISO 9000 / 9002**. Our Quality Assurance System is well implemented and meets the requirements of all important national standards and the specific requirements of manufacturers of nuclear components.

To make sure our products are safe - Quality, for us, is a matter of course.

FORMS AVAILABLE

According to thickness and tolerances required, our sheets and plates in **BÖHLER NEUTRONIT** can be supplied

- ⇒ hot rolled, heat treated, pickled (**No.1 Finish ASTM A480.8**)
- ⇒ cold rolled, heat treated, pickled (**No.2D Finish ASTM A480.8**)

For sheet / plate which are used in compact storage racks a surface grinding before final pickling / passivation is standard.

Brushing with nylon brushers after pickling is a standard fabrication step for this special grade too. A final treatment with hot air prevents mineral spots in the state of delivery.

These procedures guarantee a clean and shiny surface, free of defects. Cleaning operations can be easily carried out during life time.

Sheets and plates from our steel grade **BÖHLER NEUTRONIT** are available in essentially the same sizes and thicknesses as those made from standard stainless steels. The most widely used thicknesses, however, are within the range of 1.5 mm to 10.0 mm.

A plate length of up to 5 m, necessary for shielding in compact storage racks, is within the standard production program of Böhler Bleche.

For cutting to the ordered sizes and for cuttings as per drawing we have the facilities for **LASER-cutting**. As an alternative we can offer guillotine shearing, under water plasma cutting or cold sawing.

BOHLER SPECIAL PLATES -
DO THE JOB ALL OVER THE WORLD

 **BÖHLER**
BLECHE

LASER-cut EDGES

LASER-cut sheets and strips offer very low size tolerances, which are comparable with machined products-
but at a lower cost level.

BÖHLER BLECHE offers
size tolerances of **+0,5/-0,0 mm (+0,02/-0,0 in.)** for any size available.

LASER-cutting is a thermal cutting process. Because of the very low energy input during cutting the time on high temperature level is very short - too short for any change in analysis or structure.



BÖHLER NEUTRONIT A976 with 1,45 wt% boron

At the edge the borides are transformed to oxids during cutting.

Pickling after cutting removes the oxid layer. The remaining micro-pits are less than 0,05 mm (0,002 in.)

etched, magnification 200x

1.3.2.2 Electroless Nickel Plating Literature

Reference information describing the electroless nickel plating used for coating the carbon steel piece parts of the FuelSolutions™ W74 canister basket assembly is included in this section (pages 290 - 310).

This page intentionally left blank.

Electroless Nickel Plating

Revised by Donald W. Baudrand, MacDermid Inc.

ELECTROLESS NICKEL PLATING is used to deposit nickel without the use of an electric current. The coating is deposited by an autocatalytic chemical reduction of nickel ions by hypophosphite, aminoborane, or borohydride compounds. Two other methods have been used commercially for plating nickel without electric current, including (1) immersion plating on steel from solutions of nickel chloride and boric acid at 70 °C (160 °F) and (2) decomposition of nickel carbonyl vapor at 180 °C (360 °F). Immersion deposits, however, are poorly adherent and nonprotective, while the decomposition of nickel carbonyl is expensive and hazardous. Accordingly, only electroless nickel plating has gained wide acceptance.

Since gaining commercial use in the 1950s, electroless nickel plating has grown rapidly and now is an established industrial process. Currently, hot acid hypophosphite-reduced baths are most frequently used to plate steel and other metals, whereas warm alkaline hypophosphite baths are used for plating plastics and nonmetals. Borohydride-reduced baths are also used to plate iron and copper alloys, especially in Europe.

Electroless nickel is an engineering coating, normally used because of excellent corrosion and wear resistance. Electroless nickel coatings are also frequently applied on aluminum to provide a solderable surface and are used with molds and dies to improve lubricity and part release. Because of these properties, electroless nickel coatings have found many applications, including those in petroleum, chemicals, plastics, optics, printing, mining, aerospace, nuclear, automotive, electronics, computers, textiles, paper, and food machinery (Ref 1). Some advantages and limitations of electroless nickel coatings include:

Advantages

- Good resistance to corrosion and wear
- Excellent uniformity
- Solderability and brazability
- Low labor costs

Limitations

- Higher chemical cost than electroplating
- Brittleness

- Poor welding characteristics due to contamination of nickel plate with nickel-phosphorus deposits
- Need to copper strike plate alloys containing significant amounts of lead, tin, cadmium, and zinc before electroless nickel can be applied
- Slower plating rate, as compared to electrolytic methods

Bath Composition and Characteristics

Electroless nickel coatings are produced by the controlled chemical reduction of nickel ions onto a catalytic surface. The deposit itself is catalytic to reduction, and the reaction continues as long as the surface remains in contact with the electroless nickel solution. Because the deposit is applied without an electric current, its thickness is uniform on all areas of an article in contact with fresh solution.

Electroless nickel solutions are blends of different chemicals, each performing an important function. Electroless nickel solutions contain:

- A source of nickel, usually nickel sulfate
- A reducing agent to supply electrons for the reduction of nickel
- Energy (heat)
- Complexing agents (chelators) to control the free nickel available to the reaction
- Buffering agents to resist the pH changes caused by the hydrogen generated during deposition
- Accelerators (exultants) to help increase the speed of the reaction
- Inhibitors (stabilizers) to help control reduction
- Reaction byproducts

The characteristics of an electroless nickel bath and its deposit are determined by the composition of these components.

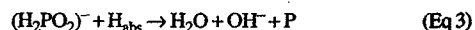
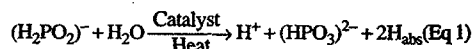
Reducing Agents

A number of different reducing agents have been used in preparing electroless nickel baths,

including sodium hypophosphite, aminoboranes, sodium borohydride, and hydrazine.

Sodium Hypophosphite Baths. The majority of electroless nickel used commercially is deposited from solutions reduced with sodium hypophosphite. The principal advantages of these solutions over those reduced with boron compounds or hydrazine include lower cost, greater ease of control, and better corrosion resistance of the deposit.

Several mechanisms have been proposed for the chemical reactions that occur in hypophosphite-reduced electroless nickel plating solutions. The most widely accepted mechanism is illustrated by the following equations:



In the presence of a catalytic surface and sufficient energy, hypophosphite ions are oxidized to orthophosphite. A portion of the hydrogen given off is absorbed onto the catalytic surface (Eq 1). Nickel at the surface of the catalyst is then reduced by the absorbed active hydrogen (Eq 2). Simultaneously, some of the absorbed hydrogen reduces a small amount of the hypophosphite at the catalytic surface to water, hydroxyl ion, and phosphorus (Eq 3). Most of the hypophosphite present is catalytically oxidized to orthophosphite and gaseous hydrogen (Eq 4) independently of the deposition of nickel and phosphorus, causing the low efficiency of electroless nickel solutions. Usually 5 kg (10 lb) of sodium hypophosphite is required to reduce 1 kg (2 lb) of nickel, for an average efficiency of 37% (Ref 2, 3).

Early electroless nickel formulations were ammoniacal and operated at high pH. Later, acid solutions were found to have several advantages over alkaline solutions. Among these are higher plating rate, better stability, greater ease of con-

Table 1 Hypophosphite-reduced electroless nickel plating solutions

Constituent or condition	Alkaline			Acid		
	Bath 1	Bath 2	Bath 3	Bath 4	Bath 5	Bath 6
Composition						
Nickel chloride, g/L (oz/gal)	45 (6)	30 (4)	30 (4)
Nickel sulfate, g/L (oz/gal)	21 (2.8)	34 (4.5)	45 (6)
Sodium hypophosphite, g/L (oz/gal)	11 (1.5)	10 (1.3)	10 (1.3)	24 (3.2)	35 (4.7)	10 (1.3)
Ammonium chloride, g/L (oz/gal)	50 (6.7)	50 (6.7)
Sodium citrate, g/L (oz/gal)	100 (13.3)
Ammonium citrate, g/L (oz/gal)	...	65 (8.6)
Ammonium hydroxide	To pH	To pH
Lactic acid, g/L (oz/gal)	28 (3.7)
Malic acid, g/L (oz/gal)	35 (4.7)	...
Amino-acetic acid, g/L (oz/gal)	40 (5.3)
Sodium hydroxyacetate, g/L (oz/gal)	10 (1.3)
Propionic acid, g/L (oz/gal)	2.2 (0.3)
Acetic acid, g/L (oz/gal)	10 (1.3)
Succinic acid, g/L (oz/gal)	10 (1.3)	...
Lead, ppm	1
Thiourea, ppm	1	...
Operating conditions						
pH	8.5-10	8-10	4-6	4.3-4.6	4.5-5.5	4.5-5.5
Temperature, °C (°F)	90-95 (195-205)	90-95 (195-205)	88-95 (190-205)	88-95 (190-205)	88-95 (190-205)	88-95 (190-205)
Plating rate, μm/h (mil/h)	10 (0.4)	8 (0.3)	10 (0.4)	25 (1)	25 (1)	25 (1)

Table 2 Aminoborane- and borohydride-reduced electroless nickel plating solutions

Constituent or condition	Aminoborane		Borohydride	
	Bath 7	Bath 8	Bath 9	Bath 10
Composition				
Nickel chloride, g/L (oz/gal)	30 (4)	24-48 (3.2-6.4)	...	20 (2.7)
Nickel sulfate, g/L (oz/gal)	50 (6.7)	...
DMAB, g/L (oz/gal)	...	3-4.8 (0.4-0.64)	3 (0.4)	...
DEAB, g/L (oz/gal)	3 (0.4)
Isopropanol, mL (fluid oz)	50 (1.7)
Sodium citrate, g/L (oz/gal)	10 (1.3)
Sodium succinate, g/L (oz/gal)	20 (2.7)
Potassium acetate, g/L (oz/gal)	...	18-37 (2.4-4.9)
Sodium pyrophosphate, g/L (oz/gal)	100 (13.3)	...
Sodium borohydride, g/L (oz/gal)	0.4 (0.05)
Sodium hydroxide, g/L (oz/gal)	90 (12)
Ethylene diamine, 98%, g/L (oz/gal)	90 (12)
Thallium sulfate, g/L (oz/gal)	0.4 (0.05)
Operating conditions				
pH	5-7	5.5	10	14
Temperature, °C (°F)	65 (150)	70 (160)	25 (77)	95 (205)
Plating rate, μm/h (mil/h)	7-12 (0.5)	7-12 (0.5)	...	15-20 (0.6-0.8)

trol, and improved deposit corrosion resistance. Accordingly, most hypophosphite reduced electroless nickel solutions are operated between 4 and 5.5 pH. Compositions for alkaline and acid plating solutions are listed in Table 1 (Ref 2-5).

Aminoborane Baths. The use of aminoboranes in commercial electroless nickel plating solutions has been limited to two compounds: N-dimethylamine borane (DMAB)— $(\text{CH}_3)_2\text{NHBH}_3$, and H-diethylamine borane (DEAB)— $(\text{C}_2\text{H}_5)_2\text{NHBH}_3$. DEAB is used primarily in European facilities, whereas DMAB is used principally in the United States. DMAB is readily soluble in aqueous systems. DEAB must be mixed with a short chain aliphatic alcohol, such as ethanol, before it can be dissolved in the plating solution.

Aminoborane-reduced electroless nickel solutions have been formulated over wide pH ranges, although they are usually operated between 6 and

9 pH. Operating temperatures for these baths range from 50 to 80 °C (120 to 180 °F), but they can be used at temperatures as low as 30 °C (90 °F). Accordingly, aminoborane baths are very useful for plating plastics and nonmetals, which is their primary application. The rate of deposition varies with pH and temperature, but is usually 7 to 12 μm/h (0.3 to 0.5 mil/h). The boron content of the deposit from these baths varies between 0.4 and 5%. Compositions and operating conditions for aminoborane baths are listed in Table 2 (Ref 2, 5, 6).

Sodium Borohydride Baths. The borohydride ion is the most powerful reducing agent available for electroless nickel plating. Any water-soluble borohydride may be used, although sodium borohydride is preferred.

In acid or neutral solutions, hydrolysis of borohydride ions is very rapid. In the presence of

nickel ions, nickel boride may form spontaneously. If the pH of the plating solution is maintained between 12 and 14, however, nickel boride formation is suppressed, and the reaction product is principally elemental nickel. One mol of sodium borohydride can reduce approximately one mol of nickel, so that the reduction of 1 kg (2 lb) of nickel requires 0.6 kg (1 lb) of sodium borohydride. Deposits from borohydride-reduced electroless nickel solutions contain 3 to 8 wt% B.

To prevent precipitation of nickel hydroxide, complexing agents, such as ethylene diamine, that are effective between 12 to 14 pH must be used. Such strong complexing agents, however, decrease the rate of deposition. At an operating temperature of 90 to 95 °C (195 to 205 °F), the plating rate of commercial baths is 25 to 30 μm/h (1 to 1.2 mil/h). Compositions of a borohydride-reduced electroless nickel bath are also shown in Table 2 (Ref 6).

During the course of reduction, the solution pH decreases, requiring constant additions of an alkali hydroxide. Spontaneous solution decomposition may occur if the bath pH is allowed to fall below 12. Because of the high operating pH, borohydride plating baths cannot be used for aluminum substrates (Ref 2, 5, 7).

Hydrazine Baths. Hydrazine has also been used to produce electroless nickel deposits. These baths operate at 90 to 95 °C (195 to 205 °F) and 10 to 11 pH. Their plating rate is approximately 12 μm/h (0.5 mil/h). Because of the instability of hydrazine at high temperatures, however, these baths tend to be very unstable and difficult to control.

Whereas the deposit from hydrazine-reduced solutions is 97 to 99% N, it does not have a metallic appearance. The deposit is brittle and highly stressed with poor corrosion resistance. The stress and brittleness are likely due to codeposition of small amounts of basic nickel salts, $\text{Ni}(\text{OH})_2$, and nitrogen. Unlike hypophosphite- and boron-reduced nickels, hardness from a hydrazine-reduced electroless nickel has very little commercial use (Ref 2).

Energy

The amount of energy or heat present in an electroless nickel solution is one of the most important variables affecting coating deposition. In a plating bath, temperature is a measure of its energy content.

Temperature has a strong effect on the deposition rate of acid hypophosphite-reduced solutions. The rate of deposition is usually very low at temperatures below 65 °C (150 °F), but increases rapidly with increased temperature (Ref 5). This is illustrated in Fig. 1, which gives the results of tests conducted using bath 3 in Table 1 (Ref 7). The effect of temperature on deposition in boron-reduced solutions is similar. At temperatures above 100 °C (212 °F), electroless nickel solutions may decompose. Accordingly, the preferred operating range for most solutions is 85 to 95 °C (185 to 205 °F).

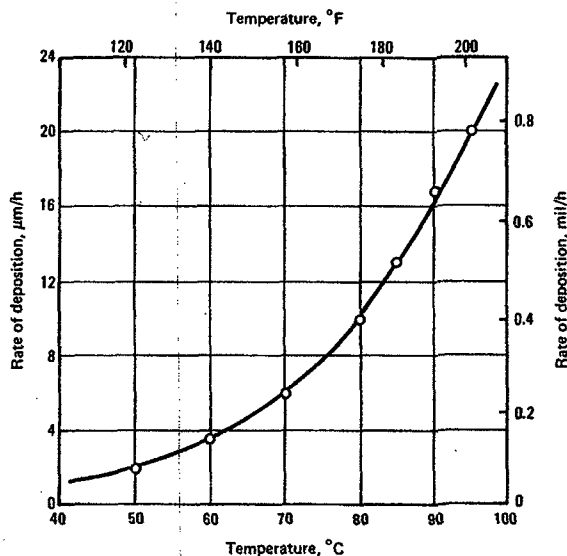


Fig. 1 Effect of solution temperature on the rate of deposition. Tests conducted on bath 3 at 5 pH

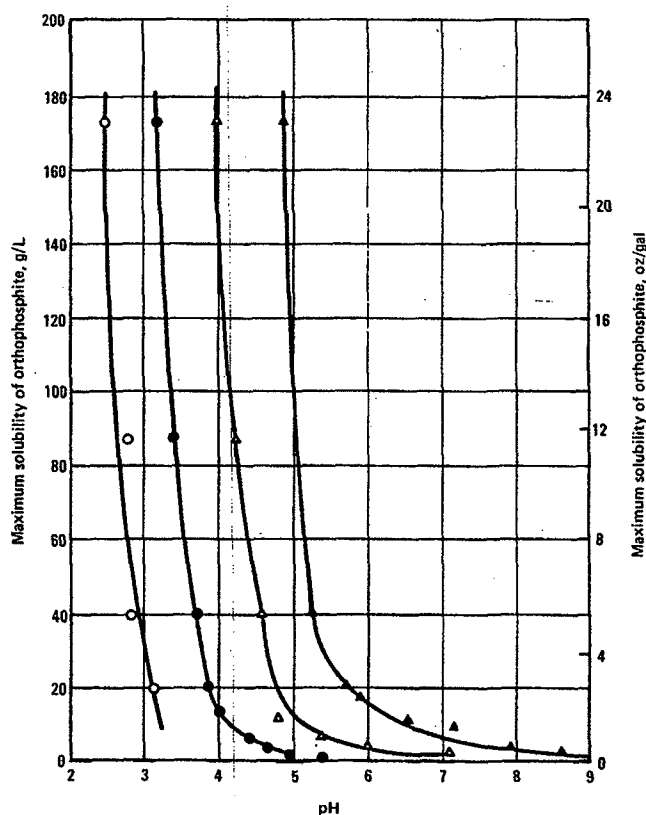


Fig. 2 Limits of solubility for orthophosphite in electroless nickel solutions. Solutions contain 30 g/L (4 oz/gal) nickel chloride (NiCl_2) and 10 g/L (1.3 oz/gal) sodium hypophosphite (NaH_2PO_2). O, without a complexing agent; ●, with 15 g/L (2 oz/gal) citric acid; Δ, with 39 g/L (5.2 oz/gal) glycolic acid; ▲, with 78 g/L (10 oz/gal) glycolic acid.

Complexing Agents

To avoid spontaneous decomposition of electroless nickel solutions and to control the reaction so that it occurs only on the catalytic surface, complexing agents are added. Complexing

agents are organic acids or their salts, added to control the amount of free nickel available for reaction. They act to stabilize the solution and to retard the precipitation of nickel phosphite.

Complexing agents also buffer the plating solution and prevent its pH from decreasing too rapidly as hydrogen ions are produced by the

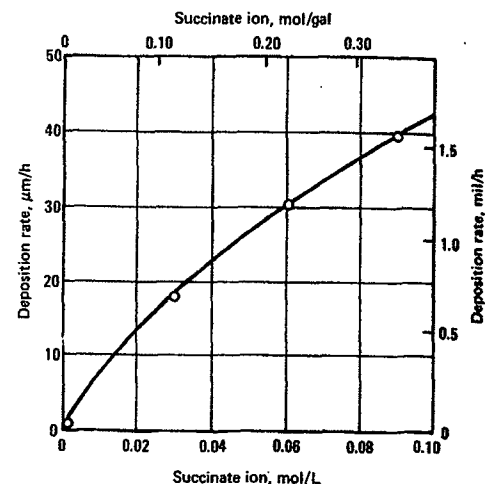


Fig. 3 Effect of succinate additions on the plating rate of an electroless nickel solution. Solutions contain 16 g/L (2.1 oz/gal) nickel chloride (NiCl_2) and 24 g/L (3.2 oz/gal) sodium hypophosphite (NaH_2PO_2), 5 g/L (0.7 oz/gal) ammonium hydroxide (NH_4OH) and 1 mg/L (4 mg/gal) lead at 5 pH and 95 °C (205 °F).

reduction reaction. Ammonia, hydroxides, or carbonates, however, may also have to be added periodically to neutralize hydrogen.

Original electroless nickel solutions were made with the salts of glycolic, citric, or acetic acids. Later baths were prepared using other polydentate acids, including succinic, glutaric, lactic, propionic, and aminoacetic. The complexing ability of an individual acid or group of acids varies, but may be quantified by the amount of orthophosphite that can be held in solution without precipitation (Ref 2, 8). This is illustrated in Fig. 2, which shows the maximum solubility of orthophosphite in solutions complexed with citric and glycolic acids as a function of pH (Ref 9). The complexing agent used in the plating solution can also have a pronounced effect on the quality of the deposit, especially on its phosphorus content, internal stress, and porosity (Ref 8).

Accelerators

Complexing agents reduce the speed of deposition and can cause the plating rate to become uneconomically slow. To overcome this, organic additives, called accelerators or exultants, are often added to the plating solution in small amounts. Accelerators are thought to function by loosening the bond between hydrogen and phosphorus atoms in the hypophosphite molecule, allowing it to be more easily removed and absorbed onto the catalytic surface. Accelerators activate the hypophosphite ion and speed the reaction shown in Eq 1 (Ref 2, 3). In hypophosphite-reduced solutions, succinic acid is the accelerator most frequently used. Other carbonic acids, soluble fluorides, and some solvents, however, have also been used (Ref 2). The effect of succinate additions upon deposition rate is illustrated in Fig. 3 (Ref 3).

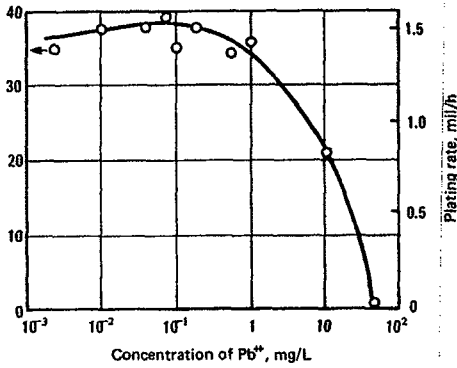


Fig. 4 Effect of lead additions on plating rate in a hypophosphite-reduced succinate-based bath. Bath at .6 pH and 95 °C (205 °F). Solutions containing less than 0.1 µg (0.4 mg/gal) Pb^{2+} were unstable.

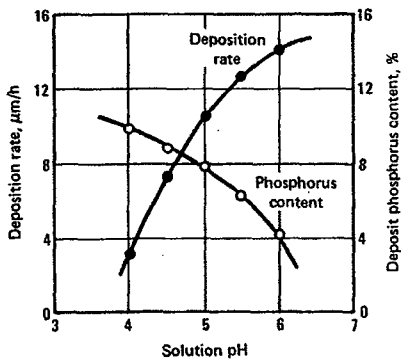


Fig. 5 Effect of solution pH on deposition rate and deposit phosphorus content

Inhibitors

The reduction reaction in an electroless nickel plating bath must be controlled so that deposition occurs at a predictable rate and only on the substrate to be plated. To accomplish this, inhibitors, also known as stabilizers, are added. Electroless nickel plating solutions can operate for hours or days without inhibitors, only to decompose unexpectedly. Decomposition is usually initiated by the presence of colloidal, solid particles in the solution. These particles may be the result of the presence of foreign matter (such as dust or blasting media), or may be generated in the bath as the concentration of orthophosphite exceeds its solubility limit. Whatever the source, the large surface area of the particles catalyzes reduction, leading to a self-accelerating chain reaction and decomposition. This is usually preceded by increased hydrogen evolution and the appearance of a finely divided black precipitate throughout the solution. This precipitate consists of nickel and either nickel phosphide or nickel boride.

Spontaneous decomposition can be controlled by adding trace amounts of catalytic inhibitors to the solution. These inhibitors are absorbed on any colloidal particles present in the solution and pre-

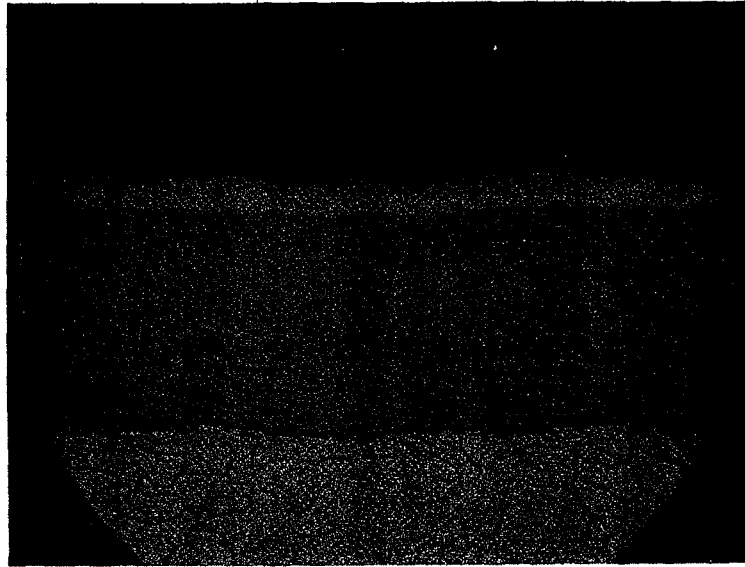


Fig. 6 Cross section of a 75 µm (3 mils) thick electroless nickel deposit. Contains approximately 10% phosphorus and less than 0.05% other elements. 400x

vent the reduction of nickel on their surface. Traditionally, inhibitors used with hypophosphite-reduced electroless nickel have been of three types: sulfur compounds, such as thiourea; oxy anions, such as molybdates or iodates; and heavy metals, such as lead, bismuth, tin, or cadmium. More recently, organic compounds, including oleates and some unsaturated acids, have been used for some functional solutions. Organic sulfide, thio compounds, and metals, such as selenium and thallium, are used to inhibit aminoborane- and borohydride-reduced electroless nickel solutions.

The addition of inhibitors can have harmful as well as beneficial effects on the plating bath and its deposit. In small amounts, some inhibitors increase the rate of deposition and/or the brightness of the deposit; others, especially metals or sulfur compounds, increase internal stress and porosity and reduce ductility, thus reducing the ability of the coating to resist corrosion and wear (Ref 2, 3, 5).

The amount of inhibitor used is critical. The presence of only about 1 mg/L (4 mg/gal) of HS^- ion completely stops deposition, whereas at a concentration of 0.01 mg/L (0.04 mg/gal), this ion is an effective inhibitor. The effect of lead additions on a hypophosphite-reduced succinate bath at pH 4.6 and 95 °C (205 °F) is shown in Fig. 4 (Ref 3). The tests illustrated in Fig. 4 also showed that baths containing less than 0.1 mg/L (0.4 mg/gal) Pb^{2+} decomposed rapidly, whereas baths containing higher concentrations were stable. Excess inhibitor absorbs preferentially at sharp edges and corners, resulting in incomplete coverage (edge pull back) and porosity.

Reaction Byproducts

During electroless nickel deposition, the byproducts of the reduction, orthophosphite or

borate and hydrogen ions, as well as dissolved metals from the substrate accumulate in the solution. These can affect the performance of the plating bath.

Orthophosphite. As nickel is reduced, orthophosphite ion (HPO_3^{2-}) accumulates in the solution and at some point interferes with the reaction. As the concentration of orthophosphite increases, there is usually a small decrease in the deposition rate and a small increase in the phosphorus content of the deposit. Ultimately the accumulation of orthophosphite in the plating solution results in the precipitation of nickel phosphite, causing rough deposits and spontaneous decomposition. Orthophosphite ion also codeposits with nickel and phosphorus, creating a highly stressed, porous deposit.

The solubility of phosphite in the solution is increased when complexing agents, such as citric or glycolic acids, are added. This effect is shown in Fig. 2. However, the use of strong complexors, in other than limited quantities, tends to reduce the deposition rate and increase the porosity and brittleness of the deposit (Ref 8).

Borates. The accumulation of metaborate ion (BO_2^-) from the reduction of borohydride or of boric acid (H_3BO_3) from the reduction of aminoboranes has little effect on electroless nickel plating baths. Both borohydride and aminoborate baths have been operated through numerous regenerations with only a slight decrease in plating rate and without decomposing. With aminoborane-reduced solutions, the solubility of boric acid is probably increased by the presence of amine through the formation of a complex aminoborate (Ref 10).

Hydrogen ions (H^+), produced by the reduction reaction, cause the pH of the bath to decrease. The amount of hydrogen produced, however, depends on the reducing agent being used. Because they are less efficient, hypophosphite-reduced solutions tend to generate more hydrogen ions than those reduced with boron compounds.

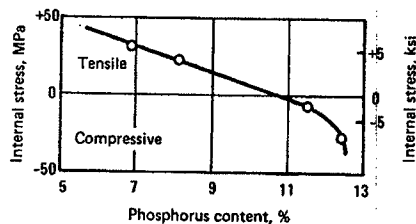


Fig. 7 Effect of phosphorus content on the internal stress of electroless nickel deposits on steel

The pH of the bath has a strong effect on both solution operation and the composition of the deposit. This is illustrated in Fig. 5, which shows the plating rate and deposit phosphorus content resulting from varying solution pH values in a bath containing 33 g/L (4.4 oz/gal) of nickel sulfate and 20 g/L (2.7 oz/gal) of sodium hypophosphite at 82 °C (180 °F) (Ref 11).

To retard pH changes and to help keep operating conditions and deposit properties constant, buffers are included in electroless nickel solutions. Some of the most frequently used buffers include acetate, propionate, and succinate salts. Additions of alkaline materials, such as hydroxide, carbonate solutions, or ammonia, are also required periodically to neutralize the acid formed during plating.

Properties of Electroless Nickel-Phosphorus Coatings

Hypophosphite-reduced electroless nickel is an unusual engineering material, because of both its method of application and its unique properties. As applied, nickel-phosphorus coatings are uniform, hard, relatively brittle, lubricious, easily solderable, and highly corrosion resistant. They can be precipitation hardened to very high levels through the use of low-temperature treatments, producing wear resistance equal to that of commercial hard chromium coatings. This combination of properties makes the coating well suited for many severe applications and often allows it to be used in place of more expensive or less readily available alloys.

Structure. Hypophosphite-reduced electroless nickel is one of the very few metallic glasses used as an engineering material. Depending on the formulation of the plating solution, commercial coatings may contain 6 to 12% P dissolved in nickel, and as much as 0.25% of other elements. As applied, most of these coatings are amorphous; they have no crystal or phase structure. Their continuity, however, depends on their composition. Coatings containing more than 10% P and less than 0.05% impurities are typically continuous. A cross section of one of these coatings is shown in Fig. 6.

Coatings with lower phosphorus content, especially those applied from baths stabilized with heavy metals or sulfur compounds, are often porous. These deposits consist of columns of amorphous material separated by cracks and holes. The presence of such discontinuities has a severe

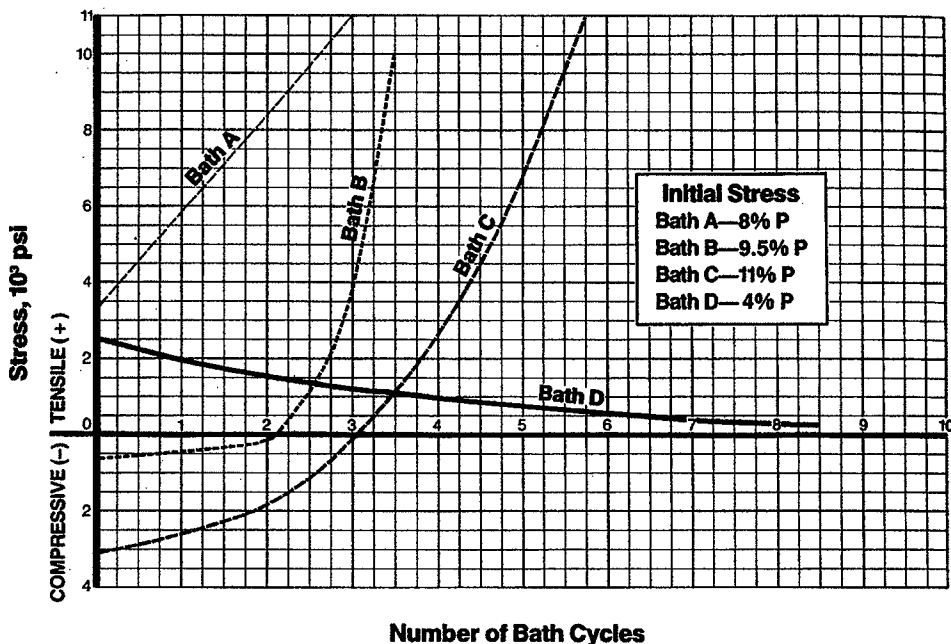


Fig. 8 Intrinsic stresses as related to bath cycles for four amounts of phosphorus in deposits from acid nickel-phosphorus solutions. A bath cycle is defined as one complete replacement of nickel in the solution (sometimes called bath turnover). Nickel content, 6 g/L (0.8 oz/gal); pH, 4.8

effect on the properties of the deposit, especially on ductility and corrosion resistance.

As electroless nickel-phosphorus is heated to temperatures above 220 to 260 °C (430 to 500 °F), structural changes begin to occur. First, coherent and then distinct particles of nickel phosphite (Ni_3P) form within the alloy. Then, at temperatures above 320 °C (610 °F), the deposit begins to crystallize and lose its amorphous character. With continued heating, nickel phosphite particles conglomerate and a two-phase alloy forms. With coatings containing more than 8% P, a matrix of nickel phosphite forms, whereas almost pure nickel is the predominant phase in deposits with lower phosphorus content. These changes cause a rapid increase in the hardness and wear resistance of the coating, but cause its corrosion resistance and ductility to be reduced (Ref 2, 12-14).

Internal stress in electroless nickel coatings is primarily a function of coating composition. As illustrated in Fig. 7, stress in coatings used on steel containing more than 10% P is neutral or compressive (Ref 15). With lower phosphorus deposits, however, tensile stresses of 15 to 45 MPa (2.2 to 6.5 ksi) develop because of the difference in thermal expansion between the deposits and the substrate. The high level of stress in these coatings promotes cracking and porosity (Ref 12).

The structural changes during heat treatment at temperatures above 220 °C (430 °F) cause a volumetric shrinkage of electroless nickel deposits of up to 4 to 6% (Ref 16). This increases tensile stress and reduces compressive stress in the coating.

Deposit stress can also be increased by the codeposition of orthophosphites or heavy metals, as well as by the presence of excess complexing

agents in the plating solution. Even small quantities of some metals can produce a severe increase in stress. The addition of only 5 mg/L (20 mg/gal) of bismuth and antimony to most baths can cause the deposit tensile stress to increase to as much as 350 MPa (50 ksi). High levels of internal stress also reduce the ductility of the coating and increase cracking (Ref 2, 16).

When using reported values for stress, it is important to know how the stress was measured. There are several methods that may yield different results. It is important to know whether intrinsic stress (internal stress of the deposit independent of basis material) or total stress of the plated system is reported. Total stress includes the effect of differences in coefficient of thermal expansion of the basis metal and the plated deposit (Ref 17).

Intrinsic stress (Fig. 8) is measured using a spiral contractometer covered by ASTM B 636. Intrinsic stress is found by taking the initial and final readings at the operating temperature of the plating solution. Reading at room temperature provides the total stress, but only for the specific basis metal used for the test. It is best to specify intrinsic stress so that comparison between deposit characteristics can be made (Ref 17).

The thickness must be constant since stress readings vary with deposit thickness. The ASTM thickness standard is 0.0006 in. (15 μm).

Uniformity. One especially beneficial property of electroless nickel is uniform coating thickness. With electroplated coatings, thickness can vary significantly depending on the shape of the part and the proximity of the part to the anodes. These variations can affect the ultimate performance of the coating, and additional finishing may be required after plating. With electroless nickel, the plating rate and

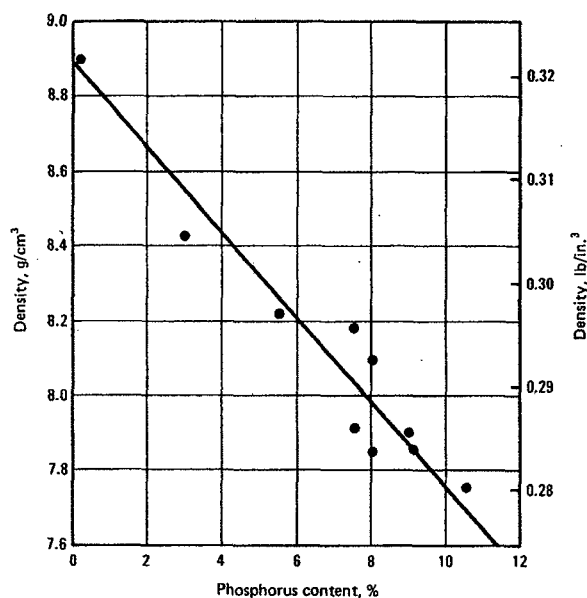


Fig. 9 Effect of phosphorus content on coating density

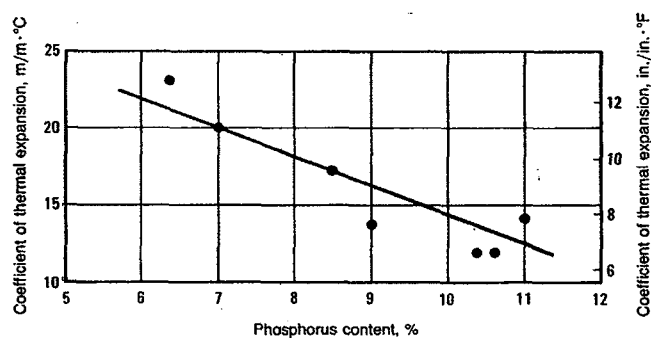


Fig. 10 Effect of deposit phosphorus content on coefficient of thermal expansion

coating thickness are the same on any section of the part exposed to fresh plating solution. Grooves and blind holes have the same amount of coating as the outside of a part.

With electroless nickel, coating thickness can be controlled to suit the application. Coatings as thin as 2.5 μm (0.1 mil) are applied for electronic components, whereas those as thick as 75 to 125 μm (3 to 5 mils) are normally used in corrosive environments. Coatings thicker than 250 μm (10 mils) are used for salvage or repair of worn or mismachined parts (Ref 12).

Adhesion of electroless nickel coatings to most metals is excellent. The initial replacement reaction, which occurs with catalytic metals, together with the associated ability of the baths to remove submicroscopic soils, allows the deposit to establish metallic as well as mechanical bonds with the substrate. The bond strength of the coating to properly cleaned steel or aluminum substrates has been found to be at least 300 to 400 MPa (40 to 60 ksi).

With noncatalytic or passive metals, such as stainless steel, an initial replacement reaction does not occur, and adhesion is reduced. With proper pretreatment and activation, however, the

bond strength of the coating usually exceeds 140 MPa (20 ksi) (Ref 2, 12, 13). With metals such as aluminum, parts baked after plating for 1½ h at 190 to 210 °C (375 to 410 °F) to increase the adhesion of the coating. These treatments relieve hydrogen from the part and the deposit and provide a very minor amount of codiffusion between coating and substrate. Baking parts is most useful where pretreatment has been less than adequate and adhesion is marginal. With properly applied coatings, baking has only a minimal effect on bond strength (Ref 2, 12, 14).

The adhesion of electroless nickel deposits depends on the quality of the cleaning and preparation steps prior to plating. Procedures for cleaning and preparation for electroless nickel plating are generally the same as those for electroplating. One exception is that electrocleaners sometimes cannot be used because of fixturing restraints, making soak cleaning more critical. See the section "Pretreatments for Electroless Nickel Coatings" in this article for more information.

Physical Properties. The density of electroless nickel coatings is inversely proportional to their phosphorus content. As shown in Fig. 9, den-

sity varies from about 8.5 g/cm³ for very low-phosphorus deposit to 7.75 g/cm³ for coatings containing 10 to 11% P (Ref 2, 13, 18-20).

The thermal and electrical properties of these coatings also vary with composition. For commercial coatings, however, electrical resistivity and thermal conductivity are generally about 50 to 90 $\mu\Omega \cdot \text{cm}$ and 0.010 to 0.013 cal/cm · s · °C (2.4 to 3.1 Btu/ft · h · °F), respectively. Accordingly, these coatings are significantly less conductive than conventional conductors such as copper or silver.

Heat treatments precipitate phosphorus from the alloy and can increase its conductivity by three to four times (Ref 2, 13). The formulation of the plating solution can also affect conductivity. Tests with baths containing sodium acetate and succinic acid showed electrical resistivities of 61 and 84 $\mu\Omega \cdot \text{cm}$, respectively (Ref 2).

Phosphorus content also has a strong effect on the thermal expansion of electroless nickel. This is shown in Fig. 10, which shows data for deposit stress measurements on different substrates (Ref 15). The coefficient of thermal expansion of high phosphorus coatings is approximately equal to that of steel. As deposited, coatings containing more than 10% P are completely nonmagnetic. Lower phosphorus coatings, however, have some magnetic susceptibility. The coercivity of 3 to 6% P coatings is about 20 to 80 Oe (1592 to 6366 A/m), while that of deposits containing 7 to 9% P is typically 1 to 2 Oe (80 to 160 A/m). Heat treatments at temperatures above 300 °C (570 °F) improve the magnetic response of electroless nickel and can provide coercivities of about 100 to 300 Oe (7958 to 23,873 A/m) (Ref 11, 21).

Mechanical Properties. The mechanical properties of electroless nickel deposits are similar to those of other glasses. They have high strength, limited ductility, and a high modulus of elasticity. The ultimate tensile strength of commercial coatings exceeds 700 MPa (102 ksi) and allows the coating to withstand a considerable amount of abuse without damage. The effect of phosphorus content on the strength and strain at fracture of electroless nickel deposits is shown in Fig. 11 (Ref 22).

The ductility of electroless nickel coatings also varies with composition. High phosphorus, high purity coatings have a ductility of about 1 to 1½% (as elongation). Although this is less ductile than most engineering materials, it is adequate for most coating applications. Thin films of deposit can be bent completely around themselves without fracture. With lower phosphorus deposits, or with deposits containing metallic or sulfur impurities, ductility is greatly reduced and may approach zero (Ref 12, 14).

Hardening type heat treatments reduce both the strength and ductility of electroless nickel deposits. Exposure to temperatures above 220 °C (428 °F) causes an 80 to 90% reduction in strength and can destroy ductility. This is illustrated by Fig. 12, which shows the effect of different 1 h heat treatments on the elongation at fracture of brass panels coated with 6% P electroless nickel (Ref 11). The modulus of elasticity of electroless nickel coatings containing 7 to 11% P is about

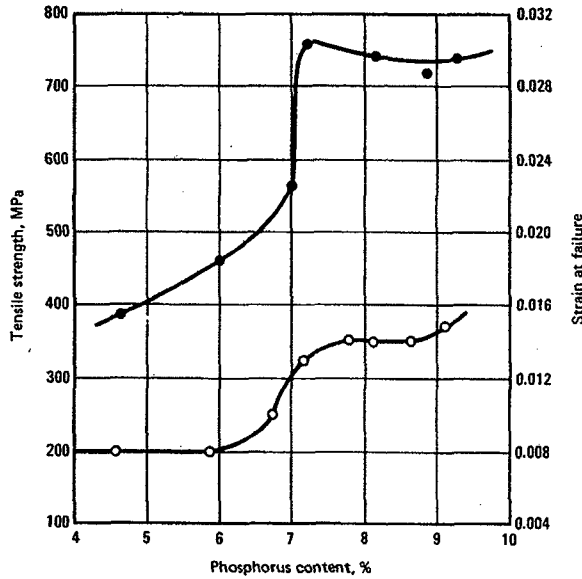


Fig. 11 Effect of deposit phosphorus content on strength and strain at fracture

200 GPa (29,000 ksi) and is very similar to that of steel.

Hardness and wear resistance are extremely important properties for many applications. As deposited, the microhardness of electroless nickel coatings is about 500 to 600 HV₁₀₀, which is approximately equal to 48 to 52 HRC and equivalent to many hardened alloy steels. Heat treatment causes these alloys to age harden and can produce hardness values as high as 1100 HV₁₀₀, equal to most commercial hard chromium coatings (Ref 2, 12). Figure 13 shows the effect of different 1-h heat treatments on the hardness of electroless nickel containing 10½% P (Ref 2).

For some applications, high-temperature treatments cannot be tolerated because parts may

warp, or the strength of the substrate may be reduced. For these applications, longer times and lower temperatures are sometimes used to obtain the desired hardness. This is illustrated in Fig. 14, which shows the effect of different treatment periods on the hardness of a coating containing 10½% P (Ref 12). ASTM specification B 578 requires that the Knoop hardness method be used for plated deposits. However, Vickers hardness numbers have been widely used (Ref 23-25).

Electroless nickel coatings also have excellent hot hardness. To about 400 °C (750 °F), the hardness of heat-treated electroless nickel is equal to or better than that of hard chromium coatings. As-deposited coatings also retain their hardness to this temperature, although at a lower level. The

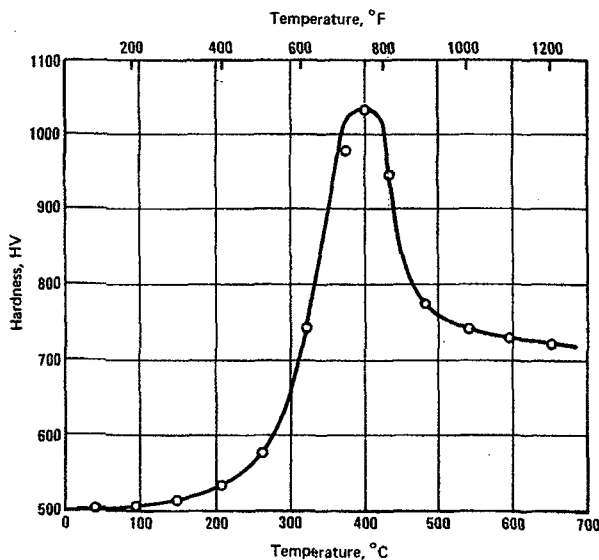


Fig. 13 Effect of heat treatment on hardness of 10½% P electroless nickel coating

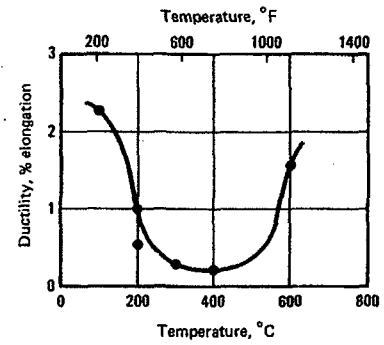


Fig. 12 Effect of heat treatment on the ductility of a 6% P electroless nickel coating

effect of elevated temperature on a 10% P coating is shown in Fig. 15 (Ref 26, 27).

Because of their high hardness, electroless nickel coatings have excellent resistance to wear and abrasion, both in the as-deposited and hardened conditions. Taber Abraser Index values for electroless nickel and for electrodeposited nickel and chromium are summarized in Table 3 (Ref 28, 29, 30).

Tests with electroless nickel-coated vee-blocks in a Falex Wear Tester have shown a similar relationship between heat treatment and wear and confirmed the coating to be equal to hard chrome under lubricated wear conditions (Ref 14, 28). The effect of phosphorus content on the wear experienced by electroless nickel coatings under lubricated conditions is summarized in Fig. 16. These rotating ball tests showed that after heat treatment, high phosphorus deposits provide the best resistance to adhesive wear (Ref 6, 31).

Frictional properties of electroless nickel coatings are excellent and similar to those of chromium. Their phosphorus content provides a natural lubricity, which can be very useful for applications

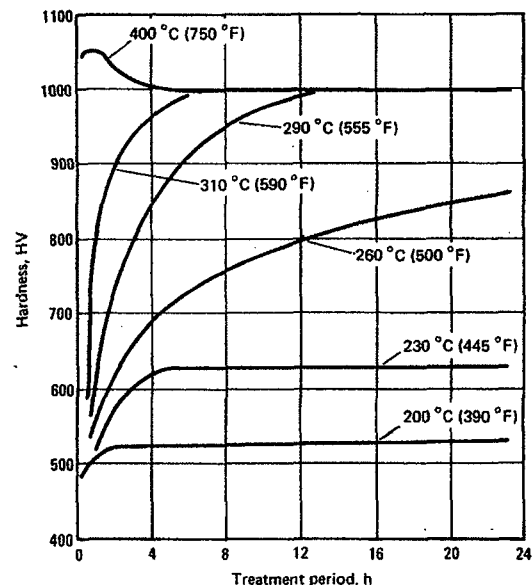


Fig. 14 Effect of different heat treatment periods on hardness of a high-phosphorus electroless nickel coating

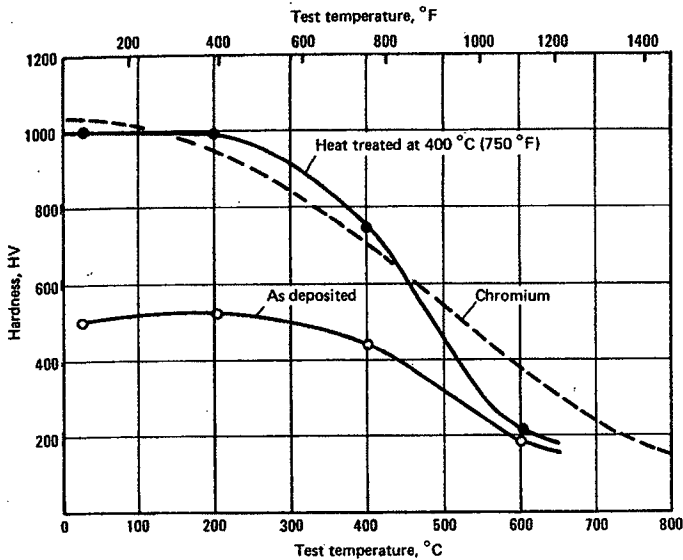


Fig. 15 Effect of temperature on the elevated-temperature hardness of a 10% P electroless nickel coating

Table 3 Comparison of the Taber abraser resistance of different engineering coatings

Coating	Heat treatment for 1 h		Taber wear index, mg/1000 cycles(a)
	°C	°F	
Watts nickel	None	None	25
Electroless Ni-P(b)	None	None	17
Electroless Ni-P(b)	300	570	10
Electroless Ni-P(b)	500	930	6
Electroless Ni-P(b)	650	1200	4
Electroless Ni-B(c)	None	None	9
Electroless Ni-B(c)	400	750	3
Hard chromium	None	None	2

(a) CS-10 abraser wheels, 1000 g load, determined as average weight loss per 1000 cycles for total test of 6000 cycles. (b) Hypophosphite-reduced electroless nickel containing approximately 9% P. (c) Borohydride-reduced electroless nickel containing approximately 5% B

such as plastic molding. The coefficient of friction for electroless nickel versus steel is about 0.13 for lubricated conditions and 0.4 for unlubricated conditions. The frictional properties of these coatings vary little with either phosphorus content or with heat treatment (Ref 2, 28, 31).

Solderability. Electroless nickel coatings can be easily soldered and are used in electronic applications to facilitate soldering such light metals as aluminum. For most components, rosin mildly activated (RMA) flux is specified along with conventional tin-lead solder. Preheating the component to 100 to 110 °C (212 to 230 °F) improves the ease and speed of joining. With moderately oxidized surfaces, such as those resulting from steam aging, activated rosin (RA) flux or organic acid is usually required to obtain wetting of the coating (Ref 2, 32).

Corrosion Resistance. Electroless nickel is a barrier coating, protecting the substrate by sealing it off from the environment, rather than using sacrificial action. Therefore, the deposit must be free of pores and defects. Because of its amorphous nature

and passivity, the coating's corrosion resistance is excellent and, in many environments, superior to that of pure nickel or chromium alloys. Amorphous alloys have better resistance to attack than equivalent polycrystalline materials, because of their freedom from grain or phase boundaries, and because of the glassy films that form on and passivate their surfaces. Some examples of the corrosion experienced in different environments are shown in Table 4 (Ref 2, 16, 30, 33). The resistance to attack in neutral and acidic environments is increased as the phosphorus content is increased in the deposit. The reverse is true in alkaline corrosive environments.

Effect of Composition. The corrosion resistance of an electroless nickel coating is a function of its composition. Most deposits are naturally passive and very resistant to attack in most environments. Their degree of passivity and corrosion resistance, however, is greatly affected by their phosphorus content. Alloys containing more than 10% P are more resistant to attack than those with lower phosphorus contents (Ref 16, 18) in neutral or acidic environments. Alloys containing low phosphorus (3 to 4%) are more resistant to strong alkaline environments than high phosphorus deposits.

Often the tramp constituents present in an electroless nickel are even more important to its corrosion resistance than its phosphorus content. Most coatings are applied from baths inhibited with lead, tin, cadmium, or sulfur. Codeposition of these elements in more than trace amounts causes the corrosion resistance to be decreased by 5 to 40 times (Ref 16).

Effect of Heat Treatment. One of the most important variables affecting the corrosion of electroless nickel is its heat treatment. As nickel-phosphorus deposits are heated to temperatures above 220 °C (430 °F), nickel phosphide particles begin to form, reducing the phosphorus content of the remaining material. This reduces the corrosion resistance of the coating. The particles

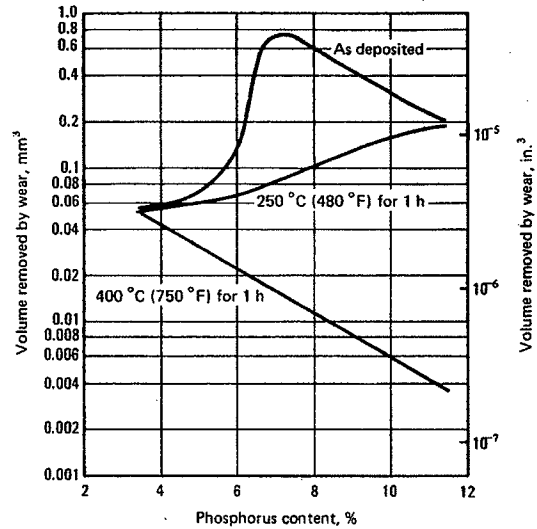


Fig. 16 Effect of phosphorus content on the wear of electroless nickel coatings in rotating ball tests

also create small active/passive corrosion cells, further contributing to the destruction of the deposit. The deposit also shrinks as it hardens, which can crack the coating and expose the substrate to attack. The effect of these changes is illustrated in Table 5, which shows the results of tests with a 10½% P deposit heat treated to represent different commercial treatments and then exposed to 10% hydrochloric acid at ambient temperature (Ref 16). Baking at 190 °C (375 °F), similar to the treatment used for hydrogen embrittlement relief, caused no significant increase in corrosion. Hardening, however, caused the corrosion rate of the deposit to increase from 15 µm/yr (0.6 mil/yr) to more than 900 µm/yr (35 mils/yr). Tests in other environments showed a similar reduction in resistance after hardening. Where corrosion resistance is required, hardened coatings should not be used (Ref 16).

Properties of Electroless Nickel-Boron Coatings

The properties of deposits from borohydride- or aminoborane-reduced baths are similar to those of electroless nickel-phosphorus alloys with a few exceptions. The hardness of nickel-boron alloys is very high, and these alloys can be heat treated to levels equal to or greater than that of hard chromium. Nickel-boron coatings have outstanding resistance to wear and abrasion. These coatings, however, are not completely amorphous and have reduced resistance to corrosive environments; furthermore, they are much more costly than nickel-phosphorus coatings. The physical and mechanical properties of borohydride-reduced electroless nickel are summarized in Table 6 (Ref 2, 6, 34). For comparison, the properties of a hypophosphite-reduced electroless nickel containing 10½% P are also listed (Ref 12).

Table 4 Corrosion of electroless nickel coatings in various environments

Environment	Temperature		Corrosion rate			
			Electroless nickel-phosphorus(a)		Electroless nickel-boron(b)	
	°C	°F	μm/yr	mil/yr	μm/yr	mil/yr
Acetic acid, glacial	20	68	0.8	0.03	84	3.3
Acetone	20	68	0.08	0.003	Nil	Nil
Aluminum sulfate, 27%	20	68	5	0.2
Ammonia, 25%	20	68	16	0.6	40	1.6
Ammonia nitrate, 20%	20	68	15	0.6	(c)	(c)
Ammonium sulfate, saturated	20	68	3	0.1	3.5	0.14
Benzene	20	68	Nil	Nil	Nil	Nil
Brine, 3½% salt, CO ₂ saturated	95	205	5	0.2
Brine, 3½% salt, H ₂ S saturated	95	205	Nil	Nil
Calcium chloride, 42%	20	68	0.2	0.008
Carbon tetrachloride	20	68	Nil	Nil	Nil	Nil
Citric acid, saturated	20	68	7	0.3	42	1.7
Cupric chloride, 5%	20	68	25	1
Ethylene glycol	20	68	0.6	0.02	0.2	0.008
Ferric chloride, 1%	20	68	200	8
Formic acid, 88%	20	68	13	0.5	90	3.5
Hydrochloric acid, 5%	20	68	24	0.9
Hydrochloric acid, 2%	20	68	27	1.1
Lactic acid, 85%	20	68	1	0.04
Lead acetate, 36%	20	68	0.2	0.008
Nitric acid, 1%	20	68	25	2
Oxalic acid, 10%	20	68	3	0.1
Phenol, 90%	20	68	0.2	0.008	Nil	Nil
Phosphoric acid, 85%	20	68	3	0.1	(c)	(c)
Potassium hydroxide, 50%	20	68	Nil	Nil	Nil	Nil
Sodium carbonate, saturated	20	68	1	0.04	Nil	Nil
Sodium hydroxide, 45%	20	68	Nil	Nil	Nil	Nil
Sodium hydroxide, 50%	95	205	0.2	0.008
Sodium sulfate, 10%	20	68	0.8	0.03	11	0.4
Sulfuric acid, 65%	20	68	9	0.4
Water, acid mine, 3.3 pH	20	68	7	0.3
Water, distilled, N ₂ deaerated	100	212	Nil	Nil	Nil	Nil
Water, distilled, O ₂ saturated	95	205	Nil	Nil	Nil	Nil
Water, sea (3½% salt)	95	205	Nil	Nil

(a) Hypophosphite reduced electroless nickel containing approximately 10½% P. (b) Borohydride reduced electroless nickel containing approximately 5% B. (c) Very rapid. Specimen dissolved during test

Table 5 The effect of heat treatment on the corrosion of a 10½% P electroless nickel deposit in 10% hydrochloric acid

Heat treatment	Deposit hardness, HV ₁₀₀	Corrosion rate	
		μm/yr	mil/yr
None	480	15	0.6
190 °C (375 °F) for 1½ h	500	20	0.8
290 °C (550 °F) for 6 h	900	1900	75
290 °C (550 °F) for 10 h	970	1400	55
340 °C (650 °F) for 4 h	970	900	35
400 °C (750 °F) for 1 h	1050	1200	47

Structure and Internal Stress. The boron content of electroless nickel reduced with DMAB or DEAB can vary from 0.2 to 4% depending on bath formulation and operation. Commercial borohydride-reduced coatings typically contain 3 to 5% B. Unlike nickel-phosphorus coatings in the as-deposited condition, electroless nickel-boron contains crystalline nickel mixed with nickel-boron (typically Ni₂B) glass. These coatings also are not totally homogeneous and consist of phases of different composition (Ref 2, 7, 35).

During heating, electroless nickel-boron age hardens in the same manner as nickel-phosphorus alloys. At temperatures over 250 °C (480 °F),

particles of nickel boride (Ni₃B) form, and at 370 to 380 °C (700 to 715 °F), the coating crystallizes. The final structure of hardened nickel-boron coatings consists of nickel-boron intermetallic compounds (principally Ni₃B and Ni₂B) and about 10% Ni (Ref 2, 7, 34).

The internal stress level of nickel-boron deposits is generally high. The effect of boron content and complexing agent on the stress in DMAB-reduced electroless nickel coatings is shown in Table 7 (Ref 10). The internal stress of borohydride-reduced coatings is typically 110 to 200 MPa (16 to 29 ksi) tensile (Ref 34).

Physical and mechanical properties of borohydride-reduced electroless nickel are summarized in Table 6 (Ref 2, 6, 34). For comparison, the properties of a hypophosphite-reduced coating containing 10½% P are also listed (Ref 12). The density of electroless nickel-boron is very similar to that of nickel-phosphorus coatings of equal alloy content. The density of borohydride-reduced coatings containing 5% B is 8.25 g/cm³ in both the as-deposited and heat-treated condition (Ref 2, 34).

The melting point of nickel-boron coatings is relatively high and can approach that of metallic nickel. Sodium borohydride reduced coatings melt at 1080 °C (1975 °F), while the melting point of DMAB-reduced coatings varies

Table 6 Physical and mechanical properties of electroless nickel-boron and nickel-phosphorus deposits

Properties are for coatings in the as-deposited condition, unless noted.

Property	Electroless nickel-boron(a)	Electroless nickel-phosphorus(b)
Density, g/cm ³ (lb/in. ³)	8.25 (2.98)	7.75 (2.8)
Melting point, °C (°F)	1080 (1980)	890 (1630)
Electrical resistivity, μΩ · cm	89	90
Thermal conductivity, W/m · K (cal/cm · s · °C)	...	4 (0.01)
Coefficient of thermal expansion (22-100 °C, or 72-212 °F), μm/m · °C (μin./in. · °F)	12.6 (7.1)	12 (6.7)
Magnetic properties	Very weakly ferromagnetic	Nonmagnetic
Internal stress, MPa (ksi)	110 (16)	Nil
Tensile strength	110 (16)	700 (100)
Ductility, % elongation	0.2	1.0
Modulus of elasticity, GPa (10 ⁶ psi)	120 (17)	200 (29)
As-deposited hardness, HV ₁₀₀	700	500
Heat-treated hardness, 400 °C (750 °F) for 1 h, HV ₁₀₀	1200	1100
Coefficient of friction vs steel, lubricated	0.12	0.13
Wear resistance, as-deposited, Taber mg/1000 cycles	9	18
Wear resistance, heat treated 400 °C (750 °F) for 1 h, Taber mg/1000 cycles	3	9

(a) Borohydride-reduced electroless nickel containing approximately 5% B. (b) Hypophosphite-reduced electroless nickel containing approximately 10½% P.

Table 7 Effect of boron content and complexing agent on internal stress in DMAB-reduced deposits

Complexing agent	Boron content, %	Internal stress(a)	
		MPa	ksi
Malonate	4.3	120	17.4
Malein-glycine	1.2	310	44.9
Pyrophosphate	0.4	480	69.6

(a) Based on tests with 12½ μm thick coatings on a Brenner-Senderoff Spiral Contractometer. Stresses are tensile.

from about 1350 to 1390 °C (2460 to 2535 °F) (Ref 2, 34).

The electrical resistivity of 5% B coatings is similar to that of nickel-phosphorus alloys ranging from 89 μΩ · cm in the as-deposited condition to 43 μΩ · cm after heat treatment at 1100 °C (2010 °F). The resistivity of 0.5% B to 1% B ranges from 10 to 20 μΩ · cm. In the as-deposited condition, nickel-boron coatings are very weakly ferromagnetic, with coercivities about 10% of that of metallic nickel. Their magnetic susceptibility, however, can be increased by heat treatments at temperatures above 370 °C (700 °F) (Ref 2, 7, 34).

The strength and ductility of nickel-boron coatings containing 5% B is only about one-fifth that

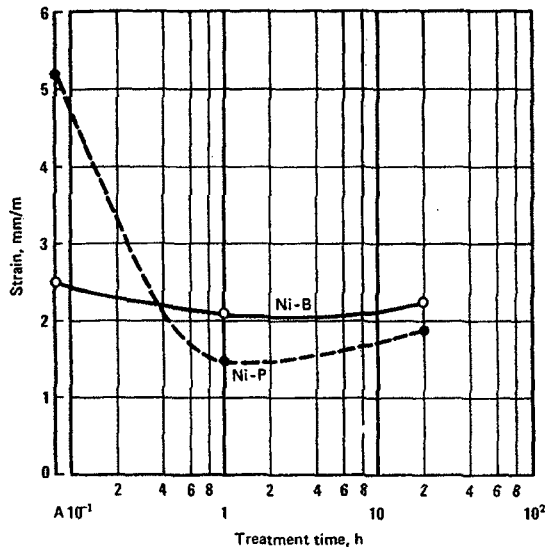


Fig. 17 Effect of heat treatments at 400 °C (752 °F) on the strain at fracture of electroless Ni-5% B and Ni-9% P coatings

of high-phosphorus deposits. Guided bend tests of panels coated with 5% Ni-B showed it strain at fracture to be 2.5 mm/m (2.5 mils/in.). In the same test, the breaking strain of a hypophosphite-reduced electroless nickel containing approximately 9% P was 5.3 mm/m (5.3 mils/in.). Unlike nickel-phosphorus coatings, however, heat treatment has little effect on the ductility of nickel-boron. As illustrated by Fig. 17, even after 12 h at 400 °C (750 °F), strain at fracture declines by only 15% (Ref 7). The modulus of elasticity of borohydride-reduced coatings ranges from 120 GPa (17,000 ksi) in the as-deposited condition to 180 GPa (26,000 ksi) for coatings heat treated at 400 °C (750 °F) for 1 h (Ref 34).

Hardness and Wear Resistance. The principle advantage of electroless nickel-boron is its high hardness and superior wear resistance. In the as-deposited condition, microhardness values of 650 to 750 HV₁₀₀ are typical for borohydride- and aminoborane-reduced coatings. After 1-h heat treatments at 350 to 400 °C (660 to 750 °F) hardness values of 1200 HV₁₀₀ can be produced. This is illustrated by Fig. 18, which shows the effect of heat treatment temperature on hardness (Ref 2, 7, 34).

Long-term treatments (30 to 40 weeks) at temperatures between 200 and 300 °C (390 and 570 °F) can produce hardness values of 1700 to 2000 HV₁₀₀. These low-temperature treatments result in a finer dispersion of nickel boride than do higher temperatures and in the formation of iron borides (such as Fe₂B and Fe₃C_{0.2}B_{0.8}) within the coating (Ref 2, 34).

The wear resistance of electroless nickel-boron is exceptional and after heat treatment equals or exceeds that of hard chromium coatings. Typical Taber wear test results for a 5% B coating is shown in Tables 3 and 6. The effect of heat treatment and hardness on the wear experienced in rotating ring and block tests (similar to the Alpha LFW-1 test described in ASTM D 2714) (Ref 35)

under nonlubricated conditions is also shown in Fig. 18. Nickel-boron deposits containing 2.5 to 3% B exhibit similar wear characteristics.

Electroless nickel-boron coatings are naturally lubricious. Their coefficient of friction versus steel is typically 0.12 to 0.13 in the lubricating conditions, and 0.43 to 0.44 for dry wear (Ref 2, 34).

Corrosion Resistance. In general, the corrosion resistance of electroless nickel-boron coatings is less than that of high-phosphorus alloys. That is illustrated by Table 4, which compares the attack experience by hypophosphite- and borohydride-reduced coatings in different media. In environments that cause little corrosion of nickel-phosphorus, such as alkalis and solvents, electroless nickel-boron is also very resistant. In environments, however, that cause moderate attack of nickel-phosphorus, such as acids and ammonia solutions, nickel-boron coatings can be severely corroded. In strongly oxidizing media, of course, neither coating is satisfactory.

Effect of Electroless Nickel Coatings on the Fatigue Strength of Steel

Because of their tendency to crack under cyclic loads, electroless nickel coatings can cause a significant reduction in the fatigue strength of steel substrates. The magnitude of the reduction, however, depends on the composition, heat treatment, and thickness of the coating, as well as the original fatigue strength of the steel. Several investigations have shown that the use of electroless nickel coatings causes a 10 to 50% reduction in the fatigue strength and endurance limit of steel substrates (Ref 6, 7, 36-38). In these tests, fatigue strength of notched specimens was reduced by at least 15%, whereas unnotched samples showed relatively small reductions.

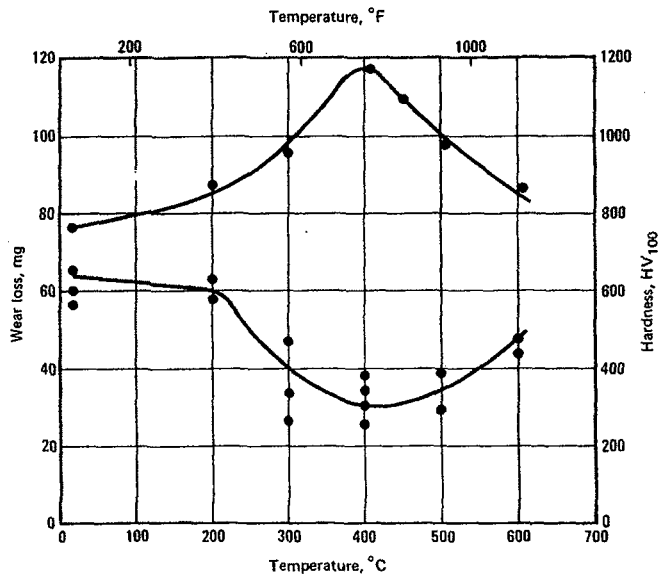


Fig. 18 Effect of different 1h heat treatments on the hardness and wear resistance of borohydride-reduced electroless nickel

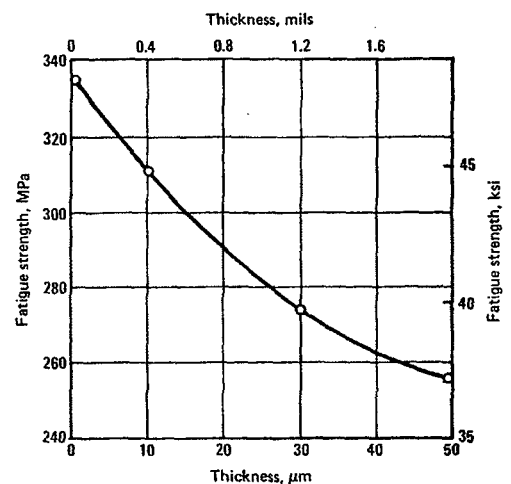


Fig. 19 Effect of coating thickness on the fatigue strength of a carbon-manganese steel

The loss of fatigue strength has principally been a problem with hypophosphite-reduced coatings containing less than 10% P, and with nickel-boron alloys. These deposits contain high levels of internal tensile stress and under cyclic stress conditions tend to crack and initiate fatigue failures. Other tests have implied that this is not a significant problem with high-phosphorus deposits (Ref 39, 40). Coatings containing 10½% or more phosphorus are compressively stressed on steel and tend to resist cracking.

Heat treatment of electroless nickel coatings tends to exacerbate the decrease in fatigue strength. Heat-treated coatings tend to be more highly stressed than as-deposited coatings and have a greater tendency to crack. Heat treating a high phosphorus, compressively stressed coating can cause it to become tensilely stressed (Ref 14). Coatings heat treated at temperatures above 340

Table 8 Effect of heat treatment of an electroless nickel-5% B coating on the fatigue strength of steel

Condition	Fatigue strength	
	MPa	ksi
Not coated	350	51
As-deposited	270	39
250 °C (480 °F) for 1 h	260	38
350 °C (660 °F) for 1 h	245	36
400 °C (750 °F) for 1 h	270	39

°C (650 °F) also tend to be cracked because of the shrinkage of the alloy. These cracks act as stress risers and further reduce fatigue resistance. Table 8 shows the effect of different 1-h heat treatments on the fatigue strength of a 0.42% C steel (C45, Werkstoff 1.0503) coated with 30 µm (1.2 mils) of borohydride-reduced electroless nickel (Ref 6). Heat treatments at very high temperatures, 650 to 800 °C (1200 to 1470 °F), produce a thick diffusion zone between the coating and the substrate, which may eliminate or at least greatly reduce the effect of the coating on fatigue strength.

The reduction in fatigue strength produced by electroless nickel deposits is also affected by the thickness of the coating. Thicker deposits have the greatest effect on fatigue strength. This is illustrated in Fig. 19, which shows the reduction in strength of a carbon-manganese steel (St52, Werkstoff 1.0580) produced by different thicknesses of a 5% B nickel coating (Ref 6).

Pretreatment for Electroless Nickel Coatings

Proper pretreatment can be as important to the successful application of an electroless nickel coating as the actual deposit. Inadequate cleaning can result in lack of adhesion, roughness, coating porosity, and early failure. The methods used to clean and prepare a metal surface for electroless nickel plating are similar to those used for conventional electroplating, although more care and control are required. One penetrant that is unique to electroless nickel plating is the application of a strike copper plate to alloys containing significant amounts of lead, tin, cadmium, or zinc. This ensures adequate coverage and prevents contamination of the electroless solution.

Pretreatment for Ferrous Alloys

To prepare ferrous alloys properly for electroless nickel plating, the combination of solvent and alkaline degreasing, acid activation, and electrocleaning are required, with intermediate water rinses. These steps are discussed in other articles in this Volume. Recommended pretreatment procedures for different ferrous alloys are summarized below:

Carbon and low-alloy steel

1. Soak clean for 10 to 30 min

2. Rinse
3. Electroclean at 5 V for 60 to 120 s
4. Rinse
5. Dip in 30% HCl for 30 to 60 s. Alternatives: 10 to 20% sulfuric acid avoids leaving chloride ions in pores and thus can improve salt spray resistance. Sulfamic acid and citric acids are also used beneficially.
6. Rinse
7. Electroclean at 5 V for 30 to 60 s
8. Rinse
9. Plate to thickness

Alloy steel (Cr or Ni > 1½%)

1. Soak clean for 10 to 30 min
2. Rinse
3. Electroclean at 5 V for 60 to 120 s
4. Rinse
5. Dip in HCl acid for 30 to 60 s
6. Rinse
7. Electroclean at 5 V for 30 to 60 s
8. Rinse
9. Dip in 30% HCl for 30 to 60 s
10. Rinse
11. Nickel strike at 2 A/dm² (20 A/ft²) for 60 s
12. Rinse
13. Plate to thickness

300 or 400 series stainless steel

1. Soak clean for 10 to 30 min
2. Rinse
3. Electroclean at 5 V for 60 to 120 s
4. Rinse
5. Dip in 30% HCl for 60 s
6. Rinse
7. Nickel strike at 2 A/dm² (20 A/ft²) for 60 s
8. Rinse
9. Plate to thickness

300 series stainless steel (complex shapes)

1. Soak clean for 10 to 30 min
2. Rinse
3. Electroclean at 5 V for 60 to 120 s
4. Rinse
5. Dip in 30% HCl for 60 s
6. Rinse
7. 10% H₂SO₄ at 60 °C (140 °F) for 30 s. Alternative: nickel strike
8. Plate to thickness

400 series stainless steel (complex shapes)

1. Soak clean for 10 to 30 min
2. Rinse
3. Electroclean at 5 V for 60 to 120 s
4. Rinse
5. Dip in 30% HCl for 60 s
6. Rinse
7. Dip in 20% HCl at 50 °C (120 °F) for 30 s. Alternative: nickel strike

8. Rinse with deionized water
9. Plate to thickness

In Step 1, all alkaline soak cleaners should be operated at their supplier's maximum recommended temperature, typically 60 to 80 °C (140 to 175 °F). Unless otherwise indicated, all other processes are at ambient temperature. In Step 3, electrocleaning is with at least three reversals of current (part, cathodic/anodic, three times) at 3 to 5 A/dm² (30 to 50 A/ft²). Except for 300 series stainless steel, the final current cycle should be with the part anodic; with 300 series stainless steels, the final current cycle should be with the part cathodic to minimize the formation of an oxide film on its surface.

Activation for Alloy Steels. Before electroless plating, stainless and alloy steel parts must be chemically activated to obtain satisfactory adhesion. For this, a low pH nickel strike is normally used. Two common strike baths are listed below:

Nickel sulfamate strike	
Nickel sulfamate	165-325 g/L (22-43 oz/gal)
Nickel (as metal)	35-75 g/L (5-10 oz/gal)
Sulfamic acid (~20 g/L, or 2.7 oz/gal)	to pH 1-1.5
Boric acid	30-34 g/L (4-4.5 oz/gal)
Hydrochloric acid (20° Bé)	12 mL/L (1.5 fluid oz/gal)
Temperature	Room temperature
Cathode current density	1-10 A/dm ² (10-100 A/ft ²)
Time	30-60 s
Anodes (bagged)	Sulfur depolarized nickel
Operating pH	0.8-1.5
Woods nickel strike	
Nickel chloride	240 g/L (32 oz/gal)
Hydrochloric acid	250 mL/L (32 fluid oz/gal)
Temperature	Room temperature
Cathode current density	2-10 A/dm ² (20-100 A/ft ²)
Time	30-120 s
Anodes	Rolled depolarized nickel

Caution: Insoluble anodes cannot be used. Chlorine gas would be liberated from insoluble anodes.

Nickel strikes should not be used to cover up improper pretreatment of plain or low-alloy steel. Nickel-strike activation should be considered, however, when processing steel with chromium or nickel contents of over 1.5% carburized or nitrided steels, and stainless steels. Nickel-strike processing should follow acid activation to avoid drag-in of alkaline materials into the strike (Ref 41-46).

Pretreatment for Aluminum Alloys

Like steel, aluminum is catalytic to electroless nickel deposition and could be plated after only a simple cleaning. Aluminum is very reactive, however, and oxides form very rapidly on its surface during rinsing or exposure to air. The

oxide films that develop prevent metallic bonds from forming between the coating and the substrate and can result in adhesion failure. To avoid this problem, special processing procedures are required, including deoxidizing and zincating or acid zinc immersion. Processing procedures for aluminum alloys are discussed in the article on cleaning and finishing of aluminum alloys in this Volume.

Pretreatment for Copper Alloys

Copper-base alloys are prepared for electroless nickel plating using procedures similar to those for steel, alkaline cleaning and acid deoxidizing. Two important differences exist, however:

- ▶ Copper is not catalytic to the chemical reduction of electroless nickel, and its alloys must be activated chemically or electrolytically before they can be plated.
- ▶ Lead in amounts of 1/2 to 10% is often added to copper alloys to make them easier to machine. Unless the free lead present on the surface of the part is removed, adhesion failures and coating porosity result.

Processing procedures for copper alloys are given in the article on cleaning and finishing of copper and copper alloys in this Volume.

Activation. Once a copper alloy surface is clean and oxide-free, it must be activated before electroless nickel can deposit. To prevent reoxidation, this activation should be initiated without long intermediate delays. The preferred method for initiating deposition is an electrolytic strike in the electroless nickel bath. Using a nickel anode, the parts are made cathodic at 5 V for 30 to 60 s. This applies a thin, electrolytic nickel-phosphorus coating and provides a catalytic surface. After the current is removed, the electroless deposition can continue.

Another method for initiating electroless deposition on copper alloy surfaces is to preplate surfaces with electrolytic nickel. One disadvantage of this method is that blind holes, internal surfaces, or low current density areas may not be coated by the strike, resulting in incomplete coverage or unplated areas. The use of nickel chloride strikes also may result in chloride contamination of the electroless nickel bath through drag-in.

A third method of activating copper alloys in electroless nickel solutions is to touch them with a piece of steel or with another part already coated with electroless nickel after they have been immersed in the bath. This creates a galvanic cell, producing an electric current to initiate the electroless reaction. Deposition spreads until the whole part is covered with electroless nickel. However, two problems can occur with galvanic activation:

- ▶ Galvanic currents do not travel well around sharp curves, such as those on threads or cor-

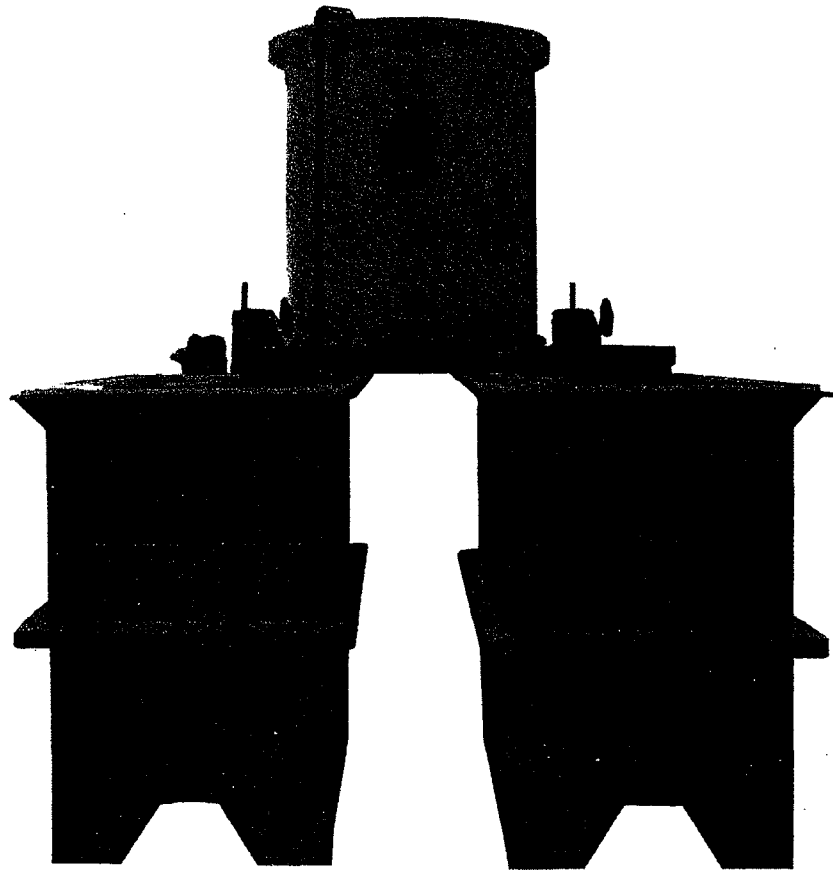


Fig. 20 Twin tank system for electroless nickel plating. Tanks are used alternately. While one tank is being used to plate, the second is being passivated. Cylindrical tank is used to store 30% nitric acid for passivation.

- ners, and can leave bare spots or areas of reduced thickness
- Passivation of the copper can occur before the deposit spreads across the entire surface leading to poor adhesion

Other methods include immersion for 15 to 30 s in dilute solutions of palladium chloride (0.05 to 0.1 g/L), and nickel-boron nickel strike processes that use DMAB reducing agent.

Leaded Alloys. Unlike other elements added to brass or bronze, lead does not combine with copper to form an alloy. Instead, it remains in the metal as globules. The lead exposed during cutting or machining acts as a lubricant by flowing or smearing across the surface. Electroless nickel does not deposit on lead. Unless lead smears are removed, the applied coating is porous with poor adhesion. Lead remaining on the surface of parts can also contaminate electroless nickel solutions, causing a rapid decline in plating rate and deposit quality.

Surface lead is best removed by immersing parts for 30 s to 2 min in a 10 to 30% solution of fluoboric acid at room temperature. Sulfamic acid, citric acid, and dilute nitric acid have also been reported to be effective solutions for removing lead. The removal of lead must occur before deoxidizing or bright dipping in the pretreatment cycle, and it is not a substitute for these steps (Ref 2, 41, 47).

Equipment for Electroless Nickel Plating

Because electroless nickel is applied by a chemical reaction rather than by electrolytic deposition, special attention to design and construction of the tanks and auxiliary equipment is required to ensure trouble-free operation and quality coatings.

Plating Tanks

Cylindrical or bell-shaped tanks have been used for electroless nickel plating, although rectangular tanks have been found to be the most convenient to build and operate. Rectangular tanks have been constructed from various materials in many different sizes. A common electroless nickel plating system is shown in Fig. 20.

Physical Dimensions. The following factors should be considered when selecting the size of an electroless nickel plating tank:

- Size of the part to be plated
- Number of parts to be plated each day
- Plating thickness required
- Plating rate of the solution (most conventional electroless nickel solutions deposit between 12 and 25 $\mu\text{m/h}$, or 0.5 and 1 mil/h)

- Type of rack, barrel, or basket used to support parts
- Number of production hours available each day to process parts
- Nominal recommended work load of 1.2 dm²/L (0.5 ft²/gal) of working solution

The size of the part or the size of the supporting rack, barrel, or basket usually defines the minimum size tank that can be used. The minimum dimension of the tank should be at least 15 cm (6 in.) greater than the maximum dimension of the part or its support to allow proper agitation and the flow of fresh solution to all surfaces. The size of the tank may have to be increased, however, to accommodate the volume of the parts required or to provide a more suitable work area to solution volume ratio.

Construction Materials. The following factors should be considered when selecting construction materials for a plating tank:

- Operating temperature of the electroless nickel plating solutions, usually 85 to 95 °C (185 to 205 °F)
- Tendency of tank material to become sensitized to the deposition of electroless nickel
- Cost of tank material, including both initial construction cost and its life in a production environment

With continued exposure to heated electroless nickel solutions, almost any surface eventually becomes sensitized or receptive to deposition of the coating. The more inert or passive the material selected, the less likely that plate out can occur. All material in contact with the plating solution must be repassivated periodically with 30 vol% nitric acid to minimize deposition on its surface.

The most widely used materials for tank construction have been polypropylene, stainless steel, and steel or aluminum with a 635 µm (25 mil) thick polyvinyl chloride bag liner. Contamination from bleedout of oils or other plasticizers can have harmful effects on the plating solution. Leaching linings prior to use is recommended. However, the contaminants continue to migrate to the surface and enter the solution (Ref 48). Although all of these materials have been used successfully, a 6 to 12 mm (0.25 to 0.5 in.) thick polypropylene liner installed in a steel or fiberglass support tank, has proven to be the most troublefree material and has gained the widest acceptance. Polypropylene is relatively inexpensive and is very resistant to plate out. The smooth surface of polypropylene also reduces the possibility of deposit nucleation.

When constructing a polypropylene tank, only stress relieved, unfilled virgin material should be used. Welds should be made under an inert gas shield, such as nitrogen, to prevent oxidation of the polypropylene and incomplete fusion. All welds should be spark tested at 20,000 V before use to ensure integrity.

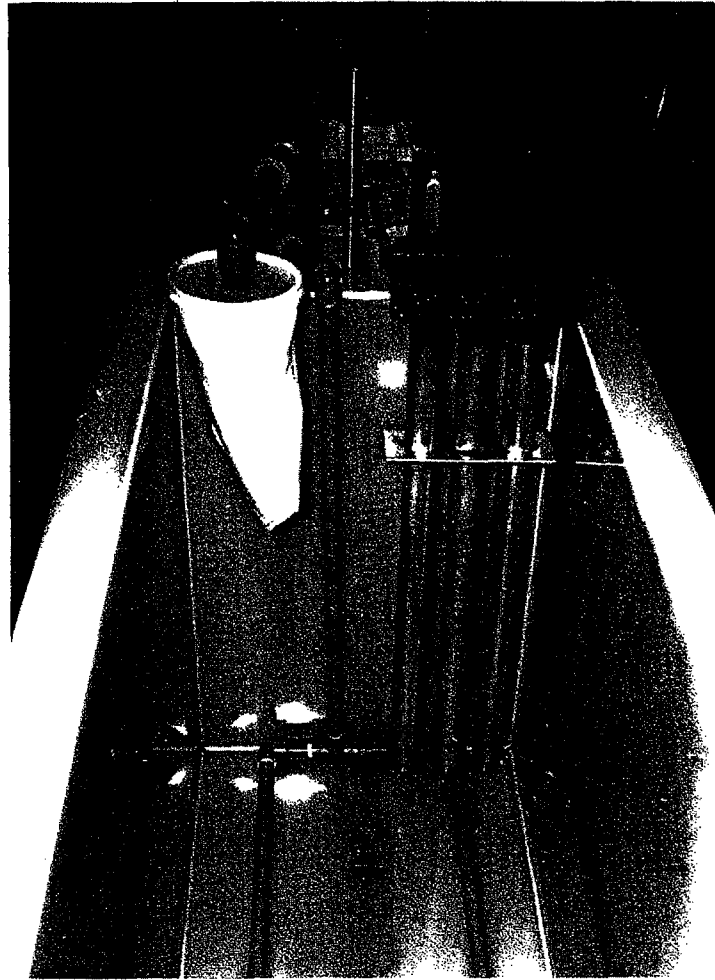


Fig. 21 Electric immersion heater

Heating the Solution

Steam and electricity are the two most common sources of power for heating plating solutions. Although the capital expenditures for steam or pressurized hot water are somewhat higher than that for electricity, the operating costs for steam are considerably less.

Steam. Heating with steam is accomplished using immersion coils or external heat exchangers. The most common immersion coils are those made of Teflon or stainless steel.

Teflon heat exchanger coils are made of many small diameter Teflon tubes looped into the tank between manifolds. Because of the poor conductivity of the plastic, a much larger coil surface area must be used than would be needed with a metal heater. Teflon tubes are delicate, and the tubes must be protected from mechanical damage.

Stainless steel panel coils are constructed of plates joined together with internal passages for the flow of heating medium. These coils are very efficient and economical. Their primary disadvantage is that they are easily galvanically activated and are prone to plate out. To prevent this,

coils are often coated with Teflon. This, however, reduces their heat transfer and their efficiency.

Anodic passivation is also sometimes used to prevent stainless steel coils from plating. With this technique, a slight positive charge is applied to the coil preventing the deposition of electroless nickel. If the work is suspended too close to an anodically passivated coil, however, stray currents from the coil may affect the quality of the plating. Static electricity discharges from steam coils to the work can also cause nonuniform or pitted coatings. To avoid this, coils should be isolated from the steam piping with dielectric couplings.

Steam can also be used to heat the plating solution through a heat exchanger, which is mounted outside the tank. The heat exchangers are usually of shell and tube or plate coil design and are constructed of stainless steel. The solution is pumped through exchangers and returned to the tank, often through a filter. To prevent the inside of the exchanger from plating, the solution velocity must be maintained above 2½ m/s (8 ft/s).

Electric. Heating with electricity is usually accomplished with tube immersion heaters. The resistance heating elements are sheathed in quartz,

Table 9 Comparison of piping and valve materials for electroless nickel plating systems

Material	Resistance to plating temperatures	Resistance to plate out	Relative cost	Availability
Piping				
Stainless steel	High	Low	High	Good
Kynar	High	High	Moderate	Poor
CPVC	Moderate	Moderate	Low	Good
Polypropylene	Low	High	Low	Limited
Valves				
Stainless steel	High	Low	Moderate	Good
CPVC	Moderate	Moderate	Moderate	Good
Polypropylene	Moderate	High	Moderate	Good

titanium, or stainless steel. Stainless steel is the most economical material and is usually preferred. Either type 304 or 316 stainless steel is acceptable. Occasionally electropolished stainless steel or Teflon-coated heaters are also used. The cost of these additions, however, cannot usually be justified for most applications. An electric immersion heater is shown in Fig. 21.

Pumps

Pumps are used in electroless nickel plating systems for solution transfer and filtration. The following factors should be considered when selecting pumps for electroless nickel plating systems:

- Operating temperature of the plating solution, usually 85 to 95 °C (185 to 205 °F)
- Chemicals being handled in both the electroless nickel plating solution and the 30% nitric acid solution used for passivation
- Volume flow rate (liters per minute) required to allow the total tank volume to be filtered approximately ten times each hour

Two materials, CPVC plastic and type 304 stainless steel, have been proven to be satisfactory for electroless nickel pumps. CPVC plastic is more resistant to plate out than stainless steel and is less expensive. However, large plastic pumps lack the capacity and mechanical strength needed to provide proper filtration in electroless nickel systems. Accordingly, plastic pumps are used for flow rates less than 300 L/min (80 gal/min), whereas stainless steel is used for higher flow applications.

Vertical Pumps. Vertical centrifugal pumps are now the most commonly used pumps for electroless nickel systems. These pumps can be mounted so only the impeller is below the solution level and shaft seals are not required. Consequently, maintenance of this pump is minimized. Some vertical pumps can also be mounted outside the tank, providing the maximum area for plating.

With CPVC plastic pumps, the impeller should be machined or molded; glued impellers should not be used. All gaskets and O-rings for electroless nickel systems should be fluorocarbon rubber.

The velocity of the solution through the pump should be at least 2½ m/s (8 ft/min) to prevent the solution from plating out on the pump housing, especially when stainless steel is used. To accomplish this, a pump speed of 1750 rev/min is required.

Piping and Valves

Piping and valves available for electroless nickel systems are of four principal types: stainless steel, polyvinylidene fluoride, CPVC plastic, and polypropylene. The advantages and disadvantages of each of these materials are summarized in Table 9.

Piping components in electroless nickel plating systems are used for air agitation spiders, tank outlet, pump inlet, and discharge pipes, solution manifolds, and deionized water fill lines. These pipes must be sized to minimize restrictions and provide proper agitation and filtration. The diameter of the tank outlet piping should be at least as large as the pump inlet connection to avoid cavitation and increased pump wear. CPVC plastic is normally used for pipe exposed to the plating solution.

Although CPVC or other plastic pipe may be joined by solvent welding, threaded joints are preferred. Threaded connections are easier to make and more trouble-free, allowing repairs or modifications to be accomplished quickly. When threading plastic pipe, a plug should be inserted inside the pipe end to support the pipe and prevent collapse or thread breakage. Threads should be wrapped with Teflon tape before joining to prevent potential leakage from the galling of the plastic.

Valves. Almost all of the valves used for electroless nickel systems are a ball and seat design. Because of prolonged exposure to stagnant plating solutions, inertness or resistance to deposit plate out is of primary importance with these valves. Accordingly, polypropylene is used most often. The reduced strength of polypropylene at plating temperatures is not a problem with valves, because of their compactness and greater thickness.

CPVC plastic valves are also used occasionally for electroless nickel systems, although their reduced resistance to deposit plate out makes them more prone to seizure and failure due to deposit buildup than polypropylene. Because of their

somewhat higher cost and tendency to activation and deposition, stainless steel valves are not normally used. For valves in agitation air supply lines, plain PVC plastic valves may be used if they are mounted at least 200 mm (8 in.) away from hot plating solution. Valves and piping for steam services should be steel or stainless steel.

Agitation

Agitation of parts and solution is necessary during electroless nickel plating to provide a fresh supply of solution to the part and to remove the hydrogen produced during deposition. Without consistent renewal of plating solution, localized depleted areas can occur, resulting in nonuniform coating thickness. Hydrogen bubbles, if allowed to remain on the surface of the part, tend to mask plating and can cause pitting or fisheyes in the coating.

Agitation is accomplished by moving the part mechanically through the solution, by solution movement (preferably by discharge of solution from a suitable filter and distributed by a sparger throughout the tank), or by bubbling air through the bath to move the solution past the part. A typical air agitation spider is shown in Fig. 21. For air agitation, a clean low-pressure air source, such as is provided by centrifugal blowers, is preferred. High-pressure air from compressors can introduce oil or other contaminants into the bath and affect deposit quality.

Filtration

Two types of filtration are used for electroless nickel systems, cartridge filters and filter bags. Both require the use of an external circulation pump, and both should be capable of removing particles larger than 5 µm (0.2 mil) in size. Wound cartridge filters are supported in CPVC or polypropylene chambers located outside of the tank. The installation cost of these filters is high, however, and replacement of the cartridges is a large maintenance cost. Also the added back pressure of the filter can significantly reduce the flow of the pump and often its life.

Woven polypropylene bags are now being used to filter electroless nickel solutions. These bags are mounted above the plating tank itself, allowing the solution to flow through the bag by gravity. Filter bags are relatively inexpensive and result in only a minimum restriction on the discharge of the pump. When bags become soiled or begin to plate out, the change is obvious to the operator, and the bags can be quickly and easily replaced. Filter bags with stainless steel support rings rather than plated steel rings should be used. Plated rings can introduce cadmium or zinc into the bath and slow or stop deposition. A filter assembly is shown in Fig. 21.

Filter cartridges and bags should be washed using hot water prior to use for electroless nickel. Antistatic agents often found in these filter media can be harmful to the plating solution.

For extremely critical applications such as memory disks, filtration should be through a 1 μM filter cartridge followed by a 0.2 μM cartridge using flow rates sufficient to turn over the volume of plating solution 10 to 20 times per hour. Filter discharge is best done through a sparger to distribute the solution uniformly in the tank, and not impinge on the parts being plated.

Racking for Electroless Nickel Plating

Because electroless nickel is applied by chemical reduction, anode to cathode area relationships and current density considerations, usually of concern in electrolytical applications, are usually not important. This simplifies rack design.

Construction Materials. Racks for plating ferrous and copper alloys should be capable of carrying 3 to 6 A/dm^2 (30 to 60 A/ft^2) of part surface during electrocleaning and striking without overheating or excessive voltage loss. Suitable materials for racks include steel, stainless steel, copper, and titanium. Of these, steel or plastic coated steel is most often used. Stainless steel and titanium can be cleaned easily in the nitric acid, but are rarely used because of high cost and limited current carrying capability. The cost of copper racks is reasonable and current capacity is excellent. With copper, however, all submerged surface, except the contact points, should be coated to avoid copper contamination of the cleaning and plating solutions and to minimize stripping of the coating from the frame.

Because electrolytic steps are not required when processing aluminum alloys, plastics as well as metals can be used to support parts. The materials used for racks for aluminum alloys include polypropylene, CPVC, aluminum, and stainless steel. Polypropylene and CPVC are especially useful, because they are easily constructed, inexpensive, and highly resistant to plating. Iron, nickel, or copper alloys are not suitable, because they are rapidly attacked by the oxidizing and desmutting solutions used for aluminum alloys.

Coatings for racks and fixtures used in electroless nickel plating have only limited life. The high temperatures and harsh chemicals used during pretreatment and stripping can cause rapid degradation of vinyls, epoxies, and phenolics. Coatings, however, do reduce current requirements during cleaning and striking operations and can reduce unwanted deposition on the racks.

Fixturing. When fixturing and positioning a part, the following factors should be considered:

- **Hydrogen evolution:** During the deposition of electroless nickel, hydrogen gas is evolved at the surface of the part. As the hydrogen bubble grows and rises, it should be able to free itself from the part. If hydrogen becomes trapped in any area of the part, such as an inverted hole, it masks the surface and can reduce or prevent plating.
- **Electrical contact:** Good contact is needed between the support and the part to ensure adequate and uniform current for electrocleaning

and striking. Proximity to anodes is not usually very important with these operations, although in extreme cases, such as deep holes, internal anodes may be required.

- **Rinsing:** Easy rinsing is necessary to minimize dragout of the pretreatment cleaners and to prevent drag-in of contaminants to the electroless nickel bath.

A rack should be designed to allow blind holes to drain easily or to allow holes to be rinsed thoroughly with a hose. Some racks are designed to be tipped or turned upside down to ensure rinsing and to control dragout. During plating, these holes must be positioned vertically to allow hydrogen gas to escape.

Bulk and Barrel Plating

The uniform plating thickness of electroless nickel coatings allows many parts that would have to be racked if they were finished electrolytically to be bulk plated. Because of the resulting labor savings, coatings such as chromium can sometimes be replaced with electroless nickel at a lower overall finished cost, although the chemical cost is higher. Four principal types of bulk plating are used:

- **Soldier-style racking:** Parts are placed so close together that complete coverage would be difficult, if not impossible, with an electrolytic process.
- **Baskets:** Many bulk plating jobs can be run efficiently in baskets made of polypropylene or stainless steel, especially in smaller electroless nickel tanks. Baskets occupy much less space than barrels and allow more loads to be run. When compared to using barrels, baskets have the disadvantage of not mechanically agitating parts during plating. Accordingly, baskets should be shaken and moved periodically to allow fresh plating solution to circulate around parts.
- **Trays:** Many jobs, such as small shafts and bars, can be run most easily using egg crate or test tube rack trays. In addition, many parts, because of their finish or design, must be separated during processing to keep them from touching or nesting. Separated trays accomplish this successfully and allow good solution transfer, minimizing the labor required for fixturing. Trays are most often constructed of polypropylene, steel, or stainless steel.
- **Barrels:** Where very large volumes of parts are to be plated or continuous mechanical agitation is necessary, barrels usually provide the most efficient and economical methods of processing.

Barrels for electroless nickel plating should be made from nonfilled, nonpigmented polypropylene. If added strength is required, glass-filled polypropylene construction is preferred. Polypropylene gears, rather than a belt drive, should be used to turn the barrel. Plastisol-coated steel barrels are not successful for electroless

nickel plating, because they are prone to coating failures, plate out, possible contamination by bleedout of plasticizers or preplate preparation solutions, and occasional drive failures. For electroless nickel plating, the barrel speed should be 1 to 2 rev/min. Higher-speed barrels may be required, however, where the solution must be pumped through internal passages or holes in a part. The drive mechanism should allow the barrel to rotate, both in the processing tanks and in transfer stages, to ensure free rinsing and minimize dragout. To allow adequate solution transfer in and out of the barrel, the hole size should be as large as possible and should be just capable of containing parts.

All racks, baskets, trays, and barrels used for electroless nickel plating should be used exclusively for this operation. The use of equipment from other plating systems can result in contamination of the electroless nickel plating solution, in decomposition, or in reduced deposit quality.

Solution Control

To ensure a quality deposit and consistent plating rate, the composition of the plating solution must be kept relatively constant. This requires periodic analyses for the determination of pH, nickel content, and hypophosphite and orthophosphite concentrations, as well as careful temperature control. With modern premixed solutions, only checks of nickel content and pH are required. The frequency with which these analyses should be made depends on the quantity of work being plated and the volume and type of solution being used.

Hydrogen Embrittlement Relief

Hydrogen embrittlement is the failure that results from the absorption of hydrogen into metals. Hydrogen embrittlement usually occurs in combination with residual or applied stresses in a part, happening most frequently in high-strength steels and occasionally in other high-strength alloys.

Hydrogen can be introduced into a metal by processes such as pickling, electrocleaning, acid activation, electroplating, or electroless deposition. Although the hydrogen produced by electroless nickel plating is much less than that produced by an electrolytic process, such as cadmium or hard chrome plating, it can be enough to cause cracking of high-strength steels. To prevent this, components are baked at 200 \pm 10 $^{\circ}\text{C}$ (390 \pm 18 $^{\circ}\text{F}$) to diffuse the absorbed hydrogen out of the steel. This usually restores the mechanical properties of the steel almost completely, helping to ensure against failure.

The time required to remove hydrogen from a steel and avoid embrittlement depends on the strength of the steel. Longer relief treatment periods or higher temperatures are needed as the strength of the steel increases. Recommendations for embrittlement relief of steels on different strength levels are summarized in Table 10. Longer times may be required for parts with de-

Table 10 Heat treatment of steels to relieve hydrogen embrittlement

Maximum specified tensile strength	Heat treatment at 190 to 210 °C (375 to 410 °F), h	
	MPa	ksi
≤1050	≤152	Not required
1051-1450	152-210	2
1451-1800	210-260	18
>1800	>260	24

posit thickness greater than 1 mil. Deposits are amorphous, thus there are no grain boundaries for the hydrogen to follow. Shorter times may be used if unplated areas are present. Temperature ramp-up times should be longer than for hydrogen relief of other metal deposits. Hydrogen embrittlement relief treatment should begin within 4 h of the completion of electroless nickel plating (Ref 2, 49, 50).

Applications

Electroless nickel is applied for five different applications: corrosion resistance, wear resistance, lubricity, solderability, or buildup of worn or overmachined surfaces. To varying degrees, these properties are used by all segments of industry, either separately or in combination. Applications of these coating are given in Table 11.

Applications for electroless nickel-boron deposits in the electronics industry include wire bonding for IC chips, soldering, brazing, laser welding, low electrical resistivity, and as a diffusion barrier.

Specifications

The published specifications for electroless nickel-phosphorus currently available in the United States include:

- AMS 2404, Electroless Nickel Plating (Ref 51)
- ASTM B 656, Autocatalytic Nickel Deposition on Metals for Engineering Use (Ref 43)
- Military Specification Requirements for Electroless Nickel Coatings (Ref 52)

In addition, an international standard has been drafted by the International Standards Organization (Ref 50). Published standards for electroless nickel-boron coatings for engineering purposes are not available.

Although these standards are good guidelines for testing and quality control, none include any real requirements for structural quality, corrosion resistance, or wear resistance. The standards consist primarily of a visual examination and simple tests for thickness and adhesion. Often this forces industrial users to develop their own internal specifications for coating quality. These in-house specifications can be relatively simple with requirements for only a few desired properties, or very detailed with requirements for substrate pre-

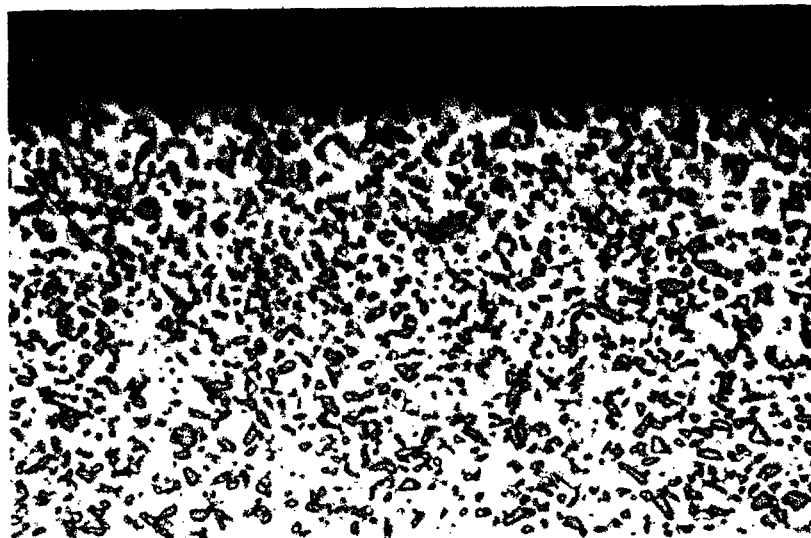


Fig. 22 Cross-sectional view of a typical silicon carbide composite coating. Heater mounted in a 200 L (50 gal) electroless nickel plating tank. A bag filter is mounted on the filtration pump discharge. 1000x

treatment, bath operation, equipment design, deposit chemistry, and properties.

Electroless Nickel Composite Coatings

Composites are one of the most recently developed types of electroless nickel coatings. These cermet deposits consist of small particles of intermetallic compounds, fluorocarbons, or diamonds dispersed in an electroless nickel-phosphorus matrix. These coatings have a high apparent hardness and superior wear and abrasion resistance.

Chemistry. Most composite coatings are applied from proprietary baths. Typically, they consist of 20 to 30 vol% of particles entrapped in an electroless nickel containing 4 to 11% P. Most commonly silicon carbide, diamond particles, fluorinated carbon powders, and PTFE are used, although calcium fluoride is also occasionally codeposited. The particles are carefully sized and are normally 1 to 3 μm in diameter (Ref 53-55) for silicon carbide and diamonds and 0.35 μm for PTFE. A micrograph of a typical silicon carbide composite coating is shown in Fig. 22 (Ref 56). The baths used for composite plating are conventional sodium hypophosphite reduced electroless nickel solutions, with the desired particles suspended in them. These baths, however, are heavily stabilized to overcome or inhibit the very high surface area produced by the particles. The baths otherwise are operated normally and the nickel-phosphorus matrix is produced by the traditional hypophosphite reduction of nickel. The particles are merely caught or trapped in the coating as it forms. Their bond to the coatings is purely mechanical.

Hardness and Wear. The primary use for electroless nickel composite coating is for applications requiring maximum resistance to wear and abrasion. The hardnesses of diamond and silicon carbide are 10,000 and 4500 HV, respectively. In addition, the coatings are normally heat treated to provide maximum hardness (1000 to 1100 HV₁₀₀) of the electroless nickel matrix. The resulting apparent surface hardness of the composite is 1300 HV₁₀₀ or more (Ref 53, 56).

The wear surface of a composite coating consists of very hard mounds separated by lower areas of hard electroless nickel. During wear, the mating surface usually rides on the particles and slides over the matrix. Thus, the wear characteristics of these coatings approach that of the particle material (Ref 53). Typical wear test results for a silicon carbide composite coating are shown in Table 12 (Ref 56).

Frictional properties of composite coatings are similar to those of other electroless nickels. Typically, the coefficient of friction of these materials is about 0.13 in the lubricated condition and 0.3 to 0.4 in the unlubricated condition (Ref 53, 54).

Corrosion Resistance. In general, the corrosion resistance of composite coatings is significantly less than that of other electroless nickel coatings. The electroless nickel matrix contains large amounts of codeposited inhibitor, which reduces the alloy's passivity and corrosion resistance. Also, heat treated coatings are less protective than are as-applied coatings, both because of the conversion of the amorphous deposit to crystalline nickel and Ni₃P and because of cracking of the coating (Ref 53, 56). With composites, this problem is amplified because of the presence of the diamond or intermetallic particles. The mixture of phosphides, nickel, and particles creates a very strong galvanic

Table 11 Applications of electroless nickel plating

Application	Base metal	Coating thickness(a)		Reason for use
		µm	mils	
Automotive				
Heat sinks	Aluminum	10	0.4	Corrosion resistance, solderability, uniformity
Carburetor components	Steel	15	0.6	Corrosion resistance
Fuel injectors	Steel	25	1.0	Corrosion and wear resistance
Ball studs	Steel	25(b)	1.0(b)	Wear resistance
Differential pinion ball shafts	Steel	25(b)	1.0(b)	Wear resistance
Disc brake pistons and pad holders	Steel	25(b)	1.0(b)	Wear resistance
Transmission thrust washers	Steel	25(b)	1.0(b)	Wear resistance
Syncromesh gears	Brass	30	1.2	Wear resistance
Knuckle pins	Steel	38(b)	1.0(b)	Wear resistance
Exhaust manifolds and pipes and mufflers	Steel	25	1.0	Corrosion resistance
Shock absorbers	Steel	10	0.4	Corrosion resistance and lubricity
Lock components	Steel	10	0.4	Wear and corrosion resistance and lubricity
Hose couplings	Steel	5	0.2	Wear and corrosion resistance
Gears and gear assemblies	Carburized steel	25(c)	1.0(c)	Buildup of worn surfaces and wear resistance
Fuel pump motors	Steel	12	0.5	Corrosion, wear resistance
Aluminum wheels	Aluminum	25	1	Corrosion resistance
Water pump components	Steel	20	0.8	Corrosion resistance
Steering column tilt wheel components	Powdered metal	15	0.6	Ease of movement
Air bag hardware	Steel	10	0.4	Ease of movement
Air conditioning compressor components	Steel	25	1	Low friction
Decorative plastics	Plastics (ABS, etc)	2	0.1	Base coat
Slip yokes	Steel	15	0.6	...
Aircraft/aerospace				
Bearing journals	Aluminum	38(d)	1.5(d)	Wear resistance and uniformity
Servo valves	Steel	18	0.7	Corrosion resistance, uniformity and lubricity
Compressor blades	Alloy steel	25(e)	1.0(e)	...
Hot zone hardware	Alloy steel	25	1.0	Corrosion and wear resistance
Piston heads	Aluminum	25	1.0	Wear resistance
Engine main shafts and propellers	Steel	>38	>1.5	Buildup of worn surfaces and wear resistance
Hydraulic actuator splines	Steel	25(b)	1.0(b)	Wear resistance
Seal snaps and spacers	Steel	20(e)	0.8(e)	Wear and corrosion resistance
Landing gear components	Aluminum	>125	>5.0	Buildup of mis-machined surfaces
Struts	Stainless steel	>25	>1.0	Buildup of mis-machined or worn surfaces
Pitot tubes	Brass/stainless steel	12	0.5	Corrosion and wear resistance
Gyro parts	Steel	12	0.5	Wear resistance and lubricity
Engine mounts	4140 Steel	25	1.0	Wear and corrosion resistance
Oil nozzle components	Steel	25	1.0	Corrosion resistance and uniformity
Turbine front bearing cages	Alloy steel	25	1	Corrosion, wear resistance
Engine mount insulator housing	Alloy steel	25	1	Corrosion resistance
Flanges	Alloy steel	20	0.8	Corrosion, wear resistance
Sun gears	Alloy steel	25	1	Wear resistance
Breech caps	Alloy steel	15	0.6	Corrosion, wear resistance
Shear bolts	Alloy steel	50	2	Corrosion resistance
Engine oil feed tubes	Steel, stainless steel	10	0.4	Corrosion resistance
Flexible bearing supports	Steel	25	1	Corrosion resistance
Break attach bolts	Alloy steel	25	1	Corrosion resistance
Antirotational plates	Alloy steel	25	1	Wear resistance
Wing flap universal joints	Alloy steel	20	0.8	Corrosion, low friction
Titanium thruster tracks	Titanium	25	1	Wear and corrosion resistance, low friction
Printing				
Printing rolls	Steel/cast iron	38	1.5	Corrosion and wear resistance
Press beds	Steel/cast iron	38	1.5	Corrosion and wear resistance
Textiles				
Feeds and guides	Steel	50(b)	2.0(b)	Wear resistance
Fabric knives	Steel	12(b)	0.5(b)	Wear resistance
Spinnerettes	Stainless steel	25	1.0	Corrosion and wear resistance
Loom ratchets	Aluminum	25	1.0	Wear resistance
Knitting needles	Steel	12	0.5	Wear resistance
Molds and dies				
Zinc die cast dies	Alloy steel	25	1.0	Wear resistance and part release
Glass molds	Steel	50	2.0	Wear resistance and part release
Plastic injection molds	Alloy steel	15	0.6	Corrosion and wear resistance and part release
Plastic extrusion dies	Alloy steel	25	1.0	Corrosion and wear resistance and part release
Military				
Fuse assemblies	Steel	12	0.5	Corrosion resistance
Mortar detonators	Steel	10	0.4	Corrosion resistance
Tank turret bearings	Alloy steel	30	1.2	Wear and corrosion resistance
Radar wave guides	Aluminum	25	1.0	Corrosion resistance and uniformity
Mirrors	Aluminum/beryllium	>75	>3.0	Uniformity and reflectivity
Firearms				
Commercial and military firearms	Steel	8	0.3	Corrosion and wear resistance and lubricity

(continued)

Table 11 Applications of electroless nickel plating (continued)

Application	Base metal	Coating thickness(a)		Reason for use
		µm	mils	
Marine				
Marine hardware	Brass	25	1.0	Corrosion resistance
Pumps and equipment	Steel/cast iron	50	2.0	Corrosion and wear resistance
Electronics				
Heat sinks	Aluminum	10	0.4	Corrosion resistance and solderability
Computer drive mechanisms	Aluminum	18	0.7	Corrosion and wear resistance
Memory drums and discs	Aluminum	25	1.0	Corrosion and wear resistance and uniformity
Terminals and lead wires	Alloy steel	2	0.1	Solderability
Chassis	Aluminum/steel	12	0.5	Corrosion resistance and solderability
Connectors	Steel/aluminum	25	1.0	Corrosion and wear resistance and solderability
Diode and transistor cans	Steel	5	0.2	Corrosion resistance and solderability
Interlocks	Steel/brass	12	0.5	Corrosion and wear resistance
Junction fittings	Aluminum/plastic	10	0.4	Corrosion and wear resistance, solderability and conductivity
Printed circuit boards	Plastic	5	0.2	Solderability and weldability
Railroad				
Tank cars	Steel	90(f)	3.5(f)	Corrosion resistance
Diesel engine shafts	Steel	>25	>1.0	Wear and fretting resistance and buildup of worn surfaces
Car hardware	Powder iron	20	0.8	Corrosion and wear resistance
Electrical				
Motor shafts	Steel	12	0.5	Wear and corrosion resistance
Rotor blades	Steel/aluminum	25(b)	1.0(b)	Wear and corrosion resistance
Stator rings	Steel/aluminum	25	1.0	Wear and corrosion resistance
Chemical and petroleum				
Pressure vessels	Steel	50	2.0	Corrosion resistance
Reactors	Steel	100(f)	4.0(f)	Corrosion resistance and product purity
Mixer shafts	Steel	38	1.5	Corrosion resistance
Pumps and impellers	Cast iron/steel	75	3.0	Corrosion and erosion resistance
Heat exchangers	Steel	75	3.0	Corrosion resistance
Filters and components	Steel	25	1.0	Corrosion and erosion resistance
Turbine blades and rotor assemblies	Steel	75	3.0	Corrosion and erosion resistance
Compressor blades and impellers	Steel/aluminum	125(d)	5.0(d)	Corrosion and erosion resistance
Spray nozzles	Brass/steel	12	0.5	Corrosion and wear resistance
Ball, gate, plug, check and butterfly valves	Steel	75	3.0	Corrosion resistance and lubricity
Valves	Stainless steel	25(b)	1.0(b)	Wear and galling resistance and protection against stress-corrosion cracking
Chokes and control valves	Steel/stainless steel	75	3.0	Corrosion and wear resistance and protection against stress-corrosion cracking
Oil field tools	Steel	75	3.0	Corrosion and wear resistance
Oil well packers and equipment	Alloy steel	75	3.0	Corrosion and erosion resistance
Oil well tubing and pumps	Steel	50	2.0	Corrosion and wear resistance
Drilling mud pumps	Alloy steel	75	3.0	Corrosion resistance and protection against stress-corrosion cracking
Hydraulic systems and actuators	Steel	75	3.0	Corrosion and wear resistance and lubricity
Blowout preventers	Alloy steel	75	3.0	Corrosion and wear resistance
Medical and pharmaceutical(g)				
Disposable surgical instruments and equipment	Steel/aluminum	12	0.5	Corrosion resistance and ease of operation
Sizing screens	Steel	20	0.8	Corrosion resistance and cleanliness
Pill sorters	Steel	20	0.8	Corrosion resistance and cleanliness
Feed screws and extruders	Steel	25	1.0	Corrosion and wear resistance and cleanliness
Food(g)				
Pneumatic canning machinery	Steel	25	1.0	Corrosion and wear resistance and cleanliness
Baking pans	Steel	25	1.0	High temperature resistance, cleanliness, and ease of release
Molds	Steel	12	0.5	Cleanliness, corrosion resistance and ease of release
Grills and fryers	Steel	12	0.5	Cleanliness, corrosion resistance and ease of release
Mixing bowls	Steel	25	1.0	Cleanliness and corrosion and wear resistance
Bun warmers	Steel	12	0.5	Cleanliness and ease of release
Feed screws and extruders	Steel	25	1.0	Cleanliness and corrosion and wear resistance
Material handling				
Hydraulic cylinders and shafts	Steel	25	1.0	Corrosion and wear resistance and lubricity
Extruders	Alloy steel	75(b)	3.0(b)	Wear and corrosion resistance
Link drive belts	Steel	12	0.5	Wear and corrosion resistance and lubricity
Gears and clutches	Steel	>25	>1.0	Wear resistance and buildup of worn surfaces
Mining				
Hydraulic systems	Steel	60	2.4	Corrosion and abrasion resistance
Jetting pump heads	Steel	60	2.4	Corrosion and erosion resistance
Mine engine components	Steel/cast iron	30	1.2	Corrosion and wear resistance
Piping connections	Steel	60	2.4	Corrosion resistance
Framing hardware	Steel	30	1.2	Corrosion resistance
Wood and paper				
Knife holder corer plates	Steel	30	1.2	Corrosion and abrasion resistance
Abrading plates	Steel	30	1.2	Corrosion and abrasion resistance
Chopping machine parts	Steel	30	1.2	Corrosion and abrasion resistance

(continued)

Table 11 Applications of electroless nickel plating (continued)

Application	Base metal	Coating thickness(a)		Reason for use
		µm	mils	
Miscellaneous				
Chain saw engines	Aluminum	25	1.0	Wear and corrosion resistance
Drill and taps	Alloy steel	12(b)	0.5(b)	Wear resistance and ease of use
Precision tools	Alloy steel	12	0.5	Wear resistance and cleanliness
Shaver blades and heads	Steel	8	0.3	Wear resistance and smoothness
Pen tips	Brass	5	0.2	Corrosion resistance

(a) Many components are heat treated at 190 to 210 °C (375 to 410 °F) for 1 to 3 h to improve adhesion or to relieve hydrogen embrittlement. (b) Heat treated for 1 h at 400 °C (750 °F) for maximum hardness. (c) Heat treated for 6 h at 135 °C (275 °F) for hydrogen embrittlement relief. (d) Heat treated for 10 h at 290 °C (550 °F) for maximum hardness. (e) Cadmium plated after electroless nickel and then heat treated for 2 h at 340 °C (640 °F) to diffuse cadmium into the nickel. (f) Heat treated for 1 h at 620 °C (1150 °F) to diffuse coating into basis metal. (g) For medical, pharmaceutical, and food applications, coatings must be free of toxic heavy metals such as lead, cadmium, mercury, or thallium.

Table 12 Comparison of the Taber abraser resistance of silicon carbide composite coatings with other engineering materials

Material	Hardness	Taber wear index, Mg 11,000 cycles
400-C stainless steel	57 HRC	5.6
A2 tool steel	60-62 HRC	5.0
Electroless nickel (hardened)	900-1000 HV	3.7
Hard chromium	1000-1100 HV	3.0
Tungsten carbide	1300 HV	2.0
Electroless nickel and silicon carbide composite	1300 HV	0.18-0.22

Note: Taber wear index determined for an average of three 5000-cycle runs with 100 g load and CS17 abrasive test wheels

couple accelerating attack. For applications requiring good corrosion resistance, electroless nickel composite coatings are not normally used.

Plating on Plastics

Except for ferrous alloys, plastics are probably the substrate most commonly electroless nickel plated. The coating is typically applied to non-metals as a conductive base for subsequent electroplating of both decorative and functional deposits. Occasionally, electroless nickel is used by itself for applications requiring resistance to abrasion or environmental attack (Ref 2). Because plastics are nonconductive and are not catalytic to the chemical reduction of nickel, special processing steps are required to ensure adequate adhesion and to initiate deposition. With synthetics, metallic bonds cannot form between the coating and the substrate. Thus, adhesion results only from mechanical bonding of the coating to the substrate surface. To improve adhesion, plastics are typically etched in acidic solutions or organic solvents to roughen their surface and to provide more bonding sites.

In order to initiate electroless nickel plating on plastics (or other nonmetals) their etched surfaces must first be catalyzed with stannous chloride and palladium chloride and then accelerated in acid. This produces palladium nucleation sites on the surface for deposition. A typical pretreatment sequence for plastics is:

- Degreasing
- Etching
- Neutralization
- Catalyzation
- Acceleration
- Electroless nickel deposition

Thorough rinsing after each processing step is essential. After the electroless nickel layer has been completed, the part may be plated conventionally with any desired electrolytic coating (Ref 2, 57).

Degreasing. When necessary, light soil or fingerprints can be removed from plastic parts by immersion in a mildly alkaline soak cleaner for 2 to 5 min. A typical degreasing solution contains 25 g/L each of sodium carbonate and trisodium phosphate and is operated at 50 to 70 °C (120 to 160 °F). Alkaline cleaning is not always required, provided the plastic is carefully handled after molding and is not allowed to become excessively soiled. Fingerprints and loose dust or dirt are normally removed by the etching solution.

Etching solutions for plastics are typically strongly oxidizing acids that cause a microscopic roughening of the part's surface. These solutions also alter the chemical character of the surface and cause it to become hydrophilic. Etching not only improves mechanical bonding and adhesion of the coating to the plastic substrate, but also improves access of subsequent processing solutions to the surface. Most commercially used etching solutions are formulated with either chromic acid or mixtures of sulfuric acid and chromic acid or dichromate salt. These solutions are typically operated at 50 to 70 °C (120 to 160 °F) with immersion times of 3 to 10 min. Chromic acid based solutions are particularly effective with ABS plastics, but are also used for polyethylene, polypropylene, PVC, polyesters, and other common polymers.

Neutralizing. After the plastic has been properly etched and rinsed, it should be neutralized to remove residual chromium ions, which may interfere with subsequent catalyzation. Neutralizers are rinsing aids and are typically dilute acid or alkaline solutions, often containing complexing and reducing agents. Ionic surfactants are sometimes added to increase the absorption of the catalyst on the surface. Neutralizing solutions are normally operated at 40 °C (105 °F) with immersion times of 1 to 2 min.

Catalyzing. In order to initiate deposition of the electroless nickel coating on plastics, their surfaces must be catalyzed. This is normally accomplished by chemically depositing small amounts of palladium. The original commercial catalyzing procedures required two processing steps. In the first step, stannous chloride was absorbed onto the surface from a solution of SnCl₂ and HCl. After rinsing, the part was immersed in a solution of PdCl₂ and HCl, and palladium chloride was absorbed onto the surface. The stannous ions then reduced the palladium ions leaving discrete sites of metallic palladium. Currently, a one-step catalyzing procedure is normally used. For this, a solution of stannous chloride and palladium chloride in hydrochloric acid is used. The solution consists of tin/palladium complexes and colloids stabilized by excess stannous chloride. The chloride content of the solution is critical and must be carefully controlled. During immersion, globules of tin/palladium colloid absorb onto the plastic surface. After rinsing, nuclei of metallic palladium surrounded by hydrolyzed stannous hydroxide, are left attached to the surface.

Acceleration. With one-step catalyzation, a further step is required to remove excess stannous hydroxide from the surface and to expose the palladium nuclei. This step is called acceleration and is accomplished by immersing the part in a dilute solution of hydrochloric acid or an acid salt. The acid reacts with the insoluble stannous hydroxide forming soluble stannous and stannic chloride. After rinsing, there surface is free of tin and active catalytic sites are present. Acceleration solutions are typically operated at a temperature of 50 °C (120 °F) and are agitated with air. The parts are normally immersed for 30 to 60 s.

Electroless Nickel Deposition. Most electroless nickel solutions operate at too high a temperature for plastics. High temperatures may cause plastics to warp. In addition, the large difference in coefficient of thermal expansion between plastics and electroless nickel may cause adhesion failures during cooling from bath temperatures. Electroless nickel solutions for plating on plastics, thus, are formulated to operate at low temperatures—typically 20 to 50 °C (70 to 120 °F). These solutions are normally alkaline and reduced with sodium hypophosphite, although some DMAB solutions are also used. Ammonia-based plating baths are preferred because of their ability to complex excess palladium dragged in with the part and to avoid spontaneous

decomposition. While most of these solutions are proprietary, some typical formulations (Ref 2) are:

Composition	Bath 1		Bath 2	
	g/L	oz/gal	g/L	oz/gal
Nickel chloride	119	15
Nickel sulfate	50	6.5
Sodium hypophosphite	106	14	50	6.5
Sodium pyrophosphate	100	13
Ammonium citrate	65	8
Ammonia, mL/L (fluid oz/gal)	45	5.8
Sodium hydroxide	To pH	
Operating conditions	Bath 1		Bath 2	
pH	10		10	
Temperature, °C (°F)	30-50 (85-120)		25 (77)	
Typical plating rate, μm/h (mils/h)	3-11 (0.12-0.44)		3 (0.12)	

Plastic parts are normally immersed in the electroless nickel solution for 5 to 10 min to provide a uniform metal film about 0.25 to 0.50 μm thick. This coating is sufficient to cover the surface of the plastics and to make them conductive for subsequent electroplating. These deposits typically contain 2 to 6% P. After proper treatment the peel strength of 25 mm (1 in.) width strips of these coatings on plastics like ABS and polypropylene is on the order of 50 to 100 N (Ref 2, 57).

REFERENCES

1. K. Parker, "Recent Advances in Electroless Nickel Deposits, 8th Interfinish Conference," 1972 (Basel)
2. G.G. Gawrilov, *Chemical (Electroless) Nickel Plating*, Portcullis Press, Redhill, England, 1979
3. G. Gutzeit, An Outline of the Chemistry Involved in the Process of Catalytic Nickel Deposition from Aqueous Solution, *Plat. Surf. Finish.*, Vol 46 (No. 10), 1959, p 1158
4. A. Brenner and G. Riddell, Deposition of Nickel and Cobalt by Chemical Reduction, *J. Res. Natl. Bur. Stand.*, Vol 39 (No. 11), 1947, p 385
5. G.O. Mallory, The Electroless Nickel Plating Bath, Electroless Nickel Conference, Cincinnati, Nov 1979
6. K. Stallman and H. Speckhardt, Deposition and Properties of Nickel-Boron Coatings, *Metaloberfl.; Angew. Elektrochem.*, Vol 35 (No. 10), 1981, p 979
7. K.M. Gorbunova and A.A. Nikiforova, *Physicochemical Principles of Nickel Plating*, Izdatel'stvo Akademii Nauk SSSR, Moscow, 1960
8. G.O. Mallory, Influence of the Electroless Plating Bath on the Corrosion Resistance of the Deposits, *Plating*, Vol 61 (No. 11), 1974, p 1005
9. C.E. deMinjer and A. Brenner, Studies on Electroless Nickel Plating, *Plating*, Vol 44 (No. 12), 1957, p 1297
10. G.O. Mallory, The Electroless Nickel-Boron Plating Bath; Effects of Variables on Deposit Properties, *Plating*, Vol 58 (No. 4), 1971, p 319
11. C. Baldwin and T.E. Such, The Plating Rates and Physical Properties of Electroless Nickel/Phosphorus Alloy Deposits, *Trans. Inst. Met. Finish.*, Vol 46 (No. 2), 1968, p 73
12. R.N. Duncan, Properties and Applications of Electroless Nickel Deposits, *Finish. Manage.*, Vol 26 (No. 3), 1981, p 5
13. W.H. Metzger, Characteristics of Deposits, *Symposium on Electroless Nickel Plating*, STP 265, ASTM, 1959
14. K. Parker, Effects of Heat Treatment on the Properties of Electroless Nickel Deposits, *Plat. Surf. Finish.*, Vol 68 (No. 12), 1981, p 71
15. K. Parker and H. Shah, Residual Stresses in Electroless Nickel Plating, *Plating*, Vol 58 (No. 3), 1971, p 230
16. R.N. Duncan, Performance of Electroless Nickel Coatings in Oil Field Environments, CORROSION/82 Conference, National Association of Corrosion Engineers, March 1982
17. J. Horner and B. Durkin, "Experiences with Measuring Properties of Electroless Nickel Deposits," Electroless Nickel Conf. (Sulihill, UK), British Electroless Nickel Society, 1991
18. G.D.R. Jarrett, Electroless Nickel Plating, *Ind. Finish.* (London), Vol 18 (No. 218), 1966, p 41
19. L.G. Fitzgerald, Chemical Nickel Plating Products, *Finishing* (London), Vol 13 (No. 5), 1960, p 68
20. W.H. Roberts, "Coating Beryllium with Electroless Nickel," Report RFP478, U.S. Atomic Energy Commission, 1964
21. L.F. Spencer, Electroless Nickel Plating—A Review, *Met. Finish.*, Vol 72 (No. 12), 1974, p 58
22. A.H. Graham, R.W. Lindsay, and H.J. Read, The Structure and Mechanical Properties of Electroless Nickel, *J. Electrochem. Soc.*, Vol 112 (No. 4), 1965, p 401
23. J. Horner, Microhardness Testing of Plated Coatings; Recent Round Experiences, STP 947, ASTM, 1987
24. J. Horner, "Microhardness Testing of Plated Coatings; Defining Precision and Bias," Int. Tech. Conf. Proc. AESF Surf./Finish., 1992
25. L. Weisenberger and J. Greene, "Hardness versus Wear Resistance of Electroless Nickel Alloys," Electroless Nickel Conf. Proc. on Products Finishing, 1989
26. K. Nemoto et al., The Study on Hardness of Non-Electrolytically Plated Ni-P Deposits at High Temperatures and Effects Given by Heat Treatments, *J. Met. Finish. Soc. Jpn.*, Vol 16 (No. 3), p 106
27. L. Domnikov, Chromium and Electroless Nickel Deposits, Hardness at High Temperatures, *Met. Finish.*, Vol 60 (No. 1), 1962, p 67
28. K. Parker, Hardness and Wear Resistance Tests of Electroless Nickel Deposits, *Plating*, Vol 61 (No. 9), 1974, p 834
29. Industrial Nickel Plating and Coating, International Nickel Company, New York, 1976
30. H.G. Klein et al., *Metaloberfl.; Angew. Elektrochem.*, Vol 25 (No. 9), 1971; Vol 26 (No. 1), 1972
31. J.P. Randin and H.E. Hintermann, Electroless Nickel Deposited at Controlled pH; Mechanical Properties as a Function of Phosphorus Content, *Plating*, Vol 54 (No. 5), 1967 p 523
32. D.W. Baudrand, Use of Electroless Nickel to Reduce Gold Requirements, *Plat. Surf. Finish.*, Vol 68 (No. 12), 1981, p 57
33. R.N. Duncan, "Corrosion Control with Electroless Nickel Coatings," Electroless Plating Symposium, American Electroplaters' Society, March 1982 (St. Louis, MO)
34. "Technical Information about Electroless of Chemical Nickel Plating by the Nibodur Method," Paul Anke KG, Essen, West Germany
35. "Calibration and Operation of the Alpha Model LFW-1 Friction and Wear Testing Machine," Part 24, D 2714, *Annual Book of ASTM Standards*, ASTM, 1978
36. H. Spahn, The Effect of Internal Stress on the Fatigue and Corrosion Fatigue Properties of Electroplated and Chemically Plated Nickel Deposits, Proc. 6th Int. Metal Finish. Conf., *Trans. Inst. Met. Finish.*, Vol 42, 1964, p 364
37. E.F. Jungslager, Electroless Deposition of Nickel, *Tijdschr. Oppervlakte Tech. Metalen*, Vol 9 (No. 1), 1965, p 2
38. E.W. Turns and J.W. Browning, Properties of Electroless Nickel Coatings on High Strength Steels, *Plating*, Vol 60 (No. 5), 1973
39. G. Reinhardt, "Potential Applications of Electroless Nickel in Airline Maintenance Operations," Electroless Nickel Conference, 6-7 Nov 1979 (Cincinnati)
40. S. Izumi and Kondo, "The Fatigue Strength of Electroless Nickel Plated Steel," The 18th Japan Conf. Mater. Res., March 1975
41. S. Spring, *Industrial Cleaning*, Prism Press, Melbourne, 1974
42. J. Kuczma, How to Operate Electroless Nickel More Efficiently, *Prod. Finish. (Directory)*, Vol 44 (No. 12A), 1980, p 158
43. "Autocatalytic Nickel Deposition on Metals for Engineering Use," Part 9, B 656, *Annual Book of ASTM Standards*, ASTM, 1981
44. "Preparation of Low-Carbon Steel for Electroplating," Part 9, B 183, *Annual Book of ASTM Standards*, ASTM, 1981
45. "Preparation of High-Carbon Steel for Electroplating," Part 9, B 242, *Annual Book of ASTM Standards*, ASTM, 1981
46. "Preparation of and Electroplating on Stainless Steel," Part 9, B 254, *Annual Book of ASTM Standards*, ASTM, 1981
47. "Preparation of Copper and Copper-Base Alloys for Electroplating," Part 9, B 281, *Annual Book of ASTM Standards*, 1981
48. C.P. Steinecker, Evaluation of PVC Tank Liners for Electroless Nickel Plating, *Met. Finish.*, Vol 90 (No. 5), May 1992
49. *Metals Handbook*, 9th ed., Vol 1, American Society for Metals, 1978

310 / Plating and Electroplating

50. "Autocatalytic Nickel-Phosphorus Coatings," ISO 4527, International Standards Organization
51. "Electroless Nickel Plating," AMS 2404B, Society of Automotive Engineers, 1977
52. "Military Specification—Coatings, Electroless Nickel, Requirements for," MIL-C-26074B, U.S. Government Printing Office, 1959 and 1971
53. J.M. Scale, Wear Resistance of Silicon Carbide Composite Coatings, *Met. Prog.*, Vol 115 (No. 4), 1979, p 44
54. D.J. Kenton et al., "Development of Dual Particle Multifunction Electroless Nickel Composite Coatings," Electroless Plating Symposium, American Electroplaters' Society, 1982 (St. Louis, MO)
55. N. Feldstein et al., "The State of the Art in Electroless Composite Plating," Electroless Plating Symposium, American Electroplaters' Society, 1982 (St. Louis, MO)
56. W.B. Martin et al., "Electroless Nickel Composites—The Second Generation of Chemical Plating," Electroless Nickel Conference, Nov 1979 (Cincinnati, OH)
57. J.K. Dennis and T.E. Such, *Nickel and Chromium Plating*, Newnes-Butterworths, 1972, p 287

1.3.3 Glossary of Terms

Bottom Plate Forging – The bottom end of the FuelSolutions™ TS125 Transportation Cask body, which consists of a plate that closes the end of the cask and a short section of interfacing shell for attaching the inner and outer cask shells.

Canister – The FuelSolutions™ canister is a sealed, metallic container for maintaining multiple SNF assemblies and any non-fuel bearing components in a dry, inert environment for interim storage, transport, and, for some canister designs, geologic disposal.

Canister Basket Assembly – The FuelSolutions™ canister internal components that maintain geometric spacing and provide structural support and criticality control for the SNF assemblies and any non-fuel bearing components.

Canister Class – Some FuelSolutions™ canisters have two similar canister designs, including a design that is suitable for storage and transport and a design that incorporates alternative materials of construction that is also suitable for disposal. The FuelSolutions™ “M” class canisters are for storage, transport, and disposal. The FuelSolutions™ “T” class canisters are for storage and transportation, but not for disposal.

Canister Shell Assembly – The FuelSolutions™ canister components that provide the on-site storage and transfer confinement boundary and axial gamma shielding for both storage and transport.

Canister Type – FuelSolutions™ canisters that accommodate more than one SNF assembly class and require the use of short (S) and/or long (L) canister shells and steel (S), lead (L) or depleted uranium (D) shield plugs are assigned a designator (e.g., LS), which is termed the canister type.

Cask – The FuelSolutions™ TS125 Transportation cask body with closure lid without the impact limiters.

Cask Body – The FuelSolutions™ TS125 Transportation Cask without the closure lid or impact limiters.

Cask Cavity Spacer – A structural element used to fill the void in the FuelSolutions™ TS125 Transportation Cask cavity when a short FuelSolutions™ canister is transported within the cask.

Closure Bolts or Closure Lid Bolts – Fasteners that secure the closure lid to the FuelSolutions™ TS125 Transportation Cask body.

Closure Lid – The removable plate that closes the top end of the FuelSolutions™ TS125 Transportation Cask cavity and that contains a vent port, a seal test port, and grooves for both the containment (inner) O-ring seal and the test (outer) O-ring seal.

Containment Boundary – Consists of the FuelSolutions™ TS125 Transportation Cask inner shell, the bottom plate forging, the top ring forging, the closure lid, the containment (inner) O-ring seal, the drain port (and O-ring sealing device), and the vent port (and O-ring sealing device).

Containment Seal – The innermost O-ring seal, inserted into a groove in the FuelSolutions™ TS125 Transportation Cask closure lid, which forms a part of the containment boundary.

Drain Port – An opening in the FuelSolutions™ TS125 Transportation Cask bottom plate forging, communicating with the cask cavity, which facilitates draining the cask cavity following canister fuel loading operations and is sealed closed during transport.

Dynamic Load Factor – The ratio of dynamic component response to static response.

Fuel Assembly Spacer – A structural element used to provide an appropriate guide tube cavity cross section and/or length for some classes of SNF assemblies.

FuelSolutions™ Spent Fuel Management System – The BFS canister-based, fully integrated system of compatible components and equipment that is designed for efficient storage, transport, and disposal of SNF assemblies from commercial power reactors in the contiguous United States.

Gamma Shield – The cast lead that fills the annulus between the FuelSolutions™ TS125 Transportation Cask inner and outer shells.

Gamma Shield Cavity – The volume formed by the FuelSolutions™ TS125 Transportation Cask inner and outer structural shells and the top and bottom cask forgings.

Guide Rails – Two flat strips of anti-galling stainless steel material, welded to the FuelSolutions™ TS125 Transportation Cask cavity, on which the FuelSolutions™ canister assembly slides and rests during horizontal canister transfer and subsequent transport.

Guide Tube – A stainless steel tube that lines the fuel cell opening, which facilitates fuel loading operations and maintains the position of the neutron absorber material.

Impact Limiter – A device used to limit the impact deceleration of the FuelSolutions™ TS125 Transportation Cask due to a free drop.

Inner Shell – The inner wall of the FuelSolutions™ TS125 Transportation Cask body, which is welded at each end to the bottom plate forging and the top ring forging.

Intermodal Transportation Skid – The skid used to secure the FuelSolutions™ TS125 Transportation Package to the conveyance during transport and to facilitate cask handling operations prior to and subsequent to transport.

Neutron Absorber – A panel of borated aluminum or stainless steel attached to the canister basket guide tube to provide criticality control.

Neutron Shield – A hydrogenous material, cast into place within the neutron shield cavity.

Neutron Shield Cavity – A cavity into which the neutron shield is cast, formed by the FuelSolutions™ TS125 Transportation Cask outer shell, the neutron shield jacket, and the tiedown rings.

Neutron Shield Jacket – A steel shell that forms the outer boundary of the neutron shield cavity.

Neutron Shield Support Angles – V-section members welded to the FuelSolutions™ TS125 Transportation Cask outer shell and to the neutron shield jacket, which aid in transmitting heat from the cask interior to the ambient through the neutron shield material.

Outer Shell – The outer wall of the FuelSolutions™ TS125 Transportation Cask body, which is welded at each end to the bottom plate forging and the top ring forging.

Package – The FuelSolutions™ transportation packaging with its radioactive contents, or payload, as presented for transport.

Packaging – The FuelSolutions™ transportation packaging consists of a FuelSolutions™ TS125 Transportation Cask with impact limiters and a FuelSolutions™ canister.

Payload – The radioactive contents of a FuelSolutions™ canister including the SNF.

Personnel Barrier – The perforated fabrication that allows free air circulation, which is placed over the FuelSolutions™ TS125 Transportation Cask body between impact limiters to prevent personnel access to the cask exterior.

Shear Block – A block that forms a pocket, located at the bottom of a horizontally oriented FuelSolutions™ TS125 Transportation Cask during transport and welded to the cask outer shell, which interfaces with the intermodal transportation skid to provide longitudinal support for shock and vibration loads during transport.

SNF Assembly Class – Commercial SNF assemblies are identified by class (e.g., PWR SNF includes WE 17 x 17, B&W 15x15, etc., and BWR SNF includes GE 7 x 7, GE 8 x 8).

SNF Assembly Type – Commercial SNF assembly designs within an SNF assembly class are identified by type (e.g., WE 17 x 17 OFA, B&W 15 x 15 Mark B, etc.).

Spacer Plate – Canister basket assembly circular plate with machined openings for guide tubes to provide geometric separation and transverse support for the SNF.

Spent Nuclear Fuel (SNF) – Fuel that has been withdrawn from a nuclear reactor following irradiation, in which the constituent elements have not been separated by reprocessing.

Support Rod (or Tube) – Canister basket assembly rod or tube that positions and provides axial support for the spacer plates.

Test Port – An opening in the closure lid, communicating with the annular region between the containment and test O-ring seals, which facilitates helium leak testing of the containment seal and is sealed closed during transport.

Test Seal – The outermost O-ring, inserted into a groove in the closure lid, which facilitates helium leak testing of the containment seal.

Tiedown Ring – A solid steel ring oriented radially outward from the FuelSolutions™ TS125 Transportation Cask outer shell, located at each end of the neutron shield cavity, which provides a bearing surface for interfacing with the intermodal transportation skid to provide transverse support for shock and vibration loads during transport.

Transportation Cask – see Cask.

Trunnion Attachment Bolts – Fasteners that attach the lifting and handling trunnions.

Trunnion Mounting Boss – A provision in the FuelSolutions™ TS125 Transportation Cask outer shell for mounting of the bolt-on trunnions.

Trunnion Seal – An elastomeric O-ring seal used to keep spent fuel pool water from entering the area between the trunnion and cask body when the cask is immersed for loading.

Trunnions – Lifting attachments, each bolted to a trunnion mounting boss, which are used to lift and/or rotate the FuelSolutions™ TS125 Transportation Cask.

Types of FuelSolutions™ Canisters – Within each class of FuelSolutions™ canisters, each separate and unique canister design is called a type of FuelSolutions™ canister.

Top Ring Forging – The top end of the FuelSolutions™ TS125 Transportation Cask body wall, to which both the inner and outer cask shells are welded, contains threaded holes to interface with the closure lid and upper impact limiter.

Vent Port – An opening in the closure lid, communicating with the FuelSolutions™ TS125 Transportation Cask cavity, which allows gas exchange within the cask interior during opening and closing operations and is sealed closed during transport.

2. STRUCTURAL EVALUATION

This chapter presents the structural evaluation that demonstrates that the FuelSolutions™ W74 canisters, transported in the FuelSolutions™ TS125 Transportation Cask,¹ satisfy the standards specified in 10CFR71,² Subpart E, under the conditions specified in 10CFR71, Subpart F. The effects of the Normal Conditions of Transport (NCT) test specified in 10CFR71.71, Hypothetical Accident Conditions (HAC) specified in 10CFR71.73, and special requirements specified for irradiated nuclear fuel shipments in 10CFR71.61, are evaluated by analysis in accordance with Regulatory Guide 7.9.³ In accordance with 10CFR71.71(a), the NCT load conditions are evaluated separately. In accordance with 10CFR71.73(a), the HAC load conditions are evaluated sequentially to determine their cumulative effects on the package.

The W74 canisters are evaluated using a combination of computer programs and classical manual calculations. The calculations included in the structural evaluation are presented in sufficient detail to allow the results to be verified. All structural finite element analyses are performed using the ANSYS⁴ general purpose finite element program. The ANSYS program is used extensively throughout the industry and has been proven to provide accurate results when used properly. The finite element models used for the structural evaluation of the W74 canister have been generated using proven element types, good modeling practices, and mesh densities with sufficient refinement to accurately calculate the structural responses of interest. Sensitivity studies have been performed to confirm the suitability of the finite element model mesh densities. In accordance with the BFS Quality Assurance Program, the ANSYS program has been verified to provide accurate solutions to numerous problems with classical closed-form solutions. In addition, the specific finite element models used for the structural evaluation of the W74 canister are validated by comparing the results to those obtained from closed-form calculations. Detailed descriptions of the finite element models used for the structural analysis of the W74 canisters are included in Section 2.12.4.

Detailed descriptions of the W74 canister assembly structural evaluation are provided for each NCT and HAC load condition in Sections 2.6 and 2.7, respectively. Separate evaluations are performed for each of the major structural components of the W74 canister. In many cases, discrete models of the individual canister components are used for the structural evaluations, considering the structural interactions with the interfacing canister components. For conditions that include a range of loads, the worst-case combination of loading is evaluated. For instance, the structural evaluation of the W74 canister for the NCT and HAC free drops are performed using upper bound equivalent static acceleration loads (based on the lowest package weight with the lightest W74 canister assembly and cold ambient conditions), applied loads based on the

¹ WSNF-120, *FuelSolutions™ TS125 Transportation Cask Safety Analysis Report*, NRC Docket 71-9276, EnergySolutions Spent Fuel Division, Inc.

² Title 10, Code of Federal Regulations, Part 71 (10CFR71), *Packaging and Transportation of Radioactive Materials*, U.S. Nuclear Regulatory Commission, October 2004.

³ Regulatory Guide 7.9, *Standard Format and Content of Part 71 Applications for Approval of Packaging of Radioactive Material*, U.S. Nuclear Regulatory Commission, Revision 2 (draft), 1986.

⁴ ANSYS/Mechanical, Versions 5.4 and 5.5, ANSYS Inc., Houston, Pennsylvania.

heaviest SNF assemblies accommodated within each W74 canister type, and lower bound allowable stresses based on the maximum temperatures within the canister for the hot ambient condition.

For transport conditions, the transportation cask provides containment of all radioactive materials, and no credit is taken for containment or confinement of the radioactive materials provided by the canister shell. As such, the structural analysis of the canister shell is limited to the controlling HAC load conditions, including the HAC end drop and HAC oblique drop slapdown. For these conditions, it need only be demonstrated that the canister shell assembly does not experience any gross failure that would induce loads onto the canister basket or SNF assemblies that are not otherwise accounted for in the structural evaluation. The canister shell assembly failure modes considered for the transportation free drop conditions include:

- Excessive stresses in the canister shell assembly due to a HAC end drop or a HAC oblique drop slapdown impact.
- Failure of the top end shield plug assembly or its supports due to a bottom end drop.
- Buckling of the canister shell due to a top or bottom end drop.

The structural evaluation of the W74 damaged fuel canister for transportation conditions is based on the structural evaluation of the W74 guide tube assembly due to the similarity of their designs, loadings, and support conditions. As discussed in Section 2.1.1.3, the damaged fuel can is essentially a guide tube with screened ends. Since the damaged fuel canister is continuously supported inside the support tubes, its stresses for the controlling NCT and HAC free drop conditions are substantially lower than those of the W74 guide tubes, which are supported intermittently by the spacer plate ligaments. Therefore, the stresses in the W74 damaged fuel can due to transportation conditions are conservatively assumed equal to those in the W74 guide tube.

The FuelSolutions™ W74 canisters are evaluated and shown to provide adequate support for the SNF assembly payload for all design bases conditions. NCT and HAC evaluations are performed in accordance with the requirements of 10CFR71 for the FuelSolutions™ W74 canisters. The analytic methods used comply with those presented in Regulatory Guides 7.6⁵ and 7.8.⁶ The minimum design margins for the FuelSolutions™ W74 canisters for NCT and HAC are summarized in Table 2.1-1 and Table 2.1-2.

⁵ Regulatory Guide 7.6, *Design Criteria for the Structural Analysis of Shipping Cask Containment Vessels*, Revision 1, U.S. Nuclear Regulatory Commission, Office of Standards Development, March 1978.

⁶ Regulatory Guide 7.8, *Load Combinations for the Structural Analysis of Shipping Casks for Radioactive Material*, Revision 1, U.S. Nuclear Regulatory Commission, Office of Standards Development, March 1989.

2.1 Structural Design

2.1.1 Discussion

The FuelSolutions™ W74 canisters, which are designed for transport in the FuelSolutions™ TS125 Transportation Cask with impact limiters, are comprised of a shell assembly and upper and lower internal basket assemblies. The shell assembly is designed as the confinement boundary for on-site storage conditions, although no credit is taken for confinement or containment of radioactive materials provided by the canister shell during transport. The basket assembly, which is sealed inside the canister shell assembly cavity, maintains the positions of the SNF assemblies and neutron absorbing materials, thus providing subcriticality control.

As discussed in Section 1.2.3.1, intact BRP MOX and partial fuel assemblies are transported in the FuelSolutions™ W74 canister in the same manner as intact UO₂ fuel assemblies. Damaged MOX and UO₂ fuel may also be transported in the FuelSolutions™ W74 canister inside of specially designed FuelSolutions™ W74 damaged fuel can assemblies. Section 2.1.1.3 describes the principal structural members of the FuelSolutions™ W74 damaged fuel can that are used to accommodate BRP damaged fuel within the W74 canisters.

2.1.1.1 Shell Assembly

The shell assembly consists of a right circular shell with redundant welded closure plates and a shield plug assembly at the top end; and a bottom closure plate, bottom shield plug, and bottom end plate at the bottom of the canister. The shell assembly components (including the shell, top end inner closure plate, top end outer closure plate, bottom closure plate, vent and drain port bodies and covers, and top outer closure plate leak test port cover) are fabricated from Type 316 stainless steel for the W74M class canisters and Type 304 stainless steel for the W74T class canisters. Optionally, Type 304 stainless steel with a reduced carbon content may be used for the W74T class canister. The shell assembly stainless steel material provides excellent corrosion protection and has minimum susceptibility to weld sensitization.

Each shell assembly contains carbon steel shield plugs at the top and bottom ends. The bottom shield plug is a solid shield plate encased by the canister bottom closure plate, cylindrical shell extension, and bottom end plate. The top shield plug may either be fabricated from a solid shield plate or a partitioned shield plate and individual shield caps (plugs) for each basket fuel cell. The shield caps are captured inside the sealed canister between the shield plate and top end inner closure plate. The top shield plate includes integral vent and drain ports. All exposed surfaces of the top shield plug assembly are plated with electroless nickel (EN) to provide corrosion protection.

2.1.1.2 Basket Assembly

Each FuelSolutions™ W74 canister includes an upper and lower basket assembly. The upper and lower basket assemblies are similar in construction. Each assembly consists of a series of spacer plates, support tube assemblies, and guide tube assemblies. In addition, the upper basket assembly includes an engagement spacer plate that supports the SNF assemblies in the upper basket assembly for normal vertical transfer and storage. The guide tube assemblies provide lateral support for the SNF assemblies and maintain the position of the neutron absorbing

material. The spacer plates maintain the relative spacing between guide tubes and provide structural support for the basket assembly and SNF assemblies in the lateral direction. The spacer plates are positioned and supported longitudinally by four support tube assemblies. The W74M and W74T basket assembly designs are shown on the general arrangement drawings included in Section 1.3.1 of this SAR.

The W74M upper and lower basket assemblies include 14 spacer plates each. The top and bottom end spacer plates of each W74M basket assembly, referred to as long-term performance (LTP) spacer plates, are fabricated from 2-inch thick SA-240, Type XM-19 stainless steel. All interior spacer plates, referred to as general spacer plates, are fabricated from 0.75-inch thick SA-517 or A514, Grade P or Grade F carbon steel.

The W74T upper and lower basket assemblies each contain 13 general spacer plates fabricated from 0.75-inch thick SA-517 or A514, Grade P or Grade F carbon steel. The dimensions of all spacer plate cutouts are identical. Each spacer plate includes thirty-three 7.25-inch by 7.40-inch guide tube openings and four 9.05-inch square support tube openings. The rows and columns of guide tube openings are aligned relative to their centerlines with the orientations of adjacent guide tube openings rotated 90° relative to one another. The support tube openings are located in the diagonal positions furthest from the center of the plate.

Each basket assembly includes four support tube assemblies that maintain the longitudinal spacing of the spacer plates and provide longitudinal support of the basket assembly. The support tube assemblies consist of a full-length support tube and support sleeves. The support sleeves are positioned over the support tube and between spacer plates, as shown in Figure 2.1-1. For the W74M basket assemblies, the top and bottom end LTP spacer plates are welded to the support tubes to maintain the longitudinal positions of the spacer plates, as shown in Figure 2.1-1. The W74T upper and lower basket assembly top and bottom end spacer plates are captured using stainless steel sleeves that are inserted over and welded to the support tubes, as shown in Figure 2.1-1. The W74M and W74T support tubes and support sleeves are fabricated from SA-240 Type, XM-19 stainless steel and SA-240, Type 304 stainless steel, respectively.

The W74M and W74T guide tube assembly design dimensions and materials are identical. Each guide tube assembly consists of a 13 gage (0.090-inch thick) inner guide tube and either one or two 14 gage (0.075-inch thick) neutron absorber sheets, depending on the location within the basket assembly. Each neutron absorber sheet is positioned on the guide tube by two non-structural shear keys and attached to the guide tube using seven 20 gage (0.036-inch thick) stainless steel neutron absorber sheet retainers. Each retainer fits within a small hole in the neutron absorber sheet and is welded to the guide tube to capture and support the neutron absorber sheet prior to insertion into the basket assembly. The retainers are relied on to maintain the positions of the neutron absorber sheets on the guide tube under all NCT and HAC loadings.

Each W74M guide tube assembly is secured to the bottom end LTP spacer plate within each basket assembly with two attachment brackets to maintain their positions during normal operations and prevent removal of the guide tube during fuel unloading operations. A nominal 0.1-inch clearance is provided between the bottom end of the guide tubes and the bottom end of the support tubes. The clearance is provided to assure that the guide tubes do not support the weight of the basket assemblies under normal handling and storage conditions. The guide tube attachment brackets are designed to fail when subjected to large longitudinal loads, such as those resulting from the HAC end drop. The designed failure mode of the W74M guide tube

attachment brackets prevents overloading of the bottom end spacer plates and the associated welds.

Each W74T guide tube assembly is secured within the basket assembly by a stainless steel retainer clip. A single retainer clip is welded to the side of each guide tube just below the top spacer plate. The retainer clips are designed to secure the guide tube assemblies to the basket assembly in order to maintain criticality control in the unlikely event that it becomes necessary to apply an increased pull force to remove a jammed fuel assembly during fuel retrieval. However, the W74T guide tube retainer clips are designed with sufficient longitudinal clearance between the adjacent spacer plates to allow the guide tube assemblies to move in the longitudinal direction within a sealed canister without imposing out-of-plane loading on the basket assembly spacer plates.

The W74M and W74T guide tubes are fabricated from SA-240, Type 316 stainless steel. For both the W74M and W74T guide tube assemblies, the neutron absorber sheet retainers are fabricated from SA-240, Type 304 stainless steel, and the neutron absorber sheets are fabricated from A887, Type 304 B5 borated stainless steel. The borated neutron absorber materials used in the basket assemblies are not relied on for structural support of other structural components, but are considered to only support their own self weight.

2.1.1.3 Damaged Fuel Can

The FuelSolutions™ W74 canister is designed to accommodate up to eight damaged fuel assemblies. Each damaged fuel assembly is placed inside a FuelSolutions™ W74 damaged fuel can within the upper or lower basket assembly support tubes. The FuelSolutions™ W74 damaged fuel can is designed to contain damaged or undamaged BRP fuel assemblies during all NCT and HAC loadings. The FuelSolutions™ W74 damaged fuel can, containing a damaged BRP fuel assembly, is designed to be handled vertically.

The FuelSolutions™ W74 damaged fuel can, shown in Figure 2.1-2, consists of a damaged fuel can and a removable top lid assembly. The structural design of the damaged fuel can is similar to that of the FuelSolutions™ W74 guide tube assembly. The damaged fuel can consists of a 13 gage (0.090-inch thick) tube and a 12 gage (0.105-inch thick) bottom end plate. The bottom end of the damaged fuel can includes screened holes to allow for water drainage. The damaged fuel can includes borated stainless steel neutron absorber sheets on all four faces of the tube. The damaged fuel can neutron absorber sheet attachment detail is similar to that of the guide tubes.

The principal structural members of the damaged fuel can top lid assembly include the handle, base plate, and attachment hardware. As shown in Figure 2.1-2, the top lid assembly handle has four legs that are each 0.25-inch thick by 2-inch wide. Each leg of the handle is attached to the base plate using full penetration groove welds. The top lid assembly base plate consists of a 6.7-inch square by 3/8-inch thick plate, with a 5.5-inch long by 1.25-inch wide rectangular cutout in the center to accommodate the fuel assembly bail handle. The base plate also includes eight slotted holes to accommodate the attachment hardware.

The top lid assembly attachment hardware consists of four attachment bars or “dogs.” The top lid attachment dogs are used to secure and lock the top lid assembly to the damaged fuel can after insertion of the damaged fuel assembly. Each attachment dog is secured to the top lid base plate using two cap screws. Slotted holes in the base plate allow the attachment dogs to be retracted

for insertion into the damaged fuel can. Once inserted, the attachment dogs are extended to engage the slotted holes in the corners of the damaged fuel can and secured with the cap screws. In the extended position, the heads of the cap screws are positioned in recessed holes to prevent the attachment dogs from inadvertently retracting.

2.1.2 Design Criteria

This section identifies the codes and standards that are applicable to the design of the FuelSolutions™ W74 canisters. The basic allowable stress design criteria for the W74 canister shell and basket are defined in Section 2.1.2.1. The NCT and HAC load combinations are defined in Section 2.1.2.2. Miscellaneous structural design criteria for brittle fracture, fatigue, and buckling are defined in Section 2.1.2.3. The function and design code for each of the W74 canister assembly structural components are summarized in Table 2.1-3.

2.1.2.1 Basic Design Criteria

Canister Shell Assembly

The allowable stress design criteria of Section III, Division 1, Subsection NB,⁷ of the ASME B&PV Code are applied to all structural components of the canister shell assembly that provide confinement under 10CFR72. These components include the canister cylindrical shell, inner and outer closure plates, bottom closure plate, and all associated seam welds and closure welds. The top shield plug assembly, bottom shield plug, bottom shell extension, and bottom end plate are designed in accordance with the allowable stress criteria of Section III, Division 1, Subsection NF⁸ of the ASME B&PV Code. The allowable stresses for the canister shell containment components and shield plugs are summarized in Table 2.1-4. Buckling of the canister shell is evaluated in accordance with ASME Code Case N-284-1.⁹

Basket Assembly

The basket assembly criticality control components, which are relied on to maintain the relative positions of the fissile and neutron absorbing materials, are designed in accordance with Section III, Subsection NG¹⁰ of the ASME B&PV Code. These include components within the basket assemblies such as the spacer plates, support tubes, support sleeves, and the guide tubes. In addition, the W74 damaged fuel canisters are designed in accordance with Section III, Subsection NG, of the ASME B&PV Code. The allowable stress design criteria for components evaluated on an elastic basis are conservatively used for all NCT and HAC loading conditions. In addition, plastic analyses are also provided for the basket assembly criticality control

⁷ American Society of Mechanical Engineers (ASME) Boiler and Pressure Vessel Code, Section III, Division 1, Subsection NB, *Class 1 Components*, 1998 Edition.

⁸ American Society of Mechanical Engineers (ASME) Boiler and Pressure Vessel Code, Section III, Division 1, Subsection NF, *Supports*, 1998 Edition.

⁹ Code Case N-284-1, *Metal Containment Shell Buckling Design Methods*, American Society of Mechanical Engineers (ASME) Boiler and Pressure Vessel Code, 1998 Code Cases, Nuclear Components, 1998 Edition.

¹⁰ American Society of Mechanical Engineers (ASME) Boiler and Pressure Vessel Code, Section III, Division 1, Subsection NG, *Core Support Structures*, 1998 Edition.

components that experience stress levels in excess of the material yield strength for the purpose of determining maximum permanent deformations to be considered in the criticality evaluation. A summary of the allowable stress design criteria used for the structural evaluation of the W74 canister criticality components is presented in Table 2.1-5.

The W74 basket assembly neutron absorber panels and their attachments to the W74 guide tubes are designed in accordance with the allowable stress design criteria of Subsection NG of the ASME B&PV Code. As discussed in Section 2.3, the neutron absorber panel allowable stresses are calculated assuming that the borated stainless steel material from which they are fabricated has strength properties equal to those of SA-240, Type 304 stainless steel.

The buckling design criteria of NUREG/CR-6322¹¹ and Article F-1331.5(a)(1)¹² of the ASME B&PV Code are used for the buckling evaluation of the basket assembly criticality control components. Buckling evaluations are performed for the basket assembly criticality control components considering both elastic buckling behavior and general plastic instability. For the elastic buckling evaluations, the basket assembly components are evaluated using the beam-column buckling interaction equations of NUREG/CR-6322. For general plastic instability, the maximum load is limited to two-thirds of the buckling load determined by a plastic stability analysis in accordance with F-1334.3(a)(1).

2.1.2.2 Load Combinations

Table 2.1-6 and Table 2.1-7 show the NCT and HAC load combinations for which the FuelSolutions™ W74 canisters are evaluated. The NCT and HAC load combinations are developed in accordance with Table 1 of Regulatory Guide 7.8. In addition, the load combinations include intermediate values for initial conditions that could result in a more limiting case for the W74 canister design. For example, the cold environment (i.e., -40°F ambient temperature) is evaluated in combination with maximum decay heat, since this combination may be most limiting for differential thermal expansion and thermal stress.

Each NCT load condition is evaluated separately in accordance with the requirements of 10CFR71.71(a). Each HAC load condition is applied sequentially in accordance with 10CFR71.73(a) to determine the maximum cumulative damage resulting from the HAC load conditions specified in 10CFR71.73(c). These include a 30-foot free drop onto a horizontal essentially unyielding surface, followed by a 40-inch free drop onto a 6-inch diameter mild steel puncture bar, followed by exposure to a 30-minute fire. The cumulative damage sustained by the W74 canister from the sequential application of the HAC load conditions is discussed in Section 2.7.7. The 2 MPa (290 psi) external pressure load of 10CFR71.61 is evaluated separately, as discussed in Section 2.8.

Each NCT and HAC loading is evaluated along with the applicable initial conditions, including ambient temperature, insolation, decay heat, internal pressure, and fabrication stresses. Since no credit is taken for containment provided by the canister shell during transport and the canister

¹¹ NUREG/CR-6322, *Buckling Analysis of Spent Fuel Basket*, U.S. Nuclear Regulatory Commission, UCRL-ID-119697, May 1995.

¹² American Society of Mechanical Engineers (ASME) Boiler and Pressure Vessel Code, Section III, Division 1, Appendix F, *Rules for Evaluation of Service Loadings with Level D Service Limits*, 1998 Edition.

basket assembly does not retain pressure loads, the W74 canister is not evaluated for internal pressure loading. The processes used for the fabrication of the W74 canisters assure that there are no significant residual stresses due to fabrication. These fabrication processes include the use of multi-pass welds and weld filler metals with a minimum delta ferrite content of 5FN for shop welds and 10FN for field closure welds to minimize weld distortion. Therefore, fabrication stresses are not considered in the load combination evaluation.

2.1.2.3 Miscellaneous Structural Failure Modes

Brittle Fracture

The FuelSolutions™ W74M and W74T canister shell and basket assemblies are designed using materials that provide degrees of safety against failure due to brittle fracture, which are appropriate for the intended uses. The fracture toughness requirements used for the W74 canisters are based on a Lowest Service Temperature (LST) for all NCT and HAC loadings, which produce significant dynamic tensile stress levels in the canister components. The results of the W74 canister structural evaluation show that the only conditions that produce significant dynamic stresses in the canister shell and basket assembly structural components are the NCT and HAC free drop loadings. A conservative LST of -20°F is used to establish the fracture toughness requirements for the W74 canister assemblies.

With the exception of the top and bottom end shield plugs, the FuelSolutions™ W74 canister shell assembly components are designed in accordance with the fracture toughness requirements of ASME NB-2300. The FuelSolutions™ W74 canister shell assembly components are fabricated entirely from SA-240, Type 304 and Type 316 austenitic stainless steels. These materials do not undergo a ductile-to-brittle transition in the temperature range of interest (i.e., down to -20°F), and thus are not susceptible to brittle fracture. Accordingly, impact testing is not required for austenitic stainless steels in accordance with NB-2311(a)(6).

The W74 carbon steel shield plugs are designed in accordance with the fracture toughness requirements of ASME NF-2300. Per NF-2311(b)(7), impact testing is not required for materials for which the maximum stress does not exceed 6,000 psi tension or is compressive since brittle fracture failure under these conditions is not credible. As shown in the W74 canister shell structural evaluation, the maximum stress in the bottom carbon steel shield plug is less than 6,000 psi for the HAC end drop. Therefore, brittle fracture failure of the W74 canister carbon steel bottom shield plugs is not a credible failure mode, and impact testing of these materials is not required. For the W74 top shield plugs, impact testing will be performed in accordance with NF-2300 to assure adequate fracture toughness of the material.

The FuelSolutions™ W74 canister basket assembly and the W74 damaged fuel can are designed in accordance with the fracture toughness requirements of NG-2300, except that the impact testing requirements of NUREG/CR-1815¹³ are used in lieu of NG-2330. Since the basket assembly components do not provide containment, the fracture toughness testing requirements from NUREG/CR-1815 for Category II steel are used. These requirements assure that the fracture toughness of the material is sufficient to prevent fracture initiation of pre-existing cracks

¹³ NUREG/CR-1815, *Recommendations for Protection Against Failure by Brittle Fracture in Ferritic Steel Shipping Containers Up to Four Inches Thick*, U.S. Nuclear Regulatory Commission, June 15, 1981.

under dynamic loading. The basket assembly structural components are fabricated from SA-240, Type 316, Type 304, and Type XM-19 austenitic stainless steels and SA-517 or A514, Grade P or Grade F, carbon steels. Austenitic stainless steel materials do not undergo a ductile-to-brittle transition in the temperature range of interest (i.e., down to -20°F), and thus are not susceptible to brittle fracture. Accordingly, impact testing of austenitic stainless steels is not required by ASME NG-2311(a)(5).

The W74 general spacer plate material (i.e., 0.75-inch thick SA-517, Grades F or P, or A514, Grades F or P carbon steel plate) experiences a ductile-to-brittle transition at a temperature lower than the NUREG/CR-1815 prescribed maximum Nil Ductility Transition (NDT) temperature. Drop weight testing of the general spacer plate material in accordance with ASTM E-208 will be performed to demonstrate that the NDT temperature (T_{NDT}) is at or below the T_{NDT} test temperature. The T_{NDT} test temperature for the general spacer plate material is established based on the material thickness and the LST using Figure 7 of NUREG/CR-1815 as follows:

$$T_{NDT} = LST - A = -30^{\circ}\text{F}$$

where:

LST = -20°F, LST for all on-site storage and transfer conditions for which the cask drop and tip-over accidents are postulated to occur

A = 10°F, offset temperature established using Figure 7 (curve KID/(yd) of NUREG/CR-1815

The effects of irradiation on material toughness properties is considered in accordance with the requirements of ASME NG-2332(d). The evaluation is based on an exposure of 100 years, conservatively assuming no decay of the neutron source. The total neutron fluence (8.81E+14 n/cm² for E>1.0 MeV and 3.97E+15 n/cm² for E>0.1 MeV) results in 1.88E-06 dpa iron atom displacements. According to Figure 3-1 of NUREG-1509,¹⁴ the entire neutron energy spectrum of 1.88E-06 dpa will not change the fracture toughness properties of SA-517 or A514 carbon steels.

Fatigue

Fatigue failure of the W74 canister shell and basket for transportation is evaluated in accordance with Articles NB-3222.4(d) and NG-3222.4(d) of the ASME Code, respectively. The detailed fatigue evaluation is presented in Section 2.6.1.4. As discussed in Section 2.6.1.4, the analyses of the FuelSolutions™ W74 canister shell assembly and basket assembly demonstrate that cyclical loads occurring during normal transportation and storage conditions do not present a fatigue concern for the FuelSolutions™ W74 canister components.

Buckling

The stability of the canister shell for transport conditions is evaluated in accordance with ASME Code Case N-284-1. The evaluation includes factors to account for geometric and loading eccentricities in the shell. The end drop condition produces the most severe buckling loads in the canister shell. The buckling evaluation of the canister shell is presented in Section 2.7.1.1.5.3.

¹⁴ NUREG-1509, *Radiation Effects on Reactor Vessel Supports*, U.S. Nuclear Regulatory Commission.

The buckling criteria of NUREG/CR-6322 and Article F-1331.5(a)(1) of the ASME Code are used for the basket assembly criticality control components. Buckling evaluations are performed for the basket assembly criticality control components considering both elastic buckling behavior and general plastic instability. For the elastic buckling evaluations, the basket assembly components are evaluated using the beam-column buckling interaction equations of NUREG/CR-6322. For general plastic instability, the maximum load is limited to two-thirds of the buckling load determined by a plastic stability analysis in accordance with F-1334.3(a)(1).

**Table 2.1-1 - FuelSolutions™ W74 Canister Minimum Design Margins
for NCT Loading Conditions**

Canister Component	Controlling Stress Type	Governing Condition	Minimum Design Margin⁽¹⁾	Reference SAR Section
LTP Spacer Plate	Buckling	NCT Side Drop + NCT Thermal	+0.35	2.6.7.1
General Spacer Plate	P_m+P_b	NCT Side Drop	+0.32	2.6.7.1
Engagement Plate	P_m+P_b+Q	NCT Side Drop + NCT Thermal	+2.51	2.6.7.2
Support Tube	P_m+P_b	NCT Side Drop	+26.2	2.6.7.3
Support Tube Longitudinal Seam Weld	Shear	NCT Side Drop	+16.9	2.6.7.3
W74M Support Tube/LTP Spacer Plate Weld	Shear	NCT Side Drop + NCT Thermal	+3.52	2.6.7.3
W74T Support Tube/Attachment Sleeve Weld	Shear	NCT Thermal	+1.11	2.6.1.3.3
Support Sleeve	Buckling	NCT Thermal	+3.27	2.6.1.3.3
Guide Tube	P_m+P_b	NCT Side Drop	+0.84	2.6.7.4
Guide Tube Longitudinal Seam Weld	P_m+P_b	NCT Side Drop	+0.85	2.6.7.4
Guide Tube Neutron Absorber Panel	P_m+P_b	NCT Side Drop	+19.3	2.6.7.4
Guide Tube Neutron Absorber Panel Attachment Weld	Shear	NCT Side Drop	+1.64	2.6.7.4

Note:

⁽¹⁾ Design margin is equal to (Allowable/Stress) - 1.

Table 2.1-2 - FuelSolutions™ W74 Canister Minimum Design Margins for HAC Loading Conditions

Canister Component	Controlling Stress Type	Governing Condition	Minimum Design Margin⁽¹⁾	Reference SAR Section
LTP Spacer Plate	Buckling	HAC Side Drop + NCT Thermal	+0.04	2.7.1.2.1
General Spacer Plate	Buckling	HAC Oblique Drop Slapdown + NCT Thermal	+0.27	2.7.1.4.1
Engagement Plate	P_m	HAC End Drop	+0.73	2.7.1.1.2
Support Tube	Buckling	HAC End Drop	+0.16	2.7.1.1.3
Support Tube Longitudinal Seam Weld	Shear	HAC Oblique Drop Slapdown	+5.47	2.7.1.4.3
W74M Support Tube/LTP Spacer Plate Weld	Shear	HAC End Drop	+2.68	2.7.1.1.3
W74T Support Tube/Attachment Sleeve Weld	Shear	HAC End Drop	+0.36	2.7.1.1.3
Support Sleeve	Buckling	HAC End Drop	+0.41	2.7.1.1.3
Guide Tube	P_m+P_b	HAC Oblique Drop Slapdown	+0.06	2.7.1.4.4
Guide Tube Longitudinal Seam Weld	P_m+P_b	HAC Oblique Drop Slapdown	+0.32	2.7.1.4.4
Guide Tube Neutron Absorber Panel	P_m+P_b	HAC Oblique Drop Slapdown	+10.7	2.7.1.4.4
Guide Tube Neutron Absorber Panel Attachment Weld	Shear	HAC Oblique Drop Slapdown	+0.34	2.7.1.4.4
Canister Shell	P_m+P_b	HAC Oblique Drop Slapdown	+0.16	2.7.1.4.5
Top Shield Plug	P_m+P_b	HAC End Drop	+0.47	2.7.1.1.5
Alignment Bar Welds (Top Shield Plug Supports)	Shear	HAC End Drop	+0.46	2.7.1.1.5

Note:

⁽¹⁾ Design margin is equal to (Allowable/Stress) - 1.

Table 2.1-3 - Summary of FuelSolutions™ W74 Canister Component Functions and Design Codes

Assembly	Component⁽¹⁾	Function	Codes & Standards
Shell Assembly	Cylindrical Shell	Confinement ⁽²⁾	NB
	Bottom End Plate	Structural	NF
	Bottom End Shell Extension	Structural	NF
	Bottom Shield Plug	Shielding	NF
	Bottom Closure Plate	Confinement ⁽²⁾	NB
	Top End Outer Closure Plate	Confinement ⁽²⁾	NB
	Top End Inner Closure Plate	Confinement ⁽²⁾	NB
	Top Shield Plug	Shielding	NF
	Top Shield Plug Support Bars	Structural	NF
Basket Assembly	General Spacer Plates	Criticality Safety	NG
	LTP Spacer Plate (W74M)	Criticality Safety	NG
	Support Tube	Criticality Safety	NG
	Support Sleeve	Criticality Safety	NG
	Guide Tube	Criticality Safety	NG
	Neutron Absorber Panel	Criticality Safety	NG
	Neutron Absorber Panel Button	Criticality Safety	NG
	Guide Tube Attachment Bracket (W74M)	Criticality Safety	NG
	Damaged Fuel Can	Criticality Control	NG

Notes:

- (1) Components are included in both the W74M and W74T canisters, unless otherwise specified.
- (2) The canister shell provides confinement of radioactive materials for storage conditions, but is not relied on to provide containment of radioactive material for transportation conditions.

Table 2.1-4 - Canister Shell Allowable Stress Criteria

Shell Component	Stress Category	Service Condition	
		NCT (Service Level A)	HAC (Service Level D)
Shell Components (Subsection NB)	P_m	S_m	Lesser of $2.4S_m$ or $0.7S_u$
	$P_m + P_b$	$1.5S_m$	150% of P_m allowable
	$P_m + P_b + Q$	$3.0S_m$	N/A
	Pure Shear Stress	$0.6S_m$	$0.42S_u$
	Canister Shell Buckling	Per ASME Code Case N-284-1	
Shield Plugs (Subsection NF)	P_m	S_m	Greater of $1.5 S_m$ or $1.2 S_y$, not to exceed $0.7S_u$
	$P_m + P_b$	$1.5S_m$	150% of P_m Allowable
	Pure Shear Stress	$0.6S_m$	$0.42S_u$

Table 2.1-5 - Canister Basket Allowable Stress Criteria

Basket Components	Stress Category	Service Condition	
		NCT (Service Level A)	HAC (Service Level D)
Criticality Control Components ⁽¹⁾ (Subsection NG)	P_m	S_m	Lesser of: $2.4S_m$ or $0.7S_u$
	$P_m + P_b$	$1.5S_m$	150% of P_m allowable
	$P_m + P_b + Q$	$3.0S_m$	N/A
	Pure Shear Stress	$0.6S_m$	Lesser of $1.2S_m$ ⁽²⁾ or $0.42S_u$
	Buckling	Per NUREG/CR-6322 and Article F-1331.5(a)(1) of the ASME Code	

Notes:

- (1) Includes general spacer plates, LTP spacer plates, engagement spacer plate, support tubes, support sleeves, and guide tubes. Also included are the support tube attachment welds, support tube longitudinal seam welds, and guide tube longitudinal seam welds.
- (2) In accordance with NG-3225, special stress limits for Service Level D conditions are limited to twice the allowable stress for Service Level A and Level B conditions.

Table 2.1-6 - Summary of NCT Load Combinations

Loads (applied separately)	Applicable Initial Condition								
	Thermal Conditions						Internal Pressure		Fabrication Stresses
	Ambient Temp.		Insolation		Decay Heat		Max	Min	
	100°F	-20°F	Max	Zero	Max	Zero			
Hot Environment	x		x		x		x		x
Cold Environment -40°F ambient temp.				x	x	x ⁽¹⁾		x ⁽¹⁾	x
Increased External Pressure: 20 psia		x		x		x		x	x
Minimum External Pressure: 3.5 psia	x		x		x		x		x
Vibration and Shock:	x		x		x	x ⁽¹⁾		x ⁽¹⁾	x
		x		x			x ⁽²⁾		x
Free Drop: 1 foot drop	x		x		x	x ⁽¹⁾		x ⁽¹⁾	x
		x		x			x ⁽²⁾		x

Notes:

- (1) In accordance with Regulatory Guide 7.8, intermediate values of initial conditions that could possibly create a more limiting condition are evaluated.
- (2) Considered only for brittle fracture.

Table 2.1-7 - Summary of HAC Load Combinations

Loads (applied sequentially)	Applicable Initial Condition									
	Thermal Conditions							Internal Pressure		Fabrication Stresses
	Ambient Temperature			Insolation		Decay Heat		Max	Min	
	100°F	-20°F	-40°F	Max	Zero	Max	Zero			
Free Drop: 30 foot drop	x			x		x		x		x
		x			x	x ⁽¹⁾		x ⁽¹⁾		x
		x					x ⁽²⁾		x	x
Puncture: 40-inch drop	x			x		x		x		x
		x			x		x ⁽²⁾		x	x
Thermal: 1,475°F fire	x			x ⁽³⁾		x		x		x

Notes:

- (1) In accordance with Regulatory Guide 7.8, intermediate values of initial conditions that could possibly create a more limiting condition are evaluated.
- (2) Considered only for brittle fracture.
- (3) The HAC pre-fire steady-state condition is analyzed with zero insolation per 10CFR71.73(c)(3).

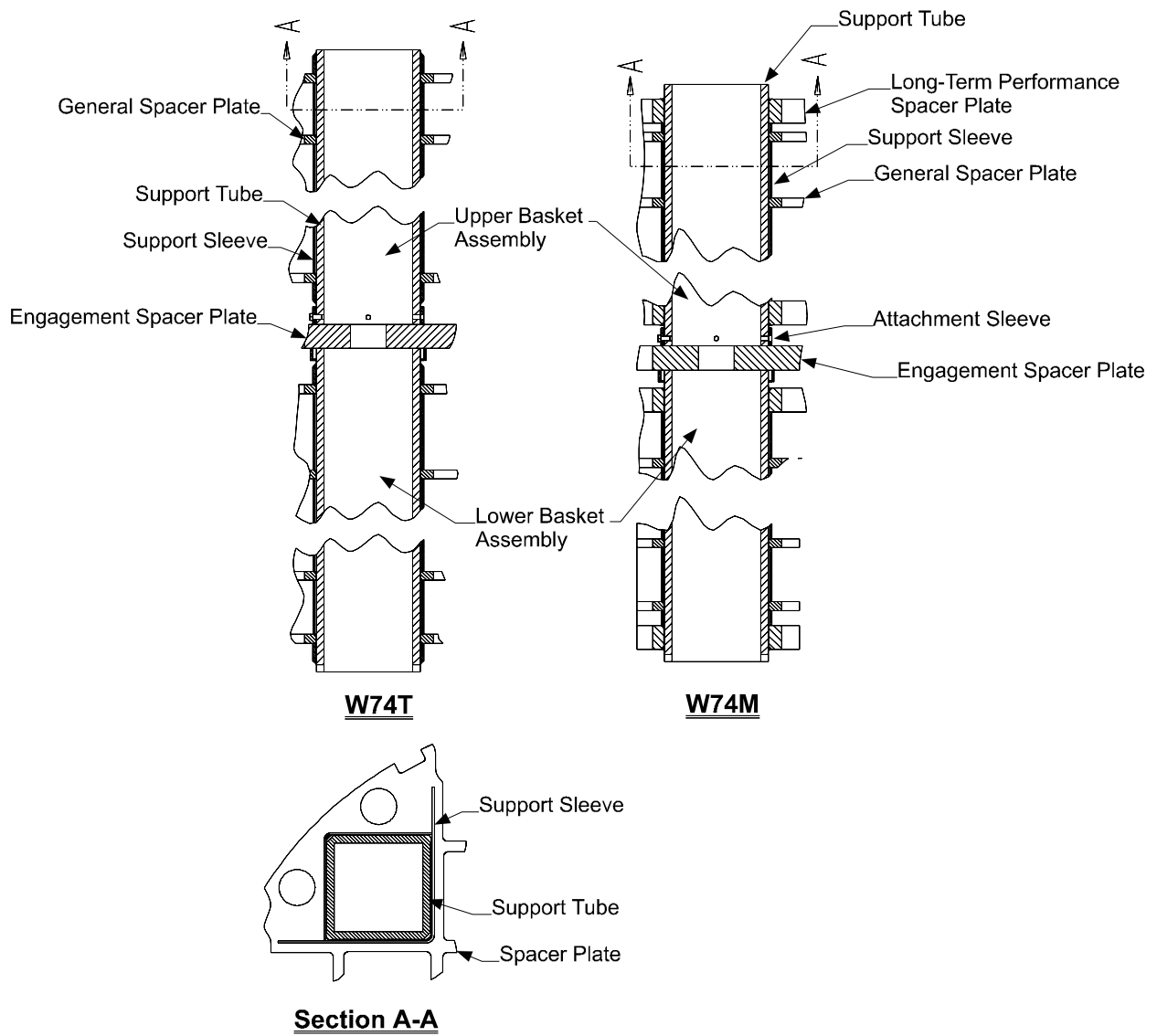


Figure 2.1-1 - FuelSolutions™ W74 Canister Support Tube Assembly Detail

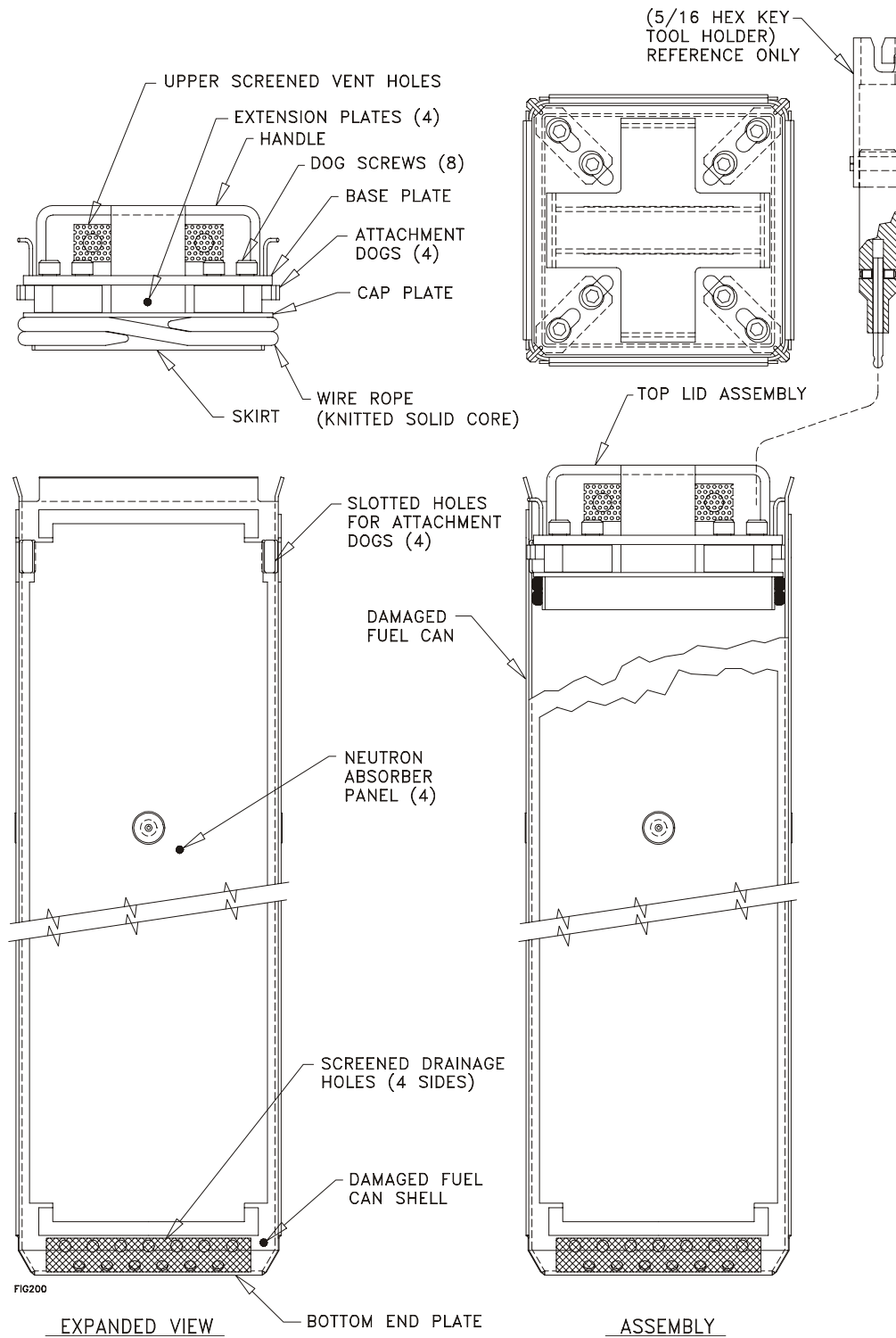


Figure 2.1-2 - FuelSolutions™ W74 Damaged Fuel Can

This page intentionally left blank.

2.2 Weights and Center of Gravity

The weights of the major FuelSolutions™ W74 canister components and payload (SNF assemblies and damaged fuel cans) are summarized in Table 2.2-1. The total weight and center of gravity of each canister configuration, with maximum payload weights, are shown for the dry storage configuration (e.g., dry sealed canister containing payload). The BRP fuel assembly weights reported in Table 2.2-1 are based on a 32 intact UO₂ BRP SNF assemblies, each with a nominal weight of 465 pounds, plus a bounding weight of 200 pounds for four damaged fuel cans in both the upper and lower baskets. The calculated weight of each damaged fuel can is 121 pounds. As shown in Table 1.2-5, the maximum weight of and BRP SNF assemblies is 485 pounds. Therefore, the maximum payload weights for the W74M and W74T canisters could be slightly higher than those reported in Table 2.2-1. However, the weight of the heaviest W74 canisters with the heaviest payload is lower than the 85,000-pound canister payload weight for which the FuelSolutions™ TS125 Transportation Package is designed.

Per Section 1.2.3.1, if less than 64 total fuel assemblies are loaded into a W74 canister, a dummy fuel assembly shall be placed into each empty canister basket guide tube. Each dummy fuel assembly shall be the approximate weight and size of the actual fuel being loaded. The dummy fuel assemblies maintain the minimum total package weight and the center of gravity near the centerline of the canister.

Table 2.2-1 - W74 Canister Weights and Centers of Gravity

Component	W74M		W74T	
	Weight (pounds)	Center of Gravity ⁽¹⁾ (in.)	Weight (pounds)	Center of Gravity ⁽¹⁾ (in.)
Canister Field Assembly	24,681	101.6	24,681	101.6
Shell Assembly	15,143	48.1	15,143	48.1
Top Shield Plug	6,673	184.9	6,673	184.9
Inner Closure Plate	955	189.5	955	189.5
Outer Closure Plate	1,910	191.0	1,910	191.0
Lower Basket Assembly	9,255	50.2	8,171	50.4
Upper Basket Assembly	10,963	132.5	9,883	131.7
Fuel in Lower Basket ⁽²⁾	15,680	50.9	15,680	50.9
Fuel in Upper Basket ⁽²⁾	15,680	138.2	15,680	138.2
Sealed Canister⁽²⁾	76,259	96.9	74,095	97.0
Heaviest Sealed Canister⁽³⁾	77,539	---	75,375	---

Notes:

- (1) Centers of gravity are relative to bottom end of canister, as shown in Figure 2.2-1.
- (2) Payload weight includes 32 SNF assemblies plus four damaged fuel canisters per basket at the support tube locations. Weights are based on nominal SNF assembly weight of 465 pounds and bounding damaged fuel canister weight of 200 pounds.

- ⁽³⁾ Payload weight includes 32 SNF assemblies plus four damaged fuel canisters per basket at the support tube locations. Weights are based on nominal SNF assembly weight of 485 pounds and bounding damaged fuel canister weight of 200 pounds.

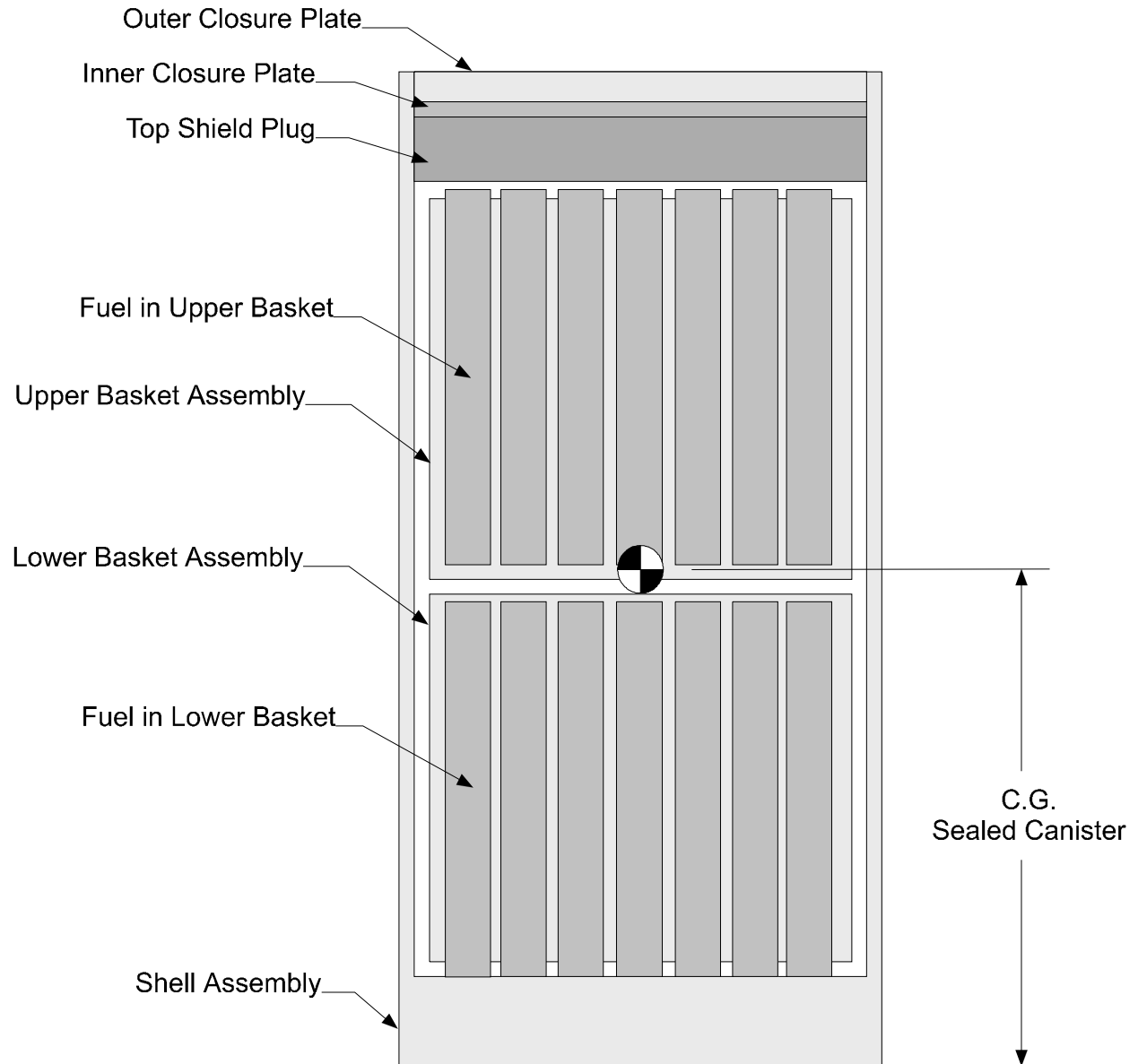


Figure 2.2-1 - FuelSolutions™ W74 Canister Center of Gravity Diagram

This page intentionally left blank.

2.3 Mechanical Properties of Materials

The FuelSolutions™ W74M and W74T canister structural components are fabricated entirely from austenitic stainless steel and carbon steel. Table 2.3-1 and Table 2.3-2 identify components, material specifications, and the corresponding material data tables for the FuelSolutions™ W74M and W74T canisters, respectively.

The weight density and Poisson's ratio for stainless steel used in the structural analysis are 0.290 lb/in³ and 0.29, respectively. Similarly, the weight density and Poisson's ratio for carbon steel used in the structural analysis are 0.283 lb/in³ and 0.3, respectively. Detailed descriptions of the FuelSolutions™ W74M and W74T canister materials of construction are included in the following paragraphs.

Both the FuelSolutions™ W74M and W74T canister shell assembly designs are of identical construction and vary only in the type of stainless steel used for the shell and closure plates. The canister shell assembly structural components for the W74M, with the exception of the top and bottom shield plugs, are all fabricated from SA-240, Type 316 austenitic stainless steel. The canister shell assembly structural components for the W74T canister are all fabricated from SA-240, Type 304 austenitic stainless steel. SA-240, Type 304 austenitic stainless steel with a reduced carbon content may also be used for the W74T canister shell assembly. The bottom shield plug is fabricated from ASTM A36 carbon steel. The bottom shield plug is encased between the bottom closure plate and the bottom end plate within the cylindrical shell extension. The top shield plug assembly consists of a shield plate and 37 shield caps. The shield plate is fabricated from ASTM A516, Grade 55 or 60 carbon steel, and the shield caps are fabricated from ASTM A36 carbon steel. Optionally, a solid shield plate fabricated from ASTM A36 carbon steel may be used for both the W74M and W74T canisters. The shield plate and shield caps are coated to provide corrosion protection.

The W74M and W74T basket assembly designs are of similar construction and vary only in the materials used for the top and bottom end spacer plates of each basket. The general spacer plates used in the W74T and W74M basket assembly are all fabricated from EN coated SA-517, Grades F or P or A514, Grades F or P carbon steel. The W74M upper and lower basket assemblies each include a top and bottom end LTP spacer plate fabricated from SA-240, Type XM-19 austenitic stainless steel.

The support tube, support sleeve, and guide tube materials are identical for the W74M and W74T basket assembly designs. The support tubes and support sleeves are fabricated from SA-240, Type XM-19 and Type 304 austenitic stainless steels, respectively. Each W74M and W74T guide tube assembly consists of a guide tube and two neutron absorber panels. The guide tubes are fabricated from SA-240, Type 316 stainless steel.

For accident drop conditions, the guide tubes are evaluated using plastic analysis. The elastic-plastic material properties for this analysis are based on information from NUREG/CR-0481.¹⁵ Since the guide tube evaluations are conservatively performed at a bounding temperature of 650°F and the stress-strain values from the report are at a maximum

¹⁵ NUREG/CR-0481, SAND77-1872, *An Assessment of Stress-Strain Data Suitable for Finite-Element Elastic-Plastic Analysis of Shipping Containers*, R-7, Rack, H. J., Knorovsky, G. A., September 1978.

temperature of 600°F, a “normalization” factor is used to determine the equivalent plastic material properties at 650°F. This factor is computed based on the ASME Code value for yield stress of Type 316 stainless steel at 650°F, divided by the report value at 0.2% strain for a temperature of 600°F. This factor is then applied to the report stress values at 600°F, to arrive at the stress vs. strain values at 650°F. These values, as presented in Table 2.3-4, are used in the plastic analysis of the guide tube.

All structural materials used for the W74 canisters are permitted for use in Section III construction per Section II, Part D and Code Case N-71-16¹⁶ of the ASME Code. The SA-517, Grade F or P and A514, Grade F or P carbon steel materials used for the general spacer plates are permitted for supports only. Use of these materials for the basket assembly spacer plates and support tubes is acceptable since there is no significant effects on the material properties for the intended service conditions. As discussed in Section 2.1.2.3, the cumulative effect of irradiation from the SNF does not significantly affect the fracture toughness of the general spacer plate carbon steel materials over the design life of the canister.

The maximum allowable temperatures of the canister materials for all normal design conditions are limited to those tabulated in ASME, Section II, Part D. Short-term elevated temperatures in excess of these allowable values may occur during loading operations or off-normal on-site transfer and storage events. The maximum temperatures in the basket assembly components remain below 1,000°F for all short-term thermal conditions. As shown in ASME Code Case N-47-33,¹⁷ the strength properties of austenitic stainless steels do not change due to exposure to 1,000°F for up to 10,000 hours. Therefore, short-term exposure to temperatures of this magnitude does not have any significant effect on mechanical properties of the basket assembly materials.

The acceptable weld metals and welding processes for all welds in the W74 canisters are shown on the general arrangement drawings included in Section 1.3.1. The weld metals specified provide equal or greater strength than the specified base material strength.

¹⁶ American Society of Mechanical Engineers (ASME) Boiler and Pressure Vessel Code, 1998 Code Cases, Nuclear Components, Case N-71-17, *Additional Materials for Subsection NF, Class 1, 2, 3, and MC Component Supports Fabricated by Welding*, 1998 Edition.

¹⁷ American Society of Mechanical Engineers (ASME) Boiler and Pressure Vessel Code, 1995 Code Cases, Nuclear Components, Case N-47-33, *Class 1 Components in Elevated Temperature Service*, 1995 Edition.

Table 2.3-1 - FuelSolutions™ W74M Canister Materials Summary

Assembly	Component	Material	Reference Table
Shell Assembly	Cylindrical Shell	SA-240, Type 316	Table 2.3-3
	Bottom Closure Plate	SA-240, Type 316	Table 2.3-3
	Bottom End Plate	SA-240, Type 316	Table 2.3-3
	Bottom Shield Plug	A36	Table 2.3-7
	Top End Inner Closure Plate	SA-240, Type 316	Table 2.3-3
	Top End Outer Closure Plate	SA-240, Type 316	Table 2.3-3
	Top Shield Plug Shield Plate ⁽¹⁾	SA-36 or A516, Grade 55 or 60	Table 2.3-7 Table 2.3-11
	Shield Caps (Top Shield Plug)	A36	Table 2.3-7
	Shield Plug Support Bars	SA-240, Type 316	Table 2.3-3
Basket Assembly	LTP Spacer Plate	SA-240, Type XM-19	Table 2.3-3
	General Spacer Plate	SA-517, Grade F or P, or A514, Grade F or P	Table 2.3-8, Table 2.3-9
	Engagement Spacer Plate	SA-240, Type XM-19	Table 2.3-3
	Support Tube	SA-240, Type XM-19	Table 2.3-6
	Support Sleeve	SA-240, Type 304	Table 2.3-5
	Guide Tube	SA-240, Type 316	Table 2.3-3
	Guide Tube Attachment Bracket	SA-240, Type 304	Table 2.3-5
	Neutron Absorber Sheet Retainer	SA-240, Type 304	Table 2.3-5
	Neutron Absorber Sheet	A887, Type 304B5	Table 2.3-10 ⁽²⁾

Notes:

- ⁽¹⁾ The top shield plug assembly consists of a shield plate and 37 shield caps. The shield plate is fabricated from ASTM A516, Grade 55 or 60 carbon steel, and the shield caps are fabricated from ASTM A36 carbon steel. Optionally, a solid shield plate fabricated from SA-36 carbon steel may be used for the W74M canisters.
- ⁽²⁾ Assumed to have the same mechanical properties as SA-240, Type 304 stainless steel.

Table 2.3-2 - FuelSolutions™ W74T Canister Material Summary

Assembly	Component	Material	Reference Table
Shell Assembly	Cylindrical Shell	SA-240, Type 304	Table 2.3-5
	Bottom Closure Plate	SA-240, Type 304	Table 2.3-5
	Bottom End Plate	SA-240, Type 304	Table 2.3-5
	Bottom Shield Plug	A36	Table 2.3-7
	Top End Inner Closure Plate	SA-240, Type 304	Table 2.3-5
	Top End Outer Closure Plate	SA-240, Type 304	Table 2.3-5
	Top Shield Plug Shield Plate ⁽¹⁾	SA-36 or SA-516, Grade 55 or 60	Table 2.3-7 Table 2.3-11
	Shield Caps (Top Shield Plug)	A36	Table 2.3-7
	Shield Plug Support Bars	SA-240, Type 304	Table 2.3-5
Basket Assembly	General Spacer Plate	SA-517, Grade F or P, or A514, Grade F or P	Table 2.3-8, Table 2.3-9
	Engagement Spacer Plate	SA-240, Type XM-19	Table 2.3-5
	Support Tube	SA-240, Type XM-19	Table 2.3-6
	Support Sleeve	SA-240, Type 304	Table 2.3-5
	Guide Tube	SA-240, Type 316	Table 2.3-3
	Neutron Absorber Sheet Retainer	SA-240, Type 304	Table 2.3-5
	Neutron Absorber Panels	A887, Type 304B5	Table 2.3-10 ⁽²⁾
	Guide Tube Retainer Clips	Type 304	Table 2.3-5

Notes:

- ⁽¹⁾ The top shield plug assembly consists of a shield plate and 37 shield caps. The shield plate is fabricated from ASTM A516, Grade 55 or 60 carbon steel, and the shield caps are fabricated from ASTM A36 carbon steel. Optionally, a solid shield plate fabricated from SA-36 carbon steel may be used for the W74T canisters.
- ⁽²⁾ Assumed to have the same mechanical properties as SA-240, Type 304 stainless steel.

Table 2.3-3 - Type 316 Stainless Steel Material Properties

Material Spec.	Temp. (°F)	Yield Strength, ⁽¹⁾ S _y (ksi)	Ultimate Strength, ⁽²⁾ S _u (ksi)	Design S.I., ⁽³⁾ S _m (ksi)	Elastic Modulus, ⁽⁴⁾ E (ksi × 10 ³)	Mean Coefficient of Thermal Expansion ⁽⁵⁾ (in/in/°F × 10 ⁻⁶)
SA-240 Type 316	-40	30.0	75.0	20.0	28.9	8.23
	-20	30.0	75.0	20.0	28.7	8.28
	70	30.0	75.0	20.0	28.3	...
	100	30.0	75.0	20.0	28.1	8.54
	200	25.9	75.0	20.0	27.6	8.76
	300	23.4	73.4	20.0	27.0	8.97
	400	21.4	71.8	19.3	26.5	9.21
	500	20.0	71.8	18.0	25.8	9.42
	600	18.9	71.8	17.0	25.3	9.60
700	18.1	71.8	16.3	24.8	9.76	

Notes:

- (1) ASME B&PV Code, Section II, Part D, Table Y-1.
- (2) ASME B&PV Code, Section II, Part D, Table U.
- (3) ASME B&PV Code, Section II, Part D, Table 2A.
- (4) ASME B&PV Code, Section II, Part D, Table TM-1, Material Group G.
- (5) ASME B&PV Code, Section II, Part D, Table TE-1, 16Cr-12Ni-2Mo, Coefficient B (mean from 70°F).

Table 2.3-4 - Type 316 Stainless Steel Plastic Material Properties

Strain	0.2%	0.273% ⁽²⁾	0.3%	0.8%	4.0%
Stress Values ⁽¹⁾ at 600°F (ksi)	21.0	21.4	21.5	25.0	37.5
Stress Values at 650°F (ksi)	---	19.7	---	23.1	34.7

Notes:

- (1) From NUREG/CR-0481, SAND77-1872, R-7, *An Assessment of Stress-Strain Data Suitable for Finite-Element Elastic-Plastic Analysis of Shipping Containers*, Figure 8(d), heat 297.
- (2) Strain corresponding to 0.2% offset yield at 700°F, equal to S_y/E + 0.002.

Table 2.3-5 - Type 304 Stainless Steel Material Properties

Material Spec.	Temp. (°F)	Yield Strength, ⁽¹⁾ S _y (ksi)	Ultimate Strength, ⁽²⁾ S _u (ksi)	Design S.I., ⁽³⁾ S _m (ksi)	Elastic Modulus, ⁽⁴⁾ E (ksi × 10 ³)	Mean Coefficient of Thermal Expansion ⁽⁵⁾ (in/in/°F × 10 ⁻⁶)
SA-240 Type 304	-40	30.0	75.0	20.0	28.9	8.21
	-20	30.0	75.0	20.0	28.7	8.26
	70	30.0	75.0	20.0	28.3	...
	100	30.0	75.0	20.0	28.1	8.55
	200	25.0	71.0	20.0	27.6	8.79
	300	22.5	66.0	20.0	27.0	9.00
	400	20.7	64.4	18.7	26.5	9.19
	500	19.4	63.5	17.5	25.8	9.37
	600	18.2	63.5	16.4	25.3	9.53
	700	17.7	63.5	16.0	24.8	9.69

Notes:

- (1) ASME B&PV Code, Section II, Part D, Table Y-1.
- (2) ASME B&PV Code, Section II, Part D, Table U.
- (3) ASME B&PV Code, Section II, Part D, Table 2A.
- (4) ASME B&PV Code, Section II, Part D, Table TM-1, Material Group G.
- (5) ASME B&PV Code, Section II, Part D, Table TE-1, 18Cr-8Ni, Coefficient B (mean from 70°F).

Table 2.3-6 - Type XM-19 Stainless Steel Material Properties

Material Spec.	Temp. (°F)	Yield Strength,⁽¹⁾ S_y (ksi)	Ultimate Strength,⁽²⁾ S_u (ksi)	Design S.I.,⁽³⁾ S_m (ksi)	Elastic Modulus,⁽⁴⁾ E (ksi × 10³)	Mean Coefficient of Thermal Expansion⁽⁵⁾ (in/in/°F × 10⁻⁶)
SA-240, Type XM-19	-40	55.0	100.0	33.3	28.9	8.05
	-20	55.0	100.0	33.3	28.7	8.08
	70	55.0	100.0	33.3	28.3	...
	100	55.0	100.0	33.3	28.1	8.30
	200	47.0	99.5	33.2	27.6	8.48
	300	43.4	94.3	31.4	27.0	8.65
	400	40.8	90.7	30.2	26.5	8.79
	500	38.8	89.1	29.7	25.8	8.92
	600	37.3	87.8	29.2	25.3	9.03
	700	36.3	86.5	28.8	24.8	9.15

Notes:

- (1) ASME B&PV Code, Section II, Part D, Table Y-1, for material annealed at 1925°F-1975°F (H1).
- (2) ASME B&PV Code, Section II, Part D, Table U.
- (3) ASME B&PV Code, Section II, Part D, Table 2A.
- (4) ASME B&PV Code, Section II, Part D, Table TM-1, Material Group G.
- (5) ASME B&PV Code, Section II, Part D, Table TE-1, 22Cr-13Ni, Coefficient B (mean from 70°F).

Table 2.3-7 - ASTM A36 Carbon Steel Material Properties

Material Spec.	Temp. (°F)	Yield Strength, ⁽²⁾ S _y (ksi)	Ultimate Strength, ⁽³⁾ S _u (ksi)	Design S.I., ⁽⁴⁾ S _m (ksi)	Elastic Modulus, ⁽⁵⁾ E (ksi × 10 ³)	Mean Coefficient of Thermal Expansion ⁽⁶⁾ (in/in/°F × 10 ⁻⁶)
A36 ⁽¹⁾	-40	36.0	57.9	19.3	30.0	5.03
	-20	36.0	57.9	19.3	29.9	5.10
	70	36.0	57.9	19.3	29.5	...
	100	36.0	57.9	19.3	29.3	5.53
	200	32.9	57.9	19.3	28.8	5.89
	300	31.9	57.9	19.3	28.3	6.26
	400	30.9	57.9	19.3	27.7	6.61
	500	29.2	57.9	19.3	27.3	6.91
	600	26.6	53.1	17.7	26.7	7.17
	700	26.0	51.9	17.3	25.5	7.41

Notes:

- (1) Material properties for ASTM A36 carbon steel based on SA-36 properties from Part D of the ASME Code.
- (2) ASME B&PV Code, Section II, Part D, Table Y-1.
- (3) Values for S_u taken as 3S_m.
- (4) ASME B&PV Code, Section II, Part D, Table 2A.
- (5) ASME B&PV Code, Section II, Part D, Table TM-1, Carbon Steels with C ≤ 0.30%.
- (6) ASME B&PV Code, Section II, Part D, Table TE-1, Material Group C, Coefficient B (mean from 70°F).

Table 2.3-8 - A514, Grades F or P Carbon Steel Material Properties

Material Spec.	Temp. (°F)	Yield Strength, ⁽¹⁾ S _y (ksi)	Ultimate Strength, ⁽²⁾ S _u (ksi)	Design S.I., ⁽³⁾ S _m (ksi)	Elastic Modulus, ⁽⁴⁾ E (ksi × 10 ³)	Mean Coefficient of Thermal Expansion ⁽⁵⁾ (in/in/°F × 10 ⁻⁶)
A514, Grade F or P	-40	100.0	110.0	36.7	30.0	5.89
	-20	100.0	110.0	36.7	29.9	5.95
	70	100.0	110.0	36.7	29.5	...
	100	100.0	110.0	36.7	29.3	6.27
	200	95.5	110.0	36.7	28.8	6.54
	300	92.5	110.0	36.7	28.3	6.78
	400	89.8	110.0	36.7	27.7	6.98
	500	87.6	110.0	36.7	27.3	7.16
	600	85.5	110.0	36.7	26.7	7.32
	650	84.3	110.0	36.5	26.1	7.41
700	83.0	107.7	35.9	25.5	7.47	

Notes:

- (1) ASME B&PV Code, Code Case N-71-17, Table 3, plate thickness up to and including 2½ inches.
- (2) ASME B&PV Code, Code Case N-71-17, Table 5.
- (3) ASME B&PV Code, Code Case N-71-17, Table 1, plate thickness up to and including 2½ inches.
- (4) ASME B&PV Code, Section II, Part D, Table TM-1, Carbon Steels with C ≤ 0.30%.
- (5) ASME B&PV Code, Section II, Part D, Table TE-1, Material Group E, Coefficient B (mean from 70°F).

Table 2.3-9 - SA-517, Grade F or P Carbon Steel Material Properties

Material Spec.	Temp. (°F)	Yield Strength, ⁽¹⁾ S _y (ksi)	Ultimate Strength, ⁽²⁾ S _u (ksi)	Design S.I., ⁽³⁾ S _m (ksi)	Elastic Modulus, ⁽⁴⁾ E (ksi × 10 ³)	Mean Coefficient of Thermal Expansion ⁽⁵⁾ (in/in/°F × 10 ⁻⁶)
SA-517, Grade F or P	-40	100.0	115.0	38.3	30.0	5.89
	-20	100.0	115.0	38.3	29.9	5.95
	70	100.0	115.0	38.3	29.5	...
	100	100.0	115.0	38.3	29.3	6.27
	200	95.5	115.0	38.3	28.8	6.54
	300	92.5	115.0	38.3	28.3	6.78
	400	89.8	115.0	38.3	27.7	6.98
	500	87.6	115.0	38.3	27.3	7.16
	600	85.5	115.0	38.3	26.7	7.32
	650	84.3	115.0	38.2	26.1	7.41
	700	83.0	112.6	37.5	25.5	7.47

Notes:

- (1) ASME B&PV Code, Section II, Part D, Table Y-1, plate thickness up to and including 2½ inches.
- (2) ASME B&PV Code, Code Case N-71-17, Table 5.
- (3) ASME B&PV Code, Section II, Part D, Table 2A, plate thickness up to and including 2½ inches.
- (4) ASME B&PV Code, Section II, Part D, Table TM-1, Carbon Steels with C ≤ 0.30%.
- (5) ASME B&PV Code, Section II, Part D, Table TE-1, Material Group E, Coefficient B (mean from 70°F).

Table 2.3-10 - Neutron Absorber Material Properties

Material Specification	Temp. (°F)	Yield Strength, S_Y (ksi)	Ultimate Strength, S_u (ksi)	Elastic Modulus, E (ksi × 10³)	Mean Coefficient of Thermal Expansion⁽²⁾ (in/in/°F × 10⁻⁶)
ASTM A887, Type 304 B5 Borated Stainless Steel ⁽¹⁾	70	30.0	75.0	28.3	---
	500	19.4	63.5	25.8	9.37
	700	17.7	63.5	24.8	9.69

Notes:

- (1) Properties based on SA-240, Type 304 stainless steel.
- (2) Mean coefficient of thermal expansion from 70°F.

Table 2.3-11 - A516, Grades 55 and 60 Carbon Steel Material Properties

Material Spec.	Temp. (°F)	Yield Strength $S_y^{(1)}$ (ksi)	Ultimate Strength $S_u^{(2)}$ (ksi)	Design S.I. $S_m^{(3)}$ (ksi)	Elastic Modulus $E^{(4)}$ (ksi × 10 ³)	Mean Coefficient of Thermal Expansion, ^(5, 6) (in/in/°F × 10 ⁻⁶)
A516, Grade 55 ⁽⁷⁾	70	30.0	55.0	18.3	29.5	---
	100	30.0	55.0	18.3	29.3	5.73
	200	27.3	55.0	18.3	28.8	6.09
	300	26.6	55.0	17.7	28.3	6.43
	400	25.7	55.0	17.2	27.7	6.74
	500	24.5	55.0	16.2	27.3	7.06
A516, Grade 60 ⁽⁷⁾	70	32.0	60.0	20.0	29.5	---
	100	32.0	60.0	20.0	29.3	5.53
	200	29.2	60.0	19.5	28.8	5.89
	300	28.3	60.0	18.9	28.3	6.26
	400	27.4	60.0	18.3	27.7	6.61
	500	25.9	60.0	17.3	27.3	6.91

Notes:

- (1) ASME B&PV Code, Section II, Part D, Table Y-1.
- (2) ASME B&PV Code, Section II, Part D, Table U.
- (3) ASME B&PV Code, Section II, Part D, Table 2A.
- (4) ASME B&PV Code, Section II, Part D, Table TM-1, Carbon Steels with C ≤ 0.30%.
- (5) SA-516, Gr. 55 (C-Si): ASME B&PV Code, Section II, Part D, Table TE-1, Material Group B, Coefficient B (mean from 70°F).
- (6) SA-516, Gr. 60 (C-Mn-Si): ASME B&PV Code, Section II, Part D, Table TE-1, Material Group C, Coefficient B (mean from 70°F).
- (7) Material properties for ASTM A516, Grades 55 and 60 are based on SA-516, Grades 55 and 60 from the ASME B&PV Code, Section II, Part D.
- (8) Values shown in *italics* are calculated using linear interpolation.

2.4 General Standards for All Packages

The FuelSolutions™ TS125 Transportation Cask SAR provides evidence that the general requirements for packages in 10CFR71.43 are met. The specific consideration of the FuelSolutions™ W74 canisters relative to the general package standards is provided in the following sections.

2.4.1 Minimum Package Size

The FuelSolutions™ W74 canisters are transported in the FuelSolutions™ TS125 Transportation Cask. The transportation package dimensions exceed the minimum allowable package size of four (4) inches.

2.4.2 Tamper Indicating Device

Since the FuelSolutions™ W74 canisters are contained within the FuelSolutions™ TS125 Transportation Cask, they do not require tamperproof indicating features.

2.4.3 Positive Closure

Since the FuelSolutions™ W74 canisters are contained within the FuelSolutions™ TS125 Transportation Cask, they do not affect the positive closure of the packaging.

2.4.4 Chemical and Galvanic Reactions

The materials and coatings of the W74 canisters are evaluated for potential chemical or galvanic reactions for its intended service conditions. The evaluation shows that no significant chemical or galvanic reactions result from its intended service conditions. In addition, the concentration of combustible gases within the W74 canisters does not exceed the specified limits for the intended service conditions.

The service conditions for the W74 canisters include short-term immersion in BWR fuel pools, vacuum drying and helium backfill conditions, on-site storage conditions, off-site transportation, and potential canister opening in a W100 transfer cask (water reflood). The potential reactions evaluated for immersion service include general aqueous corrosion and hydrogen generation from wetted surfaces. The potential reactions evaluated for on-site storage and off-site transportation include chloride induced stress corrosion cracking (SCC) of the austenitic stainless steel surfaces and intergranular stress corrosion cracking (IGSCC) of the sensitized weld heat affected zones (HAZ). In addition, possible reactions resulting from inleakage of water are considered for off-site transportation service.

FuelSolutions™ W74M and W74T canisters are constructed from austenitic stainless steel, electroless nickel (EN) coated carbon steel, uncoated carbon steel (bottom shield plug), and borated stainless steel (used for neutron absorber panels). The uncoated carbon steel is encased in stainless steel to alleviate water immersion and hydrogen generation.

The corrosion of austenitic stainless steels is generally extremely low, as these materials quickly form a protective passive film in the spent fuel pool environments. The EN coating on carbon steel spacer plates is for corrosion protection following canister fabrication, and for the brief

immersion period during fuel loading and canister sealing. Electroless nickel coatings are widely used for corrosion protection and wear resistance in the electronics, petrochemical, automotive, and food industries, most often on steel and alloy steel substrates.

During immersion in a BWR spent fuel pool and subsequent canister sealing, hydrogen production is relatively low. BWR spent fuel pools are generally filled with air saturated, demineralized water having a neutral pH (5.6 to 7.1) and low impurities. When compared to carbo-zinc or aluminum flame spray coating systems in boric acid, the hydrogen generation rate of EN is much lower than that of carbo-zinc and aluminum flame spray. Once the canister is drained, dried, sealed, and backfilled with helium, the corrosion mechanism is removed and the EN coating is inert during storage.

The W74M and W74T canisters are evaluated to determine the potential for chemical, galvanic, or other reactions in the intended service conditions, as required by NRC Bulletin 96-04.¹⁸ The hydrogen generation analysis of the W74 canisters considers the effects of radiolytic generation of spent fuel pool water and corrosion of the canister materials under the most limiting service conditions. The results of the hydrogen generation analysis show that the estimated time to reach a concentration limit of 10% of the Lower Explosive Limit (LEL) (0.4% hydrogen by volume) in the canister cavity is approximately 42 hours. Therefore, monitoring the gas in the W74 canister cavity and purging (when necessary) prior to welding the top inner closure plate to the canister shell is performed to eliminate the potential for a hydrogen gas burn event and assure the safety of the public and plant personnel. Further discussion of the procedures for monitoring and purging the canister during welding and canister opening are provided in Sections 8.1 and 8.2 of the FuelSolutions™ Storage System FSAR.¹⁹

The austenitic stainless steel for the FuelSolutions™ W74 canister is evaluated for the effects of corrosion during on-site dry storage and off-site transportation and found to provide sufficient protection against failures due to corrosion. During on-site storage and subsequent transportation service conditions, IGSCC of the sensitized weld HAZ areas will not occur. The potential for IGSCC resulting from sensitization of weld HAZ areas exists for long-term exposure to temperatures above 800°F. Since the maximum temperature of the W74 canister shell is lower than 500°F for normal on-site storage and off-site transportation conditions, sensitization of the weld HAZ areas will not occur.

During on-site storage and subsequent transportation service conditions, chloride induced SCC of the austenitic stainless steel surfaces will not occur. The potential for chloride induced SCC exists for austenitic stainless steel under long-term exposure to coastal marine areas, if wind blown sea spray containing chlorides comes into contact with the canister shell. Furthermore, the potential for chloride induced SCC of the austenitic stainless steel surfaces exists only at relatively low temperatures (below 212°F). The chloride levels anticipated in the rural environments in which the canisters are typically stored are approximately three to four orders of

¹⁸ NRC Bulletin 96-04, *Chemical, Galvanic, or Other Reactions in Spent Fuel Storage and Transportation Casks*, United States Nuclear Regulatory Commission Office of Nuclear Reactor Regulations, OMB No. 3150-0011, July 5, 1996.

¹⁹ WSNF-220, *FuelSolutions™ Storage System Final Safety Analysis Report*, NRC Docket 72-1026, BNG Fuel Solutions Corporation.

magnitude lower than the chloride levels required for chloride induced SCC. Thus, chloride induced SCC of the canister shell will not occur in rural environments. During transportation, the canister is sealed inside of the TS125 Transportation Cask containment system in an inert atmosphere and protected from exposure to chloride.

During on-site storage and subsequent transportation operations, hydrogen generation resulting from radioactive decay and potentially small amounts of moisture remaining in the canister after vacuum drying is not significant. The total volume of hydrogen gas accumulated inside the W74 canister during on-site storage and off-site transportation service is lower than regulatory limit of 5% of the free gas volume.

For transportation operations, the W74 canister is sealed inside the TS125 Transportation Cask containment system in an inert environment. The interfacing components of the W74 canister shell and the TS125 Transportation Cask are all constructed of austenitic stainless steel. During NCT, two rails fabricated from hardened stainless steel and attached to the inside of the TS125 Transportation Cask cavity support the W74 canister. Therefore, the materials of the W74 canister shell and TS125 Transportation Cask that make physical contact during NCT are not susceptible to eutectic reactions at temperatures lower than the material melting points.

For off-site transportation operations, the potential reactions resulting from inleakage of water are considered. The W74 canister materials do not experience any significant chemical, galvanic, or other reactions when exposed to a neutral water environment. The austenitic stainless steel materials in the canister shell are very stable in a neutron water environment and will not produce significant amounts of hydrogen. The EN coated carbon steel material is also very stable in a neutron water environment. The hydrogen generation rate of the canister materials in a neutral water environment is expected to be lower than the hydrogen generation rate in the BWR spent fuel pool air-saturated demineralized water environment. Given the low hydrogen generation rates of the W74 canister materials and the large free volume within the canister, the time required for the hydrogen gas to reach 5% of the free volume is substantial. Therefore, explosive concentrations of combustible gas are not expected to accumulate due to inleakage of water.

This page intentionally left blank.

2.5 Lifting and Tiedown Standards

The FuelSolutions™ TS125 Transportation Package lifting and tiedown devices are evaluated and shown to satisfy the criteria of 10CFR71.45 in Section 2.5 of the FuelSolutions™ TS125 Transportation Cask SAR. The lifting and tiedown evaluations are performed using a bounding weight of 85 kips for a loaded FuelSolutions™ canister. As shown in Section 2.2, the maximum weight of the FuelSolutions™ W74M and W74T canisters with their allowable SNF payloads is less than the maximum allowable canister weight of 85 kips specified in the FuelSolutions™ TS125 Transportation Cask SAR.

For transportation conditions, the FuelSolutions™ W74 canisters are only handled while sealed inside the FuelSolutions™ TS125 Transportation Cask. Therefore, no additional evaluation is required for the transportation cask lifting and tiedown devices. As discussed in Section 1.1, the FuelSolutions™ canisters are designed for loads associated with normal handling operations performed under the plant's 10CFR50 license, a stand-alone storage and/or cask handling facility's 10CFR72 license, or a certificate holder's 10CFR71 C of C for off-site transportation. The canister normal handling operations include both vertical or horizontal canister transfers. The structural evaluation of the FuelSolutions™ W74 canister lifting devices for normal handling operations is presented in Section 3.4.3 of the FuelSolutions™ W74 Canister Storage FSAR.²⁰ The structural evaluation of the W74 canister lifting devices demonstrates that the allowable stress design criteria of ANSI N14.6 is satisfied for all lifting conditions associated with normal handling operations. Furthermore, the W74 canister is shown to satisfy the applicable ASME B&PV Code allowable stress design criteria for loading resulting from normal and off-normal horizontal transfer operations.

²⁰ WSNF-223, *FuelSolutions™ W74 Canister Storage Final Safety Analysis Report*, NRC Docket 72-1026, BNG Fuel Solutions Corporation.

This page intentionally left blank.

2.6 Normal Conditions of Transport

When subjected to NCT tests specified in 10CFR71.71, the FuelSolutions™ W74 canisters meet the standards specified in Subpart E of 10CFR71. This is demonstrated in the following subsections where each NCT condition is addressed and shown to meet the applicable design criteria. A summary of load combinations used herein, consistent with Regulatory Guide 7.8, is provided in Section 2.1.2.2.

2.6.1 Heat

This section presents the structural evaluation of the FuelSolutions™ W74 canisters for the heat load condition of 10CFR71.71(c)(1). The structural evaluation of the FuelSolutions™ TS125 Transportation Cask for the heat load condition is presented in Section 2.6.1 of the FuelSolutions™ TS125 Transportation Cask SAR. The structural evaluation shows that the heat load condition does not compromise the structural integrity of the package.

The FuelSolutions™ W74 canisters are evaluated in the FuelSolutions™ TS125 Transportation Cask for the thermal gradients and temperatures resulting from:

1. NCT Hot thermal conditions, including an ambient temperature of 100°F, maximum fuel decay heat, and insolation in accordance with 10CFR71.71(c)(1).
2. NCT Cold thermal conditions, including an ambient temperature of -20°F, maximum fuel decay heat, and no insolation.
3. NCT Cold Environment thermal conditions, including an ambient temperature of -40°F, maximum fuel decay heat, and no insolation.

In accordance with Regulatory Guide 7.8, the stresses due to NCT thermal loads are considered in combination with internal pressure and fabrication stresses. No credit is taken for containment or confinement provided by the W74 canister. Consequently, the W74 canisters are not evaluated for internal pressure loads for transport conditions. In addition, there are no significant residual stresses in the W74 canister due to fabrication. Therefore, the only loads considered for the NCT thermal load combinations are the NCT thermal loads.

The maximum canister assembly component pressures and temperatures resulting from the NCT thermal conditions are calculated in Section 3.4 of this SAR. The bounding temperatures and pressures used for the structural evaluation of the W74 canister are summarized in Section 2.6.1.1. Differential thermal expansion between the FuelSolutions™ W74 canister shell and the TS125 Transportation Cask cavity, and between the W74 canister basket assembly and shell, are evaluated in Section 2.6.1.2. The stresses in the W74 canister due to NCT thermal loading are evaluated in Section 2.6.1.3. The results of the NCT thermal stress evaluation demonstrate that the W74 canister satisfies the appropriate design criteria for NCT thermal conditions.

2.6.1.1 Summary of Pressures and Temperatures

For transport conditions, the FuelSolutions™ TS125 Transportation Cask provides the containment function for the canister contents. Therefore, no credit is taken for the containment provided by the FuelSolutions™ W74 canister shell during transportation. As such, the canister

shell assembly is not evaluated for pressure loads associated with transport conditions. The canister basket assembly also does not retain pressure. Therefore, pressure loads are not addressed in the canister basket assembly structural analysis.

As discussed in Chapter 3, the thermal analysis of the W74 canisters is performed using the design basis SNF assembly decay heat profile shown in Figure 3.1-1. The W74 canister assembly temperatures resulting from NCT thermal conditions are calculated in Section 3.4 and summarized in Table 2.6-1. Bounding maximum and minimum temperatures are used to evaluate the differential thermal expansion of the W74 canister in Section 2.6.1.2. In addition, the bounding design temperatures at which the allowable stresses are calculated for the W74 canister are provided in Table 2.6-1. The bounding design temperatures are consistent with those temperatures expected in service, as determined in Section 3.4 of this SAR.

2.6.1.2 Differential Thermal Expansion

Differential thermal expansion between the W74 canister basket assembly, W74 canister shell assembly, and the transportation cask cavity is evaluated in the following sections, considering possible interference resulting from a reduction in gap sizes. The results of the evaluation of differential thermal expansion show that the W74 canister shell assembly expands freely within the transportation cask cavity under the NCT heat load condition. The W74 canister basket assemblies are also shown to expand freely within the W74 canister shell assembly cavity under the NCT heat load condition.

2.6.1.2.1 Canister Shell

Differential thermal expansion between the FuelSolutions™ canister shell and TS125 Transportation Cask cavity is evaluated in Section 2.6.1.2 of the FuelSolutions™ TS125 Transportation Cask SAR. The differential thermal expansion analysis conservatively assumes a uniform temperature difference of 210°F between the canister shell and cask inner shell over the entire length of the canister shell. As shown in Table 3.4-1, the maximum temperature difference between the W74 canister shell and the cask inner shell for all NCT thermal load conditions is 117°F for the NCT cold environment (i.e., -40°F ambient temperature, maximum decay heat, and no solar). Therefore, the worst-case differential thermal expansion between the W74 canister shell and the transportation cask cavity under NCT thermal loading is bounded by the evaluation presented in the FuelSolutions™ TS125 Transportation Cask SAR. Thus, positive clearances remain between the FuelSolutions™ TS125 Transportation Cask cavity and the W74 canister shell under the worst-case NCT thermal conditions.

2.6.1.2.2 Spacer Plates

The FuelSolutions™ W74 spacer plates are designed with a nominal 0.38-inch diametrical clearance inside the canister shell. This clearance is sufficient to allow free thermal expansion of the spacer plates under the worst-case NCT and HAC thermal conditions. The relative expansion between the W74 spacer plates and the canister shell is calculated using the temperature differential between the two components at the hottest axial section because the heat flux and, therefore, the temperature gradient are maximized at that section. The worst-case ΔT is obtained from Section 3.4 and corresponds to the highest canister heat load and the NCT cold environment condition. As shown in Table 2.6-1, the maximum temperature of the hottest W74

general spacer plates is much greater than the maximum temperature of the hottest LTP spacer plates for the cold environment condition. However, the LTP spacer plate mean coefficient of thermal expansion is higher than that of the general spacer plate. Therefore, the diametral differential thermal expansion (δ_D) between the canister shell and the hottest general and LTP spacer plates is calculated as follows:

$$\begin{aligned}\delta_D &= D[\alpha_{sp}(T_{sp} - 70) - \alpha_{sh}(T_{sh} - 70)] \\ &= 0.122 \text{ in. (general spacer plate)} \\ &= 0.145 \text{ in. (LTP spacer plate)}\end{aligned}$$

where:

- D = 64.75 inches, inside diameter of the canister shell
- T_{sp} = Bounding temperature of the hottest general or LTP spacer plate for NCT cold environment thermal condition
 - = 550°F (hottest general spacer plate)
 - = 500°F (hottest LTP spacer plate)
- α_{sp} = Mean coefficient of thermal expansion for the general or LTP spacer plate material at the bounding temperature
 - = 7.24×10^{-6} in/in/°F, general spacer plate (SA-517, Grade F or P or A514, Grade F or P) at 550°F
 - = 8.92×10^{-6} in/in/°F, LTP spacer plate (SA-240, Type XM-19) at 500°F
- T_{sh} = 250°F, lower bound temperature of the canister shell at the location of the hottest general and LTP spacer plates for NCT cold environment thermal condition
- α_{sh} = 8.87×10^{-6} in/in/°F, mean coefficient of thermal expansion for the W74 canister shell, conservatively based on SA-240, Type 316 stainless steel at a lower bound temperature of 250°F

This bounding differential expansion is lower than the 0.38-inch diametral gap provided between the W74 spacer plates and the canister shell. Therefore, no interference occurs.

2.6.1.2.3 Support Tubes

The FuelSolutions™ W74 support tubes are designed with sufficient axial and transverse clearances to allow free longitudinal and transverse thermal expansion within the FuelSolutions™ W74 canister shell cavity and the spacer plate support tube holes for all NCT thermal conditions. The support tube differential thermal expansion evaluation is performed using hand calculations, as described below.

Longitudinal Differential Thermal Expansion

The longitudinal differential thermal expansion evaluation of the support tubes is performed based on the temperature differential between the support tubes and the canister shell at the hottest axial section. This is conservative because it assumes that the maximum gradient is maintained along the entire cavity length. The worst-case ΔT is obtained from Section 3.4 and corresponds to the highest canister heat load and the NCT cold environment thermal condition.

The axial thermal expansion (δ_L) of the tubes relative to the canister shell is calculated as follows:

$$\delta_L = L[\alpha_t (T_t - 70) - \alpha_{sh} (T_{sh} - 70)] = 0.30\text{-inch}$$

where:

- L = 172.5 inches, combined length of support tubes in upper and lower basket assemblies, including 2-inch thick engagement spacer plate
- T_t = 508°F, maximum temperature of the support tube for the -40°F NCT cold environment (use a conservative upper bound temperature of 550°F)
- α_t = 8.98×10^{-6} in/in/°F, coefficient of thermal expansion for the support tube SA-240, Type XM-19 at the upper bound temperature of 550°F
- T_{sh} = 376°F, temperature of the canister shell corresponding at the hottest axial location of the canister for -40°F NCT cold environment (use a conservative lower bound temperature of 350°F)
- α_{sh} = 9.10×10^{-6} in/in/°F, coefficient of thermal expansion for the shell SA-240, Type 304 steel at the lower bound temperature of 350°F

The calculated axial expansion is smaller than the nominal 0.50-inch clearance provided for the support tubes. Therefore, the support tubes will expand freely within the canister shell for NCT thermal conditions.

Transverse Differential Thermal Expansion

Thermal loads within the W74 canister result in temperature gradients across the section of the W74 support tubes. These transverse thermal gradients cause the support tubes to bend inward, as shown in Figure 2.6-1, since the support tube temperatures are higher on the side nearest the basket centerline. The support tubes are designed with sufficient transverse clearance within the holes in the general spacer plates to allow free transverse thermal expansion within the spacer plate holes for all NCT and HAC thermal conditions. As shown in Table 3.4-1, the maximum lateral thermal gradient across the support tube at any axial location is 55°F for all NCT thermal conditions. A bounding 55°F gradient is conservatively assumed over the entire length of the support tube for the transverse thermal expansion evaluation. The corresponding lateral deflection of the support tube at its center is determined using hand calculations (Roark,²¹ Table 3, Case 6e) as follows:

$$\delta = (\alpha L^2 / 8 d) \Delta T = 0.048 \text{ in.}$$

²¹ W. C. Young, *Roark's Formulas for Stress and Strain*, Sixth Edition, McGraw-Hill Book Company, 1989.

where:

- L = 82.75 in., maximum distance between top and bottom spacer plate supports (weld to weld)
- α = 9.03×10^{-6} in/in/°F, mean coefficient of thermal expansion for the support tube (SA-240, Type XM-19 stainless steel) at 600°F
- d = 8.90 in., depth of the support tube section
- ΔT = 55°F, bounding transverse (through depth) temperature gradient across the support tube

The maximum lateral deflection of the support tube is within the 0.075-inch lateral clearance [(9.05 - 8.90)/2] provided between the support tubes and the holes in the general spacer plates. Therefore, the support tubes will expand freely within the general spacer plate holes under all NCT thermal loads.

2.6.1.2.4 Guide Tubes

The FuelSolutions™ W74 guide tubes are designed with sufficient axial and lateral clearances to allow free thermal expansion within the FuelSolutions™ W74 canister shell cavity and basket assembly for all NCT and HAC thermal conditions. The W74 guide tube differential thermal expansion evaluation considers both transverse differential thermal expansion between the guide tubes and the spacer plate openings and longitudinal differential thermal expansion between the guide tubes and the canister shell assembly.

The transverse differential thermal expansion between the guide tube assembly and the spacer plate opening is evaluated using hand calculations. The differential thermal expansion between the guide tube and the spacer plate opening is conservatively calculated for a temperature of 637°F, which bounds the maximum guide tube and spacer plate temperatures for all NCT and HAC thermal conditions, as shown in Sections 3.4 and 3.5. The transverse differential thermal expansion between the guide tube and spacer plate opening is calculated as follows:

$$\delta_D = D(\alpha_{gt} - \alpha_{cp})(T - 70) = 0.01 \text{ inches}$$

where:

- D = 7.40 inches, spacer plate hole long dimension
- α_{gt} = 9.68×10^{-6} in/in/°F, mean coefficient of thermal expansion for the guide tube (SA-240, Type 316) at 650°F
- α_{cp} = 7.41×10^{-6} in/in/°F, mean coefficient of thermal expansion for the SA-517, Grade P carbon steel spacer plate at 650°F

The nominal clearance between the guide tube and the spacer plate opening is 0.17 inch. The minimum clearance remaining between the guide tube and the spacer plate opening is 0.16 inch. Therefore, the W74 guide tube assemblies expand freely within spacer plates holes under NCT thermal loading.

For the longitudinal thermal expansion, the thermal expansion of the W74 guide tubes is compared to that of the W74 support tubes to assure that the longitudinal clearance provided is sufficient to permit free thermal expansion under all NCT and HAC thermal conditions. The largest differential expansion between the W74 guide tubes and the support tubes results from the NCT cold environment thermal condition because the canister thermal gradients are maximized for this condition. Therefore, a bounding differential longitudinal thermal expansion analysis is performed for the cold conditions. The evaluation is performed based on the temperature differential at the hottest axial section of the canister, which is conservative because it assumes that the maximum gradient is maintained along the entire basket length. The worst-case ΔT is obtained from Section 3.4 and corresponds to the highest canister heat load and the NCT cold environment thermal condition. As shown in Table 2.6-1, the maximum guide tube temperature and minimum support tube temperature at the hottest axial section of the canister for the NCT cold environment thermal condition are 534°F and 411°F, respectively. An upper bound guide tube temperature of 550°F and a lower bound support tube temperature of 350°F are conservatively used for the differential thermal expansion evaluation.

The axial thermal expansion (δ_L) of the guide tubes relative to the support tubes is calculated as follows:

$$\delta_L = L[\alpha_{gt}(T_{gt} - 70) - \alpha_{st}(T_{st} - 70)] = 0.18 \text{ inches}$$

where:

- L = 84.8 inches, length of the W74 guide tubes
- T_{gt} = 550°F, upper bound temperature of the guide tube for the -40°F NCT cold environment
- α_{gt} = 9.51×10^{-6} in/in/°F, mean coefficient of thermal expansion for the guide tube SA-240, Type 316 material at an upper bound temperature of 550°F
- T_{st} = 350°F, lower bound temperature of the support tube at the hottest axial location of the canister for -40°F NCT cold environment
- α_{st} = 8.72×10^{-6} in/in/°F, mean coefficient of thermal expansion for the support tube SA-240, Type XM-19 steel at the lower bound temperature of 350°F

The calculated axial expansion is smaller than the 0.375-inch nominal longitudinal clearance provided for the guide tubes. Therefore, no axial interference could occur between the guide tube and canister shell or basket assembly for all NCT and HAC thermal loadings.

2.6.1.3 Stress Calculations

This section presents the structural evaluation of the stresses in the FuelSolutions™ W74 canister for the heat load condition. In accordance with Regulatory Guide 7.8, the heat load condition is evaluated in combination with maximum internal pressure and fabrication stresses. Since the W74 canister shell is not relied on for containment during transportation conditions, internal pressure loads are not applied to the canister shell. Furthermore, there are not significant residual stresses in the W74 canister basket assembly or shell assembly resulting from

fabrication. Therefore, the only stresses in the W74 canister due to the heat load condition are those resulting from thermal gradients and thermal expansion of dissimilar materials. As shown in Section 2.6.1.2, there are no stresses in the W74 canister that result from interference of free differential thermal expansion.

Thermal stresses are categorized as either “general” or “local” in accordance with the ASME B&PV Code. General thermal stress is classified as a secondary stress and is associated with gross distortion of the structure. Local thermal stress is classified as a peak stress, which does not produce any significant distortion in the structure. Only the secondary stresses are evaluated herein. The local thermal peak stresses are considered only for fatigue.

2.6.1.3.1 General and LTP Spacer Plates

The FuelSolutions™ W74 general spacer plates and LTP spacer plates are evaluated for thermal stresses resulting from NCT thermal loading. Spacer plate thermal stresses are primarily due to radial thermal gradients. These stresses are highest for the spacer plates located in the middle of the basket assembly, since the radial thermal gradients are largest in this region. In addition, curvature of the support tubes (see Figure 2.6-1) under NCT thermal loading produces thermal stresses in the top and bottom end spacer plates in each basket assembly. The spacer plate stresses due to both of these effects are calculated separately and added together absolutely and irrespective of location to determine the maximum spacer plate thermal stresses.

The radial thermal gradients in the hottest W74 general and LTP spacer plates resulting from NCT thermal loading in the FuelSolutions™ TS125 Transportation Cask are provided in Chapter 3 of this SAR. The spacer plate radial thermal gradients and the resulting thermal stresses are generally highest for the condition with the maximum internal heat generation rate and the lowest ambient air temperature. As shown in Table 2.6-1, the highest radial thermal gradients in both the hottest general spacer plate and hottest LTP spacer plate result from the NCT cold environment thermal condition. Therefore, bounding thermal stress evaluations of the hottest W74 general spacer plate and LTP spacer plate are performed for the NCT cold environment thermal condition.

Thermal stresses in the hottest general and LTP spacer plates resulting from the NCT cold environment thermal loading are calculated using the plane stress finite element model described in Section 2.12.4.1.1, with the appropriate material properties and plate thickness. As discussed in Section 2.6.1.2.2, the spacer plates expand freely within the canister shell under all NCT thermal conditions. Consequently, the finite element model is pinned to prevent rigid body translation and allow free radial thermal expansion. The bounding thermal gradients in the hottest general and LTP spacer plates resulting from the NCT cold environment thermal condition are applied to the spacer plate model, as shown in Figure 2.6-2 and Figure 2.6-3, respectively. The temperature dependent material properties of SA-517, Grade P²² carbon steel and SA-240, Type XM-19 stainless steel are used for the W74 general and LTP spacer plate thermal stress analyses, respectively.

²² The carbon steel spacer plates are fabricated from either SA-517, Grades F or P or A514, Grades F or P carbon steel. The temperature-dependent material properties (i.e., E and α) of all these carbon steels are identical. Therefore, the thermal stress analysis is valid for all material alternatives.

The 20 highest general thermal stress intensities (i.e., membrane plus bending) in the hottest W74 general and LTP spacer plates resulting from the governing NCT radial thermal gradients are summarized in Table 2.6-2 and Table 2.6-3, respectively. The analysis results shows that the maximum general thermal stress intensity in the hottest W74 general and LTP spacer plates due to the radial thermal gradients are 19.5 ksi and 28.7 ksi, respectively.

As discussed above, thermal stresses also occur in the spacer plates at the top and bottom end of each basket assembly due to curvature of the support tubes resulting from radial thermal gradients within the support tubes. For this condition, the unrestrained angle of rotation at the ends of the support tubes, calculated assuming simply supported ends, is 0.0023 radians. The actual end rotation of the support tube is less than the unrestrained rotation since the top and bottom end spacer plates resist bending of the support tubes.

The rotation at the support tube to end spacer plate location is calculated using the principle of static equilibrium based on the relative stiffness of the support tube and spacer plate. The rotational stiffness of the W74 general and LTP spacer plates, calculated in Section 3.5.1.3.2 of the FuelSolutions™ W74 Canister Storage FSAR, are 410 in-kips/radian and 7,500 in-kips/radian, respectively. The bending stiffness of the support tube, calculated using simple beam theory for a simply supported beam subjected to equal end moments, is 166,900 inch-kips/radian. The support tube end rotations required to satisfy static equilibrium are 0.0023 radians for the W74 general spacer plate and 0.0022 radians for the W74 LTP spacer plate.

The spacer plate stresses resulting from the curvature of the support tube are determined by scaling the spacer plate stresses calculated for a unit rotation (0.001-radian) by the ratio of the support tube end rotations. As shown in Section 3.5.1.3.2 of the FuelSolutions™ W74 canister Storage FSAR, the maximum thermal membrane plus bending stress intensities due to the unit rotation at the ends of the support tubes are 1.14 ksi in the general spacer plate and 2.92 ksi in the LTP spacer plate. Therefore, the maximum spacer plate thermal stress intensities due to the calculated support tube end rotations are 2.6 ksi ($=1.14 \text{ ksi} \times 0.0023/0.001$) for the general spacer plate and 6.4 ksi ($=2.92 \text{ ksi} \times 0.0022/0.001$) for the LTP spacer plate. The maximum stress intensities resulting from the curvature of the support tube are conservatively combined with the maximum stress intensities due to the radial thermal gradients, irrespective of sign and location.

The maximum general thermal stress intensity in the general spacer plate due to the radial thermal gradient for the governing NCT thermal condition is 19.5 ksi. The maximum thermal bending stress in the general spacer plate due to the curvature of the support tubes is 2.6 ksi. Therefore, the combined thermal stress in the general spacer plate is 22.1 ksi. As discussed above, general thermal stress intensity is classified as secondary. The Service Level A allowable primary plus secondary stress intensity for the W74 general spacer plate material at a bounding design temperature of 700°F is 107.7 ksi.²³ The minimum design margin for thermal stress in the W74 general spacer plate is +3.87. Therefore, the W74 general spacer plates meet the Service Level A allowable stress design criteria for the governing NCT thermal loading.

The maximum general thermal stress intensity in the LTP spacer plate resulting from the maximum radial thermal gradient for the governing NCT thermal condition is 28.7 ksi. This

²³ Based on the lowest value for SA-517, Grades F or P and A-514, Grades F or P carbon steel.

stress is combined with the maximum membrane plus bending stress intensity of 6.4 ksi due to the thermal curvature of the support tube, as discussed above. Therefore, the maximum combined thermal stress intensity in the LTP spacer plate is 35.1 ksi. As discussed above, general thermal stress intensity is classified as secondary. The Service Level A allowable primary plus secondary stress intensity for SA-240, Type XM-19 stainless steel at the bounding design temperature of 700°F is 86.4 ksi. Therefore, the minimum design margin for thermal stress in the LTP spacer plate is +1.46. Therefore, the W74 LTP spacer plates meet the Service Level A allowable stress design criteria for the governing NCT thermal loading.

The effects of NCT thermal loading are evaluated in combination with other NCT and HAC loadings in the respective sections of this chapter.

2.6.1.3.2 Engagement Spacer Plate

The W74 engagement spacer plate stresses are calculated for all NCT thermal loadings in this section. The W74 engagement spacer plate thermal gradients resulting from NCT thermal loading are provided in Section 3.4 of this SAR. The engagement spacer plate radial thermal gradients and the resulting thermal stresses are generally highest for the condition with the maximum internal heat generation rate and the lowest ambient air temperature. As shown in Table 2.6-1, the highest engagement spacer plate thermal gradient, resulting from the NCT cold environment thermal condition, is 109°F. Therefore, the NCT cold environment is expected to result in the highest thermal stresses in the W74 engagement spacer plate.

The NCT thermal stress evaluation of the W74 engagement spacer plate is performed using the half-symmetry plane stress finite element model described in Section 2.12.4.2.1 and shown in Figure 2.12-6. The temperature gradients resulting from the NCT cold environment (-40°F ambient), NCT cold (-20°F ambient), and NCT hot (100°F ambient) thermal loadings are applied to the W74 engagement spacer plate finite element model. The applied thermal gradient for the NCT cold environment is shown in Figure 2.6-4. The material properties of SA-240, Type XM-19 stainless steel are used in the finite element model.

As shown in Section 2.6.1.2.2, the W74 spacer plates expand freely within the canister shell under all NCT thermal loadings. Therefore, the only restraint on the spacer plates for NCT thermal loading is due to the spacer plate self-constraint. Symmetry boundary constraints are applied to those nodes located on the plate vertical centerline of the finite element model (i.e. at $X=0$, $UX=0$). In addition, the model is restrained from translating in the vertical direction ($UY=0$) at the node located at the bottom centerline to prevent rigid-body translation.

The W74 engagement spacer plate thermal stress analysis results show that the maximum thermal stress intensities result from the NCT cold environment (-40°F ambient). For this condition, the maximum thermal stress intensity, including stress concentrations at structural discontinuities near the edge of the plate, is 22.9 ksi. The maximum thermal stress intensities resulting from the NCT cold and NCT hot thermal loadings are 22.8 ksi and 21.7 ksi, respectively. The maximum thermal stress intensity is conservatively compared with the Service Level A allowable primary plus secondary stress intensity.

The Service Level A allowable primary plus secondary stress intensity for SA-240, Type XM-19 stainless steel at a bounding design temperature of 500°F is 89.1 ksi. The corresponding minimum design margin for general thermal stress intensity due to NCT thermal loading is:

$$D.M. = \frac{89.1}{22.9} - 1 = +2.89$$

Therefore, the W74 engagement spacer plate thermal stresses due to NCT thermal loading are less than the Service Level A allowable primary plus secondary stress intensity. Thermal stresses in the W74 engagement spacer plate are evaluated in combination with the stresses resulting from NCT vibration and NCT free drop in the respective sections of this SAR.

2.6.1.3.3 Support Tubes and Support Sleeves

The W74M and W74T support tubes and support sleeves are evaluated for thermal stresses due to NCT thermal loading. The W74 support tube and support sleeve stresses resulting from longitudinal differential thermal expansion of the basket assembly components and from radial thermal gradients through the cross section of the support tube are evaluated in this section using hand calculations. In addition, the stresses in the W74T support sleeve attachment welds and W74M LTP spacer plate attachment welds resulting from NCT thermal loading are evaluated in this section.

Support Tube and Support Sleeve Stress Evaluation

The longitudinal differential thermal expansion of the W74 support tubes, support sleeves, and spacer plates produces axial compressive stress in the support sleeves and tensile stress in the support tubes. As shown in Chapter 3 of this SAR, the maximum support tube temperatures result from the NCT hot thermal condition. The maximum temperature at the hottest axial section of the support tubes for this condition is 599°F. The stresses in the W74 support tubes and support sleeves due to longitudinal differential thermal expansion are calculated for a bounding design temperature of 600°F.

The largest differential thermal expansion between the support tubes, support sleeves, and spacer plates in the upper and lower basket assemblies for the bounding temperature of 600°F are 0.00975-inch for the W74T (lower basket assembly) and 0.01033-inch for the W74M (lower basket assembly). The axial load in the support tube and support sleeves due to the differential thermal expansion is calculated based on the principle of static equilibrium. The axial load is equal to the product of the differential thermal expansion and the equivalent axial stiffness of the support tube, support sleeves, and spacer plates. The equivalent axial stiffness of the system is calculated assuming the support sleeves, spacer plates, and attachment sleeves (W74T only) act as springs in series, and together they act in parallel with the support tube stiffness. The resulting maximum axial loads are 17.05 kips for the W74T support tubes and support sleeves, and 17.99 kips for the W74M support tube and support sleeves.

The 17.05 kip axial load in the W74T results in a tensile stress of 0.73 ksi in the support tube, and a compressive axial stress of 2.27 ksi in the support sleeve. Similarly, the 17.99 kip axial load in the W74M results in a tensile stress of 0.77 ksi in the support tube, and a compressive axial stress of 2.40 ksi in the support sleeve.

The results of the thermal evaluation presented in Chapter 3 of this SAR show that under NCT thermal loading, the temperature on the sides of the support tube facing inward are higher than the temperature on the outward facing sides. As a result, the support tubes will curve inward

slightly, as shown in Figure 2.6-1. For the W74M basket assemblies, the curvature of the support tubes is resisted by the top and bottom end LTP spacer plates that are welded to the support tubes. Similar restraint is conservatively assumed for the W74T basket assemblies. Since the bending stiffness of the support tubes is much larger than the bending stiffness of the basket assembly end spacer plates, the moment reactions at the ends of the support tube resulting from the thermal curvature are small and the associated support tube stresses are negligible. However, the stresses in the welds that connect the support tubes to the LTP spacer plates (W74M) or the attachment sleeves (W74T) are evaluated to assure the structural integrity of the connections. The weld thermal stress evaluations are discussed in the following paragraphs.

W74T Support Sleeve Attachment Weld Stresses

The top and bottom end support sleeves in both the W74T upper and lower basket assemblies are welded to the support tubes with all-around ¼-inch fillet welds to capture the basket assembly spacer plates and interior support sleeves. The stresses in these welds due to normal thermal loading are evaluated using hand calculations. The weld stress evaluation addresses thermal stresses due to differential thermal expansion of dissimilar materials and thermal gradients within the basket assembly.

As discussed above, differential thermal expansion of the W74T basket assembly due to NCT thermal conditions results in an axial load of 17.05 kips. The resulting average shear stress in the support sleeve attachment weld is 3.26 ksi. Additional shear stresses occur in these welds due to the moment reaction resulting from thermal curvature of the support tubes. As discussed in Section 2.6.1.3.1, the maximum rotation of the W74T support tube attachment weld joint is 0.0023 radians. The resulting moment reaction at the W74T support tube attachment weld resulting from thermal curvature of the support tubes is equal to the joint rotation multiplied by the bending stiffness of the W74 general spacer plate (410 in-kips/radian per Section 2.6.1.3.1), or 0.94 in-kips (= 0.0023 x 410). The moment reaction is carried in shear through the weld, resulting in a maximum weld shear stress of 0.06 ksi. The combined weld shear stress is equal to 3.32 ksi. The corresponding Service Level A allowable average shear stress intensity is 7.0 ksi, based on SA-240, Type XM-19 material properties at 600°F and including a 40% weld efficiency factor for a single-sided fillet weld with surface PT examination, in accordance with Table NG-3352-1 of the ASME Code. Therefore, the minimum design margin for shear stress in the W74T support sleeve attachment weld due to the controlling NCT thermal load condition is +1.11.

W74M Support Tube/LTP Spacer Plate Weld Stresses

The top and bottom end LTP spacer plates in both the W74M upper and lower basket assemblies are welded to the support tubes with all-around ½-inch groove welds with ¼-inch cover fillet welds. The stresses in these welds due to normal thermal loading are evaluated using hand calculations. The weld stress evaluation addresses thermal stresses due to differential thermal expansion of dissimilar materials and thermal gradients within the basket assembly.

As discussed above, differential thermal expansion of the W74M basket assembly due to NCT thermal loading results in an axial load of 17.99 kips. The resulting average shear stress in the LTP spacer plate attachment weld is 1.09 ksi. Additional shear stresses occur in these welds due to the moment reaction resulting from thermal curvature of the support tubes. As discussed in Section 2.6.1.3.1, the maximum rotation of the W74M support tube attachment weld joint is

0.0022 radians. The resulting moment reaction at the LTP spacer plate attachment weld resulting from thermal curvature of the support tubes is equal to the joint rotation multiplied by the bending stiffness of the W74 LTP spacer plate (7,500 in-kips/radian per Section 2.6.1.3.1), or 16.5 in-kips (= 0.0022 x 7,500). The moment reaction is carried in shear through the weld, resulting in a maximum weld shear stress of 0.35 ksi. Therefore, the combined shear stress in the weld is 1.44 ksi. The corresponding Service Level A allowable average shear stress is 7.0 ksi, based on SA-240, Type XM-19 stainless steel material properties at 600°F and including a 40% weld efficiency factor for a single groove weld with surface PT examination, in accordance with Table NG-3352-1 of the ASME Code. Therefore, the minimum design margin for shear stress in the W74M LTP spacer plate attachment weld due to normal thermal loading is +3.86.

Support Sleeve Buckling Evaluation

The stability of the support sleeves is evaluated for NCT thermal loading using plate buckling theory, as described in Section 5.3 of NUREG/CR-6322. As discussed above, the controlling NCT thermal condition produces axial compressive stresses of 2.27 ksi and 2.40 ksi in the W74T and W74M support sleeves, respectively. The allowable buckling stress is limited to ½ of the theoretical buckling stress for NCT, in accordance with the requirements of NUREG/CR-6322. The theoretical buckling stress of the support sleeve walls is conservatively calculated treating the support sleeve as a plate subjected to uniaxial compressive loading, with one edge free and the other edge simply supported (NUREG/CR-6322, Figure 8, Case E). The theoretical buckling stress for this condition (NUREG/CR-6322, Case E, Eq. 11) is calculated as follows:

$$\sigma_e = k_c \frac{\pi^2 D}{b^2 h} = 20.5 \text{ ksi}$$

where:

k_c = 5.0, buckling coefficient corresponding to $a/b=0.46$ from Figure 8 of NUREG/CR-6322

a = 6.38 in., maximum support sleeve length

b = 14.0 in., width of support sleeve angle

h = 0.1875 in., support sleeve plate thickness

$D = \frac{Eh^3}{12(1-\nu^2)}$, plate cylindrical stiffness
 = 15.3 in-kips

ν = 0.3, Poisson's ratio for stainless steel

E = 25.3(10)⁶ psi, modulus of elasticity of SA-240, Type 304 stainless steel at 600°F

The allowable buckling stress is limited to ½ of the theoretical buckling stress for NCT, in accordance with the requirements of NUREG/CR-6322. Therefore, the allowable buckling stress for the W74 support sleeve is 10.25 ksi for NCT. The minimum design margin for buckling of the most heavily loaded W74 support sleeve for NCT thermal loading is:

$$DM = \frac{10.25}{2.40} - 1 = +3.27$$

Therefore, the W74M and W74T support sleeves meets the buckling design criteria of NUREG/CR-6322 for NCT thermal loading.

2.6.1.3.4 Guide Tubes

As discussed in Section 2.6.1.2.4, the W74 guide tubes expand freely within the W74 basket assemblies and canister shell cavity during all NCT thermal conditions. Therefore, the W74 guide tubes will not experience any significant thermal stresses.

2.6.1.4 Fatigue Evaluation

Shell Assembly

The W74 canister confinement components, consisting of the cylindrical shell, top end inner closure plate, top end outer closure plate, bottom closure plate, and all associated seam welds and closure welds are evaluated for cyclical loading in accordance with the requirements of NB-3222.4. Specifically, the six conditions specified in NB-3222.4(d) are evaluated to demonstrate that a detailed fatigue analysis of the W74 canister shell for cyclical service is not required. These criteria are discussed below:

1. *Atmospheric to Service Pressure Cycle*: The conditions of NB-3222.4(d)(1) are satisfied if the specified number of times (including startup and shutdown) that the pressure will be cycled from atmospheric pressure to service pressure and back to atmospheric pressure during normal service does not exceed the number of cycles on the applicable fatigue curve corresponding to a S_a value for the material at service temperature.

The maximum number of pressure cycles associated with startup and shutdown is limited to 30,000 for the W74 canister shell. This is based on the fatigue curve from Figure I-9.2.1 of the ASME Code for $3S_m = 52.5$ ksi, where the lower bound value of S_m is conservatively taken as 17.5 ksi for the W74T canister shell Type 304 material at a service temperature of 500°F. The canister normal service includes one vacuum drying operation and one helium fill after closure. All other pressure fluctuations during transportation and storage are due to changes in atmospheric conditions. Hence, the canister is never cycled back to the atmospheric pressure during normal service. Therefore, the first condition of NB-3222.4(d) is satisfied.

2. *Normal Service Pressure Fluctuation*: The conditions of NB-3222.4(d)(2) are satisfied if the specified full range of pressure fluctuations during normal service does not exceed $1/3 \times \text{Design Pressure} \times (S_a/S_m)$, where S_a is the value obtained from the applicable design fatigue curve for the total specified number of significant pressure fluctuations, and S_m is the allowable stress intensity for the material at service temperature. Significant pressure fluctuations are those for which the total excursion exceeds the quantity $1/3 \times \text{Design Pressure} \times (S/S_m)$, where S is taken as 10^6 since the total number of pressure cycles is less than 10^6 because the pressure cycles only occur due to changes in the ambient temperature (assuming one cycle a day, obtain $1 \times 365 \times 100 = 36,500$ over the lifetime).

The design pressure for the W74 canisters is 10 psig. The W74T and W74M shell and closure plates are made out of Type 304 and Type 316 stainless steels, respectively. As discussed above for Condition (1), the lower bound value of S_m at the 500°F design temperature is 17.5 ksi. The value of S for 10^6 cycles is 28.3 ksi per Figure I-9.2.1 of the ASME B&PV Code. Therefore, the cut-off for the significant pressure fluctuation is:

$$SPF = \frac{1}{3} \times DP \times \left(\frac{S}{S_m} \right) = \frac{1}{3} \times 10 \times \left(\frac{28.3}{17.5} \right) = 5.4 \text{ psi}$$

As shown in Chapter 3 of this SAR and in Chapter 4 of the FuelSolutions™ W74 Canister Storage FSAR, the W74 canister shell internal pressure range for NCT and normal storage conditions is less than 5.4 psi. Hence, no significant pressure fluctuations are expected during transportation. Therefore, the second condition of NB-3222.4(d) is satisfied.

3. *Temperature Difference - Startup and Shutdown:* The condition of NB-3222.4(d)(3) is satisfied if the temperature difference between any two adjacent points of the structure during normal service does not exceed $S_a/(2E\alpha)$, where S_a is the value obtained from the applicable design fatigue curves for the specified number of startup-shutdown cycles, α is the value of the instantaneous coefficient of thermal expansion, and E at the mean value of the temperatures at the two points.

Under normal service conditions, the W74 canister shell will only experience one startup-shutdown cycle. However, a total of 10 startup-shutdown cycles are conservatively assumed. Per Figure I-9.2.1 of the ASME B&PV Code, the value of S_a at 10 cycles for austenitic steels is 708 ksi. At a mean temperature of 400°F, the value of E for Type 304 and Type 316 stainless steel is 26.5 ksi. Per Table TE-1 of Section II, Part D of the ASME B&PV Code, the instantaneous coefficient of thermal expansion for Type 304 and Type 316 stainless steels (Coefficient A, 16Cr-12Ni-2Mo) at 400°F is 9.95×10^{-6} in/in/°F. Therefore, the temperature difference between any two adjacent points on the canister shell during startup and shutdown is limited to:

$$\frac{S_a}{2E\alpha} = \frac{708}{2(26,500)(9.95 \cdot 10^{-6})} = 1,343^\circ\text{F}$$

Since the temperature difference between any two points in the W74 canister shell never approaches this quantity during normal transport and storage, the third condition of NB-3222.4(d) is satisfied.

4. *Temperature Difference - Normal Service:* The condition of NB-3222.4(d)(4) is satisfied if the temperature difference between any two adjacent points does not change during normal service by more than the quantity $S_a/(2E\alpha)$, where S_a is the value obtained from the applicable design fatigue curve for the total specified number of significant temperature difference fluctuations. A temperature difference fluctuation shall be considered significant if its total algebraic range exceeds the quantity $S/(2E\alpha)$, where S is the value of S_a obtained from the applicable design fatigue curve for 10^6 cycles.

As determined in (2) above, the value of S is 28.3 ksi. At the W74 canister shell service temperature of 500°F, the value of E for Type 304 and Type 316 stainless steel is 25.8 ksi. Per Table TE-1 of the ASME B&PV Code, the instantaneous coefficient of thermal expansion for Type 304 and Type 316 stainless steels (Coefficient A, 16Cr-12Ni-2Mo) at 500°F is 10.25×10^{-6} in/in/°F. Therefore, a significant temperature fluctuation for normal service is:

$$STF = \frac{S}{2E\alpha} = \frac{28.3}{2(25,800)(10.25 \cdot 10^{-6})} = 54^\circ\text{F}$$

The normal service in this criterion does not include startups and shutdowns; hence, the only temperature variations are due to changes in the ambient conditions. As shown in Chapter 4 of the FuelSolutions™ W74 Canister Storage FSAR and in Chapter 3 of this SAR, the temperature difference between any two points in the W74 canister shell does not change significantly from normal cold to normal hot conditions. Temperatures at all points drop uniformly by approximately the same amount. Therefore, there are no significant variations in the temperature gradient during normal service. The fourth condition of NB-3222.4(d) is satisfied.

5. *Temperature Difference- Dissimilar Materials:* For components fabricated from materials of differing moduli of elasticity or coefficients of thermal expansion, the condition of NB-3222.4(d)(5) is satisfied if the total algebraic range of temperature fluctuation experienced by the component during normal service does not exceed the magnitude $S_a/2(E_1\alpha_1 - E_2\alpha_2)$, where S_a is the value obtained from the applicable design fatigue curve for the total specified number of significant temperature fluctuations, E_1 and E_2 are the moduli of elasticity, and α_1 and α_2 are the values of the instantaneous coefficients of thermal expansion at the mean temperature value involved for the two materials of construction. A temperature fluctuation shall be considered to be significant if its total excursion exceeds the quantity $S/2(E_1\alpha_1 - E_2\alpha_2)$, where S is the value of S_a obtained from the applicable design fatigue curve for 10^6 cycles.

The W74 canister shell components that provide confinement of radioactive materials during storage, and are designed in accordance with Subsection NB, are fabricated entirely of Type 304 (W74T) or Type 316 (W74M) austenitic stainless steel. Hence, dissimilar materials are not used. Therefore, the fifth condition of NB-3222.4(d) is satisfied.

6. *Mechanical Loads:* The condition of NB-3222.4(d)(6) is satisfied if the specified full range of mechanical loads, excluding pressure, does not result in load stresses whose range exceeds the S_a value obtained from the applicable design fatigue curve for the total specified number of significant load fluctuations. If the total number of significant load fluctuations exceeds the maximum number of cycles defined on the applicable design fatigue curve, the S_a value corresponding to the maximum number of cycles defined on the curve may be used. A load fluctuation shall be considered to be significant if the total excursion of load stress exceeds the quantity S, where S is defined as the value of S_a obtained from the applicable design fatigue curve for 10^6 cycles if the total number of service cycles is 10^6 or less, or S is defined as the value of S_a obtained from the

applicable design fatigue curve for the total number of service cycles if the total number of service cycles exceeds 10^6 .

The W74 canister shells are fabricated from austenitic stainless steel. Assuming that the total number of service cycles due to mechanical loads is less than 10^6 , the value of S_a at 10^6 cycles from Figure I-9.2.1 of the ASME B&PV Code is 28.3 ksi. The mechanical loads specified for the W74 canister during storage include normal handling loads associated with vertical and horizontal canister transfers and vibration loading during on-site transport. The mechanical loads specified for the W74 canister during transport include shock and vibration. The only mechanical loading that qualifies as a significant load fluctuations (i.e., produces a stress in the canister shell exceeding 28.3 ksi) is the normal horizontal transfer. Since the number of horizontal transfer loading applications for each canister is expected to be fewer than 10, which is much less than 10^6 cycles, it is clear that the sixth condition of NB-3222.4(d) is satisfied.

The evaluation demonstrates that the W74 canister shell assembly confinement components meet all six conditions specified in NB-3222.4(d). Therefore, in accordance with NB-3222.4(a), no analysis of the W74 canister shell assembly for cyclic service is required.

Basket Assembly

The W74 basket assembly criticality control components include the guide tube assemblies, support tubes, support sleeves, engagement spacer plate, general spacer plates, and LTP spacer plates. Per NG-3222.4(a), these components do require a detailed fatigue evaluation if the four conditions criteria of NG-3222.4(d) are satisfied. Each of the four conditions specified in NG-3222.4(d) are evaluated below.

1. *Temperature Difference - Startup and Shutdown:* The conditions specified in NG-3222.4(d)(1) are satisfied if the temperature difference between any two adjacent points of the structure during normal service does not exceed $S_a/(2E\alpha)$, where S_a is the value obtained from the applicable design fatigue curves for the specified number of startup-shutdown cycles, α is the value of the instantaneous coefficient of thermal expansion, and E at the mean value of the temperatures at the two points.

Under normal service conditions, the W74 canister will only experience one startup-shutdown cycle. However, a total of 10 startup-shutdown cycles are conservatively assumed. Per Figure I-9.1 and Figure I-9.2.1 of the ASME B&PV Code, the value of S_a for 10 cycles is 580 ksi for the basket carbon steel components and 708 ksi for the basket stainless steel components. The temperature difference between any two adjacent points on the canister basket assembly carbon steel components during startup and shutdown is limited to:

$$S_a/2E\alpha = 580 / 2(27,300)(8.39 \cdot 10^{-6}) = 1,266^\circ\text{F}$$

where the maximum values of E and α for the basket carbon steel materials at a mean temperature of 500°F are conservatively used to obtain the minimum cut-off value. The maximum value of E for the carbon steel basket materials at 500°F is 27.3×10^6 psi. Per

Table TE-1 of the ASME B&PV Code, the maximum instantaneous coefficient of thermal expansion for the basket carbon steel materials (Coefficient A, Material Group E) at 500°F is 8.39×10^{-6} in/in/°F.

The temperature difference between any two adjacent points on the stainless steel components of the W74 canister basket assembly during startup and shutdown is limited to:

$$S_a / 2E\alpha = 708 / 2(25,800)(10.25 \cdot 10^{-6}) = 1,339^\circ\text{F}$$

where the maximum values of E and α for the basket stainless steel materials at a mean temperature of 500°F are conservatively used to obtain the minimum cut-off value. The maximum value of E for the basket stainless steel materials at 500°F is 25.8×10^6 psi. Per Table TE-1 of the ASME B&PV Code, the maximum instantaneous coefficient of thermal expansion for the basket stainless steel materials (Coefficient A, 16Cr-12Ni-2Mo) at 500°F is 10.25×10^{-6} in/in/°F.

As shown in Chapter 4 of the FuelSolutions™ W74 Canister Storage FSAR and in Chapter 3 of this SAR, the axial and radial temperature differences within the W74 basket assembly for normal storage and transportation conditions do not exceed the cut-off values calculated above. Therefore, the first of NG-3222.4(d) is satisfied.

2. *Temperature Difference - Normal Service:* The conditions specified in NG-3222.4(d)(2) are satisfied if the temperature difference between any two adjacent points does not change during normal service by more than the quantity $S_a / (2E\alpha)$, where S_a is the value obtained from the applicable design fatigue curve for the total specified number of significant temperature difference fluctuations. A temperature difference fluctuation shall be considered significant if its total algebraic range exceeds the quantity $S / (2E\alpha)$, where S is the value of S_a obtained from the applicable design fatigue curve for 10^6 cycles.

Per Figure I-9.1 and Figure I-9.2.1 of the ASME B&PV Code, the value of S_a for 10^6 cycles is 12.5 ksi for the carbon steel basket components and 28.3 ksi for the stainless steel basket components. The significant temperature fluctuation for the carbon steel basket materials is:

$$\text{STF} = 12.5 / 2(25,500)(8.39 \cdot 10^{-6}) = 29^\circ\text{F}$$

where the maximum values of E and α for the basket carbon steel materials at the assumed service temperature of 700°F are conservatively used to obtain the minimum cut-off value. The maximum value of E for the carbon steel basket materials at 700°F is 25.5×10^6 psi. Per Section II, Part D, Table TE-1 of the ASME B&PV Code, the maximum instantaneous coefficient of thermal expansion for the basket carbon steel materials (Coefficient A, Material Group E) at 700°F is 8.39×10^{-6} in/in/°F.

The significant temperature fluctuation for the stainless steel basket materials is:

$$STF = \frac{28.3}{2(24,800)(10.76 \cdot 10^{-6})} = 53^{\circ}\text{F}$$

where the maximum values of E and α for the basket stainless steel materials at the assumed service temperature of 700°F are conservatively used to obtain the minimum cut-off value. The maximum value of E for the basket stainless steel materials at 700°F is 24.8×10^6 psi. Per Section II, Part D, Table TE-1 of the ASME B&PV Code, the maximum instantaneous coefficient of thermal expansion for the basket stainless steel materials (Coefficient A, 16Cr-12Ni-2Mo) at 700°F is 10.76×10^{-6} in/in/°F.

As shown in Chapter 4 of the FuelSolutions™ W74 Canister Storage FSAR and in Chapter 3 of this SAR, the temperature difference between any two points in the W74 basket assembly does not change significantly from normal cold to normal hot conditions. The difference between the maximum spacer plate thermal gradient for normal hot and normal cold conditions varies by less than 15°F. Therefore, there are no significant variations in the temperature gradient during normal service, and the second condition of NG-3222.4(d) is satisfied.

3. *Temperature Difference- Dissimilar Materials:* For components fabricated from materials of differing moduli of elasticity or coefficients of thermal expansion, the condition of NG-3222.4(d)(3) is satisfied if the total algebraic range of temperature fluctuation experienced by the component during normal service does not exceed the magnitude $S_a/2(E_1\alpha_1 - E_2\alpha_2)$, where S_a is the value obtained from the applicable design fatigue curve for the total specified number of significant temperature fluctuations, E_1 and E_2 are the moduli of elasticity, and α_1 and α_2 are the values of the instantaneous coefficients of thermal expansion at the mean temperature value involved for the two materials of construction. A temperature fluctuation shall be considered to be significant if its total excursion exceeds the quantity $S/2(E_1\alpha_1 - E_2\alpha_2)$, where S is the value of S_a obtained from the applicable design fatigue curve for 10^6 cycles.

The cut-off value for significant temperature fluctuations is determined for both the W74M and W74T basket assemblies conservatively based on the basket assembly materials having the highest and lowest coefficients of thermal expansion. The W74 guide tube material is not considered for this evaluation, since there are no mechanical connections between the guide tubes and the other basket assembly components in the sealed canister. For the W74M and W74T basket assemblies, the significant temperature fluctuation is:

$$STF = \frac{S}{2(E_1\alpha_1 - E_2\alpha_2)} = \frac{12.5}{2(25,800 \cdot (10.25 \cdot 10^{-6}) - 27,300 \cdot (7.90 \cdot 10^{-6}))} = 128^{\circ}\text{F}$$

where S = 12.5 ksi (from Condition (2) above), and values for E and α are taken from Section II, Part D, Tables TM and TE of the ASME B&PV Code for the basket assembly material with the highest coefficient of thermal expansion (e.g. SA-240, Type 316 stainless steel) and the lowest instantaneous coefficient of thermal expansion (e.g.

SA-517, Grade F or P or A514, Grade F or P carbon steel) at the mean basket temperature of 500°F.

As shown in Chapter 4 of the FuelSolutions™ W74 Canister Storage FSAR and in Chapter 3 of this SAR, the maximum temperature fluctuation within the basket assembly between normal cold and normal hot conditions is approximately 100°F. Therefore, only a very few significant temperature fluctuations per year are possible. Assuming the number of 10 per year and a canister lifetime of 100 years, there are 1000 significant temperature fluctuations over the life of the canister. The lower bound value of S_a is 83 ksi from Table I-9.1 of the ASME B&PV Code. The range limit is:

$$\frac{S_a}{2(E_1\alpha_1 - E_2\alpha_2)} = \frac{83}{2(25,800 \cdot (10.25 \cdot 10^{-6}) - 27,300 \cdot (7.90 \cdot 10^{-6}))} = 851^\circ\text{F}$$

The temperature fluctuations in any basket component do not exceed the above values during normal service. Therefore, the third condition of NG-3222.4(d) is satisfied.

4. *Mechanical Loads*: The condition of NG-3222.4(d)(4) is satisfied if the specified full range of mechanical loads does not result in load stresses whose range exceeds the S_a value obtained from the applicable design fatigue curve for the total specified number of significant load fluctuations. If the total number of significant load fluctuations exceeds 10^6 , the S_a value at $N = 10^6$ may be used. A load fluctuation shall be considered to be significant if the total excursion of load stress exceeds the value of S_a , where S is defined as the value of S_a obtained from the applicable design fatigue curve for 10^6 cycles if the total number of service cycles is 10^6 or less, or S is defined as the value of S_a obtained from the applicable design fatigue curve for the total number of service cycles if the total number of service cycles exceeds 10^6 .

The W74 canister baskets are fabricated from carbon steel and austenitic stainless steel. Assuming that the total number of service cycles due to mechanical loads is less than 10^6 , the value of S_a at 10^6 cycles from Figures I-9.1 and I-9.2.1 of the ASME B&PV Code is 12.5 ksi for carbon steels with S_u less than 80 ksi and 28.3 ksi for austenitic stainless steels and nickel alloys. The mechanical loads specified for the W74 canister during storage include normal handling loads associated with vertical and horizontal canister transfers and 2g vertical vibration loading during on-site transport. The mechanical loads specified for the W74 canister during off-site transport include a bounding 2g vertical load due to shock and vibration. As shown in Section 2.6.5, none of the W74 basket assembly components experience significant load fluctuations due to NCT vibration loading. Therefore, the fourth condition of NG-3222.4(d) is satisfied.

The evaluation demonstrates that the W74 canister basket assembly components meet all four conditions specified in NG-3222.4(d). Therefore, a detailed fatigue analysis of the W74 canister basket assembly for cyclic service is not required.

2.6.1.5 Comparison with Allowable Stresses

The results of the thermal stress analyses presented in Section 2.6.1.3 demonstrate that the W74 canister components meet the stress acceptance criteria discussed in Section 2.1.2.1. The results of the fatigue analysis demonstrate that the fatigue performance requirements are satisfied.

The effects of thermal loading are considered in combination with NCT vibration loading and NCT free drop loading in Sections 2.6.5 and 2.6.7, respectively. The combined stresses for each load combination meet the NCT stress acceptance criteria discussed in Section 2.1.2.1.

Therefore, the FuelSolutions™ W74 canister satisfies all applicable performance requirements.

The minimum W74 canister design margins due to NCT thermal loading are summarized in Table 2.6-4 for all canister components. All design margins for the NCT thermal loading are positive. The minimum design margin for NCT thermal is +1.11 for the W74T support tube to attachment sleeve weld.

Table 2.6-1 - Summary of W74 Canister Temperatures

Canister Component	Temperatures (°F)						Design Temp. ⁽¹⁾ (°F)
	NCT Cold Environment		NCT Cold		NCT Hot		
	Max.	Min.	Max.	Min.	Max.	Min.	
General Spacer Plate	519	282	532	296	615	384	700
LTP Spacer Plate	494	262	507	277	590	366	700
Engagement Spacer Plate	364	255	377	270	462	360	500
Guide Tube	534 ⁽³⁾	(2)	547 ⁽³⁾	(2)	628 ⁽³⁾	(2)	650
Support Tubes and Sleeves	508 ⁽³⁾	411 ⁽⁴⁾	520 ⁽³⁾	424 ⁽⁴⁾	599 ⁽³⁾	501 ⁽⁴⁾	600
Canister Shell	376 ⁽³⁾	(2)	389 ⁽³⁾	(2)	475 ⁽³⁾	(2)	400

Notes:

- (1) Temperature at which allowable stresses are calculated.
- (2) Not used in structural evaluation.
- (3) Maximum temperature at hottest axial section.
- (4) Minimum temperature of support tube at the hottest axial section.

Table 2.6-2 - W74 General Spacer Plate Stress Intensities (20 Highest Values) - NCT Cold Environment Thermal Loading

Section Number ⁽¹⁾	Section Node ⁽²⁾	Stress Components (ksi) ⁽³⁾						S.I. (ksi)
		SX	SY	SZ	SXY	SYZ	SXZ	
82	I	17.18	3.53	0.00	-6.02	0.00	0.00	19.45
2	I	17.15	3.59	0.00	6.03	0.00	0.00	19.44
84	I	11.28	6.53	0.00	-8.30	0.00	0.00	17.53
4	I	11.14	6.37	0.00	8.12	0.00	0.00	17.22
96	I	3.16	14.71	0.00	-5.52	0.00	0.00	16.92
66	I	3.18	14.66	0.00	-5.53	0.00	0.00	16.89
27	I	3.14	14.67	0.00	5.50	0.00	0.00	16.88
135	I	3.17	14.63	0.00	5.52	0.00	0.00	16.86
78	I	10.66	6.31	0.00	-7.75	0.00	0.00	16.54
158	I	10.54	6.17	0.00	7.74	0.00	0.00	16.40
147	I	6.24	10.59	0.00	7.64	0.00	0.00	16.36
68	I	6.08	10.54	0.00	-7.70	0.00	0.00	16.32
15	I	6.18	10.47	0.00	7.58	0.00	0.00	16.20
94	I	6.04	10.41	0.00	-7.61	0.00	0.00	16.14
77	I	9.70	9.81	0.00	-6.30	0.00	0.00	16.05
160	I	14.06	2.47	0.00	5.14	0.00	0.00	16.01
81	I	13.97	2.39	0.00	-5.11	0.00	0.00	15.90
149	I	9.53	9.81	0.00	6.23	0.00	0.00	15.90
85	I	8.51	9.44	0.00	-5.82	0.00	0.00	14.81
13	I	8.38	9.40	0.00	5.77	0.00	0.00	14.68

Notes:

- (1) Section locations are shown in Figure 2.12-1.
- (2) The location on the section at which the maximum stress intensity occurs identified as “I” for I-node and “O” for O-node, where the section is defined starting at the I-node and ending at the O-node.

Table 2.6-3 - W74 LTP Spacer Plate Stress Intensities (20 Highest Values) - NCT Cold Environment Thermal Loading

Section Number ⁽¹⁾	Section Node ⁽²⁾	Stress Components (ksi) ⁽³⁾						S.I. (ksi)
		SX	SY	SZ	SXY	SYZ	SXZ	
96	I	6.01	24.95	0.00	-9.26	0.00	0.00	28.72
27	I	5.98	24.90	0.00	9.23	0.00	0.00	28.66
160	I	24.89	5.23	0.00	9.07	0.00	0.00	28.44
81	I	24.73	5.08	0.00	-9.01	0.00	0.00	28.23
78	I	17.67	10.40	0.00	-12.82	0.00	0.00	27.35
2	I	24.00	4.71	0.00	8.64	0.00	0.00	27.31
82	I	23.97	4.58	0.00	-8.60	0.00	0.00	27.23
158	I	17.46	10.15	0.00	12.78	0.00	0.00	27.10
147	I	10.15	17.23	0.00	12.44	0.00	0.00	26.63
68	I	9.90	17.16	0.00	-12.53	0.00	0.00	26.58
84	I	16.97	9.98	0.00	-12.57	0.00	0.00	26.53
4	I	16.78	9.80	0.00	12.32	0.00	0.00	26.10
66	I	4.31	22.71	0.00	-8.59	0.00	0.00	26.10
135	I	4.29	22.66	0.00	8.58	0.00	0.00	26.04
77	I	15.39	15.87	0.00	-10.10	0.00	0.00	25.74
15	I	9.87	16.57	0.00	12.04	0.00	0.00	25.72
94	I	9.63	16.49	0.00	-12.10	0.00	0.00	25.64
85	I	15.23	15.75	0.00	-10.00	0.00	0.00	25.49
149	I	15.11	15.84	0.00	9.99	0.00	0.00	25.47
13	I	14.98	15.73	0.00	9.90	0.00	0.00	25.26

Table 2.6-4 - Summary of W74 NCT Thermal Stress Design Margins

W74 Canister Component	Stress Type	Maximum S.I. (ksi)	Allowable S.I. (ksi)	Minimum Design Margin⁽¹⁾	Reference SAR Section
General Spacer Plate	P_m	N/A ⁽²⁾	35.9	N/A ⁽²⁾	2.6.1.3.1
	$P_m + P_b$	N/A ⁽²⁾	53.9	N/A ⁽²⁾	2.6.1.3.1
	$P_m + P_b + Q$	22.1	107.7	+3.87	2.6.1.3.1
LTP Spacer Plate	P_m	N/A ⁽²⁾	28.8	N/A ⁽²⁾	2.6.1.3.1
	$P_m + P_b$	N/A ⁽²⁾	43.2	N/A ⁽²⁾	2.6.1.3.1
	$P_m + P_b + Q$	35.1	86.4	+1.46	2.6.1.3.1
Engagement Spacer Plate	P_m	N/A ⁽²⁾	29.7	N/A ⁽²⁾	2.6.1.3.2
	$P_m + P_b$	N/A ⁽²⁾	44.6	N/A ⁽²⁾	2.6.1.3.2
	$P_m + P_b + Q$	22.9	89.1	+2.89	2.6.1.3.2
Support Tube	P_m	N/A ⁽²⁾	29.2	N/A ⁽²⁾	2.6.1.3.3
	$P_m + P_b$	N/A ⁽²⁾	43.8	N/A ⁽²⁾	2.6.1.3.3
	$P_m + P_b + Q$	0.77	87.6	+113	2.6.1.3.3
Support Sleeve	P_m	N/A ⁽²⁾	16.4	N/A ⁽²⁾	2.6.1.3.3
	$P_m + P_b$	N/A ⁽²⁾	24.6	N/A ⁽²⁾	2.6.1.3.3
	$P_m + P_b + Q$	2.40	49.2	+19.5	2.6.1.3.3
	Buckling	2.40	10.25 ⁽⁴⁾	+3.27	2.6.1.3.3
W74M Support Tube to LTP Spacer Plate Weld	Shear	1.44	7.0 ⁽⁵⁾	+3.86	2.6.1.3.3
W74T Support Tube to Attachment Sleeve Weld	Shear	3.32	7.0 ⁽⁵⁾	+1.11	2.6.1.3.3
Guide Tube	P_m	N/A ⁽²⁾	16.7	N/A ⁽²⁾	2.6.1.3.4
	$P_m + P_b$	N/A ⁽²⁾	25.0	N/A ⁽²⁾	2.6.1.3.4
	$P_m + P_b + Q$	⁽⁶⁾	50.0	⁽⁶⁾	2.6.1.3.4

Notes:

- (1) Design margin is equal to (Allowable/Stress) - 1.
- (2) General thermal stress intensity is classified as secondary in accordance with Subsection NG of the ASME B&PV Code.
- (3) Buckling interaction ratio calculated in accordance with NUREG/CR-6322.
- (4) The allowable axial compressive stress is limited to ½ of the theoretical buckling stress for NCT loading in accordance with NUREG/CR-6322.
- (5) The allowable weld stresses include a 40% weld quality factor in accordance with Table NG-3352-1 of the ASME B&PV Code.
- (6) No significant stresses in the guide tubes due to NCT thermal loading.

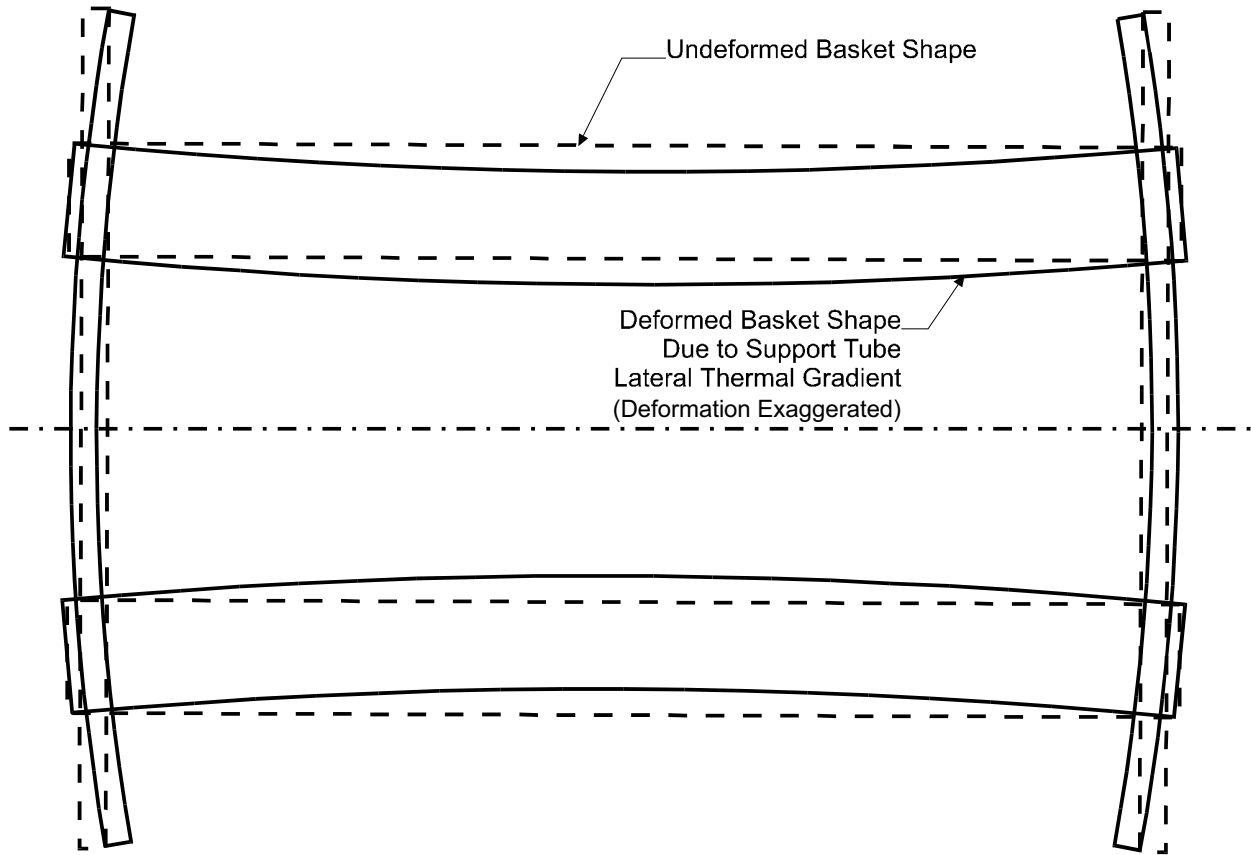
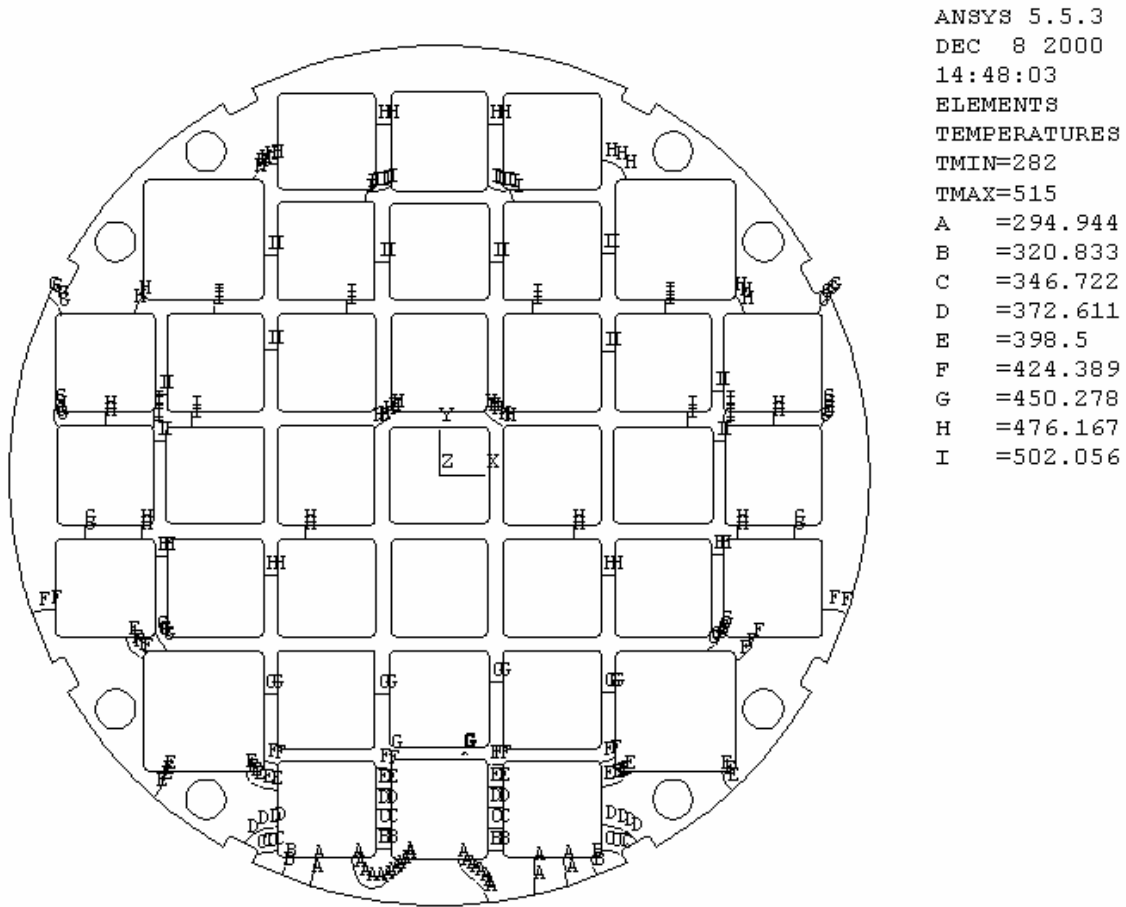
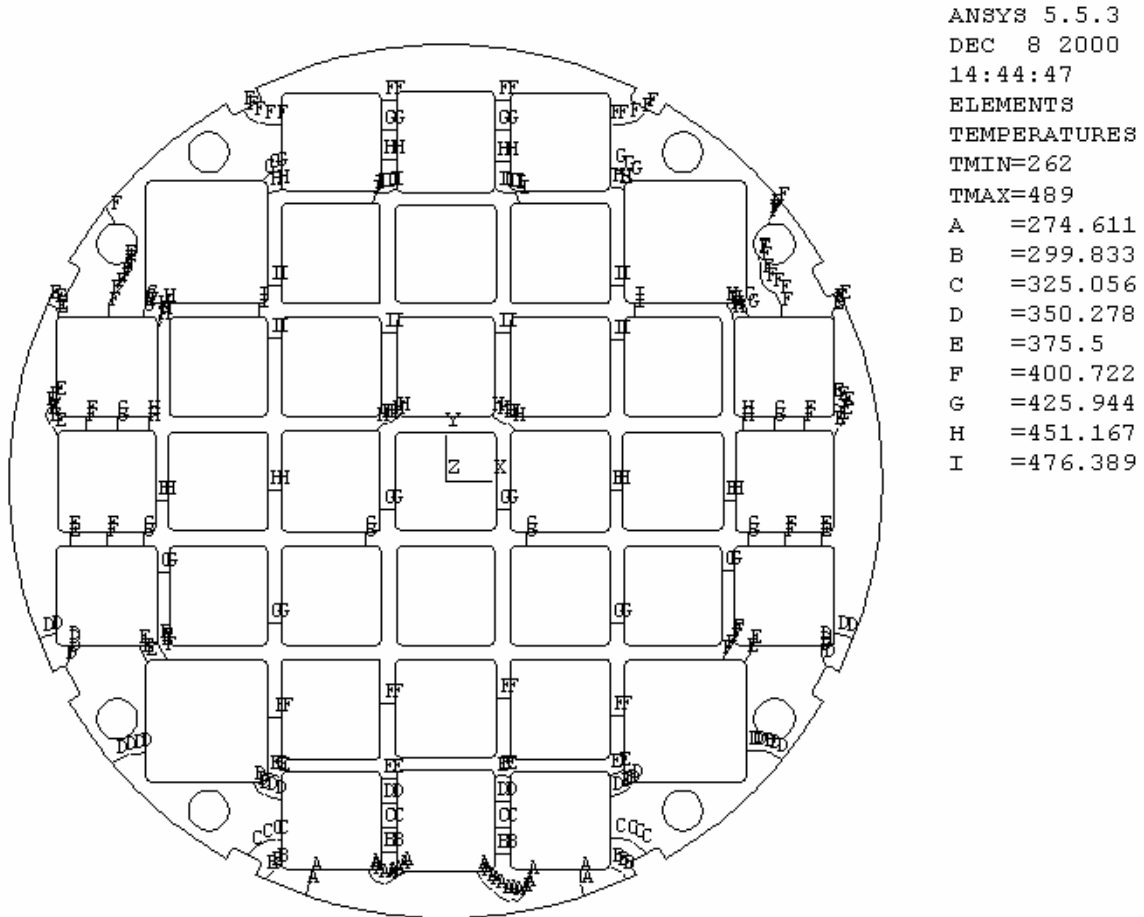


Figure 2.6-1 - W74 Canister Support Tube and End Spacer Plate Curvature Due to Lateral Thermal Gradients



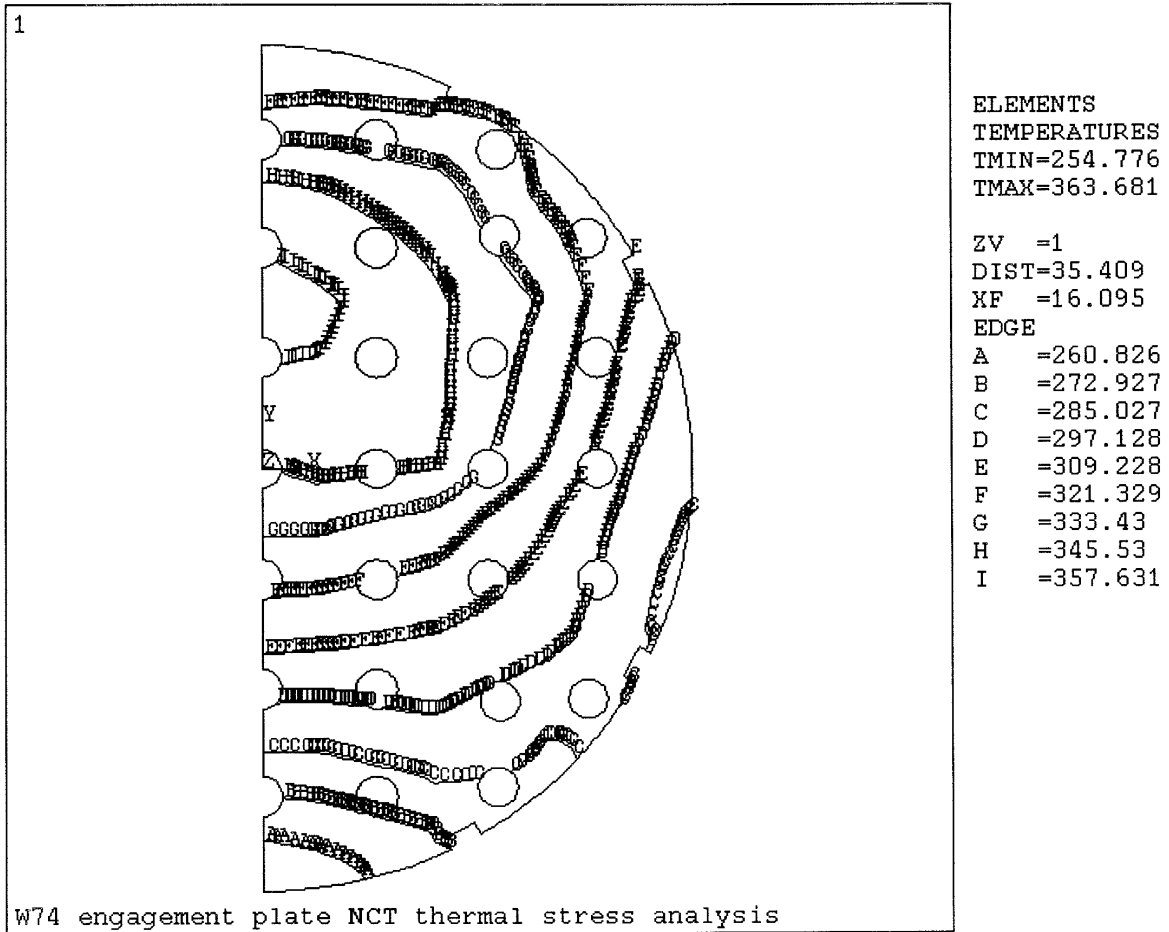
Note: Temperatures reported in °F.

Figure 2.6-2 - W74 General Spacer Plate NCT Cold Environment Thermal Gradient



Note: Temperatures reported in °F.

Figure 2.6-3 - W74 LTP Spacer Plate NCT Cold Environment Thermal Gradient



Note: Temperatures in °F.

Figure 2.6-4 - W74 Canister Engagement Spacer Plate NCT Cold Environment Thermal Gradient

2.6.2 Cold

The FuelSolutions™ W74 canisters are evaluated in the FuelSolutions™ TS125 Transportation Cask for the thermal effects of a steady-state ambient temperature of -40°F in still air and shade, in accordance with 10CFR71.71(c)(2). In accordance with Regulatory Guide 7.8, the NCT cold environment is evaluated in combination with zero insolation, zero decay heat, and zero internal pressure.

Differential thermal expansion is evaluated considering possible interference resulting from a reduction in gap sizes. As discussed in Section 2.6.1.2, transverse and longitudinal clearances are provided within the W74 canister and between the FuelSolutions™ W74 canister shell and the TS125 Transportation Cask to permit free thermal expansion under all NCT and HAC thermal conditions. The NCT cold environment with zero insolation and zero decay heat results in a uniform temperature of -40°F throughout the transportation package. The W74 canister is fabricated entirely from carbon steel and stainless steel materials. Since the coefficient of thermal expansion is similar for all W74 canister materials and the change in temperature is small ($\Delta T = -110^\circ\text{F}$), differential thermal expansion resulting from this condition will not result in any substantial reduction in gap sizes.

In addition, the evaluation considers the effect of the cold temperature on the W74 canister material properties, including possible freezing of liquids. The W74 canister is fabricated entirely from austenitic stainless steel and carbon steel. As discussed in Section 2.1.2.3, the W74 canister materials have sufficient fracture toughness to preclude brittle fracture failure for the LST of -20°F. Since the NCT cold environment is not required to be considered in combination with the NCT and HAC free drops, brittle fracture failure is not a credible failure mode for the NCT cold environment. The W74 canister is drained and backfilled with inert gas prior to being placed into service. Therefore, the W74 canister does not contain any liquids that could freeze in the NCT cold environment.

In accordance with the requirements of Regulatory Guide 7.8, the effects of the NCT cold environment in combination with zero insolation and maximum decay heat are considered in the evaluation of the NCT hot environment presented in Section 2.6.1. The results of the structural analysis of the W74 canister for the NCT hot environment demonstrate that the W74 canisters satisfy the requirements of Subpart E of 10CFR71 for the governing NCT thermal loading.

2.6.3 Reduced External Pressure

The FuelSolutions™ W74 canisters are not affected by fluctuations in atmospheric pressure for transportation conditions since they are sealed inside the FuelSolutions™ TS125 Transportation Cask, which is the pressure boundary.

2.6.4 Increased External Pressure

The FuelSolutions™ W74 canisters are not affected by fluctuations in atmospheric pressure for transportation conditions since they are sealed inside the FuelSolutions™ TS125 Transportation Cask, which is the pressure boundary.

2.6.5 Vibration

The W74 canister is evaluated for the effects of vibration normally incident to transport. Loading due to NCT shock and vibration is evaluated for each W74 canister component separately and in combination with initial conditions, in accordance with Regulatory Guide 7.8. The initial conditions considered in combination with the shock and vibration loading include thermal stress due to the effects of ambient conditions and decay heat load.

The magnitude of the vibration loads experienced during rail car transport are expected to be similar to those experienced during truck transport. For truck transport of large shipping containers weighing over 56,000 pounds, draft ANSI N14.23²⁴ identifies the peak accelerations due to vibration in the 0 Hz to 1,900 Hz range as 0.27g, 0.19g, and 0.52g in the longitudinal (i.e., direction of travel), transverse, and vertical directions, respectively. Furthermore, draft ANSI N14.23 recommends that the peak acceleration values be used for calculating the maximum inertial loading on the package. The W74 canisters are evaluated for a bounding 2g vertical vibration load. The longitudinal and transverse vibration loads are neglected since they are low in magnitude and do not produce significant stresses in the W74 canisters. The structural evaluation of the W74 canister components for the NCT vibration loading are presented in the following sections.

2.6.5.1 General and LTP Spacer Plates

The maximum stresses in the most heavily loaded FuelSolutions™ W74 general and LTP spacer plates due to the 2g vertical vibration loading are determined by scaling the maximum horizontal dead weight stresses by 2g/1g. The structural evaluation of the most heavily loaded W74 general and LTP spacer plates for horizontal dead weight loading is presented in Section 3.5.3.6.2 of the FuelSolutions™ W74 Canister Storage FSAR. The W74 spacer plate horizontal dead weight stresses are calculated using finite element methods assuming linear-elastic material behavior. The horizontal dead weight evaluation conservatively assumes that the weight of each SNF assembly loads the basket spacer plates only through the SNF assembly grid spacers.

The stress intensities in the most heavily loaded W74 general spacer plate due to horizontal dead weight loading are $P_m = 1.84$ ksi, $P_m + P_b = 3.74$ ksi, and $P_m + P_b + Q = 3.89$ ksi. Therefore, the maximum stress intensities in the most heavily loaded W74 general spacer plate for the 2g vertical vibration load are $P_m = 3.7$ ksi ($=1.84$ ksi \times 2g), $P_m + P_b = 7.5$ ksi ($=3.74$ ksi \times 2g), and $P_m + P_b + Q = 7.8$ ksi ($=3.89$ ksi \times 2g), respectively. The Service Level A allowable primary membrane, primary membrane plus bending, and primary plus secondary stress intensities for the general spacer plate material²⁵ at a bounding design temperature of 700°F are 35.9 ksi, 53.9 ksi, and 107.7 ksi, respectively. The minimum design margins for primary membrane (P_m) and primary membrane plus bending ($P_m + P_b$) stress intensity in the most heavily loaded W74 general spacer plate due to the 2g vibration loading are:

$$P_m: DM = \frac{35.9}{3.7} - 1 = +8.70$$

²⁴ ANSI N14.23, *Design Basis for Resistance to Shock and Vibration of Radioactive Material Packages Greater Than One Ton in Truck Transport*, American National Standards Institute, Inc., New York, New York, 1980.

²⁵ Based on the lowest value for SA-517, Grades F or P and A-514, Grades F or P carbon steel.

$$P_m + P_b: DM = \frac{53.9}{7.5} - 1 = +6.19$$

The stress intensities in the most heavily loaded W74 LTP spacer plate due to horizontal dead weight loading are $P_m = 0.44$ ksi, $P_m + P_b = 0.90$ ksi, and $P_m + P_b + Q = 0.93$ ksi. Therefore, the maximum stress intensities in the most heavily loaded W74 LTP spacer plate for the 2g vertical vibration load are $P_m = 0.9$ ksi ($=0.44$ ksi x 2g), $P_m + P_b = 1.8$ ksi ($=0.90$ ksi x 2g), and $P_m + P_b + Q = 1.9$ ksi ($=0.93$ ksi x 2g), respectively. The Service Level A allowable primary membrane, primary membrane plus bending, and primary plus secondary stress intensities for the LTP spacer plate SA-240, Type XM-19 stainless steel material at a bounding design temperature of 700°F are 28.8 ksi, 43.2 ksi, and 86.4 ksi, respectively. The minimum design margins for primary membrane (P_m) and primary membrane plus bending ($P_m + P_b$) stress intensity in the most heavily loaded W74 LTP spacer plate due to the 2g vibration loading are:

$$P_m: DM = \frac{28.8}{0.9} - 1 = +31.0$$

$$P_m + P_b: DM = \frac{43.2}{1.8} - 1 = +23.0$$

As discussed above, the spacer plate stresses due to NCT vibration loading are evaluated in combination with the maximum stresses due to NCT thermal loading. Since thermal stresses are classified as secondary in accordance with the ASME Code, the load combination evaluation for NCT vibration plus NCT thermal is performed only for primary plus secondary stress intensity. The NCT vibration plus NCT thermal load combination evaluation is performed by conservatively adding the maximum stress intensities due to the individual load conditions irrespective of sign and location. As shown in Section 2.6.1.3.1, the maximum general thermal stress intensities in the hottest W74 general and LTP spacer plates due to NCT thermal loading are 22.1 ksi and 35.1 ksi, respectively. Therefore, the maximum combined primary plus secondary stress intensities in the most heavily loaded W74 general and LTP spacer plates for NCT vibration plus NCT thermal loading are 29.9 ksi ($= 7.8 + 22.1$) and 37.0 ksi ($=1.9 + 35.1$), respectively. Therefore, the minimum design margin for primary plus secondary stress intensity in the W74 general and LTP spacer plate due to NCT thermal plus NCT vibration loading are:

$$P_m + P_b + Q: DM = \frac{107.7}{29.9} - 1 = +2.60 \quad (\text{W74 general spacer plate})$$

$$P_m + P_b + Q: DM = \frac{86.4}{37.0} - 1 = +1.34 \quad (\text{W74 LTP spacer plate})$$

Therefore, the most heavily loaded FuelSolutions™ W74 general and LTP spacer plates meet the Service Level A allowable stress design criteria for NCT vibration loading.

2.6.5.2 Engagement Spacer Plate

The W74 engagement spacer plate is evaluated for the effects of vibration normally incident to transport. Per Section 2.6.5, a 2g vertical acceleration load is used for the structural evaluation of the W74 canisters. The FuelSolutions™ transportation package is transported only in the horizontal orientation. Therefore, when subjected to the 2g vertical NCT vibration loading, the W74 engagement spacer plate is loaded only by its own weight.

The stresses in the engagement spacer plate due to a 2g vertical vibration load are calculated using the half symmetry plane stress finite element model used for the NCT side drop evaluation, as described in Section 2.12.4.2.1. Only the geometry of the engagement spacer plate is modeled, neglecting the attachment sleeves and engagement sleeves, which are welded to the engagement spacer plate. The edge support provided by the canister shell is modeled using radial gap elements to reflect the non-linear interface. The engagement spacer plate is supported only at the locations of those gap elements that close under NCT vibration loading.

The maximum primary plus secondary plus peak stress intensity due to NCT vibration is 1.0 ksi, occurring on the plate centerline at the point of contact with the canister shell. The maximum stress intensity is highly localized, and the stress intensities elsewhere in the engagement spacer plate are considerably lower. However, this stress intensity is conservatively compared to the Service Level A allowable primary membrane stress intensity.

The Service Level A allowable primary membrane, primary membrane plus bending, and primary plus secondary stress intensities for the W74 engagement spacer plate SA-240, Type XM-19 stainless steel material at an upper bound design temperature of 500°F are 29.7 ksi, 44.6 ksi, and 89.1 ksi, respectively. Therefore, the minimum design margins for primary membrane and primary membrane plus bending stress intensity resulting from NCT vibration loading (without thermal stress) are:

$$P_m: DM = \frac{29.7}{1.0} - 1 = +28.7$$

$$P_m+P_b: DM = \frac{44.6}{1.0} - 1 = +43.6$$

In accordance with Regulatory Guide 7.8, the effects of NCT vibration are evaluated in combination with NCT hot (100°F ambient temperature) and NCT cold (-20°F ambient temperature) thermal loading. As shown in Section 2.6.1.3.2, the maximum thermal stress intensity due to the NCT hot and NCT cold thermal loading is 22.8 ksi. Conservatively adding the maximum stress intensities due to NCT thermal and vibration irrespective of sign and location gives a combined primary plus secondary stress intensity of 23.8 ksi, compared with a Service Level A allowable primary plus secondary stress intensity of 89.1 ksi. The resulting minimum design margin for primary plus secondary stress intensity is:

$$DM = \frac{89.1}{23.8} - 1 = +2.74$$

Therefore, the maximum W74 engagement spacer plate meets the Service Level A allowable stress design criteria for NCT vibration loading.

2.6.5.3 Support Tubes and Support Sleeves

This section presents the structural evaluation of the W74M and W74T support tubes and support sleeves for NCT vibration loading.

Support Tube Stresses

The stresses in the support tubes due to the 2g NCT vibration load are determined by scaling the stresses calculated for the 60g HAC side drop load using elastic-system analyses by the ratio of the loads (i.e., 2g/60g). As shown in Section 2.7.1.2.3, the maximum primary membrane (P_m) and primary membrane plus bending (P_m+P_b) stress intensities in the W74 support tube due to the 60g HAC side drop load are 1.44 ksi and 6.44 ksi, respectively. The resulting maximum primary membrane (P_m) and primary membrane plus bending (P_m+P_b) stress intensities in the W74 support tube due to the 2g NCT vibration load are 0.05 ksi (=1.44 ksi x 2g/60g) and 0.22 ksi (=6.44 ksi x 2g/60g), respectively.

In accordance with Regulatory Guide 7.8, NCT vibration loads are evaluated in combination with NCT thermal loads. As shown in Section 2.6.1.3.3, the maximum general thermal stress intensity (P_m+P_b+Q) in the W74M and W74T support tubes due to the bounding NCT thermal condition are 0.77 ksi and 0.73 ksi, respectively. Therefore, the maximum primary plus secondary stress intensity due to NCT vibration plus NCT thermal is 0.99 ksi in the W74M support tube.

The Service Level A allowable primary membrane, primary membrane plus bending, and primary plus secondary stress intensities for the W74M and W74T support tube Type XM-19 material at a bounding design temperature of 600°F are 29.2 ksi, 43.8 ksi, and 87.6 ksi, respectively. Therefore, the minimum design margins in the W74 support tubes for primary membrane, primary membrane plus bending, and primary plus secondary stress intensity due to NCT vibration loading are:

$$P_m: DM = \frac{29.2}{0.05} - 1 = +583$$

$$P_m+P_b: DM = \frac{43.8}{0.22} - 1 = +198$$

$$P_m+P_b+Q: DM = \frac{87.6}{0.99} - 1 = +87.5$$

The results show that the W74 support tubes meet the Service Level A allowable stress design criteria for the combined effects of the NCT vibration and NCT thermal loading.

Support Tube Longitudinal Seam Weld Stresses

The stresses in the support tube corner seam welds are evaluated in the same manner as the stresses in the support tube base metal, as described above. As shown in Section 2.7.1.2.3, the maximum shear stress in the support tube corner weld due to the 60g side drop load is 1.34 ksi. Therefore, the maximum shear stress in the weld due to the 2g transverse load is 0.05 ksi (=1.34 ksi x 2g/60g).

The Service Level A allowable shear stress is 6.1 ksi, based on SA-240, Type XM-19 stainless steel at 600°F with a weld quality factor of 35% for a single fillet weld with surface visual examination, per Table NG-3352-1 of the ASME Code. Therefore, the minimum design margin in the support tube corner weld for NCT vibration loading is large.

W74M Support Tube to LTP Spacer Plate Attachment Welds

Each W74M support tube is welded to the top and bottom end LTP spacer plates using ½-inch partial penetration groove welds with ¼-inch cover fillets on all four sides of the tube. The stresses in these W74M support tube to LTP spacer plate attachment welds due to the NCT vibration loads are calculated by scaling the maximum stresses calculated for the HAC side drop loads in the same manner as the support tubes, as described in the previous section. The only significant weld stresses resulting from transverse loads are due to the shear reactions at the end spacer plates. As discussed in Section 2.7.1.2.3, the maximum shear stress in the W74M support tube attachment welds calculated for the 60g HAC side drop load using an elastic system analysis is 0.44 ksi. The resulting maximum shear stress in the W74M support tube to LTP spacer plate attachment weld due to the 2g NCT vibration load is 0.02 ksi ($=0.44 \text{ ksi} \times 2g/60g$).

In accordance with Regulatory Guide 7.8, NCT vibration loads are evaluated in combination with NCT thermal loads. As shown in Section 2.6.1.3.3, the maximum shear stress in the W74M support tube to LTP spacer plate attachment weld due to NCT thermal loading is 1.44 ksi. Therefore, the combined shear stress in the W74M support tube to LTP spacer plate attachment weld due to NCT vibration plus NCT thermal loading is 1.46 ksi.

As discussed in Section 2.6.1.3.3, the Service Level A allowable shear stress for the W74M support tube to LTP spacer plate attachment weld, based on SA-240, Type XM-19 stainless steel at 600°F with a 0.40 weld quality factor in accordance with Table NG-3352-1 of the ASME Code, is 7.0 ksi. Therefore, the minimum design margins for shear stress in the W74M support tube attachment welds for NCT vibration loading is +3.79.

Support Sleeve Stresses

As discussed in Section 2.7.1.2.3, the support sleeve stresses due to transverse loads are insignificant since the support sleeves are loaded only by their own weight in this direction. Consequently, only longitudinal loads are considered for the support sleeve NCT vibration stress evaluation. The shear stress in the support sleeve seam welds are evaluated in the same manner as the stresses in the support tube seam weld, as described above. Since longitudinal loads do not produce any significant stresses in the support sleeve seam welds, only transverse loads are considered for the weld stress evaluation. As shown in Section 2.7.1.2.3, the maximum shear stress in the support sleeve seam weld calculated for the 60g side drop load using an elastic system analysis is 2.36 ksi. Therefore, the maximum shear stress in the weld due to the 2g transverse load is 0.06 ksi ($=2.36 \text{ ksi} \times 2g/60g$). The corresponding Service Level A allowable shear stress is 3.4 ksi, based on SA-240, Type 304 stainless steel at 600°F with a weld quality factor of 35% for a single fillet weld with surface visual examination, per Table NG-3352-1 of the ASME Code. Therefore, the minimum design margin in the support sleeve seam weld for NCT vibration loading is +55.7.

2.6.5.4 Guide Tubes

The W74 guide tube assembly is loaded by its own weight and the weight of the contained fuel assembly for the 2g NCT vibration loading. The spacer plate ligaments provide vertical support along the bottom face of the guide tube assembly. The structural evaluation of the W74 guide tubes for the bounding 2g NCT vibration loading considers two assumed SNF assembly loading distributions: (1) uniform fuel load assumption (i.e., SNF assembly load applied as a uniform pressure load over the supporting face of the guide tube), and (2) concentrated load at SNF assembly grid spacers. These two conditions are evaluated in the following paragraphs.

Uniform Fuel Assembly Loading

A structural evaluation of the W74 guide tubes is performed for the NCT vibration loading assuming the weight of the SNF assembly is distributed uniformly to the bottom panel of the guide tube assembly. The stresses in the most highly loaded W74 guide tube span for 2g NCT vibration loading are determined by scaling the maximum guide tube stresses calculated for the 15g NCT side drop loading using an elastic system analysis by the ratio of the acceleration loads (i.e., 2g/15g). As shown in Section 2.6.7.4, the maximum primary membrane and primary membrane plus bending stress intensities resulting from the 15g NCT side drop load are 3.9 ksi and 13.6 ksi, respectively. Therefore, the W74 guide tube primary membrane and primary membrane plus bending stress intensities due to the 2g vertical vibration load are 0.5 ksi (= 3.9 x 2g/15g) and 1.8 ksi (= 13.6 x 2g/15g), respectively.

The NCT allowable primary membrane and primary membrane plus bending stress intensities for the SA-240, Type 316 stainless steel guide tube material are 16.7 ksi and 25.0 ksi, respectively, at a temperature of 650 °F. Therefore, the primary membrane stress intensity design margin in the W74 guide tube for the 2g vibration load is:

$$P_m: DM = \frac{16.7}{0.5} - 1 = +32.4$$

$$P_m + P_b: DM = \frac{25.0}{1.8} - 1 = +12.9$$

The W74 guide tubes include two full penetration longitudinal seam welds located on opposite faces. The longitudinal seam welds may be examined using either RT or surface PT methods. When RT examination is performed, there are no restrictions on the locations of the longitudinal seam welds since the allowable stresses for the welds are equal to those of the base material. When only surface PT examination is performed, the longitudinal seam welds must be located at ¼ the panel width to minimize the weld stress. The stresses in the W74 guide tube longitudinal seam weld located at ¼ the panel width due to the NCT vibration loading are determined by scaling the stresses calculated for the NCT side drop load by the ratio of the acceleration loads (i.e., 2g/15g). As shown in Section 2.6.7.4, the maximum primary membrane and primary membrane plus bending stress intensities in the longitudinal seam weld resulting from the 15g NCT side drop load are 1.38 ksi and 7.16 ksi, respectively. Therefore, maximum primary membrane and primary membrane plus bending stress intensities in the W74 guide tube

longitudinal seam weld due to the 2g vertical vibration loading are 0.2 ksi (= 1.28 x 2g/15g) and 1.0 ksi (= 7.16 x 2g/15g), respectively.

In accordance with Table NG-3352-1 of the ASME Code, a 65% weld efficiency factor is applied to the allowable stresses for a full penetration weld with PT examination. Therefore, the W74 guide tube seam weld Service Level A allowable primary membrane and primary membrane plus bending stress intensities are 10.8 ksi (=16.7 x 0.65) and 16.3 ksi (=25.0 x 0.65), respectively. The minimum design margins for primary membrane and primary membrane plus bending stress intensities in the W74 guide tube longitudinal seam weld due to NCT vibration are:

$$P_m: DM = \frac{10.8}{0.2} - 1 = +59.0$$

$$P_m+P_b: DM = \frac{16.3}{1.0} - 1 = +15.3$$

As discussed in Section 2.6.1.3.4, there are no significant stresses in the W74 guide tubes due to the thermal loading. Therefore, no load combination evaluation for vibration plus thermal is required for the guide tube assemblies.

Concentrated Fuel Assembly Loading

In addition to the uniform fuel loading assumption evaluated above, the loads from the SNF assembly are assumed to be applied to the guide tube as concentrated loads at the location of the SNF grid spacers. Table 2.12-3 presents the grid spacer tributary weights for the BRP fuel accommodated by the W74 canisters. The results show that the maximum grid spacer tributary weight of BRP fuel is 118 pounds. The W74M and W74T upper and lower basket assemblies all have maximum spacer plate center-to-center spacing of 7.125 inches. Stress evaluations are performed for the guide tube and the longitudinal seam welds, based on the largest guide tube span and the maximum grid spacer tributary weight.

A linear-elastic stress analysis of the W74 guide tube for the 2g NCT vibration loading is performed using the ½-symmetry multi-span finite element model described in Section 2.12.4.3. The SNF assembly loading is applied as a concentrated load over the area of the guide tube bottom panel that supports the SNF assembly grid spacer. A bounding force of 247.2 pounds is applied to the guide tube bottom panel at the location of the grid spacer. This load is approximately 5% higher than the maximum grid spacer loading of 236 pounds (=118 lb. x 2g). Since the grid spacer area of the model is split by two symmetry planes, ¼ of this load (61.8 pounds) is applied to the model. In addition, a 2g vertical acceleration load is applied to the finite element model to account for the loading due to the guide tube's own weight.

The resulting stress intensity distribution in the guide tube at the shell element middle, top, and bottom fibers are shown in Figure 2.6-5, Figure 2.6-6 and Figure 2.6-7, respectively. As shown in Figure 2.6-5, the maximum stress intensity at the middle fiber of the guide tube shell elements is 1.9 ksi. Since this stress is highly localized and is not necessary to satisfy the laws of equilibrium of external and internal forces and moments, it is not considered to be a primary stress, per NG-3213.8. The maximum primary membrane stress intensity is taken as the

maximum membrane stress intensity occurring on the short edge of the area supporting the grid spacer, or 1.1 ksi. The maximum stress intensity at the extreme fibers of the guide tube shell elements (i.e., top and bottom fibers) is 7.6 ksi, as shown Figure 2.6-6 and Figure 2.6-7. This stress intensity is localized at the corner of the area supporting the fuel grid spacer. As such, it is classified as primary plus secondary plus peak (P_m+P_b+Q+F), in accordance with NG-3213.10, since it is highly localized and cannot cause any noticeable distortion. The primary membrane plus bending stress intensity (P_m+P_b) is taken as the stress occurring on the long edge of the area supporting the grid spacer, or 1.5 ksi. The primary plus secondary stress intensity (P_m+P_b+Q) is taken as the maximum stress intensity occurring on the short edge of the area supporting the grid spacer, or 5.3 ksi. The Service Level A allowable primary membrane (P_m), primary membrane plus bending (P_m+P_b), and primary plus secondary (P_m+P_b+Q) stress intensities for SA-240, Type 316 stainless steel at 650°F are 16.7 ksi, 25.0 ksi, and 50.0 ksi, respectively. Therefore, the minimum design margins in the W74 guide tube for NCT vibration loading are:

$$P_m: DM = \frac{16.7}{1.1} - 1 = +14.18$$

$$P_m+P_b: DM = \frac{25.0}{1.5} - 1 = +15.67$$

$$P_m+P_b+Q: DM = \frac{50.0}{5.3} - 1 = +8.43$$

Therefore, the W74 guide tube stresses meet the Service Level A allowable stress design criteria for the NCT vibration loading assuming a concentrated fuel load at the grid spacer.

The W74 guide tubes include two full penetration longitudinal seam welds located on opposite faces. The longitudinal seam welds may be examined using either RT or surface PT methods. When RT examination is performed, there are no restrictions on the locations of the longitudinal seam welds since the allowable stresses for the welds are equal to those of the base material. When only surface PT examination is performed, the longitudinal seam welds must be located at ¼ the panel width to minimize the weld stress. The stresses in the W74 guide tube longitudinal seam weld due to the NCT vibration loading for the concentrated fuel load assumption are also evaluated using the maximum nodal moment reactions from the finite element solution. The guide tube longitudinal seam welds are located at the ¼ span of the panel width. The maximum stress intensities in the guide tube longitudinal seam welds are calculated using the nodal forces and moments for the model nodes at the bottom panel and side panel weld locations as follows:

$$P_m = \sqrt{\sigma_m^2 + 4\tau^2}$$

$$P_m + P_b = \sqrt{\sigma_{m+b}^2 + 4\tau^2}$$

where, for the bottom panel (X and Y interchanged for side panel):

$$\sigma_m = \text{Average stress normal to weld axis} = \frac{FX}{L_w t_w} + \frac{6MY}{L_w^2 t_w}$$

$$\sigma_{m+b} = \text{Membrane + Bending stress in weld} = \sigma_m + \frac{6MZ}{L_w t_w^2}$$

$$\tau = \text{Maximum shear stress in weld} = \sqrt{\left(\frac{FY}{L_w t_w} + \frac{6MX}{L_w^2 t_w}\right)^2 + \left(\frac{FZ}{L_w t_w}\right)^2}$$

L_w = Associated nodal length.

t_w = 0.090 in., weld throat thickness

FX, FY, FZ, MX, MY, and MZ are the nodal forces and moments from the finite element solution.

The nodal forces and moments at each node along the weld length are summarized in Table 2.6-6 and Table 2.6-7, along with the nodal tributary lengths and calculated stresses. The results show that the maximum primary membrane and primary membrane plus bending stress intensities in the W74 guide tube longitudinal seam weld due to horizontal dead weight loading (concentrated fuel load assumption) are 0.4 ksi and 1.2 ksi, respectively.

As discussed previously, the W74 guide tube seam weld Service Level A allowable primary membrane and primary membrane plus bending stress intensities are 10.8 ksi (=16.7x0.65) and 16.3 ksi (=25.0x0.65) respectively. The minimum design margin for bending stress in the W74 guide tube longitudinal seam weld for NCT vibration loading is:

$$P_m: \text{ DM} = \frac{10.8}{0.4} - 1 = +26.0$$

$$P_m+P_b: \text{ DM} = \frac{16.3}{1.2} - 1 = +12.6$$

Therefore, the W74 guide tubes meet the Service Level A allowable stress design criteria for the NCT vibration loading.

2.6.5.5 Vibration Summary

The analyses presented in the preceding sections show that the maximum stresses in the FuelSolutions™ W74 canister due to NCT vibration loading, including the Regulatory Guide 7.8 load combinations shown in Table 2.1-6, are lower than the corresponding Service Level A allowable stresses. The minimum design margins in each of the W74 canister components are summarized in Table 2.6-5. Furthermore, the W74 canisters are not susceptible to fatigue failure, as shown in Section 2.6.1.4. The minimum design margin for NCT vibration is +1.11 for primary

plus secondary stress intensity in the W74T support tube to attachment sleeve weld due to combined NCT vibration and NCT thermal loading.

Table 2.6-5 - Summary of W74 Canister NCT Vibration Design Margins

W74 Canister Component	Stress Type	Maximum S.I. (ksi)	Allowable S.I. (ksi)	Minimum Design Margin ⁽¹⁾	Reference SAR Section
General Spacer Plate	P_m	3.7	35.9	+8.76	2.6.5.1
	$P_m + P_b$	7.5	53.9	+6.19	2.6.5.1
	$P_m + P_b + Q$	29.9	107.7	+2.60	2.6.5.1
	Buckling ⁽³⁾	⁽²⁾	1.0	⁽²⁾	2.6.5.1
LTP Spacer Plate	P_m	0.9	28.8	+31.0	2.6.5.1
	$P_m + P_b$	1.8	43.2	+23.0	2.6.5.1
	$P_m + P_b + Q$	37.0	86.4	+1.34	2.6.5.1
	Buckling ⁽³⁾	⁽²⁾	1.0	⁽²⁾	2.6.5.1
Engagement Spacer Plate	P_m	1.0	29.7	+28.7	2.6.5.2
	$P_m + P_b$	1.0	44.6	+43.6	2.6.5.2
	$P_m + P_b + Q$	23.8	89.1	+2.74	2.6.5.2
Support Tube	P_m	0.05	29.2	+Large	2.6.5.3
	$P_m + P_b$	0.22	43.8	+Large	2.6.5.3
	$P_m + P_b + Q$	0.99	87.6	+87.5	2.6.5.3
Support Sleeve	P_m	0.0	16.4	+Large	2.6.5.3
	$P_m + P_b$	0.0	24.6	+Large	2.6.5.3
	$P_m + P_b + Q$	2.40	49.2	+19.5	2.6.5.3
Support Tube Longitudinal Seam Weld	Shear	0.05	6.1 ⁽⁴⁾	+121	2.6.5.3
W74M Support Tube to LTP Spacer Plate Weld	Shear	1.46	7.0 ⁽⁵⁾	+3.79	2.6.5.3
W74T Support Tube to Attachment Sleeve Weld	Shear	3.32	7.0 ⁽⁵⁾	+1.11	2.6.5.3
Guide Tube	P_m	1.1	16.7	+14.2	2.6.5.4
	$P_m + P_b$	1.8	25.0	+12.9	2.6.5.4
	$P_m + P_b + Q$	5.3	50.0	+8.43	2.6.5.4
Guide Tube Longitudinal Welds	P_m	0.4	10.8 ⁽⁶⁾	+26.0	2.6.5.4
	$P_m + P_b$	1.2	16.3 ⁽⁶⁾	+12.6	2.6.5.4

Notes:

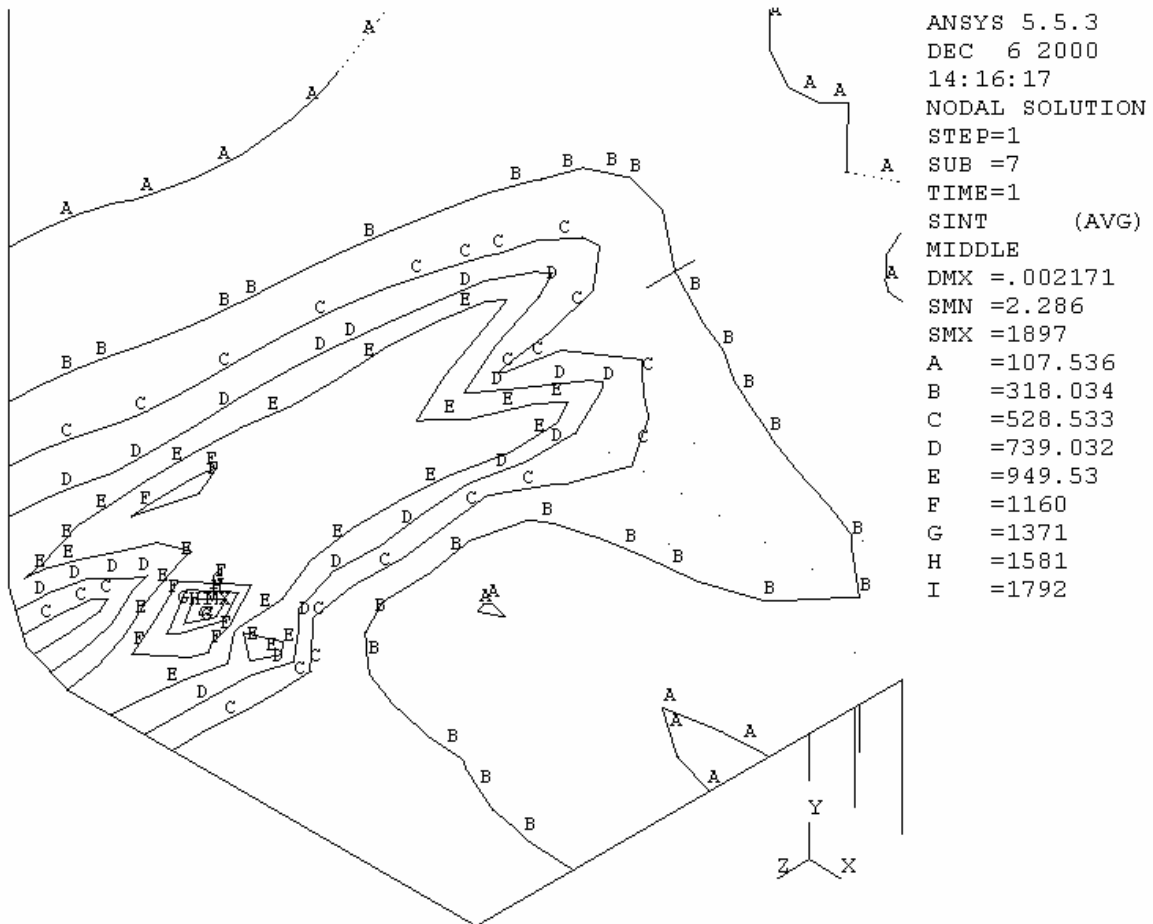
- (1) Design margin is equal to (Allowable/Stress) - 1.
- (2) Bounded by NCT side drop.
- (3) Buckling interaction ratio calculated in accordance with NUREG/CR-6322.
- (4) Includes a 35% weld quality factor for a single fillet weld with surface visual examination, in accordance with Table NG-3352-1 of the ASME B&PV Code.
- (5) Includes a 40% weld quality factor for single groove or fillet welds with surface PT examination, in accordance with Table NG-3352-1 of the ASME B&PV Code.
- (6) Includes a 65% weld quality factor for a full penetration weld with surface PT examination, in accordance with Table NG-3352-1 of the ASME B&PV Code.

Table 2.6-6 - W74 Guide Tube Longitudinal Seam Weld Stresses due to NCT Vibration Loading (Horizontal Panel)

Node No.	Forces (lbf)			Moments (in-lbf)			L _w (in)	σ _m (psi)	σ _{m+b} (psi)	τ (psi)	S.I. _m (psi)	S.I. _{m+b} (psi)
	FX	FY	FZ	MX	MY	MZ						
2	3.788	0.230	0.259	0.014	0.000	0.084	0.129	327	812	81	365	828
8	7.645	0.623	0.432	0.001	0.000	0.177	0.258	330	838	33	337	841
7	7.748	0.392	0.633	0.001	0.000	0.175	0.258	335	838	33	341	841
125	7.631	0.958	0.499	0.003	0.001	0.212	0.258	330	939	49	345	944
124	8.231	0.365	0.013	0.016	0.002	0.361	0.309	298	1164	24	301	1165
207	7.297	0.164	0.684	0.031	0.002	0.210	0.360	227	659	30	235	661
208	3.793	0.133	1.157	0.037	0.003	0.170	0.360	119	469	43	146	477
209	0.116	0.009	1.176	0.043	0.003	0.107	0.360	5	225	43	85	241
210	3.970	0.163	0.807	0.020	0.003	0.033	0.360	124	193	29	137	201
211	7.365	0.360	0.043	0.017	0.002	0.050	0.360	229	332	20	232	335
206	9.842	0.459	1.518	0.062	0.002	0.128	0.367	298	556	64	325	571
453	10.48	0.469	3.261	0.112	0.000	0.197	0.375	311	701	117	389	739
452	8.716	0.456	4.338	0.136	0.001	0.246	0.365	266	765	156	409	826
535	6.031	0.247	4.415	0.132	0.001	0.268	0.354	190	751	159	370	815
536	3.573	0.137	3.778	0.110	0.001	0.274	0.354	113	686	134	291	737
537	1.643	0.054	2.749	0.080	0.001	0.261	0.354	52	597	97	201	628
538	0.360	0.009	1.735	0.053	0.001	0.238	0.354	12	510	61	123	525
539	0.419	0.016	0.948	0.032	0.001	0.215	0.354	14	463	35	70	469
540	0.883	0.025	0.425	0.019	0.001	0.195	0.531	19	290	10	28	291
541	1.254	0.029	0.047	0.009	0.000	0.175	0.531	26	270	3	27	270
542	1.342	0.029	0.027	0.006	0.000	0.170	0.531	28	265	2	28	265
543	1.454	0.027	0.075	0.005	0.000	0.165	0.354	46	390	4	46	390
544	1.516	0.027	0.074	0.004	0.000	0.164	0.354	48	391	4	48	391
545	1.530	0.025	0.068	0.004	0.000	0.169	0.354	48	400	4	49	401
546	1.482	0.021	0.104	0.003	0.000	0.177	0.354	47	417	4	47	418
547	1.333	0.008	0.222	0.001	0.000	0.191	0.354	42	441	7	44	441
548	1.013	0.008	0.451	0.007	0.000	0.208	0.354	32	466	15	43	467
549	0.423	0.037	0.770	0.016	0.001	0.225	0.354	14	485	26	54	488
550	0.494	0.082	1.057	0.025	0.001	0.240	0.354	16	518	37	75	524
551	1.635	0.135	1.101	0.027	0.001	0.249	0.354	52	573	39	94	578
534	2.737	0.188	0.741	0.019	0.000	0.260	0.364	84	612	27	100	614
1272	1.632	0.105	0.381	0.010	0.000	0.134	0.188	97	625	33	118	629

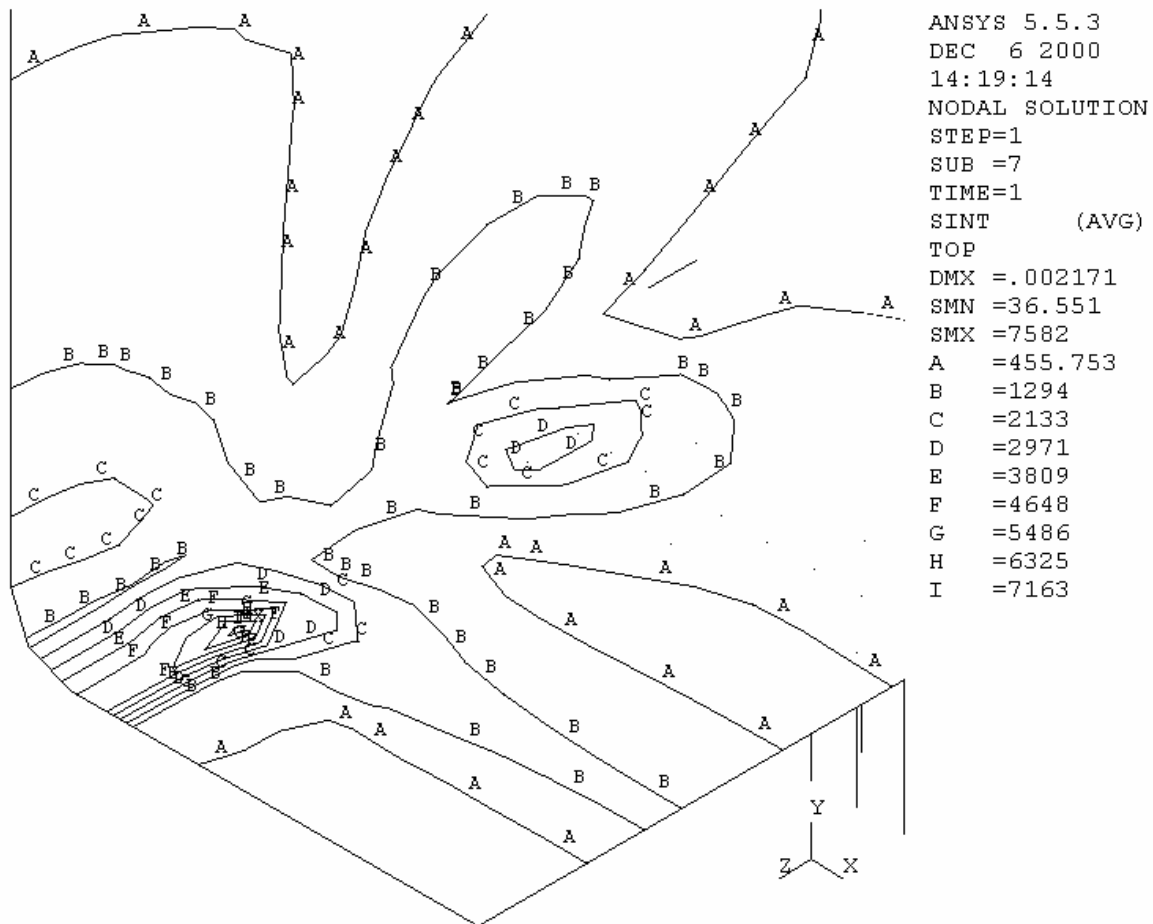
Table 2.6-7 - W74 Guide Tube Longitudinal Seam Weld Stresses due to NCT Vibration Loading (Vertical Panel)

Node No.	Forces (lbf)			Moments (in-lbf)			L _w (in)	σ _m (psi)	σ _{m+b} (psi)	τ (psi)	S.I. _m (psi)	S.I. _{m+b} (psi)
	FX	FY	FZ	MX	MY	MZ						
40	0.182	0.259	0.327	0.000	0.003	0.170	0.129	23	999	39	80	1002
45	0.362	0.450	0.616	0.000	0.005	0.334	0.258	20	980	34	70	983
44	0.338	0.285	1.141	0.000	0.012	0.320	0.258	13	934	56	112	941
151	0.327	0.102	1.528	0.001	0.017	0.297	0.258	5	859	73	146	872
150	0.321	0.010	2.162	0.001	0.030	0.314	0.309	1	754	84	169	773
285	0.299	0.093	2.726	0.002	0.044	0.301	0.360	4	624	90	180	649
286	0.171	0.503	2.860	0.002	0.050	0.221	0.360	16	471	94	188	507
287	0.050	1.122	2.938	0.002	0.049	0.136	0.360	36	315	95	192	368
288	0.083	1.791	2.998	0.002	0.037	0.053	0.360	56	166	95	198	252
289	0.182	2.338	3.076	0.001	0.016	0.024	0.360	73	122	96	205	228
284	0.271	2.614	3.261	0.001	0.014	0.095	0.367	79	270	100	215	336
479	0.300	2.375	3.410	0.000	0.046	0.158	0.375	70	383	106	222	437
478	0.287	1.551	3.218	0.001	0.069	0.201	0.365	48	456	107	220	504
769	0.231	0.552	2.778	0.001	0.080	0.227	0.354	18	493	100	202	533
770	0.180	0.331	2.241	0.001	0.082	0.245	0.531	7	348	52	105	364
771	0.100	1.153	1.391	0.001	0.068	0.248	0.531	24	371	34	73	377
772	0.077	1.335	1.134	0.001	0.062	0.246	0.531	28	372	29	64	376
773	0.042	1.486	0.767	0.001	0.049	0.237	0.354	47	543	36	87	548
774	0.019	1.515	0.550	0.000	0.038	0.226	0.354	48	521	27	72	524
775	0.003	1.495	0.452	0.000	0.029	0.217	0.354	47	500	21	63	502
776	0.006	1.467	0.435	0.000	0.022	0.210	0.354	46	484	18	59	486
777	0.011	1.455	0.466	0.000	0.017	0.206	0.354	46	476	17	57	478
778	0.013	1.465	0.519	0.000	0.012	0.206	0.354	46	477	18	58	478
779	0.011	1.496	0.570	0.000	0.007	0.210	0.354	47	486	18	60	487
780	0.005	1.539	0.595	0.000	0.003	0.217	0.354	48	502	19	61	504
781	0.005	1.571	0.573	0.000	0.003	0.227	0.354	49	524	18	61	526
782	0.022	1.556	0.484	0.000	0.009	0.239	0.354	49	548	16	59	549
783	0.046	1.449	0.333	0.000	0.014	0.250	0.354	46	568	14	53	569
784	0.074	1.229	0.157	0.000	0.017	0.259	0.354	39	581	12	46	582
785	0.101	0.929	0.021	0.000	0.016	0.266	0.354	29	586	12	37	586
768	0.128	0.675	0.028	0.000	0.010	0.277	0.364	21	584	9	27	585
1285	0.069	0.288	0.015	0.000	0.005	0.143	0.188	17	583	14	32	583



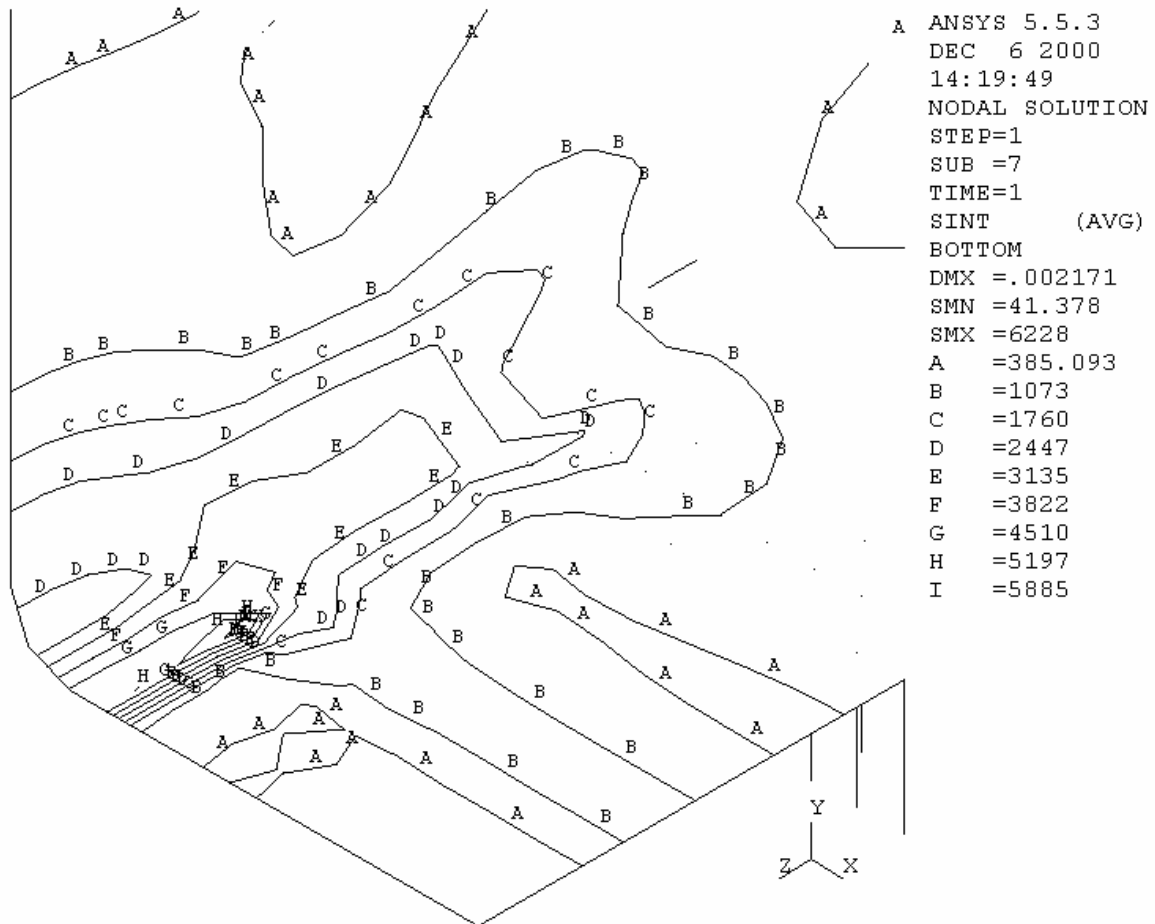
Note: Stresses in psi.

Figure 2.6-5 - W74 Guide Tube NCT Vibration S.I. Contour Plot (Middle Fiber)



Note: Stresses in psi.

Figure 2.6-6 - W74 Guide Tube NCT Vibration S.I. Contour Plot (Top Fiber)



Note: Stresses in psi.

Figure 2.6-7 - W74 Guide Tube NCT Vibration S.I. Contour Plot (Bottom Fiber)

This page intentionally left blank.

2.6.6 Water Spray

In accordance with Regulatory Guide 7.8, the water spray test of 10CFR71.71(c)(6) is not considered significant in the design of large casks. Consequently, the W74 canister, which is transported in the FuelSolutions™ TS125 Transportation Cask, need not be evaluated for the water spray condition.

2.6.7 Free Drop

In accordance with 10CFR71.71(c)(7), a one-foot free drop test is required for packages weighing more than 33,000 pounds. The FuelSolutions™ TS125 Transportation Package, including the W74 canister, weighs considerably more than 33,000 pounds, and therefore is analyzed for this postulated free drop condition. As discussed in Chapter 7 of the FuelSolutions™ TS125 Transportation Cask SAR, the only lifting and handling operations performed for the transportation package which are governed by 10CFR71 are movements between the railcar and a heavy-haul trailer. These operations are always performed with the transportation package in the horizontal orientation in which it is transported. Furthermore, the impact limiters are always installed during these operations. All other lifting and handling operations in which the transportation cask is either handled in a different orientation or without the impact limiters installed are governed by the requirements of the facility in which the cask is being handled, such as 10CFR50 or 10CFR72. Therefore, to satisfy the intent of the regulation, the FuelSolutions™ Transportation Package is analyzed for the NCT free drop only in the horizontal orientation in which it is transported.

The W74 canisters are analyzed for the NCT one-foot side drop loading using equivalent static loads. The equivalent static loads are calculated by multiplying the peak rigid body response by the appropriate dynamic load factor (DLF). As discussed in Section 2.12.2, a bounding NCT side drop equivalent static design load of 15g is conservatively used for the structural evaluation of the W74 canister.

In accordance with Regulatory Guide 7.8, NCT free drop loads are evaluated in combination with internal pressure, thermal, and fabrication stresses. Since no credit is taken for containment or confinement of the radioactive internals provided by the W74 canister shell assembly, the W74 canisters need not be evaluated for internal pressure loads. There are no significant fabrication stresses in any of the canister assembly components. Therefore, the only load condition acting in combination with the NCT side drop is thermal. Stresses in the canister components due to thermal loads are classified as secondary stresses in accordance with Subsection NG of the ASME Code. Since thermal stresses are classified as secondary, the only combined stresses to consider are primary plus secondary.

2.6.7.1 General and LTP Spacer Plates

When subjected to the NCT side drop loading, the W74 general and LTP spacer plates are loaded by their own weight, plus the tributary weight of the guide tubes, support tubes, support sleeves, damaged fuel canisters, and SNF assemblies. For this loading condition, the weights of the guide tubes, support tubes, support sleeves, and damaged fuel canisters are assumed to be distributed to the spacer plates based on the spacer plate tributary lengths. However, two loading assumptions are considered for the distribution of the SNF assembly loads:

1. Uniform SNF assembly loading - the SNF assembly weight uniformly distributed to the spacer plates based on the spacer plate tributary lengths.
2. Concentrated SNF assembly loading - the maximum SNF assembly grid spacer or end fitting tributary weight applied to each spacer plate type.

The spacer plate tributary weights are calculated in Section 2.12.1 for both SNF assembly loading assumptions. For the uniform SNF assembly loading assumption, the maximum tributary weights of the W74 general and LTP spacer plates are calculated to be 2,119 pounds and 2,043 pounds, respectively. Therefore, the total load supported by the most heavily loaded W74 general and LTP spacer plates for the uniform SNF loading assumption are 31.8 kips and 30.7 kips, respectively. For the concentrated SNF assembly loading assumption, the maximum tributary weights of the W74 general and LTP spacer plates are 4,637 pounds and 2,825 pounds, respectively. Therefore, the total load supported by the most heavily loaded W74 general and LTP spacer plates for the concentrated SNF loading assumption are 69.6 kips and 60.0 kips, respectively.

The most heavily loaded W74 general and LTP spacer plates are evaluated for the 15g NCT side drop loading using the spacer plate plane-stress finite element model described in Section 2.12.4.1.1. Elastic-system analyses are performed for both the uniform and concentrated SNF assembly loading assumptions for the most heavily loaded W74 general and LTP spacer plates. In addition, a buckling evaluation of the most heavily loaded W74 general and LTP spacer plates is performed for the bounding NCT side drop loading, both with and without NCT thermal loading superimposed, in accordance with the requirements of NUREG/CR-6322.

Figure 2.6-8 shows a loading diagram of the most heavily loaded W74 general and LTP spacer plates for the 15g NCT side drop loading. The applied loads and reactions on the most heavily loaded W74 general and LTP spacer plates due to the bounding 15g NCT side drop load are slightly higher than the maximum loads calculated above. The results of the NCT side drop stress and buckling evaluations for the most heavily loaded W74 general and LTP spacer plates are summarized in the following paragraphs.

General Spacer Plate Stress Evaluation

The maximum stress intensities in the most heavily loaded W74 general spacer plate due to the bounding 15g NCT side drop loading, assuming a uniform SNF assembly load distribution, are $P_m = 11.0$ ksi (Figure 2.12-1, Point 11), $P_m + P_b = 25.1$ ksi (Figure 2.12-1, Point 2), and $P_m + P_b + Q = 32.2$ ksi (Figure 2.12-1, Point 2), respectively. Similarly, the maximum stress intensities in the most heavily loaded W74 general spacer plate due to the bounding 15g NCT side drop loading, assuming a concentrated SNF assembly load distribution, are $P_m = 23.4$ ksi (Figure 2.12-1, Point 11), $P_m + P_b = 40.7$ ksi (Figure 2.12-1, Point 11), and $P_m + P_b + Q = 47.8$ ksi (Figure 2.12-1, Point 2), respectively. As expected, these results show that the maximum stress intensities due to the concentrated SNF assembly loading are higher than those due to the uniform SNF loading. However, the increase in stress intensities is not proportional to the increase in load. This is due to the non-linear support provided by the canister shell and cask body for transverse loading. As the loading is increased and the spacer plate deforms, the angle of contact between the spacer plate and the canister shell increases.

As discussed in Section 2.6.5.1, the Service Level A allowable primary membrane, primary membrane plus bending, and primary plus secondary stress intensities for the W74 general

spacer plate at a bounding design temperature of 700°F are 35.9 ksi, 53.9 ksi, and 107.7 ksi, respectively. Therefore, minimum design margins for primary membrane and primary membrane plus bending stress intensities in the most heavily loaded W74 general spacer plate for the bounding 15g NCT free drop are:

$$P_m: DM = \frac{35.9}{23.4} - 1 = +0.54$$

$$P_m + P_b: DM = \frac{53.9}{40.7} - 1 = +0.32$$

As discussed above, the spacer plate stresses due to NCT free drop loading are evaluated in combination with the maximum stresses due to NCT thermal loading. Since general thermal stress intensities are classified as secondary in accordance with the ASME Code, the load combination evaluation for NCT free drop plus NCT thermal is performed only for primary plus secondary stress intensity. The NCT free drop plus NCT thermal load combination evaluation is performed by conservatively adding the maximum stress intensities due to the individual load conditions irrespective of sign and location. As shown in Section 2.6.1.3.1, the maximum general thermal stress intensities in the hottest W74 general spacer plate due to NCT thermal loading is 22.1 ksi. Therefore, the maximum combined primary plus secondary stress intensities in the most heavily loaded W74 general spacer plate for NCT free drop plus NCT thermal loading is 69.9 ksi (= 47.8 + 22.1). The minimum design margin for primary plus secondary stress intensity in the W74 general spacer plate due to NCT thermal plus NCT free drop loading is:

$$P_m + P_b + Q: DM = \frac{107.7}{69.9} - 1 = +0.54$$

Therefore, the W74 general spacer plates meet the Service Level A allowable stress design criteria for the bounding 15g NCT free drop loading.

LTP Spacer Plate Stress Evaluation

The maximum stress intensities in the most heavily loaded W74 LTP spacer plate due to the bounding 15g NCT side drop loading, assuming a uniform SNF assembly load distribution, are $P_m = 4.1$ ksi (Figure 2.12-1, Point 83), $P_m + P_b = 12.7$ ksi (Figure 2.12-1, Point 2), and $P_m + P_b + Q = 15.9$ ksi (Figure 2.12-1, Point 2), respectively. Similarly, the maximum stress intensities in the most heavily loaded W74 LTP spacer plate due to the bounding 15g NCT side drop loading, assuming a concentrated SNF assembly load distribution, are $P_m = 7.5$ ksi (Figure 2.12-1, Point 11), $P_m + P_b = 20.4$ ksi (Figure 2.12-1, Point 2), and $P_m + P_b + Q = 26.0$ ksi (Figure 2.12-1, Point 2), respectively. As expected, these results show that the maximum stress intensities due to the concentrated SNF assembly loading are higher than those due to the uniform SNF loading. However, the increase in stress intensities is not proportional to the increase in load. This is due to the non-linear support provided by the canister shell and cask body for transverse loading. As the loading is increased and the spacer plate deforms, the angle of contact between the spacer plate and the canister shell increases.

The Service Level A allowable primary membrane, primary membrane plus bending, and primary plus secondary stress intensities for SA-240, Type XM-19 stainless steel at a bounding design temperature of 700°F are 28.8 ksi, 43.2 ksi, and 86.4 ksi, respectively. Therefore, minimum design margins for primary membrane and primary membrane plus bending stress intensities in the most heavily loaded W74 LTP spacer plate for bounding 15g NCT free drop are:

$$P_m: DM = \frac{28.8}{7.5} - 1 = +2.84$$

$$P_m + P_b: DM = \frac{43.2}{20.4} - 1 = +1.12$$

As discussed above, the spacer plate stresses due to NCT free drop loading are evaluated in combination with the maximum stresses due to NCT thermal loading. Since thermal stresses are classified as secondary in accordance with the ASME Code, the load combination evaluation for NCT free drop plus NCT thermal is performed only for primary plus secondary stress intensity. The NCT free drop plus NCT thermal load combination evaluation is performed by conservatively adding the maximum stress intensities due to the individual load conditions, irrespective of sign and location. As shown in Section 2.6.1.3.1, the maximum general thermal stress intensities in the hottest W74 LTP spacer plate due to NCT thermal loading is 35.1 ksi. Therefore, the maximum combined primary plus secondary stress intensities in the most heavily loaded W74 LTP spacer plate for NCT free drop plus NCT thermal loading is 61.1 ksi (= 26.0 + 35.1). Therefore, the minimum design margin for primary plus secondary stress intensity in the W74 general and LTP spacer plate due to NCT thermal plus NCT free drop loading are:

$$P_m + P_b + Q: DM = \frac{86.4}{61.1} - 1 = +0.41$$

Therefore, the W74 LTP spacer plates meet the Service Level A allowable stress design criteria for the bounding 15g NCT free drop loading.

Buckling Evaluation

The beam-column buckling evaluation of the W74 general and LTP spacer plates for the NCT side drop loading is performed in accordance with NUREG/CR-6322 for linear type supports subjected to combined axial compression and bending loads. Buckling evaluations are performed for the most highly loaded ligaments in both the W74 general and LTP spacer plates for the NCT side drop loading, both with and without the bounding NCT thermal loading superimposed.

The maximum stresses in the W74 spacer plates are evaluated using interaction equations (26), (27), and (28) of NUREG/CR-6322, defined as follows:

$$\frac{f_a}{F_a} + \frac{C_{mx} f_{bx}}{\left(1 - \frac{f_a}{F'_e}\right) F_{bx}} + \frac{C_{my} f_{by}}{\left(1 - \frac{f_a}{F'_e}\right) F_{by}} \leq 1.0 \quad (\text{Eq. 26})$$

$$\frac{f_a}{0.6S_y} + \frac{f_{bx}}{F_{bx}} + \frac{f_{by}}{F_{by}} \leq 1.0 \quad (\text{Eq. 27})$$

If $f_a/F_a \leq 0.15$, then equation (28) may be used in lieu of equations (26) and (27):

$$\frac{f_a}{F_a} + \frac{f_{bx}}{F_{bx}} + \frac{f_{by}}{F_{by}} \leq 1.0 \quad \text{if } \frac{f_a}{F_a} \leq 0.15 \quad (\text{Eq. 28})$$

The allowable axial stress, F_a , bending stress, F_b , and Euler buckling stress, F'_e , are calculated for all ligament sizes for both the W74 general (carbon steel) and LTP (stainless steel) spacer plate.

The allowable axial compressive stress for carbon steel (general spacer plate) and stainless steel (LTP spacer plate) members are calculated using Equations 22 and 24 of NUREG/CR-6322, as follows:

$$F_a = \frac{\left[1 - \frac{1}{2} \left(\frac{Kl}{rC_c}\right)^2\right]}{\frac{5}{3} + \frac{3}{8} \frac{Kl}{rC_c} - \frac{1}{8} \left(\frac{Kl}{rC_c}\right)^3} S_y \quad \text{if } \frac{Kl}{r} < C_c = \sqrt{2\pi \frac{E}{S_y}} \quad (22)$$

$$F_a = \left(0.47 - \frac{Kl/r}{444}\right) S_y \quad \text{if } \frac{Kl}{r} \leq 120 \quad (24)$$

where:

K = 0.65, effective length factor for fixed-fixed support per Figure 6 of NUREG/CR-6322

L = Unsupported length of spacer plate ligaments

r = $\sqrt{I/A_g}$, ligament radius of gyration

I = $bt^3/12$, ligament moment of inertia, for $b > t$
= $b^3t/12$, ligament moment of inertia, for $b < t$

A_g = bt , ligament gross area

b = Ligament width

- t = Spacer plate thickness
= 0.75 inch, general spacer plate
= 2.00 inch, LTP spacer plate
- S_y = Spacer plate material yield strength
= 83.0 ksi, general spacer plate at 700°F
= 36.3 ksi, LTP spacer plate at 700°F
- E = Spacer plate material elastic modulus
= 25.1x10⁶ psi, general spacer plate at 700°F
= 24.8x10⁶ psi, LTP spacer plate at 700°F
- C_m = 0.85, coefficient for members in frames where side-sway is permitted per NUREG/CR-6322

The Euler buckling stress, calculated in accordance with Section 6.22 of NUREG/CR-6322, is defined as follows:

$$F'_e = \frac{\pi^2 E}{1.92(KL/r)^2} \text{ (carbon steel - general)}$$

$$F'_e = \frac{\pi^2 E}{2.15(KL/r)^2} \text{ (stainless steel - LTP)}$$

The allowable bending stress for compact sections, F_b, is defined in Section 6.22 of NUREG/CR 6322 as:

$$F_b = 0.60S_y$$

The W74 general and LTP spacer plate ligament dimensions, section properties, and allowable stresses are calculated for each of the ligament types and are summarized in Table 2.6-9 and Table 2.6-10, respectively.

The maximum axial compressive and bending stresses in the ligaments of the most heavily loaded W74 general and LTP spacer plates due to the 15g NCT side drop loading are conservatively taken from the stress analysis results for the concentrated fuel loading assumption. For each ligament on the impacted side of the spacer plate, the NUREG/CR-6322 buckling interaction ratios are calculated both with and without the bounding NCT thermal loading superimposed. The combined stresses due to NCT side drop plus NCT thermal loading are determined by adding the stress components at each ligament section from the two analyses. The maximum axial compressive and bending stresses and the resulting buckling interaction ratios are summarized in Table 2.6-11.

The results show that the maximum buckling interaction ratios for NCT side drop loading only are 0.57 for the most heavily loaded W74 general spacer plate and 0.66 for the most heavily loaded W74 LTP spacer plate. For the combined NCT side drop and NCT thermal loading, the maximum buckling interaction ratios are 0.71 for the most heavily loaded W74 general spacer plate and 0.74 for the most heavily loaded W74 LTP spacer plate. Therefore, the minimum design margins for buckling ligaments of the most heavily loaded W74 general and LTP spacer

plates for the NCT side drop loading, including the combined effects of NCT thermal loading, are:

$$DM = \frac{1.0}{0.71} - 1 = +0.41 \text{ (General Spacer Plate)}$$

$$DM = \frac{1.0}{0.74} - 1 = +0.35 \text{ (LTP Spacer Plate)}$$

The results of the W74 spacer plate NCT side drop buckling evaluation demonstrate that the most heavily loaded general and LTP spacer plates meet the NCT buckling design criteria of NUREG/CR-6322.

2.6.7.2 Engagement Spacer Plate

The W74 engagement spacer plate is evaluated for a bounding 20g NCT side drop load using the half-symmetry plane-stress finite element model described in Section 2.12.4.2.1. Only the geometry of the engagement spacer plate is modeled, neglecting the attachment sleeves and engagement sleeves that are welded to the engagement spacer plate. The edge support provided by the canister shell is modeled using radial gap elements to reflect the non-linear interface. The engagement spacer plate is supported only at the locations of those gap elements that close under NCT free drop loading.

The maximum stress intensity in the W74 engagement spacer plate, occurring at the point of impact, is 4.5 ksi. The maximum stress intensity, which includes primary plus secondary plus peak stresses, is conservatively compared with Service Level A allowable primary membrane stress intensity. As discussed in Section 2.3, the W74M and W74T engagement spacer plates are fabricated from SA-240, Type XM-19 stainless steel. The Service Level A allowable primary membrane, primary membrane plus bending, and primary plus secondary stress intensities for this material at the bounding design temperature of 500°F are 29.7 ksi, 44.6 ksi, and 89.1 ksi, respectively. Therefore, the minimum design margins for primary stress intensities in the W74 engagement spacer plate for the bounding 20g NCT side drop load are:

$$P_m: DM = \frac{29.7}{4.5} - 1 = +5.60$$

$$P_m+P_b: DM = \frac{44.6}{4.5} - 1 = +8.91$$

In accordance with Regulatory Guide 7.8, the effects of NCT side drop loading are evaluated in combination with NCT hot (100°F ambient temperature) and NCT cold (-20°F ambient temperature) thermal loading. As shown in Section 2.6.1.3.2, the maximum thermal stress intensity due to the NCT hot and NCT cold thermal loading is 21.1 ksi. Conservatively adding the maximum stress intensities due to NCT thermal and NCT side drop irrespective of sign gives a maximum primary plus secondary stress intensity of 25.4 ksi, compared with a Service Level A allowable primary plus secondary stress intensity of 89.1 ksi. The resulting minimum design margin for primary plus secondary stress intensity is:

$$DM = \frac{89.1}{25.4} - 1 = +2.51$$

Therefore, the maximum W74 engagement spacer plate meets the Service Level A allowable stress design criteria for the NCT side drop loading.

2.6.7.3 Support Tubes

This section presents the structural evaluation of the W74M and W74T support tubes and support sleeves for NCT vibration loading.

Support Tube Stresses

The stresses in the support tubes due to the 15g NCT side drop loading are determined by scaling the stresses calculated for the 60g HAC side drop load using an elastic system analysis by the ratio of the loads (i.e., 15g/60g). As shown in Section 2.7.1.2.3, the maximum primary membrane (P_m) and primary membrane plus bending (P_m+P_b) stress intensities in the W74 support tube due to the 60g HAC side drop load are 1.44 ksi and 6.44 ksi, respectively. The resulting maximum primary membrane (P_m) and primary membrane plus bending (P_m+P_b) stress intensities in the W74 support tube due to the 15g NCT side drop loading are 0.36 ksi ($=1.44 \text{ ksi} \times 15\text{g}/60\text{g}$) and 1.61 ksi ($=6.44 \text{ ksi} \times 15\text{g}/60\text{g}$), respectively.

In accordance with Regulatory Guide 7.8, NCT free drop loads are evaluated in combination with NCT thermal loads. As shown in Section 2.6.1.3.3, the maximum general thermal stress intensity (P_m+P_b+Q) in the W74M and W74T support tubes due to the bounding NCT thermal condition are 0.77 ksi and 0.73 ksi, respectively. Therefore, the maximum primary plus secondary stress intensity due to NCT side drop plus NCT thermal loading is 2.38 ksi in the W74M support tube.

The Service Level A allowable primary membrane, primary membrane plus bending, and primary plus secondary stress intensities for the W74M and W74T support tube Type XM-19 stainless steel material at a bounding design temperature of 600°F are 29.2 ksi, 43.8 ksi, and 87.6 ksi, respectively. Therefore, the minimum design margins in the W74 support tubes for primary membrane, primary membrane plus bending, and primary plus secondary stress intensities are:

$$P_m: \frac{29.2}{0.36} - 1 = +80.1$$

$$P_m+P_b: \frac{43.8}{1.61} - 1 = +26.2$$

$$P_m+P_b+Q: \frac{87.6}{2.38} - 1 = +35.8$$

The results show that the W74 support tubes meet the Service Level A allowable stress design criteria for the combined effects of the NCT side drop and NCT thermal loading.

Support Tube Longitudinal Seam Weld Stresses

The stresses in the support tube corner seam welds are evaluated in the same manner as the stresses in the support tube base metal, as described above. As shown in Section 2.7.1.2.3, the maximum shear stress in the support tube corner weld calculated for the 60g side drop load using an elastic system analysis is 1.34 ksi. Therefore, the maximum shear stress in the weld due to the 15g transverse load is 0.34 ksi ($=1.34 \text{ ksi} \times 15\text{g}/60\text{g}$).

The Service Level A allowable shear stress is 6.1 ksi, based on SA-240, Type XM-19 stainless steel at 600°F with a weld quality factor of 35% for a single fillet weld with surface visual examination, per Table NG-3352-1 of the ASME Code. Therefore, the minimum design margin in the support tube corner weld for NCT side drop loading is +16.9.

W74M Support Tube to LTP Spacer Plate Attachment Welds

Each W74M support tubes are welded to the top and bottom end LTP spacer plates using ½-inch partial penetration groove welds, with ¼-inch cover fillets on all four sides of the tube. The stresses in these W74M support tube to LTP spacer plate attachment welds due to the NCT side drop loading are calculated by scaling the maximum stresses calculated for the HAC side drop loading in the same manner as the support tubes, as described in the previous section. The only significant weld stresses resulting from transverse loads are due to the shear reactions at the end spacer plates. As discussed in Section 2.7.1.2.3, the maximum shear stress in the W74M support tube attachment welds calculated for the 60g HAC side drop load using an elastic system analysis is 0.44 ksi. The resulting maximum shear stress in the W74M support tube to LTP spacer plate attachment weld due to the 15g NCT side drop loading is 0.11 ksi ($=0.44 \text{ ksi} \times 15\text{g}/60\text{g}$).

In accordance with Regulatory Guide 7.8, NCT free drop loads are evaluated in combination with NCT thermal loads. As shown in Section 2.6.1.3.3, the maximum shear stress in the W74M support tube to LTP spacer plate attachment weld due to NCT thermal loading is 1.44 ksi. Therefore, the combined shear stress in the W74M support tube to LTP spacer plate attachment weld due to NCT side drop plus NCT thermal loading is 1.55 ksi.

As discussed in Section 2.6.1.3.3, the Service Level A allowable shear stress for SA-240, Type XM-19 stainless steel at 600°F is 7.0 ksi. Therefore, the minimum design margins for shear stress in the W74M support tube attachment welds for NCT side drop loading is +3.52.

W74T Support Tube to Attachment Sleeve Welds

As discussed in Section 2.7.1.2.3, the stresses in the W74T support tube to attachment sleeve welds due to transverse loading, such as the NCT side drop, are insignificant. The only significant stresses in these welds for NCT load conditions are due to NCT thermal loading. As shown in Section 2.6.1.3.3, the bounding NCT thermal loading condition results in a maximum shear stress of 3.32 ksi in the W74T support tube to attachment sleeve welds, compared to a Service Level A allowable shear stress of 7.0 ksi. The resulting minimum design margin for shear stress in the weld is +1.11.

2.6.7.4 Guide Tubes

The W74 guide tube assembly is loaded by its own weight and the weight of the contained fuel assembly for the 15g NCT side drop loading. The spacer plate ligaments provide vertical support

along the bottom face of the guide tube assembly. The structural evaluation of the W74 guide tubes for the bounding 15g NCT side drop loading considers two assumed SNF assembly loading distributions: (1) uniform fuel load assumption (i.e., SNF assembly load applied as a uniform pressure load over the supporting face of the guide tube), and (2) concentrated load at SNF assembly grid spacers. These two conditions are evaluated in the following paragraphs.

Guide Tube Stress Evaluation - Uniform Fuel Loading

The stresses in the largest span of the W74 guide tube due to the 15g NCT side drop load are evaluated using the half-symmetry periodic finite element model described in Section 2.12.4.3. The model represents a segment of the W74 guide tube spanning from the centerline of a spacer plate to the mid-span between the adjacent spacer plate support, taking advantage of longitudinal symmetry. The guide tube is modeled using shell elements. The material density used for the guide tube elements is adjusted to account for the mass of the neutron absorber panels, conservatively taking no credit for structural support of the guide tube provided by the neutron absorber panels. As shown in Section 2.12.4.3, the adjusted density of the guide tube is 0.51 lb/in^3 . An equivalent static side drop load of 15g is applied to the model. The load from the fuel assembly is applied as a uniform pressure load on the supporting guide tube panel.

The guide tube stresses are determined using a linear-elastic static analysis. The resulting stress intensity distribution at the middle, top, and bottom fibers of the shell elements are shown in Figure 2.6-9, Figure 2.6-10, and Figure 2.6-11, respectively. The maximum primary membrane stress intensity is conservatively taken as the maximum stress intensity at the middle fiber, or 3.9 ksi. The maximum primary membrane plus bending stress intensity is conservatively taken as the maximum stress intensity occurring on the top and bottom fibers, or 13.6 ksi.

The Service Level A allowable primary membrane and primary membrane plus bending stress intensities for SA-240, Type 316 stainless steel at the guide tube design temperature of 650°F are 16.7 ksi and 25.0 ksi, respectively. Therefore, the minimum design margins in the W74 guide tube for the bounding 15g NCT side drop load are +3.28 for primary membrane stress intensity and +0.84 for primary membrane plus bending stress intensity.

The stresses in the guide tube longitudinal seam weld due to the 15g NCT side drop loading are also evaluated using the maximum nodal forces and moment from the finite element solution, as described in Section 2.6.5.4. The guide tube longitudinal seam welds are located at the $\frac{1}{4}$ span of the panel width. The maximum primary membrane and primary membrane plus bending stress intensities in the guide tube longitudinal seam weld due to the 15g side drop load are 1.4 ksi and 7.26 ksi, respectively.

In accordance with Table NG-3352-1 of the ASME Code, a 65% weld efficiency factor is applied to the allowable stresses for a full penetration weld with surface PT examination. Therefore, the W74 guide tube seam weld Service Level A allowable primary membrane and primary membrane plus bending stress intensities, based on SA-240, Type 316 stainless steel properties at a design temperature of 650°F, are 10.8 ksi ($=16.7 \times 0.65$) and 16.3 ksi ($=25.0 \times 0.65$), respectively. Therefore, the minimum design margins for primary membrane and primary membrane plus bending stress intensities in the W74 guide tube seam weld are +6.71 and +1.26, respectively.

Guide Tube Stress Evaluation – Concentrated Fuel Loading

The maximum stress intensities in the most heavily loaded W74 guide tube span for the bounding 15g NCT side drop loading are determined by scaling the maximum guide tube stresses calculated in Section 2.6.5.4 for a 2g NCT vibration load using an elastic system analysis by 15g/2g. Hence, maximum stress intensities in the most heavily loaded W74 guide tube for the 15g NCT side drop loading are:

$$P_m = 1.1 \cdot \left(\frac{15g}{2g} \right) = 8.3 \text{ ksi}$$

$$P_m + P_b = 1.5 \cdot \left(\frac{15g}{2g} \right) = 11.3 \text{ ksi}$$

The Service Level A allowable primary membrane (P_m) and primary membrane plus bending (P_m+P_b) stress intensities for SA-240, Type 316 stainless steel at 650°F are 16.7 ksi and 25.0 ksi, respectively. Therefore, the minimum design margins in the W74 guide tube for NCT side drop loading are:

$$P_m: \text{ DM} = \frac{16.7}{8.3} - 1 = +1.01$$

$$P_m+P_b: \text{ DM} = \frac{25.0}{11.3} - 1 = +1.21$$

Therefore, the W74 guide tube stresses meet the Service Level A allowable stress design criteria for primary stresses resulting from the NCT side drop loading assuming a concentrated fuel load at the grid spacer.

As shown in Section 2.6.5.4, the maximum primary plus secondary stress intensity in the W74 guide tube due to the 2g NCT vibration loading is 5.3 ksi. When scaled up by 15g/2g, the resulting maximum primary plus secondary stress intensity in the W74 guide tube due to the 15g NCT side drop loading is 39.8 ksi. Obviously, this stress level can be sustained in the guide tube Type 316 stainless steel material. In accordance with NG-3213.9, local yielding can satisfy the condition that causes the secondary stress to occur, and failure from one application is not to be expected. Furthermore, in accordance with NG-3228.1(b), the limits on primary plus secondary stress intensity need not be satisfied at a specific location if, when evaluated on a plastic basis, shakedown occurs (as opposed to continuing deformation). This is demonstrated by performing a plastic analysis using the W74 guide tube model described in Section 2.12.4.3 for multiple cycles of NCT free drop loading.

The plastic behavior of the W74 guide tube is modeled using the elasto-plastic stress-strain data of Type 316 stainless steel at 650°F from Table 2.3-4 with the multi-linear isotropic hardening (MISO) plasticity option. For this analysis, the SNF assembly loading is applied in the same

manner described in Section 2.6.5.4 for the 2g NCT vibration loading. A total load of 463.5 pounds (= 61.8 lb. x 15g/2g) is applied to the model at the location of the SNF assembly grid spacer. In addition, a 15g vertical acceleration load is applied to the finite element model to account for the loading due to the guide tube's own weight. The loading is then reduced to that of horizontal dead weight to complete the cycle. A total of three loading cycles are applied to the model. The results of this analysis show that the maximum permanent deformation resulting from the first load cycle is 0.0066 inch. The results also show that the maximum permanent deformation of the guide tube remains at 0.0066 inch after all subsequent loading cycles. Therefore, shakedown occurs after the first loading cycle. Consequently, the limits on primary plus secondary stress intensity need not be satisfied in accordance with NG-3228.1(b). This plastic analysis also demonstrates that the high secondary stresses are self-limiting, since the local yielding of the guide tube allows the loads to redistribute to other portions of the structure and does not result in failure or gross distortion.

The maximum stress intensities in the W74 guide tube longitudinal seam welds due to the 15g NCT side drop loading are determined by scaling the maximum weld stresses calculated in Section 2.6.5.4 for a 2g NCT vibration load by 15g/2g. Hence, maximum stress intensities in the W74 guide tube longitudinal seam weld for the 15g NCT side drop loading are:

$$P_m = 0.41 \cdot \left(\frac{15g}{2g} \right) = 3.1 \text{ ksi}$$

$$P_m + P_b = 1.17 \cdot \left(\frac{15g}{2g} \right) = 8.8 \text{ ksi}$$

As discussed previously in this section, the W74 guide tube seam weld Service Level A allowable primary membrane and primary membrane plus bending stress intensities are 10.8 ksi and 16.3 ksi, respectively. The minimum design margins for primary membrane and primary membrane plus bending stress intensities in the W74 guide tube longitudinal seam weld for 15g NCT side drop loading are:

$$P_m: \text{ DM} = \frac{10.8}{3.1} - 1 = +2.48$$

$$P_m + P_b: \text{ DM} = \frac{16.3}{8.8} - 1 = +0.85$$

The results of the structural evaluation show that the maximum stresses in the W74 guide tube due to the NCT side drop loading are less than the Service Level A allowable stresses.

Neutron Absorber Panel Stresses

The maximum bending stress in the W74 guide tube neutron absorber panel due to the NCT side drop is scaled from the maximum stress calculated for the 62g HAC oblique drop transverse load in Section 2.7.1.4.4 as follows:

$$f_b = 5.0 \left(\frac{15g}{62g} \right) = 1.2 \text{ ksi}$$

As discussed in Section 2.3, the neutron absorber panel borated stainless steel material is assumed to have the same mechanical properties as SA-240, Type 304 stainless steel. Therefore, the Service Level A allowable primary membrane plus bending stress intensity for the neutron absorber panel at 650°F is 24.3 ksi. The minimum design margin for primary membrane plus bending stress intensity in the W74 guide tube neutron absorber panel due to the bounding 15g NCT side drop loading is:

$$DM = \frac{24.3}{1.2} - 1 = +19.3$$

Therefore, the W74 guide tube neutron absorber panel stresses resulting from the bounding 15g NCT side drop load are lower than the corresponding allowable stresses.

Neutron Absorber Retainer Weld Stresses

For the NCT side drop loading, the most highly loaded retainer weld is that which supports the largest tributary length of the neutron absorber sheet. As shown in Table 2.7-14, the largest tributary length of the neutron absorber sheet supported by any of the retainers in the W74M and W74T upper and lower basket assemblies is 14.25-inches. The maximum shear stress in the 3/16-inch diameter plug welds between the W74 guide tube and the neutron absorber retainers due to the 15g NCT side drop load is determined by scaling the maximum shear stress calculated in Section 2.7.1.4.4 for the HAC oblique drop slapdown impact by the ratio of the acceleration loads. As shown in Table 2.7-14, the maximum shear stress in the retainer welds with a 14.25-inch tributary length is 3.7 ksi in retainer number 5 of the W74T lower basket assembly for a 51.7g acceleration load. Therefore, the maximum retainer weld shear stress resulting from the 15g NCT side drop load is calculated as follows:

$$f_w = 3.7 \left(\frac{15g}{51.7g} \right) = 1.1 \text{ ksi}$$

In accordance with Table NG-3352-1 of the ASME B&PV Code, a 30% weld quality factor is applied to the allowable stresses for plug welds. Therefore, the Service Level A allowable weld shear stress, based on SA-240, Type 304 stainless steel at a bounding design temperature of 650°F, is 2.9 ksi (=9.7 ksi x 0.3). Therefore, the minimum design margin for pure shear stress in the neutron absorber retainer plug weld due to the bounding 15g NCT side drop load is:

$$DM = \frac{2.9}{1.1} - 1 = +1.64$$

Therefore, the W74 guide tube neutron absorber retainer plug weld shear stress resulting from the bounding 15g NCT side drop load is lower than the corresponding Service Level A allowable shear stress.

Guide Tube Buckling

Buckling of the W74 guide tube is evaluated for the NCT side drop using the criteria of NUREG/CR-6322 for linear-type members subjected to combined axial compressive and bending loads. The maximum axial compressive and bending stresses in the side panel of the W74 guide tube are scaled from the HAC oblique drop stresses as follows:

$$f_a = 0.225 \left(\frac{15g}{62g} \right) = 0.05 \text{ ksi}$$

$$f_b = 12.95 \left(\frac{15g}{62g} \right) = 3.1 \text{ ksi}$$

The NCT allowable compressive stress is determined in accordance with Equation 46 of NUREG/CR-6322 as follows:

$$P_{EQ46} = \left(0.4 - \frac{120\lambda}{600\sqrt{2}} \right) S_y = 3.47 \text{ ksi (for } \lambda > \sqrt{2} \text{)}$$

where:

$$\lambda = \left(\frac{KL}{r} \right) \left(\frac{1}{\pi} \right) \sqrt{\frac{S_y}{E}} = 1.51$$

and,

K = 0.65, effective length factor for a fixed-slider boundary condition per NUREG/C-6322

L = 6.99 in., length of the guide tube side panel

r = $0.090/\sqrt{12} = 0.026$ inches, guide tube side panel radius of gyration

S_y = 18.5 ksi, yield strength of SA-240, Type 316 stainless steel at 650°F

E = 25.1×10^6 psi, elastic modulus of SA-240, Type 316 stainless steel at 650°F

The allowable bending stress per NUREG/CR-6322 is equal to 0.66S_y or 12.2 ksi for SA-240, Type 316 stainless steel at 650°F.

Since the ratio f_a/F_a is less than 0.15, only interaction equation 28 of NUREG/CR-6322 need be evaluated. Therefore, the maximum guide tube buckling interaction ratio for the bounding NCT side drop load is:

$$\frac{f_a}{F_a} + \frac{f_b}{F_b} = \frac{0.05}{4.43} + \frac{3.1}{12.2} = 0.27 < 1.0$$

Therefore, the W74 guide tube meets the buckling design criteria of NUREG/CR-6322 for the NCT side drop loading.

2.6.7.5 Canister Shell Assembly

As discussed in Section 2, even though the canister shell assembly is designed and fabricated in accordance with the requirements of Subsections NB and NF of the ASME Code, the transportation cask is relied upon to provide containment and no credit is taken for containment provided by the W74 canister shell assembly during transportation. The normal condition allowable stress design criteria of the ASME Code provides large safety margins against structural failure and limits the primary stresses to levels that assure that no significant permanent deformation occurs. Whereas, the accident condition allowable stress design criteria of the ASME Code provides sufficient safety margins to prevent gross structural failure, but allows local permanent deformation associated with high discontinuity stresses. Since the canister shell assembly is not relied upon to provide containment during transportation, local plastic deformation resulting from NCT loading is not detrimental to its structural integrity. As such, the structural evaluation of the W74 canister shell for transportation conditions is limited to the most severe loading conditions that present the most significant potential to cause structural failure of the canister shell. The NCT side drop and HAC side drop design loads are 15g and 60g, respectively. Clearly, the HAC side drop loads evaluated in Section 2.7.1.2 are more severe and present a greater potential to cause structural failure of the canister shell than the NCT side drop loads. As shown in Section 2.7.1.2.5, the structural integrity of the W74 canister shell assembly is sufficient to withstand the 60g HAC side drop loading without structural failure. Therefore, structural failure of the W74 canister shell assembly due to the 15g NCT side drop loading also is not credible.

2.6.7.6 Free Drop Summary

The preceding NCT free drop analyses show that the FuelSolutions™ W74 canisters have positive design margins for all the Regulatory Guide 7.8 load combinations shown in Table 2.1-6. The minimum design margin for the NCT free drop is +0.32 for primary membrane plus bending stress intensity in the most heavily loaded W74 general spacer plate.

Table 2.6-8 - Summary of W74 Canister NCT Free Drop Design Margins

W74 Canister Component	Stress Type	Maximum S.I. (ksi)	Allowable S.I. (ksi)	Minimum Design Margin ⁽¹⁾	Reference SAR Section
General Spacer Plate	P_m	23.4	35.9	+0.54	2.6.7.1
	$P_m + P_b$	40.7	53.9	+0.32	2.6.7.1
	$P_m + P_b + Q$	69.9	107.7	+0.54	2.6.7.1
	Buckling ⁽³⁾	0.71	1.0	+0.41	2.6.7.1
LTP Spacer Plate	P_m	7.5	28.8	+2.84	2.6.7.1
	$P_m + P_b$	20.4	43.2	+1.12	2.6.7.1
	$P_m + P_b + Q$	61.1	86.4	+0.41	2.6.7.1
	Buckling ⁽³⁾	0.74	1.0	+0.35	2.6.7.1
Engagement Spacer Plate	P_m	4.5	29.7	+5.60	2.6.7.2
	$P_m + P_b$	4.5	44.6	+8.91	2.6.7.2
	$P_m + P_b + Q$	25.4	89.1	+2.51	2.6.7.2
Support Tube	P_m	0.36	29.2	+80.1	2.6.7.3
	$P_m + P_b$	1.61	43.8	+26.2	2.6.7.3
	$P_m + P_b + Q$	2.38	87.6	+35.8	2.6.7.3
Support Sleeve	P_m	0.0	16.4	+Large	2.6.7.3
	$P_m + P_b$	0.0	24.6	+Large	2.6.7.3
	$P_m + P_b + Q$	2.40	49.2	+19.5	2.6.7.3
	Buckling ⁽⁴⁾	2.40	10.25	+3.27	2.6.7.3
Support Tube Longitudinal Seam Weld	Shear	0.34	6.1 ⁽⁵⁾	+16.9	2.6.7.3
W74M Support Tube to LTP Spacer Plate Weld	Shear	1.55	7.0 ⁽⁶⁾	+3.52	2.6.7.3
W74T Support Tube to Attachment Sleeve Weld	Shear	3.32	7.0 ⁽⁶⁾	+1.11	2.6.7.3
Guide Tube	P_m	8.3	16.7	+1.01	2.6.7.4
	$P_m + P_b$	13.6	25.0	+0.84	2.6.7.4
	$P_m + P_b + Q$	13.6	50.0	+2.67	2.6.7.4
	Buckling ⁽³⁾	0.27	1.0	+2.70	2.6.7.4
Guide Tube Longitudinal Welds	P_m	3.1	10.8	+2.48	2.6.7.4
	$P_m + P_b$	8.8	16.3	+0.85	2.6.7.4
Neutron Absorber Panel	$P_m + P_b$	1.2	24.3	+19.3	2.6.7.4
Neutron Absorber Attachment Weld	Shear	1.1	2.9	+1.64	2.6.7.4

Notes:

- (1) Design margin is equal to (Allowable/Stress) - 1.
- (2) Stresses in the support sleeves due to NCT vibration loading are insignificant.
- (3) Buckling interaction ratio calculated in accordance with NUREG/CR-6322.
- (4) The allowable axial compressive stress is limited to 1/2 of the theoretical buckling stress for NCT loading, in accordance with NUREG/CR-6322.
- (5) Includes a 35% weld quality factor for a single fillet weld with surface visual examination, in accordance with Table NG-3352-1 of the ASME B&PV Code.
- (6) Includes a 40% weld quality factor for single groove or fillet welds with surface PT examination, in accordance with Table NG-3352-1 of the ASME B&PV Code.

Table 2.6-9 - W74 General Spacer Plate Allowable Buckling Stresses for NCT Conditions

Spacer Plate Buckling Characteristics	Ligament Type ⁽¹⁾				
	A	Bx	By	B	C
Width, b (in.)	1.125	1.050	0.975	1.005	0.875
Thickness, t (in.)	0.75	0.75	0.75	0.75	0.75
Height, L (in.)	7.325	7.40	7.25	7.325	7.325
Gross Area, A _g (in ²)	0.84	0.79	0.73	0.75	0.66
I _{xx} (in ⁴)	0.040	0.037	0.034	0.035	0.031
r _x (in.)	0.217	0.217	0.217	0.217	0.217
Effective Length Factor, K	0.65	0.65	0.65	0.65	0.65
KI/r _x	21.99	22.22	21.77	21.99	21.99
S _y at 700°F (ksi)	83.0	83.0	83.0	83.0	83.0
E at 700°F (ksi)	25.5x10 ³	25.5x10 ³	25.5x10 ³	25.5x10 ³	25.5x10 ³
C _c	43.94	43.94	43.94	43.94	43.94
F _a (ksi)	33.8	33.6	34.1	33.8	33.8
F _b (ksi)	49.8	49.8	49.8	49.8	49.8
F _e ' (ksi)	271.0	265.6	276.7	271.0	271.0

Note:

⁽¹⁾ The location of the spacer plate ligament types are shown in Figure 2.6-8.

Table 2.6-10 - W74 LTP Spacer Plate Allowable Buckling Stresses for NCT Conditions

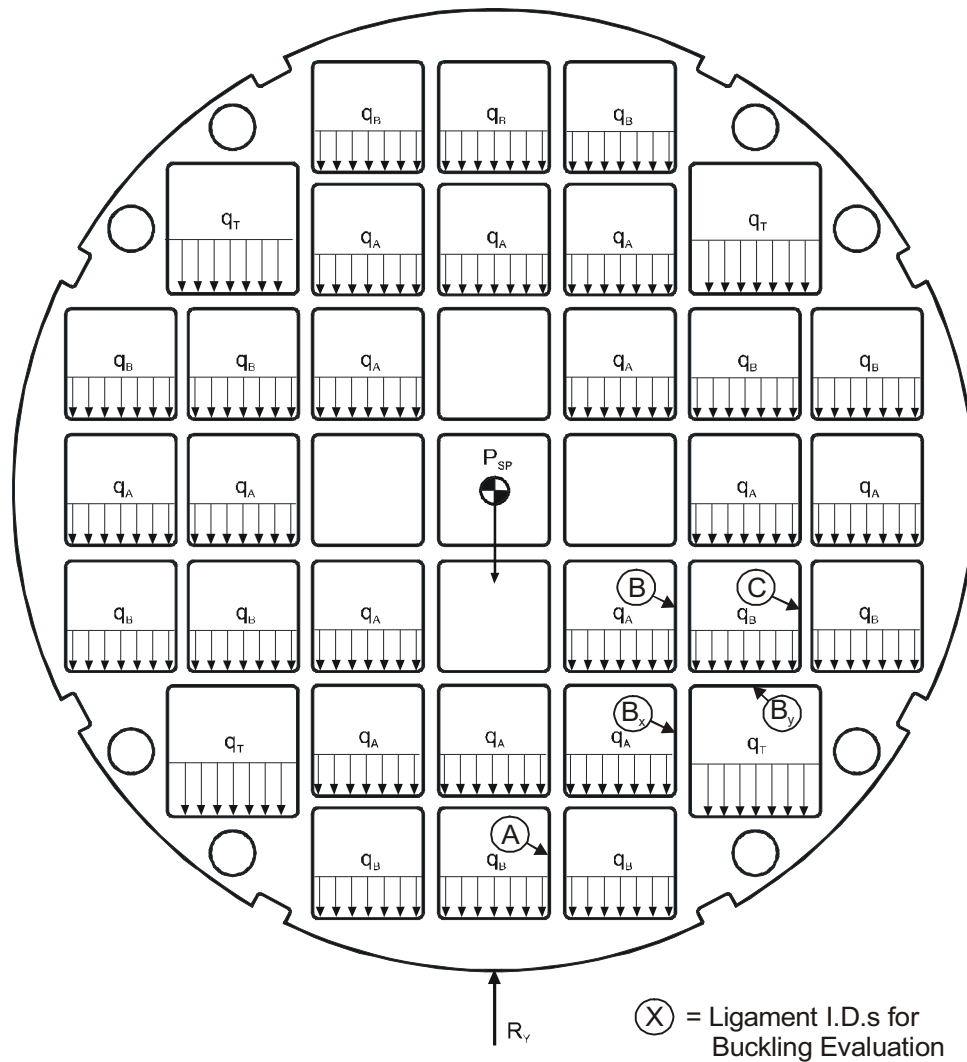
Spacer Plate Buckling Characteristics	Ligament Type ⁽¹⁾				
	A	Bx	By	B	C
Width, b (in.)	1.125	1.050	0.975	1.005	0.875
Thickness, t (in.)	2.00	2.00	2.00	2.00	2.00
Height, L (in.)	7.325	7.40	7.25	7.325	7.325
Gross Area, A _g (in ²)	2.25	2.10	1.95	2.01	1.75
I _{xx} (in ⁴)	0.237	0.193	0.154	0.169	0.112
r _x (in.)	0.325	0.303	0.281	0.290	0.253
Effective Length Factor, K	0.65	0.65	0.65	0.65	0.65
Kl/r _x	14.66	15.87	16.74	16.41	18.85
S _y at 700°F (ksi)	36.3	36.3	36.3	36.3	36.3
E at 700°F (ksi)	2.48E+04	2.48E+04	2.48E+04	2.48E+04	2.48E+04
F _a (ksi)	15.9	15.8	15.7	15.7	15.5
F _b (ksi)	21.8	21.8	21.8	21.8	21.8
F _c ' (ksi)	529.7	452.1	406.1	422.7	320.4

Notes:

⁽¹⁾ The location of the spacer plate ligament types are shown in Figure 2.6-8.

Table 2.6-11 - W74 Spacer Plate NCT Side Drop Ligament Stresses and Buckling Interaction Ratios

Loading Condition	Stresses and Interaction Ratios	Ligament Type ⁽¹⁾				
		A	B _x	B _y	B	C
General Spacer Plate						
NCT Side Drop	Axial Stress (ksi)	14.95	11.89	0.00	9.27	0.00
	Bending Stress (ksi)	5.73	7.99	21.05	16.76	27.04
	Interaction Ratio (Eq. 26)	0.55	0.50	0.36	0.57	0.46
	Axial Stress (ksi)	12.15	11.89	0.00	9.27	0.00
	Bending Stress (ksi)	8.57	7.99	21.05	16.76	27.04
	Interaction Ratio (Eq. 27)	0.42	0.40	0.42	0.52	0.54
NCT Side Drop + NCT Thermal	Axial Stress (ksi)	14.09	15.25	0.69	12.63	0.00
	Bending Stress (ksi)	10.07	10.08	23.32	18.57	23.80
	Interaction Ratio (Eq. 26)	0.60	0.64	0.42	0.71	0.41
	Axial Stress (ksi)	14.09	15.25	0.69	12.63	0.00
	Bending Stress (ksi)	10.07	10.08	23.32	18.57	23.80
	Interaction Ratio (Eq. 27)	0.49	0.51	0.48	0.63	0.48
LTP Spacer Plate						
NCT Side Drop	Axial Stress (ksi)	6.56	2.50	0.00	0.00	0.00
	Bending Stress (ksi)	5.71	3.52	5.05	9.89	14.39
	Interaction Ratio (Eq. 26)	0.64	0.30	0.20	0.39	0.56
	Axial Stress (ksi)	6.56	2.50	0.00	0.00	0.00
	Bending Stress (ksi)	5.71	3.52	5.05	9.89	14.39
	Interaction Ratio (Eq. 27)	0.56	0.28	0.23	0.45	0.66
NCT Side Drop + NCT Thermal	Axial Stress (ksi)	8.59	7.22	3.77	6.60	4.15
	Bending Stress (ksi)	4.88	4.89	6.21	6.22	8.54
	Interaction Ratio (Eq. 26)	0.74	0.65	0.48	0.67	0.61
	Axial Stress (ksi)	2.18	7.22	3.77	3.44	4.15
	Bending Stress (ksi)	12.41	4.89	6.21	10.16	8.54
	Interaction Ratio (Eq. 27)	0.67	0.56	0.46	0.62	0.58



Spacer Plate 15g NCT Side Drop Loads	General Spacer Plate		LTP Spacer Plate	
	Uniform Fuel Loading	Concentrated Fuel Loading	Uniform Fuel Loading	Concentrated Fuel Loading
Spacer Plate Self Weight, P_{SP} (kips)	3.47	3.47	9.47	9.47
Support Tube Holes, $q_T^{(1)}$ (kips) (4 plcs.)	1.87	3.43	1.37	2.57
Type A Guide Tube Holes, $q_A^{(2)}$ (kips) (14 plcs)	0.75	1.88	0.57	1.44
Type B Guide Tube Holes, $q_B^{(2)}$ (kips) (14 plcs)	0.75	1.88	0.57	1.44
Total Reaction Load, R_Y (kips)	32.0	69.7	30.8	60.2

Notes:

- (1) Total load from support tube, support sleeves, damaged fuel can, and SNF assembly.
- (2) Total load from guide tube and SNF assembly.

Figure 2.6-8 - W74 Spacer Plate NCT Free Drop Loading Diagram

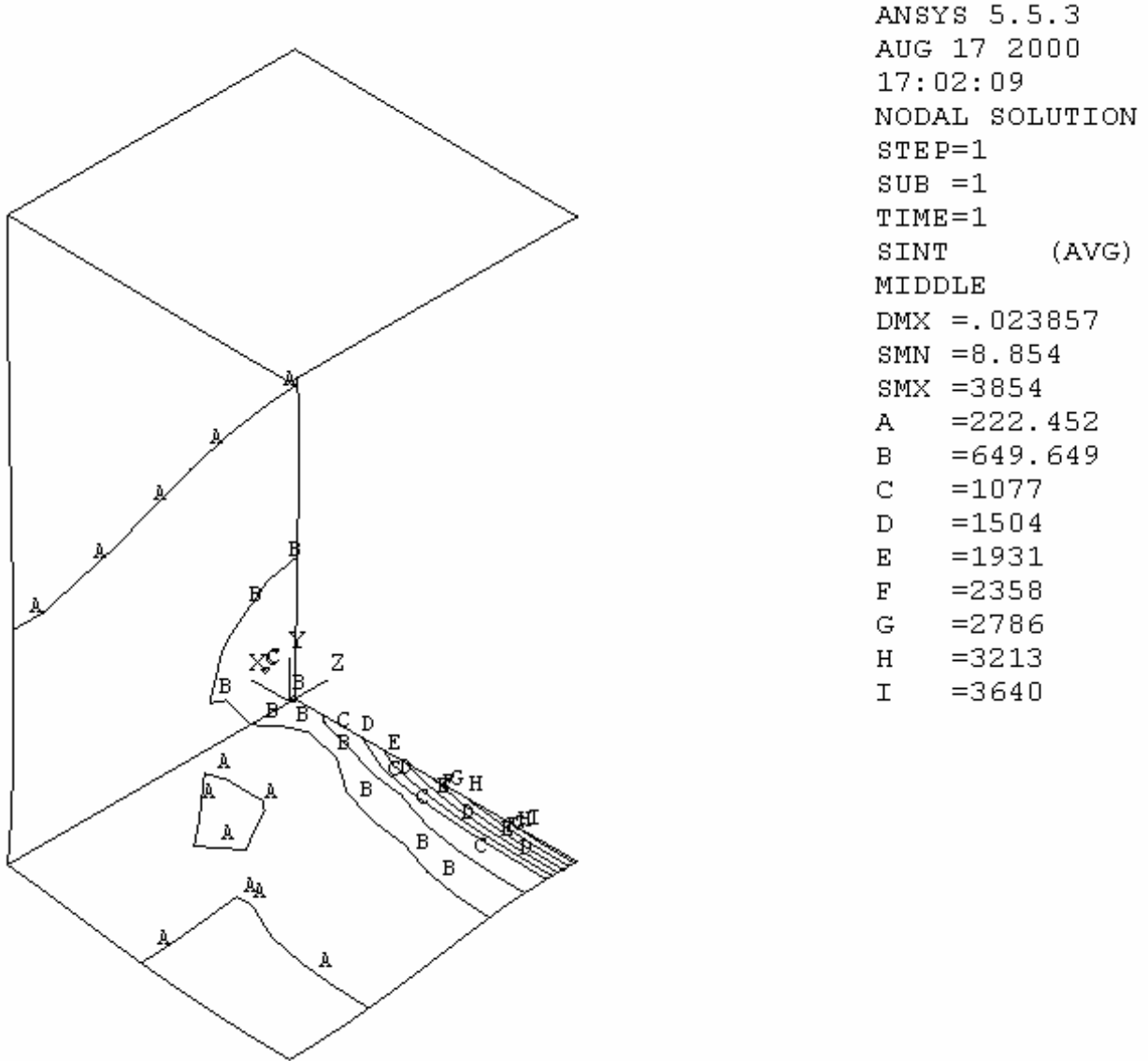
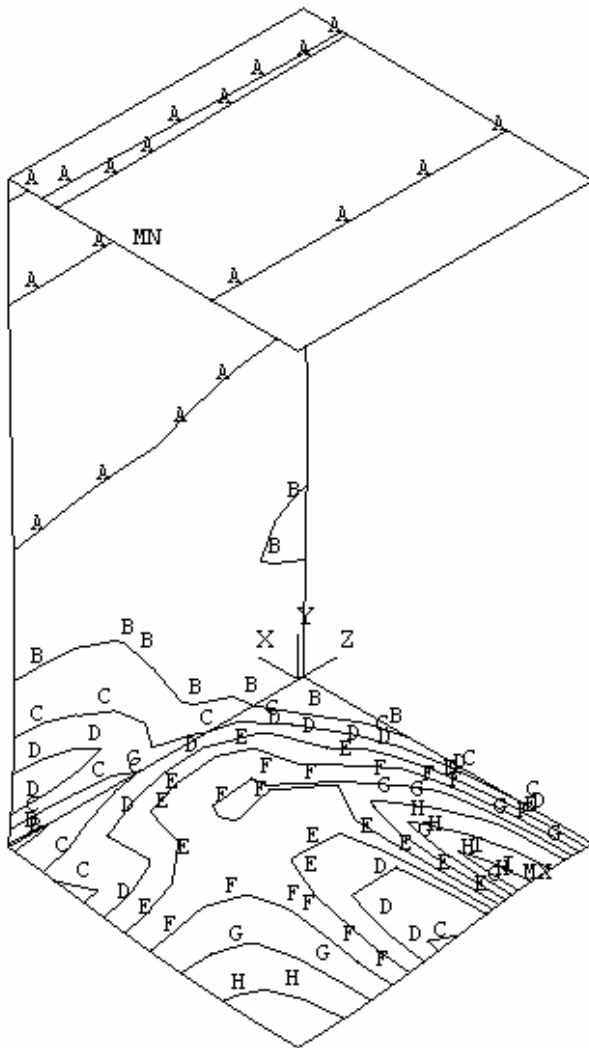


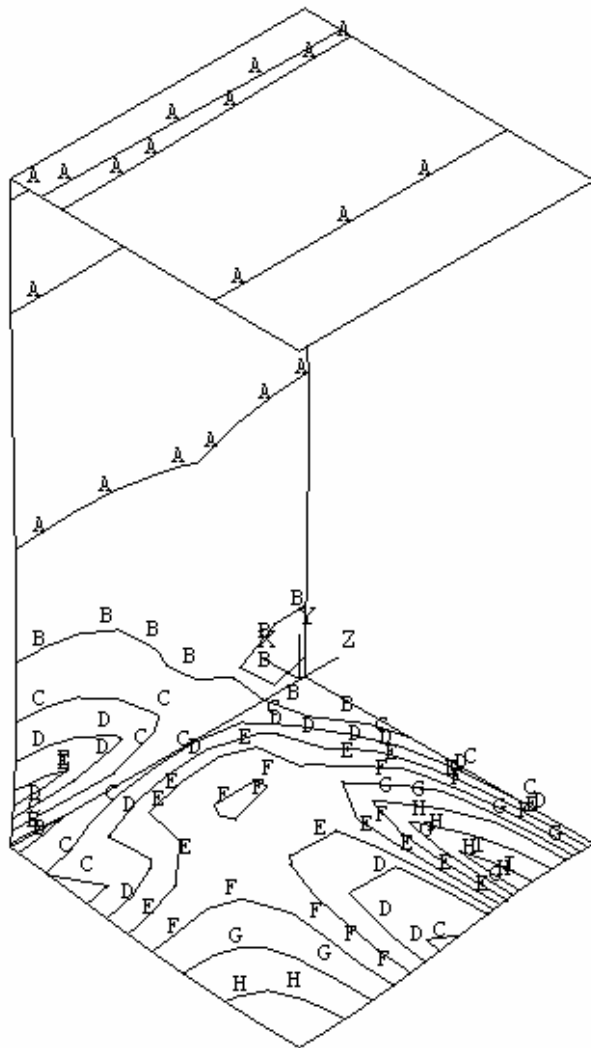
**Figure 2.6-9 - W74 Guide Tube S.I. Contour Plot (Middle Fiber) -
15g NCT Side Drop, Uniform Fuel Loading**



```
ANSYS 5.5.3  
AUG 17 2000  
17:00:08  
NODAL SOLUTION  
STEP=1  
SUB =1  
TIME=1  
SINT      (AVG)  
TOP  
DMX =.023857  
SMN =218.01  
SMX =13593
```

```
A  =961.04  
B  =2447  
C  =3933  
D  =5419  
E  =6905  
F  =8391  
G  =9877  
H  =11363  
I  =12850
```

**Figure 2.6-10 - W74 Guide Tube S.I. Contour Plot (Top Fiber) -
15g NCT Side Drop, Uniform Fuel Loading**



```
ANSYS 5.5.3  
AUG 17 2000  
17:02:33  
NODAL SOLUTION  
STEP=1  
SUB =1  
TIME=1  
SINT      (AVG)  
BOTTOM  
DMX =.023857  
SMN =189.902  
SMX =13643
```

```
A  =937.286  
B  =2432  
C  =3927  
D  =5422  
E  =6916  
F  =8411  
G  =9906  
H  =11401  
I  =12895
```

**Figure 2.6-11 - W74 Guide Tube S.I. Contour Plot (Bottom Fiber) -
15g NCT Side Drop, Uniform Fuel Loading**

This page intentionally left blank.

2.6.8 Corner Drop

The corner drop condition of 10CFR71.71(c)(8) applies only to rectangular fiberboard or wood packages weighing less than 110 pounds, or cylindrical fiberboard or wood packages weighing less than 220 pounds. Therefore, the FuelSolutions™ W74 canister need not be evaluated for the NCT corner drop.

2.6.9 Compression

The compression condition, as specified in 10CFR71.71(c)(9), applies only to packages weighing less than 5,000 pounds. The FuelSolutions™ TS125 Transportation Package exceeds a weight of 5,000 pounds, and therefore does not need to be evaluated for NCT compression.

2.6.10 Penetration

The penetration condition of 10CFR71.71(c)(10) does not apply to the FuelSolutions™ W74 canisters since they are protected against penetration by the FuelSolutions™ TS125 Transportation Cask body.

This page intentionally left blank.

2.7 Hypothetical Accident Conditions

When subjected to Hypothetical Accident Conditions (HACs) as specified in 10CFR71.73, the FuelSolutions™ W74 canisters meet the performance requirements specified in Subpart E of 10CFR71. This is demonstrated in the following subsections where the W74 canisters are evaluated for each accident condition sequentially in accordance with 10CFR71.73(a), considering the cumulative damage sustained from the preceding accident conditions, and shown to meet the applicable design criteria.

2.7.1 Free Drop

Subpart F of 10CFR71 requires that a 30-foot free drop be considered for the transportation package. The free drop is postulated to occur onto a flat, essentially unyielding, horizontal surface, and the transportation cask is to strike the surface in a position for which maximum damage is expected. This section presents the structural evaluation of the W74 canisters for the range of HAC free drop orientations expected to cause maximum damage, including:

- End Drop with the package longitudinal axis oriented vertically.
- Side Drop with the package longitudinal axis oriented horizontally.
- Corner Drop with the package center of gravity located directly over the corner of impact (i.e., 21° with respect to vertical).
- Oblique Drops, including both primary and secondary (slapdown) impacts, with the package longitudinal axis oriented at angles of 30°, 45°, 60°, and 75° with respect to vertical.

For the HAC end drop, corner drop, and oblique drops, impacts on both ends of the package are evaluated. In addition, a range of circumferential orientations are evaluated for certain W74 canister components to determine the maximum damage resulting from the HAC free drop loading.

The transportation package peak rigid body accelerations for the impact orientations considered are reported in Section 2.12.2 of the FuelSolutions™ TS125 Transportation Cask SAR. As discussed in Section 2.12.2 of the FuelSolutions™ TS125 Transportation Cask SAR, the peak rigid-body accelerations of the transportation package are calculated for both hot and cold impact conditions. The hot impact conditions consist of NCT hot thermal loading (i.e., maximum impact limiter temperature of 200°F), minimum crush strength of the impact limiter energy absorbing material considering manufacturing tolerances, and a maximum package weight of 285 kips. Conversely, the cold impact conditions consist of NCT cold thermal loading with zero decay heat (i.e., minimum impact limiter temperature of -20°F), maximum crush strength of the impact limiter energy absorbing material considering manufacturing tolerances, and a minimum package weight. The results of the drop loads evaluations show that the maximum peak rigid-body accelerations for each drop orientation result from the cold impact conditions. In order to minimize the number of specific analyses that must be performed and reviewed, upper bound design loads based on the heaviest W74 canisters and the maximum accelerations resulting from the cold impact conditions are used to determine the loads and stresses within the W74 canisters. Furthermore, the resulting stresses are compared to lower bound allowable

stresses, calculated using material properties at the upper-bound design temperatures shown in Table 2.6-1 that bound the maximum temperatures resulting from the NCT hot thermal condition.

The HAC free drop equivalent static design loads are developed as described in Section 2.12.2. The equivalent static design loads, are determined by multiplying the maximum peak rigid-body accelerations by a dynamic load factor (DLF) to account for possible dynamic amplification of the response within the structure. The derivation of the DLFs and equivalent static design loads for each HAC free drop orientation are presented in Section 2.12.2. The resulting equivalent static design loads and bounding design loads used for the structural evaluation of the W74 canisters are summarized in Table 2.12-6.

2.7.1.1 End Drop

The W74 canister is evaluated for an HAC end drop, occurring on either the top or bottom end of the package, considering the worst-case initial conditions in accordance with Regulatory Guide 7.8. As discussed in Section 2.7.1, the structural evaluation of the W74 canisters for the HAC end drop is performed using equivalent static loads that account for possible dynamic amplification within the structure. As discussed in Section 2.12.2, a bounding 60g HAC end drop equivalent static acceleration load is used for the structural evaluation of the W74 canister. The structural evaluation of the W74 canister for the bounding 60g HAC end drop design load is presented in the following sections. Each of the W74 canister components are evaluated separately, considering the boundary conditions and loading due to all other W74 canister components.

2.7.1.1.1 General and LTP Spacer Plates

For the HAC end drop, the LTP spacer plates and general spacer plates are supported by the four support tube assemblies. The SNF assemblies and damaged fuel canisters in the upper and lower basket assemblies are supported by the end of the canister shell cavity or the engagement spacer plate, depending on the end drop orientation (i.e., bottom or top). Therefore, the SNF assemblies and damaged fuel cans do not load the W74 spacer plates for the HAC end drop. The guide tubes in the W74T upper and lower basket assemblies are not mechanically fastened to the spacer plates. Instead, they are captured between the engagement spacer plate and the ends of the canister shell cavity. The guide tube assemblies in the W74M upper and lower basket assemblies are secured to the bottom end LTP spacer plate with attachment brackets. Therefore, the bottom end LTP spacer plates in the W74M upper and lower basket assemblies are loaded by their own weight, plus the weight of 28 guide tube assemblies. All other W74 general and LTP spacer plates are loaded only by their own weight.

For the HAC end drop, the W74 spacer plates are loaded in the longitudinal direction only. Consequently, the W74 spacer plate ligaments do not experience any significant axial compressive stresses and buckling is not a credible failure mode. The stress evaluation of the W74 general and LTP spacer plates for the HAC end drop loading is discussed in the following paragraphs.

General Spacer Plate

As discussed above, the W74 general spacer plates are loaded only by their own weight for the 60g HAC end drop. The maximum primary membrane and primary membrane plus bending stress intensities in the W74 general spacer plate resulting from a 60g end drop load are calculated by scaling the maximum stresses resulting from vertical dead weight loading. As shown in Section 3.5.3.2.1 of the FuelSolutions™ W74 Canister Storage FSAR, the membrane stress due to vertical dead weight loading is negligible. In addition, the maximum membrane plus bending stress intensity in the W74 general spacer plate due to vertical dead weight loading is 0.39 ksi. Therefore, the maximum membrane plus bending stress intensity in the W74 general spacer plate resulting from the 60g end drop loading is 23.4 ksi (=0.39 ksi x 60g/1g).

The Service Level D allowable membrane plus bending stress intensity for the general spacer plate carbon steel material at a bounding design temperature of 700°F is 113.1 ksi. Therefore, minimum design margin in the W74 general spacer plate for the bounding 60g HAC end drop is:

$$P_m + P_b: DM = \frac{113.1}{23.4} - 1 = +3.83$$

Therefore, the W74 general spacer plates meet the Service Level D allowable stress design criteria for the bounding 60g HAC end drop loading.

LTP Spacer Plate

As discussed in Section 2.1.1.2, the attachment brackets that secure the W74M guide tubes to the bottom end LTP spacer plates in the upper and lower basket assemblies are designed to fail when subjected to large longitudinal loading, such as those resulting from the HAC end drop. The designed failure mode of the W74M guide tube attachment brackets prevents overloading of the bottom end LTP spacer plate and its welds to the support tubes for the HAC end drop. As discussed in Section 3.7.3.2.1 of the FuelSolutions™ W74 Canister Storage FSAR, the W74M guide tube attachment brackets have an ultimate load capacity of less than 20g. Therefore, the W74M LTP spacer plates are evaluated for two end drop loading conditions: (1) a 20g end drop acceleration for which the bottom end LTP spacer plate supports its own weight and the weight of all 28 guide tubes, and (2) a 60g end drop acceleration for which the LTP spacer plate supports only its own weight.

The maximum primary membrane and primary membrane plus bending stress intensities in the W74 LTP spacer plates resulting from the end drop loading are calculated by scaling the vertical dead weight stresses by the ratio of the longitudinal g-loads. As shown in Section 3.5.3.2.1 of the FuelSolutions™ W74 Canister Storage FSAR, the membrane stress intensities in the LTP spacer plates due to vertical dead weight loading are negligible. In addition, the maximum membrane plus bending stress intensity in the W74 bottom end LTP spacer plate due to vertical dead weight loading is 0.69 ksi. Therefore, the maximum membrane plus bending stress intensity in the W74 bottom end LTP spacer plate resulting from a 20g end drop load (i.e., ultimate capacity of guide tube attachment brackets) is 13.8 ksi (=0.69 ksi x 20g/1g). As shown in Section 3.5.3.2.1 of the FuelSolutions™ W74 Canister Storage FSAR, the maximum membrane plus bending stress intensity in the W74 LTP spacer plate due to vertical dead weight loading is 0.15 ksi. Therefore, the maximum membrane plus bending stress intensities in the W74 LTP spacer plate resulting

from the 60g end drop loading is 9.0 ksi (=0.15 ksi x 60g/1g). Therefore, the maximum membrane plus bending stress intensity of 13.8 ksi occurs in the bottom end LTP spacer plate.

The Service Level D allowable membrane plus bending stress intensity for the W74M LTP spacer plate SA-240, Type XM-19 stainless steel material at a bounding design temperature of 700°F is 90.8 ksi. Therefore, minimum design margin in the W74 LTP spacer plate for the bounding 60g HAC end drop loading is:

$$P_m + P_b: DM = \frac{90.8}{13.8} - 1 = +5.58$$

Therefore, the W74 LTP spacer plates meet the Service Level D allowable stress design criteria for the bounding 60g HAC end drop loading.

2.7.1.1.2 Engagement Spacer Plate

In the event of an end drop, the W74 engagement spacer plate supports its own weight plus the entire weight of the basket assembly opposite the end of impact, including 32 fuel assemblies (i.e., the five centermost basket openings are blocked-out and contain no fuel) and four damaged fuel canisters. The engagement spacer plate is supported longitudinally by the four support tubes in the basket assembly beneath it. Since the weight of the upper basket assembly (not including the engagement spacer plate) is equal to the weight of the lower basket assembly, the engagement spacer plate loading is equal for a top end or bottom end drop. In addition, the engagement spacer plate support conditions are identical for a top or bottom end drop. Therefore, the W74 engagement spacer plate stresses are assumed to be equal for either a top or bottom end drop.

The W74 engagement spacer plate stress analysis for the HAC end drop loading is performed using the quarter symmetry finite element model described in Section 2.12.4.2.4. The inertial loads from the basket assembly, SNF assemblies, and damaged fuel canisters that rest on the engagement spacer plate are modeled as uniform pressure loads applied to the regions of the engagement spacer plate on which they bear. The applied pressure loads corresponding to the bounding 50g HAC end drop load are calculated as described in Section 2.12.4.2.4. In addition to these loads, the inertial load due to the engagement spacer plates own mass is included by applying a 50g longitudinal acceleration to the model.

Longitudinal restraint of the engagement spacer plate is provided by the support tubes on which the engagement spacer plate bears. Only those nodes in the region of the support tube that are loaded in compression are restrained such that the engagement spacer plate is not prevented from uplifting. The engagement spacer plate is assumed to pivot about the two exterior edges of the support tube, which face toward the center of the basket assembly. This is verified by HAC end drop stress analysis results, which show that the reaction forces at all constrained nodes are compressive and that the plate deflects away from the tube in all other regions.

A linear-elastic static analysis is performed to determine the engagement spacer plate stresses due to a 50g HAC end drop load. The maximum stress intensities in the W74 engagement spacer plate due to the 60g HAC end drop design loading are determined by scaling the maximum stress intensities calculated for the 50g HAC end drop loading by 60g/50g. The maximum primary membrane and primary membrane plus bending stress intensities in the engagement spacer plate

due to a 50g HAC end drop are 30.2 ksi and 37.0 ksi, respectively. Therefore, the maximum primary membrane and primary membrane plus bending stress intensities in the W74 engagement spacer plate due to a 60g HAC end drop are 36.2 ksi (=30.2 ksi x 60g/50g) and 44.4 ksi (=37.0 ksi x 60g/50g), respectively.

The W74M and W74T engagement spacer plates are fabricated from SA-240, Type XM-19 stainless steel. The Service Level D allowable primary membrane and primary membrane plus bending stress intensities for Type XM-19 stainless steel at an upper bound design temperature of 500°F are 62.4 ksi and 93.6 ksi, respectively. Therefore, the minimum design margins for the bounding 60g HAC end drop load are:

$$P_m: DM = \frac{62.4}{36.2} - 1 = +0.73$$

$$P_m + P_b: DM = \frac{93.6}{44.4} - 1 = +1.11$$

Therefore, the W74 engagement spacer plate meets the Service Level D allowable stress design criteria for the HAC end drop condition.

2.7.1.1.3 Support Tubes and Support Sleeves

Stress and buckling evaluations are performed for the most heavily loaded W74 support tubes and support sleeves for the bounding 60g HAC end drop loading in this section. In addition, the structural evaluations of the W74M and W74T support tube attachment welds are presented in this section. The structural evaluation of the W74 support tubes for HAC end drop loading is discussed in the following paragraphs.

Support Tube Stress Evaluation

When subjected to the HAC end drop loading, the basket assembly support tubes nearest the impacting end provide longitudinal support for their own weight, plus the weight of the spacer plates and sleeves, and the entire weight of the basket assembly and its SNF assemblies opposite the impacting end. The W74 support tube HAC end drop stress evaluation is performed for the most heavily loaded support tubes. As shown in Table 2.2-1, the weight of the W74M basket assemblies bounds that of the W74T basket assemblies. Therefore, since the W74M and W74T support tube cross sections are identical, the stresses in the W74M lower basket assembly support tubes bound those in the W74T lower basket support tubes. Since both the W74M and W74T support tubes are fabricated from Type XM-19 stainless steel, the minimum design margins for the HAC end drop condition are those of the W74M basket support tubes.

The stresses in the W74M basket assembly support tubes due to the bounding 60g HAC end drop acceleration are determined by scaling the maximum stresses calculated for a 50g bottom end drop load in the Section 3.7.3.2.3 of the FuelSolutions™ W74 Canister Storage FSAR by 60g/50g. As shown in Section 3.7.3.2.3 of the FuelSolutions™ W74 Canister Storage FSAR, the maximum primary membrane and membrane plus bending stress intensities in the W74 support tube due to a 50g bottom end drop are $P_m = 18.8$ ksi and $P_m + P_b = 19.7$ ksi, respectively. Therefore, the maximum primary membrane and membrane plus bending stress intensities in the

W74 support tube due to the bounding 60g HAC end drop are $P_m = 22.6$ ksi and $P_m + P_b = 23.6$ ksi, respectively.

The Service Level D allowable primary membrane and primary membrane plus bending stress intensities for SA-240, Type XM-19 stainless steel at 600°F are 61.5 ksi and 92.2 ksi, respectively. Therefore, the minimum design margins in the W74 support tubes for the bounding 60g HAC end drop loading are:

$$P_m : DM = \frac{61.5}{22.6} - 1 = +1.72$$

$$P_m + P_b : DM = \frac{92.2}{23.6} - 1 = +2.91$$

Therefore, the W74 support tubes meet the Service Level D allowable stress design criteria for the bounding 60g HAC end drop load.

Support Tube Buckling Evaluation

Buckling of the most heavily loaded W74 support tubes is evaluated for the HAC end drop using the criteria of NUREG/CR-6322 for linear-type supports subjected to combined axial compression and bending stresses. The maximum axial compressive stress in the most heavily loaded W74 support tube is determined by scaling the maximum axial compressive calculated for a 50g bottom end drop load in the Section 3.7.3.2.3 of the FuelSolutions™ W74 Canister Storage FSAR by 60g/50g. As shown in Section 3.7.3.2.3 of the FuelSolutions™ W74 Canister Storage FSAR, the maximum axial stresses in the W74M support tube due to a 50g bottom end drop is $f_a = 16.1$ ksi. Therefore, the maximum axial stress in the W74M support tubes due to the bounding 60g HAC end drop load is 19.3 ksi.

The support tube bending stress in the critical buckling span due to the combined effects of the moment reaction from the spacer plates and the P-δ effect caused by the bow in the support tube due to lateral thermal gradients is determined using hand calculations. The maximum bending moment in the support tube due to a 60g HAC end drop load (M_{SP}) is determined by multiplying the support tube moment calculated for vertical dead weight loading in the FuelSolutions™ W74 Canister Storage FSAR by 60. As shown in Section 3.5.3.4.1 of the FuelSolutions™ W74 Canister Storage FSAR, the maximum support tube moment for vertical dead weight loading is 158.7 inch-pounds. Therefore, the maximum bending moment in the support tube due to a 60g HAC end drop load is $M_{SP} = 9.5$ inch-kips. The maximum axial compressive load in the most heavily loaded W74 support tube due to a 60g HAC end drop load is determined by scaling the maximum axial compressive load calculated for a 50g bottom end drop in the FuelSolutions™ W74 Canister Storage FSAR by 60g/50g. As shown in Section 3.7.3.2.3 of the FuelSolutions™ W74 Canister Storage FSAR, the maximum axial load in the support tubes due to the 50g end drop load is 1,500 pounds, or 375 pounds per support tube. Therefore, the maximum axial compressive load in the support tube due to a 60g HAC end drop load is $P = 450$ kips.

$$f_b = \frac{(M_{SP} + P\delta)c}{I} = 0.5 \text{ ksi}$$

where M_{SP} and P are defined above, and:

- c = 4.45 in., distance from support tube centroid to outer fiber
- I = 273 in⁴, support tube moment of inertia
- δ = 0.048 in., maximum lateral deflection of support tube due to bounding NCT thermal gradient, per Section 2.6.1.2.3

Per NUREG/CR-6322, members subjected to combined compression and bending must satisfy the following equations:

$$\frac{f_a}{F_a} + \frac{C_m f_{bx}}{\left(1 - \frac{f_a}{F'_{ex}}\right) F_{bx}} + \frac{C_m f_{by}}{\left(1 - \frac{f_a}{F'_{ey}}\right) F_{by}} \leq 1.0$$

$$\frac{f_a}{2 \times 0.6 S_y} + \frac{f_{bx}}{F_{bx}} + \frac{f_{by}}{F_{by}} \leq 1.0$$

Per NUREG/CR-6322, the allowable compressive stress is defined as follows:

$$F_a = \frac{P_{EQ40}}{A_g}$$

where:

$$\begin{aligned} A_g &= \text{gross area of each support tube} \\ &= (8.90)^2 - (7.40)^2 - 4(0.75)^2 / 2 \\ &= 23.3 \text{ in}^2 \end{aligned}$$

P_{EQ40} is the allowable compressive load determined in accordance with Equation 40 of NUREG/CR-6322 as follows:

$$P_{EQ40} = \frac{(P_{EQ45})(P_{EQ33})}{P_{EQ43}} = 536 \text{ kips}$$

where P_{EQ45} , P_{EQ33} , and P_{EQ43} are the allowable compressive loads from Equations (45), (33), and (43) of NUREG/CR-6322, which are calculated as follows:

$$\lambda = \left(\frac{KL}{r}\right) \left(\frac{1}{\pi}\right) \sqrt{\frac{S_y}{E}} = 0.19$$

$$P_{EQ45} = \left(0.47 - \frac{120\lambda}{444\sqrt{2}}\right) S_y A_g = 377 \text{ kips (for } \lambda \leq \sqrt{2})$$

$$P_{EQ33} = \frac{(1-\lambda^2/4)}{1.11+0.5\lambda+0.17\lambda^2-0.28\lambda^3} S_y A_g = 712 \text{ kips (for } 0 \leq \lambda \leq 1)$$

$$P_{EQ43} = \frac{(1-\lambda^2/4)}{\frac{5}{3} + \frac{3}{8} \left(\frac{\lambda}{\sqrt{2}}\right) - \frac{1}{8} \left(\frac{\lambda}{\sqrt{2}}\right)^3} S_y A_g = 501 \text{ kips (for } \lambda \leq \sqrt{2})$$

where:

K = 0.65, effective length factor for a fixed-fixed column per Figure 6 of NUREG/CR-6322

L = 80.75 inches, unsupported length of support tube, conservatively assumed equal to distance between centerlines of the top and bottom LTP spacer plates

r = support tube radius of gyration

$$= \sqrt{\frac{I}{A_g}} = \sqrt{\frac{273}{23.3}} = 3.42 \text{ inches}$$

S_y = 37.3 ksi, yield strength of Type XM-19 stainless steel at 600°F

E = 25.3(10)⁶ psi, elastic modulus of Type XM-19 stainless steel at 600°F

Therefore, the allowable compressive stress for the most heavily loaded support tube is:

$$F_a = \frac{536 \text{ kips}}{23.3 \text{ in}^2} = 23.0 \text{ ksi}$$

The Euler buckling stress, including a 1.46 factor of safety for stainless steel material and hypothetical accident conditions, per Section 6.32 of NUREG/CR-6322, is defined as:

$$F'_e = \frac{\pi^2 E}{1.46(KL/r)^2} = 726 \text{ ksi}$$

The allowable bending stress for compact sections, F_b, is defined in NUREG/CR-6322 as:

$$F_b = fS_y = 45.5 \text{ ksi}$$

where the plastic shape factor, f, is calculated using Roark, Table 1, Case 3, as follows:

$$f = \frac{(d^3 - d_i^3)d}{8I} = \frac{((8.90 \text{ in})^3 - (7.40 \text{ in})^3)(8.90 \text{ in})}{8(273 \text{ in}^4)} = 1.22$$

Interaction equations (26) and (27) are satisfied as follows, where C_m is conservatively assumed as 1.0 for equation (26):

$$\frac{19.3}{23.0} + \frac{(1.0)(0.5)}{\left(1 - \frac{19.3}{726}\right)(45.5)} + \frac{(1.0)(0.5)}{\left(1 - \frac{19.3}{726}\right)(45.5)} = 0.86 \quad (26)$$

$$\frac{19.3}{2 \times 0.6(37.3)} + \frac{0.5}{45.5} + \frac{0.5}{45.5} = 0.45 \quad (27)$$

These results show that the W74 support tubes are adequate to withstand the HAC end drop loads. Note that the drop loads need not be combined with the thermal stresses resulting from longitudinal differential thermal expansion, because the axial thermal stress acts as a tension preload that is relieved by the HAC end drop axial compressive loading.

The minimum design margin for buckling of the W74 support tubes is:

$$DM = \frac{1.00}{0.86} - 1 = +0.16$$

Since the stresses in the W74 support tube resulting from the bounding 60g HAC end drop load are lower than the support tube yield strength, inelastic buckling is not a credible failure mode and need not be evaluated.

W74M Support Tube to LTP Spacer Plate Weld Stress Evaluation

The W74M support tubes are welded to the top and bottom end LTP spacer plates with ½-inch partial penetration groove welds, with ¼-inch cover fillets on all four sides of each support tube. For the HAC end drop, the support tube to LTP spacer plate welds nearest the impacting end are loaded by the weight of the 12 general spacer plates, the support sleeves, plus the self weight of the LTP spacer plate. The W74M lower basket weld is the most heavily loaded since the overall length of support sleeves in the lower basket (and weight) is slightly higher than that of the upper basket. The total shear load on each support tube weld due to the bounding 60g HAC end drop load is determined by scaling the maximum weld shear stress calculated for a 50g bottom end drop in the FuelSolutions™ W74 Canister Storage FSAR by 60g/50g. As shown in Section 3.7.3.2.3 of the FuelSolutions™ W74 Canister Storage FSAR, the maximum shear stress due to the 50g end drop load is 3.2 ksi. Therefore, the maximum weld shear stress due to the 60g HAC end drop load is 3.8 ksi.

In accordance with Regulatory Guide 7.8, the HAC end drop loading is evaluated in combination with NCT thermal loading. As shown in Section 2.6.1.3.3, the bounding NCT thermal loading results in a maximum shear stress of 1.44 ksi in the W74M support tube to LTP spacer plate welds. This weld shear stress is due primarily to axial loads resulting from differential longitudinal expansion of the support tubes and support sleeves. For the HAC end drop loading, the axial compressive loads resulting from the impact loads cause the support sleeves to compress. This compression relieves the preload condition caused by thermal expansion. Therefore, the weld shear stress due to NCT thermal and HAC end drop loading is not additive.

As shown above, the 3.8 ksi weld shear stress due to the HAC end drop loading is greater than that due to NCT thermal loading and is controlling for this load combination.

The allowable stresses for welds are equal to the base material allowable stress multiplied by the applicable weld quality factor from Table NG-3352-1 of the ASME B&PV Code. In accordance with Table NG-3352-1, the weld quality factor for a single groove weld with a surface PT examination is 0.40. The Service Level D allowable shear stress for SA-240, Type XM-19 stainless steel at an upper bound design temperature of 600°F is 35.0 ksi. Therefore, the Service Level D allowable shear stress for the W74M support tube to LTP spacer plate weld is 14.0 ksi (= 35.0 x 0.40). The minimum design margin for shear stress in the W74M support tube to LTP spacer plate weld due to the 60g HAC end drop loading is:

$$DM = \frac{14.0}{3.8} - 1 = +2.68$$

The W74M support tube to LTP spacer plate weld meets the Service Level D allowable stress criteria for the bounding 60g HAC end drop loading.

W74T Support Tube to Attachment Sleeve Weld Stress Evaluation

The W74T support tubes are welded to the top and bottom attachment sleeves, with ¼-inch fillet welds on all four sides of each support tube. For the HAC end drop, the support tube to attachment sleeve welds nearest the impacting end are loaded by the weight of the 13 general spacer plates, the support sleeves, plus the self weight of one attachment sleeve. The W74T lower basket weld is the most heavily loaded since the overall length of support sleeves in the lower basket (and weight) is slightly higher than that of the upper basket. The maximum shear stress in the W74T support tube to attachment sleeve weld due to the bounding 60g HAC end drop is determined by scaling the weld shear stress calculated in FuelSolutions™ W74 Canister Storage FSAR for a 50g bottom end drop condition by 60g/50g. As shown in Section 3.7.3.2.3 of the FuelSolutions™ W74 Canister Storage FSAR, the maximum weld shear stresses due to a 50g bottom end drop is 8.6 ksi. Therefore, the maximum shear stress in the W74T support tube to attachment sleeve weld due to the bounding 60g HAC end drop load is 10.3 ksi.

In accordance with Regulatory Guide 7.8, the HAC end drop loading is evaluated in combination with NCT thermal loading. As shown in Section 2.6.1.3.3, the bounding NCT thermal loading results in a maximum shear stress of 3.32 ksi in the W74T support tube to attachment sleeve welds. This weld shear stress is due primarily to axial loads resulting from differential longitudinal expansion of the support tubes and support sleeves. For the HAC end drop loading, the axial compressive loads resulting from the impact loads cause the support sleeves to compress. This compression relieves the preload condition caused by thermal expansion. Therefore, the weld shear stress due to NCT thermal and HAC end drop loading is not additive. As shown above, the 10.3 ksi weld shear stress due to the HAC end drop loading is greater than that due to NCT thermal loading and is controlling for this load combination.

The allowable stresses for welds are equal to the base material allowable stress multiplied by the applicable weld quality factor from Table NG-3352-1 of the ASME B&PV Code. In accordance with Table NG-3352-1, the weld quality factor for a single fillet weld with a surface PT examination is 0.40. The Service Level D allowable shear stress for SA-240, Type XM-19

stainless steel at an upper bound design temperature of 600°F is 35.0 ksi. Therefore, the Service Level D allowable shear stress for the W74T support tube to attachment sleeve weld is 14.0 ksi (= 35.0 x 0.40). The minimum design margin for shear stress in the W74T support tube to attachment sleeve weld due to the 60g HAC end drop loading is:

$$DM = \frac{14.0}{10.3} - 1 = +0.36$$

The W74T support tube to attachment sleeve weld meets the Service Level D allowable stress design criteria for the bounding 60g HAC end drop loading.

Support Sleeve Stress Evaluation

When subjected to the HAC end drop loading, each W74 support sleeve is loaded by its own weight, plus the weight of the support sleeves and general spacer plates within the basket assembly. The most heavily loaded support sleeve is nearest the impacting end.

The axial compressive stress in the most heavily loaded W74 support sleeve due to a bounding 60g HAC end drop load is determined using hand calculations. The 0.125-inch thick retainer portion of the sleeve is conservatively assumed to provide no structural support for axial loads. Therefore, the entire axial load is carried by the 0.1875-inch thick support sleeve angle.

The maximum axial compressive stress in the most heavily loaded W74 support sleeve is calculated as:

$$f_a = \frac{P}{A_{sl}} = 9.7 \text{ ksi}$$

where:

$$\begin{aligned} P &= \text{Total axial load from the four support sleeves and 12 spacer plates} \\ &= (W_{sp} + W_{sl})(60g) \\ &= 202.3 \text{ kips} \end{aligned}$$

$$\begin{aligned} W_{sp} &= \text{Weight of the 12 spacer plates} \\ &= 12 (230 \text{ lbs}) \\ &= 2,760 \text{ lbs} \end{aligned}$$

$$\begin{aligned} W_{sl} &= \text{Weight of the four sets of sleeve segments (including retainer angles)} \\ &= L_{sl} (A_{sl} + A_{ra}) \rho_{ss} \\ &= 611 \text{ lbs} \end{aligned}$$

$$\begin{aligned} L_{sl} &= \text{Maximum total length of the sleeve segments} \\ &= 81.50 - 2.375 - 12(0.75) \\ &= 70.125 \text{ in.} \end{aligned}$$

$$\begin{aligned} A_{sl} &= \text{Section area of four support sleeves, neglecting retainer angles} \\ &= 20.86 \text{ in}^2 \end{aligned}$$

$$\begin{aligned} A_{ra} &= \text{Section area of four retainer angles} \\ &= 4 [2(9.1 + 0.125/2)(0.125)] \\ &= 9.163 \text{ in}^2 \end{aligned}$$

$$\rho_{ss} = 0.29 \text{ lb/in}^3, \text{ weight density of stainless steel}$$

The Service Level D allowable primary membrane (P_m) and primary membrane plus bending (P_m+P_b) stress intensity for the support sleeve Type 304 stainless steel at 600°F are 39.4 ksi and 59.0 ksi, respectively. Therefore, the minimum design margins in the most heavily loaded W74 support sleeve due to the 60g HAC end drop loading are:

$$P_m : DM = \frac{39.4}{9.7} - 1 = +3.06$$

$$P_m + P_b : DM = \frac{59.0}{9.7} - 1 = +5.08$$

Therefore, the most heavily loaded W74 support sleeves meet the Service Level D allowable stress design criteria for the 60g HAC end drop loading.

In accordance with Regulatory Guide 7.8, the HAC end drop loading is evaluated in combination with NCT thermal loading. General thermal stresses in the W74 support sleeves are classified as secondary in accordance with Subsection NG of the ASME B&PV Code. For Service Level D conditions, Appendix F of the ASME B&PV Code does not require evaluation of secondary stress. However, the combined effects of thermal and impact loading are considered in the buckling evaluation of the W74 support sleeves.

Support Sleeve Buckling Evaluation

The stability of the support sleeves is evaluated for the HAC end drop using plate buckling theory as described in Section 5.3 of NUREG/CR-6322. The sleeve walls are conservatively evaluated with the boundary conditions applied per Case E of Figure 8 of NUREG/CR-6322. These boundary conditions represent a plate with uniaxial loading; one edge free and the other edge simply supported. The theoretical buckling stress for a plate with a uniaxial compressive load per Case E and equation 11 in NUREG/CR-6322 is calculated as follows:

$$\sigma_e = k_c \frac{\pi^2 D}{b^2 h} = 20.5 \text{ ksi}$$

where:

$$k_c = 5.0, \text{ buckling coefficient corresponding to } a/b=0.46 \text{ from Figure 8 of NUREG/CR-6322}$$

$$a = 6.38 \text{ in.}, \text{ maximum support sleeve length}$$

$$b = 14.0 \text{ in.}, \text{ width of support sleeve angle}$$

$$h = 0.1875 \text{ in.}, \text{ support sleeve plate thickness}$$

$$D = \frac{Eh^3}{12(1-\nu^2)}, \text{ plate cross section rigidity}$$
$$= 15.3 \text{ in-kips}$$

$$\nu = 0.3, \text{ Poisson's ratio for stainless steel}$$

$$E = 25.3(10)^6 \text{ psi, modulus of elasticity of SA-240, Type 304 stainless steel at } 600^\circ\text{F}$$

Paragraph F-1331.5 of Appendix F of the ASME Code and Section 6.5 of NUREG/CR-6322 require that the compressive stresses resulting from Service Level D loadings be limited to 2/3 of the critical buckling load. Therefore, the corresponding buckling stress limit is 2/3 of σ_c , or 13.7 ksi.

As shown above, the maximum axial compressive stress in the most heavily loaded W74 support sleeve is 9.7 ksi for the bounding 60g HAC end drop load. In accordance with Regulatory Guide 7.8, the HAC end drop loading is evaluated in combination with NCT thermal loading. As shown in Section 2.6.1.3.3, the bounding NCT thermal loading results in a maximum axial compressive stress of 2.4 ksi in the W74M support sleeves. This axial compressive stress is due primarily to axial loads resulting from differential longitudinal expansion of the support tubes and support sleeves. For the HAC end drop loading, the axial compressive loads resulting from the impact loads cause the support sleeves to compress. This compression relieves the preload condition caused by thermal expansion. Therefore, the support sleeve axial compressive stress due to NCT thermal and HAC end drop loading is not additive. As shown above, the 9.7 ksi axial compressive stress due to the HAC end drop loading is greater than that due to NCT thermal loading and is controlling for this load combination.

The minimum design margin for buckling of the most heavily loaded W74 support sleeve is:

$$\text{D.M.} = \frac{13.7}{9.7} - 1 = +0.41$$

Therefore, the most heavily loaded W74 support sleeves meet the NUREG/CR-6322 accident condition design criteria for buckling.

2.7.1.1.4 Guide Tubes

The W74 guide tubes support only their own weight for the HAC end drop loading. As discussed in Section 2.1.1.2, the W74M and W74T guide tube assemblies are equally sized and fabricated from the same materials. However, there are two different guide tube configurations, which differ in the number of neutron absorber sheets that are attached to the guide tube. All of the W74 guide tubes in the interior of the basket assemblies include two neutron absorber sheets on opposing faces, whereas the guide tubes on the perimeter of the basket assembly include only one neutron absorber sheet. Since no structural credit is taken for the support that the neutron absorber sheets provide to the guide tube, and their mass is assumed to load the guide tube, bounding structural evaluations of the W74 guide tube are performed for the interior guide tubes, which include two neutron absorber sheets.

Stress Evaluation

The guide tube stresses due to a bounding 60g HAC end drop load are determined using classical methods. The maximum stress occurs in the bottom end of the guide tubes, since it supports guide tube weight and has the smallest area due to the 1.5-inch high by 4.3-inch wide notches cut in two opposite sides of the guide tube. The uniform axial compressive stress at the bottom end of the guide tube due to a 60g HAC end drop load is calculated as follows:

$$f_a = \frac{WG}{A_{\text{bot}}} = 3.7 \text{ ksi}$$

where:

W = 83.1 lb., weight of heaviest W74 guide tube (109 lb., conservatively used)

G = 60g, equivalent static HAC end drop acceleration

A_{bot} = Cross-sectional area at the bottom of a guide tube
= 2.52 - 2(4.3)(0.09)
= 1.53 in²

Since axial compression is the only significant stress component in the guide tube for the HAC end drop, the primary membrane stress intensity is equal to 3.7 ksi.

The Service Level D allowable primary membrane stress intensity for SA-240, Type 316 stainless steel at 650°F is 40.0 ksi. Therefore, the minimum design margin in the W74 guide tube for primary membrane stress intensity due to the HAC end drop is:

$$P_m : DM = \frac{40.0}{3.7} - 1 = +9.81$$

Therefore, the W74 guide tubes meet the Service Level D allowable stress design criteria for the bounding 60g HAC end drop loading.

Buckling Evaluation

Buckling of the W74 guide tubes is evaluated in accordance with NUREG/CR-6322. The notched region at the bottom of the guide tubes has the lowest factor of safety against buckling due to the increased stresses in this region and formation of a free edge at the notch. The theoretical elastic buckling stress for the guide tube at the bottom notch region is determined using classical methods. The guide tube panel is evaluated as a rectangular plate under uniform compression of equal magnitude on the top and bottom opposing edges. The top, bottom, and corner of the plate are assumed to be simply supported and the other edge free as shown in Figure 2.7-1. The theoretical buckling stress for these conditions is determined using Roark, Table 35, Case 1d, as follows:

$$\sigma = K \frac{E}{1 - \nu^2} \left(\frac{t}{b} \right)^2 = 131.3 \text{ ksi}$$

where:

E = 25.1(10)³ ksi, elastic modulus of Type 316 stainless steel at 650°F

t = 0.090 in, thickness of the guide tube

b = 1.3 inches, width of the corner piece of guide tube panel

ν = 0.29, Poisson's ratio

K = 1.00 for a/b = 1.5/1.3 = 1.15

In accordance with NUREG/CR-6322, the allowable stress for the accident condition is limited to 2/3 of the critical stress, or 87.6 ksi. Therefore, the minimum design margin for buckling of the W74 guide tubes due to the bounding 60g HAC end drop loading is:

$$DM = \frac{3.7}{87.6} - 1 = +22.7$$

Therefore, the W74 guide tube will not buckle under a bounding 40g HAC end drop load. However, this stress does not control since the limiting stress is the P_m of 40.0 ksi evaluated above.

Neutron Absorber Panel Retainer Weld Stress Evaluation

The neutron absorber panels are attached to the guide tubes using stainless steel retainers. A minimum of seven retainers are used per neutron absorber panel. Each retainer is welded to the guide tube with a plug weld. The maximum tributary load supported by the most heavily loaded retainer for the 60g HAC end drop is bounded by the maximum tributary load due to the HAC oblique drop slapdown impact evaluated in Section 2.7.1.4.4. Therefore, no evaluation of the retainer weld stresses for the HAC end drop is required.

2.7.1.1.5 Canister Shell

This section presents the structural evaluation of the W74 canister shell for the HAC end drop. As discussed in Section 2, the W74 canister shell is evaluated for the HAC end drop to demonstrate that it does not fail or induce loading on the canister basket or SNF assemblies, which are not otherwise accounted for in the structural evaluation. The canister shell HAC end drop structural evaluation addresses the following:

- Stresses in the canister shell (not including stresses in the top shield plug) due to a top and bottom end drop.

- Stresses in the W74 canister top shield plug and its supports due to a bottom end drop.
- Buckling of the canister shell due to a top or bottom end drop.

The analysis shows that the W74 canister meets the applicable stress and buckling design criteria for the HAC end drop condition. This is demonstrated in the following sections.

2.7.1.1.5.1 Canister Shell Stresses

The W74 canister shell assembly is evaluated for a bounding 60g end drop using a combination of finite element analysis and closed form hand calculations. The stresses in all of the canister shell components, except for the top shield plug and the top shield plug support bar attachment welds, are evaluated using the axisymmetric finite element model discussed in Section 2.12.4.5. As discussed in Section 2.12.4.5, the top end shield plug assembly and shield plug supports are included in the axisymmetric model to account for the weight of the top shield plug and the loads transferred to the shell.

The load from the W74 canister contents (basket assembly and SNF assemblies) is supported on the impacted end of the transportation cask cavity. As discussed in Section 2.12.4.5, the load from the canister contents is modeled as a uniform pressure on the inner surface of the canister cavity, assuming a bounding payload weight of 57 kips. A vertical acceleration of 60g is applied to the model to account for the self weight of the shell assembly. Stress analyses are performed for a top end drop and a bottom end drop. The HAC top and bottom end drop loading is evaluated both with and without a bounding internal pressure load of 12 psig. Thermal loading is not evaluated in combination with the HAC end drop loading since the ASME Code classifies general thermal stresses as secondary and does not require evaluation of secondary stresses for accident conditions. The maximum canister shell stress intensities resulting from the 60g top and bottom end drop loads, analyzed with and without internal pressure loading, are reported in Table 2.7-2. The results show that all stresses within the canister shell are lower than the Service Level D allowable stresses.

2.7.1.1.5.2 Top Shield Plug Stresses

The W74 top shield plug assembly consists of a shield plate, 33 guide tube shield caps, and 4 support tube shield caps. The top shield plug is captured at the top end of the canister shell assembly between the canister shell top end inner closure plate and eight shield plug support bars. The most severe HAC end drop impact loading for the W74 top shield plug results from a bottom end drop. In the event of an HAC bottom end drop, the W74 top shield plug is loaded by its own weight and supported by eight shield plug support bars that are welded to the inside of the canister shell. In addition, the W74 top shield plug is conservatively assumed to support the entire weight of the canister shell inner and outer closure plates. The stresses in the W74 top shield plug and its supports are evaluated for a bounding 60g HAC bottom end drop loading.

As discussed in Section 2.1.1.1, the top shield plug may either be fabricated from a solid shield plate or a partitioned shield plate and individual shield caps (plugs) for each basket fuel cell. The maximum stresses in the solid and partitioned W74 top shield plate designs due to the bounding 60g HAC bottom end drop loading are determined by scaling the results from the on-site storage 50g bottom end drop stress evaluation by the ratio of the loads (i.e., 60g/50g).

The maximum bending stress in the solid W74 top shield plate is calculated for the 50g bottom end drop loading using hand calculations, treating the plate as simply supported with a uniform pressure load. The maximum bending stress in the solid W74 top shield plate for these conditions is 3.6 ksi. Therefore, the maximum bending stress in the solid W74 top shield plate resulting from a 60g bottom end drop load is 4.3 ksi (=3.6 ksi x 60g/50g).

As shown in Section 3.7.3.1 of the FuelSolutions™ W74 Canister Storage FSAR, the maximum primary membrane (P_m) and primary membrane plus bending (P_m+P_b) stress intensities in the partitioned W74 top shield plate resulting from a 50g bottom end drop load are 5.0 ksi and 27.1 ksi, respectively. Therefore, the maximum primary membrane (P_m) and primary membrane plus bending (P_m+P_b) stress intensities in the partitioned W74 top shield plate resulting from a 60g bottom end drop load are 6.0 ksi (=5.0 ksi x 60g/50g) and 32.5 ksi (=27.1 ksi x 60g/50g), respectively. The results show that the maximum stresses in the partitioned shield plate are substantially higher than those in the solid shield plate.

The Service Level D allowable primary membrane (P_m) and primary membrane plus bending (P_m+P_b) stress intensities for the W74 top shield plate SA-516, Grade 70 carbon steel material at a bounding design temperature of 300°F are 31.9 ksi and 47.9 ksi, respectively. Therefore, the minimum design margins in the partitioned W74 top shield plate due to the bounding 60g HAC end drop loading are:

$$P_m: DM = \frac{31.9}{6.0} - 1 = +4.32$$

$$P_m+P_b: DM = \frac{47.9}{32.5} - 1 = +0.47$$

As discussed above, the W74 top shield plug is supported by eight support bars, which are welded to the inside surface of the canister shell. Each shield plug support bar is welded to the canister shell. In the event of a bottom end drop, the shield plug support bar attachment welds are loaded in pure shear by the weight of the top shield plug assembly and the weight of the canister shell top end inner and outer closure plates. The maximum shear stress in the shield plug support bar weld due to the 60g HAC bottom end drop loading is calculated by scaling the results from the on-site storage 50g bottom end drop stress evaluation by the ratio of the loads (i.e., 60g/50g).

The maximum shear stress in the support bar welds calculated for a 50g bottom end drop load is shown to be 9.2 ksi in Section 3.7.3.1 of the FuelSolutions™ W74 Canister Storage FSAR. Therefore, the maximum shear stress in the support bar welds due to the 60g HAC bottom end drop loading is 11.1 ksi (=9.2 ksi x 60g/50g).

The Service Level D allowable shear stress for the weld is 16.2 ksi based on SA-240, Type 304 stainless steel material properties at a bounding design temperature of 300°F. Therefore, the minimum design margin for shear stress in the shield plug support bar welds due to a bounding 60g HAC bottom end drop load is:

$$DM = \frac{16.2}{11.1} - 1 = +0.46$$

The results of the W74 top shield plug stress evaluation show that the maximum stresses in the W74 top shield plug and its supports resulting from a bounding 60g HAC bottom end drop are lower than the corresponding Service Level D allowable stresses.

2.7.1.1.5.3 Canister Shell Buckling

The canister shell is evaluated for the impact loads resulting from the HAC end drop to assure that it has adequate design margin against buckling. The HAC end drop condition results in the highest axial compressive stresses in the canister shell. Internal pressure loads, which result in tensile stresses in the shell thereby offsetting the impact loads, are conservatively ignored for the buckling evaluation. For a HAC top end drop, the only significant loads on the W74 canister shell are due to its own weight and the weight of the bottom shield plug, bottom closure plate, and bottom outer plate. Similarly, for a bottom end drop, the only significant loads on the canister shell are due to its self-weight and the weight of the top shield plug assembly, top end inner closure plate, and top end outer closure plate. The load from the canister baskets and SNF assemblies does not load the canister shell, since it is supported directly by the impacting end of the canister shell. Since the weight of the W74 top end shield plug and top end inner and outer closure plates is higher than that of the bottom end shield plug and the bottom closure plate and bottom outer plate, the bottom HAC end drop condition is controlling. The buckling evaluation of the canister shell is performed in accordance with Code Case N-284-1.

The results of the canister shell 60g bottom end drop finite element analysis show that the maximum axial compressive stress in the canister shell due to a 60g bottom end drop load is 8.1 ksi. Therefore, the adjusted axial compressive stress, including a 1.34 factor of safety and a 0.207 capacity reduction factor in accordance with Code Case N-284, is 52.4 ksi ($=1.34 \times 8.1/0.207$).

The theoretical buckling stress, calculated in accordance with Paragraph –1712 of Code Case N-284 using the weaker canister shell material properties at an upper bound temperature of 400°F, is 298.4 ksi. Thus, the buckling interaction ratio for the canister shell is:

$$\frac{52.4}{298.4} = 0.18 \leq 1.0$$

The corresponding minimum design margin for buckling of the W74 canister shell due to the bounding 60g HAC end drop loading is +4.56 ($= 1.0/0.18 - 1$). Therefore, the W74 canister shell

meets the buckling design criteria of NUREG/CR-6322 for the bounding 60g HAC end drop loading.

2.7.1.1.6 HAC End Drop Summary

The results of the preceding HAC end drop structural analyses demonstrate that the W74 canisters have adequate structural integrity to satisfy the structural design criteria of Section 2.1.2 of this SAR. The results of the HAC end drop structural evaluation are summarized in Table 2.7-1.

The maximum stress intensities in each of the W74 canister components resulting from the bounding 60g HAC end drop loading meet the corresponding Service Level D allowable stress design criteria. Excluding buckling results, the lowest design margin for the HAC end drop is +0.36 for shear stress weld that connects the W74T support tubes and attachment sleeves. The minimum buckling design margin for the HAC end drop is +0.16 for the W74 support tubes. However, as shown in Figure 14 of NUREG/CR-6322, the factor of safety embedded in the buckling interaction equations for axial compressed stainless steel members is approximately 1.5 (for $\lambda \geq 0.19$). Therefore, the W74 support tubes provide a significant factor of safety against buckling.

The extent of damage sustained by the W74 canister for the HAC end drop is minimal. As discussed in Section 2.7.1.1.1, the stainless steel attachment brackets that secure the W74M guide tubes to the bottom end LTP spacer plate are designed to fail under HAC end drop loading. The resulting longitudinal shifting of the guide tube assembly relative to the SNF assembly is considered in the accident criticality evaluation presented in Chapter 6 of this SAR. The results of the criticality evaluation demonstrate that failure of the guide tube attachment brackets due to the HAC end drop loading does not affect the ability of the W74 canister to satisfy the subcriticality requirements of 10CFR71. Furthermore, the failure of the guide tube attachment brackets does not prevent retrieval of the SNF assemblies from the canister.

Table 2.7-1 - Summary of W74 Canister Basket Assembly HAC End Drop Design Margins

W74 Canister Component	Stress Type	Maximum S.I. (ksi)	Allowable S.I. (ksi)	Minimum Design Margin⁽¹⁾	Reference SAR Section
General Spacer Plate	P_m	(2)	75.4	(2)	2.7.1.1.1
	$P_m + P_b$	23.4	113.1	+3.83	2.7.1.1.1
LTP Spacer Plate	P_m	(2)	60.6	(2)	2.7.1.1.1
	$P_m + P_b$	13.8	90.8	+5.58	2.7.1.1.1
Engagement Spacer Plate	P_m	36.2	62.4	+0.73	2.7.1.1.2
	$P_m + P_b$	44.4	93.6	+1.11	2.7.1.1.2
Support Tube	P_m	22.6	61.5	+1.72	2.7.1.1.3
	$P_m + P_b$	23.6	92.2	+2.91	2.7.1.1.3
	Buckling	0.86 ⁽³⁾	1.0	+0.16	2.7.1.1.3
Support Sleeve	P_m	9.7	39.4	+3.06	2.7.1.1.3
	$P_m + P_b$	9.7	59.0	+5.08	2.7.1.1.3
	Buckling	9.7	13.7 ⁽⁴⁾	+0.41	2.7.1.1.3
W74M Support Tube to LTP Spacer Plate Weld	Shear	3.8	14.0 ⁽⁵⁾	+2.68	2.7.1.1.3
W74T Support Tube to Attachment Sleeve Weld	Shear	10.3	14.0 ⁽⁵⁾	+0.36	2.7.1.1.3
Guide Tube	P_m	3.7	40.0	+9.81	2.7.1.1.4
	Buckling	3.7	87.6 ⁽⁴⁾	+22.7	2.7.1.1.4
Canister Shell	P_m	14.1	46.2	+2.28	2.7.1.1.5.1
	$P_m + P_b$	32.6	69.3	+1.13	2.7.1.1.5.1
	Buckling	0.18 ⁽⁷⁾	1.0	+4.56	2.7.1.1.5.3
Top Shield Plug	P_m	6.0	31.9	+4.32	2.7.1.1.5.2
	$P_m + P_b$	32.5	47.9	+0.47	2.7.1.1.5.2
Alignment Bar Welds	Shear	11.1	16.2	+0.46	2.7.1.1.5.2

Notes:

- (1) Design margin is equal to (Allowable/Stress) - 1.
- (2) Membrane stress in the W74 spacer plates due to HAC end drop loading is insignificant.
- (3) Buckling interaction ratio calculated in accordance with NUREG/CR-6322.
- (4) The allowable axial compressive stress is limited to 2/3 of the theoretical buckling stress for HAC loading in accordance with NUREG/CR-6322.
- (5) The allowable weld stresses include a 35% weld quality factor in accordance with Table NG-3352-1 of the ASME B&PV Code.
- (6) The allowable stresses for the top inner closure weld include a 0.9 weld efficiency factor.
- (7) Buckling interaction ratio calculated in accordance with Code Case N-284.

**Table 2.7-2 - W74 Canister Shell HAC End Drop
Stress Analysis Results**

Shell Component	Stress Type	Allowable Stress ⁽¹⁾ (ksi)	Maximum Stress (ksi) [Location] ⁽²⁾				Minimum Design Margin
			Bottom End Drop		Top End Drop		
			Zero Internal Pressure	Max. Internal Pressure	Zero Internal Pressure	Max. Internal Pressure	
Top Outer Closure Plate	P _m	46.2	1.0 [1]	1.0 [1]	1.2 [1]	1.2 [1]	+37.5
	P _m +P _b	69.3	9.9 [1]	10.0 [1]	1.2 [1]	1.2 [1]	+5.93
Top Outer Closure Weld	P _m	37.0 ⁽³⁾	4.7 [5]	4.6 [5]	2.9 [5]	2.8 [5]	+6.87
Top Inner Closure Plate	P _m	46.2	1.9 [9]	1.8 [9]	1.5 [6]	1.5 [6]	+23.3
	P _m +P _b	69.3	19.8 [6]	17.5 [6]	1.5 [6]	1.5 [6]	+2.50
Top Inner Closure Weld	P _m	41.6 ⁽⁴⁾	12.1 [10]	11.6 [10]	1.9 [10]	1.9 [10]	+2.44
Cylindrical Shell	P _m	46.2	14.1 [14]	13.6 [14]	9.1 [22]	6.7 [22]	+2.28
	P _m +P _b	69.3	25.5 [15]	24.9 [15]	32.6 [22]	21.2 [22]	+1.13
Bottom Shell Extension	P _m	46.2	7.2 [24]	7.0 [24]	3.0 [23]	1.9 [23]	+5.42
	P _m +P _b	69.3	24.2 [25]	23.5 [25]	3.2 [23]	2.2 [23]	+1.86
Bottom End Closure	P _m	46.2	0.8 [26]	0.8 [27]	2.3 [28]	2.2 [28]	+19.1
	P _m +P _b	69.3	3.1 [28]	3.3 [28]	14.0 [26]	6.0 [26]	+3.95
Bottom End Plate	P _m	46.2	3.4 [33]	3.3 [33]	0.3 [33]	0.3 [33]	+12.6
	P _m +P _b	69.3	4.1 [33]	4.0 [33]	2.6 [32]	2.2 [32]	+15.9
Shell Extension Welds	Shear	27.7	12.3 [36]	12.0 [36]	1.1 [35]	0.9 [35]	+1.25

Notes:

- (1) Allowable stress intensities are based on the weaker of the W74M and W74T canister shell materials (SA-240, Type 304 stainless steel) properties at 300°F.
- (2) The section numbers corresponding to the locations of the maximum stresses in each canister shell assembly component are shown in Figures 2.12-19 and 2.12-20.
- (3) The allowable stresses for the top outer closure weld include a 0.8 weld efficiency factor in accordance with ISG-4.
- (4) The allowable stresses for the top inner closure weld include a 0.9 weld efficiency factor.

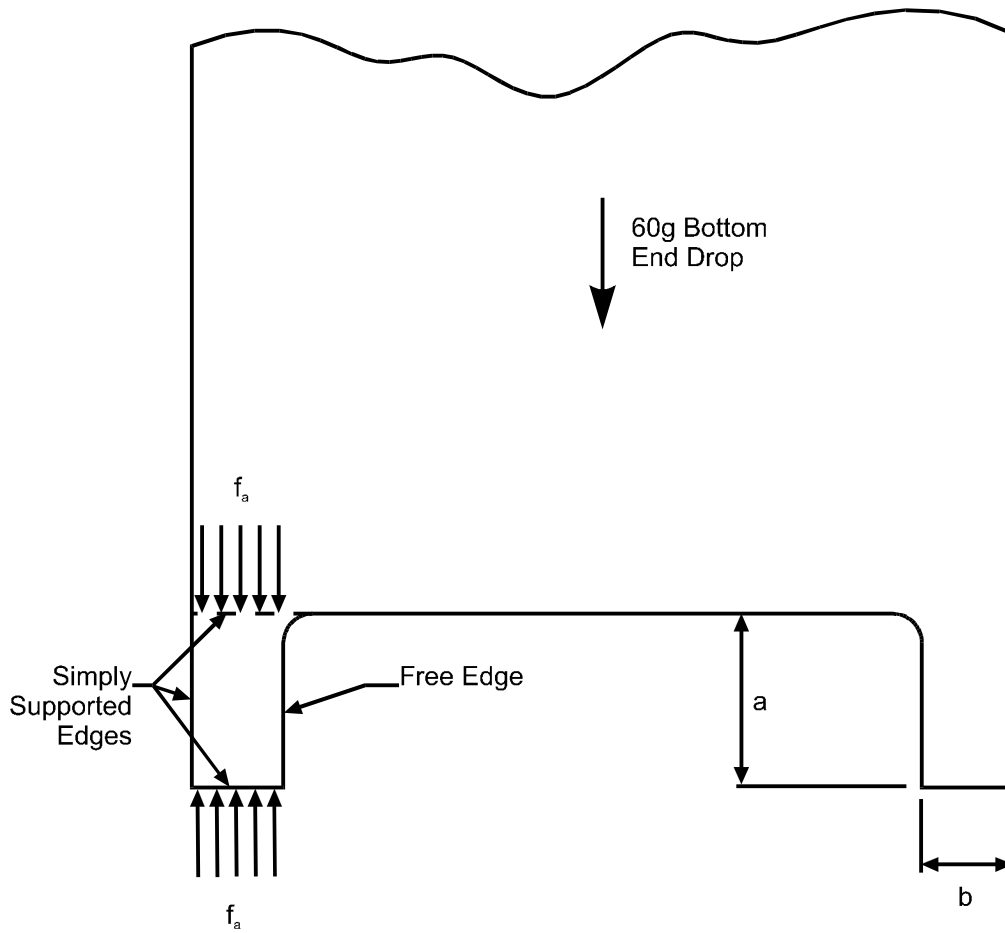


Figure 2.7-1 - W74 Canister Guide Tube HAC End Drop Buckling Evaluation Boundary Conditions

2.7.1.2 Side Drop

The HAC side drop evaluation considers a 30-foot free drop onto both impact limiters with the cask axis oriented horizontally. The FuelSolutions™ W74 canisters are evaluated for the HAC side drop considering the worst-case initial conditions in accordance with Regulatory Guide 7.8. The initial conditions considered include ambient conditions, decay heat load, internal pressure, and fabrication stresses. No credit is taken for containment or confinement provided by the canister shell transport conditions. Consequently, the W74 canisters are not evaluated for internal pressure loads. Stresses in the canister components due to thermal loads are generally classified as secondary stresses in accordance with the ASME B&PV Code. Since secondary stresses need not be evaluated for accident conditions, the combined effects of the HAC side drop and thermal loads generally need not be evaluated. Thermal loads are considered for buckling evaluations where the thermal loads result in compressive stresses in the members that reduce the factor of safety against buckling.

As discussed in Section 2.7.1, the structural evaluation of the W74 canister assembly components for the HAC side drop condition is performed using equivalent static loads. Equivalent static loads are calculated by multiplying the peak rigid body response by the appropriate DLF. As discussed in Section 2.12.2 of this SAR, the structural evaluation of the W74 canisters for the HAC side drop loading is performed using a bounding 60g equivalent static acceleration. The structural evaluations of the W74 canister components for the 60g HAC side drop loading are presented in the following sections.

2.7.1.2.1 General and LTP Spacer Plates

The most highly loaded W74 general and LTP spacer plates are evaluated for the HAC side drop loading to demonstrate their structural adequacy. For the HAC side drop loading, each W74 spacer plate supports its own weight, plus the tributary weight of the SNF assemblies, damaged fuel cans, guide tube assemblies, support tubes, and support sleeves. The W74 spacer plates are supported by the W74 canister shell in the region of impact, and the canister shell is supported by the transportation cask shells. In accordance with Regulatory Guide 7.8, the HAC side drop loading is considered in combination with NCT thermal loading. Thermal stresses are classified as secondary stresses in accordance with Subsection NG of the ASME Code and consequently need not be evaluated for accident conditions. However, thermal stresses are combined with the HAC side drop loads for the buckling evaluation of the spacer plates.

The most highly loaded W74 general and LTP spacer plates are evaluated for a 60g transfer cask side drop in Section 3.7.5.2.1 of the FuelSolutions™ W74 Canister Storage FSAR. The results of this side drop evaluation are directly applicable to the HAC side drop since the interface between the canister shell and the transfer cask cavity is identical to the interface inside the FuelSolutions™ TS125 Transportation Cask. The structural evaluation of the W74 spacer plates for the 60g side drop loading from Section 3.7.5.2 of the FuelSolutions™ W74 Canister Storage FSAR is summarized in the following paragraphs.

Elastic Stress Analysis - Uniform Fuel Loading

An elastic-system analysis is performed for the most heavily loaded W74 general and LTP spacer plates to determine the maximum spacer plate stress intensities for comparison with the

ASME B&PV Code allowable stress design criteria. The spacer plate loads for these analyses are calculated assuming that the loading from SNF assemblies is uniformly distributed along the length of the fuel assembly and distributed to each spacer plate based on its tributary length. The most heavily loaded W74 general and LTP spacer plates are identified based on a comparison of the spacer plate tributary weights in each W74 canister type.

The W74 spacer plate side drop elastic stress analysis is performed using the plane stress finite element model described in Section 3.9.2.4.1 of the FuelSolutions™ W74 Canister Storage FSAR. A total of seven side drop impact orientations are analyzed for both spacer plates, including 0°, 15°, 30°, 45°, 60°, 75°, and 90°, as shown in Figure 2.7-2. The maximum primary membrane and primary membrane plus bending stress intensities in the most heavily loaded W74 general and LTP spacer plates are summarized in Table 2.7-3 for each side drop impact orientation evaluated.

The maximum primary membrane (P_m) and primary membrane plus bending (P_m+P_b) stress intensities in the most heavily loaded W74 general spacer plate are 35.3 ksi and 78.9 ksi, respectively. The Service Level D allowable primary membrane and primary membrane plus bending stress intensities for the W74 general spacer plate material²⁶ at the bounding design temperature of 700°F are 75.4 ksi and 113.1 ksi, respectively. Therefore, the minimum design margins in the most heavily loaded W74 general spacer plate for the bounding 60g HAC side drop loading are:

$$P_m: DM = \frac{75.4}{35.3} - 1 = +1.14$$

$$P_m+P_b: DM = \frac{113.1}{78.9} - 1 = +0.43$$

The maximum primary membrane (P_m) and primary membrane plus bending (P_m+P_b) stress intensities in the most heavily loaded W74 LTP spacer plate are 17.4 ksi and 51.3 ksi, respectively. The Service Level D allowable primary membrane and primary membrane plus bending stress intensities for the W74 LTP spacer plate SA-240, Type XM-19 stainless steel material at the bounding design temperature of 700°F are 60.6 ksi and 90.8 ksi, respectively. Therefore, the minimum design margins in the most heavily loaded W74 LTP spacer plate for the bounding 60g HAC side drop loading are:

$$P_m: DM = \frac{60.6}{17.4} - 1 = +2.48$$

²⁶ The allowable stress intensities are taken as the lower values for the general spacer plate SA-517, Grade F or P carbon steel and A514, Grade F or P carbon steel.

$$P_m+P_b: DM = \frac{90.8}{51.3} - 1 = +0.77$$

The results show that the maximum stress intensities in the most highly loaded W74 general and LTP spacer plates due to the bounding 60g side drop loading are less than the corresponding Service Level D allowable stress intensities.

Permanent Deformation Analysis - Concentrated Fuel Loading at Fuel Grid Spacers

A plastic system analysis of the most heavily loaded W74 general and LTP spacer plates is performed for the 60g side drop loading to determine the maximum permanent deformation of the spacer plates for consideration in the criticality evaluation. The spacer plate loads for these analyses are calculated assuming the weight of the SNF assemblies is concentrated at the SNF assembly grid spacers and applied directly over the spacer plate ligament. For this analysis, impact orientations of 0°, 45°, and 90° are considered.

The W74 spacer plates plastic stress analyses for the 60g side drop loadings are performed using the finite element model described in Section 3.9.2.4.1 of the FuelSolutions™ W74 Canister Storage FSAR. The results of the W74 general and LTP spacer plate 60g side drop plastic analyses show that the plastic strain in the most heavily loaded spacer plates are small and occur only in localized regions. The maximum equivalent plastic strains in the most highly loaded W74 general and LTP spacer plates are 0.5% and 0.2%, respectively. The maximum permanent deformation in the most highly loaded W74 general and LTP spacer plates is 0.040 inch and 0.014 inch, respectively. The spacer plate permanent deformations resulting from the 60g side drop loading are considered in the criticality evaluation presented in Chapter 6.

Spacer Plate Buckling

The buckling evaluation of the spacer plates for the 60g side drop condition considers both beam-column buckling in accordance with NUREG/CR-6322 and general plastic instability in accordance with Appendix F of the ASME Code.

Beam-buckling of the W74 spacer plates is evaluated for the 60g side drop loading using the criteria of NUREG/CR-6322 for linear type supports subjected to combined axial compression and bending. Buckling evaluations are performed for the most highly stressed ligaments in both the W74 general and LTP spacer plates for the bounding 60g side drop loading, both with and without the bounding thermal loading superimposed. The thermal gradients used in the spacer plate buckling evaluation are those resulting from normal storage conditions. A comparison of the spacer plate thermal gradients resulting from normal storage and transportation conditions shows that the normal storage thermal gradients are bounding and produce higher thermal stresses in the spacer plates. Therefore, the results of the spacer plate buckling evaluations for combined 60g side drop and normal storage thermal loading bound those for the corresponding transportation conditions.

The results of the W74 spacer plate buckling analysis show that the highest interaction ratios in the most highly loaded general and LTP spacer plates resulting from the bounding 60g side drop loading, both with and without thermal loading superimposed, are 0.52 and 0.96, respectively. Therefore, the most highly loaded W74 spacer plates satisfy the buckling criteria of NUREG/CR-6322 for the bounding 60g side drop loading.

In addition to the elastic beam-column buckling analysis, general plastic instability of the W74 spacer plates is evaluated for the bounding 60g side drop loading, both with and without thermal loading, using plastic large deflection analyses. General instability of the W74 spacer plates occurs when the spacer plate experiences a global longitudinal plate buckling mode. Since the out-of-plane bending stiffness of the spacer plates is proportional to the plate thickness cubed, the bending stiffness of the 2.00-inch thick LTP spacer plates is much greater than that of the 3/4-inch thick general spacer plates. In addition, the results of the W74 spacer plate elastic stress analysis for the 60g side drop loading show that the spacer plate stress levels relative to the material yield strengths are comparable. Therefore, general instability will be controlled by the W74 general spacer plates and the LTP spacer plates need not be evaluated.

The W74 general spacer plate plastic large deflection buckling analysis for the 60g side drop loading is performed using the finite element model described in Section 3.9.2.4.5 of the FuelSolutions™ W74 Canister Storage FSAR. For this analysis, the loads from the SNF assemblies are conservatively applied to the supporting basket assembly structure as concentrated loads at the SNF assembly grid spacer locations. The worst-case loading for each W74 spacer plate results from the SNF fuel with the highest grid spacer tributary weight for the fuel assembly grid spacer located directly over that spacer plate. As discussed above, the maximum tributary weights for the Big Rock Point fuel in-core grid spacer and end fittings are 108.1 pounds and 54.1 pounds, respectively. The bi-linear kinematic hardening material model with a 0.1% tangent modulus is conservatively used for the spacer plate, support tube, support sleeve, and guide tube materials. For the 60g side drop loading without thermal, the material properties at 700°F are assumed. For the combined 60g side drop plus thermal loading, temperature-dependent material properties are used for the spacer plates, support tubes, support sleeves, and guide tubes. The bounding thermal gradient in the hottest W74 general spacer plate for normal cold storage conditions is conservatively used for this analysis. As discussed previously, the stresses in the spacer plates for the normal cold storage conditions bound those for NCT thermal conditions.

For the W74 general spacer plate side drop plastic large deflection buckling analysis, all in-plane loads are ramped up to 1.5 times the side drop load (i.e., 90g). The results show that the most highly loaded W74 general spacer plates do not experience plastic instability failure for side drop loading up to 90g, both with and without thermal loading superimposed. Therefore, the W74 general spacer plates provide the required factor of safety of 1.5 against buckling.

2.7.1.2.2 Engagement Spacer Plate

In the event of a side drop, the engagement spacer plate is loaded only by its own weight. The weight of the upper and lower basket assemblies and SNF fuel assemblies are supported by the transportation cask and do not load the engagement spacer plate. The W74 engagement spacer plate is evaluated for the 60g HAC side drop loading to demonstrate compliance with the ASME B&PV Code Service Level D allowable stress design criteria. In addition, a buckling evaluation of the W74 engagement spacer plate is performed for the 60g HAC side drop loading.

Stress Evaluation

The W74 engagement plate HAC side drop stress analysis is performed for impacts along the 0°, 28°, 36°, and 45° azimuths, as shown in Figure 2.7-3. Since the W74 engagement spacer plate is

symmetric with respect to the horizontal and vertical centerlines, these impact orientations encompass all of the orientations expected to cause the most severe spacer plate stresses.

The 0° impact HAC side drop evaluation is performed using the half-symmetry plane stress finite element model described in Section 2.12.4.2.1 and shown in Figure 2.12-6. A linear-elastic static stress analysis is performed using a 60g equivalent static acceleration load applied to the model along the 0° azimuth. The peak stress intensity resulting from the 0° impact HAC side drop is 9.6 ksi.

The W74 engagement spacer plate HAC side drop stress evaluation for impact azimuths of 28°, 36°, and 45° are performed using the full engagement plate plane stress finite element model described in Section 2.12.4.2.2 and shown in Figure 2.12-7. A linear-elastic static stress analysis is performed using a 60g equivalent static acceleration for each impact orientation. The peak stress intensities resulting from the 28°, 36°, and 45° HAC side drop impacts are 14.6 ksi, 16.4 ksi, and 12.2 ksi, respectively.

The HAC side drop stress analysis shows that the maximum primary plus secondary plus peak stress intensity of 16.4 ksi results from the 36° azimuth impact orientation. This stress intensity is conservatively compared with the Service Level D allowable primary membrane stress intensity. The W74M and W74T engagement spacer plates are fabricated from SA-240, Type XM-19 stainless steel. The Service Level D allowable primary membrane and primary membrane plus bending stress intensities for Type XM-19 stainless steel at 500°F are 62.4 ksi and 93.6 ksi, respectively. Therefore, the minimum design margins for the 60g HAC side drop are:

$$P_m: DM = \frac{62.4}{16.4} - 1 = +2.80$$

$$P_m+P_b: DM = \frac{93.6}{16.4} - 1 = +4.71$$

Therefore, the W74 engagement spacer plate meets the Service Level D allowable stress design criteria for the HAC side drop condition.

Buckling Evaluation

The elastic stability of the W74 engagement spacer plate is evaluated in this section for the effects of a bounding HAC free drop impact load (i.e., 60g in-plane and 45g out-of-plane) and combined NCT thermal and bounding HAC free drop impact loads. The evaluations demonstrate that the engagement spacer plate will not fail due to elastic buckling and provide the required factor of safety against buckling.

The stability of the W74 stainless steel engagement spacer plate is evaluated for the bounding HAC free drop impact loads using the half-symmetry finite element model described in Section 2.12.4.2.1. Elastic shell elements are used instead of plane-stress elements to account for both in-plane and out-of-plane response. The elastic stability is evaluated for the 0° impact

orientation only, since the bending stiffness of the engagement spacer plate does not vary significantly with respect to the in-plane impact orientation.

Two buckling analyses are performed: (1) bounding HAC free drop impact loads only (i.e., no thermal loads), and (2) combined bounding HAC free drop impact and NCT thermal loading. The results of the HAC side drop analysis show that the side drop load produces significant compressive stresses in the impact region and small tensile stresses in the interior regions. For impact loads acting alone (i.e., no thermal), the “toe” of the engagement spacer plate (i.e., the portion of the spacer plate outboard of the support tube holes) buckles first due to the high compressive loads in the region of impact. However, when thermal loads that result in compressive stresses in the interior region of the engagement spacer plate and tensile stresses in the exterior regions are combined with impact loads, other buckling modes may control.

For buckling analyses, the finite element model is limited to linear behavior. Therefore, the non-linear gap elements used to model the interface contact between the spacer plate and the canister shell are replaced with equivalent radial displacement constraints in the region where the engagement spacer plate and shell come in contact, as shown by the HAC side drop stress analysis results. Symmetry boundary constraints (i.e., $UX=ROTY=ROTZ=0$) are applied to the nodes that lie on the symmetry plane ($X=0$). Longitudinal constraints ($UZ=0$) are applied to a single node in the region of each support tube, conservatively assuming simple support conditions. For HAC free drop loading without thermal, perimeter buckling is expected to control. Therefore, for this condition longitudinal constraints are applied to the nodes located at the corners of the support tubes closest to the center of the engagement spacer plate to maximize the unsupported length at the perimeter of the plate. For combined HAC free drop and thermal loading, center buckling of the engagement spacer plate is expected to control. Therefore, for this condition, longitudinal constraints are applied to the nodes located at the corners of the support tubes furthest to the center of the engagement spacer plate to maximize the unsupported length in the center of the plate.

The engagement spacer plate buckling evaluation is performed using bounding longitudinal and transverse equivalent static accelerations of 45g and 60g, respectively. The 45g longitudinal acceleration is equivalent to that resulting from a corner drop, and the 60g transverse acceleration is equivalent to the maximum side drop acceleration. Combination of these two loads is conservative since they bound the entire range of drop loads for the corner drop, oblique drops, and side drop. For the 45g longitudinal load, the engagement spacer plate is loaded by its own weight in addition to the weight of the fuel and basket assembly opposite the side of impact. The loads from the fuel assemblies, guide tubes, and basket assembly are applied as uniform pressures of the respective regions of the model. The magnitudes of the pressure loads are determined by scaling those calculated for the 50g end drop in Section 2.12.4.2.4 by the ratio of the longitudinal g-loads (45g/50g). The resulting applied pressures are:

$$q_1 = 632.7 \text{ psi, pressure load on interior cell regions}$$

$$q_2 = 646.4 \text{ psi, pressure load on support tube interior regions}$$

$$q_3 = 4,645 \text{ psi, pressure load on support tube bearing region}$$

The material properties used in the finite element model are those of SA-240, Type XM-19. For the HAC free drop loading without thermal, material properties corresponding to a bounding temperature of 600°F are used ($E=25.3(10)^6$ psi). The temperature-dependent properties (E and α) of SA-240, Type XM-19 are used for the buckling evaluation in which thermal loading is superimposed. Poisson's ratio and the density of stainless steel are modeled as 0.29 and 0.290 lb/in³, respectively.

The factor of safety against buckling are determined via eigenvalue buckling analyses using the ANSYS general purpose finite element analysis program. The resulting factors of safety (i.e., load factors) for the 0° HAC free drop impact with and without thermal loading superimposed are 21.1 and 22.5, respectively. These factors are higher than the required factor of safety against buckling of 1.5.

In addition, the stability of the W74 engagement spacer plate is evaluated using a large deflection buckling analysis. The W74 engagement spacer plate large deflection buckling analysis is performed for the 60g HAC side drop loading (0° impact angle) with NCT thermal loading superimposed. For this analysis, the finite element model uses shell elements to allow out-of-plane displacements of the W74 engagement spacer plate. The model also includes radial gap elements modeled around the perimeter of the engagement plate (similar to those used for the side drop stress analysis). The load is gradually increased up to 6 times the HAC side drop loading of 60g. The results show that the finite element solution converges (no buckling takes place) over the entire loading range. Therefore, the critical buckling load has not yet been reached. The maximum compressive load is limited to 2/3 of the critical buckling load in accordance with F-1331.5(a)(1) of the ASME Code. Taking the limit to be 6 times the HAC side drop load limit gives an allowable g -load of 240g ($=60g \times 2/3 \times 6.0$). Hence, the results of the spacer plate buckling analysis confirm that the ASME Code buckling criteria are satisfied. The minimum design margin for buckling of the W74 engagement spacer plate is $240g/60g - 1 = +3.00$.

2.7.1.2.3 Support Tubes and Support Sleeves

The W74 support tubes and support sleeves are evaluated for a 60g side drop load in the FuelSolutions™ W74 Canister Storage FSAR. The results of this evaluation are applicable to the HAC side drop condition since the loads and support conditions for the W74 support tubes and support sleeves are equivalent. Structural evaluations are performed to determine the maximum stresses in the support tube and its longitudinal seam welds, the support tube attachment welds, and the support sleeve seam welds. The structural evaluations of the W74 support tube and support sleeve for the 60g side drop loading are summarized in the following paragraphs.

Support Tube Stress Evaluation

For the side drop loading conditions, the horizontally oriented support tubes are loaded in the vertical direction by their own weight, plus the weight of the support sleeves and the SNF assembly inside the support tube. Since the support tube is designed to contain either intact or damaged SNF assembly, the weight of the damaged fuel can is also included. As shown in Section 3.7.5.2.3 of the FuelSolutions™ W74 Canister Storage FSAR, the maximum primary membrane and primary membrane plus bending stress intensities in the W74 support tube are $P_m = 1.44$ ksi and $P_m + P_b = 6.44$ ksi.

The Service Level D allowable primary membrane and primary membrane plus bending stress intensities for the support tube SA-240, Type XM-19 stainless steel material at 600°F are 61.5 ksi and 92.2 ksi, respectively. Therefore, the minimum design margins in the W74 support tube due to the 60g HAC side drop loading are:

$$P_m : DM = \frac{61.5}{1.44} - 1 = +41.7$$

$$P_m + P_b : DM = \frac{92.2}{6.44} - 1 = +13.3$$

Therefore, the W74 support tubes meet the Service Level D allowable stress design criteria for the bounding 60g HAC side drop load.

In accordance with Regulatory Guide 7.8, the HAC side drop loading is evaluated in combination with NCT thermal loading. General thermal stresses in the W74 support tubes are classified as secondary in accordance with Subsection NG of the ASME B&PV Code. For Service Level D conditions, Appendix F of the ASME B&PV Code does not require evaluation of secondary stress.

Support Tube Longitudinal Seam Weld Stress Evaluation

As shown in Section 3.7.5.2.3 of the FuelSolutions™ W74 Canister Storage FSAR, the maximum shear stress in the W74 support tube longitudinal seam weld due to the 60g side drop loading is 1.34 ksi. In accordance with NG-3352, the allowable stresses for welds are equal to the base material allowable stress multiplied by the applicable weld quality factor from Table NG-3352-1. Per Table NG-3352-1, the weld quality factor for a single fillet weld with a surface visual examination is 0.35. The Service Level D allowable shear stress for SA-240, Type XM-19 stainless steel at an upper bound temperature of 600°F is 35.0 ksi. Therefore, the Service Level D allowable shear stress for the W74 support tube longitudinal seam weld is 12.3 ksi (= 35.0 x 0.35). The minimum design margin in the W74 support tube longitudinal seam weld due to the HAC side drop is:

$$D.M. = \frac{12.3}{1.34} - 1 = +8.18$$

Therefore, the W74 support tube longitudinal seam weld meets the Service Level D allowable stress design criteria for the bounding 60g HAC side drop load.

W74M Support Tube to LTP Spacer Plate Weld

As shown in Table 3.7-2 of the FuelSolutions™ W74 Canister Storage FSAR, the maximum shear stress in the W74M support tube to LTP spacer plate weld due to the 60g side drop loading is 0.44 ksi. In accordance with Regulatory Guide 7.8, the HAC side drop loading is evaluated in combination with NCT thermal loading. As shown in Section 2.6.1.3.3, the bounding NCT thermal loading results in a maximum shear stress of 1.44 ksi in the W74M support tube to LTP spacer plate welds. This weld shear stress is conservatively combined with the maximum weld shear stress due to the 60g HAC side drop loading. Therefore, the combined weld shear stress for this condition is 1.88 ksi.

In accordance with NG-3352, the allowable stresses for welds are equal to the base material allowable stress, multiplied by the applicable weld quality factor from Table NG-3352-1. Per Table NG-3352-1, the weld quality factor for a single groove weld with a surface visual examination is 0.40. The Service Level D allowable shear stress for SA-240, Type XM-19 stainless steel at an upper bound temperature of 600°F is 35.0 ksi. Therefore, the Service Level D allowable shear stress for the W74 support tube longitudinal seam weld is 14.0 ksi (= 35.0 x 0.40). The minimum design margin in the W74M support tube to LTP spacer plate weld due to the bounding 60g HAC side drop loading is:

$$D.M. = \frac{14.0}{1.88} - 1 = +6.45$$

Therefore, the W74M support tube to LTP spacer plate weld meets the Service Level D allowable stress design criteria for the bounding 60g HAC side drop load.

W74T Support Tube to Attachment Sleeve Weld

As shown in Table 3.7-2 of the FuelSolutions™ W74 Canister Storage FSAR, the W74T support tube to attachment sleeve weld stresses due to the 60g side drop loading are insignificant. However, in accordance with Regulatory Guide 7.8, the HAC side drop loading is evaluated in combination with NCT thermal loading. As shown in Section 2.6.1.3.3, the bounding NCT thermal loading results in a maximum shear stress of 3.32 ksi in the W74T support tube to attachment sleeve weld. This stress is bounded by the maximum weld shear stress calculated for the HAC end drop.

Support Sleeve Stresses

In the horizontal orientation, each support sleeve is loaded by its own weight and continuously supported by the support tube. As such, the stresses in the support sleeves due to the 60g side drop loading are low and do not control the design. The governing stress in the support sleeve is the shear stress in the 2-inch long by 1/8-inch single fillet weld between the sleeve retainer (i.e., small inner angle) and sleeve wall (i.e., large outer angle). As shown in Section 3.7.5.2.4 of the FuelSolutions™ W74 Canister Storage FSAR, the maximum shear stress in the support sleeve weld due to the 60g side drop loading is 2.36 ksi.

The Service Level D allowable weld shear stress, calculated based on SA-240, Type 304 stainless steel properties at 600°F with a 35% weld efficiency factor for a single fillet weld with surface visual examination, is 6.7 ksi (=19.2 ksi x 0.35). Therefore, the minimum design margin in the W74 support sleeve longitudinal seam weld for the bounding 60g side drop load is +1.85.

2.7.1.2.4 Guide Tubes

For the HAC side drop condition, the highest guide tube stresses occur in the largest unsupported spans between spacer plates. As shown in the general arrangement drawings in Section 1.3.1 of this SAR, the largest center-to-center span between general spacer plates is 7.13 inches. Stress and buckling evaluations of the W74 guide tube are presented in Section 2.7.1.4.4 for a bounding transverse acceleration load of 62g applied to the largest guide tube free span. The resulting stresses bound those due to the HAC side drop. Therefore, no additional evaluation of the W74 guide tube is required for the HAC side drop.

2.7.1.2.5 Canister Shell Assembly

The W74 canister shell assembly is evaluated for an 87g transverse load due to the HAC oblique drop slapdown impact in Section 2.7.1.4.5. The slapdown impact load is conservatively applied as a uniform acceleration over the length of the canister, thereby bounding the 60g HAC side drop condition. Therefore, the W74 canister shell stresses due to a 60g HAC side drop load are bounded by those calculated for the 87g HAC oblique drop slapdown impact load in Section 2.7.1.4.5, and need not be evaluated.

2.7.1.2.6 HAC Side Drop Summary

The results of the preceding HAC side drop structural analyses demonstrate that the W74 canister has adequate structural integrity to satisfy the structural design criteria of Section 2.1.2 of this SAR. The results of the W74 canister HAC side drop structural evaluation are summarized in Table 2.7-4 and in the following paragraphs.

The maximum stress intensities in each of the W74 canister components resulting from the bounding 60g side drop loading meet the corresponding Service Level D allowable stress design criteria. Excluding buckling, the lowest design margins in the W74 canister is +0.43 for primary membrane plus bending stress intensity in the most heavily loaded W74 general spacer plate. The minimum design margin for buckling is +0.04 in the most heavily loaded W74 LTP spacer plate. However, as shown in Figure 14 of NUREG/CR-6322, the factor of safety embedded in the buckling interaction equations for axial compressed stainless steel members is greater than 1.5 (for $\lambda \geq 0.1$). Therefore, the most heavily loaded W74 LTP spacer plates provide a significant factor of safety against buckling.

The extent of damage sustained by the W74 canister for the HAC side drop includes small permanent deformations in the W74 guide tubes and spacer plates. As discussed in Section 2.7.1.2.1, the maximum permanent deformation of the W74 general and LTP spacer plates caused by a 60g side drop load are 0.04 inch and 0.014 inch, respectively. The permanent deformation of the spacer plates is highly localized and does not affect the ability of the package to satisfy the subcriticality requirements of 10CFR71. As discussed in Section 2.7.1.2.4, the permanent deformation of the W74 guide tubes resulting from the HAC side drop is bounded by the permanent deformation resulting from the HAC oblique drop slapdown impact.

Table 2.7-3 - W74 Spacer Plate 60g Side Drop Elastic Stress Analysis Results

Impact Angle ⁽¹⁾	Maximum Stress Intensities (ksi)			
	General Spacer Plate		LTP Spacer Plate	
	P _m	P _m +P _b	P _m	P _m +P _b
0°	33.3	59.2	17.4	32.3
15°	35.3	74.1	12.7	40.8
30°	31.7	77.0	11.7	51.3
45°	25.5	78.9	10.5	51.2
60°	23.1	78.7	12.3	47.0
75°	26.5	77.6	13.7	42.1
90°	28.0	59.0	14.2	31.7

Note:

⁽¹⁾ Impact orientations are shown in Figure 2.7-2.

Table 2.7-4 - Summary of W74 Canister Basket Assembly HAC Side Drop Design Margins

W74 Canister Component	Stress Type	Maximum S.I. (ksi)	Allowable S.I. (ksi)	Minimum Design Margin ⁽¹⁾	Reference SAR Section
General Spacer Plate	P _m	35.3	75.4	+1.14	2.7.1.2.1
	P _m + P _b	78.9	113.1	+0.43	2.7.1.2.1
	Buckling	0.52 ⁽³⁾	1.0	+0.92	2.7.1.2.1
LTP Spacer Plate	P _m	17.4	60.6	+2.48	2.7.1.2.1
	P _m + P _b	51.3	90.8	+0.77	2.7.1.2.1
	Buckling	0.96 ⁽³⁾	1.0	+0.04	2.7.1.2.1
Engagement Spacer Plate	P _m	16.4	62.4	+2.80	2.7.1.2.2
	P _m + P _b	16.4	93.6	+4.71	2.7.1.2.2
	Buckling	6.0	1.5 ⁽⁴⁾	+3.00	2.7.1.2.2
Support Tube	P _m	1.44	61.5	+41.7	2.7.1.2.3
	P _m + P _b	6.44	92.2	+13.3	2.7.1.2.3
Support Sleeve	Bounded by HAC End Drop				2.7.1.2.3
Support Tube Longitudinal Seam Weld	Shear	1.34	12.3 ⁽⁵⁾	+8.18	2.7.1.2.3
W74M Support Tube to LTP Spacer Plate Weld	Shear	1.88	14.0 ⁽⁵⁾	+6.45	2.7.1.2.3
W74T Support Tube to Attachment Sleeve Weld	Bounded by HAC End Drop				2.7.1.2.3
Guide Tube	Bounded by HAC Oblique Drop Slapdown				2.7.1.2.4
Canister Shell Assembly	Bounded by HAC Oblique Drop Slapdown				2.7.1.2.5

Notes:

- (1) Design margin is equal to (Allowable/Stress) - 1.
- (2) Stresses in the support sleeves due to NCT vibration loading are insignificant.
- (3) Buckling interaction ratio calculated in accordance with NUREG/CR-6322.
- (4) The allowable axial compressive stress is limited to 2/3 of the theoretical buckling stress for HAC loading in accordance with NUREG/CR-6322. Alternatively stated, a 1.5 factor of safety against buckling is required.
- (5) Includes a 35% weld quality factor in accordance with Table NG-3352-1 of the ASME B&PV Code.

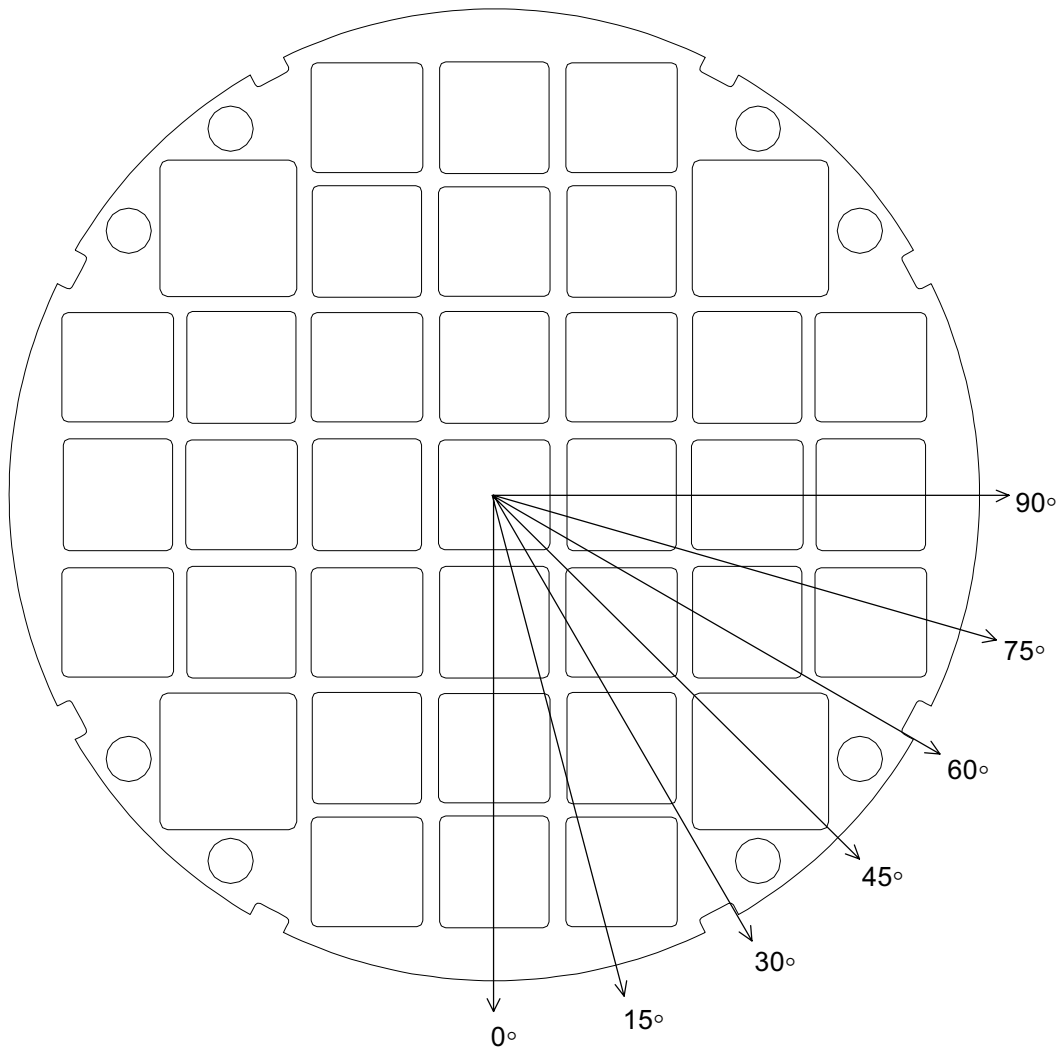


Figure 2.7-2 - W74 Canister General and LTP Spacer Plate HAC Side Drop Impact Orientations Evaluated

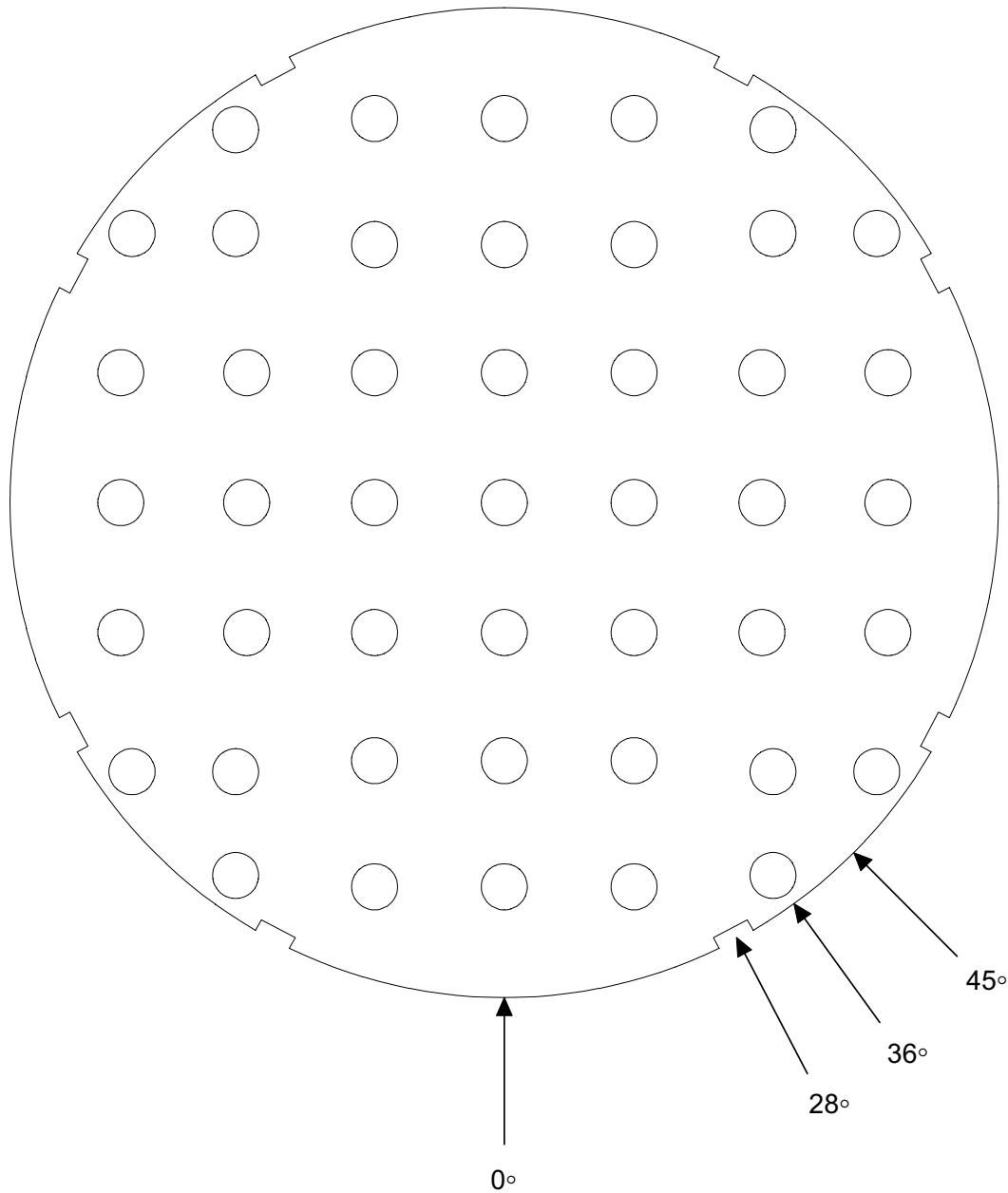


Figure 2.7-3 - W74 Canister Engagement Spacer Plate HAC Side Drop Impact Orientations Evaluated

2.7.1.3 Corner Drop

The FuelSolutions™ W74 canisters are evaluated for the 30-foot HAC free drop with the package center of gravity located directly over the point of impact (i.e., 21° from vertical), considering the worst-case initial conditions in accordance with Regulatory Guide 7.8. As discussed in Section 2.12.2 of this SAR, the structural evaluations of the W74 canisters for the HAC corner drop condition are performed using a bounding 40g equivalent static acceleration load. The bounding 40g HAC corner drop load has a longitudinal component of 37.3g and a transverse component of 14.3g. The structural evaluations of the W74 canister component for the bounding 40g HAC corner drop loading are presented in the following sections.

2.7.1.3.1 General and LTP Spacer Plates

As discussed in Section 2.7.1.4.1 of this SAR, the most heavily loaded W74 spacer plates are evaluated for the combined effects of bounding HAC oblique drop primary impact longitudinal and transverse loads of 38g and 36g, respectively. Therefore, the stresses in the W74 spacer plates due to the HAC corner drop loading are bounded by the stresses calculated for the bounding HAC oblique drop primary impact loads. Therefore, a detailed structural evaluation of the W74 spacer plates for the HAC corner drop loading is not presented in this SAR.

2.7.1.3.2 Engagement Spacer Plate

In the event of a HAC corner drop, each W74 engagement spacer plate is loaded in the transverse direction by its own weight, and in the longitudinal direction by its own self-weight plus the weight of the basket assembly, SNF assemblies, and damaged fuel canisters opposite the corner of impact. The W74 engagement spacer plate is evaluated for the HAC corner drop using equivalent static g-loads equal to the product of the peak rigid body acceleration and the engagement spacer plate DLF. As discussed in Section 2.7.1.3, the bounding HAC corner drop design load is 40g, or 37.3g in the longitudinal direction and 14.3g in the transverse direction. Bounding longitudinal and transverse g-loads of 40g and 15g are conservatively used for the W74 engagement spacer plate HAC corner drop stress evaluation.

The stresses in the most heavily loaded W74 engagement spacer plate due to the HAC corner drop loading are determined by scaling the maximum stresses calculated for the HAC end drop and the HAC side drop by the ratio of the applied loads. The resulting stresses are conservatively summed irrespective of sign and location.

The maximum primary membrane and primary membrane plus bending stress intensities due to a 50g HAC end drop load are 30.2 ksi and 37.0 ksi, respectively. The maximum primary plus secondary plus peak stress intensity due to the 60g HAC side drop, conservatively used in place of the HAC side drop maximum primary membrane and primary membrane plus bending stress intensities, is 16.4 ksi. Therefore, the maximum stresses due to the HAC corner drop are:

$$P_m = (30.2) \left(\frac{40g}{50g} \right) + (16.4) \left(\frac{15g}{60g} \right) = 28.3 \text{ ksi}$$

$$P_m + P_b = (37.0) \left(\frac{40g}{50g} \right) + (16.4) \left(\frac{15g}{60g} \right) = 33.7 \text{ ksi}$$

The Service Level D allowable primary membrane and primary membrane plus bending stress intensities for Type XM-19 stainless steel at a bounding design temperature of 500°F are 62.4 ksi and 93.6 ksi, respectively. The minimum design margin for primary membrane and primary membrane plus bending stress intensity in the W74 engagement spacer plate due to the HAC corner drop are:

$$P_m: \text{DM} = \frac{62.4}{28.3} - 1 = +1.20$$

$$P_m + P_b: \text{DM} = \frac{93.6}{33.7} - 1 = +1.78$$

Therefore, the most heavily loaded W74 engagement spacer plate meets the stress acceptance criteria for the bounding HAC corner drop load.

The engagement spacer plate elastic stability is evaluated in Section 2.7.1.2.2 for combined longitudinal and transverse g-loads of 45g and 60g, respectively. These loads bound the HAC corner drop longitudinal and transverse design g-loads of 40g and 15g, respectively. Therefore, no additional buckling evaluation is required for the HAC corner drop loading.

2.7.1.3.3 Support Tubes and Support Sleeves

The stresses in the W74 support tubes, support sleeves, and all associated welds resulting from the HAC corner drop loading are determined by scaling the stresses calculated for the 60g HAC side drop loading by the ratio of the transverse accelerations (i.e., 15g/60g) and the stresses calculated for the 60g HAC end drop loading by the ratio of the longitudinal accelerations (i.e., 38g/60g), and conservatively adding the resulting stresses absolutely and irrespective of location. The support tube, support sleeve, and associated weld stresses due to the HAC corner drop load are summarized in the following paragraphs.

Support Tube Stress Evaluation

As shown in Section 2.7.1.2.3, the maximum primary membrane and primary membrane plus bending stress intensities in the most heavily loaded W74 support tube due to the bounding 60g HAC side drop load are 1.44 ksi and 6.44 ksi, respectively. As shown in Section 2.7.1.1.3, the maximum primary membrane and primary membrane plus bending stress intensities in the most heavily loaded W74 support tube due to the bounding 60g HAC end drop load are 22.6 ksi and 23.6 ksi, respectively. Therefore, the support tube primary membrane and primary membrane plus bending stress intensities for the HAC corner drop are calculated as follows:

$$P_m = (1.44) \left(\frac{15g}{60g} \right) + (22.6) \left(\frac{38g}{60g} \right) = 14.7 \text{ ksi}$$

$$P_m + P_b = (6.44) \left(\frac{15g}{60g} \right) + (23.6) \left(\frac{38g}{60g} \right) = 16.6 \text{ ksi}$$

The Service Level D allowable primary membrane and primary membrane plus bending stress intensities for the support tube SA-240, Type XM-19 stainless steel material at 600°F are 61.5 ksi and 92.2 ksi, respectively. Therefore, the minimum design margins in the support tube due to the HAC corner drop are:

$$P_m : DM = \frac{61.5}{14.7} - 1 = +3.18$$

$$P_m + P_b : DM = \frac{92.2}{16.6} - 1 = +4.55$$

Therefore, the W74 support tubes meet the Service Level D allowable stress design criteria for the bounding HAC corner drop load.

Support Tube Longitudinal Seam Weld Stress Evaluation

As shown in Section 2.7.1.2.3, the maximum shear stress in the W74 support tube longitudinal seam weld due to the bounding 60g HAC side drop load is 1.34 ksi. Since the longitudinal loading does not result in any significant shear stress in the W74 support tube longitudinal seam weld, only the transverse component of the HAC corner drop loading is considered. The maximum shear stress in the W74 support tube longitudinal seam weld due to the HAC corner drop is calculated as follows:

$$f_v = (1.34) \left(\frac{15g}{60g} \right) = 0.3 \text{ ksi}$$

Per Section 2.7.1.2.3, the Service Level D allowable shear stress for the W74 support tube longitudinal seam weld is 12.3 ksi. The minimum design margin in the support tube longitudinal seam weld for HAC corner drop loading is:

$$DM = \frac{12.3}{0.3} - 1 = +40.0$$

Therefore, the W74 support tube longitudinal seam weld meets the Service Level D allowable stress design criteria for the HAC corner drop load.

W74M Support Tube to LTP Spacer Plate Weld Stress Evaluation

As shown in Section 2.7.1.1.3, the maximum shear stress in the W74M support tube to LTP spacer plate weld due to the 60g HAC end drop load is 3.8 ksi. Per Section 2.7.1.2.3, the maximum shear stress in the W74M support tube to LTP spacer plate weld due to the 60g HAC side drop is 0.44 ksi. Therefore, the W74M support tube to LTP spacer plate weld stress due to the HAC corner drop is calculated as follows:

$$f_v = (3.8) \left(\frac{38g}{60g} \right) + (0.44) \left(\frac{15g}{60g} \right) = 2.5 \text{ ksi}$$

In accordance with Regulatory Guide 7.8, the HAC corner drop loading is evaluated in combination with NCT thermal loading. As shown in Section 2.6.1.3.3, the bounding NCT thermal loading results in a maximum shear stress of 1.44 ksi in the W74M support tube to LTP spacer plate welds. This weld shear stress is due primarily to axial loads resulting from differential longitudinal expansion of the support tubes and support sleeves. For the HAC corner drop loading, the axial compressive loads resulting from the longitudinal impact loads cause the support sleeves to compress. This compression relieves the preload condition caused by thermal expansion. Therefore, the weld shear stress due to NCT thermal and HAC corner drop longitudinal loading is not additive. As shown above, the weld shear stress due to the 38g longitudinal component of the HAC corner drop loading ($3.8 \text{ ksi} \times 38\text{g}/60\text{g} = 2.4 \text{ ksi}$) is greater than that due to NCT thermal loading. Therefore, the combined shear stress of 2.5 ksi calculated above is controlling for this load combination.

Per Section 2.7.1.1.3, the Service Level D allowable shear stress for the W74M support tube to LTP spacer plate weld is 14.0 ksi. The minimum design margin in the W74M support tube to LTP spacer plate weld for bounding HAC corner drop load is:

$$DM = \frac{14.0}{2.5} - 1 = +4.60$$

Therefore, the W74M support tube to LTP spacer plate welds meet the Service Level D allowable stress design criteria for the bounding HAC corner drop load.

W74T Support Tube to Attachment Sleeve Weld Stress Evaluation

As shown in Section 2.7.1.1.3, the maximum shear stress in the W74T support tube to attachment sleeve weld due to the 60g HAC end drop load is 10.3 ksi. Per Section 2.7.1.2.3, the stresses in the W74T support tube to attachment sleeve weld due to the 60g HAC side drop are insignificant. Therefore, the W74T support tube to attachment sleeve weld shear stress due to the HAC corner drop is:

$$f_v = (10.3) \left(\frac{38\text{g}}{60\text{g}} \right) = 6.5 \text{ ksi}$$

In accordance with Regulatory Guide 7.8, the HAC corner drop loading is evaluated in combination with NCT thermal loading. As shown in Section 2.6.1.3.3, the bounding NCT thermal loading results in a maximum shear stress of 3.32 ksi in the W74T support tube to attachment sleeve welds. This weld shear stress is due primarily to axial loads resulting from differential longitudinal expansion of the support tubes and support sleeves. For the HAC corner drop loading, the axial compressive loads resulting from the longitudinal impact loads cause the support sleeves to compress. This compression relieves the preload condition caused by thermal expansion. Therefore, the weld shear stress due to NCT thermal and HAC corner drop longitudinal loading is not additive. As shown above, the weld shear stress due to the 38g longitudinal component of the HAC corner drop loading is greater than that due to NCT thermal loading.

Per Section 2.7.1.1.3, the Service Level D allowable shear stress for the W74T support tube to attachment sleeve weld is 14.0 ksi. Therefore, the minimum design margin in the W74T attachment sleeve weld for HAC corner drop load is:

$$DM = \frac{14.0}{6.5} - 1 = +1.15$$

Therefore, the W74T support tube to attachment sleeve welds meet the Service Level D allowable stress design criteria for the bounding HAC corner drop load.

Support Tube Buckling Evaluation

Buckling of the most heavily loaded W74 support tubes is evaluated for the HAC corner drop using the criteria of NUREG/CR-6322 for linear-type supports subjected to combined axial compression and bending stresses. As shown in Section 3.7.5.2.3 of the FuelSolutions™ W74 Canister Storage FSAR, the maximum beam bending stress (i.e., case 1) in the W74 support tubes due to the bounding 60g side drop load is 0.07 ksi. As shown in Section 2.7.1.1.3, the maximum axial compressive and bending stresses in the critical span of the most heavily loaded W74 support tube due to the bounding 60g HAC end drop load are 19.3 ksi and 0.5 ksi, respectively. Therefore, the maximum axial and bending stresses in the critical buckling span of the support tubes for the HAC corner drop are calculated as follows:

$$f_a = (19.3) \left(\frac{38g}{60g} \right) = 12.2 \text{ ksi}$$

$$f_b = (0.07) \left(\frac{15g}{60g} \right) + (0.5) \left(\frac{38g}{60g} \right) = 0.3 \text{ ksi}$$

Per NUREG/CR-6322, members subjected to combined compression and bending must satisfy the following equations:

$$\frac{f_a}{F_a} + \frac{C_m f_{bx}}{\left(1 - \frac{f_a}{F_{ex}}\right) F_{bx}} + \frac{C_m f_{by}}{\left(1 - \frac{f_a}{F_{ey}}\right) F_{by}} \leq 1.0$$

$$\frac{f_a}{2 \times 0.6 S_y} + \frac{f_{bx}}{F_{bx}} + \frac{f_{by}}{F_{by}} \leq 1.0$$

Interaction equations (26) and (27) are satisfied as follows, where C_m is conservatively assumed as 1.0 for equation (26) and the allowable stresses are defined in Section 2.7.1.1.3:

$$\frac{12.2}{23.0} + \frac{(1.0)(0.3)}{\left(1 - \frac{12.2}{726}\right)(45.5)} + \frac{(1.0)(0.3)}{\left(1 - \frac{12.2}{726}\right)(45.5)} = 0.54 \tag{26}$$

$$\frac{12.2}{2 \times 0.6(37.3)} + \frac{0.3}{45.5} + \frac{0.3}{45.5} = 0.29 \tag{27}$$

These results show that the W74 support tubes satisfy the buckling design criteria of NUREG/CR-6322 for the bounding HAC corner drop load. Note that the drop loads need not be combined with the thermal stresses resulting from longitudinal differential thermal expansion because the thermal stress acts as a tension preload that is relieved by the HAC corner drop axial compressive loading.

The minimum design margin for buckling of the W74 support tubes for the HAC corner drop is:

$$DM = \frac{1.00}{0.54} - 1 = +0.85$$

Since the stresses in the W74 support tube resulting from the HAC corner drop are lower than the support tube yield strength, inelastic buckling is not a credible failure mode. Therefore, no evaluation of inelastic buckling is required for the W74 support tubes.

Support Sleeve Evaluation

Since the W74 support sleeve stresses resulting from transverse loading are insignificant and the longitudinal acceleration due to the HAC corner drop is bounded by the HAC end drop, the W74 support sleeve stresses and buckling interaction ratio for the HAC corner drop are bounded by those calculated for the HAC end drop in Section 2.7.1.1.3.

2.7.1.3.4 Guide Tubes

In the event of an HAC corner drop, the guide tube assemblies are loaded in the transverse direction by their own inertial load and the inertial load of the SNF assembly inside the guide tube. Since the SNF assemblies are supported at the impacting end by the canister shell end plates, the guide tubes are loaded only by their own inertial load in the longitudinal direction.

The guide tube stresses due to the HAC corner drop are calculated by scaling the maximum stresses due to the HAC oblique drop transverse load by the ratio of the transverse loads (15g/62g) and the HAC end drop by the ratio of longitudinal g-loads (38g/60g). The stresses are conservatively combined irrespective of sign and location. As shown in Section 2.7.1.1.4, the HAC end drop results in a maximum primary membrane stress intensity of 3.7 ksi at the bottom end of the guide tube. The results of the HAC oblique drop evaluation, presented in Section 2.7.1.4.4, show that the maximum primary membrane and primary membrane plus bending stress intensities due to the 62g transverse load are 16.0 ksi and 56.4 ksi, respectively. Therefore, the maximum primary membrane and primary membrane plus bending stress intensities in the W74 guide tube due to the HAC corner drop are:

$$P_m = (16.0) \left(\frac{15g}{62g} \right) + (3.7) \left(\frac{38g}{60g} \right) = 6.2 \text{ ksi}$$

$$P_m + P_b = (56.4) \left(\frac{15g}{62g} \right) + (3.7) \left(\frac{38g}{60g} \right) = 16.0 \text{ ksi}$$

The Service Level D allowable primary membrane and primary membrane plus bending stress intensities for SA-240, Type 316 stainless steel at 650°F are 40.0 ksi and 60.0 ksi, respectively. The minimum design margins for primary membrane and primary membrane plus bending stress intensity in the W74 guide tube due to the HAC corner drop loading are:

$$P_m: DM = \frac{40.0}{6.2} - 1 = +5.45$$

$$P_m + P_b: DM = \frac{60.0}{16.0} - 1 = +2.75$$

Therefore, the W74 guide tubes meet the Service Level D allowable stress design criteria for the bounding HAC corner drop loading.

2.7.1.3.5 Corner Drop Summary

The results of the preceding HAC corner drop structural analyses demonstrate that the W74 canister has adequate structural integrity to satisfy the structural design criteria of Section 2.1.2 of this SAR. The results of the HAC corner drop structural evaluation are summarized in Table 2.7-5 and discussed in the following paragraphs.

The maximum stress intensities in each of the W74 canister components due to the HAC corner drop loading satisfy the Service Level D allowable stress design criteria. In general, the maximum stresses due to the HAC corner drop loading are bounded by those due to other HAC free drop orientations.

The extent of damage sustained by the W74 canister for the HAC corner drop is minimal. As discussed in Section 2.7.1.1.1, the stainless steel attachment brackets that secure the W74M guide tubes to the bottom end LTP spacer plate are designed to fail when subjected to longitudinal loads exceeding 20g. Therefore, the guide tube attachment brackets will fail in the event of an HAC corner drop. The resulting longitudinal shifting of the guide tube assembly relative to the SNF assembly is considered in the accident criticality evaluation presented in Chapter 6 of this SAR. The results of the criticality evaluation demonstrate that failure of the guide tube attachment brackets does not affect the ability of the W74 canister to satisfy the subcriticality requirements of 10CFR71. Furthermore, the failure of the guide tube attachment brackets does not prevent retrieval of the SNF assemblies from the canister.

Table 2.7-5 - Summary of W74 Canister HAC Corner Drop Design Margins

W74 Canister Component	Stress Type	Maximum S.I. (ksi)	Allowable S.I. (ksi)	Minimum D.M. ⁽¹⁾	Reference SAR Section
General Spacer Plate	Bounded by HAC oblique drop primary impact				2.7.1.3.1
LTP Spacer Plate	Bounded by HAC oblique drop primary impact				2.7.1.3.1
Engagement Spacer Plate	P _m	28.3	62.4	+1.20	2.7.1.3.2
	P _m + P _b	33.7	93.6	+1.78	2.7.1.3.2
	Buckling	Bounded by buckling evaluation presented in Section 2.7.1.2.2			2.7.1.3.2
Support Tube	P _m	14.7	61.5	+3.18	2.7.1.3.3
	P _m + P _b	16.6	92.2	+4.55	2.7.1.3.3
	Buckling	0.54 ⁽²⁾	1.0	+0.85	2.7.1.3.3
Support Sleeve	Bounded by HAC oblique drop primary impact				2.7.1.3.3
Support Tube Longitudinal Seam Weld	Shear	0.3	12.3 ⁽³⁾	+40.0	2.7.1.3.3
W74M Support Tube to LTP Spacer Plate Weld	Shear	2.5	14.0 ⁽³⁾	+4.60	2.7.1.3.3
W74T Support Tube to Attachment Sleeve Weld	Shear	6.5	14.0 ⁽³⁾	+1.15	2.7.1.3.3
Guide Tube	P _m	6.2	40.0	+5.45	2.7.1.3.4
	P _m + P _b	16.0	60.0	+2.75	2.7.1.3.4

Notes:

- ⁽¹⁾ Design margin is equal to (Allowable/Stress) - 1.
- ⁽²⁾ Buckling interaction ratio calculated in accordance with NUREG/CR-6322.
- ⁽³⁾ The allowable weld stresses include a 35% weld quality factor in accordance with Table NG-3352-1 of the ASME B&PV Code.

2.7.1.4 Oblique Drop

The FuelSolutions™ W74 canisters are evaluated for the HAC oblique drop condition considering the worst-case initial conditions in accordance with Regulatory Guide 7.8. The initial conditions considered include ambient conditions, decay heat load, internal pressure, and fabrication stresses. The canister assembly is not relied on to perform any containment function for transportation conditions. Consequently, the canister assembly need not be evaluated for internal pressure loads. Stresses in the canister and basket components due to thermal loads are classified as secondary stresses in accordance with the ASME Code. Since secondary stresses need not be evaluated for hypothetical accident conditions, the combined effects of the HAC oblique drop and thermal loads are not calculated. Thermal loads are only considered for buckling evaluations where the thermal loads result in compressive stresses in the members that reduce the critical buckling stress.

The HAC oblique drop conditions considered for the structural evaluations of the W74 canisters include both primary and secondary (i.e., slapdown) impacts. As discussed in Section 2.12.2 of the FuelSolutions™ TS125 Transportation Cask SAR, peak rigid-body acceleration loads are calculated for HAC oblique drop primary impact angles of 15°, 30°, 45°, and 60° with respect to horizontal. In addition, the peak rigid-body accelerations are calculated for the most severe secondary impact. As discussed in Section 2.12.2, the structural evaluation of the W74 canister for the HAC oblique drop primary and secondary impact loading is performed using bounding equivalent static loads. The equivalent static loads are calculated by multiplying the peak rigid-body accelerations by the appropriate DLF to account for dynamic amplification of displacements and stresses within the W74 canister. The DLFs are determined for the W74 canister based on the controlling system response frequency and the rigid body acceleration time history resulting from the cold HAC oblique drop condition. As shown in Table 2.12-6, bounding design loads of 38g longitudinal and 36g transverse are used to envelop all HAC oblique drop primary impact orientations. In addition, HAC oblique drop slapdown impact design loads of 31.8g transverse and 212 rad/s² are used for the structural evaluation of the W74 canisters. The structural evaluations of each W74 canister component for the bounding HAC oblique drop primary and secondary impact loadings are presented in the following sections.

2.7.1.4.1 General and LTP Spacer Plates

The W74 general and LTP spacer plates are evaluated for the HAC oblique drop condition to demonstrate their structural adequacy. The HAC oblique drop conditions consider both primary impacts and secondary (slapdown) impacts for a range of drop orientations. The structural evaluation of the W74 general and LTP spacer plates for the oblique drop primary and secondary impacts are presented in Sections 2.7.1.4.1.1 and 2.7.1.4.1.2, respectively.

2.7.1.4.1.1 Primary Impact Evaluation

Structural evaluations of the most highly loaded W74 general and LTP spacer plates are performed for the HAC oblique drop primary impact using two bounding fuel loading assumptions: (1) uniform fuel loading assumption (i.e., fuel weight distributed uniformly to basket assembly spacer plates), and (2) concentrated fuel loading at the fuel assembly grid spacers. The uniform fuel loading assumption is used for elastic system stress analyses in

accordance with Appendix F of the ASME Code. The concentrated fuel loading assumption is used for plastic system stress analyses to determine the maximum permanent deformation in the most highly loaded W74 general and LTP spacer plates for consideration in the criticality evaluation.

Elastic Stress Analysis - Uniform Fuel Loading

The stresses in the most heavily loaded W74 general and LTP spacer plates due to the bounding HAC oblique drop primary impact longitudinal and transverse loadings are evaluated separately. The spacer plate stress intensities resulting from the 38g longitudinal loading are determined by multiplying the maximum stresses due to vertical dead weight loading from Section 3.5.3.2.1 of the FuelSolutions™ W74 Canister Storage FSAR by 38g/1g. The spacer plate stress intensities resulting from the 36g transverse loading are calculated using finite element methods. The maximum stress intensities due to the transverse and longitudinal loads are conservatively combined, irrespective of sign and location, to determine the maximum stress intensities due to the bounding HAC oblique drop primary impact loading.

As shown in Section 3.5.3.2.1 of the FuelSolutions™ W74 Canister Storage FSAR, vertical dead weight loading results in a maximum primary membrane plus bending stress intensity of 0.39 ksi in the W74 general spacer plate. Therefore, the maximum primary membrane plus bending stress intensity in the W74 general spacer plate due to the 38g HAC oblique drop primary impact longitudinal loading is 14.8 ksi ($=0.39 \times 38g/1g$).

The maximum primary membrane plus bending stress intensities in the W74 top and bottom end LTP spacer plates are 0.15 ksi and 0.69 ksi, respectively. The vertical dead weight stress in the bottom end LTP spacer plate is higher than that in the top end spacer plate, since it supports the weight of 28 guide tube assemblies. However, as discussed in Section 3.7.3.2.1 of the FuelSolutions™ W74 Canister Storage FSAR, the attachment brackets that secure the W74M guide tube assemblies to the bottom end LTP spacer plate are designed with an ultimate capacity of less than 20g. The designed failure mode of the W74M guide tube attachment brackets prevents overloading of the bottom end LTP spacer plate and its welds to the support tubes for HAC free drops that result in high longitudinal loads. Therefore, the maximum primary membrane plus bending stress intensity in the W74 LTP spacer plate is taken as the larger of 5.7 ksi ($=0.15 \times 38g/1g$) or 13.8 ksi ($=0.69 \times 20g/1g$).

The stresses in the most heavily loaded W74 general and LTP spacer plates due to the 36g HAC oblique drop primary impact transverse loading are calculated using the plane-stress finite element model described in Section 2.12.4.1.1. The most heavily loaded W74 general and LTP spacer plates are evaluated for the HAC oblique drop primary impact loading for seven separate impact orientations, as shown in Figure 2.7-2. These include impacts along the 0°, 15°, 30°, 45°, 60°, 75°, and 90° azimuths. Since the spacer plate geometry is symmetric about both the horizontal and vertical centerlines, these seven impact orientations adequately envelop all possible impact orientations. The loads from the support tubes, support sleeves, guide tube assemblies, damaged fuel canisters, and fuel assemblies are applied to the supporting spacer plate ligaments as pressure loads. These loads are calculated as described in Section 2.12.4.1.1.

The most highly loaded W74 general and LTP spacer plates are those supporting the highest in-plane tributary weights. As discussed in Section 2.12.1, the W74 general spacer plate supporting the highest in-plane tributary weight (2,119 pounds) is the bottom end spacer plate of

the W74T upper basket assembly. Similarly, the W74 LTP spacer plate supporting the highest in-plane tributary weight (2,043 pounds) is the bottom end spacer plate of the W74M upper basket assembly. The tributary lengths of these spacer plates are 7.44 inches (general) and 5.63 inches (LTP) per Tables 2.12-1 and 2.12-2.

The maximum primary membrane and primary membrane plus bending stress intensities in the most highly loaded W74 general and LTP spacer plates are summarized in Table 2.7-6 for each impact orientation evaluated. The maximum primary membrane and primary membrane plus bending stress intensities in the most heavily loaded W74 general spacer plate are 25.5 ksi (0° impact azimuth) and 67.4 ksi (45° impact azimuth), respectively. Similarly, maximum primary membrane and primary membrane plus bending stress intensities in the most heavily loaded W74 LTP spacer plate are 10.0 ksi (30° impact azimuth) and 39.7 ksi (60° impact azimuth), respectively.

As discussed previously, the maximum stress intensities calculated for the 36g transverse loading and the 38g longitudinal loading are conservatively combined without consideration of sign and location. Therefore, the combined stress intensities in the most heavily loaded W74 general spacer plate are:

$$P_m = 25.5 + 0.0 = 25.5 \text{ ksi}$$

$$P_m + P_b = 67.4 + 14.8 = 82.2 \text{ ksi}$$

The Service Level D allowable primary membrane and primary membrane plus bending stress intensities for the W74 general spacer plate material at a bounding design temperature of 700°F are 75.4 ksi and 113.1 ksi, respectively. Therefore, minimum design margins in the most heavily loaded W74 general spacer plate for the bounding HAC oblique drop primary impact loads are:

$$P_m: \text{ DM} = \frac{75.4}{25.5} - 1 = +1.95$$

$$P_m + P_b: \text{ DM} = \frac{113.1}{82.2} - 1 = +0.38$$

The combined stress intensities in the most heavily loaded W74 LTP spacer plate for the HAC oblique drop primary impact loadings are:

$$P_m = 10.0 + 0.0 = 10.0 \text{ ksi}$$

$$P_m + P_b = 39.7 + 13.8 = 53.5 \text{ ksi}$$

The Service Level D allowable primary membrane and primary membrane plus bending stress intensities for SA-240, Type XM-19 stainless steel at a bounding design temperature of 700°F are 60.6 ksi and 90.8 ksi, respectively. Therefore, minimum design margins in the most heavily loaded W74 LTP spacer plate for the bounding HAC oblique drop primary impact loads are:

$$P_m: DM = \frac{60.6}{10.0} - 1 = +5.07$$

$$P_m + P_b: DM = \frac{90.8}{53.5} - 1 = +0.70$$

Therefore, the most heavily loaded W74 general and LTP spacer plates meet the Service Level D allowable stress design criteria for the bounding HAC oblique drop primary impact loading.

Permanent Deformation Analysis - Concentrated Fuel Loading at Fuel Grid Spacers

The results of the W74 general and LTP spacer plate stress evaluations for HAC oblique drop loading show that, with the exception of the bottom end LTP spacer plates, the slapdown impact loading results in higher stresses than the primary impact loading. Therefore, with the exception of the bottom end LTP spacer plate, the spacer plate permanent deformations calculated for the HAC slapdown loading will bound any potential permanent deformation resulting from the HAC oblique drop primary impact loading.

A plastic analysis of the most heavily loaded W74 bottom end LTP spacer plate is performed for the bounding HAC oblique drop primary impact loading. For this evaluation, the transverse loading of the LTP spacer plate is conservatively calculated based on a concentrated load at the SNF assembly bottom end fitting. For the HAC oblique drop primary impact, the bottom end LTP spacer plate in the W74M upper basket assembly is most heavily loaded. As shown in Table 2.12-4, this LTP spacer plate (i.e., spacer plate number 1 of the W74M upper basket) supports a higher in-plane tributary weight (2,825 pounds) than the bottom end LTP spacer plate in the lower W74M basket assembly. Therefore, the most heavily loaded W74 LTP spacer plate supports a total in-plane load of 101.7 kips (=2,825 lbs. x 36g) for the HAC oblique drop primary impact transverse loading.

In addition, the 28 guide tube assemblies in the upper basket assembly are secured to the bottom end LTP spacer plate by attachment brackets that have an ultimate capacity of 20g. Therefore, the bottom end LTP spacer plate supports the weight of the guide tubes up to the 20g failure load of the attachment brackets. As shown above in the elastic stress analysis, the maximum primary membrane plus bending stress intensity due to the 20g longitudinal loading with the guide tubes attached to the spacer plate is higher than the maximum primary membrane plus bending stress intensity due to the 38g longitudinal loading without the guide tubes attached. Therefore, the permanent deformation is calculated using a 20g longitudinal loading that includes the weight of the guide tubes.

Plastic analysis of the W74 bottom end LTP spacer plate for the HAC oblique drop primary impact loading are performed for impact orientations of 0° and 45° using the finite element model described in Section 2.12.4.1.2. The spacer plate in-plane loading due to the tributary weight of the guide tube assemblies, support tubes, support sleeves, and damaged fuel canisters are calculated using the formulas presented in Section 2.12.4.1.1 based on a spacer plate tributary length of 5.63 inches. The in-plane loading due to the SNF assemblies is calculated based on the maximum tributary weight of the BRP fuel lower tie plate (55.4 pounds per Table 2.12-3). The longitudinal loading from the guide tubes is applied as nodal forces at the locations of the guide tube attachment brackets. The heaviest W74 guide tube assembly weighs 84.2 pounds. Each

guide tube is secured to the bottom end LTP spacer plate with two attachment brackets. Therefore, the total longitudinal load at each attachment bracket, corresponding to the 20g ultimate load capacity, is 842 pounds (=20g x 84.2 lbs/2).

Classical bi-linear kinematic hardening law is used for the LTP spacer plate SA-240, Type XM-19 stainless steel material. The material yield strength is conservatively based on an upper bound temperature of 700°F. A 0.1% tangent modulus is conservatively used for stresses greater than the yield strength.

The results of the plastic analysis show that the plastic strain in the most heavily loaded bottom end LTP spacer plate resulting from the bounding HAC oblique drop primary impact loading is low in magnitude and highly localized. The maximum equivalent plastic strain in the most heavily loaded bottom end LTP spacer plate, resulting from the 45° impact orientation, is less than 0.5%. The maximum permanent deformation of the most heavily loaded bottom end LTP spacer plate is less than 0.015 inch. As shown in Section 2.7.1.4.1.2, the maximum permanent deformation of the most heavily loaded LTP spacer plate resulting from the HAC slapdown impact loading is 0.023 inch. Therefore, the maximum permanent deformation in the most heavily loaded LTP spacer plate resulting from the HAC oblique drop primary impact loading is lower than that resulting from the HAC oblique drop slapdown impact loading.

2.7.1.4.1.2 Secondary Impact Evaluation

The structural evaluation of the canister assembly components for the HAC oblique drop secondary impact (i.e., slapdown) is performed using equivalent static loads. Equivalent static loads are calculated by multiplying the peak rigid body response by the appropriate DLF. As discussed in Section 2.12.2 of this SAR, the structural evaluation of the W74 canisters for the HAC oblique drop slapdown impact loading is performed using bounding equivalent static accelerations of 31.9g (uniform transverse) and 211.8 rad/s² (angular). Using these bounding design acceleration loads, the transverse acceleration at the location of each spacer plate is calculated as follows:

$$G(x) = 31.9g + \frac{(211.8 \text{ rad/s}^2)(x)}{386.4 \text{ in/s}^2}$$

where x is the longitudinal distance from the package center of gravity to the spacer plate of interest. Since the HAC oblique drop secondary impact occurs at or near a horizontal orientation, there are no significant longitudinal accelerations. The structural evaluations of the W74 canister components for the HAC oblique drop slapdown impact loading are presented in the following sections.

Structural evaluations of the most highly loaded W74 general and LTP spacer plates are performed for the HAC oblique drop slapdown impact using two bounding fuel loading assumptions: (1) uniform fuel loading assumption (i.e., fuel weight distributed uniformly to basket assembly spacer plates), and (2) concentrated fuel loading at the fuel assembly grid spacers. The uniform fuel loading assumption is used for elastic system stress analyses in accordance with Appendix F of the ASME Code. The concentrated fuel loading assumption is used for plastic system stress analyses to determine the maximum permanent deformation in the

most highly loaded W74 general and LTP spacer plates for consideration in the criticality evaluation. Finally, a buckling evaluation of the W74 spacer plates is performed that considers beam-column buckling in accordance with NUREG/CR-6322 (uniform fuel load), and general instability in accordance with Appendix F of the ASME Code (concentrated fuel load).

Elastic Stress Analysis - Uniform Fuel Loading

The W74 spacer plate HAC oblique drop slapdown elastic stress analyses are performed using the plane stress finite element model described in Section 2.12.4.1.1. Only the most highly loaded W74 general and LTP spacer plates are evaluated for the HAC oblique drop slapdown impact loading. In order to identify the most heavily loaded W74 spacer plates, the total transverse load resulting from the slapdown impact loading is calculated for each spacer plate in the W74M and W74T upper and lower basket assemblies. The total transverse impact load at each spacer plate is equal to the transverse acceleration at the location of the spacer plate multiplied by the spacer plate tributary weight. The spacer plate tributary weights are defined as the portion of the SNF assembly (and damaged fuel canister, if required), guide tube, support tube, and support sleeve weights that are supported by each spacer plate in the transverse direction, combined with the spacer plate self-weight. Since the slapdown impact acceleration load varies in magnitude over the length of the basket assembly, the W74 spacer plates at the top and bottom ends of the canister experience the highest transverse g-loads. However, the spacer plates at the top end of the upper basket assembly and at the bottom end of the lower basket assembly are spaced closer together to reduce their tributary weights.

In order to identify the most highly loaded W74 general and LTP spacer plates for the HAC slapdown impact, the total in-plane load is calculated for each spacer plate in the W74M and W74T upper and lower basket assemblies. The spacer plate in-plane loads are calculated by multiplying the total tributary weights from Tables 2.12-1 and 2.12-2 by the HAC slapdown equivalent static transverse load occurring at the corresponding spacer plate location, calculated as described previously in this section. The most heavily loaded W74 general spacer plate (i.e., spacer plate no. 13 at the top end of the W74T upper basket assembly) supports a total load of 131.4 kips. The most heavily loaded W74 LTP spacer plate (i.e., spacer plate no. 14 at the top end of the W74M upper basket assembly) supports a total load of 120.6 kips.

The most heavily loaded W74 general and LTP spacer plates are evaluated for the HAC oblique drop slapdown impact loading for seven separate impact orientations, as shown in Figure 2.7-2. These include impacts along the 0°, 15°, 30°, 45°, 60°, 75°, and 90° azimuths. Since the spacer plate geometry is symmetric about both the horizontal and vertical centerlines, these seven impact orientations adequately envelop all possible impact orientations. The loads from the support tubes, support sleeves, guide tube assemblies, damaged fuel canisters, and fuel assemblies are applied to the supporting spacer plate ligaments as pressure loads. These loads are calculated as described in Section 2.12.4.1.1.

For each impact orientation, a linear-elastic static analysis is performed. The primary stress intensities in the spacer plates are evaluated as discussed in Section 2.12.3. The maximum primary membrane (P_m) and primary membrane plus bending (P_m+P_b) stress intensities in the most highly loaded W74 general and LTP spacer plates are summarized in Table 2.7-7 for each impact orientation.

The maximum primary membrane and primary membrane plus bending stress intensities in the most heavily loaded W74 general spacer plate due to the HAC oblique drop slapdown impact loading result from the 0° and 30° impact orientations, respectively. The maximum primary membrane and primary membrane plus bending stress intensities are 30.7 ksi and 88.7 ksi, respectively. The Service Level D allowable primary membrane and primary membrane plus bending stress intensities for the W74 general spacer plate material at 700°F are 75.4 ksi and 113.1 ksi, respectively. Therefore, the minimum design margins for primary membrane and primary membrane plus bending stress intensities in the most highly loaded W74 general spacer plate due to the HAC oblique drop slapdown impact loading are +1.46 and +0.28, respectively.

The maximum primary membrane and primary membrane plus bending stress intensities in the most highly loaded W74 LTP spacer plate due to the HAC side drop load result from the 0° and 45° impact orientations, respectively. The maximum primary membrane and primary membrane plus bending stress intensities are 15.2 ksi and 50.1 ksi, respectively. The Service Level D allowable primary membrane and primary membrane plus bending stress intensities for SA-240, Type XM-19 stainless steel at 700°F are 60.6 ksi and 90.8 ksi, respectively. Therefore, the minimum design margins for primary membrane and primary membrane plus bending stress intensities in the most highly loaded W74 LTP spacer plate due to the HAC oblique drop slapdown impact loading are +2.98 and +0.81, respectively.

Permanent Deformation Analysis - Concentrated Fuel Loading at Fuel Grid Spacers

In addition to the uniform fuel load case, the loads from the SNF assemblies are conservatively applied to the supporting basket assembly structure as concentrated loads at the fuel grid spacer locations. The worst-case loading for each W74 spacer plate results from the SNF fuel with the highest grid spacer tributary weight for the fuel assembly grid spacer located directly over that spacer plate. As shown in Table 2.12-3, the maximum tributary weights for the BRP fuel in-core grid spacer and end fittings are 118.0 pounds and 90.6 pounds, respectively.

In order to identify the most highly loaded W74 general and LTP spacer plates for the HAC slapdown impact, the total in-plane load is calculated for each spacer plate in the W74M and W74T upper and lower basket assemblies. The spacer plate in-plane loads are calculated by multiplying the total tributary weights from Tables 2.12-4 and 2.12-5 by the HAC slapdown equivalent static transverse load occurring at the corresponding spacer plate location, calculated as described previously in this section. Based on the results of these calculations, spacer plate number 10 in the W74M upper basket is the most highly loaded general spacer plate, with a 67.3g transverse acceleration and a total in-plane load of 299.8 kips. Similarly, the bottom LTP spacer plate in the W74M lower basket assembly is the most highly loaded LTP spacer plate, with a 79.0g transverse acceleration and a total in-plane load of 213.3 kips.

Plastic stress analyses of the most highly loaded W74 general and LTP spacer plates for the HAC oblique drop slapdown impact loading are performed for impact orientations of 0° and 45° using the full plane-stress finite element model described in Section 2.12.4.1.1. The plane-stress finite element model includes a single spacer plate only, conservatively taking no credit for the support tubes and guide tubes that provide load sharing with the adjacent spacer plates. The most highly loaded W74 general spacer plate is modeled with a 0.75-inch thickness and a tributary length of 6.13 inches (i.e., spacer plate no. 10 in the W74M upper basket assembly). The LTP spacer plate is modeled with a 2.00-inch thickness and a tributary length of 3.63 inches (i.e.,

spacer plate no. 1 in the W74M lower basket assembly). The spacer plate loading due to the tributary weight of the guide tubes, support tubes, support sleeves, and damaged fuel canisters plus the fuel assembly grid spacer tributary weights are applied to the model as pressure loads on the supporting spacer plate ligaments. These loads are calculated as described in Section 2.12.4.1.1. The bounding HAC slapdown loading is applied to the finite element model and then reduced to 1g in order to determine the spacer plate permanent deformations.

Classical bi-linear kinematic hardening law is used for the general and LTP spacer plate materials. The material yield strength is conservatively based on an upper bound temperature of 700°F. A 0.1% tangent modulus is conservatively used for stresses greater than the yield strength.

The results of the W74 general spacer plate plastic analyses show that no permanent deformation of the most highly loaded W74 general spacer plates results from the HAC slapdown loading. The maximum equivalent plastic strain in the most highly loaded W74 LTP spacer plate is less than 0.3% for all impact orientations. The maximum permanent deformation in the most highly loaded W74 LTP spacer plate results from the 45° impact orientation and is 0.023 inch.

Spacer Plate Buckling

The buckling evaluation of the spacer plates for the HAC oblique drop slapdown impact considers both beam-column buckling in accordance with NUREG/CR-6322 and general plastic instability in accordance with Appendix F of the ASME Code. For the beam-buckling condition, the W74 spacer plates are evaluated for buckling using the criteria of NUREG/CR-6322 for linear type supports subjected to combined axial compression and bending loads. Buckling evaluations are performed for the most highly loaded ligaments in both the W74 general and LTP spacer plates for the HAC oblique drop slapdown impact loading, both with and without the bounding NCT thermal loading superimposed.

The maximum stresses in the W74 spacer plates are evaluated using interaction equations (26), (27), and (28) of NUREG/CR-6322, defined as follows:

$$\frac{f_a}{F_a} + \frac{C_{mx} f_{bx}}{\left(1 - \frac{f_a}{F'_{ex}}\right) F_{bx}} + \frac{C_{my} f_{by}}{\left(1 - \frac{f_a}{F'_{ey}}\right) F_{by}} \leq 1.0 \quad (\text{Eq. 26})$$

$$\frac{f_a}{2 \times 0.6S_y} + \frac{f_{bx}}{F_{bx}} + \frac{f_{by}}{F_{by}} \leq 1.0 \quad (\text{Eq. 27})$$

If $f_a/F_a \leq 0.15$, then equation (28) may be used in lieu of equations (26) and (27):

$$\frac{f_a}{F_a} + \frac{f_{bx}}{F_{bx}} + \frac{f_{by}}{F_{by}} \leq 1.0 \quad \text{if } \frac{f_a}{F_a} \leq 0.15 \quad (\text{Eq. 28})$$

The allowable axial stress, F_a , bending stress, F_b , and Euler buckling stress, F_e' , are calculated for all ligament sizes for both the W74 general (carbon steel) and LTP (stainless steel) spacer plate. Per NUREG/CR-6322, the allowable compressive stress for carbon steel is defined as follows:

$$F_a = \frac{P_{33}}{A_g} \text{ (carbon steel - general)}$$

$$F_a = \frac{P_{40}}{A_g} \text{ (stainless steel - LTP)}$$

where, A_g is the gross area of the spacer plate ligament, and P_{33} and P_{40} are the maximum allowable axial compressive loads for carbon steel and stainless steel, respectively, determined in accordance with NUREG/CR-6322, as follows:

$$P_{33} = \frac{(1 - \lambda^2/4)}{1.11 + 0.5\lambda + 0.17\lambda^2 - 0.28\lambda^3} \cdot S_y A_g \text{ (for } 0 \leq \lambda \leq 1)$$

and,

$$P_{40} = \frac{(P_{45})(P_{33})}{P_{43}}$$

where:

$$\lambda = \left(\frac{KL}{r_x} \right) \left(\frac{1}{\pi} \right) \sqrt{\frac{S_y}{E}}$$

$$P_{43} = \frac{(1 - \lambda^2/4)}{\frac{5}{3} + \frac{3}{8} \left(\frac{\lambda}{\sqrt{2}} \right) - \frac{1}{8} \left(\frac{\lambda}{\sqrt{2}} \right)^3} \cdot S_y A_g \text{ (for } \lambda \leq \sqrt{2})$$

$$P_{45} = \left(0.47 - \frac{120\lambda}{444\sqrt{2}} \right) \cdot S_y A_g \text{ (for } \lambda \leq \sqrt{2})$$

where:

$K = 0.65$, effective length factor for fixed-fixed support per Figure 6 of NUREG/CR-6322

$L = 7.40$ in., unsupported length of spacer plate ligaments

$r_x = \sqrt{\frac{I_x}{A_g}}$ in., ligament radius of gyration

- $I = bt^3/12$, ligament moment of inertia, for $b > t$
 $= b^3t/12$, ligament moment of inertia, for $b < t$
- $A_g = bt$, ligament gross area
- $b =$ Ligament width
- $t =$ Spacer plate thickness
 $= 0.75$ in., general spacer plate
 $= 2.00$ in., LTP spacer plate
- $S_y =$ Spacer plate material yield strength
 $= 83.0$ ksi, general spacer plate at 700°F
 $= 38.8$ ksi, LTP spacer plate at 500°F
- $E =$ Spacer plate material elastic modulus
 $= 25.5 \times 10^6$ psi, general spacer plate at 700°F
 $= 25.8 \times 10^6$ psi, LTP spacer plate at 500°F
- $C_m = 0.85$, coefficient for members in frames where side-sway is permitted per NUREG/CR-6322

The Euler buckling stress, calculated in accordance with Section 6.32 of NUREG/CR-6322, is defined as follows:

$$F'_e = \frac{\pi^2 E}{1.30(KL / r_x)^2} \text{ (carbon steel - general)}$$

$$F'_e = \frac{\pi^2 E}{1.46(KL / r)^2} \text{ (stainless steel - LTP)}$$

The allowable bending stress for compact sections, F_b , is defined in NUREG/CR-6322 as:

$$F_b = fS_y$$

where the plastic shape factor is $f=1.5$ for a solid rectangular section per Roark, Table 1, Case 2.

The allowable stresses are calculated for each of the W74 general and LTP spacer plate ligament types and summarized in Table 2.7-8 and Table 2.7-9.

As discussed previously, the spacer plate stresses used for the NUREG/CR-6322 buckling evaluation are calculated on a linear-elastic basis using the W74 spacer plate plane stress finite element model described in Section 2.12.4.1.1. The spacer plate stresses are determined for the HAC oblique drop slapdown impact loading, both with and without NCT thermal loading superimposed. The HAC oblique drop slapdown impact loading for the spacer plates are calculated and applied to the finite element models as described in Section 2.12.4.1.1. The thermal gradient in the hottest W74 general spacer plate for NCT cold thermal loading is used for the general spacer plate buckling evaluation. The buckling evaluation of the LTP spacer plate is performed using the thermal gradient in the bottom end spacer plate of the W74M lower basket assembly resulting from the NCT cold thermal loading.

The maximum axial compressive and bending stresses in the ligaments of the most heavily loaded W74 general and LTP spacer plates for the HAC oblique drop slapdown impact loading, both with and without the bounding NCT thermal loading superimposed, are summarized in Table 2.7-10 through Table 2.7-13 along with the resulting interaction ratios. The results of the analysis show that the highest interaction ratios resulting from the HAC oblique drop slapdown impact loading are 0.79 for the W74 general spacer plate and 0.94 for the W74 LTP spacer plate. Therefore, the minimum design margins for ligament buckling of the most highly loaded W74 general and LTP spacer plates for the HAC oblique drop slapdown impact loading are +0.27 and +0.06, respectively.

In addition to the elastic beam-column buckling analysis, general plastic instability of the most heavily loaded W74 general and LTP spacer plates is evaluated for the HAC oblique drop slapdown impact loading, both with and without NCT thermal loading, using plastic large deflection analyses. The W74 general spacer plate plastic large deflection buckling analyses are performed using the multi-span finite element model described in Section 2.12.4.1.3. This model is similar in most respects (e.g., cross-section dimensions, applied loading, and material properties) to the finite element model used to evaluate permanent deformation of the W74 general spacer plate for the HAC slapdown loading. However, the buckling model includes the support tubes and adjacent spacer plate, which provide additional support to the loaded spacer plate. For these analyses, the loads from the SNF assembly grid spacers are conservatively applied to the ligaments of the loaded spacer plate. As discussed in the permanent deformation evaluation, the most heavily loaded W74 general spacer plate is spacer plate number 10 in the W74M upper basket assembly. The total HAC slapdown transverse impact load for the most heavily loaded W74 general spacer plate is 299.8 kips.

The W74 LTP spacer plate plastic large deflection buckling analysis is performed using the finite element model described in Section 2.12.4.1.1 with plastic shell elements (SHELL43) to permit longitudinal deformation of the spacer plate. For this analysis, the loads from the SNF assemblies are conservatively applied to the supporting basket assembly structure as concentrated loads at the SNF assembly grid spacer locations. As discussed above in the LTP spacer plate permanent deformation evaluation, the most heavily loaded W74M LTP spacer plate for the HAC slapdown loading is at the bottom end of the W74M lower basket assembly. The total HAC slapdown transverse impact load for the most heavily loaded W74M LTP spacer plate is 240.0 kips.

The NCT thermal loading and a 10g longitudinal load are initially applied to the finite element models. The spacer plate in-plane loads are then applied and ramped up to 1.5 times the HAC oblique drop slapdown impact loading. The results show that the most heavily loaded W74 general and LTP spacer plate remain stable up to 1.5 times the bounding HAC oblique drop slapdown impact loading, both with and without NCT thermal loading superimposed. Therefore, the most heavily loaded W74 general and LTP spacer plates satisfy the buckling design criteria of NUREG/CR-6322.

2.7.1.4.2 Engagement Spacer Plate

In the event of an oblique drop primary impact, the W74 engagement spacer plate is loaded in the transverse direction by its own weight, and in the longitudinal direction by its own self-weight plus the weight of the basket assembly, damaged fuel canisters, and SNF assemblies

opposite the end of impact. The W74 engagement spacer plate is evaluated for the oblique drop using equivalent static g -loads equal to the product of the peak rigid body acceleration and the engagement spacer plate DLF. As shown in Section 2.12.2, bounding equivalent static longitudinal and transverse acceleration loads 38g and 36g are used for the W74 canister HAC oblique drop primary impact evaluation. For the HAC oblique drop slakedown impact, the loading on the W74 engagement spacer plate is lower than the HAC oblique drop primary impact loading since W74 engagement spacer plate is located near the package center of gravity.

The stresses in the most heavily loaded W74 engagement spacer plate due to the bounding oblique drop primary impact loads are evaluated by scaling the stresses calculated for the HAC end drop and the HAC side drop by the ratio of the applied loads. The resulting stresses are conservatively summed absolutely and irrespective of location.

The maximum primary membrane and primary membrane plus bending stress intensities due to the 60g HAC end drop are 36.2 ksi and 44.4 ksi, respectively. The maximum primary plus secondary plus peak stress intensity due to the 60g HAC side drop, conservatively used in place of the HAC side drop maximum primary membrane and primary membrane plus bending stress intensities, is 16.4 ksi. Therefore, the maximum stresses due to the HAC oblique drop are:

$$P_m = (36.2) \left(\frac{38g}{60g} \right) + (16.4) \left(\frac{36g}{60g} \right) = 32.8 \text{ ksi}$$

$$P_m + P_b = (44.4) \left(\frac{38g}{60g} \right) + (16.4) \left(\frac{36g}{60g} \right) = 38.0 \text{ ksi}$$

The Service Level D allowable primary membrane and primary membrane plus bending stress intensities for Type XM-19 stainless steel at a temperature of 500°F are 62.4 ksi and 93.6 ksi, respectively. The minimum design margins for primary membrane and primary membrane plus bending stress intensity due to the bounding HAC oblique drop loading are:

$$P_m: \text{ DM} = \frac{62.4}{32.8} - 1 = +0.90$$

$$P_m + P_b: \text{ DM} = \frac{93.6}{38.0} - 1 = +1.46$$

Therefore, the W74 engagement spacer plate meets the Service Level D allowable stress design criteria for the bounding HAC oblique drop loading.

The engagement spacer plate elastic stability is evaluated in Section 2.7.1.2.2 for combined longitudinal and transverse g -loads of 45g and 60g, respectively. These loads bound the HAC

oblique drop longitudinal and transverse design g-loads of 38g and 36g, respectively. Therefore, no additional buckling evaluation is required for the HAC oblique drop loading.

2.7.1.4.3 Support Tubes and Support Sleeves

A bounding HAC oblique drop condition is used for the support tube evaluation, combining the highest longitudinal acceleration and the highest transverse acceleration. As discussed in Section 2.7.1.4, the bounding longitudinal equivalent static acceleration load, resulting from the 60° oblique drop primary impact, is 32.4g. The bounding transverse equivalent static acceleration, occurring at the end of the basket for the HAC oblique drop slapdown impact, is 81.1g. For conservatism, bounding HAC oblique drop longitudinal and transverse equivalent static acceleration loads of 35g and 85g are used in the W74 support tube structural evaluation.

The support tube stresses resulting from the HAC oblique drop loads are determined by scaling the stresses calculated for the 60g HAC side drop loading by the ratio 85g/60g and the stresses calculated for the 60g HAC end drop load by 35g/60g, and conservatively adding the resulting stresses absolutely and irrespective of location. The support tube, support sleeve, and associated weld stresses due to the HAC oblique drop load are summarized in the following paragraphs.

Support Tube Stress Evaluation

As shown in Section 2.7.1.2.3, the maximum primary membrane and primary membrane plus bending stress intensities in the most heavily loaded W74 support tube due to the bounding 60g HAC side drop load are 1.44 ksi and 6.44 ksi, respectively. As shown in Section 2.7.1.1.3, the maximum primary membrane and primary membrane plus bending stress intensities in the most heavily loaded W74 support tube due to the bounding 60g HAC end drop load are 22.6 ksi and 23.6 ksi, respectively. Therefore, the support tube primary membrane and primary membrane plus bending stress intensities for the bounding HAC oblique drop are calculated as follows:

$$P_m = (1.44) \left(\frac{85g}{60g} \right) + (22.6) \left(\frac{35g}{60g} \right) = 15.2 \text{ ksi}$$

$$P_m + P_b = (6.44) \left(\frac{85g}{60g} \right) + (23.6) \left(\frac{35g}{60g} \right) = 22.9 \text{ ksi}$$

The Service Level D allowable primary membrane and primary membrane plus bending stress intensities for the support tube SA-240, Type XM-19 stainless steel material at 600°F are 61.5 ksi and 92.2 ksi, respectively. Therefore, the minimum design margins in the W74 support tube due to the bounding HAC oblique drop are:

$$P_m : DM = \frac{61.5}{15.2} - 1 = +3.05$$

$$P_m + P_b : DM = \frac{92.2}{22.9} - 1 = +3.03$$

Therefore, the W74 support tubes meet the Service Level D allowable stress design criteria for the bounding HAC oblique drop load.

Support Tube Longitudinal Seam Weld Stress Evaluation

As shown in Section 2.7.1.2.3, the maximum shear stress in the W74 support tube longitudinal seam weld due to the bounding 60g HAC side drop load is 1.34 ksi. Since the longitudinal loading does not result in any significant shear stress in the W74 support tube longitudinal seam weld, only the transverse component of the HAC oblique drop loading is considered. The maximum shear stress in the support tube longitudinal seam weld due to the HAC oblique drop is calculated as follows:

$$f_v = (1.34) \left(\frac{85g}{60g} \right) = 1.9 \text{ ksi}$$

Per Section 2.7.1.2.3, the Service Level D allowable shear stress for the W74 support tube longitudinal seam weld is 12.3 ksi. The minimum design margin in the support tube longitudinal seam weld for HAC oblique drop loading is:

$$DM = \frac{12.3}{1.9} - 1 = +5.47$$

Therefore, the W74 support tube longitudinal seam weld meets the Service Level D allowable stress design criteria for the bounding HAC oblique drop load.

W74M Support Tube to LTP Spacer Plate Weld Stress Evaluation

As shown in Section 2.7.1.1.3, the maximum shear stress in the W74M support tube to LTP spacer plate weld due to the 60g HAC end drop load is 3.8 ksi. Per Section 2.7.1.2.3, the maximum shear stress in the W74M support tube to LTP spacer plate weld due to the 60g HAC side drop is 0.44 ksi. Therefore, the W74M support tube to LTP spacer plate weld stress due to the bounding HAC oblique drop is calculated as follows:

$$f_v = (3.8) \left(\frac{35g}{60g} \right) + (0.44) \left(\frac{85g}{60g} \right) = 2.8 \text{ ksi}$$

In accordance with Regulatory Guide 7.8, the HAC oblique drop loading is evaluated in combination with NCT thermal loading. As shown in Section 2.6.1.3.3, the bounding NCT thermal loading results in a maximum shear stress of 1.44 ksi in the W74M support tube to LTP spacer plate welds. This weld shear stress is due primarily to axial loads resulting from differential longitudinal expansion of the support tubes and support sleeves. For the HAC oblique drop loading, the axial compressive loads resulting from the longitudinal impact loads cause the support sleeves to compress. This compression relieves the preload condition caused by thermal expansion. Therefore, the weld shear stress due to NCT thermal and HAC oblique drop longitudinal loading is not additive. As shown above, the weld shear stress due to the 35g longitudinal component of the HAC oblique drop loading ($3.8 \text{ ksi} \times 35g/60g = 2.2 \text{ ksi}$) is greater than that due to NCT thermal loading. Therefore, the combined shear stress of 2.8 ksi calculated above is controlling for this load combination.

Per Section 2.7.1.1.3, the Service Level D allowable shear stress for the W74M support tube to LTP spacer plate weld is 14.0 ksi. The minimum design margin in the W74M support tube to LTP spacer plate weld for bounding HAC oblique drop load is:

$$DM = \frac{14.0}{2.8} - 1 = +4.00$$

Therefore, the W74M support tube to LTP spacer plate welds meet the Service Level D allowable stress design criteria for the bounding HAC oblique drop load.

W74T Support Tube to Attachment Sleeve Weld Stress Evaluation

As shown in Section 2.7.1.1.3, the maximum shear stress in the W74T support tube to attachment sleeve weld due to the 60g HAC end drop load is 10.3 ksi. Per Section 2.7.1.2.3, the stresses in the W74T support tube to attachment sleeve weld due to the 60g HAC side drop are insignificant. Therefore, the W74T support tube to attachment sleeve weld shear stress due to the bounding HAC oblique drop is:

$$f_v = (10.3) \left(\frac{35g}{60g} \right) = 6.0 \text{ ksi}$$

In accordance with Regulatory Guide 7.8, the HAC oblique drop loading is evaluated in combination with NCT thermal loading. As shown in Section 2.6.1.3.3, the bounding NCT thermal loading results in a maximum shear stress of 3.32 ksi in the W74T support tube to attachment sleeve welds. This weld shear stress is due primarily to axial loads resulting from differential longitudinal expansion of the support tubes and support sleeves. For the HAC oblique drop loading, the axial compressive loads resulting from the longitudinal impact loads cause the support sleeves to compress. This compression relieves the preload condition caused by thermal expansion. Therefore, the weld shear stress due to NCT thermal and HAC oblique drop longitudinal loading is not additive. As shown above, the weld shear stress due to the 35g longitudinal component of the HAC oblique drop loading is greater than that due to NCT thermal loading.

Per Section 2.7.1.1.3, the Service Level D allowable shear stress for the W74T support tube to attachment sleeve weld is 14.0 ksi. The minimum design margin in the W74T attachment sleeve weld for bounding HAC oblique drop load is:

$$DM = \frac{14.0}{6.0} - 1 = +1.33$$

Therefore, the W74T support tube to attachment sleeve welds meet the Service Level D allowable stress design criteria for the bounding HAC oblique drop load.

Support Tube Buckling Evaluation

Buckling of the most heavily loaded W74 support tubes is evaluated for the HAC oblique drop using the criteria of NUREG/CR-6322 for linear-type supports subjected to combined axial compressive and bending stresses. As shown in Section 3.7.5.2.3 of the FuelSolutions™ W74 Canister Storage FSAR, the maximum beam bending stress (i.e., case 1) in the W74 support

tubes due to the bounding 60g side drop load is 0.07 ksi. As shown in Section 2.7.1.1.3, the maximum axial compressive and bending stresses in the critical span of the most heavily loaded W74 support tube due to the bounding 60g HAC end drop load are 19.3 ksi and 0.5 ksi, respectively. Therefore, the maximum axial compressive and bending stresses in the critical buckling span of the support tubes for the bounding HAC oblique drop loading are calculated as follows:

$$f_a = (19.3) \left(\frac{35g}{60g} \right) = 11.3 \text{ ksi}$$

$$f_b = (0.07) \left(\frac{85g}{60g} \right) + (0.5) \left(\frac{35g}{60g} \right) = 0.4 \text{ ksi}$$

Per NUREG/CR-6322, members subjected to combined compression and bending must satisfy the following equations:

$$\frac{f_a}{F_a} + \frac{C_m f_{bx}}{\left(1 - \frac{f_a}{F_{ex}}\right) F_{bx}} + \frac{C_m f_{by}}{\left(1 - \frac{f_a}{F_{ey}}\right) F_{by}} \leq 1.0$$

$$\frac{f_a}{2 \times 0.6 S_y} + \frac{f_{bx}}{F_{bx}} + \frac{f_{by}}{F_{by}} \leq 1.0$$

Interaction equations (26) and (27) are satisfied as follows, where C_m is conservatively assumed as 1.0 for equation (26) and the allowable stresses are defined in Section 2.7.1.1.3:

$$\frac{11.3}{23.0} + \frac{(1.0)(0.4)}{\left(1 - \frac{11.3}{726}\right)(45.5)} + \frac{(1.0)(0.4)}{\left(1 - \frac{11.3}{726}\right)(45.5)} = 0.50 \quad (26)$$

$$\frac{11.3}{2 \times 0.6(37.3)} + \frac{0.4}{45.5} + \frac{0.4}{45.5} = 0.27 \quad (27)$$

These results show that the W74 support tubes are adequate to withstand the bounding HAC oblique drop loading. Note that the drop loads need not be combined with the primary thermal stresses resulting from longitudinal differential thermal expansion because the thermal stress acts as a tension preload that is relieved by the HAC oblique drop axial compressive loading.

The minimum design margin for buckling of the W74 support tubes for the bounding HAC oblique drop loading is:

$$DM = \frac{1.00}{0.50} - 1 = +1.00$$

Since the stresses in the W74 support tube resulting from the HAC oblique drop are lower than the support tube yield strength, inelastic buckling is not possible. Therefore, no evaluation of inelastic buckling is required for the W74 support tubes.

Support Sleeve Evaluation

Since the W74 support sleeve stresses resulting from transverse loading are insignificant and the longitudinal acceleration due to the HAC oblique drop is bounded by the HAC end drop, the W74 support sleeve stresses and buckling interaction ratio for the HAC oblique drop are bounded by those calculated for the HAC end drop in Section 2.7.1.1.3.

2.7.1.4.4 Guide Tubes

As discussed in Section 2.7.1.4, the W74 canisters are evaluated for bounding HAC oblique drop primary and secondary (slapdown) impact loadings. For the HAC oblique drop primary impact, the W74 guide tube assemblies are subjected to both longitudinal (38g) and transverse (36g) loading. Whereas, the HAC oblique drop slapdown impact loading consists of a uniform transverse acceleration of 31.8g and an angular acceleration of 212 rad/s² and results in a transverse acceleration load of over 80g at the end of the canister. The guide tubes are loaded in the transverse direction by their own inertial load and the inertial load of the SNF assembly. Since the SNF assemblies are supported longitudinally at the impacting end by the canister shell end plates, the guide tubes are loaded only by their own inertial load in the longitudinal direction. As shown in Section 2.7.1.1.4, the 60g HAC end drop loading results in a maximum axial compressive stress of 3.7 ksi at the bottom end of the guide tube. Since guide tube stresses due to longitudinal loading are low and the HAC oblique drop primary impact transverse loading is significantly lower than that resulting from the slapdown impact, the slapdown impact loading will produce higher stresses in the W74 guide tube than the primary impact loading. Therefore, the structural evaluation of the W74 guide tubes for the HAC oblique drop is performed only for the bounding slapdown impact loading.

The structural evaluation of the W74 guide tube for the HAC oblique drop slapdown impact loading is performed for two fuel loading assumptions: (1) uniform distribution of the SNF assembly weight along the entire length of the guide tube, and (2) concentrated loads on the guide tube only at the locations of the SNF assembly grid spacers.

An elastic-system analysis is performed in Section 2.7.1.4.4.1 using the uniform fuel loading assumption to demonstrate that the W74 guide tubes meet the Service Level D allowable stress design criteria of Subsection NG for the HAC oblique drop slapdown loading. The elastic-system analysis includes a finite element analysis to determine the maximum stress intensities in the guide tube. Hand calculations are performed to determine the maximum stresses in the neutron absorber panels and their attachments to the guide tubes. In addition, buckling of the guide tube is evaluated in accordance with NUREG/CR-6322 for the HAC slapdown loading.

A plastic-system analysis is performed in Section 2.7.1.4.4.2 to determine the maximum permanent deformation of the guide tube resulting from the HAC slapdown impact loading. The plastic analysis is performed using the concentrated SNF loading assumption, since this condition results in the largest permanent deformation of the guide tube. The resulting guide tube permanent deformation is considered in the criticality evaluation presented in Chapter 6.

2.7.1.4.4.1 Guide Tube Elastic-System Analysis

Guide Tube Stress Evaluation

The guide tube transverse loads are proportional to the transverse acceleration. For the HAC oblique drop conditions, the transverse acceleration increases with the moment arm from the package center of gravity. As shown in Section 2.12.2, the transverse accelerations resulting from the HAC slapdown impact varies from 31.8g at the package center of gravity to over 80g near the ends of the canister (i.e., at a distance of 90 inches from the package center of gravity). The increase in loading on the guide tube spans further from the package center of gravity are offset by the smaller free span distances. The guide tube span in which the highest stresses occur is identified by comparing the relative stresses in each guide tube span due to the HAC oblique drop 15° secondary impact. For this evaluation, the guide tubes panels, upon which the SNF assembly is supported, are treated as flat rectangular plates with fixed edges, subjected to a uniform pressure load.

The stress in a flat plate loaded by a uniform pressure is a function of the plate dimension, support conditions, and the magnitude of the pressure load. The maximum bending stress for a rectangular plate fixed on all edges is given in Table 26, Case 8a, of Roark, as:

$$\sigma = -\beta_1 q (b/t)^2$$

Since the guide tube thickness (t), fuel line load (w), and plate width (a) are the same for both W74M and W74T designs, the following relationship is true for the guide tube:

$$\sigma \approx \beta_1 G b^2$$

where:

- β_1 = Stress parameter (varies as function of the plate aspect ratio a/b)
- a = Larger of the guide tube panel width (6.99 in.) or span length (varies)
- b = Smaller of the guide tube panel width (6.99 in.) or span length (varies)
- G = Equivalent static acceleration at center of each guide tube span
= 31.9g + [(211.8 rad/s² x d)/386.4 in/s²]
- d = Longitudinal distance from the package c.g. to the center of the guide tube span

The value of the $\beta_1 G b^2$ is calculated for all W74M and W74T guide tube free spans for the HAC slapdown impact loading. The results show that the maximum bending stress due to the HAC slapdown impact occurs in span number 8 of the W74M lower basket assembly (i.e., between the 5th and 6th general spacer plates from the bottom end of the basket). The equivalent static transverse acceleration at this span is 62g. The guide tube stress and buckling evaluations are performed for this governing guide tube span using a bounding transverse acceleration load of 62g.

The stresses in the governing span of the W74 guide tube due to the 62g HAC slapdown impact transverse load are evaluated using the half-symmetry periodic finite element model described in Section 2.12.4.3. The model represents a segment of the W74 guide tube spanning from the centerline of a spacer plate to the mid-span between the adjacent spacer plate support, taking advantage of longitudinal symmetry. The guide tube is modeled using shell elements. The material density used for the guide tube elements is adjusted to account for the mass of the neutron absorber panels, conservatively taking no credit for structural support of the guide tube provided by the neutron absorber panels. As shown in Section 2.10.4.3, the adjusted density of the guide tube is 0.51 lb/in³.

The load from the SNF assembly is applied as a uniform pressure load on the supporting guide tube panel. The SNF assembly pressure load due to the 62g HAC slapdown transverse loading is:

$$q_F = \left(\frac{w_f}{a} \right) (62g) = 50.7 \text{ psi}$$

where;

$$\begin{aligned} w_f &= 5.72 \text{ lb/inch, bounding line load (weight per unit length) for BRP fuel} \\ &= 485 \text{ lb./84.8 inches} \end{aligned}$$

$$a = 6.99 \text{ inches, width of guide tube}$$

The guide tube stresses are determined using a linear-elastic static analysis. The maximum primary membrane and primary membrane plus bending stress intensities in the guide tube due to the bounding 62g slapdown loading are 16.0 ksi and 56.4 ksi, respectively. Stress intensity contour plots at the middle, top, and bottom fibers of the shell are shown in Figure 2.7-4 through Figure 2.7-6.

The Service Level D allowable primary membrane and primary membrane plus bending stress intensities for Type 316 stainless steel at 650°F are 40.0 ksi and 60.0 ksi, respectively. Therefore, the minimum design margins for primary membrane and primary membrane plus bending stress intensities due to the HAC oblique drop slapdown impact are:

$$P_m: \text{ DM} = \frac{40.0}{16.0} - 1 = +1.50$$

$$P_m + P_b: DM = \frac{60.0}{56.4} - 1 = +0.06$$

The W74 guide tubes include two full penetration longitudinal seam welds located on opposite faces. The longitudinal seam welds may be examined using either RT or surface PT methods. When RT examination is performed, there are no restrictions on the locations of the longitudinal seam welds since the allowable stresses for the welds are equal to those of the base material. When only surface PT examination is performed, the longitudinal seam welds must be located at ¼ the panel width to minimize the weld stress. The stresses in the guide tube longitudinal seam weld resulting from the 62g slakedown loading are evaluated using the maximum nodal forces and moments from the finite element solution. The equations used for this evaluation are the same as those used for the NCT vibration loading in Section 2.6.5.4. The results show that the maximum primary membrane and primary membrane plus bending stress intensities, occurring in the bottom horizontal panel at mid-span, are 5.7 ksi and 29.6 ksi, respectively.

In accordance with Table NG-3352-1 of the ASME Code, a 65% weld efficiency factor is applied to the allowable stresses for a full penetration weld with PT examination. Therefore, the W74 guide tube seam weld Service Level D allowable primary membrane and primary membrane plus bending stress intensities are 26.0 ksi (=40.0 x 0.65) and 39.0 ksi (=60.0 x 0.65), respectively. The minimum design margins for primary membrane and primary membrane plus bending stress intensities in the W74 guide tube longitudinal seam weld due to the bounding 62g slakedown transverse load are:

$$P_m: DM = \frac{26.0}{5.7} - 1 = +3.56$$

$$P_m + P_b: DM = \frac{39.0}{29.6} - 1 = +0.32$$

Therefore, the W74 guide tubes meet the Service Level D allowable stress design criteria for the bounding HAC oblique drop loads.

Guide Tube Buckling Evaluation

Buckling of the W74 guide tube is evaluated for the HAC oblique drop using the criteria of NUREG/CR-6322 for linear-type members subjected to combined axial compressive and bending loads. The axial compressive stress and bending stress in the side panels of the W74 guide tube are determined using classical solutions. The side panel is evaluated as a fixed-fixed span, assuming half of the panel weight is applied at the end (top panel contribution) and the self-weight of the side panel is distributed along its length. As a result, the axial compression is not constant but varies along the side panel length. Since the theoretical buckling stress for linearly varying axial compressive stress in a column is higher than that of a column subjected to a uniform axial compressive stress on which the NUREG/CR-6322 acceptance criteria are based, an equivalent value of axial stress is calculated for use in the interaction equations. The

equivalent axial load corresponding to the theoretical buckling stress of the guide tube side panel is determined using Roark, Table 34, Case 3a, assuming $a/l = 1$ and $P/pl = 0.5$. The critical load pa is calculated to be $3.94(\pi^2EI/L^2)$ for the total of $5.9(\pi^2EI/L^2)$ at the base of the panel (i.e., $1.5pa$). This compares to a critical axial compressive load $4\pi^2EI/L^2$ for a linear member with a uniform axial compressive stress distribution. Therefore, the equivalent axial stress in the side panel is calculated as follows:

$$f_a = \frac{4}{5.9} \left(L + \frac{L}{2} \right) \rho G = 225 \text{ psi}$$

where:

$G = 62g$, bounding HAC oblique drop slapdown load

$L = 6.99$ in., width of the guide tube panel

$\rho = 0.51$ lb/in³, effective guide tube density accounting for the weight of neutron absorber panel, as calculated above

The maximum bending stress in the guide tube side panel due to moment reactions from the top and bottom panels is calculated based on the maximum guide tube bending stress in the top and bottom panel due to the 62g HAC oblique drop slapdown load. Since buckling is a global effect, the bending stress is averaged over the span between the spacer plates. The average stress intensity along the bottom edge of the side panel due to a 62g transverse acceleration load is approximately 12.93 ksi, as shown in Figure 2.7-5 and Figure 2.7-6.

The allowable axial and bending stresses for the guide tube are calculated in accordance with NUREG/CR-6322 for linear members subjected to combined axial compressive and bending loads. The allowable axial stress for austenitic stainless steel members is calculated as follows:

$$F_a = \frac{(P_{EQ46})(P_{EQ35})}{P_{EQ44}} = 4.43 \text{ ksi}$$

where P_{EQ46} , P_{EQ35} , and P_{EQ44} are the allowable compressive stresses from Equations (46), (35), and (44) of NUREG/CR-6322, which are calculated as follows:

$$\lambda = \left(\frac{KL}{r} \right) \left(\frac{1}{\pi} \right) \sqrt{\frac{S_y}{E}} = 1.51$$

$$P_{EQ46} = \left(0.4 - \frac{120\lambda}{600\sqrt{2}} \right) S_y = 3.46 \text{ ksi (for } \lambda > \sqrt{2} \text{)}$$

$$P_{EQ35} = \frac{2}{3\lambda^2} S_y = 5.41 \text{ ksi (for } \lambda > \sqrt{2} \text{)}$$

$$P_{EQ44} = \frac{1}{1.92\lambda^2} S_y = 4.23 \text{ ksi (for } \lambda > \sqrt{2})$$

where:

K = 0.65, effective length factor for a fixed-slider boundary condition

L = 6.99 inches, length of the panel

r = $0.090/\sqrt{12} = 0.026$ inches, radius of gyration

S_y = 18.5 ksi, yield strength of Type 316 stainless steel at 650°F

E = 25.1x10⁶ psi, elastic modulus of Type 316 stainless steel at 650°F

The ratio of f_a / F_a (0.225/4.43) is equal to 0.051. Since this ratio is less than 0.15, equation (28) of NUREG/CR-6322 may be used.

The allowable bending stress per NUREG/CR-6322 is F_b = fS_y or 27.75 ksi, where f=1.5 is the plastic shape factor for rectangular cross-section. Therefore, the interaction ratio for equation (28) of NUREG/CR-6322 is calculated as follows:

$$\frac{f_a}{F_a} + \frac{f_b}{F_b} = 0.051 + \frac{12.95}{27.75} = 0.52 < 1$$

The minimum guide tube design margin against buckling is:

$$DM = \frac{1.00}{0.52} - 1 = +0.92$$

No thermal stresses exist in the guide tube because sufficient clearances are provided. Therefore, the guide tube is adequate to withstand the HAC oblique drop without buckling.

Neutron Absorber Panel Stress Evaluation

The maximum bending stress and average bearing stress in the neutron absorber panel resulting from the HAC oblique drop are evaluated using hand calculations. The W74 guide tube neutron absorber panels are designed to support their own weight over the span between each spacer plate in case of a HAC oblique drop. The maximum bending moment and bending stress in the panel at the governing span are calculated for a fixed-fixed beam as follows:

$$M = 62g \cdot \frac{wl^2}{12} = 4.58 \text{ in} - \text{lbs/in}$$

$$f_b = \frac{6M}{t_{NA}^2} = 5.0 \text{ ksi}$$

where:

$l = 6.375$ in., maximum clear span between spacer plates

$w = \rho t_{NA}$, self-weight load on the neutron absorber panel
 $= 0.29 \text{ lb/in}^3 \times 0.075 \text{ in.}$
 $= 0.0218 \text{ psi}$

$t_{NA} = 0.075$ in., neutron shield panel thickness

The shear stress in the neutron absorber panels due to the 62g transverse loading is not significant (less than 0.1 ksi). Therefore, the maximum bending stress is compared to the Service Level D allowable primary membrane plus bending stress intensity. As discussed in Section 2.3, the neutron absorber panels are assumed to have the same mechanical properties as SA-240, Type 304 stainless steel. Therefore, the Service Level D allowable primary membrane plus bending stress intensity at 650°F is 58.3 ksi. The minimum design margin for primary membrane plus bending stress in the neutron absorber panel due to the 62g slapping loading is:

$$DM = \frac{58.3}{5.0} - 1 = +10.7$$

The maximum bearing stress in neutron absorber panel occurs at the carbon steel spacer plate because its tributary load is close to that of the stainless spacer but the thickness is much lower. The bearing stress is determined as follows:

$$f_p = G \cdot \frac{W_{\text{fuel}} + W_{\text{tube}}}{bt} = 62g \cdot 7.125 \cdot \frac{5.72 + 0.51 \times 2.52}{6.4 \times 0.75} = 645 \text{ psi}$$

where the area of the guide tube section is taken as $4 \times 6.99 \times 0.090 = 2.52 \text{ in}^2$, and the other parameters are defined above.

Although evaluation of bearing stress is not required per the ASME Code for accident conditions, the bearing stress in the neutron absorber panel is considered to assure that no local damage results from the slapping impact. As discussed in Section 2.3, the W74 guide tube neutron absorber panels are assumed to have the same mechanical properties as SA-240, Type 304 stainless steel. The yield strength of Type 304 stainless steel at 650°F is 18.5 ksi. Therefore, the bearing stress level in the neutron absorber sheets due to the 62g HAC oblique drop slapping impact loading is not sufficient to cause any damage to the neutron absorber panels.

Neutron Absorber Panel Retainer Weld Stress Evaluation

The neutron absorber panels are attached to the guide tubes using stainless steel retainers. A minimum of seven retainers are used per neutron absorber panel, with variable center-to-center spacing. Each retainer is welded to the guide tube with a 3/16-inch plug weld. Shear plug welds are relied on to support the maximum neutron absorber sheet retainer shear load due to the

tributary weight of the neutron absorber sheet on the vertical side of the guide tube. The maximum weld shear stress is:

$$f_w = \frac{Gw(D_{NA}S)}{\pi d^2/4} = 5.05GS$$

where:

- G = transverse slapdown equivalent static acceleration load at center of tributary length for each retainer, per Table 2.7-14
 = 1.13 x [28.2g + (187.4 rad/s²)(x)/(386.4 in/s²)]
- x = longitudinal moment arm, assumed equal to distance from center of engagement spacer plate to the center of the length of neutron absorber sheet tributary to the retainer
- w = 0.0218 psi, self-weight load on the neutron absorber panel
 = 0.29 lb/in³ x 0.075 in.
- D_{NA} = 6.4 inches, width of the neutron absorber sheet
- S = tributary length for each weld, per Table 2.7-14
- d = 0.1875 inches, plug weld diameter

The tributary length, S, of neutron absorber sheet supported by each retainer and the equivalent static acceleration load, G, due to the slapdown impact, along with the resulting weld shear stresses, are summarized in Table 2.7-14 for the W74M and W74T upper and lower basket assemblies. The results show that the maximum retainer weld shear stress due to the HAC oblique drop slapdown impact is 4.4 ksi, occurring in the top retainer (number 7) of the W74M upper basket assembly.

In accordance with Table NG-3352-1 of the ASME B&PV Code, a 30% weld quality factor is applied to the allowable stresses for plug welds. Therefore, the Service Level D allowable weld shear stress, based on SA-240, Type 304 stainless steel at a bounding design temperature of 650°F, is 5.9 ksi (=19.5 ksi x 0.3). The minimum design margin for shear stress in the neutron absorber sheet retainer plug weld for the HAC oblique drop is:

$$DM = \frac{5.9}{4.4} - 1 = +0.34$$

Therefore, the stresses in the plug weld between the neutron absorber panel retainers and the guide tubes meet the Service Level D allowable stress design criteria for the HAC oblique drop loading.

2.7.1.4.4.2 Guide Tube Plastic Analysis

In addition to the linear-elastic stress analysis performed in Section 2.7.1.4.4.1, the W74 guide tubes are evaluated for the bounding HAC oblique drop slapdown impact loading on a plastic basis to determine the maximum guide tube permanent deformation. For this analysis, the guide tube span that experiences the highest loads from the SNF assembly grid space is evaluated. In order to identify the governing guide tube span, the loading from each SNF grid spacer is calculated for the HAC slapdown impact. The grid spacer loading is calculated as follows:

$$F_{gs} = W_{gs}G$$

where:

W_{gs} = Grid spacer tributary weights from Tables 2.12-4 and 2.12-5

G = Transverse acceleration at the location of each grid spacer
= $31.8g + (212 \text{ rad/s}^2)(d)/(386.4 \text{ in/s}^2)$

d = Longitudinal distance from the package c.g. to the center of the grid spacer

The maximum grid spacer loads are shown to occur at the top in-core grid spacer in the W74T upper basket assembly, located at a distance of 59.2 inches from the package center of gravity. The tributary weight of this grid spacer is 118 pounds (Table 2.12-3) and the transverse slapdown g-load at this location is 64.3g. The location of this grid spacer coincides with the location of a spacer plate. However, it is conservatively assumed that the grid spacer loading is applied to the guide tube at the center of the span between spacer plates number 9 and 10. The guide tube span length at this location is 6.50 inches.

The evaluation of the W74 guide tube for the bounding 64.5g slapdown impact loading, with the SNF assembly weight applied as a concentrated load at the location of the SNF grid spacer, is performed using the finite element model described in Section 3.9.2.6.2 of the FuelSolutions™ W74 Canister Storage SAR.¹⁹ The SNF assembly load is applied to the model at the mid-span of the largest guide tube span (i.e., midway between spacer plate supports), since this results in the largest guide tube deformations for a given load. The applied loads include: (1) a 64.5g acceleration applied to account for the guide tube self-weight, (2) a grid spacer protrusion displacement imposed on the guide tube bottom panel nodes in the region of the grid spacer, and (3) a uniform pressure load applied to those spans that do not have the imposed displacement loading, to account for the balance of the fuel weight not accounted for by the imposed displacement.

The magnitude of the imposed displacement is based on the maximum protrusion of the BRP fuel grid spacer beyond the fuel rod envelope (i.e., distance from edge of grid spacer to outermost fuel rod), recognizing that the displacement of the guide tube is limited by this fuel parameter. The maximum grid spacer protrusion is 0.148 inch. A bounding 0.15-inch displacement is imposed onto the guide tube bottom panel in the area of the grid spacer support. In addition, a uniform pressure load of 44 psig is applied to the guide tube span without the imposed displacement load.

The total vertical reaction load from the finite element solution is 2,354 pounds, compared to the expected reaction load of 2,308 lbs. ($=64.5g [118 \text{ lb.} + 1.29 \text{ lb./inch} \times 19.5 \text{ inches}]/4$). The resulting stress intensity distributions in the guide tube shell elements at the middle, top, and bottom shell fibers are shown in Figure 2.7-7, Figure 2.7-8, and Figure 2.7-9, respectively. The results show that the maximum stress intensity and maximum equivalent plastic strain at the middle fiber of the guide tube shell elements are 19.0 ksi and 2.1%, respectively. The maximum stress intensity and equivalent plastic strain at the extreme fibers (i.e., top and bottom) of the guide tube shell elements are 27.5 ksi and 7.7%, respectively. The plastic strain in the guide tube only exceeds 1% in a small region near the edge of the grid spacer support area. Furthermore, the maximum plastic strain resulting from the HAC slapdown impact loading is much lower than the maximum elongation of SA-240, Type 316 stainless steel. The maximum permanent deformation of the W74 guide tube, occurring at the location of the concentrated grid spacer loading, is 0.125 inch. The deformed shape of the W74 guide tube resulting from the concentrated fuel loading is shown in Figure 2.7-10.

2.7.1.4.5 Canister Shell

The W74 canister shell assembly is evaluated for an 87g transverse load resulting from the HAC oblique drop slapdown impact using the three-dimensional half-symmetry finite element model described in Section 2.12.4.6. This model represents the top end region of the canister shell and basket assembly. The top end shield plug and basket assembly spacer plates are included in the finite element model and connected to the canister shell with gap elements in order to accurately capture the non-linear interaction between these components and the canister shell for the slapdown loading. In addition, radial gap elements are used to model the non-linear support interface between the outside of the canister shell and the inside of the cask cavity.

For the W74 canister shell slapdown evaluation, the inertial loads of the canister shell, top end outer and inner closure plates, the shield plug, and the self weight of the spacer plates are accounted for by applying an appropriate acceleration in the direction of the loading. The inertial loads of the fuel assembly and the guide tube are applied as uniform pressure loads over the width of the supporting spacer plate ligaments. The ligament pressure loads are calculated for each spacer plate based on the guide tube and fuel tributary weights.

The stresses in the canister shell due to the 87g HAC oblique drop slapdown impact loading are calculated using a linear-elastic static analysis. The HAC oblique drop slapdown loading is evaluated both with and without a bounding internal pressure load of 12 psig. Thermal loading is not evaluated in combination with the HAC oblique drop slapdown loading since the ASME Code classifies general thermal stresses as secondary and does not require evaluation of secondary stresses for accident conditions. The resulting stress intensities in the canister shell, analyzed with and without internal pressure loading, are shown in Figure 2.7-11. In general, the stress intensities within the canister shell due to the 87g HAC oblique drop slapdown impact loading are relatively low (less than 10 ksi). As shown in Figure 2.7-11, the only significant canister shell stresses occur on the bottom centerline (i.e., impact line) near the top end inner and outer closure plates. These higher stresses, which are highly localized, are due primarily to concentrated bearing loads that produce high bearing stresses. Bearing stress is not expected to cause gross structural failure of the shell. Furthermore, the ASME B&PV Code does not require evaluation of bearing stresses for Service Level D conditions. The maximum stress intensities in each of the canister shell assembly components are summarized in Table 2.7-15. The results of

the canister shell slapdown stress analysis show that the maximum stresses are less than the corresponding Service Level D allowable stresses.

The maximum primary membrane stress intensity, occurring in the inner cylindrical shell, is 39.6 ksi compared to a Service Level D allowable primary membrane stress intensity of 46.2 ksi. The corresponding minimum design margin in the canister shell for primary membrane stress intensity due to the bounding 87g HAC oblique drop slapdown impact load is +0.17. The maximum primary membrane plus bending stress intensity, occurring in the cylindrical shell, is 59.9 ksi versus a Service Level D allowable primary membrane plus bending stress intensity of 69.3 ksi. The corresponding minimum design margin in the canister shell for primary membrane plus bending stress intensity due to the bounding 87g HAC oblique drop slapdown impact load is +0.16. Therefore, the maximum stress intensities in the W74 canister shell due to the HAC oblique drop slapdown impact loading are less than the corresponding Service Level D allowable stress intensities.

2.7.1.4.6 Oblique Drop Summary

The results of the preceding HAC oblique drop structural analyses demonstrate that the W74 canister has adequate structural integrity to satisfy the structural design criteria of Section 2.1.2 of this SAR. The results of the HAC oblique drop structural evaluation are summarized in Table 2.7-16 and discussed in the following paragraphs.

The maximum stress intensities in each of the W74 canister components due to the HAC oblique drop loading satisfy the Service Level D allowable stress design criteria. Excluding buckling, the lowest design margins in the W74 canister is +0.06 for primary membrane plus bending stress intensity in the most heavily loaded span of the W74 guide tube. The minimum design margin for buckling is +0.06 in the most heavily loaded W74 LTP spacer plate for the combined HAC oblique drop slapdown impact plus NCT thermal loading. However, as shown in Figure 14 of NUREG/CR-6322, the factor of safety embedded in the buckling interaction equations for axial compressed stainless steel members is greater than 1.5 (for $\lambda \geq 0.1$). Therefore, the most heavily loaded W74 LTP spacer plates provide a significant factor of safety against buckling.

The extent of damage sustained by the W74 canister for the HAC oblique drop includes small permanent deformations in the W74 guide tubes and LTP spacer plates. In addition, failure of the stainless steel attachment brackets that secure the W74M guide tubes to the bottom end LTP spacer plate will occur for the HAC oblique drop primary impact.

As discussed in Section 2.7.1.4.1, the maximum permanent deformation of the most heavily loaded W74 LTP spacer plates caused by HAC oblique drop loading is 0.023 inch. The permanent deformation of the LTP spacer plates is highly localized and does not affect the ability of the package to satisfy the subcriticality requirements of 10CFR71. As shown in Section 2.7.1.4.4.2, the maximum permanent deformation of the guide tube is 0.125 inch. The 0.125-inch permanent deformation occurs only at the locations of the SNF assembly grid spacers (approximately every third guide tube span) with no permanent deformation in the guide tube spans between grid spacers.

The longitudinal shifting of the guide tube assembly relative to the SNF assembly resulting from failure of the attachment brackets is considered in the accident criticality evaluation presented in Chapter 6 of this SAR. The results of the criticality evaluation demonstrate that failure of the

guide tube attachment brackets does not affect the ability of the W74 canister to satisfy the subcriticality requirements of 10CFR71. Furthermore, the failure of the guide tube attachment brackets does not prevent retrieval of the SNF assemblies from the canister.

Table 2.7-6 - W74 Canister General and LTP Spacer Plate Maximum Stress Intensities for 36g Transverse Loading

Impact Azimuth ⁽¹⁾	Maximum General Spacer Plate Stress Intensities (ksi) ⁽²⁾ [Location] ⁽³⁾		Maximum LTP Spacer Plate Stress Intensities (ksi) ⁽²⁾ [Location] ⁽³⁾	
	P _m	P _m + P _b	P _m	P _m + P _b
0°	25.5 [11]	44.6 [11]	9.4 [11]	23.2 [2]
15°	17.9 [10]	59.1 [104]	9.7 [10]	33.9 [90]
30°	16.0 [10]	65.2 [118]	10.0 [26]	38.3 [16]
45°	13.6 [10]	67.4 [131]	8.9 [26]	39.2 [28]
60°	14.2 [26]	64.5 [42]	9.8 [11]	39.7 [33]
75°	17.5 [11]	60.8 [51]	8.5 [24]	35.0 [51]
90°	23.8 [65]	42.4 [27]	8.8 [65]	23.6 [27]

Notes:

- (1) Impact azimuths are shown in Figure 2.7-2.
- (2) Maximum stress intensities are shown in **bold**.
- (3) The section numbers corresponding to the location of the maximum stress intensities are shown in Figure 2.12-1.

Table 2.7-7 - W74 Canister General and LTP Spacer Plate Maximum Stresses for HAC Oblique Drop Secondary Impact

Impact Azimuth ⁽¹⁾	Maximum General Spacer Plate Stress Intensities (ksi) ⁽²⁾ [Location] ⁽³⁾		Maximum LTP Spacer Plate Stress Intensities (ksi) ⁽²⁾ [Location] ⁽³⁾	
	P _m	P _m + P _b	P _m	P _m + P _b
0°	30.7 [11]	62.5 [2]	15.2 [11]	31.5 [2]
15°	30.4 [88]	88.4 [114]	12.6 [10]	44.9 [104]
30°	26.8 [88]	88.7 [114]	11.6 [10]	49.9 [118]
45°	23.3 [4]	84.1 [131]	10.2 [10]	50.1 [42]
60°	27.1 [65]	87.5 [55]	10.6 [11]	49.9 [42]
75°	30.3 [65]	86.9 [55]	12.1 [11]	45.2 [51]
90°	30.0 [27]	63.8 [27]	14.1 [65]	32.1 [27]

Notes:

- (1) Impact azimuths are shown in Figure 2.7-2.
- (2) Maximum stress intensities are shown in **bold**.
- (3) The section numbers corresponding to the location of the maximum stress intensities are shown in Figure 2.12-1.

Table 2.7-8 - W74 General Spacer Plate Allowable Buckling Stresses

Spacer Plate Buckling Characteristics	Ligament Type ⁽¹⁾				
	A	Bx	By	B	C
Width, b (in.)	1.125	1.050	0.975	1.005	0.875
Thickness, t (in.)	0.75	0.75	0.75	0.75	0.75
Height, L (in.)	7.325	7.40	7.25	7.325	7.325
Gross Area, A _g (in ²)	0.84	0.79	0.73	0.75	0.66
I _{xx} (in ⁴)	0.040	0.037	0.034	0.035	0.031
r _x (in.)	0.217	0.217	0.217	0.217	0.217
Effective Length Factor, K	0.65	0.65	0.65	0.65	0.65
Kl/r _x	21.99	22.22	21.77	21.99	21.99
S _y at 700°F (ksi)	83.0	83.0	83.0	83.0	83.0
E at 700°F (ksi)	25.5x10 ³	25.5x10 ³	25.5x10 ³	25.5x10 ³	25.5x10 ³
Lambda	0.399	0.403	0.395	0.399	0.399
P ₃₃ (kips)	51.0	47.5	44.3	45.5	39.7
P ₄₃ (kips)	N/A	N/A	N/A	N/A	N/A
P ₄₅ (kips)	N/A	N/A	N/A	N/A	N/A
P ₄₀ (kips)	N/A	N/A	N/A	N/A	N/A
F _a (ksi)	60.4	60.3	60.6	60.4	60.4
F _b (ksi)	124.5	124.5	124.5	124.5	124.5
F _e ' (ksi)	400.3	392.2	408.6	400.3	400.3

Note:

⁽¹⁾ Ligament IDs are shown in Figure 2.6-8.

Table 2.7-9 - W74 LTP Spacer Plate Allowable Buckling Stresses

Spacer Plate Buckling Characteristics	Ligament Type ⁽¹⁾				
	A	Bx	By	B	C
Width, b (in.)	1.125	1.050	0.975	1.005	0.875
Thickness, t (in.)	2.00	2.00	2.00	2.00	2.00
Height, L (in.)	7.325	7.40	7.25	7.325	7.325
Gross Area, A _g (in ²)	2.25	2.10	1.95	2.01	1.75
I _{xx} (in ⁴)	0.237	0.193	0.154	0.169	0.112
r _x (in.)	0.325	0.303	0.281	0.290	0.253
Effective Length Factor, K	0.65	0.65	0.65	0.65	0.65
Kl/r _x	14.66	15.87	16.74	16.41	18.85
S _y at 500°F (ksi)	38.8	38.8	38.8	38.8	38.8
E at 500°F (ksi)	25.8E+03	25.8E+03	25.8E+03	25.8E+03	25.8E+03
Lambda	0.181	0.196	0.207	0.203	0.233
P ₃₃ (kips)	71.9	66.6	61.4	63.5	54.4
P ₄₃ (kips)	50.5	47.0	43.5	44.9	38.8
P ₄₅ (kips)	38.0	35.2	32.6	33.6	28.9
P ₄₀ (kips)	54.1	50.0	46.0	47.6	40.5
F _a (ksi)	24.0	23.8	23.6	23.7	23.2
F _b (ksi)	58.2	58.2	58.2	58.2	58.2
F _e ' (ksi)	811.4	692.6	622.1	647.6	490.9

Note:

⁽¹⁾ The locations of the different spacer plate ligament types are shown in Figure 2.6-8.

Table 2.7-10 - W74 General Spacer Plate Buckling Interaction Ratios for HAC Slapdown Impact Loading without Thermal

Impact Orientation	Stresses and Interaction Ratios	Ligament Type ⁽¹⁾				
		A	B _x	B _y	B	C
0°	Axial Stress (ksi)	23.41	22.90	0.74	18.60	6.80
	Bending Stress (ksi)	6.54	11.73	35.96	24.70	33.12
	Interaction Ratio (Eq. 26)	0.43	0.46	0.26	0.48	0.34
	Axial Stress (ksi)	23.41	22.90	0.74	18.60	6.80
	Bending Stress (ksi)	6.54	11.73	35.96	24.70	33.12
	Interaction Ratio (Eq. 27)	0.29	0.32	0.30	0.39	0.33
15°	Axial Stress (ksi)	14.24	22.81	0.00	13.71	5.40
	Bending Stress (ksi)	60.22	29.55	61.98	68.37	53.24
	Interaction Ratio (Eq. 26)	0.66	0.59	0.42	0.71	0.46
	Axial Stress (ksi)	14.24	22.81	0.00	11.57	0.00
	Bending Stress (ksi)	60.22	29.55	61.98	73.64	63.15
	Interaction Ratio (Eq. 27)	0.63	0.47	0.50	0.71	0.51
30°	Axial Stress (ksi)	12.52	19.58	0.00	9.34	0.00
	Bending Stress (ksi)	64.75	24.68	64.54	76.25	64.57
	Interaction Ratio (Eq. 26)	0.66	0.50	0.44	0.69	0.44
	Axial Stress (ksi)	12.52	19.58	0.00	9.34	0.00
	Bending Stress (ksi)	64.75	24.68	64.54	76.25	64.57
	Interaction Ratio (Eq. 27)	0.65	0.39	0.52	0.71	0.52
45°	Axial Stress (ksi)	8.31	15.49	0.00	6.12	0.00
	Bending Stress (ksi)	73.31	19.02	60.91	73.45	65.78
	Interaction Ratio (Eq. 26)	0.65	0.39	0.42	0.61	0.45
	Axial Stress (ksi)	8.31	0.00	0.00	5.89	0.00
	Bending Stress (ksi)	73.31	44.03	60.91	74.05	65.78
	Interaction Ratio (Eq. 27)	0.67	0.35	0.49	0.65	0.53
60°	Axial Stress (ksi)	10.43	3.81	15.56	9.07	9.46
	Bending Stress (ksi)	70.23	39.87	28.64	76.88	45.45
	Interaction Ratio (Eq. 26)	0.66	0.34	0.46	0.69	0.47
	Axial Stress (ksi)	10.43	0.00	0.00	9.07	0.00
	Bending Stress (ksi)	70.23	46.24	53.51	76.88	66.23
	Interaction Ratio (Eq. 27)	0.67	0.37	0.43	0.71	0.53
75°	Axial Stress (ksi)	13.96	3.46	19.09	13.30	13.22
	Bending Stress (ksi)	61.67	46.61	35.22	71.15	52.44
	Interaction Ratio (Eq. 26)	0.67	0.38	0.57	0.72	0.59
	Axial Stress (ksi)	13.96	3.46	19.09	11.31	13.22
	Bending Stress (ksi)	61.67	46.61	35.22	73.89	52.44
	Interaction Ratio (Eq. 27)	0.64	0.41	0.47	0.71	0.55
90°	Axial Stress (ksi)	22.99	0.00	24.31	17.91	6.70
	Bending Stress (ksi)	4.49	30.11	11.61	26.05	30.83
	Interaction Ratio (Eq. 26)	0.41	0.21	0.49	0.48	0.32
	Axial Stress (ksi)	18.73	0.00	24.31	17.85	6.70
	Bending Stress (ksi)	10.85	30.11	11.61	26.18	30.83
	Interaction Ratio (Eq. 27)	0.28	0.24	0.34	0.39	0.31

Note:

⁽¹⁾ The locations of the different spacer plate ligament types are shown in Figure 2.6-8.

Table 2.7-11 - W74 General Spacer Plate Buckling Interaction Ratios for Combined HAC Slapdown Impact and NCT Thermal Loading

Impact Orientation	Stresses and Interaction Ratios	Ligament Type ⁽¹⁾				
		A	B _x	B _y	B	C
0°	Axial Stress (ksi)	25.43	26.60	3.72	22.24	9.73
	Bending Stress (ksi)	4.90	13.92	36.95	26.90	35.58
	Interaction Ratio (Eq. 26)	0.46	0.54	0.32	0.56	0.41
	Axial Stress (ksi)	21.27	26.60	3.72	22.24	9.73
	Bending Stress (ksi)	10.84	13.92	36.95	26.90	35.58
	Interaction Ratio (Eq. 27)	0.30	0.38	0.33	0.44	0.38
15°	Axial Stress (ksi)	16.09	26.82	2.44	16.45	8.10
	Bending Stress (ksi)	63.87	26.58	62.76	73.34	57.46
	Interaction Ratio (Eq. 26)	0.72	0.64	0.47	0.79	0.53
	Axial Stress (ksi)	16.09	22.28	2.44	14.39	8.10
	Bending Stress (ksi)	63.87	33.65	62.76	76.92	57.46
	Interaction Ratio (Eq. 27)	0.67	0.49	0.53	0.76	0.54
30°	Axial Stress (ksi)	14.30	23.55	0.34	12.09	6.71
	Bending Stress (ksi)	71.00	21.97	66.85	81.91	57.43
	Interaction Ratio (Eq. 26)	0.74	0.55	0.46	0.78	0.51
	Axial Stress (ksi)	14.30	18.59	0.34	12.09	2.19
	Bending Stress (ksi)	71.00	29.24	66.85	81.91	65.60
	Interaction Ratio (Eq. 27)	0.71	0.42	0.54	0.78	0.55
45°	Axial Stress (ksi)	10.81	19.43	1.21	8.87	10.54
	Bending Stress (ksi)	79.05	16.39	63.42	79.29	47.94
	Interaction Ratio (Eq. 26)	0.73	0.44	0.45	0.70	0.51
	Axial Stress (ksi)	10.81	0.00	1.21	8.87	0.00
	Bending Stress (ksi)	79.05	43.71	63.42	79.29	70.15
	Interaction Ratio (Eq. 27)	0.74	0.35	0.52	0.73	0.56
60°	Axial Stress (ksi)	12.95	6.98	16.00	10.75	13.83
	Bending Stress (ksi)	76.09	40.87	35.45	82.21	55.08
	Interaction Ratio (Eq. 26)	0.75	0.40	0.52	0.75	0.62
	Axial Stress (ksi)	12.95	6.98	2.11	10.75	13.83
	Bending Stress (ksi)	76.09	40.87	56.12	82.21	55.08
	Interaction Ratio (Eq. 27)	0.74	0.40	0.47	0.77	0.58
75°	Axial Stress (ksi)	16.54	6.66	20.24	14.61	17.66
	Bending Stress (ksi)	67.06	47.53	37.98	76.19	62.64
	Interaction Ratio (Eq. 26)	0.75	0.44	0.61	0.78	0.74
	Axial Stress (ksi)	16.54	6.66	20.24	14.61	17.66
	Bending Stress (ksi)	67.06	47.53	37.98	76.19	62.64
	Interaction Ratio (Eq. 27)	0.70	0.45	0.51	0.76	0.68
90°	Axial Stress (ksi)	26.35	2.20	27.33	20.80	10.20
	Bending Stress (ksi)	4.09	32.00	14.44	29.81	35.19
	Interaction Ratio (Eq. 26)	0.47	0.26	0.56	0.56	0.42
	Axial Stress (ksi)	21.62	1.94	27.33	20.80	10.20
	Bending Stress (ksi)	14.38	32.55	14.44	29.81	35.19
	Interaction Ratio (Eq. 27)	0.33	0.28	0.39	0.45	0.39

Note:

⁽¹⁾ The locations of the different spacer plate ligament types are shown in Figure 2.6-8.

Table 2.7-12 - W74 LTP Spacer Plate Buckling Interaction Ratios for HAC Slapdown Impact Loading without Thermal

Impact Orientation	Stresses and Interaction Ratios	Ligament Type ⁽¹⁾				
		A	B _x	B _y	B	C
0°	Axial Stress (ksi)	10.88	6.76	0.60	5.44	3.49
	Bending Stress (ksi)	5.64	5.82	11.37	11.47	14.63
	Interaction Ratio (Eq. 26)	0.54	0.37	0.19	0.40	0.37
	Axial Stress (ksi)	10.88	6.76	0.60	5.44	0.00
	Bending Stress (ksi)	5.64	5.82	11.37	11.47	18.98
	Interaction Ratio (Eq. 27)	0.33	0.25	0.21	0.31	0.33
15°	Axial Stress (ksi)	6.66	10.34	0.00	0.00	0.00
	Bending Stress (ksi)	31.61	18.43	19.95	41.91	40.96
	Interaction Ratio (Eq. 26)	0.74	0.71	0.29	0.61	0.60
	Axial Stress (ksi)	6.66	10.34	0.00	0.00	0.00
	Bending Stress (ksi)	31.61	18.43	19.95	41.91	40.96
	Interaction Ratio (Eq. 27)	0.69	0.54	0.34	0.72	0.70
30°	Axial Stress (ksi)	3.67	9.14	4.83	5.57	5.41
	Bending Stress (ksi)	44.65	17.18	12.37	35.67	23.70
	Interaction Ratio (Eq. 26)	0.81	0.64	0.39	0.76	0.58
	Axial Stress (ksi)	3.67	9.14	0.00	1.57	0.00
	Bending Stress (ksi)	44.65	17.18	22.85	44.93	39.92
	Interaction Ratio (Eq. 27)	0.85	0.49	0.39	0.81	0.69
45°	Axial Stress (ksi)	4.27	7.67	6.71	4.49	4.37
	Bending Stress (ksi)	44.20	14.83	13.82	41.22	29.38
	Interaction Ratio (Eq. 26)	0.83	0.54	0.49	0.80	0.62
	Axial Stress (ksi)	4.27	7.67	0.00	4.49	0.46
	Bending Stress (ksi)	44.20	14.83	23.98	41.22	35.35
	Interaction Ratio (Eq. 27)	0.85	0.42	0.41	0.80	0.62
60°	Axial Stress (ksi)	5.62	5.82	8.27	7.04	6.01
	Bending Stress (ksi)	39.93	11.60	14.68	32.32	32.42
	Interaction Ratio (Eq. 26)	0.82	0.42	0.57	0.77	0.74
	Axial Stress (ksi)	3.55	5.82	8.27	3.17	0.00
	Bending Stress (ksi)	44.14	11.60	14.68	42.47	40.66
	Interaction Ratio (Eq. 27)	0.83	0.32	0.43	0.80	0.70
75°	Axial Stress (ksi)	8.71	0.51	9.64	8.04	6.83
	Bending Stress (ksi)	26.26	14.75	15.06	18.18	22.75
	Interaction Ratio (Eq. 26)	0.75	0.24	0.63	0.61	0.63
	Axial Stress (ksi)	4.90	0.27	9.64	0.00	0.00
	Bending Stress (ksi)	32.79	15.08	15.06	39.15	41.52
	Interaction Ratio (Eq. 27)	0.67	0.26	0.47	0.67	0.71
90°	Axial Stress (ksi)	10.82	0.00	6.92	5.29	3.43
	Bending Stress (ksi)	5.05	10.18	6.35	11.56	13.31
	Interaction Ratio (Eq. 26)	0.52	0.15	0.39	0.39	0.34
	Axial Stress (ksi)	10.82	0.00	6.92	5.12	0.00
	Bending Stress (ksi)	5.05	10.18	6.35	11.85	19.65
	Interaction Ratio (Eq. 27)	0.32	0.17	0.26	0.31	0.34

Note:

⁽¹⁾ The locations of the different spacer plate ligament types are shown in Figure 2.6-8.

Table 2.7-13 - W74 LTP Spacer Plate Buckling Interaction Ratios for Combined HAC Slapdown Impact and NCT Thermal Loading

Impact Orientation	Stresses and Interaction Ratios	Ligament Type ⁽¹⁾				
		A	B _x	B _y	B	C
0°	Axial Stress (ksi)	12.20	10.27	4.30	9.05	6.64
	Bending Stress (ksi)	4.29	6.69	9.44	10.66	15.88
	Interaction Ratio (Eq. 26)	0.57	0.53	0.32	0.54	0.52
	Axial Stress (ksi)	12.20	10.27	4.30	9.05	6.64
	Bending Stress (ksi)	4.29	6.69	9.44	10.66	15.88
	Interaction Ratio (Eq. 27)	0.34	0.34	0.25	0.38	0.42
15°	Axial Stress (ksi)	8.37	14.01	2.78	11.51	5.50
	Bending Stress (ksi)	31.06	15.67	19.51	19.24	31.42
	Interaction Ratio (Eq. 26)	0.81	0.82	0.40	0.77	0.70
	Axial Stress (ksi)	8.37	14.01	2.78	2.65	0.43
	Bending Stress (ksi)	31.06	15.67	19.51	41.10	37.98
	Interaction Ratio (Eq. 27)	0.71	0.57	0.40	0.76	0.66
30°	Axial Stress (ksi)	5.57	12.82	7.95	9.21	7.81
	Bending Stress (ksi)	42.79	14.70	11.44	35.99	24.86
	Interaction Ratio (Eq. 26)	0.86	0.76	0.51	0.92	0.71
	Axial Stress (ksi)	5.57	12.82	4.22	4.70	2.15
	Bending Stress (ksi)	42.79	14.70	20.58	43.93	37.45
	Interaction Ratio (Eq. 27)	0.85	0.53	0.44	0.86	0.69
45°	Axial Stress (ksi)	6.10	11.37	9.77	8.14	7.00
	Bending Stress (ksi)	40.47	12.36	12.74	40.45	32.89
	Interaction Ratio (Eq. 26)	0.85	0.66	0.60	0.94	0.79
	Axial Stress (ksi)	4.93	11.37	3.19	8.14	7.00
	Bending Stress (ksi)	43.37	12.36	24.13	40.45	32.89
	Interaction Ratio (Eq. 27)	0.85	0.46	0.48	0.87	0.72
60°	Axial Stress (ksi)	6.77	9.56	11.31	9.98	8.63
	Bending Stress (ksi)	41.69	9.23	13.57	32.78	36.02
	Interaction Ratio (Eq. 26)	0.90	0.54	0.68	0.91	0.91
	Axial Stress (ksi)	6.19	5.89	3.82	6.85	8.63
	Bending Stress (ksi)	42.72	17.84	25.07	41.60	36.02
	Interaction Ratio (Eq. 27)	0.87	0.43	0.51	0.86	0.80
75°	Axial Stress (ksi)	9.27	4.30	12.68	10.99	9.32
	Bending Stress (ksi)	30.12	17.00	13.73	19.63	27.23
	Interaction Ratio (Eq. 26)	0.83	0.43	0.74	0.76	0.81
	Axial Stress (ksi)	8.25	4.30	5.87	3.53	0.00
	Bending Stress (ksi)	32.65	17.00	24.19	39.03	40.04
	Interaction Ratio (Eq. 27)	0.74	0.38	0.54	0.75	0.69
90°	Axial Stress (ksi)	13.00	2.76	10.81	8.81	5.90
	Bending Stress (ksi)	4.93	11.56	8.19	13.39	16.43
	Interaction Ratio (Eq. 26)	0.61	0.29	0.58	0.57	0.50
	Axial Stress (ksi)	11.23	2.76	10.81	8.81	5.90
	Bending Stress (ksi)	7.90	11.56	8.19	13.39	16.43
	Interaction Ratio (Eq. 27)	0.38	0.26	0.37	0.42	0.41

Note:

⁽¹⁾ The locations of the different spacer plate ligament types are shown in Figure 2.6-8.

**Table 2.7-14 - Guide Tube Neutron Absorber Sheet Retainer Weld
Shear Stresses – HAC Oblique Drop Slapdown Impact**

W74 Basket Assembly	Retainer Number	Longitudinal Moment Arm, d (in.)⁽¹⁾	Neutron Absorber Sheet Tributary Length, S (in.)	Equivalent Static Acceleration, G (g)	Plug Weld Shear Stress, f_w (ksi)
W74M Upper Basket	7	79.48	11.50	75.4	4.4
	6	67.69	12.07	69.0	4.2
	5	54.98	13.35	62.0	4.2
	4	41.24	14.16	54.5	3.9
	3	27.04	14.25	46.7	3.4
	2	14.96	9.91	40.1	2.0
	1	5.87	8.28	35.1	1.5
W74M Lower Basket	7	7.31	10.57	35.9	1.9
	6	19.41	13.63	42.5	2.9
	5	33.35	14.25	50.1	3.6
	4	47.45	13.97	57.9	4.1
	3	60.83	12.78	65.2	4.2
	2	71.90	9.38	71.3	3.4
	1	81.06	8.94	76.3	4.5
W74T Upper Basket	7	80.55	9.16	76.0	3.5
	6	70.08	11.78	70.3	4.2
	5	57.67	13.04	63.5	4.2
	4	44.17	13.97	56.1	4.0
	3	30.06	14.25	48.3	3.5
	2	16.95	11.97	41.2	2.5
	1	6.30	9.34	35.3	1.7
W74T Lower Basket	7	8.47	12.70	36.5	2.3
	6	21.95	14.25	43.9	3.2
	5	36.20	14.25	51.7	3.7
	4	50.18	13.72	59.4	4.1
	3	63.24	12.41	66.5	4.2
	2	73.82	8.75	72.3	3.2
	1	81.91	7.44	76.8	2.9

Notes:

⁽¹⁾ Axial location relative to the middle of the engagement spacer plate.

Table 2.7-15 - W74 Canister Shell Assembly HAC Oblique Drop Slapdown Impact Stress Analysis Results

Shell Component	Stress Type	Allowable Stress ⁽¹⁾ (ksi)	Maximum Stress (ksi)		Minimum Design Margin
			Zero Internal Pressure	Max. Internal Pressure	
Top Outer Closure Plate	P _m	46.2	18.9 ⁽²⁾	18.8 ⁽²⁾	+1.44
	P _m +P _b	69.3	31.4 ⁽²⁾	31.9 ⁽²⁾	+1.17
Top Outer Closure Weld	P _m	37.0 ⁽³⁾	13.8 ⁽⁴⁾	13.6 ⁽⁴⁾	+1.68
Top Inner Closure Plate	P _m	46.2	26.2 ⁽²⁾	25.2 ⁽²⁾	+0.76
	P _m +P _b	69.3	52.3 ⁽²⁾	54.0 ⁽²⁾	+0.28
Top Inner Closure Weld	P _m	41.6 ⁽⁵⁾	16.9 ⁽⁴⁾	17.7 ⁽⁴⁾	+1.35
Cylindrical Shell	P _m	46.2	39.6 ⁽⁶⁾	38.9 ⁽⁶⁾	+0.17
	P _m +P _b	69.3	59.9 ⁽⁷⁾	59.9 ⁽⁷⁾	+0.16

Notes:

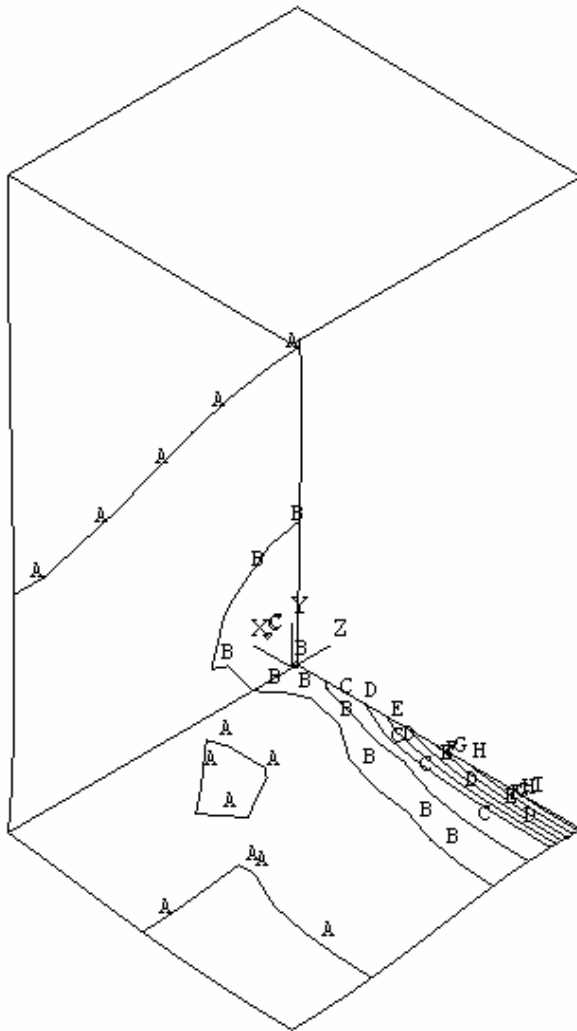
- (1) Allowable stress intensities are based on the weaker of the W74M and W74T canister shell materials (SA-240, Type 304 stainless steel) properties at 300°F.
- (2) The maximum stress intensities occur along the bottom centerline near the line of impact.
- (3) The allowable stresses for the top outer closure weld include a 0.8 weld efficiency factor in accordance with ISG-4.
- (4) The maximum primary stress intensities in the closure welds are taken at 11.4° from the line of impact (i.e., bottom centerline) to avoid the region of high bearing stresses which need not be evaluated for accident conditions in accordance with Appendix F of the ASME BPVC.
- (5) The allowable stresses for the top inner closure weld include a 0.9 weld efficiency factor.
- (6) The maximum primary membrane stress intensities in the cylindrical shell occur along the line of impact (i.e., bottom centerline) in the region of the top inner closure plate.
- (7) The maximum primary membrane plus bending stress intensities in the cylindrical shell occur along the line of impact (i.e., bottom centerline) in the region of the top outer closure plate.

Table 2.7-16 - Summary of W74 Canister HAC Oblique Drop Design Margins

W74 Canister Component	Stress Type	Maximum S.I. (ksi)	Allowable S.I. (ksi)	Minimum D.M. ⁽¹⁾	Reference SAR Section
General Spacer Plate	P _m	30.7	75.4	+1.46	2.7.1.4.1.2
	P _m + P _b	88.7	113.1	+0.28	2.7.1.4.1.2
	Buckling	0.79 ⁽³⁾	1.0	+0.27	2.7.1.4.1.2
LTP Spacer Plate	P _m	15.2	60.6	+2.98	2.7.1.4.1.2
	P _m + P _b	53.5	90.8	+0.70	2.7.1.4.1.1
	Buckling	0.94 ⁽³⁾	1.0	+0.06	2.7.1.4.1.2
Engagement Spacer Plate	P _m	32.8	62.4	+0.90	2.7.1.4.2
	P _m + P _b	38.0	93.6	+1.46	2.7.1.4.2
	Buckling	(2)	(2)	(2)	2.7.1.4.2
Support Tube	P _m	15.2	61.5	+3.05	2.7.1.4.3
	P _m + P _b	22.9	92.2	+3.03	2.7.1.4.3
	Buckling	0.50 ⁽³⁾	1.0	+1.00	2.7.1.4.3
Support Sleeve	Bounded by HAC end drop				2.7.1.4.3
Support Tube Longitudinal Seam Weld	Shear	1.9	12.3 ⁽⁴⁾	+5.47	2.7.1.4.3
W74M Support Tube to LTP Spacer Plate Weld	Shear	2.8	14.0 ⁽⁴⁾	+4.00	2.7.1.4.3
W74T Support Tube to Attachment Sleeve Weld	Shear	6.0	14.0 ⁽⁴⁾	+1.33	2.7.1.4.3
Guide Tube	P _m	16.0	40.0	+1.50	2.7.1.4.4
	P _m + P _b	56.4	60.0	+0.06	2.7.1.4.4
	Buckling ⁽³⁾	0.52	1.0	+0.92	2.7.1.4.4
Guide Tube Longitudinal Welds	P _m	5.7	26.0 ⁽⁵⁾	+3.56	2.7.1.4.4
	P _m + P _b	29.6	39.0 ⁽⁵⁾	+0.32	2.7.1.4.4
Neutron Absorber Panels	P _m + P _b	5.0	58.3	+10.7	2.7.1.4.4
NAP Retainer Welds	Shear	4.4	5.9 ⁽⁶⁾	+0.34	2.7.1.4.4
Canister Shell Assembly	P _m	39.6	46.2	+0.17	2.7.1.4.5
	P _m + P _b	59.9	69.3	+0.16	2.7.1.4.5

Notes:

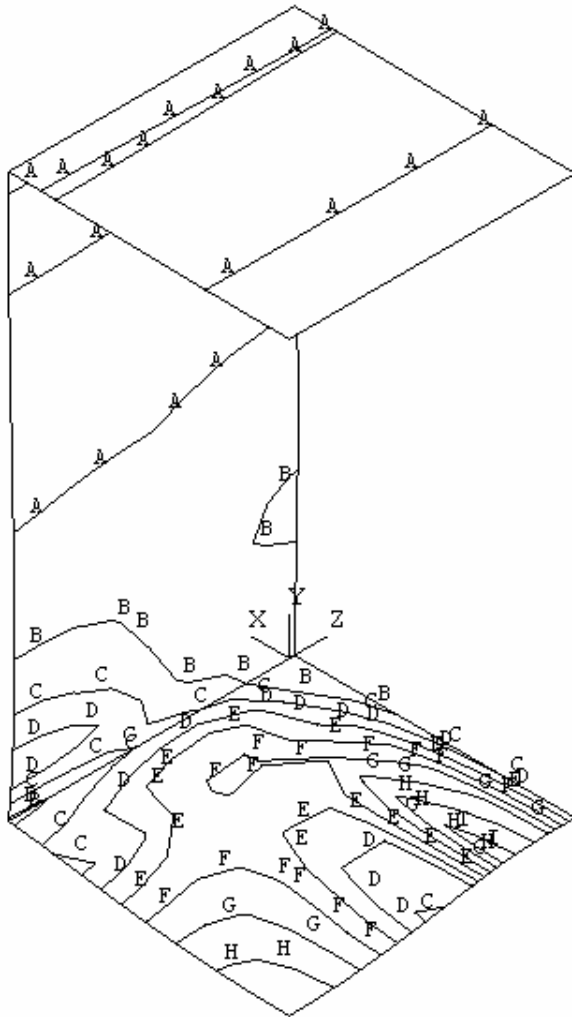
- (1) Design margin is equal to (Allowable/Stress) - 1.
- (2) Bounded by buckling evaluation presented in Section 2.7.1.2.2.
- (3) Buckling interaction ratio calculated in accordance with NUREG/CR-6322.
- (4) Includes a 35% weld quality factor for single sided groove welds and fillet welds with surface PT examination in accordance with Table NG-3352-1 of the ASME B&PV Code.
- (5) Includes a 65% weld quality factor for a full penetration weld with surface PT examination in accordance with Table NG-3352-1 of the ASME B&PV Code.
- (6) Includes a 30% weld quality factor for plug welds in accordance with Table NG-3352-1 of the ASME B&PV Code.



```
ANSYS 5.5.3  
AUG 17 2000  
17:06:46  
NODAL SOLUTION  
STEP=1  
SUB =1  
TIME=1  
SINT      (AVG)  
MIDDLE  
DMX =.098607  
SMN =36.596  
SMX =15928  
A  =919.47  
B  =2685  
C  =4451  
D  =6217  
E  =7982  
F  =9748  
G  =11514  
H  =13280  
I  =15045
```

Note: All stresses are in psi.

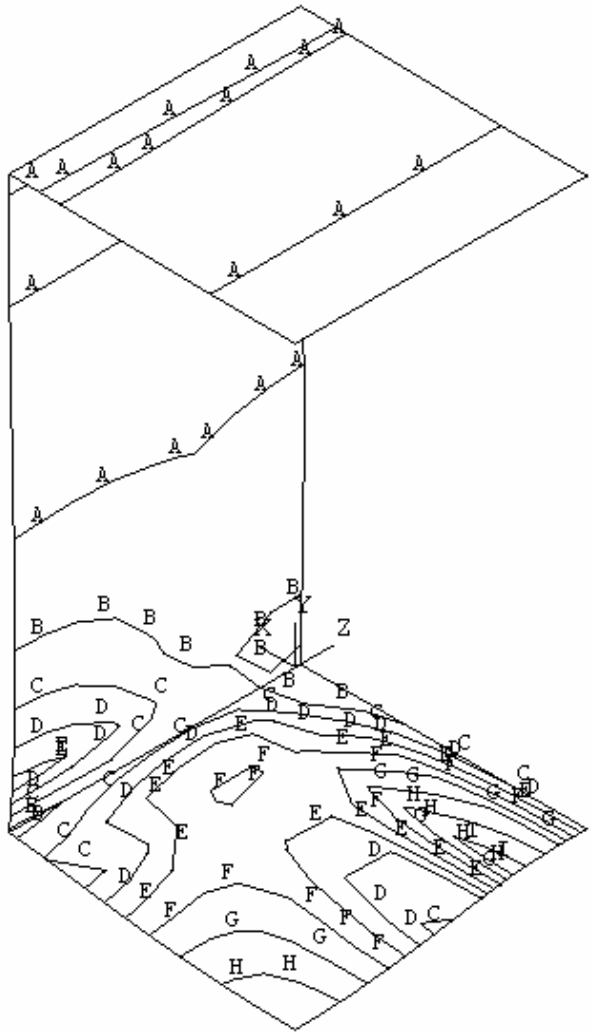
**Figure 2.7-4 - W74 Guide Tube S.I. Contour Plot (Middle Fiber) -
62g Slapdown, Uniform SNF Loading, Elastic Analysis**



```
ANSYS 5.5.3  
AUG 17 2000  
17:06:08  
NODAL SOLUTION  
STEP=1  
SUB =1  
TIME=1  
SINT      (AVG)  
TOP  
DMX =.098607  
SMN =901.11  
SMX =56183  
  
A   =3972  
B   =10115  
C   =16257  
D   =22399  
E   =28542  
F   =34684  
G   =40827  
H   =46969  
I   =53111
```

Note: All stresses are in psi.

**Figure 2.7-5 - W74 Guide Tube S.I. Contour Plot (Top Fiber) -
62g Slapdown, Uniform SNF Loading, Elastic Analysis**

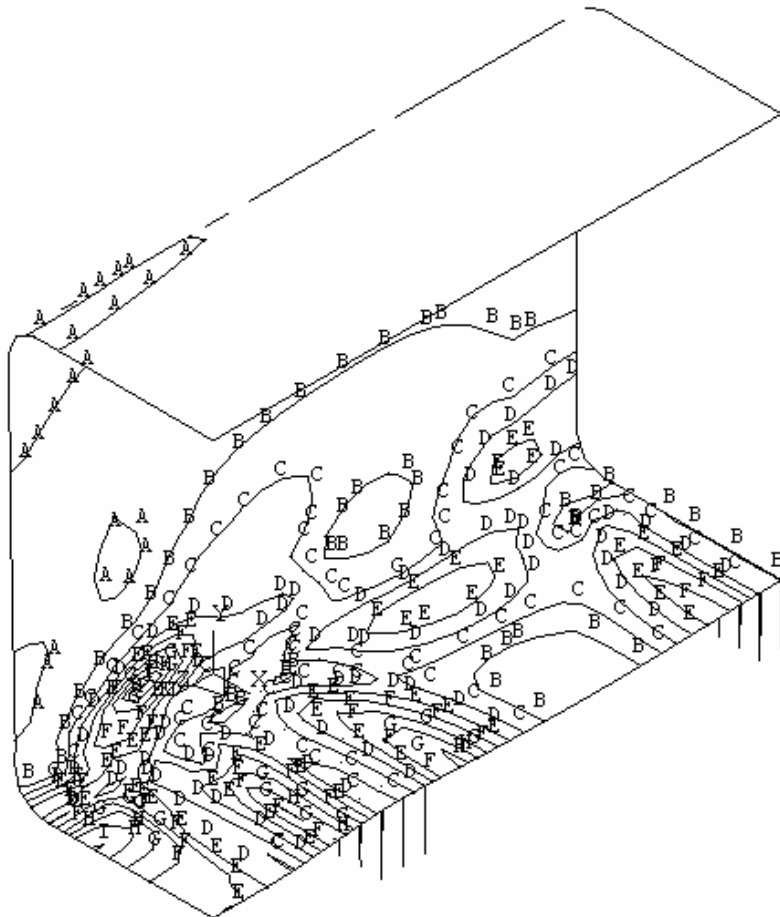


```
ANSYS 5.5.3  
AUG 17 2000  
17:06:26  
NODAL SOLUTION  
STEP=1  
SUB =1  
TIME=1  
SINT      (AVG)  
BOTTOM  
DMX =.098607  
SMN =784.926  
SMX =56390
```

```
A   =3874  
B   =10052  
C   =16231  
D   =22409  
E   =28588  
F   =34766  
G   =40944  
H   =47123  
I   =53301
```

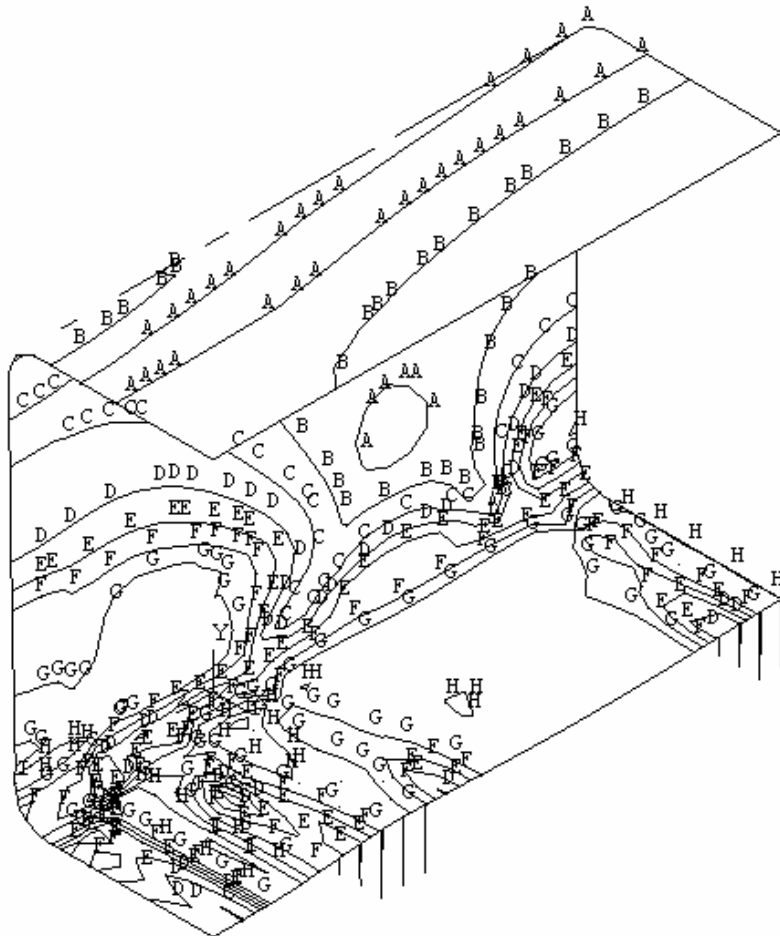
Note: All stresses are in psi.

**Figure 2.7-6 - W74 Guide Tube S.I. Contour Plot (Bottom Fiber) -
62g Slapdown, Uniform SNF Loading, Elastic Analysis**



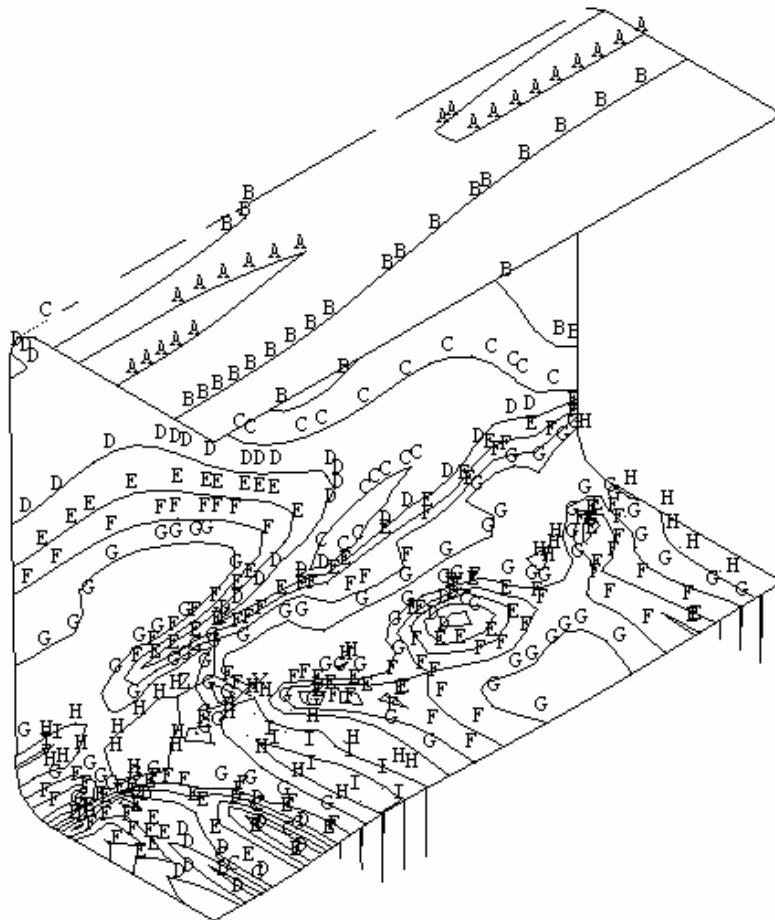
```
ANSYS 5.5.3  
AUG 17 2000  
17:09:34  
NODAL SOLUTION  
STEP=5  
SUB =7  
TIME=5  
SINT (AVG)  
MIDDLE  
DMX =.150043  
SMN =124.144  
SMX =18955  
A =1170  
B =3263  
C =5355  
D =7447  
E =9539  
F =11632  
G =13724  
H =15816  
I =17909
```

Figure 2.7-7 - W74 Guide Tube S.I. Contour Plot (Middle Fiber) - 64.5g Slapdown Load, Concentrated SNF Loading, Plastic Analysis



```
ANSYS 5.5.3  
AUG 17 2000  
17:10:11  
NODAL SOLUTION  
STEP=5  
SUB =7  
TIME=5  
SINT      (AVG)  
TOP  
DMX =.150043  
SMN =722.349  
SMX =27442  
A  =2207  
B  =5176  
C  =8145  
D  =11113  
E  =14082  
F  =17051  
G  =20020  
H  =22989  
I  =25958
```

**Figure 2.7-8 - W74 Guide Tube S.I. Contour Plot (Top Fiber) -
64.5g Slapdown Load, Concentrated SNF Loading, Plastic Analysis**



```
ANSYS 5.5.3  
AUG 17 2000  
17:09:04  
NODAL SOLUTION  
STEP=5  
SUB =7  
TIME=5  
SINT      (AVG)  
BOTTOM  
DMX =.150043  
SMN =283.349  
SMX =26956  
A  =1765  
B  =4729  
C  =7692  
D  =10656  
E  =13619  
F  =16583  
G  =19547  
H  =22510  
I  =25474
```

Figure 2.7-9 - W74 Guide Tube S.I. Contour Plot (Bottom Fiber) - 64.5g Slapdown Load, Concentrated SNF Loading, Plastic Analysis

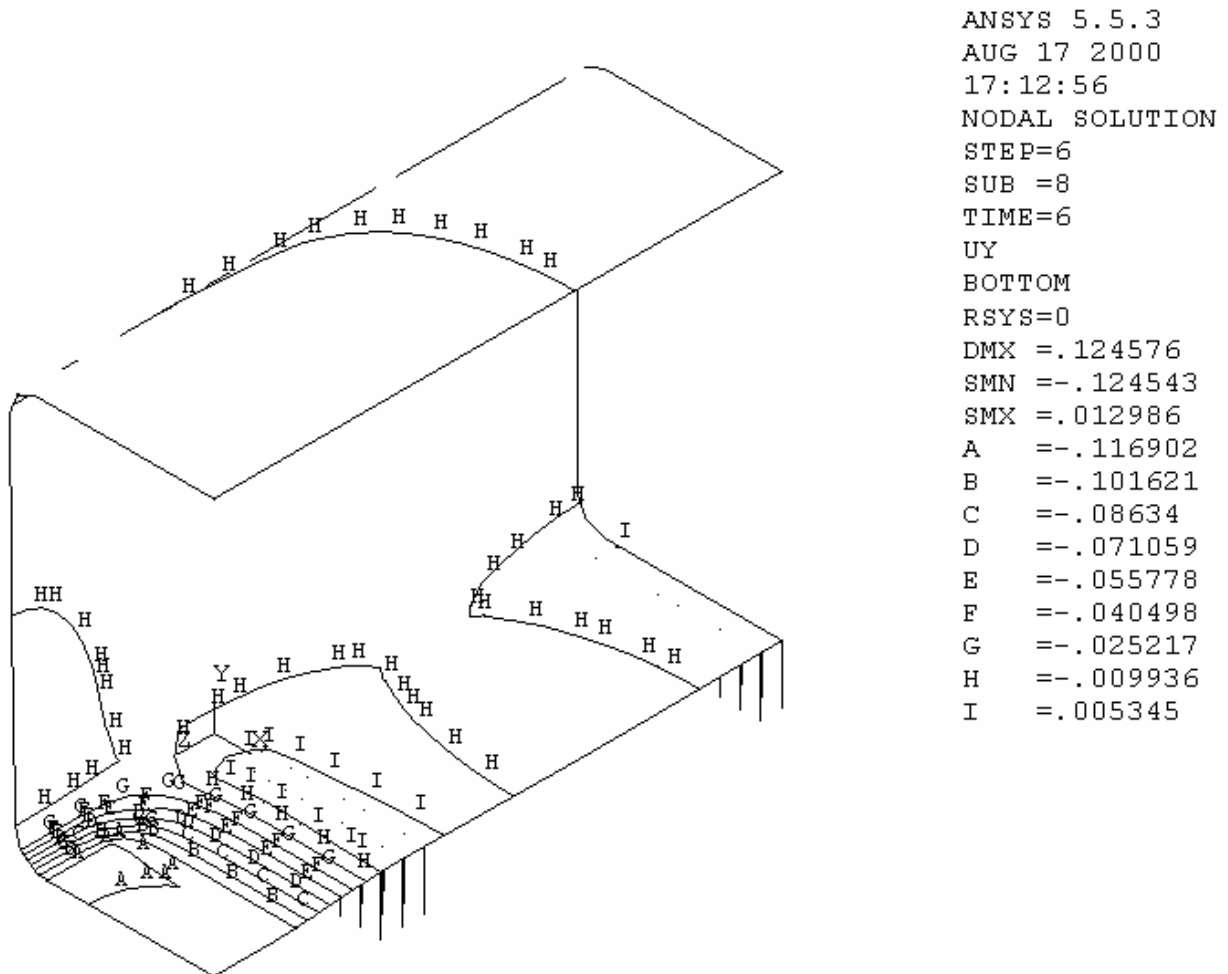
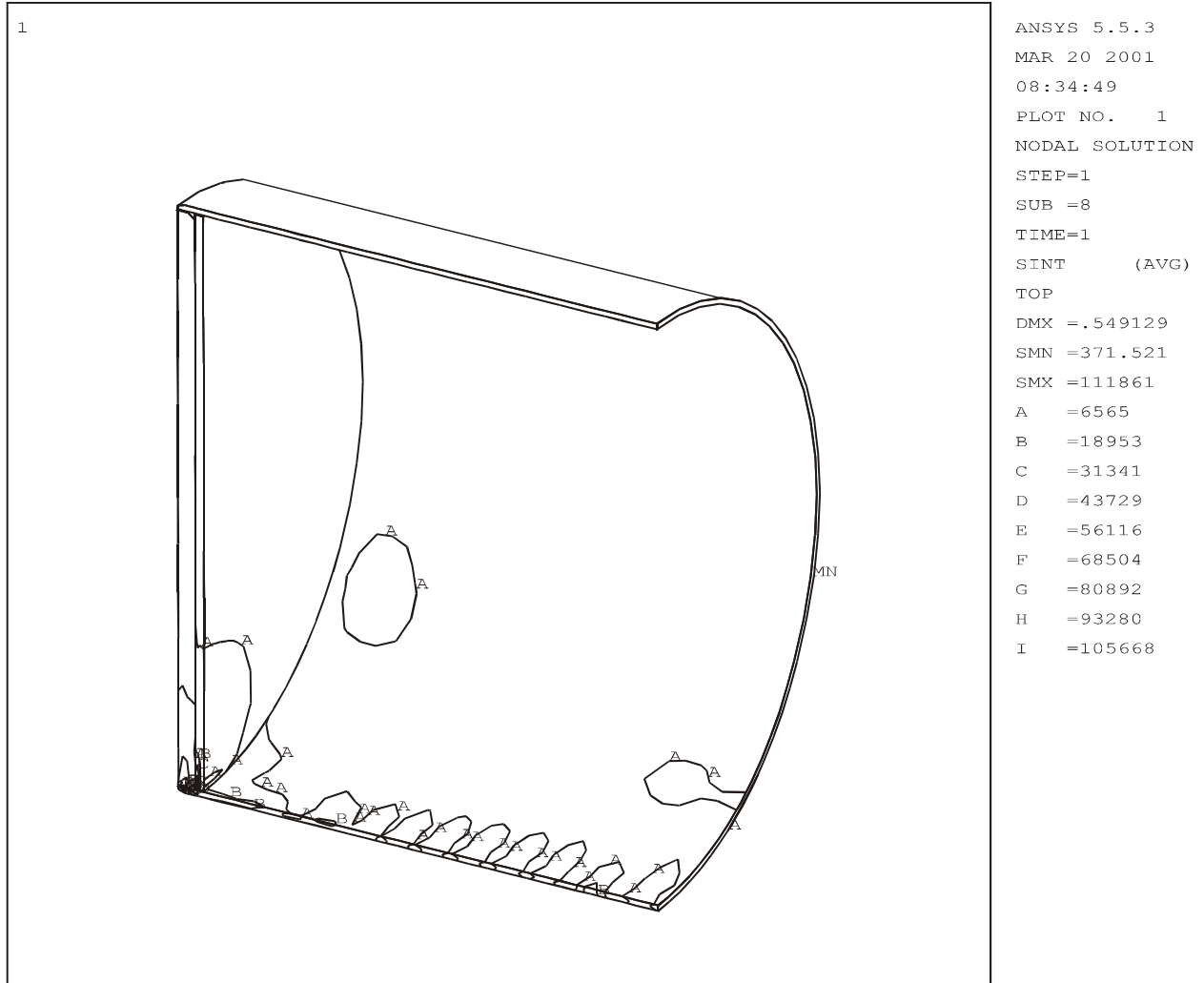


Figure 2.7-10 - W74 Guide Tube Permanent Deformation Resulting from HAC Slapdown Impact Loading



Note: Top shield plug and basket assembly not shown for clarity.

**Figure 2.7-11 - Canister Shell Stress Intensity Contour Plot for 87g
HAC Slapdown Load**

2.7.2 Crush

The crush test of 10CFR71.73(c)(2) is required only when the specimen has a mass not greater than 500 kg (1100 lbs) and an overall density not greater than 1000 kg/m³ (62.4 lb/ft³) based on external dimensions. Since the mass of the FuelSolutions™ TS125 Transportation Package is greater than 500 kg (1100 lbs), the crush test does not apply to the FuelSolutions™ TS125 Transportation Package.

2.7.3 Puncture

The HAC 40-inch puncture drop requirement of 10CFR71.73(c)(3) is evaluated in the FuelSolutions™ TS125 Transportation Cask SAR to demonstrate the puncture resistance of the external cask surfaces. The transportation cask is shown to provide adequate protection against puncture, and thus protects the canister assembly from local damage due to the HAC puncture. In accordance with 10CFR71.73(a), the HAC tests are applied sequentially, considering the cumulative damage sustained from the preceding HAC loads. The HAC free drop loading precedes the HAC puncture loading. As discussed in Section 2.7.7, the extent of damage sustained by the W74 canister from the HAC free drop loading is minimal and does not affect the canister's ability to withstand the HAC puncture drop. Since the package rigid-body acceleration loads resulting from the HAC free drop condition bound the package decelerations resulting from the HAC puncture condition, no further analysis is required to demonstrate the structural adequacy of the FuelSolutions™ W74 canisters for the HAC puncture load.

2.7.4 Thermal

The FuelSolutions™ Transportation Package, containing the FuelSolutions™ W74 canister, is designed to withstand a 30-minute fire of 1,475°F per 10CFR71.73(c)(4). In accordance with 10CFR71.73(a), the HAC tests are applied sequentially, considering the cumulative damage sustained from the preceding HAC loads. The HAC free drop and HAC puncture precede the HAC fire. As discussed in Section 2.7.7, the extent of damage sustained by the W74 canister from the HAC free drop and HAC puncture loading is minimal and does not affect the canister's ability to withstand the HAC fire.

As shown in Section 3.5, the HAC fire does not significantly effect the W74 canister temperatures due to the insulation provided by the FuelSolutions™ TS125 Transportation Cask. The maximum temperatures of the W74 canister components during the HAC fire are slightly higher than those due to the NCT hot thermal condition but do not exceed the NCT design temperatures shown in Table 2.6-1 of this SAR. In addition, the thermal gradients within the W74 canister due to controlling NCT thermal condition bound the thermal gradients during the HAC fire. Therefore, the thermal stresses in the W74 canister due to controlling NCT thermal condition bound those due to the HAC fire.

2.7.5 Immersion - Fissile Material

The criticality evaluation presented in Chapter 6 of this SAR considers the effect of water in-leakage. Thus, the immersion test requirement of 10CFR71.73(c)(4) does not apply to the W74 canister.

2.7.6 Immersion - All Packages

No credit is taken for containment or confinement provided by the FuelSolutions™ W74 canister. Therefore, the immersion test requirement of 10CFR71.73(c)(5) does not apply to the W74 canister.

2.7.7 Summary of Damage

The W74 canister structural evaluation results show that the canister would incur only minimal damage for the HAC loads specified in 10CFR71.73. The extent of damage incurred by the W74 canister will not prevent it from satisfying the containment, shielding, subcriticality, and temperature requirements of 10CFR71, Subpart E. In accordance with 10CFR71.73(a), the evaluation of cumulative damage to the transportation package for the HAC of 10CFR71.73(c) is based on the sequential application of the 30-foot free drop, puncture, and thermal (fire). In accordance with 10CFR71.73(a), the water immersion test of 10CFR71.73(c)(6) is not evaluated in sequence.

The structural evaluation of the canister shell assembly demonstrates that no gross failure of the canister shell assembly components occurs due to the HAC free drop that would result in additional loading on the basket assembly components. The evaluation of the basket assembly criticality control components shows that the spacer plates, support tubes, support sleeves, and guide tube assemblies do not buckle under the most severe HAC free drop loads. Furthermore, the stresses in the W74 canister meet the accident condition allowable stress design criteria specified in Section 2.1.2.

The extent of damage sustained by the FuelSolutions™ TS125 Transportation Package, including the W74 canister, as a result of the HAC loads specified in 10CFR71.73 is minimal. The extent of damage sustained by the TS125 Transportation Cask and impact limiters due to the HAC load conditions is discussed in Section 2.7.7 of the FuelSolutions™ TS125 Transportation Cask SAR. The extent of damage sustained by the W74 canisters due to the HAC load conditions is summarized in the following paragraphs.

HAC Free Drop

As discussed in Sections 2.7.1.1.6, 2.7.1.3.5, and 2.7.1.4.6, the HAC end drop, corner drop, and oblique drop primary impacts will result in failure of the brackets that secure the W74M guide tubes to the bottom end LTP spacer plates in the upper and lower basket assemblies. The failure of the guide tube attachment brackets results in possible axial shifting of the guide tube assemblies relative to the SNF assemblies, which is considered in the criticality evaluation presented in Chapter 6. The results of the W74 canister criticality evaluation demonstrate that failure of the guide tube attachment brackets due to HAC free drop loading does not affect the ability of the W74 canisters to satisfy the subcriticality requirements of 10CFR71, Subpart E. Furthermore, the failure of the guide tube attachment brackets does not prevent retrieval of the SNF assemblies from the canister.

As discussed in Sections 2.7.1.2.6 and 2.7.1.4.6, the HAC side drop and HAC oblique drops result in small permanent deformations of the W74 guide tubes and spacer plates. The results show that the maximum permanent deformations of the W74 guide tubes resulting from the HAC side drop and HAC oblique drop slapdown impact loading are similar in magnitude. For a

uniform fuel loading assumption, the guide tube maximum permanent deformation resulting from the 60g HAC side drop loading is 0.066 inch in each span. However, if the weight of the SNF assemblies is assumed to act at the locations of the grid spacers (i.e., concentrated loading), then the maximum guide tube permanent deformation resulting from the HAC oblique drop slapdown impact is 0.125 inch. Unlike the permanent deformation resulting from the uniform fuel loading assumption, this permanent deformation occurs only in every third span of the guide tube, with no significant guide tube permanent deformation in the intermediate spans. The maximum permanent deformation of the most heavily loaded W74 general and LTP spacer plates due to the HAC side drop and HAC oblique drop slapdown impact loading are 0.04 inch and 0.023 inch, respectively. The permanent deformations of the W74 guide tubes and spacer plates are considered in the criticality evaluation presented in Chapter 6. The results of the W74 canister criticality evaluation demonstrate that the permanent deformations in the W74 basket due to HAC free drop loading do not affect the ability of the W74 canisters to satisfy the subcriticality requirements of 10CFR71, Subpart E.

HAC Puncture

The W74 canisters are subjected to the HAC puncture loading considering the damage sustained from the HAC free drop loading. The damage to the W74 canister sustained during the HAC 30-foot free drops of 10CFR71.73(c)(1) does not affect the canister's ability to withstand the HAC puncture drop of 10CFR71.73(c)(3). As discussed in Section 2.7.3, the W74 canisters are adequately protected by the FuelSolutions™ TS125 Transportation Cask against local damage due to HAC puncture drop. In addition, the acceleration loads experienced by the W74 canisters in the event of an HAC puncture drop are significantly lower than those resulting from the HAC 30-foot free drops. Consequently, the HAC puncture drop is not expected to cause any additional damage to the W74 canisters.

HAC Thermal

The W74 canisters are subjected to the HAC thermal (fire) loading considering the damage sustained from the HAC 30-foot free drop and HAC puncture drop conditions. The damage to the W74 canister sustained during the HAC 30-foot free drops of 10CFR71.73(c)(1) and HAC puncture drop of 10CFR71.73(c)(3) does not affect the canister's ability to withstand the HAC thermal condition of 10CFR71.73(c)(4). As discussed in Section 2.7.4, the W74 canister is protected from the effects of the HAC fire loading by the FuelSolutions™ TS125 Transportation Cask. The stresses in the W74 canister during the HAC fire event are expected to be bounded by those calculated for the bounding NCT thermal loading. Therefore, the HAC fire is not expected to cause any additional damage to the W74 canisters.

This page intentionally left blank.

2.8 Special Requirements for Irradiated Nuclear Fuel Shipments

In accordance with 10CFR71.61, a Type B package containing more than 10^5 A₂ must be designed so that its undamaged containment system can withstand an external pressure of 2 MPa (290 psi) for a period of not less than one hour without collapse, buckling, or inleakage of water. The structural analysis of the FuelSolutions™ TS125 Transportation Cask containment system that demonstrates compliance with the requirements of 10CFR71.61 is presented in Section 2.8 of the FuelSolutions™ TS125 Transportation Cask SAR. As discussed in Section 2.1.1.1, no credit is taken for containment provided by the W74 canister for transportation conditions.

This page intentionally left blank.

2.9 Internal Pressure Test

In accordance with 10CFR71.85(b), where the MNOP will exceed 35 kPa (5 psi) gauge, the containment system shall be tested at 150% of the MNOP to verify the capability of that system to maintain its structural integrity at that pressure. The structural analysis of the FuelSolutions™ TS125 Transportation Cask containment system for a test pressure equal to 150% of MNOP is presented in Section 2.9 of the FuelSolutions™ TS125 Transportation Cask SAR. As discussed in Section 2.1.1.1, no credit is taken for containment provided by the W74 canister for transportation conditions.

This page intentionally left blank.

2.10 Special Form

The FuelSolutions™ W74 canisters are not designed to carry radioactive material of special form designation per 10CFR71.75.

This page intentionally left blank.

2.11 Fuel Rods

Containment of the radioactive materials is provided by the cask containment boundary, as defined in Chapter 4 of this SAR. The analysis of the cask containment boundary presented in the FuelSolutions™ TS125 Transportation Cask SAR demonstrates that the TS125 Transportation Cask containment will not be breached.

The structural integrity of the fuel rod cladding is maintained throughout the canister design life. The structural evaluation of the fuel cladding considers thermally induced failures and structural failure (i.e., buckling) due to the HAC free drop loadings.

The risk of gross cladding failure in intact zircaloy-clad fuels is effectively eliminated by maintaining peak cladding temperatures sufficiently low to limit creep in dry storage. As shown in Chapter 3 of this SAR and Chapter 4 of the FuelSolutions™ W74 Canister Storage FSAR, the peak fuel cladding temperatures for all SNF accommodated in the FuelSolutions™ W74 canisters do not exceed the allowable cladding temperatures for on-site storage and off-site transportation conditions. As discussed in Chapter 4 of this SAR, the allowable cladding temperatures for all BRP MOX, partial, and damaged fuel assemblies is greater than or equal to the allowable cladding temperature of intact UO₂ fuel. In addition, the maximum cladding temperature for BRP MOX, partial, and damaged fuel assemblies is bounded by the maximum cladding temperature of intact UO₂ fuel. Therefore, the risk of gross cladding failure in all BRP intact zircaloy, MOX, partial, and damaged fuel assemblies is effectively eliminated.

In addition to thermally induced cladding failure, structural failure of intact zircaloy and MOX fuel cladding due to the HAC free drops is evaluated. The FuelSolutions™ W74 canister is designed to withstand a bounding end drop load of 60g and a bounding side drop load 60g. For transverse impact loads resulting from the side drop, studies indicate that damage to SNF rods will not occur for loads less than 63g.²⁷ Therefore, the structural integrity of the intact zircaloy and MOX fuel cladding will be maintained in the event of the HAC side drop.

Structural failure of the BRP zircaloy and MOX fuel cladding for the HAC end drop is evaluated using classical hand calculations. The Euler buckling load is calculated for each BRP fuel type conservatively assuming that the entire weight of the fuel assembly, including the weight of the fuel pellets, is supported by the cladding tubes. The longest unsupported span of the fuel rod is taken as the maximum distance between the fuel assembly grid spacers. The Euler buckling evaluation of the fuel cladding tube is conservatively performed assuming pinned end conditions. The results of this evaluation show that the lower bound buckling load for all BRP SNF types is 61.0g. Since this is greater than the 60g HAC end drop design load, the BRP fuel cladding structural integrity will be maintained in the event of a storage cask bottom end drop.

For partial BRP fuel assemblies, the axial compressive load supported by each fuel rod is approximately equal to that of the intact BRP fuel assemblies. Therefore, the critical end drop buckling load for partial BRP fuel assemblies is equal to that of intact BRP fuel.

²⁷ UCID-21246, *Dynamic Impact Effects on Spent Fuel Assemblies*, Chun, Witte, and Schwartz, Lawrence Livermore National Laboratory, September 1987.

The structural integrity of damaged BRP fuel is not required for the HAC free drops since these fuel assemblies are placed inside damaged fuel canisters. As discussed in Chapter 6, the criticality evaluation of BRP damaged fuel assumes that the fuel rod cladding fails under HAC free drop loading. The W74 canister is shown to satisfy the criticality design requirements for all possible post-accident configurations with damaged BRP fuel assemblies. The damaged fuel canisters provide a means to retrieve damaged BRP fuel assemblies after a HAC free drop condition.

2.12 Appendices

2.12.1 General and LTP Spacer Plate Tributary Weights

The spacer plate in-plane tributary weights are defined as the portion of the SNF assembly, guide tube, damaged fuel canister, support tube, and support sleeve weights that are supported by each spacer plate in the transverse direction, combined with the spacer plate self-weight. The W74 spacer plate tributary weights are calculated assuming the W74 upper and lower basket assemblies are each loaded with 32 Big Rock Point (BRP) SNF assemblies and four (4) damaged fuel canisters. The spacer plate in-plane tributary weights are calculated assuming that the mass of the SNF assemblies is; (1) uniformly distributed along its length to the supporting spacer plates, and (2) distributed as concentrated loads only at the locations of the SNF assembly grid spacers and end fittings. In general, the spacer plate in-plane tributary weights that are calculated based on the uniform SNF assembly load distribution are used for elastic-system analyses that form the bases of the spacer plate stress qualification for the NCT and HAC free drop loadings. The spacer plate in-plane tributary weights that are calculated based on the concentrated SNF fuel loads at the grid spacers are used for plastic-system analyses performed to determine the maximum permanent deformation of the spacer plates and demonstrate general stability of the spacer plates for the HAC free drop loadings. In addition, the spacer plate tributary weights based on concentrated SNF fuel loads at the grid spacers are used for the evaluation of NCT vibration loading.

The tributary weight is calculated for each spacer plate by multiplying the basket assembly component line loads by the spacer plate tributary width, adding the self-weight of the corresponding spacer plate, and then adding the tributary weight of the SNF assemblies. The tributary width of each spacer plate is taken as half the span on each side of the spacer plate, except for the spacer plates that are located at each end of the basket. For the spacer plates at the top and bottom ends of the basket, the entire span on the outboard side of the spacer plate is considered in conjunction with the half-span on the opposite side. The calculation of the basket assembly component tributary weights and SNF assembly tributary weights, using both uniform and concentrated fuel loading assumptions are performed as follows:

Basket Assembly Component Tributary Weights

The weights of each W74 general spacer plate and LTP spacer plate are 229 pounds and 627 pounds, respectively.

Each W74 basket assembly includes 18 Type A guide tube assemblies and 10 Type B guide tube assemblies. The cross-section dimensions of the guide tubes are identical, but the Type A guide tubes include two neutron absorber panels each, and the Type B guide tubes only include one neutron absorber panel each. The line load used for the Type A W74M and W74T guide tubes is calculated as follows:

$$w_g = (A_g + A_n)\rho_{ss} = 1.01 \text{ lb / in. (Type A) or } 0.87 \text{ lb / in. (Type B)}$$

where:

$$\begin{aligned} A_g &= \text{Cross-section area of guide tube} \\ &= 4(6.90 + 0.090)(0.090) \\ &= 2.52 \text{ in}^2 \end{aligned}$$

$$\begin{aligned} A_n &= \text{Cross-section area of neutron absorber panels} \\ &= 2(6.40)(0.075) = 0.96 \text{ in}^2 \text{ (Type A)} \\ &= 1(6.40)(0.075) = 0.48 \text{ in}^2 \text{ (Type B)} \end{aligned}$$

$$\rho_{ss} = 0.29 \text{ lb/in}^3, \text{ density of stainless steel and borated stainless steel}$$

The total weight of guide tubes tributary to the top end spacer plate and to each interior spacer plate is equal to 18 times the Type A guide tube line load multiplied by the spacer plate tributary length, plus 10 times the Type B guide tube line load multiplied by the spacer plate tributary length. The support sleeve tributary weight for the bottom end spacer plates in each basket assembly is calculated in a similar manner, except 1.5 inches is subtracted from the spacer plate tributary length to account for the cutouts in the bottom end of each guide tube.

The line load used for the four support tubes in each of the W74M and W74T basket assemblies is calculated as follows:

$$w_t = A_t \rho_{ss} = 26.88 \text{ lb/in.}$$

where ρ_{ss} is as defined previously and:

$$\begin{aligned} A_t &= \text{Cross-section area of four support tubes} \\ &= 4(8.90^2 - 7.40^2 - 4(0.8^2)/2) \\ &= 92.7 \text{ in}^2 \end{aligned}$$

The total weight of support tubes tributary to each spacer plate is equal to the support tube line load multiplied by the spacer plate tributary width.

The line load used for the support sleeves in each of the W74M and W74T basket assemblies is calculated as follows:

$$w_s = A_s \rho_{ss} = 8.73 \text{ lb/in.}$$

where ρ_{ss} is as defined previously and:

$$\begin{aligned} A_t &= \text{Cross-section area of four support sleeves} \\ &= 4[2(14)(0.1875) + 2(9.1)(0.125)] \\ &= 30.1 \text{ in}^2 \end{aligned}$$

The total weight of support sleeves tributary to each interior spacer plate is equal to the support sleeve line load multiplied by the spacer plate tributary length less the spacer plate thickness.

The support sleeve tributary weight for the top and bottom end spacer plates is equal to the support sleeve line load multiplied by one half of the length of the support sleeve interior to the spacer plate.

SNF Assembly Tributary Weights – Uniform Loading

The spacer plate tributary weights are calculated assuming both the upper and lower basket assemblies are loaded with 32 SNF assemblies each. The maximum weight for a single BRP fuel assembly with channels is 485 pounds. The irradiated length of BRP fuel is 84.80 inches. Therefore, the line load for Big Rock Point fuel with channels is 5.72 lb/inch. It is also assumed that fuel assemblies at all four support tube locations are placed into 200-pound damaged fuel cans, which results in the additional line load of 2.36 lb/inch at those locations. The total weight of payload tributary to each spacer plate is equal to the total line load multiplied by the spacer plate tributary length.

The W74M and W74T spacer plate in-plane tributary weights calculated based on the uniform SNF assembly loading assumption are shown in Table 2.12-1 and Table 2.12-2, respectively. The maximum tributary weights of the W74 general and LTP spacer plates are 2,119 pounds (W74T upper basket, spacer plate no. 1) and 2,043 pounds (W74M upper basket, spacer plate no. 1), respectively.

SNF Assembly Tributary Weights – Concentrated Loads at Grid Spacers

The portion of the SNF assembly weight that is supported by each spacer plate in the transverse direction depends on location of SNF grid spacer or end fitting and spacer plate itself. The SNF assembly weight that is tributary to each SNF assembly grid spacer and end fitting is calculated as the tributary length of the grid spacer or end fitting, multiplied by the BRP fuel line load from above. The SNF grid spacer tributary length is taken as half the span on each side of the grid spacer. For the SNF top and bottom end fittings, the entire span on the top or bottom side of the end fitting is considered in conjunction with the half-span on the interior side.

The SNF assembly grid spacer and end fitting tributary weights are conservatively assumed to load only the single spacer plate that is closest to the location of the SNF grid spacer or end fitting. Therefore, some of the spacer plates are not loaded from SNF assembly weights. In those cases where the grid space is located between two spacer plates, the full tributary weight at the grid spacer or end fitting is conservatively applied to both spacer plate. The enveloping SNF assembly tributary weights are then combined with the spacer plate tributary weight due to the basket components. The W74M and W74T spacer plate in-plane tributary weights calculated based on the concentrated SNF assembly loading assumption are shown in Table 2.12-4 and Table 2.12-5, respectively. The maximum tributary weights of the W74 general and LTP spacer plates are 4,637 pounds and 2,825 pounds, respectively.

**Table 2.12-1 - W74M Spacer Plate Tributary Weights –
 Uniform Fuel Loading**

Basket Assembly	Spacer Plate	Bottom to Centerline Distance (in.)	Spacer Plate Thick. (in.)	Tributary Length (in.)	Tributary Weights (lbs.)				Total Tributary Weight (lbs.)
					Spacer Plate	Fuel Assy.	Guide Tube	Spt.Tubes, Sleeves & Fuel Cans	
W74M Upper Basket	14	170.30	2.00	3.68	627	589	99	232	1,546
	13	168.18	0.75	3.50	229	560	94	231	1,115
	12	162.68	0.75	5.63	229	901	151	375	1,657
	11	156.93	0.75	5.88	229	941	158	392	1,720
	10	150.93	0.75	6.13	229	981	164	409	1,784
	9	144.68	0.75	6.50	229	1,041	174	435	1,880
	8	137.93	0.75	6.94	229	1,111	186	465	1,991
	7	130.80	0.75	7.13	229	1,141	191	477	2,039
	6	123.68	0.75	7.13	229	1,141	191	477	2,039
	5	116.55	0.75	7.13	229	1,141	191	477	2,039
	4	109.43	0.75	7.13	229	1,141	191	477	2,039
	3	102.30	0.75	7.13	229	1,141	191	477	2,039
	2	95.18	0.75	5.81	229	931	156	388	1,704
	1	90.05	2.00	5.63	627	901	151	365	2,043
W74M Lower Basket	14	82.75	2.00	5.49	627	879	147	355	2,008
	13	77.50	0.75	5.88	229	941	158	392	1,720
	12	70.38	0.75	7.13	229	1,141	191	477	2,039
	11	63.25	0.75	7.13	229	1,141	191	477	2,039
	10	56.13	0.75	7.13	229	1,141	191	477	2,039
	9	49.00	0.75	7.13	229	1,141	191	477	2,039
	8	41.88	0.75	7.13	229	1,141	191	477	2,039
	7	34.75	0.75	7.13	229	1,141	191	477	2,039
	6	27.63	0.75	6.56	229	1,051	176	439	1,895
	5	21.63	0.75	6.00	229	961	161	401	1,752
	4	15.63	0.75	5.88	229	941	158	392	1,720
	3	9.88	0.75	5.50	229	881	148	367	1,625
	2	4.63	0.75	3.63	229	581	97	240	1,147
	1	2.00	2.00	3.63	627	581	97	229	1,533

**Table 2.12-2 - W74T Spacer Plate Tributary Weights –
Uniform Fuel Loading**

Basket Assembly	Spacer Plate No.	Bottom to Centerline Distance (in.)	Spacer Plate Thick. (in.)	Tributary Length (in.)	Tributary Weights (lbs.)				Total Tributary Weight (lbs.)
					Spacer Plate	Fuel Assy.	Guide Tube	Spt.Tubes, Sleeves & Fuel Cans	
W74T Upper Basket	13	170.13	0.75	5.74	229	919	154	383	1685
	12	165.00	0.75	5.44	229	871	146	363	1609
	11	159.25	0.75	5.75	229	921	154	384	1688
	10	153.50	0.75	6.00	229	961	161	401	1752
	9	147.25	0.75	6.38	229	1021	171	426	1848
	8	140.75	0.75	6.69	229	1071	179	448	1927
	7	133.88	0.75	7.00	229	1121	188	469	2007
	6	126.75	0.75	7.13	229	1141	191	477	2039
	5	119.63	0.75	7.13	229	1141	191	477	2039
	4	112.50	0.75	7.13	229	1141	191	477	2039
	3	105.38	0.75	7.13	229	1141	191	477	2039
	2	98.25	0.75	7.13	229	1141	191	477	2039
1	91.13	0.75	7.44	229	1191	200	499	2119	
W74T Lower Basket	13	81.88	0.75	6.94	229	1111	186	465	1991
	12	74.75	0.75	7.13	229	1141	191	477	2039
	11	67.63	0.75	7.13	229	1141	191	477	2039
	10	60.50	0.75	7.13	229	1141	191	477	2039
	9	53.38	0.75	7.13	229	1141	191	477	2039
	8	46.25	0.75	7.13	229	1141	191	477	2039
	7	39.13	0.75	7.13	229	1141	191	477	2039
	6	32.00	0.75	6.81	229	1091	183	456	1959
	5	25.50	0.75	6.38	229	1021	171	426	1848
	4	19.25	0.75	6.00	229	961	161	401	1752
	3	13.50	0.75	5.63	229	901	151	375	1657
	2	8.00	0.75	5.38	229	861	144	359	1593
1	2.75	0.75	5.38	229	861	144	359	1593	

Table 2.12-3 - BRP Fuel Grid Spacer Positions and Tributary Weights

BRP SNF Assembly Component	Tributary Dimensions		Location in Basket (in.)	
	Length (in.)	Trib. Wt. (lbs)	Upper Basket	Lower Basket
Upper Tie Plate	15.84	90.60	167.28	80.03
Spacer	20.63	117.99	145.48	58.23
Spacer	18.90	108.09	126.59	39.34
Spacer	18.92	108.21	107.69	20.44
Lower Tie Plate	9.69	55.42	89.16	1.91

**Table 2.12-4 - W74M Spacer Plate Tributary Weights –
Concentrated Fuel Loading**

Basket Assembly	Spacer Plate No.	Distance to Spacer Plate Centerline (in.) ⁽¹⁾	Distance to SNF Assy. Grid Spacer (in.) ⁽²⁾	Grid Spacer Tributary Length (in.)	Grid Spacer Tributary Weight (lbs)	Basket Component Tributary Weight (lbs)	Total Tributary Weight (lbs)
Upper Basket Assy.	14	170.30				839	839
	13	168.18	167.28	15.84	3,048	441	3,489
	12	162.68				574	3,622
	11	156.93				590	590
	10	150.93	145.48	20.63	3,970	605	4,575
	9	144.68				629	4,599
	8	137.93				656	656
	7	130.80	126.59	18.90	3,637	668	4,304
	6	123.68				668	4,304
	5	116.55				668	668
	4	109.43	107.69	18.92	3,641	668	4,309
	3	102.30				668	4,309
	2	95.18				586	586
	1	90.05	89.16	9.69	1,865	960	2,825
Lower Basket Assy.	14	82.75	80.03	15.84	3,048	952	4,000
	13	77.50				590	3,638
	12	70.38				668	668
	11	63.25	58.23	20.63	3,970	668	4,637
	10	56.13				668	4,637
	9	49.00				668	668
	8	41.88	39.34	18.90	3,637	668	4,304
	7	34.75				668	668
	6	27.63				633	633
	5	21.63	20.44	18.92	3,641	597	4,238
	4	15.63				590	4,231
	3	9.88				566	566
	2	4.63				449	449
	1	2.00	1.91	9.69	1,865	835	2,700

Notes:

- (1) Longitudinal distance from the bottom of the lower basket assembly support tubes to the centerline of the spacer plate.
- (2) Longitudinal distance from the bottom of the lower basket assembly support tubes to the centerline of the SNF assembly end fitting or grid spacer.

**Table 2.12-5 - W74T Spacer Plate Tributary Weights –
Concentrated Fuel Loading**

Basket Assembly	Spacer Plate No.	Distance to Spacer Plate Centerline (in.) ⁽¹⁾	Distance to SNF Assy. Grid Spacer (in.) ⁽²⁾	Grid Spacer Tributary Length (in.)	Grid Spacer Tributary Weight (lbs)	Basket Component Tributary Weight (lbs)	Total Tributary Weight (lbs)
Upper Basket Assy.	13	170.13	167.28	15.84	3,048	581	3,629
	12	165.00				562	3,610
	11	159.25				582	582
	10	153.50				597	597
	9	147.25	145.48	20.63	3,970	621	4,591
	8	140.75				640	4,610
	7	133.88				660	660
	6	126.75	126.59	18.90	3,637	668	4,304
	5	119.63				668	4,304
	4	112.50	107.69	18.92	3,641	668	4,309
	3	105.38				668	4,309
	2	98.25				668	668
1	91.13	89.16	9.69	1,865	687	2,552	
Lower Basket Assy.	13	81.88	80.03	15.84	3,048	656	3,704
	12	74.75				668	668
	11	67.63				668	668
	10	60.50	58.23	20.63	3,970	668	4,637
	9	53.38				668	4,637
	8	46.25	39.34	18.90	3,637	668	4,304
	7	39.13				668	4,304
	6	32.00				648	648
	5	25.50	20.44	18.92	3,641	621	4,262
	4	19.25				597	4,238
	3	13.50				574	574
	2	8.00				558	558
1	2.75	1.91	9.69	1,865	558	2,423	

Notes:

- ⁽¹⁾ Longitudinal distance from the bottom of the lower basket assembly support tubes to the centerline of the spacer plate.
- ⁽²⁾ Longitudinal distance from the bottom of the lower basket assembly support tubes to the centerline of the SNF assembly end fitting or grid spacer.

2.12.2 Free Drop Equivalent Static Design Loads

This section presents the calculations to determine the bounding equivalent static accelerations used for the NCT and HAC free drop structural evaluations. The FuelSolutions™ W21 canisters are evaluated for the NCT and HAC free drop conditions using equivalent static loads, which account for dynamic amplification of the peak rigid body response. The equivalent static accelerations for each impact orientation are calculated by multiplying the peak rigid-body acceleration by the corresponding Dynamic Load Factor (DLF). The DLF for each impact orientation is calculated based on the controlling fundamental frequencies of the structural system, considering the participating vibration modes. The calculation of the fundamental system frequencies are presented in Section 2.12.2.1. The determination of the corresponding DLFs and the resulting equivalent static accelerations for the NCT and HAC drop conditions are discussed in Section 2.12.2.2.

2.12.2.1 W74 Canister Frequency Analysis

2.12.2.1.1 Longitudinal Response Frequencies

The longitudinal modes of vibration considered in the structural evaluation of the W74 canister include:

- W74 general and LTP spacer plate out-of-plane bending
- Engagement spacer plate out-of-plane bending
- Support tube longitudinal compression/extension
- Guide tube longitudinal compression/extension
- Canister shell longitudinal compression/extension
- Top shield plug out-of-plane bending.

These modes are evaluated in the following paragraphs.

General and LTP Spacer Plate Longitudinal Bending Mode

The out-of-plane (longitudinal) general spacer plate frequencies are calculated using finite element analysis techniques. The modal analysis of the W74 general spacer plate is performed using the spacer plate shell model described in Section 2.12.4.1.1, with quadrilateral shell elements (SHELL63) instead of plane stress elements to capture the out-of-plane bending response of the spacer plates. The spacer plate is modeled with a 0.75-inch uniform thickness. Longitudinal displacements constraints (i.e., $U_Z=0$) are applied to the nodes around the perimeter of the support tube holes where support is provided by the support sleeves. The spacer plate supports only its own self weight in the longitudinal direction. The mass of the spacer plate is inherently modeled by application of a mass-density material specification and the appropriate plate thickness. The material properties used in the model are based on a bounding temperature of 700°F. The modal analysis results indicate that the lowest out-of-plane frequency of the W74 general spacer plate is 99 Hz.

The longitudinal vibration frequency of the W74 LTP spacer plate is higher than that of the W74 general spacer plate due to its greater thickness. However, it is conservatively assumed that the W74 LTP spacer plate longitudinal frequency is equal to that of the W74 general spacer plate for the purpose of determining maximum DLFs.

Support Tube Longitudinal Compression/Extension Mode

When subjected to longitudinal impact loads, the weight of the W74 basket assembly and fuel opposite the impacting end is supported longitudinally by the W74 basket assembly support tubes nearest the impacting end. Under these conditions, the lowest longitudinal vibration frequency of the structural system is assumed to be the compression/extension frequency of the support tubes on the impacting end. The fundamental longitudinal compression/extension frequency of the W74 basket assembly support tubes is evaluated using hand calculations. The system frequency is calculated assuming the support tubes behave as a uniform bar, fixed on one end and free on the other, with a uniform load w per unit length equal to the self weight of the support tubes, plus a concentrated load W at the free end (Table 36, Case 7C, of Roark), as follows:

$$f_1 = \frac{1}{2\pi} \sqrt{\frac{AEg}{Wl + (wl^2/3)}} = 98 \text{ Hz}$$

where;

- A = Total cross section area of all four support tubes
 = $4[(8.90)^2 - (7.40)^2 - 4(0.75)^2/2]$
 = 93.3 in²
- E = 25.3(10)⁶ psi, elastic modulus of the support tube SA-240, Type XM-19 stainless steel at a bounding temperature of 600°F
- g = 386.4 in/sec², gravitational constant
- W = 27,526 pounds, weight of W74M upper basket assembly and fuel, and top end 2.00-inch thick stainless steel spacer plate of lower basket assembly, plus additional weight of the four damaged fuel cans at the support tube fuel cells
 = 10,567 + 15520 + 639 + 4(200)
- w = 27.06 lb./inch, weight per unit length of four support tubes
 = (0.290 lb./in³)(93.3 in²)
- l = 85.25 in., length of support tube

Engagement Spacer Plate Longitudinal Bending Mode

The engagement spacer plate fundamental longitudinal bending frequency is calculated using the quarter-symmetry finite element model described in Section 2.12.4.2.3 and shown in Figure 2.12-8. A reduced subspace modal analysis with 1000 master degrees of freedom is performed using the ANSYS general purpose finite element code. A maximum of 20 modes are

extracted up to a maximum frequency of 500 Hz. The results show that the lowest out-of-plane (Z direction) mode with significant mass participation occurs at 78 Hz. The mass participating in this mode is approximately 28% (=5.142 /18.71) of the total system mass. The other significant out-of-plane modes, occurring at 153.6 Hz, 274.7 Hz, and 411.3 Hz, account for 40%, 2%, and 3% of the total system mass, respectively. For the purpose of the engagement spacer plate end drop evaluation, it is conservatively assumed that the entire mass of the system responds at a frequency of 78 Hz.

Guide Tube Longitudinal Compression/Extension

The W74 guide tube supports only its own weight and that of the neutron absorber in the longitudinal direction. The guide tube axial compression/extension frequency is evaluated using hand calculations. Using Table 36, Case 7b, of Roark, the axial frequency of the guide tube assembly is calculated assuming the guide tube assemblies behave as a uniform bar vibrating along its longitudinal axis, with the bottom end fixed and the top end free, subjected to a uniform load, w, per unit length (including the neutron absorber panel weight) as follows:

$$f_1 = \frac{1.57}{2\pi} \sqrt{\frac{AEg}{wL^2}} = 462 \text{ Hz}$$

where:

- A = 2.52 in², cross-section area of a guide tube
- E = 25.1x10⁶ psi, elastic modulus of Type 316 stainless steel at 650°F
- g = 386.4 inch/s², gravitational acceleration
- L = 84.8 inches, length of the W74 guide tube assemblies
- w = 0.993 lbs./inch, W74 guide tube weight per unit length
= 84.2 lb./84.8 inches

2.12.2.1.2 Transverse Response Frequencies

The transverse vibration modes considered in the structural evaluation of the W74 canister include the following:

- General and LTP spacer plate in-plane vibration modes
- Guide tube panel bending mode
- Transportation cask beam bending mode.

These modes are evaluated in the following paragraphs.

Spacer Plate In-Plane Vibration Modes

For transverse impact loads, each W74 general and LTP spacer plate supports its own weight, plus the tributary weight of the fuel assemblies, damaged fuel cans, guide tubes, support tubes, and support sleeves. The in-plane tributary weights for each W74M and W74T basket assembly spacer plate are calculated in Section 2.12.1. The largest tributary weights for the W74 general and LTP spacer plates are 2,017 pounds and 1,973 pounds, respectively. Since cross-section

geometry of the W74 general and LTP spacer plates are identical and the elastic moduli are very close, the in-plane stiffness of the spacer plates is approximately proportional to the plate thickness. Therefore, the in-plane stiffness of the LTP spacer plate is greater than that of the general spacer plate. In addition, the maximum tributary weight supported by the LTP spacer plate is less than that of the general spacer plate. Consequently, the fundamental frequency of the LTP spacer plate is greater than that of the general spacer plate. As shown in Section 2.12.5 of the FuelSolutions™ TS125 Transportation Cask SAR, the HAC free drop DLFs generally decrease as the frequency increases. Therefore, the lower bound frequency of the W74 general spacer plate is conservatively used to determine the bounding DLFs for the spacer plate HAC drop stress evaluation.

The in-plane modal analysis of the W74 general spacer plate is performed using the two-dimensional plane-stress finite element model described in Section 2.12.4.1.1. Modal analyses are performed for impact orientations of 0° and 45°, in order to determine the lowest in-plane frequency. The mass of the tributary components is modeled using 2-D lumped mass elements (MASS21). The tributary mass of the guide tubes, support tubes, support sleeves, fuel, and damaged fuel cans are calculated for a maximum general spacer plate tributary length of 7.13 inches. The maximum fuel assembly weight of 485 pounds is used for the spacer plate modal analysis. Therefore, the calculated spacer plate frequencies are conservatively lower than the actual spacer plate frequencies.

The tributary mass of each guide tube assembly and the associated fuel assembly weight is distributed evenly to the nodes on the supporting spacer plate ligaments. Similarly, the tributary mass of the support tube/sleeve assembly and associated fuel assembly/damaged fuel can weight is distributed evenly to the nodes supporting edges of the support tube hole openings. The mass of the spacer plate is inherently modeled by application of a mass-density material specification and the appropriate plate thickness “real constant.” The material properties used in the model are conservatively based on a bounding design temperature of 700°F.

The boundary conditions applied to the spacer plate finite element model for the modal analysis are based on the results of the HAC drop evaluation. Since gap elements are not permitted for modal analyses, the spacer plate support conditions are modeled using nodal displacement constraints. For each orientation evaluated, the spacer plate is supported radially (UX=0) over a region that is approximately equal to the region shown to be supported in the HAC oblique drop secondary impact stress analysis. The results show that the lowest in-plane frequency of the W74 general spacer plate is 110 Hz for the 45° orientation. This lower bound frequency is conservatively used to determine the maximum DLFs for the W74 general and LTP spacer plates for all HAC free drop transverse impact loads. The lowest spacer plate frequency for the 0° impact orientation is 129 Hz. This frequency is used to determine the maximum DLF for the NCT side drop.

Transport Cask Beam Bending Mode

For transverse drop loads, the W74 canister is supported by the FuelSolutions™ TS125 Transportation Cask body, which is supported by the impact limiters. The fundamental frequency of the cask body is evaluated in the FuelSolutions™ TS125 Transportation Cask SAR using hand calculations. The transportation cask inner and outer shells are conservatively evaluated as a simply supported beam, with the entire mass of the transportation cask and

canister distributed uniformly over the length of the transportation cask. The results of this evaluation show that the frequency of the FuelSolutions™ TS125 Transportation Cask is 100 Hz.

2.12.2.2 Equivalent Static Accelerations

The W74 general and LTP spacer plates are evaluated for the HAC 30-foot drop loads using equivalent static loads, which account for dynamic amplification of the peak rigid body response. The dynamic amplification experienced in each spacer plate is expressed as a DLF. The DLF is a function of the response frequency of the system and the characteristics of the acceleration time-history for each drop orientation. Section 2.12.2.1 presents the calculation of the system response frequencies used to derive the equivalent static design loads for the W74 canister structural analysis. The DLF for each free drop condition is conservatively taken as the highest value for all frequencies greater than or equal to the lowest relevant system response frequency. The governing system response frequencies for the W74 general and LTP spacer plates and the corresponding DLFs from Section 2.10.5 of the FuelSolutions™ TS125 Transportation Cask SAR are summarized in Table 2.12-6.

Table 2.12-6 - W74 Canister Equivalent Static Free Drop G-Loads

Free Drop Condition	Participating Component Vibration Modes	Natural Frequency (Hz)	Dynamic Load Factor ⁽¹⁾	Peak Rigid-Body G-Load ⁽²⁾	Equivalent Static G-Load ⁽³⁾	Bounding Design G-Load
NCT Side Drop	Cask Beam Bending Spacer Plate In-Plane	100 110	1.05	10.2g	10.7g	15g
HAC End Drop	Spacer Plate Bending Engagement Plate Bending Support Tube Longitudinal Guide Tube Longitudinal	99 78 98 462	1.34	42.9g	57.5g	60g
HAC Side Drop	Cask Beam Bending Spacer Plate In-Plane	100 110	1.11	49.7g	55.2g	60g
HAC Corner Drop	Cask Beam Bending Spacer Plate (Trans./Long.) Engagement Plate Bending Support Tube Longitudinal Guide Tube Longitudinal	101 110/99 78 98 462	1.06	36.6g	38.8g	40g
HAC Oblique Drop (Primary Impact)	Cask Beam Bending Spacer Plate (Trans./Long.) Engagement Plate Bending Support Tube Longitudinal Guide Tube Longitudinal	100 110/99 78 98 462	1.34	22.4g (75°) ⁽⁴⁾ 30.9g (60°) 28.9g (45°) 32.3g (30°)	35.9g (Trans.) 37.5g (Long.)	36g (Trans.) 38g (Long.)
HAC Oblique Drop (Slapdown)	Cask Beam Bending Spacer Plate In-Plane	100 110	1.13	$a_{cg}=28.2g$ $\alpha=187.4 \text{ rad/s}^2$ $a_{lat,end}=71.8g^{(5)}$	$a_{cg}=31.9g$ $\alpha=211.8 \text{ rad/s}^2$ $a_{lat,end}=81.1g$	$a_{cg}=31.9g$ $\alpha=211.8 \text{ rad/s}^2$ $a_{lat,end}=81.1g$

Notes:

- (1) DLFs are calculated in Section 2.12.3 of the FuelSolutions™ TS125 Transportation Cask SAR.
- (2) Peak rigid-body accelerations for each free drop condition are calculated in Section 2.12.2 of the FuelSolutions™ TS125 Transportation Cask SAR. The peak g-loads are conservatively based on a lower bound package weight of 260 kips.
- (3) The equivalent static g-load is equal to the peak g-load multiplied by the maximum DLF for all participating component vibration modes.
- (4) The HAC oblique drop primary impact vertical g-loads at the package c.g. are reported for each oblique drop orientation evaluated. The corresponding transverse and longitudinal accelerations are determined by multiplying the vertical g-load by the cosine and sine of the impact angle. The c.g. acceleration is considered separately from the rotational acceleration for the 75° primary impact since the peaks occur at different times.
- (5) The peak transverse acceleration at a distance of 90 inches from the package center of gravity.

2.12.3 General and LTP Spacer Plate Stress Evaluation Points

The W74 general and LTP spacer plates are evaluated using the finite element models described in Section 2.12.4.1 of this report. The section stresses at all critical spacer plate locations are evaluated for each loading condition. A total of 160 stress sections are considered, as shown in Figure 2.12-1. In general, the section stresses are evaluated at each end of the spacer plate ligaments and at the thinnest ligaments located along the outside edge of the spacer plate.

Section stresses are used to determine the average membrane, linearized membrane plus bending, and total (primary plus secondary plus peak) stress distribution across each section for comparison with the stress limits defined in the ASME Code. Section stresses are determined using the stress linearization routine described in the ANSYS User's Theory Manual. For each section, the linearized stresses are determined at the innermost radial position of the section ("I"), the center of the section ("C"), and the outermost radial position of the section ("O"). For analyses that use shell elements, linearizations are determined at three additional section locations; the top ("T"), middle ("M"), and bottom ("B") surfaces of the elements.

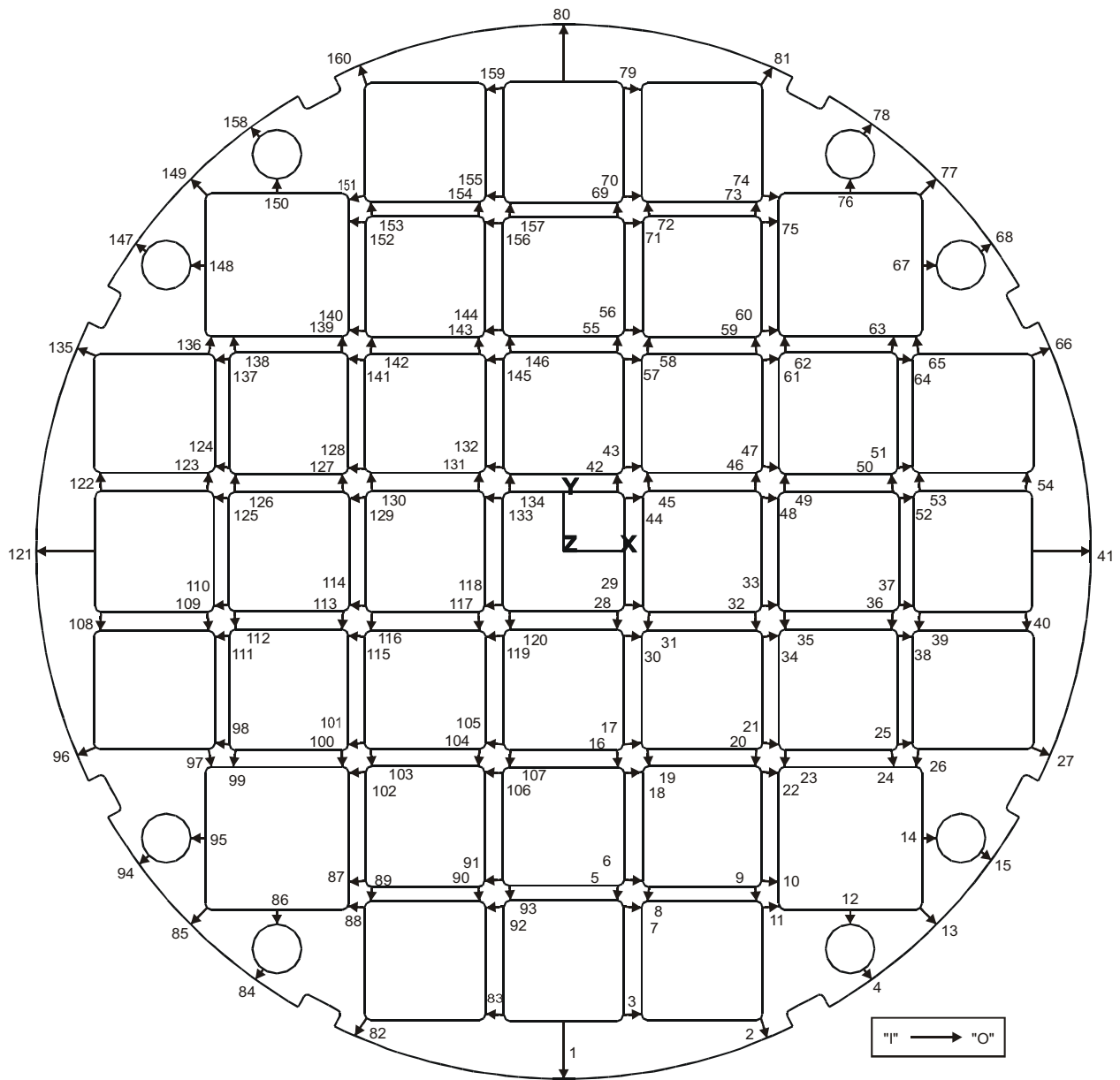


Figure 2.12-1 - W74 Canister General and LTP Spacer Plate Stress Evaluation Points

2.12.4 Finite Element Model Descriptions

Finite element evaluations of the W74 canister components are performed using ANSYS, a general purpose finite element code. The following sections provide basic descriptions of the finite element models used for the W74 canister structural evaluations including: model construction, boundary conditions, material properties, and applied loading.

2.12.4.1 General and LTP Spacer Plate Models

2.12.4.1.1 Spacer Plate Plane Stress Model

The structural analysis of the W74 general and LTP spacer plates for NCT thermal, NCT vibration, NCT free drop, and HAC oblique drop in-plane loads is performed using the two-dimensional plane-stress finite element model shown in Figure 2.12-2. Details of the W74 spacer plate plane-stress finite element model are provided in the following paragraphs.

Model Construction

The W74 spacer plate plane-stress finite element model includes plane-stress elements, gap elements, and spring elements. The spacer plate is modeled using PLANE42 elements (4-node quadrilateral) with the spacer plate thickness input as a real constant. Three-dimensional node-to-node gap elements (CONTAC52) are included around the perimeter of the spacer plate for NCT vibration, NCT side drop, and HAC drop conditions to model the non-linear support provided by the canister shell. The gap elements are modeled with a uniform 3/16-inch nominal radial gap size and a contact stiffness of 9×10^5 pounds/inch (based on shell compliance). When the spacer plate loading is initially applied, the spacer plate is moved into contact with the ground nodes at the initial point of contact with the canister shell, and the gap element sizes are updated based on the new node locations.

In order to provide numerical stability, three spring elements (COMBIN14) are attached to the perimeter of the spacer plate model at the 0° , $+45^\circ$, and $+90^\circ$ azimuths. The spring elements are modeled with a small spring stiffness of 100 pounds/inch and do not have any significant effect on the stress solution.

Boundary Conditions

The “ground” nodes of each gap and spring element are restrained in all directions. Additionally, to prevent rigid body rotation of the model, the node on the perimeter of the model at the impact location is restrained in the “theta” direction.

Material Properties

The W74 general and LTP spacer plates are modeled with the material properties of A514, Grade F or P carbon steel and SA-240, Type XM-19 stainless steel, respectively. The material properties for an upper bound design temperature of 700°F are used for all load conditions, except those including thermal loads. Temperature-dependent material properties are used for those conditions including thermal loading.

Loading

For inertial load conditions, the spacer plate loading consists of its own inertial load plus the inertial load corresponding to the tributary weight of the fuel assemblies, guide tube assemblies, support tubes, and support sleeves. Since the spacer plate is modeled directly, the spacer plate's own inertial load is accounted for by applying an acceleration load in the direction of impact.

The inertial load of the SNF assemblies, damaged fuel canisters, guide tube assemblies, support tubes, and support sleeves are modeled as uniform pressure loads over the width of the supporting spacer plate ligaments, as shown in Figure 2.12-3. The pressure load on each of the supporting support tube hole or guide tube hole ligaments in the global X and Y directions due to an applied acceleration G is determined as follows:

Support Tube Holes:
$$P_{T,X} = (W_F + W_C + W_T)(G)(\sin(\theta))/A_{lig}$$

$$P_{T,Y} = (W_F + W_C + W_T)(G)(\cos(\theta))/ A_{lig}$$

Guide Tube Holes:
$$P_{G,X} = (W_F + W_G)(G)(\sin(\theta))/A_{lig}$$

$$P_{G,Y} = (W_F + W_G)(G)(\cos(\theta))/ A_{lig}$$

where;

- W_F = Tributary weight of the fuel assembly (pounds)
- W_C = Tributary weight of the damaged fuel can (pounds)
- W_T = Tributary weight of the support tube and support sleeve (pounds)
- W_G = Tributary weight of the guide tube assembly (pounds)
- A_{lig} = Ligament surface area over which the pressure is applied (in²)
- G = Resultant in-plane equivalent static load (g's)
- θ = Angle of resultant load vector G measure CCW relative to 0° azimuth (degrees)

For the concentrated SNF assembly loading assumption, different tributary lengths are specified for the basket components (i.e., guide tubes, support tubes, support sleeves) and the SNF assembly, to account for fuel grid spacer pitch in different locations. Unlike the uniform fuel loading, the concentrated fuel loading assumes that the SNF assembly weight acts (through the grid spacers) only on those spacer plates nearest the grid spacer location. The in-plane spacer plate loads due to each NCT and HAC load condition are discussed further in the respective sections of this SAR.

2.12.4.1.2 General Spacer Plate Full Multi-Span Shell Model

The full spacer plate multi-span shell model shown in Figure 2.12-4 and described in this section is used for the 0° and 45° HAC oblique drop slapdown impact plastic large deflection analysis of the W74 general spacer plates.

Model Construction

The W74 general spacer plate full multi-span finite element model includes three general spacer plates; the center spacer plate over which the fuel grid spacers are assumed to be positioned, and the adjacent spacer plates on either side. The W74 spacer plates are modeled with nominal cross-section dimensions. All three general spacer plates are modeled with a ¾-inch thickness and a uniform pitch (i.e., longitudinal spacing) according to the respective conditions. The W74 guide tubes and support tubes extend 3.5625 inches beyond the centerlines of the outer spacer plates on each side.

The spacer plates are modeled using plastic shell elements (SHELL43), which permit treatment of longitudinal deflections. The W74 guide tubes and support tubes are also modeled using plastic shell elements (SHELL43). The guide tubes are modeled with a 0.090-inch thickness, conservatively neglecting the structural capacity of the guide tube neutron absorber sheets. However, an adjusted weight density is used for the guide tube material to account for the weight of the neutron absorber sheets, conservatively addressing two neutron absorber sheets per guide tube. The adjusted weight density of the guide tube is calculated as follows:

$$\rho = \frac{\rho_{ss}(A_{GT} + A_N)}{A_{GT}} = 0.40 \text{ lbs/in}^3$$

where:

$$\rho_{ss} = 0.290 \text{ lbs/in}^3, \text{ weight density of stainless steel}$$

$$A_{GT} = 2.52 \text{ in}^2, \text{ guide tube cross-sectional area} \\ = 4(6.90 + 0.090)(0.090)$$

$$A_N = 0.96 \text{ in}^2, \text{ cross-sectional area of 2 neutron absorber panels} \\ = 2(6.4)(0.075)$$

Two dimensional node-to-node gap elements (CONTAC12) are included between the bottom of the guide and support tubes and the supporting spacer plate ligaments, in order to provide the proper guide tube and support tube to spacer plate interface for the cask drop events. The normal contact stiffness of 1×10^6 lbs/inch is used for these gap elements.

The W74 support sleeves are modeled using three dimensional structural solid elements (SOLID45). Nonlinear spring elements (COMBIN39), having a stiffness in compression of 1×10^7 lbs/inch and a stiffness in tension of 10 lbs/inch, are included between the nodes of the support sleeves at their interface with the spacer plate and the corresponding spacer plate nodes. Three dimensional point-to-surface contact elements (CONTAC49), having a normal contact stiffness of 1×10^6 lbs/inch, are included between the extended portions of the sleeves at their interface with the spacer plate and the associated spacer plate nodes.

Three dimensional node-to-node gap elements (CONTAC52) are included around the perimeter of each spacer plate for the transfer cask side drop condition to model the non-linear support provided by the canister shell. These gap elements are modeled with a uniform 3/16-inch nominal gap size and a normal contact stiffness of 9.0×10^5 lbs/inch. The gap contact stiffness is based on a compliance analysis of the canister shell. When the spacer plate loading is initially applied, the spacer plates are moved into contact with the ground nodes at the initial point of

contact with the canister shell. The gap element sizes are updated based on the new node locations.

Soft spring elements (COMBIN14) are placed on the perimeter of each spacer plate at locations of 0°, -45° and -90° in the global cylindrical coordinate system (CSYS=1) for added numerical stability. The stiffness of the soft springs is specified as 100 lbs/in., such that their presence has no significant effect on the accuracy of the solution. These springs are also used to maintain stability of the guide tubes and support tubes during solution convergence.

Material Properties

The W74 general spacer plates are modeled using the material properties of SA-517, Grade F or P carbon steel. The W74 guide tubes are modeled using SA-240, Type 316 stainless steel material properties. The W74 support tubes are modeled using SA-240, XM-19 stainless steel material properties. The W74 support sleeves are modeled using SA-240, Type 304 stainless steel material properties. Bi-linear kinematic hardening with a 0.1% tangent modulus is assumed for all materials. For the oblique drop and side drop conditions without thermal loading, uniform material properties at a bounding design temperature of 700°F are used. The weight density and Poisson's ratio are taken as 0.283 lbs/in³ and 0.3 for carbon steel and 0.290 lbs/in³ and 0.3 for stainless steel.

Boundary Conditions

For the HAC oblique drop slapdown impact evaluation, the “ground” nodes of each spacer plate perimeter gap element are restrained in all directions. Additionally, to prevent rigid body rotation of the model, the node on the model edge at the impact location is restrained in the “theta” direction.

Symmetry boundary constraints are applied to the model nodes located on the half-symmetry plane (i.e. UX = ROTY = ROTZ = 0) for spacer plate and guide tube elements. Symmetry boundary conditions (i.e. UZ=ROTX=ROTY = 0) are also applied to the nodes on the end planes of the guide tubes and support tubes.

Loading

The model loading includes the self-weight of the spacer plates, guide tubes, support tubes and support sleeves, in addition to the loads from the weight of the fuel assemblies (including damaged fuel cans). Since the spacer plates, guide tubes, support tubes, and support sleeves are discretely modeled, an acceleration load is applied to the model to account for their load due to their self-weight. The loads due to the weight of the SNF assemblies are modeled as concentrated loads at the SNF assembly grid spacers. The SNF assembly loads are applied to directly above the W74 general spacer plate ligaments at the center of the finite element model.

2.12.4.1.3 General Spacer Plate Multi-Span Buckling Shell Model

The general spacer plate multi-span buckling shell model shown in Figure 2.12-5 and described in this section is used for the 0° and 45° HAC oblique drop slapdown impact plastic large deflection buckling analysis of the W74 general spacer plates. This model is similar to the W74 general spacer plate full multi-span model described in Section 2.12.4.1.2, with simplifications to reduce computer run times. These simplifications are described in the following paragraphs.

Model Construction

The W74 general spacer plate multi-span buckling finite element model includes two general spacer plates; the one general spacer plate on the symmetry plane over which the fuel grid spacers are assumed to be positioned, and the adjacent general spacer plate on one side. The W74 general spacer plates are modeled with nominal cross-section dimensions, a uniform thickness of 3/4-inch, and uniform longitudinal spacing between spacer plates. Unlike the full multi-span model described in Section 2.12.4.1.2, the W74 guide tubes are included in the buckling model. To further reduce a complexity, instead of direct modeling of the support sleeves, displacement boundary constraints are applied to the spacer plates at the support sleeve locations.

The spacer plates are modeled using plastic shell elements (SHELL43), which permit treatment of longitudinal deflections. The W74 support tubes are also modeled using plastic shell elements (SHELL43).

Three dimensional node-to-node gap elements (CONTAC52) are included between all faces of the support tubes and the supporting spacer plate ligaments, in order to provide the proper support tube to spacer plate interface for the cask drop events. The normal contact stiffness of 1×10^6 lbs/inch is used for these gap elements.

Three dimensional node-to-node gap elements (CONTAC52) are included around the perimeter of each spacer plate for the transfer cask side drop condition to model the non-linear support provided by the canister shell. These gap elements are modeled with a uniform 3/16-inch nominal gap size and a normal contact stiffness of 9.0×10^5 lbs/in. The gap contact stiffness is based on a compliance analysis of the canister shell. When the spacer plate loading is initially applied, the spacer plates are moved into contact with the ground nodes at the initial point of contact with the canister shell. The gap element sizes are updated based on the new node locations.

Soft spring elements (COMBIN14) are placed on the perimeter of each spacer plate at locations of 0° , -45° and -90° in the global cylindrical coordinate system (CSYS=1) for added numerical stability. The stiffness of the soft springs is specified as 100 lbs/in., such that their presence has no significant effect on the accuracy of the solution. These springs are also used to maintain stability of the support tubes during solution convergence.

Material Properties

The W74 general spacer plates are modeled using the material properties of SA-517, Grade F or P carbon steel. The W74 support tubes are modeled using SA-240, Type XM-19 stainless steel material properties. Bi-linear kinematic hardening with a 0.1% tangent modulus is assumed for all materials. For drop conditions without thermal loading, uniform material properties at a bounding design temperature of 700°F are used. The weight density and Poisson's ratio are taken as 0.283 lbs/in^3 and 0.3 for carbon steel and 0.290 lbs/in^3 and 0.3 for stainless steel.

Boundary Conditions

The "ground" nodes of each spacer plate perimeter gap element are restrained in all directions. Additionally, to prevent rigid body rotation of the model, the node on the model edge at the

impact location is restrained in the “theta” direction. Symmetry boundary conditions (i.e., $UZ=ROTX=ROTY = 0$) are applied to the nodes on the end planes of the support tubes. However, symmetry boundary conditions are not applied to the general spacer plate lying on the support tube symmetry plane. This permits longitudinal displacement associated with out-of-plane buckling of the general spacer plate.

As discussed above, the support sleeves are not modeled discretely. It is conservatively assumed that support sleeves does not constrain spacer plates during buckling. In order to provide longitudinal constraint without rotational constraint, constraint equation are applied to the nodes around the perimeter of the support tube holes.

Loading

The model loading includes the self-weight of the spacer plates and support tubes, in addition to the loads from the weight of the guide tubes, support sleeves, and SNF assemblies (including damaged fuel cans). Since the spacer plates and support tubes are discretely modeled, an acceleration load is applied to the model to account for their load due to their self-weight. The loads due to the combined weight of the SNF assemblies, guide tube assemblies, support sleeves, and damaged fuel cans are modeled as concentrated forces on the supporting spacer plate ligaments.

2.12.4.2 Engagements Spacer Plate Finite Element Models

2.12.4.2.1 Half-Symmetry Plane Stress Model

The W74 engagement spacer plate is evaluated for the NCT thermal stress, NCT vibration, NCT side drop, and HAC 0° side drop using the half-symmetry plane stress finite element model shown in Figure 2.12-6. Details of the finite element model are provided in the following paragraphs.

Model Construction

The finite element model includes two-dimensional isoparametric plane stress elements (PLANE42), representing the geometry of the engagement spacer plate. Each plane stress element has four nodes, each node having two degrees of freedom (UX and UY). The finite element mesh consists mostly of four node elements, minimizing the use of triangular (constant strain) elements (which are too stiff) and consequently should be avoided where practical, particularly in areas of high stress gradients. The engagement spacer plate plane stress elements are modeled with a uniform thickness of 2.00 inches. The spacer plate thickness is input as a real constant.

The non-linear contact support provided by the canister shell is modeled using 3-D point-to-point contact (gap) elements (CONTAC52). The gap elements are modeled with the nominal radial gap size based on the engagement spacer plate and shell element ground nodes being initially concentric. The engagement spacer plate is then moved to close the gap in the region of initial contact, and the gap elements sizes are updated based on the new node locations. This effectively models the variation in the size of the gap between the engagement spacer plate and canister shell around the perimeter of the engagement spacer plate. The gap element contact stiffness is modeled as $9(10)^5$ pounds per inch. Friction between the spacer plate and the canister shell is conservatively ignored in the gap elements.

Boundary Conditions

Symmetry boundary displacement constraints are applied to the engagement spacer plate model nodes lying on the half-symmetry plane (e.g., $UX=0$ at $X=0$). In addition, the gap element ground nodes used for the NCT vibration, NCT side drop, and HAC 0° side drop evaluations are fixed. For the NCT thermal evaluation, the gap elements are not used and the model is restrained from vertical translation at the bottom centerline location.

Material Properties

The material properties used in the finite element model are those of SA-240, Type XM-19 at a design temperature of 600°F, as reported in Section 2.3 of this SAR. Poisson's ratio and the density of stainless steel are modeled as 0.29 and 0.290 lb/in³, respectively. The modulus of elasticity used in the model is 25.3(10)⁶ psi.

Loading

For the NCT thermal condition, temperature constraints are applied to the model as described in Section 2.6.1.3.2. For NCT vibration, NCT side drop, and HAC side drop conditions, the W74 engagement spacer plate is loaded only by its own weight. Acceleration loads are used to apply the inertial loads due to the engagement plate self weight.

2.12.4.2.2 Full Plane Stress Model

The W74 engagement spacer plate 28°, 36°, and 45° impact HAC side drop evaluations are performed using the full engagement plate plane stress finite element model shown in Figure 2.12-7. The model geometry is developed by reflecting the engagement spacer plate finite element mesh of the half-symmetry plane stress finite element model described in Section 2.12.4.2.1 about the vertical centerline (i.e., YZ plane). The gap elements used to model the non-linear contact between the engagement spacer plate and the canister shell are modeled using the same approach discussed in Section 2.12.4.2.1. Gap elements are generated for all nodes along the perimeter of the plate in the lower right hand quadrant (i.e., 270° to 360°). The model material properties and loading are identical to those discussed in Section 2.12.4.2.1. The boundary conditions applied to the full model are similar to those used for the half-symmetry model, without symmetry boundary constraints.

2.12.4.2.3 Solid Quarter-Symmetry Modal Analysis Model

The W74 engagement spacer plate longitudinal fundamental frequency is calculated using the quarter symmetry finite element model shown in Figure 2.12-8. Details of the finite element model are provided in the following paragraphs.

Model Construction

The W74 engagement spacer plate solid quarter-symmetry modal analysis model, which includes the engagement spacer plate and the attachment sleeve, consists entirely of 8-node solid brick elements. Each node of the brick elements includes three translational degrees of freedom (UX, UY, and UZ).

The mass of those components that are supported by the engagement spacer plate are included in the model by applying equivalent adjusted mass density to the elements in the respective model

regions. Four separate equivalent mass densities are used to model the various regions of the engagement spacer plate, as shown in Figure 2.12-9. The equivalent mass densities for each region are calculated as follows:

Region I: Interior Fuel Cells: A single intact SNF assembly and guide tube assembly is supported by the engagement spacer plate in the region of each fuel cell. The adjusted weight density (ρ'_1) used for these regions is calculated as follows:

$$\rho'_1 = \rho_{ss} + \frac{(m_{fa} + m_{gt})}{V_{fc}} = 0.01894 \text{ lb-s}^2 / \text{in}^4$$

where:

$$\begin{aligned} \rho_{ss} &= 7.505(10)^{-4} \text{ lb-s}^2/\text{in}^4 \text{ (0.290 lb/in}^3\text{), mass density of stainless steel} \\ m_{fa} &= 1.2552 \text{ lb-s}^2/\text{in} \text{ (485 lb.), maximum mass of fuel assembly} \\ m_{gt} &= 0.2200 \text{ lb-s}^2/\text{in} \text{ (85 lb.), bounding mass of guide tube assembly} \\ V_{fc} &= \text{volume in fuel cell region, assumed equal to region within guide tube i.d.} \\ &= [6.90^2 - \pi(1.50)^2] \times 2.00 \\ &= 81.08 \text{ in}^3 \end{aligned}$$

Region II: Support Tube Fuel Cells: A single payload unit (i.e., intact SNF assembly, failed fuel assembly, or GTCC waste) is supported by the engagement spacer plate in the region of each support tube cell. The adjusted weight density (ρ'_2) used for this regions is calculated as follows:

$$\rho'_2 = \rho_{ss} + \frac{m_p}{V_{st}} = 0.01934 \text{ lb-s}^2 / \text{in}^4$$

where:

$$\begin{aligned} \rho_{ss} &= 7.505(10)^{-4} \text{ lb-s}^2/\text{in}^4 \text{ (0.290 lb/in}^3\text{), mass density of stainless steel} \\ m_p &= 1.7728 \text{ lb-s}^2/\text{in} \text{ (485 lb + 200 lb.), maximum mass of cell payload (SNF assembly and damaged fuel can)} \\ V_{st} &= \text{Volume in support tube cell region, assumed equal to region within support tube i.d.} \\ &= [7.40^2 - \pi(1.50)^2] \times 2.00 \\ &= 95.38 \text{ in}^3 \end{aligned}$$

Region III: Support Tube Bearing (Basket Weight): One quarter of the basket assembly weight is applied to the region in which the support tube bears on the engagement spacer plate. The adjusted weight density (ρ'_3) used for this region is calculated as follows:

$$\rho'_2 = \rho_{ss} + \frac{m_b}{V_{stb}} = 0.1343 \text{ lb-s}^2 / \text{in}^4$$

where:

$$\begin{aligned} \rho_{ss} &= 7.505(10)^{-4} \text{ lb-s}^2/\text{in}^4 \text{ (0.290 lb/in}^3\text{), mass density of stainless steel} \\ m_b &= 5.823 \text{ lb-s}^2/\text{in} \text{ (2,250 pounds for } \frac{1}{4} \text{ symmetry model), bounding mass of} \\ &\quad \text{W74M basket assembly} \\ V_{stb} &= \text{Volume in support tube bearing region, modeled as area between} \\ &\quad \text{attachment sleeve i.d. and support tube i.d.} \\ &= [8.75^2 - 7.40^2] \times 2.00 = 43.61 \text{ in}^3 \end{aligned}$$

Region IV: No Density Adjustment: The regions of the engagement spacer plate that do not support any external mass are modeled with the mass density of stainless steel, $\rho_{ss} = 7.505(10)^{-4} \text{ lb-s}^2/\text{in}^4 \text{ (0.290 lb/in}^3\text{)}$.

The total mass included in the quarter symmetry model is 18.71 lb-s²/inch (7,230 pounds). This is equivalent to a total supported weight of 28,920 pounds. The combined weight of W74M upper basket assembly, including guide tubes, fuel, and damaged fuel cans, is 26,887 pounds. Therefore, the model mass is approximately 8% higher than the bounding design mass, which results in a conservatively low natural frequency. The mass difference is due to the bounding weights assumed for the upper basket assembly and guide tubes.

Material Properties

With the exception of the equivalent adjusted material densities, all other material properties used in the end drop modal analysis finite element model are those of SA-240, Type XM-19 stainless steel at a design temperature of 600°F, as reported in Section 2.3 of this SAR. Poisson's ratio is modeled as 0.29. The modulus of elasticity used in the model is 25.3(10)⁶ psi.

Boundary Conditions

Symmetry displacement constraints are applied to the nodes lying on the engagement spacer plate symmetry boundaries (i.e., UX=0 for all nodes at X=0 and UY=0 for all nodes at Y=0). Longitudinal restraint (UZ=0) of the engagement spacer plate is provided by the support tubes on which the engagement spacer plate bears. The extent of the constraint applied (i.e., fixed vs. pinned) to the modal analysis model is consistent with those boundary conditions used for the end drop stress analysis. As shown in the HAC end drop stress evaluation, the engagement spacer plate pivots about the two exterior edges of the support tube, which face toward the center of the basket assembly. No other contact is developed between the engagement spacer plate and the supporting tube. This is verified in the end drop stress analysis by assuring that the reaction forces at all constrained nodes are compressive and that the plate deflects away from the tube in all other regions.

2.12.4.2.4 Solid Quarter-Symmetry Stress Analysis Model

The engagement spacer plate HAC end drop stress analysis is performed using the solid quarter symmetry finite element model shown in Figure 2.12-10 and Figure 2.12-11. Details of the finite element model are provided in the following paragraphs.

Model Construction

The engagement spacer plate end drop stress analysis model is similar to that used for the modal analysis in Section 2.12.4.2.3, but has greater refinement to more accurately calculate the resulting stresses. As shown in Figure 2.12-10, the model includes two elements through the plate thickness, which is adequate to accurately calculate the linear through-thickness bending stresses within the plate. However, this mesh density may not be sufficient to accurately determine peak stresses, but since evaluation of peak stresses for accident conditions is not required, the mesh density is adequate. The nominal dimensions of the engagement spacer plate are used in the finite element model. The end drop stress analysis model, which includes the engagement spacer plate and the attachment sleeve, consists entirely of 8-node solid brick elements. Each node of the brick elements includes three translational degrees of freedom (UX, UY, and UZ). The model does not include the engagement sleeve, since these components are not relied on for structural support in the HAC end drop.

Material Properties

The material properties used in the end drop finite element model are those of SA-240, Type XM-19 stainless steel at a design temperature of 600°F, as reported in Section 2.3 of this SAR. Poisson's ratio and the density of stainless steel are modeled as 0.29 and 0.290 lb/in³, respectively. The modulus of elasticity used in the model is 25.3(10)⁶ psi.

Boundary Conditions

The finite element model boundary conditions are shown in Figure 2.12-10 and described below. Symmetry displacement constraints are applied to the nodes lying on the engagement spacer plate symmetry boundaries (i.e., UX=0 for all nodes at X=0 and UY=0 for all nodes at Y=0). Longitudinal restraint of the engagement spacer plate is provided by the support tubes on which the engagement spacer plate bears. Only those nodes in the region of the support tube that are loaded in compression are restrained, such that the engagement spacer plate is not prevented from uplifting. Based on preliminary analyses, the engagement spacer plate was shown to pivot about the two exterior edges of the support tube, which face toward the center of the basket assembly. No other contact is developed between the engagement spacer plate and the supporting tube. This is verified by examining the end drop stress analysis results, which show that the reaction forces at all constrained nodes are compressive and that the plate deflects away from the tube in all other regions.

Loading

The finite element model applied HAC end drop loads are shown in Figure 2.12-11 and described in the following paragraphs. As discussed in Section 2.7.1.1.2, a bounding equivalent static HAC end drop acceleration of 50g is conservatively used for the structural evaluation of the W74 engagement spacer plate. An acceleration of 50g is applied to the model to account for the self weight of the engagement spacer plate. The loading of those components that are

supported by the engagement spacer plate are modeled as uniform pressure loads applied to the respective model regions, corresponding to the regions shown in Figure 2.12-9. The applied pressure loading for each region is calculated as follows:

Region I: Interior Fuel Cells: A single intact SNF assembly and guide tube assembly is supported by the engagement spacer plate in the region of each fuel cell. The uniform end drop pressure load (q_1) applied over these regions is calculated as follows:

$$q_1 = \frac{50g \times (W_{fa} + W_{gt})}{A_{fc}} = 703.0 \text{ psi}$$

where:

- W_{fa} = 485 lb., maximum weight of fuel assembly
- W_{gt} = 85 lb., bounding weight of guide tube assembly
- A_{fc} = Area in fuel cell region, assumed equal to area within guide tube i.d.
 = $6.90^2 - \pi(1.50)^2 = 40.54 \text{ in}^2$

Region II: Support Tube Fuel Cells: A single payload unit (i.e., intact SNF assembly, failed fuel assembly, or GTCC waste) is supported by the engagement spacer plate in the region of each support tube cell. The applied end drop pressure load (q_2) used for this regions is calculated as follows:

$$q_2 = \frac{50g \times W_p}{A_{st}} = 718.2 \text{ psi}$$

where:

- W_p = 685 lb., maximum weight of cell payload (485 lbs SNF assembly + 200 lbs damaged fuel can)
- A_{st} = Area of support tube cell region, assumed equal to area within support tube i.d.
 = $[7.40^2 - \pi(1.50)^2] = 47.69 \text{ in}^2$

Region III: Support Tube Bearing (Basket Weight): One quarter of the basket assembly weight is supported by applied to the region in which the support tube bears on the engagement spacer plate. The applied pressure load (q_3) used for this region is calculated as follows:

$$q_3 = \frac{50g \times W_b}{A_{stb}} = 5,161 \text{ psi}$$

where:

$$W_b = 2,250 \text{ lb.}, \frac{1}{4} \text{ of bounding basket assembly weight (9,000 pounds)}$$

$$A_{stb} = \text{Area in support tube bearing region, modeled as area between attachment sleeve ID and support tube ID}$$

$$= 8.75^2 - 7.40^2 = 21.80 \text{ in}^2$$

2.12.4.3 Guide Tube Half-Symmetry Periodic Model

The FuelSolutions™ W74 guide tube assembly is evaluated for transverse loads resulting from the HAC oblique drop using the half-symmetry periodic model shown in Figure 2.12-12. The model represents the segment of the guide tube in which the highest stresses are shown to occur. The model spans from the centerline of a spacer plate ligament support to the mid-span between the adjacent spacer plate ligament support, taking advantage of longitudinal symmetry. Details of the finite element model are provided in the following paragraphs.

Model Construction

The guide tube is modeled with plastic shell elements (SHELL43) having three translational (UX, UY, UZ) and three rotational degrees of freedom (ROTX, ROTY, ROTZ) at each node. The shell elements include both membrane and bending capabilities. The plastic capabilities of these shell elements are not used for the guide tube linear-elastic stress analysis, but only for the evaluation of the guide tube permanent deformations. The guide tube assembly model includes only the guide tube for structural support, conservatively neglecting the structural contributions of the borated stainless steel neutron absorber panels. The load on the guide tube due to the neutron absorber panels is accounted for by adjusting the weight density of the guide tube as discussed below.

Material Properties

For the linear-elastic stress analysis, the guide tube is modeled with the elastic modulus of SA-240, Type 316 material properties at 700°F. The guide tube plastic analysis is performed using elastic-plastic stress-strain curve for Type 316 stainless steel at 700°F, based on NUREG/CR-0481, as discussed in Section 2.3 of this SAR. For both analyses, Poisson's ratio is taken as 0.29. As discussed above, the guide tube density is adjusted to account for the load on the guide tube due to the weight of the neutron absorber panels. The adjusted weight density is calculated as follows:

$$w = \rho \times \left(\frac{t_{NA} a_{NA}}{t_{GT} a} + 1 \right) = 0.51 \text{ lbs / in}^3$$

where:

$$\rho = 0.290 \text{ lb/in}^3, \text{ weight density of stainless steel}$$

$$a_{NA} = 6.40 \text{ in.}, \text{ width of neutron absorber panel}$$

$a = 6.99$ in., guide tube span width

$t_{NA} = 0.075$ in., thickness of neutron absorber panel

$t_{GT} = 0.09$ in., thickness of guide tube

Boundary Conditions

The model includes symmetry boundary constraints along the half-symmetry plane and along the vertical plane passing through the nodes located at the spacer plate support. Vertical displacement constraints are applied to the guide tube nodes at the location of the spacer plate ligament support.

Loading

The guide tube loading for the HAC oblique drop evaluation is described in Section 2.7.1.4.4.1.

2.12.4.4 Canister Top Shield Plug Model

The W74 top shield plug assembly is evaluated for the HAC end drop using the quarter symmetry finite element model shown in Figure 2.12-13. Details of the finite element model are provided in the following paragraphs.

Model Construction

The W74 top shield plug model includes only the shield plate with the guide tube and support tube shield cap cutouts, and the support bar recess cutouts. The model does not include the vent/drain ports since they have no significant effect on the stresses shield plate. The guide tube shield caps and support tube shield caps are not included in the model. The loading on the shield plate due to the weight of the shield caps plus the weight of the canister shell top end inner and outer closure plates is modeled by adjusting the density of the shield plate elements as discussed below.

Material Properties

The W74 shield plate is modeled using the elastic modulus of SA-516, Grade 70 carbon steel at 400°F and Poisson's ratio of 0.30. As discussed above, the density of the shield plate elements are adjusted to include the weight of the shield caps and the top end inner and outer closure plates. The weight of the top end inner and outer closure plates is distributed evenly over the entire area of the top shield plug. The weight of the shield caps is distributed to the center region of the shield plate (Region 2 in Figure 2.12-14) around the shield cap holes. An adjusted density is used for the shield plate elements. Therefore, the adjusted density used in the perimeter region of the shield plate (i.e., region 1 of Figure 2.12-14) is:

$$\rho_1 = \frac{(0.283)(7.38) + (0.290)(3.00)}{7.38} = 0.401 \text{ lb / in}^3$$

A bounding material density of 0.5 lb/in³ is conservatively used for region 1 of the W74 canister top shield plug model.

The adjusted density used in the ligament elements (i.e., region 2 of Figure 2.12-14) is calculated as follows:

$$\rho'_2 = (0.283) \left(\frac{W_{\text{solid}} + W_{\text{cls}}}{W_{\text{lig}}} \right) = 1.705 \text{ lb / in}^3 \text{ (conservatively assume } 1.71 \text{ lb / in}^3 \text{)}$$

where, with reference to Figure 2.12-14:

$$\begin{aligned} W_{\text{solid}} &= \text{Weight of solid steel section inside ligament region} \\ &= (0.283)(7.38)[(43.0)^2 + 4(28.73-21.50)(24.4)] \\ &= 5,336 \text{ lb.} \end{aligned}$$

$$\begin{aligned} W_{\text{cls}} &= \text{Weight of closure plates inside ligament region} \\ &= (0.290)(3.00)[(43.0)^2 + 4(28.73-21.50)(24.4)] \\ &= 2,223 \text{ lb.} \end{aligned}$$

$$\begin{aligned} W_{\text{lig}} &= \text{Weight of ligaments inside ligament region} \\ &= 5,336 - 4(0.283)[(8.00)^2(3.06) + (7.50)^2(4.32)] - \\ &\quad 33(0.283)[(7.50)^2(3.06) + (7.00)^2(4.32)] \\ &= 1,254 \text{ lb.} \end{aligned}$$

Boundary Conditions

Symmetry boundary conditions are applied to the shield plug quarter symmetry finite element model (i.e., UX=0 for all nodes at X=0 and UY=0 for all nodes at Y=0). Longitudinal displacement constraints (UZ=0) are applied to a single line of nodes at the top of each support bar access cutout, assuming the shield plate pivots about the inner edge of each support bar.

Loading

Since the model densities are adjusted to include the weight of the shield caps and closure plates, the only loading applied to the model is a longitudinal acceleration load.

2.12.4.5 Canister Shell Axisymmetric Finite Element Model

The two-dimensional axisymmetric finite element model described in this section and shown in Figure 2.12-15 is used for analyzing all components of the W74 canister shell assembly, with the exception of the top end shield plug, for the HAC top end drop and HAC bottom end drop. The top end shield plug is evaluated using the finite element model described in Section 2.12.4.4.

Two different bounding canister shell axisymmetric models are used for the W74 canister shell assembly structural evaluation. The basic geometry of the W74 canister shell assemblies is similar to all other FuelSolutions™ canister shell assemblies with carbon steel shield plugs, with the exception of the top end shield plug assembly and its supports. The canister shell

axisymmetric models both include a 5/8-inch thick cylindrical shell, 2.0-inch thick outer closure plate, 1.0-inch thick inner closure plate, 1.0-inch thick bottom closure, and 1.75-inch thick bottom end plate. The model used for the bottom end drop analysis is based on a canister shell assembly design that includes lead top and bottom shield plugs with bounding weights. The total modeled weights of the top and bottom end shield plugs are 6,790 pounds and 6,328 pounds, respectively. The canister shell stresses calculated using this bounding canister shell model bound those in the W74 canister shell, since the lead shield plugs included in the bounding model have a bounding weights and lower stiffness (i.e., lower elastic modulus).

The bounding canister shell assembly axisymmetric model used for the top end drop analysis is identical to the bounding model used for the bottom end drop analysis, except it includes 5.75-inch thick carbon steel bottom shield plug. The use of the lead top shield plug for the HAC top end drop evaluation is conservative since it is heavier than the carbon steel top shield plug design. Furthermore, the stresses in the top carbon steel shield plug due to the HAC end drop loading are evaluated separately using closed-form hand calculations rather than by finite element methods.

The shell assembly axisymmetric model is comprised primarily of 2-D structural solid (PLANE42) elements. These elements are used to model the bottom end plate, bottom shield plug, bottom closure plate, bottom end shell extension, cylindrical shell, top end shield plug assembly and supports, top end inner closure plate, and top end outer closure plate. Each PLANE42 element is defined by four nodes, with two translational degrees of freedom (UX and UY) per node. The partial penetration groove weld, which attaches the top end outer closure plate to the canister shell, is modeled discretely using PLANE42 elements. All other canister shell partial penetration welds are modeled by coupling the degrees of freedom (radial and axial) at the coincident nodes of the connected parts. The resulting nodal forces at the coupled locations are used to compute the weld shear stresses and stress intensities for the weld stress evaluation. The canister shell welds are all modeled with the minimum acceptable weld throats.

Non-linear 2-D point to point contact (CONTAC12) elements are used to model the interface between adjacent surfaces that may maintain or break physical contact, including the top closure plates and closure shield plug, and the bottom end plate, bottom closure plate, and bottom shield plug. The contact elements transfer only compressive loads normal to the contact surface and have no stiffness in tension. The contact surfaces between the cover plates and shield plugs are modeled using CONTAC12 elements with a contact stiffness of $1.0(10)^{10}$ lb/inch. The initial gap size and orientation angles are defined by real constants. All gaps are assumed initially closed and not sliding. Gap friction is conservatively ignored.

Material Properties

The shell assembly is modeled using linear-elastic material properties at an average shell temperature of 300°F. The canister shell stainless steel components are modeled using an elastic modulus of 27×10^6 psi and a weight density of 0.29 lb/in³. As discussed above, the canister shell models used for the HAC end drop evaluation include a lead shield plug at the top end. In order to bound the weight of the W74 canister top shield plug assembly, a weight density of 0.42 lb/in³ is used for the lead material in the top shield plug. For the bottom end drop analysis, the bottom end shield plug is modeled as a 3.125-inch thick lead plug with a weight density of 0.53 lb/in³, such that the modeled weight of the bottom shield plug bounds the weight of the W74 canister

bottom shield plug. For the top end drop, the 5.75-inch thick carbon steel bottom shield plug used in the W74 canister design is modeled. The lead materials in the top and bottom end shield plugs are modeled using an elastic modulus of 2×10^6 psi. The carbon steel bottom shield plug is modeled with an elastic modulus of 28.3×10^6 psi, a density of 0.283 lb/in^3 , and Poisson's ratio of 0.3.

Boundary Conditions and Loading

For the bottom end drop analysis, the nodes on the outer surface of the bottom end plate of the canister shell axisymmetric finite element model are constrained from translating in the axial direction ($UZ=0$). Similarly, for the top end drop analysis, the nodes on the outer surface of the top end outer closure plate of the canister shell axisymmetric finite element model are constrained from translating in the axial direction ($UZ=0$).

For the top and bottom end drop analysis, the weight of the W74 canister basket assemblies and SNF assemblies is modeled as a uniform pressure load on the supporting end of the canister cavity. A bounding weight of 57 kips is assumed for the canister internals for calculating the applied pressure loading used in the models. The load is applied over a circular area with a 31.625-inch radius. The applied pressure load due to a 60g HAC end drop is 1,088 psi ($= 60g \times 57,000 / (\pi \times 31.625^2)$).

2.12.4.6 Canister Shell Half-Symmetry Finite Element Model

The W74 canister shell assembly stresses due to the HAC oblique drop slapdown loads are evaluated using the three dimensional half-symmetry finite element model shown in Figure 2.12-16 through Figure 2.12-18. This model, which represents the top end region of the W21M-LS canister assembly, is used to provide a bounding stress analysis for the W74 canister shell assembly. The W21M-LS canister assembly stresses are bounding since the total weight of the basket assembly and SNF assemblies are significantly higher than that of the W74 canisters (i.e., 56.1 kips versus 51.6 kips).

The top end of the canister shell assembly is modeled because the stresses in the top end region are expected to bound those in the bottom end region, since the top shield plug is heavier than the bottom shield plug. Also, the bottom shield plug is sandwiched between the two closure plates, and the upper shield plug is captured between the top end inner closure plate and the shield plug support ring. The top eleven spacer plates of the W21M-LS basket assembly are included in the model, with the two top end 3/4-inch thick plates modeled as a single 1.5-inch thick plate, as shown in Figure 2.12-16.

The W21M-LS canister shell three-dimensional half-symmetry model includes the canister shell, top end inner and outer closure plates and welds, top end shield plug, and the basket assembly spacer plates. The canister shell assembly top end inner and outer closure plates, top shield plug, and cylindrical shell are modeled using brick shell elements (SOLID45), as shown in Figure 2.12-17. The top end outer closure weld is modeled discretely. The top inner closure partial penetration weld is modeled as a pinned connection, since this weld is not designed as a moment connection. The stresses in the top inner and outer closure welds are evaluated in the same manner as described for the canister shell axisymmetric finite element model.

The assembly spacer plates are modeled using elastic shell elements (SHELL63). Since the spacer plates are included in this model only for the purpose of accurately modeling their loads

on the canister shell, a coarse mesh is used for the spacer plates, as shown in Figure 2.12-18. The spacer plate mesh in the bottom region is adjusted to align the nodes radially with the corresponding nodes on the canister shell.

Radial gap elements are placed between the basket assembly spacer plates and inside of the canister shell, and between the top shield plug and the inside of the canister shell, to model the non-linear interface between these components. The shield plug and spacer plate gap elements are modeled with an initial radial gap sizes of 0.1875 inch and 0.175 inch, respectively. The gap element radial orientation is maintained throughout the analyses. The element status (open or closed) and the gap size for each gap element are continuously updated through an iterative solution. For each increment of loading applied to the model, the solution iterates until the convergence criteria has been satisfied (i.e., forces are balanced). At the end of each substep, each gap element size and status is updated based on the locations of the gap element end nodes. For gap elements that are open, there is no associated stiffness. The gap element contact stiffness is modeled as 1×10^7 lb/inch. Friction at the gap interfaces is conservatively ignored.

For the HAC slapdown load conditions, the canister assembly is supported by the inner shell of the transportation cask (i.e., cylinder within a cylinder). Radial gap elements are used to model the non-linear interface between the outside of the canister shell and the inside of the cask inner shell. These gap elements are similar to those used between the spacer plates and canister shell, but have an initial radial gap size of 0.5 inch and a contact stiffness of 1×10^8 lb/inch.

Boundary Conditions

The global Z coordinate system goes from the bottom end to the top end. The half model is represented from the top (0° azimuth) to the bottom (180° azimuth). Along the half-symmetry plane, the nodes are restrained from translating along the X-axis and rotating about Y-axis and Z-axis. Another plane of symmetry is located on the bottom end of the model, near the last spacer plate. The canister shell nodes at this location are restrained from translating along the Z-axis and rotating about X-axis (radial) and Y-axis (circumferential). The gap element ground nodes are fixed. To maintain model stability for the spacer plate, the top and bottom nodes of the spacer plates are restrained from translation in the Z direction.

Material Properties

The canister shell, top end outer closure plate and weld, the top end inner closure plate, and the spacer plates are modeled with an elastic modulus of 27.0×10^6 lb/in², a density of 0.29 lb/in³, and a Poisson's ratio of 0.29. The carbon steel plug is modeled with an elastic modulus of 27.0×10^6 lb/in², a density of 0.284 lb/in³, and a Poisson's ratio of 0.29.

Applied Loading

The inertial loads of the canister shell, top end outer and inner closure plates, the shield plug, and the self weight of the spacer plates are accounted for by applying an appropriate acceleration in the direction of the loading. The inertial loads of the fuel assembly and the guide tube are applied as uniform pressure loads over the width of the supporting spacer plate ligaments, as shown in Figure 2.12-18. The ligament pressure loads are scaled using the appropriate acceleration applicable in the selected loading condition.

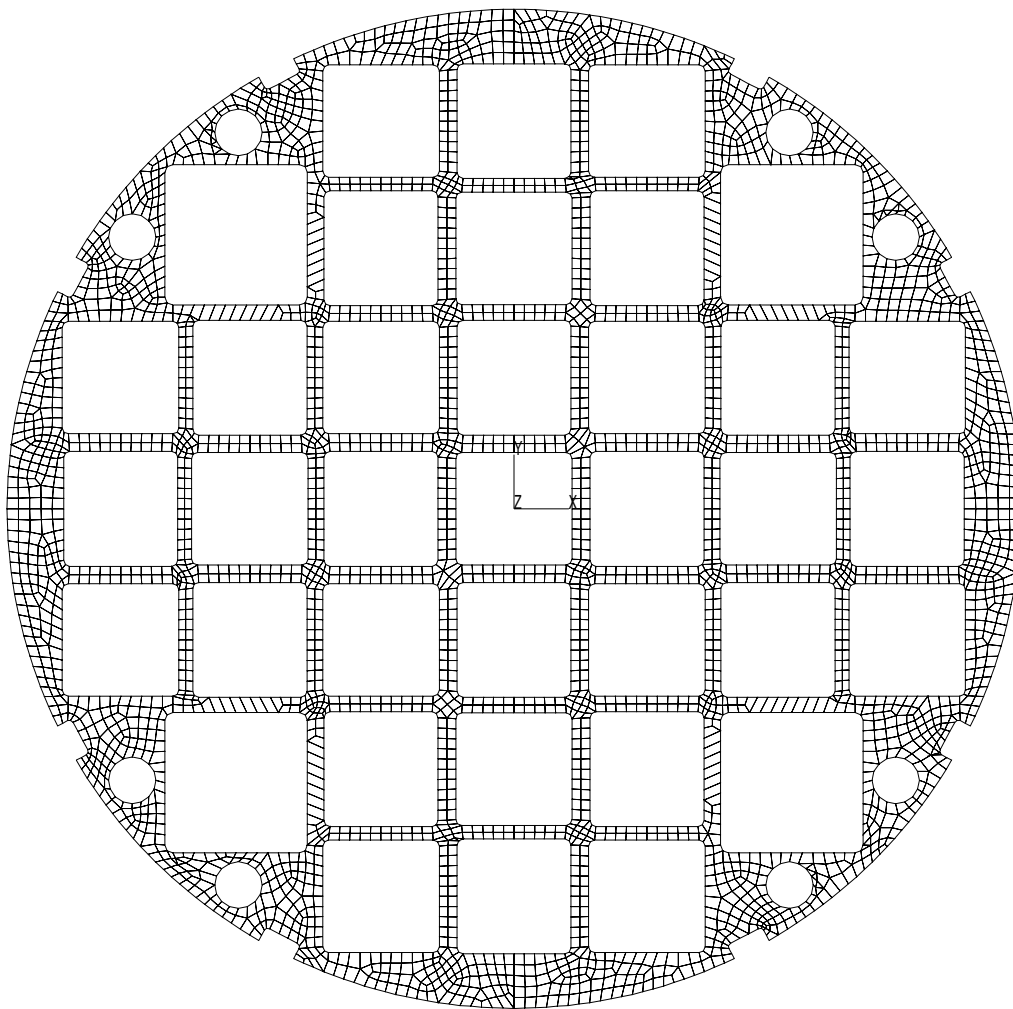


**Figure 2.12-2 - W74 Canister General and LTP Spacer Plate
Plane-Stress Finite Element Model**

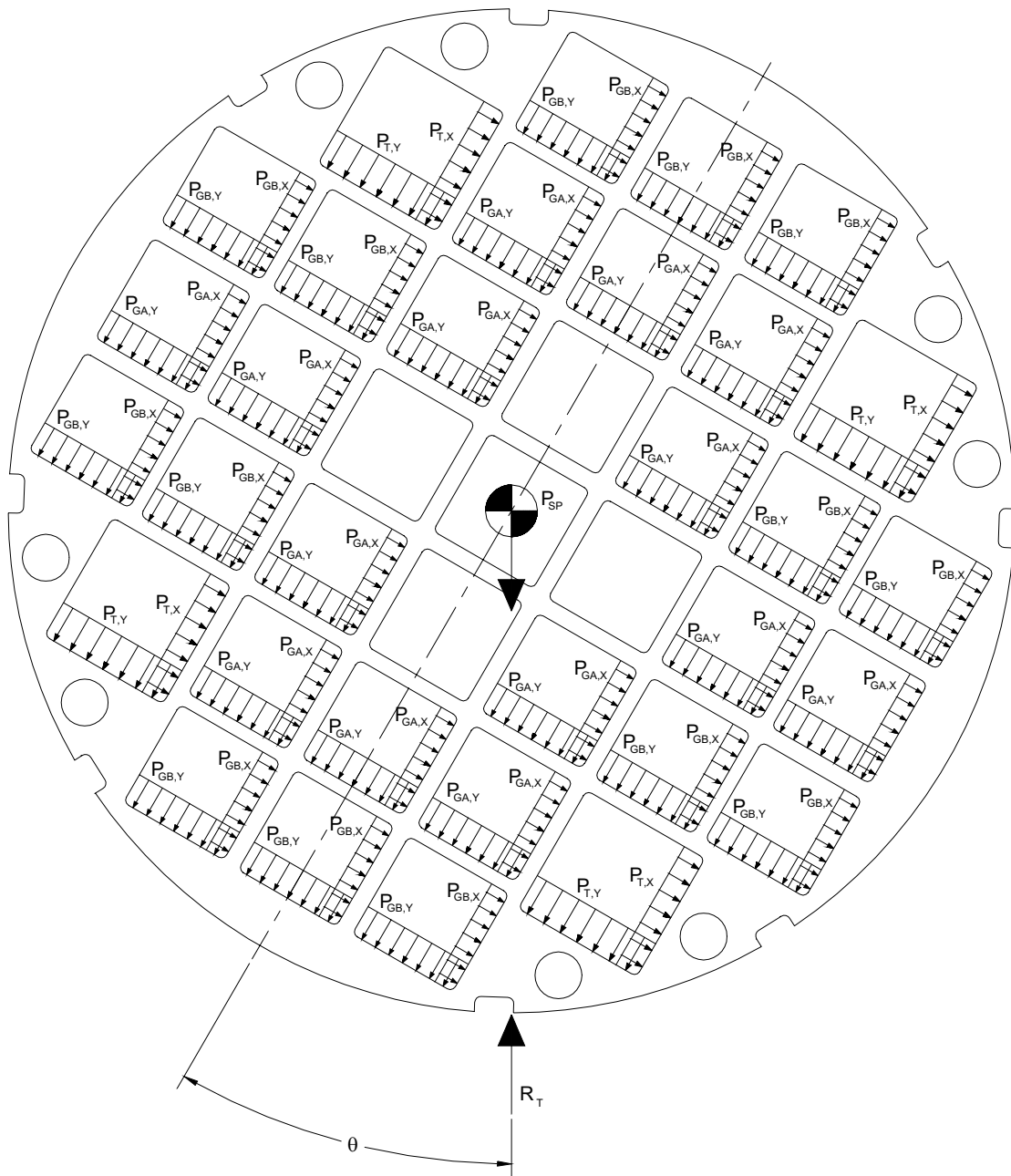


Figure 2.12-3 - W74 Canister General and LTP Spacer Plate Loading Diagram

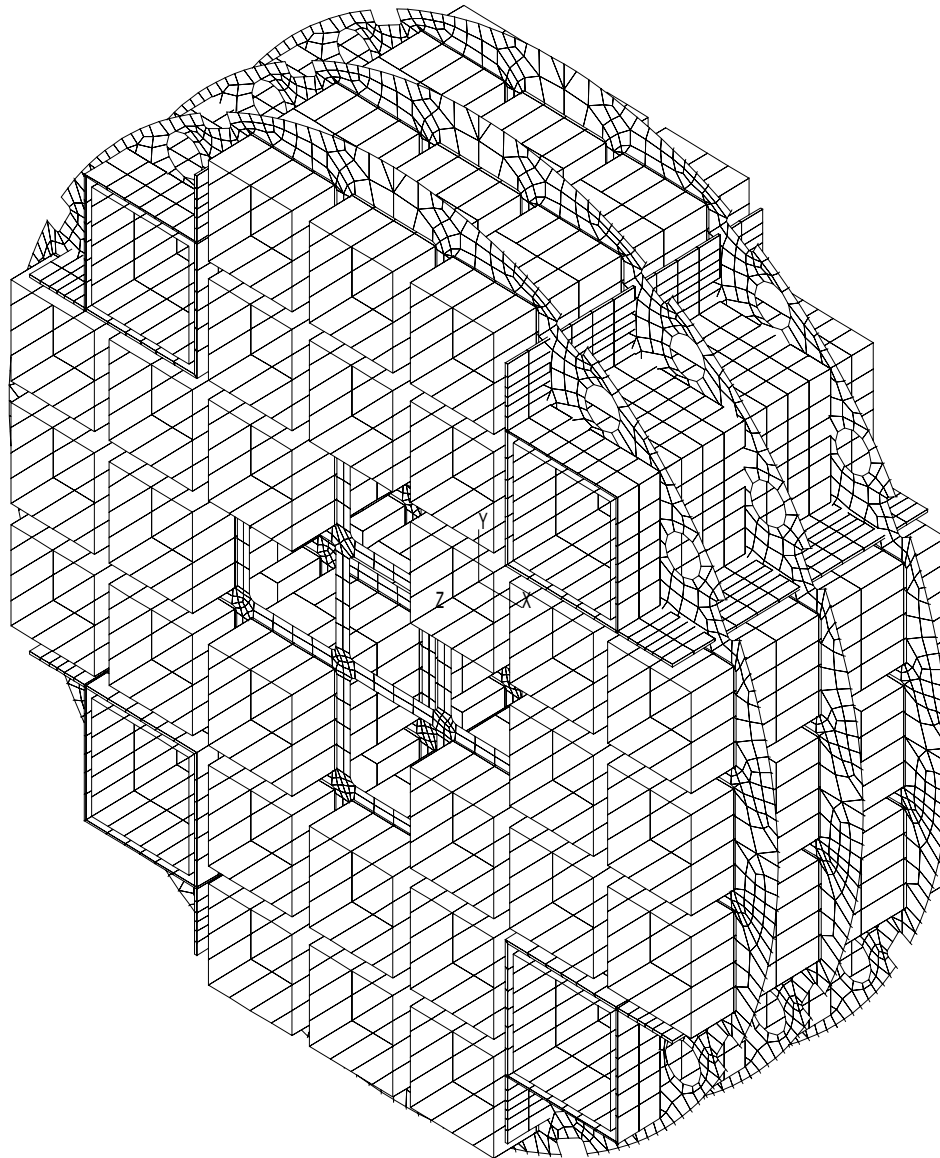


Figure 2.12-4 - W74 General Spacer Plate Full Multi-Span Finite Element Model

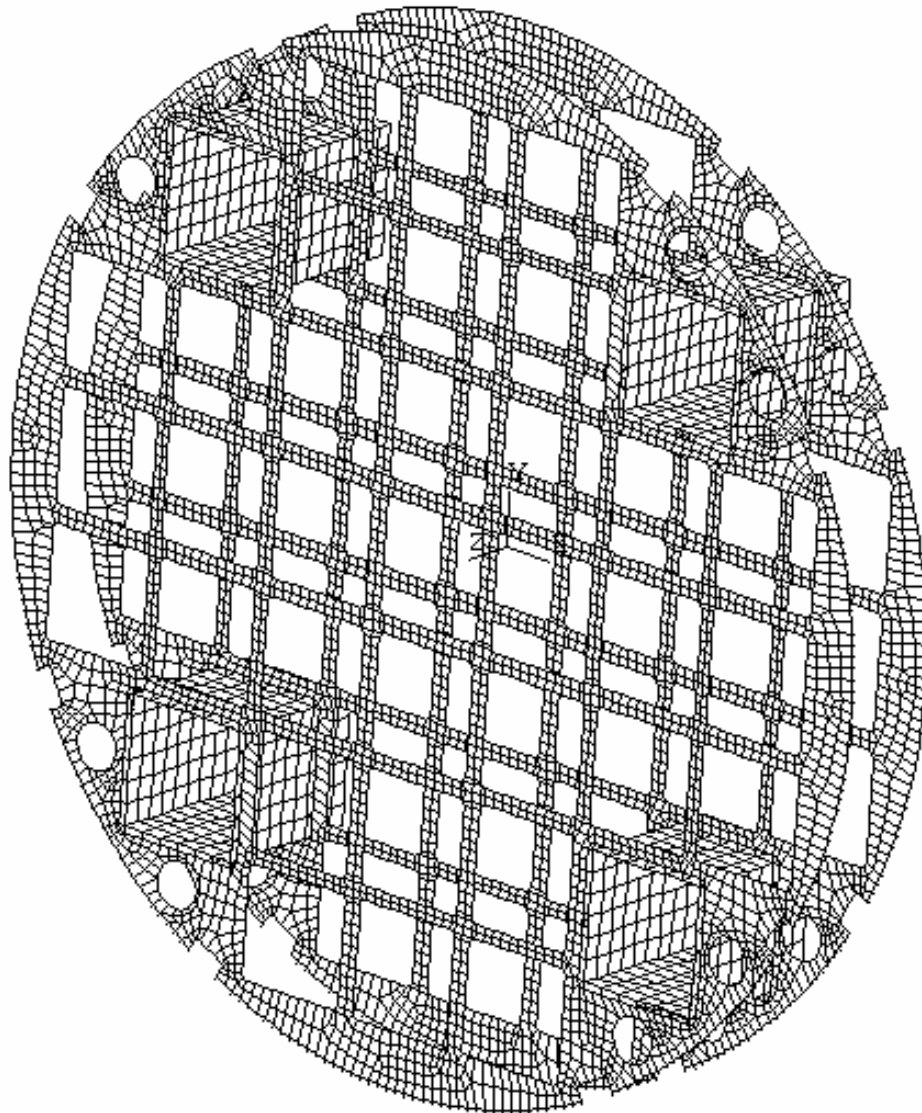
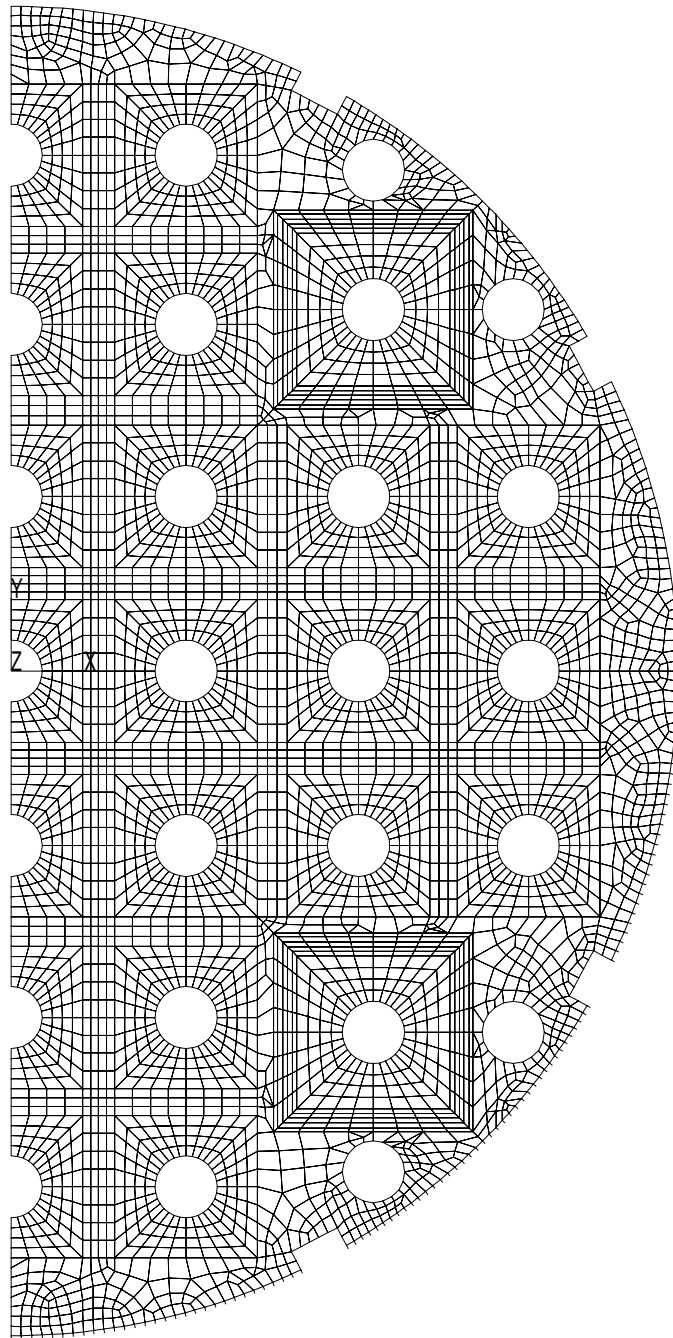
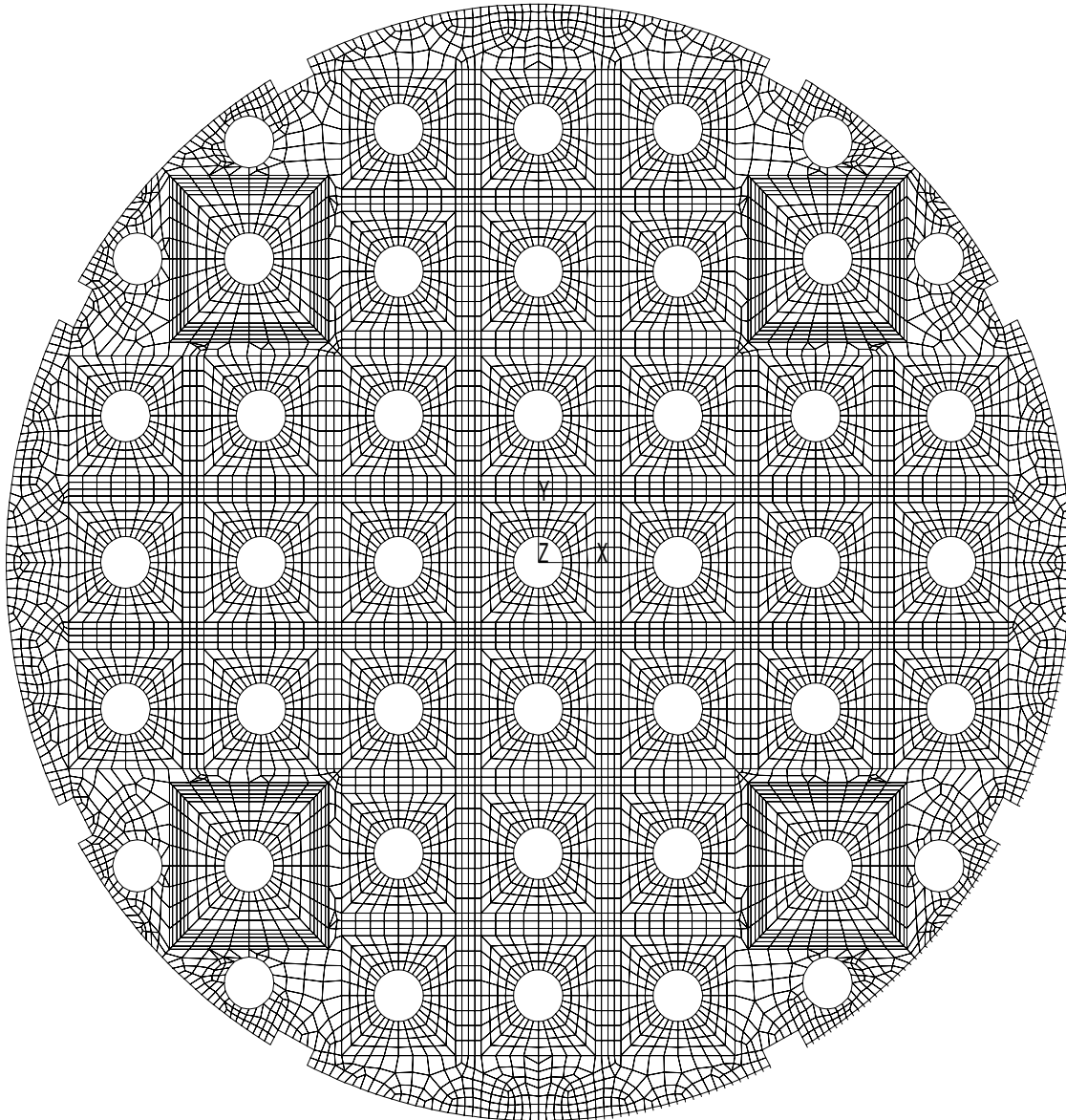


Figure 2.12-5 - W74 General Spacer Plate Buckling Shell Finite Element Model



**Figure 2.12-6 - W74 Canister Engagement Spacer Plate
Half-Symmetry Plane-Stress Finite Element Model**



**Figure 2.12-7 - W74 Canister Engagement Spacer Plate Full
Plane-Stress Finite Element Model**

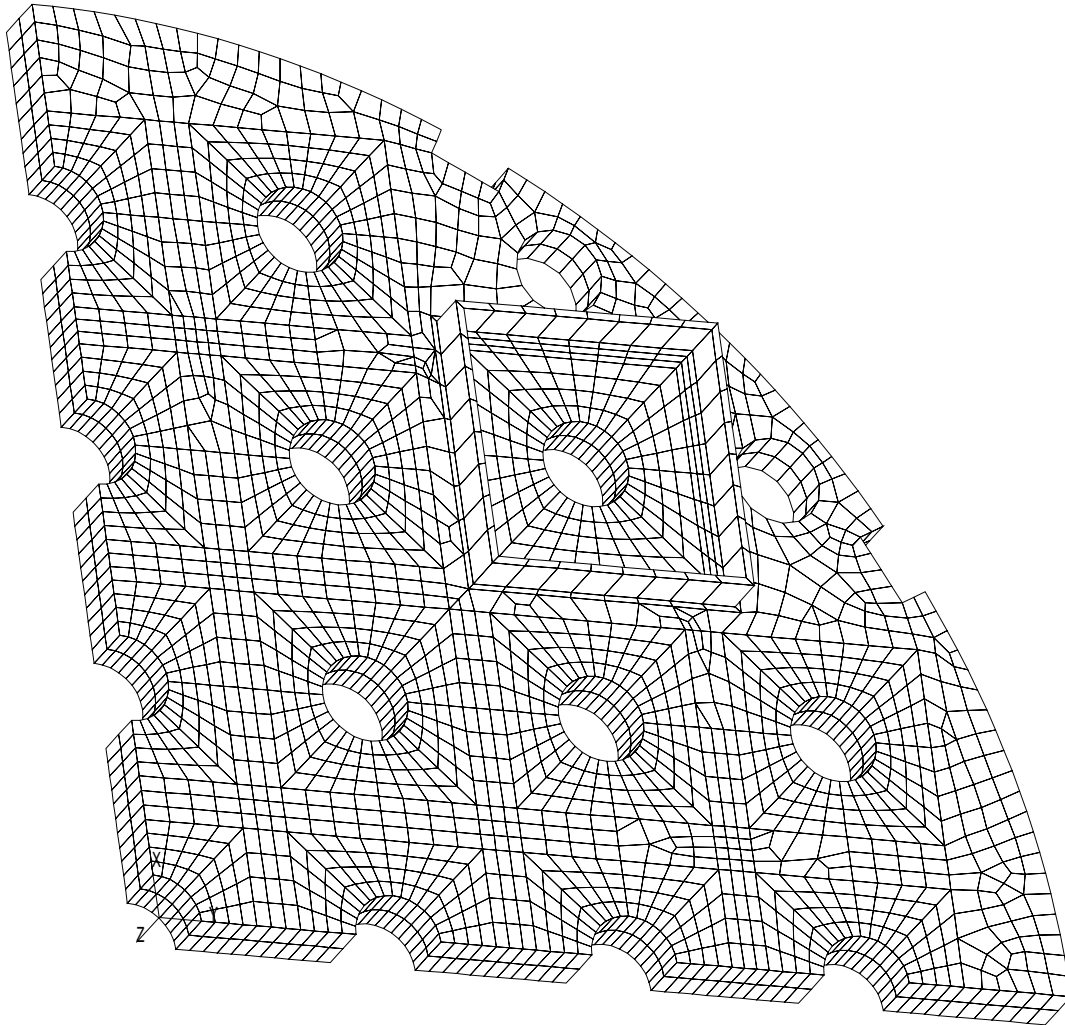


**Figure 2.12-8 - W74 Canister Engagement Spacer Plate Solid
Quarter-Symmetry Modal Analysis Model**

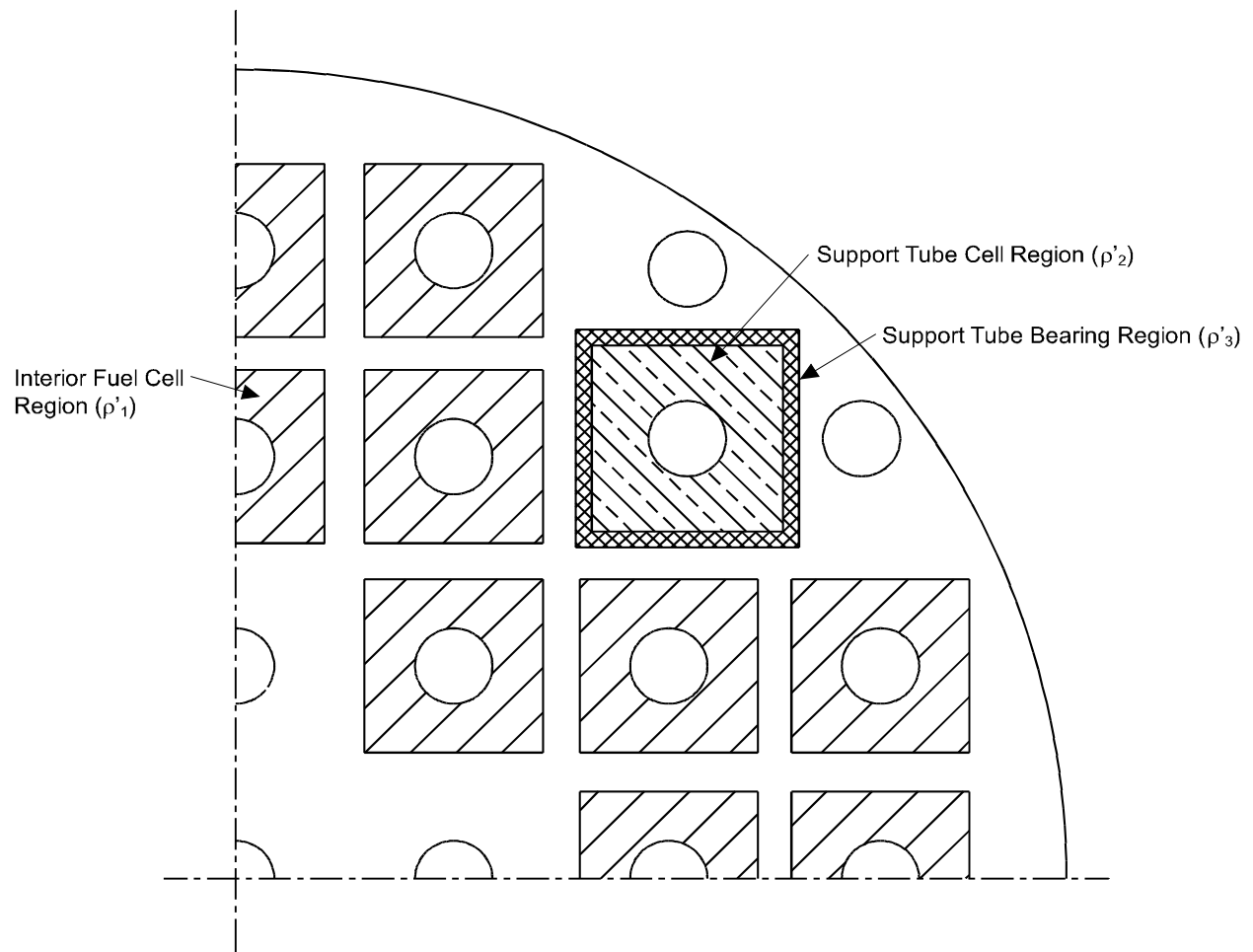


Figure 2.12-9 - W74 Canister Engagement Spacer Plate HAC End Drop Modal Analysis Mass Distribution

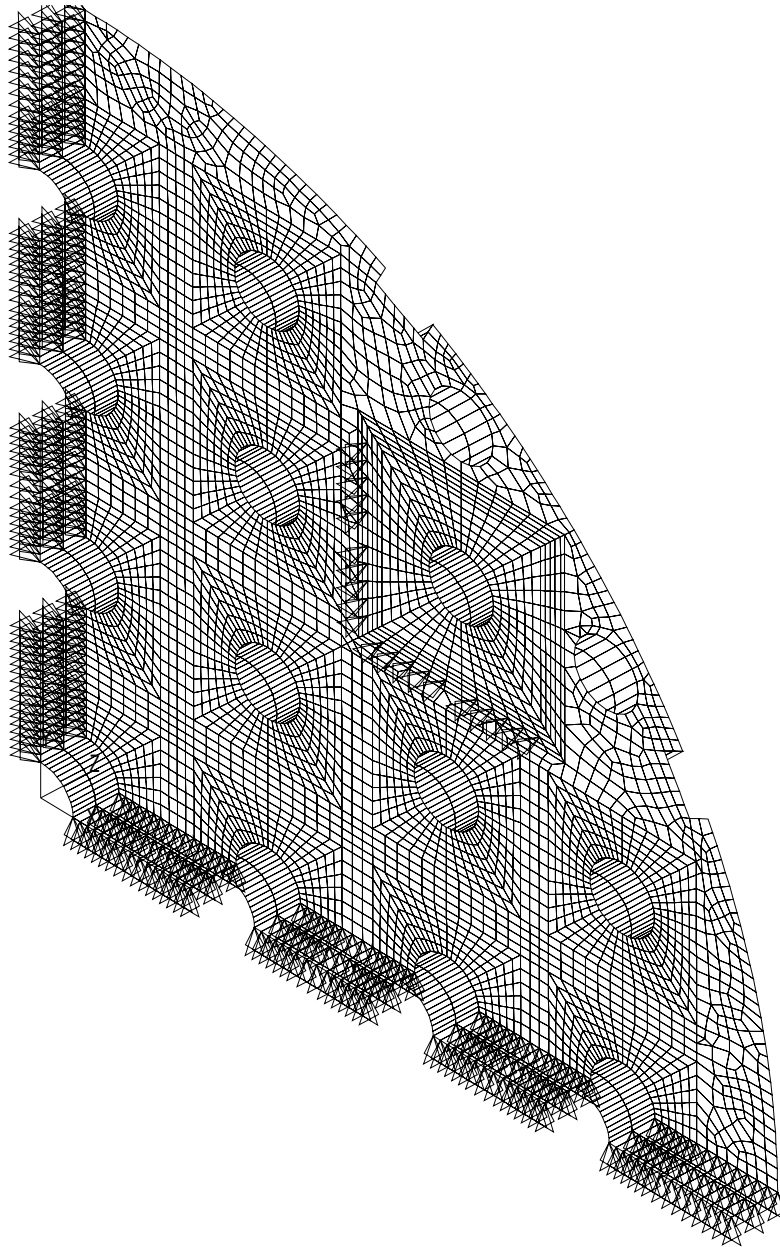


Figure 2.12-10 - W74 Canister Engagement Spacer Plate HAC End Drop Solid Quarter-Symmetry Model Boundary Conditions

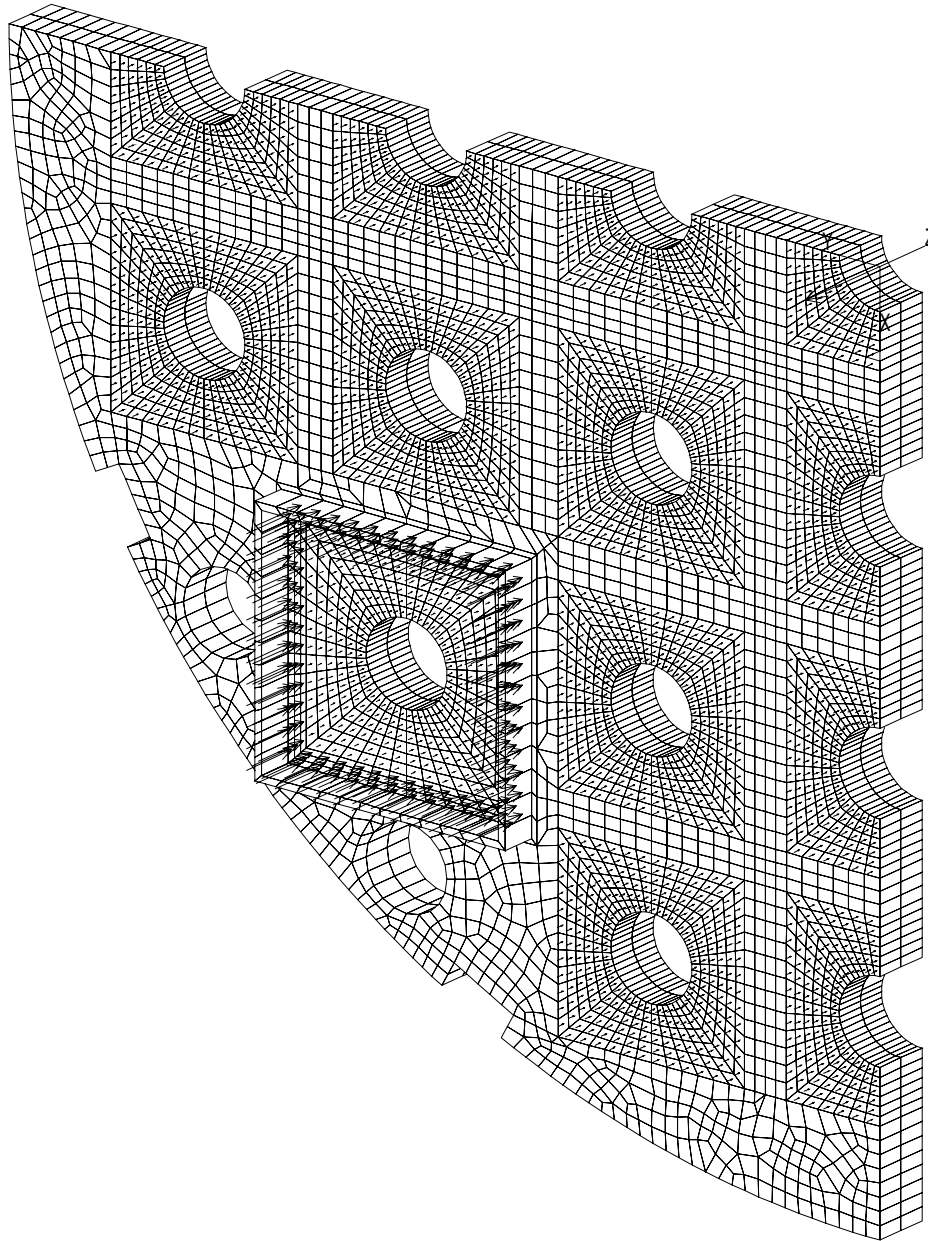


Figure 2.12-11 - W74 Canister Engagement Spacer Plate HAC End Drop Solid Quarter-Symmetry Model Pressure Loading

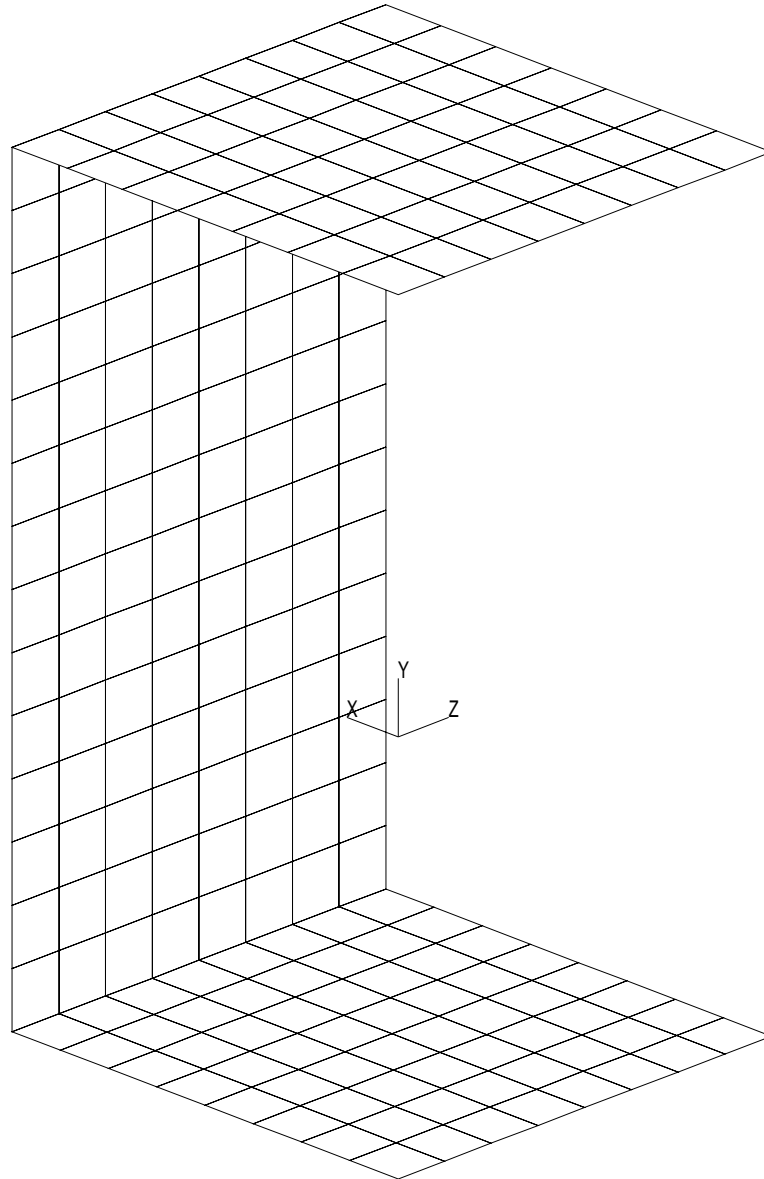
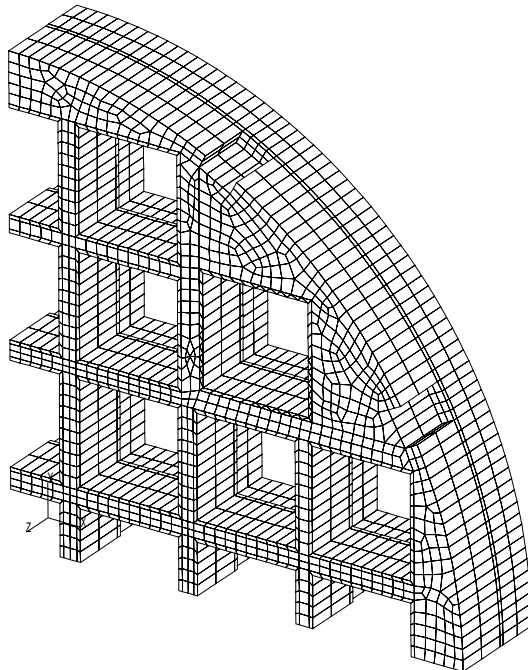
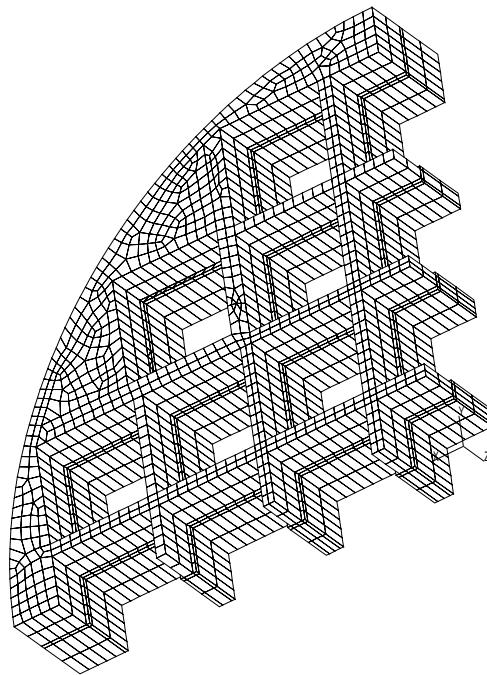


Figure 2.12-12 - W74 Canister Guide Tube Finite Element Model



View from Bottom



View from Top

**Figure 2.12-13 - W74 Canister Top Shield Plug
Quarter Symmetry Model**

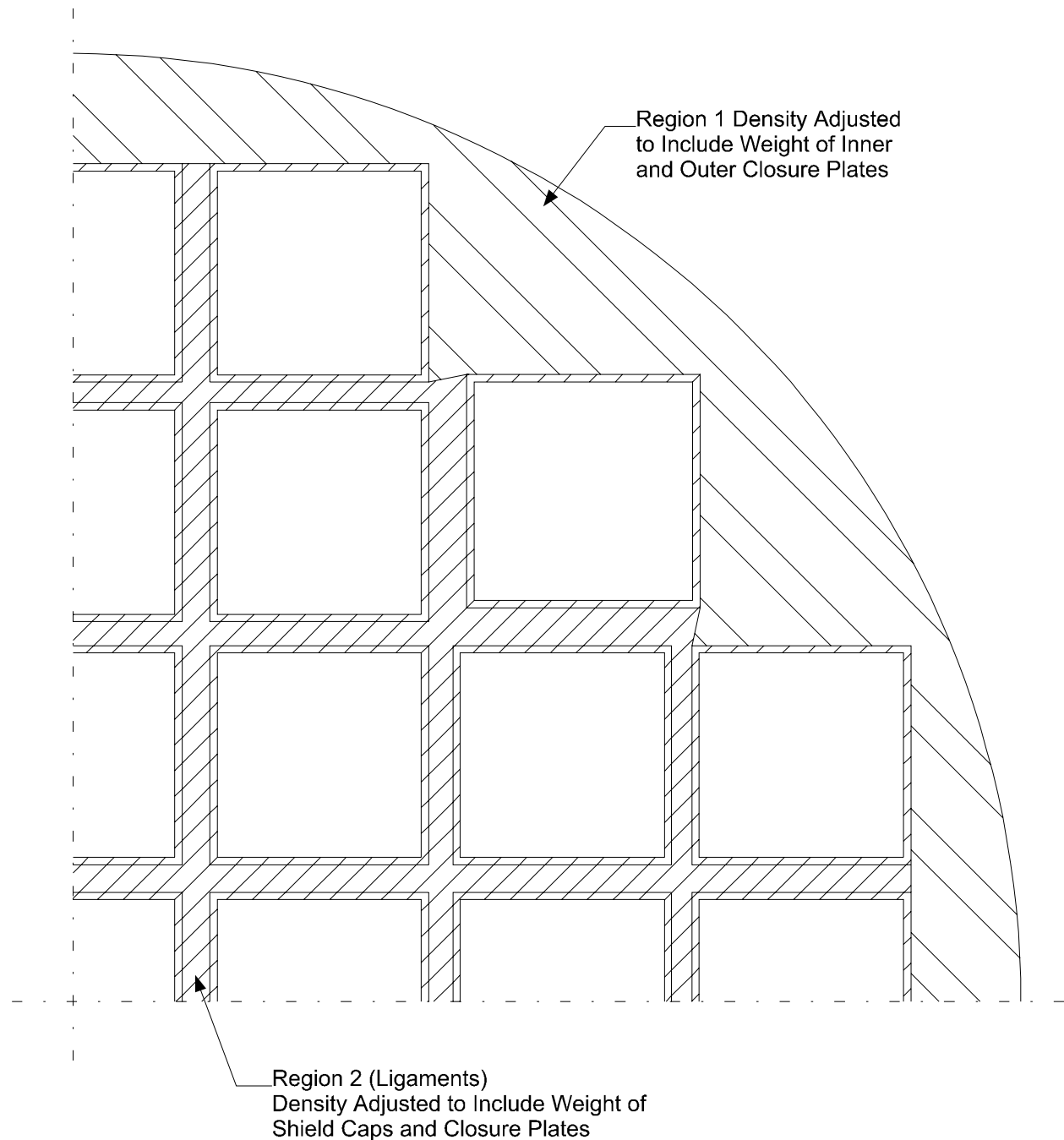


Figure 2.12-14 - W74 Canister Top Shield Plug Quarter Symmetry Model Adjusted Density Regions

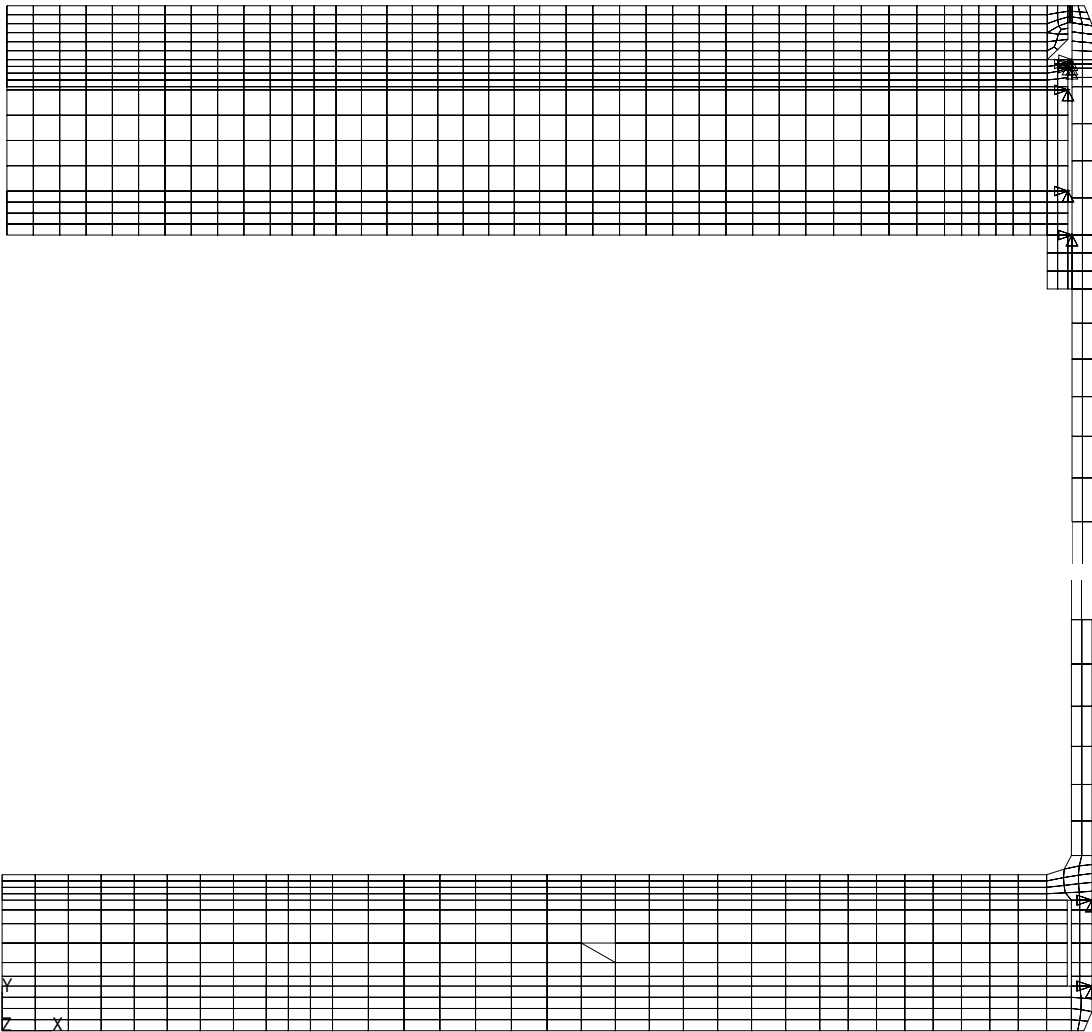


Figure 2.12-15 - Bounding Canister Shell Assembly Axisymmetric Finite Element Model

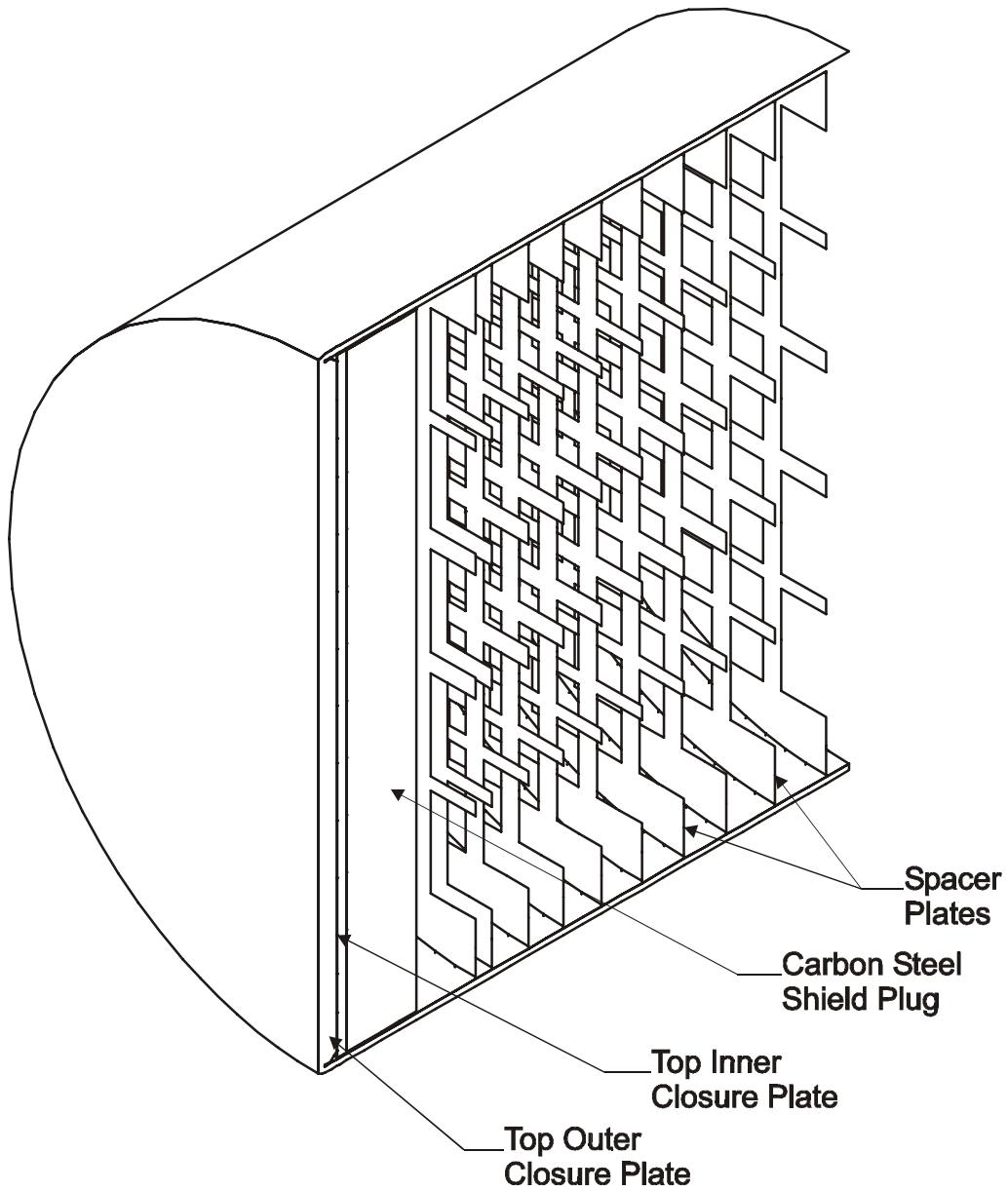


Figure 2.12-16 - Canister Shell Half-Symmetry Finite Element Model

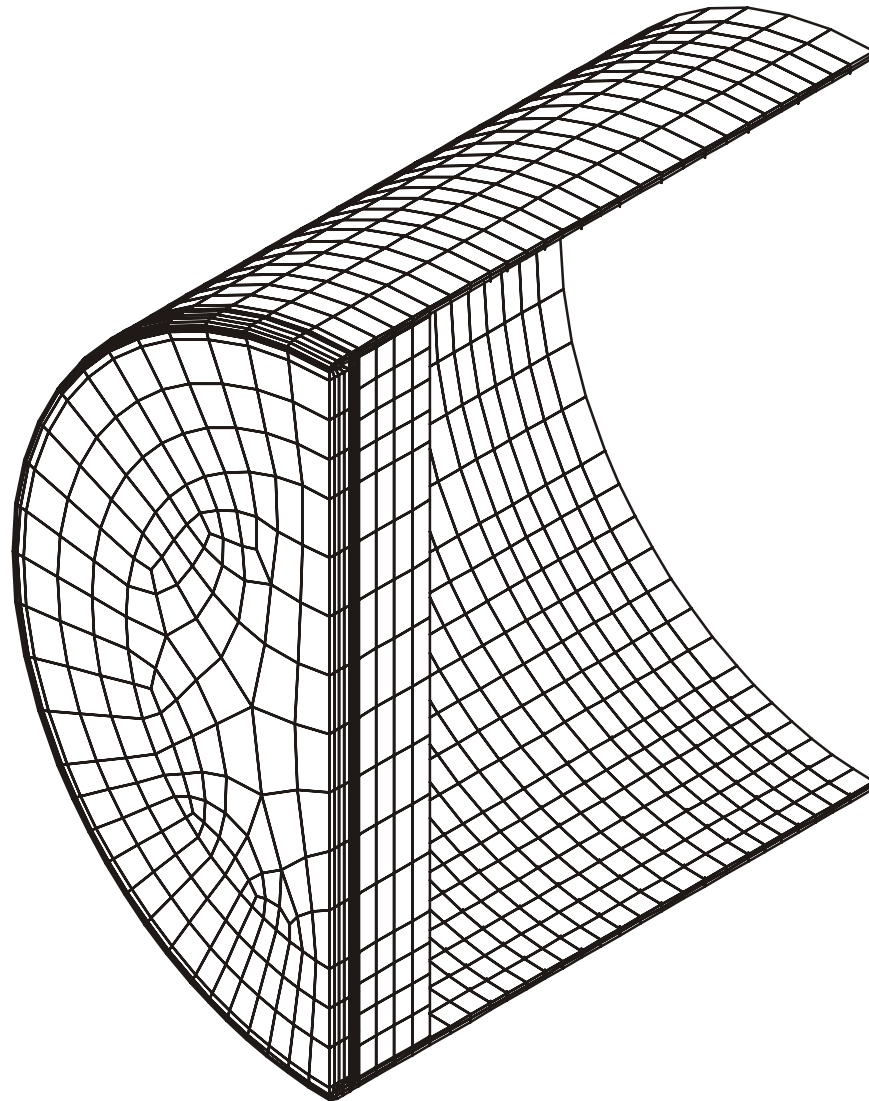


Figure 2.12-17 - Canister Shell Assembly Half-Symmetry Finite Element Model, Shell Assembly Mesh

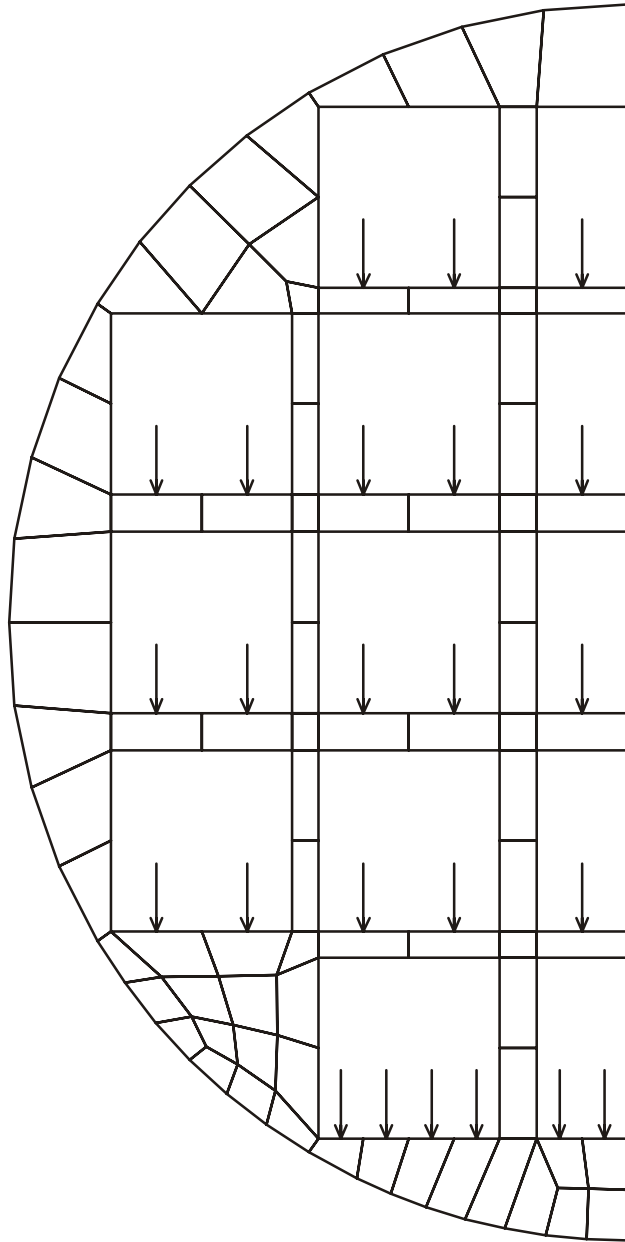


Figure 2.12-18 - Canister Shell Assembly Half-Symmetry Finite Element Model - Spacer Plate Mesh and Loading

2.12.5 Canister Shell Stress Evaluation Points

The W74 canister shell structural evaluation is performed using the axisymmetric and three-dimensional finite element models described in Sections 2.12.4.5 and 2.12.4.6. Linearized section stresses are used to determine the average membrane, linearized membrane plus bending, and total (primary plus secondary plus peak) stress distribution at the critical sections of the canister shell for comparison with the stress limits defined in the ASME Code. Section stresses are determined using the stress linearization routine described in the ANSYS User's Theory Manual. For each section, the linearized stresses are determined at the innermost radial position of the section ("I"), the center of the section ("C"), and the outermost radial position of the section ("O"). For consistency, the "I" and "O" nodes are defined on the inside and outside surfaces of the canister shell.

For the canister shell assembly structural evaluations performed using the axisymmetric finite element model described in Section 2.12.4.5, a total of 36 locations are evaluated. The canister shell stress evaluation locations in the top and bottom regions and the cavity region of the axisymmetric model are shown in Figure 2.12—19 and Figure 2.12—20. The stress evaluation locations selected include all of the regions of the canister shell in which the highest stresses occur. Stress evaluation sections are provided at the center and edge of each end plate, as well as at intermediate locations. Stress evaluation sections are also provided in the shell cavity region and in the shell end regions at the junction of the end plates. The stresses in all canister shell partial penetration welds are also evaluated using the finite element analysis results. The top outer closure weld, which is discretely modeled, is evaluated using section stresses as described above. All other canister shell partial penetration weld connections are modeled by coupling the nodes of the connected components at the location of the weld. For these welds, the weld shear stress and membrane stress intensity are calculated based on the nodal forces from the finite elements solution. The weld shear stress is calculated as the resultant nodal force divided by the minimum effective weld throat and the primary membrane stress intensity is equal to twice the shear stress.

For the canister shell structural evaluation performed using the three-dimensional half-symmetry model described in Section 2.12.4.6, the linearized stresses are evaluated at all locations on the lower half of the shell. The shear stress and membrane stress intensity in the inner closure weld, which is modeled as a pinned connection between the inner closure plate and cylindrical shell, are calculated using the nodal forces, as described above.

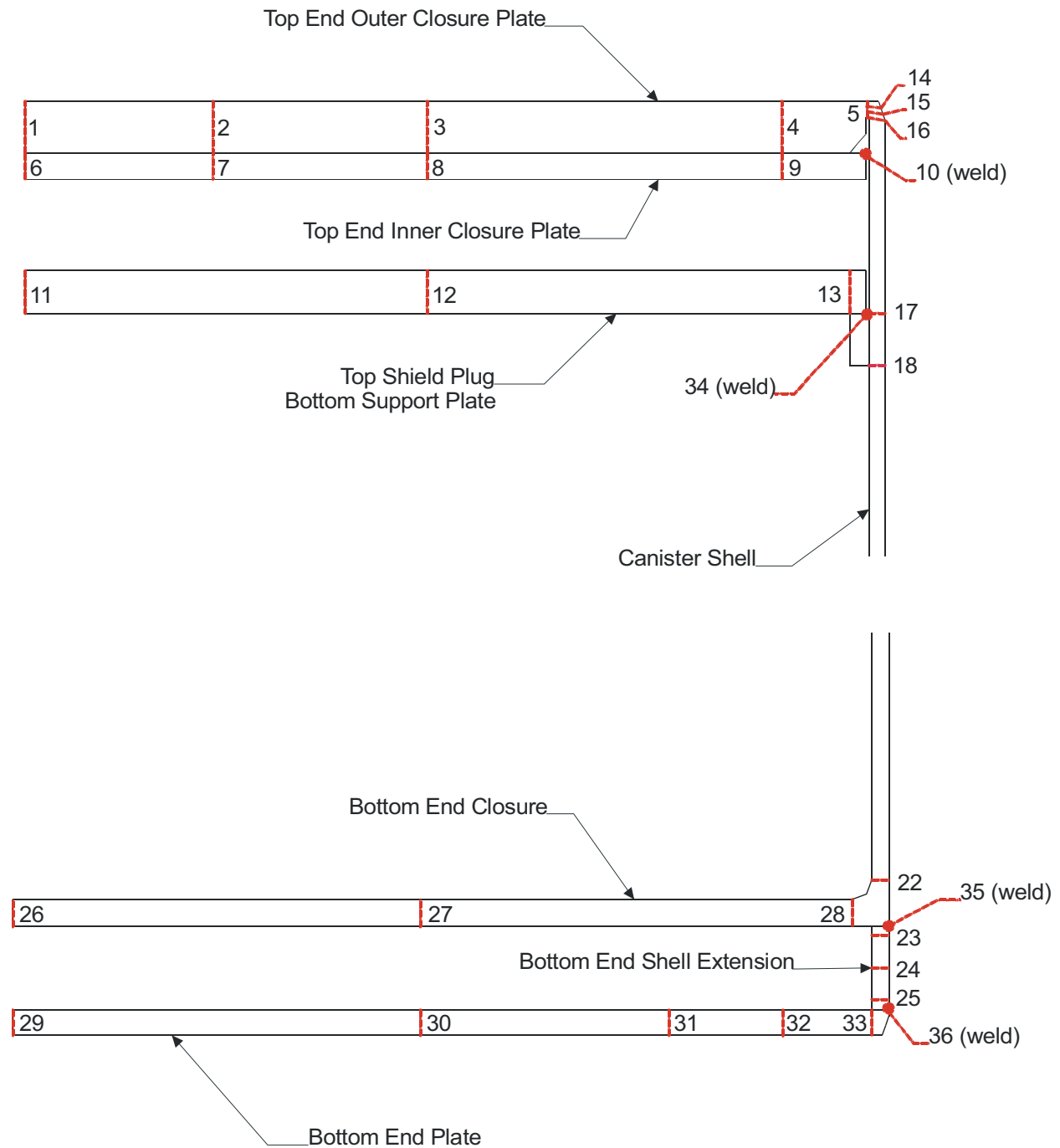


Figure 2.12—19 - Canister Shell Axisymmetric Model Stress Evaluation Locations - Top and Bottom End Regions

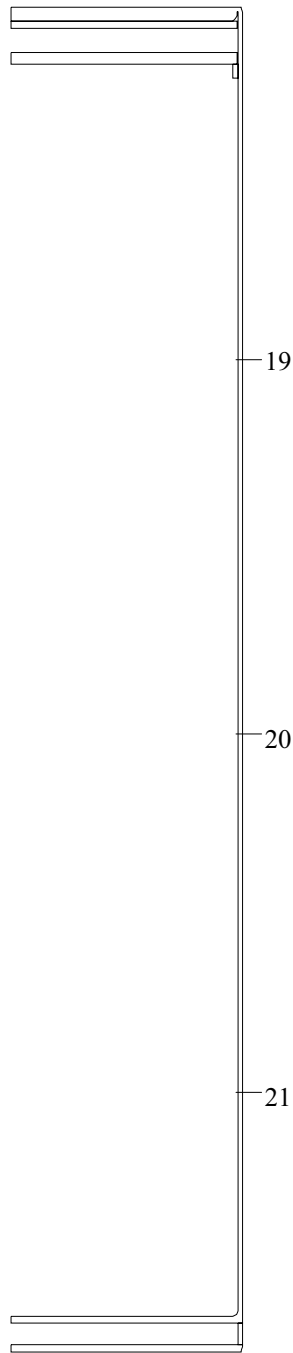


Figure 2.12—20 - Canister Shell Axisymmetric Model Stress Evaluation Locations - Cavity Region

This page intentionally left blank.

3. THERMAL EVALUATION

This chapter presents the evaluations which demonstrate that the FuelSolutions™ W74 canister meets the thermal requirements of 10CFR71.¹ The FuelSolutions™ W74 canister basket assembly is designed to maintain the geometry of the SNF assemblies during transportation within the FuelSolutions™ TS125 Transportation Cask. Containment of the SNF assemblies during transportation is provided by the TS125 Transportation Cask. The thermal design and safety evaluation for the transportation cask are provided in Chapter 3 of the FuelSolutions™ TS125 Transportation Cask SAR.² The thermal evaluation of the FuelSolutions™ W74 canister presented in this chapter is compared with the results presented in the FuelSolutions™ TS125 Transportation Cask SAR to assure that the thermal interface criteria for the transportation cask defined in Chapter 3 of that SAR are met.

The evaluations presented in this chapter assure that the thermal performance of the combined FuelSolutions™ W74 canister and TS125 Transportation Cask system complies with the applicable regulatory safety requirements during normal conditions of transportation (NCT) and hypothetical accident conditions (HAC). Compliance is demonstrated using analytic techniques complying with the methodology presented in Regulatory Guide 7.6³ and Regulatory Guide 7.8.⁴

The maximum thermal ratings for the FuelSolutions™ W74 canister are limited by the applicable allowable temperatures for the materials of the W74 canister, the transportation cask and impact limiters, and the SNF assembly cladding. This assures that the canister/cask component temperatures are maintained below their respective allowable temperatures throughout transportation operations, and that the fuel cladding is protected against degradation and gross ruptures. In addition, the W74 canister may not be loaded in the transportation cask unless the SNF assembly heat generation profile is compliant with the thermal requirements of the transportation cask, as defined in Section 3.1.3.3 of the FuelSolutions™ TS125 Transportation Cask SAR. In this manner, the thermal safety of both the canister and the transportation cask is assured.

This chapter presents FuelSolutions™ W74 canister thermal evaluation results for the design basis NCT and HAC cases. Section 3.2 provides the thermal properties for the W74 canister materials, and Section 3.3 provides the corresponding material specifications. Transportation cask material properties and specifications are presented in the FuelSolutions™ TS125 Transportation Cask SAR. W74 canister analytical model descriptions and thermal results are given in Sections 3.4 and 3.5 for NCT and HAC, respectively. The transportation cask analytical

¹ Title 10, Code of Federal Regulations, Part 71 (10CFR71), *Packaging and Transportation of Radioactive Materials*, U.S. Nuclear Regulatory Commission, October 2004.

² WSNF-120, *FuelSolutions™ TS125 Transportation Cask Safety Analysis Report*, NRC Docket 71-9276, EnergySolutions Spent Fuel Division, Inc.

³ Regulatory Guide 7.6, *Design Criteria for the Structural Analysis of Shipping Cask Containment Vessels*, Revision 1, U.S. Nuclear Regulatory Commission, March 1978.

⁴ Regulatory Guide 7.8, *Load Combinations for the Structural Analysis of Shipping Casks for Radioactive Material*, Revision 1, U.S. Nuclear Regulatory Commission, March 1989.

model, which interfaces with the W74 canister model, is described in the FuelSolutions™ TS125 Transportation Cask SAR. Supplemental data are presented in the Section 3.6 appendices.

As discussed in Chapter 4 of this SAR, containment of all radioactive materials is provided by the transportation cask containment boundary. The transportation cask maximum internal pressure is dependent on the characteristics of the specific FuelSolutions™ W74 canister and SNF payload contained within the cask. Conservative predictions of transportation cask internal pressure for NCT and HAC are provided in Sections 3.4 and 3.5, respectively. Sections 3.6.4, 3.6.5, and 3.6.6 give the thermal evaluations for any amount of Big Rock Point (BRP) mixed-oxide (MOX) assemblies, up to eight damaged fuel assemblies, and partial fuel assemblies, respectively. The evaluation for damaged fuel assemblies includes an assessment of the thermal effects imposed by the presence of the damaged fuel can.

3.1 Discussion

The FuelSolutions™ W74 canister, as part of the FuelSolutions™ Transportation Package, is designed to safely transport Big Rock Point SNF assemblies. The transportation package consists of the FuelSolutions™ TS125 Transportation Cask together with its energy-absorbing impact limiters, personnel barrier, and the FuelSolutions™ W74 canister payload. Thermal loads imposed on the FuelSolutions™ W74 canister arise from the decay heat of the SNF assemblies and from the external environment, including insolation. Since a loaded W74 canister is always surrounded by the cask and impact limiters during transportation operations, it is not directly subjected to ambient conditions. The W74 canister is designed to passively dissipate the decay heat from the SNF to the transportation cask, while maintaining component material temperatures and fuel assembly cladding temperatures within their allowable values, as presented in Section 3.3. The effects of ambient conditions on the W74 canister, including insolation acting on the surrounding transportation cask, are addressed under NCT and HAC analysis in Sections 3.4 and 3.5, respectively. Cold temperature conditions are also included in the package design and are specifically considered under NCT and HAC.

The thermal analysis of the FuelSolutions™ W74 canister is performed for NCT and HAC using the Thermal Desktop®⁵ and SINDA/FLUINT®⁶ computer program. An overview of the Thermal Desktop® and SINDA/FLUINT® computer programs are presented in Section 3.6.

This section provides a description of the thermal design features for the FuelSolutions™ W74 canister, the interface conditions with the transportation cask, the design basis ambient conditions used, the design basis SNF heat generation profile, the thermal modes of operation, and the canister thermal ratings. These descriptions, the bases of analysis, and the canister thermal ratings remain valid for the transportation of MOX, partial, and damaged fuel assemblies within the FuelSolutions™ W74 canister. The specific assumptions, modeling approach, and predicted thermal performance relating to MOX, damaged, and partial fuel assemblies are respectively given in Sections 3.6.4, 3.6.5, and 3.6.6.

3.1.1 Design Features

The FuelSolutions™ W74 canister design features are described in Section 1.2 of this SAR. The transportation cask design features are described in Section 1.2 of the FuelSolutions™ TS125 Transportation Cask SAR.² The configuration of the W74 canister is shown in Figure 1.2-2. Drawings of the W74 canister are provided in Section 1.3.1 of this SAR. This section summarizes the W74 canister design features that affect thermal performance. Since the W74 canister is always placed in the cavity of the transportation cask during transportation operations, a brief description of the transportation cask design features that affect the thermal performance of the canister is also included here.

⁵ Thermal Desktop®, Version 3.1, prepared for NASA, Johnson Spacecraft Center, Contracts NAS8-40560 and NAS8-97009, by Cullimore and Ring Technologies, Inc., Littleton, Colorado, 1999.

⁶ SINDA/FLUINT®, *Systems Improved Numerical Differencing Analyzer and Fluid Integrator*, Version 4.1, prepared for NASA, Johnson Spacecraft Center, Contracts NAS9-19365 and NAS9-97017, by Cullimore and Ring Technologies, Inc., Littleton, Colorado, 1999.

3.1.1.1 W74 Canister

The FuelSolutions™ W74 canister subsystem includes two classes of FuelSolutions™ canister assembly configurations (i.e., the W74M and W74T). A discussion of the canister types and the differences between them is presented in Section 1.2 of this SAR. While the canister basket configurations may vary somewhat in the number, placement, and spacer plate materials, both configurations share the same basic heat transfer characteristics in that each canister configuration uses a spacer plate and guide tube type of basket assembly to position and support the fuel assemblies within the canister. The W74 canister is unique to other FuelSolutions™ canisters in that the W74 canister contains an upper and a lower basket assembly designed specifically for shorter length Big Rock Point BWR fuel. Since the basket assemblies are not mechanically attached to the canister wall, the principal means of heat transfer between the fuel assemblies and the canister shell is via radiation and convection. The following paragraphs provide a brief overview of the thermal similarities and differences between the W74M and W74T class canister configurations.

The following general design features are used to enhance the thermal performance of both canister assembly configurations:

- Carbon steel spacer plates are used for increased thermal conductance.
- Basket assembly layouts are configured to maximize convective flow areas for the horizontal transportation configuration.
- Helium gas is used to backfill the canister to an internal pressure of 24 psia at the normal hot storage condition (100°F ambient within the FuelSolutions™ W150 Storage Cask) to enhance both conduction and convection heat transfer across void spaces in the basket.

Although the W74 canister can physically accommodate a total of seventy-four Big Rock Point BWR fuel assemblies, a physical barrier attached to the basket prevents fuel assemblies from being loaded in the center five cell locations of each basket. As such, the W74 canister fuel loading is limited to a maximum of 32 fuel assemblies in each of the upper and lower baskets for a total of up to 64 fuel assemblies for each FuelSolutions™ W74 canister configuration. The fuel assemblies are structurally intact zircaloy-clad fuel. The fuel assembly acceptance basis for the FuelSolutions™ W74 canister, which satisfies the thermal requirements presented in this chapter, are presented in Section 1.2.3 of this SAR.

Both classes of FuelSolutions™ W74 canisters consist of the same canister shell and basket assembly components. These include a right cylindrical shell, top end inner closure plate, top end outer closure plate, bottom closure plate, bottom outer plate, top and bottom end shield plugs, and vent and drain ports. The W74T canister shells are fabricated of Type 304 stainless steel versus the Type 316 steel used in the W74M canister shell. Both the W74M and W74T canister designs include only the long (192-inch) canister shell configuration. Additionally, both canister classes use only carbon steel material for the top and bottom end shield plugs.

The W74T upper and lower basket assemblies use carbon steel spacer plates to position and support the fuel assemblies. In addition, the W74T upper basket includes a stainless steel engagement plate at its lower end to provide a structural interface with the lower basket assembly. The W74M canister design uses a similar number of spacer plates, but substitutes a stainless steel spacer plate in lieu of the carbon steel plates at the top and bottom ends of both the upper and

lower baskets. The W74M upper basket also includes a stainless steel engagement plate for interface between the baskets.

Both the W74T and W74M basket assemblies use stainless steel support tubes and sleeves to align and separate the spacer plates. Both canister types use stainless steel guide tubes in the upper and lower baskets.

3.1.1.2 Transportation Cask

The thermal design features of the FuelSolutions™ TS125 Transportation Cask are discussed in Section 3.1.1 of the FuelSolutions™ TS125 Transportation Cask SAR.² A summary of the primary thermal design features of the transportation cask as they relate to the FuelSolutions™ W74 canister subsystem includes:

- The FuelSolutions™ W74 canister transfers the decay heat from the fuel assemblies to the transportation cask through a combination of conduction, radiation, and convection. Since the inside diameter of the transportation cask cavity is larger than the canister outside diameter by 1.0 inch, a nominal 0.5-inch annulus will exist between the canister and the cask. Two 0.125-inch high rails attached to the cask inner shell are used to support the canister within the cask cavity when in the horizontal orientation. The low height of the rails will result in the canister being eccentric to the cask centerline when the cask is in the horizontal orientation.
- The side wall region of the transportation cask consists of a series of concentric cylinders or shells. The inner stainless steel shell is surrounded by a cylinder of chemical copper lead for attenuating gamma radiation. This gamma shield is formed by a controlled lead pour procedure that minimizes the residual gap between the lead and the outer shell of the cask. The differential thermal expansion between steel and lead will assure that an intimate interface will occur between the gamma shield and the inner cask shell. A thick outer stainless steel shell surrounds the lead gamma shield and provides additional structural support.
- Neutron shielding is provided by an approximately 6-inch thick shell of NS-4-FR material surrounding the outer shell. Thirty-two A-516, Grade 70 carbon steel support angles are spaced lengthwise between the cask outer shell and neutron shield jacket to enhance heat transfer through the solid NS-4-FR neutron shielding material to the ambient environment. The carbon steel support angles are welded to the cask outer shell and outer jacket using a continuous weld seam.
- The neutron shield jacket is fabricated of 3/16-inch thick A-516, Grade 70 carbon steel. The outer surface of the jacket is coated with an epoxy-based coating to protect the jacket from corrosion, raise its emissivity, and lower its solar absorptance. The continuous weld seam used to attach the jacket to the steel support angles provides a high heat transfer rate between the support angles and the jacket. The relatively high thermal conductivity of the carbon steel jacket then distributes the heat around the exterior of the cask for efficient transfer to the ambient environment.
- The most thermally sensitive transportation cask material is the solid neutron shielding material. The use of Helicoflex[®] metallic seals at the containment boundaries of closure

lid and bottom end regions of the cask reduces the thermal sensitivity of these regions substantially due to the wide temperature capability exhibited by these seals.

- The annulus between the W74 canister and the transportation cask is backfilled with helium gas to enhance heat transfer from the canister.
- The transportation cask provides the containment boundary for the W74 canister and its SNF payload.
- The Cross-Core® aluminum honeycomb used in the impact limiters provides a relatively efficient heat transfer path between the cask ends and the ambient environment (in comparison to impact limiters that use polyurethane foam), while shielding the cask from the high impact loads and heat fluxes associated with the hypothetical accident event.
- A personnel barrier is used with the intermodal skid and railcar to provide a physical barrier between personnel and the transportation cask. Approximately 28 inches of clearance is provided between the cask exterior and the personnel barrier. The design of the personnel barrier provides a minimum 60% free opening for a nearly unobstructed flow of air around the transportation cask for convection cooling and radiation heat transfer to the ambient environment. The barrier is fabricated of uncoated, stainless steel.

3.1.2 Design Basis Thermal Load Conditions

The FuelSolutions™ W74 canister is evaluated within the transportation cask in accordance with 10CFR71 and Regulatory Guide 7.8 for all applicable NCT and HAC thermal loads. The thermal analyses of the W74 canister within the transportation cask presented herein are based on conservative assumptions and methodologies. Because of this approach, the actual thermal response of the canister to the design basis events is expected to produce larger positive design margins than reported herein (i.e., lower temperatures, gradients, and thermal stresses).

Table 3.1-1 presents the design basis initial conditions used in the evaluation of the FuelSolutions™ W74 canister. These load combinations are defined as follows:

- *NCT Hot*: An ambient temperature of 100°F is used to evaluate the maximum temperatures within the canister with maximum decay heat and maximum insolation, per 10CFR71.71(c)(1), averaged over 24 hours.
- *NCT Hot (no solar)*: This case is the same as NCT Hot, but without insolation. The steady-state results are used as initial conditions for the HAC Fire (hot) described below. Additionally, NCT Hot (no solar) serves as the basis for evaluation of the maximum temperature at the transportation cask personnel barrier in accordance with 10CFR71.43(g).
- *NCT Cold*: An ambient temperature of -20°F is used to evaluate the temperatures within the canister with maximum decay heat and no insolation. The steady-state results are used as initial conditions for the HAC Fire (cold) described below.
- *NCT Cold (no heat)*: This case is the same as NCT Cold, but without decay heat. This analytically trivial case addresses minimum material temperatures for the brittle fracture evaluation presented in Section 2.6.2 of this SAR.

- *NCT Cold Environment*: A -40°F steady-state ambient temperature with maximum decay heat and zero insolation. This case is used for evaluation of the maximum thermal gradients and is not combined with other structural loads.
- *NCT Cold Environment (no heat)*: This case is the same as NCT Cold Environment, but without decay heat. Similar to NCT Cold (no heat), this analytically trivial case establishes minimum material temperatures for material compatibility and for the brittle fracture evaluation presented in Section 2.6.2.
- *HAC Fire (cold)*: Thermal conditions are evaluated as a steady-state ambient temperature of -20°F with maximum decay heat and zero insolation prior to the event, followed by a thirty-minute transient with an ambient temperature of 1475°F with maximum decay heat, and then back to a steady-state ambient temperature of -20°F with maximum decay heat and zero insolation. This case is used for evaluation of the thermal gradients expected under the HAC fire conditions. Comparison with the results from the HAC Fire (hot) case below provides an indication of the sensitivity of the package thermal response to the HAC event with the initial starting temperature.
- *HAC Fire (hot)*: Thermal conditions are evaluated as a steady-state ambient temperature of 100°F with maximum decay heat and zero insolation prior to the event, followed by a thirty-minute transient with an ambient temperature of 1475°F with maximum decay heat and maximum insolation, and then back to a steady-state ambient temperature of 100°F with maximum decay heat and maximum insolation, per 10CFR71.71(c)(1), averaged over 24 hours. This load case evaluates the peak temperature achieved for the various cask components under the HAC fire event and the associated thermal stresses.

The 10CFR71.71(c)(1) insolation values are applied to the transportation cask as discussed in Section 3.1.2 of the FuelSolutions™ TS125 Transportation Cask SAR,² and their effects are included in the W74 canister thermal evaluations provided herein. The insolation values are applied to the transportation package as a 24-hour average. Transient insolation modeling is not considered^{7,8} due to the large thermal inertia of the transportation package and the relative magnitude of the insolation load compared to the heat load provided by the SNF.

3.1.3 Design Basis Axial Heat Generation Profile

The FuelSolutions™ W74 canister is designed to accommodate only Big Rock Point BWR fuel. In order to assure that the W74 canister design configurations presented in Section 1.2 of this SAR are qualified to accommodate the worst-case thermal loads, a conservative design basis axial heat generation profile is used in the thermal analysis. The axial heat generation profile and, hence, the temperature profile within the FuelSolutions™ W74 canister are dependent on the variation in the heat load and axial location of the fuel assembly loaded within each basket. The distribution of the heat load within the canister is a function of: (1) the SNF assembly class (i.e., Big Rock Point BWR), (2) the corresponding heavy metal content, burnup, and cooling time,

⁷ Brown, N., Gianoulakis, S., and Lake, W., *Comparison of 10 CFR 71 Normal Conditions with Bounding US "Hot Day" Extremes*, Sandia Report SAND91-2255C, October 1992.

⁸ Manson, S., and Gianoulakis, S., *Comparison of Spent Fuel Shipping Cask Response to 10 CFR 71 Normal Conditions and Realistic Hot Day Extremes*, Sandia Report SAND94-0812, April 1994.

(3) the number of SNF assemblies in the canister, (4) the active length of the SNF assemblies, and (5) the axial position of the SNF assembly active fuel length within the canister. The above variables are set by the canister type and the characteristics of the specific Big Rock Point fuel to be loaded. Sections 3.1.3.1 and 3.1.3.2 describe how the design basis heat generation profile is determined and applied.

In order to address the axial heat profile variations with fuel assembly class and burnup, two thermal acceptance criteria are used for the W74 canister thermal rating qualification. These thermal acceptance criteria are: (1) the maximum heat load rating (Q), and (2) the maximum linear heat generation rate (LHGR) on a per unit length basis. Both thermal criteria are needed to define the allowable W74 canister thermal loading. Although the total heat load is the major determining factor in the overall temperature levels within the W74 canister, the temperature levels at any specific location are more directly affected by the LHGR. This is especially true where the cask and/or canister design and the material thermal conductivity combine to limit the axial spreading of localized heat effects.

3.1.3.1 Development of the Design Basis Axial Heat Generation Profile

Development of PWR and BWR axial heat generation profiles is addressed in detail in Section 3.1.3 of the FuelSolutions™ TS125 Transportation Cask SAR.² The variation in LHGR within the W74 canister is a function of the axial location of the active fuel within the canister. To create a design basis canister axial heat generation profile for use in analyzing the W74 canister, the design basis peaking factor curve for the generic BWR fuel type (Figure 3.1-1 of the FuelSolutions™ TS125 Transportation Cask SAR) is adjusted for the location and length of the active fuel region of the Big Rock Point fuel assemblies within the upper and lower baskets in the W74 canister. Using this profile, a W74 canister-specific axial heat profile is developed. This design basis W74 canister profile, termed the “Big Rock Point” profile (see Figure 3.1-1), envelops the worst-case axial heat profile expected from the fuel to be stored within the W74 canister.

The “Big Rock Point” profile assumes a burnup of 29 GWd/MTU. Burnup for a given fuel assembly class determines the SNF assembly’s total heat load (kW) at the time of reactor discharge and the profile of the heat load versus fuel axial position. A uniform burnup over the entire active fuel length would result in a flat axial heat profile with no peaks (i.e., a peaking factor of 1.0). Since fuel does not burn uniformly over the entire axial length, the heat generation from the fuel will exhibit a peak in the center region of the assembly. A curve fit through the maximum peaking factor observed as a function of burnup is presented in Figure 3.1-2 for generic BWR fuel. Because of the variation in peaking factor versus burnup level, an adjustment/penalty factor is included for low burnup fuels to extend the required SNF cooling times even if the total canister maximum heat load rating (Q_{max}) meets the thermal rating criteria established for the transportation cask and the canister type. SNF assemblies with burnups less than the nominal values are essentially de-rated to normalize the lower burnup peaks with the baseline. Although appropriate, an adjustment/credit is conservatively not applied for SNF assemblies with burnups greater than the nominal values.

The active fuel length of an individual Big Rock Point fuel assembly is 70 inches. Thus, the total active fuel length of the fuel in the upper and lower baskets is 140 inches. However, a 72-inch active fuel length is used for the fuel in the upper basket assembly for the design basis axial heat

generation profile shown in Figure 3.1-1. This results in a slight difference between the upper and lower fuel heat generation profiles that does not significantly affect the results of the thermal evaluation. The composite heat loads in the upper and lower baskets each represent approximately one half of the total W74 canister heat load. Since the W74 canister is designed specifically to accommodate only Big Rock Point fuel and since shorter BWR fuels do not exist, there is no need for a shorter “max. thermal gradient” profile, as used in the thermal analysis of other FuelSolutions™ canisters. Therefore, only the “Big Rock Point” profile is needed to bound all possible W74 canister fuel loadings.

Table 3.1-2 presents in tabular form the design basis “Big Rock Point” canister axial heat profile illustrated in Figure 3.1-1. The same axial heat profile is applicable to the MOX, damaged, and partial fuel assemblies.

3.1.3.2 Application of Axial Heat Profiles for Canister Analysis

The FuelSolutions™ W74 canister analytical model used for the thermal evaluation includes simulation of the individual fuel assemblies within the upper and lower baskets. The local decay heat (Q_{local}) at any specific axial location within the fuel assemblies is determined using the Big Rock Point axial profile in Figure 3.1-1 as follows:

$$Q_{Local} = \left(\frac{Q_{Assy}}{AFL} \right) \cdot N(z) \cdot L$$

where:

- Q_{Local} = Local fuel assembly heat load at the nodal location
- Q_{Assy} = Total fuel assembly heat load (kW) for the given axial profile
- AFL = Active fuel length in inches for the associated axial profile (i.e., 70 inches)
- $N(z)$ = Normalized heat generation at the center of the region being modeled (from Figure 3.1-1 or Table 3.1-2)
- L = Axial length in inches of the region being modeled

For determination of the allowable W74 canister thermal rating within the transportation cask, the value of Q_{Assy} is increased until one or more of the canister or cask allowable material temperatures or the allowable fuel cladding temperature are reached. The maximum value of Q_{Assy} that meets all canister/cask allowable temperatures is multiplied by the total number of assemblies (64) to determine the maximum heat load rating (Q_{Total}) for the canister. The corresponding maximum LHGR for each profile is equal to the average heat load ($Q_{Total}/(2 \times AFL)$) multiplied by the peaking factor (PF). In this case, the active fuel length is multiplied by a factor of 2 since there are two baskets inside the W74 canister. In addition, a peaking factor of 1.22 is used for Big Rock Point fuel.

The calculated maximum heat load rating (Q_{Total}) and maximum LHGR become the thermal ratings for the W74 canister. Via this methodology, any combination of fuel cooling time, active length, or burnup that increases the heat load above the qualified Q_{Total} and LHGR values for the canister will restrict the loading of that candidate fuel assembly until sufficient additional cooling time has occurred to reduce the heat load.

3.1.3.3 Compliance with Transportation Cask Thermal Requirements

As discussed in Section 3.1.3.3 of the FuelSolutions™ TS125 Transportation Cask SAR, any FuelSolutions™ canister that is to be transported in the TS125 Transportation Cask must have a design basis canister heat load that does not exceed 22.0 kW, and that does not produce a peak temperature in the inner shell of the TS125 Transportation Cask exceeding that calculated for the transportation cask's Q_{\max} thermal profile.

The design basis BRP profile used for the thermal evaluation of the W74 canister has a maximum heat load of 22.0 kW and a maximum LHGR of 0.192 kW/inch. As shown in Table 3.1-3, the BRP profile is compliant with the maximum allowable canister heat load of 22.0 kW for the TS125 transportation cask. However, the maximum LHGR of the BRP profile (0.192 kW/inch) exceeds the maximum LHGR of the Q_{\max} profile upon which the TS125 transportation cask thermal rating is based. Comparison of the peak temperature in the TS125 transportation cask from the W74 thermal analysis with those from Chapter 3 of the FuelSolutions™ TS125 Transportation Cask SAR shows that the BRP profile produces lower peak temperatures in the cask inner shell than those calculated for the Q_{\max} profile in Chapter 3 of the FuelSolutions™ TS125 Transportation Cask SAR. Therefore, the W74 canister design basis BRP axial heat generation profile satisfies the canister thermal requirements specified in Section 3.1.3.3 of the FuelSolutions™ TS125 Transportation Cask SAR.

3.1.4 Temperature Summary

The maximum allowable material temperatures for the W74 canister components are presented in Section 3.3.1, while the SNF cladding allowable temperature is presented in Section 3.3.2. The canister system temperatures under the various bounding thermal load conditions for transportation are presented in Sections 3.4 and 3.5 for NCT and HAC, respectively. These system temperatures are determined by applying either the maximum W74 canister thermal ratings presented in Table 3.1-3 or zero decay heat, depending on the applicable thermal load condition summarized in Table 3.1-1.

The figures and tables in Section 3.4 provide a comprehensive overview of the thermal performance of the W74 canister in the TS125 cask under NCT conditions. As the thermal analysis of Section 3.4 demonstrates, all of the temperatures and temperature distributions noted from the analysis are well within the established thermal limits for both the canister and the cask. The predicted peak fuel cladding temperature is 656°F (347°C), or 96°F below the conservatively established allowable temperature for the fuel cladding. The peak spacer plate temperature is 615°F, and the peak canister shell temperature is 475°F.

The predicted peak cask shell temperature is 363°F, or 437°F below the established allowable temperature for the structural steel. The maximum predicted temperature of the lead material forming the gamma shield is 354°F, or 266°F below the established melting point for the lead. The bulk average temperature for the lead shield under the bounding NCT load condition is 334°F. The bulk average temperature of the solid neutron shield material is 261°F, or 39°F below the 300°F limitation established to limit the loss of hydrogen from the material.

Likewise, the thermal evaluations for HAC conditions presented in Section 3.5 demonstrate that the canister and cask component temperatures will remain below their respective accident allowable temperatures. Despite conservative assumptions for emissivity and absorptivity and

the worst-case modeling for potential damage to the impact limiters, the thermal evaluations demonstrate that fuel cladding, spacer plates, and other canister components remain within their long-term allowable temperatures, the cask containment boundary remains intact, and that the lead will remain well below its established melting point. The predicted peak fuel cladding temperature is 350°C, or only 7°C above its pre-fire level. Likewise, the peak spacer plate temperature and the peak canister shell temperatures are only 20 and 35°F, respectively, above their pre-fire temperature levels.

The peak cask component temperatures seen for HAC conditions are within their allowable limits. A full discussion of the performance of the TS125 cask under HAC conditions is provided in the FuelSolutions™ TS125 Transportation Cask SAR.²

3.1.5 Transportation Cask Internal Pressure Summary

Although designed as a confinement boundary for storage conditions, the FuelSolutions™ W74 canister shell assembly is not considered a containment boundary for transportation conditions. Instead, the transportation cask serves this function. In addition to the cask cavity backfill gas, the transportation cask is conservatively assumed to be pressurized due to a postulated release of fuel rod fill gas, fuel rod fission gas, and canister backfill gas directly to the transportation cask cavity. As discussed in Chapter 7 of this SAR, the W74 canister is backfilled with helium during closure operations. The quantity in moles of inert gas needed for canister cavity backfill is determined in order to achieve 10 psig (1.68 atm) in the canister cavity under normal hot storage conditions (i.e., 100°F ambient at the W74 thermal rating for storage within the FuelSolutions™ W150 Storage Cask) with 1% rod failures. The transportation cask cavity is conservatively assumed to be backfilled with helium to achieve 1 atm at room temperature (70°F). Since it can safely be assumed that the canister/cask temperatures will be above 70°F at the time of backfill, the actual cask cavity pressures will be less than those determined based on this assumed quantity of helium backfill gas.

The transportation cask maximum internal pressure is dependent on the characteristics of the specific FuelSolutions™ W74 canister and its SNF payload. A FuelSolutions™ TS125 Transportation Cask design pressure of 75 psig has been established to bound the maximum pressures resulting from the worst-case combination of canister and SNF. Conservative predictions of transportation cask internal pressure for NCT and HAC are provided in Sections 3.4 and 3.5, respectively. The calculations for NCT assume the rupture of 3% of the SNF and PWR control component rods, while those for HAC assume the rupture 100% of the SNF and PWR control component rods.⁹ The release of 100% of the rod fill gas, 30% of the SNF rod fission gas, and 30% of the gas generated within PWR control components is conservatively assumed for each postulated failed rod.

The maximum normal operating pressure (MNOP) for NCT hot and NCT cold conditions and HAC pressure are presented in Table 3.1-5. As shown, both the MNOP and the HAC pressure

⁹ Table 4-1, NUREG-1617, *Standard Review Plan for Transportation Packages for Spent Nuclear Fuel*, Spent Fuel Project Office, Office of Nuclear Material Safety and Safeguards, U.S. Nuclear Regulatory Commission, Washington, D.C. 20555-0001, March 2000.

generated with a bounding W74 canister remains within the design pressure rating for the FuelSolutions™ TS125 Transportation Cask.

Table 3.1-1 - Transportation Design Basis Thermal Conditions

Case	Description	Applicable Conditions				
		Ambient Temperature (°F)	Insolation		Decay Heat	
			Max. ⁽¹⁾	Zero	Max.	Zero
1	NCT Hot ⁽²⁾	100	x		x	
2	NCT Hot (no solar) ^(2,3,6)	100		x	x	
3	NCT Cold ^(2,3)	-20		x	x	
4	NCT Cold (no heat) ⁽⁴⁾	-20		x		x
5	NCT Cold Environment ⁽⁵⁾	-40		x	x	
6	NCT Cold Environment (no heat) ⁽⁴⁾	-40		x		x
7	HAC Fire (cold) ⁽³⁾	-20/1475/-20		x	x	
8	HAC Fire (hot) ⁽³⁾	100/1475/100	x		x	

Notes:

- (1) Insolation in accordance with 10CFR71.71(c)(1), averaged over 24 hours.
- (2) Thermal conditions used to evaluate thermal acceptance criteria and for structural load combinations.
- (3) For the HAC fire event, a transient consisting of an initial steady-state initial conditions (i.e. Case 2 or Case 3), followed by a 30-minute fire event, and concluded with a post-fire transient analysis to establish the peak temperatures.
- (4) NCT Cold and Cold Environment are evaluated without decay heat to establish minimum material temperatures for material compatibility and brittle fracture considerations.
- (5) NCT Cold Environment evaluated with maximum decay heat to establish the worst-case spacer plate thermal gradients.
- (6) NCT Hot (no solar) used to assure compliance with 10CFR71.43(g) criteria for accessible surface temperature.

Table 3.1-2 - W74 Canister Design-Basis Axial Heat Profile

Axial Location⁽¹⁾ (Inches)	Big Rock Fuel Profile Peaking Factor⁽²⁾
0 – 12.99	0
13	0.21
17.4	0.76
20	0.99
30	1.19
40	1.21
50	1.19
60	1.13
70	0.99
80	0.4889
83 – 97.99	0
98	0.21
102	0.76
110	1.14
120	1.20
130	1.20
140	1.16
150	1.08
160	0.81
164	0.70
168	0.21
170 - 192	0

Notes:

- (1) Axial location is given with respect to the bottom end of the canister.
- (2) Intermediate values are determined by linear interpolation.

Table 3.1-3 - W74 Canister Maximum Thermal Ratings for Transportation

Component	Maximum Canister Heat Load, Q_{Total} (kW)	Maximum LHGR (kW/in)
W74 Canister BRP Profile	22.0	0.192
TS125 Transportation Cask Q_{max} Profile ⁽¹⁾	22.0	0.1606
W74 Canister Thermal Rating ⁽²⁾	22.0	0.192

Notes:

- (1) The design basis canister heat generation profile that is used for the TS125 transportation cask thermal evaluation in the FuelSolutions™ TS125 Transportation Cask SAR.
- (2) As discussed in Section 3.1.3.3, the W74 canister LHGR thermal rating, which exceeds that of the TS125 transportation cask Q_{max} profile, is compliant with the thermal requirements of the TS125 transportation cask since it does not produce higher peak temperatures in the transportation cask inner shell than those in the FuelSolutions™ TS125 Transportation Cask SAR.

Table 3.1-4 - W74 Canister Thermal Ratings vs. SNF Burnup

Burnup (GWd/MTU)	Burnup Value For Group (GWd/MTU)	Peaking Factor, PF	De-rating Factor	Maximum LHGR (kW/in)	Q_{Total} (kW)
0 to 15	7.50	1.459	0.836	0.192	18.3 ⁽¹⁾
15 to 20	17.50	1.305	0.935	0.192	20.5 ⁽¹⁾
20 to 25	22.50	1.263	0.966	0.192	21.2 ⁽¹⁾
25 to 29	27.50	1.231	0.991	0.192	21.8 ⁽¹⁾
> 29	-	1.22	1.00	0.192	22.0 ⁽²⁾

Notes:

- (1) Thermal rating limited by the W74 canister's maximum LHGR of 0.192 kW/inch. The corresponding maximum canister heat load, Q_{Total} , is limited to (0.192 kW/inch x 140 inches)/PF.
- (2) Canister rating limited by maximum thermal rating of 22.0 kW for TS125 Transportation Cask.

Table 3.1-5 - Transportation Cask Internal Pressures with Loaded W74 Canister

Condition	Transportation Cask Pressure	Max. Design Pressure
MNOP ⁽¹⁾	10.7 psig	75 psig
MNOP Cold ⁽²⁾	8.5 psig	75 psig
Max. HAC Internal Pressure	28.3 psig	75 psig

Notes:

- (1) At maximum canister rating and with 100°F ambient and solar.
- (2) At maximum canister rating and with -20°F ambient and no solar.

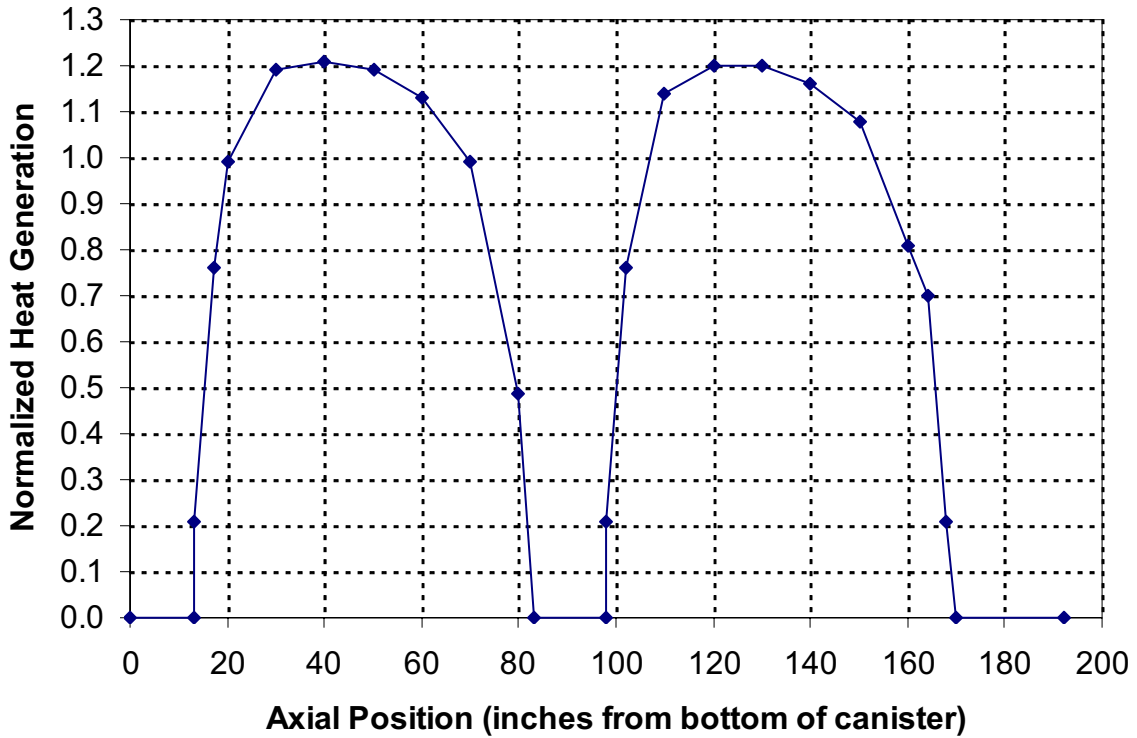


Figure 3.1-1 - Design Basis Axial Heat Profile for W74 Canister Analysis

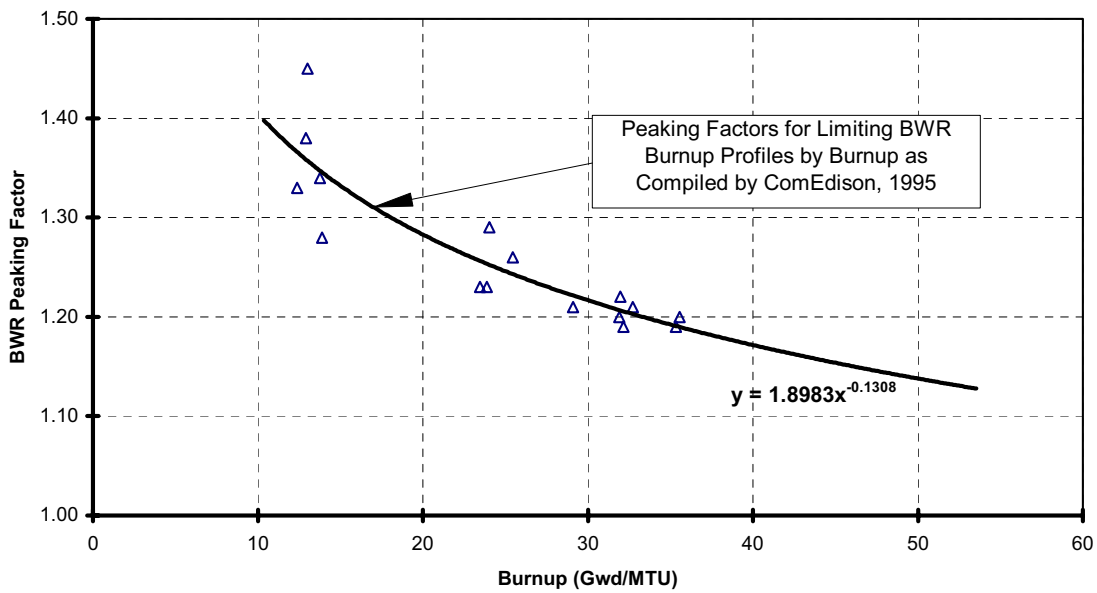


Figure 3.1-2 - Max. Peaking Factor vs. Burnup for BWR Fuel

This page intentionally left blank.

3.2 Summary of Thermal Properties of Materials

The analysis of the W74 canister heat transfer within the transportation cask requires that thermal properties be defined for the materials used in their fabrication. Table 3.2-1 tabulates the relevant thermal properties for the materials used in the fabrication of the FuelSolutions™ W74 canister. The materials used in the fabrication of the transportation cask are presented in Section 3.2 of the FuelSolutions™ TS125 Transportation Cask SAR.² Table 3.2-2 provides a summary of the W74 canister material emissivity values used for radiation heat transfer analyses. Table 3.2-3 provides a summary of the fluid material properties used for thermal analysis. The material properties required for the determination of thermal stresses (i.e., modulus of elasticity, coefficient of thermal expansion, etc.) are presented in Chapter 2.

Material properties presented in this section are taken from technical references that are established and recognized within the thermal analysis field. Realistic material properties are used for the thermal analyses presented in Sections 3.4 and 3.5. As indicated in the tables, the variation of key thermal properties within the temperature range encountered during transportation is modeled as a function of temperature. The effects of material property uncertainties are accounted for by conservatism in the analytical methods presented in Sections 3.4 and 3.5.

The emissivity values presented in Table 3.2-2 are conservative for the materials and surface finishes considered. These values may increase, with a corresponding enhancement in radiation heat transfer and canister thermal performance, if oxidation occurs prior to loading, during vacuum drying, or for the canister exterior during time in the storage cask. Due to conservative analytical assumptions, no controls or limits are necessary to maintain canister material emissivity values over the W74 canister lifetime.

Sections 3.6.4.3, 3.6.5.3, and 3.6.6.2 present the modeling approach for determining the effective thermal conductivity for BRP MOX, damaged, and partial fuel assemblies. Given that the fuel pellets are conservatively ignored when computing the effective thermal conductivity of the fuel assemblies, the thermal properties for UO₂ and MOX fuel are not required for this analysis.

3.2.1 W74 Canister

The FuelSolutions™ W74 canister shell assemblies are fabricated from stainless steel and have carbon steel shield plugs at the ends. The W74M and W74T basket assemblies each contain spacer plates fabricated from carbon steel. The W74M basket also contains stainless steel spacer plates. The basket guide tube assembly is fabricated with a stainless steel inner sleeve and with borated stainless steel neutron-absorbing material attached on one side or two sides, depending on the guide sleeve location within the baskets. Both the W74M and W74T basket support tubes and support sleeves are fabricated of stainless steel. The damaged fuel can is fabricated from Type 304 and Type 316 stainless steel. Further discussion of the FuelSolutions™ W74 canister design is provided in Section 1.2 of this SAR.

The void spaces within the W74 canister cavity and in the annulus between the transportation cask inner shell and canister are filled with helium gas to create an inert environment and to enhance heat transfer. At the time of SNF loading, the W74 canister cavity is backfilled with helium gas to achieve a canister internal pressure of 10 psig, assuming the design basis W74 heat

load for storage, 1% fuel rod failures, and steady-state normal hot storage conditions (100°F ambient). Following W74 canister loading in the transportation cask, the annulus between the W74 canister shell and the transportation cask cavity is backfilled with helium to achieve 1 atm (0 psig). The quantity of helium gas required for this is conservatively estimated assuming room temperature (70°F) conditions. Since it can safely be assumed that the canister/cask temperatures will be above 70°F at the time of backfill, the actual cask cavity pressures will be less than those determined based on this assumed quantity of helium backfill gas.

3.2.2 Big Rock Point Fuel

The individual components of the BWR fuel assemblies are not discretely modeled; rather, the fuel assemblies are included as composite thermal masses with an effective radial thermal conductance based on the work of Manteufel and Todreas.¹⁰ Specifically, the non-linear form of the lumped $k_{\text{eff}}/h_{\text{edge}}$ model for a typical BWR assembly, as presented in Equations (31) and (32) and Table II of Manteufel and Todreas, is used. These equations relate the maximum temperature within the fuel assembly (T_M) to the temperature at the edge of the assembly (T_E) via the equation:

$$Q = 17.38(T_M - T_E) + 3.60E - 8(T_M^4 - T_E^4)$$

and from the edge of the assembly (T_E) to the temperature at the guide tube surface (T_W) via the equation:

$$Q = 36.54(T_E - T_W) + 2.49E - 8(T_E^4 - T_W^4)$$

where Q is in terms of watts, and T_M , T_E , and T_W are in degrees Kelvin.

Before their use in the thermal model, the equation coefficients are modified to remove the assumed 1.2 peaking factor correction, since the effects of peaking factor are computed directly within the thermal model, and to replace the assumed helium gas thermal conductivity of 0.2 W/m-K with a temperature-dependent value. Incorporation of these changes results in the above equations becoming:

$$Q / \text{meter} = 7.122951 \cdot k_{\text{Helium}} \cdot (T_M - T_E) + 2.95082E - 9(T_M^4 - T_E^4)$$

and

$$Q / \text{meter} = 14.97541 \cdot k_{\text{Helium}} \cdot (T_E - T_W) + 2.039904E - 9(T_E^4 - T_W^4)$$

where “Q/meter” represents the net heat transfer between the fuel assembly and a meter length of each guide tube wall. Axial conductance within the fuel assemblies is limited to that which will occur within the thickness of the zircaloy cladding.

These equations are valid for the case where helium is used as the backfill gas. Since the above equations are for an active fuel length of 144 inches, the equations are scaled as needed to match the specific active fuel length of the assembly being modeled. Axial conductance within the fuel assemblies is limited to that which occurs within the thickness of the cladding.

The thermal mass of the fuel assembly used in the thermal analysis is based on a typical Big Rock Point fuel assembly that has a total assembly weight of 457 pounds, an active fuel length of

¹⁰ Manteufel, R. D., and Todreas, N. E., *Effective Thermal Conductivity and Edge Conductance Model for a Spent-Fuel Assembly*, Nuclear Technology, Vol. 105, pp. 421-440, March 1994.

70 inches, and an effective specific heat of 0.03 BTU/lb-°F.¹¹ These parameters are conservative for thermal mass determination and bound all Big Rock Point fuel assemblies, including MOX and partial fuel assemblies. The thermal properties for damaged fuel assemblies are presented in Section 3.6.5.3.

¹¹ NUREG/CR-6150, *SCDAP/RELAP5/MOD3.2 Code Manual, Volume IV: MATPRO – A Library of Materials Properties For Light-Water-Reactor Accident Analysis*, Revision 1, Volume IV, Idaho National Engineering and Environmental Laboratory, October 1997.

**Table 3.2-1 - W74 Canister Homogenous Material Properties
(2 pages)**

Material	Temperature (°F)	Thermal Conductivity (BTU/hr-ft-°F)	Density⁽¹⁾ (lb/ft³)	Specific Heat (BTU/lb-°F)
Type 304/304L Stainless Steel ⁽²⁾	-40	8.2 ⁽⁴⁾	503	0.111 ⁽⁴⁾
	70	8.6		0.113
	100	8.7		0.114
	200	9.3		0.119
	300	9.8		0.122
	400	10.4		0.125
	600	11.3		0.129
	800	12.2		0.132
	1000	13.2		0.135
	1200	14.0		0.137
	1500	15.3		0.141
Type 316 Stainless Steel ⁽²⁾	-40	6.9 ⁽⁴⁾	502	0.110 ⁽⁴⁾
	70	7.7		0.114
	100	7.9		0.116
	200	8.4		0.119
	300	9.0		0.124
	400	9.5		0.125
	600	10.5		0.129
	800	11.5		0.132
	1000	12.4		0.134
	1200	13.3		0.136
	1500	14.6		0.140
Type XM-19 Stainless Steel ⁽²⁾	-40	5.7 ⁽⁴⁾	494	0.103 ⁽⁴⁾
	70	6.4		0.113
	100	6.6		0.115
	250	7.40		0.121
	400	8.2		0.126
	600	9.3		0.132
	800	10.4		0.136
	1000	11.4		0.138
	1200	12.5		0.142
	1500	14.0		0.148

**Table 3.2-1 - W74 Canister Homogenous Material Properties
 (2 pages)**

Material	Temperature (°F)	Thermal Conductivity (BTU/hr-ft-°F)		Density ⁽¹⁾ (lb/ft ³)	Specific Heat (BTU/lb-°F)	
		Grade F	Grade P		Grade F	Grade P
SA-514/517 Carbon Steel ⁽²⁾	-40	21.1 ⁽⁴⁾	19.8 ⁽⁴⁾	501	0.096 ⁽⁴⁾	0.097 ⁽⁴⁾
	70	21.8	21.3		0.103	0.105
	150	22.3	22.2		0.109	0.111
	250	22.4	22.9		0.115	0.117
	350	22.4	23.3		0.120	0.123
	400	22.3	23.3		0.122	0.125
	500	22.0	23.1		0.127	0.130
	600	21.5	22.7		0.132	0.135
	800	20.4	21.6		0.143	0.149
	1000	19.2	20.2		0.157	0.167
Type A36 or A516 Carbon Steel ⁽²⁾	-40	22.9 ⁽⁴⁾		489	0.096 ⁽⁴⁾	
	70	23.6			0.110	
	200	24.4			0.118	
	300	24.4			0.123	
	400	24.2			0.128	
	600	23.1			0.136	
	800	21.7			0.149	
	1000	20.0			0.165	
	1500	15.1			0.183	
1.25% Borated Stainless Steel ⁽³⁾	77	8.55		487	0.118	
	212	9.25			0.124	
	302	9.65			0.127	
	392	10.00			0.128	
	482	10.40			0.129	
	752	11.50			0.132	
	932	12.25			0.133	

Table 3.2-1 Notes:

- (1) Single values are shown for homogeneous material density, since this material property does not vary significantly with temperature.
- (2) Material properties are obtained from ASME Boiler and Pressure Vessel Code, Section II, Part D, 1998 Edition.
- (3) Micro-Melt® NeutroSorb PLUS®, *Alloy Data for Modified Type 304 Stainless with Boron ASTM A887-89 Grade "A" Alloys*, Document #1-94/5M, Carpenter Technology Corporation, 1994.
- (4) Extrapolated value.

Table 3.2-2 - W74 Canister Surface Emissivities

Material	Conditions	Emissivity (ϵ)
Spacer Plates & Canister Shell (304/304L & XM-19 ^(1,2))	slightly oxidized, 250-500°F	0.40
Fuel Guide Tubes & BORAL™ Wrappers (304/304L & Borated Stainless Steel ^(1,2))	oxidized, >500°F	0.45 ⁽⁴⁾
Spacer Plates (SA-564 Grade 630 Stainless Steel (17-4 PH) ⁽¹⁾)	as-received, <600°F	0.40
Spacer Plates & Canister Shield Plugs (A-36 and SA-514/517 Grade F/P Carbon Steel ^(1,3))	Electroless nickel plated	0.11

Notes:

- (1) Gubareff, G. G., Janssen, J. E., and Torborg, R. H., *Thermal Radiation Properties Survey*, 2nd Edition, Honeywell Research Center, 1960.
- (2) Frank, R. C., and Plagemann, W. L., *Emissivity Testing of Metal Specimens*, Boeing Analytical Engineering coordination sheet No. 2-3623-2-RF-C86-349, August 21, 1986.
- (3) Siegel, R., and Howell, J. R., *Thermal Radiation Heat Transfer*, 3rd Edition, Hemisphere Publishing Corporation, Washington, D.C., 1992.
- (4) Components such as the neutron absorber sheet attachment buttons and retainer clips could have an emissivity range of 0.15 to 0.45.

Table 3.2-3 - W74 Canister Material Properties, Fluids

Material	Temp. (°F)	Thermal Conductivity (BTU/hr-ft-°F)	Specific Heat (BTU/lb-°F)	Density (lb/ft ³) ⁽¹⁾	Viscosity (centipoise)
Air ^(1,2,3,7,8)	-99	0.010	0.239	Use ideal gas law	0.01336
	81	0.015	0.240		0.01853
	261	0.019	0.242		0.02294
	441	0.023	0.246		0.02682
	621	0.026	0.251		0.03030
	801	0.030	0.257		0.03349
	981	0.033	0.262		0.03643
	1161		0.267		0.03918
	1341	0.039	0.272		0.04177
	1701		0.280		0.04650
Helium ^(4,5,6,7,8)	-99	0.067	1.24	Use ideal gas law	0.0150
	81	0.087	1.24		0.0199
	261	0.104	1.24		0.0243
	441	0.122	1.24		0.0283
	621	0.143	1.24		0.0320
	801	0.161	1.24		0.0355
	981	0.177	1.24		0.0388
	1161	0.194	1.24		0.0420
	1341	0.210	1.24		0.0450
	1701	0.240	1.24		0.0508

Notes:

- (1) Eckert, E. R.G., and Drake, Jr., R. M., *Analysis of Heat and Mass Transfer*, McGraw-Hill Book Company, New York, 1972.
- (2) Rohsenow, Hartnett, and Ganic, *Handbook of Heat Transfer Fundamentals*, 2nd edition, McGraw-Hill Publishers.
- (3) Kreith, F., *Principles of Heat Transfer*, 3rd Edition, Harper & Row Publishers.
- (4) Touloukian, Y.S., *Specific Heat - Nonmetallic Liquids and Gases*, Thermophysical Properties of Matter, the TPRC Data Series, Vol. 6, 1970.
- (5) Touloukian, Y.S., *Thermal Conductivity - Nonmetallic Liquids and Gases*, Thermophysical Properties of Matter, the TPRC Data Series, Vol. 3, 1970.
- (6) Touloukian, Y.S., *Viscosity - Nonmetallic Liquids and Gases*, Thermophysical Properties of Matter, the TPRC Data Series, Vol. 11, 1970.
- (7) The associated Prandtl number at each temperature point can be computed from the given table values via the equation: Prandtl number = specific heat*viscosity*2.41909/conductivity.
- (8) The coefficient of thermal expansion for an ideal gas is 1/(T+459.67), where T is the gas temperature in degrees F.

This page intentionally left blank.

3.3 Technical Specification of Components

This section provides the material specifications for components of the W74 canister and the SNF. Since the W74 canister is entirely passive, the only applicable material specifications are the maximum allowable temperatures. The material specifications for the transportation cask components are presented in the FuelSolutions™ TS125 Transportation Cask SAR.²

3.3.1 W74 Canister

The FuelSolutions™ W74 canister materials that are considered temperature sensitive are the zircaloy cladding on the SNF assembly rods, the borated stainless steel, and the canister structural components. W74 canister component maximum allowable temperatures are summarized in Table 3.3-1 for the applicable thermal load condition. The minimum allowable service temperature for all W74 canister components is less than -40°F.

Since the borated stainless steel is not used for structural purposes, its maximum temperature for continuous operation is 1200°F¹² or less in order to prevent material changes due to annealing, etc. The actual melting point is approximately 2550°F. No minimum allowable temperature is needed for the cold conditions.

Carbon and stainless steel exhibit material property variations within the operating temperature range of the canister. In compliance with the ASME B&PV Code,¹³ the maximum allowable temperature of carbon and stainless steel used for structural purposes is 700°F and 800°F, respectively. Both carbon and stainless steel have a melting point well above 2500°F (1371°C).^{14,15} The ASME allowable temperatures apply only to thermal loading conditions under which material properties are relied on for structural loads postulated to occur within the respective operating mode or load combination (e.g., NCT and HAC drop accidents). The HAC fire accident thermal condition exists for a short duration and does not need to be combined with an off-normal structural load condition, since the HAC drop is postulated to occur prior to the HAC fire. For the HAC fire condition, higher allowable material temperatures are established to assure that the ASME material long-term material properties are not impacted. As shown in the ASME Code,¹⁶ the strength properties of steels do not change due to short-term exposure up to 1,000°F. Therefore, since short-term exposure to the temperatures of this magnitude does not have any significant effect on mechanical properties of the materials, 1,000°F is the selected short-term allowable temperature for the structural ASME carbon and stainless steel in the W74 canister.

¹² Micro-Melt® NeutroSorb PLUS®, *Alloy Data for Modified Type 304 Stainless with Boron ASTM A887-89 Grade "A" Alloys*, Document #1-94/5M, Carpenter Technology Corporation, 1994.

¹³ ASME Boiler and Pressure Vessel Code, Section III, Division 1 - Subsections NB and NG, 1998 Edition.

¹⁴ ASME Boiler and Pressure Vessel Code, Table NF-2, Section II, Part D, 1998 Edition.

¹⁵ *Material Engineering*, Penton Publishing, December 1991.

¹⁶ Section III, Division I, Subsection NH, *Class 1 Components in Elevated Temperature Service*, American Society of Mechanical Engineers (ASME) Boiler and Pressure Vessel Code, 1998 Edition.

The W74T basket assemblies use SA-517 Grade P carbon steel material for the support tubes. This material has a maximum allowable temperature of 700°F if it is used for structural purposes. Although the W74M support tube material (XM-19 stainless steel) has a higher allowable temperature (800°F), the SA-517 Grade P maximum allowable temperature is applied in order to thermally bound all W74 basket assemblies. Similar to the carbon and stainless steel discussion above, a higher allowable temperature of 1000°F is established for the W74M support tube material during the HAC fire accident thermal condition.

These component specifications remain valid and bounding for the analysis of the BRP MOX, partial, and damaged fuel assemblies within the FuelSolutions™ W74 canister.

3.3.2 Fuel Cladding Allowable Temperatures

Thermal conditions within the transportation cask are considered short-term thermal conditions since the W74 canister will not remain within the transportation cask for durations longer than a year. The bounding short-term allowable SNF cladding temperature is established as 570°C¹⁷ for all NCT conditions within the transportation cask. In order to confirm that this short-term allowable cladding temperature is valid for burnups above 28 GWd/MTU (as specified in NUREG-1536¹⁸), the worst-case rod stress is calculated using a Big Rock Point assembly under 40 GWd/MTU burnup conditions for peak internal pressure and cladding oxidation. The ANF 9x9 assembly has the highest rod diameter (D) to cladding thickness (t) ratio. Since hoop stress is proportional to the D/t ratio, the fuel assembly with the highest D/t ratio will bound the other BRP BWR types.

This calculated maximum cladding stress is compared with the tabulation of failure mode observations presented in EPRI Report TR-103949.¹⁹

$$\sigma_{\infty} = \frac{PD_{mid}}{2t} = \frac{(11.9 \text{ MPa})(0.5295 \text{ in})}{2(0.033 \text{ in})} = 95.5 \text{ MPa}$$

where:

$$P = (1200 \text{ psi}) \frac{(570^{\circ} \text{ C} + 273 \text{ K})}{(311^{\circ} \text{ C} + 273 \text{ K})} \left(\frac{6894.75 \text{ Pa}}{\text{psi}} \right) \left(\frac{\text{MPa}}{10^6 \text{ Pa}} \right) = 11.9 \text{ MPa}$$

$$D_{mid} = 0.5625 \text{ in} - 0.033 \text{ in} = 0.5295 \text{ in}$$

$$t = (0.034 \text{ in} - 0.000984 \text{ in}) = 0.033 \text{ in}$$

$$311^{\circ} \text{ C} = \text{Assumed plant operating temperature for BRP BWR fuel}$$

$$1200 \text{ psi} = \text{Bounding rod pressure at the plant operating temperature}$$

¹⁷ PNL-4835, *Technical Basis for Storage of Zircaloy-Clad Spent Fuel in Inert Gases*, Pacific Northwest Laboratory, September 1983.

¹⁸ NUREG-1536, *Standard Review Plan for Dry Cask Storage Systems*, U.S. Nuclear Regulatory Commission, January 1997.

¹⁹ EPRI TR-103949, *Temperature Limit Determination for the Inert Dry Storage of Spent Nuclear Fuel*, Electric Power Research Institute, May 1994.

The maximum short-term cladding stress calculated above (95.5 MPa) is conservative due to the conservatism of the 40 GWd/MTU rod pressure, and the use of the peak instead of the average rod temperature for the rod pressure calculation.

Regardless, the calculated maximum short-term cladding stress is much lower than the average rod stress (395 MPa) reported in EPRI Report TR-103949,¹⁹ Table A-1, for stress-rupture observations of irradiated zircaloy. The calculated maximum stress is also much less than the lowest rod stress reported for Zr-2 clad BWR fuel (337 MPa). Additionally, no rod failures were reported by PNL-4835¹⁷ for rods tested up to 570°C, and only pinhole defects (no gross failures) were observed for unirradiated rods tested up to 800°C. This provides additional assurance that the 570°C short-term allowable temperature is conservative, and that no gross cladding failures will occur if short-term temperatures are maintained below this value.

This short-term allowable cladding temperature would nominally apply during all thermal conditions within the transportation cask. However, the FuelSolutions™ W74 Canister Storage FSAR²⁰ based the long-term allowable cladding temperature on cladding degradation due to material creep behavior. This methodology is a result of more recent testing for SNF with burnups to 60 GWd/MTU (herein referred to as the “creep methodology”). The creep methodology is in accordance with 10CFR72.72(h)²¹ and NUREG-1536,¹⁸ wherein the degradation of fuel cladding that results in gross cladding failure is to be prevented throughout the entire storage life. Gross cladding failure can be characterized as a type of cladding breach, such as axial splits or ductile fracture, where irradiated UO₂ particles may be released. The design intent is to avoid cladding rupture and maintain sufficient cladding structural integrity to allow handling at the end of storage life. Both UCID-21181²² and EPRI Report TR-103949¹⁹ agree that the SNF cladding allowable temperature for dry storage should be determined primarily by the creep properties of the cladding.

Currently it is not feasible to uniquely define the effects on creep associated with changes in hydriding and annealing characteristics of Zircaloy-2 and Zircaloy-4 fuel assembly cladding during a post-transportation, dry storage period, if the necessary transportation cycle operations entail lengthy periods with temperatures above 400°C (752°F). Therefore, the allowable fuel cladding temperature is established as 400°C (752°F) to assure that the total cladding creep is less than 1% for all NCT operations of the W74 canister within the transportation cask. A 570°C (1058°F) fuel cladding temperature limitation will apply for all HAC events.

The MOX fuel rods used at Big Rock Point have design operating parameters that are equal to or bounded by those for conventional UO₂ fuel rods. As such, the bounding operational temperature (e.g., in-reactor) experience of the two fuel rod configurations is similar. Further, since the 35 GWd/MTU burnup value of the BRP MOX fuel is below the design basis 40 GWd/MTU burnup for the conventional BRP fuel, the MOX fuel internal rod pressures and operating

²⁰ WSNF-223, *FuelSolutions™ W74 Canister Storage Final Safety Analysis Report*, NRC Docket 72-1026, BNG Fuel Solutions Corporation.

²¹ Title 10, Code of Federal Regulations, Part 72 (10CFR72), *Licensing Requirements for the Independent Storage of Spent Nuclear Fuel and High-Level Radioactive Waste*, U.S. Nuclear Regulatory Commission, 1995.

²² UCID-21181, *Spent Fuel Cladding Integrity during Dry Storage*, Lawrence Livermore National Laboratory, September 1987.

temperature effects will be bounded by those for the conventional BRP fuel. Although the BRP MOX fuel assemblies have lower internal rod pressures and, therefore, lower cladding stress levels than the design basis BRP fuel assemblies, the same long-term allowable cladding allowable temperature is used for both fuel types as a bounding value. Section 3.6.4.4 presents the basis for this assumption.

Table 3.3-1 - W74 Canister Component Allowable Temperatures

Canister Component	Applicable Thermal Criteria (°F)	
	NCT ⁽¹⁾	HAC Fire and Post-fire ⁽²⁾
Peak Fuel Cladding	752 (400°C)	1058 (570°C)
Structural Carbon Steel	-40 to 700	-40 to 1000
Structural Stainless Steel	-40 to 800	-40 to 1000
Borated Stainless Steel	-40 to 1200	-40 to 1200

Notes:

⁽¹⁾ Cases 1 through 6 in Table 3.1-1.

⁽²⁾ Cases 7 and 8 in Table 3.1-1.

This page intentionally left blank.

3.4 Thermal Evaluation for Normal Conditions of Transport

This section provides a discussion of the thermal analysis methodology and results for the FuelSolutions™ W74 canister within the FuelSolutions™ TS125 Transportation Cask under NCT. The applicable canister assembly thermal ratings, temperature distributions, and thermal performance are evaluated to verify that the canister and transportation cask thermal design features adequately perform their intended functions under the NCTs defined in 10CFR71.71. The thermal evaluations of the W74 canister in the transportation cask are performed using conservative analytical techniques. Canister and cask thermal ratings are established to assure that all materials are maintained within their applicable minimum and maximum allowable temperatures during all modes of operation.

To validate the performance of the FuelSolutions™ W74 canister within the TS125 Transportation Cask under NCT, the combined thermal model for the W74 canister and the transportation cask is evaluated for the design basis NCT cases presented in Table 3.1-1 using the enveloping W74 canister heat generation profile presented in Section 3.1.3. The analysis presented herein is designed to establish a thermal rating and to demonstrate that the W74 canister and transportation cask allowable material temperatures are not exceeded.

The thermal model of the W74 canister is described in this section along with a discussion of how the canister thermal model interfaces with that for the transportation cask. The specifics of the thermal model for the FuelSolutions™ TS125 Transportation Cask are presented in Section 3.4.1 of the FuelSolutions™ TS125 Transportation Cask SAR² and are not repeated here.

The thermal analysis methodology and results for the FuelSolutions™ W74 canister with BRP MOX, damaged, and partial fuel assemblies are presented in Sections 3.6.4, 3.6.5, 3.6.6, respectively.

3.4.1 Thermal Models

3.4.1.1 Analytical Thermal Models

The analytical thermal model of the W74 canister assembly is developed for use with the SINDA/FLUINT^{®6} computer program. Section 3.6.7 presents an overview of the SINDA/FLUINT[®] program and its past use for the analysis of nuclear systems. The thermal modeling of the W74 canister assembly is presented in the following paragraphs.

Canister Modeling Approach

The basic thermal modeling approach used for the W74 canister is to divide the basket assembly into common geometric segments, such as a spacer plate and the sections of guide tubes, and the canister shell extending from that spacer plate to the next spacer plate. By defining the basic thermal model in this manner, the thermal mass and conductance for all other sections of the basket are modeled by applying a set of scaling factors as a function of the spacer plate thickness and the distance between the spacer plates. This approach not only simplifies the thermal modeling, but eases the verification process by minimizing the amount of original coding required to provide a complete thermal representation of the system. Precisely how this feature is used for this analysis is explained below.

The FuelSolutions™ W74 canister includes the shell and basket assembly components. The canister shell assembly components include the cylindrical shell, top end inner closure plate, top end outer closure plate, bottom closure plate, bottom outer plate, top and bottom end shield plugs, and vent and drain ports.

From a thermal point of view, the differences between the W74M and W74T versions of the FuelSolutions™ W74 canister are slight. The use of two additional carbon steel spacer plates in the W74T version over those used in the W74M version has essentially no impact on the thermal performance. This is due to the fact that the thicker stainless steel spacer plates and the lower emissivity associated with the electroless nickel plated carbon steel plates combine to effectively cancel the higher thermal conductivity of SA-517 carbon steel over Type 316 stainless steel.

Taken together, the design differences between the W74M and W74T versions of the basket assemblies result in no significant impact on the thermal performance of the baskets. Therefore, the thermal model documented herein is for the W74M version of the FuelSolutions™ W74 canister design, but is also applicable to the W74T version of the canisters.

Three general categories of analytical thermal submodels are used to analyze the performance of the W74 canister assembly within the transportation cask. These submodels are:

- A typical spacer plate or group of spacer plates within the W74 basket assembly, including the associated sections of the SNF assemblies and guide tubes.
- The bottom end of the canister assembly, together with the bottom end shield plug and the associated basket assembly spacer plate sections.
- The top end of the canister assembly, together with the closure end shield plug and the associated basket assembly spacer plate sections.

Program features within SINDA/FLUINT®⁶ are used to combine the thermal modeling of these common elements to complete the thermal modeling for every other section within the basket. The individual thermal sections, or submodels, are thermally connected to complete a full-length representation of the W74 canister configuration. A total of eight submodels are used in the thermal model of the W74 canister assembly.

Figure 3.4-1 illustrates the placement and extent of the submodels used in the thermal model of the W74M canister. Each thermal submodel represents a 90-degree section of the basket assembly and canister shell assembly. Since the W74 canister is horizontal within the transportation cask, these 90-degree segments are extended to 180 degrees by adding an additional 90-degree model segment to represent the bottom half of the basket assembly. For simplicity, the 180-degree modeling is limited to those portions of the basket assembly that experience the highest temperature gradients within the spacer plates. The sections of the basket outside of this region are represented with 90-degree model segments, which conservatively use heat transfer coefficients that are applicable to the upper half (i.e., the hottest portion) of the basket assembly. This modeling approach captures both the hottest temperatures and the maximum thermal gradients within the basket assembly.

The thermal model of each canister configuration consists of submodels “SA,” “SB,” “SC,” “SD,” “SE,” and “SF” through the mid-section of the canister and basket assembly, and model sections “END” at the bottom end and “LID” at the top end of the canister. Figure 3.4-2 through

Figure 3.4-8 present the layout of the thermal sections and nodes used within each of the model submodels.

Taken together, the submodels and their associated thermal sections provide a quasi-three-dimensional thermal model of the entire FuelSolutions™ W74M canister. The model is referred to as “quasi-three-dimensional” because it uses a combination of two-dimensional and three-dimensional modeling to represent different segments of the canister. Those portions of the assemblies (i.e., the interior of the basket assemblies and the canister side wall) that have significant variation in heat transfer in all three dimensions (“r,” “ θ ,” and “z”) are represented with a three-dimensional model. The bottom end and closure lid shield plugs are represented with axisymmetric modeling (i.e., “r” and “z” dimensions only), since the temperature variation in the “ θ ” direction (e.g., around the circumference) is small for the thermal boundary conditions imposed by the casks.

Modeling of the entire length of the canister permits simulation of the axial variation in decay heat within the fuel assemblies, the ability to model differences in axial placement of the fuel assemblies within the canister, and an accurate determination of the thermal end effects introduced by the canister shield plugs and the variation in decay heat with axial position.

The approach used to model the canister assembly is further illustrated by examining the makeup of the thermal modeling for the “END” submodel. The “END” submodel encompasses the canister bottom, the shield plug, and the first three spacer plate sections of the basket assembly. Figure 3.4-2 illustrates the section of the canister assembly covered by the “END” submodel and the thermal node layout in the canister bottom and shield plug. Thermal nodes at six radial locations are used to provide temperature resolution within the bottom outer plate, the shielding material, and the bottom closure plate. In addition to the nodes shown, an additional five thermal nodes are used on the inner surface of the bottom closure plate to represent surface temperatures. The thermal modeling in the shield plug represents an axisymmetric model of these components, which is appropriate for the expected temperature variation within the components.

Canister Modeling Basis

A 1.0-inch space is assumed to separate the bottom closure plate and the bottom of the first spacer plate. This dimension represents the 1-inch distance where the support tubes extend below the spacer plate. Heat transfer between the inside surface of the shield plug and the first spacer plate is via radiation and conduction/convection through the helium gas. No direct contact is assumed between the basket and the shield plug.

Temperature-dependent properties for specific heat and thermal conductivity are used for all components of the shield plug. No direct contact is assumed between the bottom outer plate and the shield material, or between the shield material and the bottom closure plate. Instead, an air gap of 0.060 inch (1.5 mm) is assumed between each pair of materials. This modeling approach provides a conservative estimate of the internal canister temperatures and the axial thermal gradient within the shield plug.

Figure 3.4-3 to Figure 3.4-5 illustrate the thermal modeling used for the fuel assemblies, the guide tubes, and the spacer plates in this section of the canister assembly. Figure 3.4-3 presents the thermal node layout used for the typical modeling of the fuel assemblies and the basket assembly in the region between spacer plates. A 90-degree segment of the basket is represented

by the modeling. An additional 90-degree segment can be added to simulate the lower half of the basket when the canister is in the horizontal orientation. The temperature of each fuel assembly is simulated by one thermal node representing the peak fuel cladding temperature and a node at each face of the fuel assembly to provide the edge temperatures. This node layout complies with the lumped $k_{\text{eff}}/h_{\text{edge}}$ model described in Manteufel and Todreas¹⁰ (see Section 3.2.2). Helium gas is assumed as the medium within the canister.

A single node is used to represent the temperature within each wall of the guide tube, despite the fact that the guide tube wall is actually composed of up to two separate layers (e.g., the guide tube wall and the borated steel neutron absorber sheet) on one or two faces of the guide tube. This level of modeling is appropriate based on hand calculations showing that the heat transfer through the combined thickness of the materials and the direct contact between the materials limits the temperature difference across the composite layers to less than 1 or 2 degrees Celsius. This small temperature difference is deemed an acceptable margin of error. Additionally, this level of temperature difference assumes an effective conductivity through the material of only 1.0 Btu/hr-ft-°F or greater, while the actual effective conductivity is in excess of 3 Btu/hr-ft-°F. Therefore, the modeling approach is validated.

Each guide tube is conservatively assumed to be centered in its respective spacer plate cutout (i.e., no credit is taken for direct contact between the guide tube and spacer plate surfaces), and each fuel assembly is conservatively assumed to be centered within the guide tubes. This assumption is used for the horizontal orientation to account for possible imperfect contact, high centering between a series of spacer plates, etc.

The thermal modeling provides temperature resolution for the peak cladding temperature in the fuel assembly (i.e., nodes 10, 20, 30, ... 340), the edge of the fuel assemblies (i.e., nodes 12, 13, 21, 22, ... 344), the walls of the guide tubes (i.e., nodes 16, 17, 25, 26, ... 348), the support sleeves (i.e., nodes 355 to 358), and the canister shell (i.e., nodes 502 to 522) at each spacer plate section in the basket assembly. To differentiate between the various sections of the basket assembly being modeled in the SINDA/FLUINT[®] program, the node numbers are incremented in steps of 1000 for each spacer plate section within the submodel (i.e., node 1502 is a section of the canister side wall between the first two spacer plates, 2502 is between the second and third spacer plates, etc.).

Figure 3.4-4 illustrates the modification to the typical thermal modeling of the fuel assemblies and guide tubes to simulate the short loading of the W74 canisters to achieve a total of 64 SNF assemblies per canister. As seen in the figure, not only are the center five fuel assemblies not present, but the associated guide tubes are also absent from the basket assembly. This basket configuration results in a void region in the center of the basket assembly.

Figure 3.4-5 illustrates the thermal node layout used at each spacer plate. Again, the modeling represents a 90-degree segment of the spacer plate over either the 3/4-inch thickness of the SA-517 carbon steel spacer plate or the 2-inch thickness of the Type 316 stainless steel spacer plate. Forty-eight nodes (i.e., nodes 202 to 283) are used to simulate portions of the spacer plate within the 90-degree segment. An additional 90-degree model segment is used to represent the bottom section of the spacer plate. This modeling level provides thermal resolution within the

spacer plate, while limiting the overall complexity of the model. As indicated in the figure, the same thermal nodes used to represent the fuel assemblies and guide tubes between the spacer plates are used to simulate these components at the spacer plates. While the presence of the spacer plate results in a local decrease in the temperature of these components, the amount of the decrease is small because of the thickness of the plates in comparison with their separation distances. As such, the added complexity required to capture this effect is deemed unnecessary.

Heat transfer from the guide tubes to the spacer plates is assumed to be via conduction and radiation across a gap. For conservatism, direct contact between the guide tube and spacer plate is not assumed. Heat transfer within the spacer plates is calculated using temperature-dependent properties. As such, the heat transfer between the circumference of the spacer plates and the canister side wall is via conduction and radiation across a gap. A view factor of 1.0 is assumed, together with a thermal emissivity of 0.40 for the edge of the stainless steel plates, 0.11 for the electroless nickel plated carbon steel plates, and 0.40 for the canister shell.

Canister Model Presentation

Figure 3.4-6 presents an isometric view of the node layout as it would appear between the first and second spacer plate in each thermal submodel. Axial conductors are used to complete the three-dimensional modeling of the basket assembly by providing thermal communication between the thermal nodes at one spacer plate section and those at the next. A similar modeling approach to that depicted in Figure 3.4-3 and Figure 3.4-5 is used to represent the basket components in the other thermal submodels.

Figure 3.4-7 illustrates the thermal submodel used for the typical mid-body section (i.e., submodels “SA,” “SB,” “SC,” “SD,” “SE,” and “SF”) in the canister assembly. The length of each thermal submodel is selected to encompass three to four spacer plate sections within the W74M basket assembly. The modeling of the fuel and basket assembly region between the spacer plates is similar to that shown in Figure 3.4-3, except that the length is adjusted as required to match the separation distance between spacer plates. The thermal model at the individual spacer plates is the same as shown in Figure 3.4-5. Axial conductors within the canister shell, the guide tubes, and the fuel assemblies are used to tie the various submodels together.

As illustrated in Figure 3.4-8, the thermal submodel at the top end of the canister is similar to that used at the bottom end. The differences include the added layers of steel used in the closure and the differences in the basket layout. The thermal node layout for the spacer plates and the basket assembly between plates is similar to that shown in Figure 3.4-3 and Figure 3.4-5. Again, axial conductors within the canister shell, the guide tubes, and the fuel assemblies are used to provide thermal communication between the various submodels. Although the W74 top shield plug assembly includes a shield plate with 37 individual plugs, it is modeled as a solid plate. This approach is appropriate for a combination of reasons. First, the tight fit-up between the individual plugs and the shield plate in which they fit means that the thermal resistance between the plugs and the shield plate is relatively low. Second, the relatively low heat flux at this location results in an associated low thermal gradient in the radial direction. Taking these facts together, treating the top shield plug assembly as a solid plate yields a temperature distribution

that is sufficient for the purposes of this calculation. The heat transfer in the axial direction through the shield plug is largely unaffected by the presence of the individual plugs in the shield plate.

The modeling of the heat transfer within the basket assembly consists of a series of heat exchanges between the fuel assemblies, the guide tubes, the spacer plates, the support tubes, and the canister side wall. The heat transfer modeling used to simulate the heat transfer modes for each set of spacer plates and the sections of guide tubes between them forms another layer of thermal submodeling within the SINDA/FLUINT® program. This thermal submodel is repeated and scaled as appropriate to represent other spacer plate sections of the basket assembly. The following paragraphs describe the approach used to simulate the combined heat transfer mechanisms from the fuel assemblies to the canister side wall for a single spacer plate section.

Radiation Heat Transfer

The radiation view factor program RadCAD®²³ is used to compute the radiation exchange factors from the guide tubes to adjacent guide tubes, the spacer plates, and the canister shell. Likewise, radiation heat transfer is modeled from the spacer plates to the adjacent spacer plates and to the canister shell. The emissivity values for the surfaces are taken from material properties listed in Section 3.2. The number of thermal nodes used to simulate the various surfaces of the guide tubes, spacer plates, and canister side wall results in approximately 500 radiation conductors interconnecting the various surfaces between the typical spacer plate section of the basket assembly, or somewhere between 14,000 and 15,000 radiation conductors for the entire basket assembly.

Convection Heat Transfer

Beyond conduction and radiation heat transfer, the principal heat transfer mode within the basket assembly is convection. The fundamental approach and equations used to compute the convection heat transfer within the basket assembly are presented Section 3.6.1. Figure 3.4-9 presents the modeled flow pattern within the horizontal orientation of the canister. The convection heat transfer that occurs between the fuel assemblies and the guide tubes is included as part of the Manteufel and Todreas¹⁰ non-linear form of the lumped $k_{\text{eff}}/h_{\text{edge}}$ model for a typical BWR fuel assembly (see Section 3.2.2).

Canister to Transportation Cask Model

The W74 canister thermal model described above is combined with the TS125 Transportation Cask thermal model to allow thermal analysis of the composite transportation package. The transportation cask assembly thermal model is described in detail in Section 3.4.1 of the FuelSolutions™ TS125 Transportation Cask SAR.² The modeling of the W74 canister in the transportation cask is accomplished using the Thermal Desktop®⁵ program to define the geometric relationship between the TS125 Transportation Cask thermal model and the W74 canister thermal model. Once defined, the Thermal Desktop® program automatically computes

²³ RadCAD®, *CAD Based Thermal Radiation Analyzer*, Version 2.0, prepared for NASA, Johnson Spacecraft Center, Contract NAS8-40560, by Cullimore and Ring Technologies, Inc., Littleton, Colorado, 1997.

the conduction and radiation links between the various thermal nodes representing the W74 canister shell and those representing the interior of the TS125 Transportation Cask.

The canister does not sit symmetrically within the transportation cask, but rests on two 1/8-inch thick guide rails attached to the transportation cask inner shell. Since this configuration results in eccentric positioning of the canister within the cask, the Thermal Desktop® conservatively calculated the gap conductance between the canister shell and the inner shell of the cask as a function of the position around the canister's circumference. The contact conductance²⁴ between the canister and the guide rails is computed based on the weight of the canister and the area of contact between the canister and the guide rails.

Impact of Fission Gases on the Thermal Performance of the Canister and Cask

The predicted change in gas mixture properties as a function of fission gas concentration is made using the mole fractions of the various constituents of the gas mixture and a complex function of viscosities and molecular weights. The estimation technique is based on the kinetic theory of gases. The evaluation, presented in Section 3.6.3, demonstrates that the fission gas release associated with a 3% fuel rod failure rate for NCT conditions will have no effect on the safety analysis for the FuelSolutions™ W74 canister in the TS125 Transportation Cask. The evaluation also demonstrates that a 100% fuel rod failure rate under accident conditions will have only marginal effects on the predicted temperatures within the W74 canister.

3.4.1.2 Test Thermal Model

In accordance with 10CFR71.41, and as presented herein, detailed thermal analyses of the W74 canister within the transportation cask are performed to demonstrate compliance with the NCT tests specified in 10CFR71.71. As a result, subsequent transportation package or scale model thermal testing is not required. However, thermal acceptance testing of the transportation cask will be performed as discussed in Section 8.1.6 of the FuelSolutions™ TS125 Transportation Cask SAR.²

3.4.2 Maximum Temperatures

The FuelSolutions™ W74 design basis thermal load cases are summarized in Table 3.1-1. For the determination of the W74 canister thermal rating, only steady-state NCT hot (case 1) is considered. The combined W74 canister and transportation cask thermal model is exercised using the NCT hot boundary conditions (100°F ambient w/solar) for determination of the W74 canister thermal rating.

The methodology discussed in Section 3.1.3.2 is implemented for the thermal rating case. The design basis canister axial heat profile for Big Rock Point fuel in Figure 3.1-1 is applied as a boundary condition for NCT hot. The allowable material temperatures in Table 3.3-1 are assumed and the total canister heat load (Q_{Total}) is gradually increased until an allowable material temperature is reached. The W74 canister maximum heat load ratings determined via this approach are presented in Table 3.1-3.

²⁴ Based on Curve #11 in Figure 8, page 4-19, Rohsenow, Harnett, and Ganic, *Handbook of Heat Transfer Fundamentals*, 2nd Edition, McGraw-Hill, Inc., 1989.

Comparisons of the resulting canister and cask component temperatures with the allowable component temperatures for operations at the qualified W74 canister thermal rating are presented in Table 3.4-1 under the NCT Case 1 column. Figure 3.4-10 presents the sensitivity of the W74 canister and transportation cask components to variations in heat load. As indicated in Table 3.4-1 and Figure 3.4-10, the controlling component for the W74 canister and TS125 cask assembly is the NS-4-FR neutron shielding material. Both the maximum allowable temperature of 338°F and the maximum radial average allowable temperature of 300°F are reached at a heat load of approximately 23.5 kW. The temperatures for the remaining canister and cask components show significant thermal margin at this heat load. A W74 canister heat load of 23.5 kW yields a LHGR of 0.205 kW/inch.

Since the analysis of the FuelSolutions™ TS125 Transportation Cask with a generic canister presented in the FuelSolutions™ TS125 Transportation Cask SAR² determined that a maximum canister heat load of 22.0 kW can be accommodated, the thermal rating for the W74 canister is also limited to 22.0 kW for administrative reasons. The higher thermal capacity of the W74 canister/TS125 Transportation Cask combination versus that seen for the generic canister analysis occurs because the design heat generation profile for the W74 canister is spread over a greater axial length due to its double stack of fuel baskets than the heat load profile used for the generic canister. In contrast, the LHGR of 0.192 kW/inch, corresponding to the BRP heat generation profile having a total heat generation of 22.0 kW, is not encompassed by the maximum LHGR of the Q_{\max} heat generation profile upon which the FuelSolutions™ TS125 Transportation Cask thermal rating is based. However, as discussed in Section 3.1.3.3, the BRP profile is compliant with the TS125 transportation cask thermal requirements since it does not produce peak temperatures in the cask's inner shell that exceed those calculated for the Q_{\max} profile in the FuelSolutions™ TS125 Transportation Cask SAR.

The FuelSolutions™ W74 canister maximum thermal ratings within the TS125 Transportation Cask are applied for the full range of NCT cases presented in Table 3.1-1 in order to determine the resultant transportation package system temperatures. Maximum component temperatures are presented in Table 3.4-1. All W74 canister component temperatures are within their material allowable temperatures for each load case. Note that the maximum temperatures presented in the table are based on operations at the thermal rating for the W74 canister only. A presentation of the bounding transportation cask temperatures at the cask thermal ratings is provided in the FuelSolutions™ TS125 Transportation Cask SAR.²

Figure 3.4-11 illustrates the axial temperature distributions at Q_{\max} within the SNF assemblies, spacer plates, and canister side wall for NCT hot (i.e., case 1, 100°F w/solar). The temperature distributions are along the hottest portion of the canister and through the top of the cask. The variation in the heat load profile in the double stack of Big Rock Point fuel is clearly visible in the plots. Figure 3.4-12 illustrates a similar distribution, except that the cask temperatures are taken along a radial cut 15° above the bottom of the cask. The presence of the cask's shear block can be clearly seen by its impact on the temperature distribution near the cask's mid-length. Figure 3.4-13 illustrates the associated radial temperature distributions for selected axial positions. The presence of the helium gap between the canister and the cask's inner shell, and the assumed air gap between the lead gamma shield and the cask's outer shell, can be seen in the large thermal gradients at these locations.

Figure 3.4-14 and Figure 3.4-15 illustrate the axial and radial temperature distributions, respectively, at the Q_{\max} heat load for NCT cold (i.e., case 3, -20°F w/o solar).

Figure 3.4-16 through Figure 3.4-18 present the temperature distributions for the hottest stainless steel spacer plate, hottest carbon steel spacer plate, and the engagement plate, respectively, for NCT hot (i.e., 100°F w/solar). Figure 3.4-19 through Figure 3.4-21 present the temperature distributions in these same components for NCT cold (i.e., case 3, -20°F w/o solar).

3.4.3 Minimum Temperatures

The minimum temperatures in the W74 canister and transportation cask components under the NCT cold environment (i.e., case 5, -40°F w/o solar) are listed in Table 3.4-1. Note that the temperatures shown are at the design basis canister thermal rating and, therefore, do not represent the lowest expected component temperatures. This case creates the maximum thermal gradient.

The low temperature compatibility of the W74 canister and transportation cask components is also evaluated for the bounding NCT cases with -20°F and -40°F ambient temperature, zero decay heat load, and no insolation (Table 3.1-1, cases 4 and 6). The steady-state temperatures of the W74 canister and transportation cask components for these analytically trivial cases are -20°F and -40°F, respectively. These temperature levels are within the allowable minimum temperatures for all components.

3.4.4 Maximum Internal Pressures

The W74 canister and transportation cask MNOP pressures for NCT are presented in Table 3.4-2. The W74 canister and transportation cask helium bulk temperatures and pressures are presented for the NCT hot and NCT cold thermal load conditions. The listed canister and cask pressures assume containment by the canister shell pressure boundary and no cladding failures. The MNOP is based on the initial cask helium backfill, the canister backfill, SNF rod fill gas, SNF fission gases, and no containment by the canister shell pressure boundary. Since SNF fill and fission gas quantities depend on the specific SNF assembly type, the maximum pressure is calculated for each SNF assembly type that can be accommodated by the W74 canister.

Internal gas pressure is determined within the SINDA/FLUINT^{®6} thermal model using a volume weighted average for each condition. The W74 canister cavity is assumed to be backfilled with helium to achieve an internal pressure of 24.7 psia under normal hot storage conditions. The transportation cask annulus is assumed to be backfilled with helium to achieve a pressure of 14.7 psia at room temperature (70°F). Since it can safely be assumed that the canister/cask temperatures will be above 70°F at the time of backfill, the actual cask cavity pressures will be less than those determined based on this assumed quantity of helium backfill gas.

The W74 canister and transportation cask temperatures presented in Section 3.4.2 are determined based on assumed canister and cask initial internal pressures without SNF rod failures. The MNOP presented below considers postulated SNF rod failures, but conservatively uses the helium temperatures determined by the thermal analysis. The assumption of no SNF rod failures for the thermal modeling is conservative since the increased canister gas pressure resulting from such

failures enhances convection heat transfer and results in lower canister temperatures and a corresponding lower calculated MNOP.

The pressure in the cask cavity is based on the initial cask helium backfill, the canister backfill, SNF rod fill gas, and SNF fission gases. Specifically, the transportation cask MNOP with a loaded W74 canister is determined assuming (1) no containment by the canister shell pressure boundary, (2) an NCT environment (100°F ambient w/solar or -20°F ambient w/o solar), (3) an initial cask annulus helium backfill of 14.7 psia (at 70°F), (4) an initial canister backfill pressure of 24.7 psia (at normal hot storage conditions with 1% rod failures), (5) minimum cask and canister void volumes, and (6) postulated failure of 3% of the SNF rods. For each postulated rod failure, 100% of the rod fill gas, 30% of the SNF fission gas yield, and 30% of the gas generated in PWR control components are assumed to be released into the cavity.

The average gas temperature inside the cask is determined by using volume weighted averaging of the canister bulk helium temperature and the cask annulus bulk helium temperature. Since SNF fill and fission gas quantities depend on the specific Big Rock Point fuel assembly type, the maximum pressure is calculated for each SNF assembly type that can be accommodated within the W74 canister.

Fission gas generation depends primarily on the fuel assembly MTU loading and burnup level. For the purpose of rod pressure determination, the only significant fission gas contributors are Krypton (Kr) and Xenon (Xe). All isotopes of Kr and Xe are considered for fission gas generation. Other fission products are neglected because they either exist in insignificant quantities or do not exist in the gaseous form at NCT temperatures.

The smallest loaded W74 canister free volume, based on worst-case geometry tolerances, is conservatively used. Both W74 canister configurations and fuel loading options are evaluated to determine the limiting free volumes for each fuel class and type. Both canister configurations have the same outer dimensions. Worst-case canister shell and cask tolerances are considered to conservatively determine the smallest resultant transportation cask annulus volume.

The effects of phase changes, gas generation, or chemical decomposition have been neglected for the pressure evaluation since the canister is drained and vacuum dried prior to closure, the cask annulus is drained prior to transport, and both the canister and cask annulus are backfilled with inert gas (helium).

Although the quantity of helium in the SNF rods will increase slightly due to fission product decay over the post-irradiation time period prior to transportation, the reduction in canister decay heat load, corresponding cask average helium temperature, and resultant internal pressure will offset this effect.

3.4.4.1 Fuel Rod Fill Gas

The total moles of helium fill gas within each fuel assembly depends on the assembly specific fuel rod total free volume and the fill gas pressure. Since the rods are backfilled during fabrication and prior to irradiation or exposure to elevated temperatures, the nominal rod dimensions are used. The ideal gas law applies for determination of fuel rod fill gas moles:

$$N_{Fill} = \frac{P_{Fill} V_{rod}}{RT}$$

where:

- P_{Fill} = Rod fill gas pressure (atm)
- V_{rod} = Fuel assembly rod internal free volume (liters)
- R = Ideal Gas Constant (0.0821 atm-liter/gmole-°K)
- T = Temperature at rod backfill (294°K)

Table 3.4-3 provides a summary of the moles of rod fill gas moles within the Big Rock Point fuel assemblies.

3.4.4.2 Fuel Rod Fission Gas Generation

Fission gas generation is primarily dependent on the fuel MTU loading and burnup level. For Big Rock Point Fuel, only 40 GWd/MTU burnup is evaluated. For rod fission and fill gas yield calculations, loading of 74 assemblies is conservatively assumed instead of the 64 assembly loading limit for the W74 canister.

Two independent methods are used to determine the fission gas generation. The first method uses the RADDB²⁵ to obtain the quantity of Kr and Xe gases generated for the given burnup levels, assuming standard enrichment and a representative 5-year decay. The second method is a direct calculation of the moles of Kr and Xe fission gas using standard industry constants and fuel specific burnup and MTU loading. The method that results in the largest quantity of fission gas generation is conservatively used in the pressure calculations. Basic methodologies are described below:

Fission Gas Yield from RADDB

$$N_{\text{Kr}} = (m_{\text{Kr}} \frac{\text{grams}}{\text{MTIHM}}) (\frac{\text{mole}}{83.8 \text{grams Kr}}) (\frac{\text{MTU}}{\text{assy}}) (\frac{74 \text{assy}}{\text{canister}})$$

$$N_{\text{Xe}} = (m_{\text{Xe}} \frac{\text{grams}}{\text{MTIHM}}) (\frac{\text{mole}}{131.3 \text{grams Xe}}) (\frac{\text{MTU}}{\text{assy}}) (\frac{74 \text{assy}}{\text{canister}})$$

$$N_{\text{Fission}} = N_{\text{Kr}} + N_{\text{Xe}}$$

where:

- N_{Kr} = gmoles of Kr/canister
- N_{Xe} = gmoles of Xe/canister
- m_{Kr} = grams Kr/MTIHM (from RADDB)
- m_{Xe} = grams Xe/MTIHM (from RADDB)
- MTU/assy = Fuel assembly class-specific

²⁵ LWR Radiological Data Base (RADDB) v 1.1, U.S. Department of Energy, Office of Civilian Radioactive Waste Management, prepared by Oak Ridge National Laboratory, July 1992.

Calculation of Fission Gas Yield

$$N_{Fission} = \left(\frac{GWd}{MTU}\right) \left(1.0 \cdot 10^9 \frac{W}{GW}\right) \left(86,400 \frac{sec}{day}\right) \left(\frac{MeV}{1.602 \cdot 10^{-13} Joules}\right) \left(\frac{1 fission}{207 MeV}\right) \left(0.303 \frac{atoms Kr + Xe}{fission}\right) \cdot \left(\frac{mole}{6.02 \cdot 10^{23} atoms}\right) \left(\frac{MTU}{assy}\right) \left(\frac{74 assy}{canister}\right)$$

where:

$N_{Fission}$ = gmoles of Kr and Xe fission gas/canister

MTU/assy = Fuel assembly class-specific

Industry constants:

207 MeV/fission²⁶

0.303 moles Kr and Xe/fission²⁷

Moles of rod fission gas for the 40 GWd/MTU burned Big Rock Point fuel are summarized in Table 3.4-3.

3.4.4.3 Transportation Cask MNOP

The transportation cask MNOP is calculated as follows:

$$MNOP = \frac{N_{Cask} RT_{NCT}}{V_{Cask}}$$

$$N_{Cask} = N_{Cask Annulus} + N_{Canister} + N_{SNF}$$

$$N_{SNF} = 0.03 \cdot \left[N_{SNF fill} + 0.30 \cdot N_{SNF fission} \right]$$

where:

$N_{Cask Annulus}$ = Total moles cask annulus backfill gas

$N_{Canister}$ = Total moles canister cavity backfill gas

$N_{SNF Fill}$ = Total moles SNF rod fill gas within canister

$N_{SNF Fission}$ = Total moles SNF rod fission gas yield (30% released) within canister

R = Ideal Gas Constant (0.0821 atm-liter/gmole-°K)

V_{Cask} = Combined canister and cask cavity free volume (liters)

T_{NCT} = Volume weighted average helium temperature within cask (°K)

²⁶ Lamarsh, John R., *Introduction to Nuclear Engineering*, Addison-Wesley Publishing Company, 1977.

²⁷ Olander, Donald R., *Fundamental Aspects of Nuclear Reactor Fuel Elements*, Energy Research and Development Administration, 1976.

The FuelSolutions™ TS125 Transportation Cask MNOP with the W74 canister and 40 GWd/MTU Big Rock Point fuel is 10.7 psig, as presented in Table 3.4-2. Significant margin exists between this calculated MNOP and the transportation cask design pressure of 75 psig. Table 3.4-4 presents the calculated MNOP for each fuel assembly class that may be accommodated in the W74 canister.

3.4.5 Maximum Thermal Stresses

Section 2.3 of this SAR gives thermo-mechanical properties of the W74 canister materials that may cause temperature-induced stresses in the transportation package. Using the temperature distributions determined from the NCT thermal analyses, thermal stress analyses of the FuelSolutions™ W74 canister are presented in Sections 2.6.1 and 2.6.2 of this SAR. The impact of differential thermal expansion on clearances between transportation package components is specifically addressed. These structural analyses demonstrate the ability of the packaging components to maintain positive design margins for all combinations of NCT loads.

3.4.6 Evaluation of Package Performance for Normal Conditions of Transport

The steady-state thermal analysis results demonstrate that the W74 canister, transportation cask, and impact limiter allowable material temperatures under NCT hot environment are met for the maximum W74 canister thermal rating presented in Table 3.1-3. Additionally, the minimum material temperatures under the NCT cold environment with zero decay heat also meet material specifications. The MNOP resulting from the NCT hot environment and conservative assumptions is within the transportation cask maximum design pressure. Therefore, the W74 canister is suitable for transportation of Big Rock Point SNF within the FuelSolutions™ TS125 Transportation Cask.

Analysis results for NCT hot (case 1) shown in Table 3.4-1, Figure 3.4-11 through Figure 3.4-13, and Figure 3.4-16 through Figure 3.4-18 are used for the NCT shock and vibration, and the 1-foot drop structural evaluations presented in Sections 2.6.5 and 2.6.7 of this SAR, respectively. Analysis results for NCT cold (case 3, -20°F) presented in Figure 3.4-14 through Figure 3.4-15, and Figure 3.4-19 through Figure 3.4-21 are also considered in the structural analyses presented in Sections 2.6.5 and 2.6.7 of this SAR.

Table 3.4-1 - FuelSolutions™ W74 Canister Maximum System Temperatures for NCT

Component	NCT Thermal Load Condition ⁽¹⁾			Maximum Allowable Temperature
	Case 1 (100°F/Solar) ⁽²⁾	Case 3 (-20°F/No Solar) ⁽³⁾	Case 5 (-40°F/No Solar)	
Peak Fuel Cladding	346.7°C/656.1°F	305.9°C/582.6°F	299.5°C/571.1°F	400°C/752°F
Guide Tube	628°F	547°F	534°F	800°F
Spacer Plates				
Stainless Steel	590°F	507°F	494°F	800°F
Carbon Steel	615°F	532°F	519°F	700°F
Support Tube	599°F	520°F	508°F	700°F
Avg. Canister Gas	528°F	445°F	431°F	N/A
Canister Shell	475°F	389°F	376°F	800°F
Avg. Canister-Cask Gas	379°F	287°F	272°F	N/A
Inner Cask Shell ⁽⁴⁾	363°F	273°F	259°F	800°F
Gamma Shield (Lead) ⁽⁴⁾				
Maximum	354°F	263°F	248°F	620°F
Bulk Average	334°F	240°F	226°F	620°F
Outer Cask Shell	328°F	227°F	211°F	800°F
NS-4-FR Shield ^(4,5)				
Max. Radial Avg.	289°F	186°F	169°F	300°F
Bulk Average	261°F	156°F	139°F	300°F
Neutron Shield Jacket ^(4,6)				
Near Shear Block	284°F	179°F	162°F	350°F
Elsewhere	213°F	108°F	91°F	350°F
Personnel Barrier	139°F	-7°F	-28°F	185°F
Impact Limiter ⁽⁷⁾				
Max. Honeycomb	165°F	30°F	10°F	300°F
Bulk Avg. Honeycomb	151°F	14°F	-7°F	200°F
Cask Metallic Seals				
Cask Closure	246°F	137°F	121°F	932°F
Vent & Drain Ports	262°F	154°F	138°F	662°F

Notes:

- (1) All temperatures in this table are based on heat loads of 22.0 kW with Big Rock Point Axial Heat Profile.
- (2) W74 canister heat load qualification is based on NCT hot conditions.
- (3) NCT hot (100°F) and NCT cold (-20°F) conditions with maximum decay heat and no solar apply as initial conditions for the HAC fire evaluation presented in Section 3.5.
- (4) Temperatures computed along an axial cut plane that passes through the “rub rails” to capture the peak temperatures noted in the cask. Lower temperatures are noted at the other cask circumference positions.
- (5) The solid neutron shield material temperature is presented in two forms: a radial average temperature at the axial location with the highest temperature and as bulk average temperature across the length of the neutron shield. Both averages are limited to 300°F or less for out gas considerations from the material. Per the heat load qualification process illustrated in Figure 3.4-10, the maximum neutron shield material temperature is below 338°F.
- (6) A 350°F limit used based on the maximum operating temperature for the epoxy coating. The operating limit for the carbon steel material is 700°F.
- (7) A 300°F limit used to provide a 50°F margin below the cure temperature for the thermoset adhesive used in the fabrication of the honeycomb material. A 200°F limit used for bulk average temperature for structural considerations.

Table 3.4-2 - Transportation Package NCT Internal Pressures

Parameter	Case 1 (100°F/Solar)	Case 3 (-20 °F/No Solar)
Canister Helium Bulk Temperature ⁽¹⁾	528°F	445°F
Canister Helium Bulk Pressure ^(1,2)	24.4 psia	22.3 psia
Cask Annulus Helium Bulk Temperature ⁽¹⁾	379°F	287°F
Cask Annulus Helium Bulk Pressure ⁽²⁾	23.3 psia	20.7 psia
Average Mixed Volume Helium Bulk Temperature ⁽³⁾	522°F	438°F
MNOP ⁽⁴⁾	25.4 psia (10.7 psig)	23.2 psia (8.5 psig)

Notes:

- (1) Temperatures are based on heat loads of 22.0 kW with the Big Rock Point axial heat profile.
- (2) Canister and cask pressures assuming no breach in the canister pressure boundary and no fuel cladding failures. Estimated canister pressure is based on an initial canister backfill of 10 psig under normal hot storage conditions (100°F within the W150 Storage Cask and with 1% SNF rod failures) and the ideal gas law. The estimated cask annulus pressure conservatively assumes a gas backfill to one atmosphere at a mean temperature of 70°F.
- (3) Average mixed volume helium bulk temperature is computed based on a volume-weighted average of the canister and cask annulus gas temperatures assuming no containment by the canister shell pressure boundary. The average temperature is presented for the specific Big Rock Point fuel assembly type that results in the highest MNOP.
- (4) Maximum Normal Operating Pressure (MNOP) is determined for the hot environment assuming no containment by the canister shell and 3% SNF fuel rod failures. The cold environment is considered to support the fatigue evaluation.

Table 3.4-3 - W74 Canister SNF Gas

Fuel Class	Rod Fill Gas/Canister (moles)	Rod Fission Gas/Canister (moles)⁽¹⁾
GE 9x9	7.7	153.1
GE 11x11	7.4	137.8
ANF 11x11	13.2	146.4
ANF/Jersey 9x9	34.9	140.9
NFS 11x11	22.4	143.1

Note:

⁽¹⁾ Fission gas generation based on 40 GWd/MTU burned BWR fuel. Values shown are the maximum postulated to be released into the canister-cask free volume under 100% rod failure (30% of generated quantity).

Table 3.4-4 - W74 Canister Free Volume and MNOP⁽¹⁾

Fuel Class	Canister Type	Total Free Volume (liters)⁽²⁾	Canister Backfill Gas (moles)⁽³⁾	Cask Annulus Backfill Gas (moles)⁽⁴⁾	Average Helium Gas Temperature (°F)⁽⁵⁾	MNOP (psig)
GE 9x9	74M	6391.7 + 278.1	240.5	11.5	522	10.6
GE 11x11	74M	6359.3 + 278.1	239.5	11.5	522	10.6
ANF 11x11	74M	6359.3 + 278.1	239.3	11.5	522	10.6
ANF/Jersey 9x9	74M	6385.0 + 278.1	240.1	11.5	522	10.7
NFS 11x11	74M	6419.0 + 278.1	241.5	11.5	522	10.6

Notes:

- (1) Quantities are shown for the limiting fuel assembly type and canister free volume that results in the highest calculated MNOP
- (2) Total free volume is the canister internal free volume combined with the canister-cask annulus free volume.
- (3) Canister backfill moles are based on 10 psig at normal hot storage (100°F in the W150 Storage Cask) conditions with 1% SNF rod failures.
- (4) Cask annulus backfill moles are based on 1 atm at room temperature (70°F).
- (5) Average helium temperature is the volume weighted average of the canister bulk helium (528°F) and cask annulus helium (379°F) temperatures for NCT Hot.

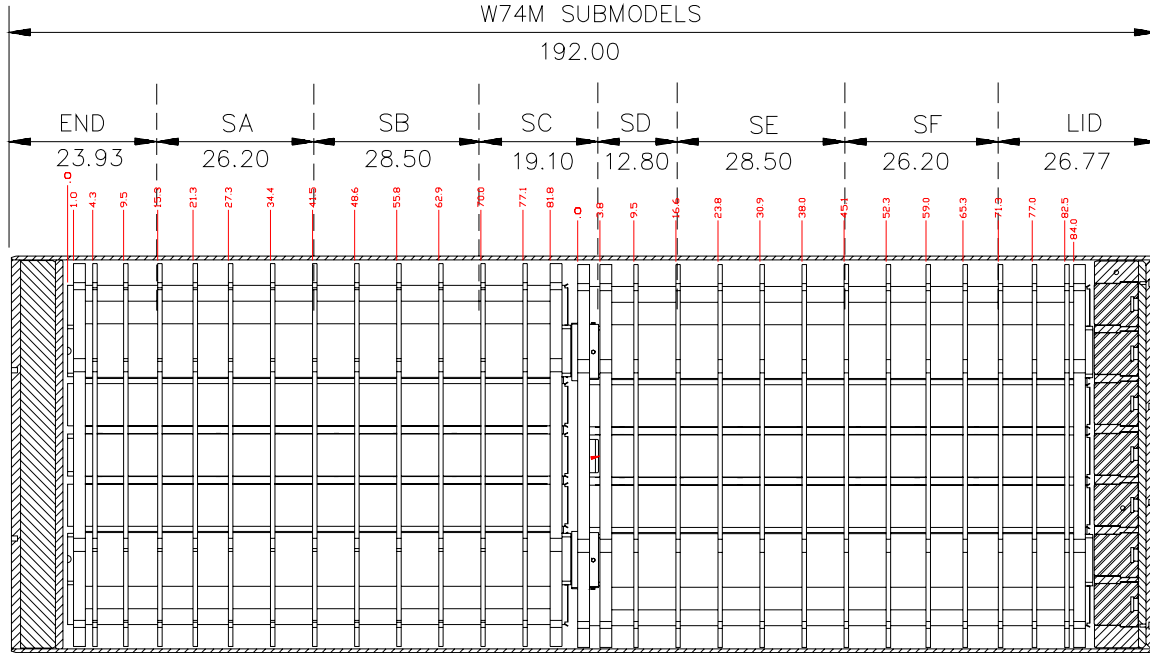


Figure 3.4-1 - FuelSolutions™ W74M Canister Thermal Submodel Layout

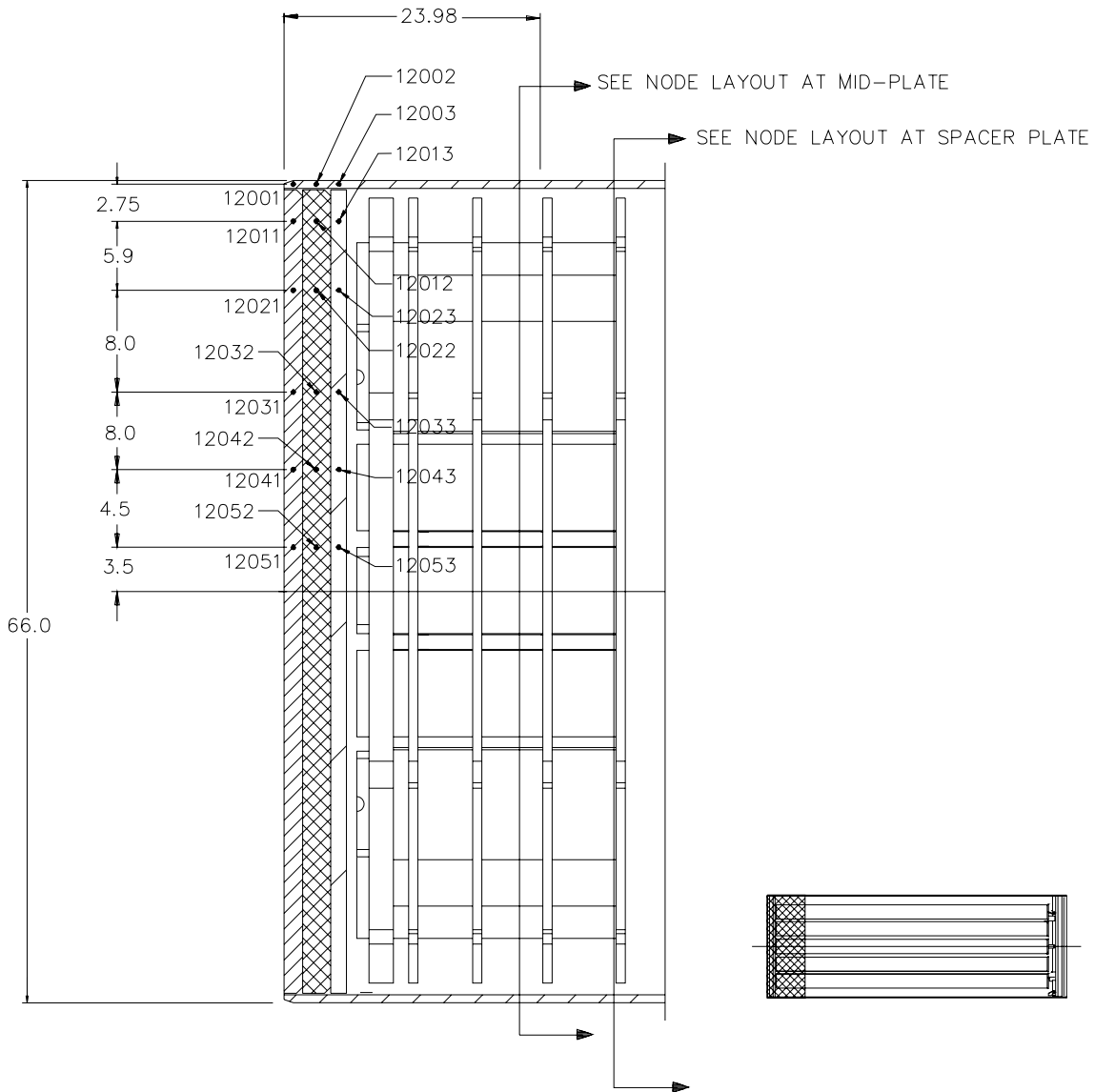


Figure 3.4-2 - Node Layout for W74 Canister Bottom End

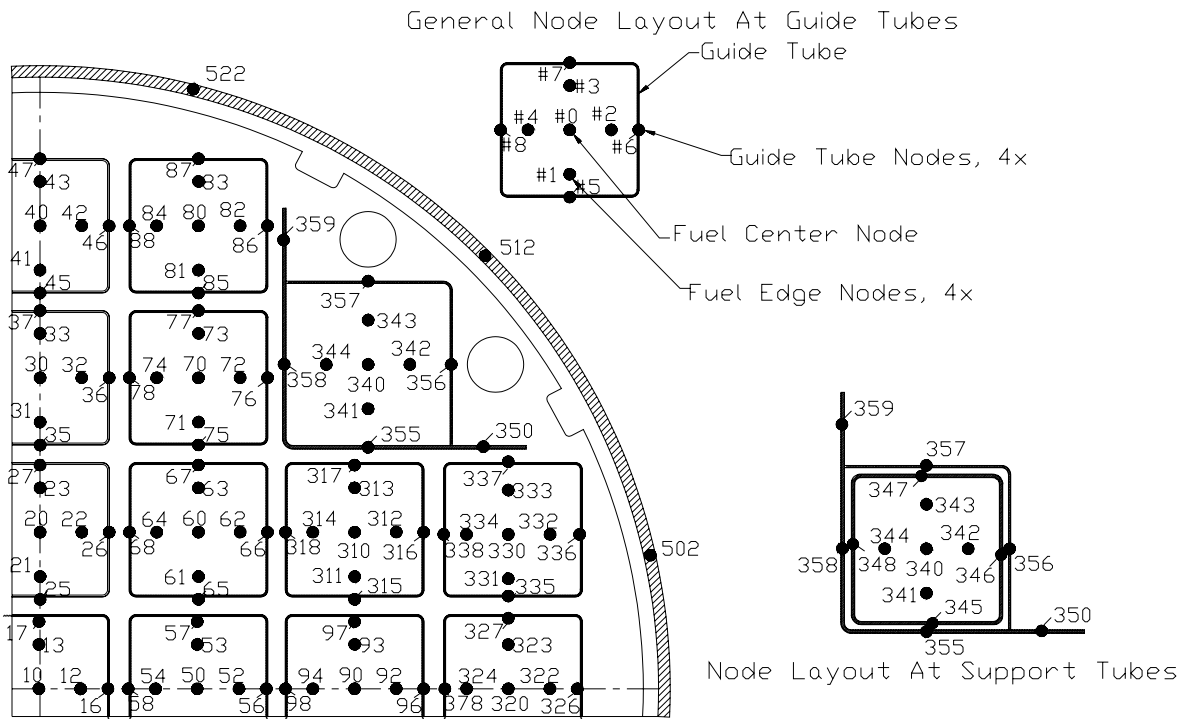


Figure 3.4-3 - Typical Node Layout Between W74 Spacer Plates

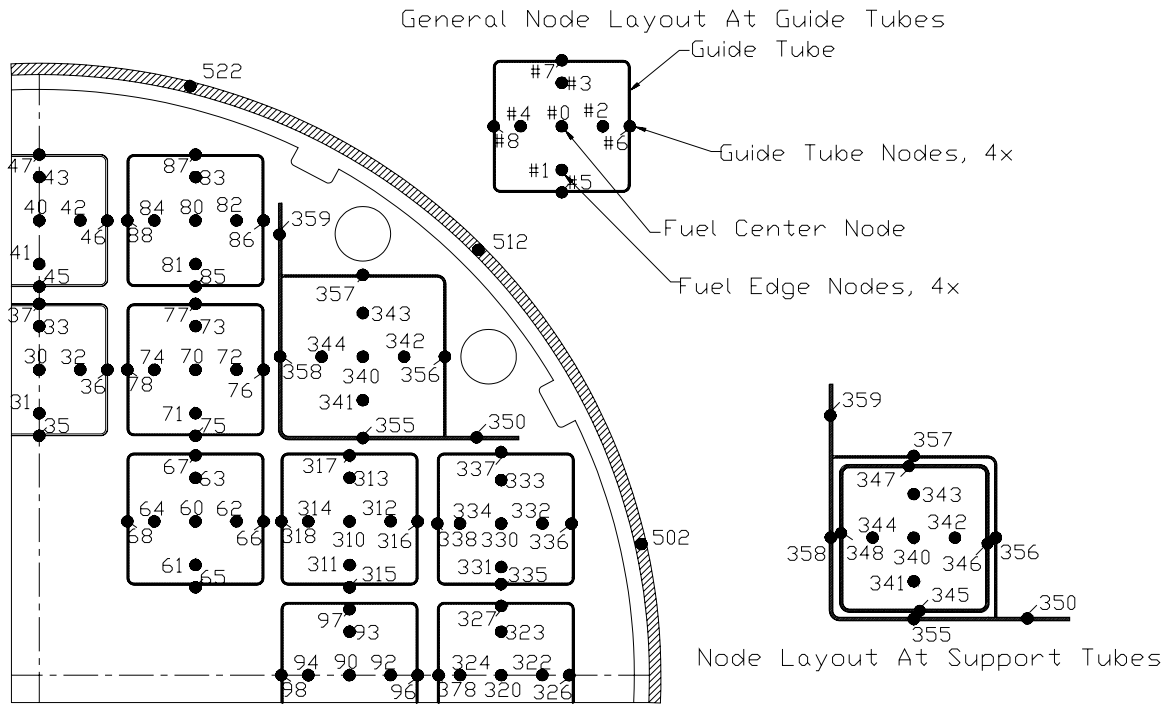


Figure 3.4-4 - Node Layout for W74 Canister Fuel Load Configuration

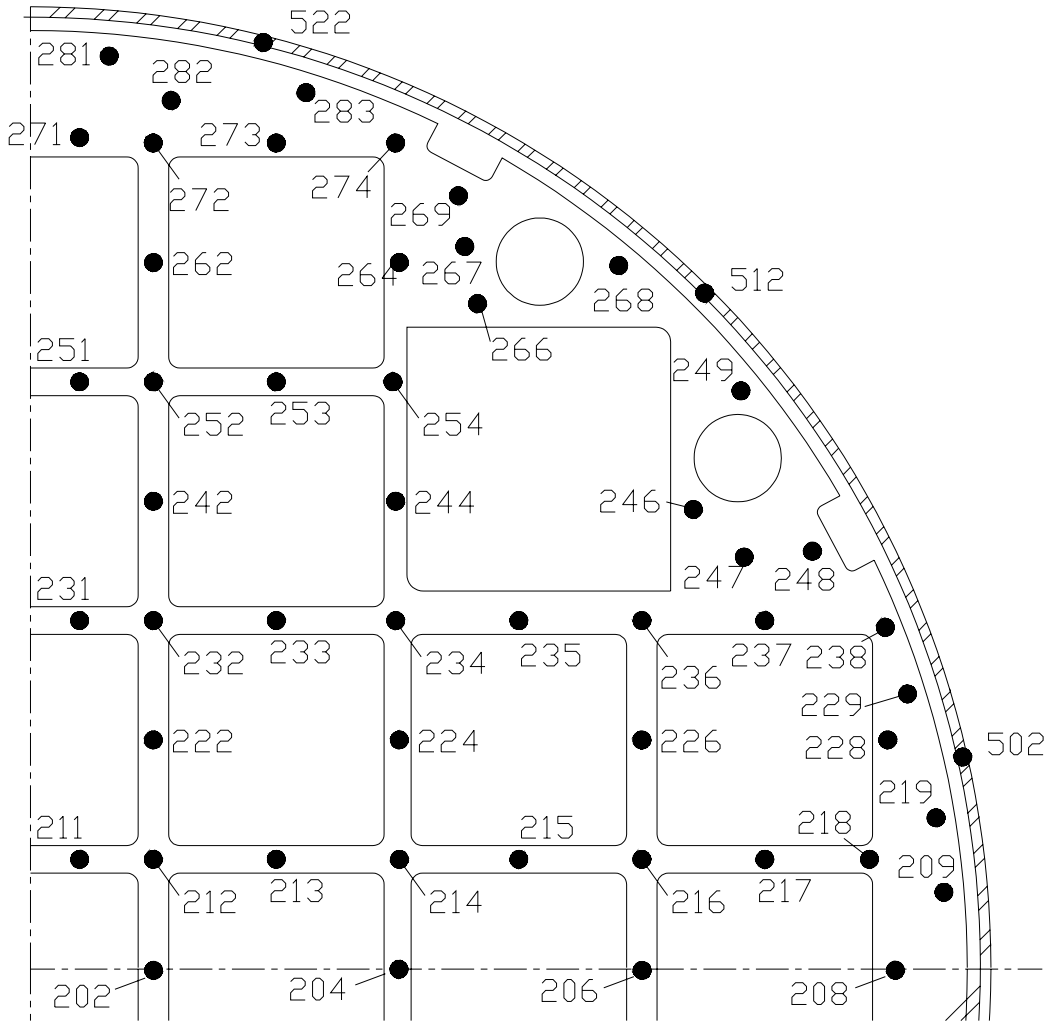


Figure 3.4-5 - Typical Node Layout for W74 Spacer Plate

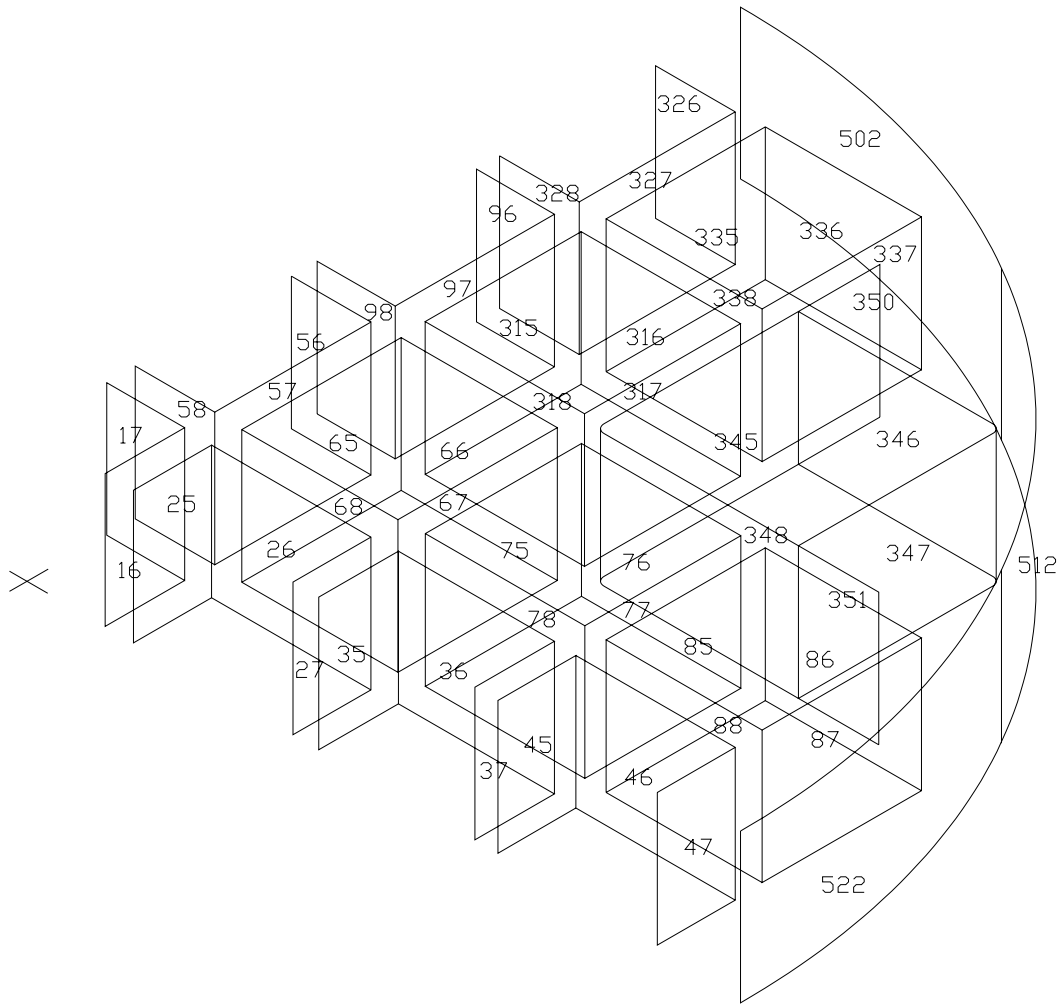


Figure 3.4-6 - Isometric View of Node Layout Between Typical Set of W74 Spacer Plates

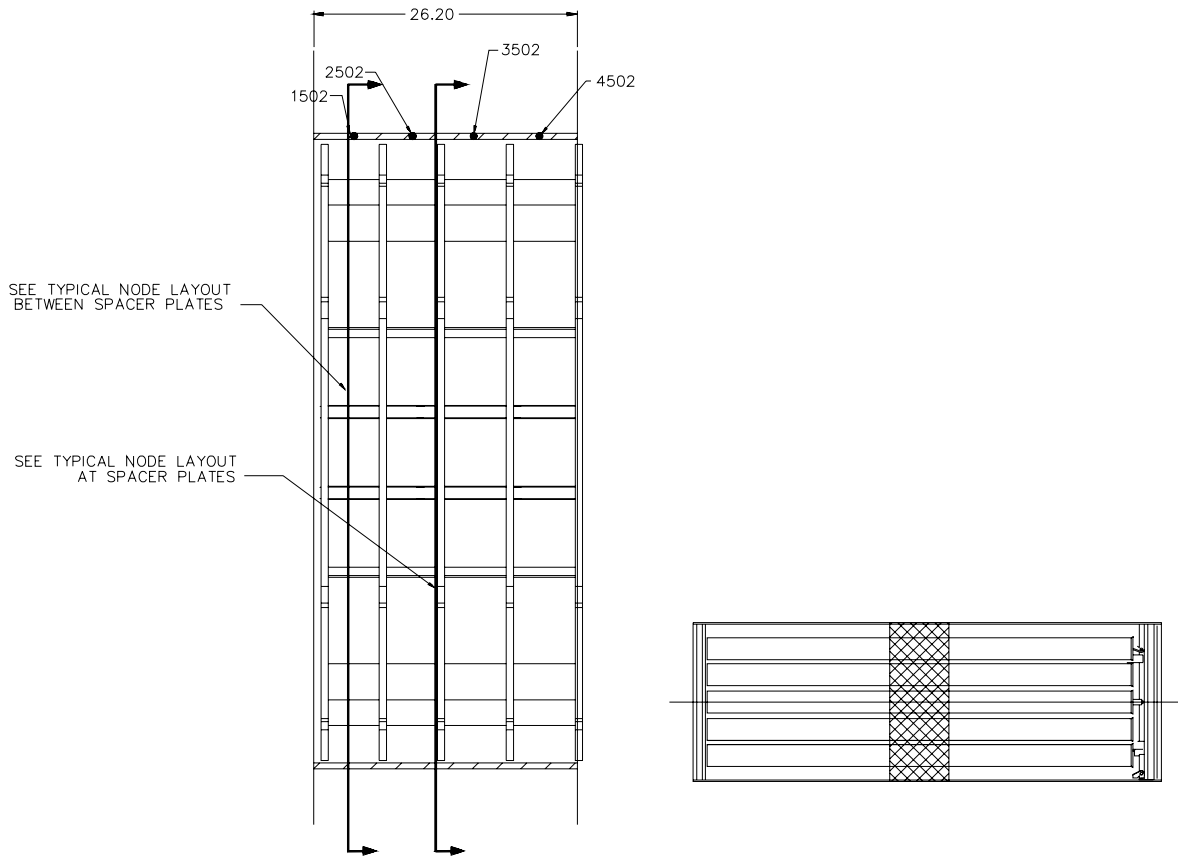


Figure 3.4-7 - Node Layout for W74 Canister Mid-Length Section

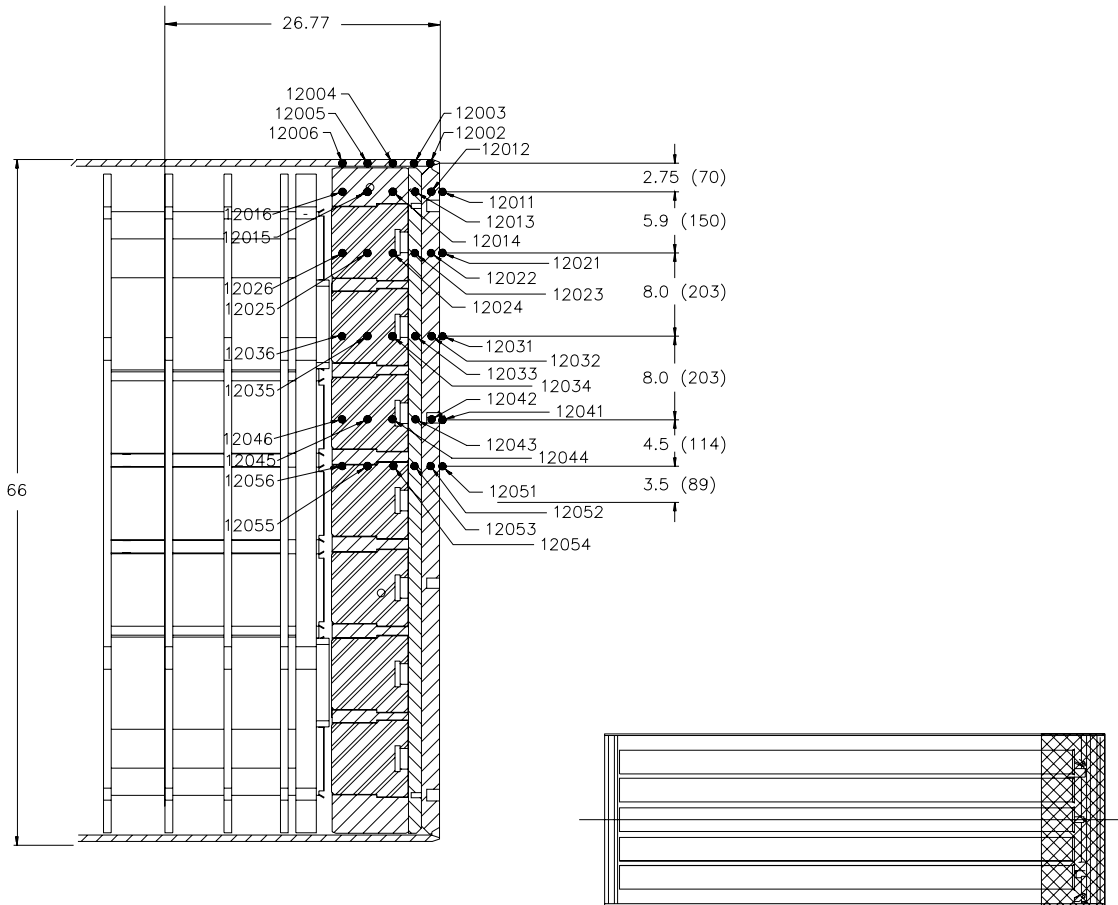


Figure 3.4-8 - Node Layout for W74 Top End

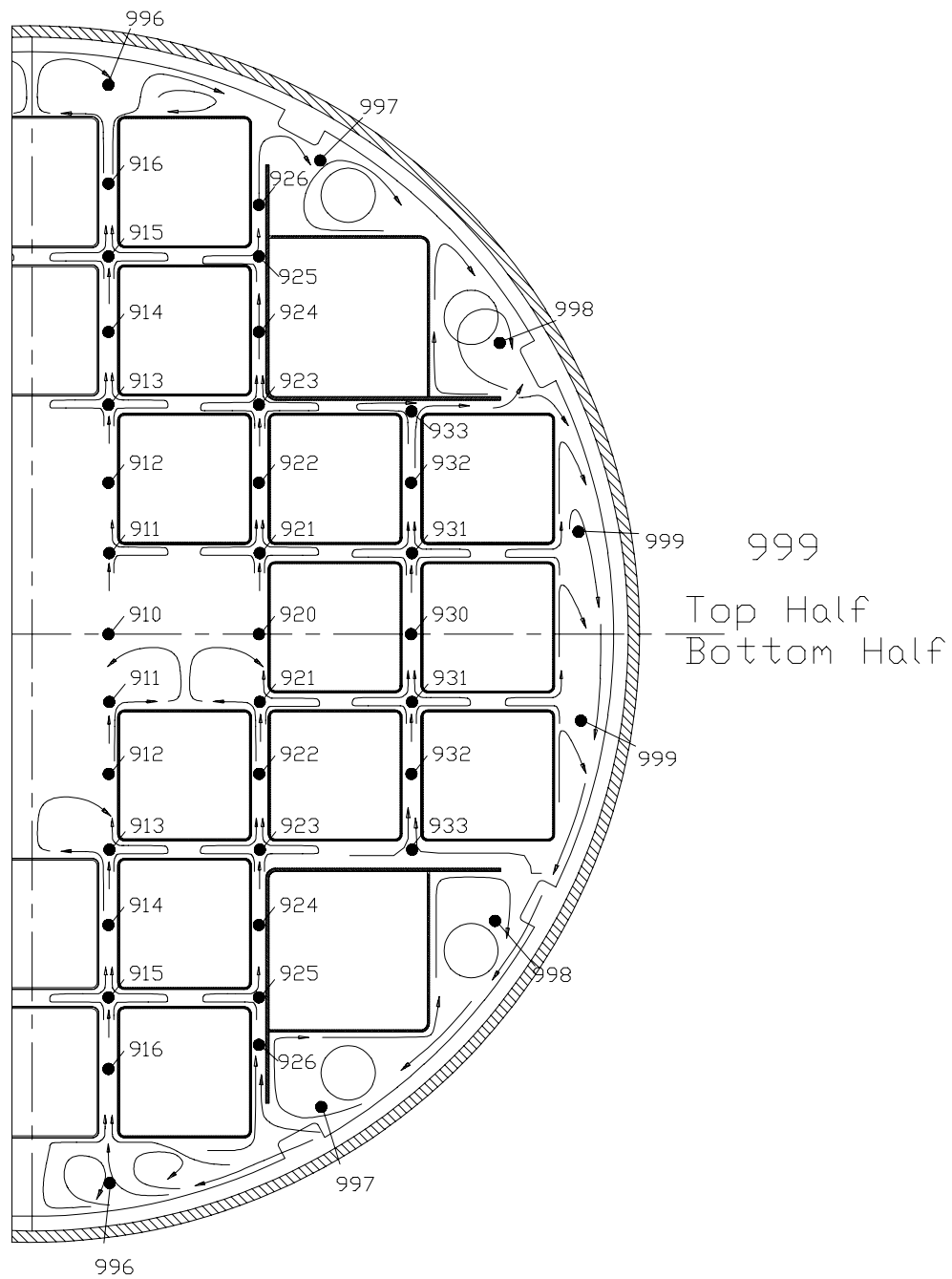


Figure 3.4-9 - Assumed Flow Pattern within Horizontal Canister

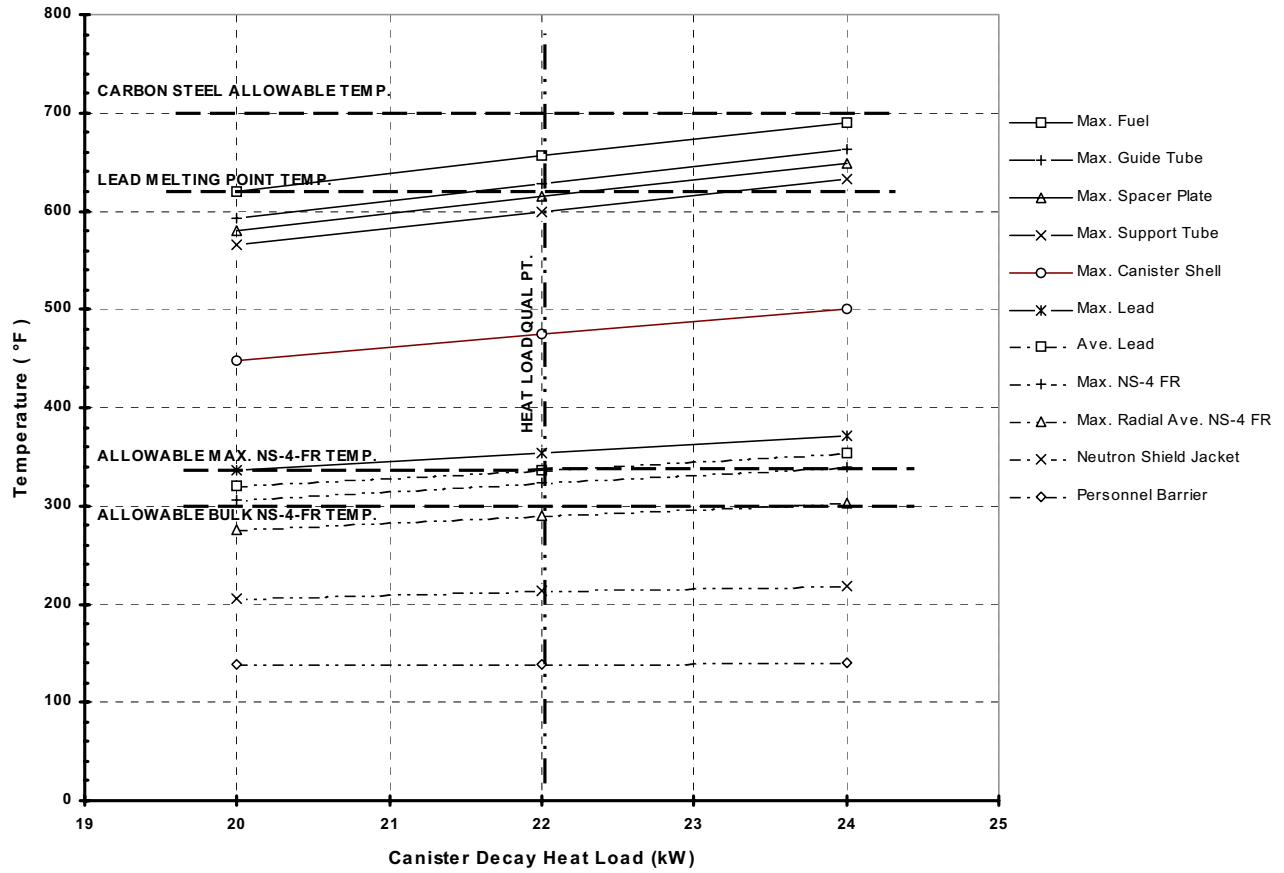
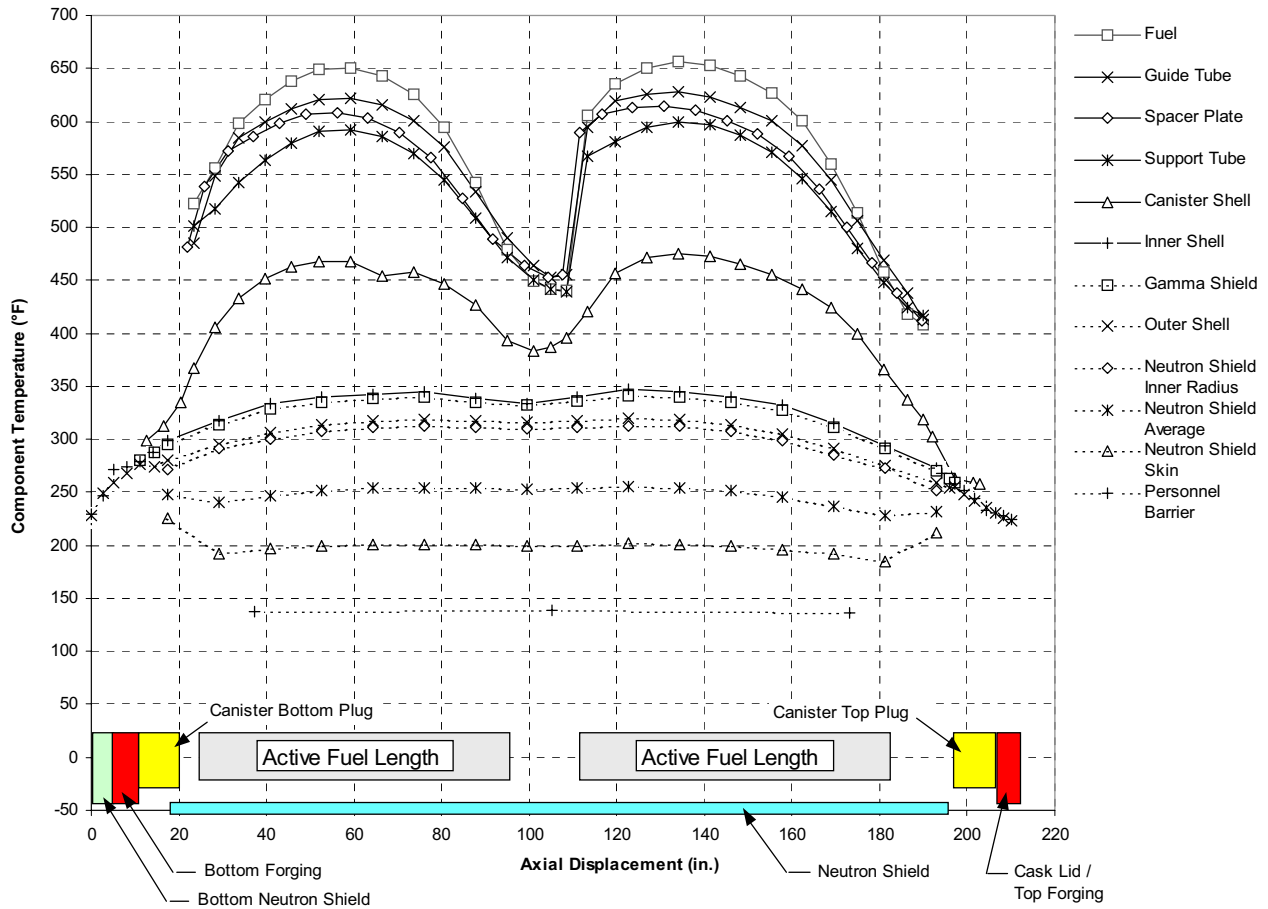


Figure 3.4-10 - Sensitivity of W74 Canister and TS125 Transportation Cask Components to Heat Load



**Figure 3.4-11 - W74/TS125 Axial Temperature Distribution;
 NCT Hot (100°F), 180° Rotation From Bottom²⁸**

²⁸ Note: The temperatures for the canister and interior components represent the maximum temperatures and are not a function of the rotational “cut line” through the cask sidewall.

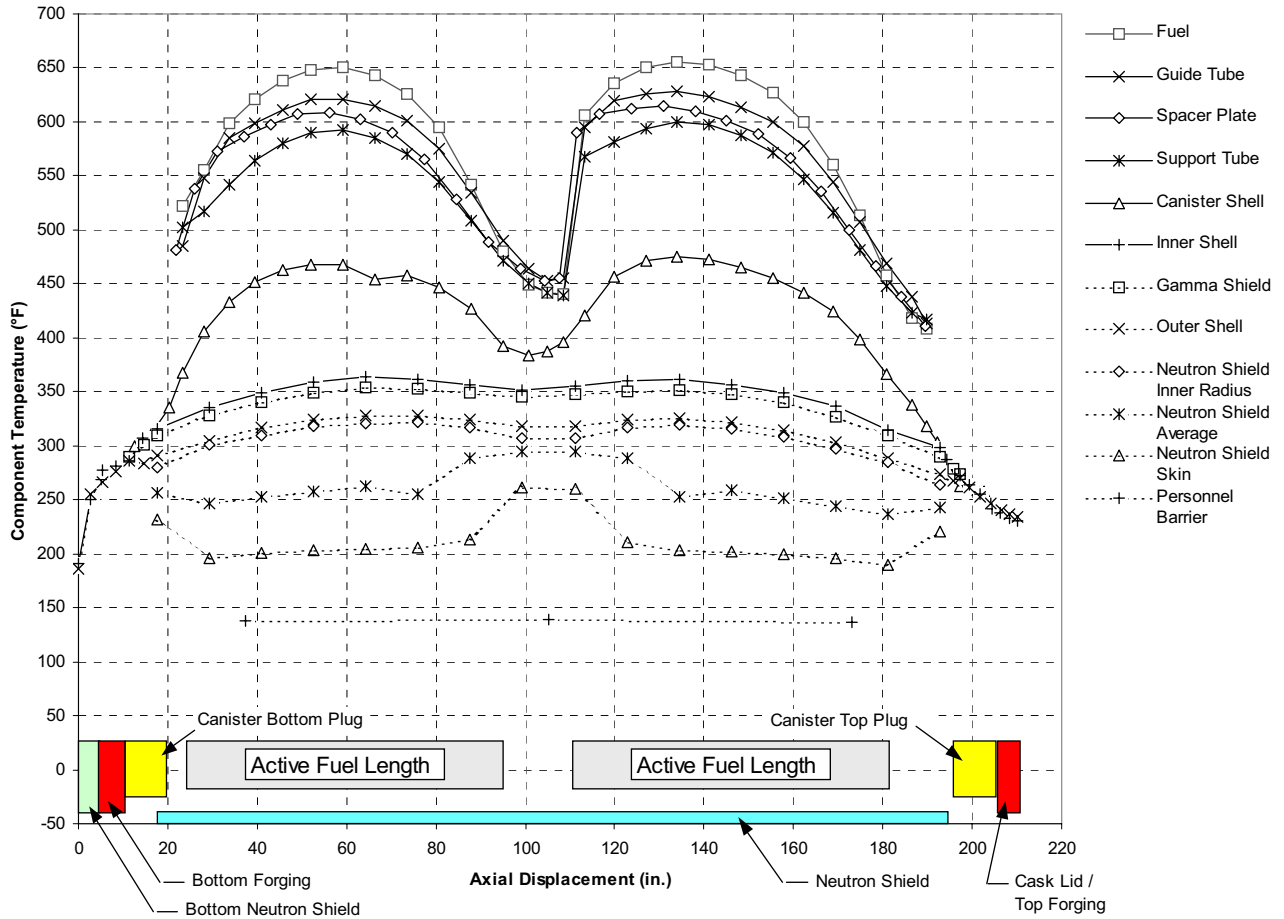


Figure 3.4-12 - W74/TS125 Cask Axial Temperature Distribution; NCT Hot (100°F), 15° Rotation From Bottom²⁹

²⁹ Note: The temperatures for the canister and interior components represent the maximum temperatures and are not a function of the rotational “cut line” through the cask sidewall.

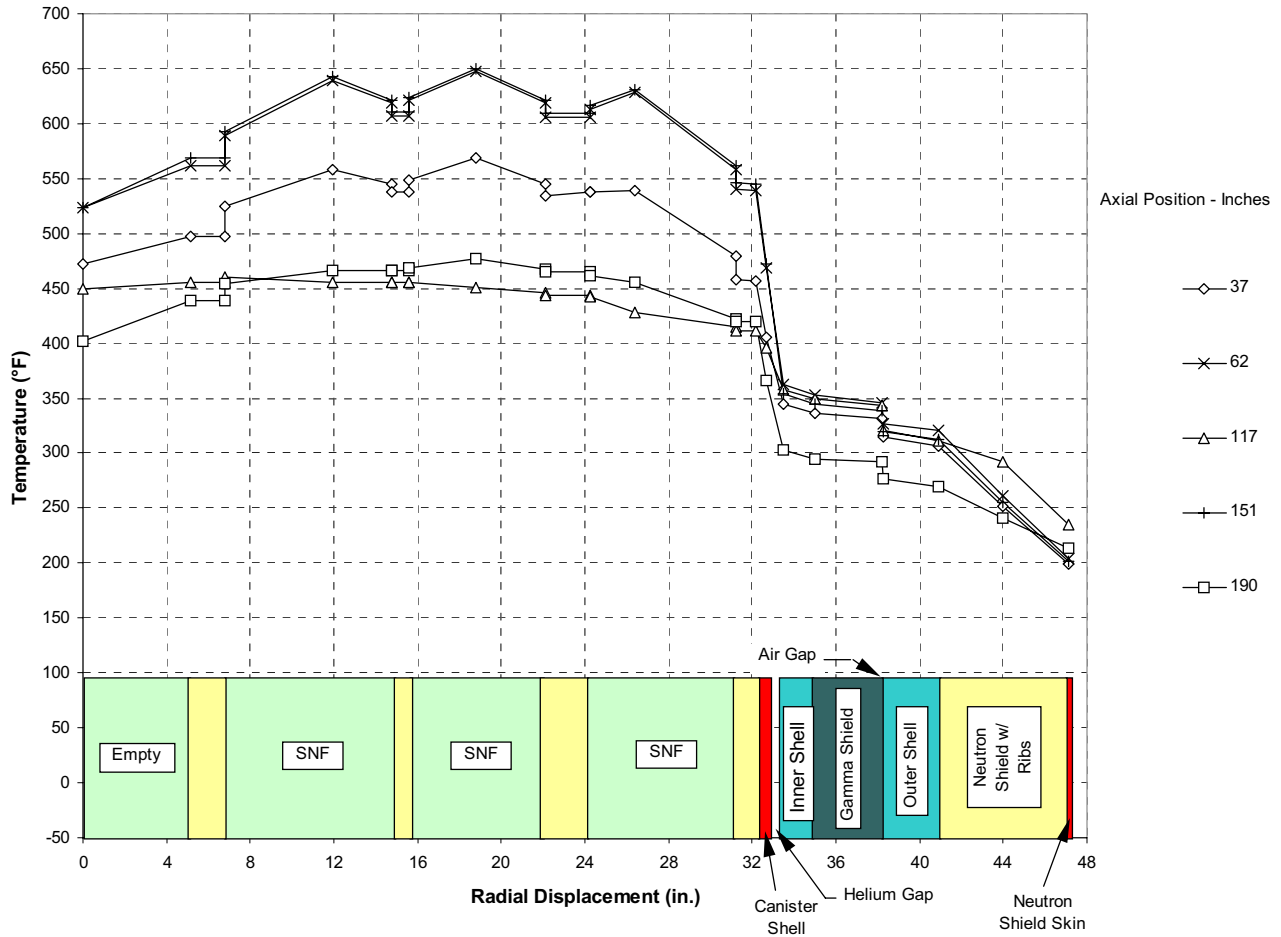
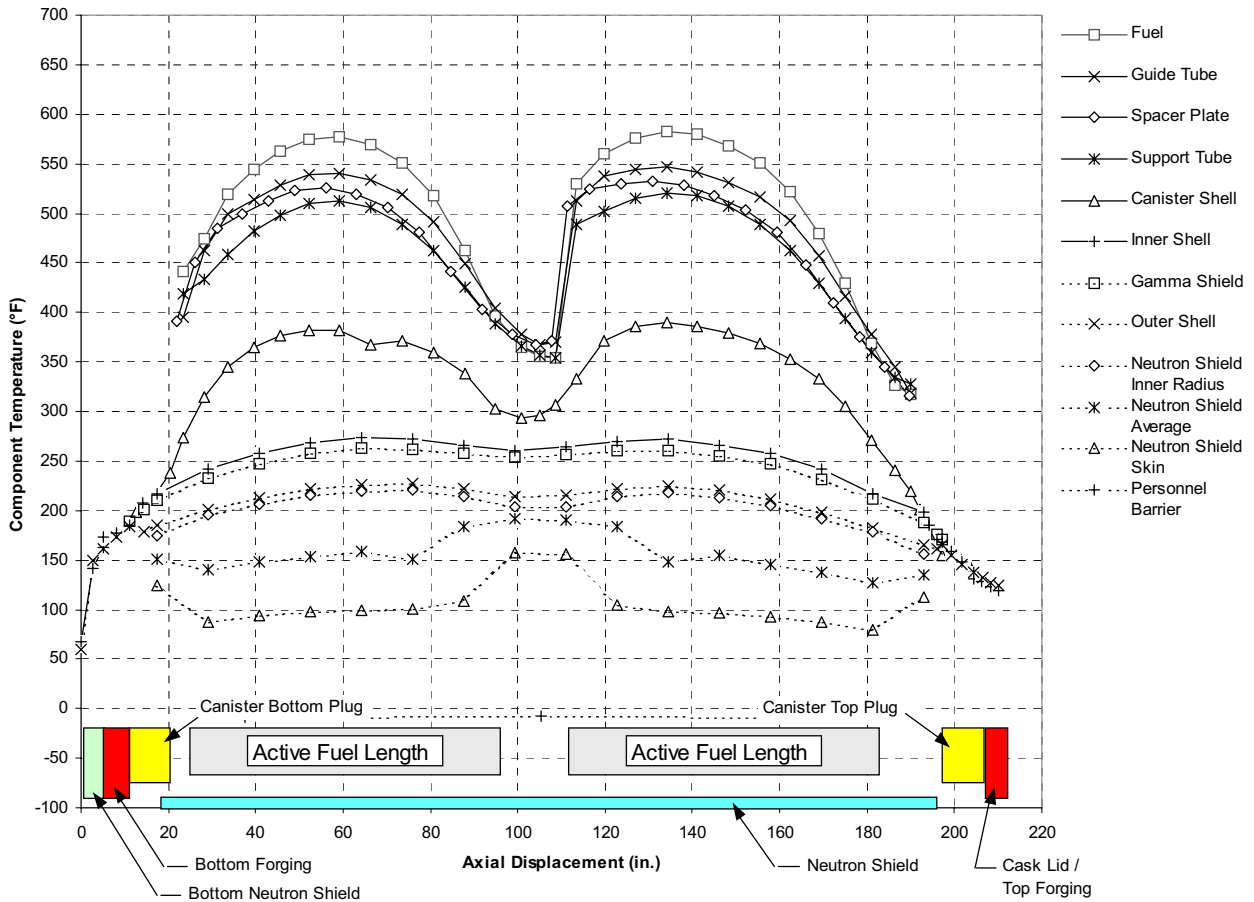


Figure 3.4-13 - W74/TS125 Cask Radial Temperature Distribution; NCT Hot (100°F), 15° Rotation From Bottom³⁰

³⁰ Note: The temperatures for the canister and interior components represent the temperatures along a “cut line” extending vertically from the center of the canister, while the rotational “cut line” through the cask sidewall is as indicated. This was done to capture the peak temperatures in the canister and the cask.



**Figure 3.4-14 - W74/TS125 Cask Axial Temperature Distribution;
 NCT Cold (-20°F), 15° Rotation From Bottom³¹**

³¹ Note: The temperatures for the canister and interior components represent the maximum temperatures and are not a function of the rotational “cut line” through the cask sidewall.

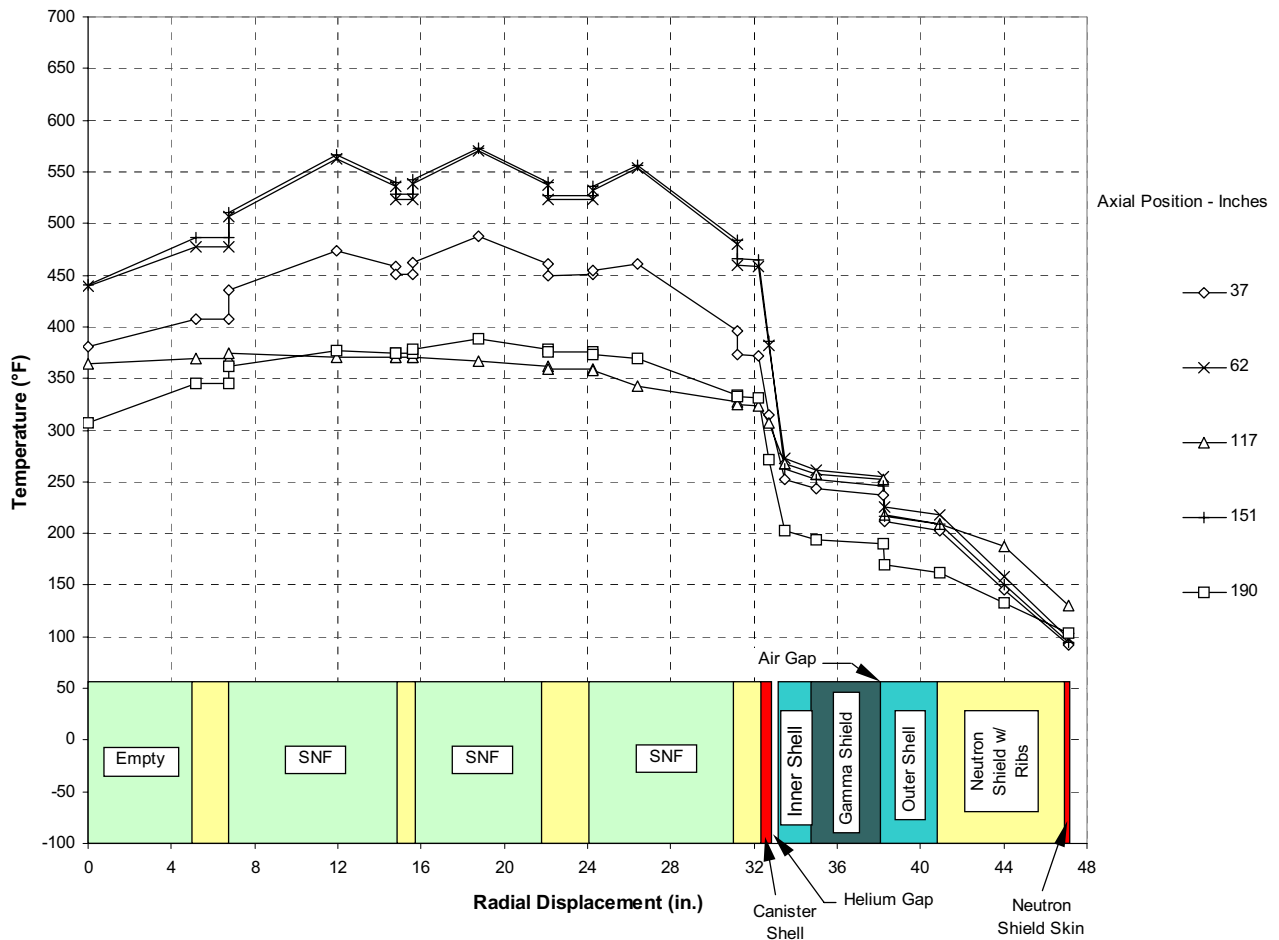


**Figure 3.4-15 - W74/TS125 Cask Radial Temperature Distribution;
 NCT Cold (-20°F), 15° Rotation From Bottom³²**

³² Note: The temperatures for the canister and interior components represent the temperatures along a “cut line” extending vertically from the center of the canister, while the rotational “cut line” through the cask sidewall is as indicated. This was done to capture the peak temperatures in the canister and the cask.

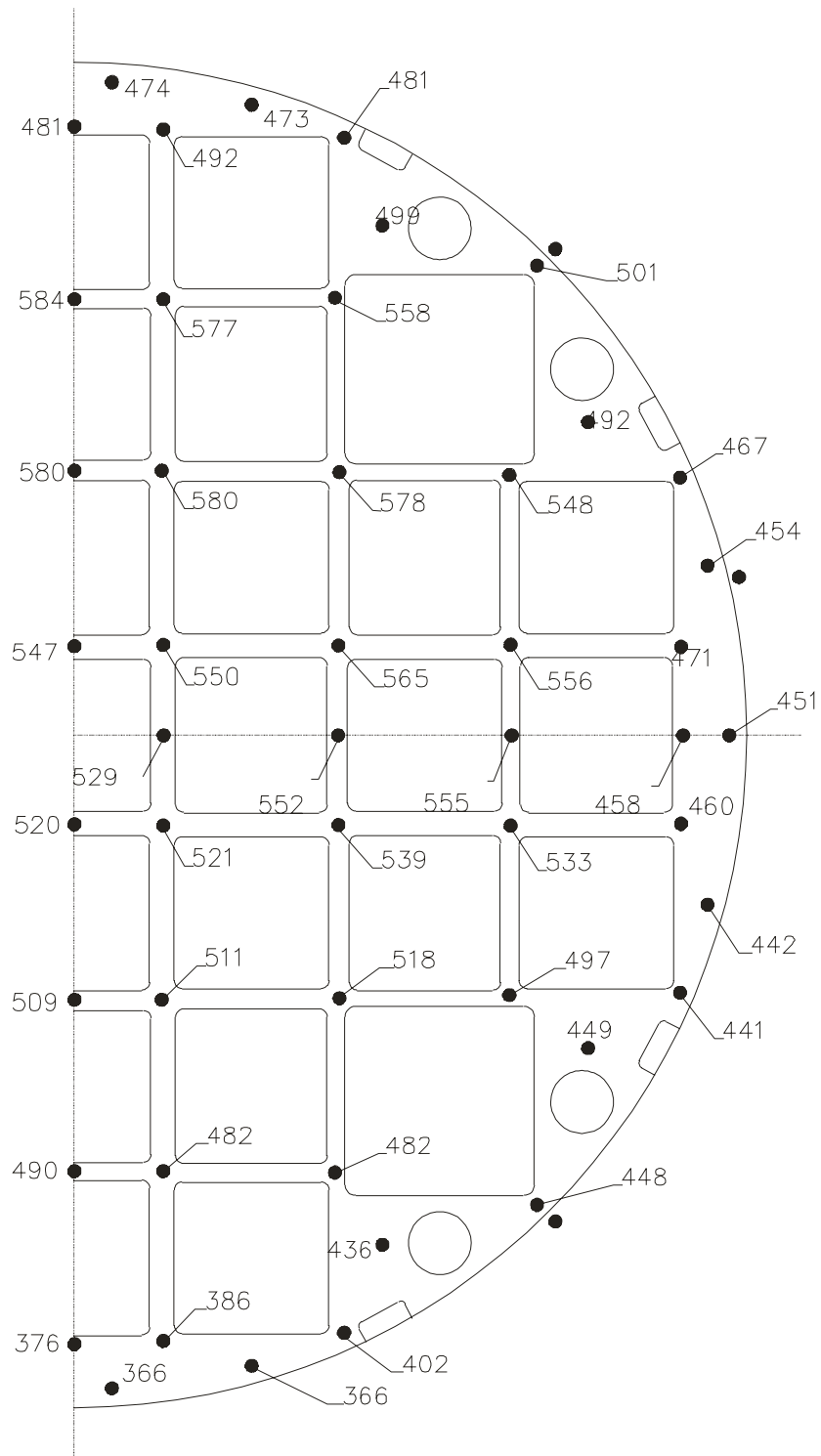


Figure 3.4-16 - Hottest W74 Stainless Steel Spacer Plate Temperature Distribution, NCT Hot (100°F)

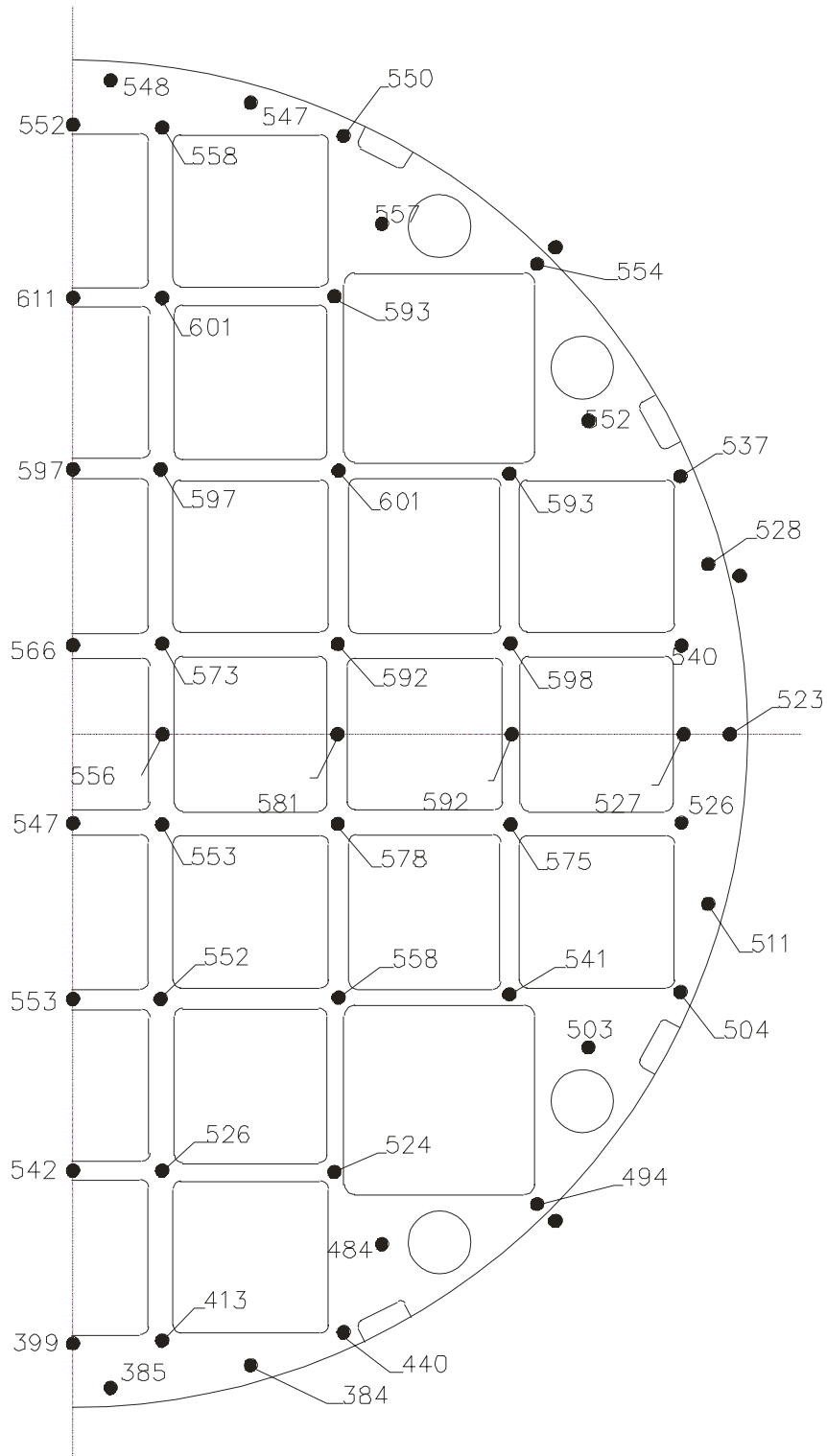


Figure 3.4-17 - Hottest W74 Carbon Steel Spacer Plate Temperature Distribution, NCT Hot (100°F)

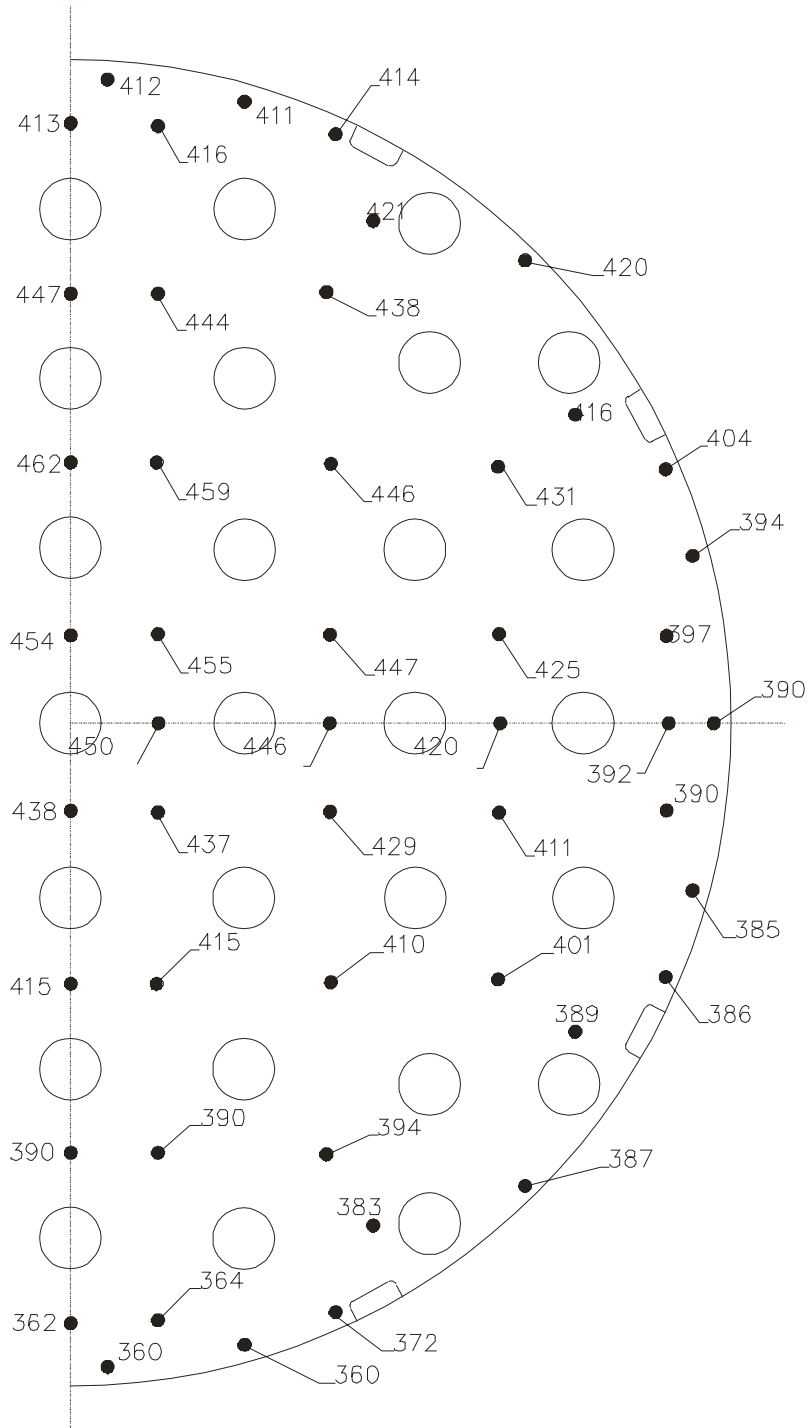


Figure 3.4-18 - W74 Engagement Plate Temperature Distribution, NCT Hot (100°F)

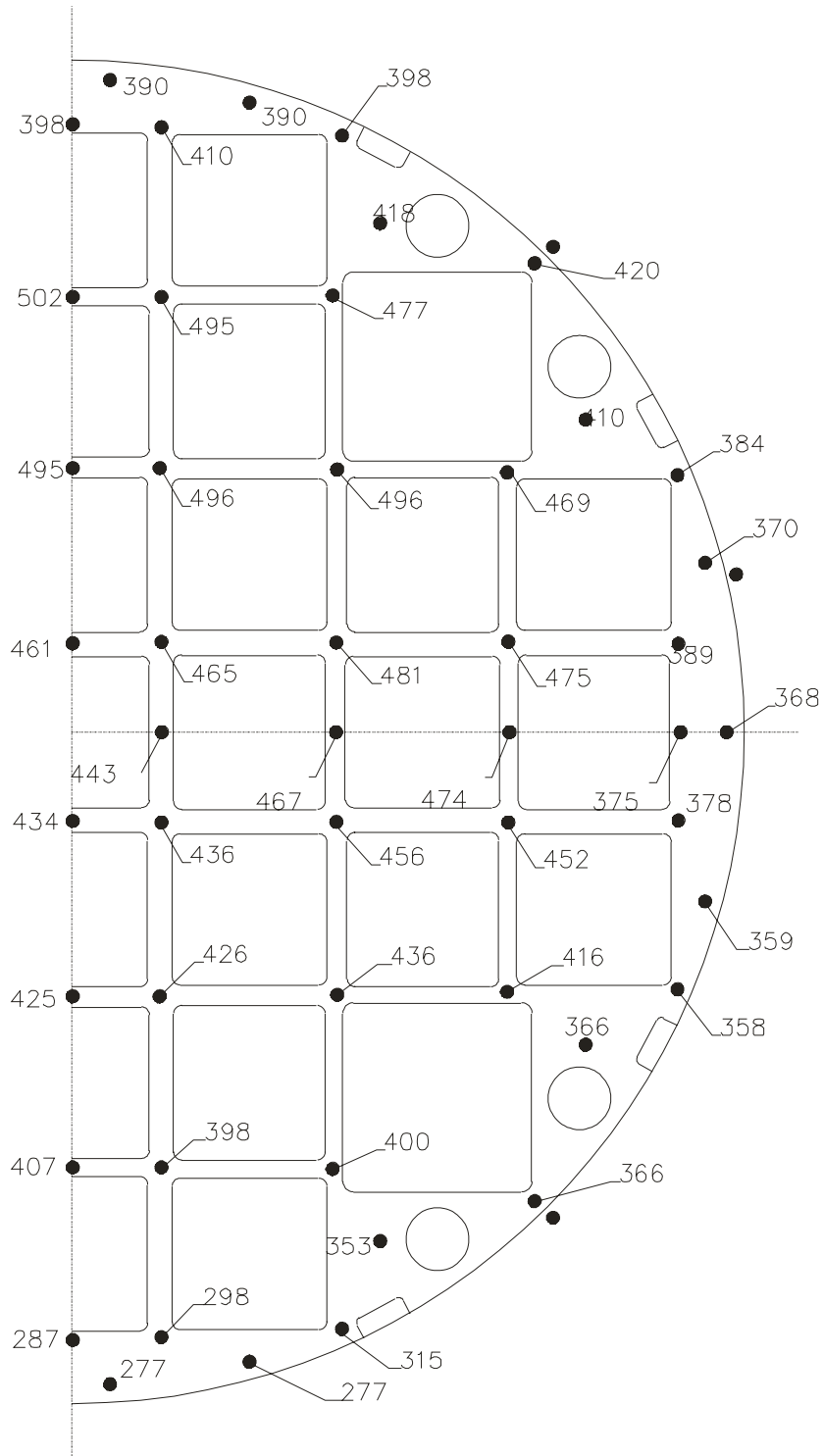


Figure 3.4-19 - Hottest W74 Stainless Steel Spacer Plate Temperature Distribution, NCT Cold (-20°F)

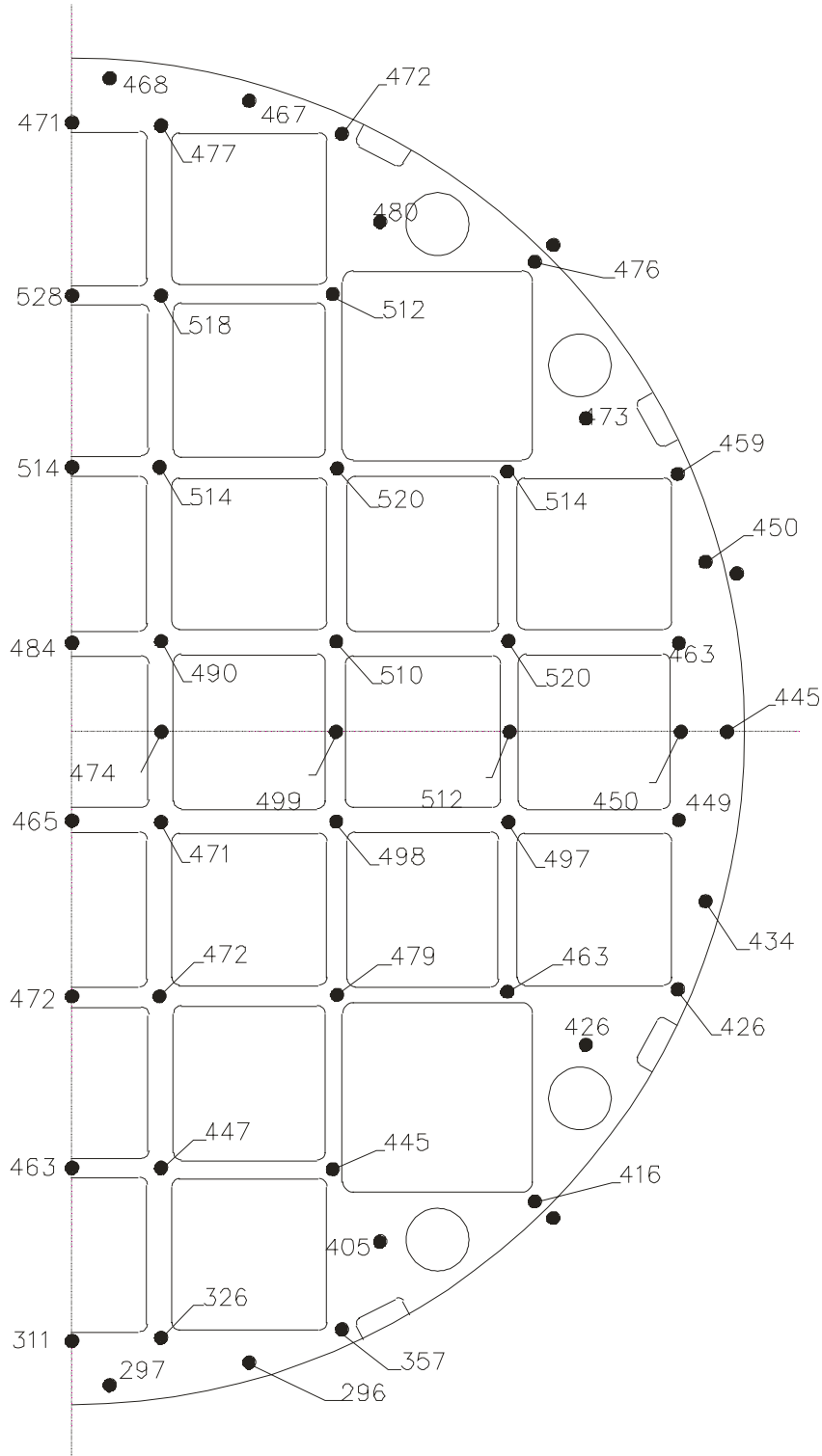


Figure 3.4-20 - Hottest W74 Carbon Steel Spacer Plate Temperature Distribution, NCT Cold (-20°F)

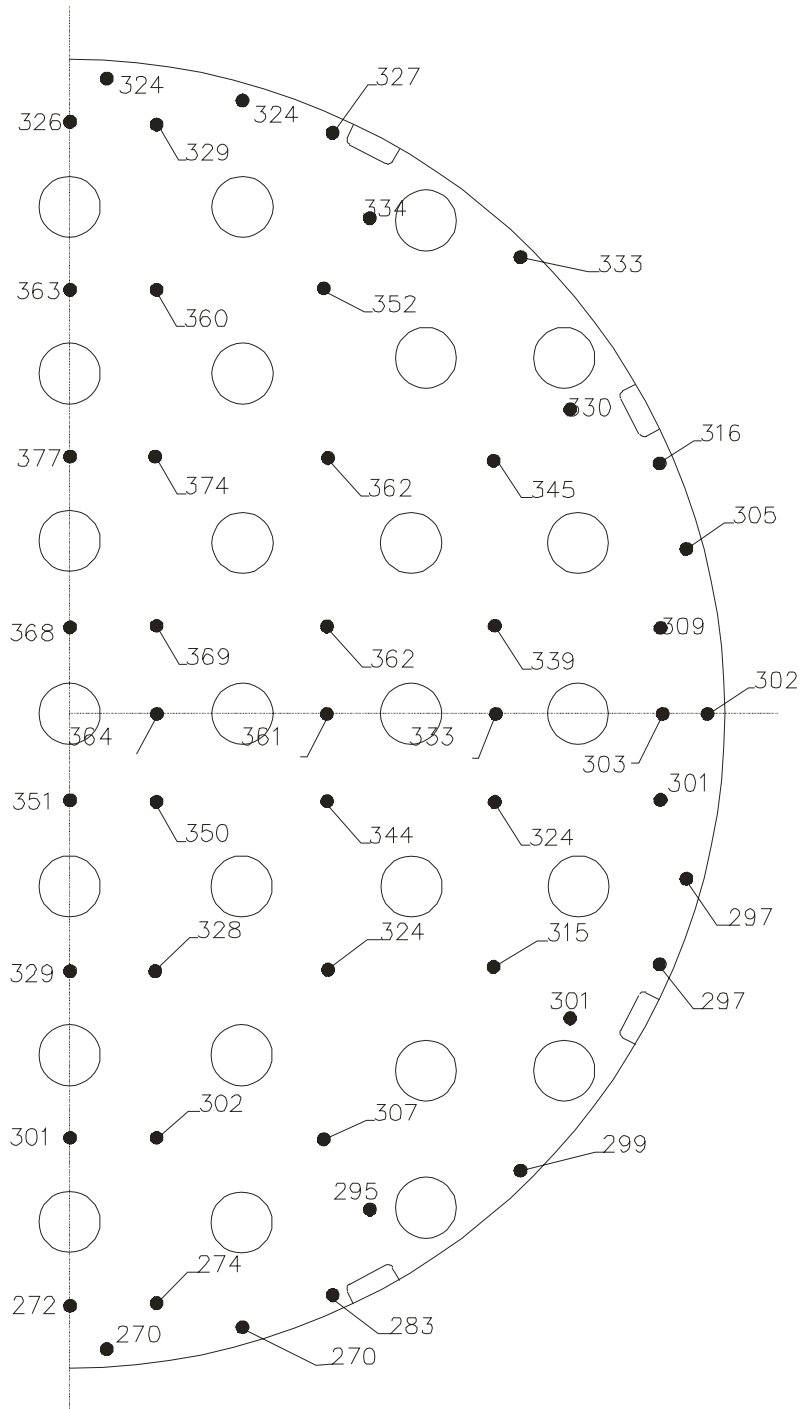


Figure 3.4-21 - W74 Engagement Plate Temperature Distribution, NCT Cold (-20°F)

3.5 Thermal Evaluation for Hypothetical Accident Conditions

This section provides a discussion of the thermal analysis methodology and results for the FuelSolutions™ W74 canister when used in conjunction with the FuelSolutions™ T125 Transportation Cask under accident conditions. The applicable canister assembly thermal ratings, temperature distributions, and thermal performance are evaluated to verify that the canister and cask thermal design features adequately perform their intended functions.

The conclusions presented in Sections 3.6.4, 3.6.5, and 3.6.6 demonstrate that the following results for hypothetical accident conditions with intact BRP UO₂ fuel assemblies are bounding for the FuelSolutions™ W74 canister with BRP MOX, damaged, and partial fuel assemblies.

3.5.1 Thermal Model

3.5.1.1 Analytical Thermal Model

This section presents the HAC fire event thermal analysis for the FuelSolutions™ W74 canister within the transportation package, as specified in 10CFR71.73(c)(4). Thermal performance of the package is evaluated analytically using a three-dimensional thermal model. Modifications to the transportation cask model to account for the combined damage sustained from the HAC 30-foot drop and puncture events are presented in Section 3.5.1 of the FuelSolutions™ TS125 Transportation Cask SAR.² A summary of the cask model changes implemented for HAC conditions is as follows:

1. Credit is taken for the presence of the NS-4-FR material in the solid neutron during the fire transient and ignored after the 30-minute fire. This approach conservatively maximizes the heat input to the cask and conservatively bounds the heat loss from the cask after the fire.
2. The shear block modeling is increased in complexity to conservatively capture the level of radiation and convection heat transfer between the cask and the ambient for the HAC event. This complexity was conservatively ignored for NCT conditions since the shear block provides a relatively low thermal resistance for heat loss from the cask.
3. The intermodal skid, the railcar, and the personnel barrier are considered to be absent during and after the HAC fire event. This assumption maximizes the view factor to the fire and reduces the effective thermal mass of the package.
4. The surface absorptivity and emissivity of all external surfaces are set to 0.9. The 0.9 value represents an upper range value for emissivity of the neutron shield's epoxy coating, and a conservative absorptivity value to account for possible sooting of the surfaces during the fire.
5. To conservatively bound the thermal effects of a damaged set of impact limiters, the thermal modeling approach used assumed that the impact limiters are absent during the 30-minute fire, but are in place and undamaged during the post-fire cool down. This approach maximizes the heat input into the cask structure from the fire and minimizes the post-fire cool down rate.

The W74 canister, including the basket and SNF assemblies, is not expected to be damaged as a result of the HAC 30-foot drop and puncture bar events. As such, the thermal model of the W74

canister for the HAC events is the same as that presented in Section 3.4.1 for the NCT evaluations.

3.5.1.2 Test Thermal Model

In accordance with 10CFR71.41, detailed thermal analyses of the W74 canister within the transportation cask have been performed to demonstrate compliance with the HAC tests specified in 10CFR71.73. As a result, subsequent transportation package or scale model thermal testing under simulated HAC fire conditions is not required.

3.5.2 Package Conditions and Environment

The initial temperature distribution in the package is taken from the steady-state conditions determined in Section 3.4 for two ambient temperatures, -20°F (case 3) and 100°F (case 2), maximum decay heat, and no insolation. Per 10CFR71.73(c)(4),¹ the transportation package is exposed to a convective and radiative heat flux based on ambient air at 1475°F, with an effective emissivity of 0.9 during the HAC fire event. Although insolation does not need to be applied during the HAC fire, it is conservatively assumed to be present during the HAC hot analysis. The duration of the HAC fire event is 30 minutes, after which time the thermal boundary conditions are returned to the original ambient temperature; either -20°F without insolation or 100°F, with insolation. Following the end of the HAC fire event, the thermal transient analysis is continued for a sufficient time to determine the maximum temperatures for all components.

The convection coefficients between the cask assembly and the ambient are calculated using natural convection correlations before and after the 30-minute fire event. The appropriate level of forced convection to be used during the simulation of the fire event is based on a full-scale pool fire test conducted at Sandia National Laboratories, with the express intent of assessing the gas velocities and temperatures arising from such an event.³³ The results at four heights above the level of the pool (e.g., approximately 1.5 to 5.3 meters) indicate a wide variation in velocities primarily due to the effects of wind and turbulence generated by the fire. While the peak velocity varied from approximately 5 to 15 meters/second, a constant value of 10 meters per second (33 feet per second) is seen as being appropriate for capturing the convection coefficients. This is especially true for the 2.6 to 4 meters above the pool, which is the range of interest for this cask.

An evaluation presented in Section 3.6.3 demonstrates that the bounding safety analysis for the FuelSolutions™ W74 canister in the TS125 Transportation Cask will be achieved if the effects of fission gas release are ignored. While the thermal conductivity of the canister gas mixture could be significantly reduced if the fuel rod fission gas is released, the mass transport properties of the resultant gas mixture will also improve. Until the fission gas concentration, on a mole fraction basis, is greater than about 42%, the overall effect will be an increase in the convection heat transfer rates. The estimation technique used to reach this conclusion is based on the kinetic theory of gases, and computes the change in gas mixture properties as a function of the mole fractions of the various constituents of the gas mixture and a complex function of viscosities and molecular weights.

³³ Schneider, M.E., and Kent, L.A., *Measurements of Gas Velocities and Temperatures In A Large Open Pool Fire*, Heat and Mass Transfer in Fire - HTD Vol. 73, ASME, New York, New York 10017.

3.5.3 Package Temperatures

The tabulated data in Table 3.5-1 presents the W74 canister and transportation cask initial and peak temperatures for the evaluated initial ambient conditions of 100°F (case 8) and -20°F (case 7), and at the maximum W74 canister thermal rating of $Q_{\max} = 22.0$ kW. The peak temperatures for the impact limiters are not reported since the analysis approach used assumes the limiters are not present during the fire. Figure 3.5-1 and Figure 3.5-2 present the temperature history results for the evaluation of the HAC fire event under HAC hot (100°F) and HAC cold (-20°F) ambient conditions. Figure 3.5-1 presents the temperature history results for the evaluation of the HAC fire event under the HAC hot (100°F, case 8) conditions, while Figure 3.5-2 presents the same temperature history results for the HAC cold (-20°F, case 7) ambient condition. The elapsed time periods from the beginning of the fire transient to the occurrence of the peak material temperatures noted in Table 3.5-1 are apparent in the Figure 3.5-1 and Figure 3.5-2 trend lines.

Due to the conservative modeling approach used for the HAC simulation, which assumes that the impact limiters are not in place during the 30-minute fire event, the maximum inner shell, gamma shield (lead), and outer shell temperatures occur at the junction with the top and bottom forgings. However, as can be seen in the axial temperature profiles presented in Section 3.5.3 of the FuelSolutions™ TS125 Transportation Cask SAR,² these peak temperatures occur only at the ends of these components and are not representative of the general temperature levels reached during the HAC event. Therefore, the maximum inner and outer shell temperatures reported in Table 3.5-1 are for axial locations that lie underneath the neutron shield. Since the potential for melting within the lead shield is always a concern during HAC events, the maximum temperature reported for the gamma shield is the maximum that occurs anywhere within the model. As such, the reported maximum gamma shield temperatures do not coincide with the same locations as those for the maximum inner and outer shell temperatures, as reported in Table 3.5-1. A detailed evaluation of the transportation cask assembly temperatures resulting from exposure to the HAC fire event at the transportation cask thermal rating is presented in Section 3.5.3 of the FuelSolutions™ TS125 Transportation Cask SAR.²

All W74 canister and transportation cask components, with the exception of the drain port seal, remain below the respective short-term allowable temperatures and exhibit substantial thermal margin during the fire. This is expected given the relatively high thermal mass of the cask and the relatively thin shell of the solid neutron shield, which acts as a radiation shield to limit the amount of heat transferred into the cask during the HAC event. As a result, little temperature impact is seen by the W74 canister or SNF payload from the presence of the fire.

Although the maximum temperature predicted for the drain port seal comes within 14°F of its 662°F temperature limit, the actual thermal margin will be substantially larger. The predicted maximum seal temperatures are conservatively high since the analysis method assumes that the impact limiters are not present during the fire. In reality, the impact limiters will remain attached during the drop events, and the shells of the impact limiters will act like thermal shields during the fire. In addition, the heat flux applied through a drop-damaged or puncture-damaged impact limiter will be substantially less than the levels calculated herein.

The post-fire, steady-state temperature distribution for the canister and cask assembly is bounded by those for the NCT hot (case 1) and NCT cold (case 3) conditions presented in Section 3.4.2.

This conclusion is reached due to the following facts: (1) the assumed absence of the personnel barrier will increase the radiative heat exchange with the ambient over and above the associated increase in insulation load, (2) the assumed damage to the impact limiters will reduce their overall thermal resistance, thus increasing the heat loss at the cask ends, and (3) no significant cask side wall or canister payload damage is projected to occur that would act to increase the temperature rise from the canister shell to the ambient.

3.5.4 Maximum Internal Pressures

With the exception of the assumed fuel rod failure rate, the calculation of the maximum HAC pressure is similar to the MNOP calculation presented in Section 3.4.4. The FuelSolutions™ TS125 Transportation Cask maximum internal pressure during the HAC fire with a loaded W74 canister is based on the initial cask helium backfill, the canister backfill, SNF rod fill gas, and SNF fission gases. Specifically, the pressure in the cask cavity is determined assuming (1) no containment by the canister shell pressure boundary, (2) hot ambient (100°F), (3) an initial cask annulus helium backfill of 14.7 psia (at 70°F), (4) an initial canister backfill pressure of 24.7 psia (at normal hot storage conditions with 1% rod failures), (5) minimum cask and canister void volumes, and (6) postulated failure of 100% of the SNF rods. For each postulated SNF rod failure, 30% of the fission gas yield and 100% of the rod fill gas are assumed to be released into the canister cavity.

The average gas temperature inside the cask is determined by using volume weighted averaging of the canister bulk helium temperature and the cask annulus bulk helium temperature. Since SNF fill and fission gas quantities depend on the specific Big Rock Point fuel assembly type, the maximum pressure is calculated for each SNF assembly type that can be accommodated within the W74 canister.

The quantities of SNF rod gas, canister total free volume, canister backfill gas, and cask annulus backfill gas are presented in Table 3.4-3.

The transportation cask peak internal pressure during the HAC fire event with the W74 canister and 40 GWd/MTU Big Rock Point fuel is 28.3 psig, as presented in Table 3.5-2. Significant margin exists between this calculated maximum internal pressure and the transportation cask design pressure of 75 psig.

3.5.5 Maximum Thermal Stresses

Thermal stress analyses of the FuelSolutions™ W74 canister using the temperature distributions determined from the HAC fire analyses are presented in Section 2.7.4 of this SAR.

3.5.6 Evaluation of Package Performance for Hypothetical Accident Conditions

The results of the HAC fire transient analyses demonstrate that the W74 canister and transportation cask allowable material temperatures during the HAC fire event are met for the maximum W74 canister thermal rating presented in Table 3.1-3. The maximum internal pressure resulting from the HAC fire environment and conservative assumptions is within the transportation cask maximum design pressure. The analysis presented in this section demonstrates compliance with the HAC

thermal test requirements of 10CFR71.73. Therefore, the W74 canister is suitable for transportation of Big Rock Point SNF within the FuelSolutions™ TS125 Transportation Cask.

The HAC fire analysis results in Table 3.5-1, Figure 3.5-1, and Figure 3.5-2 are used for the structural evaluations presented in Section 2.7.4 of this SAR.

Table 3.5-1 - W74/TS125 System Temperature For HAC Fire

Component	Case 7⁽¹⁾ (-20°F ambient), Initial/Peak	Case 8⁽¹⁾ (100°F ambient), Initial/Peak	Max. Allowable Temperature
Peak Fuel Cladding	305.9°C / 314.4°C	343.2°C / 350°C	400°C / 570°C
Guide Tube	547°F / 566°F	621°F / 637°F	800°F / 1000°F
Spacer Plates			
Stainless Steel	507°F / 517°F	583°F / 596°F	800°F / 1000°F
Carbon Steel	532°F / 552°F	608°F / 624°F	700°F / 1000°F
Support Tube	520°F / 534°F	593°F / 605°F	700°F / 1000°F
Avg. Canister Gas	445°F / 472°F	520°F / 545°F	n/a
Canister Shell	389°F / 424°F	467°F / 499°F	800°F / 1000°F
Avg. Canister-Cask Gas	287°F / 345°F	371°F / 423°F	n/a
Inner Cask Shell	273°F / 319°F	356°F / 402°F	800°F / 1000°F
Gamma Shield (Lead)			
Max. Temperature	263°F / 402°F	344°F / 485°F	620°F / 620°F
Avg. Temperature	240°F / 295°F	326°F / 378°F	620°F / 620°F
Outer Cask Shell	227°F / 345°F	320°F / 422°F	800°F / 1000°F
Solid Neutron Shield ⁽³⁾			
Max. Radial Ave. Temp.	186°F / 624°F	281°F / 693°F	300°F / 1472°F
Bulk Avg. Temperature	156°F / 546°F	252°F / 617°F	300°F / 1472°F
Shear Block	203°F / 1128°F	298°F / 1156°F	800°F / 2700°F
Neutron Shield Jacket	108°F / 1286°F	193°F / 1303°F	350°F / 2700°F ⁽⁴⁾
Personnel Barrier	-7°F / n/a	115°F / n/a	185°F / n/a
Impact Limiter			
Max. Honeycomb	30°F / n/a	157°F / n/a	350°F / n/a ⁽⁵⁾
Bulk Avg. Honeycomb	14°F / n/a	133°F / n/a	200°F / n/a ⁽⁵⁾
Cask Metallic Seals ⁽²⁾			
Cask Closure	137°F / 459°F	233°F / 536°F	932°F / 932°F
Vent & Drain Ports	154°F / 581°F	251°F / 648°F	662°F / 662°F

Notes:

- (1) Temperatures in this table are based on a heat load of 22.0 kW with the Big Rock Point axial heat generation profile.
- (2) The closure seal temperatures are conservatively estimated assuming the impact limiters are not present to shield the cask ends from the fire event. This assumption conservatively bounds potential loss in thermal shielding resulting from HAC drop damage to the impact limiters.
- (3) The solid neutron shield material temperature is presented in two forms: a radial average temperature at the axial location with the highest temperature and as bulk average temperature across the length of the neutron shield.
- (4) The shear block and neutron shield jacket short-term allowable temperature is based on the melting point of XM-19 stainless steel and A-516, Grade 70 carbon steel (>2700°F). Pre-fire shear block temperature presented for a location coincident with maximum temperature during the fire, not the location of the pre-fire maximum temperature.
- (5) Impact limiter material strength properties are not relied on during and following the HAC fire event.

Table 3.5-2 - W74 Canister and Transportation Cask Internal Pressures for HAC Fire Event

Parameter	Case 7 (-20°F ambient), Peak	Case 8 (100°F ambient), Peak
Canister Helium Bulk Temperature ⁽¹⁾	472°F	545°F
Cask Annulus Helium Bulk Temperature ⁽¹⁾	359°F	399°F
Average Mixed Volume Helium Bulk Temperature ⁽²⁾	n/a	538°F
Max. HAC Pressure ⁽³⁾	n/a	44.0 psia (29.3 psig)

Notes:

- (1) Temperatures are based on heat loads of 22.0 kW with the Big Rock Point axial heat profile.
- (2) Average mixed volume helium bulk temperature is computed based on a volume-weighted average of the canister and cask annulus gas temperatures assuming no containment by the canister shell pressure boundary. The average temperature is presented for the specific Big Rock Point fuel assembly type that results in the highest HAC pressure.
- (3) Maximum HAC pressure is determined for the hot environment only, assuming no containment by the canister shell and 100% SNF fuel rod failures.

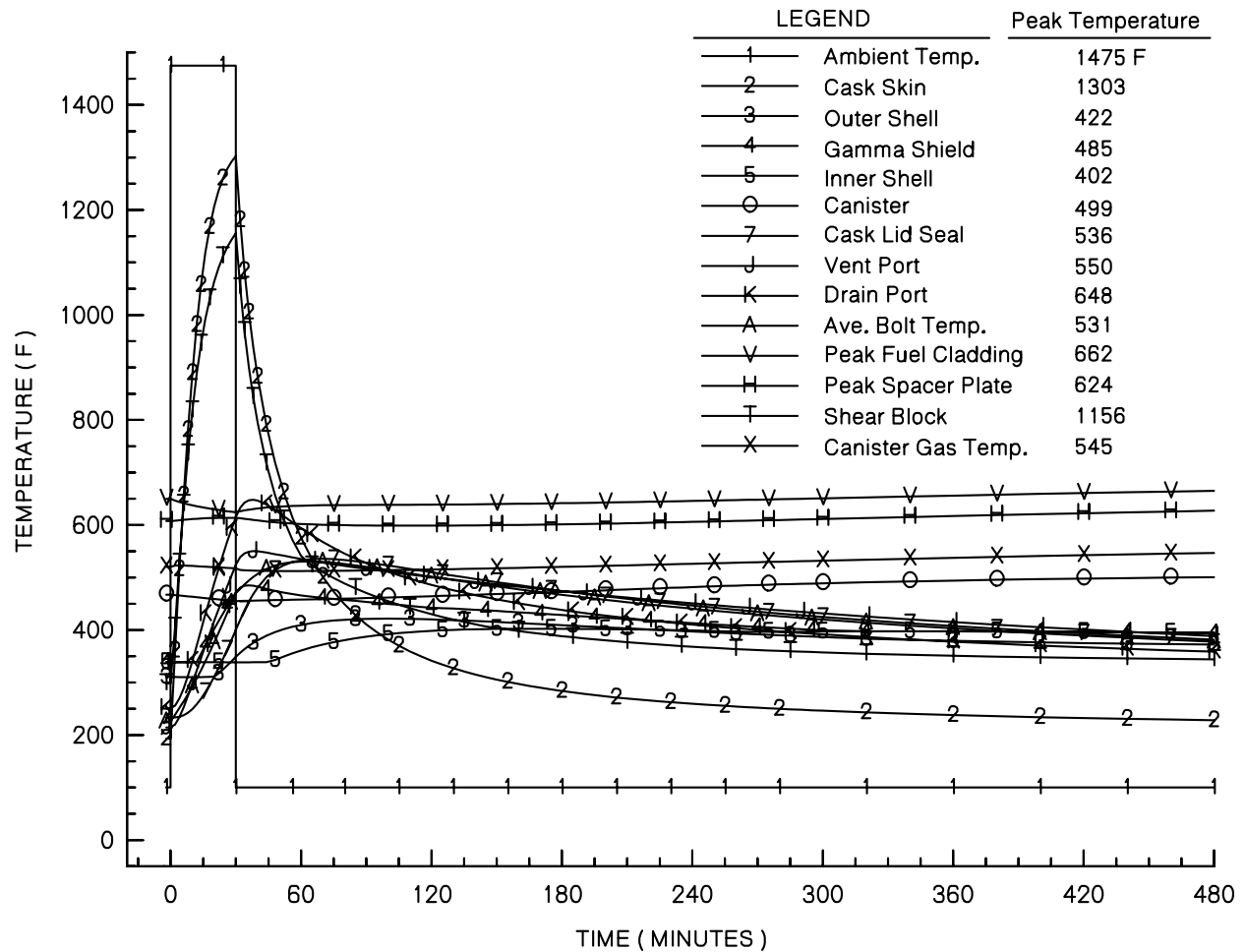


Figure 3.5-1 - HAC Fire Transient, FuelSolutions™ W74 Canister, Hot Initial Conditions³⁴

³⁴ The plotted inner and outer shell temperatures are for axial locations that coincide with the neutron shield and do not reflect the maximum temperatures reached at the ends of the cask.

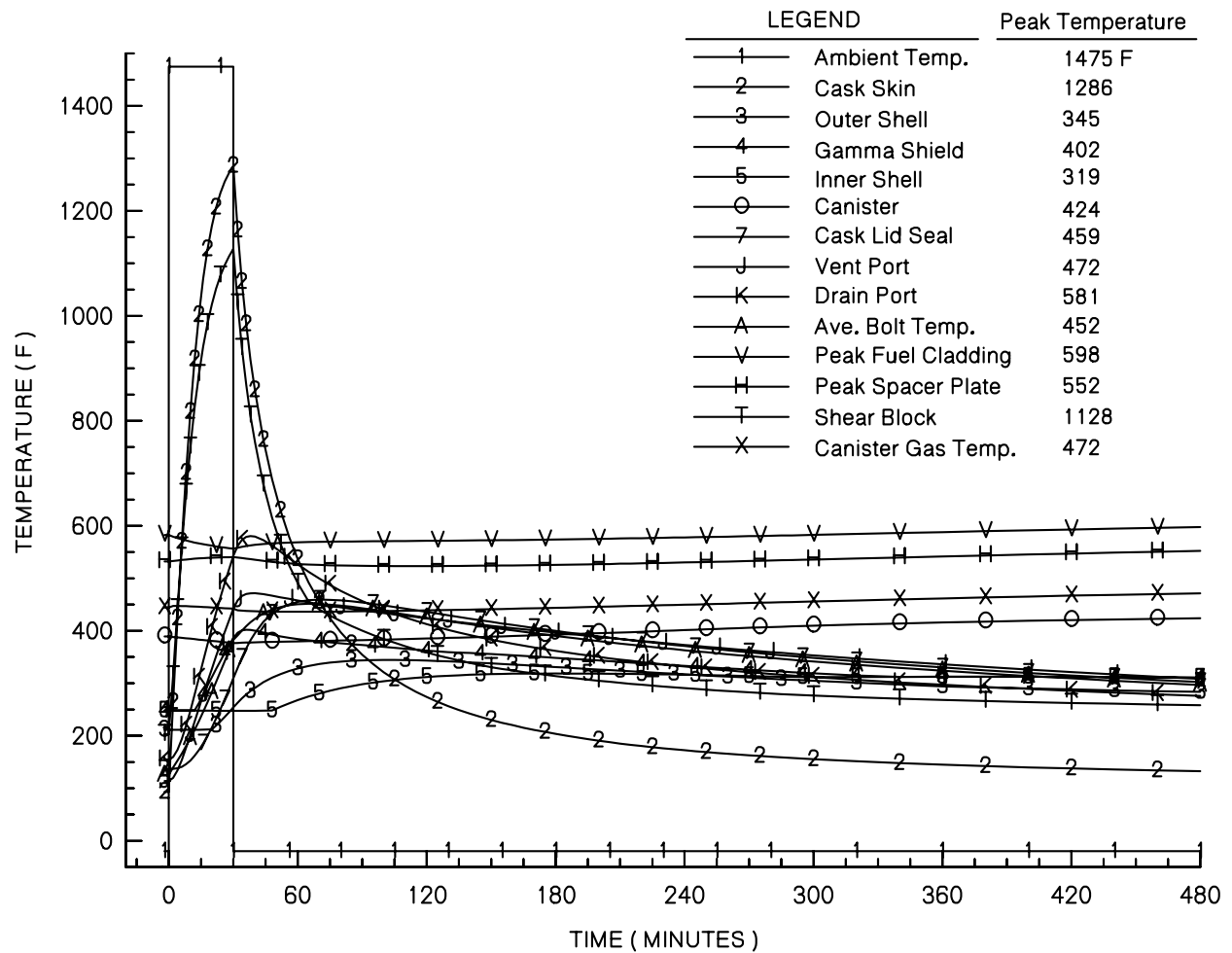


Figure 3.5-2 - HAC Fire Transient, FuelSolutions™ W74 Canister, Cold Initial Conditions³⁵

³⁵ The plotted inner and outer shell temperatures are for axial locations that coincide with the neutron shield and do not reflect the maximum temperatures reached at the ends of the cask.

This page intentionally left blank.

3.6 Appendices

3.6.1 Canister Internal Convection

Beyond conduction and radiation heat transfer, the principal heat transfer mode within the horizontal basket assembly is convection. The following paragraphs provide a more specific description of the approach and equations used for the W74 basket assembly.

To account for the natural convection heat transfer interaction within the W74 basket assembly, the internal flow environment is divided into a series of related flow regions, and the results from each region are superimposed on the global solution to arrive at a unified result. Convection heat transfer coefficients are determined for each flow region based on its particular physical and behavioral characteristics. The analytical algorithms used to determine these coefficients are computed as a function of the local environment (i.e., geometry, temperatures, and pressures) and are incorporated into the SINDA/FLUINT® thermal model iterative solution.

The fact that the basket assemblies are keyed within the canister and the canister is aligned within the transportation cask assures that the global orientation of the fuel assemblies essentially remains constant for each transportation cycle. As such, the analysis of the fluid flow due to convection within a horizontally oriented basket is approached as an analysis of a series of vertically oriented channels. The general flow pattern is one where the helium blanket gas is transported upward under buoyancy forces through the basket and then downward along the inside circumference of the canister. Superimposed on this predominant flow pattern is a series of sub-flow paths at each of the double open-ended cavities created between the upper and lower edges of adjacent guide tubes.

A representation of the assumed flow pattern for the W74 basket assembly is presented in Figure 3.6-1. The two main underlying assumptions for this type of buoyancy-driven recirculating flow field are that it is incompressible and that the flow is nominally two-dimensional. Although discontinuities occur at the upper and lower edges of each guide tube, the vertical channels formed between pairs of guide tubes can be analytically treated as smooth wall channels for the purposes of determining the governing convection heat transfer rates. This is a result of the relatively close spacing of the guide tubes and the estimated flow velocities yielding Reynolds numbers on the order of 100. The assumed flow pattern and the smooth wall channel assumption are confirmed by the measured flow velocities from the testing conducted on a similar basket layout by Kawasaki Heavy Industries.³⁶ The results of this testing are summarized by Figure 3.6-2 and Figure 3.6-3.

Based on these assumptions, the natural convection in vertical channels with symmetric and uniform wall heat flux is estimated using equations 3.65 and 3.66 of Bar-Cohen,³⁷ where the

³⁶ Nishimura, M., et al., *Natural Convection Heat Transfer in the Horizontal Dry Storage System for the LWR Spent Fuel Assemblies*, Journal of Nuclear Science and Technology, Vol. 33, No. 11, pp. 821-828, November 1996.

³⁷ Bar-Cohen, A., and Kraus, A.D., *Advances In Thermal Modeling of Electronic Components and Systems*, Hemisphere Publishing Corporation, Vol. 1, 1988.

characteristic length is the height of the channel. These equations are applicable over the range of $3 \times 10^{-1} < Ra^* < 3 \times 10^4$ and are as follows:

$$Nu_{\frac{L}{2}} = \frac{h_c L}{k} = \left\{ \left(\frac{12}{Ra^*} \right) + \frac{17}{70} \right\}^{-1} 3 \times 10^{-1} < Ra^* < 3 \times 10^4$$

for the mean value on each wall and:

$$Nu_L = \frac{h_c L}{k} = \left\{ \left(\frac{48}{Ra^*} \right) + \frac{17}{70} \right\}^{-1} 3 \times 10^{-1} < Ra^* < 3 \times 10^4$$

for the exit region value on each wall. Ra^* is defined as:

$$Ra^* = Gr \cdot Pr = \frac{g \beta q b^5 \mu C_p}{L v^2 k^2}$$

where:

- g = Gravitational acceleration
- β = Coefficient of thermal expansion
- q = Heat flux density
- b = Channel gap width
- μ = Dynamic viscosity
- C_p = Specific heat
- L = Height of the channel
- v = Kinematic viscosity
- k = Thermal conductance

The wall heat flux, q , used in the equations is computed using the surface area of the guide tube over the active length of the fuel, and then adjusted at each specific basket location to account for the placement of the fuel within the basket and the fuel peaking factor along the length of the fuel assembly. The computed heat flux is further adjusted to account for the fact that any heat dissipated out the horizontal surfaces of the guide tubes ultimately ends up in the vertical channel and is available to feed the buoyancy-driven flow.

Radiation and conduction from the guide tubes into the spacer plates results in the spacer plate temperatures being significantly above the local gas temperature. As such, the characteristic heat transfer coefficients determined for the guide tube walls are also applied to the adjacent spacer plate surfaces. Although this assumption of two-dimensional flow behavior is not necessarily conservative, it is offset by the assumption that the flow within the vertical channels is fully developed and by the fact that the channel flow correlation includes the flow that is within an enclosure. In reality, based on a Reynolds analogy, the approximate flow development length within the largest vertical channel for the W74 basket assembly is approximately half of the

channel height. This means that higher than predicted convection heat transfer will actually exist within the channels.

The convection heat transfer rates from the upper and lower surfaces of each guide tube pair are addressed using a correlation for the average Nusselt number within horizontal cavities. The correlation is developed using the findings presented in several papers pertaining to buoyancy-driven flow from open-ended cavities.

The correlation includes the effects of the cavity configuration, the Rayleigh number (Ra), and aspect ratio (A), defined as:

$$A = \frac{H}{L}$$

where H is the separation distance between the guide tubes, and L is one-half the width of the guide tubes.

The cavity Rayleigh number is defined as:

$$Ra = Gr \cdot Pr$$

where:

$$Gr = \frac{g\beta(T_w - T_\infty)H^3}{\nu^2}$$

and

$$Pr = \frac{\mu C_p}{\kappa} = \frac{\nu}{\alpha}$$

The cavity configuration depicted in Figure 3.6-4 is the most similar to the horizontally oriented double open-ended cavities occurring in the W74 basket geometry. The correlation selected for the double open-ended cavities within the W74 basket assembly is:

$$\overline{Nu}_H = \frac{h_c L}{k} = 0.110 \cdot ((A)^{\frac{3}{2}} \cdot Ra)^{0.345}$$

where:

$$60 \leq Ra \leq 2 \times 10^3$$

where the characteristic length is one-half of the width of the guide tube. This correlation is evaluated in the SINDA/FLUINT® thermal model based on the local thermal properties and cavity aspect ratio for each horizontal cavity formed by the upper and lower surfaces of the guide tubes. The resulting Nusselt number is used to compute a convective heat transfer rate from the horizontal surfaces of the guide tubes and the local gas temperature within the vertical channels.

The convection heat transfer from the guide tube and spacer plate surfaces that lie outside of the basket interior are computed using the isolated surface correlations for flat plates in the horizontal and vertical orientation. The same correlations are used for the canister shell surfaces.

3.6.2 Other Modes of Heat Transfer

Convection From Isolated Surfaces

Natural convection from a discrete vertical surface is computed using Equations 6-39 to 6-42 of Rohsenow,³⁸ where the characteristic length is the height of the surface. These equations are applicable over the range $1 < Ra < 10^{12}$ as follows:

$$Nu^T = \bar{C}_L Ra^{1/4}$$

$$\bar{C}_L = \frac{4}{3} \left[\frac{0.503}{\left(1 + (0.492/Pr)^{9/16}\right)^{4/9}} \right]$$

$$Nu_L = \frac{2.8}{\ln(1 + 2.8/Nu^T)}$$

$$Nu_t = C_t^V Ra^{1/3}$$

$$C_t^V = \frac{0.13 Pr^{0.22}}{\left(1 + 0.61 Pr^{0.81}\right)^{0.42}}$$

$$Nu = \frac{h_c L}{k} = \left[(Nu_L)^6 + (Nu_t)^6 \right]^{1/6}$$

Natural convection from upward facing horizontal surfaces is computed from Equations 7-21 and 7-22 of Kreith,³⁹ where the characteristic dimension (L) is typically the width of the surface, or for non-square shapes, the characteristic length may be calculated from $L = 0.9$ diameter for disk shapes and $L =$ mean of the length and the width for rectangles. These equations are applicable over the range $10^5 < Ra < 3 \times 10^{10}$ as follows:

$$Nu = \frac{h_c L}{k} = 0.54 Ra^{1/4} 10^5 < Ra < 2 \times 10^7$$

³⁸ Rohsenow, Harnett, and Ganic, *Handbook of Heat Transfer Fundamentals*, 2nd Edition, McGraw-Hill, Inc., 1989.

³⁹ Kreith, F., *Principles of Heat Transfer*, 3rd Edition, Intext Press, Inc., 1973.

$$Nu = \frac{h_c L}{k} = 0.14 Ra^{1/3} \quad 2 \times 10^7 < Ra < 3 \times 10^{10}$$

Natural convection from downward facing horizontal surfaces is computed from Equation 7-23a of Kreith. The characteristic length is the length of the surface. This equation is applicable over the range $3 \times 10^5 < Ra < 3 \times 10^{10}$ as follows:

$$Nu = \frac{h_c L}{k} = 0.27 Ra^{1/4} \quad 3 \times 10^5 < Ra < 3 \times 10^{10}$$

Natural convection from horizontal cylindrical surfaces is computed from Equation 3-43 of Chapter 1 from Guyer.⁴⁰ The characteristic length is the diameter of the cylinder. This equation is applicable over the range $10^{-5} < Ra < 10^{12}$ and is as follows:

$$Nu = \frac{h_c d}{k} = \left\{ 0.60 + \frac{0.387 Ra^{1/6}}{\left[1 + (0.559/Pr)^{9/16} \right]^{8/27}} \right\}^2 \quad 10^{-5} < Ra < 10^{12}$$

Radiation Heat Transfer

Radiation heat transfer is computed using standard gray-body equations. Shape factors between the fuel assemblies, the basket assembly surfaces, the canister shell, and the transportation cask are computed using either pre-defined relationships or the string method for standard geometric configurations. For complex, non-standard shapes, the RadCAD[®] program is used to calculate the radiation view factors. Once the view factor F_{1-2} is obtained by either method, it is used to compute the Hottel script factor, F_{1-2} , which represents the combined geometric shape and emissivity effects in a single factor. The factor is computed via the equation on page 262 of Kreith.³⁹

$$\text{Hottel script } F_{1-2} = \frac{1}{\left(\frac{1}{\varepsilon_1} - 1 \right) + \left(\frac{1}{F_{1-2}} \right) + \left(\frac{A_1}{A_2} \right) \left(\frac{1}{\varepsilon_2} - 1 \right)}$$

The heat transferred via radiation interchange, where σ is the Stefan-Boltzmann constant, is computed via the Equation 1-8 of Kreith:³⁹

$$q = \sigma A_1 F_{1-2} (T_1^4 - T_2^4)$$

Values of $(A_1 F_{1-2})$ are provided in the SINDA/FLUINT[®] input deck for each radiation conductor. The program automatically computes the T^4 values using the absolute temperature and adds the Stefan-Boltzmann constant σ .

The modes of heat transfer discussed in detail within this section are used for the W74 canister thermal analysis discussed in Sections 3.4 and 3.5, for NCT and HAC, respectively.

⁴⁰ Guyer, E.C., *Handbook of Applied Thermal Design*, McGraw-Hill, Inc., 1989.

3.6.3 Impact Of Fission Gas Release On Thermal Performance

This analysis estimates the effect upon heat transport within the FuelSolutions™ W74 canister and the TS125 Transportation Cask caused by the addition of the radioactive fission gases, xenon and krypton, to the backfill helium. The major transport parameters of interest are the Rayleigh number and the thermal conductivity. The appropriate and the most completely developed theory for the calculation of gas transport properties is based on the assumption that the only forces acting between the gaseous molecules are the intermolecular potential forces, an assumption closely satisfied if four conditions are approximately met:

- The gas is sufficiently dilute so that only binary collisions occur (as opposed to the simultaneous impact of three or more molecules).
- Collisions between molecules can be described by classical mechanics.
- These collisions are elastic.
- The intermolecular potential functions are spherically symmetrical.

The first three conditions are standard for the application of results stemming from the kinetic theory of gases, and the last is satisfied by monatomic gases such as are considered here (although only minor corrections are required for dealing with polyatomic bipolar molecules).

Based on the data used to determine the W74 canister internal pressure, the bounding fuel assembly (relative to canister pressurization) is the ANF 9x9. Sixty-four assemblies with a burnup of 40 GWd/MTU are predicted to contain 34.9 moles of fill gas (helium) and 140.9 moles of fission gases that are available for release upon cladding failure. The canister is estimated to contain 224.8 moles of helium at the time of loading, while the cask backfill is estimated to be 11.5 moles of helium. As such, the amount of fission gases released under 3% and 100% rod failure rates are as follows:

Rod Failure Rate:	<u>3%</u>	<u>100%</u>
Helium from rod fill:	1.05 moles	34.9 moles
Fission gases:	4.23 moles	140.9 moles
Helium from canister backfill:	224.8 moles	224.8 moles
Helium from cask backfill:	<u>11.5 moles</u>	<u>11.5 moles</u>
TOTALS	241.6 moles	412.1 moles

Under each of these rod failure rates, the maximum percentage of fission gas occupying the canister void space will be 1.75% and 34.2%, respectively, assuming the worst-case (i.e., smallest) void volume within the canister. Other fuel/canister combinations will result in larger canister void volumes and a lower percentage of fission gas to canister backfill gas. Further, the fission gases within the ANF 9x9 assemblies are assumed to be composed of 11% krypton and 89% xenon. These fission gas mole fractions increase to 1.8% and 35.2%, respectively, if the canister containment boundary is not breached. For conservatism, the gas mole fractions associated with the ANF 9x9 assemblies with no canister breach are used in the following evaluations.

The parameters governing the gaseous heat transport within the cask and canister are the thermal conductivity, k , and the Rayleigh number, Ra ; the former parameter is associated with pure

conduction and the latter with “free” or natural convection. The potential effect of fission gas release upon the heat transfer mechanisms within the canister is addressed by evaluating the change in relative impact of each of these parameters, taken separately and in combination, with and without the inclusion of fission gases.

Taking the Rayleigh number as the product of the Grashof number Gr , and the Prandtl number, Pr , the equation is expressed as follows:

$$Ra = Gr \cdot Pr = \left(\frac{g \cdot \beta \cdot (T_{surface} - T_{gas}) \cdot L^3}{\nu^2} \right) \cdot \left(\frac{\mu \cdot c_p}{k} \right)$$

where:

- g = the gravitational constant
- β = coefficient of thermal expansion
- $T_{surface}$ = temperature of surfaces
- T_{gas} = temperature of the gas mixture
- L = characteristic length
- ν = kinematic viscosity
- ρ = gas density
- $\mu = \rho \cdot \nu$ = dynamic viscosity
- c_p = specific heat at constant pressure
- κ = thermal conductivity of the gas mixture

It is apparent that the gas properties that must be evaluated as functions of the gas composition are β , ρ , c_p , and κ . Since the formula for calculating properties of a mixture requires a means of calculating the individual component properties, a calculation method⁴¹ was developed that yields reasonable values for the properties of helium, Xe, and Kr, as functions of temperature. The accuracy of these equations was validated against calculated values and the experimental data for viscosity and thermal conductivity.^{42, 43, 44}

Figure 3.6-5 presents the sensitivity of the thermal conductivity for the gas mixture versus the mole fraction of fission gases contained in the mixture. As expected, the thermal conductivity decreases significantly as the mole fraction of fission gases increases.

While the trend line in Figure 3.6-5 illustrates the impact on those regions of the canister and cask thermal models that are dependent on conduction through a gas layer, it does not accurately reflect the effect for those regions where convection is present. Examination of the equation for the Rayleigh number above shows that, for a given geometry and temperature difference, the

⁴¹ Reid, R.C., J.M. Prausnitz, and B.E. Poling, *The Properties of Gases and Liquids*, 4th Edition, McGraw-Hill, New York City, New York, 1987.

⁴² Neufeld, P.S., Janzen, A.R., and Aziz, R.A., *J. Chem. Phys.*, Vol. 57, 1972.

⁴³ Weast, R.C., Editor, *CRC Handbook of Chemistry and Physics*, 61st Edition, 1981.

⁴⁴ Washburn, E.W., Editor, *International Critical Tables*, McGraw-Hill, 1926.

value of the Rayleigh number (and thus the strength of the associated convection stream) will increase if either density or specific heat increases, or if viscosity or thermal conductivity decreases, or for any combination thereof. As Figure 3.6-6 illustrates, while the viscosity of the gas mixture remains essentially constant with fission gas content, the density of the gas mixture will increase significantly with higher fission gas content. Therefore, the total buoyancy force available for a given temperature difference will also increase.

Given the non-linear effects on the individual property values, the overall effect of the addition of fission gases upon the heat transport within the canister must be examined through a combined evaluation of the changes in Rayleigh number and thermal conductivity. Figure 3.6-7 shows that, until the fission gas concentration (on a mole fraction basis) that may be released into the canister is greater than about 42%, the overall effect will be an increase in the convection heat transfer rates. Since the maximum fission gas concentration for the W74 canister will be 35%, it is expected that those portions of the canister that permit convection heat transfer will see a net thermal performance improvement upon the release of any fission gases. For conservatism, this potential for improved heat transfer is ignored within the evaluations for NCT and HAC. The supposition that the potential release of the fission gases will not result in gross cladding failure of fuel stored within the W74 canister is supported by an independent analysis⁴⁵ sponsored by the NRC.

The potential effect of fission gas release on the thermal performance within the W74 canister was examined for the bounding evaluation of 100% fuel rod failure under accident conditions. The same calculation methodology used for the case with no fuel rod failure was used, with the exception that the thermal properties of the helium fill gas were modified to reflect a mixture of 65% helium and 35% fission gas.

Table 3.6-1 presents a comparison of predicted canister and cask component temperatures with and without inclusion of fission gas effects. All canister component temperatures remain within their allowable limits under the conservative combination of 100% fission gas release and a breach in the canister pressure boundary. In fact, the thermal gradients within the canisters show a decrease due to the thermal enhancement that the fission gas provides to convection heat transfer. The peak fuel cladding temperature increases by 27.5°C, primarily due to the assumption of no convection within and from the fuel assembly to the fuel guide tube. Therefore, the lower thermal conductivity associated with the fission gas release greatly increases the delta temperatures required in these regions of the thermal model. However, since in reality convection will exist in these regions as well, the observed temperature increases are expected to be less than predicted due to the presence of the fission gases. Nevertheless, the predicted peak cladding temperature remains well within the conservative 400°C limit established for the maximum allowable temperature for undamaged fuel.

As expected, the canister shell temperature shows an increase in peak temperature due to the assumed presence of fission gas in the canister-cask annulus. However, the increase is slight (i.e. 45°F), partially as a result of the increased convection within the canister that reduces the thermal stratification, and partially due to the increase in radiation heat transfer occurring at the

⁴⁵ *Safety Evaluation Report*, Docket No. 72-1026, FuelSolutions™ Storage System, Certificate of Compliance 1026, U.S. Nuclear Regulatory Commission, Washington D.C.

higher temperature levels. The peak cask component temperatures show an increase in the vicinity of the rub strip due to the decreased heat transfer rate across the canister-cask annulus with a fission gas mixture. However, as evidenced by the temperatures listed in the third column for the side of the cask (i.e., the 90° position on the cask), the component temperatures over the majority of the cask's circumference are near or below those seen for the case with no fission gas release. Furthermore, unless both the fuel rod cladding and the canister shell pressure boundary were to fail, the canister shell and cask component temperatures would show essentially no change from the case that does not consider the influence of fission gases.

In conclusion, the presence of a bounding amount of fission gases within the canister is expected to yield only marginal component temperature increases. Further, both the fuel cladding and the canister pressure boundary must fail to yield this predicted increase in temperature. Therefore, ignoring its potential presence for both the NCT and HAC evaluations of the canister thermal performance is appropriate.

3.6.4 Big Rock Point Mixed-Oxide (MOX) Fuel

The thermal evaluations provided in this chapter address UO₂ 9x9 and 11x11 BRP fuel assemblies. The analysis for UO₂ fuel bounds the condition of a FuelSolutions™ W74 canister loaded with any number of MOX fuel assemblies. The BRP MOX fuel assemblies are similar to the UO₂ assemblies with respect to all assembly physical characteristics (including fuel mass, fuel density, fuel rod cladding dimensions, cladding material, rod fill pressures, and active fuel height) except initial fuel material composition. In addition, as discussed in Section 3.6.4.4, the design operating parameters of MOX fuel is equal to or bounded by those for conventional UO₂ fuel assemblies. All existing BRP MOX fuel has a burnup level under 35 GWd/MTIHM and an assembly cooling time of at least 15 years.

3.6.4.1 Heat Generation of BRP MOX Fuel

Assembly heat generation levels are explicitly calculated for BRP MOX fuel using the ORIGEN 2.1 point-depletion code (see Section 5.5.2 of the FuelSolutions™ W74 Canister Storage FSAR²⁰). Based on this analysis, the maximum heat generation level for any existing BRP MOX fuel assembly is less than 150 watts/assembly. This is 56% less than the design basis maximum assembly heat generation level of 343.75 watts/assembly that forms the basis of the canister thermal rating given in Table 3.1-3.

3.6.4.2 Axial Heat Generation Profile of BRP MOX Fuel

The design basis axial heat generation profile discussed in Section 3.1.3 of this SAR is applicable to both MOX and UO₂ BRP fuel assemblies. The physical dimensions (such as active fuel height) of the MOX assemblies are the same as those of the corresponding UO₂ assemblies. Furthermore, the MOX and UO₂ fueled BRP assemblies are irradiated in the same reactor core, often in close proximity to each other, and they have similar linear heat ratings, maximum clad operating temperatures, etc. The BRP MOX fuel assemblies also contain a large number of UO₂ fuel rods around their periphery. For these reasons, the axial heat generation profile is expected to be very similar for BRP UO₂ and MOX assemblies.

3.6.4.3 Effective Thermal Conductivity of BRP MOX Fuel

As discussed in Section 3.4.1 of this SAR, the intact UO₂ fuel assembly is modeled as a homogenous mass that has an effective radial and axial conductivity. Given that the cladding dimensions (i.e., diameter and thickness), the number of fuel rods, and the fuel rod pitch are essentially the same for UO₂ and MOX fuel assemblies, the only significant difference between the UO₂ and MOX assembly types is the fuel material within the fuel rods. However, the fuel material does not contribute significantly to the overall axial or radial assembly conductivity⁴⁶ because the fuel material conductivity is lower than that of the fuel rod cladding. Additionally, there are potential gaps between the individual fuel pellets and between the fuel pellets and the cladding. With respect to the effective radial assembly conductivity, the majority of the thermal resistance occurs between the fuel rods, as opposed to within or across the fuel rods.

The temperature difference across the individual fuel rods is very small, even if only conduction through the cladding is considered. Therefore, the fuel material's thermal properties are conservatively neglected in the methodology used to compute the fuel assembly's axial and effective radial thermal conductivity (see Section 3.4.1). As such, the calculated axial and radial conductivities for UO₂ and MOX BRP fuel are the same.

3.6.4.4 Allowable Cladding Temperature for BRP MOX Fuel

Based on proprietary data in Jersey Nuclear and Exxon Nuclear design reports, the design operating parameters of MOX fuel assemblies used at Big Rock Point are equal to or bounded by those for conventional UO₂ fuel assemblies. As such, the bounding operational temperature (e.g., in-reactor) experience of the two fuel rod configurations are similar. Further, since the 35 GWd/MTU burnup value of the BRP MOX fuel is below the design basis 40 GWd/MTU burnup for the conventional BRP fuel, the MOX fuel internal rod pressures and operating temperature effects will be bounded by those for the conventional BRP fuel.

The peak BRP fuel rod pressure is based on a generated fission gas quantity of about 8 moles per fuel assembly. The data presented in Table 3.1-5 assume a 30% release fraction; therefore, the total fission gas quantity available for release is about 2.4 moles per assembly.

The generated fission gas inventory for all BRP MOX fuel is less than 6 moles per assembly due to its lower burnup value (under 35 GWd/MTU versus a design basis UO₂ fuel burnup of 40 GWd/MTU). Assuming a 30% release fraction, the quantity of fission gas available for release would be less than 1.8 moles per assembly. Therefore, the MOX fission gas available for release is bounded. It is also noted that the longer assembly cooling time (a minimum of 15 years) yields lower rod temperatures and, thus, rod pressures.

Given that other parameters such as cladding dimensions, gas plenum volume, and fill gas pressure are similar for the MOX and UO₂ assemblies, and given the lower MOX fuel internal rod pressure, the cladding stress levels determined for design basis BRP UO₂ fuel at any given temperature are bounding for BRP MOX fuel. Because the cladding stress levels are lower for MOX fuel, the allowable cladding temperature based on the creep methodology is bounding for all BRP MOX fuel.

⁴⁶ Manteufel, R. D. and Todreas, N. E., *Effective Thermal Conductivity and Edge Conductance Model for a Spent-Fuel Assembly*, Nuclear Technology, Vol. 105, March 1994.

3.6.4.5 Canister Internal Pressure for BRP MOX Fuel

Since the BRP MOX fuel assemblies have lower fission gas quantities and, therefore, lower internal rod pressures than the design basis BRP assemblies, the canister internal pressures calculated in Sections 3.4.4.3 and 3.5.4 of this SAR are bounding for a canister containing any amount of MOX fuel.

3.6.4.6 Thermal Summary for BRP MOX Fuel

BRP MOX fuel assemblies have an axial heat generation profile, an effective assembly thermal conductivity (axial and radial), and an assembly heat generation decay curve that are similar to those of BRP design basis (UO₂ fueled) assemblies. Furthermore, the BRP MOX fuel assemblies have lower internal rod pressures, 56% lower heat generation levels due to lower burnup level, and much longer cooling times than the BRP design basis assemblies. For these reasons, BRP MOX fuel assemblies will produce lower peak fuel cladding temperatures (when loaded into the canister), while having fuel rod cladding allowable temperatures that are at least as high as those of BRP design basis fuel assemblies.

As such, the thermal evaluations for normal and accident conditions of transportation presented in Sections 3.4 and 3.5 of this SAR are valid and bounding for canisters containing BRP MOX fuel assemblies. Therefore, it is concluded that all existing BRP MOX fuel assemblies are thermally qualified for loading into the FuelSolutions™ W74 canister and no further thermal or assembly heat generation calculations need to be performed.

3.6.5 Big Rock Point Damaged Fuel

The thermal evaluations provided in this chapter assume intact fuel assemblies. However, the analysis bounds the assumption of a canister loaded with up to eight damaged fuel assemblies. Damaged includes fuel rod damage in excess of hairline cracks or pinhole leaks. Fuel assemblies with damaged grid spacers (defined as damaged to a degree where fuel rod structural integrity cannot be assured, or where grid spacers have shifted vertically from their design position) will also be stored in damaged fuel cans. The relatively minor nature of the fuel assembly damage contained within this definition supports the basic assumption that the fuel assemblies to be placed in the damaged fuel cans have the basic geometric configuration of an undamaged fuel assembly and are expected to retain this geometry throughout normal and accident transportation events.

The evaluation for damaged fuel assemblies includes an assessment of the thermal effects imposed by the presence of the damaged fuel can. The effect of the damaged fuel can on the overall (smeared) heat transfer coefficient of the damaged fuel assemblies is deemed negligible. Because the damaged fuel has the same design heat generation rate as intact fuel, the steady-state effect would be a slight increase in the damaged fuel cladding temperatures and would not result in a change in the spacer plate temperature distribution (see Section 3.6.5.5).

Since it is not possible to definitively know the full extent of damage to each fuel assembly, the evaluation for damaged fuel also includes an assessment of the predicted temperatures within the damaged fuel can and within the W74 canister in response to a potential reconfigured fuel assembly within the damaged fuel can(s).

3.6.5.1 Heat Generation of BRP Damaged Fuel

Assembly heat generation levels are calculated for BRP damaged UO₂ and damaged MOX fuel assemblies using the ORIGEN 2.1 point-depletion code (see Section 5.5.2 of the FuelSolutions™ W74 Canister Storage FSAR²⁰). The maximum heat generation level permitted for any BRP damaged fuel assembly to be loaded into the FuelSolutions™ W74 canister is equal to the design basis maximum assembly heat generation level of 343.75 watts/assembly. Per Section 3.6.4.1, damaged MOX fuel assemblies have heat loads that are 56% less than those of the design basis assembly. The design basis heat generation rate forms the basis of the canister thermal rating given in Section 3.1.4 of this SAR.

3.6.5.2 Axial Heat Generation Profile of BRP Damaged Fuel

The design basis axial heat generation profile discussed in Section 3.1.3 is applicable for damaged and intact UO₂ and MOX BRP fuel assemblies. The physical dimensions (such as active fuel height) of the damaged fuel assemblies are the same as those of the corresponding intact assemblies. The damaged fuel assemblies are also irradiated in the same reactor core as the intact fuel assemblies. Therefore, for given burnup and cooling time, the BRP damaged fuel axial heat generation profile is the same as that for the BRP intact fuel assemblies.

The axial heat generation profile associated with a potential reconfigured damaged fuel assembly is addressed in the following section.

3.6.5.3 Effective Thermal Conductivity of BRP Damaged Fuel

Given the level of damage expected for BRP damaged fuel, the thermal resistance between the damaged fuel can and the damaged fuel assembly is expected to be encompassed by that used for the evaluation of the intact fuel assemblies. As discussed in Section 3.2.2, the fuel assembly is modeled as a homogenous mass that has an effective radial and axial conductivity. The effective radial and axial conductivities are assumed to be the same for both the UO₂ and MOX damaged fuel assemblies (see Section 3.6.4.3). A mis-positioned grid spacer, or damage in the excess of a pinhole leak or hairline crack in a few rods will not affect the overall pin-to-pin heat transfer via radiation or conduction/convection that characterizes an intact fuel assembly. Also, the loss of a rod's internal gas pressure due to a defect will not affect the computed effective conductivity for the assembly because the presence of both the fill gas and the fuel material is conservatively ignored by the methodology used (see Section 3.2.2).

Since damaged rods will have released their gas prior to placement within the canister, there will be no introduction of fission gas from the damaged fuel into the canister atmosphere. Further, analysis has shown that the presence of fill gas constituents within the canister environment will not adversely affect the overall heat transfer rates.

Therefore, damaged BRP fuel will not have an effect on the overall (smeared) fuel assembly effective thermal conductivity. For these reasons, the effective thermal conductivity of the BRP damaged fuel is predicted to be bounded by the UO₂ and MOX intact fuel assemblies (refer also to the discussion on the effective thermal conductivity of MOX fuel in Section 3.6.4.3). However, since it is not possible to definitively know the full extent of damage to each fuel assembly, the evaluation for damaged fuel also includes an assessment of the predicted

temperatures within the damaged fuel can and within the W74 canister in response to a potential reconfigured fuel assembly within the damaged fuel can(s).

A reconfigured fuel assembly is expected only as the result of an accident condition. The two credible accident scenarios that could yield significant failure to the damaged fuel assemblies are a side drop or an end drop. A side drop accident could result in damage levels ranging from nothing, to a bounding scenario involving the fracture and collapse of the fuel assembly against the wall of the damaged fuel can. Given that only a nominal 0.35 inch of space exists between the edges of the fuel assembly and the walls of the damaged fuel can, and that the effective radial thermal conductivity for the intact fuel assembly (see Section 3.2.2) takes no credit for convection within the fuel assembly or contact between the assembly and the damaged fuel can walls, a partial collapse of the fuel assembly will not significantly affect the heat transfer within the damaged fuel can.

The bounding side drop damage scenario, which involves the fracture and collapse of the fuel assembly against the wall of the damaged fuel can, will yield a situation where the fuel rod sections are in direct contact with one another and/or the wall of the damaged fuel can. The heat transfer within this reconfigured fuel assembly would actually improve due to the direct contact between the individual fuel rods and the increase in surface area as the debris spreads across the width of the fuel can. Combined with the direct contact between the fuel assembly and the wall of the damaged fuel can, this would yield an overall improvement in the heat transfer and temperature distribution within the damaged fuel can and the W74 canister. This conclusion is confirmed by the end drop scenario analysis results discussed in Section 3.6.5.6.

A key assumption in the above side drop damage scenario is that the axial distribution of heat within the reconfigured fuel assembly will be consistent with the undamaged fuel assembly. The antithesis to this assumption is that the fuel debris collects in a concentrated rubble pile. The most credible event leading to this situation will occur if the canister is upended subsequent to the side drop induced damage, and the broken sections of fuel are concentrated at the bottom of the damaged fuel can. A bounding scenario for the concentrated rubble pile is addressed below as part of the end drop scenario.

The second credible accident scenario that could yield significant failure to the damaged fuel assemblies is an end drop. An end drop could ultimately result in a damaged fuel assembly fracturing and ending up in a pile at the bottom of the damaged fuel can. A similar geometry would result if a canister containing a fuel assembly damaged from a side drop is upended. Based on the bounding minimum solid volume presented by the range of BRP fuel, the fuel assembly could ultimately collapse to occupy the lower 38.7 inches of the damaged fuel can. This volume is based on the absence of flow channels (removed prior to loading) and a porosity of 0.45 (based on the minimum value typical for granular material). A shorter height is not feasible based on the use of the minimum solid volume and porosity. Contrarily, a larger height dimension would yield a lower decay heat density within the rubble and a larger surface area to transfer the heat. Conservatively, the decay heat within this shortened rubble pile is distributed using the same peaking factor curve used for the undamaged fuel assemblies.

Heat transfer within the rubble pile is evaluated three ways: as a tightly packed group of rods, as a loosely packed group of rods,⁴⁷ or as a porous media.⁴⁸ Table 3.6-2 shows the effective thermal conductivity as a function of temperature for these three means of representing the rubble pile. The lowest effective heat transfer coefficient among these three options (i.e., a loosely packed group of rods) is used to compute the temperatures within the rubble pile. The void space above the rubble pile is treated as a combination of convection and radiation between the walls of the damaged fuel can.

3.6.5.4 Allowable Cladding Temperature for BRP Damaged Fuel

The appropriate allowable temperature for BRP damaged fuel is the same as that for the intact fuel assemblies since, despite the presence of the damaged fuel can, the design goal is to avoid any additional failures. Sections 3.3.2 and 3.6.4.4 address the allowable cladding temperatures for intact UO₂ and MOX fuel assemblies. The cladding temperature for the BRP damaged fuel is estimated in Section 3.6.5.5.

3.6.5.5 Estimated Cladding Temperature for BRP Damaged Fuel

It is concluded that the damaged fuel assemblies will not exceed the cladding allowable temperature for the reasons summarized below. As noted in Table 3.4-1 of this SAR, the NCT Hot temperature difference between the peak intact fuel rod and the hottest guide tube wall is approximately 28°F (i.e., 656°F - 628°F). This temperature difference is essentially the same as the 26°F (i.e., 625°F - 599°F) temperature difference seen at the support tube location where a damaged fuel can would be placed. The added thermal resistance created by the presence of the damaged fuel can walls will act to slightly increase this required delta temperature.

Given the same assembly decay heat load, a similar temperature difference (i.e., 26°F) will exist between the damaged fuel assemblies and the walls of the damaged fuel can. This assumption is justified because, with the exception of its vented top and bottom covers, the cross-section of the damaged fuel can has a similar geometry and surface finish properties as a guide tube and because the heat transfer mechanisms from the damaged fuel assembly and the damaged fuel can are the same as for the intact fuel assembly and the basket support tube walls. Although this assumption is based on a damaged fuel assembly that maintains a similar geometry as an intact fuel assembly, considerable latitude exists. For example, a missing or bowed fuel rod will increase the radiation and convection exchange between the interior of the fuel assembly and the walls of the can.

The presence of the damaged fuel can within the support tube will introduce an added thermal resistance due to the additional need to transfer heat from the damaged assembly to the support tube walls. This thermal resistance can be conservatively estimated assuming conduction across the gap between the walls of the damaged fuel can and the basket support tube. This gap is a nominal 0.085 inches [i.e., (7.4 inches - 7.23 inches)/2]. Given a damaged fuel can width of

⁴⁷ License Application Design Selection Feature Report: Rod Consolidation, OCRWM Report #B00000000-0717-2.200-0210, Rev. 0, June 1999.

⁴⁸ Kaviany, M, *Principles of Heat Transfer in Porous Media*, 2nd Edition, Springer-Verlag, New York, New York, 1995.

7.23 inches and a conservatively high peak heat generation rate of 22 kw/64 assemblies/70-inch active fuel length*1.21 peaking factor = 5.94 watts/inch. The delta T required to pass this heat generation rate across the gap between the damaged fuel can wall and the support tube wall via conduction alone is:

$$\Delta T = QL/(kA) * \text{ratio of interior to local heat generation}$$

where:

ΔT = Temperature difference

Q = Heat generation rate (5.94 watts/inch)

L = Gap width (0.085 inches)

K = Thermal conductivity for helium (~0.122 BTU/hr-ft-F)

A = Area per unit length (4 sides x 7.23 inches)

$$\begin{aligned}\Delta T &= 5.94 \text{ watts/inch} * 3.413 \text{ BTU/hr/watt} * 0.085 \text{ inches} / \\ & [0.122 \text{ BTU/hr-ft-F} * 4 * 7.23 \text{ inches} / 12] \\ &= 5.9 \text{ }^\circ\text{F} \\ &= 3.3 \text{ }^\circ\text{C}\end{aligned}$$

This estimated temperature increase would be less if the contribution of radiation heat transfer had been included. Based on this analysis, the peak rod temperature within the damaged fuel assembly is conservatively estimated to be 6°F higher than an intact fuel assembly at the same location, or 631°F at the NCT Hot condition (i.e., 625°F + 6°F or 333°C). This is well within the allowable cladding temperature established for BRP fuel.

For similar reasons, the presence of damaged fuel cans in the support tubes will not significantly affect the peak fuel rod temperatures within the basket. Only a small fraction of the heat from the other assemblies in the basket flows through the support tube interior (i.e., as evidenced by the 28°F/26°F ratio of interior to local temperature differences). Most of the heat travels around the support tubes via convection or through the thick (0.75-inch) steel support tube walls.

Similar arguments apply to all other normal and accident conditions for the FuelSolutions™ W74 canister. A sufficient thermal margin between the hottest fuel cladding location and the 400°C fuel cladding limit to accommodate the added 3.3°C due to the presence of the damaged fuel can. In reality, since the support tube is not the location of the hottest fuel cladding, an even greater thermal margin will exist. Therefore, it can be concluded that a canister loaded with damaged fuel assemblies would not approach the fuel cladding allowable temperature for any case.

3.6.5.6 Estimated Cladding Temperature for BRP Fuel Rubble

An alternative analysis examines the temperatures within the damaged fuel can and W74 canister assuming the BRP damaged fuel is reconfigured due to an accident scenario. The damaged fuel can serves to confine the resulting sections of fuel assembly within the can, with the material occupying the lower 38.7 inches of the damaged fuel can. This rubble volume is based on the dimensions of the damaged fuel can, the minimum feasible solid volume for the intact fuel

assembly, and the minimum porosity for granular material. Larger rubble volumes will act to decrease temperatures due to a reduction in the decay heat density and an increase in the surface area available for heat transfer.

The thermal model of the W74 canister described in Section 3.4.1 of this SAR was modified to simulate the presence of the damaged fuel can and the fuel rubble at the four basket locations where damaged fuel cans may be placed. The modifications consisted of replacing the thermal conductivity for intact fuel assemblies with that for the fuel rubble discussed in Section 3.6.5.3, and with the damaged fuel can discussed in Section 3.6.5.5 over the lower 38.7 inches of each damaged fuel can location. Heat transfer above this height was treated as convection and radiation across an empty damaged fuel can.

Previous thermal modeling with simulated BRP fuel rubble for the “Off-Normal Hot” conditions of transfer within the FuelSolutions™ W150 Transfer Cask presented in the FuelSolutions™ W74 Canister Storage FSAR²⁰ can also be used to estimate the impact of this fuel configuration for the transportation condition. Since both conditions involve the canister in the horizontal position, similar differences between the temperatures for the undamaged and damaged conditions will exist. Figure 3.6-8 illustrates the temperature comparison for the “Off-Normal Hot” conditions of transfer between a canister full of intact fuel assemblies and a canister with reconfigured, damaged fuel assemblies. The parameters chosen for comparison are the intact fuel cladding temperatures at the peak location (near the basket center), the maximum temperature around the support tube, and the temperature of the cladding/failed fuel at the support tube location. As seen from the figure, the presence of the reconfigured fuel within the failed fuel can is clearly seen by the downward shift and shortening of the temperature distribution at this location. The peak fuel cladding temperature within the canister was seen to increase by only 10°F due to the presence of the damaged fuel can and the reconfigured fuel, while the peak cladding/failed fuel temperature at the support tube location increases by 30°F.

Assuming a similar change in temperature levels for a W74 canister within the TS125 Transportation Cask, it can be concluded that the presence of the damaged fuel can will not cause the W74 canister component temperatures to exceed their allowables, whether the damaged fuel remains intact or even if, conservatively, the fuel reconfigures into a pile as a result of an accident scenario.

3.6.5.7 Canister Internal Pressure for BRP Damaged Fuel

The intact fuel rods within the BRP damaged fuel assemblies are assumed to have the same internal rod pressures as the design basis BRP assemblies. As such, the canister interior pressures calculated in Sections 3.4.4 and 3.5.4 of this SAR are bounding for any canister containing damaged fuel assemblies because the gas released from the damaged fuel rods prior to loading will not contribute to canister pressurization.

3.6.5.8 Thermal Summary for BRP Damaged Fuel Assemblies

For the above reasons, it is concluded that the thermal analyses for BRP intact assemblies presented in Sections 3.4 and 3.5 of this SAR bound the damaged fuel assemblies with respect to thermal considerations. Therefore, the canister thermal rating and the canister de-rating as a

function of assembly burnup given in Table 3.1-3 and Table 3.1-4 of this SAR apply for both intact and damaged BRP fuel assemblies.

3.6.6 Big Rock Point Partial Fuel Assemblies

Partial assemblies have fuel rods missing from the design basis assembly array. The thermal evaluations previously provided in this chapter assume intact fuel assemblies. However, the analysis bounds the assumption of a canister loaded with any number of partial fuel assemblies.

3.6.6.1 Maximum Canister Thermal Rating for BRP Partial Fuel Assemblies

Table 3.1-3 and Table 3.1-4 in this SAR specifies the maximum thermal rating for the W74 canister and the canister derating as a function of assembly burnup.

For a given assembly burnup, initial enrichment, and cooling time, a lower number of fuel rods results in a lower assembly fuel loading, and therefore a lower level of assembly heat generation. The maximum thermal rating and canister derating presented in Table 3.1-3 and Table 3.1-4 are based on a heat load of no more than 22 kW for a FuelSolutions™ W74 canister completely loaded with intact BRP assemblies. For a canister loaded with one or more partial BRP assemblies, the required cooling time will always yield a canister heat load lower than the allowable value of 22 kW.

3.6.6.2 Effective Thermal Conductivity of BRP Partial Fuel Assemblies

The effective thermal conductivities for BRP partial assemblies are similar to and bounded by those of intact BRP fuel assemblies. In fact, missing fuel rods will increase the effective radiative conductivity of the assembly due to higher values of radiation heat exchange within the assembly.

Radiative heat transfer between fuel rods is a primary mode of heat transfer across the assembly fuel rod array.⁴⁶ Each row of rods effectively forms a radiation barrier; that is, it adds to the overall thermal resistance of the assembly. For a given rate of heat flow across the assembly, there is a given temperature drop (required to move the heat via radiation and conduction) between each row of fuel rods. The lower the number of “jumps” the heat has to make while crossing the assembly, the higher the effective assembly thermal conductivity. Thus, the removal of fuel rods allows heat transfer via radiation to pass directly through those fuel rod locations to the rods on the other side. This reduction in the need for absorption and re-radiation will enhance the overall radiative heat transfer across the assembly.

It is also true that removing rods opens up larger void spaces between rods that will allow for greater convective heat transfer across the assembly. While the conductivity within an individual fuel rod is greater than the conductivity of the helium that would occupy that location if the rod were removed, the enhanced radiative and convective heat transfer that results from the removal of a fuel rod offsets the increased local value of thermal conductivity due to the rod’s presence. For these reasons, the removal of fuel rods will enhance the effective conductivity of a fuel assembly, as well as reduce the assembly heat generation level.

3.6.6.3 Thermal Summary for BRP Partial Fuel Assemblies

For the above reasons, it is concluded that BRP intact assemblies bound partial assemblies with respect to thermal considerations. Therefore, the canister thermal rating given in Table 3.1-3 and

the canister de-rating as a function of burnup given in Table 3.1-4 of this SAR apply for both intact and partial BRP fuel assemblies. The thermal evaluations for normal and accident conditions of transportation presented in Sections 3.4 and 3.5 of this SAR are valid and bounding for canisters containing partial fuel assemblies.

3.6.7 Computer Code Descriptions

3.6.7.1 Thermal Desktop® Computer Code

The analytical thermal model for the FuelSolutions™ TS125 Transportation Cask is developed using the Thermal Desktop® computer code.⁴⁹ Thermal Desktop® provides a CAD-based, PC environment for generating geometric thermal models and visualizing results. Thermal models can be generated using finite elements, finite difference meshes, lumped parameter (arbitrary) networks, or all three at once. Available CAD drawings can be used to aid the building of the thermal models. The code automatically calculates the model areas, lengths, etc. that are required to construct the various thermal conductors needed to define the problem. The results of these computations are exported to a file format that is suitable for use as an input stream to the SINDA/FLUINT® heat transfer code (see below). Included with this thermal model definition are the ability to assign thermo-physical properties, including constant and temperature dependent capacitance and conductivity, anisotropic conductivity, etc.

The computation of radiation heat exchange conductors is handled within the Thermal Desktop® computer code using the RadCAD® analyzer. RadCAD® is a fast thermal radiation analyzer that uses Monte Carlo Ray Tracing to calculate form factors, radiation conductors, and heating rates for true conic surface representations. If required, the RadCAD® code is capable of computing radiation exchange factors for specular and diffuse surfaces and surfaces with angular dependent properties.

Both the Thermal Desktop® computer code and its embedded RadCAD® analyzer have been validated for use under the EnergySolutions Spent Fuel Division Quality Assurance program.

3.6.7.2 SINDA/FLUINT® Computer Code

The analytical thermal models for the W74 canister and the transportation cask are developed using the SINDA/FLUINT® heat transfer code.⁵⁰ This finite difference, lumped parameter code was developed under the sponsorship of the NASA Johnson Space Center and has been evaluated and validated for simulating the thermal response of transportation packages.⁵¹ The program is available as either a public domain code from the government software libraries, or in one of several forms from private vendors. The program is validated for use per the BFS Quality Assurance program.

⁴⁹ Thermal Desktop®, Version 3.1, prepared for NASA, Johnson Spacecraft Center, Contracts NAS8-40560 and NAS8-97009, by Cullimore and Ring Technologies, Inc., Littleton, Colorado, 1999.

⁵⁰ SINDA/FLUINT®, *Systems Improved Numerical Differencing Analyzer and Fluid Integrator*, Version 4.1, Prepared for NASA, Johnson Spacecraft Center, Contracts NAS9-19365 and NAS9-97017, by Cullimore and Ring Technologies, Inc., Littleton, Colorado, 1999.

⁵¹ Glass, R.E., et al., *Standard Thermal Problem Set for the Evaluation of Heat Transfer Codes Used in the Assessment of Transportation Packages*, SAND88-0380, Sandia National Laboratories, August 1988.

In addition, the code has been used for the analysis and subsequent licensing of several other transportation packages for nuclear material, including the RTG transportation package⁵² and the TRUPACT-II transportation package.⁵³

The SINDA/FLUINT® code provides the capability to simulate steady-state and transient temperatures using temperature-dependent material properties and heat transfer via conduction, convection, and radiation. Heat transfer solutions for one-, two-, or three-dimensional problems may be programmed. Complex algorithms may be programmed into the solution process for the purposes of computing the various heat transfer coefficients as a function of geometry, fluid, and temperatures; or, for example, to estimate the effects of buoyancy-driven heat transfer. Standard algorithms are used for computing the convection heat transfer from common surfaces (i.e., vertical and horizontal plates, cylinders, etc.) as a function of the surface geometry, the fluid properties, and the temperatures.

A major feature of the SINDA/FLUINT® code used for this modeling is the ability to use thermal submodels to represent common geometry sections of the canister shell, guide tubes, spacer plates, etc. A thermal submodel is defined as a thermal model that contains the necessary information to be independently solved for the temperatures of the components that it simulates, but which depends on one or more other thermal submodels for some or all of its boundary conditions. Thermal interconnections are provided to allow the various thermal submodels to “communicate” with each other. This thermal modeling approach simplifies the modeling and verification process by minimizing the amount of original coding required to provide a complete thermal representation of the system.

3.6.7.3 RadCAD® Computer Code

The radiation exchange thermal conductors for the W74 Canister are developed using the RadCAD® computer code. RadCAD®, developed under the sponsorship of the NASA Johnson Space Center, is a software system designed to calculate radiation exchange factors from complex geometries for use with the SINDA/FLUINT® thermal analyzer. It uses the AutoCAD® computer program as the 3-D visualization and mesh generation engine. Options are available for specifying the radiation properties of each surface, specifying whether a surface is active or inactive, etc. The same nodal layout illustrated for the SINDA/FLUINT® thermal model in Section 3.4 of this SAR is used for the surface generation within the RadCAD® computer code. Additional meshing is used to sub-divide these surfaces and achieve greater computational accuracy.

⁵² DOE Docket No. 94-6-9904, *Radioisotope Thermoelectric Generator Transportation System Safety Analysis Report for Packaging*, WHC-SD-RTG-SARP-001, prepared for the U.S. Department of Energy, Office of Nuclear Energy, under Contract No. DE-AC06-87RL10930 by Westinghouse Hanford Company, Richland, Washington.

⁵³ NRC Certificate of Compliance Number 9218 for TRUPACT-II Package, Docket Number 71-9218, prepared for the U.S. Nuclear Regulatory Commission by Nuclear Packaging Inc., Federal Way, Washington, March 3, 1989.

Table 3.6-1 - FuelSolutions™ W74 Canister Maximum System Temperatures With and Without Fission Gas Release

Component	NCT Thermal Load Condition ⁽¹⁾		
	Case 2 (100°F/No Solar) w/ No Rod Failure	Case 2 (100°F/No Solar) w/ 100% Rod Failure	
Peak Fuel Cladding	343.2°C	370.7°C	
Guide Tube	621°F	658°F	
Spacer Plates			
Stainless Steel	583°F	593°F	
Carbon Steel	608°F	636°F	
Support Tube	593°F	627°F	
Avg. Canister Gas	520°F	557°F	
Canister Shell	467°F	512°F	496°F ⁽²⁾
Avg. Canister-Cask Gas	371°F ⁽³⁾	406°F ⁽³⁾	383°F ⁽²⁾
Inner Cask Shell	356°F ⁽³⁾	399°F ⁽³⁾	347°F ⁽²⁾
Gamma Shield (Lead)			
Maximum	344°F ⁽³⁾	379°F ⁽³⁾	342°F ⁽²⁾
Bulk Average	326°F ⁽³⁾	354°F ⁽³⁾	320°F ⁽²⁾
Outer Cask Shell	320°F ⁽³⁾	344°F ⁽³⁾	320°F ⁽²⁾
NS-4-FR Shield			
Max. Radial Avg.	281°F ⁽³⁾	301°F ⁽³⁾	253°F ⁽²⁾
Bulk Average	252°F ⁽³⁾	269°F ⁽³⁾	245°F ⁽²⁾
Shear Block ⁽⁴⁾	309°F	334°F	-
Neutron Shield Jacket	215°F ⁽³⁾	212°F ⁽³⁾	196°F ⁽²⁾
Personnel Barrier	115°F	117°F	117°F

Notes:

- (1) All temperatures in this table are based on heat loads of 22.0 kW, with the design basis BRP profile.
- (2) Temperatures computer along an axial cut plane that passes through the 90-degree position on the cask.
- (3) Temperatures computed along an axial cut plane that passes through the “rub rails” to capture the peak temperatures noted in the cask. Lower temperatures are noted at the other cask circumference positions.
- (4) Shear block temperature presented for a location coincident with maximum temperature, not the same location used for the HAC analysis.

Table 3.6-2 - W74 Damaged Fuel Effective Conductivity

Material	Temperature (°F)	Effective Thermal Conductivity (BTU/hr-ft-°F)	Density ⁽¹⁾ (lb/ft ³)	Specific Heat (BTU/lb-°F)
Loosely Packed Consolidated Fuel Rods	77	0.324 ⁽¹⁾	Not needed	Not needed
	122	0.347		
	212	0.393		
	302	0.451		
	392	0.509		
	482	0.572		
	572	0.636		
	662	0.711		
	752	0.786		
Tightly Packed Consolidated Fuel Rods	77	0.416 ⁽¹⁾	Not needed	Not needed
	122	0.480		
	212	0.624		
	302	0.780		
	392	0.954		
	482	1.133		
	572	1.306		
	662	1.474		
	752	1.630		
Porous Media	392	2.040 ⁽²⁾	Not needed	Not needed
	572	1.699		
	752	1.560		

Notes:

⁽¹⁾ Table 5-1, *License Application Design Selection Feature Report: Rod Consolidation*, OCRWM Report #BOOOOOOOO-0717-2.200-0210, Rev. 0, June 1999.

⁽²⁾ Based on the thermal conductivity of helium and uranium oxide and the methodology presented in *Principles of Heat Transfer in Porous Media*, 2nd Edition, M. Kaviany, Springer-Verlag, New York, New York, 1995.

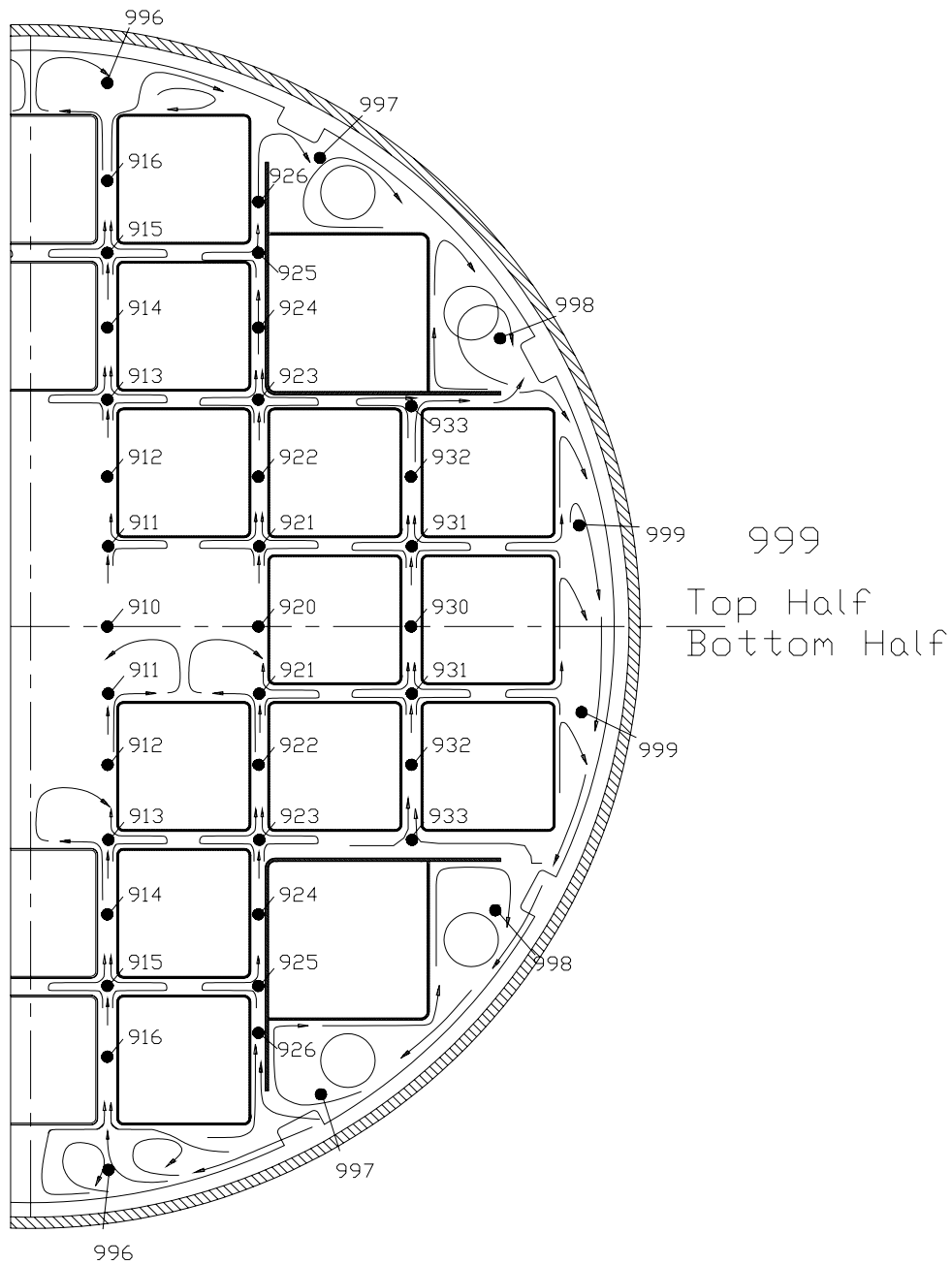


**Figure 3.6-1 - Gas Node and Flow Pattern
in a Horizontal Canister**

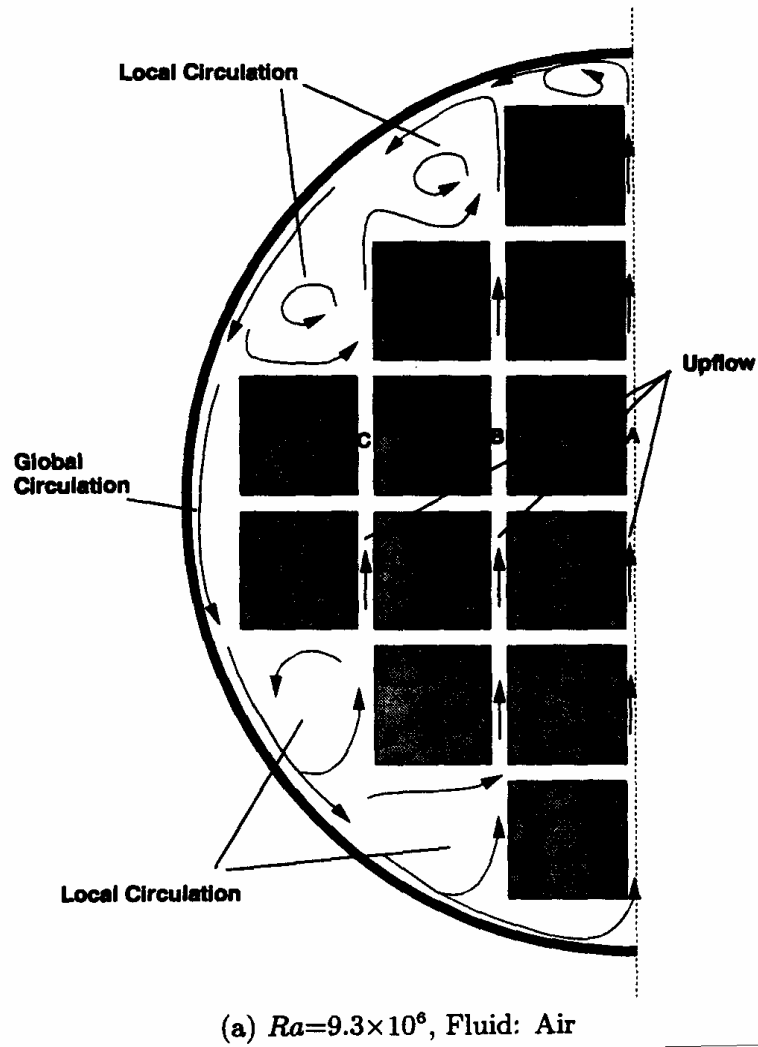


Figure 3.6-2 - Circulation Pattern within NUHOMS® 24 Unit DSC

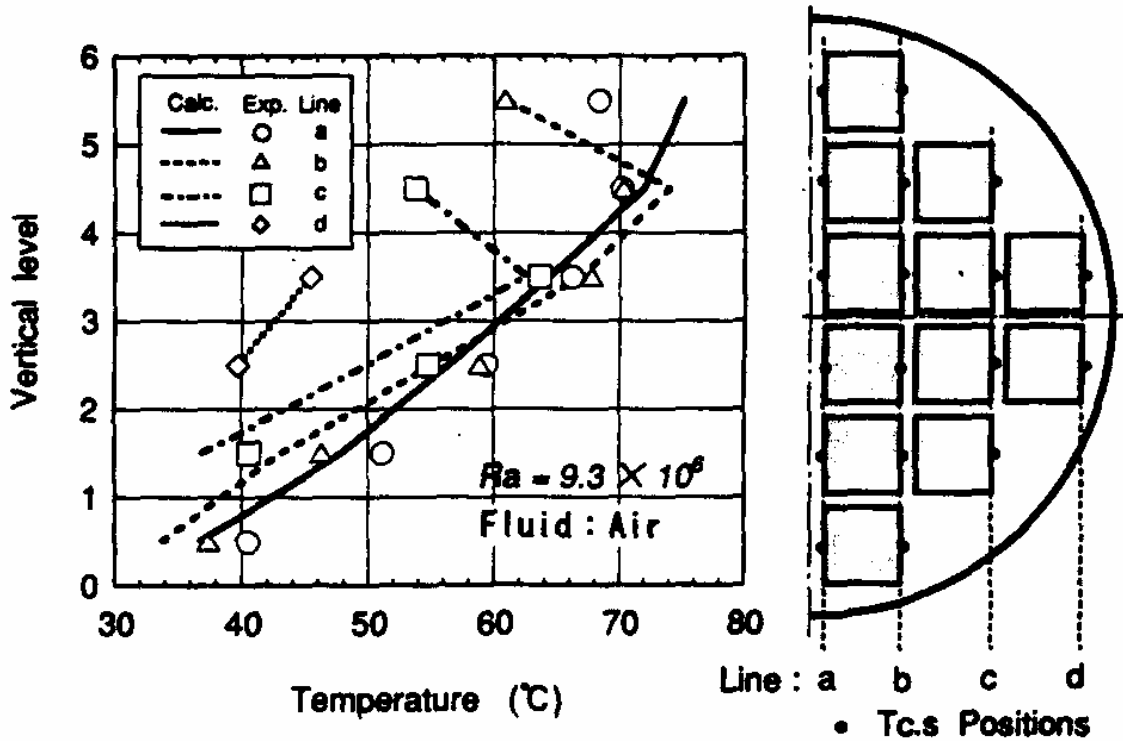


Figure 3.6-3 - Temperature Distribution in NUHOMS® 24 Unit Basket

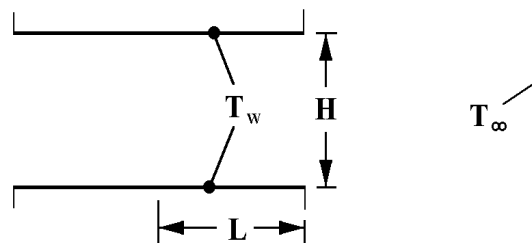


Figure 3.6-4 - Double Open-Ended Cavity with Two Heated Walls

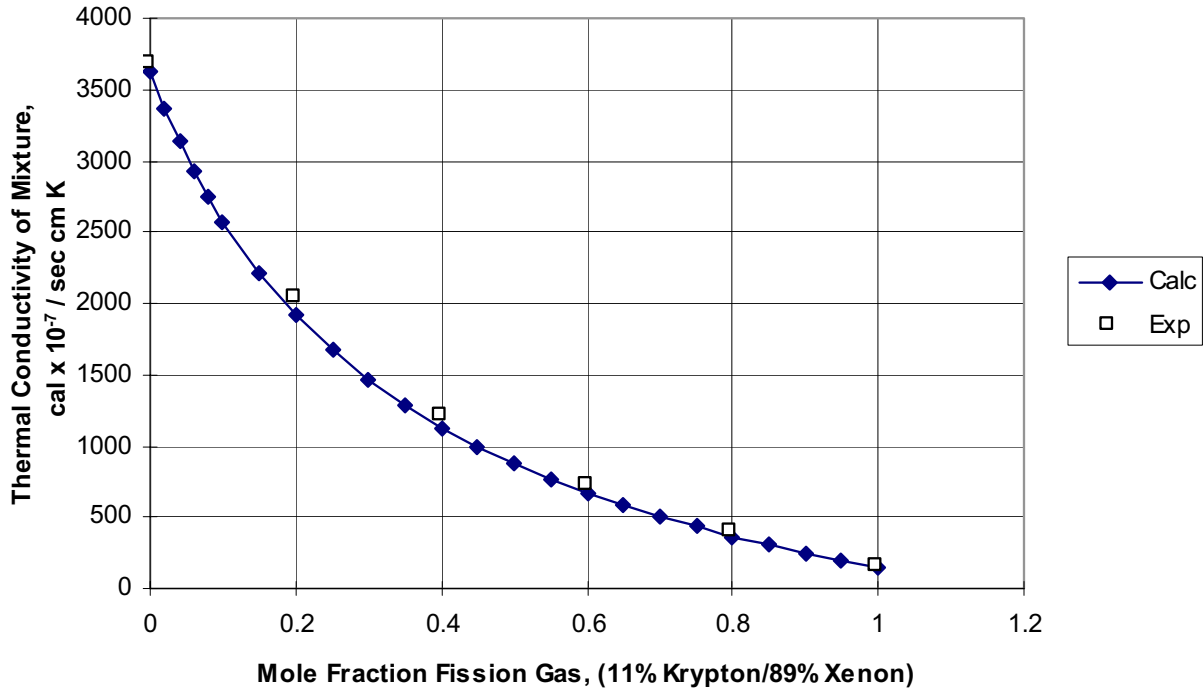


Figure 3.6-5 - Gas Mixture Thermal Conductivity vs. Fission Gas Mole Fraction

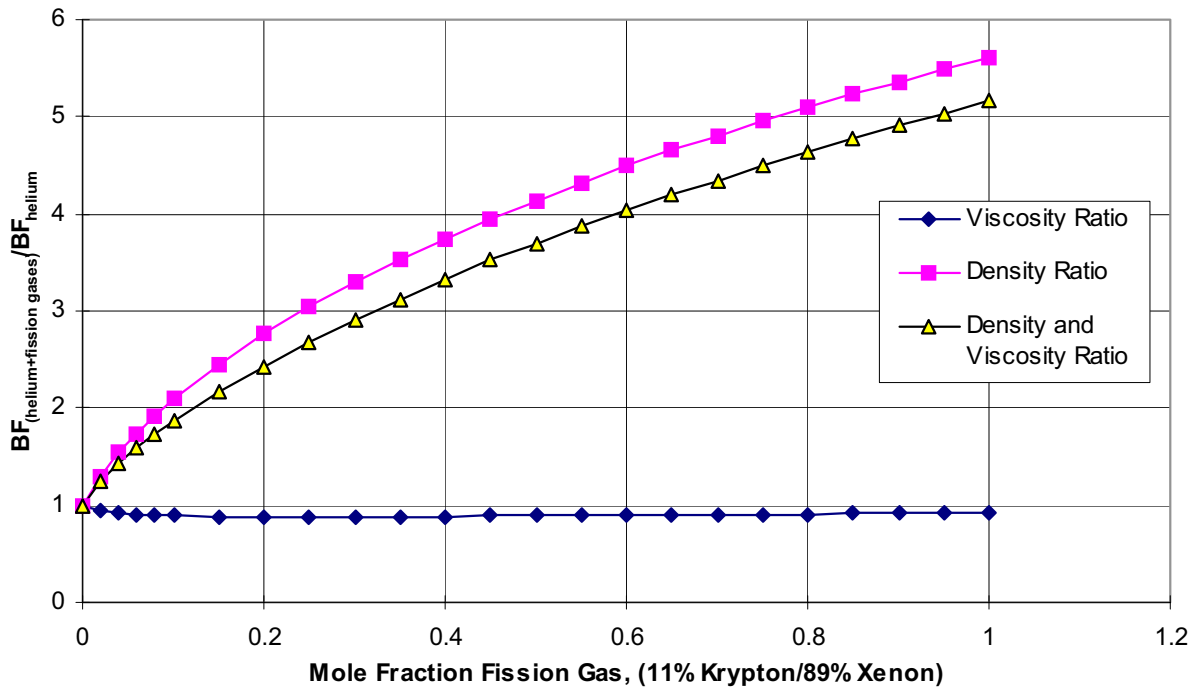


Figure 3.6-6 - Change in Buoyancy Forces Due to Addition of Fission Gases To Helium Backfill Gases

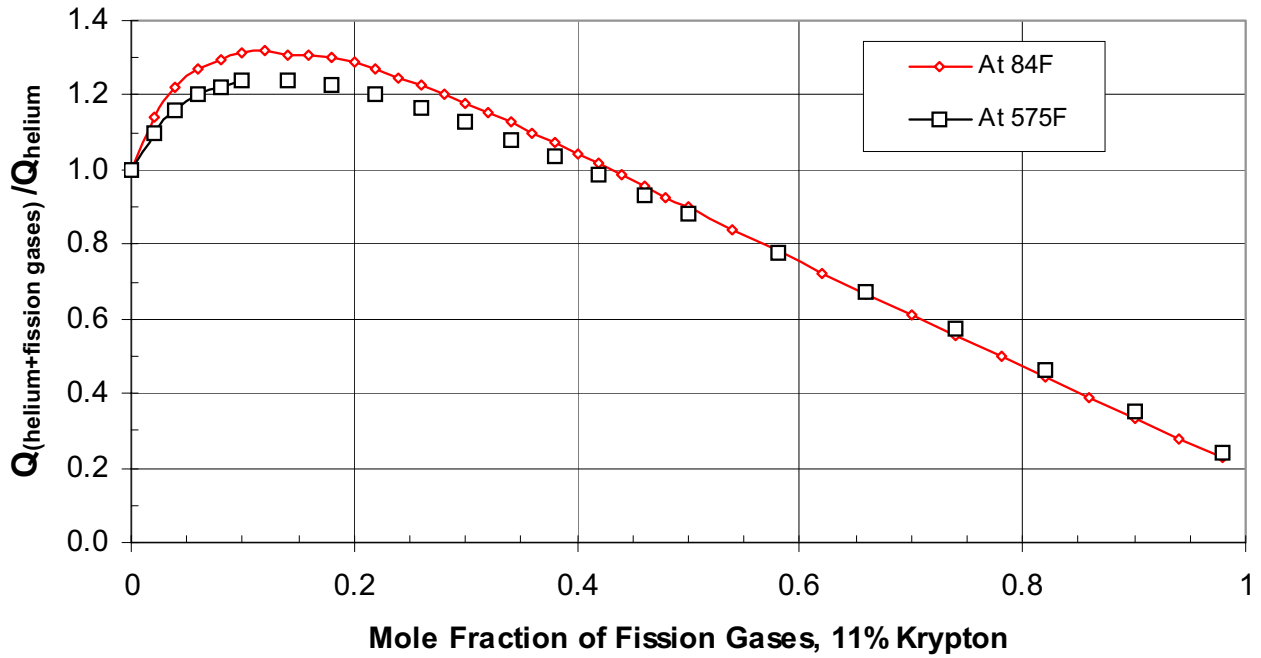


Figure 3.6-7 - Combined Effect on Convection Heat Transfer Due to Addition of Fission Gases

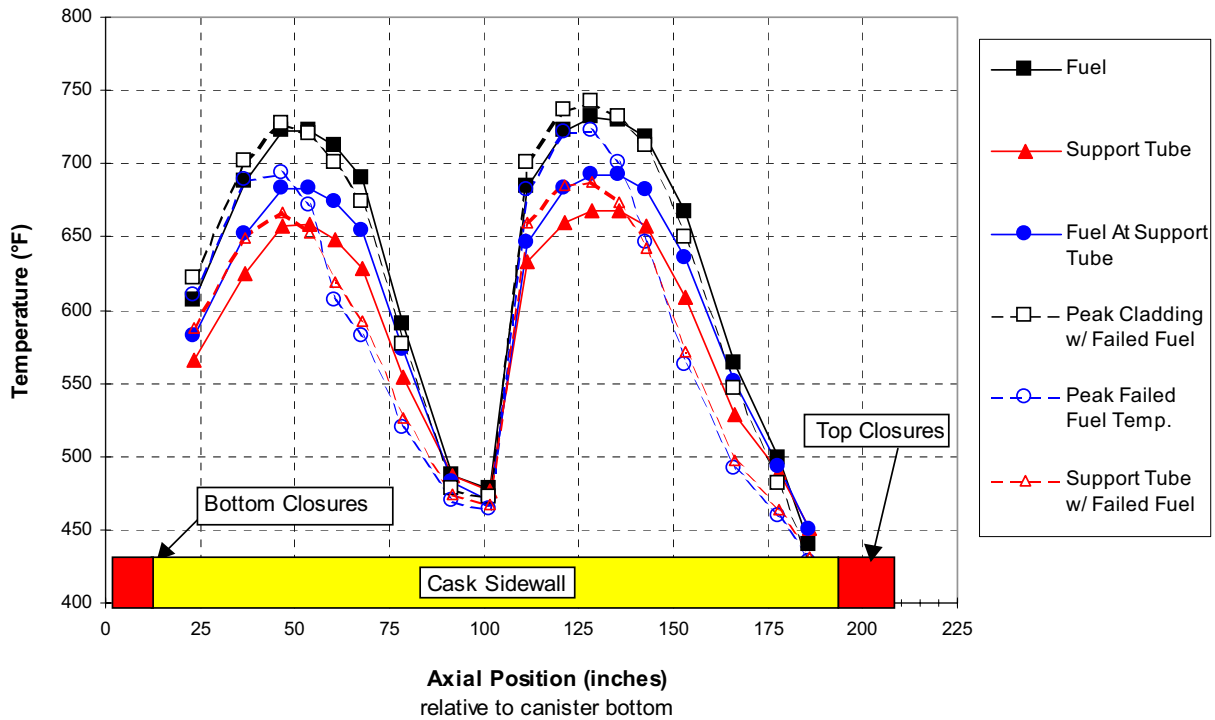


Figure 3.6-8 - Effect of Reconfigured, Damaged Fuel on W74 Canister Temperatures Within W150 Transfer Cask

This page intentionally left blank.

4. CONTAINMENT

Containment of all radioactive materials in the FuelSolutions™ W74 canister, including the SNF assemblies, is provided by the FuelSolutions™ TS125 Transportation Cask. The cask containment evaluation is provided in Chapter 4 of the FuelSolutions™ TS125 Transportation Cask SAR.¹

¹ WSNF-120, *FuelSolutions™ TS125 Transportation Cask Safety Analysis Report*, NRC Docket No. 71-9276, EnergySolutions Spent Fuel Division, Inc.

This page intentionally left blank.

4.1 Description of Containment System

Chapter 4 of the FuelSolutions™ TS125 Transportation Cask SAR describes the containment system. This chapter discusses any canister-specific features or differences from the discussion in Chapter 4 of the FuelSolutions™ TS125 Transportation Cask SAR.

The materials of construction for the FuelSolutions™ W74 canister are evaluated and selected to avoid chemical, galvanic, or other reactions. FuelSolutions™ canisters and the TS125/canister cavity are backfilled with inert gas to further assure that the materials of construction and SNF assemblies are protected from degradation due to chemical, galvanic reactions, or other reactions. Section 2.4.4 presents the materials evaluation for the W74 canister.

4.1.1 Containment Boundary

See Chapter 4 of the FuelSolutions™ TS125 Transportation Cask SAR.

The W74 canister does not include an inner containment system (for loading more than 20 curies of plutonium per canister of damaged fuel debris, etc.).

4.1.2 Codes and Standards

See Chapter 4 of the FuelSolutions™ TS125 Transportation Cask SAR.

The codes, standards, and criteria for the damaged fuel cans are the same as those of the W74 basket assembly, since the cans also support neutron attenuation sheets. The damaged fuel cans are designed in accordance with Section III, Subsection NG of the ASME B&PV Code,² and the buckling design criteria of NUREG/CR-6322³ and Article F-1331.5(a)(1).² The allowable stresses are discussed in Section 2.1.2.1 of this SAR.

4.1.3 Special Requirements for Damaged Spent Nuclear Fuel

Spent nuclear fuel assembly records are evaluated to determine that the condition of the fuel is suitable for loading. Fuel that is known or suspected to be damaged is visually inspected prior to loading. If the visual inspection indicates that damage exists greater than a hairline crack or pinhole leak, the fuel must be considered damaged.

Damaged fuel may be loaded into the FuelSolutions™ W74 canister. The damaged fuel assemblies are canned in special overpacks to facilitate handling and confine gross fuel particles to a known subcritical volume under NCT and HAC conditions. Figure 4.1-1 shows the damaged fuel can. Damaged fuel cans are designed with screened openings to allow easy flow of water to and from the can during fuel loading and unloading operations, NCT, and HAC. The screens are 0.05-inch mesh stainless steel to permit adequate flow of water to and from the cans while confining any potential fuel pellets for fuel fines that may be postulated to occur as a result of

² American Society of Mechanical Engineers (ASME) Boiler and Pressure Vessel Code, Section III, *Rules for Construction of Nuclear Power Plant Components*, 1998 Edition.

³ NUREG/CR-6322, *Buckling Analysis of Spent Fuel Basket*, U.S. Nuclear Regulatory Commission, UCRL-ID-119697, May 1995.

accident conditions. The top of the can is removable and it is “sealed” by using wire rope to prohibit transfer of fuel fines from the can. When the top is inserted and locked into the can body, the wire rope is pressed tightly against the side of the can. Chapter 6 of this SAR presents the criticality analyses that demonstrate subcriticality for canned fuel.

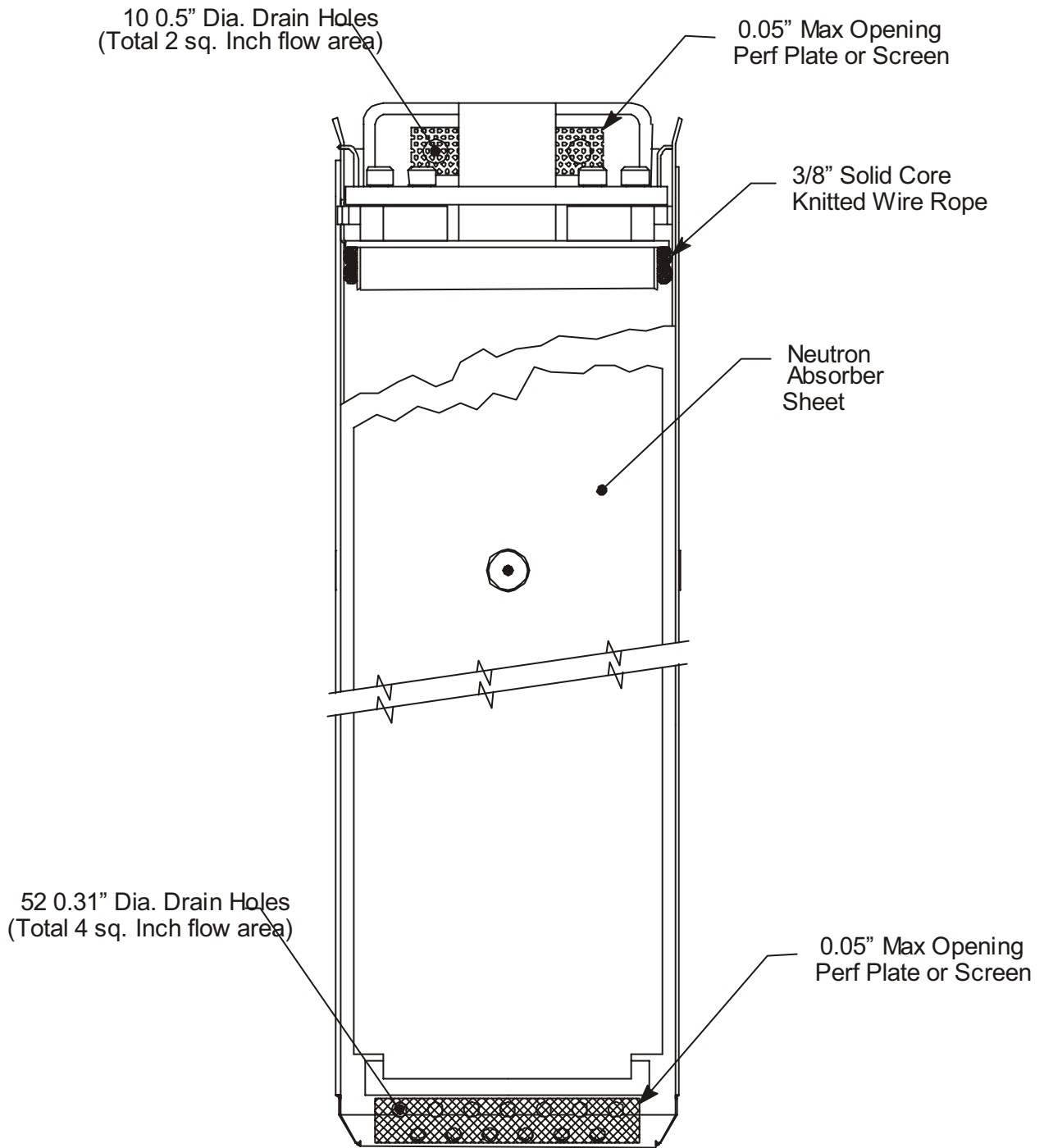


Figure 4.1-1 - W74 Damaged Fuel Can

This page intentionally left blank.

4.2 Containment Under Normal Conditions of Transport

Since no credit is taken for the canister containment boundary, see Section 4.2 of the FuelSolutions™ TS125 Transportation Cask SAR.

4.2.1 Pressurization of Containment Vessel

The FuelSolutions™ TS125 Transportation Cask is designed for a maximum normal operating pressure (MNOP) of 75 psig. The calculated NCT MNOP for the W74 canister is 10.7 psig, assuming the canister is breached and all the pressure is retained by the TS125 cask containment boundary. Section 3.4.4 of this SAR describes the details of the MNOP calculation assumptions and methodology.

4.2.2 Containment Criteria

See Section 4.2.2 of the FuelSolutions™ TS125 Transportation Cask SAR.

4.2.3 Compliance with Containment Criteria

See Section 4.2.3 of the FuelSolutions™ TS125 Transportation Cask SAR.

This page intentionally left blank.

4.3 Containment Under Hypothetical Accident Conditions

Since no credit is taken for the canister containment boundary, see Section 4.3 of the FuelSolutions™ TS125 Transportation Cask SAR.

4.3.1 Pressurization of Containment Vessel

The FuelSolutions™ TS125 Transportation Cask is designed for a MNOP of 75 psig. The calculated HAC internal pressure for the W74 canister is 29.3 psig, assuming the canister is breached and all the pressure is retained by the TS125 cask containment boundary. Section 3.4.4 of this SAR describes the details of the HAC internal pressure calculation assumptions and methodology.

4.3.2 Containment Criteria

See Section 4.3.2 of the FuelSolutions™ TS125 Transportation Cask SAR.

4.3.3 Compliance with Containment Criteria

See Section 4.3.3 of the FuelSolutions™ TS125 Transportation Cask SAR.

This page intentionally left blank.

5. SHIELDING EVALUATION

This chapter identifies, describes, discusses, and analyzes the principal shielding design of the FuelSolutions™ TS125 Transportation Package, when it is configured with a FuelSolutions™ W74 canister, to demonstrate compliance with the performance requirements specified in 10CFR71.47 and 10CFR71.51. This chapter, together with Chapter 5 of the FuelSolutions™ TS125 Transportation Cask SAR,¹ provides the complete shielding evaluation.

This chapter contains the following information:

- Descriptions of the FuelSolutions™ W74 canister shielding design features.
- The acceptable SNF burnup, enrichment, and cooling time for transportation in the W74 canister.
- A discussion of the W74 canister-specific shielding calculations.
- The results of the W74 canister-specific shielding calculations.

Chapter 5 of the FuelSolutions™ Transportation Cask SAR contains:

- A description of the TS125 transportation cask body and its shielding features.
- A description of the differences between the TS125 transportation cask body under the conditions specified in 10CFR71.71 (Normal Conditions of Transport) and 71.73 (Hypothetical Accident Conditions).
- A description of the TS125 transportation cask body radial and axial shielding configuration model used in the FuelSolutions™ package models presented in the individual Canister Transportation SARs.
- The shielding regional densities used to model the TS125 transportation cask body in each of the canister-specific FuelSolutions™ package models.
- A shielding calculation to evaluate the generic impact of the cask shear key on calculated gamma and neutron dose rates.
- A shielding calculation to evaluate the generic impact of post-accident lead slump and radial neutron shield damage on calculated gamma and neutron dose rates.
- A shielding calculation to evaluate the generic impact of neutron streaming through the heat transfer fins present within the cask radial neutron shield.

¹ WSNF-120, *FuelSolutions™ TS125 Transportation Cask Safety Analysis Report*, NRC Docket No. 71-9276, EnergySolutions Spent Fuel Division, Inc.

This page intentionally left blank.

5.1 Discussion and Results

The FuelSolutions™ W125 Transportation Package is designed for exclusive use shipment by railcar, barge, or heavy-haul vehicle. It is designed, constructed, and prepared for shipment so that under the tests specified in 10CFR71.71 (NOC), there would be no significant increase in external radiation levels. Furthermore, since it is a Type B package, it is designed so that no external radiation dose rate would exceed 1 rem/hr at 1 meter from the external surface of the package one week after hypothetical accident conditions. Both the normal and accident condition dose rates described below are based on calculational models that reflect the post-test package conditions.

The shielding analysis is performed using established codes and standards applicable to transportation cask shielding design such as ANSI/ANS 6.1.1-1977,² ANSI/ANS-10.4,³ and applicable portions of ANSI/ANS-6.6.1.⁴

5.1.1 FuelSolutions™ TS125 Transportation Cask Shielding Design Features

Section 5.1.1 of the FuelSolutions™ TS125 Transportation Cask SAR describes the shielding features of the FuelSolutions™ transportation cask. The shielding analyses presented in this chapter and Chapter 5 of the FuelSolutions™ TS125 Transportation Cask SAR show that the transportation cask, when loaded with a FuelSolutions™ W74 canister containing SNF with the parameters described in Section 1.2.3, meets the radiological requirements of 10CFR71.⁵ Table 5.1-1 summarizes these results.

5.1.2 FuelSolutions™ W74 Canister Shielding Design Features

The FuelSolutions™ W74 canister has thick metal shield plugs located at both ends of the canister that provide substantial gamma radiation shielding in the axial directions. This axial shielding maintains radiation exposures ALARA during canister sealing operations, canister transfer operations, dry storage, and transportation. Although the canister provides containment during dry storage, no credit is taken for containment during transportation.

The FuelSolutions™ W74 canister differs from other FuelSolutions™ canister designs because of its stacked upper and lower basket arrangement and segmented top shield plug. Although operationally dissimilar from other FuelSolutions™ canisters, the shielding design features of the W74 canister are the same because the axial shielding and canister shell are similar.

² ANSI/ANS-6.1.1-1977, "Neutron and Gamma-Ray Fluence-to-Dose Factors."

³ ANSI/ANS-10.4-1987, "Guidelines for the Verification and Validation of Scientific and Engineering Computer Programs for the Nuclear Industry."

⁴ ANSI/ANS-6.6.1-1987, "Calculation and Measurement of Direct and Scattered Gamma Radiation from LWR Nuclear Power Plants."

⁵ Title 10, Code of Federal Regulations, Part 71 (10CFR71), *Packaging and Transportation of Radioactive Materials*, U.S. Nuclear Regulatory Commission, October 2004.

The FuelSolutions™ W74 canister is available in two classes: the W74M and W74T, as described in Section 1.2.1.1. The only difference between the canister classes is the materials of construction used for certain basket components. Table 5.1-2 summarizes the FuelSolutions™ W74 canister classes and types, and the shield plate materials and thicknesses. Drawings for the FuelSolutions™ W74 canister are provided in Section 1.3.1 of this SAR. Both classes of canisters are similar from a shielding safety standpoint since they have the same cylindrical shells and closure plates, the same axial shields, and very similar internal basket components.

5.1.3 Shielding Results

The shielding calculations demonstrate that the FuelSolutions™ W125 Transportation Package, when configured with a FuelSolutions™ W74 canister, meets 10CFR71 dose rate limits for normal and accident conditions when normally occupied areas of the vehicle are four meters or greater away from the ends of the impact limiters. Table 5.1-1 shows the final shielding results for the package surfaces, as defined in Section 5.3.1.4. The results are presented in further detail in Section 5.4.2. These results are valid for the contents specified in Section 1.2.3 of this SAR, and described in detail in Section 5.2.

Table 5.1-1 - Summary of W125/W74 Maximum Dose Rates

Location	Maximum Dose Rate (mrem/hr)			10CFR71 Limit
	Gamma ⁽¹⁾	Neutron ⁽¹⁾	Total	
Normal Conditions of Transport				
10CFR71.47(b)(1) - External Surface of Package				
Package Side	2.11	112.93	115.04	1000
Package Top End	0.45	19.96	20.41	
Package Bottom End	0.54	0.23	0.77	
10CFR71.47(b)(2) - Outside Conveyance⁽²⁾				
Package Side	6.91	19.62	26.53	200
Package Top End	0.45	19.96	20.41	
Package Bottom End	0.54	0.23	0.77	
Underneath Railcar ⁽³⁾	11.89	80.42	92.31	
10CFR71.47(b)(3) - 2 Meters Away from Conveyance				
Vertical Planes	7.30	1.90	9.20	10
Package Top End	0.24	5.21	5.44	
Package Bottom End	0.54	0.11	0.65	
10CFR71.47(b)(4) - Normally Occupied Areas⁽⁴⁾				
Top or Bottom of Package	0.1	1.6	1.7	2
Hypothetical Accident Case				
10CFR71.51(a)(2) - 1 Meter Away from Package Surface				
Package Side	31.57	477.83	509.40	1000
Package Top End	1.04	58.28	59.31	
Package Bottom End	3.15	148.85	152.00	

Notes:

- (1) Gamma and neutron contributions to total dose rate vary with assembly burnup and cooling time. The presented values correspond to the case that yields the highest total dose rate.
- (2) Conveyance envelope consists of the cylindrical surface defined by the impact limiter diameter, and the planes at the package top and bottom ends.
- (3) This dose rate corresponds to the conveyance surface at the point directly under the shear key penetration in the neutron shield. The neutron dose rate is increased due to the presence of the shear key.
- (4) These are defined as the locations two meters from the package bottom end and/or four meters from the package top end. The presented dose rate corresponds to the four-meter top end location. Other calculations, presented in the above row, show that the dose rates are under 2 mrem/hr two meters from the package bottom.

Table 5.1-2 - W74 Canister Shielding Design Features

Canister Class and Type								
<i>Class</i> ⁽¹⁾ →	W74M				W74T			
<i>Type</i> ⁽²⁾ →	-LD	-LS	-SD	-SS	-LL	-LS	-SL	-SS
Shell	0.63" Stainless Steel (all types)							
<i>Top Closure</i>								
Outer Closure Plate	2.00" Stainless Steel (all types)							
Inner Closure Plate	1.00" Stainless Steel (all types)							
Shield Plug (Top Plate)	--	N/A	--	--	--	N/A	--	--
Shield Plug (Material)	--	7.25" Steel	--	--	--	7.25" Steel	--	--
Shield Plug (Bottom Plate)	--	N/A	--	--	--	N/A	--	--
<i>Bottom Closure</i>								
Closure Plate	--	1.0" Steel	--	--	--	1.0" Steel	--	--
Shield Plug (Material)	--	5.8" Steel	--	--	--	5.8" Steel	--	--
End Plate	--	1.8" Steel	--	--	--	1.8" Steel	--	--

Notes:

⁽¹⁾ M = MPC, T = Transport/Storage.

⁽²⁾ The W74 canister is only available with a long canister shell/steel axial shields.

5.2 Source Specification

The dose rate results presented in Table 5.1-1 are based on Monte-Carlo MCNP calculations performed for the FuelSolutions™ TS125 Transportation Cask with a FuelSolutions™ W74 canister. The canister is assumed to contain 64 BWR SNF assemblies with worst-case fuel parameters for shielding.

The FuelSolutions™ W74 canister accommodates the Big Rock Point (BRP) fuel assembly class. Since Big Rock Point is permanently shut down, the state of all SNF assemblies is known and no further assemblies will be irradiated. During its operation, Big Rock Point produced spent UO₂ and mixed-oxide (MOX) fuel assemblies. The W74 canister is designed to accommodate all existing BRP fuel assemblies, including both UO₂ and MOX fuel designs. For clarity, this section discusses the development of the intact UO₂ fuel assembly source terms, which are used in the shielding models. Section 5.5 qualifies the BRP MOX fuel assemblies and discusses the acceptability of partial fuel assemblies and damaged fuel.

The design basis UO₂ fuel parameters are 32 GWd/MTU, 3.0% initial enrichment, 2.9 grams of initial cobalt per assembly in the assembly core zone, and a six-year cooling time. The burnup, initial enrichment, and cobalt content bound all BRP fuel assemblies (3.0% enrichment is a lower bound—this is conservative because it maximizes the neutron source terms). Six years is the minimum cooling time that yields acceptable dose rates for the transportation cask. These worst-case fuel parameters are translated to corresponding radiological source terms by first constructing the generic (per metric ton) library of gamma and neutron source strengths, which is described in the following section.

5.2.1 FuelSolutions™ Generic Decay Library

A generic BWR decay library for FuelSolutions™ UO₂ sources is created using ORIGEN-2.1. The data in the libraries is generated on a per MTIHM basis for BWR fuel, and includes gamma sources, gamma energy spectra, neutron sources, decay heat generation rates, and a radionuclide inventory for cooling times varying from one to eighty years. Although the physical design and materials of construction vary from fuel assembly vendor to vendor or by fuel class, these differences have very little influence on the radiological properties of SNF.⁶ Two BWR ORIGEN-2.1 data libraries⁷ are used (only the first is needed for the BRP fuel):

- Standard BWR library (BWR-US) for burnups from 15,000-34,000 MWd/MTU (this ORIGEN-2.1 library is created using a 27,500 MWd/MT reactor model).
- Extended BWR library (BWR-UE) for burnups from 34,000-60,000 MWd/MTU (this ORIGEN-2.1 library is created using a 40,000 MWd/MT reactor model).

Table 5.2-1 describes the assumptions and parameters used in the generic BWR fuel source term calculations. Cycle burnup and enrichment values are specified as the desired parametric ranges

⁶ *Characteristics of Potential Repository Wastes*, DOE/RW-0184-R1, Oak Ridge National Laboratory, Oak Ridge, Tennessee, July 1992.

⁷ Ludwig, S. B., Renier, J. P., *Standard- and Extended-Burnup BWR and BWR Reactor Models for the ORIGEN2.1 Computer Code*, ORNL/TM-11018, Oak Ridge National Laboratories Oak Ridge, Tennessee, December 1989.

as needed for the decay library. Although based on particular plant conditions, these input assumptions represent a reasonable basis for the generic source term calculations. These parameters are used only for generating the generic library. The shielding analyses assume bounding values for parameters such as uranium loading, core region cobalt quantity, and non-fuel region gamma source strengths.

Source terms for the W74 canister shielding calculations are derived using this generic library. The generic library source terms for the design basis fuel parameters must be multiplied by 0.1421 MTU/assembly, then again multiplied by 64 assemblies per canister in order to arrive at the final source term per canister. The resulting source terms are valid for the W74 canister.

5.2.2 Gamma Source Terms

Gamma sources from SNF include primary gammas from fission products in the irradiated fuel and activated components of the SNF assemblies and non-fuel hardware, plus secondary gammas generated throughout the system by neutron interactions within the SNF and the shielding materials. The primary gammas are accounted for separately in the shielding calculations by modeling the SNF assemblies as four axial regions. The secondary gammas are accounted for in separate neutron models.

5.2.2.1 Active Fuel Primary Gamma Sources

UO₂ Fuel Primary Gamma Sources

Table 5.2-2 tabulates the fuel material (UO₂) primary gamma source strengths by energy group for the W74 canister design basis fuel parameters. The fuel gamma source strengths, per MTU, from the generic source term library are multiplied by the amount of heavy metal per assembly (0.1421 MTU/assembly) and number of fuel assemblies per canister (64) to obtain a base gamma source and spectrum.

Table 5.2-2 presents the gamma source strengths in the same ORIGEN2 group structure as is presented in the ORIGEN2.1 output and used in the shielding analyses. Therefore, no rebinning of the gamma spectrum is performed. The lower and upper bound gamma energies are shown for each group in the first two columns of Table 5.2-2. The shielding analyses model the entire gamma source strength corresponding to each energy group as being emitted at the exact group midpoint energy shown for that group in the third column of Table 5.2-2.

Although the generic source term library tabulates the gamma source strengths over all gamma energies (as a function of burnup, enrichment, and cooling time), the shielding analyses treat only the gamma energies between 0.575 and 3.5 MeV. Table 5.2-2 presents the gamma source strengths for these energies only. Gamma sources with energies below 0.575 MeV or above 3.5 MeV are known to not contribute significantly to transportation cask external dose rates. The lower energy gammas do not penetrate the thick cask shielding. The higher energy gammas are not produced in significant numbers by SNF. The fact that the very low and very high gamma energies do not contribute to cask external dose rates has been recognized and accepted by the NRC.⁸

⁸ NUREG/CR-1536, *Standard Review Plan for Dry Storage Cask Systems*, Spent Fuel Projects Office, U.S. Nuclear Regulatory Commission, 1997.

The fuel gamma source strengths shown for each gamma energy line in the fourth column of Table 5.2-2 are divided by the total gamma source strength (at the bottom of the fourth column) to yield normalized gamma source strengths. This normalized fuel gamma source spectrum is presented in the far right column of Table 5.2-2.

MOX Fuel Primary Gamma Sources

See Section 5.5.

5.2.2.2 End Fitting and Plena Region Gamma Sources

The gamma source strengths presented in the generic library are based on a single metric ton of UO₂ and do not include gamma sources from activated non-UO₂ fuel assembly hardware, such as fuel rod cladding, grid spacers, assembly top and bottom nozzles, and other non-fuel assembly hardware. The gamma sources from these assembly hardware materials are almost entirely due to the decay of ⁶⁰Co. Therefore, the source spectrum from these gamma sources is 50% 1.173 MeV gammas and 50% 1.333 MeV gammas.

The shielding analyses separately model the activated assembly hardware gamma sources in four axial regions of the assembly (the active fuel region, the bottom end region, the gas plenum region, and the top end region). Table 5.2-3 summarizes these source strengths by axial assembly region for the design basis W74 fuel parameters analyzed in the shielding analysis.

The gamma source strengths from activated assembly hardware are calculated using the ORIGEN2.1 point-depletion code, the same code used to calculate the fuel gamma source strengths in the generic library. ORIGEN2.1 calculations specifying one gram of cobalt within the assembly core zone are performed. The ORIGEN2.1 calculations output the gamma source strength due to the specified gram of cobalt.

As illustrated in Table 5.2-3, four steps are used to calculate the assembly hardware gamma sources for each axial assembly zone and for each combination of assembly burnup, initial enrichment, and cooling time considered in the shielding calculations. These four steps consist of the following:

1. Using ORIGEN2.1, calculate the ⁶⁰Co activity, per gram of initial cobalt, in the active fuel region as a function of assembly burnup and initial enrichment. For 32 GWd/MTU BWR fuel, this is 167.22 Ci ⁶⁰Co activity/g initial cobalt at discharge.
2. Decay this ⁶⁰Co activity to the desired fuel assembly cooling time (six years), using the ⁶⁰Co half-life of 5.27 years. This results in an activity multiplication factor of 0.4543.
3. For each of the three non-fuel axial assembly zones, adjust the above active fuel zone ⁶⁰Co activity (per gram of initial cobalt) by the appropriate neutron flux factor⁶ to account for the reduced neutron flux in the region of interest (0.15 for the bottom end, 0.2 for the gas plena, or 0.1 for the top end).
4. Multiply the final per gram ⁶⁰Co activity by the initial cobalt quantity of the assembly zone, the number of assemblies (64), and 7.4 x 10¹⁰ (the number of gammas emitted per Ci of ⁶⁰Co) to obtain the total canister gamma source for the axial region of interest.

5.2.2.3 Secondary Gamma Sources

Secondary gamma rays are produced by (n,γ) reactions in the SNF assemblies, and the canister and transportation cask materials of construction. The code and cross-sections used to perform the shielding calculations account for secondary gamma reproduction by creating and tracking gamma ray particle histories in the coupled neutron-gamma models. The results of the neutron models therefore include all contributions from secondary gamma sources.

5.2.2.4 Axial Distribution of Gamma Sources

UO₂ Fuel Axial Source Distribution

Due to the axial flux profile in the nuclear reactor core, the local fuel burnup level in the assembly active fuel zone varies with axial location. In spent fuel, gamma source strengths for a given initial enrichment and assembly cooling time are roughly directly proportional to fuel burnup level. The gamma source strength in the SNF therefore varies with axial position, along with the local burnup level. To account for this phenomenon, the active fuel zone of each fuel assembly is subdivided into 24 axial subsections of roughly equal height, each subsection having a different gamma source strength. The W74 canister actually has two layers of fuel assemblies stacked on top of each other (i.e., the lower and upper baskets). Thus, there are a total of 48 axial source subsections over the entire height of the canister (within the two active fuel regions of the two assembly layers).

The axial gamma source strength profiles modeled in the shielding analyses are described in Table 5.2-4. To avoid duplication, Table 5.2-4 provides the axial profile of one fuel assembly layer (i.e., one of the baskets), since the assemblies in the lower and upper baskets have identical axial gamma source strength profiles. Therefore, Table 5.2-4 (left column) describes 24, as opposed to 48, axial zones. For each axial subsection, the axial coordinates that define the top and bottom end of the section are shown. The axial coordinates are defined relative to the bottom of the active fuel region of the assembly.

Each axial subsection has a different “relative” gamma source strength, which is defined as the gamma source density within that axial subsection as compared with the average gamma source density over the entire assembly fuel zone. These relative gamma source strengths are shown in the center column of Table 5.2-4. Note that the weighted average of the relative source strengths (weighted by the heights of the axial subsections) equals 1.0. (The weighted average is the sum of the relative source strengths times the fraction of the overall height [177.8 cm] covered by the corresponding axial subsection. Since the axial subsections are of nearly equal height, the sum of relative source strengths shown in column two of Table 5.2-4, divided by 24, also yields almost exactly 1.0. To be precise, however, the weighted average approach is required.)

The shielding analyses require as input a set of source fractions for each of the axial subsections defined in the left column of Table 5.2-4. The fraction of the total gamma source strength in the overall model that exists within each axial subsection must be defined and input. The source fraction for each axial subsection is equal to the relative gamma source strength for the subsection times the fraction of the overall source zone height covered by that subsection. Since the shielding analyses model the entire W74 canister, including both the upper and lower baskets, the overall source zone height is 355.6 cm, as opposed to 177.8 cm. Therefore, for each axial subsection described in Table 5.2-4, the gamma source strength fraction is equal to the

relative gamma source strength (shown in the second column) times the axial span of the subsection (shown in the first column), divided by the overall height of 355.6 cm. The resulting gamma source fractions are presented in the right column of Table 5.2-4.

An axial source profile identical to the one described above is used for the fuel (UO₂) and non-fuel (assembly hardware) gamma sources present in the active fuel zone of the assembly. Gamma sources for the fuel assembly bottom end, gas plenum, and top end regions are assumed to have a flat axial distribution.

MOX Fuel Axial Source Distribution

Because the BRP reactor core flux profile is similar for UO₂ and MOX fuel, Table 5.2-4 is appropriate for MOX fuel as well.

5.2.3 Neutron Source Terms

5.2.3.1 Neutron Source Strengths

Neutron sources in SNF include spontaneous fission of actinides, (α , n) reactions, and subcritical multiplication. All significant neutron production comes from the active fuel region of the SNF assemblies. These neutron sources are modeled in the FuelSolutions™ W74 shielding analysis in two ways.

Spontaneous fission and (α , n) sources are extracted from the generic decay library discussed in Section 5.2.1. To obtain the per-canister neutron source strengths for the shielding calculations, the neutron source term from the generic decay library is multiplied by the maximum uranium loading of 0.1421 MTU/assembly, then by the payload of 64 assemblies. The resulting neutron source term is 3.153×10^9 neutrons/s-canister (total for both layers).

The W74 shielding analysis accounts for subcritical multiplication neutrons by using a subcritical neutron multiplication factor of 1.587 for each neutron dose rate calculated by MCNP. The factor is based on criticality calculations for a dry canister full of fresh (unburned) fuel for which the effective neutron multiplication factor is 0.37. Using the definition of the effective multiplication factor, the subcritical multiplication factor is $1/(1-0.37) = 1.587$. This approach is extremely conservative since the design basis W74 fuel assembly is much less reactive than a fresh assembly.

The neutron source input to MCNP includes the base value of 3.153×10^9 neutrons/s-canister times the subcritical multiplication factor of 1.587, times a factor of 1.327 to account for the effects of the axial burnup profile described in Section 5.2.3.3.

5.2.3.2 Neutron Energy Spectrum

Most neutrons produced by SNF (~98%) arise from the spontaneous fission of ²⁴⁴Cm. Neutron spectra for the shielding calculations are therefore based on the ²⁴⁴Cm spontaneous fission energy spectrum. Table 5.2-5 presents the normalized neutron energy spectrum along with the energy group structure used to specify the neutron sources.

5.2.3.3 Axial Neutron Distribution

As with the gamma source strength, the neutron source strength varies with the axial position within the assembly fuel zone due to the axial variation in local burnup level. Unlike the gamma source strength, however, the neutron source strength varies with burnup in a strong, non-linear fashion (the source strength is roughly proportional to the burnup to the 4th power). The axial variation in the neutron source strength is treated by the shielding analysis models in a manner similar to that used for the gamma source strength variation. The fuel zone source region of the assemblies (in both the upper and lower baskets) is subdivided into 24 axial subsections of roughly equal height, each subsection having a different neutron source strength. The neutron source strength present in each axial subsection is determined as discussed below.

The relative burnup level of each axial subsection is determined by dividing the local burnup level for that section by the assembly average burnup level. (Since the local gamma source strength is assumed to be directly proportional to local burnup level, the relative gamma source strengths shown in the second column of Table 5.2-4 are equal to the relative burnup levels of each axial subsection.) The relative neutron source strength for each axial subsection is determined by raising the relative burnup level for that subsection to the 4th power.

The neutron source strength profile is described Table 5.2-6. The left column presents the axial spans covered by each of the 24 axial subsections that are defined in the shielding models. The second column shows the relative neutron source strength present in each axial subsection (determined as described above). The relative neutron source strength, for each axial subsection, is defined as the local neutron source strength within that subsection, divided by the local neutron source strength corresponding to the assembly average burnup level.

The sum of the relative neutron source strengths over the axial sections is 1.327. Due to the fourth power dependence of neutron source strength on burnup, the sum of the relative neutron source strengths exceeds 1.0. This value corresponds to the increase in the overall neutron source strength of the fuel assembly due to the presence of the axial burnup profile. Due to the non-linear dependence of neutron source strength on burnup, the axial profile in assembly burnup yields an increase in the overall neutron source strength of the assembly. In other words, the overall neutron source strength of the actual assembly is greater than total assembly source strength would be if it were calculated at the assembly average burnup level (or, if the assembly has a flat burnup profile).

The shielding analyses require as input a set of source fractions for each of the axial subsections defined in the left column of Table 5.2-6. The fraction of the total neutron source strength that exists within each axial subsection in the overall model must be defined and input. The source fraction for each axial subsection is equal to the relative neutron source strength for that subsection, times the fraction of the overall source region height covered by that subsection. The set of relative source strengths first must be “normalized,” so they average out to 1.0, before being multiplied by the subsection height fraction. Also, since the shielding analyses model the entire W74 canister, including both the upper and lower baskets, the overall source region height is 355.6 cm, as opposed to the 177.8 cm height of one assembly’s fuel zone. Therefore, for each axial subsection presented in Table 5.2-6, the neutron source strength fraction is calculated by dividing the relative neutron source strength (shown in the second column) by 1.327, multiplying

the result by the height of the axial subsection (shown in the first column), and dividing that result by 355.6 cm. The resulting neutron source fractions are presented in the right column of Table 5.2-6.

The total neutron source strength of 3.153×10^9 neutrons/sec-canister given in Section 5.2.3.1 corresponds to the assembly average burnup level. Because the set of axial neutron source fractions shown in the right column of Table 5.2-6 is normalized, it does not account for the overall source strength increase. Therefore, the total neutron source strength of 3.153×10^9 neutrons/sec-canister must be multiplied by the axial profile effect factor of 1.327. Thus, due to the effects of the axial burnup profile in the fuel, the actual total neutron source strength for the W74 canister is 4.184×10^9 neutrons/sec-canister. Sub-critical neutron multiplication further increases the overall neutron source produced within the canister to 6.64×10^9 neutrons/sec-canister.

Table 5.2-1 - BWR Source Term Calculation Input Parameters

Parameter	Assumed Value/Rationale
Assembly Thermal Power	23.51 MWt/assembly
Fuel Assembly Type	UO ₂ 8x8 in Zircaloy-4 Channels with Two Water Rods (GE-5 8x8 assembly)
Assembly Rod Pitch	0.64 inch
Fuel Rod O.D.	0.483 inch
Clad Thickness	0.032 inch
Fuel Pellet O.D.	0.410 inch
Fuel Pellet Density	95% UO ₂ theoretical
Equilibrium cycle length	Range of Values Assumed ⁽¹⁾
Uranium Enrichment (Active Fuel)	Range of Values Assumed ⁽¹⁾
Fuel Loading Pattern ⁽²⁾	Four-Region Equilibrium Cycle
Downtime Between Cycles ⁽²⁾	None
Operating Fuel Temperature	1000 K
ORIGEN Decay Library	bwrus.lib (≤ 34,000 MWd/MTU) bwrue.lib (> 34,000 MWd/MTU)

Notes:

- ⁽¹⁾ Ranges for burnup and initial enrichment are varied to cover the ranges in the canister fuel cooling tables.
- ⁽²⁾ The ORIGEN-2.1 decay libraries are generated assuming a three-cycle power history. The ORIGEN-2.1 calculations, however, are conservatively performed based on a single burn period with no downtimes.

Table 5.2-2 - W74 UO₂ Fuel Gamma Sources

Gamma Energies (MeV) ⁽¹⁾			Gamma Source Strength (Gammas/sec per canister)	Energy Group Gamma Source Strength Fraction
Group Lower Energy	Group Upper Energy	Group Midpoint Energy		
0.45	0.70	0.575	3.906E+16	8.117E-01
0.70	1.0	0.85	7.195E+15	1.495E-01
1.0	1.5	1.25	1.803E+15	3.747E-02
1.5	2.0	1.75	4.690E+13	9.747E-04
2.0	2.5	2.25	1.396E+13	2.901E-04
2.5	3.0	2.75	5.448E+11	1.132E-05
3.0	4.0	3.5	7.004E+10	1.456E-06
-	-	Total	4.812E+16	1.000E+00

Notes:

- (1) These energies correspond to the lower, upper, and midpoint energies of the ORIGEN2 gamma energy group structure. The entire gamma source strength presented for each group is modeled at the midpoint line energy shown in the third column.

Table 5.2-3 - W74 Assembly Hardware Gamma Source Strengths

	Fuel Zone	Top End	Plenum Region	Bottom End
Core ⁶⁰ Co Activation at Assembly Discharge (Ci/initial g cobalt)	167.2	167.2	167.2	167.2
⁶⁰ Co Decay Factor (6 yr.)	0.4543	0.4543	0.4543	0.4543
Neutron Flux Factor	1.0	0.1	0.2	0.15
Cobalt Quantity (grams)	2.9	5.81	0.04	1.55
⁶⁰ Co Activity (Ci/assy) ⁽¹⁾	220.28	44.13	0.61	17.66
Gamma Source (γ/s-can) ⁽²⁾	1.043E+15	2.090E+14	2.878E+12	8.634E+13

Notes:

- (1) The initial (assembly discharge) core zone ⁶⁰Co activation level of 167.2 Ci per gram cobalt is decayed 6 years to 75.96 Ci per gram. This value is multiplied by the neutron flux factors and the assembly zone cobalt quantities to yield the assembly zone ⁶⁰Co activities (shown in this row).
- (2) The assembly zone ⁶⁰Co activities, in Ci, are multiplied by the canister capacity of 64 assemblies, and by 7.4×10^{10} (γ/sec per Ci of ⁶⁰Co) to yield the total gamma source strength of each assembly non-fuel zone, in γ/s-can.

Table 5.2-4 - BWR Fuel Axial Gamma Profiles

Axial Position (cm)		Relative Gamma Source Strength ⁽¹⁾	Gamma Source Fraction ⁽²⁾
0.00	- 7.47	0.23	0.0048
7.47	- 14.85	0.77	0.0160
14.85	- 22.23	0.99	0.0205
22.23	- 29.69	1.09	0.0229
29.69	- 37.07	1.13	0.0234
37.07	- 44.45	1.16	0.0241
44.45	- 51.92	1.17	0.0246
51.92	- 59.30	1.18	0.0245
59.30	- 66.68	1.18	0.0245
66.68	- 74.14	1.18	0.0248
74.14	- 81.52	1.18	0.0245
81.52	- 88.90	1.18	0.0245
88.90	- 96.37	1.18	0.0248
96.37	- 103.75	1.17	0.0243
103.75	- 111.13	1.16	0.0241
111.13	- 118.59	1.14	0.0239
118.59	- 125.97	1.12	0.0232
125.97	- 133.35	1.1	0.0228
133.35	- 140.82	1.07	0.0225
140.82	- 148.20	1.02	0.0212
148.20	- 155.58	0.94	0.0195
155.58	- 163.04	0.81	0.0170
163.04	- 170.42	0.63	0.0131
170.42	- 177.80	0.23	0.0048

Notes:

- (1) Equal to the relative burnup level for that axial subsection (i.e., equal to the axial burnup profile).
- (2) Equal to the relative gamma source strength, times the height of the axial subsection, divided by the overall fuel source region height of 355.6 cm. This set of source strength fractions applies for both fuel source zones, each 177.8 cm high, that are present in the shielding analysis model, which includes the lower and upper W74 baskets. The total gamma source strength applied to the model corresponds to the entire canister, i.e., both baskets. For this reason, the set of source strength fractions summarized here for a single basket sums to 0.5.

Table 5.2-5 - W74 Normalized Neutron Source Spectrum

Group Upper Energy (MeV)	Neutron Source Strength Fraction		Group Upper Energy (MeV)	Neutron Source Strength Fraction
1.733E+01	3.897E-05		2.972E-01	2.716E-02
1.419E+01	1.798E-04		1.832E-01	1.407E-02
1.221E+01	1.149E-03		1.111E-01	6.833E-03
1.000E+01	2.805E-03		6.738E-02	3.282E-03
8.607E+00	6.455E-03		4.087E-02	9.268E-04
7.408E+00	1.865E-02		3.183E-02	5.299E-04
6.065E+00	3.564E-02		2.606E-02	1.613E-04
4.966E+00	9.194E-02		2.418E-02	1.890E-04
3.679E+00	8.411E-02		2.188E-02	5.036E-04
3.012E+00	4.671E-02		1.503E-02	4.519E-04
2.725E+00	4.854E-02		7.102E-03	1.471E-04
2.466E+00	2.055E-02		3.355E-03	4.782E-05
2.365E+00	4.113E-03		1.585E-03	1.948E-05
2.346E+00	2.475E-02		4.540E-04	2.383E-06
2.231E+00	7.378E-02		2.144E-04	7.738E-07
1.921E+00	7.109E-02		1.013E-04	2.890E-07
1.653E+00	8.733E-02		3.727E-05	7.028E-08
1.353E+00	1.103E-01		1.068E-05	8.597E-09
1.003E+00	5.884E-02		5.043E-06	3.211E-09
8.209E-01	2.523E-02		1.855E-06	6.228E-10
7.427E-01	4.287E-02		8.764E-07	2.022E-10
6.081E-01	3.395E-02		4.140E-07	8.566E-11
4.979E-01	3.746E-02		1.000E-07	1.153E-11
3.688E-01	1.921E-02			

Table 5.2-6 - W74 Axial Neutron Source Profiles

Axial Position (cm)	Relative Neutron Source Strength⁽¹⁾	Neutron Source Fraction⁽²⁾
0.00 - 7.47	0.003	0.000044
7.47 - 14.85	0.352	0.0055
14.85 - 22.23	0.961	0.0150
22.23 - 29.69	1.412	0.0223
29.69 - 37.07	1.630	0.0255
37.07 - 44.45	1.811	0.0283
44.45 - 51.92	1.874	0.0297
51.92 - 59.30	1.939	0.0303
59.30 - 66.68	1.939	0.0303
66.68 - 74.14	1.939	0.0307
74.14 - 81.52	1.939	0.0303
81.52 - 88.90	1.939	0.0303
88.90 - 96.37	1.939	0.0307
96.37 - 103.75	1.874	0.0293
103.75 - 111.13	1.811	0.0283
111.13 - 118.59	1.689	0.0267
118.59 - 125.97	1.574	0.0246
125.97 - 133.35	1.464	0.0229
133.35 - 140.82	1.311	0.0207
140.82 - 148.20	1.082	0.0169
148.20 - 155.58	0.781	0.0122
155.58 - 163.04	0.430	0.0068
163.04 - 170.42	0.158	0.0025
170.42 - 177.80	0.003	0.000044

Notes:

⁽¹⁾ Equal to the relative burnup level for that axial subsection, raised to the 4th power.

⁽²⁾ Equal to the relative neutron source strength, divided by a profile normalization factor of 1.327, times the height of the axial subsection, divided by the overall fuel source region height of 355.6 cm. This set of source strength fractions applies for both fuel source zones, each 177.8 cm high, that are present in the shielding analysis model, which includes the lower and upper W74 baskets. The total neutron source strength applied to the model corresponds to the entire canister, i.e., both baskets. For this reason, the set of source strength fractions summarized here for a single basket sums to 0.5.

This page intentionally left blank.

5.3 Model Specification

5.3.1 Description of Radial and Axial Shielding Configuration

5.3.1.1 Overview

Table 5.3-1 is a road map to the W74 shielding models. Six different MCNP models are necessary to represent normal and accident conditions, for neutron and gamma radiation. All models represent the W74M-LS or W74T-LS canister design (they are identical for the purpose of shielding calculations). The FuelSolutions™ W74 shielding results are therefore valid for both W74 canister configurations.

The primary shielding analyses are azimuthally symmetrical R-Z models of the cask system. These models can accurately treat the canister shell and transportation cask, whose major geometry features are all azimuthally symmetrical. The components in the canister interior (fuel assemblies, assembly guide tubes, etc.), which are not azimuthally symmetrical, are smeared into homogenous materials that fill defined, azimuthally symmetrical sub-volumes within the canister interior.

Table 5.3-2 and Table 5.3-3 show the canister and source region dimensions used in the shielding models. To conservatively account for axial positioning of the assemblies within the canister cavity in a single model, the canister is shortened in the model so that its ends are in contact with both ends of the design basis SNF assembly.

Like the canister, the cask is shortened in the model so that its ends are in contact with both ends of the canister to account for the effects of axial positioning. Removing a “slice” from the mid-plane of the cask does this without altering the geometry at the ends of the cask where gamma streaming is an important factor. This artificial shortening of the canister and cask yields conservatively high cask exterior dose rates since it maximizes the degree to which the source regions “peek” over the axial ends of the gamma and neutron shields.

Although the FuelSolutions™ TS125 Transportation Package is designed for exclusive use transport, the shielding models do not take credit for the presence of the railcar, skid, or other transport hardware. The conveyance surface and two-meter dose rates correspond to the model surfaces described in Section 5.3.1.4.

5.3.1.2 Treatment of Voids, Streaming Paths, and Other Geometry Irregularities

The shielding models are carefully designed to maximize the effects of radiation streaming through voids, streaming paths, and other geometry irregularities such as occurred near the edges of the transportation cask radial neutron shield, gamma shield, and impact limiters as discussed above.

Some features of the transportation cask are simplified or omitted from the shielding models. Omitted features that have potentially significant effects are accounted for using the results of sensitivity studies described in the FuelSolutions™ TS125 Transportation Cask SAR. Treatment of these features is as follows:

- The steel ribs in the neutron shield are not modeled discretely. They are instead smeared into the neutron shield mixture. A sensitivity study to evaluate the effects of the neutron shield ribs is included in Section 5.4.1.1 of the FuelSolutions™ TS125 Transportation Cask SAR. The results of the MCNP calculations are increased to account for these effects.
- The neutron shield shear key cutout is not modeled. A sensitivity study to evaluate the effects of the shear key is included in Section 5.4.1.2 of the FuelSolutions™ TS125 Transportation Cask SAR. The results of the MCNP calculations are increased to account for these effects.

The lifting trunnion penetrations through the neutron shield are not modeled. Since the trunnion bosses do not displace a large amount of neutron shielding material, and since the lifting trunnion covers are “potted” with neutron absorber, dose rates at the locations of interest are not greatly affected by the presence of the penetrations.

5.3.1.3 Differences Between Normal and Accident Models

Section 5.3.1.2 of the FuelSolutions™ TS125 Transportation Cask SAR discusses differences in the transportation cask body shielding model resulting from the conditions specified in 10CFR71.71 (Normal Conditions of Transport) and 71.73 (Hypothetical Accident Conditions). Model changes account for some of the differences between normal and accident conditions (e.g., loss of impact limiters); and the correction factors described in Section 5.3.1.2 of the FuelSolutions™ TS125 Transportation Cask SAR account for others (e.g., lead slump and neutron shield damage).

The FuelSolutions™ W74 canister and contents are not notably different between normal and accident conditions.

5.3.1.4 Dose Point Locations

The shielding results presented in Table 5.1-1 come from MCNP area detectors defined on the various surfaces at zero, one, and two meters from the package surface, consistent with the requirements of 10CFR71.47 and 71.51. The locations of these area detectors are illustrated in Figure 5.3-1 and Figure 5.3-2 for the normal and accident condition models, respectively. Since MCNP area detectors return area-averaged dose rates, special attention is given to assure that the size and location of the area detectors is sufficient to accurately represent peak surface dose rates on the package surfaces.

The package surface is defined, for the purpose of the shielding analysis, as a cylinder that extends the length of the cask and impact limiters, with a diameter equal to the outer radius of the neutron shield, or the cask impact limiters, depending on the axial location.

For dose rates on the conveyance surface, the MCNP detectors are located on a cylindrical surface that extends the length of the cask and impact limiters and has a diameter equal to the impact limiters. This represents the accessible surface of the package because a personnel barrier extends between the impact limiters when the cask is configured for shipment. For conservatism, it is assumed that the conveyance only extends between the ends of the impact limiters in the axial direction.

The two-meter surface is simply defined as a concentric cylinder two meters larger in radius and four meters longer than the conveyance surface (i.e., two meters from all conveyance surfaces).

The accident one-meter surface is defined as a cylinder whose radius is one meter greater than the outside of the cask neutron shield, and two meters longer than the length of the cask (sans impact limiters). Thus, the one-meter surface lies at least one meter from all cask surfaces.

5.3.1.5 TS125 Cask Body Geometry

Section 5.3.1 of the FuelSolutions™ TS125 Transportation Cask SAR discusses the shielding model for the TS125 cask body, including the differences between normal and accident condition models.

5.3.1.6 W74 Canister Geometry

Six MCNP models are necessary to perform the W74 shielding calculations:

- Two R-Z models for side (radial) gamma calculations for normal and accident conditions.
- Two R-Z models for neutron calculations for normal and accident conditions.
- Two infinite slab gamma models for the top and bottom ends (used for both normal and accident conditions).

The canister internals are divided into identical upper and lower zones. Each of these zones is subdivided into the following azimuthally symmetrical regions:

- A cylindrical central zone to represent the central area of each basket that contains structural materials but no fuel.
- Four annular source zones including the fuel assembly top end, gas plena, active fuel, and bottom end regions.
- A fifth annular zone that lies outside the fuel zone, but inside the canister wall (this fifth zone is not modeled in the infinite slab models). For conservatism, the spacer plates are ignored and the models are specified with void in this region.

The central zone and source zone outer radii, which form the boundaries between the three radial sections of the canister interior (the central zone, source zone, and edge zone) are shown in Table 5.3-3. The source zone represents the canister interior area covered by the 37 guide tubes loaded with fuel assemblies. The central zone represents the canister interior area covered by the five guide tubes at the center of the basket, which do not contain fuel assemblies. The edge zone represents the remaining area in the basket, which lies outside all of the canister guide tubes.

The source zone radius is calculated as follows. A perimeter is drawn that extends along the outer surfaces of all the guide tubes that lie along the outer edge of the basket. The area inside that perimeter is roughly equal to the area of a cylinder with a radius equal to the source zone radius shown in Table 5.3-3. Similarly, a perimeter is drawn around the five center guide tube locations in the W74 basket. The area inside this perimeter is roughly equal to the area of a cylinder with a radius equal to the central zone radius shown in Table 5.3-3. Thus, the areas covered by the central and source zone regions in the shielding models are roughly equal to the areas covered by the corresponding guide tubes, full or empty, in the actual canister interior. This

approach allows the different canister interior regions to be modeled in an azimuthally symmetrical fashion, on an equal area basis, in the R-Z shielding analyses.

Several key modeling assumptions are common to the models:

- Minimum thickness values allowed by cask system dimensional tolerances are assumed for all significant cask shielding components.
- Conservatively large gaps over the gamma and neutron shields are assumed, along with conservatively large accident condition lead slump gaps.
- Canisters and casks are artificially shortened to a “snug fit” condition in order to maximize limiting dose rates.
- All spacer plate steel inside the four W74 fuel assembly source zones is neglected.
- Several regions of the aluminum honeycomb impact limiters are not modeled in several calculations, and the steel outer skin of the impact limiters is conservatively neglected.
- UO₂ fuel assemblies are modeled. The shielding calculations qualify MOX fuel by comparing source strength ratios only as discussed in Section 5.4.

Side Gamma Model for Normal Conditions

Figure 5.3-3 shows the R-Z model used to calculate gamma ray dose rates on the side of the package (i.e., in the radial direction only) for the normal condition package configuration.

Because of the very thick gamma shielding at the ends of the package, the MCNP particle statistics from this model are poor at the end surfaces. The package end dose rates are therefore determined using the two infinite slab models described below. Void zones are specified at the top and bottom ends of this model to kill particles that exit the cask ends since they are not tallied.

Neutron Model for Normal Conditions

Figure 5.3-4 shows the R-Z model used to calculate neutron dose rates on the side and ends of the package for the normal condition package configuration.

Side Gamma Model For Accident Conditions

Figure 5.3-5 shows the R-Z model used to calculate gamma ray dose rates on the side of the package (i.e., in the radial direction only) for the accident condition package configuration.

Because of the very thick gamma shielding at the ends of the package, the MCNP particle statistics from this model are poor at the end surfaces. The package end dose rates are therefore determined using the two infinite slab models described below. Void zones are specified at the top and bottom ends of this model to kill particles that exit the cask ends since they are not tallied.

Neutron Model for Accident Conditions

Figure 5.3-5 shows the R-Z model used to calculate neutron dose rates on the side and ends of the package for the accident condition package configuration. The HAC neutron model geometry is identical to the side HAC gamma model, except that the void (particle killing) zones at the ends of the cask are not present. The void zones are not used, since the neutron model shown in Figure 5.3-5 is used to calculate both side and end HAC neutron dose rates.

Bottom End Gamma Model for Normal and Accident Conditions

Figure 5.3-6 shows the infinite slab model used to calculate gamma dose rates on the bottom end of the package for both the normal and accident condition package configurations. No credit is taken for geometric fall off in gamma dose rate for detector locations away from the cask end surfaces, as this effect cannot be treated by the infinite slab model. Thus, the gamma dose rates calculated on the bottom surface of the aluminum honeycomb material (as shown in Figure 5.3-6) are used for the package, conveyance, and two meter cask bottom NCT locations. For accident conditions (HAC), the impact limiter is assumed to be removed. A second gamma dose rate is tallied on the bottom surface of the cask underneath the impact limiter (the interface between the steel and the honeycomb material shown in Figure 5.3-6). This dose rate is conservatively used for the HAC gamma dose rate one meter from the cask bottom. This calculated dose rate is conservative in that it does not take credit for geometric effects and because any gamma backscatter (from the honeycomb material actually present in the model) will cause the calculated dose rate to increase.

Top End Gamma Model for Normal and Accident Conditions

Figure 5.3-7 shows the infinite slab model used to calculate gamma dose rates on the top end of the package for both the normal and accident condition package configurations. As with the bottom end infinite slab model, the gamma dose rate tallied on the top surface of the impact limiter honeycomb material (as shown in Figure 5.3-7) is used for the package, conveyance, and two meter cask top NCT locations. The gamma dose rate tallied underneath the impact limiter is used for the one meter HAC cask bottom dose rate.

5.3.2 Shield Regional Densities

5.3.2.1 FuelSolutions™ W125 Transportation Cask Shield Regional Densities

Section 5.3.2 of the FuelSolutions™ TS125 Transportation Cask SAR describes the materials that make up the transportation cask, such as stainless steel, impact limiter aluminum honeycomb, lead, and neutron shield material, used for the FuelSolutions™ shielding analyses.

5.3.2.2 FuelSolutions™ W74 Canister Shield Regional Densities

The materials of construction for the FuelSolutions™ W74 canister are durable and resistant to degradation by corrosive, galvanic, and chemical reactions in the anticipated service environment. There are no canister materials whose density or other material characteristics require special measures to assure continued shielding efficacy, nor are any temperature-sensitive canister materials. The thermal analyses described in Section 3.4.2 show that no temperature limits are exceeded for shielding materials; therefore, the shielding is expected to perform as designed under the normal conditions of transport as well as accident conditions.

Table 5.3-4 shows the atom densities used for the raw materials of construction. These are used for pure materials (e.g., steel canister shell, canister axial shield plugs, etc.), and to convert the volume fractions of mixtures into partial atom densities.

Inside the canister cavity, there are five material zones modeled: the top end zone, gas plena zone, active fuel zone, bottom end zone, and the “center zone,” which is a smear of the basket

structural material, sans fuel, used to represent the central unfueled region in the upper and lower basket assemblies.

Table 5.3-5 shows the specification for the active fuel region mixture. Uranium dioxide, fuel cladding, steel basket guide tubes, and borated steel neutron absorber sheets are considered in the volume fractions indicated at the top of the table. There is no credit taken for spacer plates steel within the zone.

Table 5.3-6 shows the specification for the gas plenum region mixture. Fuel cladding, steel basket guide tubes, and borated steel neutron absorber sheets are considered in the volume fractions indicated at the top of the table. No credit is taken for spacer plate steel within the zone.

Table 5.3-7 shows the specification for the bottom end region mixture. Bottom end fittings, steel basket guide tubes, and borated steel neutron absorber sheets are considered in the volume fractions indicated at the top of the table. There is no credit taken for spacer plates steel within the zone.

Table 5.3-8 shows the specification for the top end region mixture. Top end fittings, steel basket guide tubes, and borated steel neutron absorber sheets are considered in the volume fractions indicated at the top of the table. There is no credit taken for spacer plates steel within the zone.

Table 5.3-9 shows the specification for the central zone mixture. Steel basket guide tubes and borated steel neutron absorber sheets are considered in the volume fractions indicated at the top of the table. No credit is taken for spacer plate steel within the zone. The central zone material mixture corresponds to the active fuel region mixture, shown in Table 5.3-5, except that the UO₂ and zircaloy materials have been removed since the five center guide tube locations contain no fuel assemblies.

Void is specified for the edge zone, thus conservatively neglecting attenuation in the spacer plates.

Table 5.3-1 - Roadmap to W74 Shielding Models

Rad.	Location	Condition	Figure
Gamma	Side	Normal	Figure 5.3-3
Neutron	All	Normal	Figure 5.3-4
Gamma	Side	Accident	Figure 5.3-5
Neutron	All	Accident	
Gamma	Bottom	All	Figure 5.3-6
Gamma	Top	All	Figure 5.3-7

Table 5.3-2 - W74 Canister Component Dimensions

W74 Canister Component	Nominal Dimensions (in.)	Modeled Dimensions (in.)
Canister Shell I.R.	32.375	32.375
Canister Shell Thickness	0.625	0.615
Canister Shell O.R.	33.00	32.99
Inner Closure Plate Thickness	1.00	0.99
Outer Closure Plate Thickness	2.00	1.99
Bottom End Plug Bottom Plate	1.75	1.74
Bottom End Carbon Steel Shield Plug	5.75	5.74
Bottom End Plug Top Plate	1.00	0.99
Top End Carbon Steel Shield Plug	7.25	7.24

Table 5.3-3 - Canister Interior Source Zone Dimensions (in.)

Axial Assembly Region	Length (in)
Bottom Nozzle	2.0
Active Fuel	70.0
Upper Gas Plenum	4.5
Top Nozzle	9.0
Source Zone Radius ⁽¹⁾	28.485
Central Zone Radius ⁽²⁾	9.598

Notes:

- (1) This radius corresponds to a cylinder with an area equal to that covered by all of the guide tubes inside the W74 canister (see Section 5.3.1.6 discussion).
- (2) This radius corresponds to a cylinder with an area equal to that covered by five empty guide tubes at the center of the W74 canister (see Section 5.3.1.6 discussion).

Table 5.3-4 - Raw Material Atom Densities

	Atom Density ⁽¹⁾ (atoms/b-cm ²)						
	UO ₂	Zircaloy	SS-304	SS-316	Inc-718	Borated Steel	Carbon Steel
¹⁰ B	-	-	-	-	-	1.291E-03	-
¹¹ B	-	-	-	-	-	5.195E-03	-
C	-	-	-	-	-	-	-
O	4.590E-02	-	-	-	-	-	-
Al	-	-	-	-	-	-	-
Si	-	-	1.721E-03	1.721E-03	-	1.248E-03	-
Ti	-	-	-	-	9.271E-04	-	-
Cr	-	-	1.767E-02	1.581E-02	1.803E-02	1.708E-02	-
Mn	-	-	1.760E-03	1.760E-03	-	1.701E-03	-
Fe	-	-	5.887E-02	5.670E-02	1.716E-02	5.293E-02	8.447E-02
Ni	-	-	8.236E-03	9.883E-03	4.413E-02	1.075E-02	-
Zr	-	4.271E-02	-	-	-	-	-
Mo	-	-	-	1.260E-03	1.569E-03	-	-
Sb	-	4.660E-04	-	-	-	-	-
U	2.294E-02	-	-	-	-	-	-
Total	6.884E-02	4.318E-02	8.826E-02	8.713E-02	8.182E-02	9.020E-02	8.447E-02

Table 5.3-5 - W74 Active Fuel Region Densities

Element or Nuclide	Atom Density ⁽¹⁾ (atoms/b-cm ²)				
	UO ₂	Zircaloy	SS-316	Borated Steel	Total
Vol. Frac:	0.1925	0.0772	0.0365	0.0102	0.3164
¹⁰ B	-	-	-	1.317E-05	1.317E-05
¹¹ B	-	-	-	5.299E-05	5.299E-05
O	8.836E-03	-	-	-	8.836E-03
Si	-	-	6.282E-05	1.273E-05	7.555E-05
Cr	-	-	5.771E-04	1.742E-04	7.513E-04
Mn	-	-	6.424E-05	1.735E-05	8.159E-05
Fe	-	-	2.070E-03	5.399E-04	2.609E-03
Ni	-	-	3.607E-04	1.097E-04	4.704E-04
Zr	-	3.297E-03	-	-	3.297E-03
Mo	-	-	4.599E-05	-	4.599E-05
Sb	-	3.598E-05	-	-	3.598E-05
U	4.416E-03	-	-	-	4.416E-03

Notes:

- ⁽¹⁾ Elemental densities are calculated by multiplying the full material densities in Table 5.3-4 by the volume fractions in the first row of the table.

Table 5.3-6 - W74 Plenum Region Densities

Element or Nuclide	Atom Density ⁽¹⁾ (atoms/b-cm ²)			
	Zircaloy	SS-316	Borated Steel	Total
Vol. Frac:	0.0772	0.0365	0.0102	0.1239
¹⁰ B	-	-	1.317E-05	1.317E-05
¹¹ B	-	-	5.299E-05	5.299E-05
C	-	-	-	-
Si	-	6.282E-05	1.273E-05	7.555E-05
Ti	-	-	-	-
Cr	-	5.771E-04	1.742E-04	7.513E-04
Mn	-	6.424E-05	1.735E-05	8.159E-05
Fe	-	2.070E-03	5.399E-04	2.609E-03
Ni	-	3.607E-04	1.097E-04	4.704E-04
Zr	3.297E-03	-	-	3.297E-03
Mo	-	4.599E-05	-	4.599E-05
Sb	3.598E-05	-	-	3.598E-05

Notes:

- ⁽¹⁾ Elemental densities are calculated by multiplying the full material densities in Table 5.3-4 by the volume fractions in the first row of the table.

Table 5.3-7 - W74 Bottom End Densities

Element or Nuclide	Atom Density ⁽¹⁾ (atoms/b-cm ²)			
	SS-304	SS-316	Borated Steel	Total
Vol. Frac:	0.1070	0.0365	0.0102	0.1537
¹⁰ B	-	-	1.317E-05	1.317E-05
¹¹ B	-	-	5.299E-05	5.299E-05
Si	1.841E-04	6.282E-05	1.273E-05	2.597E-04
Cr	1.891E-03	5.771E-04	1.742E-04	2.642E-03
Mn	1.883E-04	6.424E-05	1.735E-05	2.699E-04
Fe	6.299E-03	2.070E-03	5.399E-04	8.909E-03
Ni	8.813E-04	3.607E-04	1.097E-04	1.352E-03
Mo	-	4.599E-05	-	4.599E-05

Notes:

- (1) Atom densities are calculated by multiplying the atom densities in Table 5.3-4 by the volume fractions in the first row of this table.

Table 5.3-8 - W74 Top End Densities

Element or Nuclide	Atom Density ⁽¹⁾ (atoms/b-cm ²)				
	SS-304	SS-316	Inc-718	Borated Steel	Total
Vol. Frac:	0.0313	0.0365	0.0070	0.0102	0.0850
¹⁰ B	-	-	-	1.317E-05	1.317E-05
¹¹ B	-	-	-	5.299E-05	5.299E-05
Si	5.387E-05	6.282E-05	-	1.273E-05	1.294E-04
Ti	-	-	6.490E-06	-	6.490E-06
Cr	5.531E-04	5.771E-04	1.262E-04	1.742E-04	1.431E-03
Mn	5.509E-05	6.424E-05	-	1.735E-05	1.367E-04
Fe	1.843E-03	2.070E-03	1.201E-04	5.399E-04	4.572E-03
Ni	2.578E-04	3.607E-04	3.089E-04	1.097E-04	1.037E-03
Mo	-	4.599E-05	1.098E-05	-	5.697E-05

Notes:

- ⁽¹⁾ Atom densities are calculated by multiplying the atom densities in Table 5.3-4 by the volume fractions in the first row of this table.

Table 5.3-9 - W74 “Center” Region Densities⁽¹⁾

Element or Nuclide	Atom Density ⁽²⁾ (atoms/b-cm ²)		
	SS-316	Borated Steel	Total
Vol. Frac:	0.0365	0.0102	0.0467
¹⁰ B	-	1.317E-05	1.317E-05
¹¹ B	-	5.299E-05	5.299E-05
Si	6.282E-05	1.273E-05	7.555E-05
Cr	5.771E-04	1.742E-04	7.513E-04
Mn	6.424E-05	1.735E-05	8.159E-05
Fe	2.070E-03	5.399E-04	2.609E-03
Ni	3.607E-04	1.097E-04	4.704E-04
Mo	4.599E-05	-	4.599E-05

Notes:

- (1) The center region densities are equal to the active fuel region densities (shown in Table 5.3-5), with the UO₂ and zircaloy materials removed.
- (2) Atom densities are calculated by multiplying the atom densities in Table 5.3-4 by the volume fractions in the first row of this table.

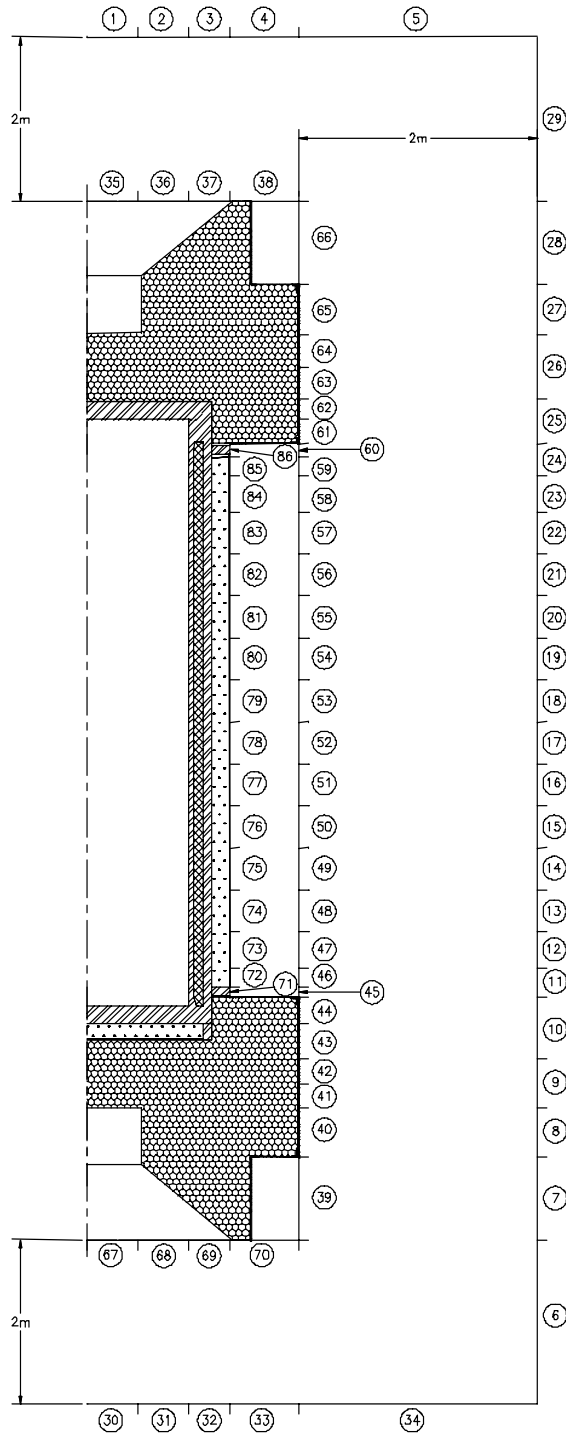


Figure 5.3-1 - Normal Condition Detector Locations

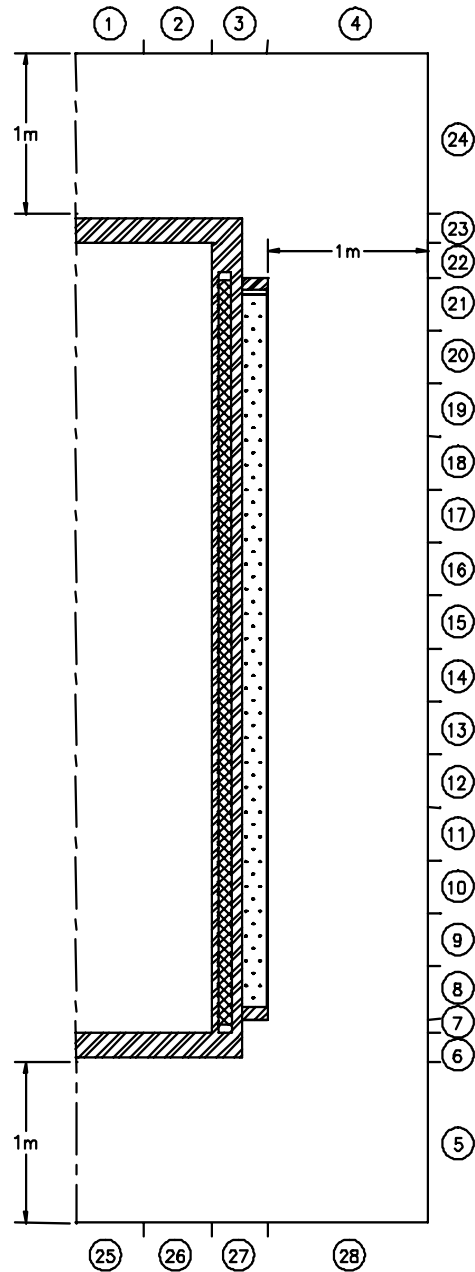


Figure 5.3-2 - Accident Condition Detector Locations

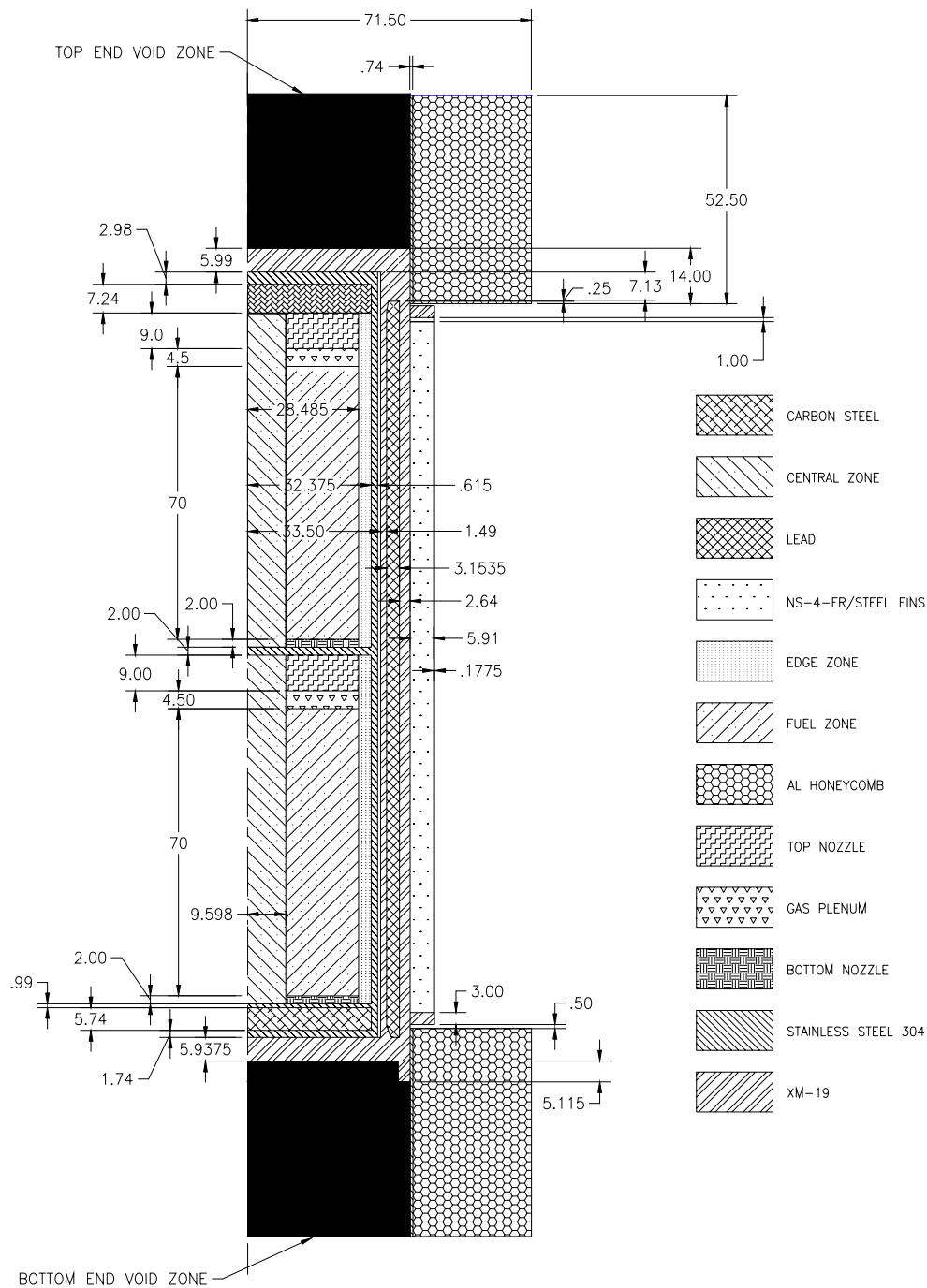


Figure 5.3-3 - W74 Side R-Z Gamma Model (normal conditions)

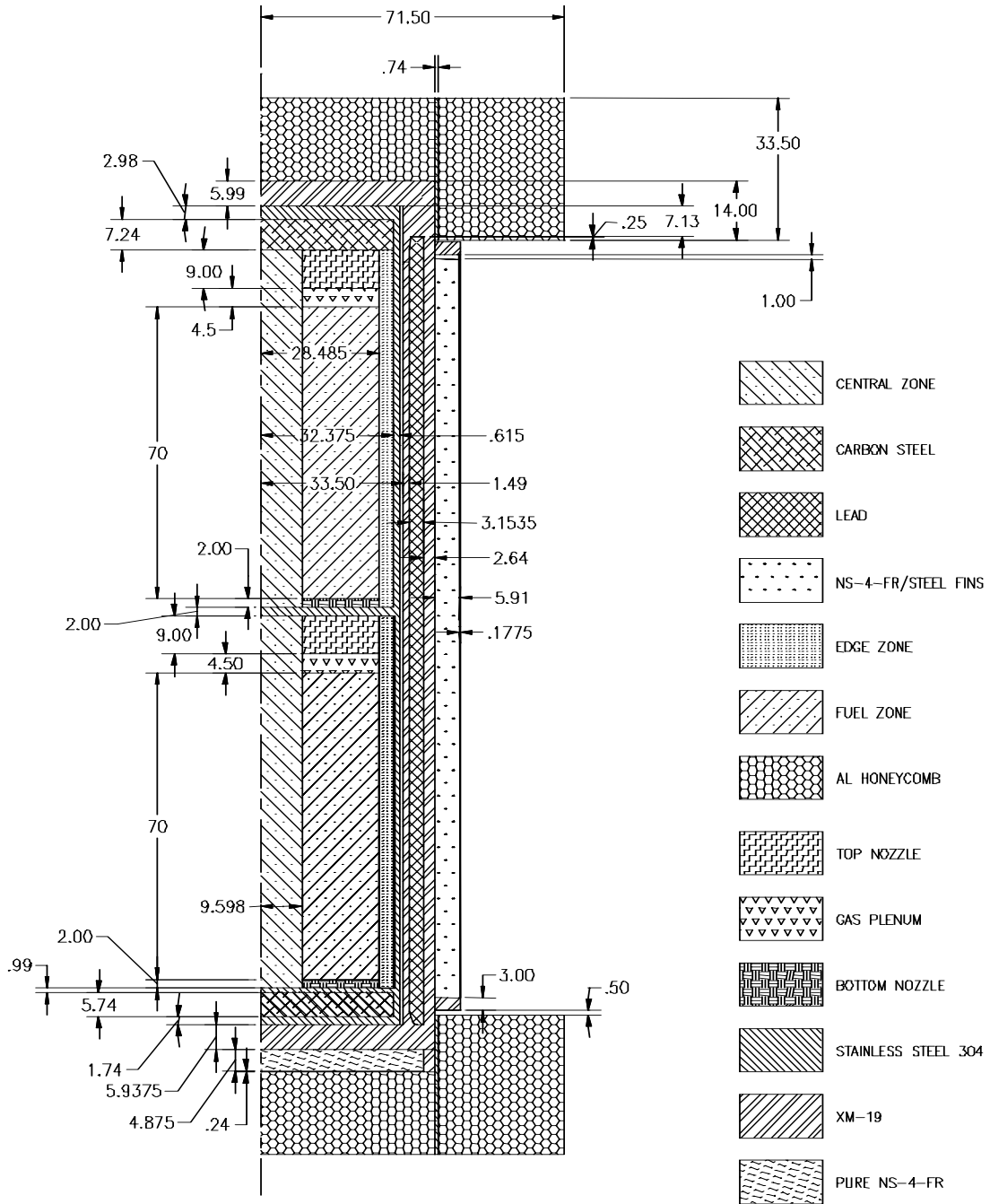


Figure 5.3-4 - W74 Neutron R-Z Model (normal conditions)

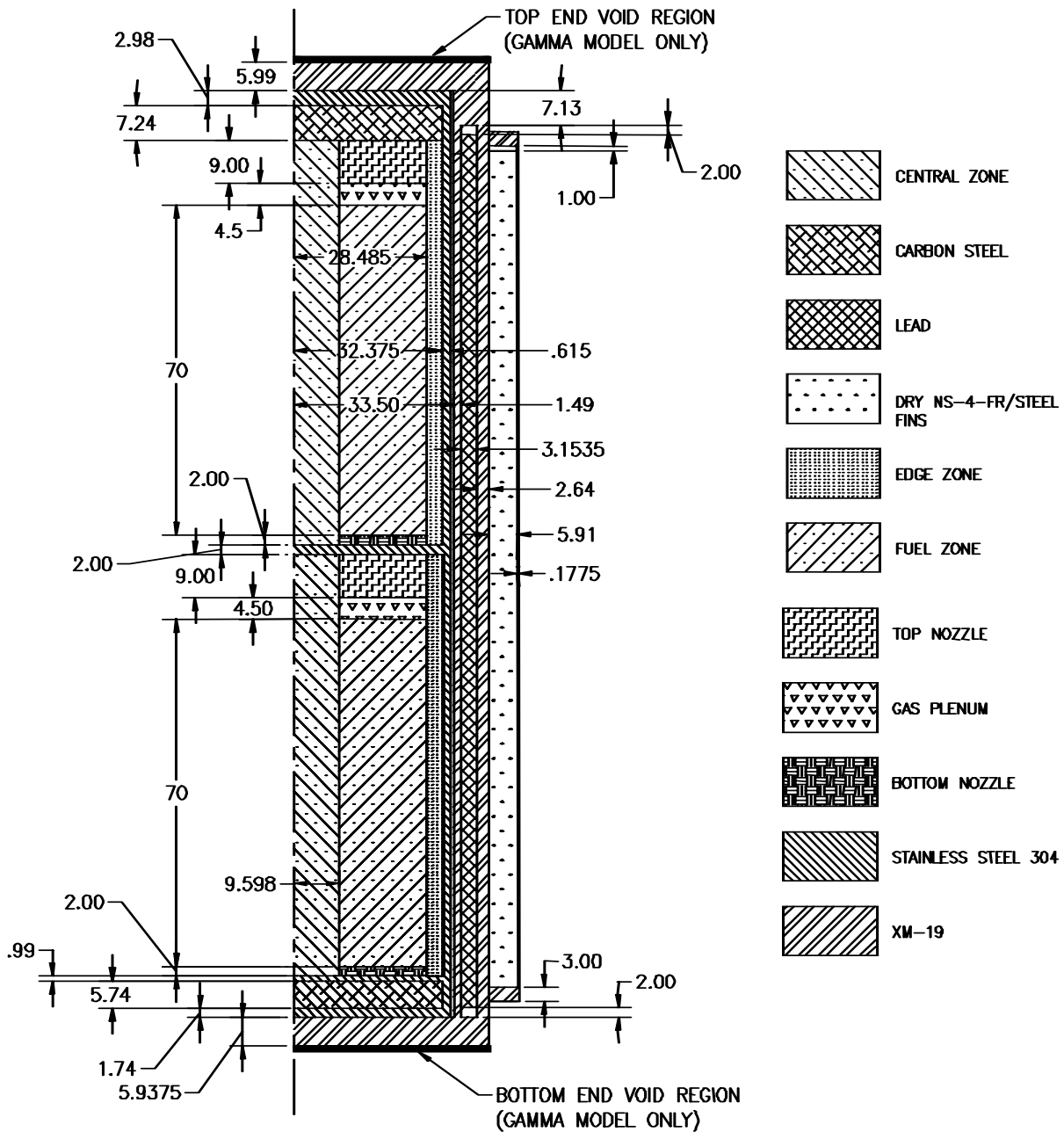
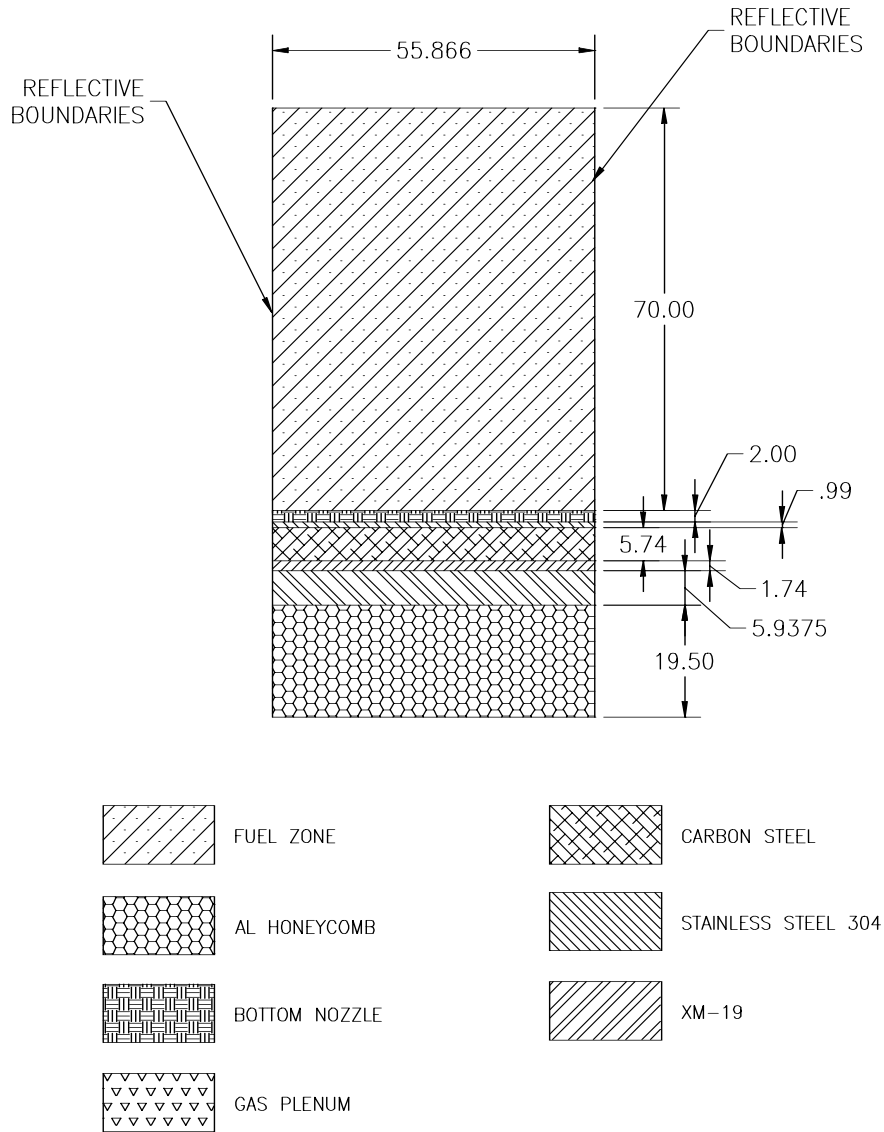
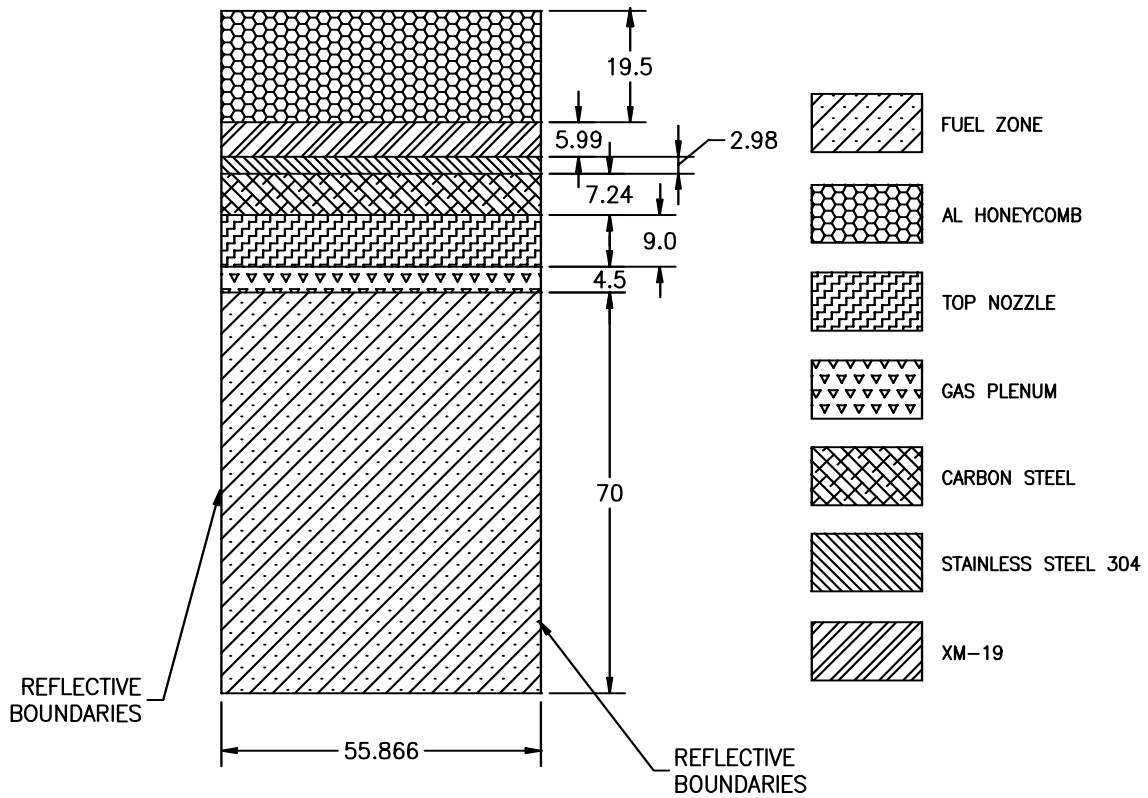


Figure 5.3-5 - W74 Gamma and Neutron R-Z Model
 (accident conditions)



**Figure 5.3-6 - W74 Bottom End Gamma Model
 (normal and accident conditions)**



**Figure 5.3-7 - W74 Top End Gamma Model
 (normal and accident conditions)**

5.4 Shielding Evaluation

5.4.1 Methodology

The shielding calculations are performed using MCNP,⁹ a general-purpose, continuous-energy, generalized geometry, coupled neutron-photon-electron Monte-Carlo transport code system. MCNP treats an arbitrary one-, two-, or three-dimensional configuration of materials in geometric cells bounded by first- and second-degree surfaces and some special fourth-degree surfaces. MCNP is used for the FuelSolutions™ shielding calculations because of its ability to model the desired geometries, source distributions, and tallies. MCNP is an industry-standard shielding code that is commonly used for SNF applications and has been extensively benchmarked under a wide range of problem classes.^{10,11} The MCNP pointwise continuous-energy cross section data¹² are used for all calculations. This cross section data set is used because of its ability to perform coupled neutron-gamma calculations, and its suitability for deep-penetration shielding problems.

The shielding calculations are performed using 2-D (R-Z) and 1-D (infinite slab) MCNP shielding models. The R-Z models are radially symmetric. Two-dimensional models are adequate because the effects of azimuthal variations in cask geometry are treated with supplemental analyses and appropriate adjustment factors, as described in Section 5.4 of the FuelSolutions™ W125 Transportation Cask SAR. The analyses calculate dose rate contributions from fuel gamma sources, fuel assembly hardware gamma sources (from both the fuel and non-fuel axial zones of the assembly), primary neutron sources, subcritical neutron multiplication sources, and secondary gamma sources. The dose rate contributions from the fuel gammas, the assembly hardware gammas, the primary neutron source, and from secondary gammas are calculated separately, multiplied by certain adjustment factors, then summed for presentation in the dose rate results tables. Dose rates are calculated directly within MCNP by specifying the ANSI/ANS 6.1.1-1977 flux-to-dose conversion factors. (See Section 5.5.1 of the FuelSolutions™ Transport Cask SAR for a listing of the factors.)

Surfaces are defined on or around the cask exterior where gamma and neutron fluxes are tallied. These surfaces correspond to the locations at which 10CFR71 regulations specify dose rate limits. Since a Monte-Carlo code is used, dose rates are tallied over areas, as opposed to point detectors. Since the models are radially symmetric, the detector areas are bands that extend over the full circumference of the cylindrical detector surface (around the cask sides). Each band

⁹Briesmeister, J., *MCNP-4A General Monte Carlo Code N-Particle Transport Code Version 4A*, LA-12625-M, November 1993.

¹⁰ Whalen, D., et al., “*MCNP: Photon Benchmark Problems*,” LA-12196, Los Alamos National Laboratory, Los Alamos, New Mexico, September 1991.

¹¹ Whalen, D., et al., “*MCNP: Neutron Benchmark Problems*,” LA-12212, Los Alamos National Laboratory, Los Alamos, New Mexico, November 1991.

¹² *MCNPXS: Standard Neutron, Photon, and Electron Data Libraries for MCNP4B*, RSICC Data Library DLC-189, Radiation Shielding Information Code Center, Oak Ridge, Tennessee.

covers a specified axial length. The cask end surfaces are vertical planes. The end detectors are a disk with surrounding annular areas.

The detector areas are small enough to give an adequate description of the spatial variance of the dose rates, but large enough to yield good particle statistics. In areas where the cask shield region geometry features are changing, smaller detector areas are generally defined. Detectors are specifically defined which cover areas of interest in the cask geometry, such as over gaps in the shielding or at the axial ends of the gamma and neutron shields. The central disk detector at the cask ends (where the peak dose rates are expected to occur) has a radius of half the radius of the source zone within the canister. The dose rate profile on the end of a cask is generally relatively flat inside this radius, so the central disk detector will give an adequate measure of peak cask end dose rate. On and over the cask side, the detectors cover an axial height of 12 inches, for a total of 12 detector areas over the active fuel region. In the area of peak dose rate (over the peak burnup section of the fuel), the dose rate differences between axial detector areas are a few percent. Given that this is the case, the axial variation within the peak dose rate detector area (i.e., the actual peak over the area average value for the peak detector) is only on the order of 1.0%. This is about an order of magnitude less than the margin of at least ~10% (versus the regulatory limit) that exists for all detector locations. Thus, the cask side detector areas are considered small enough to give an accurate calculation of peak dose rates.

A sufficient number of particle histories is run to give very low levels of statistical error. On the cask sides, the statistical error level in the MCNP gamma and neutron dose rate results is less than 1%. For some of the smaller detectors that are defined over the cask ends, error levels are as high as ~10%. The dose rates there, however, are significantly less than other regions on the cask side.

On the cask ends, the error levels in the primary gamma and neutron dose rates are only a few percent. This is a very adequate level of error given that the total dose rates on the cask ends are lower than their regulatory margins by a very wide margin (over a factor of two). For the secondary gamma dose rates, the error levels on the cask top end are a few percent. On the cask bottom end, higher error levels (up to 20%) are found for the secondary gammas. This is because an insignificant number of gammas penetrate the thick bottom shielding. The calculated secondary gamma dose rate values are extremely small (orders of magnitude lower than the regulatory limit), so the particle statistics may be considered adequate.

5.4.2 Results

The raw MCNP output gamma and neutron dose rates are adjusted by several factors. Each factor is designed to be bounding for its set of conditions.

Neutron dose rates are multiplied as follows:

1. All neutron dose rates are multiplied by the subcritical multiplication factor of 1.587 that is discussed in Section 5.2.3.1.
2. All neutron dose rates are multiplied by the axial profile effects factor of 1.327 that is discussed in Section 5.2.3.3.
3. All normal condition cask side neutron dose rates are multiplied by the fin neutron streaming factors of 1.215, 1.046, or 1.040 (for the package, conveyance, and two-meter

surfaces respectively). (See Section 5.4.1 of the FuelSolutions™ TS125 Transportation Cask SAR for the discussion of these factors.)

4. The normal condition neutron dose rate shown for the “underneath railcar” location in Table 5.1-1 is multiplied by the shear key penetration factor of 7.34. (See Section 5.4.1 of the FuelSolutions™ TS125 Transportation Cask SAR for the discussion of this factor.)
5. All accident condition cask side neutron dose rates, for locations that lie over the radial neutron shield, are multiplied by the neutron shield damage factor of 1.503. (See Section 5.4.2 of the FuelSolutions™ TS125 Transportation Cask SAR for the discussion of this factor.)

Gamma ray dose rates are multiplied as follows:

1. All secondary gamma dose rates are multiplied by the subcritical multiplication factor of 1.587 that is discussed in Section 5.2.3.1.
2. All accident condition cask side gamma dose rates, at locations that lie over the radial gamma shield, are multiplied by the lead slump and neutron shield damage factor of 6.288. (See Section 5.4.2 of the FuelSolutions™ TS125 Transportation Cask SAR for the discussion of this factor.)

There are no damage mechanisms that would occur as a result of normal condition tests that are anticipated to result in a significant increase in external radiation levels. The damage that is presumed to occur as a result of the hypothetical accident conditions is localized and will not result in a significant increase in external radiation levels. In order to demonstrate compliance with 10CFR71, the approach is to apply these factors in bulk fashion over entire surfaces of the package. This is, of course, grossly conservative with respect to the actual dose rates to be expected in the accident condition.

Figure 5.3-1 and Figure 5.3-2 illustrate the location of the normal and accident condition detector zones, respectively. Table 5.4-1 shows the normal condition results for each of these detectors, including all of the adjustment factors listed above. Table 5.4-2 shows the corresponding accident condition results. Each results table lists the dose rate contribution from each of the source contributors, along with the total dose rate and the corresponding 10CFR71 dose rate limit that applies for the detector location of interest.

The results in the two tables show that the FuelSolutions™ W74 canister meets the dose rate requirements at all locations, for all the Big Rock Point UO₂ fuel assemblies. Section 5.5.1 demonstrates that all Big Rock Point MOX fuel assemblies are also qualified for shipment.

In order to establish the minimum required distance for “normally occupied” sections of the vehicle, where the required dose rate is 2 mrem/hr or less, further evaluation of the cask end dose rates is necessary. At the top end of the package, which has the highest dose rates, the surface dose rate of 9.50 mrem/hr falls off to 2.80 mrem/hr at 2 m. For the MOX fuel case (discussed in Section 5.5.1), the cask top surface and two-meter dose rates are 20.41 and 5.44 mrem/hr, respectively. Based on this rate of spatial attenuation, the dose rate four meters from the end of the package will be less than the two mrem/hr limit. “Normally occupied” areas should therefore be at least four meters from the ends of the packages.

Table 5.4-1 - W74 Normal Condition Results (3 pages)

Detector No.	Normal Condition Dose Rate (mrem/hr)						
	Fuel Gamma	Fuel Zone Hardware Gamma	Non-Fuel Zone Gamma	Fuel Neutron	Secondary Gamma	Total	10CFR71 Limit
1	0.04	0.01	0.38	2.33	0.03	2.79	10
2	0.04	0.01	0.38	2.33	0.04	2.80	10
3	0.04	0.01	0.38	2.19	0.04	2.65	10
4	0.04	0.01	0.38	1.90	0.03	2.36	10
5	0.04	0.01	0.38	1.23	0.03	1.68	10
6	0.12	0.05	0.07	0.23	0.04	0.51	10
7	0.37	0.15	0.14	0.43	0.12	1.21	10
8	0.69	0.29	0.22	0.69	0.19	2.08	10
9	1.16	0.48	0.36	0.97	0.26	3.23	10
10	1.65	0.68	0.59	1.24	0.34	4.50	10
11	2.16	0.89	0.81	1.61	0.39	5.85	10
12	2.62	1.06	1.01	1.79	0.44	6.91	10
13	2.84	1.18	1.21	1.88	0.48	7.59	10
14	3.04	1.26	1.47	1.89	0.52	8.17	10
15	3.12	1.30	1.77	1.89	0.54	8.63	10
16	3.25	1.32	2.00	1.90	0.55	9.03	10
17	3.18	1.32	2.24	1.90	0.56	9.20	10
18	3.20	1.33	2.23	1.89	0.55	9.20	10
19	3.16	1.31	2.14	1.90	0.54	9.06	10
20	3.19	1.29	2.08	1.90	0.53	8.99	10
21	2.93	1.21	2.03	1.90	0.49	8.56	10
22	2.63	1.11	2.04	1.90	0.45	8.13	10
23	2.29	0.94	2.10	1.87	0.42	7.62	10
24	1.85	0.76	2.21	1.81	0.36	6.99	10
25	1.36	0.57	1.71	1.53	0.30	5.47	10
26	0.95	0.39	0.92	1.26	0.24	3.76	10
27	0.58	0.25	0.47	1.13	0.18	2.61	10
28	0.34	0.14	0.25	1.07	0.12	1.94	10
29	0.12	0.05	0.10	1.01	0.06	1.34	10
30	0.17	0.05	0.31	0.11	0.01	0.65	10
31	0.17	0.05	0.31	0.12	0.00	0.65	10
32	0.17	0.05	0.31	0.11	0.00	0.65	10
33	0.17	0.05	0.31	0.11	0.00	0.64	10
34	0.17	0.05	0.31	0.14	0.01	0.67	10
35	0.04	0.01	0.38	8.94	0.13	9.50	200

Table 5.4-1 - W74 Normal Condition Results (3 pages)

Detector No.	Normal Condition Dose Rate (mrem/hr)						10CFR71 Limit
	Fuel Gamma	Fuel Zone Hardware Gamma	Non-Fuel Zone Gamma	Fuel Neutron	Secondary Gamma	Total	
36	0.04	0.01	0.38	7.97	0.12	8.52	200
37	0.04	0.01	0.38	6.51	0.10	7.04	200
38	0.04	0.01	0.38	4.53	0.07	5.02	200
39	0.02	0.01	0.01	0.21	0.00	0.26	200
40	0.05	0.02	0.02	0.23	0.01	0.32	200
41	0.18	0.05	0.04	0.39	0.01	0.67	200
42	0.26	0.11	0.09	1.57	0.07	2.10	200
43	0.56	0.24	0.17	5.97	0.32	7.25	200
44	1.77	0.70	0.59	6.14	0.57	9.77	200
45	3.51	1.44	1.58	8.47	0.83	15.83	200
46	5.53	2.29	1.92	8.36	1.11	19.20	200
47	8.53	3.56	1.33	6.70	1.45	21.58	200
48	10.35	4.23	0.88	5.89	1.69	23.04	200
49	10.39	4.24	1.31	5.18	1.76	22.89	200
50	8.96	3.75	3.15	4.39	1.70	21.96	200
51	6.75	2.85	7.12	3.56	1.61	21.89	200
52	5.41	2.22	10.91	3.21	1.60	23.35	200
53	6.50	2.72	8.93	3.50	1.64	23.28	200
54	8.90	3.72	4.14	4.13	1.75	22.64	200
55	10.37	4.34	1.93	4.70	1.80	23.15	200
56	10.39	4.29	1.74	4.91	1.71	23.04	200
57	8.88	3.65	3.23	4.88	1.49	22.12	200
58	6.04	2.51	6.97	5.40	1.15	22.08	200
59	3.29	1.36	10.76	7.48	0.84	23.73	200
60	2.02	0.79	11.95	8.79	0.67	24.21	200
61	1.23	0.49	5.09	6.30	0.44	13.55	200
62	0.48	0.21	2.27	6.35	0.25	9.56	200
63	0.18	0.07	1.21	5.87	0.17	7.51	200
64	0.07	0.03	0.57	4.35	0.10	5.12	200
65	0.03	0.02	0.18	3.91	0.07	4.21	200
66	0.02	0.01	0.05	4.02	0.06	4.17	200
67	0.17	0.05	0.31	0.23	0.01	0.76	200
68	0.17	0.05	0.31	0.23	0.01	0.77	200
69	0.17	0.05	0.31	0.23	0.01	0.76	200
70	0.17	0.05	0.31	0.20	0.01	0.73	200
71	0.59	0.23	0.82	50.59	0.64	52.87	1000

Table 5.4-1 - W74 Normal Condition Results (3 pages)

Detector No.	Normal Condition Dose Rate (mrem/hr)						10CFR71 Limit
	Fuel Gamma	Fuel Zone Hardware Gamma	Non-Fuel Zone Gamma	Fuel Neutron	Secondary Gamma	Total	
72	8.66	3.54	7.25	9.91	2.15	31.52	1000
73	18.83	7.79	0.72	10.14	3.23	40.70	1000
74	20.67	8.64	0.04	11.28	3.82	44.45	1000
75	20.28	8.37	0.05	10.40	3.86	42.95	1000
76	18.29	7.64	0.27	7.88	3.29	37.36	1000
77	10.68	4.60	7.88	4.56	2.57	30.29	1000
78	2.55	1.05	37.36	2.78	2.26	46.00	1000
79	8.72	3.55	17.28	4.69	2.65	36.89	1000
80	18.44	7.78	0.80	8.23	3.44	38.69	1000
81	20.45	8.73	0.08	10.31	3.97	43.54	1000
82	20.39	8.51	0.11	10.29	3.76	43.05	1000
83	18.74	7.73	0.44	8.19	3.03	38.13	1000
84	11.12	4.54	8.04	5.30	2.09	31.10	1000
85	2.33	0.90	37.53	6.65	1.43	48.83	1000
86	0.29	0.13	25.07	43.70	0.73	69.92	1000

Table 5.4-2 - W74 Accident Condition Results

Detector No.	Accident Condition Dose Rate (mrem/hr)						10CFR71 Limit
	Fuel Gamma	Fuel Zone Hardware Gamma	Non-Fuel Zone Gamma	Fuel Neutron	Secondary Gamma	Total	
1	0.07	0.02	0.69	26.11	0.34	27.23	1000
2	0.07	0.02	0.69	20.27	0.28	21.33	1000
3	0.07	0.02	0.69	16.05	0.22	17.05	1000
4	0.07	0.02	0.69	15.10	0.14	16.02	1000
5	8.43	3.70	2.47	58.90	0.34	73.83	1000
6	24.31	9.89	6.92	98.38	0.56	140.06	1000
7	32.10	12.93	10.42	109.72	0.64	165.81	1000
8	46.06	19.62	14.06	136.79	0.78	217.31	1000
9	67.44	28.92	13.25	176.18	0.97	286.77	1000
10	79.88	34.06	13.61	201.39	1.11	330.04	1000
11	82.14	34.94	20.01	210.54	1.22	348.84	1000
12	75.92	32.06	36.08	209.68	1.24	354.97	1000
13	65.15	27.43	58.86	202.59	1.27	355.30	1000
14	57.59	25.17	74.62	200.60	1.25	359.23	1000
15	63.85	27.23	67.43	204.37	1.23	364.12	1000
16	75.97	32.17	43.16	211.45	1.23	363.98	1000
17	83.64	35.48	27.92	214.08	1.20	362.33	1000
18	82.72	34.90	25.34	202.44	1.11	346.52	1000
19	71.51	29.99	37.07	177.78	1.04	317.39	1000
20	52.56	21.91	55.15	147.07	0.87	277.56	1000
21	31.11	13.40	11.34	108.89	0.66	165.40	1000
22	19.30	7.82	9.16	79.36	0.52	116.16	1000
23	13.19	5.34	7.27	66.31	0.42	92.53	1000
24	4.90	2.12	3.81	38.96	0.24	50.04	1000
25	1.02	0.34	2.22	66.69	0.76	71.02	1000
26	1.02	0.34	2.22	54.54	0.59	58.70	1000
27	1.02	0.34	2.22	39.06	0.41	43.04	1000
28	1.02	0.34	2.22	26.68	0.26	30.51	1000

This page intentionally left blank.

5.5 Supplemental Data

5.5.1 BRP Mixed-Oxide (MOX) Fuel Assembly Qualification

The design basis W74 UO₂ fuel is 32 GWd/MTU, 3.0% enriched, 6-year cooled. These fuel parameters are bounding for the entire Big Rock Point UO₂ fuel inventory with respect to radiation source strengths. There are also MOX fuel assemblies at Big Rock Point that must be qualified. The gamma source strengths for all BRP MOX fuel are expected to be much lower than those of the UO₂ fuel design basis, because all BRP MOX fuel has a cooling time of at least 15 years, versus the 6-year design basis UO₂ fuel cooling time. Due to the higher actinide content of MOX fuel, however, the neutron source strength is higher than UO₂ fuel.

In order to qualify MOX fuel, the MOX source terms are evaluated, then the gamma and neutron dose rate results for UO₂ fuel are multiplied by the ratio of MOX to UO₂ source terms. The sum of the gamma and neutron dose rates is then compared to allowable dose rates to determine acceptability.

MOX Fuel Source Terms

There are three BRP MOX fuel assembly designs, the J2 (9x9) assembly, the DA (11x11) assembly, and the G-Pu (11x11) assembly. These assemblies are described in detail in Section 6.6.1 of this SAR. The BRP MOX assembly arrays contain a mixture of one or more types of MOX fuel rods and UO₂ fuel rods of multiple ²³⁵U enrichment levels. Figures 6.6-1 through 6.6-3 of this SAR illustrate the fuel rod array for the three MOX fuel assembly types. The locations of the different rod types are shown, along with their ²³⁵U enrichment levels and their fuel material plutonium weight fractions.

Point-depletion calculations are performed with the ORIGEN 2.1 code¹³ to determine bounding fuel gamma and neutron source strengths for each of the three MOX fuel assembly designs. The calculations are performed using the BWRPUU.LIB cross-section library. This ORIGEN 2.1 cross-section library is tailored to model a mixture of plutonium and uranium fuels within a BWR reactor. This best characterizes BRP MOX fuel, which contains a mixture of MOX and UO₂ fuel pins.

Table 5.5-1 shows the fuel parameters for each of the three BRP MOX fuel assembly designs. ORIGEN 2.1 code calculates fuel gamma and neutron source strengths on a per assembly basis, as a function of assembly cooling time for each set of fuel parameters. Table 5.5-2 shows the bounding total fuel gamma source strengths on a gammas/sec-assembly basis. The gamma source strengths are presented in the ORIGEN energy group structure. The BRP MOX fuel assembly with the highest gamma and neutron source strengths is the G-Pu MOX design. The source strengths calculated for this assembly are conservatively based on a cooling time of 15 years, which corresponds to the assembly's cooling time as of January 2000.

The bounding MOX fuel gamma source strengths are shown in Table 5.5-3 for each significant gamma energy line. The design basis UO₂ fuel gamma source strengths are included in

¹³ BWRPUU.LIB, *ORIGEN 2.1 - Isotope Generation and Depletion Code, Matrix Exponential Method*, RSICC Computer Code Collection CCC-371, Oak Ridge National Laboratory, Oak Ridge, Tennessee, February 1996.

Table 5.5-3 for comparison. Comparison of the MOX fuel and design basis UO₂ fuel gamma source strengths shows that the design basis source strengths (used as the basis for the W74 shielding analyses) are higher than the MOX fuel source strengths for all gamma energy lines. Furthermore, the MOX fuel gamma source strength is at most 0.583 times the design basis source strength. The highest fraction occurs for the 0.575 MeV energy line (a relatively unimportant energy line). Therefore the cask external gamma dose rates for bounding BRP MOX fuel are at most 0.583 times the dose rates calculated by the W74 shielding analyses. In fact, the actual dose rate ratio will be closer to 0.327, the ratio corresponding to the (dominant) 1.25 MeV gamma energy line. For this reason, the W74 UO₂ fuel gamma dose rates presented in Section 5.4.2 may be multiplied by 0.583 to yield the gamma dose rates for BRP MOX fuel in the next section.

The neutron source strengths for the three BRP MOX fuel assembly designs are shown in Table 5.5-4. The source strengths are presented on a per MTU and a per assembly basis, with the per assembly source strengths equaling the per MTU source strengths times the BRP MOX assembly uranium loadings shown in Table 5.5-1. The bounding (primary) fuel neutron source strength for BRP MOX fuel is the G-Pu assembly source strength of 7.738×10^8 neutrons/sec-MTU. The W74 UO₂ shielding analysis primary neutron source strength (given in Section 5.2.3.1) is 3.467×10^8 neutrons/sec-MTU. Thus, the MOX fuel neutron source strength is 2.232 times that of the design basis UO₂ BRP assembly modeled in the W74 shielding analyses. For this reason, the W74 UO₂ fuel gamma dose rates presented in Section 5.4.2 may be multiplied by 2.232 to yield the neutron dose rates for BRP MOX fuel in the next section.

For both UO₂ and MOX BRP fuel, the neutron source strength is almost entirely due to spontaneous fission of ²⁴⁴Cm. The ORIGEN2.1 calculations that determine the total neutron source strengths for the BRP MOX fuel assemblies show that spontaneous fission of ²⁴⁴Cm is responsible for over 98% of the overall MOX fuel neutron source strength. This nuclide yields a similar fraction of the neutron source strength for the bounding UO₂ BRP fuel case, as discussed in Section 5.2.3.2. For this reason, the same neutron energy spectrum (the spontaneous fission spectrum of ²⁴⁴Cm) is assumed for both UO₂ and MOX BRP fuel assemblies. Since the source spectrum is the same, the neutron dose rates for the MOX case are determined by scaling the UO₂ case dose rates, using the ratio of total neutron source strengths as discussed above.

As discussed in Section 5.2.2, it is assumed that the assembly hardware gamma source strengths are similar for BRP MOX fuel and UO₂ fuel, for a given set of fuel parameters (i.e., burnup and cooling time). The burnup levels for the bounding BRP MOX and UO₂ fuel assemblies are similar (34.2 vs. 32 GWd/MTU). There is a large difference in cooling time, however (15 years for the MOX vs. 6 years for the UO₂). Nine additional years of cooling time would reduce gamma source strengths ~0.3 times their original value, based on a 5.27-year (Co-60) half-life. This exceeds the small difference in burnup levels.

The fuel and non-fuel region assembly hardware gamma dose rate contributions calculated for the design basis UO₂ BRP assembly case are adjusted downward by a factor of three to yield the BRP MOX fuel assembly hardware gamma dose rate contributions. This correction factor (0.33) is about 10% higher than the correction factor determined above (0.30). This elevated factor is used to account for any differences in hardware activity due to the slight difference in burnup level (34.2 vs. 32 GWd/MTU), and to account for any small differences in hardware activation between UO₂ and MOX BRP fuel.

MOX Fuel Dose Rates

Thus, in summary, the UO₂ fuel gamma and neutron results shown in Table 5.4-1 and Table 5.4-2 are multiplied by 0.583 and 2.232, respectively, to yield the bounding BRP MOX fuel gamma and neutron dose rates presented in Table 5.5-5 and Table 5.5-6. The assembly hardware gamma dose rate contributions shown in Table 5.5-5 and Table 5.5-6 are divided by a factor of three to yield the corresponding MOX fuel values.

Since all dose rates for MOX fuel are within their allowable limits, all BRP MOX fuel is qualified for transportation in the W74 canister. The dose rates four meters from the cask ends will fall below 2 mrem/hr for the MOX fuel case, as discussed in Section 5.4.2.

5.5.2 BRP Partial Fuel Assembly Qualification

Partial fuel assemblies have one or more fuel rods missing from the design basis assembly array. A number of partial BRP assemblies are known to exist.

The gamma and neutron source strengths per MTU of BRP fuel are a function of the burnup, cooling time, and initial enrichment of the fuel. The W74 canister shielding calculations are based on these per MTU source strengths and an upper bound BRP assembly uranium loading of 0.1421 MTU/assembly. A larger assembly uranium loading yields a proportionally larger gamma and neutron source strength on a per assembly basis. Shielding sensitivity calculations show that the increase in gamma and neutron source strengths causes an increase in cask surface gamma and neutron dose rates, despite the increase in assembly self-shielding due to the increased uranium mass. Thus, assuming a maximum assembly uranium loading is conservative.

Removing fuel rods from the assembly array reduces the assembly uranium loading. The gamma and neutron source strengths for each fuel rod remain the same for a given assembly burnup, cooling time, and initial enrichment. Thus, partial fuel assemblies are equivalent to assemblies with a lower uranium loading. Their uranium mass is lower and their gamma and neutron source strengths are proportionally lower. For a given set of fuel parameters, for both partial assemblies and low uranium loading assemblies, the gamma and neutron source strengths per MTU of fuel are the same as those of the (maximum loading) design basis BRP fuel assembly. As discussed above, lower uranium loading assemblies are shown by calculation to produce lower cask external dose rates, for a given burnup, enrichment, and cooling time. Therefore, partial BRP assemblies produce lower cask external dose rates than intact BRP fuel assemblies.

For the above reasons, the W74 shielding analyses, which are based on intact BRP fuel assemblies with an upper bound uranium loading, are bounding for all partial BRP fuel assemblies.

5.5.3 BRP Damaged Fuel Assembly Qualification

Damaged assemblies are assemblies with damage in excess of pinhole leaks or hairline cracks.¹⁴ Fuel assemblies with damaged grid spacers (defined as damaged to a degree where fuel rod

¹⁴ ISG-1, *Damaged Fuel*, Spent Fuel Project Office Interim Staff Guidance, United States Nuclear Regulatory Commission, November 1998.

structural integrity cannot be assured, or where grid spacers have shifted vertically from their design position) will also be stored in damaged fuel cans.

All BRP assemblies classified as damaged must be placed inside a damaged fuel can, which is then loaded into one of the eight support tube locations of the W74 basket. The damaged fuel can is similar to a W74 canister guide tube, with 0.09-inch thick stainless steel walls and 0.075-inch thick borated stainless steel poison sheets attached to each of the four walls.

With respect to all assembly parameters that affect shielding, damaged fuel assemblies must meet all of the same limitations as intact assemblies. The required cooling times apply for both damaged and undamaged (i.e., intact or partial) BRP fuel assemblies.

Assembly damage does not affect the quantity of fuel or assembly hardware materials, or the radiation source strengths of a given quantity of fuel or hardware materials. Thus, assembly damage does not affect the radiation source strengths. Bent fuel rods would not significantly affect the source strength distribution. Therefore, the shielding analyses for intact BRP assemblies are applicable for damaged BRP assemblies.

If some fuel rods in a damaged assembly have missing pellets or sections that have broken off, they effectively have a missing rod over some section of the axial length. As discussed in Section 5.5.2, assemblies with missing rods have lower source terms than design basis assemblies and are, therefore, bounded by the intact assembly shielding analyses.

Furthermore, damaged fuel assemblies must be placed in the damaged fuel cans, which have stainless steel walls and borated stainless steel poison sheets. These damaged fuel can materials provide additional shielding within the canister interior that is not present for canisters loaded with intact fuel. Due to this additional shielding, the dose rates for canisters containing damaged fuel are bounded by those calculated for the intact fuel case.

Rod fragments and/or loose pellets (i.e., fuel debris) are not qualified for loading into the damaged fuel cans in the W74 canister.

Table 5.5-1 - ORIGEN 2.1 Data for BRP MOX Fuel Assemblies

Assembly Parameter	J2 Assembly Value	DA Assembly Value	G-Pu Assembly Value
Cooling Time (years)	22	22	15
Maximum Burnup (GWd/MTIHM)	22.82	21.85	34.22
Assembly Thermal Power (MW/assy.)	2.86	2.86	2.86
Total Heavy Metal Loading (MT/assy.) ⁽¹⁾	0.124	0.126	0.127
²³⁵ U Quantity (gram/assembly) ⁽¹⁾	3193	2714	3926
²³⁸ U Quantity (gram/assembly) ⁽¹⁾	119,409	121,205	122,041
²³⁹ Pu Quantity (gram/assembly) ⁽¹⁾	1072	1354	1074
²⁴⁰ Pu Quantity (gram/assembly) ⁽¹⁾	280	328	249
²⁴¹ Pu Quantity (gram/assembly) ⁽¹⁾	81	122	108
²⁴² Pu Quantity (gram/assembly) ⁽¹⁾	16	30	23

Note:

- ⁽¹⁾ Representative value for assemblies of that type. Small variations in these masses (on the order of one percent) may occur between individual BRP MOX assemblies. The analyses are still applicable for all assemblies of each type, as discussed in Section 5.5.1.

Table 5.5-2 - BRP MOX Fuel Gamma Source Strengths

ORIGEN Group	Average Energy (MeV)	22-Year Old J2 MOX Fuel Source (g/s-assy.)	22-Year Old DA MOX Fuel Source (g/s-assy.)	15-Year Old G-Pu MOX Fuel Source (g/s-assy.)
1	0.01	1.12E+14	1.04E+14	2.01E+14
2	0.025	2.19E+13	2.01E+13	4.01E+13
3	0.0375	2.73E+13	2.57E+13	5.18E+13
4	0.0575	2.78E+13	2.75E+13	4.30E+13
5	0.085	1.18E+13	1.09E+13	2.25E+13
6	0.125	9.35E+12	8.65E+12	2.08E+13
7	0.225	9.84E+12	8.66E+12	1.87E+13
8	0.375	4.11E+12	3.71E+12	7.91E+12
9	0.575	1.97E+14	1.91E+14	3.56E+14
10	0.85	2.95E+12	2.82E+12	1.27E+13
11	1.25	2.58E+12	2.50E+12	9.21E+12
12	1.75	8.68E+10	8.35E+10	2.87E+11
13	2.25	7.44E+06	8.59E+06	1.78E+08
14	2.75	1.01E+07	1.11E+07	4.95E+07
15	3.5	2.51E+06	3.17E+06	1.21E+07
16	5.0	1.06E+06	1.35E+06	4.26E+06
17	7.0	1.23E+05	1.55E+05	4.91E+05
18	9.5	1.41E+04	1.78E+04	5.64E+04
Gamma Source		4.26E+14	4.06E+14	7.84E+14

Table 5.5-3 - BRP MOX Fuel Gamma Source Strength Comparison

Mean Energy (MeV)	Fuel γ Source Strength (γ /sec-canister)		Ratio
	Bounding MOX Fuel	UO ₂ Design Basis Fuel	
0.575	2.278 E+16	3.906 E+16	0.583
0.85	8.128 E+14	7.195 E+15	0.113
1.25	5.894 E+14	1.803 E+15	0.327
1.75	1.837 E+13	4.690 E+13	0.392
2.25	1.139 E+10	1.396 E+13	0.001
2.75	3.168 E+09	5.448 E+11	0.006
3.5	7.744 E+08	7.005 E+10	0.011

Note:

- (1) Fuel gamma dose rates from UO₂ shielding calculations are multiplied by $2.278 \text{ E}+16 / 3.906 \text{ E}+16 = 0.583$ to determine the equivalent dose rate for MOX fuel.

Table 5.5-4 - BRP MOX Assembly Total Neutron Source Strengths

Assembly Type	Max Burnup (GWd/MTU)	Cooling Time (years)	Neutron Source Strength	
			(n/sec-assy) ⁽¹⁾	(n/sec-MTIHM)
J2 MOX Assembly	22.82	22	2.512E+07	2.025E+08
DA MOX Assembly	21.85	22	3.169E+07	2.519E+08
G-Pu MOX Assembly	34.22	15	9.861E+07	7.738E+08
Limiting UO ₂ Assembly	32.00	6	4.927E+08	3.467E+08

Note:

- ⁽¹⁾ Neutron and secondary gamma dose rates from UO₂ shielding calculations are multiplied by $7.738E+08 / 3.467E+08 = 2.232$, to determine the equivalent dose rate for MOX fuel.

**Table 5.5-5 - W74 MOX Fuel Normal Condition Results
(3 pages)**

Detector No.	Normal Condition Dose Rate (mrem/hr)						10CFR71 Limit
	Fuel Gamma	Fuel Zone Hardware Gamma	Non-Fuel Zone Gamma	Fuel Neutron	Secondary Gamma	Total	
1	0.02	0.00	0.13	5.20	0.08	5.43	10
2	0.02	0.00	0.13	5.21	0.08	5.44	10
3	0.02	0.00	0.13	4.89	0.08	5.12	10
4	0.02	0.00	0.13	4.25	0.07	4.48	10
5	0.02	0.00	0.13	2.75	0.06	2.96	10
6	0.07	0.02	0.02	0.50	0.10	0.71	10
7	0.22	0.05	0.05	0.96	0.27	1.55	10
8	0.40	0.10	0.07	1.55	0.42	2.54	10
9	0.68	0.16	0.12	2.17	0.58	3.70	10
10	0.96	0.23	0.20	2.76	0.75	4.90	10
11	1.26	0.30	0.27	3.58	0.86	6.27	10
12	1.52	0.35	0.34	3.99	0.99	7.19	10
13	1.66	0.39	0.40	4.20	1.07	7.72	10
14	1.77	0.42	0.49	4.21	1.15	8.05	10
15	1.82	0.43	0.59	4.22	1.20	8.28	10
16	1.90	0.44	0.67	4.23	1.22	8.46	10
17	1.86	0.44	0.75	4.23	1.25	8.53	10
18	1.86	0.44	0.74	4.22	1.23	8.50	10
19	1.84	0.44	0.71	4.24	1.21	8.44	10
20	1.86	0.43	0.69	4.24	1.17	8.40	10
21	1.71	0.40	0.68	4.25	1.10	8.13	10
22	1.54	0.37	0.68	4.23	1.01	7.83	10
23	1.33	0.31	0.70	4.18	0.94	7.47	10
24	1.08	0.25	0.74	4.04	0.80	6.91	10
25	0.79	0.19	0.57	3.41	0.68	5.64	10
26	0.56	0.13	0.31	2.81	0.54	4.34	10
27	0.34	0.08	0.16	2.52	0.40	3.50	10
28	0.20	0.05	0.08	2.40	0.27	3.01	10
29	0.07	0.02	0.03	2.26	0.13	2.51	10
30	0.10	0.02	0.10	0.26	0.01	0.49	10
31	0.10	0.02	0.10	0.26	0.01	0.49	10
32	0.10	0.02	0.10	0.25	0.01	0.48	10
33	0.10	0.02	0.10	0.25	0.01	0.48	10
34	0.10	0.02	0.10	0.30	0.02	0.54	10

**Table 5.5-5 - W74 MOX Fuel Normal Condition Results
(3 pages)**

Detector No.	Normal Condition Dose Rate (mrem/hr)						10CFR71 Limit
	Fuel Gamma	Fuel Zone Hardware Gamma	Non-Fuel Zone Gamma	Fuel Neutron	Secondary Gamma	Total	
35	0.02	0.00	0.13	19.96	0.30	20.41	200
36	0.02	0.00	0.13	17.79	0.27	18.21	200
37	0.02	0.00	0.13	14.54	0.23	14.92	200
38	0.02	0.00	0.13	10.10	0.16	10.42	200
39	0.01	0.00	0.00	0.47	0.01	0.50	200
40	0.03	0.01	0.01	0.52	0.01	0.57	200
41	0.10	0.02	0.01	0.87	0.03	1.03	200
42	0.15	0.04	0.03	3.50	0.16	3.88	200
43	0.33	0.08	0.06	13.33	0.71	14.50	200
44	1.03	0.23	0.20	13.71	1.27	16.44	200
45	2.05	0.48	0.53	18.91	1.86	23.82	200
46	3.22	0.76	0.64	18.65	2.48	25.75	200
47	4.98	1.19	0.44	14.96	3.23	24.80	200
48	6.03	1.41	0.29	13.14	3.78	24.66	200
49	6.06	1.41	0.44	11.57	3.92	23.40	200
50	5.22	1.25	1.05	9.81	3.80	21.13	200
51	3.93	0.95	2.37	7.95	3.60	18.80	200
52	3.15	0.74	3.64	7.16	3.57	18.26	200
53	3.79	0.91	2.98	7.82	3.66	19.15	200
54	5.19	1.24	1.38	9.22	3.91	20.94	200
55	6.05	1.45	0.64	10.49	4.02	22.65	200
56	6.06	1.43	0.58	10.96	3.82	22.84	200
57	5.18	1.22	1.08	10.89	3.31	21.67	200
58	3.52	0.84	2.32	12.06	2.57	21.32	200
59	1.92	0.45	3.59	16.69	1.88	24.53	200
60	1.18	0.26	3.98	19.62	1.49	26.53	200
61	0.72	0.16	1.70	14.06	0.98	17.62	200
62	0.28	0.07	0.76	14.17	0.57	15.84	200
63	0.10	0.02	0.40	13.10	0.39	14.03	200
64	0.04	0.01	0.19	9.72	0.21	10.17	200
65	0.02	0.01	0.06	8.73	0.16	8.97	200
66	0.01	0.00	0.02	8.97	0.14	9.15	200
67	0.10	0.02	0.10	0.50	0.02	0.74	200
68	0.10	0.02	0.10	0.52	0.02	0.75	200
69	0.10	0.02	0.10	0.51	0.02	0.75	200

**Table 5.5-5 - W74 MOX Fuel Normal Condition Results
(3 pages)**

Detector No.	Normal Condition Dose Rate (mrem/hr)						10CFR71 Limit
	Fuel Gamma	Fuel Zone Hardware Gamma	Non-Fuel Zone Gamma	Fuel Neutron	Secondary Gamma	Total	
70	0.10	0.02	0.10	0.44	0.01	0.67	200
71	0.35	0.08	0.27	112.93	1.42	115.04	1000
72	5.05	1.18	2.42	22.13	4.80	35.57	1000
73	10.98	2.60	0.24	22.63	7.21	43.64	1000
74	12.05	2.88	0.01	25.18	8.53	48.65	1000
75	11.82	2.79	0.02	23.20	8.61	46.45	1000
76	10.66	2.55	0.09	17.59	7.34	38.23	1000
77	6.23	1.53	2.63	10.18	5.73	26.30	1000
78	1.49	0.35	12.45	6.20	5.04	25.53	1000
79	5.09	1.18	5.76	10.47	5.91	28.41	1000
80	10.75	2.59	0.27	18.36	7.67	39.65	1000
81	11.92	2.91	0.03	23.01	8.86	46.73	1000
82	11.89	2.84	0.04	22.97	8.39	46.11	1000
83	10.92	2.58	0.15	18.27	6.76	38.68	1000
84	6.48	1.51	2.68	11.84	4.67	27.19	1000
85	1.36	0.30	12.51	14.85	3.18	32.19	1000
86	0.17	0.04	8.36	97.53	1.63	107.73	1000

Table 5.5-6 - W74 MOX Fuel Accident Condition Results

Detector No.	Accident Condition Dose Rate (mrem/hr)						10CFR71 Limit
	Fuel Gamma	Fuel Zone Hardware Gamma	Non-Fuel Zone Gamma	Fuel Neutron	Secondary Gamma	Total	
1	0.04	0.01	0.23	58.28	0.76	59.31	1000
2	0.04	0.01	0.23	45.24	0.63	46.15	1000
3	0.04	0.01	0.23	35.82	0.50	36.59	1000
4	0.04	0.01	0.23	33.71	0.32	34.31	1000
5	0.78	1.23	0.82	131.46	0.75	135.05	1000
6	2.25	3.30	2.31	219.58	1.24	228.68	1000
7	2.98	4.31	3.47	244.89	1.42	257.08	1000
8	4.27	6.54	4.69	305.32	1.74	322.56	1000
9	6.25	9.64	4.42	393.24	2.16	415.71	1000
10	7.41	11.35	4.54	449.49	2.48	475.27	1000
11	7.62	11.65	6.67	469.92	2.72	498.57	1000
12	7.04	10.69	12.03	468.00	2.76	500.51	1000
13	6.04	9.14	19.62	452.19	2.83	489.82	1000
14	5.34	8.39	24.87	447.74	2.80	489.14	1000
15	5.92	9.08	22.48	456.16	2.75	496.39	1000
16	7.04	10.72	14.39	471.95	2.74	506.85	1000
17	7.76	11.83	9.31	477.83	2.68	509.40	1000
18	7.67	11.63	8.45	451.85	2.49	482.09	1000
19	6.63	10.00	12.36	396.80	2.33	428.11	1000
20	4.87	7.30	18.38	328.25	1.94	360.75	1000
21	2.88	4.47	3.78	243.04	1.47	255.64	1000
22	1.79	2.61	3.05	177.13	1.16	185.74	1000
23	1.22	1.78	2.42	148.00	0.94	154.37	1000
24	0.45	0.71	1.27	86.97	0.54	89.94	1000
25	0.59	0.11	0.74	148.85	1.71	152.00	1000
26	0.59	0.11	0.74	121.73	1.31	124.49	1000
27	0.59	0.11	0.74	87.18	0.91	89.53	1000
28	0.59	0.11	0.74	59.56	0.58	61.58	1000

6. CRITICALITY EVALUATION

This chapter presents an evaluation that demonstrates that the FuelSolutions™ W74 canister meets the criticality safety requirements of 10CFR71¹ and is acceptable for use as an integral part of the FuelSolutions™ Transportation Package. The FuelSolutions™ W74 canister satisfies the criticality safety acceptance criteria stated in Chapter 6 of the FuelSolutions™ Transportation Cask SAR.²

The criticality safety evaluation for the FuelSolutions™ W74 canister presented in this chapter demonstrates the following:

- The effective neutron multiplication factor (k_{eff}), including all biases and uncertainties at a 95% confidence level, does not exceed 0.95 under all credible normal and accident conditions.
- No credible event or sequence of events could cause criticality in the FuelSolutions™ W74 canister, because the maximum allowable enrichment specified for the W74 bounds the maximum planar-averaged enrichment for all fuel assemblies in the Big Rock Point (BRP) spent fuel inventory.

In addition to presenting the evaluations necessary to demonstrate that the criticality safety criteria are satisfied, this chapter describes FuelSolutions™ W74 canister criticality control design features, specifies the limiting characteristics for fuel assembly acceptance, and documents the criticality analysis method verification. The general approach used to perform the criticality safety evaluation for the FuelSolutions™ W74 canister is described in Chapter 6 of the FuelSolutions™ Transportation Cask SAR.

¹ Title 10, U.S. Code of Federal Regulations, Part 71 (10CFR71), *Packaging and Transportation of Radioactive Material*, U.S. Nuclear Regulatory Commission, October 2004.

² WSNF-120, *FuelSolutions™ TS125 Transportation Cask Safety Analysis Report*, NRC Docket No. 71-9276, EnergySolutions Spent Fuel Division, Inc.

This page intentionally left blank.

6.1 Discussion and Results

Criticality control for the FuelSolutions™ W74 canister design is based on both favorable geometry and fixed borated neutron absorber materials (poison). The criticality safety evaluation credits only 75% of the manufacturer's minimum assured boron content and the continued efficacy of fixed neutron absorber materials is demonstrated.

As specified in Section 1.2.3 of this SAR, the criticality acceptance criteria are demonstrated to be satisfied for the range of BRP assembly classes without reliance on credit for fuel burnup or fuel-related burnable neutron absorbers. To qualify for transport in the FuelSolutions™ W74 canister, BRP fuel assemblies must meet the fuel acceptance criteria listed in Table 6.1-1. The maximum allowable assembly average enrichment is 4.1 weight percent (w/o) ^{235}U . The ^{235}U enrichment limit is derived from calculations that demonstrate the highest calculated k_{eff} , less than or equal to 0.95, that might occur under any design condition. This maximum allowable enrichment value applies for all intact UO_2 fueled BRP assemblies. The assembly average enrichment is defined as the average enrichment of the existing fuel rods in the assembly array. If this average enrichment varies with axial position, the highest value that occurs for any axial position is used.

Since the BRP fuel assemblies contain multiple pin enrichments, a maximum pin-weighted average enrichment is calculated considering all radial cross-sections along the axis of the assembly. The maximum pin-weighted enrichment is then compared to the enrichment limit specified in Table 6.1-1 to verify fuel acceptance. As shown in Figure 6.3-1, loading of up to 64 fuel assemblies is permitted in the FuelSolutions™ W74 basket guide tube locations.

The BRP criticality evaluation includes analyses for the Siemens 11x11 and General Electric/Siemens 9x9 fuel assembly designs. Based on case studies (see Section 6.4) involving all BRP fuel configurations, the Siemens 11x11 fuel assembly design is established to be the most reactive in the FuelSolutions™ W74 canister. Therefore, the Siemens 11x11 fuel assembly design is used to establish the maximum allowable ^{235}U enrichment for the transport of BRP fuel in the W74 canister.

The only difference between the three analyzed 11x11 BRP assembly configurations is the number of solid zircaloy pins in the fuel rod array (0, 1, or 4). The three analyzed 9x9 BRP assembly configurations are: a case with no water holes in the array, a case with one water hole in the array center, and a case with no water holes and a pellet diameter of 0.4715 inch (as opposed to 0.471 inch). The 9x9 and 11x11 assembly arrays are otherwise identical to each other.

The analyses show that all of the configurations meet the criticality requirements, and that replacing fuel rods with solid zircaloy rods always causes k_{eff} to decrease. For this reason, 11x11 assemblies with any number of solid zircaloy rods are qualified for loading in the W74 canister.

The analyses assume a uniform rod enrichment assembly array with fuel rods in all four corners. As discussed in Section 6.6.2, this assumption is bounding for assemblies with any number of fuel rods missing from the four array corner locations. Thus, the intact assembly analyses are applicable for assemblies with any number of array corner fuel rods. The number of non-corner

water holes specified in Table 6.1-1 is the maximum number of non-corner water holes that an assembly may have if it is to be classified as intact (vs. partial). This is discussed below.

Specific criticality analyses are performed for all existing intact and partial BRP mixed-oxide (MOX) assemblies. The MOX fuel criticality analyses described in Section 6.6.1 show that all existing BRP MOX fuel assemblies are significantly less reactive than the design basis 4.1 w/o enriched UO₂ assemblies. Thus, all existing BRP MOX fuel assemblies are qualified for loading into the W74 canister.

Section 6.6.2 determines a separate enrichment criterion for partial BRP assemblies that have fuel rods missing from the design basis assembly configuration. Since BRP assemblies are under-moderated, partial assemblies may be significantly more reactive than intact assemblies. The maximum allowable assembly average enrichment values for BRP partial assemblies are 3.55 w/o (GE 9x9) and 3.6 w/o (Siemens 11x11), versus the 4.1 w/o value established for all intact BRP assemblies. As discussed in Section 6.6.2, the lower enrichment limits only apply for BRP assemblies with fuel rods missing from locations other than the four corner locations of the rod array. Also, the 4.1 w/o enrichment limit still applies for 9x9 BRP assemblies that have up to one fuel rod missing from non-corner locations. Table 6.1-1 lists the partial assembly maximum allowable enrichment criteria for each of the BRP assembly designs. Table 6.1-1 specifies that the partial assembly enrichment limits apply for all assemblies that have more than the maximum allowable number of missing non-corner fuel rods (also specified in Table 6.1-1).

Criticality analyses for damaged BRP fuel assemblies are described in Section 6.6.3. These analyses model damaged fuel cans inside each of the eight W74 canister support tubes. The damaged fuel cans have stainless steel walls, each of which has an attached borated stainless steel poison sheet. Each damaged fuel can contains a damaged BRP fuel assembly. The analyses model optimum configurations of fissile material inside each damaged fuel can. The analyses establish a maximum allowable fuel material enrichment (for any given fuel pellet within the assembly) of 4.61 w/o for the W74 damaged fuel can contents. As discussed in Section 6.6.3, the analyses also qualify all combinations of enriched uranium and plutonium that exist for the fuel material in BRP MOX fuel assemblies. Thus, both damaged MOX and damaged UO₂ BRP assemblies are qualified for loading into the damaged fuel cans.

Since the damaged fuel analyses model (and establish) the most reactive possible configuration of fissile material within the damaged fuel cans, undamaged assemblies, including assemblies that do not meet the dimensional parameter specifications for BRP fuel, may be loaded into the W74 canister damaged fuel cans. The maximum fuel pellet enrichment value of 4.61 w/o applies for all such assemblies. Additionally any type of MOX assembly can be loaded into the damaged fuel can, as long as all MOX fuel material within the assembly corresponds to one of the four MOX fuel material descriptions given in the first four columns of Table 6.6-2. Such assemblies have to physically fit inside the damaged fuel can. They also have to meet the overall assembly weight and uranium loading specifications for BRP fuel in order to satisfy structural, thermal, and shielding requirements.

Table 6.1-1 - W74 Canister Fuel Specification for Big Rock Point

Fuel Assembly Array	GE 9x9	Siemens 9x9	Siemens 11x11	Siemens 11x11
Clad Material	Zr	Zr	Zr	Zr
Initial ²³⁵ U Enrichment ⁽¹⁾	≤ 4.10	≤ 4.10	≤ 4.10	≤ 4.10
Initial ²³⁵ U Enrichment for Partial BRP Assemblies ^{(1) (2)}	≤ 3.55	≤ 3.55	≤ 3.60	≤ 3.60
Pellet Stack UO ₂ Density ⁽³⁾	≤ 96.5%	≤ 96.5%	≤ 96.5%	≤ 96.5%
Number of Fuel Rods	≤ 81	≤ 81	≤ 121	≤ 121
Clad O.D. (in)	0.5625	0.5625	0.449	0.449
Clad Thickness (in)	0.040	0.040	0.034	0.034
Pellet Diameter (in)	0.471	0.4715	0.3715	0.3735
Fuel Rod Pitch (in)	0.707	0.707	0.577	0.577
Active Fuel Length (in)	≤ 70	≤ 70	≤ 70	≤ 70
Number of Array Corner Rods ⁽⁴⁾	0-4	0-4	0-4	0-4
Number of Non-Corner Water Holes ⁽⁵⁾	≤ 1	0	0	0
Number of Inert Rods ⁽⁶⁾	≥ 0	≥ 0	≥ 0	≥ 0
Bottom Tie Plate Height (in)	≥ 1.25	≥ 1.25	≥ 1.25	≥ 1.25

Notes:

- (1) To qualify BRP fuel assemblies that have multiple pin enrichments, a maximum pin-weighted average enrichment is calculated considering all radial cross-sections along the axis of the assembly. The maximum pin-weighted enrichment is compared to the specified enrichment limit to verify fuel acceptance. No individual pin enrichment shall exceed 4.61 w/o ²³⁵U.
- (2) Partial BRP assemblies are defined as assemblies that contain more non-corner water holes than the maximum amount listed in this table (3rd row from the bottom). The pin-weighted average enrichment is determined by averaging over the *remaining* rods in the array.
- (3) The density is expressed as a percentage of the theoretical UO₂ density of 10.97 g/cc.
- (4) All BRP assemblies can contain any number of fuel rods in the four array corner locations and still qualify for the 4.1% maximum allowable enrichment. The four corner locations may also contain any number of inert rods (as discussed below in Note 6) or any other object that meets the “water hole” definition given below in Note 5.
- (5) A water hole is defined as an empty array location, a partial length fuel rod, a hollow (water) rod, a smaller fuel rod, or any other object that displaces less water than a standard fuel rod. Such objects do not qualify as water holes if they are in any of the four corner locations of the fuel rod array.
- (6) Inert rods are defined as solid steel or zircaloy rods that have a diameter and length that are equal to or greater than those of a fuel rod.

This page intentionally left blank.

6.2 Package Fuel Loading

The criticality safety evaluation for the FuelSolutions™ W74 canister includes analysis of the BRP fuel assembly designs listed in Table 6.2-1. Based on the analysis for fuel assembly types described in Table 6.2-1, the Siemens 11x11 fuel assembly design is established to be the most reactive in the FuelSolutions™ W74 basket array, as described in Section 6.4. A maximum initial enrichment of 4.1 w/o ²³⁵U is established to satisfy the $k_{\text{eff}} \leq 0.95$ criticality acceptance criterion for a full loading of up to 64 BRP fuel assemblies.

The criticality analysis assumes that fuel pins in BRP fuel assemblies contain a uniform enrichment, even though all BRP fuel assembly designs incorporate multiple fuel pin enrichments. Section 6.4 shows that modeling the BRP fuel assembly configurations in this manner is conservative. The assembly configuration with a uniform enrichment has a higher relative neutron leakage, since the BRP fuel assembly designs with multiple fuel pin enrichments have lower enriched fuel pins on the periphery. The increased leakage results in an increase in fuel assembly interaction within the FuelSolutions™ W74 canister and a corresponding increase in system reactivity.

In the criticality analysis, the maximum enrichment listed in Table 6.1-1 is applied over the entire length of each fuel stack, and the fuel is assumed to be undamaged. No credits are taken for fuel pellet dishing, fuel burnup, or fuel-related burnable neutron absorbers. The maximum uranium loading is not used directly in the criticality analysis, which instead assumes BRP fuel assemblies have pellets with an average nominal density that is 96.5% of UO₂ theoretical density. The UO₂ density is bounding for all BRP fuel assemblies and is listed in Table 6.1-1 as one of the fuel acceptance criteria.

The BRP MOX fuel assemblies contain combinations of MOX fuel rods and UO₂ fuel rods with several different enrichment levels. The specific MOX fuel criticality analyses, described in Section 6.6.1, explicitly model the fuel material mixtures present in each of the fuel rods in the assembly. Thus, no assembly averaging of fuel rod enrichments is performed. No maximum allowable assembly average enrichment is determined by the MOX fuel analyses. Instead, it is explicitly shown that all existing BRP MOX fuel assemblies are qualified for loading into the W74 canister.

The maximum uranium loading is not used directly in any of the MOX fuel criticality analyses. Instead the pellet geometry and percent theoretical densities shown in Table 6.1-1 are used. No credits are taken for fuel burnup or fuel-related burnable neutron absorbers.

The partial assembly criticality analyses described in Section 6.6.2 assume assembly average enrichments. In the case of partial assemblies, the assembly average enrichment is defined as the average enrichment of the remaining fuel rods. The partial assembly criticality analyses establish a maximum allowable assembly average enrichment for any given axial section of the fuel assembly. The maximum allowable assembly average enrichments for partial BRP fuel assemblies are given in Sections 6.1 and 6.6.2.

The damaged assembly criticality analyses described in Section 6.6.3 model arrays of fissile material inside the damaged fuel cans, including pure UO₂ fuel material and several different MOX fuel material mixtures. In all cases, a uniform material composition is modeled over the

entire fissile material configuration. The damaged fuel analyses model either partial or intact BRP assembly configurations (at their corresponding maximum enrichments) inside the other (guide tube) fuel locations of the canister. These partial or intact assemblies have pure UO₂ fuel. The enrichment of the fissile material configuration inside the damaged fuel cans (for the UO₂ fuel case) is 4.61%, as discussed in Section 6.1. The MOX fuel compositions that are analyzed for the fissile material configuration are described in Section 6.6.3.

Table 6.2-1 - Specific Fuel Assembly Parameters

Parameter	GE 9x9	GE 9x9	Siemens 9x9	Siemens 11x11	Siemens 11x11	Siemens 11x11	Siemens 11x11
Number of Fuel Rods per Assembly	80	81	81	121	120	117	121
Assembly Pin Pitch (in.)	0.707	0.707	0.707	0.577	0.577	0.577	0.577
Fuel Rod Clad Outer Diameter (in)	0.5625	0.5625	0.5625	0.449	0.449	0.449	0.449
Fuel Rod Clad Inner Diameter (in)	0.4825	0.4825	0.4825	0.381	0.381	0.381	0.381
Fuel Pellet Outer Diameter (in)	0.471	0.471	0.4715	0.3715	0.3715	0.3715	0.3735
Fuel Pellet Density (% Theo. UO ₂)	96.5	96.5	96.5	96.5	96.5	96.5	96.5
Fuel Pellet Dishing Factor (%)	0	0	0	0	0	0	0
Number of Inert (Zr) Rods / Assembly	0	0	0	0	1	4	0
Solid Zr Rod Outer Diameter (in)	N/A	N/A	N/A	N/A	0.449	0.449	N/A
Number of Water Holes / Assembly	1	0	0	0	0	0	0
Active Fuel Length (in)	70	70	70	70	70	70	70
Bottom Tie Plate Height (in)	1.25	1.25	1.25	1.25	1.25	1.25	1.25

This page intentionally left blank.

6.3 Model Specification

6.3.1 Description of Calculational Model

The analytical models used in the criticality analysis include cases for normal and hypothetical accident conditions applicable to the FuelSolutions™ Transportation Cask. The FuelSolutions™ W74 canister includes a stackable upper and lower basket assembly and a shell assembly, as described in Section 1.2.1 of this SAR. Drawings for the FuelSolutions™ W74 canister are provided in Section 1.3.1 of this SAR. Separate overpack casks are used for on-site transfer, dry storage, and off-site transportation, as described in Chapter 1 of the FuelSolutions™ Storage System FSAR³ and FuelSolutions™ TS125 Transportation Cask SAR.

The FuelSolutions™ W74 canister basket consists of an array of guide tube assemblies, support tubes, and spacer plates arranged in a manner to provide structural integrity and to prevent criticality of the stored fuel assemblies. The FuelSolutions™ W74 basket cross-section is depicted in Figure 6.3-1 with nominal dimensions provided. Figure 6.3-1 is a top view of the basket that is sliced horizontally through an axial point that passes through one of the spacer plates. The spacer plates provide a minimum separation between the guide tube assemblies. There are two types of guide tube assemblies used in the FuelSolutions™ W74 basket. Figure 6.3-2 shows the Type A guide tube assembly, which has two borated stainless steel panels, located on two opposing sides of the guide tube. Figure 6.3-3 shows the Type B guide tube assembly, which has only one borated stainless steel panel located on one side of the guide tube. In Figure 6.3-1, the borated stainless steel panel orientations within the FuelSolutions™ W74 basket are denoted by arrows except for the center non-fuel positions, which are modeled as water holes.

As discussed in Section 6.3.1.3, there are differences between the primary (intact fuel) criticality analysis model (illustrated in Figure 6.3-1) and the actual W74 canister geometry. These differences include poison sheet boron concentration, number of poison sheets, support tube location, and support tube wall thickness. With respect to all of these canister geometry differences, the configuration modeled in the criticality analyses is conservative (i.e., more reactive) than the actual W74 canister configuration.

The geometric arrangement of the guide tube assemblies within the FuelSolutions™ W74 basket is shown in Figure 6.3-1. In basket regions between the guide tubes, a water gap is formed. The water gap is bounded in the axial direction by spacer plates, on one side by a borated stainless steel poison sheet, and on the other side by the outer wall of the adjacent guide tube.

The FuelSolutions™ W74 canister criticality calculations show that moving the spacer plates closer together axially, or increasing the spacer plate thickness in the FuelSolutions™ W74 basket leads to a decrease in system reactivity. Since there is no borated stainless steel sheet on one side of the water gap in the FuelSolutions™ W74 basket, the replacement of water in that region with spacer plate material reduces reactivity. The relatively high thermal neutron flux in

³ WSNF-220, *FuelSolutions™ Storage System Final Safety Analysis Report (FSAR)*, Docket No. 72-1026, BNG Fuel Solutions Corporation.

the FuelSolutions™ W74 water gap results in a higher probability of resonance absorption by the iron and manganese present in the spacer plates, providing a negative reactivity impact.

Both FuelSolutions™ W74M and W74T canister basket and shell assembly types are considered in the criticality analysis. The two designs differ with respect to the materials used for the alignment bars, vent/drain port covers, outer closure plates, inner closure plates, canister shells, and engagement spacer plates. In the W74M, SS-316 is used for these components, while in the W74T, the material is SS-304. In addition to the material differences in the FuelSolutions™ W74M and W74T, the number, separation distances, and thickness of the spacer plates in each canister basket are also different. The spacer plate thickness and axial location have a significant influence on the reactivity of the basket since they affect the neutron physics in the water gaps between adjacent guide tubes. The effects of the material and spacer plate differences between the two FuelSolutions™ W74 versions on criticality control effectiveness are evaluated in Section 6.3. Based on the evaluation in Section 6.3, the FuelSolutions™ W74T configuration is modeled in subsequent design basis criticality calculations.

The criticality analyses are based on cask models that include an infinite array of FuelSolutions™ W74T basket and shell assemblies inside a representative transportation cask configuration. The FuelSolutions™ W74 canister shell assembly and representative transportation cask body cross-section is shown in Figure 6.3-4. This representative transportation cask configuration is different from the actual FuelSolutions™ TS125 Transportation Cask geometry, which is shown in Figure 6.3-5. However, the canister overpack (i.e., transportation cask) configuration has little effect on the reactivity of the package, due to the large water reflection region around the edge of the canister interior. There is relatively little reflection of neutrons back into the canister from the cask materials, and little neutronic interaction between the canisters in the infinite cask array. Calculations presented in Section 6.6.4 show that there is no statistically significant difference in reactivity (k_{eff}) between W74 canisters inside the analyzed configuration (shown in Figure 6.3-4), and W74 canisters inside the actual FuelSolutions™ TS125 Transportation Cask (shown in Figure 6.3-5). Therefore, the results of the W74 canister criticality analyses, which are based on the Figure 6.3-4 transportation cask configuration, are applicable for W74 canisters inside the FuelSolutions™ TS125 Transportation Cask.

Criticality of fuel assemblies in the FuelSolutions™ W74 canister is prevented by the mechanical design of the canister. Neutronic interaction between fuel assemblies is limited by favorable geometry (fixing the minimum separation between fuel assemblies) and the use of borated neutron absorber panels. The design basis for criticality prevention is to demonstrate that the effective neutron multiplication factor of the fuel assemblies within the FuelSolutions™ canister is less than the Upper Subcritical Limit (USL)⁴ established using the analysis methodology presented in NUREG/CR-5661⁵ and a diverse set of critical experiments (see Section 6.5).

⁴ Lichtenwalter, J. J., et al., *Criticality Benchmark Guide for Light-Water-Reactor Fuel in Transportation and Storage Packages*, ORNL/TM-13211 NUREG/CR-6361, March 1997.

⁵ Dyer, H. R., and Parks, C. V., *Recommendations for Preparing the Criticality Safety Evaluation of Transportation Packages*, NUREG/CR-5661, Oak Ridge National Laboratory, Oak Ridge, Tennessee, April 1997.

Both normal conditions of transport (NCT) and hypothetical accident conditions (HAC) are considered in the criticality analysis for the FuelSolutions™ W74 canister. The normal condition for the FuelSolutions™ W74 canister conservatively includes: complete flooding with water at a density that results in optimum moderation, worst-case asymmetric assembly placement within the guide tubes, and application of worst-case material and fabrication tolerances. The HAC for the FuelSolutions™ W74 canister includes all the normal conditions, plus a bounding 0.08-inch permanent deformation of the guide tubes resulting from a hypothetical cask drop accident, axial detachment of the guide tubes from the basket structure, and removal of the transportation cask neutron shield assembly. The deformation and detachment of the guide tubes and the loss of the transportation cask neutron shield are consistent with the physical conditions of the package after being subjected to the worst-case HAC defined in 10CFR71.¹

The structural calculations show that, as a result of the nine-meter drop specified in 10CFR71, the only significant permanent changes (relative to criticality) to the W74 canister and cask geometry are the deformation of the basket assembly guide tubes and their detachment from the basket internals. In the FuelSolutions™ W74 models, a 0.08-inch deformation is assumed to occur throughout the entire length of the basket guide tubes, reducing the center-to-center spacing between assemblies. The 0.08-inch maximum deformation is based on a uniform axial assembly loading of the guide tubes. A localized loading of the guide tube from the fuel assembly grid spacers results in an increase in the maximum localized guide tube deformation to ~0.125 inch. However, this deformation occurs only in every third span between spacer plates, and the maximum deformation in other spans is negligible. In Section 6.4, modeling the deformation at 0.08 inch over the entire length of the guide tube is demonstrated to be more conservative than modeling a 0.125-inch maximum deflection within axial spans that contain fuel assembly mid-grids.

The MCNP 4a code package⁶ is used for the criticality analysis of the FuelSolutions™ W74 canister to demonstrate that the transportation of the fuel assembly types identified in Table 6.2-1 satisfies the USL acceptance criterion. MCNP models are developed for the FuelSolutions™ W74 canister under NCT and HAC. The FuelSolutions™ W74 canister analytical models used include single-package models and a worst-case multiple-package array model. The worst-case multiple-package array model is conservatively used to establish the maximum acceptable enrichment and the corresponding design basis k_{eff} value for each fuel assembly design described in Table 6.2-1.

The following assumptions are used to develop the analytical models for the criticality safety evaluation of the FuelSolutions™ W74 canister:

- FuelSolutions™ W74 canister models are analyzed for the BRP fuel types identified in Table 6.2-1 in the unchanneled configuration. All fuel assemblies modeled contain UO_2 with a uniform pin enrichment of 4.1 w/o ^{235}U . The enrichments are applied over the entire length of each fuel stack, and the fuel is assumed to be undamaged.

⁶ Briesmeister, J., *MCNP-4A General Monte Carlo Code N-Particle Transport Code*, Version 4A, LA-12625-M, November 1993.

- The fuel pellets are conservatively modeled assuming a 96.5% theoretical density of UO₂ and no dishing fraction. This assumption is conservative since actual pellets are chamfered and manufactured to a UO₂ theoretical density of 95% or less.
- Unirradiated fuel conditions are assumed (fresh fuel isotopic concentrations). No credit is taken for any ²³⁴U or ²³⁶U in the fuel, nor is any credit taken for the buildup of fission product poison material.
- No credit is taken for any spacer grids, spacer sleeves, or top and bottom tie plates. In addition, the top and bottom tie plates displace moderator from an array and are manufactured from stainless steel 304, which removes neutrons by radiative capture.
- No credit is taken for any burnable absorber in the fuel rods.
- Fully flooded conditions are assumed, including water present in the fuel rod-cladding gap. The fully flooded conditions are the most conservative since the FuelSolutions™ W74 canister is an under-moderated system. The moderator is assumed to be pure water at a density of 1.0 g/cm³, which is shown to produce the most reactive conditions (see the Section 6.4.2 case studies for further discussion).
- In the intact and partial analyses, a nominal loading of 1.0 w/o of natural boron is used as the analysis basis for the borated stainless steel, versus the manufacturer's minimum specified boron concentration of 1.25 w/o that is verified during material manufacture. This loading corresponds to a minimum ¹⁰B areal density of 3.1 mg/cm², including consideration of thickness, density, and poison content. Credit is taken for only 75% of the assumed 1.0 w/o boron in borated stainless steel.
- Worst-case material and fabrication tolerance dimensions are applied to the nominal dimensions for the FuelSolutions™ W74 canister model. The tolerances are summarized in Table 6.3-1.
- A full 64-assembly loading configuration for the FuelSolutions™ W74 canister is analyzed. As shown in Figure 6.3-1, the design basis loading configuration requires the 5 central guide tube positions of both the upper and lower baskets to remain empty. These locations are modeled as water-filled holes, and no assemblies or other materials are assumed to be loaded into these locations. The W74 canister configuration employs a mechanical block-out structure over the openings of the five central guide tube positions to prevent the inadvertent loading of fuel assemblies into these locations.
- The radial boundary is defined as either the intact cask body (NCT) or the cask body with the neutron shield assembly removed (HAC). The single-package model is surrounded by twelve inches of water for reflection. The multiple-package array model consists of an infinite number of FuelSolutions™ W74 canisters in a closely packed arrangement (triangular pitch array), with the adjacent casks in contact with one another.
- The FuelSolutions™ W74 canister is modeled axially from the middle of the bottom end shield plug to a point just below the top shield plug assembly. Reflected planes are conservatively inserted at these points to prohibit neutron leakage thus maximizing k_{eff}.
- The engagement spacer plate is modeled using SS-304. The actual material specified for the engagement spacer plate is XM-19. The substitution of SS-304 for XM-19 as the

engagement spacer plate material is suitable since SS-304 and XM-19 interact similarly with neutrons.

- Fuel assembly positions within guide tubes are assumed to be shifted radially in such a manner as to maximize system reactivity. The worst-case fuel position configuration is demonstrated by analysis (see the Section 6.4 case studies for further discussion).
- Both NCT and HAC for transportation are evaluated. The NCT models of the FuelSolutions™ W74 canister system include consideration of: (1) complete flooding with water at a density sufficient for optimum moderation, (2) worst-case asymmetric assembly placement within the guide tubes, and (3) application of worst-case material and fabrication tolerances. The HAC models for the FuelSolutions™ W74 canister system include all the normal conditions, as well as the addition of a 0.08-inch permanent deformation of the guide tubes between spacer plates and the axial detachment of the guide tubes from the basket structure. The loss of the transportation cask neutron shield structure is also assumed. The 0.08-inch guide tube deformation, which occurs as a result of a cask side drop, is the only significant change in the basket structure that occurs for any hypothetical transportation accident events or event sequences.

6.3.1.1 Hypothetical Accident Conditions

The HAC modeled for the FuelSolutions™ W74 canister system includes the following worst-case assumptions:

- Complete flooding with water at a density that produces optimum moderation.
- Worst-case asymmetric fuel assembly placement within the guide tubes.
- Application of worst-case material and fabrication tolerances.
- Consideration of a bounding 0.08-inch permanent deformation of guide tubes between spacer plates and the axial detachment of the guide tubes from the basket structure.
- Loss of the transportation cask body neutron shield.

The deformation and detachment of the guide tubes and the removal of the outer cask neutron shield are consistent with the physical condition of the FuelSolutions™ W74 canister after being subjected to the HAC specified in 10CFR71.

The HAC model is an accurate representation of the FuelSolutions™W74 lower and upper baskets. The canister is modeled axially from the middle of the bottom end shield plug to a point just below the top shield plug assembly. Reflected planes are inserted at these points preventing axial leakage of neutrons from the canister. Figure 6.3-6 shows a horizontal cross-section of MCNP model. Figure 6.3-7, Figure 6.3-8, and Figure 6.3-9 show vertical cross-section views of the accident condition model that has been sliced with vertical planes to expose the lower, middle, and upper portions of the canister. As shown in Figure 6.3-7, the lower portion of the model begins at the middle of the bottom end shield plug. Next, the bottom closure plate is modeled followed by the water gap between the bottom closure plate and the bottom of the fuel stack.

The bottom of the fuel in the lower basket begins at an elevation of 1.895 inches above the bottom closure plate. The bottom of the lower basket guide tubes and the borated stainless steel

poison sheets are conservatively positioned at an elevation of 2.5 inches above the bottom closure plate. The position of the bottom of the borated stainless steel panels relative to the bottom of the fuel leaves about 0.61 inch of fuel in a non-poisoned region of the lower basket, which maximizes system reactivity. The lower basket guide tubes are modeled axially to the top of the borated stainless steel sheets, as shown in Figure 6.3-8. Water is placed between the top of the lower basket guide tubes and the bottom of the engagement spacer plate, which separates the lower and upper baskets in the FuelSolutions™ W74 canister. The axial placement of the guide tubes within the basket is consistent with the damage expected to occur from a nine-meter drop in a representative transportation cask (as specified for the hypothetical accident in 10CFR71.

The axial placement of the guide tubes within the upper basket is also consistent with the damage incurred from a nine-meter drop specified for the hypothetical accident in 10CFR71. The bottoms of the upper basket guide tubes and the borated stainless steel poison sheets are positioned at an elevation of 3.525 inches above the top of the engagement spacer plate, as shown in Figure 6.3-8.

The position for the bottom of the fuel stack in the upper basket is 1.895 inches above the top of the engagement spacer plate. The position of the bottom of the borated stainless steel sheets relative to the bottom of the fuel leaves about 1.63 inches of fuel in a non-poisoned region of the upper basket, which maximizes system reactivity. The upper basket guide tubes are modeled axially to the top of the borated stainless steel sheets, as shown in Figure 6.3-9. The top of the guide tubes in the upper basket extends through the top spacer plate. Water is placed between the top of the upper basket guide tubes and the bottom of the top shield plug assembly.

As a result of a nine-meter drop, the guide tubes separate from the basket internals and are free to move in the axial plane within the boundaries of the spacer plate holes. To maximize the effect of the guide tube relocation on system reactivity, the tops of the lower basket guide tubes are modeled resting against the bottom of the engagement spacer plate, and the tops of the upper basket guide tubes are modeled resting against the bottom of the top shield plug assembly. This results in a vertical guide tube shift of approximately 0.5 inch for the lower basket and 1.4 inches for the upper basket. The guide tube shift is maximized in the upper basket since it results in more fuel exposure in the middle of the canister. If the shift has been maximized in the lower basket, the fuel exposure results in a high probability for the loss of neutrons from the system by leakage.

To further maximize reactivity by exposing more fuel below the borated stainless steel sheets, the flared ends at the top of the guide tubes are also assumed to flatten during the accident resulting in an additional upward shift of 0.5 inch. Figure 6.3-9 shows the position of the top of the borated stainless steel sheets when the tops of the upper basket guide tubes rest against the top shield plug assembly. The final positions for the bottom of the borated stainless steel sheets after the accident is 2.5 inches above the bottom closure plate for the lower basket guide tubes and 3.525 inches above the engagement spacer plate for the upper basket guide tubes.

The active fuel stack for all BRP fuel is conservatively modeled beginning at a height of 1.895 inches and ending at a height of 71.895 inches. This represents an active fuel length of 70 inches, which is equivalent to the active fuel length of the fuel assembly types considered for transport in the FuelSolutions™ W74 canister. The position of the fuel stack bottom assumes a bottom tie plate height of 1.25 inches and a bottom end plug height of 0.645 inch. The fuel stack in the lower basket could have been shifted upward to decrease the distance between the fuel in

the upper and lower baskets of the FuelSolutions™ W74 canister; however, the length of the top tie plate and the plenum region of the fuel results in more than 12 inches of separation between the two systems. Therefore, the decision is made to maximize the amount of fuel exposed below the borated stainless steel in both the upper and lower baskets.

The nominal dimensions for the guide tubes, neutron absorber panels, spacer plates, spacer plate openings, support tubes, and support sleeves as well as material and fabrication tolerances are summarized in Table 6.3-1. The factors that primarily affect the reactivity of the FuelSolutions™ system are radiative neutron absorption and fuel assembly separation. Two parameters that affect radiative neutron absorption are the neutron absorber panel thickness and the spacer plate thickness. The parameters that affect fuel assembly separation include fuel assembly position, spacer plate opening size and location, guide tube wall thickness, guide tube inside width, and neutron absorber panel thickness. Tolerances are applied to the FuelSolutions™ W74 canister components in such a manner to maximize system reactivity as follows:

- The radiative neutron absorption within the FuelSolutions™ W74 canister system is influenced by the thickness of both the neutron absorber panel and the spacer plates. The application of the material and fabrication tolerances that decrease the neutron absorber and spacer plate thickness result in a decrease in the radiative neutron absorption of the system. The decrease in the radiative neutron absorption within the system results in an increase in the neutrons available for fission that correspondingly increases system reactivity.
- As fuel assemblies are brought closer together in the FuelSolutions™ W74 canister, the neutron interaction between assemblies increases, resulting in a higher system reactivity. In conjunction with assuming worst-case asymmetric assembly placement within the guide tubes, fuel assembly interaction is maximized in the FuelSolutions™ W74 canister models by shifting guide tube assemblies within the spacer plate openings and applying worst-case component material and fabrication tolerances. Three separate fuel/guide tube assembly shift configurations are analyzed to determine a worst-case configuration for use in the FuelSolutions™ W74 canister model. The three configurations considered are shown in Figure 6.3-10 through Figure 6.3-12. The worst-case configuration determined through analysis is the configuration depicted by Figure 6.3-12 (see the Section 6.3 case studies for further discussion). As shown in Figure 6.3-12, the fuel assemblies are moved into the corner of each guide tube as indicated, and the guide tubes are correspondingly relocated within the spacer plate opening in the same direction. The tolerances that further minimize separation of the fuel assemblies are then applied as follows: (1) the spacer plate opening size is increased, (2) the spacer plate opening locations are moved within allowed fabrication tolerances in the indicated directions, (3) the thickness of the neutron absorber panel is decreased, (4) the thickness of the guide tube wall is decreased, and (5) the inside width of the guide tube is increased.
- Another adjustment is made to the guide tube walls to incorporate the bounding 0.08-inch permanent deformation that occurs for the basket *g*-loads expected under a hypothetical nine-meter transportation cask drop. These assumed *g*-loads are bounding for all transportation conditions and drop events. The lower face on each guide tube wall is deflected downward along the full length of the guide tube. This is a conservative representation of the permanent guide tube deformation, since the actual deformation

does not occur over the full length of the guide tube (i.e., deformation is limited to regions between basket spacer plates). The effect of the guide tube deflection in the HAC model is to further decrease the center-to-center spacing of the fuel assemblies in the FuelSolutions™ W74 model. An illustration of the damaged fuel cell geometry is provided in Figure 6.3-13. The figure illustrates how the bottom edges of the guide tubes have moved downward in relation to a given assumed cask drop direction. As shown in Figure 6.3-13, this downward movement allows the fuel assemblies in the upper half of the basket (the top three assembly rows) to move closer to the assemblies in the bottom three rows and the middle row of the basket. The assemblies in the bottom three rows of the basket are conservatively pushed up against the top (non-deformed) guide tube edge, while the assemblies in the middle row are vertically centered within their guide tubes.

The neutron shield assembly for the canister overpack (i.e., the solid neutron shielding material, support ribs, and outer jacket), shown in Figure 6.3-4, is expected to experience damage during a hypothetical nine-meter cask drop. For this reason, it is completely removed in the HAC model.

6.3.1.2 Normal Conditions of Transport

The HAC model for the FuelSolutions™ W74 canister includes the following: complete flooding with water with a density that results in optimum moderation, worst-case asymmetric assembly placement within the guide tubes, and application of worst-case material and fabrication tolerances.

The HAC model is an accurate representation of the FuelSolutions™W74 lower and upper baskets. The canister is modeled axially from the middle of the bottom end shield plug to a point just below the top shield plug assembly. Reflected planes are inserted at these points preventing axial leakage of neutrons from the canister. Figure 6.3-14, Figure 6.3-15, and Figure 6.3-16 show side views of the FuelSolutions™ W74 normal operating conditions model that has been sliced with vertical planes to expose the lower, middle, and upper portions of the canister.

As shown in Figure 6.3-14, the lower portion of the model begins at the middle of the bottom end shield plug. Next, the bottom closure plate is modeled followed by the water gap between the bottom closure plate and the bottom of the active fuel. The bottom of the active fuel is modeled just below the bottom spacer plate at an elevation of 1.895 inches above the bottom spacer plate. The bottom of the borated stainless steel panel is conservatively located at an elevation of 1.5 inches above the bottom closure plate. The actual elevation of the borated stainless steel panel bottom is only 0.375 inch off the bottom closure plate. The bottoms of the lower basket guide tubes are modeled at a height of 1.5 inches above the bottom closure plate, which is a conservative placement since the guide tube faces with borated stainless steel sheets attached begin at the surface of the bottom closure plate. The lower basket guide tubes are modeled axially to the top of the borated stainless steel panels as shown in Figure 6.3-15. Water is placed between the tops of the lower basket guide tubes and the bottom of the engagement spacer plate, which separates the lower and upper baskets in the FuelSolutions™ W74 canister.

The bottom of the active fuel in the upper basket is located at an elevation of 1.895 inches above the top of the engagement spacer plate. The bottoms of the upper basket guide tubes and the borated stainless steel panels are both conservatively positioned at an elevation of 1.5 inches above the top of the engagement spacer plate. The upper basket guide tubes are modeled axially

to the top of the borated stainless steel panels, as shown in Figure 6.3-16. Water completely fills the region between the tops of the upper basket guide tubes and the bottom of the top shield plug assembly, with the exception of the volume containing the top spacer plate.

The active fuel stack for all BRP fuel is modeled beginning at a height of 1.895 inches and ending at a height of 71.895 inches. This represents an active fuel length of 70 inches, which is equivalent to the actual active fuel length of the fuel assembly types considered for transport in the FuelSolutions™ W74 canister. The position of the fuel stack bottom assumes a bottom tie plate height of 1.25 inches and a bottom end plug height of 0.645 inch.

The nominal dimensions for the guide tubes, neutron absorption panels, spacer plates, spacer plate openings, support tubes, and support sleeves are shown in Figure 6.3-1 through Figure 6.3-3, and on the drawings provided in Section 1.5.3 of this SAR. Material and fabrication tolerances are specifically evaluated for effects on system reactivity in case studies presented in Section 6.3. Worst-case material and fabrication tolerances are summarized in Table 6.3-1. The factors that primarily affect the reactivity of the FuelSolutions™ W74 canister system are radiative neutron absorption and fuel assembly separation. Two parameters that affect radiative neutron absorption are the neutron absorber panel thickness and the spacer plate thickness. The parameters that affect fuel assembly separation include fuel assembly position, spacer plate opening size and location, guide tube wall thickness, guide tube inside width, and neutron absorber panel thickness. With the exception of the accident-induced guide tube deformation and axial detachment, fuel assemblies are positioned and tolerances are applied in the NCT model consistent with the description provided in Section 6.3.1.1 for accident conditions.

6.3.1.3 Criticality Models for MOX, Partial, and Damaged BRP Fuel

The primary model geometry differences between the MOX, partial, and damaged BRP assembly criticality analyses, and the intact BRP assembly criticality analyses described earlier in this section, pertain to the fuel assemblies (i.e., there are few differences in the cask or canister model geometry). The modeled MOX, partial, and damaged BRP assembly configurations are described in Sections 6.6.1, 6.6.2, and 6.6.3, respectively.

There are, however, some minor differences in the W74 basket geometry modeled in the intact, MOX, partial, and damaged BRP assembly criticality analyses. These minor differences in modeled basket geometry are due to recent revisions in the actual basket geometry that were made after some of the criticality analyses had already been performed. The original W74 basket geometry is illustrated in Figure 6.3-1. The actual (current) W74 basket configuration is illustrated in Figure 6.3-17.

The actual (current) W74 basket geometry differs from the original W74 basket geometry as follows:

- Whereas the original W74 basket geometry has a support tube centerline distance (from the basket center) of 44.45 cm (17.5 inches), the actual basket geometry has a centerline distance of 44.831 cm (17.65 inches).
- Whereas the original W74 basket geometry has a support tube wall thickness of 0.625 inch, the actual basket geometry has a wall thickness of 0.75 inch.

- Whereas the original W74 basket geometry contains borated stainless steel poison sheets with a boron concentration of only 1.0 w/o, the actual basket geometry uses poison sheets with a boron concentration of 1.25 w/o.
- The actual (revised) W74 basket geometry contains four additional poison sheets that were not present in the original design. These four poison sheets are mounted on the four guide tube walls that face the upper or lower walls of the (larger) support tubes. As shown in Figure 6.3-1, the original basket has no poison sheets attached to the adjacent guide tube walls directly below the upper two support tubes and directly above the lower two support tubes (the adjacent guide tubes have single arrows pointing away from the support tubes). Thus, these adjacent guide tubes are shown as being Type B guide tubes, when they are actually Type A guide tubes. The actual W74 basket geometry (shown in Figure 6.3-17) has Type A guide tubes (with poison sheets facing the support tube walls) in these four locations.

The partial assembly criticality analyses model the original basket configuration (shown in Figure 6.3-1), whereas the MOX and damaged assembly criticality analyses model the current basket configuration (Figure 6.3-17). The current revision of the intact assembly criticality analyses models some, but not all, of the recent W74 basket changes. The intact analyses model the increased support tube centerline distance of 44.831 cm, and the increased support tube thickness of 0.75 inch, but they do not model the four additional poison sheets, or the increase in the poison sheet boron concentration (i.e., the 1.0 w/o concentration is modeled). The modeling of the four basket features that differ between the analyses are summarized in Table 6.3-2.

It should be noted that the poison sheet boron concentrations referred to in Figure 6.3-1 and Figure 6.3-17, and in Table 6.3-2, correspond to the actual boron concentrations in the poison sheet. These concentrations are then reduced by a factor of 0.75 in the criticality analyses, in accordance with the analysis methodology recommended in NUREG-1536.⁷ Thus, the intact and partial assembly criticality analyses actually model a boron concentration of 0.75%, and the MOX and damaged assembly analyses actually model a boron concentration of 0.9375%.

All of the criticality analyses are based on either accurate or conservative values for the four revised basket geometry features shown in Table 6.3-2. Reducing the support tube wall thickness, moving the support tube in toward the basket center, reducing the poison sheet boron concentration, and neglecting the presence of four poison sheets all cause reactivity (k_{eff}) to increase. For this reason, the partial and intact assembly analyses are based on a conservative (i.e., more reactive) basket geometry model, whereas the MOX and damaged assembly analyses are based on an accurate basket geometry model.

The damaged assembly criticality analyses have one additional W74 basket model geometry difference (in addition to the differences in the modeled assembly geometries). The damaged fuel can is also modeled inside each of the eight support tubes of the W74 canister. The damaged fuel can geometry is shown in Figure 6.3-18. The damaged fuel can is identical to a W74 canister guide tube, with four 0.09-inch-thick stainless steel walls, and an inner cavity width of 6.9 inches. A 0.075-inch thick borated stainless steel poison sheet is attached to each of the four walls of the damaged fuel can. The poison sheets contain 1.25 w/o boron. These poison sheets

⁷ NUREG-1536, *Standard Review Plan for Dry Storage Cask Systems*, U.S. Nuclear Regulatory Commission, January 1997.

have the same dimensions and material composition (i.e., boron concentration) as the poison sheets attached to the other guide tubes in the W74 basket. The cross-sectional damaged fuel can geometry shown in Figure 6.3-18 is modeled over the entire axial length of the support tube.

The damaged BRP assembly analyses model several fissile material configurations inside the damaged fuel can interior. The analyses establish the most reactive possible fissile material configuration. These fissile material configurations are described in more detail in Section 6.6.3. In the other fuel locations of the canister, the analyses model either the optimum partial assembly configuration (described in Section 6.6.1), or an intact 11x11 BRP assembly configuration.

6.3.2 Package Regional Densities

The number densities used to model moderator materials and the FuelSolutions™ W74 canister basket, shell, and reflector materials are presented in Table 6.3-3 through Table 6.3-13. These material properties are used in all FuelSolutions™ W74 canister single-package and multiple-package array models.

The FuelSolutions™ W74 canister basket incorporates panels of borated stainless steel neutron-absorbing material. The borated stainless steel alloy incorporates a minimum of 1.25 w/o natural boron. As discussed in Section 6.3.1.3, the intact and partial BRP assembly criticality analyses conservatively model a boron concentration of only 1.0 w/o, whereas the MOX and damaged BRP assembly analyses model the actual value of 1.25 w/o. Therefore, material descriptions for both 1.0 w/o and 1.25 w/o borated stainless steel are presented in Table 6.3-7 and Table 6.3-8, respectively.

Stainless steel alloys are ideally suited for use in fuel pools containing demineralized or borated water, and for long-term dry storage and transportation cask radiation and thermal environments. Product literature for this type of material is provided in Section 1.5.2 of this SAR.

The borated stainless steel is manufactured and verified under the control and surveillance of the QA program described in Chapter 13 of the FuelSolutions™ TS125 Transportation Cask SAR.

Homogeneous dispersion of boron throughout the borated stainless steel alloy is demonstrated by the process controls under which the material is manufactured and verified. Several sheet samples from each heat of material are tested by wet chemical analysis and/or neutron attenuation testing to verify B-10 areal density. For the borated stainless steel sheets used in the W74 canister, a minimum B-10 areal density of 3.1 mg/cm² shall be verified. Neutron attenuation testing will account for any reduction in neutron attenuation due to heterogeneous dispersion of boron with the sheet. The material composition assumed in the criticality analyses (Table 6.3-7 and Table 6.3-8) is based on a 25% reduction in the minimum B-10 areal density that is verified by the testing program. This reduction is sufficient to account for the effects of heterogeneous dispersion of boron in borated stainless sheets. Borated stainless steel sheets, which are actually boron alloys of stainless steel, have a much more homogenous distribution of boron (i.e., smaller grain size) than mixed particulate poison sheets such as BORAL®.

The effects of long-term exposure to neutron flux from irradiated fuel is negligible because the thermal neutron flux during dry storage and/or transportation is low. This fact, coupled with the use of the minimum boron concentration specified by the material manufacturer (rather than the

nominal) and further reducing the concentration by 25%, more than accounts for any boron depletion that may occur over the 100-year design life of the FuelSolutions™ W74 canister.

**Table 6.3-1 - Worst-Case Material and Fabrication Tolerances
 for the FuelSolutions™ W74 Canister**

Parameter	Nominal (inches)	Tolerance (inches)
Borated Stainless Steel Thickness	0.0751	- 0.007
Borated Stainless Steel Width	6.40	- 0.05
Spacer Plate Thickness	0.75	- 0.03
Spacer Plate Opening Width	7.40 x 7.25	+ 0.015
Spacer Plate Opening Location ⁽¹⁾	varies	± 0.015
Guide Tube Thickness	0.090	- 0.008
Guide Tube Inner Dimension	6.90	+ 0.05
Support Tube Thickness (in)	0.75	- 0.055
Support Tube Inner Dimension	7.4	+ 0.05

Note:

- ⁽¹⁾ The arrows in Figure 6.3-10 through Figure 6.3-12 indicate the direction of application for the spacer plate opening location tolerance.

Table 6.3-2 - W74 Basket Model Differences Between Intact, Partial, MOX, and Damaged BRP Assembly Criticality Analyses

W74 Basket Feature	Intact Assembly Analyses	Partial Assembly Analyses	MOX Assembly Analyses	Damaged Assembly Analyses
Poison Sheet Boron Concentration (w/o)	1.0 ⁽¹⁾	1.0 ⁽¹⁾	1.25 ⁽²⁾	1.25 ⁽²⁾
Poison Sheets Adjacent to Support Tubes?	No ⁽¹⁾	No ⁽¹⁾	Yes ⁽²⁾	Yes ⁽²⁾
Support Tube Center Location (cm) ⁽³⁾	44.831 ⁽²⁾	44.45 ⁽¹⁾	44.831 ⁽²⁾	44.831 ⁽²⁾
Support Tube Wall Thickness (inch)	0.75 ⁽²⁾	0.625 ⁽¹⁾	0.75 ⁽²⁾	0.75 ⁽²⁾
Basket Geometry Model Illustration	Figure 6.3-1 ⁽⁴⁾	Figure 6.3-1	Figure 6.3-17	Figure 6.3-17

Notes:

- (1) Conservative value. Yields higher reactivity than actual basket design value.
- (2) Actual W74 basket design value.
- (3) Defined as the distance, in both the X and Y directions, between the support tube centerline and the basket centerline.
- (4) With the exception of the 44.45 cm dimension shown in Figure 6.3-1. For the intact analyses, a value of 44.831 cm applies.

Table 6.3-3 - UO₂ Number Densities as a Function of Enrichment

²³⁵ U Enrichment (w/o)	Number Density (atoms/b-cm)				UO ₂ Material Density (atoms/b-cm)
	UO ₂	²³⁵ U	²³⁸ U	O	
4.0	0.0235956	0.0009554	0.0226402	0.0471912	0.0707867
4.1	0.0235958	0.0009793	0.0226166	0.0471917	0.0707875
4.2	0.0235961	0.0010032	0.0225929	0.0471922	0.0707883
4.3	0.0235964	0.0010271	0.0225693	0.0471928	0.0707891
4.4	0.0235966	0.0010509	0.0225457	0.0471933	0.0707899
4.5	0.0235969	0.0010748	0.0225221	0.0471938	0.0707907
4.6	0.0235972	0.0010987	0.0224985	0.0471943	0.0707915
4.7	0.0235974	0.0011226	0.0224748	0.0471949	0.0707923
4.8	0.0235977	0.0011465	0.0224512	0.0471954	0.0707931
4.9	0.023598	0.0011704	0.0224276	0.0471959	0.0707939
5.0	0.0235982	0.0011942	0.022404	0.0471965	0.0707947

Table 6.3-4 - Water Number Densities as a Function of Density

H₂O Density (g/cm³)	H₂O Molecular Weight (g/mole)	H Number Density (atoms/b-cm)	O Number Density (atoms/b-cm)	H₂O Material Density (atoms/b-cm)
1.0	18.01528	0.066863	0.033432	0.1002949
0.9	18.01528	0.060177	0.030088	0.0902654
0.8	18.01528	0.053491	0.026745	0.0802359
0.7	18.01528	0.046804	0.023402	0.0702064
0.6	18.01528	0.040118	0.020059	0.0601769
0.5	18.01528	0.033432	0.016716	0.0501474
0.4	18.01528	0.026745	0.013373	0.0401179
0.3	18.01528	0.020059	0.010029	0.0300885
0.2	18.01528	0.013373	0.006686	0.020059
0.1	18.01528	0.006686	0.003343	0.0100295
0.08	18.01528	0.005349	0.002675	0.0080236
0.06	18.01528	0.004012	0.002006	0.0060177
0.04	18.01528	0.002675	0.001337	0.0040118
0.02	18.01528	0.001337	0.000669	0.0020059

Table 6.3-5 - Zircaloy-4 Number Densities

Element	Zirc-4 Density (g/cm³)	Element Molecular Weight (g/mole)	Weight Percent	Number Density (atoms/b-cm)
Sn	6.56	118.71	1.45	0.000483
Fe	6.56	55.847	0.21	0.000149
Cr	6.56	51.9961	0.10	7.6 E-05
Zr	6.56	91.224	98.0975	0.042487
O	6.56	15.9994	0.12	0.000296
C	6.56	12.011	0.014	4.61 E-05
Si	6.56	28.0855	0.0085	1.2 E-05
Zirc-4 Material Density (atoms/b-cm)				0.043548

Table 6.3-6 - 304 Stainless Steel Number Densities

Element	304 SS Density (g/cm³)	Element Molecular Weight (g/mole)	Weight Percent	Number Density (atoms/b-cm)
Fe	8.027	55.847	69.75	0.06038
Mn	8.027	54.93805	2.0	0.00176
Cr	8.027	51.9961	19.0	0.017666
Ni	8.027	58.69	9.25	0.00762
304 SS Material Density (atoms/b-cm)				0.087426

**Table 6.3-7 - Borated Stainless Steel Number Densities
(1.0 w/o natural boron)**

Element or Isotope	Borated Stainless Steel Density (g/cm ³)	Element or Isotope Weight Percent	Element or Isotope Number Density (atoms/b-cm)	¹⁰ B & ¹¹ B 75% Adjusted Number Densities (atoms/b-cm)
¹⁰ B	7.76	0.184311	0.000860	0.000645
¹¹ B	7.76	0.815692	0.003463	0.002597
Fe	7.76	64.1025	0.053646	--
Mn	7.76	1.98	0.001684	--
Si	7.76	0.7425	0.001236	--
Cr	7.76	18.81	0.016907	--
Ni	7.76	13.365	0.010643	--
Borated Stainless Steel Material Density (atoms/b-cm)				0.087359

**Table 6.3-8 - Borated Stainless Steel Number Densities
(1.25 w/o natural boron)**

Element or Isotope	Borated Stainless Steel Density (g/cm ³)	Element or Isotope Weight Percent	Element or Isotope Number Density (atoms/b-cm)	¹⁰ B & ¹¹ B 75% Adjusted Number Densities (atoms/b-cm)
¹⁰ B	7.76	0.230389	0.001075	0.000807
¹¹ B	7.76	1.019615	0.004328	0.003246
Fe	7.76	63.9406	0.053510	--
Mn	7.76	1.975	0.001680	--
Si	7.76	0.7406	0.001232	--
Cr	7.76	18.76	0.016865	--
Ni	7.76	13.331	0.010616	--
Borated Stainless Steel Material Density (atoms/b-cm)				0.0879567

Table 6.3-9 - 316 Stainless Steel Number Densities

Element	SS-316 Density (g/cm³)	Element Molecular Weight (g/mole)	Element Weight Percent	Number Density (atoms/b-cm)
Fe	8.027	55.847	65.75	0.056918
Mn	8.027	54.93805	2.0	0.00176
Si	8.027	28.0855	0.75	0.001291
Cr	8.027	51.9961	17.0	0.015806
Ni	8.027	58.69	12.0	0.009885
Mo	8.027	95.94	2.5	0.00126
316 SS Material Density (atoms/b-cm)				0.086920

Table 6.3-10 - 517 P Carbon Steel Number Densities

Element	Carbon Steel Density (g/cm³)	Element Weight Percent	Element Molecular Weight (g/mole)	Element Number Density (atoms/b-cm)
Fe	7.86	96.51	55.847	0.0818076
Mn	7.86	0.59	54.93805	0.0005084
Cr	7.86	1.025	51.9961	0.0009332
Mo	7.86	0.525	95.94	0.0002590
Ni	7.86	1.35	58.69	0.0010889
517 P CS Material Density (atoms/b-cm)				0.0845971

Table 6.3-11 - XM-19 Stainless Steel Number Densities

Element	XM-19 Density (g/cm³)	Element Weight Percent	Element Molecular Weight (g/mole)	Element Number Density (atoms/b-cm)
Fe	8.027	57.5	55.847	0.049776
Mn	8.027	5.0	54.93805	0.004400
Si	8.027	0.75	28.0855	0.001291
Cr	8.027	22.0	51.9961	0.020455
Ni	8.027	12.5	58.69	0.010297
Mo	8.027	2.25	95.94	0.001134
XM-19 SS Material Density (atoms/b-cm)				0.087353

Table 6.3-12 - Depleted Uranium Number Densities

Isotope	Depleted Uranium Density (g/cm³)	Isotope Weight Percent	Isotope Molecular Weight (g/mole)	Isotope Number Density (atoms/b-cm)
²³⁵ U	18.9	0.22	235.043924	0.000106545
²³⁸ U	18.9	99.78	238.050785	0.047712715
Depleted Uranium Material Density (atoms/b-cm)				0.04781926

Table 6.3-13 - Solid Neutron Shield Number Densities

Material Type	Element or Isotope	Heterogeneous Material Number Densities (atoms/b-cm)	Heterogeneous Material Volume Fractions (w/o)	Neutron Shield Region Mixture Number Densities (atoms/b-cm)
NS-4	C	0.0224074	0.942	0.0211078
	O	0.0255763	0.942	0.0240929
	H	0.0569188	0.942	0.0536176
	N	0.0013653	0.942	0.0012861
	Al	0.0076192	0.942	0.0071773
	¹⁰ B	0.0002109	0.942	0.0001987
	¹¹ B	0.0008491	0.942	0.0007998
SS-304 Bars	Fe	0.0603800	0.026	0.0015699
	Mn	0.0017600	0.026	0.0000458
	Cr	0.0176660	0.026	0.0004593
	Ni	0.0076200	0.026	0.0001981
Copper Ribs	Cu	0.0847400	0.032	0.0027117
Total Number Density (atoms/b-cm)				0.1132650

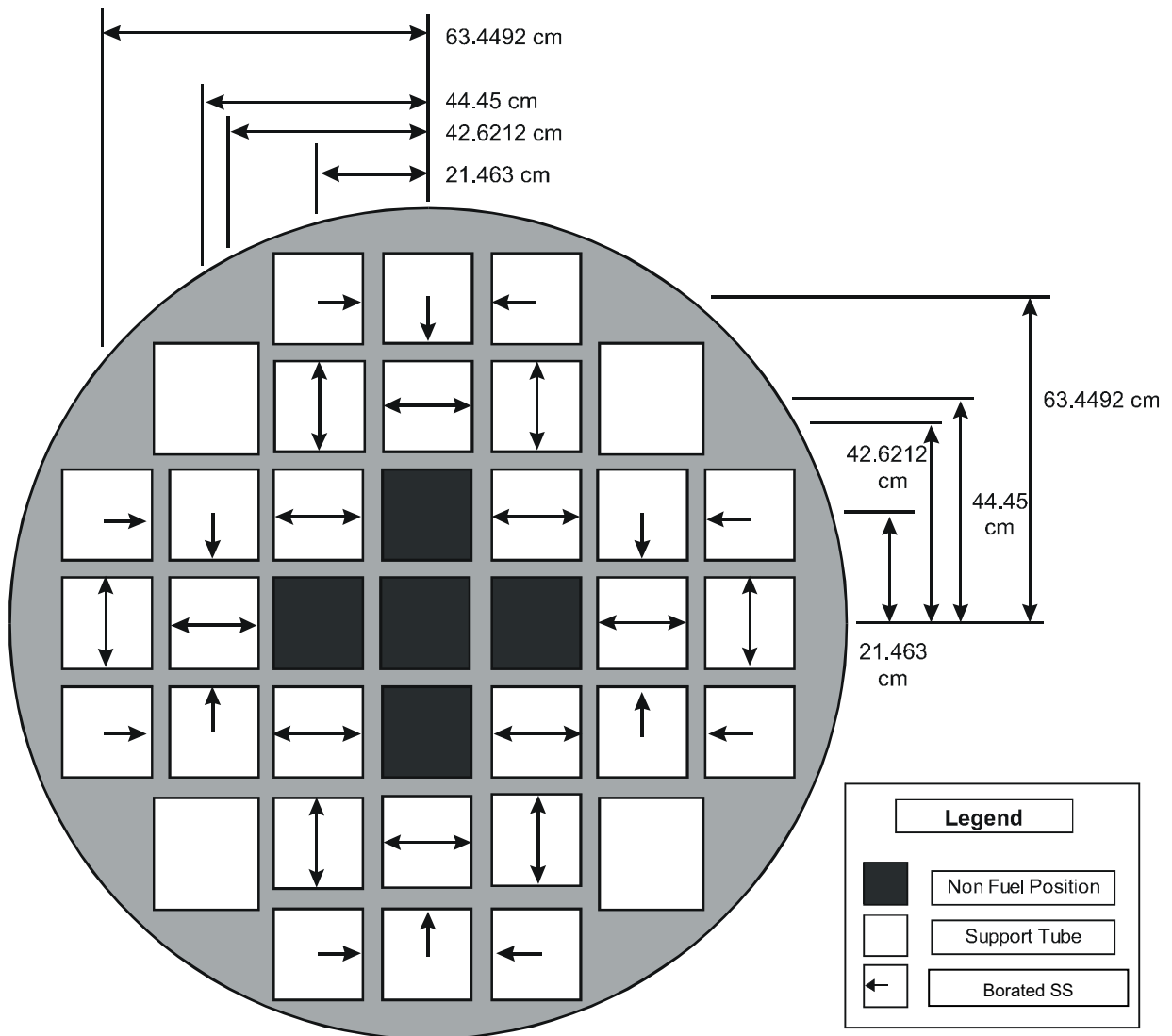
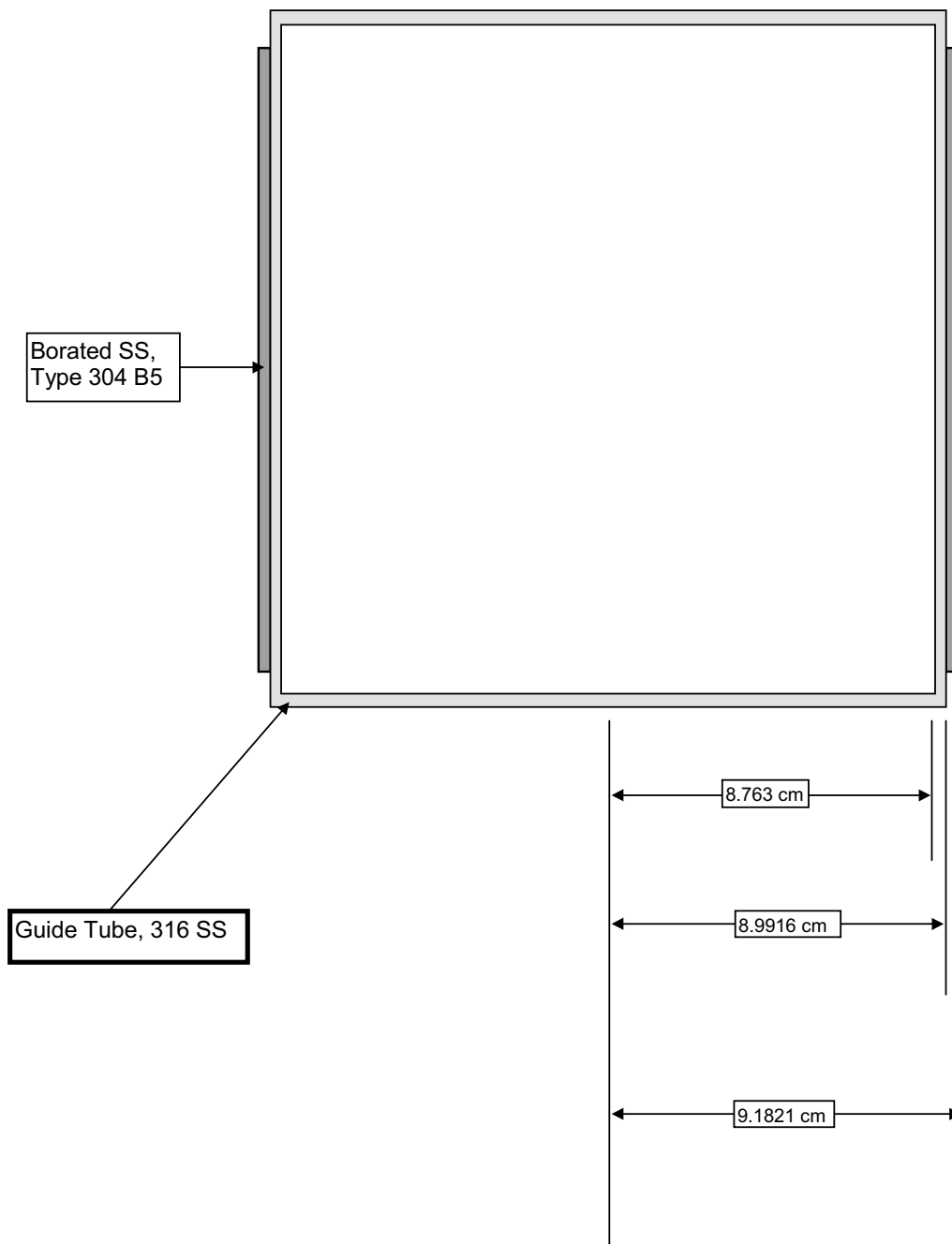
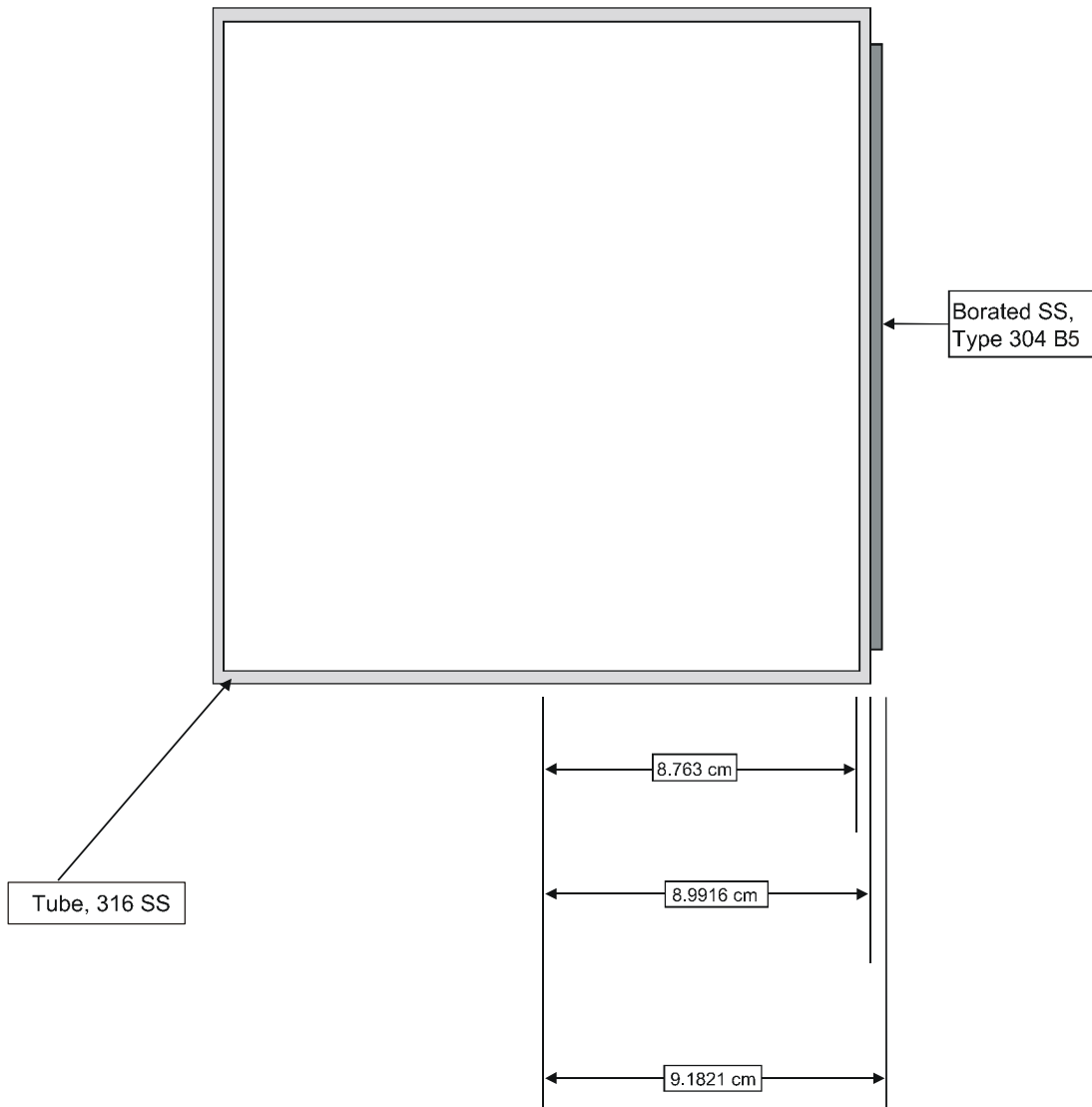


Figure 6.3-1 - FuelSolutions™ W74 Basket (Nominal Dimensions)



**Figure 6.3-2 - FuelSolutions™ W74 Type A Guide Tube Assembly
(Nominal Dimensions)**



**Figure 6.3-3 - FuelSolutions™ W74 Type B Guide Tube Assembly
(Nominal Dimensions)**

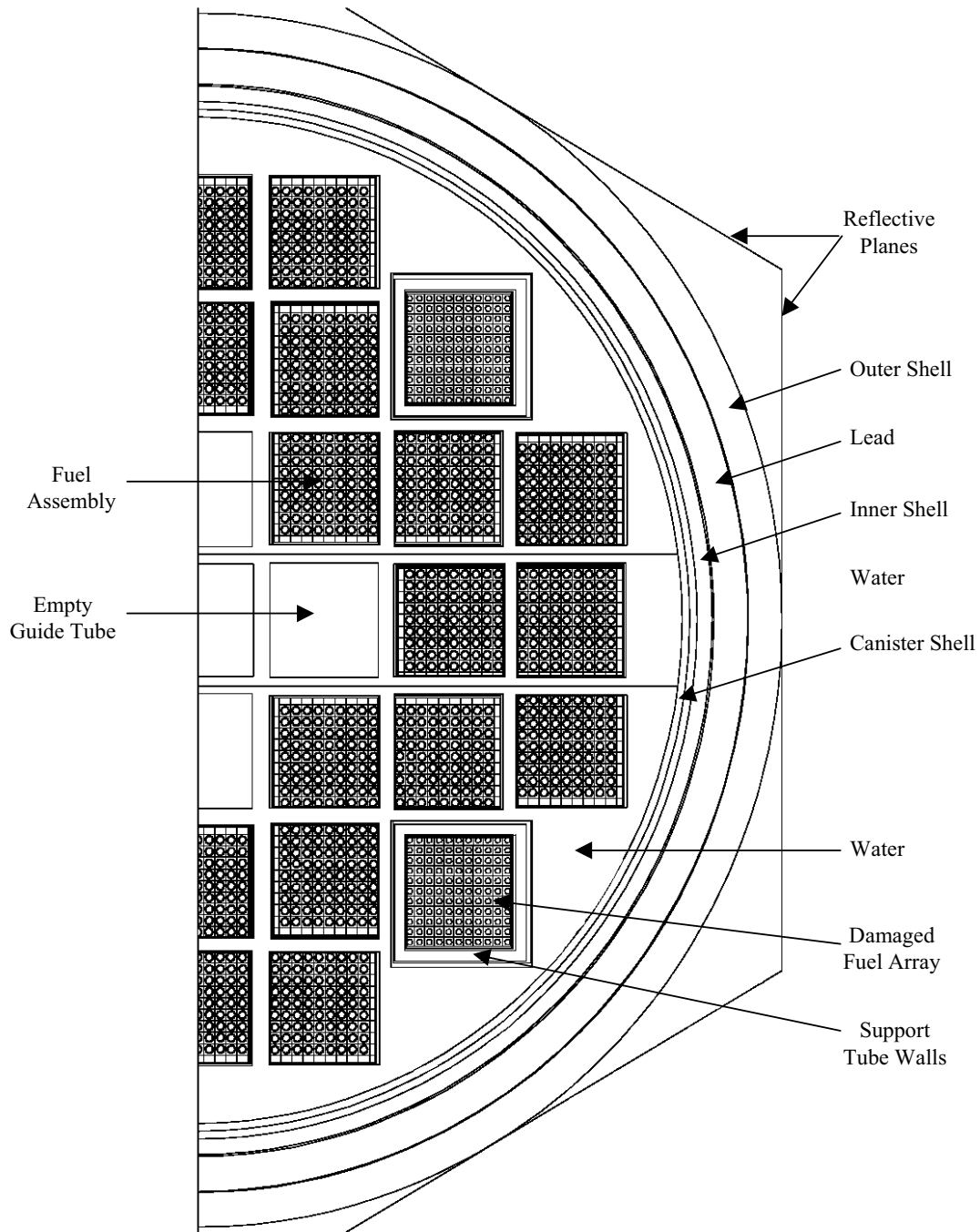


Figure 6.3-6 - Horizontal Cross-Section of MCNP Model

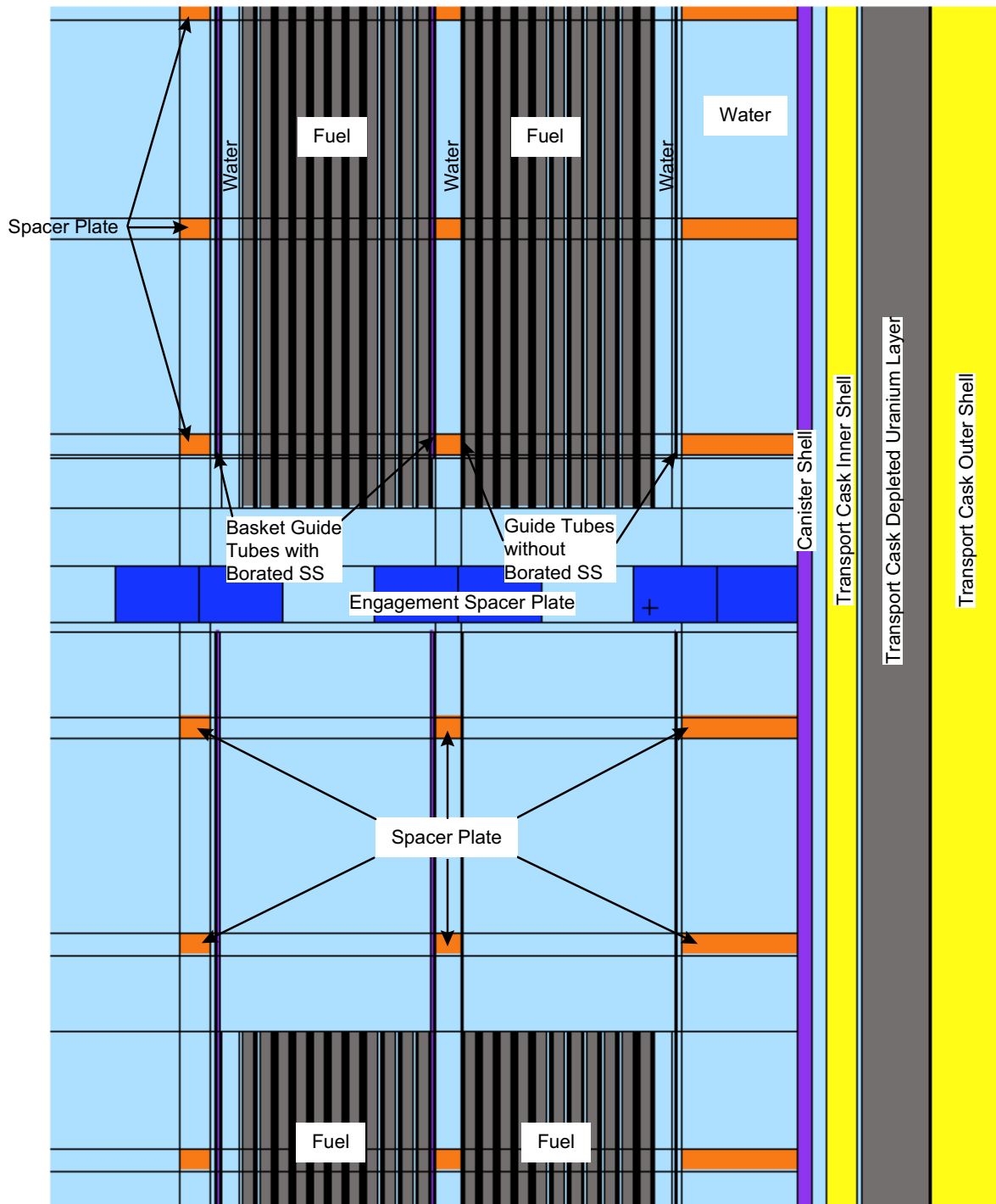


Figure 6.3-8 - Side View of Middle Portion of the FuelSolutions™ W74 HAC Model (cut-away)

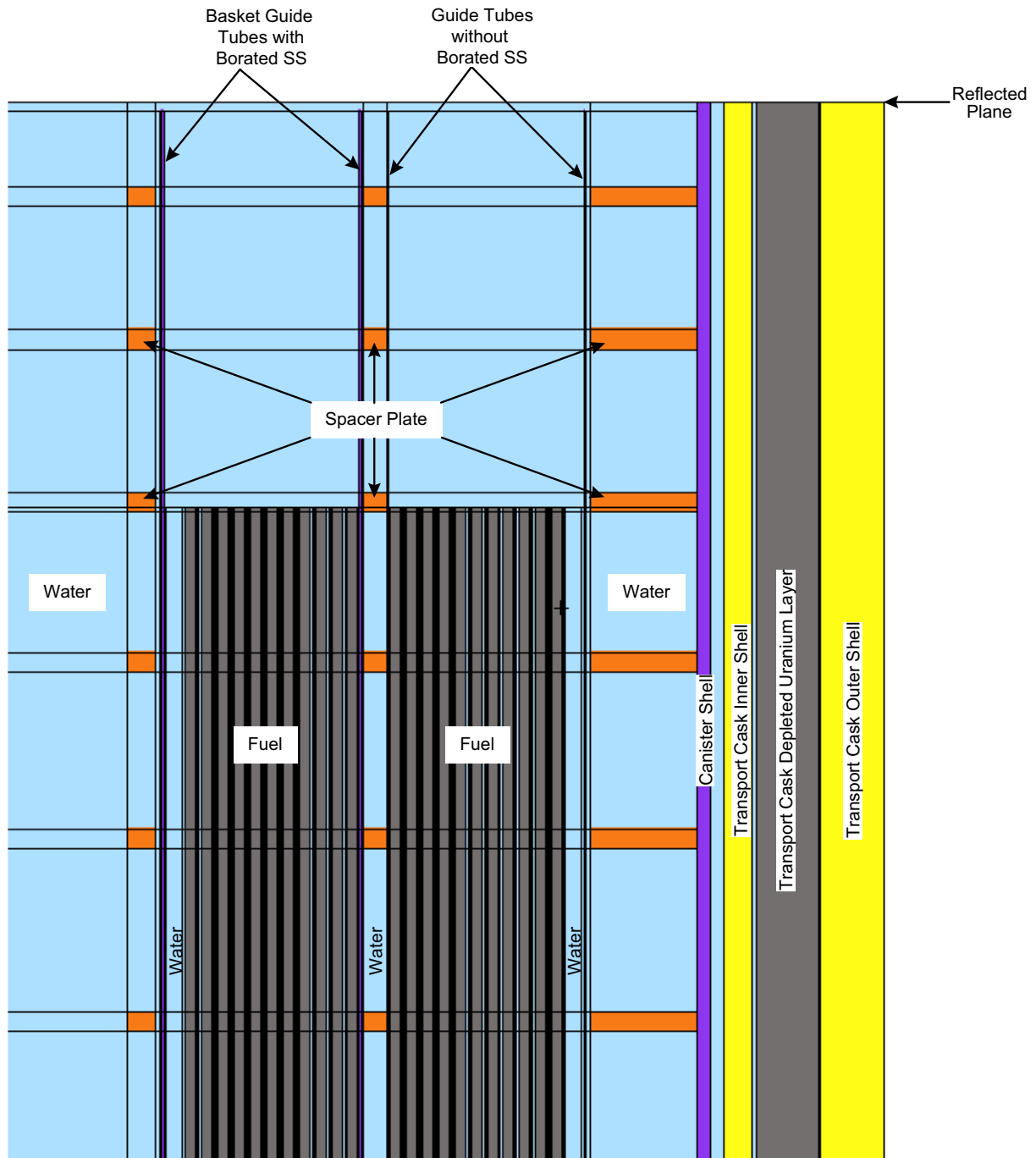
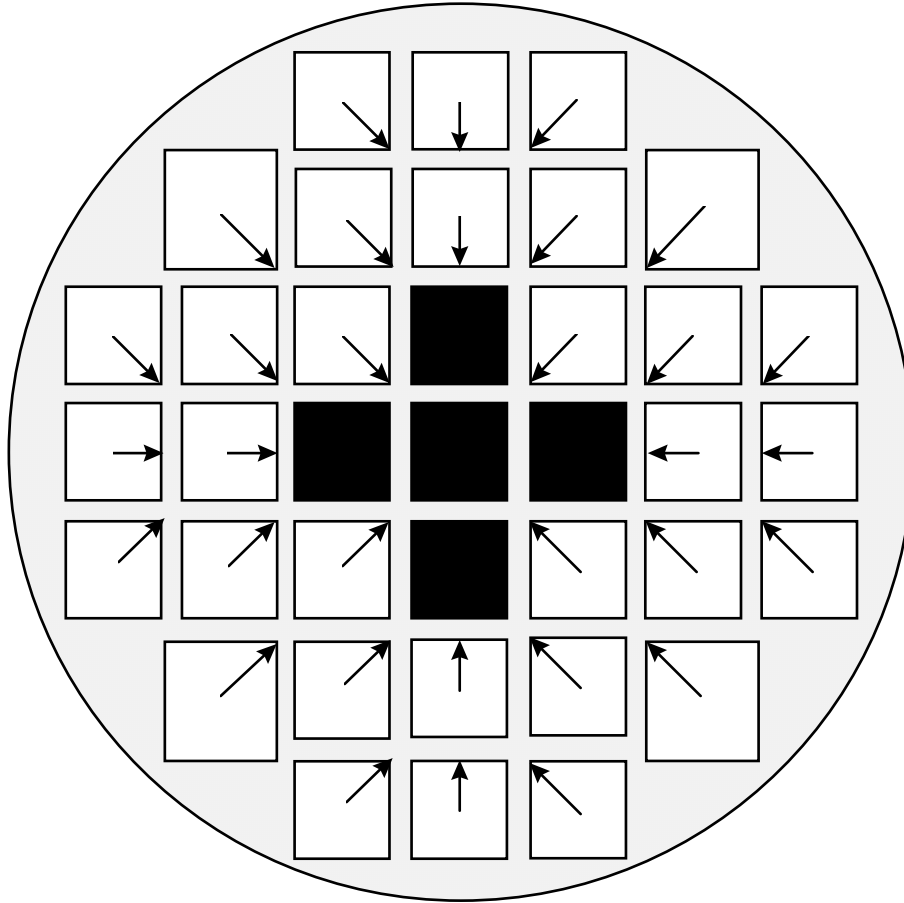
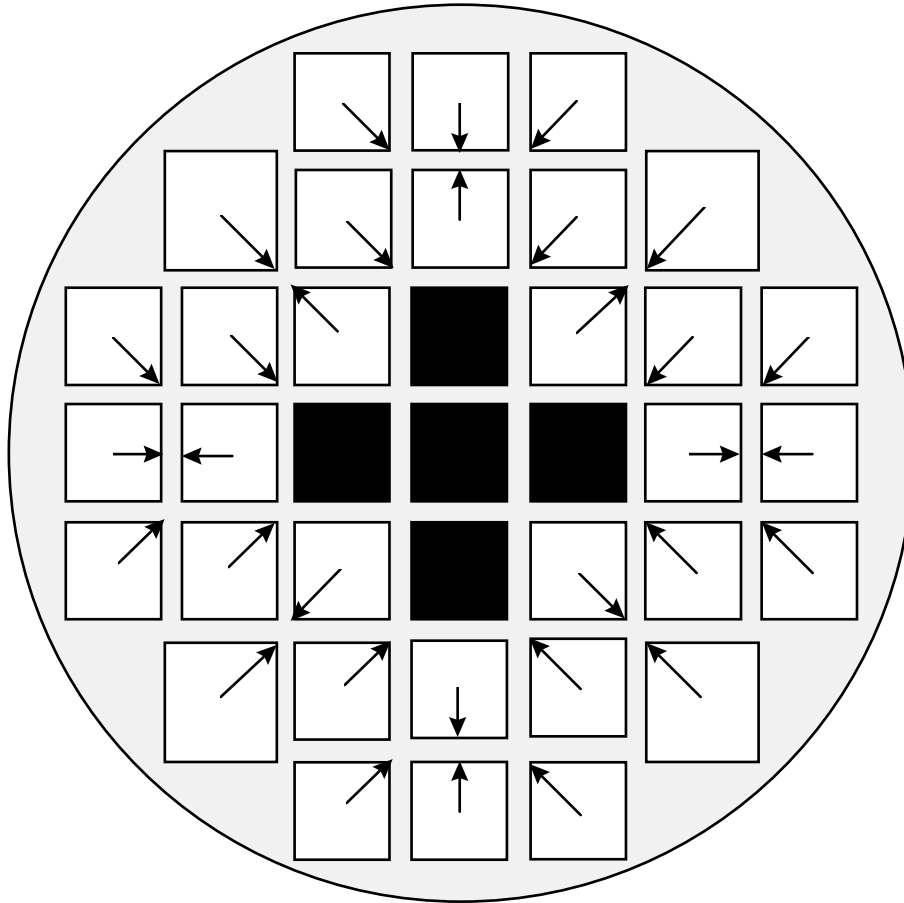


Figure 6.3-9 - Side View of Upper Portion of the FuelSolutions™ W74 HAC Model (cut-away)



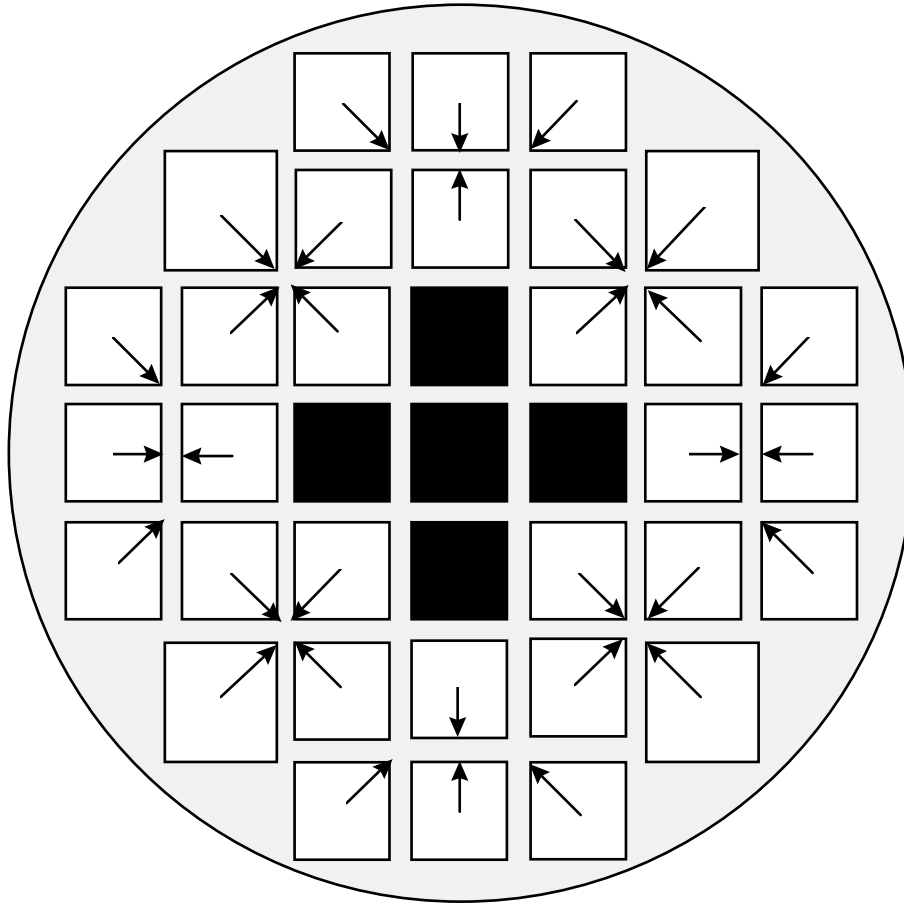
Note: The arrows indicate the direction of application for the spacer plate opening location tolerance.

Figure 6.3-10 - FuelSolutions™ W74 Fuel Pattern No. 1 Basket Configuration



Note: The arrows indicate the direction of application for the spacer plate opening location tolerance.

Figure 6.3-11 - FuelSolutions™ W74 Pattern No. 2 Basket Configuration



Note: The arrows indicate the direction of application for the spacer plate opening location tolerance.

Figure 6.3-12 - FuelSolutions™ W74 Pattern No. 3 Basket Configuration

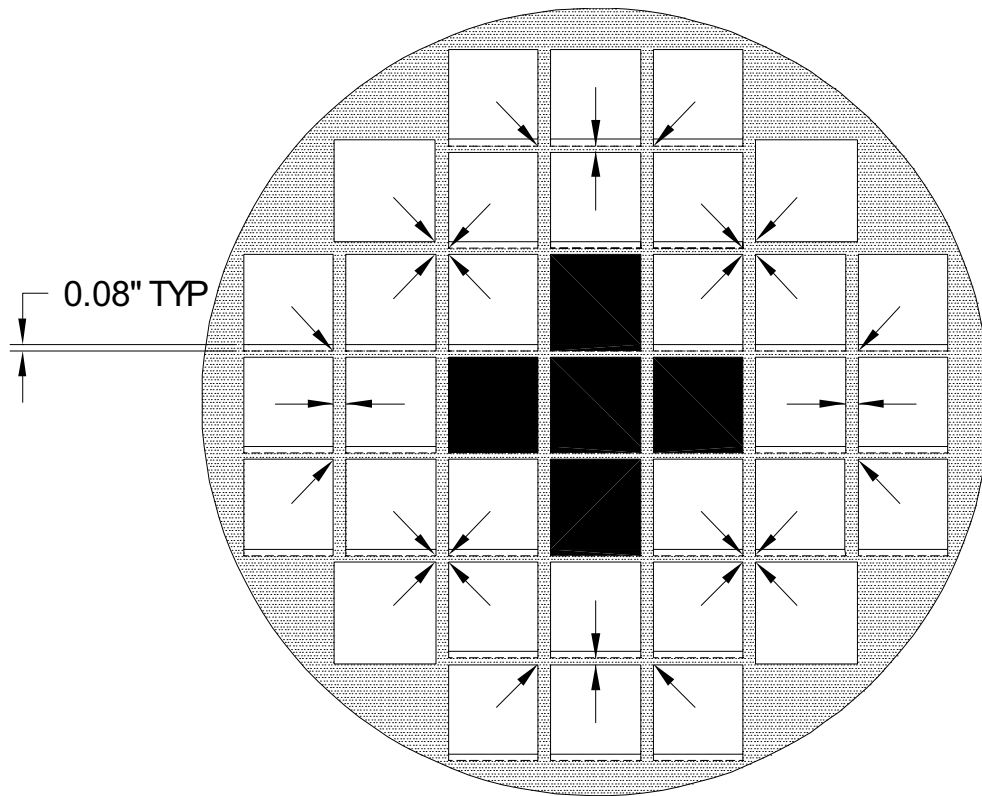


Figure 6.3-13 - W74 Canister Post-Drop Guide Tube Deformation

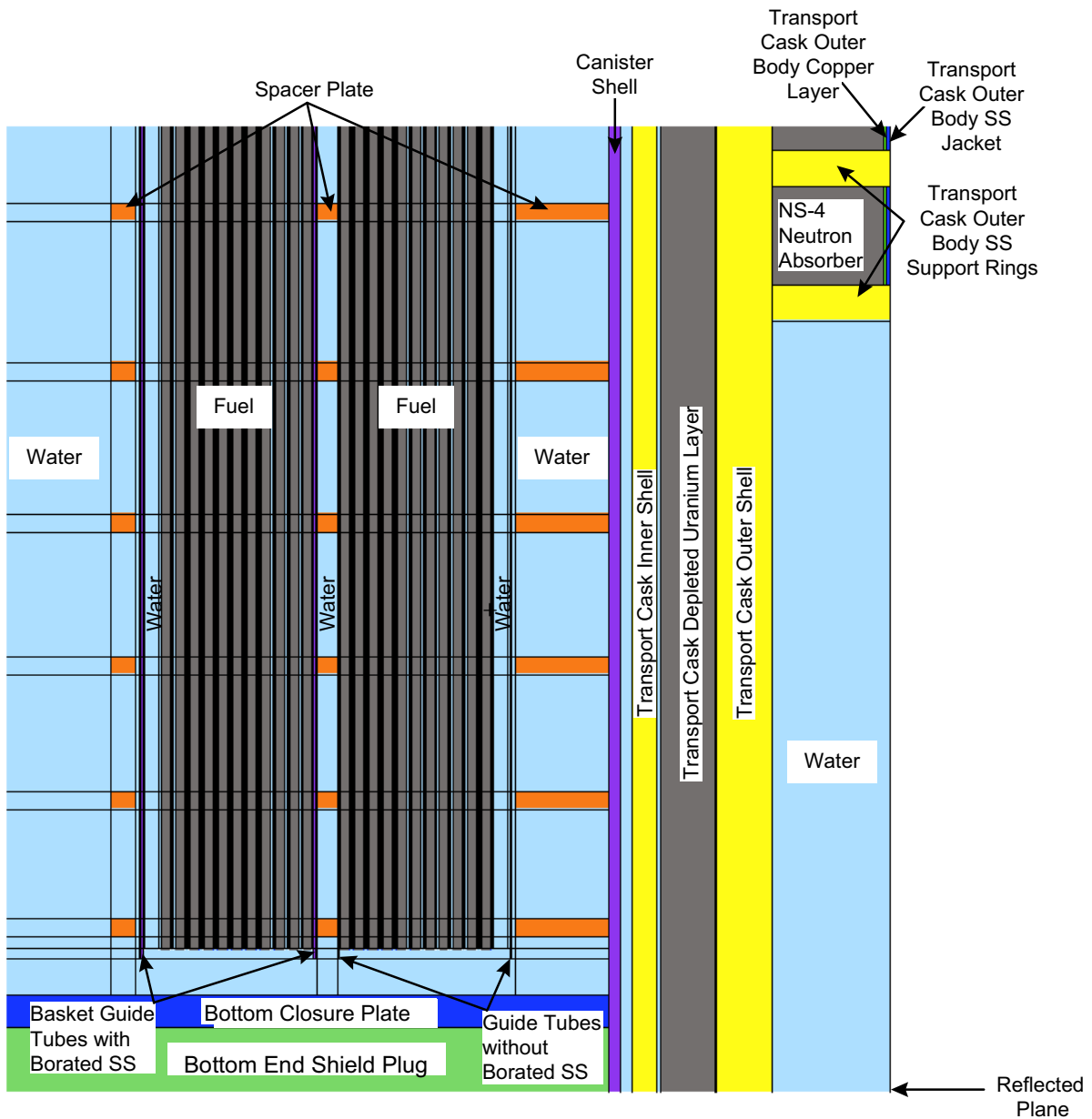


Figure 6.3-14 - Side View of Lower Portion of FuelSolutions™ W74 NCT Model (cut-away)

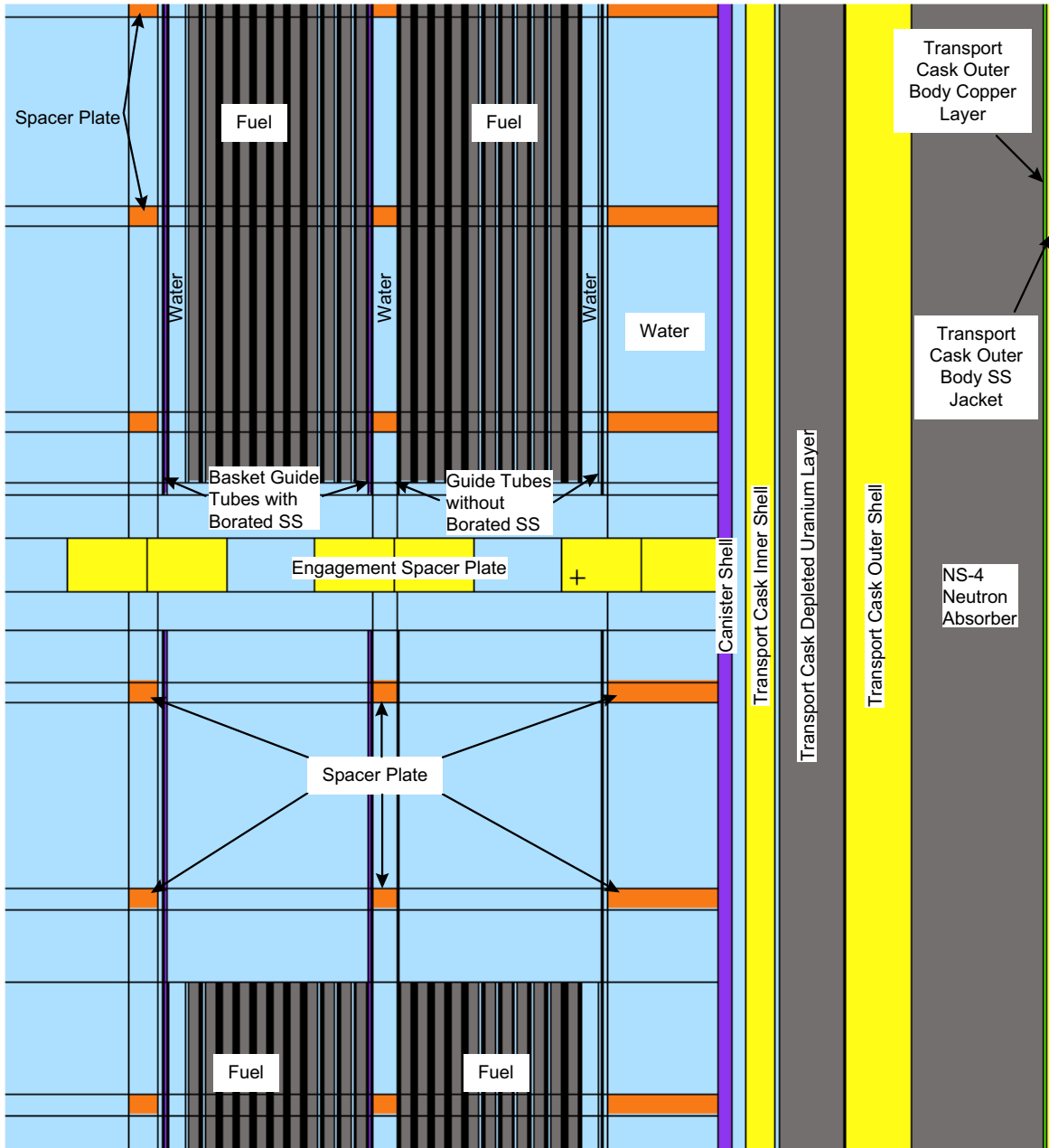


Figure 6.3-15 - Side View of Middle Portion of FuelSolutions™ W74 NCT Model (cut-away)

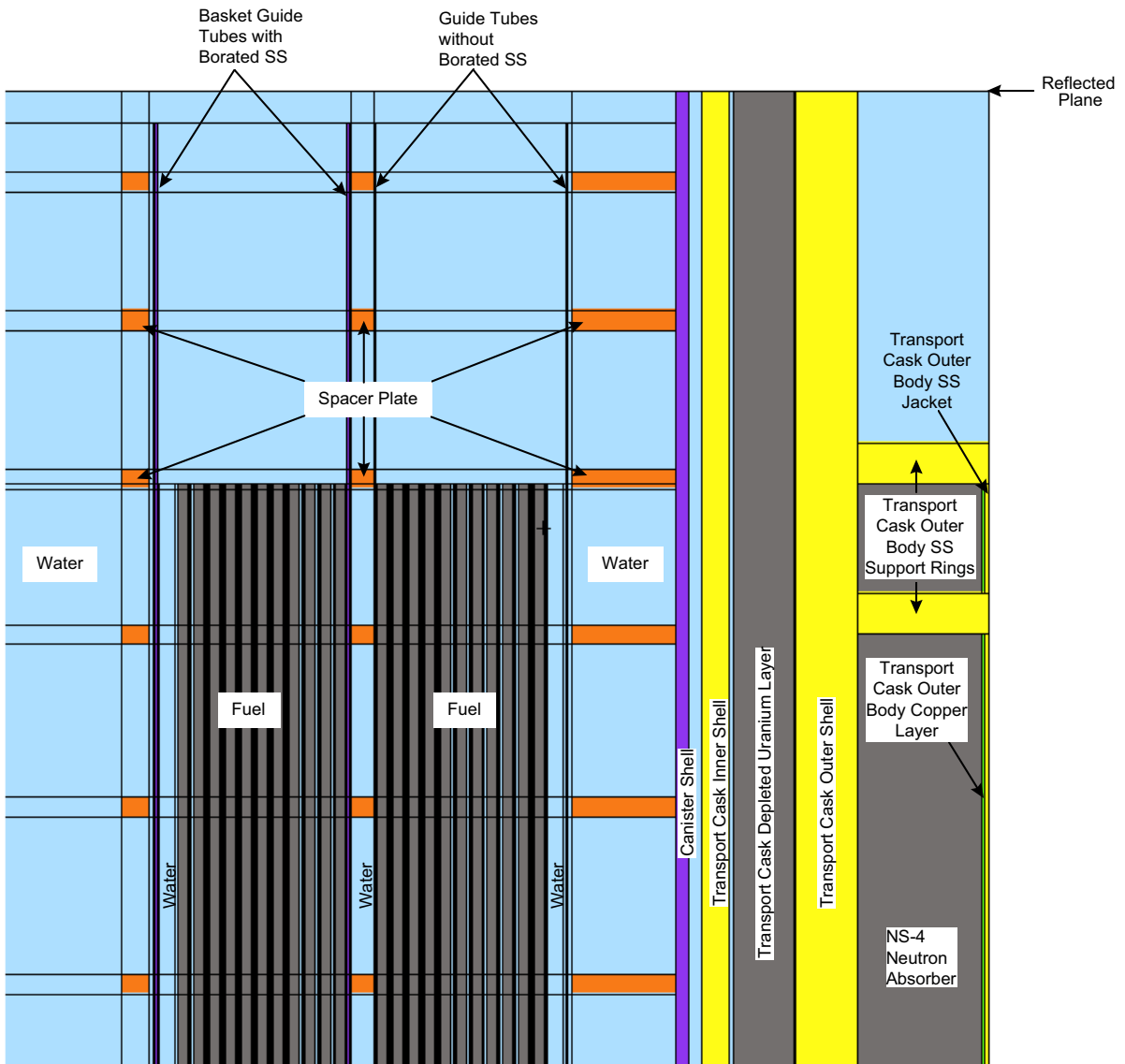


Figure 6.3-16 - Side View of Upper Portion of the FuelSolutions™ W74 NCT Model (cut-away)

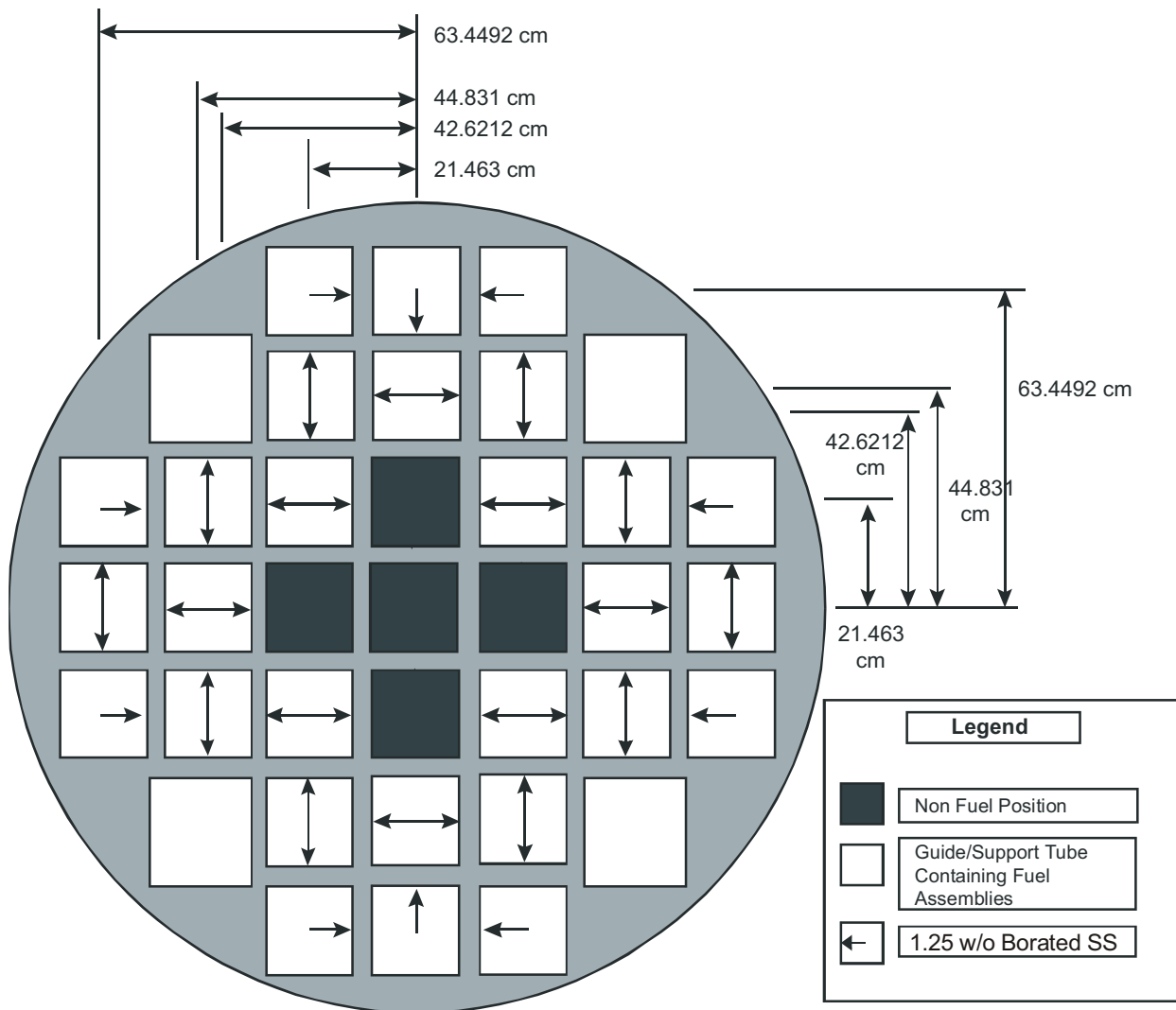


Figure 6.3-17 - FuelSolutions™ W74 Basket Model for MOX and Damaged Assembly Analyses (Nominal Dimensions)

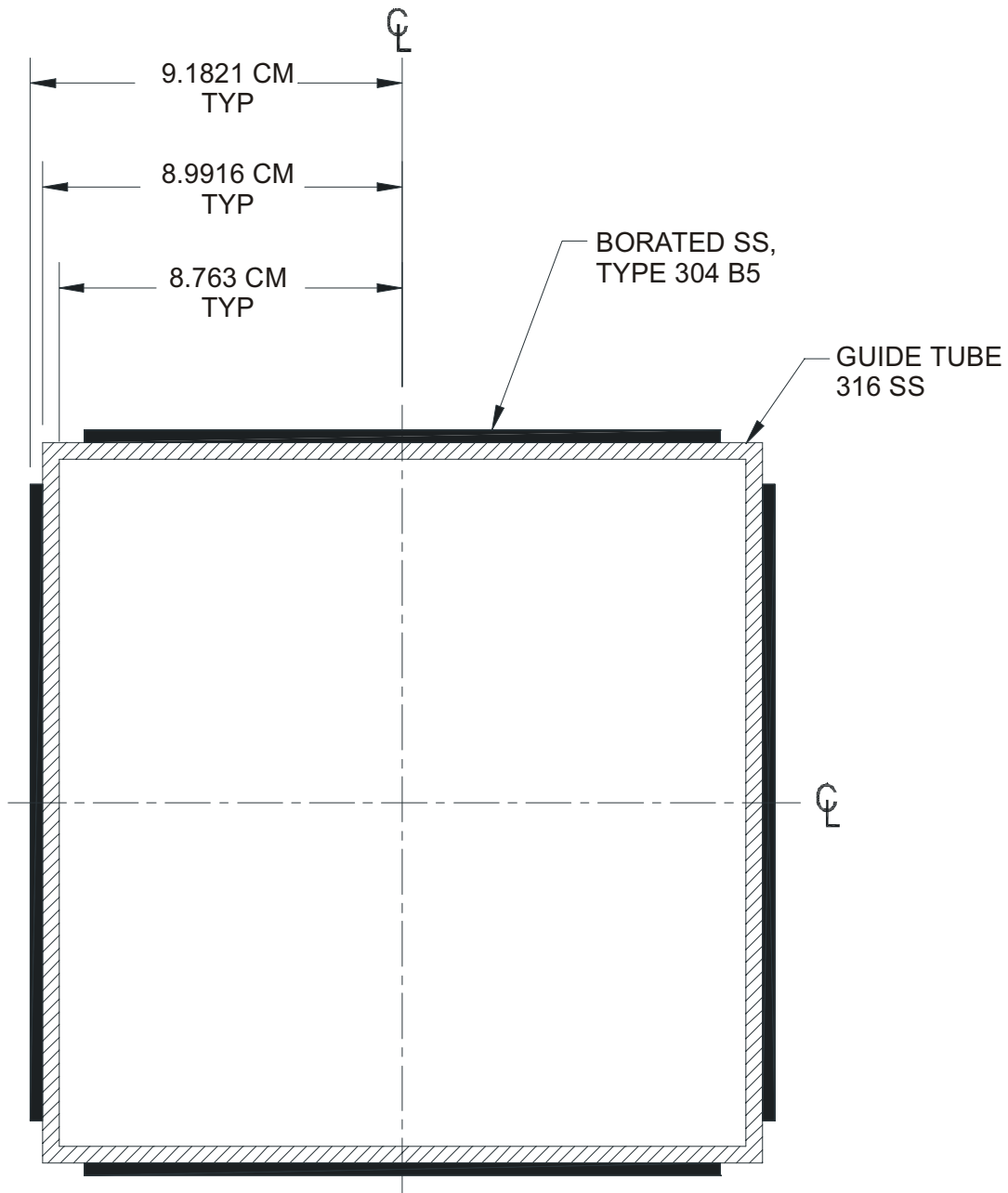


Figure 6.3-18 - W74 Damaged Fuel Can Configuration

This page intentionally left blank.

6.4 Criticality Evaluation

6.4.1 Calculational Method

The design method for the FuelSolutions™ W74 canister system analysis uses the MCNP 4a⁶ code package for reactivity determination to assure the criticality safety of stored fuel assemblies. MCNP is a general purpose Monte-Carlo code that can be used for neutron, photon, electron, or coupled neutron/photon/electron transport. It is suitable for criticality analysis since it has the capability to calculate eigenvalues for critical systems. MCNP treats an arbitrary three dimensional configuration of materials in geometric cells bounded by first and second degree surfaces.

To calculate the effective multiplication factor, MCNP uses three separate estimators: collision, absorption, and track length. The three estimators are statistically combined to provide the best estimate confidence interval for k_{eff} . The primary sources of nuclear data for MCNP are evaluations from the Evaluated Nuclear Data File (ENDF) system, the Evaluated Nuclear Data Library (ENDL), the Activation Library (ACTL) compilations from Lawrence Livermore Laboratory, and evaluations from the Applied Nuclear Science (T-2) Group at Los Alamos. The information from these various sources is incorporated into continuous energy nuclear and atomic data libraries that MCNP uses during a calculation. The primary cross-section data file used for the FuelSolutions™ criticality analysis is the ENDF/B-V.

All of the W74 MCNP criticality analyses are performed using 2000 particles per generation, and 400 cycles (or generations). Fifty generations are skipped before tallying the k_{eff} results. This assures adequate source convergence, particularly in zones of interest, such as the small axial zone at the bottom of the W74 canister where the fuel is not covered by the poison sheets.

6.4.2 Fuel Loading Optimization

6.4.2.1 Package Array

The FuelSolutions™ criticality analyses model infinite arrays of canisters inside a representative transportation cask geometry. These package array models are developed to meet the requirements of 10CFR71.

The array model consists of an infinite number of FuelSolutions™ W74 canisters/casks with adjacent casks in contact with one another in a close packed (triangular pitch) arrangement with interspersed moderator. Case studies are first presented to establish:

- The worst-case canister configuration.
- The limiting case between the uniform enrichment and the multiple pin enrichment configurations.
- The limiting BRP fuel assembly design configuration.

The hypothetical accident and the normal conditions of operation models, which provide the analytical basis for the initial enrichment fuel acceptance criterion, are analyzed for the design basis fuel loading case of up to 64 Siemens 11x11 fuel assemblies.

6.4.2.1.1 Case Studies

6.4.2.1.1.1 Canister Configuration

Two canister designs, designated FuelSolutions™ W74M and FuelSolutions™ W74T, are considered for the FuelSolutions™ W74 models. The two designs differ with respect to the materials used for the support tubes, alignment bars, vent/drain port covers, bottom end plates, bottom closure plates, canister shell assemblies, and engagement spacer plates. In the W74M, SS-316 is used for these components, while in the W74T, the material is SS-304. Since SS-316 and SS-304 undergo similar interaction with neutrons, the material differences between the two canister designs are not expected to produce appreciable reactivity differences.

In addition to the material differences in the FuelSolutions™ W74M and W74T, the number, separation distances, and thickness of the spacer plates in each canister basket are also different. The spacer plate thickness and axial location have a significant influence on the reactivity of the basket. The FuelSolutions™ W74 basket is not a true “flux trap” design, as it does not have poison sheets on both sides of its water gaps.

The spacer plate thickness and axial locations influence the size and the physics of the water gaps in the FuelSolutions™ W74 basket and, therefore, have an impact on the reactivity of the system. Since there is no borated stainless steel sheet on one side of the water gap in the FuelSolutions™ W74 basket, the replacement of water in that region with spacer plate material is a reactivity benefit. The relatively high thermal neutron flux in the FuelSolutions™ W74 water gap results in a higher probability of resonance absorption by the iron and manganese present in the spacer plates, providing a negative reactivity impact.

To validate the discussion of spacer plate impact on system reactivity, three cases are run using the package array, hypothetical accident case model for the FuelSolutions™ W74 canister. Each model contains the Siemens 11x11 fuel assembly at a uniform pin enrichment of 4.10 w/o ²³⁵U. The first case is an infinite axial model with 3.0 inches of water separating each spacer plate. The second case involves the same infinite axial model with 5.0 inches of water separating each spacer plate. The final case includes the infinite axial model with 7.0 inches of water separating each spacer plate.

The results of the spacer plate study are shown in Table 6.4-1. As evident from the results in Table 6.4-1, the spacer plates reduce the reactivity of the system by their presence in the water gaps of the FuelSolutions™ W74 basket.

Since the spacer plate study shows that maximum spacer plate spacing increases system reactivity, the FuelSolutions™ W74M and W74T basket configurations are compared to determine which one contains spacer plates with maximum axial separation. From the comparison, it is evident that the W74T basket has slightly larger axial spacing for its spacer plates in some regions; however, the difference is so small that it is considered to have a negligible impact on reactivity. Because the spacer plate spacing in the FuelSolutions™ W74M and W74T canister designs are so similar for the two basket configurations, neither design configuration is expected to dominate the other with respect to reactivity. If any discernible differences in reactivity exist, the FuelSolutions™ W74T design is expected to be slightly more reactive than the W74M design since it has fewer spacer plates and contains Type A spacer plates that are 0.75-inch thick and provide less absorption of neutrons than the two-inch thick

Type A spacer plates in the W74M design. Therefore, the FuelSolutions™ W74T design is chosen for the remaining criticality calculations.

Three fuel assembly placement patterns are investigated to determine the worst-case asymmetric placement of assemblies and the worst-case applications of the spacer plate hole location tolerances. The three patterns are shown in Figure 6.3-10 through Figure 6.3-12. Figure 6.3-10 presents the Pattern 1 basket configuration in which the assemblies and spacer plate holes are shifted toward the center of the basket. Figure 6.3-11 depicts the Pattern 2 basket configuration in which the assemblies and spacer plate holes immediately adjacent to the flat surfaces of the non-fuel positions are shifted away from the center of the basket, while all other assemblies and spacer plate holes are shifted toward the center of the basket. Figure 6.3-12 shows the Pattern 3 basket configuration in which assemblies and spacer plate holes on the periphery are shifted toward the center of the basket, while those in the center are shifted toward the periphery of the basket. MCNP models are developed for the three assembly placement patterns and runs are performed to determine the most reactive configuration. The MCNP models are constructed using the Siemens 11x11 fuel assembly in the package array under HAC.

The results of the assembly placement calculations are shown in Table 6.4-1. Based on the results in Table 6.4-1, the Pattern 3 assembly placement is demonstrated to yield the highest reactivity. Therefore, the Pattern 3 assembly placement configuration is used in subsequent criticality calculations.

The Pattern 3 asymmetric assembly placement is used to determine a bounding configuration for the damage incurred by the FuelSolutions™ W74 basket from a nine-meter transportation cask drop (which is bounding for all transportation cask drop events or accident sequences). Structural calculations indicate that the damage consists of a maximum guide tube deflection of ~0.125 inch within the basket spans containing fuel assembly mid-grids. There are no guide tube deformations within any of the other axial spans between basket spacer plates. To simplify the MCNP models for subsequent calculations, two MCNP runs are made to demonstrate that modeling the deformation at 0.08 inch over the entire length of the guide tube is more conservative than modeling a 0.125-inch maximum deflection within axial spans that contain fuel assembly mid-grids. The first model contains four spacer plates with reflected boundary conditions for the top and bottom spacer plates, resulting in an infinite axial model. The bounding radial configuration from the asymmetric assembly placement is used for the first model. This configuration incorporates an 0.08-inch deflection over the entire length of the guide tube. The second model is identical to the first except that a 0.125-inch maximum guide tube deflection is incorporated in every third span between spacer plates.

The results from the two MCNP runs are shown in Table 6.4-1 and are compared to determine the bounding representation of guide tube damage incurred from the nine-meter drop. As shown in Table 6.4-1, the case with a 0.08-inch deflection over the entire length of the guide tube bounds the case with a maximum guide tube deflection of 0.125 inch in every third span between spacer plates. Therefore, it is conservative in subsequent models to use the 0.08-inch deflection over the entire length of the guide tube to represent the damage incurred by the W74 basket in a nine-meter drop.

6.4.2.1.1.2 Material and Manufacturing Tolerance Scoping Analyses for the FuelSolutions™ W74T Canister Design

The material and manufacturing tolerances applied to the MCNP models for the FuelSolutions™ W74 criticality analysis are listed in Table 6.3-1. To demonstrate that these variations from the canister nominal dimensions result in worst-case reactivity conditions, the Siemens 11x11 fuel assembly is placed into the infinite array, hypothetical accident case model, and an MCNP run is initiated. The results from this run, which is designated the base case, are compared to six other tolerance cases.

The six other tolerance cases are created from the base case model by successively incorporating the opposing tolerance limit for the guide tube inside and outside dimensions, the borated stainless steel width and thickness, and the support tube inside and outside dimensions. The spacer plate thickness, hole width, and hole location tolerances are not studied in the Material and Manufacturing Tolerance Scoping Analysis. The impact of spacer plate thickness on system reactivity is inferred from the results of the spacer plate scoping calculations. The spacer plate hole location tolerances are investigated during the asymmetric assembly placement study. The spacer plate hole width is chosen to decrease the fuel assembly center-to-center spacing, thus increasing fuel assembly interaction and overall reactivity. The final results for the tolerance scoping analysis are shown in Table 6.4-2. Based on the results in Table 6.4-2, the tolerances listed in Table 6.3-1 are demonstrated to be worst case.

6.4.2.1.1.3 Optimum Moderator Density Scoping Analyses for the FuelSolutions™ W74T Canister Design

The HAC and NCT models for the FuelSolutions™ W74 canister are completely flooded with water at a density sufficient for optimum moderation. Optimum moderation is the condition that produces the highest k_{eff} value over the range of moderation conditions. In the FuelSolutions™ W74 multiple-package array models, water is present inside the containment boundary of the canisters and in between casks. Therefore, two cases are considered for the optimum moderation calculations: the interspersed moderator case in which the moderator density is varied outside the containment boundary, and the interior moderator case in which the moderator density is varied inside the containment boundary.

For the interspersed moderator case, the Siemens 11x11 bounding fuel assembly is placed into the HAC, multiple-package array model; and the moderator density outside the containment boundary is varied between 0.0 and 1.0 g/cc. The assumptions listed in Section 6.3.1 are used for the model, and the fuel is modeled with uranium dioxide at a uniform pin enrichment of 4.10 w/o ^{235}U over the entire length of each fuel stack.

MCNP calculations are performed for each interspersed moderator density case, and the results are shown in Table 6.4-3. As shown in Table 6.4-3, the system is essentially insensitive to optimum interspersed moderator density. Although there is no statistically significant trend, the maximum k_{eff} occurs at a water density of 1.0 g/cc. Based on these results, all multiple-package array calculations are made using an interspersed water density of 1.0 g/cc.

For the interior moderator case, the Siemens 11x11 bounding fuel assembly is placed into the HAC, multiple-package array model; and the moderator density inside the containment boundary is varied between 0.0 and 1.0 g/cc. The assumptions listed in Section 6.3.1 are used for the

model, and the fuel is modeled with uranium dioxide at a uniform pin enrichment of 4.10 w/o ^{235}U over the entire length of each fuel stack.

MCNP calculations are performed for each interior moderator density case, and the results are shown in Table 6.4-4. As shown in Table 6.4-4, optimum interior moderation occurs at a water density of 1.0 g/cc. Based on these results, all calculations for the FuelSolutions™ W74 canisters are made with an interior water density of 1.0 g/cc.

6.4.2.1.1.4 Uniform Pin Enrichment Analysis

The fuel assembly designs that are considered for transport in the FuelSolutions™ W74 canister have multiple pin enrichments rather than a single enrichment for the entire fuel assembly. For fuel qualification, it is desirable to specify a single enrichment limit for a fuel assembly type of interest without including fuel rod enrichment patterns. A uniform enrichment may be determined for a fuel assembly that contains multiple fuel rod enrichments by calculating a pin weighted average enrichment for any radial cross-section along the axis of the fuel assembly. In order to use the pin weighted average enrichment to qualify fuel with multiple pin enrichments, it must be demonstrated that the average enrichment applied uniformly throughout the assembly is an adequate or conservative representation of the multiple pin enrichments present in that fuel assembly.

Among the BRP fuel assemblies that contain uranium (no mixed oxide fuel), eight multiple fuel rod enrichment patterns are identified. Four of the multiple enrichment patterns are associated with General Electric 9x9/Siemens fuel assemblies and are shown in Figure 6.4-1 through Figure 6.4-4. The remaining four patterns are affiliated with the Siemens 11x11 fuel assembly type and are shown in Figure 6.4-5 through Figure 6.4-8. The uniform enrichment used to represent these fuel assemblies is calculated in the following manner:

- The number of fuel rods at a particular enrichment is multiplied by that enrichment, and the result is divided by the total number of fuel rods in the assembly.
- The sum of the results for all enrichments within an assembly gives the desired uniform enrichment.
- The burnable absorber present in certain fuel rods within the assemblies is neglected for the purposes of establishing the uniform enrichment. The fuel rods with burnable absorbers are treated as though they contain only UO_2 .
- The cobalt rod locations in the corners of some fuel assemblies are filled with UO_2 rods at the highest enrichment present in the assembly. As a result, these locations, which are currently empty, can be filled with fuel rods prior to loading the assembly in the FuelSolutions™ W74 canister, as long as the assembly meets the specified uniform enrichment limit with the fuel rods in place.

Once the uniform enrichments for the eight BRP fuel assembly patterns are established, two sets of MCNP calculations are made using the infinite array, hypothetical accident case model. The first set of MCNP calculations consist of eight separate models in which the FuelSolutions™ W74 canister is filled with each fuel assembly type depicted in Figure 6.4-1 through Figure 6.4-8. The second set of MCNP calculations consist of eight models in which the FuelSolutions™ W74 canister is filled with each fuel assembly type at the calculated uniform

enrichment for the patterns shown in Figure 6.4-1 through Figure 6.4-8. The results of the first set of calculations is shown in Table 6.4-5 and is compared to the results of the second set of calculations shown in Table 6.4-6. Based on a comparison of the results in Table 6.4-5 and Table 6.4-6, the uniform pin enrichment cases bound the appropriate multiple pin enrichment cases. Therefore, a single enrichment may be specified as an acceptance criterion for BRP fuel assemblies with multiple pin enrichments. To be qualified for transport in the FuelSolutions™ W74 canister, BRP fuel assemblies must have a maximum lattice enrichment less than or equal to the specified limit, where lattice enrichment means the highest pin-weighted enrichment average along the axial length of the fuel.

6.4.2.1.2 W74 HAC Analyses

Using the assumptions listed in Section 6.3.1, a multiple-package array HAC model is developed for each BRP fuel assembly design listed in Table 6.2-1. MCNP calculations are performed to determine the bounding fuel assembly design, which will be used to calculate the maximum allowable ^{235}U enrichment for BRP fuel in the FuelSolutions™ W74 canister. The results of the MCNP runs are shown in Table 6.4-7. Table 6.4-7 shows the calculated final k_{eff} results for the HAC calculations, along with the limiting (lowest) USL value and the margin between the final k_{eff} and the limiting USL value, for each specific assembly configuration listed in Table 6.2-1.

The analyses results show that the maximum final calculated k_{eff} value, as well as the lowest margin versus the limiting USL value, occurs for the Siemens 11x11 fuel assembly with all 121 lattice locations filled with fuel rods. The results presented in Table 6.4-7 also show that the final calculated k_{eff} values remain under the limiting USL value for each of the specific assembly designs. Thus, the analyses verify that at the maximum allowable enrichment defined in Table 6.1-1, the criticality requirements are met for all BRP fuel assemblies.

For all BRP fuel assemblies, either the water/fuel or pin pitch USL is the limiting USL value. The water/fuel USL is the limiting value for the General Electric and Siemens 9x9 fuel assembly designs, while the pin pitch USL is limiting for the Siemens 11x11 fuel assembly designs. Thus, either the water/fuel or pin pitch USL value is presented in Table 6.4-7 and is used to determine the criticality margins shown in that table. Simple formulas shown in Section 6.5 give the USL values as a function of assembly pin pitch, enrichment, water-to-fuel volume ratio, and H-to- ^{235}U ratio. For each of these four USL parameters, the ranges covered by the specific fuel assembly types described in Table 6.2-1 are presented in Table 6.4-8. Table 6.4-8 also presents the corresponding USL value range for each of the four parameters.

6.4.2.1.3 W74 NCT Analyses

Using the assumptions listed in Section 6.3.1, a multiple-package array NCT model is developed for the Siemens 11x11 BRP fuel assembly design. MCNP calculations are performed to demonstrate that the maximum allowable ^{235}U enrichments calculated in Section 6.4.2.1.2 for a FuelSolutions™ W74 canister loading of 64 bounding Siemens 11x11 BRP fuel assemblies is acceptable under HAC. The result of the NCT calculation is shown in Table 6.4-9. Comparison of the final calculated k_{eff} value for normal operating conditions, to the accident condition k_{eff} value shown in Table 6.4-7, shows that the accident condition is more reactive (i.e., bounding). The USL values do not change between accident and normal operating conditions, so the

calculated k_{eff} values may be compared directly to determine which case is more limiting with respect to criticality.

6.4.2.1.4 Criticality Safety Index

The criticality safety index is calculated to determine the maximum number of casks placed into an array while still maintaining a subcritical configuration. 10CFR71.59 defines the criticality safety index as the number fifty divided by a value “N.” N is defined as the maximum number of packages (divided by either five or two depending on the physical conditions) that would remain subcritical if placed together in an array. The calculations made to support this SAR analyze an infinite sized array of casks. Table 6.4-7 and Table 6.4-9 list subcritical results for the multiple-package array cases. Therefore, the value of N is equivalent to infinity and the value of the criticality safety index is effectively zero.

6.4.2.2 Single Package

The single-package models demonstrate that a FuelSolutions™ W74 canister remains adequately subcritical. The assumptions listed in Section 6.3.1 are used to develop the HAC and NCT models for a single FuelSolutions™ W74 canister. The Siemens 11x11 BRP fuel assembly design is selected as a representative fuel type for the single-package model.

6.4.2.2.1 W74 HAC Analyses

Using the assumptions listed in Section 6.3.1, three single-package HAC models are developed assuming a FuelSolutions™ W74 canister loading of 64 Siemens 11x11 BRP fuel assemblies. The Siemens 11x11 BRP fuel assembly is the bounding assembly design for the FuelSolutions™ W74 canister.

The first single-package model is a model of the full cask (and canister) surrounded by full water reflection. The second model consists of the W74 canister inside the transportation cask inner shell (the containment boundary), surrounded by full water reflection. The third model consists of a canister surrounded by the inner shell plus the depleted uranium gamma shield. These three analyses provide an evaluation of the most reactive reflector configuration, as required by 10CFR71.55(b)(3).

MCNP calculations are performed using the above HAC models, and the results are shown in Table 6.4-10 (Cases 1–3). These results are compared to the Siemens 11x11 (121 rod) assembly results shown in Table 6.4-7 for the multiple-package array configuration. This comparison shows that the multiple-package array case bounds all single-package cases for accident conditions.

Given that the applicable USL does not change between the package array and single-package models, the criticality margin of the package array case is bounding (i.e., no higher than) the margin for all the single-package cases. Additionally, the difference in margin is so small as to be statistically insignificant. This finding indicates that the fuel assemblies within a canister are effectively isolated from the fuel assemblies in an adjacent container. It also indicates that any single-package configuration, surrounded by optimum reflector conditions, has a reactivity that is equal to or less than that of an infinite package array.

6.4.2.2.2 W74 NCT Analyses

Using the assumptions listed in Section 6.3.1, two single-package NCT models are developed assuming a FuelSolutions™ W74 canister loading of 64 Siemens 11x11 BRP fuel assemblies. The Siemens 11x11 BRP fuel assembly is the bounding assembly for the FuelSolutions™ W74 canister.

The first single-package model is a model of the full cask (and canister) surrounded by full water reflection. The second model consists of the canister surrounded by the inner shell and the depleted uranium gamma shield. The accident condition analyses (discussed in Section 6.4.2.2.1) show that a canister surrounded by the cask inner shell and gamma shield is more reactive than a canister surrounded by the inner shell only. These two analyses provide an evaluation of the most reactive reflector configuration, as required by 10CFR71.55(b)(3).

MCNP calculations are performed using the above NCT models, and the results are shown in Table 6.4-10 (Cases 4–5). These results are compared to the Siemens 11x11 (121 rod) assembly results from the normal condition multiple-package array configuration, shown in Table 6.4-9. This comparison shows that the multiple-package array case bounds all single-package cases for normal conditions.

Given that the applicable USL does not change between the package array and single-package models, the criticality margin of the package array case is bounding (i.e., no higher than) the margin for all the single-package cases. The difference in margin is also so small as to be statistically insignificant. This finding indicates that the fuel assemblies within a canister are effectively isolated from the fuel assemblies in an adjacent container, and that any single-package configuration, surrounded by optimum reflector conditions, has a reactivity that is equal to or less than that of an infinite package array.

The accident condition multiple-package array case, which is presented for the Siemens 11x11 (121 rod) assembly in Table 6.4-7, is even more reactive than the normal condition multiple-package array. Therefore, the accident condition multiple-package array, upon which all maximum allowable enrichment results are based, clearly bounds all single-package configurations for both normal and accident conditions.

6.4.3 Criticality Results

The FuelSolutions™ TS125 Transportation Cask and W74 canister were analyzed in several parametric studies to assure that the most reactive configuration is selected for reporting NCT and HAC case results.

Table 6.4-1 through Table 6.4-6 show the results of sensitivity cases used to establish the most reactive canister, cask, and fuel assembly configuration. The sensitivity analyses consider the following effects:

- Spacer plate spacing (Table 6.4-1)
- Assembly position within the guide tubes (Table 6.4-1)
- Guide tube deformation due to cask drops (Table 6.4-1)
- Canister material and fabrication tolerances (Table 6.4-2)

- Interspersed moderation between casks in the HAC infinite array (Table 6.4-3)
- Canister internal moderator density (Table 6.4-4)
- Multiple fuel rod enrichments (Table 6.4-5 and Table 6.4-6).

Table 6.4-7 shows the results for the HAC multiple-package array cases. This suite of MCNP runs determined that the BRP Siemens 11x11 fuel design (with no zircaloy rods) is the most reactive in the package. Table 6.4-9 and Table 6.4-10 show the results for the NCT multiple and single-package cases, respectively.

Application of the benchmark bias is performed using the USL method described in Section 6.5. The calculated k_{eff} values in Table 6.4-7, Table 6.4-9, and Table 6.4-10 are below the USLs shown in Section 6.5; therefore, it is demonstrated that the package design provides sufficient subcritical margin. Table 6.4-8 shows the value ranges covered by the W74 canister cases for each of the four USL parameters discussed in Section 6.5. For each parameter, the value range shown in Table 6.4-8 lies within the applicable range defined for that parameter in Section 6.5.

Table 6.4-1 - MCNP Results for the Canister Design Case Studies

Case	Description	²³⁵U Enrichment (w/o)	k_{eff}	Uncertainty	k_{eff} + 2σ
1	W74T - HAC - Spacer Plate Spacing 3.0"	4.10	0.94220	0.00083	0.94386
2	W74T - HAC - Spacer Plate Spacing 5.0"	4.10	0.94467	0.00092	0.94651
3	W74T - HAC - Spacer Plate Spacing 7.0"	4.10	0.94638	0.00087	0.94812
4	W74T - HAC Asymmetric Assembly Pattern 1	4.10	0.91986	0.00087	0.92160
5	W74T - HAC Asymmetric Assembly Pattern 2	4.10	0.93622	0.00089	0.93800
6	W74T - HAC Asymmetric Assembly Pattern 3	4.10	0.93831	0.00088	0.94007
7	W74T - HAC Asymmetric Assembly Pattern 3, 0.08" Guide Tube Deformation	4.10	0.94758	0.00087	0.94932
8	W74T - HAC Asymmetric Assembly Pattern 3, 0.125" Guide Tube Deformation	4.10	0.94450	0.00084	0.94618

**Table 6.4-2 - Material and Fabrication Tolerance Results
 for the FuelSolutions™ W74 Canister**

Case	Description	²³⁵ U Enrichment	k _{eff}	Uncertainty	k _{eff} +2σ
1	Siemens 11x11, Pattern 3 Base Case	4.10	0.93831	0.00088	0.94007
2	11x11 Array, Borated SS Thickness tolerance + 0.007"	4.10	0.93129	0.00092	0.93313
3	11x11 Array, Borated SS Width tolerance + 0.05"	4.10	0.93536	0.00092	0.93720
4	11x11 Array, Guide Tube Inner Dimension tolerance - 0.05"	4.10	0.93436	0.00085	0.93606
5	11x11 Array, Guide Tube Outer Thickness tolerance + 0.008"	4.10	0.93280	0.00091	0.93462
6 ⁽¹⁾	11x11 Array, Support Tube Inner Dimension tolerance - 0.05"	4.10	0.93697	0.00090	0.93877
7	11x11 Array, Support Tube Outer Thickness tolerance + 0.055"	4.10	0.93430	0.00091	0.93612

Note:

⁽¹⁾ The difference between the results for this case and the base case is statistically insignificant.

**Table 6.4-3 - Optimum Interspersed Moderator Case Results
 for the FuelSolutions™ W74 Canister**

Case	Moderator Density (g/cm ³)	²³⁵ U Enrichment (w/o)	k _{eff}	Uncertainty	k _{eff} + 2σ
1	1.0	4.10	0.93831	0.00088	0.94007
2	0.8	4.10	0.93754	0.00087	0.93928
3	0.6	4.10	0.93686	0.00093	0.93872
4	0.4	4.10	0.93618	0.00096	0.93810
5	0.2	4.10	0.93717	0.00090	0.93897
6	0.1	4.10	0.93572	0.00087	0.93746
7	0.08	4.10	0.93610	0.00090	0.93790
8	0.06	4.10	0.93687	0.00088	0.93863
9	0.04	4.10	0.93520	0.00093	0.93706
10	0.02	4.10	0.93676	0.00094	0.93864
11	0.00	4.10	0.93704	0.00091	0.93886

**Table 6.4-4 - Optimum Interior Moderator Case Results
 for the FuelSolutions™ W74 Canister**

Case	Moderator Density (g/cm ³)	²³⁵ U Enrichment (w/o)	k _{eff}	Uncertainty	k _{eff} + 2σ
1	1.0	4.10	0.93831	0.00088	0.94007
2	0.8	4.10	0.89845	0.00092	0.90029
3	0.6	4.10	0.84791	0.00087	0.84965
4	0.4	4.10	0.77633	0.00088	0.77809
5	0.2	4.10	0.67329	0.00077	0.67483
6	0.1	4.10	0.59582	0.00063	0.59708
7	0.08	4.10	0.57204	0.00060	0.57324
8	0.06	4.10	0.54017	0.00059	0.54135
9	0.04	4.10	0.49778	0.00053	0.49884
10	0.02	4.10	0.44076	0.00049	0.44174
11	0.00	4.10	0.42738	0.00046	0.42830

Table 6.4-5 - MCNP Results for the FuelSolutions™ W74 Canister and Big Rock Point Fuel Assemblies with Variable Fuel Rod Enrichments

Case	Fuel Pattern	²³⁵ U Enrichment (w/o)	k _{eff}	Uncertainty	k _{eff} + 2σ
1	GE 9x9/ Figure 6.4-1	2.50, 3.40, 4.50	0.89783	0.00087	0.89957
2	GE 9x9/ Figure 6.4-2	2.50, 3.299, 4.50	0.89839	0.00087	0.90013
3	GE 9x9/ Figure 6.4-3	2.50, 3.299, 4.50	0.90114	0.00086	0.90286
4	Siemens 9x9/ Figure 6.4-4	2.55, 3.30, 4.50	0.89946	0.00089	0.90124
5	Siemens 11x11/ Figure 6.4-5	2.30, 3.20, 4.60	0.91266	0.00090	0.91446
6	Siemens 11x11/ Figure 6.4-6	1.50, 2.52, 3.82	0.86146	0.00089	0.86324
7	Siemens 11x11/ Figure 6.4-7	1.66, 2.79, 4.24	0.88098	0.00087	0.88272
8	Siemens 11x11/ Figure 6.4-8	1.80, 2.80, 4.18	0.88099	0.00091	0.88281

Table 6.4-6 - MCNP Results for the FuelSolutions™ W74 Canister and Big Rock Point Fuel Assemblies with Lattice Average Fuel Rod Enrichments

Case	Fuel Pattern	²³⁵ U Enrichment (w/o)	k _{eff}	Uncertainty	k _{eff} + 2σ
1	GE 9x9/ Figure 6.4-1	3.58	0.90743	0.00087	0.90917
2	GE 9x9/ Figure 6.4-2	3.57	0.90662	0.00086	0.90834
3	GE 9x9/ Figure 6.4-3	3.56	0.90718	0.00092	0.90902
4	Siemens 9x9/ Figure 6.4-4	3.58	0.90647	0.00092	0.90831
5	Siemens 11x11/ Figure 6.4-5	3.90	0.92325	0.00081	0.92487
6	Siemens 11x11/ Figure 6.4-6	3.14	0.87741	0.00083	0.87907
7	Siemens 11x11/ Figure 6.4-7, Figure 6.4-8	3.43	0.89664	0.00091	0.89846

Table 6.4-7 - Multiple-Package Array, Hypothetical Accident Condition Results to Determine the Bounding Fuel Assembly Configuration (4.1% Enriched Fuel)

Fuel Assembly Type	Calculated k_{eff}	Uncertainty	Final k_{eff} ($k_{eff} + 2\sigma$)	Minimum USL	Δ
GE-9x9 81 Fuel Rods	0.93478	0.00084	0.93646	0.94358	0.00712
GE-9x9 1 Water Pin	0.93569	0.00085	0.93739	0.94358	0.00619
Siemens 9x9 81 Fuel Rods	0.93308	0.00093	0.93494	0.94358	0.00864
Siemens 11x11 121 Fuel Rods	0.93831	0.00088	0.94007	0.94286	0.00279
Siemens 11x11 4 Zirc Rods	0.93253	0.00083	0.93419	0.94286	0.00867
Siemens 11x11 1 Zirc Rod	0.93658	0.00084	0.93826	0.94286	0.00460
Siemens 11x11 0.3735" Pellet	0.93533	0.00094	0.93721	0.94286	0.00565

Table 6.4-8 - Big Rock Point Fuel Assembly USL Value Ranges

USL Parameter	Parameter Range	USL Value Range
Pin Pitch (cm)	1.47 - 1.80	0.94286 - 0.94382
Enrichment (w/o ^{235}U)	4.10	0.94470
Water-to-Fuel Volume Ratio	1.49 - 1.66	0.94358 - 0.94368
H-to- ^{235}U Ratio	101.507 - 113.510	0.94417 - 0.94421

**Table 6.4-9 - Multiple-Package Array,
Normal Operating Condition Results**

Fuel Assembly	²³⁵ U Enrichment (w/o)	k _{eff}	Uncertainty	Final k _{eff} (k _{eff} + 2σ)
Siemens 11x11, 121 Fuel Rods	4.10	0.93599	0.00091	0.93781

Table 6.4-10 - MCNP Results for the Single-Package Models

Case	Description	²³⁵ U Enrichment (w/o)	k _{eff} ⁽¹⁾	Uncertainty	k _{eff} + 2σ
1	Siemens 11x11 (121 rods) Accident Conditions All Cask Shells Present	4.10	0.93716	0.00085	0.93886
2	Siemens 11x11 (121 rods) Accident Conditions Cask Inner Shell Only	4.10	0.93612	0.00093	0.93798
3	Siemens 11x11 (121 rods) Accident Conditions Inner Shell + DU Shield	4.10	0.93753	0.00092	0.93937
4	Siemens 11x11 (121 rods) Normal Conditions All Cask Shells Present	4.10	0.93422	0.00089	0.93600
5	Siemens 11x11 (121 rods) Normal Conditions Inner Shell + DU Shield	4.10	0.93529	0.00094	0.93717

Note:

- ⁽¹⁾ The calculated k_{eff} values of all five single-package cases are compared to the calculated k_{eff} value presented in Table 6.4-7 (infinite HAC cask array case) for the Siemens 11x11 (121 fuel rods) assembly. The infinite array case calculated k_{eff} value (0.93831) is higher than all of the calculated k_{eff} values for the single-package cases. Therefore, the infinite accident condition cask array configuration is bounding (the most reactive) for BRP assemblies in the W74 canister.

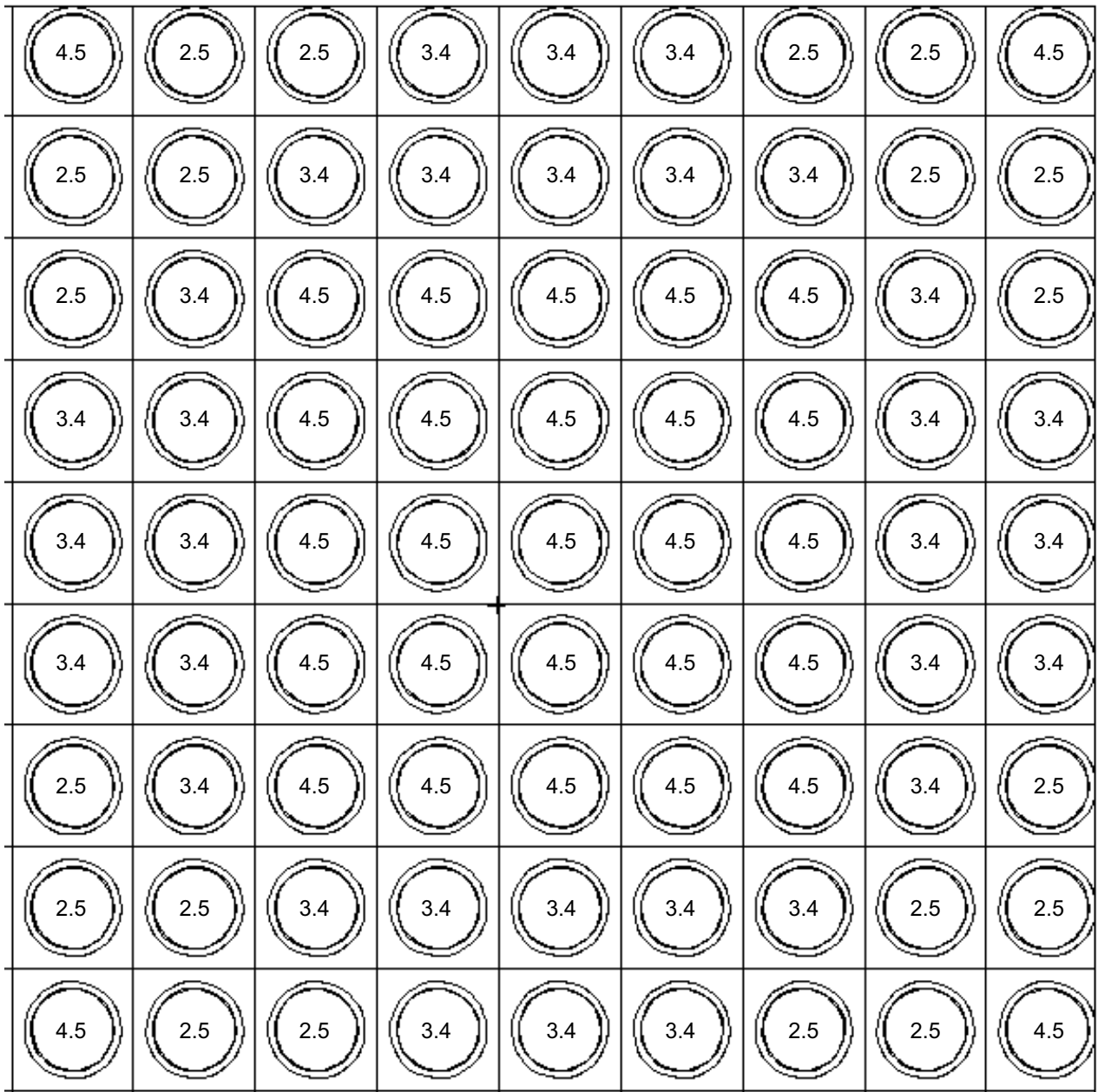


Figure 6.4-1 - Multiple Pin Enrichment Pattern 1 for the Big Rock Point GE 9x9 Fuel

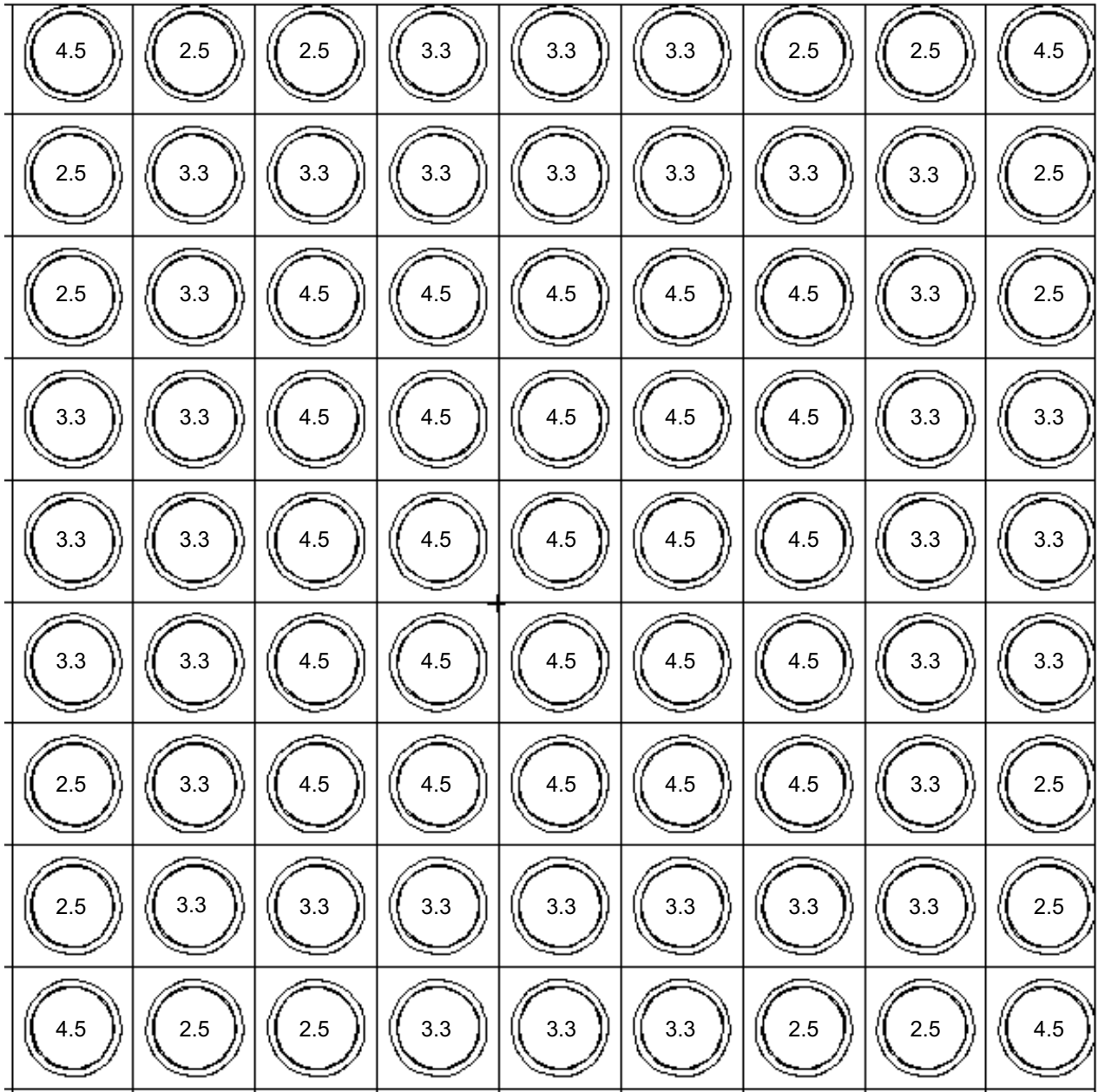


Figure 6.4-2 - Multiple Pin Enrichment Pattern 2 for the Big Rock Point GE 9x9 Fuel Assembly.

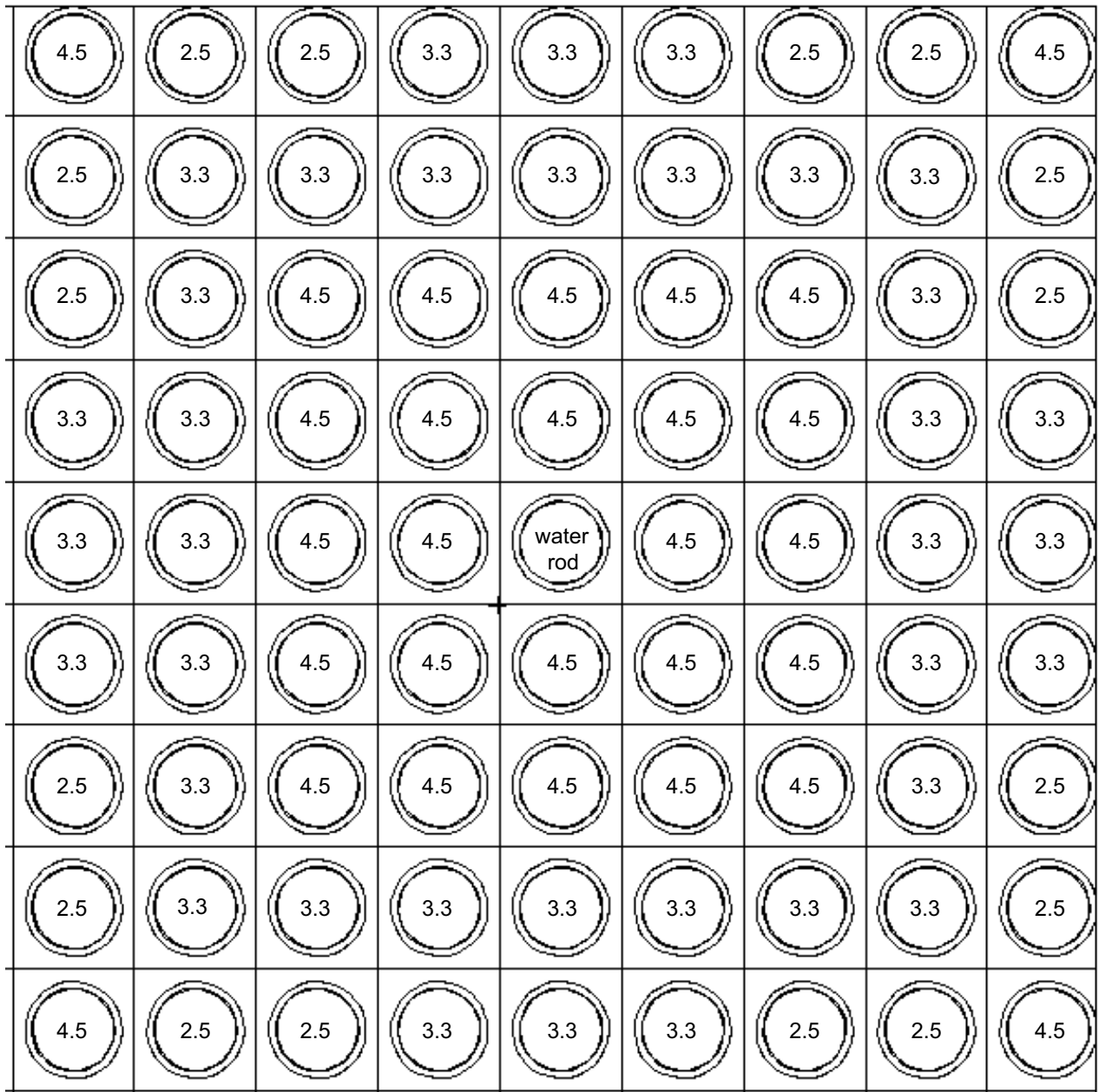


Figure 6.4-3 - Multiple Pin Enrichment Pattern 3 for the Big Rock Point GE 9x9 Fuel Assembly

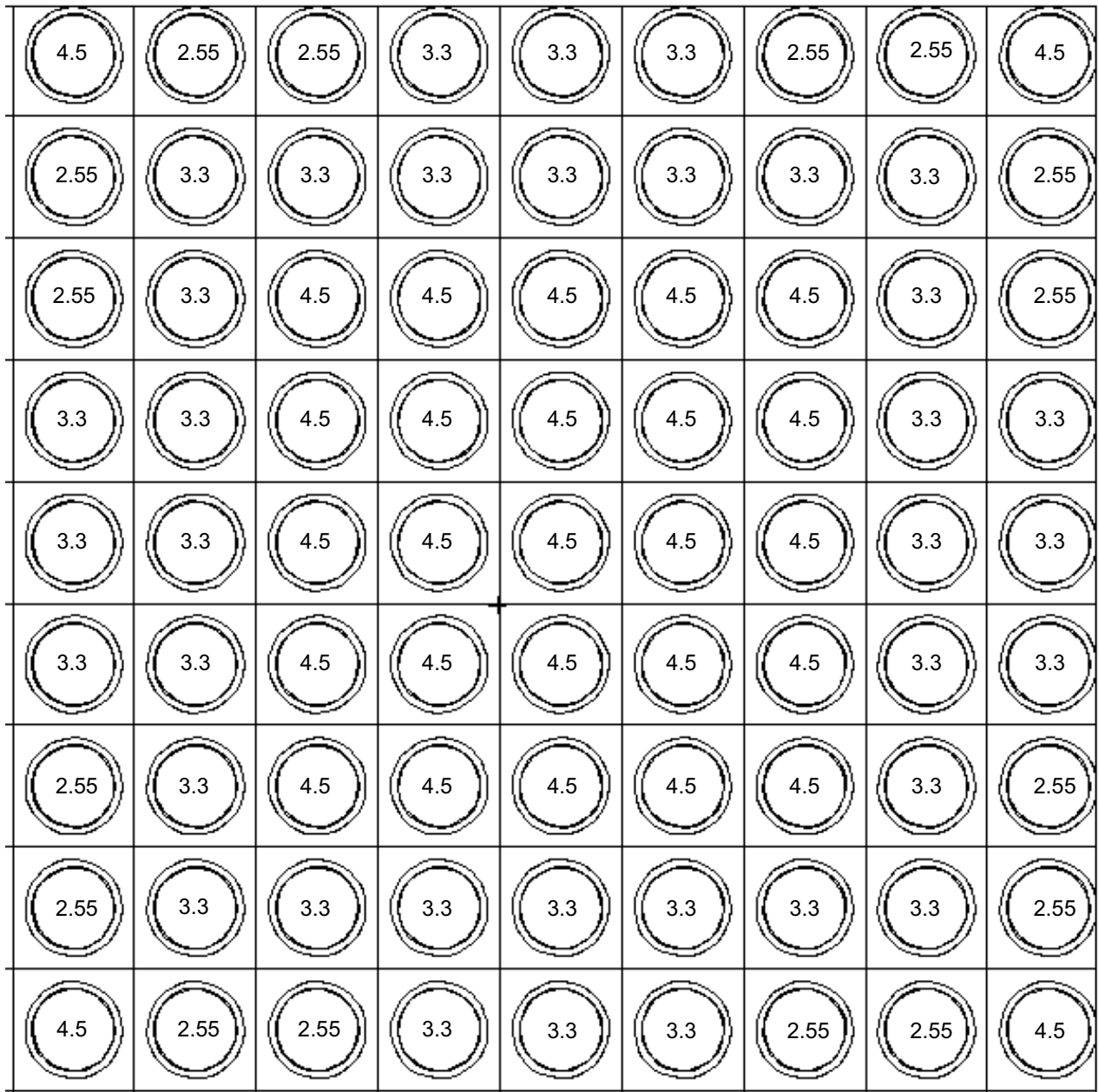


Figure 6.4-4 - Multiple Pin Enrichment Pattern 4 for the Big Rock Point Siemens 9x9 Fuel Assembly

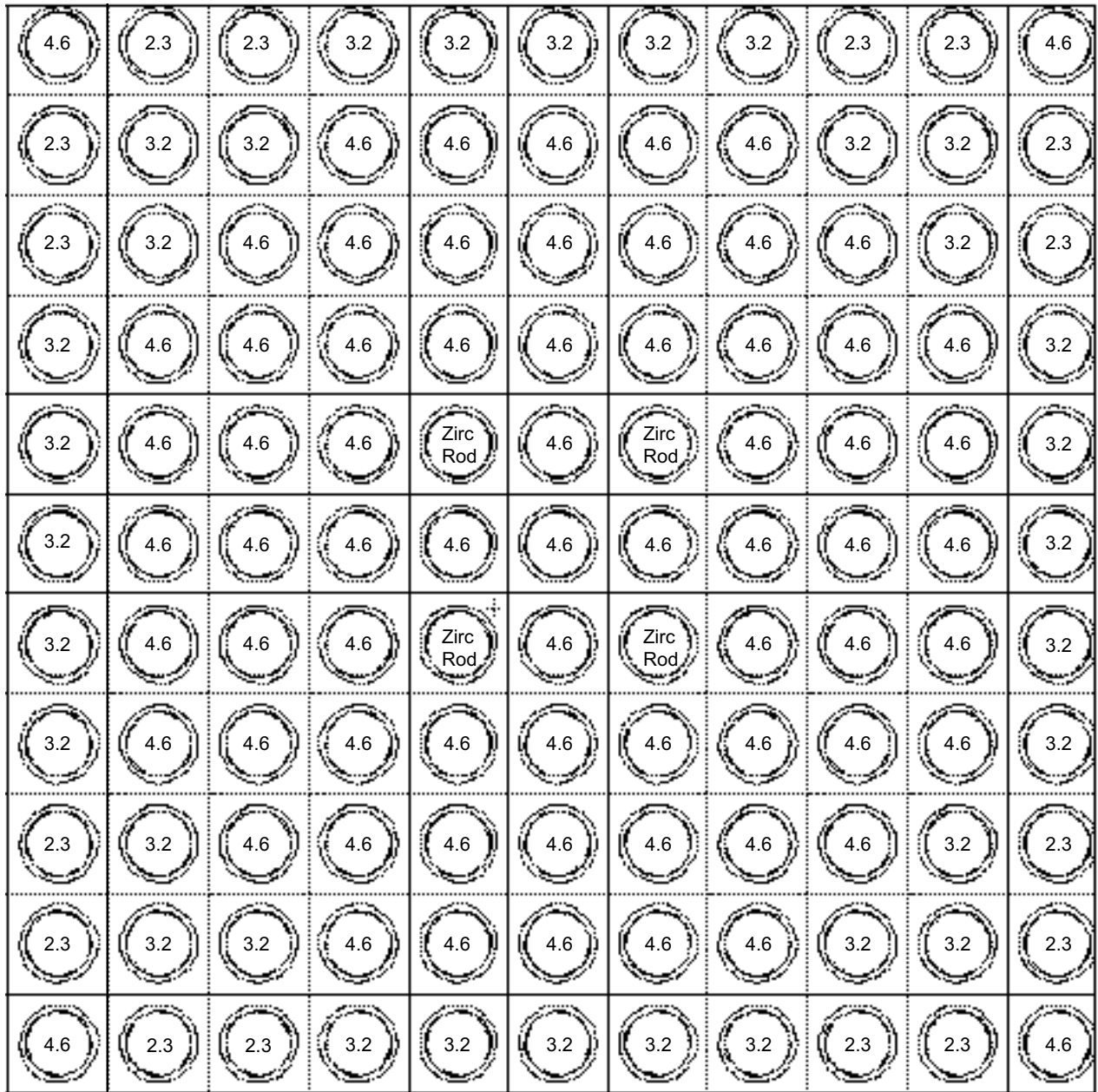


Figure 6.4-5 - Multiple Pin Enrichment Pattern 1 for the Big Rock Point Siemens 11x11 Fuel Assembly

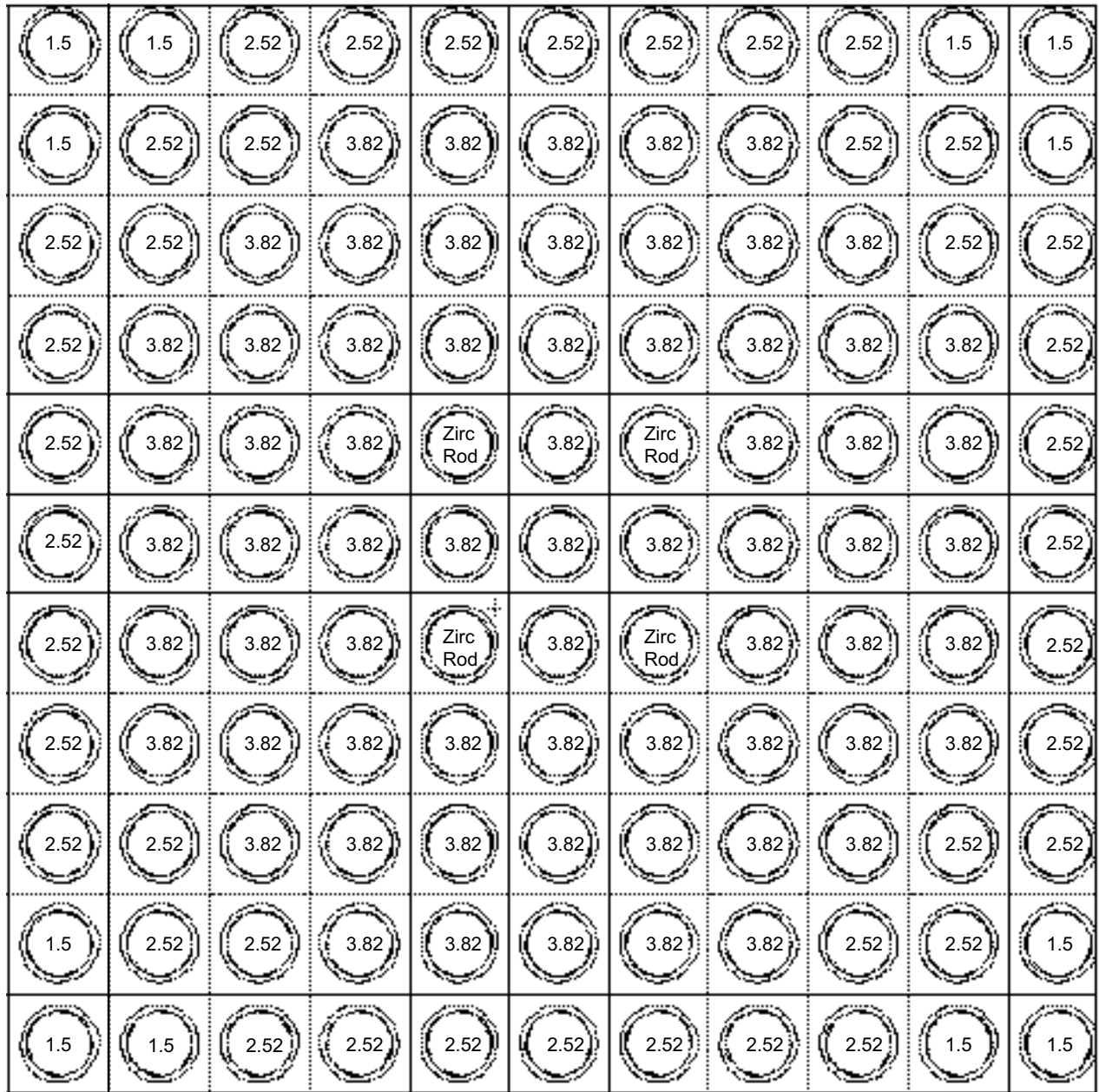


Figure 6.4-6 - Multiple Pin Enrichment Pattern 2 for the Big Rock Point Siemens 11x11 Fuel Assembly

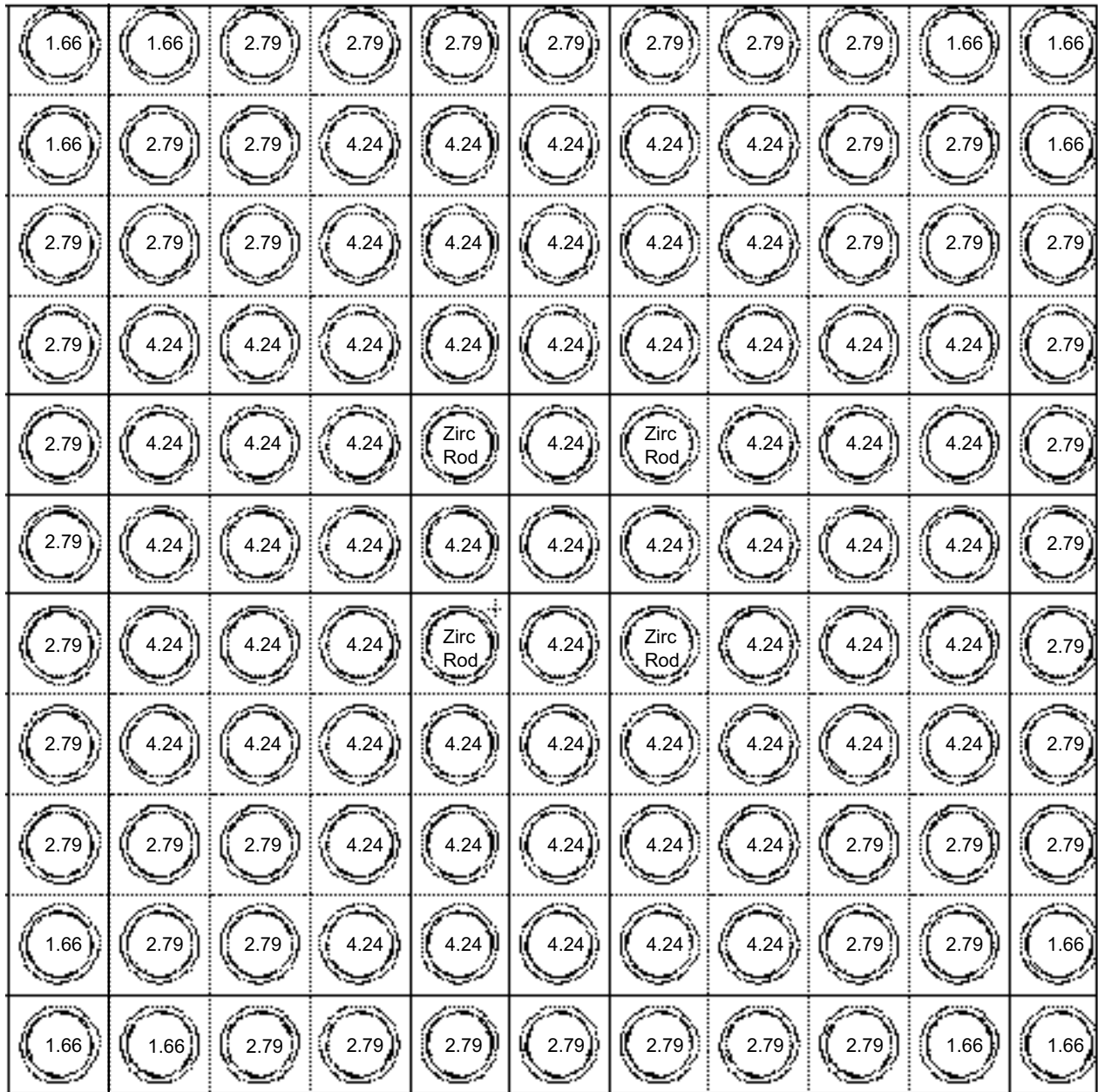


Figure 6.4-7 - Multiple Pin Enrichment Pattern 3 for the Big Rock Point Siemens 11x11 Fuel Assembly

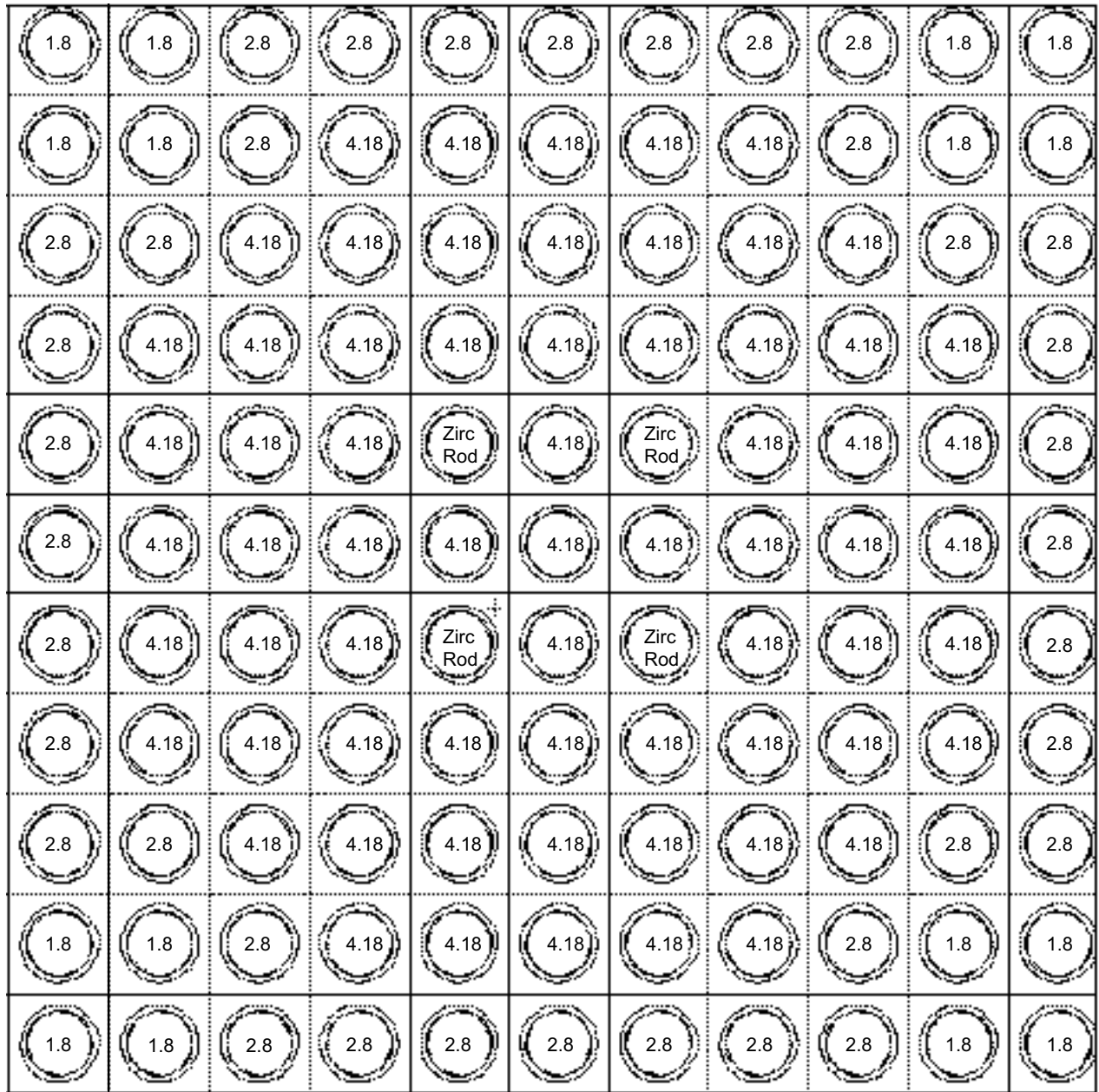


Figure 6.4-8 - Multiple Pin Enrichment Pattern 4 for the Big Rock Point Siemens 11x11 Fuel Assembly

This page intentionally left blank.

6.5 Criticality Benchmark Experiments

The criticality calculation method is verified by comparison with critical experiment data that is sufficiently diverse to establish that the method bias and uncertainty are applicable to canister conditions considered in the criticality analysis of the FuelSolutions™ Transportation System. A set of 49 critical experiments is analyzed using MCNP to demonstrate its applicability to criticality analysis and to establish a set of USLs that define acceptance criteria. Benchmark experiments are selected with compositions, configurations, and nuclear characteristics that are comparable to those encountered in a FuelSolutions™ W74 canister loaded with fuel as described in Table 6.1-1. The experiments analyzed are summarized in Table 6.5-1. The critical experiments are described in detail in NUREG/CR-6361.⁸

Forty-nine critical benchmark cases are selected for their similarity to the FuelSolutions™ system casks and canisters. The cases include different combinations of fixed neutron absorber materials and reflector wall materials. Sixteen of the benchmark experiments have BORAL[®], borated stainless steel, or unborated stainless steel absorbing plates with no reflecting walls. Twenty-five of the cases have steel or depleted uranium reflecting walls with no neutron-absorbing panels. Five of the cases have both neutron-absorbing panels and reflecting walls. Three of the cases are simple lattices without neutron-absorbing panels or reflectors. The fuel pins in the experiments have enrichments of 2.35, 4.31, or 4.74 w/o ²³⁵U. A comparison of FuelSolutions™ system attributes with these experiments demonstrates the wide range of applicability of the criticality calculation method.

A set of USLs is determined using the results from the 49 critical experiments and USL Method 1, Confidence Band with Administrative Margin, described in Section 4 of NUREG/CR-6361. The USL Method 1 applies a statistical calculation of the method bias and its uncertainty plus an administrative margin (0.05 Δk) to a linear fit of the critical experiment benchmark data. The USLs are determined as a function of the critical experiment system parameters; enrichment, water-to-fuel ratio, hydrogen-to-²³⁵U ratio, and pin pitch.

The following equation is determined for the USL as a function of enrichment:

$$\text{USL} = 0.94082 + (9.4676 \times 10^{-4})x \quad \text{for all } x$$

The applicable range for enrichment is $2.35 \leq x \leq 5.00$.

The following equation is determined for the USL as a function of water-to-fuel ratio:

$$\text{USL} = 0.94272 + (5.8009 \times 10^{-4})x \quad \text{for all } x$$

The applicable range for water-to-fuel ratio is $1.44 \leq x \leq 3.88$.

The following equation is determined for the USL as a function of hydrogen-to-²³⁵U:

$$\text{USL} = 0.94458 - (3.6041 \times 10^{-6})x \quad \text{for all } x$$

The applicable range for hydrogen-to-²³⁵U ratio is $80.895 \leq x \leq 398.7$.

⁸ NUREG/CR-6361, *Criticality Benchmark Guide for Light-Water-Reactor Fuel in Transportation and Storage Packages*, ORNL/TM-13211, March 1997.

The following equation is determined for the USL as a function of pin pitch:

$$\text{USL} = 0.93854 + (2.9355 \times 10^{-3})x \quad \text{for } x < 2.412$$

$$\text{USL} = 0.94562 \quad \text{for } x \geq 2.412$$

The applicable range for pin pitch is $1.24 \leq x \leq 2.54$.

The preceding equations are used to determine a minimum USL for each fuel assembly type considered for use with the FuelSolutions™ W74 canister (see Table 6.2-1). USL values are calculated as a function of the various parameters presented above for each candidate fuel design. The k_{eff} for a canister containing each specific fuel assembly type is compared to the minimum USL established for that fuel assembly to assure subcriticality. The following equation is used to develop the k_{eff} for the transport of fuel in the FuelSolutions™ canister:

$$k_{\text{eff}} = k_{\text{case}} + 2\sigma_{k_{\text{eff}}}$$

where:

k_{case} = MCNP k_{eff} for a particular case of interest

$\sigma_{k_{\text{eff}}}$ = uncertainty in calculated MCNP k_{eff} for a particular case of interest

Table 6.5-1 - Benchmark Critical Experiments (2 Pages)

Name	K _{eff}	Sigma	Enrich	Pitch	H ₂ O/Fuel	H/X	Plate	B (w/o)	Plate thick	Wall	Wall thick
nse71sq	0.99903	0.00110	4.74	1.26	1.823	110	-	-	-	-	-
nse71w1	0.99632	0.00115	4.74	1.26	1.823	110	-	-	-	-	-
nse71w2	0.99554	0.00108	4.74	1.26	1.823	110	-	-	-	-	-
p2438ba	1.00049	0.00096	2.35	2.032	2.918	398.7	B	28.7	0.713	-	-
p2438ss	0.99822	0.00092	2.35	2.032	2.918	398.7	SS	-	0.485	-	-
p2615ba	1.00007	0.00096	4.31	2.54	3.883	256.1	B	28.7	0.713	-	-
p2615ss	0.99893	0.00105	4.31	2.54	3.883	256.1	SS	-	0.485	-	-
p3314ba	0.99853	0.0011	4.31	1.892	1.6	105.4	B	28.7	0.713	-	-
p3314bc	1.00053	0.00112	4.31	1.892	1.6	105.4	B	31.9	0.231	-	-
p3314bs1	0.9967	0.001	2.35	1.684	1.6	218.6	SS	1.1	0.298	-	-
p3314bs2	0.9936	0.001	2.35	1.684	1.6	218.6	SS	1.6	0.298	-	-
p3314bs3	0.99733	0.00107	4.31	1.892	1.6	105.4	SS	1.1	0.298	-	-
p3314bs4	1.00069	0.00109	4.31	1.892	1.6	105.4	SS	1.6	0.298	-	-
p3314ss1	0.99508	0.00104	4.31	1.892	1.6	105.4	SS	-	0.302	-	-
p3314ss2	1.00132	0.00111	4.31	1.892	1.6	105.4	SS	-	0.302	-	-
p3314ss3	0.99387	0.00105	4.31	1.892	1.6	105.4	SS	-	0.485	-	-
p3314ss4	0.99837	0.00103	4.31	1.892	1.6	105.4	SS	-	0.485	-	-
p3314ss5	0.99454	0.00097	2.35	1.684	1.6	218.6	SS	-	0.302	-	-
p3314ss6	0.99928	0.00116	4.31	1.892	1.6	105.4	SS	-	0.302	-	-
p3602bb	0.99809	0.0011	4.31	1.892	1.6	105.4	B	30.4	0.292	SS	1.96
p3602bs1	1.00125	0.00096	2.35	1.684	1.6	218.6	SS	1.1	0.298	SS	1.32
p3602bs2	1.00064	0.00111	4.31	1.892	1.6	105.4	SS	1.1	0.298	SS	1.96
p3602n11	0.99677	0.00094	2.35	1.684	1.6	218.6	-	-	-	SS	-
p3602n12	0.99822	0.00094	2.35	1.684	1.6	218.6	-	-	-	SS	0.66
p3602n13	0.99767	0.00096	2.35	1.684	1.6	218.6	-	-	-	SS	1.68
p3602n14	0.99563	0.00098	2.35	1.684	1.6	218.6	-	-	-	SS	3.91
p3602n21	0.99907	0.00091	2.35	2.032	2.918	398.7	-	-	-	SS	2.62
p3602n22	0.99895	0.00091	2.35	2.032	2.918	398.7	-	-	-	SS	0.66
p3602n31	1.00072	0.00106	4.31	1.892	1.6	105.4	-	-	-	SS	0
p3602n32	1.00028	0.00112	4.31	1.892	1.6	105.4	-	-	-	SS	0.66
p3602n33	1.00361	0.00117	4.31	1.892	1.6	105.4	-	-	-	SS	1.32
p3602n34	1.00233	0.00113	4.31	1.892	1.6	105.4	-	-	-	SS	1.96
p3602n35	1.00068	0.0011	4.31	1.892	1.6	105.4	-	-	-	SS	2.62
p3602n36	0.99925	0.00102	4.31	1.892	1.6	105.4	-	-	-	SS	5.41

Table 6.5-1 - Benchmark Critical Experiments (2 Pages)

Name	K_{eff}	Sigma	Enrich	Pitch	H ₂ O/Fuel	H/X	Plate	B (w/o)	Plate thick	Wall	Wall thick
p3602n41	1.00211	0.00103	4.31	2.54	3.883	256.1	-	-	-	SS	-
p3602n42	1.0016	0.00104	4.31	2.54	3.883	256.1	-	-	-	SS	1.32
p3602n43	1.00014	0.00107	4.31	2.54	3.883	256.1	-	-	-	SS	2.62
p3602ss1	1.00077	0.00101	2.35	1.684	1.6	218.6	SS	-	0.302	SS	1.32
p3602ss2	0.99815	0.0011	4.31	1.892	1.6	105.4	SS	-	0.302	SS	1.96
p2827u1	0.9955	0.00086	2.35	2.032	2.918	398.7	-	-	-	U	-
p2827u2	0.99426	0.00091	2.35	2.032	2.918	398.7	-	-	-	U	1.96
p2827u3	0.99946	0.00099	4.31	2.54	3.883	256.1	-	-	-	U	-
p2827u4	0.99939	0.00101	4.31	2.54	3.883	256.1	-	-	-	U	1.96
p3926u1	0.99408	0.00091	2.35	1.684	1.6	218.6	-	-	-	U	-
p3926u2	0.99664	0.00094	2.35	1.684	1.6	218.6	-	-	-	U	1.32
p3926u3	0.99786	0.00086	2.35	1.684	1.6	218.6	-	-	-	U	3.91
p3926u4	0.99799	0.00104	4.31	1.892	1.6	105.4	-	-	-	U	-
p3926u5	0.9994	0.00102	4.31	1.892	1.6	105.4	-	-	-	U	1.96
p3926u6	0.99896	0.0011	4.31	1.892	1.6	105.4	-	-	-	U	3.28

6.6 Supplemental Analyses

6.6.1 Big Rock Point Mixed-Oxide Fuel Assembly Criticality Evaluation

Criticality analyses are performed to show that all existing BRP mixed-oxide (MOX) fuel assemblies are qualified for loading into the FuelSolutions™ W74 canister. Specific analyses are performed for each existing MOX fuel assembly configuration. The analyses show that every existing MOX assembly is much less reactive than the design basis 4.1% enriched UO₂ fueled assembly, and that a W74 canister loaded with any of these assembly types meets all 10CFR71 criticality requirements by a wide margin.

6.6.1.1 MOX Fuel Criticality Analyses

There are three existing types of BRP MOX assemblies: the J2 (9x9) assembly, the DA (11x11) assembly, and the G-Pu (11x11) assembly. These three BRP MOX fuel assembly designs are illustrated in Figure 6.6-1 through Figure 6.6-3. The three figures illustrate the different types of rods, describe their fuel material composition, and give the locations of each fuel rod type within the assembly array. The locations of any dummy rods or water rods are specifically indicated.

In addition to the three MOX fuel assembly designs, two UO₂ fueled assemblies have had two of their fuel rods replaced by MOX fuel rods (assemblies E65 and E72). The configuration for both of these assemblies is shown in Figure 6.6-4.

The geometric dimensions of the 9x9 and 11x11 MOX fuel assemblies are almost identical to those presented in Table 6.1-1 for the design basis UO₂ 9x9 and 11x11 assemblies. One exception is that the J2 9x9 MOX assembly has a fuel pellet diameter of 0.4715 inch, as opposed to 0.471 inch (the diameter shown for 9x9 fuel in Table 6.1-1). It is noted that some J2 assemblies have a pellet diameter of 0.4515 inch and a clad inner diameter of 0.4626 inch, as opposed to the J2 assembly values of 0.4715 and 0.4825, respectively. Thus, 0.02 inch of cladding replaces 0.02 inch of fuel. Replacing fuel with cladding causes reactivity to decrease, so these assemblies are bounded by the J2 assembly configuration modeled in the criticality analyses. Another exception is that the two MOX fuel rods inserted into assemblies E65 and E72 may contain three types of fuel pellets: solid (cylindrical) pellets, or annular fuel pellets with a central void region diameter of either 0.1 or 0.2 inches. The fuel pellet outer diameter and cladding dimensions for the pairs of MOX fuel rods are the same as those of a standard 9x9 BRP assembly (as shown in Table 6.1-1).

The primary difference between the MOX assemblies and the design basis UO₂ assemblies is the fuel material compositions within the rods. Each of the three MOX fuel assembly types has several different types of fuel rods in the assembly array, and each contains a different fuel material composition. All three MOX fuel types contain a number of MOX fuel rods in the center of the assembly array, and UO₂ fuel rods of two to three different enrichment levels around the edge of the assembly array, with the lower enriched UO₂ rods closest to the assembly edge. Each of the three MOX assembly types has a different set of plutonium and uranium isotope concentrations in its MOX fuel rods. The DA assemblies have two different types of MOX fuel rod, each with its own set of heavy metal isotope concentrations.

The three MOX fuel assembly types also contain dummy (solid zircaloy) fuel pins in locations different from those of the design basis UO_2 assemblies. The diameter of these dummy rods is the same as the fuel rod diameter. Also, the DA 11x11 MOX fuel assembly has four “water rods” near the center of the assembly array. These rods are modeled as hollow, water-filled zircaloy rods with the same clad O.D. and I.D. as the fuel rods.

The UO_2 fuel material description for each of the enrichment levels that occur for UO_2 rods within the MOX fuel assemblies is given in Table 6.6-1. The material description for each of the four MOX fuel rod types shown in Figure 6.6-1 through Figure 6.6-3 is given in Table 6.6-2. The partial densities (in a/b-cm) are given for each uranium and plutonium isotope. BRP MOX fuel assembly data give the plutonium isotope distribution (i.e., the percentage of the total Pu in the form of each Pu isotope) for each of the MOX fuel rod types. The isotope partial densities shown in Table 6.6-2 are calculated based on this data, the fuel rod plutonium weight percentages given in Figure 6.6-1 through Figure 6.6-3, and a conservative assumed fuel material density of 10.586 g/cc (96.5% of UO_2 theoretical density). The uranium isotope densities given for the UO_2 fuel rods in Table 6.6-1 are calculated based on this same fuel material density and the applicable UO_2 fuel rod enrichment level.

Figure 6.6-4 shows total plutonium mass per rod, as opposed to a plutonium weight percentage. The Pu in the rods is very conservatively assumed to consist entirely of ^{241}Pu , the most reactive Pu isotope. This overall plutonium mass applies for all three fuel pellet types that occur in the E65 and E72 assembly MOX rods, even though the fuel material volume varies between the three cases. The plutonium concentration is increased for the annular pellet cases, so that the overall plutonium mass is retained. An upper bound metal-oxide density of 95% of UO_2 theoretical is modeled for the E65 and E72 MOX rods. The material composition for each of the E65 and E72 MOX fuel pellet types is shown in the right three columns of Table 6.6-2.

The fuel material descriptions given for the MOX fuel assemblies in Table 6.6-1 and Table 6.6-2 correspond to fresh MOX fuel. No credit is taken for MOX fuel burnup. However, credit is taken in the MOX fuel criticality analyses for ^{241}Pu decay. It is assumed that exactly half of the ^{241}Pu has decayed (into ^{241}Am). Since the half-life of ^{241}Pu is approximately 15 years, this assumption corresponds to an assumed MOX fuel assembly cooling time of approximately 15 years. All MOX fuel assemblies are at least 15 years old (as specified in Chapter 12), so the above ^{241}Pu decay assumption is valid and conservative. Table 6.6-2 therefore shows a ^{241}Pu density that is half of the initial ^{241}Pu density.

Although ^{241}Pu decays into ^{241}Am , an absorber nuclide, the buildup of ^{241}Am (and the associated neutron absorption) is conservatively neglected in the criticality analyses. No ^{241}Am density is modeled. As discussed above, all the Pu in the two inserted MOX fuel rods shown in Figure 6.6-4 is assumed to be ^{241}Pu . It is conservatively assumed that no ^{241}Pu decay occurs in these rods.

The assembly geometry data given in Table 6.1-1, the fuel material data given in Table 6.6-1 and Table 6.6-2, and the fuel rod array descriptions given in Figure 6.6-1 through Figure 6.6-4 are sufficient to completely describe the BRP MOX fuel assemblies with respect to the criticality models. (The zircaloy material description given in Section 6.3 of this SAR is assumed for BRP MOX fuel.)

The actual design basis G-Pu MOX assembly does not have fuel rods in any of the four array corner positions. However, there are several modified G-Pu MOX assemblies that do contain additional UO₂ fuel rods in some or all of the corner locations. As shown in Section 6.6.2.1 (for UO₂ fueled assemblies), adding fuel rods to the corners increases assembly reactivity. Thus, these modified assemblies are more reactive than the design basis G-Pu assembly. The criticality model of the G-Pu MOX fuel assembly includes four 4.6% enriched UO₂ fuel rods in each of the four corners of the assembly array. As shown in Figure 6.6-1 through Figure 6.6-4, this is the maximum UO₂ fuel rod enrichment for all MOX fuel. With four maximum enrichment UO₂ fuel rods in the corners of the assembly array, the criticality model of the G-Pu MOX assembly bounds all of the modified G-Pu assemblies. Figure 6.6-3 includes these four corner fuel rods (i.e., the figure corresponds to the assembly modeled in the criticality analyses, as opposed to the actual design basis assembly).

Some of the fuel rods in the J2 and G-Pu MOX fuel assembly arrays contain a gadolinium burnable poison. These poisoned fuel rods are illustrated and described in Figure 6.6-1 through Figure 6.6-4. However, as with the UO₂ assembly criticality analyses (see Section 6.3.1), no credit is taken for this absorber material in the MOX fuel criticality analyses. In the analyses, these rods are modeled as pure UO₂ fuel rods at the ²³⁵U enrichment level shown for the poisoned rods in Figure 6.6-1 through Figure 6.6-4.

There are also four “partial” BRP MOX fuel assemblies that have one or more fuel rods missing from locations other than the four corners of the assembly array (two J2 assemblies and two G-Pu assemblies). Fuel rods missing from non-corner locations may cause the assembly reactivity to increase, as discussed in Section 6.6.2.2. Thus, these four partial MOX fuel assemblies are potentially more reactive than their design basis assemblies. For this reason, separate, specific criticality analyses are performed on these four partial MOX fuel assembly configurations.

The two partial J2 MOX fuel assembly configurations (D72 and D73) are illustrated in Figure 6.6-5 and Figure 6.6-6. The two partial G-Pu MOX fuel assembly configurations (G01 and G02) are illustrated in Figure 6.6-7 and Figure 6.6-8. These partial MOX fuel assembly configurations are identical to their corresponding design basis MOX fuel assembly configurations, except that fuel rods are removed from certain locations in the rod array. The only other difference is that zircaloy dummy rods are placed in some additional locations within the G-Pu assembly array, as illustrated in Figure 6.6-8. Thus, very minor changes to the criticality models are required for the partial MOX assembly analyses.

Specific criticality analyses are performed for each of the three design basis MOX fuel assembly types, and for each of the four partial MOX fuel assembly configurations. Three criticality analyses, one for each of the three MOX fuel pellet configurations discussed earlier, are performed for the E65 and E71 assembly configuration, which consists of UO₂ 9x9 assemblies with two inserted MOX fuel rods. All existing Big Rock Point MOX fuel assemblies are identical to one of these ten MOX assembly configurations that are specifically analyzed. The only exceptions to this are G-Pu assemblies that have either no fuel rod or a lower enriched UO₂ fuel rod in one or more of the corner locations where the G-Pu assembly criticality model has maximum enrichment UO₂ fuel rods. In this case, the modeled G-Pu assembly configuration is clearly bounding. Other specific G-Pu assemblies have zircaloy dummy pins in place of fuel rods at some array locations. Replacing fuel rods with dummy pins, however, always reduces

assembly reactivity. Finally, some specific J2 and G-Pu assemblies (including the “D72” and “D73” assemblies) have UO_2 fuel rods in certain non-corner array locations that have a lower enrichment level than that which exists (for that array location) in the analyzed (design basis) configurations (as shown in Figure 6.6-1, Figure 6.6-3, Figure 6.6-5, and Figure 6.6-6). Since lowering the enrichment of a given fuel rod in the assembly array will clearly reduce assembly reactivity, these assemblies are also clearly bounded by the analyzed G-Pu assembly configuration. Therefore, analyzing the ten assembly configurations described above is sufficient to qualify all existing BRP MOX fuel for loading into the W74 canister.

The MCNP-4a code is used for the MOX fuel assembly criticality analyses, with the bounding criticality model described in Sections 6.3 and 6.1. The W74 canister geometry models described in Sections 6.3 and 6.1 are used for the MOX fuel analyses presented here. In each of the analyses, a W74 canister is modeled that is completely filled with the MOX fuel assembly configuration being analyzed. An infinite cask array under HAC is modeled. The worst-case set of assembly and guide sleeve positions is modeled along with the worst-case set of dimensions and material thicknesses (i.e., worst-case tolerances). Full water density (1.0 g/cc) is assumed for the canister interior. This canister and cask configuration is shown by analysis to be bounding for all possible transport conditions. The 11x11 and 9x9 assembly models are used to perform the DA, the G-Pu, and the J2 MOX fuel assembly analyses, respectively. The only change made to the UO_2 fuel assembly models is in the fuel material descriptions. All geometric features of the model are left unchanged, except the fuel pellet diameter of the J2 9x9 MOX assembly, which is increased from 0.471 inch to 0.4715 inch. The material descriptions in Section 6.3.2 are used in the MOX fuel criticality models. The fuel material descriptions for MOX fuel are given in Table 6.6-1 and Table 6.6-2.

Almost all modeling assumptions for the UO_2 BRP assembly criticality analyses in Section 6.3.1 are made for the MOX fuel analyses as well. The only exception is the assumption for the assembly average enrichment in the UO_2 fuel analyses. The UO_2 fuel analyses assume a single average enrichment for all of the fuel rods in the assembly array. The MOX fuel criticality analyses, however, explicitly model the fuel material properties of each individual fuel rod within the assembly array (as described in Figure 6.6-1 through Figure 6.6-3). The MOX fuel rods, as well as the different types of UO_2 fuel rods (each with a different uranium enrichment level), are explicitly modeled.

The results of the specific criticality analyses for the three intact MOX fuel designs and the four partial MOX assembly configurations are presented in Table 6.6-3. Table 6.6-3 also presents the criticality results for the two BRP assemblies that contain two inserted MOX rods, with separate results shown for each of the three MOX fuel pellet geometries present in the inserted MOX rods. Criticality analysis results for W74 canisters filled with 4.1% enriched intact 9x9 and 11x11 UO_2 BRP fuel assemblies are also given for comparison. The two UO_2 fuel assemblies presented in Table 6.6-3 correspond to the most reactive 9x9 and 11x11 assemblies presented in Table 6.4-7 (i.e., the GE 9x9 assembly with one water pin, and the Siemens 11x11 assembly with 121 fuel rods). The MOX fuel USL value is discussed in Section 6.6.1.2. The UO_2 assembly USLs are taken from Table 6.4-7.

The UO_2 assembly configurations modeled in the 9x9 and 11x11 UO_2 assembly cases shown in Table 6.6-3 are identical to the corresponding intact UO_2 BRP assembly configurations described in Section 6.2. The UO_2 assembly analyses presented in Table 6.6-3, however, model a

different W74 basket configuration than the analyses described in Section 6.3 (results of which are presented in Table 6.4-7). As discussed in Section 6.3.1.3, there are differences between the basket configuration modeled in the intact UO₂ assembly analyses and in the MOX assembly analyses. Most significantly, the UO₂ assembly analyses model a poison sheet boron density fraction of only 1% (a conservative value), whereas the MOX analyses model the correct density fraction of 1.25%. The conservative basket geometry modeled in the UO₂ analyses is significantly more reactive than the more accurate basket geometry modeled in the MOX analyses. To provide an accurate reactivity comparison between the MOX fuel and the bounding UO₂ fuel, the bounding case analyses for the two UO₂ assembly types (9x9 and 11x11) are re-performed with the same basket configuration that is assumed in the MOX analyses.

The results of the UO₂ assembly analyses performed with the MOX analysis basket configuration are presented in Table 6.6-3. A comparison of the two UO₂ assembly results shown in Table 6.6-3 with the corresponding results in Table 6.4-7 shows that the conservative basket geometry modeled in the UO₂ assembly analyses (including the 1% poison sheet boron density) is significantly more reactive than the more accurate basket geometry modeled in the MOX assembly analyses (~1.5% in k_{eff}).

The MOX assembly analysis results show that the BRP MOX fuel assembly configurations are much less reactive than the design basis 4.1% UO₂ fueled BRP assemblies. The most reactive MOX fuel assembly configuration is the design basis G-Pu assembly, which has a final calculated k_{eff} value of ~0.883. This value is much lower than the final k_{eff} value of ~0.923 given in Table 6.6-3 for design basis (4.1% enriched, 11x11) UO₂ fuel. In addition, since the maximum calculated k_{eff} value for MOX fuel is ~6% less than the minimum USL value for MOX fuel, all existing MOX fuel is shown to meet the 10CFR71 criticality requirements by a wide margin.

The primary reason that the MOX fuel is so much less reactive than the design basis UO₂ fuel is the decay of ²⁴¹Pu, coupled with the long cooling time that exists for all BRP MOX fuel assemblies. After a cooling time of 15 years, half of the ²⁴¹Pu, the most reactive of the fissile nuclides present in the MOX fuel, decays into ²⁴¹Am, greatly decreasing MOX fuel assembly reactivity. If a MOX fuel assembly has an initial reactivity level that is similar to that of a design basis UO₂ fuel assembly, it will be significantly less reactive than a UO₂ fuel assembly after 15 years, due to the ²⁴¹Pu decay effect.

The two specific UO₂ fueled BRP assemblies that have two inserted MOX rods are much less reactive than design basis UO₂ BRP fuel because their assembly average enrichment level is much lower than the design basis value of 4.1%. The two inserted MOX fuel rods do not significantly affect the reactivity of those two assemblies.

An additional set of criticality analyses is performed to verify that a maximum canister interior moderator density produces the maximum reactivity level for MOX fuel, as it does for UO₂ fuel. The G-Pu MOX assembly criticality model was run at several canister interior water density levels. The 11x11 G-Pu assembly was selected for this analysis because it has a higher water-to-fuel volume ratio than the 9x9 MOX fuel assembly. The 11x11 assembly is therefore less under-moderated, and is more likely to become more reactive at lower moderator densities. The results of the canister interior moderator density analyses are shown in Table 6.6-4. The results show that, as with BRP UO₂ fuel, maximum reactivity occurs at maximum water density. Although it has a higher water-to-fuel volume ratio than the 9x9 assembly, the 11x11 MOX

assembly is still somewhat under-moderated at full water density, so maximum reactivity occurs at maximum water density.

The criticality analysis results verify that a W74 canister loaded with BRP UO₂ or MOX fuel meets the criticality requirements. Additional analyses also verify that canisters filled with mixtures of UO₂ and MOX fuel meet the criticality requirements. These additional analyses confirm that the MOX and UO₂ assemblies do not neutronically affect each other in a way that would increase canister reactivity.

Criticality analyses are performed for four mixed loading patterns of BRP MOX and UO₂ assemblies within the W74 canister. These patterns include checkerboard loading patterns, which maximize neutronic interaction between the MOX and UO₂ assemblies. The analyses show that combinations of MOX and UO₂ fuel within the W74 canister also meet the criticality requirements. As expected, the calculated k_{eff} values for mixtures of UO₂ and MOX fuel are ~0.91, which lies roughly halfway between the calculated k_{eff} value for UO₂ fuel (~0.923) and the calculated k_{eff} value for MOX fuel (~0.883). Thus, the results indicate that the UO₂ and MOX assemblies do not significantly affect each other's reactivity.

Also of note is the fact that the maximum final k_{eff} value for the FuelSolutions™ W74 canister loaded with design basis BRP UO₂ fuel (0.92308) is below the MOX fuel USL value of 0.94141, as well as the minimum UO₂ fuel USL value of 0.94286. Section 6.6.1.2 states that the lower of the two USL values, MOX or UO₂, is conservatively used if any MOX at all is present within the W74 canister. If a tiny amount of MOX were present, the calculated k_{eff} value for the canister would be very near the UO₂ fuel value of 0.92308. However, this calculated k_{eff} value would still be under the USL value even if the lower MOX fuel USL value of 0.94141 were applied. As more MOX is added to the system, the calculated k_{eff} value would decrease. Thus, even when the lowest USL value is used, any mixture of MOX and UO₂ fuel in the W74 canister meets the criticality requirements.

In conclusion, specific criticality analyses are performed on all existing BRP MOX fuel assembly configurations. These analyses explicitly show that all existing MOX fuel assemblies are significantly less reactive than the design basis UO₂ fueled assembly modeled in the criticality analyses described in Sections 6.3 and 6.1. The analyses also explicitly show that all MOX fuel assembly configurations meet 10CFR71 criticality requirements by a wide margin. Furthermore, the analyses show that any combination of MOX and UO₂ assemblies loaded into the W74 canister will meet the criticality requirements. Thus, all existing MOX assemblies and MOX/UO₂ combination assemblies are qualified for loading into the FuelSolutions™ W74 canister. With respect to criticality requirements, there are no restrictions on canister loading location for MOX fuel, or on the quantities of MOX and/or UO₂ BRP assemblies loaded into the canister.

A fuel assembly specification for BRP MOX fuel is given in Table 6.6-5. This table gives geometry specifications for each of the three BRP MOX fuel assembly types, and for the BRP UO₂ assemblies that contain two inserted MOX fuel rods (the E65 and E72 assemblies). This table also specifies the fuel material composition for each of the MOX assembly fuel rods, which is described in more detail in Figure 6.6-1 through Figure 6.6-3 and Table 6.6-2.

Table 6.6-5 also clarifies that the four specific J2 and G-Pu partial assembly configurations (shown in Figure 6.6-5 through Figure 6.6-8) are the only partial assembly configurations

covered by the criticality analyses. These partial assembly configurations are modeled with missing non-corner rods and are the only such MOX assembly configurations qualified for loading the W74 canister. All BRP MOX assemblies must meet the assembly geometry and fuel material specifications shown in Table 6.6-5 to qualify for loading in the W74 canister. All of the MOX fuel assemblies at Big Rock Point meet the specifications given in Table 6.6-5 and qualify for loading in the W74 canister.

6.6.1.2 MOX Fuel Criticality Benchmarks

A set of 24 MOX fuel critical experiments is analyzed with the MCNP code to verify the accuracy and applicability of the code for MOX fuel criticality analyses. Based on the MCNP calculated k_{eff} values for the 24 MOX fuel critical experiments, USL values are determined using the same NUREG/CR-6361 methodology that is used for UO₂ fuel, as described in Section 6.5.

As with the UO₂ fuel benchmark calculations, USLs are calculated as a function of assembly pin pitch, water-to-fuel volume ratio, enrichment, and hydrogen-to-²³⁵U ratio. For MOX fuel, the “enrichment” is more generally defined as the fissile material percentage, which is the percentage of the overall heavy metal mass in the form of fissile material. Based on this definition, the fissile material percentage is simply the ²³⁵U enrichment for pure UO₂ fuel. For MOX fuel, the fissile material percentage includes the masses of the fissile plutonium nuclides, ²³⁹Pu and ²⁴¹Pu. Thus, for MOX fuel, the USL is calculated as a function of fissile material percentage, as opposed to ²³⁵U enrichment. Similarly, for MOX fuel, the hydrogen-to-²³⁵U ratio is generalized as the hydrogen-to-fissile nuclide ratio.

The set of MOX fuel experiments consists of regular square arrays of MOX fuel rods with full water reflection. The experiments cover a wide range of pin pitch values. Due to the range of pin pitches, the experiments also cover a wide range of water-to-fuel ratio and hydrogen-to-fissile nuclide ratio values. In addition, the experiments cover a very wide range of fissile material percentages (from roughly 2.5% to over 20%). The fissile material is mostly plutonium for all of the experiments.

The 24 MOX fuel critical experiments are described in Table 6.6-6. For each experiment, the value for each of the four physical parameters described above is listed along with the MCNP calculated k_{eff} value for that experiment. The statistical error level (1σ) is also listed for each experiment. Table 6.6-6 contains all the data necessary to perform the NUREG/CR-6361 USL calculations for each of the four system parameters. Table 6.6-6 also lists a fifth physical parameter, the percentage of fissile material that is plutonium (as opposed to uranium), for each MOX fuel experiment. The use of this parameter is discussed below.

USLs are calculated as a function of each of the four physical parameters described previously, based on the 24 MOX fuel critical experiments. USLs are also calculated for the combined set of MOX and UO₂ critical experiments. The set of 24 MOX fuel critical experiments described in Table 6.6-6, and the 49 UO₂ fuel critical experiments described in Table 6.5-1, are combined to form a mixed set of 73 critical experiments. As a function of each of the four system parameters, USLs are calculated for this combined set of 73 critical experiments. The USLs for the MOX fuel experiment case, the combined experiment case, and the UO₂ fuel experiment case are compared for each of the four parameters, and the lowest of the three USLs is selected.

This approach is used for several reasons. First, this approach increases the number of critical experiments that form the statistical basis of the calculated USLs. Second, this assures that the final MOX fuel USL values are based on a set of experiments that feature a wider range of physical features, reflector materials, and absorber materials. The set of UO₂ experiments covers a wider range of these features than do the MOX fuel experiments. Using this approach, the USL based on the combined set of experiments (which includes all the UO₂ experiments) would be used if it is lower than the MOX fuel only USL.

The MOX fuel USLs are to be applied to criticality analyses on systems that contain mixtures of MOX fuel and UO₂ fuel. The BRP MOX fuel assemblies contain mixtures of MOX and UO₂ fuel rods. As discussed in Section 6.6.1.1, loading the W74 canister with a mixture of MOX and UO₂ BRP assemblies is to be allowed. Therefore, if the USLs calculated for the set of UO₂ experiments or the combined set of MOX and UO₂ fuel experiments are lower than those calculated for the MOX fuel experiments only, then the UO₂ or combined set USL values clearly must be used if mixed loading is to be allowed. Otherwise, a situation would exist where the applied USL would suddenly increase just because a small amount of MOX fuel material was added to the system. If the MOX fuel only USL values are lower, however, then they are to be applied if any amount of MOX material is present in the system. Thus, the applied USL values would suddenly drop if even a small amount of MOX fuel were added to the system. This is clearly a conservative approach.

Finally, analyzing the combined set of MOX and UO₂ experiments allows one to evaluate whether or not there is any shift in the MCNP code bias between uranium and plutonium fuels. A fifth physical system parameter, the percentage of fissile material that is plutonium (as opposed to uranium) is defined. A fifth USL is calculated as a function of this parameter for the combined set of MOX and UO₂ fuel experiments. For all the UO₂ experiments, the value of this parameter is zero. For all of the MOX fuel experiments, the fissile material is primarily plutonium. The value of the plutonium percentage parameter varies from 73% to just over 97% in the MOX experiments (as shown in Table 6.6-6). Thus, this parameter does not vary over a wide range in either the set of UO₂ fuel experiments or the set of MOX fuel experiments. However, when the two sets of experiments are contrasted to each other, this parameter varies over a very wide range (from 0% to almost 100%). By calculating a USL function for this fifth parameter for the combined set of MOX and UO₂ fuel experiments, the variance in MCNP code bias between uranium and plutonium fuels will be adequately evaluated and treated.

The USL value functions calculated for each of the five system physical parameters are listed in Table 6.6-7. For each parameter, the USL function (which gives the USL value as a function of the parameter value) is listed. For each parameter, the USL function for the set of MOX experiments, and for the combined set of MOX and UO₂ experiments are shown. In addition, the USL function for the set of 49 UO₂ experiments (taken directly from Section 6.5) is also shown. For the fifth parameter, the percentage of fissile material that is plutonium, a USL function is only calculated for the combined set of UO₂ and MOX fuel experiments, for the reasons discussed above.

Final USL functions are determined for each parameter by selecting the case (UO₂ only, MOX only, or combined UO₂ plus MOX) that yields the lowest USL values. If different cases are lower over different sections of the parameter range, then the parameter range is divided into

those sections and the USL formula that yields the lowest USL values is applied over each section.

Using the above approach, five final USL equations could be determined, one for each of the studied physical parameters. In some cases, these equations would be sub-divided into several sections of the parameter range, with different linear formulas applying over each section. However, examination of the set of USL functions shown in Table 6.6-7 shows that a simpler final result can be obtained. In fact, a single final USL formula, which bounds all of the USL formulas shown in Table 6.6-7 can be determined. Fortunately, the nature of the USL formulas is such that a single bounding formula can be applied without a significant amount of unnecessary conservatism.

The MOX only case USLs for fissile material percentage and hydrogen-to-fissile nuclide ratio are approximately 0.942 over the entire parameter range. The MOX only case water-to-fuel volume ratio USL is 0.94141 at the minimum water-to-fuel volume ratio value of 1.195. The first simplifying step in this process is to establish a USL upper bound of 0.94141. This assumption does not result in a large amount of conservatism because the MOX only USLs for fissile material percentage and hydrogen-to-fissile nuclide ratio would never allow a USL value over 0.942 anyway (for any set of system parameter values). Examination of the Table 6.6-7 USL formulas show that the USLs for all parameters other than pin pitch are over 0.94141 over their entire parameter ranges for all three cases (MOX only, UO₂ only, and combined UO₂ plus MOX).

Examination of the pin pitch USL formulas show that the MOX only and MOX plus UO₂ USLs both reach a value of 0.94141 at a pin pitch of 1.32 cm. The USL values are under 0.94141 for pin pitch values under 1.32 cm. The pin pitch USL for the UO₂ only case is higher than the MOX only or combined case USLs for all pin pitch values of 1.32 or less (and it is higher than 0.94141 at a pin pitch of 1.32 cm). For pin pitch values under 1.32 cm, the MOX only pin pitch USL formula yields lower USL values than the mixed case pin pitch USL formula. Thus, the MOX only pin pitch formula applies (i.e., is lowest) for all pin pitch values under 1.32 cm. For pin pitch values over 1.32 cm, the upper bound USL value of 0.94141 applies.

The final result of this analysis is a single USL formula, shown below, that gives the USL value solely as a function of pin pitch. The pin pitch of the analyzed system is determined and entered into the formula to calculate a final, lower bound USL value to be used for the criticality calculation. USL values determined using any of the formulas shown in Table 6.6-7 are bounded by this single USL formula, regardless of the physical parameter values of the system, given that the system's physical parameters are within the ranges covered by the set of critical experiments.

$$\begin{aligned} \text{USL} &= 0.93372 + (5.8336 \times 10^{-3})x && \text{for } x < 1.32 \\ \text{USL} &= 0.94141 && \text{for } x \geq 1.32 \end{aligned}$$

where "x" is the pin pitch of the fuel assemblies, in cm.

As shown in Table 6.1-1, the minimum pin pitch for BRP fuel assemblies is 0.577 inches, or 1.466 cm. Since this is higher than 1.32 cm, the upper bound USL value of 0.94141 is to be applied for all BRP MOX fuel criticality analyses.

In order for the above USL value to be applicable, however, it must be verified that the physical parameters of the FuelSolutions™ W74 canister containing BRP MOX fuel lie within the ranges

covered by the combined set of MOX and UO₂ fuel critical experiments. Table 6.6-8 lists the minimum and maximum values that occur in the MOX and UO₂ critical experiments for each of the five analyzed physical system parameters. The table then lists the minimum and maximum values that occur for those parameters in the entire inventory of BRP MOX fuel assemblies. For the BRP MOX fuel assembly inventory, the minimum and maximum values calculated for the fissile material percentage, the hydrogen-to-fissile nuclide ratio, and the fissile plutonium percentage, are conservatively based on individual fuel rods, as opposed to assembly averages. Since the BRP MOX fuel assemblies contain different types of fuel rods with material properties that vary over wide ranges, the rod by rod approach yields a much wider range of parameter values than would an assembly average approach.

The Table 6.6-8 results show that, with respect to pin pitch, water-to-fuel volume ratio, and hydrogen-to-fissile atom ratio, the ranges covered by the BRP MOX fuel inventory are bounded by the ranges covered by both the set of UO₂ critical experiments and the set of MOX fuel critical experiments. The fraction of fissile material that is plutonium ranges from approximately 33% to 86% in the BRP MOX fuel rods. These values are bounded by those of the combined set of UO₂ and MOX fuel critical experiments (from which the plutonium percentage USL was calculated), which range from 0% to 97.3%.

The pairs of MOX fuel rods in the E65 and E72 assemblies have a fissile material percentage of 2.0%. The G-Pu MOX assemblies also contain a small number of 2.3% enriched UO₂ fuel rods near the corners of the assembly array. The DA assemblies contain a larger number of MOX fuel rods with a fissile material percentage of 2.33%. These enrichment / fissile percentage values are slightly less than the minimum value that occurs in either the MOX or the UO₂ critical experiments.

This is not an issue for the following reasons. NUREG/CR-6361 allows for USL formulas to be extrapolated for parameter values that lie “slightly” outside the range covered by the set of critical experiments. If a fissile percentage value of 2.0% is entered into any of the three fissile percentage USL formulas (MOX only, UO₂ only, or combined), the resulting USL values are all above the upper bound USL value of 0.94141. Thus, if such an extrapolation were applied, it would have no effect on the final applied USL value. Furthermore, these minimum fissile material percentages of 2.0–2.3% are based on worst-case individual fuel rods. The assembly average fissile material percentage is over 3.0% for all BRP MOX fuel, which is well within the range covered by either set of critical experiments (UO₂ or MOX). The MCNP code bias is more likely to be governed by the assembly average fissile material percentage. It should be noted that the USL formulas show a very weak dependence of code bias (i.e., USL value) on the fissile material percentage. Finally, the criticality analysis results presented in Table 6.6-3 show that the most reactive BRP MOX fuel assembly produces a final k_{eff} value that is under the USL value by over 6%. Thus, the criticality requirements are met by a very wide margin. A low fissile material percentage occurring in a few individual fuel rods within the assembly arrays will not cause the MCNP code bias or USL values to shift by more than 6% in k_{eff} .

The E65 and E72 assembly MOX rod pairs may also contain annular fuel pellets (with 0.1-inch or 0.2-inch central void zone diameters). The MOX fuel benchmark analyses (and associated USL values) are also applicable for these annular pellet configurations, because the central void zones cause the neutron spectrum within the fuel to soften (generally resulting in lower code bias values), and they cause the physical system parameter values to move closer to the centers of the

ranges covered by the benchmark configuration. All of the physical system parameters lie within the ranges covered by the benchmark analyses, for both solid-pellet and annular-pellet MOX rods, except for the fissile material percentage, which is slightly under the minimum covered value (as discussed in the preceding paragraphs).

In conclusion, the MCNP code is accurate and applicable for BRP MOX fuel criticality analyses. A single USL value of 0.94141 is applicable and bounding for all such analyses.

6.6.2 Big Rock Point Partial Fuel Assembly Criticality Evaluation

The primary criticality analyses described in Sections 6.3 and 6.1 model BRP 9x9 and 11x11 assemblies that have fuel rods in all four corners of the assembly array. Partial assemblies have fuel rods missing from the design basis assembly array. Most BRP partial assemblies have fuel rods missing from one or more of the four corner locations, with the rest of the assembly array being intact. A smaller number of BRP assemblies have fuel rods missing from locations other than the four corners.

Two sets of criticality analyses are performed for the two different types of BRP partial assemblies. The two sets of analyses use different approaches as described below in Sections 6.6.2.1 and 6.6.2.2.

As discussed in Section 6.3, the partial assembly analyses conservatively model a poison sheet boron concentration of 1.0 w/o (as opposed to the actual value of 1.25 w/o), and conservatively neglect the four guide tube poison sheets that face the support tubes. Thus, the partial assembly analyses use the same basket geometry model (shown in Figure 6.3-1) that is used for the intact BRP assembly analyses. As these conservative analysis assumptions cause canister reactivity to increase, the results of the partial assembly analyses are bounding and applicable for the actual W74 basket configuration.

As with the intact BRP assembly analyses, the models are based on accident conditions, an infinite array of transportation casks, the worst-case set of canister interior dimensions, tolerances, and assembly positions (as described in Section 6.3), and a maximum canister internal moderator density of 1.0 g/cc. These conditions are modeled because they yield the maximum reactivity for the W74 canister.

6.6.2.1 Partial Assemblies with Missing Corner Rods

The first set of analyses shows that BRP 9x9 and 11x11 assemblies with one or more fuel rods missing from the four corner locations are less reactive than the design basis BRP assemblies analyzed in the primary criticality analyses. Thus, the assembly average enrichment limit of 4.1% that applies for intact BRP assemblies will also apply for all BRP assemblies with fuel rods missing from any of the four corner locations.

Two criticality analyses are performed to verify that BRP assemblies with array corner rods missing are less reactive than design basis BRP assemblies: one for the 9x9 assembly, and one for the 11x11 assembly. In each analysis, a W74 canister completely loaded with the analyzed partial BRP assembly is modeled. In each case, all four corner fuel rods are removed from the assembly array. Other than the removed corner rods, these two models are identical to the bounding primary BRP 9x9 and 11x11 criticality models presented in Sections 6.3 and 6.1. As with the primary criticality analyses, the partial BRP assemblies in these analyses are modeled

with a uniform UO_2 fuel enrichment of 4.1%. Calculations show that a uniform enrichment assumption is conservative for all BRP fuel (i.e., for all fuel rod enrichment patterns that occur for BRP fuel).

The results of the missing corner rod criticality analyses are presented in Table 6.6-9. K_{eff} values are determined for BRP 9x9 and 11x11 assemblies with all four corner rods missing. Table 6.4-7 and Section 6.1 give calculated k_{eff} values of 0.93739 and 0.94007 for the design basis 9x9 and 11x11 assemblies, respectively. The calculated k_{eff} values for the assemblies with all four corner rods missing are significantly lower than the design basis assembly values.

It is assumed that since assemblies with all four corner rods removed are significantly less reactive than design basis assemblies with all four corner rods present, then assemblies with any number of the corner rods removed are also bounded by the design basis assembly. It is therefore concluded that the design basis BRP assemblies bound any BRP assemblies with any number of fuel rods missing from the corners of the rod array. The design basis assembly average enrichment limit of 4.1% applies for all such assemblies. Note that for partial assemblies, the assembly average enrichment is defined as the enrichment averaged over the rods that remain in the assembly.

Since the calculated k_{eff} values for the BRP assemblies with missing corner rods are lower than those of the design basis BRP assemblies, the assemblies with missing corner rods will meet all 10CFR71 criticality requirements, as long as the USL values applied to the analysis results do not change. This is the case, as discussed below.

The set of USL values (as discussed in Section 6.5) that apply to the design basis BRP assemblies also apply to the assemblies with corner rods missing. The assemblies with missing corner rods were analyzed at the same design basis enrichment level of 4.1%, so the enrichment USL value does not change. The assembly pin pitch does not change with the removal of corner rods, so the pin pitch USL value does not change. Also, since the rods are removed from the corners of the fuel rod array, the effective water-to-fuel ratio and H-to- ^{235}U ratio do not change. The effective H-to- ^{235}U ratio for the assembly is not affected unless rods are removed from internal array locations. Therefore, the USL values shown in Section 6.5 are applicable to the missing corner rod assemblies.

In conclusion, BRP 9x9 and 11x11 assemblies that have any number of rods missing from the four corner positions of the assembly array are less reactive than the design basis 9x9 and 11x11 assemblies analyzed in the primary criticality analyses. Thus, the maximum allowable BRP assembly enrichment level of 4.1% that was determined in the primary criticality analyses also applies for all BRP fuel with missing corner rods.

BRP assemblies that have fuel rods missing from non-corner locations of the rod array are treated by the analyses described in Section 6.6.2.2.

It should be noted that one of the design basis BRP 9x9 assembly configurations analyzed in the intact assembly criticality analyses presented in this SAR has a water hole (i.e., a missing fuel rod) in the center of the rod array. This is the array location where a single water hole will cause the maximum increase in assembly reactivity. The intact assembly analyses qualified this assembly configuration at the maximum intact assembly enrichment level of 4.1%. For this reason, a BRP 9x9 assembly may have up to one water hole, in any array location, and still be

classified as “intact.” BRP 9x9 assemblies with two or more non-corner water holes, or BRP 11x11 assemblies with any non-corner water holes, are classified as “partial” assemblies.

6.6.2.2 Partial Assemblies with Missing Array-Interior or Array-Edge Rods

As shown in Section 6.6.2.1, removing fuel rods from the corners of the BRP 9x9 and 11x11 assembly arrays reduces their reactivity level. A different situation exists when rods are removed from the interior or sides of the assembly arrays. Removal of rods from non-corner array locations effectively increases the H-to-²³⁵U ratio of the assembly. Since the BRP assemblies are under-moderated, this causes the reactivity of the assembly to increase. Thus, partial BRP assemblies with fuel rods missing from non-corner array locations tend to be more reactive than the design basis BRP assemblies.

Due to the large number of fuel rod locations in the BRP assembly arrays, an extremely large number of partial array configurations is possible, each with a different overall reactivity level. For simplicity, a bounding (optimum) assembly array is found for each of the two BRP assembly types (9x9 and 11x11). These bounding arrays are the most reactive possible geometry (or arrangement) for any number of 9x9 or 11x11 fuel rods.

To determine the bounding fuel rod arrays for the BRP 9x9 and 11x11 assemblies, the fuel rods are arranged into a regular square-pitched array. Criticality calculations are performed that determine k_{eff} values for rod arrays with various rod pitch values. The pitch of this array is varied until maximum reactivity is achieved. In other words, the pitch is varied until the optimum H-to-²³⁵U ratio is reached.

These optimum rod pitch calculations are performed for rod arrays surrounded by full water reflection. The fuel rods contain 4.1% enriched UO₂ fuel. The rod arrays are limited in size to the envelope volumes of the corresponding BRP assembly. The assembly envelope volume has a square cross-section with a width that is equal to the assembly’s nominal pitch times the number of rods on each side of the array. Thus, the fuel rod arrays for the BRP 9x9 assembly are confined to a square area with a width of 6.363 inches (9 rods times a nominal rod pitch of 0.707). The rod array for the BRP 11x11 assembly is limited to a square area with a width of 6.347 inches (11 rods times a nominal rod pitch of 0.577 inch).

Since the BRP assemblies are under-moderated, the optimum pitches for the bounding fuel rod arrays are larger than the assembly nominal pitches. The bounding array criticality analyses start with the nominal assembly pitch and increase the pitch from there. As the fuel rod pitch is increased, a smaller number of rods fit into the fixed assembly envelope area. Thus, as the pitch is increased, the number of fuel rods in the assembly array is reduced. Despite this, however, the fuel rod array reactivity increases as the rod pitch is increased over the assembly nominal value.

For each assembly case, several rod pitch values are studied, starting with the nominal assembly pitch value. The pitch values in the tables are expressed relative to the nominal assembly pitch value (e.g., “1.09 times the nominal pitch”), as well as in inches. For all cases, the fuel rod dimensions are those shown for the 9x9 and 11x11 assemblies in Table 6.1-1. A pellet diameter of 0.3715 is assumed for the 11x11 assembly analyses. Some BRP 11x11 assemblies have a fuel pellet diameter of 0.3735 inch, 0.5% larger than the standard diameter. This very small change in fuel pellet diameter will not significantly affect the reactivity of the optimum partial array configuration, so the results of the partial assembly analyses are considered applicable for these

assemblies. For each analyzed case, the tables also present the water-to-fuel volume ratio and the H-to-²³⁵U ratio. These parameters are calculated based on the analyzed pitch, the fuel rod dimensions from Table 6.1-1, a fuel material density of 96.5% UO₂ theoretical density, and a UO₂ fuel enrichment level of 4.1%.

The results of the optimum fuel rod pitch analyses for the 9x9 and 11x11 assemblies are presented in Table 6.6-10 and Table 6.6-11, respectively. The optimum pitch analysis results are also presented graphically in Figure 6.6-9 and Figure 6.6-10. The figures show a curve fit to the data points given in Table 6.6-10 and Table 6.6-11 that gives k_{eff} versus H-to-²³⁵U ratio.

The results show that, for an array of 9x9 assembly fuel rods, the optimum H-to-²³⁵U ratio (determined from the formula given in Figure 6.6-9) is 139.6. The corresponding fuel rod pitch is approximately 1.09 times that of the 9x9 assembly nominal pitch of 0.707 inch. The optimum H-to-²³⁵U ratio for an array of 11x11 assembly fuel rods (taken from the formula in Figure 6.6-10) is 146.3. The corresponding optimum rod pitch is approximately 1.08 times the 11x11 assembly nominal pitch of 0.577 inch.

These optimum pitch arrays represent the most reactive possible configuration of fuel rods within the assembly envelope. The optimum arrays also contain the optimum number of fuel rods that may occur within the given assembly envelope area. The most reactive number of rods is less than the number of rods present in the intact BRP assembly, because the assemblies are under-moderated and the optimum pitch is greater than the nominal assembly pitch. Partial BRP assemblies, however, may actually have this optimum lower number of rods, so the optimum pitch arrays must be modeled in order to bound all possible partial assembly configurations.

Analyses are performed to verify that the regular, square, optimum pitch arrays of fuel rods described in this section are bounding for all actual partial BRP assembly configurations. A series of calculations is performed where a single fuel rod is removed from various locations of the BRP assembly array. These calculations determine which rods have the greatest reactivity worth (i.e., which rods increase assembly reactivity by the greatest amount when they are removed). Then a set of analyses is performed to determine assembly reactivity as a function of the number of fuel rods removed. Rods are removed from the highest reactivity worth locations first. Then the rods with the next highest worth are removed, and so on. Rods are removed until the assembly H-to-²³⁵U ratio is the same as that of the optimum pitch fuel rod array determined by the analyses presented earlier in this section.

These analyses show two things. First, the reactivity level of the actual assembly arrays with removed rods remains significantly below that of the optimum pitch fuel rod array (by over 2% in k_{eff}), for any number of removed rods. Second, the actual assembly arrays reach maximum reactivity at a lower H-to-²³⁵U ratio (i.e., at a lower number of removed rods) than that which occurs for the optimum pitch fuel rod array. When a sufficient number of rods was removed so that the H-to-²³⁵U ratio equaled that of the optimum pitch rod array, the k_{eff} values were already sloping downwards. For this reason, assembly configurations with greater numbers of removed rods did not have to be studied. Thus, this set of analyses confirms that the optimum pitch rod arrays are a bounding model for any actual partial BRP assembly configuration. In fact, the analyses show that the optimum pitch rod arrays are a very conservative model for any BRP partial assembly, with a reactivity level on the order of 2% (in k_{eff}) higher than that of any actual partial BRP assembly that could possibly exist. The optimum pitch rod arrays are more reactive

than actual partial assembly arrays with a similar H-to-²³⁵U ratio because the water is more evenly distributed around the fuel rods.

Once the optimum pitch arrays are determined for each of the two assembly types, criticality analyses are performed to determine the maximum allowable enrichment for BRP partial 9x9 and 11x11 assemblies. These criticality models are identical to the primary criticality models described in Sections 6.3 and 6.1, except that the intact BRP assemblies contained in each of the 64 loaded fuel sleeves are replaced with the optimum pitch fuel rod arrays described in this section. Thus, the models effectively consider a W74 canister that is fully loaded with worst-case (i.e., as reactive as possible) BRP partial assemblies.

Due to the more reactive assembly geometry, the maximum allowable enrichment level for BRP partial assemblies is lower than that of intact assemblies. The results of the maximum allowable enrichment calculations are presented in Table 6.6-12. The maximum allowable enrichment for 9x9 partial assemblies is 3.55%. The maximum allowable enrichment for 11x11 partial assemblies is 3.6%. Table 6.6-12 also lists the optimum fuel rod array pitch, water-to-fuel volume ratio, and H-to-²³⁵U ratio for each assembly case.

The optimum fuel rod array pitch analyses determine an optimum fuel rod pitch and an optimum H-to-²³⁵U ratio for arrays of 4.1% enriched UO₂ fuel rods. If the enrichment of the fuel rods is lowered to 3.55% or 3.6%, the H-to-²³⁵U ratio for an array of a given rod pitch will increase. It is assumed (and verified as discussed later) that maximum reactivity occurs at the optimum H-to-²³⁵U ratio determined in the optimum array analyses, as opposed to the optimum fuel rod pitch (i.e., the H-to-²³⁵U ratio is the more important parameter, which must be kept at its optimum value). For the criticality analyses that are run with fuel rod enrichment levels of 3.55% and 3.6%, the fuel rod pitches in the optimum rod arrays are reduced in order to keep the H-to-²³⁵U ratios constant. As shown (in boldface) in Table 6.6-12, the H-to-²³⁵U ratios for the optimum 9x9 assembly (3.55%) case and the optimum 11x11 assembly (3.6%) case are the same as the optimum ratios determined for those assemblies in the optimum rod pitch analysis (presented in Table 6.6-10 and Table 6.6-11). The fuel rod pitch and water-to-fuel volume ratios, however, are lower than those shown in Table 6.6-10 and Table 6.6-11.

The final calculated k_{eff} values shown in Table 6.6-12 are compared to all applicable USL values using the methodology discussed in Section 6.5. In the final criticality analyses of the partial assemblies, all of the physical parameters of the analyzed assemblies (or rod arrays) are different from those of the design basis BRP assemblies. The analyzed enrichment levels are lower, the pin pitch values of the optimum pitch fuel rod arrays are higher. Due to the higher pin pitch values, the water-to-fuel and H-to-²³⁵U ratios are also higher for the optimum pitch rod arrays. The applicable USL values will change for the partial assembly analysis for all four physical assembly parameters treated in Section 6.5. The USL values that apply for the partial BRP assembly analyses are given in Table 6.6-13. For each of the two BRP assembly types, and for each of the four studied physical assembly parameters, Table 6.6-13 lists the value of the physical parameter along with the corresponding USL value.

The bounding final calculated k_{eff} values for partial 9x9 and 11x11 BRP fuel shown in Table 6.6-12 are lower than all of the corresponding partial assembly USL values shown in Table 6.6-13. Section 6.5 also lists the range of USL formula applicability for each of the four parameters. The parameter values for the optimum pitch fuel rod arrays (for both 9x9 and 11x11 fuel) shown in Table 6.6-13 lie within these ranges of applicability. Therefore, it is concluded

that 3.55% enriched partial 9x9 BRP assemblies and 3.6% enriched partial 11x11 assemblies meet all 10CFR71 criticality requirements. Note that since the optimum pitch fuel rod arrays modeled in the partial assembly criticality analyses are significantly more reactive than any actual partial BRP assembly, the enrichment limits specified above actually meet the 10CFR71 criticality requirements by a wide margin for all BRP partial fuel assemblies.

Additional criticality analyses are performed to confirm that the optimum H-to-²³⁵U ratio determined for 4.1% enriched BRP assembly fuel rods also applies for 3.55% and 3.6% enriched fuel rods. These analyses also confirm that the optimum H-to-²³⁵U ratio based on a single assembly array surrounded by full water reflection is also the optimum H-to-²³⁵U ratio for arrays of rods within the guide sleeves of the W74 canister. Models of arrays of 3.55% enriched 9x9 assembly fuel rods and 3.6% enriched 11x11 assembly fuel rods in each guide sleeve of the W74 canister are run with different fuel rod array pitch values and, therefore, different H-to-²³⁵U ratios. In addition to the optimum H-to-²³⁵U ratio, a case with a lower H-to-²³⁵U ratio and a case with a higher H-to-²³⁵U ratio are run for each of the two fuel rod types (9x9 and 11x11). These additional analyses show that if the rod pitch and/or H-to-²³⁵U ratio values are either reduced or increased from the optimum values shown in boldface in Table 6.6-12, the W74 canister k_{eff} value decreases. Thus, the results indicate that the optimum H-to-²³⁵U ratios determined by the single, water-reflected assembly analysis (with 4.1% enriched fuel) are also applicable for lower enrichment fuel inside the W74 canister.

In conclusion, criticality analyses are performed on a W74 canister containing optimum pitch fuel rod arrays in place of intact design basis BRP fuel assemblies. These optimum pitch rod arrays are shown to be more reactive than any possible partial assembly configuration. These analyses show that the maximum allowable fuel rod enrichment level for a W74 canister loaded with optimum pitch arrays of 9x9 assembly fuel rods is 3.55%. For a canister loaded with optimum 11x11 assembly fuel rod arrays, the maximum allowable enrichment level is 3.6%. Therefore, a maximum allowable assembly average fuel enrichment level of 3.55% is established for all partial 9x9 BRP assemblies. A maximum allowable assembly average enrichment level of 3.6% is established for all partial 11x11 BRP assemblies. The assembly average enrichment is defined as the enrichment level averaged over the remaining fuel rods in the partial assembly array.

The maximum allowable enrichments for partial BRP assemblies are listed in Table 6.1-1. These lower enrichment limits apply for all assemblies that have more fuel rods missing from non-corner assembly array locations than the maximum allowable number shown for that assembly type in Table 6.1-1.

6.6.3 Big Rock Point Damaged Fuel Assembly Criticality Evaluation

Damaged BRP assemblies are defined as assemblies with fuel rod damage in excess of pinhole leaks or hairline cracks. The fuel rod damage criterion is based on NRC guidance.⁹ Fuel assemblies with damaged grid spacers (defined as damaged to a degree where fuel rod structural integrity cannot be assured, or where grid spacers have shifted vertically from their design position) will also be stored in damaged fuel cans.

⁹ ISG-1, *Damaged Fuel*, Spent Nuclear Fuel Project Office Interim Staff Guidance, U.S. Nuclear Regulatory Commission, November 1998.

All damaged BRP assemblies must be placed into damaged fuel cans that are then loaded into one of the eight support tube locations in the W74 canister. These damaged fuel cans (discussed in Section 6.3 and illustrated in Figure 6.3-18) are similar to a standard W74 canister guide tube, with standard W74 canister poison sheets attached to all four walls of the guide tube.

Fuel debris or fuel rod fragments are not qualified for loading into the W74 damaged fuel cans. These are pellets or fuel rod segments that are no longer attached to (or confined within) the fuel assembly.

With respect to criticality, it is conservatively assumed that damaged fuel assemblies do not maintain their geometry during transport in the W74 canister. Thus, the W74 canister, when fully loaded with fresh water, is required to remain sub-critical for any assembly geometry configuration within the damaged fuel cans. The canister must remain sub-critical with damaged fuel cans in all eight support tube locations.

6.6.3.1 W74 Canister Model for the Damaged Assembly Analyses

Criticality analyses are performed to determine the most reactive possible configuration of fissile material within the damaged fuel can interior volume. These analyses are performed using a full model of the W74 canister. The same canister and cask configuration (and assumptions) used in the intact BRP assembly criticality analyses (described in Sections 6.3 and 6.1) are used for these analyses. This configuration is shown in the intact assembly analyses to be bounding for all conditions of transport for the W74 canister.

These analyses model various fissile material configurations, inside damaged fuel cans, in all eight support tube locations. The other (guide tube) locations in the W74 canister are filled with the most reactive partial BRP assembly configuration, which is determined as discussed in Section 6.6.2.2. This configuration is a regular square array of 3.55% enriched 11x11 BRP assembly fuel rods with an H/²³⁵U ratio of 139.64. This partial assembly configuration is more reactive than the design basis (4.1% enriched) intact BRP assembly configuration.

Since a full canister model is used to determine the most reactive fissile material configuration for the damaged fuel can interiors, the same analyses can be used to verify that the most reactive fissile material configuration remains sub-critical (i.e., meets all 10CFR71 criticality requirements) when loaded into the damaged fuel cans that are placed within the W74 canister. As these analyses are also used to verify compliance with the criticality requirements, the most reactive possible contents of the other (guide tube) fuel locations must also be modeled. The bounding partial BRP assembly configuration described above is modeled in the other canister fuel locations for that reason.

After the most reactive fissile material configuration is determined, additional analyses that model the bounding intact BRP assembly configuration (a 4.1% enriched 11x11 BRP assembly) in the other (guide tube) fuel locations are performed. These analyses verify that the case with partial assemblies in the other fuel locations is the bounding case, and that all 10CFR71 criticality requirements are met whether bounding intact BRP fuel assemblies or bounding partial BRP fuel assemblies are loaded into the other fuel locations.

6.6.3.2 Damaged Fuel Can Contents Model Description

It is conservatively assumed that, during drop events, damaged fuel rods break into segments and/or break open and release their fuel pellets into the damaged fuel can interior. Screens at the bottom end of the cans will prevent any fissile material from leaving the damaged fuel can interior volume. Grid spacers are also assumed to fail, allowing any spacing between rods to occur. In theory, it would be remotely possible for all fuel rods to fail and release all of their pellets. Then, the fuel rods and all other assembly hardware would break apart and fall into a pile at one end of the damaged fuel can interior. This would leave an array of fuel pellets occupying the rest of the damaged fuel can interior. To cover this extremely unlikely scenario, an extremely conservative assumption is made for the damaged assembly criticality analyses. The damaged fuel can interior is assumed to be occupied by a mixture of pure (unburned) fuel material and full density water. Thus, all assembly hardware materials, including the fuel rod cladding, are conservatively neglected. As these materials absorb neutrons and displace a large amount of water, this assumption greatly increases the reactivity of the modeled fissile material configuration.

The bulk of the damaged assembly analyses are performed to determine the most reactive possible configuration of fuel material and water that may occupy the interior of the damaged fuel cans. The analyses consider several different arrays of fuel pellets and water. In all cases, these fuel pellet arrays are assumed to fill the entire damaged fuel can interior. The damaged fuel can geometry shown in Figure 6.3-18 is modeled over the entire axial length of the support tube in the criticality models. Thus, the fissile material configuration is also assumed to extend over the entire axial length. The end geometry of the damaged fuel cans is not modeled in the analyses, as the full length geometry assumption is bounding.

The analyses model pure 4.61% enriched UO_2 fuel, with a density that is 96.5% of UO_2 theoretical density, over the entire fuel material configuration in the damaged fuel can interior. Three types of array configurations are analyzed, a hexagonal array of fuel spheres, a hexagonal array of fuel cylinders, and a square array of fuel cylinders. The fuel cylinders in the arrays are oriented along the Z-axis of the canister, and extend over the full axial length of the support tube. The cylinders are arranged in a square or hexagonal array in the horizontal direction. The array of fuel spheres is arranged in a hexagonal array in the horizontal direction. The spheres are then evenly spaced (in columns) in the axial direction, at a spacing equal to the pitch value of the horizontal array. Thus, the spacing between the spheres is the same in all directions.

The primary fuel sphere array analysis is performed assuming a fuel sphere diameter of 0.9 cm., a particle size similar to that of a single 0.3715-inch diameter fuel pellet. The primary fuel cylinder array analyses are performed for two cylinder diameters: 0.471 inch and 0.3715 inch. These diameters correspond to the pellet diameters of the BRP 9x9 and 11x11 assemblies, respectively.

Since two diameters are analyzed for each of the two fuel cylinder arrays (hexagonal and square), there are a total of five array types that are analyzed. For each analyzed array type, the spacing between the fuel cylinders (or spheres) is varied over a wide range. The array pitch value that yields the maximum canister k_{eff} value is then determined. This corresponds to the optimum $\text{H}/^{235}\text{U}$ ratio for the array. After the optimum pitch value is determined for each of the five array types, the calculated k_{eff} value (at the optimum array pitch) is compared for the five array types.

The array type that yields the highest calculated k_{eff} value is selected as the most reactive possible configuration of fuel material inside the damaged fuel can interior.

As discussed earlier, the arrays are assumed to completely fill the damaged fuel can interior, so the volume of the fissile material array is fixed. Thus, as the array pitch is increased, the number of fuel cylinders (or spheres) in the array decreases. Since the diameter of the fuel cylinders (or spheres) is constant, the quantity of fuel material within the damaged fuel can interior also varies with the pitch value. Since the pitch value that yields maximum reactivity (considering these effects) is determined, the optimum fissile material configuration (at the optimum pitch value) is bounding for any quantity of fuel material inside the damaged fuel can interior.

It is assumed that an array with a regular spacing of fuel particles that fills the damaged fuel can interior volume, with no other assembly materials present, is the most reactive possible configuration. Materials other than fuel or water clearly reduce reactivity. There are an infinite number of irregular configurations of fuel material that could occur within the damaged fuel can. A regular array at an optimum spacing, or pitch (i.e., an optimum H/²³⁵U ratio) should bound all such irregular configurations, however. Whereas an optimum regular array would have the optimum H/²³⁵U ratio at all locations within the array, an irregular geometry would have sections with ratios that are too high and sections with ratios that are too low (i.e., over-moderated and under-moderated sections). Thus, all such configurations will have reactivity levels that are similar to or lower than those of the analyzed regular arrays. Any small differences in reactivity levels that could occur between the infinite number of possible configurations that have an optimum H/²³⁵U ratio are much smaller than the increase in reactivity created in these analyses by the (ultra-conservative) removal of all other assembly materials. It is therefore concluded that analyzing both types of regular arrays (hexagonal and square), using both basic types of fuel particle geometry (sphere and cylinder), is sufficient to establish the most reactive possible fuel material configuration.

Although fuel debris is not allowed for loading in the W74 damaged fuel can, it is possible that fuel pellets may break apart during accident events, thereby creating smaller fuel particles. For this reason, supplementary analyses are performed to evaluate the effects of particle size on k_{eff} . Two sets of fuel particle size evaluations are performed, one for cylinders and one for spheres. The cylinder study models square arrays of cylinders. The results of the primary cylinder array analyses (discussed below in Section 6.6.3.3) show that square arrays of cylinders are more reactive than hexagonal arrays of cylinders. For spheres, a hexagonal array is modeled (as in the primary analyses).

The supplementary analyses consider a wide range of cylinder and sphere diameters. Cylinder diameters ranging from 0.05 inches to 0.471 inches (the maximum whole pellet diameter for BRP fuel) are considered in the analyses. Sphere diameters range from 0.2 cm to 2.0 cm. For each studied fuel particle diameter, a wide range of pitch values (and corresponding H/²³⁵U ratios) are analyzed. The optimum pitch (i.e., H/²³⁵U ratio) is determined for each particle diameter. Then the peak k_{eff} values (at the optimum pitch for each case) are tabulated for each particle diameter. Comparison of these peak k_{eff} values, for each particle diameter, allows the most reactive particle diameter to be determined. Finally, the peak k_{eff} values between the most reactive cylinder case and the most reactive sphere case are compared to determine the most reactive particle type (cylinder or sphere). This most reactive particle diameter (and particle type), at its associated optimum pitch, is the most reactive possible fuel material configuration

for the damaged fuel can interior. The associated final k_{eff} value is the maximum reactivity for the W74 canister.

6.6.3.3 Damaged Assembly Criticality Analysis Results

The results of the primary optimum fissile material array calculations are presented in Table 6.6-14 through Table 6.6-18. For each of the five array types (described in Section 6.6.3.2), calculated k_{eff} values are presented for several analyzed array pitch values. For each array pitch value, the corresponding $H/^{235}\text{U}$ ratio for the array is presented. For each case, the k_{eff} value calculated by MCNP, the statistical error level in the MCNP result (1σ), and the final k_{eff} value (calculated as $k_{\text{eff}} + 2\sigma$) are presented. The analyses' results are also presented graphically in Figure 6.6-11 through Figure 6.6-15. The graphs show 2nd order polynomial curve fits to the k_{eff} data from Table 6.6-14 through Table 6.6-18. Thus the plots show function curves giving k_{eff} as a function of $H/^{235}\text{U}$ ratio for each of the five analyzed array types.

As shown in Table 6.6-14 through Table 6.6-18, the most reactive configuration of (whole) fuel pellets inside the damaged fuel can is a square array of 0.3715-inch diameter fuel cylinders (corresponding to 11x11 BRP assembly fuel pellets), at a pitch value of 0.655 inch and an $H/^{235}\text{U}$ ratio of 180. The analyses also show that hexagonal arrays are somewhat less reactive than square arrays since the maximum k_{eff} values for the hexagonal arrays are lower than the corresponding square arrays by a statistically significant amount (i.e., by more than two times the statistical error level in the results). The results also show that there is no measurable difference in reactivity between the two BRP fuel assembly pellet sizes. (The difference between the maximum final k_{eff} values for the two pellet diameter cases being one fifth of the statistical error level of the criticality code.)

An additional set of analyses, which model the square array of 0.3715-inch fuel cylinders in the damaged fuel can interior, are performed assuming design basis intact BRP assemblies (i.e., 4.1% enriched 11x11 BRP assemblies) in the other fuel locations in the W74 canister (as discussed in Section 6.6.3.1). These analyses are performed for the same set of array pitches shown in Table 6.6-15. The results of these analyses are presented in Table 6.6-19. These analyses show a maximum k_{eff} value at the same array pitch (0.655 inch) and $H/^{235}\text{U}$ ratio (180) shown for the partial assembly configuration case in Table 6.6-15. The analyses also show that the maximum k_{eff} value for the 4.1% enriched intact 11x11 assembly case is lower than that of the 3.55% enriched partial 9x9 assembly case. This is expected since the intact, 4.1% enriched assembly configuration is somewhat less reactive than the optimum partial, 3.55% enriched assembly configuration (as shown by comparing the k_{eff} results shown for the intact assembly in Table 6.4-7 with the results shown for the partial 9x9 assembly in Table 6.6-12).

The maximum calculated k_{eff} values for the damaged BRP assembly analyses are compared to their corresponding USL values in Table 6.6-20. The cases shown correspond to the most reactive fuel material configuration in the damaged fuel can interior, i.e., a square array of 0.3715-inch diameter fuel cylinders with a pitch of 0.655 inch, and a fuel enrichment of 4.61%. Damaged fuel cans containing this configuration are modeled in all eight W74 support tube locations. Two cases are shown in Table 6.6-20. One corresponds to an optimum, 3.55% enriched, partial 9x9 BRP assembly configuration modeled in the other fuel locations, and the other corresponds to a design basis, intact, 4.1% enriched, 11x11 BRP assembly configuration modeled in the other fuel locations.

The overall reactivity of the canister is governed by the contents of the other 56 fuel locations in the W74 canister, as opposed to the contents of the damaged fuel cans loaded in the eight support tube locations that lie at the edge of the W74 canister. This is true even though the analyses show that the presence of the damaged fuel cans increases the overall reactivity of the W74 canister somewhat. For this reason, the USL values that apply for the W74 canister are governed by the parameters of the configurations modeled in the other fuel locations, as opposed to the damaged fuel can interiors. Therefore, the limiting USL values shown in Table 6.6-20 correspond to the optimum partial 9x9 BRP assembly configuration and the intact 11x11 BRP assembly configuration. The intact assembly minimum USL value is taken from Table 6.4-7. The minimum USL value for the partial assembly configuration is taken from Table 6.6-13.

The data in Table 6.6-20 shows that the final k_{eff} values are below the corresponding minimum USL values for both the partial and intact assembly cases. Thus, the results show that all 10CFR71 criticality requirements are met for a W74 canister loaded with up to eight damaged fuel cans containing the most reactive possible assembly configuration inside each damaged fuel can. This conclusion applies even if all of the other fuel locations in the canister are loaded with the most reactive allowable contents, including the most reactive allowable intact BRP assembly configuration (a 4.1% enriched 11x11 assembly), and/or the most reactive partial BRP assembly configuration (a 3.55% enriched 9x9 assembly).

As discussed in Section 6.6.3.2, the analyses model a uniform fuel enrichment of 4.61% over the entire fuel material array inside the damaged fuel can. Thus, these analyses qualify a maximum fuel enrichment level of 4.61% for the contents of the damaged fuel can. Although extremely unlikely, it is theoretically possible for a group of maximum enrichment pellets to escape their fuel rods and congregate in one section of the damaged fuel can interior. For this reason, the analyses conservatively assume that the fuel enrichment modeled for the damaged fuel can interior array corresponds to the maximum enrichment of any individual fuel pellet within the assembly. Thus, the maximum enrichment limit of 4.61% applies for each individual fuel pellet in any candidate assembly. Therefore, in conclusion, any fuel assembly that has no fuel pellets with enrichment levels over 4.61% may be loaded into a damaged fuel can that may then be loaded into one of the support tube locations of the W74 canister.

As discussed in Section 6.6.3.2, supplementary analyses are performed to thoroughly evaluate the effects of fuel particle size on reactivity. The primary damaged fuel array analyses discussed in this section determine the most reactive configuration of whole fuel pellets within the W74 damaged fuel can interior. However, since fuel pellets may break up into smaller particles during accident events, a wide range of particle sizes must be considered, and the most reactive particle size must not yield final k_{eff} values that exceed the applicable minimum USL value.

Therefore, analyses are performed which consider a wide range of diameters for cylindrical and spherical fuel particles. The analyses consider square arrays of fuel cylinders because the primary analyses show the square array to be more reactive, as discussed earlier in this section. Hexagonal arrays of fuel spheres are considered. For each considered fuel particle diameter, a wide range of array pitches (and corresponding H/²³⁵U ratios) is analyzed. The optimum pitch and corresponding maximum k_{eff} value are calculated for each analyzed cylinder and sphere diameter.

The results of the fuel cylinder diameter evaluations are presented in Table 6.6-21 and Table 6.6-22. For each studied cylinder diameter, various array sizes are considered. In each

case, the array completely fills the damaged fuel can interior. The left column of Table 6.6-21 shows the array size (i.e., the number of fuel cylinders on each side of the square array). Each array size has a corresponding rod pitch, which corresponds to the number of fuel cylinders for that array, evenly distributed over the width of the damaged fuel can interior. Based upon this rod pitch and the diameter of the fuel cylinders, the corresponding $H/^{235}U$ ratio is determined. Table 6.6-21 shows the $H/^{235}U$ ratios that correspond to each combination of array size and fuel cylinder diameter that is considered in the analyses. Table 6.6-21 also presents $H/^{235}U$ ratios for the four types of BRP MOX fuel rods. The damaged MOX fuel analysis is discussed in Section 6.6.3.5.

For each fuel cylinder diameter, a finite range of array sizes (and corresponding $H/^{235}U$ ratios) is analyzed. The studied range is sufficient to locate the most reactive $H/^{235}U$ ratio, and to demonstrate clearly decreasing reactivity levels for $H/^{235}U$ ratios on either side of the optimum value. The range of evaluated array sizes varies greatly with particle diameter because smaller particle sizes require larger array sizes to produce similar $H/^{235}U$ ratios. The range of $H/^{235}U$ ratios that are considered for each cylinder diameter is relatively similar for all cases.

Table 6.6-22 presents the k_{eff} results of the fuel cylinder diameter evaluation. For each fuel cylinder diameter (shown in the top row of the table), several array sizes and corresponding $H/^{235}U$ ratios are analyzed. The array size for each analyzed case is given in the first column of Table 6.6-22. The $H/^{235}U$ ratio for each case in Table 6.6-22 (i.e., each combination of array size and fuel cylinder diameter) is given in Table 6.6-21. The final k_{eff} value for each case, as presented in Table 6.6-22, equals the k_{eff} value calculated by MCNP, plus two times the level of statistical error. The particle size analyses all have a level of statistical error (~ 0.0009) that is similar to that of the primary analyses presented in Table 6.6-14 through Table 6.6-20. Additionally, Table 6.6-22 presents final k_{eff} values for the four types of BRP MOX fuel rod. The damaged MOX fuel analysis is discussed in Section 6.6.3.5.

For each fuel cylinder diameter, a number of array sizes (i.e., $H/^{235}U$ ratio) are analyzed to establish the optimum $H/^{235}U$ ratio. For each diameter, the results show a peak k_{eff} value (occurring at some array size), and at least two array sizes on each side of the peak, which show descending k_{eff} values. In all cases, the k_{eff} values at both ends of the analyzed range are lower than the peak k_{eff} value by a statistically significant amount (i.e., by at least 0.002, which is more than two times the level of statistical error in the calculated k_{eff} results). These two characteristics – at least two descending points on either side of the maximum and k_{eff} values which fall to more than two standard deviations below the peak value – are sufficient to establish the optimum $H/^{235}U$ ratio and the corresponding maximum k_{eff} value.

As shown in Table 6.6-22, the k_{eff} values remain well under the applicable USL value of 0.94375 (shown in Table 6.6-20) for all cylinder diameters and all $H/^{235}U$ ratios (or rod pitches). Additionally, the margin between the peak k_{eff} values and the USL is relatively large compared to the level of variation in k_{eff} that occurs between various cylinder diameters and $H/^{235}U$ ratios. The peak final k_{eff} values for each cylinder diameter (at the optimum $H/^{235}U$ ratio) range from ~ 0.936 to ~ 0.939 over the very wide range of studied diameters, whereas the applicable USL value is ~ 0.944 . For each of the analyzed diameters, $H/^{235}U$ ratios are increased or decreased until the k_{eff} value is lower than the peak value by 0.002 (twice the level of statistical error) or more. By contrast, the applicable USL is greater than the maximum final k_{eff} value (calculated for any cylinder diameter and $H/^{235}U$ ratio combination) by more than 0.005 (i.e., by five times

the level of statistical error). Thus, the results show that the calculated k_{eff} value remains well under the applicable USL for all possible combinations of fuel cylinder diameter and $\text{H}/^{235}\text{U}$ ratio (i.e., pitch).

The results of the fuel sphere diameter evaluation are presented in Table 6.6-23. For the fuel sphere evaluation, a consistent set of seven $\text{H}/^{235}\text{U}$ ratios, ranging from 120 to 250, is analyzed for all fuel sphere diameters. Fuel sphere diameters ranging from 0.2 cm to 2.0 cm are considered. Table 6.6-23 presents the final k_{eff} value (the MCNP calculated k_{eff} value plus two times the level of statistical error) for each analyzed combination of $\text{H}/^{235}\text{U}$ ratio and fuel sphere diameter. As with the fuel cylinder runs, all of the fuel sphere diameter analyses have a statistical error level of ~ 0.0009 in the calculated k_{eff} results.

In a few cases the final k_{eff} values do not smoothly (monotonically) decrease from the peak k_{eff} value because the analyzed $\text{H}/^{235}\text{U}$ ratios are relatively close together for the fuel sphere evaluation. Instead, k_{eff} may increase somewhat as the $\text{H}/^{235}\text{U}$ ratio increases or decreases from its optimum value (i.e., the value at which the peak k_{eff} occurs). This increase in k_{eff} does not affect the overall trend of decreasing final k_{eff} values moving away from the peak k_{eff} value and is attributed to random statistical fluctuation in the final k_{eff} results. In all cases where k_{eff} increases, the amount of increase (from the previous k_{eff} value) is roughly equal to the statistical error level of the results (one sigma) or less. The k_{eff} values at the ends of the $\text{H}/^{235}\text{U}$ ratio range are lower than the peak k_{eff} value by a statistically significant amount (i.e., by over twice the level of statistical error in the k_{eff} values) in all but one case. Furthermore, the analyses in general demonstrate that the fuel sphere arrays are less reactive than the fuel cylinder arrays more than 0.002 in k_{eff} (i.e., by over twice the statistical error in the code results). The k_{eff} values for the sphere cases peak at ~ 0.936 for most of the diameter cases studied, whereas the cylinder case k_{eff} values peak at ~ 0.939 .

As with the cylinder case, the Table 6.6-23 data show that the final k_{eff} value remains well under the applicable USL value for the entire range of sphere diameters and $\text{H}/^{235}\text{U}$ ratios considered in the analysis. The margin between the peak k_{eff} value and the USL value is shown to be large relative to the level of variation in the k_{eff} results.

Thus, the sphere analyses show final k_{eff} values that are less than those of the cylinder cases and that are much lower than the applicable USL value of 0.94375, over the entire, wide range of considered sphere diameters and $\text{H}/^{235}\text{U}$ ratios. The results demonstrate the existence of broad peaks in k_{eff} (for each diameter case) over the range of $\text{H}/^{235}\text{U}$ ratios studied, with k_{eff} generally falling off at the ends of the $\text{H}/^{235}\text{U}$ ratio range.

The final results of the particle (cylinder and sphere) diameter evaluation are summarized in Table 6.6-24, which shows the peak k_{eff} value for each analyzed particle diameter, at the $\text{H}/^{235}\text{U}$ ratio that yields the highest result (i.e., the highest k_{eff} values shown in Table 6.6-22 and Table 6.6-23 for each particle diameter). Table 6.6-24 lists each studied cylinder and sphere diameter, the $\text{H}/^{235}\text{U}$ ratio that yields the highest k_{eff} value for that diameter, and the maximum k_{eff} value for that diameter.

The Table 6.6-24 results do not show any clear trend in optimum $\text{H}/^{235}\text{U}$ ratio with particle diameter. At most, there may be a slight, vague tendency of optimum $\text{H}/^{235}\text{U}$ ratio to increase with decreasing particle diameter. The results also show that the cylinder arrays are more reactive than sphere arrays over the entire range of particle diameters. The cylinder case k_{eff}

values are, in general, more than 0.002 higher than the sphere cases (i.e., more than twice the statistical error level of the k_{eff} results). The peak k_{eff} value shown for cylinder arrays is 0.93885, as compared to the maximum sphere array k_{eff} value of 0.93594 (a difference of ~ 0.003).

Additionally, the Table 6.6-24 results demonstrate a maximum in peak (optimum H^{235}U) k_{eff} that occurs within the range of studied particle diameters, for both cylinders and spheres. The cylinder results show a clear peak in reactivity at a diameter of 0.35 inches. Statistically significant reductions in peak k_{eff} are seen on each side of the optimum diameter. The sphere analyses show a broad (virtually flat) maximum in peak k_{eff} that occurs for sphere diameters between 0.7 and 1.3 cm. All of the peak k_{eff} values within this diameter range fall between 0.9353 and 0.9360, i.e., they all fall within the (one sigma) level of statistical error. Peak k_{eff} drops to ~ 0.9350 for the diameters of 0.5 and 1.5 cm, and then drops significantly (to ~ 0.9330) for the 0.2 and 2.0 cm diameters. Thus, the sphere results show a broad flat peak in k_{eff} over most of the analyzed diameter range, with k_{eff} then falling off at the ends of the range.

The optimum (i.e., most reactive) fuel cylinder diameter of 0.35 inches is in good agreement with previously published criticality evaluations. Table VII of DP-1014¹⁰ gives the minimum critical volume for cylindrical and slab shaped arrays of UO_2 fuel rods (i.e., cylinders, without cladding) in water. For 5.0% UO_2 fuel, the minimum array volumes occur for fuel rod diameters of 0.9 cm, or ~ 0.35 inches.

6.6.3.4 Damaged Fuel Can Preferential Flooding Analysis

The preceding calculations verify that any arrangement of fuel pellets with a pellet enrichment of 4.61% or less within the damaged fuel can does not cause the criticality requirements to be exceeded. These analyses are based on full moderator (water) density within the damaged can interior and within the rest of the W74 canister interior. In general, for cask systems containing unpoisoned water, this is the most reactive case. Calculations verify that the most reactive uniform water density for the canister interior is 1.0 g/cc (full density).

However, since screens are employed by the damaged fuel cans, it may be possible for preferential flooding to occur. That is to say that a situation may arise where the water density within the damaged fuel can is not the same as the water density outside the damaged fuel can (i.e., in the rest of the W74 canister interior). For this reason, additional analyses are performed that consider various combinations of damaged fuel can interior and exterior water densities. These criticality models are identical to those presented in the preceding sections, other than the water densities present in the canister and the damaged fuel can.

Two sets of analyses are performed. In the first set of analyses, the canister interior water density is maintained at 1.0 g/cc while the damaged can interior water density is varied from 1.0 g/cc down to 0.0 g/cc. In the second set of analyses, the damaged can interior water density is maintained at 1.0 g/cc while the canister interior water density is varied from 1.0 g/cc down to 0.0 g/cc.

The results of the preferential flooding analyses are presented in Figure 6.6-16. The results show that full water density inside the damaged fuel can and in the rest of the canister interior is

¹⁰ DP-1014, *Critical and Safe Masses and Dimensions of Lattices of U and UO_2 Rods in Water*, February 1966, Savannah River Laboratory, Aiken, S.C.

indeed the most reactive case. If the water density is reduced in either region, k_{eff} decreases. As expected, the k_{eff} dependence was stronger for the canister interior (damaged fuel can exterior) water, since it occupies a much larger fraction of the overall canister interior volume.

Thus, the damaged fuel criticality results and enrichment limits remain valid after considering preferential flooding effects.

6.6.3.5 Damaged BRP MOX Assembly Analyses

Some damaged BRP MOX fuel may require transport inside the W74 canister. Therefore, damaged fuel analyses, similar to those described earlier in this section, are performed for each of the MOX fuel compositions present in BRP MOX fuel. There are four MOX fuel rod types present in BRP MOX fuel, each type containing a specific MOX fuel material composition. These four material compositions are presented in Table 6.6-2. Damaged fuel analyses for these MOX fuel compositions qualify the specific MOX fuel material present in each of the four BRP MOX fuel rod types (G-Pu, DA-1, DA-2, and J2) for loading in the W74 damaged fuel can. These analyses show that k_{eff} remains below its applicable limits for all possible geometric configurations of each MOX fuel material within the damaged fuel can interior.

These analyses, however, do not qualify the MOX fuel material within the two MOX rods in the E65 and E72 BRP assemblies (the material described in the far right column of Table 6.6-2) for loading inside the damaged fuel can. BRP assemblies E65 and E72 are only analyzed in the intact MOX assembly evaluations presented in Section 6.6.1 and cannot be loaded into the W74 damaged fuel can. Plant records indicate that these two assemblies are undamaged.

These analyses determine the most reactive geometric configuration for the four BRP MOX fuel materials (described above) within the damaged fuel can interior volume. The criticality analyses presented (for UO_2 fuel) in Section 6.6.3.3 show that square arrays of fuel cylinders are more reactive than hexagonal pitch arrays, or arrays of fuel spheres. The Section 6.6.3.3 analyses also show maximum reactivity for a fuel cylinder diameter of 0.35 inches. Therefore, to qualify the BRP assembly MOX fuel compositions for loading into the W74 damaged fuel can, criticality analyses are performed that model square arrays of 0.35-inch diameter cylinders of MOX fuel within the damaged fuel can interior. These arrays are regularly spaced and completely fill the damaged fuel can interior volume.

Because of the differences in neutronic behavior between MOX fuel and UO_2 fuel, it is not clear that the optimum ratio of hydrogen to fissile isotopes for MOX fuel is the same as the optimum ratio of hydrogen to ^{235}U (i.e., the optimum H-to- ^{235}U ratio) for UO_2 fuel. For this reason, the optimum H-to-fissile atom ratio is recalculated for each of the four MOX fuel material compositions.

The H-to-fissile-atom ratio is defined as the ratio of the number of hydrogen atoms (within the fuel assembly lattice) to the total number of fissile isotope atoms in the fuel. The H-to-fissile ratio is similar to the H-to- ^{235}U ratio for UO_2 fuel, except that the total number of fissile atoms includes the number of ^{239}Pu and ^{241}Pu atoms, in addition to the number of ^{235}U atoms present in the MOX fuel.

For each analyzed MOX fuel composition, the pitch of the square, 0.35-inch diameter cylinder array is varied to analyze a wide range of H-to-fissile atom ratios. The range of analyzed pitch values is sufficient to establish the optimum H-to-fissile ratio for each MOX fuel composition.

As with the UO₂ fuel cylinder analyses presented in Section 6.6.3.3, at least five H-to-fissile ratios are analyzed. In each case, a peak k_{eff} value is presented (at the optimum H-to-fissile ratio) with at least two descending k_{eff} values on each side of the peak. Also, as with the UO₂ analyses, the k_{eff} values presented at the maximum and minimum H-to-fissile ratios are lower than the peak k_{eff} value by at least 0.002 in k_{eff} (i.e., by over twice the level of statistical error in the k_{eff} results). Thus, the analysis results demonstrate that k_{eff} decreases as the H-to-fissile ratio is either increased or decreased from the optimum value (the value at which the peak k_{eff} value occurs).

The results of the damaged MOX fuel criticality analyses are presented in Table 6.6-21 and Table 6.6-22. The four MOX fuel composition cases are shown in the four right columns of the tables. As with the UO₂ fuel cylinder analyses, several array sizes are analyzed (from 8x8 to 14x14 for the four MOX composition cases). For each array size case, the array is evenly distributed within the damaged fuel can interior volume. By varying the array size, the rod pitch is varied, which in turn varies the H-to-fissile atom ratio within the lattice.

Table 6.6-21 presents the H-to-fissile atom ratio for each analyzed MOX fuel array size and MOX fuel composition. The ratios are based upon the array dimension, the size of the damaged fuel can interior, the 0.35-inch diameter of the fuel cylinders, and the total density of fissile atoms (²³⁵U, ²³⁹Pu, and ²⁴¹Pu) within each of the MOX fuel materials. The array size is shown in the left column of the table. The four right columns of Table 6.6-21 correspond to the four BRP MOX fuel compositions described in Table 6.6-2.

The results of the damaged MOX fuel criticality analyses are presented in the four right columns of Table 6.6-22. The array size of each case is given in the left column of the table. The corresponding H-to-fissile ratios for each array size and MOX fuel composition are given in the four right columns of Table 6.6-21. The final k_{eff} values (equal to the calculated k_{eff} value plus twice the statistical error level in the results) for each analyzed combination of H-to-fissile ratio and MOX fuel composition are presented in the four right columns of Table 6.6-22.

The k_{eff} results presented for the four MOX fuel compositions in Table 6.6-22 show reactivity maxima at corresponding optimum H-to-fissile ratios, with decreasing reactivity for higher and/or lower H-to-fissile ratios. The results also show that the peak k_{eff} values remain well below the applicable USL values for all analyzed combinations. The maximum final k_{eff} value shown in Table 6.6-22 (for the G-Pu composition, H-to-fissile ratio = 271 case) is ~0.937, whereas the minimum USL value, applicable for W74 canisters containing any MOX fuel material, is ~0.941. Thus, the minimum criticality margin is ~0.004, over four times the level of statistical error in the k_{eff} results.

The k_{eff} results presented in Table 6.6-22 also show that for most BRP MOX fuel, maximum reactivity occurs at an array size (and corresponding array pitch) that is similar to that which yields maximum reactivity for 4.61% enriched UO₂ fuel. Maximum reactivity occurs at an array size of 12x12 for the DA-1 and J2 MOX fuel compositions, an array size of 11x11 for the DA-2 MOX fuel composition, and an array size of 10x10 for the G-Pu MOX fuel composition. Maximum reactivity is achieved at an array size of 12x12 (which corresponds to an array pitch of 0.6 inches) for the UO₂ fuel case.

For a given array pitch, however, the H-to-fissile ratio for the BRP MOX fuel compositions is greater than the H-to-²³⁵U ratio for 4.61% enriched UO₂ fuel. This difference in the two ratios exists because the fissile atom density within the MOX fuel compositions is lower than the ²³⁵U

atom density within 4.61% enriched UO₂ fuel. The most reactive H-to-fissile ratio for the DA-1, DA-2, J2, and G-Pu MOX fuel compositions is 330, 235, 217, and 271, respectively, whereas the most reactive H-to-²³⁵U ratio for the 4.61% enriched UO₂ fuel array (of 0.35 inch diameter cylinders) is 166. Thus, maximum reactivity occurs at higher H-to-fissile atom ratios for the BRP MOX fuel than it does for the UO₂ fuel.

The analyses presented in Table 6.6-21 and Table 6.6-22 demonstrate that, under any geometric configuration within the damaged fuel can interior, none of the four MOX fuel compositions presented in Table 6.6-2 can cause the W74 canister criticality limits to be exceeded. Therefore, damaged (or undamaged) BRP assemblies that contain any number of any one of the four MOX fuel rod types described in Table 6.6-2 may be loaded into the W74 damaged fuel can.

6.6.3.6 Other Allowable Damaged Fuel Can Contents

As discussed in Section 6.6.3.3, a maximum allowable enrichment of 4.61% is established for all assemblies to be loaded into the W74 canister damaged fuel cans. This enrichment limit applies for each individual fuel pellet within the assembly. This criterion is intended to apply for all damaged BRP assemblies that are to be loaded into the damaged fuel cans of the W74 canister.

However, the damaged assembly criticality analyses presented in this section may also be used to qualify a very broad range of possible contents for the damaged fuel cans. As discussed in Section 6.6.3.3, it is concluded that the analyses presented determine the most reactive possible configuration of fissile material inside the damaged fuel cans, given a maximum fuel enrichment of 4.61% and a maximum fuel density of 96.5% UO₂ theoretical. The calculations do not merely determine the most reactive possible configuration for a damaged BRP assembly. The conclusions of the analysis are much broader.

Other than the enrichment and fuel density limits discussed above, all assembly parameters that may affect criticality in a standard (intact assembly) criticality analysis are clearly bounded, over all possible values, by these analyses. These analyses determine the optimum pitch (and optimum H/U ratio) for the fissile material array, so all possible assembly pitch values are covered. All possible fuel rod array layouts (number and location of water holes, etc.) are also covered for the same reason. The analyses also cover all possible fuel particle sizes (diameters). Since these analyses very conservatively neglect all assembly cladding and hardware materials, all values of cladding thickness, clad material, and clad diameter are clearly bounded by these analyses. Since these analyses model the fissile material array as completely filling the damaged fuel can interior volume, all values for assembly array size and active fuel length are clearly bounded by these analyses (given that the assembly can physically fit inside the damaged fuel can).

For the above reasons, these analyses show that virtually any assembly geometry may be loaded into the damaged fuel cans of the W74 canister while meeting all 10CFR71 criticality requirements. Therefore, the only assembly parameters that will be specified (for loading into the damaged fuel cans) are the maximum fuel pellet enrichment level and the maximum fuel material density. The maximum allowable pellet enrichment is 4.61% and the maximum allowable fuel density is 96.5% of theoretical UO₂ density. These are the only two parameters that need to be specified to assure compliance with the criticality requirements. Other parameters such as assembly weight, assembly width, uranium loading, uranium loading per inch of fuel height, burnup, cooling time, etc. would have to be specified in order to meet the structural,

thermal, and shielding requirements. However, none of the assembly array dimensions (which are generally specified to meet the criticality requirements) will have to be specified.

Thus, the damaged fuel cans placed in the W74 canister support tubes may perform a second function. As well as accommodating all damaged BRP fuel, these cans may accommodate any assembly configuration, discovered at BRP, that does not meet the assembly geometry specifications for intact or partial BRP fuel assemblies. Any assembly geometry (damaged or undamaged) may be loaded into the damaged fuel cans as long as the maximum enrichment is under 4.61% and the fuel density is under 96.5% theoretical (given that the assembly physically fits inside the cans).

For MOX fuel, any assembly that meets the fuel density requirement and contains any one of the MOX fuel compositions described in the first four columns of Table 6.6-2 (or any mixture thereof) may be loaded into the damaged fuel can. A MOX fuel assembly that contains any MOX fuel material with a composition that is not described in Table 6.6-2 may not be loaded into the damaged fuel can.

6.6.4 The W74 Canister Inside the TS125 Transportation Cask

The FuelSolutions™ W74 canister transportation criticality calculations are performed using a model of an infinite array of W74 canisters inside a representative transportation cask configuration. This transportation cask configuration is shown in Figure 6.3-4. This representative transportation cask configuration differs from that of the actual FuelSolutions™ TS125 Transportation Cask, whose geometry is illustrated in Figure 6.3-5.

However, as discussed in Section 6.3.1, the transportation cask configuration is not expected to have a significant impact on system criticality. This is because the canister interior is neutronically de-coupled from the cask materials (and other canisters in the infinite array) by a large water reflection region present around the edge of the basket structure.

To demonstrate that the change in transportation cask configuration has no measurable effect on reactivity, a set of criticality analyses are performed for W74 canisters inside the actual TS125 Transportation Cask configuration. These analyses are performed for a sample of the cases analyzed in the primary W74 criticality analyses. These comparison analyses are performed for the bounding (i.e., lowest criticality margin) case for each BRP assembly type. The comparison runs are performed for the accident condition (infinite package array) case, as this is the bounding condition. The comparison runs are also performed assuming the bounding assembly and canister configuration, as determined by the scoping analyses presented in Section 6.4.2.1.1.

The specific cases for which comparison analyses (between the representative transportation cask configuration and the actual TS125 cask configuration) are performed are listed below. The list describes the case that is analyzed, and shows which result in the Section 6.1 and 6.6 tables the case in question corresponds to:

- The bounding intact BRP 9x9 assembly case (the 2nd case in Table 6.4-7)
- The bounding intact BRP 11x11 assembly case (the 4th case in Table 6.4-7)
- The bounding partial BRP 9x9 assembly configuration (the 1st case in Table 6.6-12)
- The bounding partial BRP 11x11 assembly configuration (the 2nd case in Table 6.6-12)

- The intact J2 MOX assembly configuration (the 1st case in Table 6.6-3)
- The intact DA MOX assembly configuration (the 2nd case in Table 6.6-3)
- The intact G-Pu MOX assembly configuration (the 3rd case in Table 6.6-3)
- The bounding damaged UO₂ fuel assembly configuration (the 12x12 array, 0.35-inch cylinder diameter case in Table 6.6-22)
- The bounding damaged MOX fuel assembly configuration (the 10x10 array, G-Pu MOX fuel case in Table 6.6-22).

In each of the comparison analyses described above, the only change made to the criticality model is to change the transportation cask configuration from that shown in Figure 6.3-4 to the actual FuelSolutions™ TS125 Transportation Cask configuration shown in Figure 6.3-5. The calculated k_{eff} values for the TS125 cask cases are then compared to those of the corresponding original cases. The results of the comparison analyses are presented in Table 6.6-25. For each case, the calculated k_{eff} value and level of statistical error is presented for the TS125 cask case and the corresponding original case. The difference in the calculated k_{eff} values (Δk_{eff}) is also presented for each case. The Δk_{eff} value is defined as the k_{eff} value of the TS125 cask case minus the k_{eff} value for the original (base) case. Thus, a negative Δk_{eff} value indicates that the TS125 cask case was less reactive than the original case.

Examination of the distribution of Δk_{eff} values for the 10 comparison analyses yields the following: the average Δk_{eff} value (over the 10 cases) is only 0.00010. This mean Δk_{eff} value is roughly one tenth the level of statistical error in the individual calculated k_{eff} results presented in. Also, the distribution of Δk_{eff} values lies within the range of statistical error in the individual k_{eff} results. The standard deviation for the distribution of Δk_{eff} values is 0.00118, which is close to the (one sigma) statistical error level listed for the individual calculated k_{eff} results.

Therefore, it is concluded that the distribution of Δk_{eff} values seen in Table 6.6-25 is purely due to statistical variation in the calculated k_{eff} results. It is therefore concluded that the change in transportation cask configuration has no measurable effect on the overall reactivity of the W74 canister system.

It should also be noted that any differences in reactivity between the two transportation cask configurations (shown above to be much smaller than the level of statistical error in the calculated k_{eff} results) is much smaller than the criticality margin that exists for all of the analyzed cases presented in Sections 6.1 and 6.6. The lowest criticality margin shown for the damaged fuel analyses is 0.00268 for a USL of 0.94375 (as shown in Section 6.6.3.5). This is greater than the average Δk_{eff} value of 0.0001 (determined above) by a factor of ~27. The criticality margin for the intact MOX fuel analyses is extremely large (over 0.06). As discussed in Section 6.3.1.3, the intact and partial assembly analyses are extremely conservative in that they model a poison sheet boron concentration of 1.0 w/o (versus the actual value of 1.25 w/o), and they neglect four poison sheets in the W74 basket. Thus, the real criticality margin for the intact and partial assembly analyses is actually much greater than that of the damaged assembly analyses.

For these reasons, it is concluded that any reactivity effects of a change in transportation cask configuration are much smaller than the margin that exists for all analyzed BRP assembly cases.

Therefore, the criticality results (i.e., BRP assembly enrichment limits) calculated based on the representative transportation cask configuration shown in Figure 6.3-4 are applicable for W74 canisters inside the FuelSolutions™ TS125 Transportation Cask.

As discussed in Section 6.4.2.2, 10CFR71.55 requires that analyses be performed to evaluate the relative reactivity of various reflector configurations that may be present around a single package with full water reflection. For this reason, analyses are presented in Section 6.4.2.2 which consider a single canister surrounded by the whole transportation cask, surrounded by only the cask inner liner, and surrounded by the cask inner liner and the gamma shield, with full water reflection around each of those three configurations. The analyses presented above in this section confirm that the cask geometry and materials have no measurable effect on canister reactivity. Therefore, reactivity will not significantly differ between the representative transportation cask and the actual TS125 transportation cask. However, it is difficult to assume that the results and conclusions of the single-package evaluation, which is performed for the representative cask configuration in Section 6.4.2.2, remain applicable for the TS125 transportation cask, since the single-package evaluations are performed specifically to evaluate the effects of cask geometry and materials (i.e., reflector properties).

For that reason, the single-package evaluations presented for the representative transportation cask in Section 6.4.2.2 are repeated for the actual TS125 cask geometry. The results of the TS125 cask single-package evaluations are presented in this section. The only difference between the criticality models used for this evaluation and the single-package criticality models described in Section 6.4.2.2 is that the cask geometry surrounding the canister is switched from the representative cask configuration shown in Figure 6.3-4 to the actual TS125 cask configuration shown in Figure 6.3-5. The set of single-package evaluations shown for the representative cask configuration in Table 6.4-10 are repeated for the TS125 cask. (A sixth case – a normal condition W74 canister inside the transportation cask inner shell only – is also considered.) The results of the TS125 cask single-package analyses are presented in Table 6.6-26.

As in the Section 6.4.2.2 analyses, the TS125 cask single-package analyses model a W74 canister loaded with Siemens 11x11 (121 rod) assemblies. Analyses are run for both normal and accident conditions. As in the Section 6.4.2.2 analyses, all of the single-package results presented in Table 6.6-26 are compared with the infinite HAC cask array case for the Siemens 11x11 assembly. This case (the “bounding intact 11x11 assembly” case) is presented for the TS125 cask in Table 6.6-25.

The highest calculated k_{eff} value shown in Table 6.6-26 for any of the single-package cases is 0.93638. This is very slightly higher than the calculated k_{eff} value of 0.93560 shown in Table 6.6-25 for the bounding (Siemens) intact 11x11 assembly (the TS125 cask case). The difference in k_{eff} (0.00078) is less than the (one sigma) statistical error level in the criticality analysis results. The maximum single-package k_{eff} value of 0.93638 also remains well below its allowable (USL) value of 0.94286, as shown in Table 6.4-7. The difference between the maximum single-package and infinite cask array k_{eff} values (0.00078) is smaller than the statistical error in the analysis results, whereas the criticality margin (0.00648) is much larger than the statistical error in the analysis results. (The margin is ~7 times the statistical error level.)

Therefore, there is no statistically significant difference in reactivity between the infinite HAC cask array configuration and any of the single-package configurations. Based upon that

conclusion, the results of the infinite-package array analyses are considered applicable for all possible cask configurations (including all single-package configurations).

As demonstrated by the above evaluation and the cask comparison evaluation discussed earlier in this section, the final criticality results presented in Section 6.4.3, which are based upon an infinite HAC array of the representative transportation cask geometry shown in Figure 6.3-4, remain fully applicable for a W74 canister inside the TS125 transportation cask.

Table 6.6-1 - Uranium Isotope Atom Densities for UO₂ Fuel Rods in BRP MOX Assemblies

UO₂ Rod Enrichment (w/o ²³⁵U)⁽¹⁾	BRP MOX Assembly Type	²³⁵U Atom Density (atom/barn-cm)	²³⁸U Atom Density (atom/barn-cm)
2.3	G-Pu	5.504 E-04	2.309 E-02
2.4	DA	5.743 E-04	2.306 E-02
2.5	E65/E72 ⁽²⁾	5.983 E-04	2.304 E-02
2.55	J2	6.102 E-04	2.303 E-02
3.2	G-Pu	7.658 E-04	2.287 E-02
3.3	J2	7.897 E-04	2.285 E-02
3.4	E65/E72 ⁽²⁾	8.136 E-04	2.283 E-02
4.5	J2	1.077 E-03	2.257 E-02
4.6	G-Pu	1.101 E-03	2.254 E-02

Notes:

- ⁽¹⁾ UO₂ rod enrichments are shown for each BRP MOX assembly type in Figure 6.6-1 through Figure 6.6-8.
- ⁽²⁾ Two UO₂ assemblies that each have two inserted MOX fuel rods.

Table 6.6-2 - BRP Assembly MOX Fuel Pin Isotope Densities (atom/barn-cm)

Isotope	J2 Assembly MOX Fuel Pin 0.711% ²³⁵ U 3.65% PuO ₂	DA Assembly MOX Fuel Pin #1 1.56% ²³⁵ U 1.03% PuO ₂	DA Assembly MOX Fuel Pin #2 2.4% ²³⁵ U 2.45% PuO ₂	G-Pu Assembly MOX Fuel Pin 0.711% ²³⁵ U 5.45% PuO ₂	E65/E72 Assembly MOX Fuel Pins 0.711% ²³⁵ U + 25.4 grams/rod Pu		
					Solid Pellet (cylindrical)	Annular Pellet (0.1" hole)	Annular Pellet (0.2" hole)
²³⁵ U	1.639 E-04	3.695 E-04	5.603 E-04	1.609 E-04	1.651 E-04	1.650 E-04	1.645 E-04
²³⁸ U	2.260 E-02	2.302 E-02	2.250 E-02	2.218 E-02	2.276 E-02	2.275 E-02	2.269 E-02
²³⁸ Pu	3.665 E-06	1.314 E-06	3.126 E-06	8.242 E-06	-	-	-
²³⁹ Pu	6.548 E-04	1.777 E-04	4.227 E-04	9.255 E-04	-	-	-
²⁴⁰ Pu	1.397 E-04	4.313 E-05	1.026 E-04	2.314 E-04	-	-	-
²⁴¹ Pu	2.478 E-05	7.979 E-06	1.898 E-05	4.635 E-05	3.318 E-04	3.471 E-04	4.058 E-04
²⁴² Pu	1.000 E-05	3.901 E-06	9.280 E-06	2.254 E-05	-	-	-

**Table 6.6-3 - MCNP Calculated Keff Values for W74 Baskets
Fully Loaded with BRP MOX Fuel
(Full Water Density)**

Computer Run ID	BRP Assembly	Calculated k_{eff}	Relative Error	Final k_{eff}	Limiting USL	Criticality Margin
W74_J2	J2 (9x9)	0.83953	0.00094	0.84141	0.94141	0.10000
W74_DA	DA (11x11)	0.82292	0.00091	0.82474	0.94141	0.11667
W74_G-Pu	G-Pu (11x11)	0.88136	0.00092	0.88320	0.94141	0.05821
W74_D72	D72 (partial J2)	0.85021	0.00087	0.85195	0.94141	0.08946
W74_D73	D73 (partial J2)	0.85594	0.00093	0.85780	0.94141	0.08361
W74_G01	G01 (partial G-Pu)	0.84593	0.00089	0.84771	0.94141	0.09370
W74_G02	G02 (partial G-Pu)	0.85121	0.00092	0.85305	0.94141	0.08836
W74_EG0	E65 / E72 ⁽¹⁾	0.85684	0.00088	0.85860	0.94141	0.08281
W74_EG1	E65 / E72 ⁽¹⁾	0.85699	0.00093	0.85885	0.94141	0.08256
W74_EG2	E65 / E72 ⁽¹⁾	0.85808	0.00090	0.85988	0.94141	0.08153
W74_U09	UO ₂ (9x9) ⁽²⁾	0.92106	0.00092	0.92290	0.94358 ⁽⁴⁾	0.02068
W74_U11	UO ₂ (11x11) ⁽³⁾	0.92130	0.00089	0.92308	0.94286 ⁽⁴⁾	0.01978

Notes:

- (1) Two UO₂ assemblies that each have two inserted MOX fuel rods. The “EG0”, “EG1”, and “EG2” cases refer to MOX fuel pellets with inner void region diameters of 0.0, 0.1, and 0.2 inches, respectively.
- (2) This case corresponds to the “GE 9x9, 1 Water Pin” assembly (shown in Table 6.4-7), analyzed inside the current W74 basket configuration. (See Section 6.6.1.1.)
- (3) This case corresponds to the “Siemens 11x11, 121 Fuel Rods” assembly (shown in Table 6.4-7), analyzed inside the current W74 basket configuration. (See Section 6.6.1.1.)
- (4) UO₂ assembly USLs are taken from Table 6.4-7.

**Table 6.6-4 - MCNP Calculated K_{eff} for MOX Fuel
vs. W74 Interior Water Density
(G-Pu Fuel Assemblies)**

Moderator Density (% of FD)	Calculated k_{eff}	Relative 1σ Error	Final k_{eff}
0	0.37418	0.00033	0.37484
10	0.58745	0.00064	0.58873
20	0.64368	0.00077	0.64522
40	0.72842	0.00086	0.73014
60	0.79271	0.00083	0.79437
70	0.81818	0.00086	0.81990
80	0.84037	0.00088	0.84213
90	0.86133	0.00088	0.86309
95	0.87062	0.00084	0.87230
100	0.88136	0.00092	0.88320

Table 6.6-5 - W74 Canister MOX Fuel Specifications

Fuel Assembly Array	DA Assembly	J2 Assembly	G-Pu Assembly	E65/E72 Assemblies
Clad Material	Zr	Zr	Zr	Zr
Number of Fuel Rods	≤ 113	≤ 77	≤ 120	77
Clad O.D. (in)	0.449	0.5625	0.449	0.5625
Clad Thickness (in)	0.034	0.040 ⁽¹⁾	0.034	0.040
Pellet Diameter (in)	0.3715	0.4715 ⁽¹⁾	0.3715	0.4715
Fuel Rod Pitch (in)	0.577	0.707	0.577	0.707
Active Fuel Length (in)	≤ 70	≤ 70	≤ 70	≤ 70
Number of Water Rods ⁽²⁾	4 ⁽²⁾	0	0	0
Number of Inert Rods ⁽³⁾	≥ 0	≥ 0	≥ 1	≥ 0
Number of Corner Rods	0	0	0-4	0
Number of Non-Corner Water Holes ⁽⁴⁾	0	≤ 7 ⁽⁵⁾	≤ 8 ⁽⁶⁾	0
Bottom Tie Plate Height (in)	≥ 1.25	≥ 1.25	≥ 1.25	≥ 1.25
Fuel Pellet Stack Density ⁽⁷⁾	≤ 96.5%	≤ 96.5%	≤ 96.5%	≤ 96.5%
Fuel Material Composition	Varies by pin ⁽⁸⁾	Varies by pin ⁽⁸⁾	Varies by pin ⁽⁸⁾	Varies by pin ^{(8), (9)}

Table Notes on following page

Notes for Table 6.6-5:

- (1) J2 MOX assemblies with a clad thickness of 0.05 inches and a pellet diameter of 0.4515 inches are also acceptable for loading.
- (2) Water rods are identical to fuel rods except that they are filled with water, as opposed to fuel pellets. The DA fuel assembly is only qualified for four water rods in the specific locations shown in Figure 6.6-2.
- (3) Inert rods are defined as solid steel or zircaloy rods that have a diameter and length that are equal or greater than that of a fuel rod.
- (4) A water hole is defined as an empty array location, a hollow (water) rod, a smaller fuel rod, or any other object that displaces less water than a standard fuel rod.
- (5) The two specific assembly configurations shown in Figure 6.6-5 and Figure 6.6-6 are the only J2 assembly configurations containing non-corner water holes that are qualified for loading.
- (6) The two specific assembly configurations shown in Figure 6.6-7 and Figure 6.6-8 are the only G-Pu assembly configurations containing non-corner water holes that are qualified for loading.
- (7) The density is expressed as a percentage of the theoretical UO₂ density of 10.97 g/cc.
- (8) The layout of fuel rod types for the J2, DA, and G-Pu assemblies, and the BRP assemblies with two inserted MOX fuel rods is shown in Figure 6.6-1 through Figure 6.6-4, respectively. For each array location, a UO₂ fuel rod must have an enrichment level that is equal to or less than the enrichment shown for that location in the figures. Gd₂O₃ need not be present in any rods. For MOX rod array locations (as shown in the figures), any fuel rod that is present must contain the MOX fuel material that is described in Table 6.6-2 for that location. Figure 6.6-1 through Figure 6.6-3 give the location, and the uranium and plutonium oxide weight percentages for each MOX fuel rod type. Table 6.6-2 gives the actual isotopic densities within the fuel material for each MOX fuel rod type described in the figures.
- (9) The two MOX fuel rods in the E65 and E72 assemblies may contain solid (cylindrical) pellets, or annular pellets with central void zone diameters of 0.1 or 0.2 inches. In any given MOX fuel rod, the entire pellet stack must contain the same pellet type (i.e., solid, 0.1-inch annular, or 0.2-inch annular).

Table 6.6-6 - MOX Fuel Benchmark Critical Experiments

Name	K _{eff}	Sigma	Fissile % ⁽¹⁾	Pitch	H ₂ O/Fuel	H/Fissile ⁽²⁾	Pu % ⁽³⁾
M1-1	0.99649	0.00092	20.354	0.9525	3.335	50.4	97.3
M1-2	0.99818	0.00091	20.354	1.2588	6.868	103.9	97.3
M1-3	1.00177	0.00096	20.354	1.5342	10.881	164.6	97.3
M1-4	1.00598	0.00090	20.354	1.905	17.534	265.2	97.3
M2-30	0.99771	0.00085	2.571	1.778	1.195	146.2	73.0
M2-31	0.99893	0.00086	2.571	1.778	1.195	146.2	73.0
M2-32	1.00393	0.00083	2.571	2.2091	2.525	309.0	73.0
M2-33	1.00988	0.00084	2.571	2.2091	2.525	308.8	73.0
M2-34	1.00588	0.00080	2.571	2.5145	3.641	445.6	73.0
M2-35	1.00903	0.00079	2.571	2.5145	3.641	445.4	73.0
M3-1	0.99633	0.00091	6.698	1.3208	1.681	73.9	90.1
M3-2	0.99827	0.00094	6.698	1.4224	2.164	95.3	90.1
M3-3	0.99848	0.00095	6.698	1.4224	2.164	95.2	90.1
M3-4	1.00465	0.00089	6.698	1.8679	4.706	206.8	90.1
M3-5	1.00315	0.00089	6.698	2.0116	5.672	249.7	90.1
M3-6	1.00679	0.00085	6.698	2.6416	10.754	473.1	90.1
M4-1	0.99692	0.00089	2.962	1.825	2.42	407.1	76.7
M4-5	0.99897	0.00084	2.962	1.825	2.42	409.6	76.7
M4-6	0.99719	0.00090	2.962	1.956	2.976	500.6	76.7
M4-10	0.99933	0.00086	2.962	1.956	2.976	505.3	76.7
M4-11	0.99897	0.00081	2.962	2.225	4.239	712.6	76.7
M4-15	0.99994	0.00074	2.962	2.225	4.239	717.6	76.7
M4-16	1.00214	0.00077	2.962	2.474	5.552	933.6	76.7
M4-18	1.00055	0.00074	2.962	2.474	5.552	936.9	76.7

Notes:

- ⁽¹⁾ Defined as the mass of fissile nuclides (²³⁵U, ²³⁹Pu, and ²⁴¹Pu) over the total heavy metal mass.
- ⁽²⁾ Defined as the ratio of the number of hydrogen atoms over the total number of fissile nuclide atoms within the fuel assembly array.
- ⁽³⁾ Defined as the percentage of fissile material within the assembly that is plutonium as opposed to uranium.

Table 6.6-7 - Upper Sub-Critical Limit Formulas for the MOX Only, UO₂ Only, and MOX + UO₂ Sets of Critical Experiments

System Physical Parameter	Critical Experiment Set	Min. Value	Max. Value	USL Equation ("x" = parameter value)
Pin Pitch (cm)	MOX Only	0.9525	2.6416	0.93372 + (5.8336 x 10 ⁻³ * x); for (x < 1.72) 0.94375 ; for (x ≥ 1.72)
Pin Pitch (cm)	UO ₂ Only	1.24	2.54	0.93854 + (2.9355 x 10 ⁻³ * x); for (x < 2.412) 0.94562 ; for (x ≥ 2.412)
Pin Pitch (cm)	MOX + UO ₂	0.9525	2.6416	0.93555 + (4.4440 x 10 ⁻³ * x); for (x < 2.05) 0.94466 ; for (x ≥ 2.05)
Water-to-Fuel Volume Ratio	MOX Only	1.195	17.534	0.94093 + (4.2845 x 10 ⁻⁴ * x); for (x < 1.75) 0.94168 ; for (x ≥ 1.75)
Water-to-Fuel Volume Ratio	UO ₂ Only	1.44	3.88	0.94272 + (5.8009 x 10 ⁻⁴ * x); for all x values
Water-to-Fuel Volume Ratio	MOX + UO ₂	1.195	17.534	0.94143 + (5.8269 x 10 ⁻⁴ * x); for (x < 3.93) 0.94372 ; for (x ≥ 3.93)
Fissile Material %	MOX Only	2.57	20.354	0.94197 ; for all x values
Fissile Material %	UO ₂ Only	2.35	5.00	0.94082 + (9.4676 x 10 ⁻⁴ * x); for all x values
Fissile Material %	MOX + UO ₂	2.35	20.354	0.94260 + (1.1082 x 10 ⁻⁴ * x); for (x < 9.926) 0.94370 ; for (x ≥ 9.926)
H-to-Fissile Ratio	MOX Only	50.4	936.9	0.94199 ; for all x values
H-to-Fissile Ratio	UO ₂ Only	80.9	398.7	0.94458 - (3.6041 x 10 ⁻⁶ * x); for all x values
H-to-Fissile Ratio	MOX + UO ₂	50.4	936.9	0.94230 + (3.8900 x 10 ⁻⁶ * x); for (x < 398.5) 0.94385 ; for (x ≥ 398.5)
Fissile Pu Percentage	MOX + UO ₂	0.0	97.3	0.94304 + (3.1082 x 10 ⁻⁵ * x); for (x < 46) 0.94449 ; for (x ≥ 46)

Table 6.6-8 - Parameter Ranges Covered by Critical Experiments and BRP MOX Fuel Assemblies

Physical Parameter	MOX Fuel Experiments		UO ₂ Fuel Experiments		BRP MOX Fuel Assemblies ⁽¹⁾	
	Min. Value	Max. Value	Min. Value	Max. Value	Min. Value	Max. Value
Pin Pitch (cm)	0.9525	2.6416	1.24	2.54	1.46	1.8
Water-to-Fuel Ratio	1.195	17.534	1.44	3.88	1.44	1.61
Fissile Material %	2.57	20.354	2.35	5.00	2.3 ⁽²⁾	5.3
H-to-Fissile Ratio	50.4	936.9	80.9	398.7	89.5	196
Fissile Pu %	73.0	97.3	0.0	0.0	0.0	87.3

Notes:

- (1) Limiting BRP assembly fissile material %, H-to-fissile, and fissile Pu % parameters are calculated based on individual fuel rods, as opposed to assembly average values.
- (2) Based on the two MOX fuel rods in the E65 and E72 assemblies. A small number of individual 2.3% UO₂ fuel rods also occur in the G-Pu MOX assembly. The DA assembly also contains a larger number of 2.33% UO₂ fuel rods. The assembly average fissile material % for the G-Pu assembly is over 3.9%. The lowest assembly average fissile material % for BRP MOX fuel is 3.02%, which occurs for the DA assembly.

Table 6.6-9 - Calculated K_{eff} Values for BRP Assemblies with Missing Array Corner Rods

BRP Assembly Type	Enrichment (w/o ^{235}U)	Calculated k_{eff}	Relative Error Level	Final k_{eff}
GE 9x9	4.1%	0.90893	0.00086	0.91065
Siemens 11x11	4.1%	0.92090	0.00097	0.92284

Table 6.6-10 - Calculated K_{eff} vs. Fuel Rod Pitch for 4.1% Enriched GE 9x9 BRP Assembly Fuel Rods (Single Assembly with Full Water Reflection)

Fuel Rod Pitch (vs. Nominal Value)	Rod Pitch (inches)	Water-to-Fuel Volume Ratio	H-to- ^{235}U Ratio	Calculated k_{eff}	Relative Error	Final k_{eff}
1.00 x Nominal	0.707	1.492	101.9	0.74223	0.00084	0.74391
1.05 x Nominal	0.742	1.786	121.9	0.77288	0.00089	0.77466
1.09 x Nominal	0.772	2.043	139.5	0.78395	0.00093	0.78581
1.10 x Nominal	0.778	2.094	143.0	0.78234	0.00080	0.78394
1.125 x Nominal	0.795	2.254	153.9	0.77764	0.00084	0.77932
1.25 x Nominal	0.885	3.118	212.9	0.74595	0.00085	0.74765

**Table 6.6-11 - Calculated k_{eff} vs. Fuel Rod Pitch for
4.1% Enriched Siemens 11x11 BRP Assembly Fuel Rods
(Single Assembly with Full Water Reflection)**

Fuel Rod Pitch (vs. Nominal Value)	Rod Pitch (inches)	Water-to-Fuel Volume Ratio	H-to- ²³⁵ U Ratio	Calculated k_{eff}	Relative Error	Final k_{eff}
1.00 x Nominal	0.577	1.663	113.5	0.74679	0.00094	0.74867
1.05 x Nominal	0.606	1.977	135.0	0.77607	0.00089	0.77785
1.08 x Nominal	0.621	2.144	146.4	0.77934	0.00083	0.78100
1.09 x Nominal	0.629	2.240	153.0	0.77673	0.00088	0.77849
1.10 x Nominal	0.635	2.308	157.5	0.77413	0.00091	0.77595
1.125 x Nominal	0.649	2.478	169.2	0.76248	0.00083	0.76414
1.14 x Nominal	0.658	2.583	176.3	0.75376	0.00083	0.75542

**Table 6.6-12 - Calculated k_{eff} for BRP Partial Assemblies
at Maximum Allowable Enrichment
(Optimum Pitch⁽¹⁾ Fuel Rod Arrays Inside the W74 Canister)**

BRP Assembly Type	Rod Pitch (inches)	Rod Enrichment (w/o ²³⁵ U)	Water/Fuel Volume Ratio	H / ²³⁵ U Ratio	Calculated k_{eff}	Relative Error	Final k_{eff}
GE 9x9	0.713	3.55%	1.545	121.8	0.93322	0.00086	0.93494
GE 9x9	0.741	3.55%	1.771	139.6	0.94113	0.00099	0.94311
GE 9x9	0.762	3.55%	1.952	153.9	0.93539	0.00087	0.93713
Siemens 11x11	0.567	3.60%	1.555	120.9	0.93360	0.00082	0.93524
Siemens 11x11	0.597	3.60%	1.882	146.3	0.93797	0.00082	0.93961
Siemens 11x11	0.630	3.60%	2.257	175.5	0.93699	0.00089	0.93877

Notes:

- ⁽¹⁾ The optimum pitch (or H-to-U ratio) cases are shown in bold. Two additional cases are shown for each rod type which demonstrate that k_{eff} decreases if the H-to-U ratio is increased or reduced from the optimum value.

**Table 6.6-13 - Physical Parameters and USL Values
for the Optimum BRP Fuel Rod Arrays**

Rod Array Physical Parameter	GE 9x9 Fuel Rod Array		Siemens 11x11 Fuel Rod Array	
	Parameter Value	USL Value	Parameter Value	USL Value
Pin Pitch (in.)	0.741	0.94406	0.597	0.94300
Water-to-Fuel Ratio	1.771	0.94375	1.882	0.94381
H-to- ²³⁵ U Ratio	139.6	0.94408	146.3	0.94405
Fuel Rod Enrichment	3.55%	0.94418	3.6%	0.94423

**Table 6.6-14 - Calculated K_{eff} Values for a W74 Canister w/
Eight Damaged Fuel Cans Containing a Square Array of
0.471-inch Diameter Fuel Cylinders
(Guide Tubes Contain Partial 9x9 BRP Assembly Configurations)**

Array Pitch (in.)	H / ²³⁵ U Ratio	MCNP Calculated K_{eff}	Statistical Error (1 σ)	Final K_{eff} ($k_{eff} + 2\sigma$)
0.679	100	0.92862	0.00087	0.93036
0.777	150	0.93436	0.00086	0.93608
0.795	160	0.93455	0.00091	0.93637
0.830	180	0.93390	0.00083	0.93556
0.864	200	0.93061	0.00091	0.93243

**Table 6.6-15 - Calculated K_{eff} Values for a W74 Canister w/
 Eight Damaged Fuel Cans Containing
 a Square Array of 0.3715-inch Diameter Fuel Cylinders
 (Guide Tubes Contain Partial 9x9 BRP Assembly Configurations)**

Array Pitch (in.)	H / ^{235}U Ratio	MCNP Calculated K_{eff}	Statistical Error (1σ)	Final K_{eff} ($k_{eff} + 2\sigma$)
0.535	100	0.92592	0.00091	0.92774
0.613	150	0.93385	0.00088	0.93561
0.655	180	0.93487	0.00087	0.93661
0.682	200	0.93449	0.00093	0.93635
0.720	230	0.93217	0.00091	0.93399

**Table 6.6-16 - Calculated K_{eff} Values for a W74 Canister w/
 Eight Damaged Fuel Cans Containing
 a Hexagonal Array of 0.471-inch Diameter Fuel Cylinders
 (Guide Tubes Contain Partial 9x9 BRP Assembly Configurations)**

Array Pitch (in.)	H / ^{235}U Ratio	MCNP Calculated K_{eff}	Statistical Error (1σ)	Final K_{eff} ($k_{eff} + 2\sigma$)
0.729	100	0.92779	0.00086	0.92951
0.794	130	0.93091	0.00086	0.93263
0.892	180	0.93103	0.00091	0.93285
0.929	200	0.92947	0.00084	0.93115

**Table 6.6-17 - Calculated K_{eff} Values for a W74 Canister w/
 Eight Damaged Fuel Cans Containing
 a Hexagonal Array of 0.3715-inch Diameter Fuel Cylinders
 (Guide Tubes Contain Partial 9x9 BRP Assembly Configurations)**

Array Pitch (in.)	H / ^{235}U Ratio	MCNP Calculated K_{eff}	Statistical Error (1σ)	Final K_{eff} ($k_{eff} + 2\sigma$)
0.575	100	0.92557	0.00088	0.92733
0.627	130	0.92911	0.00084	0.93079
0.704	180	0.93218	0.00093	0.93404
0.732	200	0.92992	0.00091	0.93174
0.812	260	0.92901	0.00089	0.93079

**Table 6.6-18 - Calculated K_{eff} Values for a W74 Canister w/
 Eight Damaged Fuel Cans Containing
 a Hexagonal Array of 0.9 cm Diameter Fuel Spheres
 (Guide Tubes Contain Partial 9x9 BRP Assembly Configurations)**

Array Pitch (in.)	H / ^{235}U Ratio	MCNP Calculated K_{eff}	Statistical Error (1σ)	Final K_{eff} ($k_{eff} + 2\sigma$)
1.134	140	0.92973	0.00090	0.93153
1.170	160	0.93269	0.00091	0.93451
1.204	180	0.93363	0.00089	0.93541
1.237	200	0.93381	0.00091	0.93563
1.311	250	0.92957	0.00085	0.93127

**Table 6.6-19 - Calculated K_{eff} Values for a W74 Canister w/
 Eight Damaged Fuel Cans Containing
 a Square Array of 0.3715-inch Diameter Fuel Cylinders
 (Guide Tubes Contain Intact 11x11 BRP Assembly Configurations)**

Array Pitch (in.)	H / ^{235}U Ratio	MCNP Calculated K_{eff}	Statistical Error (1σ)	Final K_{eff} ($k_{eff} + 2\sigma$)
0.535	100	0.91782	0.00091	0.91966
0.655	150	0.92742	0.00091	0.92924
0.682	180	0.92927	0.00088	0.93103
0.720	230	0.92719	0.00092	0.92903

**Table 6.6-20 - W74 Damaged Assembly 10CFR71
 Criticality Margin Calculation
 (0.655-inch Pitch Square Array of 0.3715-inch Diameter
 Fuel Cylinders in All Damaged Fuel Cans)**

Contents of Other (guide tube) Fuel Locations	MCNP Calculated K_{eff}	Statistical Error (1σ)	Final K_{eff} ($k_{eff} + 2\sigma$)	Limiting USL ⁽¹⁾	Criticality Margin
Optimum Partial (9x9) BRP Assembly	0.93487	0.00087	0.93661	0.94375	0.00714
Most Reactive Intact (11x11) BRP Assembly	0.92927	0.00088	0.93103	0.94286	0.01183

Note:

⁽¹⁾ Limiting USL for optimum partial assembly case is taken from Table 6.6-13. The intact assembly USL is taken from Table 6.4-7.

**Table 6.6-21 - H-to-²³⁵U Ratio vs. Array Dimension
 for Various UO₂ Fuel Rod Diameters and MOX Fuel Rod Material Compositions⁽¹⁾**

Cylinders per Side Of Array	UO ₂ Fuel Rod Diameter (inches) (4.61 w/o ²³⁵ U)							MOX Fuel Rod Material Type ⁽²⁾ (0.35" diameter cylinders)			
	0.05	0.1	0.2	0.3	0.35	0.3715	0.471	DA-1	DA-2	J2	G-Pu
7	-	-	-	-	-	-	346	-	-	-	-
8	-	-	-	-	-	-	238	-	-	-	486
9	-	-	-	-	-	318	168	732	405	482	359
10	-	-	-	-	279	239	120	553	306	364	271
11	-	-	-	-	214	182	86	425	235	280	208
12	-	-	-	253	166	140	-	330	183	217	162
13	-	-	-	203	130	108	-	258	143	170	127
14	-	-	-	164	102	83	-	202	112	133	-
15	-	-	389	133	80	-	-	-	-	-	-
16	-	-	-	108	-	-	-	-	-	-	-
17	-	-	283	88	-	-	-	-	-	-	-
19	-	-	211	-	-	-	-	-	-	-	-
21	-	-	159	-	-	-	-	-	-	-	-
25	-	-	92	-	-	-	-	-	-	-	-
26	-	520	-	-	-	-	-	-	-	-	-
30	-	371	-	-	-	-	-	-	-	-	-
35	-	253	-	-	-	-	-	-	-	-	-
40	-	178	-	-	-	-	-	-	-	-	-
45	-	127	-	-	-	-	-	-	-	-	-
50	-	90	-	-	-	-	-	-	-	-	-
60	362	-	-	-	-	-	-	-	-	-	-
70	249	-	-	-	-	-	-	-	-	-	-
75	208	-	-	-	-	-	-	-	-	-	-
80	175	-	-	-	-	-	-	-	-	-	-
90	125	-	-	-	-	-	-	-	-	-	-
100	90	-	-	-	-	-	-	-	-	-	-

Note:

⁽¹⁾ For the MOX fuel rod cases, the H-to-²³⁵U ratio actually refers to the ratio of hydrogen atoms to the total fissile atoms in the fuel (i.e., ²³⁵U, ²³⁹Pu, and ²⁴¹Pu).

Table 6.6-22 - Final k_{eff} vs. Fuel Cylinder Diameter and H-to- ^{235}U Ratio⁽¹⁾

Cylinders per Side Of Array ⁽²⁾	UO ₂ Fuel Rod Diameter (inches) (4.61 w/o ^{235}U)							MOX Fuel Rod Material Type (0.35" diameter cylinders)			
	0.05	0.1	0.2	0.3	0.35	0.3715	0.471	DA-1	DA-2	J2	G-Pu
7	-	-	-	-	-	-	0.92487	-	-	-	-
8	-	-	-	-	-	-	0.93247	-	-	-	0.92812
9	-	-	-	-	-	0.92884	0.93648	0.91928	0.92609	0.92747	0.93439
10	-	-	-	-	0.93263	0.93358	0.93630	0.92173	0.93274	0.93007	0.93686
11	-	-	-	-	0.93371	0.93787	0.93248	0.92254	0.93389	0.93134	0.93621
12	-	-	-	0.93556	0.93885	0.93723	-	0.92406	0.93162	0.93163	0.93539
13	-	-	-	0.93670	0.93607	0.93603	-	0.92298	0.93143	0.92988	0.93319
14	-	-	-	0.93793	0.93381	0.92992	-	0.92282	0.92813	0.92598	-
15	-	-	0.92934	0.93703	0.93180	-	-	-	-	-	-
16	-	-	-	0.93401	-	-	-	-	-	-	-
17	-	-	0.93442	0.93141	-	-	-	-	-	-	-
19	-	-	0.93788	-	-	-	-	-	-	-	-
21	-	-	0.93518	-	-	-	-	-	-	-	-
25	-	-	0.93134	-	-	-	-	-	-	-	-
26	-	0.92297	-	-	-	-	-	-	-	-	-
30	-	0.92832	-	-	-	-	-	-	-	-	-
35	-	0.93748	-	-	-	-	-	-	-	-	-
40	-	0.93651	-	-	-	-	-	-	-	-	-
45	-	0.93316	-	-	-	-	-	-	-	-	-
50	-	0.93029	-	-	-	-	-	-	-	-	-
60	0.92974	-	-	-	-	-	-	-	-	-	-
70	0.93398	-	-	-	-	-	-	-	-	-	-
75	0.93596	-	-	-	-	-	-	-	-	-	-
80	0.93313	-	-	-	-	-	-	-	-	-	-
90	0.93002	-	-	-	-	-	-	-	-	-	-
100	0.92938	-	-	-	-	-	-	-	-	-	-

Notes:

- ⁽¹⁾ For the MOX fuel rod cases, the H-to- ^{235}U ratio actually refers to the ratio of hydrogen atoms to the total fissile atoms in the fuel (i.e., ^{235}U , ^{239}Pu , and ^{241}Pu).
- ⁽²⁾ The H-to- ^{235}U ratios that correspond to the number of cylinders per side, for each of the diameter and MOX rod cases, are given in Table 6.6-21.

Table 6.6-23 - Final k_{eff} vs. H-to-²³⁵U Ratio for Various Fuel Sphere Diameters

H-to- ²³⁵ U Ratio ⁽¹⁾	UO ₂ Fuel Sphere Diameter (inches) (4.61 w/o ²³⁵ U)							
	0.2	0.5	0.7	0.9	1.1	1.3	1.5	2.0
120	0.93019	0.93160	0.93332	0.93206	0.93142	0.93262	0.93470	0.92944
140	0.93014	0.93176	0.93409	0.93153	0.93537	0.93463	0.93361	0.93062
160	0.93090	0.93401	0.93326	0.93451	0.93519	0.93594	0.93354	0.93235
180	0.93124	0.93494	0.93579	0.93541	0.93428	0.93240	0.93412	0.93254
200	0.93334	0.93496	0.93323	0.93563	0.93368	0.93357	0.93524	0.93203
220	0.93185	0.93345	0.93119	0.93406	0.93014	0.93154	0.93040	0.92920
250	0.93119	0.93121	0.92983	0.93127	0.93170	0.92932	0.93073	0.92780

Notes:

⁽¹⁾ Defined as the ratio of hydrogen atoms to ²³⁵U atoms within the area covered by the fuel rod array.

Table 6.6-24 - Final k_{eff} vs. Particle Diameter for UO₂ Fuel Cylinders and Spheres (at optimum H-to-²³⁵U ratio)

Cylinders			Spheres		
Diameter (inches)	Optimum H-to- ²³⁵ U	Final k_{eff}	Diameter (inches)	Optimum H-to- ²³⁵ U	Final k_{eff}
0.05	208	0.93596	0.2	200	0.93334
0.10	253	0.93748	0.5	200	0.93496
0.20	211	0.93788	0.7	180	0.93579
0.30	164	0.93793	0.9	200	0.93563
0.35	166	0.93885	1.1	140	0.93537
0.3715	182	0.93787	1.3	160	0.93594
0.471	168	0.93648	1.5	200	0.93524
-	-	-	2.0	180	0.93254

**Table 6.6-25 - Transportation Cask Comparison Case Results
 for the FuelSolutions™ W74 Canister**

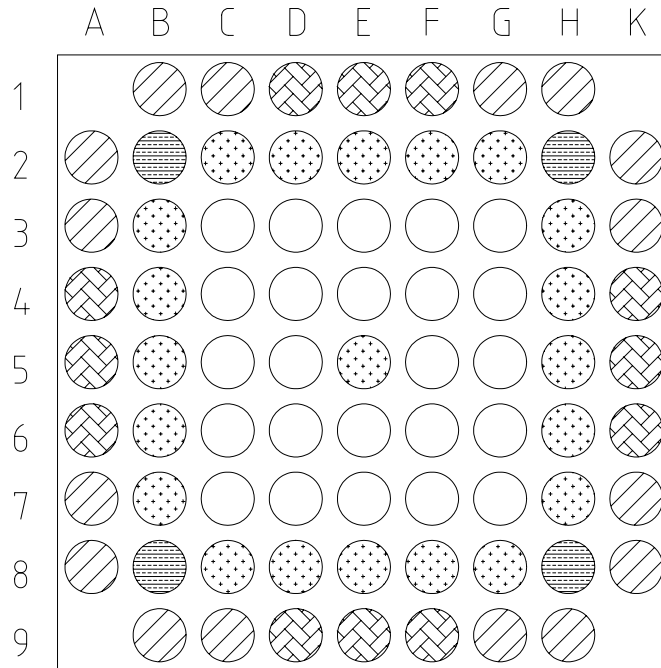
Case	Description	FuelSolutions™ TS125 Cask Configuration (Figure 6.3-5)		Original (Representative) Cask Configuration (Figure 6.3-4)		Δk_{eff}
		k_{eff}	Uncertainty	k_{eff}	Uncertainty	
1	Bounding Intact 9x9 Assembly	0.93715	0.00091	0.93569	0.00085	0.00146
2	Bounding Intact 11x11 Assembly	0.93560	0.00084	0.93831	0.00088	-0.00271
3	Bounding Partial 9x9 Assembly	0.94157	0.00103	0.94113	0.00099	0.00044
4	Bounding Partial 11x11 Assembly	0.93739	0.00083	0.93797	0.00082	-0.00058
5	Intact J2 MOX Assembly	0.83886	0.00108	0.83953	0.00094	-0.00067
6	Intact DA MOX Assembly	0.82422	0.00088	0.82292	0.00091	0.00130
7	Intact G-Pu MOX Assembly	0.87851	0.00111	0.88136	0.00092	-0.00285
8	Bounding Damaged UO ₂ Fuel Configuration	0.93621	0.00087	0.93701	0.00092	-0.00080
9	Bounding Damaged MOX Fuel Configuration	0.93213	0.00087	0.93506	0.00090	-0.00293

**Table 6.6-26 - MCNP Results for the TS125 Cask
Single-Package Models**

Case	Description	²³⁵U Enrichment (w/o)	k_{eff}⁽¹⁾	Uncertainty
1	Siemens 11x11 (121 rods) Accident Conditions All Cask Shells Present	4.10	0.93602	0.00084
2	Siemens 11x11 (121 rods) Accident Conditions Cask Inner Shell Only	4.10	0.93638	0.00094
3	Siemens 11x11 (121 rods) Accident Conditions Inner Shell + Pb Shield	4.10	0.93602	0.00084
4	Siemens 11x11 (121 rods) Normal Conditions All Cask Shells Present	4.10	0.93427	0.00085
5	Siemens 11x11 (121 rods) Normal Conditions Cask Inner Shell Only	4.10	0.93478	0.00092
6	Siemens 11x11 (121 rods) Normal Conditions Inner Shell + Pb Shield	4.10	0.93478	0.00092

Note:

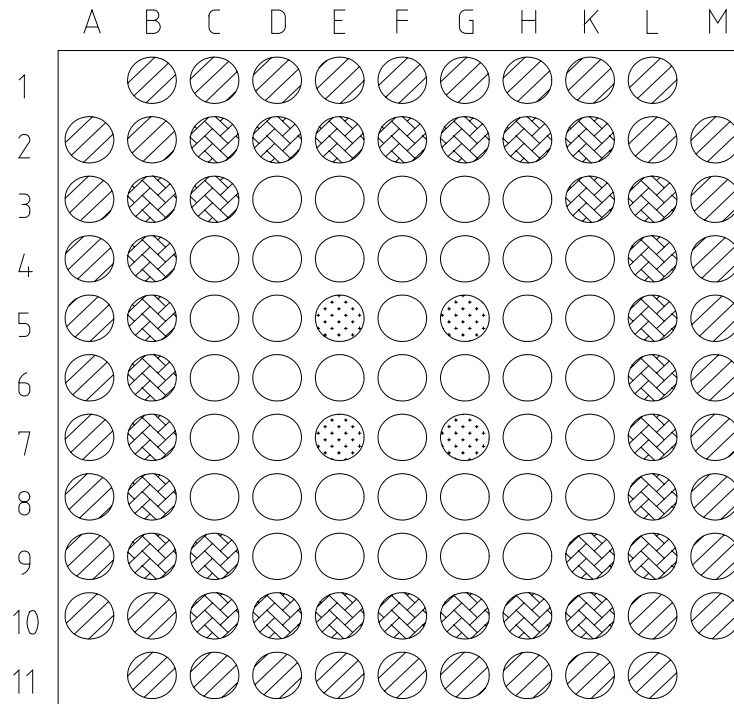
⁽¹⁾ The calculated k_{eff} values of all five single-package cases are compared to the calculated k_{eff} value presented for Case 2 in Table 6.6-25.



Fuel Pin Compositions

- | | | | |
|---|----------------|---|---|
|  | 2.55 Wt% U-235 |  | 3.30 Wt% U-235 and
1.00 % Gd203 in UO2 |
|  | 3.30 Wt% U-235 |  | 0.711 Wt% U-235
3.65 % PuO2 |
|  | 4.50 Wt% U-235 | | |

Figure 6.6-1 - J2 (9x9) BRP MOX Assembly Array

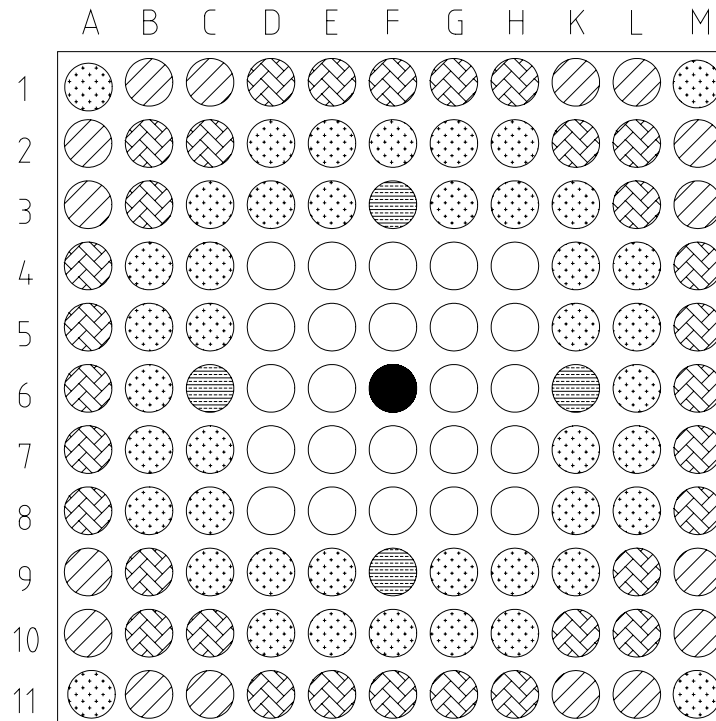


Fuel Pin Compositions

- | | | | |
|---|---|---|---------------------------|
|  | 2.40 Wt% U-235 |  | 2.40 Wt% U-235 |
|  | 1.56 Wt% U-235
1.03 Wt% PuO ₂ |  | 2.45 Wt% PuO ₂ |
| | |  | Water Rods |

Note: Water rods have the same diameter and cladding thickness as fuel rods, but they do not contain fuel pellets.

Figure 6.6-2 - DA (11x11) BRP MOX Assembly Array

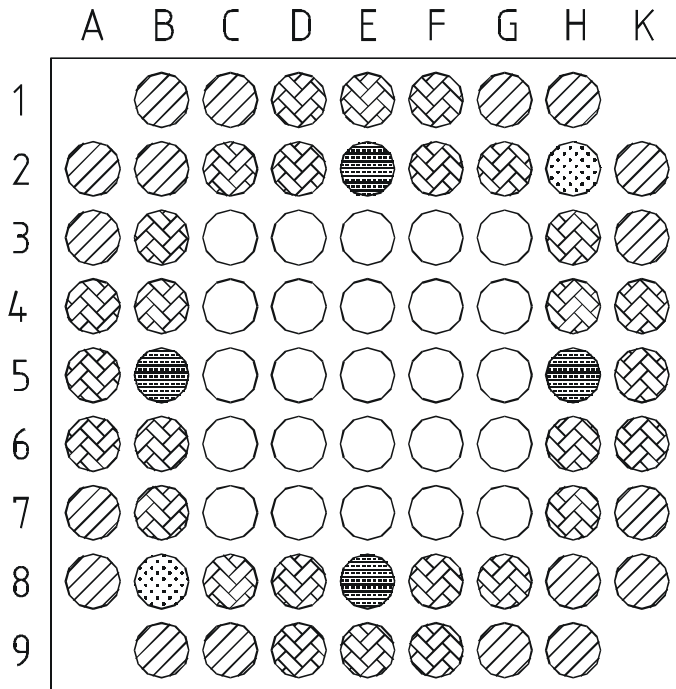


Fuel Pin Compositions

- | | | | |
|---|----------------|---|---------------------------|
|  | 2.30 Wt% U-235 |  | 4.60 Wt% U-235 |
|  | 3.20 Wt% U-235 |  | 0.711 Wt% U-235 |
|  | 4.60 Wt% U-235 |  | Solid Zirc Rod |
| | | | 5.45 Wt% PuO ₂ |

Note: G-Pu assemblies may have any number of fuel rods missing (or present) in the four corner array locations.

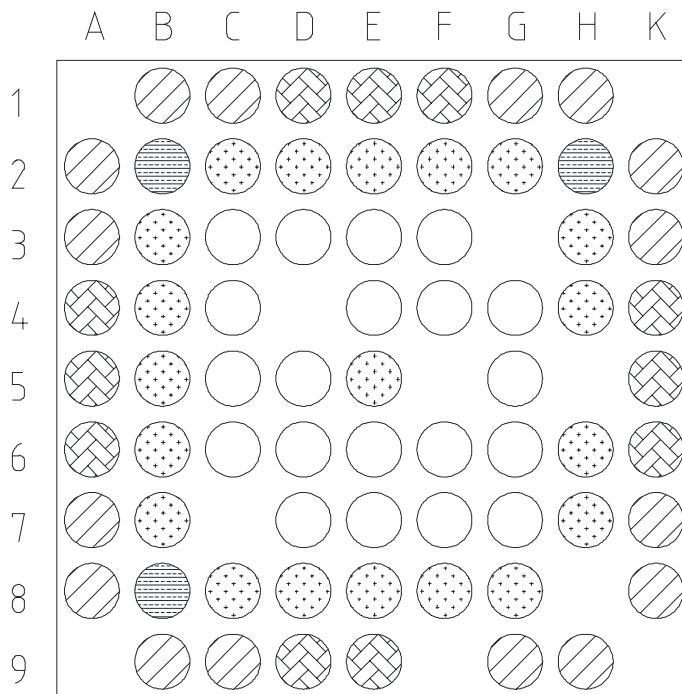
Figure 6.6-3 - G-Pu (11x11) BRP MOX Assembly Array



Fuel Pin Compositions

- | | | | |
|--|----------------|--|-----------------------|
| | 2.50 Wt% U-235 | | 3.40 Wt% U-235 |
| | 3.40 Wt% U-235 | | 2.00 Wt% Gd203 in UO2 |
| | 4.5 Wt% U-235 | | |
- 25.4 g/rod Pu

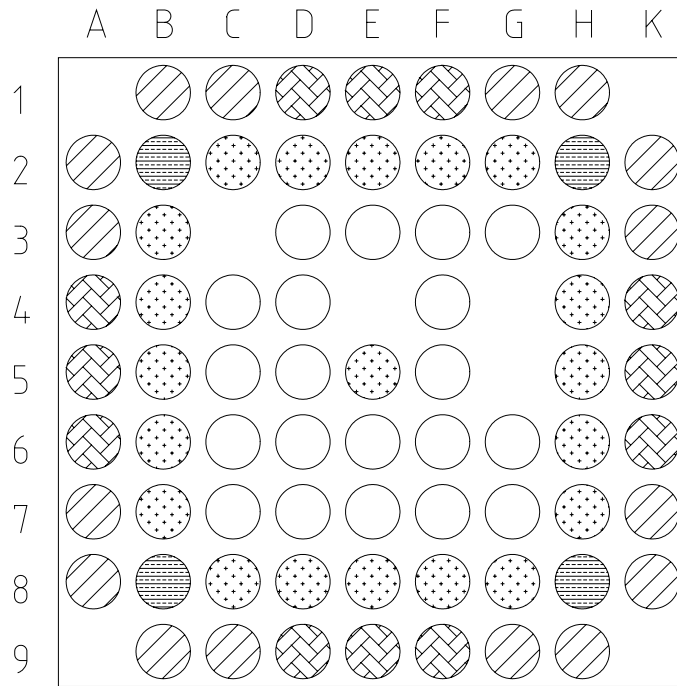
Figure 6.6-4 - UO₂ 9x9 BRP Assembly with Two Inserted MOX Rods



Fuel Pin Compositions

- | | | | |
|---|----------------|---|--|
|  | 2.55 Wt% U-235 |  | 3.30 Wt% U-235 and
1.00% Gd203 in UO2 |
|  | 3.30 Wt% U-235 |  | 0.711% U-235
3.65% PuO2 |
|  | 4.50 Wt% U-235 | | |

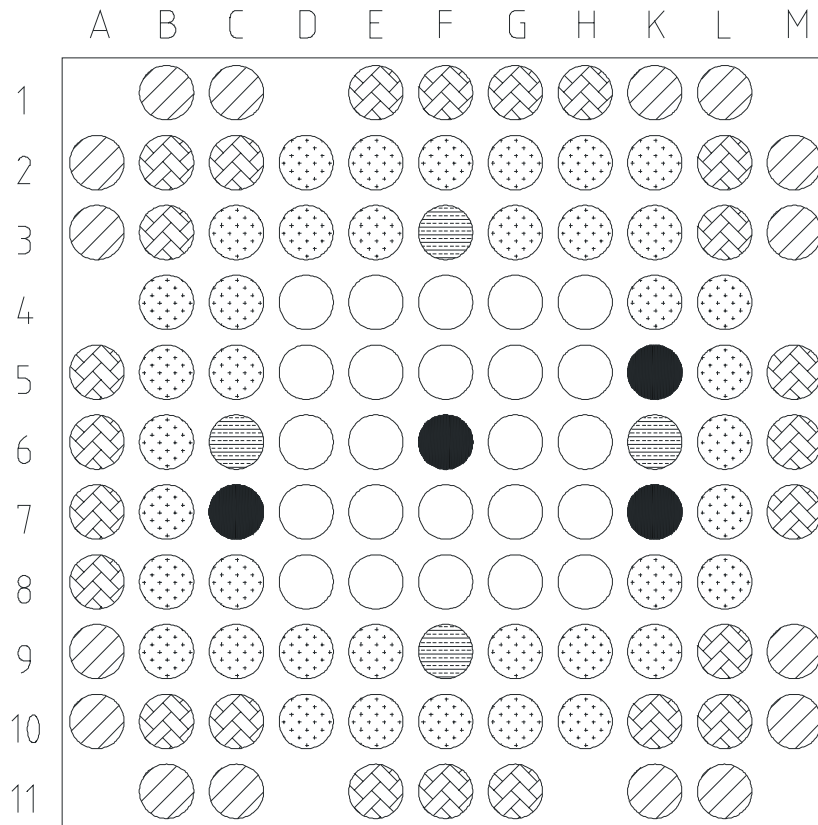
Figure 6.6-5 - D72 Partial Assembly Array - J2 Assembly Type



Fuel Pin Compositions

- | | | | |
|---|----------------|---|---|
|  | 2.55 Wt% U-235 |  | 3.30 Wt% U-235 and
1.00 % Gd203 in UO2 |
|  | 3.30 Wt% U-235 | | |
|  | 4.50 Wt% U-235 |  | 0.711 Wt% U-235
3.65 % PuO2 |

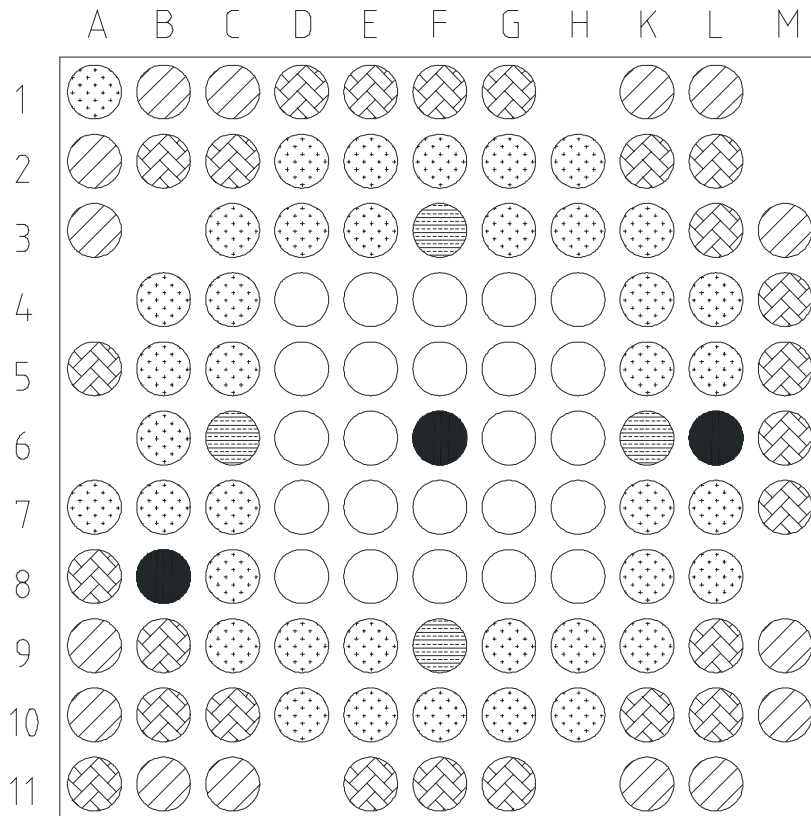
Figure 6.6-6 - D73 Partial Assembly Array - J2 Assembly Type



Fuel Pin Compositions

- | | | | |
|--|----------------|--|-----------------|
| | 2.30 Wt% U-235 | | 4.60 Wt% U-235 |
| | 3.20 Wt% U-235 | | 1.20 Wt% Gd203 |
| | 4.60 Wt% U-235 | | 0.711 Wt% U-235 |
| | Solid Zirc Rod | | 5.45 Wt% PuO2 |

Figure 6.6-7 - G01 Partial Assembly Array - G-Pu Assembly Type



Fuel Pin Compositions

- | | | | |
|---|----------------|---|-----------------|
|  | 2.30 Wt% U-235 |  | 4.60 Wt% U-235 |
|  | 3.20 Wt% U-235 |  | 1.20 Wt% Gd2O3 |
|  | 4.60 Wt% U-235 |  | 0.711 Wt% U-235 |
|  | Solid Zirc Rod |  | 5.45 Wt% PuO2 |

Figure 6.6-8 - G02 Partial Assembly Array - G-Pu Assembly Type

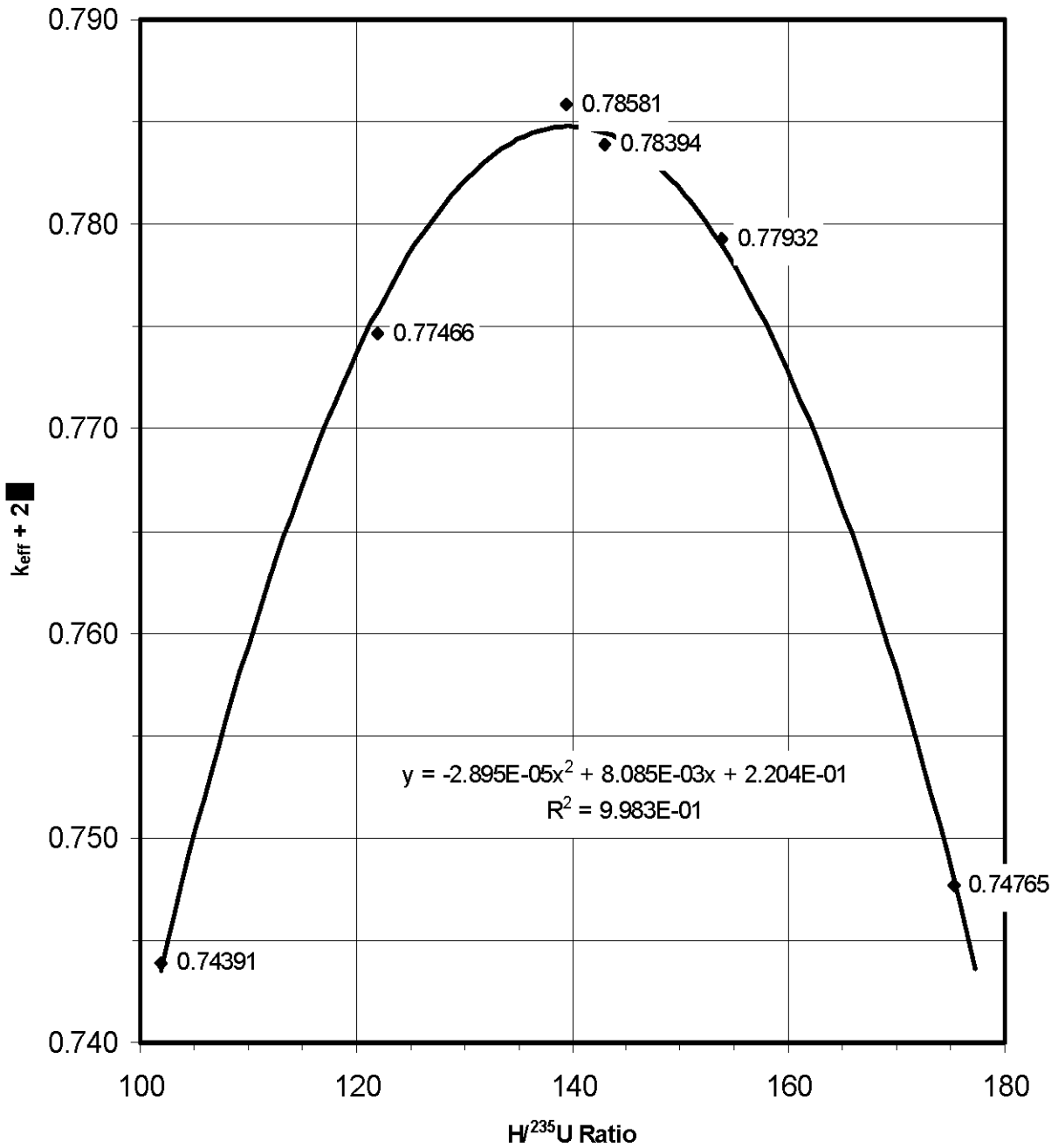


Figure 6.6-9 - K_{eff} vs. H-to-²³⁵U Ratio for GE 9x9 BRP Fuel Rod Arrays (Single Assembly Sized Fuel Rod Array with Full Water Reflection)

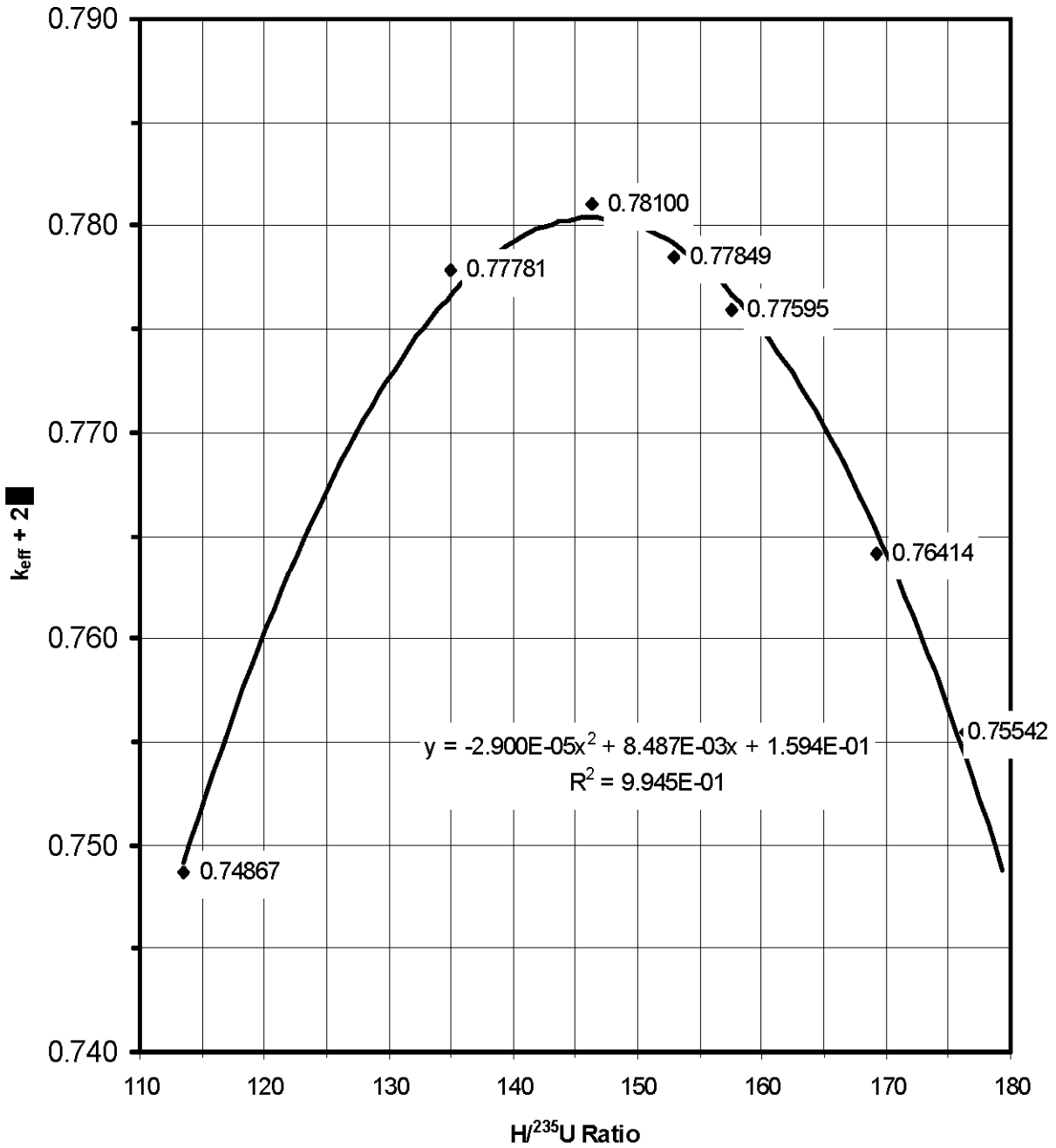


Figure 6.6-10 - K_{eff} vs. H-to-²³⁵U Ratio for Siemens 11x11 BRP Fuel Rod Arrays (Single Assembly Sized Fuel Rod Array with Full Water Reflection)

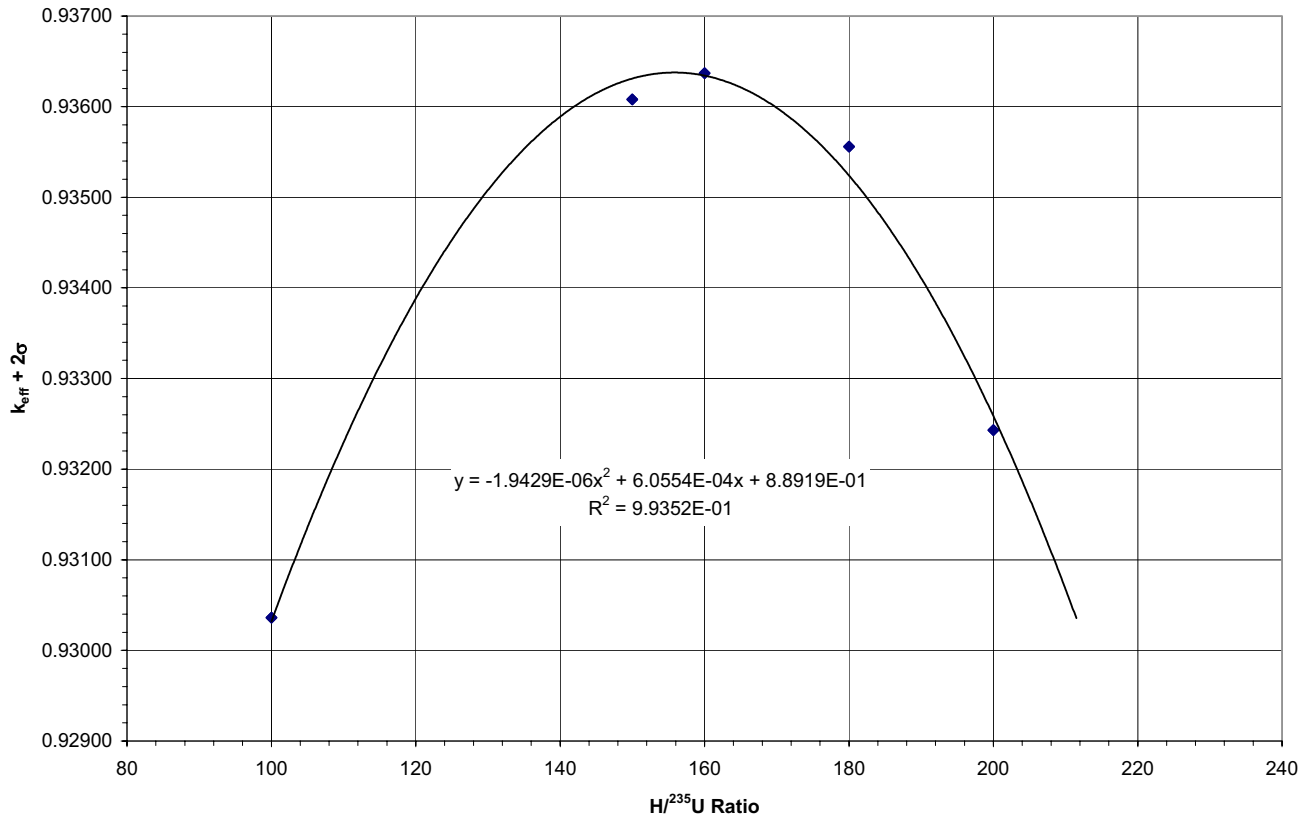


Figure 6.6-11 - K_{eff} vs. H / ²³⁵U Ratio for a Square Array of 0.471-inch Diameter Fuel Cylinders

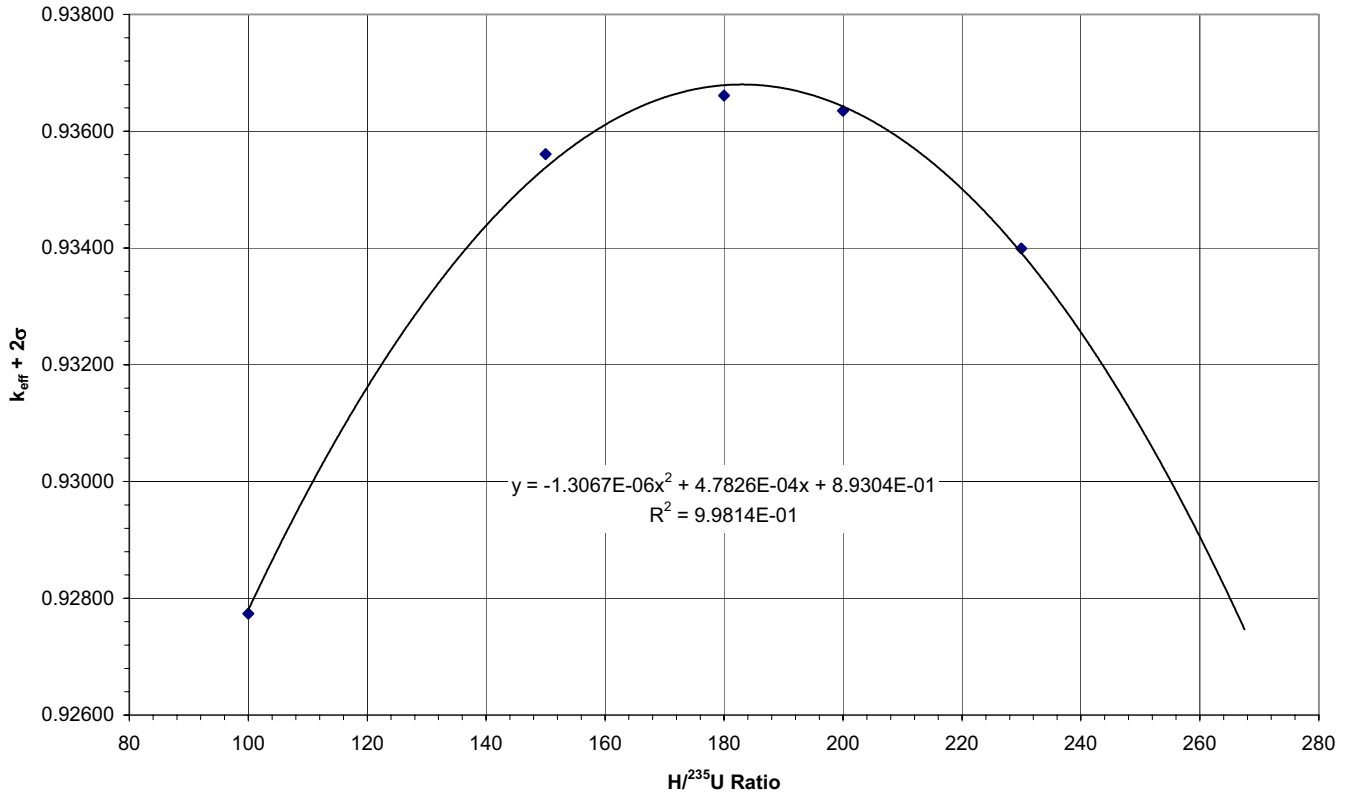


Figure 6.6-12 - K_{eff} vs. $\text{H} / ^{235}\text{U}$ Ratio for a Square Array of 0.3715-inch Diameter Fuel Cylinders

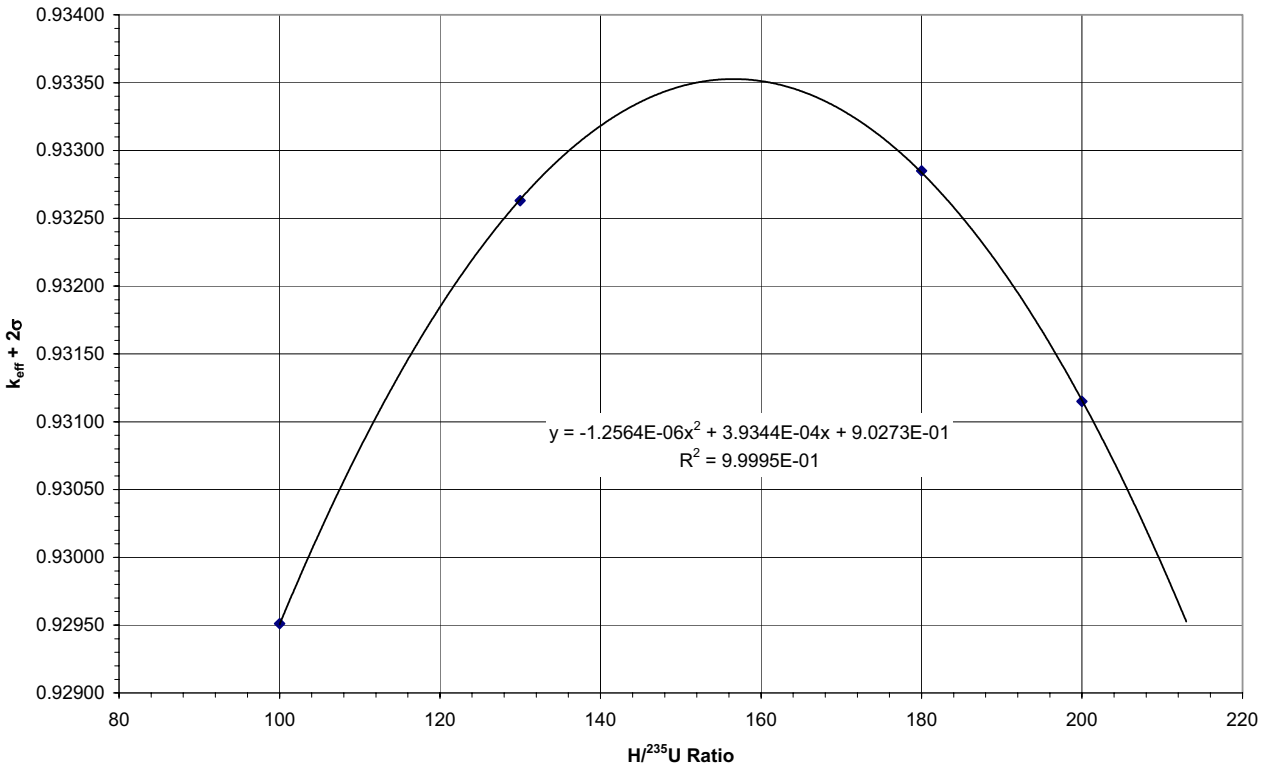


Figure 6.6-13 - K_{eff} vs. H / ²³⁵U Ratio for a Hexagonal Array of 0.471-inch Diameter Fuel Cylinders

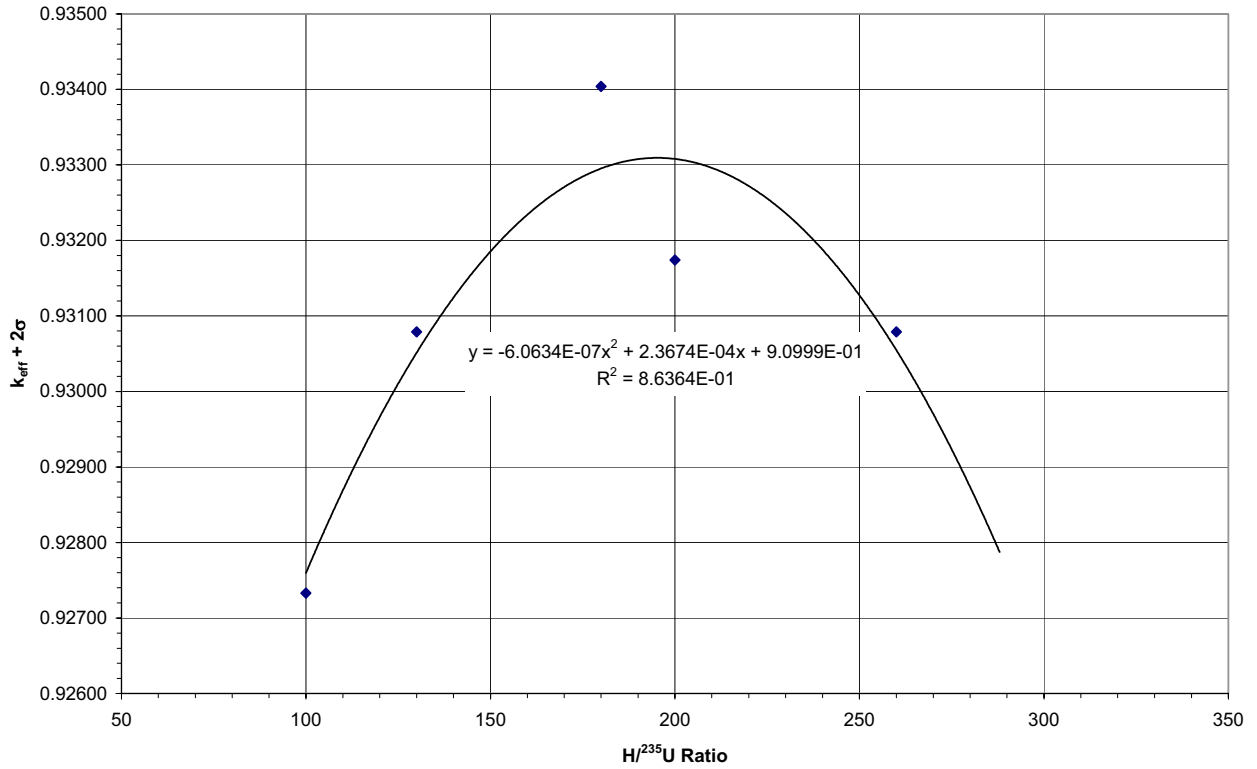


Figure 6.6-14 - K_{eff} vs. H / ²³⁵U Ratio for a Hexagonal Array of 0.3715-inch Diameter Fuel Cylinders

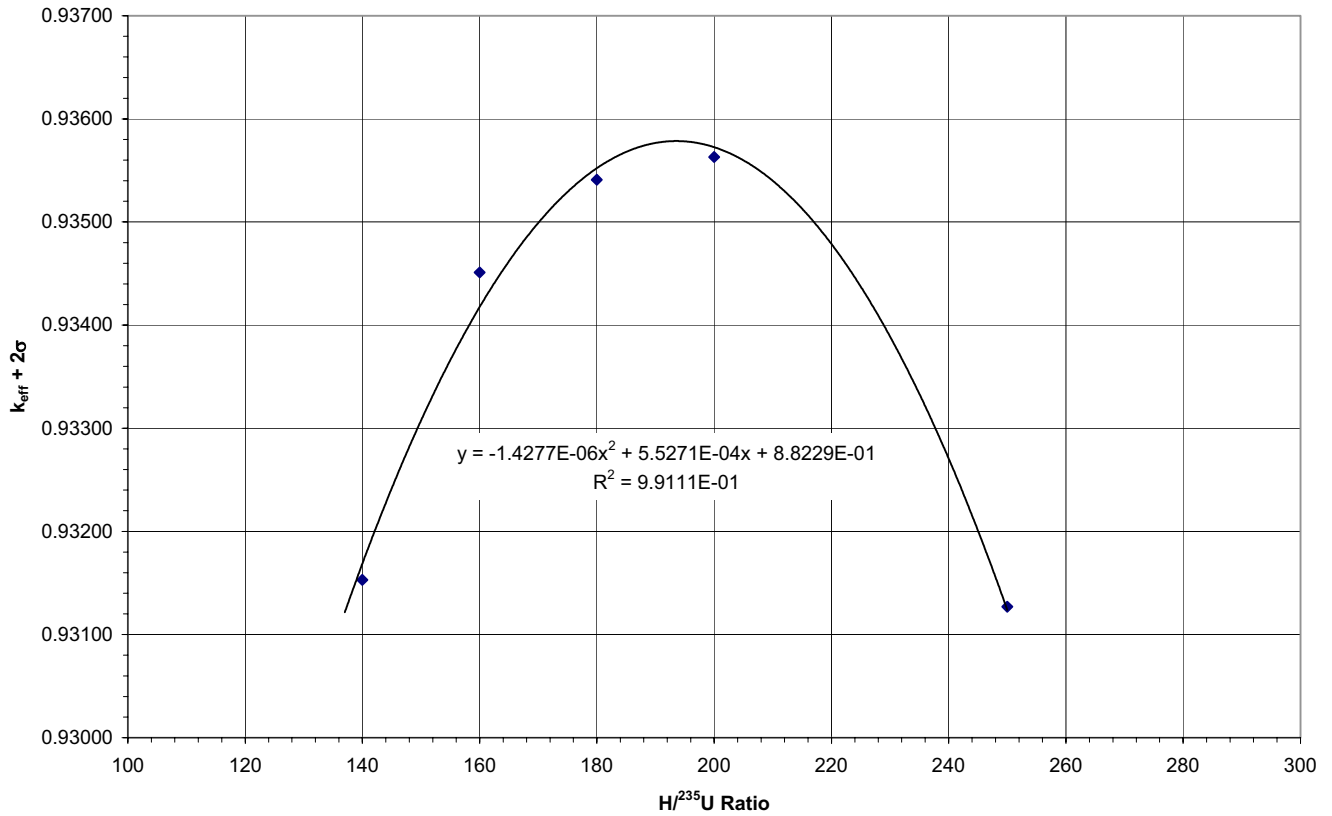


Figure 6.6-15 - K_{eff} vs. H / ²³⁵U Ratio for a Hexagonal Array of 0.9 cm Diameter Fuel Spheres

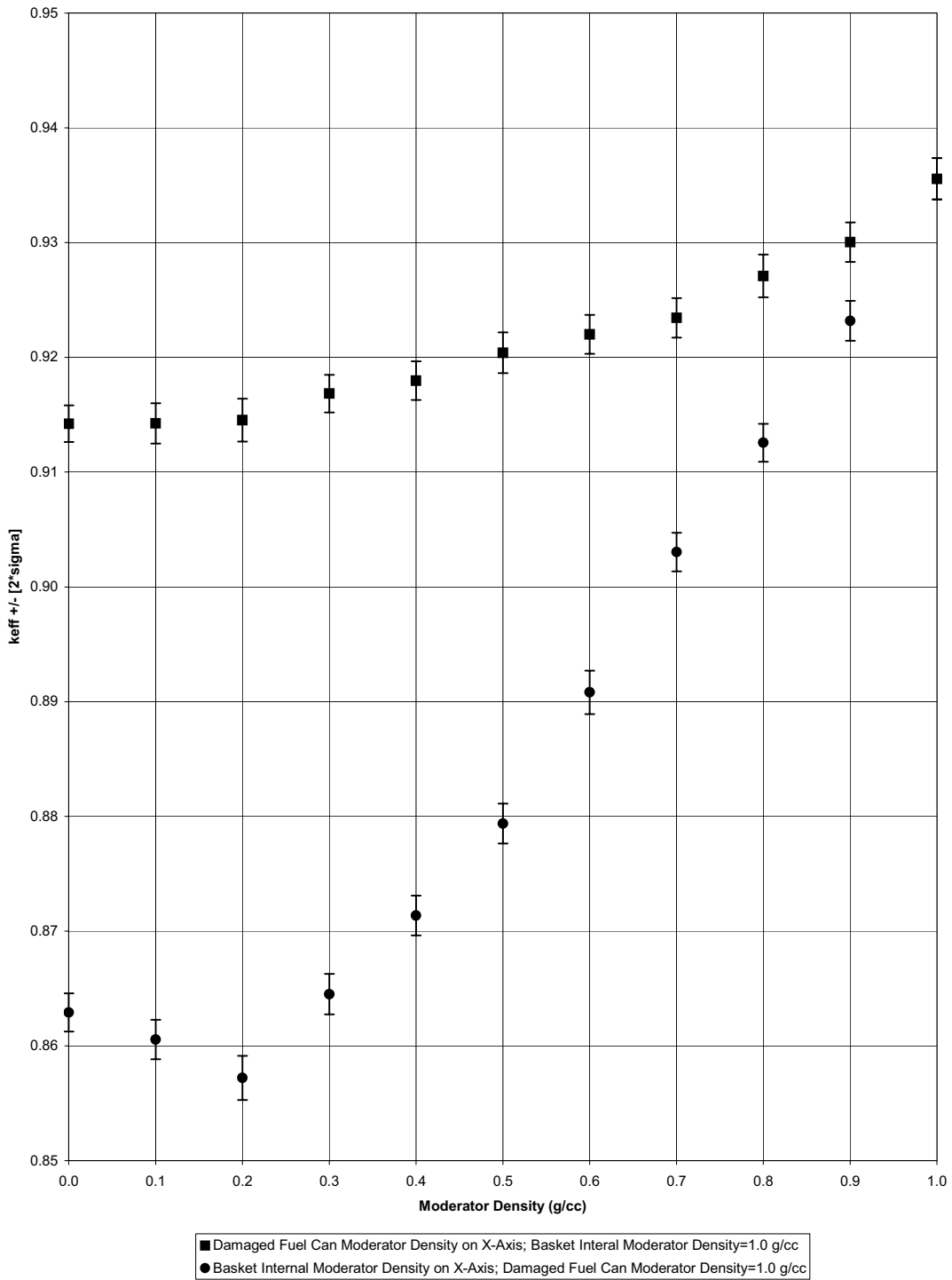


Figure 6.6-16 - W74 Canister k_{eff} vs. Damaged Fuel Can Interior and Canister Interior Moderator Densities

This page intentionally left blank.

7. OPERATING PROCEDURES

The generic operating procedures for the FuelSolutions™ Transportation System are presented in Chapter 7 of the FuelSolutions™ TS125 Transportation Cask SAR.¹ The associated procedures that are applicable to the FuelSolutions™ W74 canister include the following:

- Horizontal transfer of the FuelSolutions™ canister from the transfer cask to the transportation cask (Section 7.1.5).
- Vertical transfer of the FuelSolutions™ canister from the transfer cask to the transportation cask inside the fuel building (Section 7.1.6).

Procedures for other transportation cask handling operations that are applicable to the FuelSolutions™ W74 canister are also provided in Sections 7.1.1, 7.1.2, 7.1.8, and 7.1.9 of the FuelSolutions™ TS125 Transportation Cask SAR.

Procedures for fuel loading of a FuelSolutions™ W74 canister in a spent fuel pool are provided in Section 7.1.3 of the FuelSolutions™ TS125 Transportation Cask SAR,¹ except as noted in this chapter. Procedures for fuel loading of a FuelSolutions™ W74 canister outside the spent fuel pool in the plant's cask receiving bay using a shuttle cask and a shielded loading collar are described in Section 8.3 of the FuelSolutions™ W74 Canister Storage FSAR.² These operations are accomplished using the FuelSolutions™ support equipment described in Section 1.2.1.7 of the FuelSolutions™ TS125 Transportation Cask SAR and Section 1.2.1.4 of the FuelSolutions™ Storage System FSAR.³

The generic operating procedures provided in the FuelSolutions™ TS125 Transportation Cask SAR are applicable to the FuelSolutions™ W74 canister, as noted above. The following sections outline the operating procedures for the FuelSolutions™ Transportation System using the FuelSolutions™ W74 canister, referring to the generic procedures when applicable. These procedures have been developed to assure that all operations required for canister loading, unloading, transfer, and transport are performed safely, minimize personnel exposure, and optimize the sequence of steps required to complete the subject operations. In preparing site-specific procedures, the licensee may determine that acceptable alternate means may be available to accomplish the same operational objective.

¹ WSNF-120, *FuelSolutions™ TS125 Transportation Cask Safety Analysis Report*, NRC Docket No. 71-9276, EnergySolutions Spent Fuel Division, Inc.

² WSNF-223, *FuelSolutions™ W74 Canister Storage Final Safety Analysis Report (FSAR)*, Docket No. 72-1026, BNG Fuel Solutions Corporation.

³ WSNF-220, *FuelSolutions™ Storage System Final Safety Analysis Report (FSAR)*, Docket No. 72-1026, BNG Fuel Solutions Corporation.

This page intentionally left blank.

7.1 Procedures for Loading the Cask in the Spent Fuel Pool

The major procedural steps for loading SNF assemblies into a FuelSolutions™ canister placed in a FuelSolutions™ TS125 Transportation Cask in a spent fuel pool are outlined in Section 7.1.4 of the FuelSolutions™ Transportation Cask SAR. This section outlines specific differences in the operation of the FuelSolutions™ W74 canister during fuel loading in a spent fuel pool. All other operations are the same as those described in Section 7.1.4 of the FuelSolutions™ Transportation Cask SAR.

7.1.1 Preparation of an Empty Canister for Fuel Loading

These procedures are provided in Section 7.1.4.1 of the FuelSolutions™ TS125 Transportation Cask SAR. However, Steps 1 through 7 of Section 7.1.4.1 are augmented as follows for preparation of a W74 canister for loading (Step 8), and for loading a W74 canister with damaged fuel assemblies (Steps 9 and 10):

8. Verify that the upper basket assembly of the FuelSolutions™ W74 canister is not inside the canister. Remove the upper basket assembly, if present.
9. Examine the empty damaged fuel can and its lid for any physical damage that might have occurred since its on-site receipt inspection was performed. The damaged fuel can and its lid should be clean, and any packaging material or loose debris removed.
10. Test fit the lid inside its associated damaged fuel can and assure that its engagement finger locking devices operate correctly and freely under remote grapple conditions.

7.1.2 Installing an Empty Canister into the Transportation Cask

These procedures are provided in Section 7.1.4.2 of the FuelSolutions™ TS125 Transportation Cask SAR. However, Steps 1 through 3 of Section 7.1.4.2 are augmented as follows for installation of damaged fuel cans into the lower and upper basket assemblies: If the W74 canister's lower basket assembly is to be loaded with damaged fuel assemblies, place a damaged fuel can in each of the selected support tubes.

4. Remove the lid from each damaged fuel can.
5. Repeat Steps 4 and 5 for the W74 canister upper basket assembly.
6. Place the W74 upper basket assembly in a suitable staging area.

7.1.3 Load Fuel into the Canister

These procedures are provided in Section 7.1.4.4 of the FuelSolutions™ TS125 Transportation Cask SAR. However, Steps 1 through 6 of Section 7.1.4.4 are augmented as follows for loading of the FuelSolutions™ W74 canister upper basket assembly:

7. After completion of loading SNF into the lower basket assembly, if damaged fuel has been loaded, use a manual grapple to lower the lid of each damaged fuel can into place. The assistance of an underwater video camera or other device may be required.

8. Using a manual grapple with a fixed hex-head ball driver, manipulate the damaged fuel can's lid engagement fingers to lock the lid of each damaged fuel can into place.
9. Repeat Steps 7 and 8 for each damaged fuel can in the lower basket assembly.
10. Install the upper basket assembly containing any required damaged fuel cans and/or dummy fuel assemblies into the canister.

CAUTION: Rigging and handling operations must comply with the plant's NUREG-0612/ANSI N14.6 commitments.

11. Repeat Steps 1 through 6 for each SNF assembly to be loaded into the upper basket assembly.
12. Repeat Steps 7 and 8 for each damaged fuel can in the upper basket assembly.

7.1.4 Drain and Backfill Canister with Helium

The procedure for draining and backfilling the W74 canister with helium are provided in Section 7.1.4.8 of the FuelSolutions™ TS125 Transportation Cask SAR. This section defines the specific requirements for the vacuum drying time limits and the required helium backfill density for the W74 canister.

The procedure for vacuum drying the W74 canister is provided in Section 7.1.4.8, Step 6, of the FuelSolutions™ TS125 Transportation Cask SAR. The initial vacuum drying time for a FuelSolutions™ W74 canister is limited to 7 hours. If additional vacuum drying time is required, the controlled vacuum drying process will require at least 4 hours of cooling under helium gas backfill prior to initiating another vacuum drying period of 4 hours. Repeat this cycle of cooling under helium backfill and re-evacuating as many times as required to satisfy the canister vacuum pressure limit, within the time limit specified for vacuum drying operations.

The FuelSolutions™ W74 canister helium backfill density shall be in the range of 0.0376 ± 0.0010 g-moles/liter. The required helium backfill quantities to achieve the required helium backfill density for the FuelSolutions™ W74 canister with each SNF assembly class are provided in Table 7.1-1. Placement of partial fuel assemblies, dummy fuel assemblies, or fuel assemblies in damaged fuel cans requires adjustment of the free volume and corresponding adjustment of the canister backfill quantity to meet the helium backfill density, as described in Section 7.1.4.8 of the FuelSolutions™ TS125 Transportation Cask SAR.

Table 7.1-1 - Helium Backfill Gas Quantities for the FuelSolutions™ W74 Canister

Fuel Assembly Class	Average Payload Free Volume, V_{PAYLOAD} (liters/assembly)⁽¹⁾	Canister Free Volume, V_{FREE} (liters)⁽¹⁾	Quantity of Canister Backfill Helium, m_{He} (grams)^(1, 2)
BRP 9x9	32.6	5981	900
BRP 11x11	32.6	5981	900

Note:

- (1) Payload free volume and canister free volume are based on intact fuel assemblies. Placement of partial fuel assemblies, dummy fuel assemblies, or fuel assemblies in damaged fuel cans requires adjustment of the free volume and corresponding adjustment of the canister backfill quantity to meet the helium backfill density, as described in Section 7.1.4.8 of the FuelSolutions™ TS125 Transportation Cask SAR.
- (2) Tolerance: +/- 25 grams.

This page intentionally left blank.

7.2 Procedures for Unloading Package

The major procedural steps for unloading a FuelSolutions™ canister transported by a FuelSolutions™ TS125 Transportation Cask are outlined in Section 7.2 of the FuelSolutions™ TS125 Transportation Cask SAR. Because of the configuration of the FuelSolutions™ TS125 Transportation Cask, opening a FuelSolutions™ canister and unloading the fuel assemblies from the canister inside this cask is typically performed in a shielded hot cell or using a dry cask-to-cask transfer system. Procedures for shielded hot cell and dry cask-to-cask transfer operations are not provided in this SAR. A FuelSolutions™ canister that is to be unloaded in a spent fuel pool is first transferred either vertically or horizontally to the FuelSolutions™ W100 Transfer Cask prior to unloading. Accordingly, the associated procedures for canister opening, reflooding, and fuel assembly removal are not associated with the regulatory requirements of 10CFR71⁴ and are provided in Section 8.4 of the FuelSolutions™ W74 Canister Storage FSAR.

⁴Title 10, Code of Federal Regulations, Part 71 (10CFR71), *Packaging and Transportation of Radioactive Materials*, U.S. Nuclear Regulatory Commission, October 2004.

This page intentionally left blank.

7.3 Preparation of Empty Package for Transport

The major procedural steps for the preparation of an empty FuelSolutions™ TS125 Transportation Cask for transport are outlined in Section 7.3 of the FuelSolutions™ TS125 Transportation Cask SAR.

This page intentionally left blank.

7.4 Appendix

The major procedural steps for assembly verification leak tests of a loaded FuelSolutions™ TS125 Transportation Cask in preparation for transport are outlined in Section 7.4 of the FuelSolutions™ TS125 Transportation Cask SAR.

This page intentionally left blank.

8. ACCEPTANCE TESTS AND MAINTENANCE PROGRAM

There are no acceptance test or maintenance program requirements for a sealed FuelSolutions™ canister relative to transport operations in a FuelSolutions™ TS125 Transportation Cask. The acceptance tests and maintenance programs to be performed on a FuelSolutions™ W74 canister for on-site storage and transfer operations are contained in Chapter 9 of the FuelSolutions™ W74 Canister Storage FSAR.¹ If a W74 canister is to be loaded in the spent fuel pool using the TS125 Transportation Cask (in accordance with Section 7.1.4 of the FuelSolutions™ TS125 Transportation Cask SAR)² and directly shipped off-site, perform the following inspection: Prior to placing the empty canister into the transportation cask, visually inspect the empty canister in accordance with Section 7.1.4.1 of the FuelSolutions™ TS125 Transportation Cask SAR.

¹ WSNF-223, *FuelSolutions™ W74 Canister Storage Final Safety Analysis Report*, Docket No. 72-1026, BNG Fuel Solutions Corporation.

² WSNF-120, *FuelSolutions™ TS125 Transportation Cask Safety Analysis Report*, NRC Docket No. 71-9276, EnergySolutions Spent Fuel Division, Inc.

This page intentionally left blank.